EDITED BY
PÉTER HEDVIG AND
RÓBERT SCHILLER

PROCEEDINGS OF THE FOURTH TIHANY SYMPOSIUM ON RADIATION CHEMISTRY

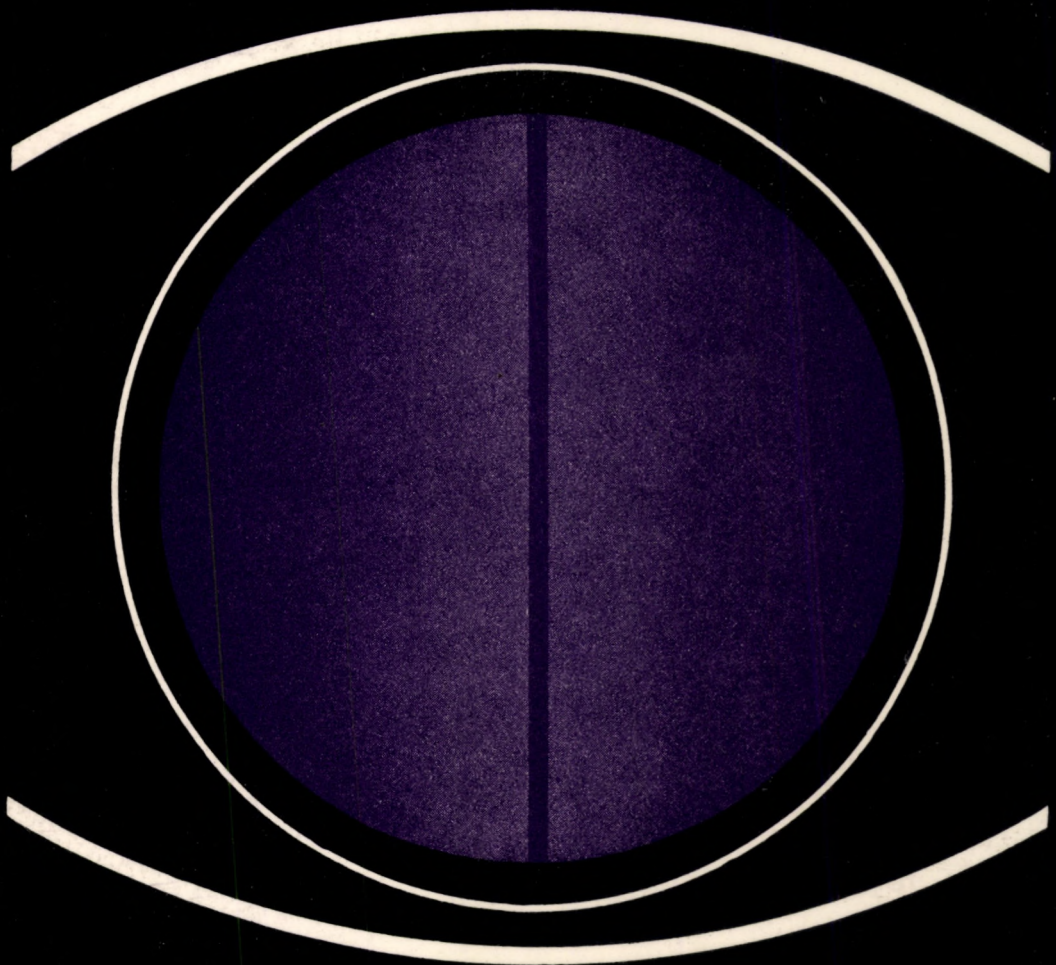

AKADÉMIAI KIADÓ, BUDAPEST

PROCEEDINGS OF THE FOURTH TIHANY SYMPOSIUM ON RADIATION CHEMISTRY

The fourth of the traditional international meetings on radiation chemistry followed the success of the previous ones. New results on the radiolysis of organic materials, polymers and aqueous solutions were presented by distinguished speakers from all over the world. 141 papers were discussed in three sections. 173 participants were present from 22 countries.

This volume contains the full text of the papers and discussions.

Besides the basic ideas and techniques of radiation chemistry, some industrial applications formed part of the programme. In contrast with the earlier meetings, biophysical and biochemical problems were also presented and discussed.

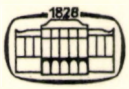

AKADÉMIAI KIADÓ • BUDAPEST

ISBN 963 05 1259 9

PROCEEDINGS OF
THE FOURTH TIHANY SYMPOSIUM
ON

RADIATION CHEMISTRY

The symposium, held at Keszthely, 1–6 June 1976,
was organized by the Hungarian Chemical Society
in co-operation with
the International Atomic Energy Agency, Vienna

HONORARY PRESIDENTS

GY. HARDY

G. SCHAY

CHAIRMAN

G. FÖLDIÁK

SCIENTIFIC SECRETARY

Á. SOMOGYI

SCIENTIFIC COMMITTEE

GY. CSERÉP

J. DOBÓ

J. FARKAS

P. HEDVIG

G. PUTIRSZKAJA

M. RODER

R. SCHILLER

L. WOJNAROVITS

ORGANIZING COMMITTEE

K. BEREI

L. BOTÁR

ZS. HORVÁTH

I. KISS

L. KISS

PROCEEDINGS OF THE FOURTH TIHANY SYMPOSIUM ON RADIATION CHEMISTRY

Edited by

PÉTER HEDVIG

and

RÓBERT SCHILLER

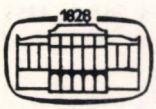

AKADÉMIAI KIADÓ · BUDAPEST 1977

ISBN 963 05 1259 9

© Akadémiai Kiadó, Budapest 1977

Printed in Hungary

CONTENTS

Opening Address 13

List of Participants 15

Preface 25

PART ONE

ORGANIC MATERIALS

M. SHIOTANI, S. MURABAYASHI, J. SOHMA
Spin trapping of radicals formed in γ-irradiated MTHF 29

L. VASÁROS, K. BEREI
Cage reactions of radioactive atoms? 39

J. GAWLOWSKI, J. NIEDZIELSKI, J. SOBKOWSKI
Neutralization of ions in the gas-phase radiolysis of ethane and propane 49

Zs. HORVÁTH, P. AUSLOOS, G. FÖLDIÁK
Comparison between liquid phase photolysis and radiolysis of C_3–C_4 hydrocarbon mixtures 57

P. CLAES, B. TILQUIN
Free radical distribution in the radiolysis of solid n–pentane 67

T. BRYL-SANDELEWSKA, R. K. BROSZKIEWICZ
The influence of NH_3 and C_2H_5OH on the yields of radiolytic products in gamma-irradiated liquid pentanes 73

E. N. AVDONINA
The mechanism of liquid n-hexane radiolysis 83

I. GYÖRGY, G. FÖLDIÁK
Effect of molecular structure on the radiolysis of binary hexane mixtures 93

J. KROH, J. MAYER, M. SZADKOWSKA
The isothermal luminescence of γ-irradiated 3-methylpentane glass doped with aromatic admixtures 101

A. OWCZARCZYK, W. STACHOWICZ
Transient species in the radiolysis of frozen (77 K) cis-pentene-2 111

J. KROH, E. SZAJDZIŃSKA, W. ŚWIĄTKOWSKI
Differential thermal analysis of γ-irradiated frozen methylcyclohexane 119

A. KOVÁCS, G. FÖLDIÁK
Radiolysis of aliphatic alkene-diene mixtures 125

J. KOLLÁR, G. FÖLDIÁK
Radiolysis of benzene, styrene and their binary mixtures 133

J. KROH, A. RUCIŃSKA-STAROSTA, S. KAROLCZAK
Structural effects in the radiolysis of saturated hydrocarbons 139

GY. CSERÉP, G. FÖLDIÁK
Effect of molecular structure on the radiolysis of alkenes 147

G. PEREZ
Gas-phase radiation chemistry of D_2-alkylbenzene mixtures 155

R. A. HOLROYD
Energetics and rates of electron attachment reactions in non-polar liquids 163

I. KALINOWSKI, J. G. RABE, W. F. SCHMIDT
Radiation-induced conductivity in saturated long chain liquid hydrocarbons 171

L. NYIKOS, E. ZÁDOR, R. SCHILLER
Temperature dependence of electron mobility in liquid hydrocarbons 179

H. J. ACHE, R. E. WILD, L. J. BARTAL
Interactions of positrons and positronium with inorganic compounds in solution 189

H. HEUSINGER, P. SCHULER
Comparison of the radiolytic and photolytic product formation of the CT-complex benzene–fumaric-nitrile 201

M. SPERANZA, F. CACACE
Gas-phase reactivity of radiolytically formed Brønsted acids toward aromatic halogenated substrates 209

G. G. CHIRAKADZE, H. M. NANOBASHVILI, G. V. KATSADZE
Radiolysis of mercapto- and thioacids 219

M. V. PANCHVIDZE, H. M. NANOBASHVILI, N. Z. DALAKISHVILI
The radiolysis of some compounds with −S−, −SH, −OH functional groups 227

Z. ŁUCZYŃSKI, H. WINCEL
Gas phase reactions of ions formed by electron irradiation of organic compounds 235

L. SH. NADIRASHVILI
Radiation phenomena in the ethane–silicon oxide system in the reactor nuclear radiation field 243

J. O. DZIĘGIELEWSKI, B. JEŻOWSKA-TRZEBIATOWSKA, E. KALECIŃSKA, J. KUDUK-JAWORSKA, J. KALECIŃSKI, J. NAVOJSKA
Gamma radiolysis of peptide and macrolide antibiotics in the solid state 249

B. G. DZANTIEV, A. N. ERMAKOV, V. N. POPOV
The role of H atoms in the radiolysis of hydrogen-containing substances 263

G. M. Zimina, N. A. Bach
Radical products of methanol radiolysis. Some dose rate effects 271

M. K. Abdullakhtov, G. A. Akopov, L. N. Lazarev, R. I. Lyubtsev,
Effect of alpha and gamma irradiation on the tributyl phosphate–CCl_4–HNO_3 extraction system 279

A. L. Karasev
Study of the liquid phase radiolysis of ethylene glycol by the spin trapping technique 289

I. Dvornik, M. Živadinović, S. Miščević, U. Zec, D. Ražem, F. Ranogajec, S. Makra, T. Pálfalvi
Radiation chemical response of the system isooctane–ethanol–chlorobenzene irradiated by neutrons of various spectra 295

M. Irie, T. Yorozu, K. Yoshida, K. Hayashi
Radiation induced racemization of 1, 1'-binaphthyl in tetrahydrofuran and toluene 303

PART TWO

POLYMERS

M. Dole, G. N. Patel, V. M. Patel, C. S. Hsu
Kinetics of chain allyl free radical decay in irradiated bulk film, hydrogenated and extended chain polyethylene 313

A. A. Dubinsky, O. Ya. Grinberg, Ya. S. Lebedev
Primary processes by radiolysis of solid paraffins: Formation of radical pairs and isolated radicals 325

A. Charlesby, R. Folland
Pulsed NMR studies of irradiated silicone fluids 335

P. Hedvig
Dielectric depolarization study of irradiated polypropylene 351

J. Dobó, P. Forgács, Á. Somogyi, M. Rőder
Some properties of radiation crosslinked polyethylene and ethylene–vinyl acetate copolymer 359

Gy. Hardy, F. Cser, K. Nyitrai, N. Fedorova
Investigation in the field of solid state polymerization XXXVIII
Radiation-induced polymerization of vinyl monomers with long chain substituents 365

L. Mahr, F. Cser, G. Kovács, Gy. Hardy
Effect of inhibitors on the gamma ray initiated solid state polymerization of acenaphthylene 377

A. Országh, P. Romiszowski
The modelling of solid-state polymerization by means of the Monte Carlo method 387

W. Pękala, I. Zuchowicz
γ-radiation-induced copolymerization of N-vinyl carbazole and acrylamide in the solid state 393

J. Żurakowska-Országh, A. Gumułka
Effect of temperature on kinetics of radiation induced solid-state polymerization of substituted acrylamides 401

H. P. Bohlmann, Ch. Schneider
Radiation induced polymerization and copolymerization of isobutene and isobutene-vinylidene chloride in thiourea canal complexes 411

L. Kiss, M. Irie, K. Hayashi
Study of the γ-ray produced paramagnetic species in the urea–acrylonitrile channel complex at low temperature 419

H. Kashiwabara, S. Shimada, H. Hori, H. Imamura, J. Itoh
Temperature dependence of the irradiation effects in polytetrafluoroethylene 431

V. M. Dziedziela, J. Rosiak
Some aspects of radiation-induced transformations of cellulose 439

D. Lindenau, G. Beck, U. Hagen, W. Schnabel
Kinetic studies of the degradation of polymers in solution 449

M. Bär, K. Friese, H. Rehor, J. Reinhardt
Fundamentals of a radiation-induced process for PVC chlorination 457

V. M. Goryaev, G. G. Ryabchikova, A. E. Chalykh, G. M. Plavnik
Radiolysis and polyamides, protection from ionizing radiation 465

M. Pietrzak, M. Wojciechowska
Influence of γ-irradiation on aromatic polyimides 471

E. Jaworska, L. Stolarczyk
The influence of the dose rate on the isomerization of cis-1,4-polyisoprene in natural rubber latex 477

A. Charlesby
Thermoluminescence in irradiated polymers 485

V. Ya. Kabanov, L. P. Sidorova, R. E. Aliev, V. I. Rudneva
The kinetics and mechanism of radiation–induced ionic graft polymerization 497

M. Pešek, J. Jarkovský, F. Pultar
Modification of inorganic materials with polymers by ionizing radiation 507

I. Yu. Babkin, A. I. Krasnogorov, K. N. Kitaev, G. V. Solovyeva
Diffusion of low molecular weight substances into radiation-grafted polymer films 513

V. K. Milinchuk, V. P. Kirjuhin, E. R. Klinshpont
Effect of high pressure on the formation of free radicals in radiolysis of polymers 521

A. S. Kuzminskii, T. S. Fedoseeva
Radiation graft–polymerization of polyfunctional substances in elastic matrix 527

G. Zeppenfeld, R. Kiessig
Investigation of electron beam cured unsaturated polyester resins 535

G. V. Shiryaeva, K. G. Glashkova, E. R. Klinshpont
Behaviour of free radicals in cured polyester resins 545

T. Czvikovszky
Pilot-scale experiments on radiation processing of wood–plastic composites 551

A. Bartl, L. Wuckel
On the grafting of polyethylene initiated by pre-irradiation in air 561

M. Barić, I. Dvornik, F. Ranogajec, J. Dobó
Apparent and true grafts in polyethylene–styrene system grafted by preirradiation in vacuo and in air 569

G. G. Ryabchikova, G. V. Zdolnikova, P. Ya. Glazunov, P. V. Vlasov, V. I. Spitsyn
Some problems of modification of fabrics by means of vapour phase radiation grafting 577

V. S. Ivanov, E. N. Konstantinova, I. I. Migunova, E. S. Oparina, V. K. Smirnova, E. E. Kever
The intensification of radiation-induced polymerization through complexation of monomers 583

S. Egusa, S. Arai, A. Kira, M. Imamura, Y. Tabata
Cationic polymerization of styrene by means of pulse radiolysis 591

A. Sugawara, S. Tagawa, Y. Tabata
Cationic polymerization of N-vinylcarbazole by means of pulse radiolysis 599

H. Heusinger, E. Wipfelder, J. Heinzl, H. Zott
Radiation induced polymerization of the system cyclohexene–N–ethylmaleimide 613

Binh Dinh-Ngoc, W. Schnabel
Radiation-induced polymerisation of β-nitrostyrene 623

M. Kerekes, J. Varga
Solid state polymerization of N-vinylphthalimide 631

A. P. Meleshevich, Yu. V. Vishev, A. E. Nesterov
Radiation-induced polymerisation of glycidyl methacrylate at low temperatures 641

V. P. Gordienko, K. A. Suprunenko, V. N. Doroshenko, A. M. Kabakchi
Radiation-chemical processes in polyethylene containing fillers of different nature 649

B. K. Pasalsky, Ja. I. Lavrentovich, V. A. Vonsyatzki, A. M. Kabakchi
LET effect on formation and stabilization of radicals in polymers 655

M. K. Asamov, Kh. U. Usmanov, A. A. Yulchibaev, T. S. Syrlybaev, S. G. Yulchibaeva, A. Valiev
Radiation polymerization of vinyl fluoride and vinylidene fluoride and their grafting to some fibres and films 663

PART THREE

AQUEOUS SOLUTIONS

J. Kroh, A. Płonka
Quantum effects in radiolysis at cryogenic temperatures 673

J. Kroh, J. Mayer, P. Polewoj
The electron transfer processes in X-irradiated alkaline ice at 77K 679

J. Grodowski, Z. P. Zagórski
Spectral sensitivity of photoconductivity effect in frozen alkaline solutions 685

A. M. Raitsimring, R. I. Samoilova, V. M. Moralev, Yu. D. Tsvetkov
Spatial distribution of trapped electrons and O^- in β- and γ-irradiated NaOH glasses at 77K 691

Z. Gasyna, S. Bachman, S. Galant, S. Witkowski
One-electron reactions in frozen aqueous solutions of cystine-containing biochemical systems 701

J. Kaleciński
Gamma radiolysis of alkali and alkaline earth nitrates in concentrated aqueous solutions in frozen and liquid states 711

B. V. Bol'shakov, M. P. Fuks, V. A. Tolkatchev, A. I. Burstein
Kinetic peculiarity of H-atom abstraction by methyl radicals in solid state 723

O. P. Stepanova, F. G. Nichiporov
Possible reactions of H_2O^+ ions and "dry" electrons in the radiolysis of aqueous solutions 731

I. Kraljić
Some regularities in OH rate constants 739

Z. Stuglik, Z. P. Zagórski
Radiation induced precipitation of ferric compounds from neutral aqueous ferrous salts solutions 747

S. Gordon, J. C. Sullivan, W. A. Mulac, D. Cohen, K. H. Schmidt
Pulse radiolysis of the lanthanide and actinide elements 753

H. M. Nanobashvili, M. V. Mamaladze
Radiation-chemical transformation of arsenic ions 761

R. K. Broszkiewicz
Radiation chemistry of the chlorocomplexes of the platinum group metals 767

M. V. Vladimirova, I. A. Kulikov, A. A. Ryabova, A. S. Milovanova
Radiation-chemical reduction of metal ions in HNO_3 solutions by γ- and α-radiolysis 777

Z. P. Zagórski, J. Grodkowski, Z. Zimek, K. Bobrowski
Pulse radiolysis of hydrates: relation to the radiation chemistry of aqueous solutions 787

W. Stiller, R. Schmidt
Polarization interactions in diffusion-controlled reactions of hydrated electrons with molecules 793

B. Hickel
Activation energy for the recombination of hydrated electrons in H_2O and D_2O 801

H. Büchler, R. E. Bühler
Transient ion-pairs in pulse irradiated alkyl iodides 809

M. S. Matheson, J. R. Miller, C. D. Jonah
Picosecond pulse radiolysis studies of hydrated electron reactions 819

H. Żegota, S. Bachman
Radiolysis of aqueous solutions of mono- and diphosphates of fructose 827

Yu. A. Panin, S. P. Buslaeva, R. V. Dzhagatspanyan, N. G. Konkov, L. M. Makarochkina, L. B. Upadyshev. M. T. Filippov
The radiolysis of a surfactant in the foam using ionizing radiation 837

K. Y. Al-Yamoor, A. Garner, K. M. Idriss Ali, G. Scholes
Reactions of pyrimidine radicals in irradiated aqueous systems: intermediate role of carbocations 845

T. Söylemez, T. I. Balkas
Studies on the reactions between aliphatic hydrocarbon radicals and radiolytically formed hydrogen peroxide 853

L. I. Kartasheva, Z. M. Potapova, A. K. Pikaev, T. V. Kharlamov
Pulse radiolysis of aqueous solutions of sodium o-iodhippurate 861

C. L. Greenstock, C. Banerjee, G. W. Ruddock
Interactions of drugs with biological macromolecules as studied by pulse radiolysis 871

J. Bös, O. Brede, W. Helmstreit, R. Mehnert
Application of pulse radiolysis and laser photolysis technique in studies of radiation induced processes in liquid phase 881

E. Kroó, L. Kovács, G. V. Putirskaya
A comparative study of radiation induced oxidation of heptene-1 in the pure organic phase and aqueous emulsion 891

M. Colosimo
Radiolysis of organic compounds in deaerated aqueous solutions. 2-Propanol and acetone in the presence of ferrous and ferric ions 897

I. Matus, G. V. Putirskaya
Radiolytic oxidation of p-xylene in water-emulsion 903

J. P. Suwalski, K. Bobrowski, Z. P. Zagórski
Regularities in the O^-, O_2^- and O_3^- reactions with homologues of organic cations 911

S. E. Gvilava, H. M. Nanobashvili, S. G. Ignatashvili
A study of radiolysis of thioacetamide and acetamide 917

V. A. Sharpatyi, N. V. Zakatova
Formation and conversion of radicals in irradiated aqueous DNP solutions 923

D. Bunn, R. C. Das
Radiolysis of aqueous solution of ethylene glycol in the presence of ferrous sulphate, sulphuric acid and excess oxygen 931

PART FOUR

MISCELLANEOUS PAPERS

R. F. Khairutdinov, K. I. Zamaraev
The role of long range tunnelling in electron transfer processes with particles other than trapped electrons 941

F. Q. H. Ngo, S. Noda, L. Kevan
Matrix endor studies of the orientation of amine molecules around trapped electrons in γ-irradiated amine glasses 951

I. I. Gromova, Kh. M. Islamova, N. A. Lebedev, N. G. Zaitseva
Chemical states of radioactive lanthanide atoms in Pr and Nd fluorinated beta-diketonates 963

Yu. A. Berlin
A theory of ion pair recombination taking into account tunnelling decay of trapped electrons 973

V. L. Tal'roze, Yu. A. Berlin, I. K. Larin
On the theory of radiation-induced initiation of chain processes 981

V. A. Zhigunov, G. I. Khaikin
On the possibility of solvation of an excess electron in liquid hydrogen chloride 991

G. R. Freeman, G. L. Bolton
Kinetics of presolvated electron reactions in concentrated solutions 999

B. Lévay, O. E. Mogensen
Correlation between inhibition of positronium formation by and chemical reaction rate of electrons with scavenger molecules in nonpolar liquids 1009

V. E. Zubarev, V. N. Belevskii, L. T. Bugaenko
Quantitative studies in the γ-radiolysis of liquid and solid alcohols by spin trapping method 1017

M. Roder, K. Pintér, K. Ritvay
On the radiation stability of some liquid crystals 1027

N. Grecz, G. Suchanek, T. Miura
Role of N-methylmaleimide in thermorestoration of radiation damage to hydrated bacterial spores 1037

E. A. Borisov, I. G. Kaplan, A. M. Miterev
Study of track structure of multicharged ion 1043

I. G. Kaplan, A. P. Markin
Interaction of high-energy electromagnetic radiation with molecules 1053

L. Botár, T. Vidóczy, I. Nemes
Stochastic treatment of diffusion controlled reactions in the case of non-homogeneous concentration of the reactants 1061

A. P. Meleshevich, E. G. Furman
Correlation between radiation-induced chemical transformation of some epoxides and their structure determined by the molecular orbital method 1071

Subject Index 1079

During the last quarter of a century, scientific research has, as we all know, developed by leaps and bounds. This progress has not, however, been uniform in all fields of research. There have been wide variations not only in the extent but also in the rate of development.

This uneven development has also been apparent in the application of isotopes and irradiation. Twenty years ago miracles were anticipated; ten years ago, just ten years after our earlier optimism, the future seemed to be more than a little bleak. Since the Fourth Conference on the Peaceful Uses of Atomic Energy organized by the United Nations in Geneva, i.e. during the last five years, a more realistic picture of the successful application of isotopes in research, in agriculture, in technical development (e.g. in the pharmaceutical and in the food industry), has emerged.

More or less the same tendency has been observable in radiation research and technology. We have already learnt that commonly used technologies based on thermal and catalytic processes and on those of photochemistry cannot be substituted by irradiation. On the other hand, in some industrial processes such as the crosslinking of polymers, e.g. in polyethylene, and in the sterilization of medical items, radiation technology provides an overwhelming improvement compared with traditional methods.

Knowledge gained in radiation research has been of no little benefit in the development of the chemical industry. New ideas have been supplied, such as the possibility of polymer grafting by irradiation, among others, and this idea has now become an integral process within the chemical industry. We are proud that this method was introduced by radiation chemists but this pride is tinged with a trace of envy that this problem has been industrialized by a cheaper, chemical method using peroxides.

With atomic power stations providing more and more spent fuel elements, radiating material of many, many megacuries activities as a byproduct in reprocessing will become available. More than twenty years ago, when radiation chemistry was in its infancy, everybody argued for the future on the basis of this cheap radiation supply anticipated by using such materials in the chemical industry. Although a somewhat controversial matter, nowadays the use of radiation sources such as

^{85}Kr, ^{90}Sr, ^{137}Cs, prepared from spent fuel elements is completely neglected, in radiation sterilization ^{60}Co activated from non-radioactive cobalt target by neutron flux is used, while the polymer industry requires mainly electron accelerators. A very important task of ours seems to be to solve this contradiction.

This latter problem is not the only one. I am deeply convinced that we are very far from a complete understanding of the possibilities of irradiation in obtaining valuable information about the structure and reaction mechanism of organic compounds. A breakthrough here would be of immense help in the development of theoretical organic chemistry as in this way "classical" organic chemistry would be able to get its hands on valuable information through which the chemical industry would again gain benefit. Thus, radiation chemistry would once more contribute to industrial development.

The more extensive elucidation of chemical mechanisms is promoted by the quick development of experimental methods. As one of the most important examples, the application of the pulse technique may be mentioned. By using this method many physical and physico-chemical processes preceding the chemical reaction can be studied. At the same time, this success due to the physics-oriented attitude in radiation research can be shaded by the recession of the chemical way of thinking

I think it is clear to everyone that the path of research is beset by obstacles and perhaps this symposium will help us to find the way to surmount them. This may give us cause for optimism.

Gábor Földiák

LIST OF PARTICIPANTS

AUSTRIA

Fowler, E.	International Atomic Energy Agency, Kärtnerring 11, Wien
Gehringer, P.	Österreichische Studiengesellschaft für Atomenergie, Lenaugasse 10, Wien
Schaudy, R.	Österreichische Studiengesellschaft für Atomenergie, Lenaugasse 10, Wien

BELGIUM

Tilquin, B.	University of Louvain, Bat. Lavoisier 1348, Louvain-la-Neuve

BULGARIA

Karaivanov, I.	Institute of Nuclear Research and Nuclear Energy, Academy of Sciences, Boul. Lenin 72, Sofia

CANADA

Freeman, G.	Chemistry Department, University of Alberta, Edmonton
Greenstock, C.	Atomic Energy of Canada Ltd, Medical Biophysics Branch, Pinawa, Manitoba

CZECHOSLOVAKIA

Benes, J.	Czechoslovak Academy of Sciences, Isotope Laboratory of the Institute for Biology Research, Budejovická, Prague
Haberda, D.	Vysoke Skolny Doprovnej, Zilina

Kopoldová, J.	Czechoslovak Academy of Sciences, Isotope Laboratory, Budejovická, Prague
Kourim, P.	Nuclear Research Institute, Řež
Pesek, M.	Institute for Research, Application and Uses of Radioisotopes, Pristavni 24, Prague
Spurny, Z.	Laboratory for Radiological Dosimetry, Na Truhlarce 39, Praha
Schweiner, Z.	Czechoslovak Atomic Energy Commission, Slezská 9, Praha

FEDERAL REPUBLIC OF GERMANY

Heinzl, J.	Institut für Radiochemie, Technische Universität, München, Garching
Heusinger, H.	Institut für Radiochemie, Technische Universität, München, Garching
Merwitz, O.	Institut für Biophysikalische Chemie, Kernforschungsanlage, Jülich, 5170 Jülich
Schneider, Ch.	Institute of Physical Chemistry, University of Cologne, Luxemburger Str. 116, Köln
Schreyer, M.	Institut für Radiochemie, Technische Universität, München, Garching
Wipfelder, E.	Institut für Radiochemie, Technische Universität, München, Garching

FRANCE

Delaire, J.	Laboratoire de Physico-Chimie des Rayonnements, Université de Paris XI 91405 Orsay
Hickel, B.	Commissariat à l'Energie Atomique, Centre d'Études Nucléaires de Saclay 91190 Gif-sur-Yvette
Kraljić, I.	Université de Paris-Sud, Laboratoire de Physico-Chimie des Rayonnements, 91405 Orsay
Magat, M.	Université de Paris Sud, Centre d'Orsay, 91405 Orsay
Puig, J.	Commissariat à l'Énergie Atomique, Centre d'Études Nucléaires de Saclay, 91190 Gif-sur-Yvette

GERMAN DEMOCRATIC REPUBLIC

Bartl, A.	Zentralinstitut für Festkörperphysik und Werkstofforschung, Helmholtzstr. 20, Dresden

Bär, M.	Zentralinstitut f. Isotopen und Strahlenforschung der AdW, Permoserstr. 15, Leipzig
Bös, J.	Zentralinstitut für Isotopen und Strahlenforschung der AdW, Permoserstr. 15, Leipzig
Hannig, H.	Staatliches Amt Für Atomsicherheit und Strahlenschutz, Waldowallee 117, Berlin
Heise, K. -H.	Zentralinstitut für Kernforschung der AdW, Dresden
Ihme, B.	Institut für Technologie der Fasern der AdW, Hohe Str. 6, Dresden
Kreiselmeier, G.	Forschungsinstitut für Textiltechnologie, Annaberger Str. 240, Karl-Marx-Stadt
Krumbiegel, P.	Isocommerz GmbH, Leipzig
Prösch, Ul.	Humboldt Universität, Hess Str. L. 1. Berlin
Reif, J.	Forschungsinstitut für Textiltechnologie, Annaberger Str. 240, Karl-Marx-Stadt
Redich, J.	Academy of Science of the GDR, Helmholtzstr. 20, Dresden
Stiller, H.	Zentralinstitut für Isotopen und Strahlenforschung der AdW, Permoserstr. 15, Leipzig
Wittig, F.	Institut für Technologie der Fasern der AdW, Hohe Str. 6, Dresden
Wuckel, L.	Zentralinstitut für Festköperphysik und Werkstofforschung, Helmholtzstr. 20, Dresden
Zeppenfeld, G.	Institut für Technologie der Fasern der AdW, Hohe Str. 6, Dresden

HUNGARY

Balázs, G.	Department of Plastics and Rubber, Technical University, Budapest, Stoczek u. 2, Budapest
Berei, K.	Central Research Institute for Physics of the Hungarian Academy of Sciences, Konkoly Thege út, Budapest
Botár, L.	Central Research Institute for Chemistry of the Hungarian Academy of Sciences, Pusztaszeri út 57, Budapest
Czvikovszky, T.	Research Institute for Plastics, Hungária krt 114, Budapest
Cser, F.	Research Institute for Plastics, Hungária krt. 114, Budapest

Cserép, Gy.	Institute of Isotopes of the Hungarian Academy of Sciences, Konkoly Thege út, Budapest
Daróczy, E.	MEDICOR Works, Hámán K. u. 98, Debrecen
Dobó, J.	Research Institute for Plastics, Hungária krt. 114, Budapest
Forgács, P.	Research Institute for Plastics, Hungária krt. 114, Budapest
Földiák, G.	Institute of Isotopes of the Hungarian Academy of Sciences, Konkoly Thege út 114, Budapest
Forster, P.	Factory of Plastics and Insulators, Budapest
Baranovics, P.	Factory of Plastics and Insulators, Budapest
Guczy, L.	Institute of Isotopes of the Hungarian Academy of Sciences, Konkoly Thege út, Budapest
György, I.	Institute of Isotopes of the Hungarian Academy of Sciences, Konkoly Thege út, Budapest
Hardy, Gy.	Research Institute for Plastics, Hungária krt. 114, Budapest
Hedvig, P.	Research Institute for Plastics, Hungária krt. 114, Budapest
Horváth, Zs.	Institute of Isotopes of the Hungarian Academy of Sciences, Konkoly Thege út, Budapest
Kálmán, I.	Research Institute for Plastics, Hungária krt. 114, Budapest
Kerecsen, J.	MEDICOR Works, Hámán K. u. 98, Debrecen
Kiss, L.	Research Institute for Plastics, Hungária krt. 114, Budapest
Kollár, J.	Institute of Isotopes of the Hungarian Academy of Sciences, Konkoly Thege út, Budapest
Kovács, A.	Institute of Isotopes of the Hungarian Academy of Sciences, Konkoly Thege út, Budapest
Kovács, G.	Research Institute for Plastics, Hungária krt. 114, Budapest
Kovács, L. P.	Central Research Institute for Chemistry of the Hungarian Academy of Sciences, Pusztaszeri út, 57, Budapest
Kroó, E.	Central Research Institute for Chemistry of the Hungarian Academy of Sciences, Pusztaszeri út, 57, Budapest

Levay, B.	Department of Physical Chemistry, Eötvös Loránd University, Puskin u. 11, Budapest
Mahr, L.	Research Institute for Plastics, Hungária krt. 114, Budapest
Matus, I.	Central Research Institute for Chemistry of the Hungarian Academy of Sciences, Pusztaszeri út 57, Budapest
Menczel, J.	Department of Plastics and Rubber, Technical University of Budapest, Stoczek u. 2., Budapest
Nagy, Á. G.,	Central Research Institute for Physics of the Hungarian Academy of Sciences, Konkoly Thege út, Budapest
Nagy, G.	Department of Plastics and Rubber, Technical University of Budapest, Stoczek u. 2., Budapest
Nyikos, L.	Central Research Institute for Physics of the Hungarian Academy of Sciences, Konkoly Thege út, Budapest
Nyitrai, K.	Research Institute for Plastics, Hungária krt. 114, Budapest
Putirszkaja, G.	Central Research Institute for Chemistry of the Hungarian Academy of Sciences, Pusztaszeri út 57, Budapest
Roder, M.	Central Research Institute for Physics of the Hungarian Academy of Sciences, Konkoly Thege út, Budapest
Said, F.	Institute of Isotopes of the Hungarian Academy of Sciences, Konkoly Thege út, Budapest
Schay, G.	Central Research Institute for Chemistry of the Hungarian Academy of Sciences, Pusztaszeri út 57, Budapest
Schiller, R.	Central Research Institute for Physics of the Hungarian Academy of Sciences, Konkoly Thege út, Budapest
Sipos, M.	MEDICOR Works, Hámán K.u. 98, Debrecen
Sipos, T.	Research Institute for Leather, Synthetic Leather and Shoe Industry, Paksi J. u. 43, Budapest
Somogyi, Á.	Research Institute for Plastics, Hungária krt. 114, Budapest
Stenger, V.	Institute of Isotopes of the Hungarian Academy of Sciences, Konkoly Thege út, Budapest
Szegő, É	Research Institute for the Textile Industry, Gyömrői út 86, Budapest
Takács, E.	Research Institute for Plastics, Hungária krt. 114, Budapest

Varga, J.	Department of Plastics and Rubber, Technical University of Budapest, Stoczek u. 2, Budapest
Vass, Sz.	Central Research Institute for Physics of the Hungarian Academy of Sciences, Konkoly Thege ut, Budapest
Vértes, A.	Department of Physical Chemistry, Eötvös Loránd University, Puskin u. 11, Budapest
Zádor, E.	Central Research Institute for Physics of the Hungarian Academy of Sciences, Konkoly Thege út, Budapest

IRAQ

Ai-Yamoor	School of Chemistry, University of Newcastle upon Tyne, Newcastle upon Tyne (present address)

ITALY

Castello, G.	Università di Genova, Istituto Chimica Industriale, Via Patore 3, Genova
Colosimo, M.	Laboratorio di Chimica Nucleare del CNR, Area della Ricerca di Roma, Monterotondo Stazione
Perez, G.	Laboratorio Chimica Nucleare, Area della Ricerca di Roma, Monterotondo Stazione
Speranza, M.	Laboratorio di Chimica Nucleare del CNR, Area della Ricerca di Roma, Monterotondo Stazione

JAPAN

Egusa, Sh.	University of Tokyo, Faculty of Engineering, Bunkyo-kum, Tokyo
Kashiwabara, H.	Nagoya Institute of Technology, Showa-kum, Nagoya
Sohma, J.	Hokkaido University, College of Engineering, Kitaku, Sapporo
Tabata, Y.	University of Tokyo, Faculty of Engineering, Bunkyo-kum, Tokyo

NETHERLANDS

Buitenhuis, R.	Institute for Nuclear Physics Research, Amsterdam

POLAND

Ambroz, H	Institute of Nuclear Research, Otwock-Swierk
Bobrowski, K	Institute of Nuclear Research, Dept. of Radiation Chemistry, Dorodna 16, Warszawa
Broszkiewicz, R.	Institute of Nuclear Research, Dept. of Radiation Chemistry, Dorodna 16, Warszawa
Dziedziela, W.	Institute of Applied Radiation Chemistry, Łódź
Dziegielewski, J.	The University Institute of Chemistry, Wrocław
Galant, S.	Technical University, Institute of Applied Radiation Chemistry, Łódź
Gawlowski, J.	Warsaw University, Laboratory of Radiochemistry, Warszawa
Grodkowski, J.	Institute of Nuclear Research, Dept. Radiation Chemistry, Dorodna 16, Warszawa
Jaworska, E.	Institute of Nuclear Research, Dept. of Radiation Chemistry, Dorodna 16, Warszawa
Kalecinski, J.	Polish Academy of Sciences, Institute for Low Temperature and Structure Research, Wrocław
Kroh, J.	Institute of Radiation Chemistry, Łódź
Mayer, J.	Institute of Applied Radiation Chemistry, Technical University, Łódź
Nagler-Kalecinska, E.	The University Institute of Chemistry, Wrocław
Országh, A.	University of Warsaw, Faculty of Chemistry, Warszawa
Ostrycharz, E.	Institute of Nuclear Research, Dept. of Radiation Chemistry, Dorodna 16, Warszawa
Parus, A.	Institute of Applied Radiation Chemistry, Technical University of Łódź, Łódź
Pekala, W.	Institute of Applied Radiation Chemistry, Technical University of Łódź, Łódź
Pietrzak, M.	Institute of Applied Radiation Chemistry, Technical University of Łódź, Łódź
Plonka, A.	Institute of Applied Radiation Chemistry, Technical University of Łódź, Łódź
Rucinska-Starosta, A.	Institute of Applied Radiation Chemistry, Technical University of Łódź, Łódź

Sobkowski, J.	Laboratory of Radiochemistry, Warsaw University, Zwirki i Wigury 101, Warszawa
Spodenkiewicz-Izycka, T.	Instytut Włókiennictwa, Łódź
Szajdzinska, E.	Institute of Applied Radiation Chemistry, Technical University, Łódź
Wincel, H.	Institute of Nuclear Research, Dept, of Radiation Chemistry, Dorodna 16, Warszawa
Zagórski, Z.	Institute of Nuclear Resarch, Dorodna 16, Warszawa
Zegota, H.	Institute of Applied Radiation Chemistry, Technical University of Łódź, Łódź
Zurakowska-Országh, J.	University of Warsaw, Faculty of Chemistry, Warszawa

SWEDEN

Christensen, H.	AB Atomenergi, Studsvik Nyköping
Lind, J.	Royal Institute of Technology, Department of Nuclear Chemistry, Stockholm

SWITZERLAND

Bühler, R.	Swiss Federal Institute of Technology, Laboratory of Physical Chemistry, Zürich

TURKEY

Söylemez, T.	Middle East Technical University, Marine Science Dept., Ankara

UNION OF SOVIET SOCIALIST REPUBLICS

Albin, A.	Karpov Institute of Physical Chem., Moscow
Akopov, G.	Leningrad
Avdonina, E.	Moscow State University, Moscow
Babkin, I.	The Branch of Karpov Institute of Physical Chemistry, Obninsk
Belevskii, W.	Moscow State University, Moscow
Berlin Yu, A	Institute of Chemical Physics, Academy of Sciences, of the USSR, Moscow
Bolkshakov, B.	Institute of Chemical Kinetics and Combustion, Novosibirsk

Chirakadze, G.	Institute of Inorganic Chemistry and Electrochemistry, Tbilisi
Dikanov, S.	Institute of Chemical Kinetics and Combustion, Novosibirsk
Dzantiev, B.	Institute of Physical Chemistry, Academy of Sciences of the USSR, Moscow
Karasev, A.	Moscow
Khairutdinov, R.	Institute of Chemical Physics, Academy of Sciences of the USSR, Moscow
Kuzminski, A. S.	Moscow
Lebedev, Ya.	Institute of Chemical Physics, Academy of Sciences of the USSR, Moscow
Mamaladze, M.	Institute of Inorganic Chemistry and Electrochemistry, Tbilisi
Nadirashvili, L.	Institute of Inorganic Chemistry and Electrochemistry, Tbilisi
Natroshvili, G.	Institute of Inorganic Chemistry and Electrochemistry, Tbilisi
Panin, Yu. A.	Institute of Radiation Technique, Moscow
Pikaev, A. K.	Institute of Physical Chemistry, Academy of Sciences of the USSR, Moscow
Ramadze, N.	Institute of Inorganic Chemistry and Elecrochemistry, Tbilisi
Romanzev, M.	Petroleum Institute, Moscow
Safonov, V.	Moscow
Stepanova, O.	Institute of Physics, Moscow
Tolkatchev, V.	Institute of Chemical Kinetics and Combustion, Novosibirsk
Tsvetkov, Y.	Institute of Chemical Kinetics and Combustion, Novosibirsk
Vladimirova, M. V.	Institute of Atomic Energy, Moscow
Zaitseva, N.	Joint Institute for Nuclear Research, Moscow
Zakatova, N.	Institute of Chemical Physics, Academy of Sciences of the USSR, Moscow
Zhigunov, V. A.	Institute of Electrochemistry, Academy of Sciences of the USSR, Moscow
Zimina, G.	Institute of Electrochemistry, Academy of Sciences of the USSR, Moscow

UNITED KINGDOM

Gardner, A.	School of Chemistry, University of Newcastle upon Tyne, Newcastle upon Tyne
Scholes, G.	School of Chemistry, University of Newcastle upon Tyne, Newcastle upon Tyne
Charlesby, A.	Department of Physics, The Royal Military College of Science, Shrivenham, Swindon, Wilts.
May, R.	Atomic Energy Authority, AERE, Harwell, Didcot

UNITED STATES OF AMERICA

Ache, H.	Department of Chemistry, Virginia Polytechnic Institute and State University, Blacksburg, Virginia
Dole, M.	Dept. of Chemistry, Baylor University, Waco, Texas
Gordon, Sh.	Argonne National Laboratory, Argonne, Illinois
Grecz, N.	Illinois Institute of Technology, Chicago
Holroyd, R.	Hahn Meitner Institut für Kernforschung GmbH, 1000 Berlin 39, Glienicker Str. 100, (present address) Brookhaven National Laboratory, Upton, N.Y., USA
Kevan, L.	Wayne State University, Department of Chemistry, Detroit, Michigan

WEST BERLIN

Kalinowski, I.	Hahn Meitner Institut für Kernforschung GmbH, 1000 Berlin 39. Glienicker Str. 100
Lindenau, D.	Hahn Meitner Institut für Kernforschung GmbH, 1000 Berlin 39, Glienicker Str. 100

YUGOSLAVIA

Dvornik, I	Institute "Ruder Boskovic", Zagreb
Ranogajec, F.	Institute "Ruder Boskovic", Zagreb

PREFACE

It is for the fourth time that an international symposium on radiation chemistry has been held at Lake Balaton – somewhat pompously called the Hungarian Sea – and the present volume is the fourth in the series of the Proceedings published after the symposia.

The publication of conference proceedings is often severely questioned. In print, the great advantage of personal encounters, the lively exchange of information, the thought-provoking atmosphere of the debates, all these fade away and only a random ensemble of papers is left which could have been published in a number of journals. This must be particularly true in the case of a volume which deals with a subject as vast as radiation chemistry is today. One of the reviewers of an earlier member of this series justly called it a method rather than a discipline.

Indeed, only a rare bird of a scientist would find the food of his interest in such far-lying fields as, for example, the fabrication of wood-plastic composites, the theory of tunnelling, the radioresistance of bacteria and the field of positron annihilation. So one is tempted to think that it is only local tradition and a general predilection for using the once shining, heartening and clear-cut term radiation chemistry that prompted us to publish these Proceedings.

It would be unfair to deny completely the role of such feeling. We have, however, some more realistic excuses too if an excuse is truly needed for our endeavour. We offer in the following pages a survey which has been made comprehensive in a certain sense. The organizers of the symposium welcomed all the works submitted the subjects of which have been developed from, or the results of which might contribute to the main body of radiation chemistry. It is to be hoped that besides the report of their present activity, the volume may give some information about what radiation chemists offer to other branches of science and what they can learn from them.

The second feature of the Tihany meeting was its truly international character. The opening of the barriers of languages and national journals could, we hope, justify in itself the publication of the present work.

As little edition as was compatible with general intelligibility and the rules of the Publisher was performed both on lectures and discussion notes. We tried to keep a balance between aggressive intrusion upon the authors' style and uncontrolled freedom in language or notation.

The Editors

PART ONE

ORGANIC MATERIALS

SPIN TRAPPING OF RADICALS FORMED IN γ-IRRADIATED MTHF

M. Shiotani, S. Murabayashi, J. Sohma
Faculty of Engineering, Hokkaido University, Sapporo 060, Japan

Introduction

ESR is one of the powerful experimental methods in radiation chemistry, however, it has a big disadvantage in that this method always needs a long time for observation and is not suitable either for pulse radiolysis or for detection of short-lived free-radicals in a liquid phase. A system from which ESR spectrum can be observed must be in the solid phase in order to trap unstable radicals. If ESR can be applied to radiation chemistry in liquid phase by a simple technique, interesting information on reaction initiated by radiation in liquid phase can be obtained. One of the promising methods for this purpose is spin-trapping /1/. A spin-trap, S, which has been dissolved in a system, is attacked by an unstable free-radical, R·, to form a long-lived radical RS·, which is called a spin-adduct. ESR spectrum is observed from the radical RS·, which is long-lived even in a liquid phase. The radical species of RS can be identified by an analysis of the observed spectrum and therefore the unstable free-radical R· is now determined. This is a spin-trapping technique. Since ESR observation can be made for a spin-adduct in liquid phase, an observed spectrum is so well resolved generally that analysis of the spectrum can be done more clearly. Thus, identification of a radical based on the spectral analysis is much less ambiguous than that on a spectrum observed from a solid system. At first, this method was applied by Wargon and Williams /2/ to the radiolysis of liquid methanol with the use of t-butylnitroxide as a spin-trap. Mao and Kevan /3/ applied this method to the radiolysis of the same system by using a different spin-trap, phenyl-t-butylnitrone, in their case. Both groups have proved that the spin-trapping method is useful for studies in radiation chemistry, although they reached different conclusions on the radiolysis mechanism of methanol. It seemed to us that different conclusions in the above studies come from the differences in the relative stability of the produced spin adducts, RS·, and/or the relative reactivity between the spin trapping reagents and the radical species formed by radiation. Thus, we have carried out more detailed study on radiolysis of methanol by using another spin-trap, 2, 4, 6, tri-t-butylnitrosobenzene, /4/ (BNB),

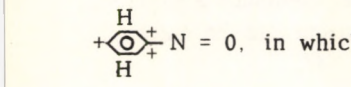

N = O, in which + represents a t-butyl group. $(CH_3)_3C-$. If this spin-

trap is attacked by a bulky radical R_1, a formed spin-adduct is an anilino-type radical, $R_1-O-\dot{N}-\phi$, in which ϕ stands for  group of BNB. If an unstable radical R_2 is not so bulky, the formed spin-adduct is a nitroxide-type radical $R_2-\overset{|}{\underset{O}{N}}-\phi$.

Experimental

2, 4, 6, tri-tert butylnitrosobenzene (BNB) was synthesized by Inamoto and his associates /5/ and the used BNB in this experiment was kindly supplied to us by Prof. Inamoto of Tokyo University. BNB solutions of MTHF were prepared and introduced into 2 mm i. d. quartz ESR tube in vacuum. The concentration of BNB was varied from 0. 01 to 0. 1 mol%. In order to avoid any complication resulting from a build-up of radiolysis products, low irradiation doses of less than 0, 1 Mrad were employed. After irradiation the samples were stored at liquid nitrogen temperature up to the moment of ESR measurement. ESR spectra were recorded in the temperature range of $-196\ ^{o}C$ to $0\ ^{o}C$ with JEOL JEX-1 spectrometer attached variable temperature control unit, operating at 9. 4 GHz with 100 KHz modulation. The signal of Mn^{2+} in MgO was used for the calibration of the magnetic field and the relative intensities of spectra.

Experimental Results and Identification of the Spin-adducts

Methanol

Before going into the main part of this communication, a good example of the spin trapping should be mentioned, that is the spin-adducts formed from the irradiated methanol in liquid phase. The spectrum observed at $-20\ ^{o}C$ from the BNB 0. 1 mol % solution of methanol, which was irradiated at $-78\ ^{o}C$, is shown as Fig. 1-A. This observed spectrum consists of three different spectra marked I, II, and III in the figure. The spectra shown as B, C and D are the theoretical spectra from the three different species of the spin-adducts, $\phi-\overset{|}{\underset{O}{N}}-CH_2OH$, $\phi-\overset{|}{\underset{O}{N}}-H$ and $\phi-\overset{|}{\underset{O}{N}}-OCH_3$, respectively. Close similarities between each of the three components, I, II and III, and each of the spectra, B, C and D, lead us to the conclusion that the spectrum I is ascribed to the spin-adduct $\phi-\overset{|}{\underset{O}{N}}-CH_2OH$, II to $\phi-\overset{|}{\underset{O}{N}}-H$ and III to $\phi-\overset{|}{\underset{O}{N}}-OCH_3$. These identifications of the spin-adducts prove formation of the three different radicals, $\cdot CH_2OH$, $\cdot H$ and $\cdot OCH_3$, in the γ-irradiated methanol. It is worthwhile noting that the presence of hydrogen atom in irradiated liquid methanol is experimentally verified. Detailed discussion on both the identifications and the mechanism of radiolysis of liquid methanol is described elsewhere /4/.

2-MTHF (tetrahydro-2-methylfuran)

2-MTHF is an interesting system in radiation chemistry because this system is frequently used as a matrix for a trapped electron. The two kinds of MTHF radicals,  and  , were reported by several researchers /6-9/ based on the ESR studies on irradiated MTHF in a solid phase. However, no ESR studies have been reported on irradiated MTHF in liquid phase, and little is known on radical species produced by γ-irradiation in a liquid phase. The spectrum observed at $-30^{\circ}C$ from the BNB 0.1 mol % solution of MTHF, which was irradiated at $-196^{\circ}C$, is shown as Fig. 2-1. The spectrum at $20^{\circ}C$ after warming the sample to $80^{\circ}C$ is shown as (2) in the same figure. By this heat treatment the peaks marked with the arrows in Fig. 2-1 disappeared. This vanished spectrum is quite similar to the triple-double triplet spectrum, C, in Fig. 1. Thus, one can ascribe this vanished spectrum to the hydrogen-adduct  . The spectrum, Fig. 2-2, consists of two components, triple-triplet (T), and triple-quartet (Q), as shown with the stick diagrams in the same figure. The T spectrum is attributed to the anilino-type spin-adduct  in which the triplet with large separation and equal intensities comes from the coupling of the nitrogen and the 1:2:1 triplet with the small separation from the coupling with the two metha-hydrogens of the phenyl ring of BNB. The spectrum Q may be attributed to the radical species having weak and same coupling of the three hydrogens, and there are spin-adducts from five possible MTHF radicals (Q radicals), from which the spin-adducts to give the Q spectrum are formed:  ,  ,  , and . The above-mentioned analyses of the components of the observed spectrum indicate the formation of hydrogen and the five species of the MTHF radicals by γ-irradiation at 77/K:  (T),  (Q-1), (Q-2), (Q-3), (Q-4). Among these species only the species (T) has been reported in the literatures /6-9/.

The observed spectrum from the dilute MTHF solution of BNB (0.01 mol %) is shown in Fig. 3-1. The relative intensity of the T component to the Q was found to increase with the decreased concentration. After the heat treatment at $80^{\circ}C$ the spectrum observed at $50^{\circ}C$ is reproduced as Fig. 3-2. Apparently the spectrum is the triple-triplet, which is identical to the T. This fact confirms that the original spectrum is a superposition of the T and the Q and the latter is less stable than the former.

It was found that the spectrum of the BNB 0. 1 mol % solution of MTHF irradiated in liquid phase is same to the spectrum of Fig. 2-2. This identity in the spectrum means that the radical species produced in a liquid phase by γ-irradiation are same to those in a solid phase, except for the hydrogen formation, which had decayed out in Fig. 2-2. Thus, one can say that the radicals produced by irradiation of liquid MTHF are, probably, T, Q-1, Q-2, Q-3 and Q-4. It was also found that BNB concentration dependence of the yield ratio of the T component to the Q one is same to that in the solid phase.

Discussion

In the last section it has been mentioned that species responsible for the Q spectrum is either one of the Q-radicals or all Q s. No spectrum was found to be attributed the spin adduct of methyl radical, which is the partner radical of the Q-1 when a direct scission is assumed. Thus, it is not likely that the Q-1 species is an origin of the Q spectrum. It is known /10/ that the hydrogen attached to the site adjacent to the oxygen is less stable and therefore it is more probable that the radical Q-3 is more easily formed than the others, Q-2, and Q-4. Accordingly one may assume that a predominant radical is presumably Q-3.

It is reasonable to assume that an unstable intermediate R· is either attacked by the spin-trap, S, or converted to a secondary species, R', that is

$$R\cdot + S \longrightarrow RS\cdot \qquad /1/$$

$$R\cdot + MTHF \longrightarrow R'\cdot + R-H \qquad /2/$$

$$R'\cdot + S \longrightarrow R'S\cdot \qquad /3/$$

and these two processes, (1) and (2), compete with each other. If the BNB concentration is high, reaction (1) proceeds more easily than the other and therefore concentration of RS· is larger than that of R'S· in this case. It was found in both liquid and solid phases that the ratio, Q/T, increased with the increased BNB concentration. Interpreting the experimental result with this competitive reactions one can say that the radical species Q-3 (or other Qs) is a precursor to the T radical. That is,

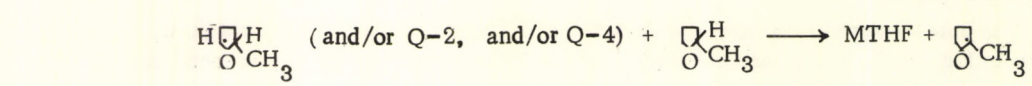

The lower stability of the Q spectrum, which is shown in Fig. 3, supports our interpretation that the radical species T is the product from the Q radicals and more stable than the others. The data and considerations presented above can be used to reach a conclusion that the radical species,  , which was reported

in the literature, is not always the primary product but the secondary one produced through the above process.

Strong electron affinity was found for BNB in the studies of irradiated methanol /4/, and the BNB anion could be converted into the hydrogen adduct through the two probable processes, a proton transfer

$$R'H + BNB^{\cdot -} \longrightarrow R'^{\cdot -} \text{ (non-radical)} + BNBH\cdot$$

and a neutralization

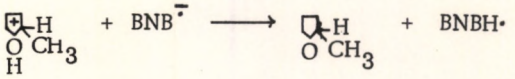

It was found that the spectrum from the hydrogen adduct was increased gradually with the decreases of the $BNB^{\cdot -}$ spectrum. And photochemical experiments showed that BNBH· was produced from $BNB^{\cdot -}$ in the absence of MTHF cation. These results indicate that the hydrogen adducts results from the neutralization process as well as the addition of the free-hydrogen.

Acknowledgement. The authors wish to express their cordial thanks to Prof. Inamoto, Tokyo University, for his kindness in having supplied us with BNB.

References

/1/ E. G. Janzen, Accounts Chem. Res, 4, 31 (1971)
/2/ J. A. Wargon, F. Wiliams, J. Am. Chem. Soc., 94, 7917 (1972)
/3/ S. W. Mao, L. Kevan, J. Phys. Chem., 78, 91 (1974)
/4/ M. Shiotani, S. Murabayashi, J. Sohma, Int. J. Radiation Phys. Chem. (in press)
/5/ N. Inamoto et al., Bull. of Chem. Soc. Japan, 42, 3559 (1969)
/6/ D. R. Smith, J. Pierori, Can. J. Chem., 43, 2141 (1965)
/7/ T. Iwamoto et al., Int. J. Rad. Phys. Chem., 1, 1 (1969)
/8/ J. Lin, K. Tsuji, F. Williams, Trans, Fard. Soc., 64, 2896 (1968)
/9/ T. Shiga et al., Ann. Rept. of Res. Inst. Kyoto Univ., 3, 19 (1970)
/10/ W. T. Dixon, R. O. C. Norman, J. Chem. Soc, 4850 (1964)

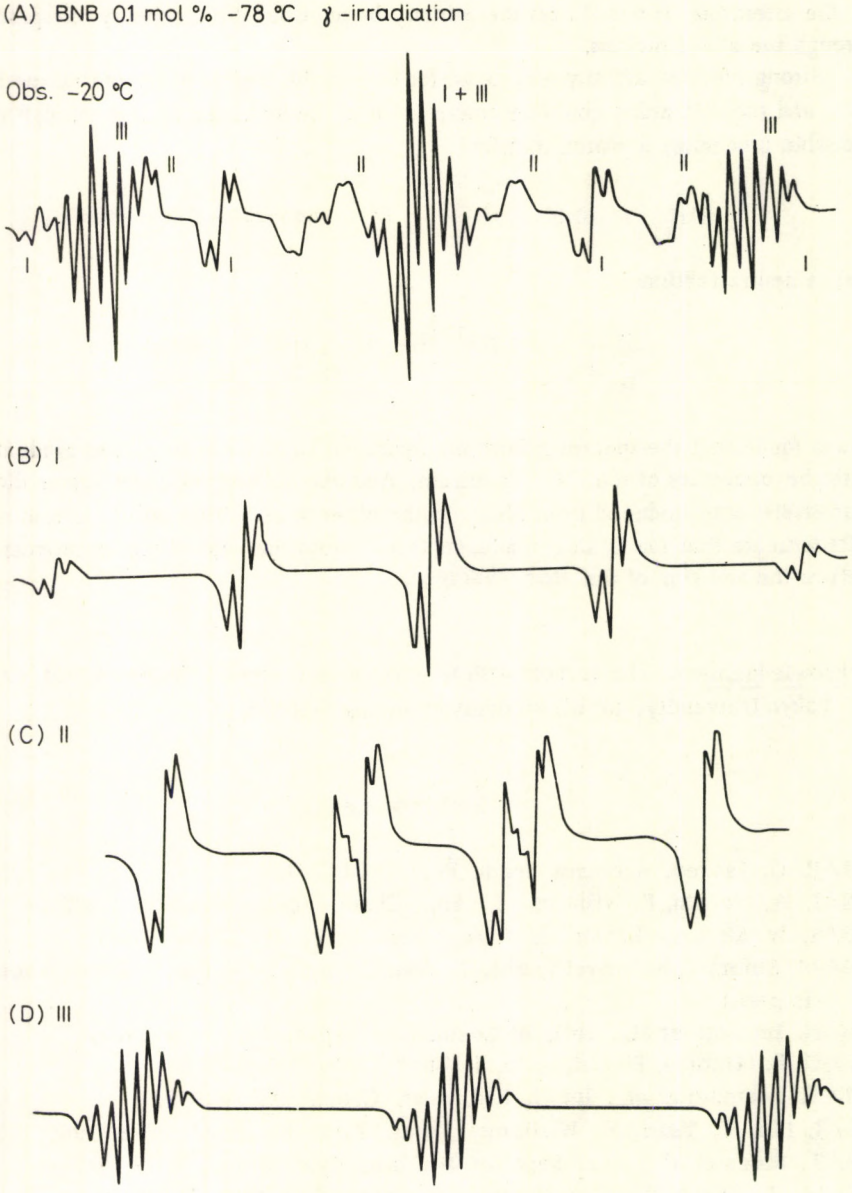
(A) BNB 0.1 mol % -78 °C γ-irradiation
Obs. -20 °C
I + III
III
II
II
II
II
III
I
I
I
I
(B) I
(C) II
(D) III

Fig. 1

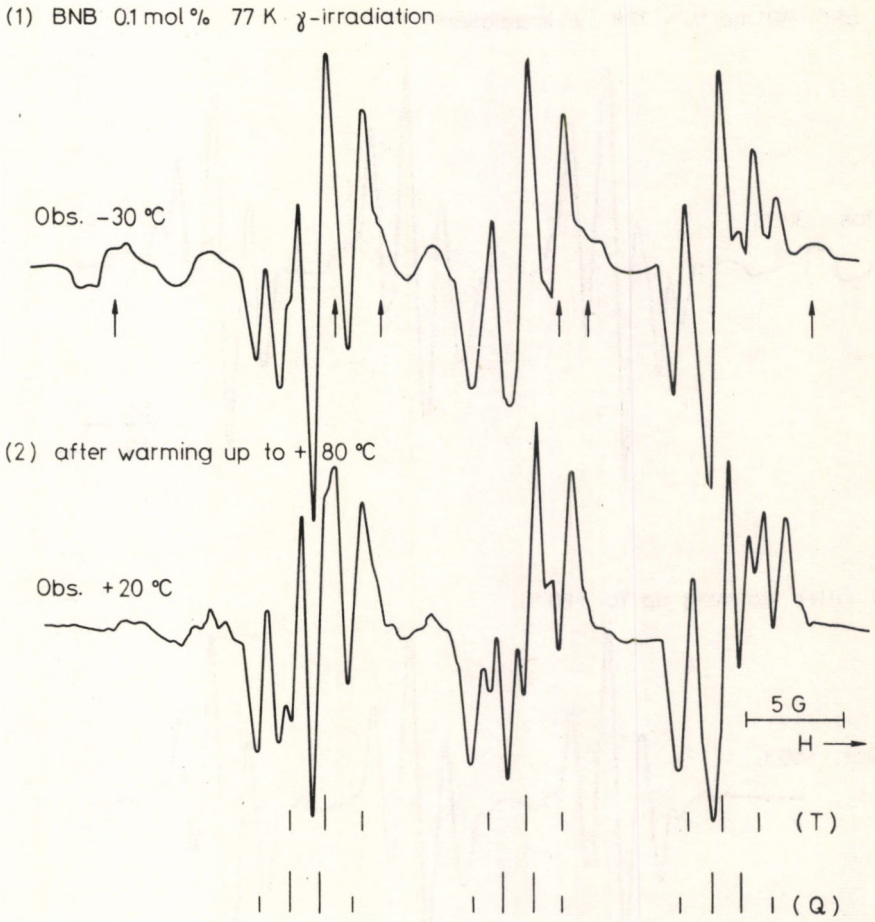
(1) BNB 0.1 mol % 77 K γ-irradiation
Obs. -30 °C
(2) after warming up to + 80 °C
Obs. +20 °C
5 G
H
(T)
(Q)

Fig. 2

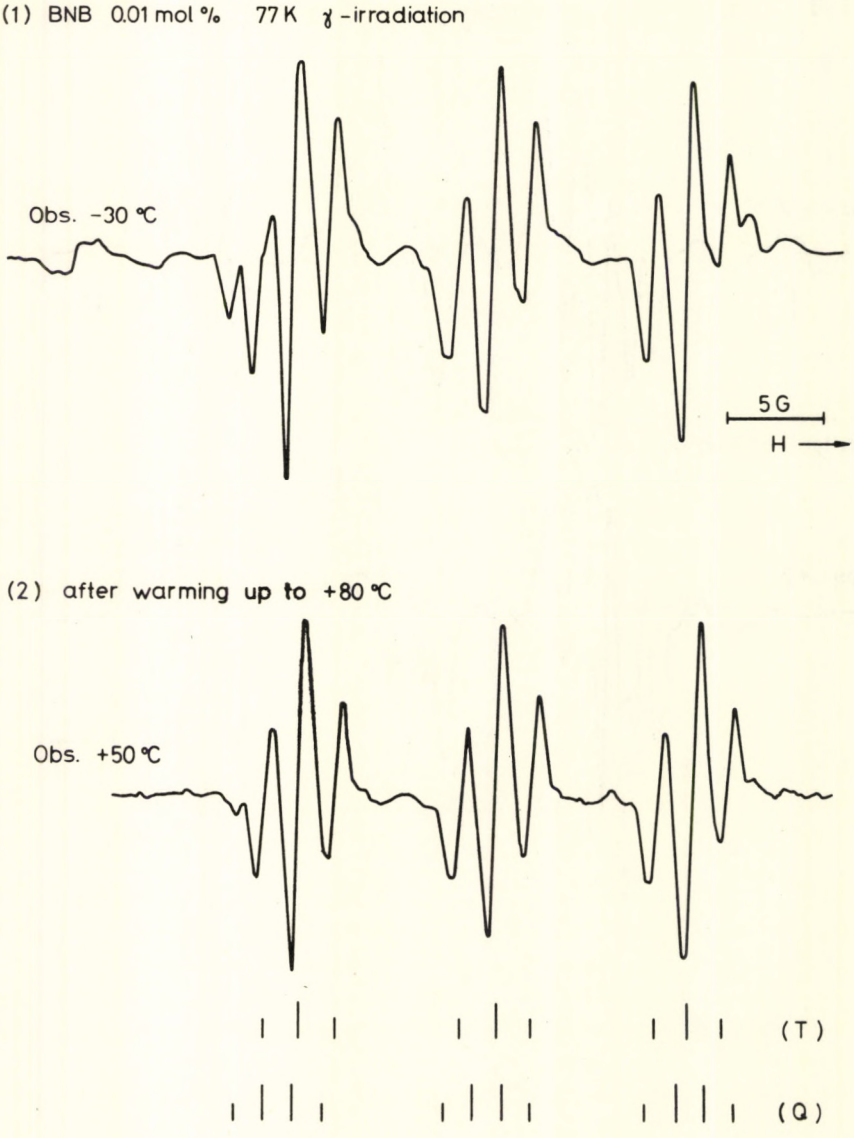
(1) BNB 0.01 mol % 77 K γ-irradiation
Obs. -30 °C
5 G
H
(2) after warming up to +80 °C
Obs. +50 °C
(T)
(Q)

Fig. 3

L. KEVAN

1) How stable is BNB to UV radiation? Nitroso compounds are usually quite unstable to UV.

2) Are your results any different if you γ-irradiate at room temperature instead of 77 K?

3) It is interesting that you find the

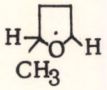

radical (I) as we did in our study of γ-irradiated MTHF in adamantane (J. Phys. Chem. 1976) However, I would like to comment that our hyperfine constants for either or both radical I and radical II

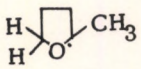

do not reproduce the ESR spectrum of the radical seen in γ-irradiated MTHF glass at 77 K after visible bleaching. Thus it appears that the "radical" spectrum in MTHF glass is apparently due to more than one radical and is still not understood.

J. SOHMA

1) We have never checked the stability of BNB against UV. However, it was found that BNB trapped the radicals produced by the reaction with the electrons, which were liberated from TMPD by UV illumination. From this fact I could say that not all of BNB were decomposed by UV and BNB survived sufficiently to produce spin adducts even under UV illumination.

2) The ESR spectrum observed from the spin adducts after γ-irradiation at room temperature is identical to that I presented in the slide except for the complete disappearance of the spectrum from the hydrogen adduct. That is, the spectrum consists of the A and T components.

3) I agree with you on the point that the hyperfine couplings of the spin adducts are not directly connected to the couplings of the original radicals. But I believe that both types of radicals may exist in γ-irradiated MTHF at 77 K.

CAGE REACTIONS OF RADIOACTIVE ATOMS?

László Vasáros, Klara Berei
Chemistry Department, Central Research Institute for Physics, Budapest, Hungary

The recombination of radicals formed in pairs is usually much faster than one would expect on the basis of their bulk concentration. This phenomenon discovered by Franck and Rabinowitsch /1/ and usually called "cage effect" may render misleading results in the study of hot atom reactions in condensed systems. Thus thermal combination with one of the radicals produced in the neighbourhood, e.g. by collision with hot atom $[Y]^{\neq}$, may result in formation of the same compound as that originated from its hot replacement reaction. The processes (1) and (2) lead to the same product.

$$[Y]^{\neq} + RX \longrightarrow [R^{\cdot} + X^{\cdot} + Y^{\cdot}]_{cage} \longrightarrow RY + X^{\cdot} \qquad (1)$$

$$[Y]^{\neq} + RX \longrightarrow RY + X^{\cdot} \qquad (2)$$

Despite frequent discussions on the "caging effect" postulated originally by Willard /2/ in the early days of hot atom chemistry and investigated by a number of authors /3-8/, its exact role remained highly speculative in actual systems. This is largely due to scavenger techniques usually applied which are inappropriate to distinguish between hot reactions and thermal processes occurring in the solvent cage.

The most straightforward approach to this problem seems to be the study of the yields of major products as a function of increasing density which varies continuously from the gas to the liquid state /9-13/. These investigations led, however, to diverging results and contradictory conclusions. Hence the role of the cage recombination remains one of the most enigmatic questions in the field of hot replacement reactions occurring in condensed phases, as was pointed out by Stöcklin /14/ in a review lecture at the Panel Meeting on Hot Atom Chemistry held in Vienna two years ago.

The aim of the present work is to attempt a differentiation between hot replacement and cage reactions in systems consisting of substituted hydrocarbons and ^{38}Cl atoms produced by (n,γ) nuclear reactions. We try to study the incidence of cage effect in two different ways.

(1) Compounds which were previously known to be produced only by thermal radical recombination and never by hot replacement, e.g. isomerization products are searched.

(2) The validity of conventional reaction kinetics for the formation of major radioactive products is investigated, those laws being thought to prevail only if the reactants are homogeneously distributed.

Experimental

Irradiatons were carried out in the beryllium reflector of the WWRS reactor with a neutron flux of 10^{13} cm^{-2} s^{-1} for a duration of about 1-3 s using a pneumatic tube. The administered γ-dose was not higher than 10^4 rad.

The inorganic and organic activities were determined by means of phase separation between carbon tetrachloride and aqueous NaOH solution which contained Na_2SO_3 as a reducing agent. The individual organic products were separated by radio gas chromatography, Gas chromatographic columns were: 20% Igepal CO-880 or 20% Polyethylene glycol-1500 on Chromosorb P-AW and 20% SF-96+6% Betone 34 on Chromosorb W-AW DMCS for aromatic and 20% Apiezon L on Chromosorb P-AW for aliphatic systems. The activity of each fraction was measured by a NaI (T1) well-type scintillation counter under identical conditions.

Results and discussion

The replacement yields of ^{38}Cl for F, Cl, NO_2 in liquid disubstituted benzene derivatives are summarized in Table 1. No perceptible yield of any isomerization product was found, although considerable yields for replacement in the original positions were observed. Even if 50 mole % of carbon tetrachloride was added, a compound likely to hinder the escape of thermal chlorine atoms from the liquid cage, no isomerization products could be detected in o-$C_6H_4ClNO_2$.

This is well in line with our earlier results /15/ obtained for hydrogen replacement by halogen atoms in fluorobenzene and chlorobenzene which did not show any major contribution of thermal radical reactions either. The isomer distribution of the replacement was nearly statistical and the small deviation from the random values (higher para, lower meta yields) was just opposite to that which one would expect of thermal radical reactions.

For a more detailed study two compounds, 1,1,-$C_2H_4Cl_2$ and o-$C_6H_4Cl_2$ were selected which could be regarded as good representatives of those aliphatic and aromatic compounds, respectively, which were most often used in our investigations. In one part of the experiments the conditions were varied to promote the cage effect: addition of CCl_4, irradiation in the solid state. In the other part hindering of this effect was intended by addition of aliphatic alcohols which are known as excellent scavengers of thermal chlorine atoms. A number of data concerning the yields of different stabilization products of ^{38}Cl were obtained from these systematic investigations. But isomerization products, i. e. meta or para-C_6H_4Cl ^{38}Cl and

Table 1

^{38}Cl replacement yields in liquid disubstituted benzene derivatives

SYSTEM		YIELD /% of total activity/					
		ortho	meta	para	ortho	meta	para
		$^{38}Cl \longrightarrow Cl$			$^{38}Cl \longrightarrow F$		
C_6H_4ClF	ortho	24.4±0.5	0.3	0.4	3.0±0.1	<0.3	<0.3
	meta	0.3	22.5±0.5	<0.3	<0.3	3.8±0.3	<0.3
	para	0.4	0.3	23.4±0.8	<0.3	0.3	3.5±0.2
		$^{38}Cl \longrightarrow Cl$			$^{38}Cl \longrightarrow NO_2$		
$C_6H_4ClNO_2$ + 50 mole % CCl_4	ortho	4.3±0.3	<0.3	0.3	15.5±0.8	0.3	0.4
		2.3±0.2	<0.3	<0.3	6.9±0.5	<0.3	<0.3
	meta	<0.3	3.5±0.1	<0.3	0.3	12.6±0.5	0.3
	para	<0.3	<0.3	3.5±0.3	<0.3	0.3	9.4±0.2
		$^{38}Cl \longrightarrow Cl$					
$C_6H_4Cl_2$	ortho	29.3±0.8	0.4	0.4			
	meta	0.5	28.6±0.6	0.4			
	para	0.4	0.3	38.1±1.1			

Table 2

^{38}Cl replacement yields in o-$C_6H_4Cl_2$ and its mixtures with CCl_4, CH_3OH and C_2H_5OH

SYSTEM		YIELD /% of total activity/		
		ortho	$C_6H_4Cl^{38}Cl$ meta	para
o-$C_6H_4Cl_2$	L	28.9 ± 0.8	0.4	0.3
	Cr.	11.1 ± 0.5	0.6	0.5
o-$C_6H_4Cl_2$ + CCl_4				
50 mole % L		24.5 ± 1.0	0.5	0.5
70 mole % L		23.3 ± 0.9	0.4	0.3
90 mole % L		20.2 ± 0.8	0.3	0.6
95 mole % L		15.8 ± 0.9	<0.3	<0.3
o-$C_6H_4Cl_2$ + CH_3OH				
10 mole % L		20.1 ± 1.0	0.4	0.3
90 mole % L		1.9 ± 0.1	<0.3	<0.3
mole % Gl.		1.7 ± 0.1	<0.3	<0.3
mole % Cr.		11.2 ± 0.7	0.5	0.4
o-$C_6H_4Cl_2$ + C_2H_5OH				
90 mole % L		1.2 ± 0.04	<0.3	<0.3
mole % Gl.		1.1 ± 0.03	<0.3	<0.3
mole % Cr.		9.2 ± 0.4	0.5	0.6

Abbreviations: L- Liquid, Gl. – glassy, Cr. – crystalline

1,2-$C_2H_4Cl\ ^{38}Cl$ for irradiated ortho-$C_6H_4Cl_2$ and 1,1-$C_2H_4Cl_2$, respectively, could not be detected in any of these systems. Thus a direct demonstration of the cage effect in the systems studied could not be given.

Now the question emerged whether the radioactive products obtained in measurable amounts are formed partly in cage recombination processes. If this is not the case, i. e. the reactants are homogeneously distributed, the established laws of

Table 3

Major products of ^{38}Cl in liquid 1,1-$C_2H_4Cl_2$ – CCl_4 binary system

CCl_4 mole %	YIELD /% of total activity/			
	1,1-$C_2H_4Cl^{38}Cl$	1,2-$C_2H_4Cl^{38}Cl$	$CCl_3{}^{38}Cl$	$CH_2Cl^{38}Cl$
0	9.7±0.3	0.4	–	1.8±0.04
10	7.3±0.4	<0.3	2.0±0.1	1.4±0.1
30	6.1±0.1	<0.3	7.7±0.1	1.3±0.04
50	4.0±0.1	<0.3	12.2±0.5	1.1±0.04
70	2.5±0.1	<0.3	20.0±0.3	0.9±0.02
85	1.2±0.05	<0.3	21.6±0.9	0.5±0.03
90	0.8±0.05	<0.3	26.5±0.4	0.4±0.04

conventional chemical kinetics are applicable to the reactions. Accordingly, if R_1 is a radioactive product originating from one of the components, $-C_1$ in the binary mixture, its formation rate depends on the concentration of this component. $[C_1]$ and on that of the radioactive atom, in the present case of ^{38}Cl.

$$\frac{d[R_1]}{dt} = k_1[C_1][^{38}Cl] \tag{3}$$

$[^{38}Cl]$, according to the steady-state approximation of Bodenstein, is constant, thus

$$\frac{d[^{38}Cl]}{dt} = \phi.\sigma.h - \sum_{i=1}^{L} k_i.[C_1][^{38}Cl] - \sum_{j=L+1}^{N} k_j.[C_2][^{38}Cl] = 0 \tag{4}$$

$$[^{38}Cl] = \frac{\phi.\sigma.h}{[C_1]\sum_{i=1}^{L} k_i + [C_2]\sum_{j=L+1}^{N} k_j} \tag{5}$$

where $\phi.\sigma.h$ is the rate of ^{38}Cl formation, k_i and k_j are the rate constants of the radioactive products formed from the two components C_1 and C_2, respectively.

From Eqs (3) and (5) the rate of R_1 formation can be expressed:

$$\frac{d[R_1]}{dt} = k_1 [C_1] \frac{\phi . \sigma . h}{[C_1] \sum_{i=1}^{L} k_i + [C_2] \sum_{j=L+1}^{N} k_j} \tag{6}$$

Since $[C_1]$ and $[C_2]$ are practically constant throughout the process, Eq. (6) is easy to integrate.

$$[R_1] = \phi . \sigma . h . t \frac{k_1 [C_1]}{[C_1] \sum_{i=1}^{L} k_i + [C_2] \sum_{j=L+1}^{N} k_j} \tag{7}$$

One can rewrite Eq. (7) in the following form

$$\frac{1}{[R_1]} = \frac{1}{\phi . \sigma . h . t} \frac{\sum_{i=1}^{L} k_i}{k_1} + \frac{\sum_{j=L+1}^{N} k_j [C_2]}{k_1 [C_1]} \tag{8}$$

i. e. a linear dependence between $\frac{1}{[R_1]}$ and $\frac{[C_2]}{[C_1]}$ can be found.

This is true only if the values of $k_{i,j}$ are independent of the composition of the system. This latter condition implies that the relative reaction probabilities are not influenced by the variation in the moderation-properties of the system which is brought about by the changes in composition.

As it is shown in Figs 1 and 2 an approximate linear relationship was found between $\frac{1}{[R_1]}$ and the ratio $\frac{C_2}{[C_1]}$ for the formation of 1, 1-$C_2H_4Cl\,^{38}Cl$, $CH_2Cl\,^{38}Cl$ in binary mixtures of 1, 1-dichloroethane with both ethyl alcohol and carbon tetrachloride and similarly for that of o-$C_6H_4Cl\,^{38}Cl$ and $C_6H_5\,^{38}Cl$ binary mixtures of o-dichlorobenzene and nitrobenzene /16/ with carbon tetrachloride.

Since the equation of homogeneous kinetics were applied in the deduction of Eq (8) these results give evidence that cage recombination is unimportant in the formation of radioactive products listed above.

Figure 3 shows a typically non-linear $\frac{1}{[R_1]}$ versus $\frac{[C_2]}{[C_1]}$ dependence for the formation of $CCl_3\,^{38}Cl$ in binary systems of carbon tetrachloride - ROH

Table 4

Major products of ^{38}Cl in 1,1-$C_2H_4Cl_2$ – C_2H_5OH binary system

C_2H_5OH mole %		YIELD /% of total activity/			
		1,1-$C_2H_4Cl^{38}Cl$	1,2-$C_2H_4Cl^{38}Cl$	$C_2H_5{}^{38}Cl$	$CH_2Cl^{38}Cl$
0	L	9.7±0.3	0.4	–	1.8±0.4
	Cr	13.7±0.2	0.6	–	1.7±0.1
10	L	5.4±0.1	<0.3	0.3	1.0±0.02
	Cr	13.1±0.3	<0.3	0.7±0.1	1.7±0.1
20	L	4.2±0.2	<0.3	0.5±0.02	0.8±0.03
	Cr	12.8±0.4	<0.3	0.8±0.04	1.5±0.03
40	L	2.8±0.1	<0.3	0.7±0.05	0.5±0.02
	Gl	5.1±0.1	<0.3	0.9±0.05	1.0±0.03
	Cr	10.8±0.4	<0.3	1.1±0.2	1.4±0.1
60	L	1.8±0.1	<0.3	1.2±0.1	0.3
	Gl	3.0±0.1	<0.3	1.5±0.1	0.6
80	L	0.9±0.01	<0.3	1.3±0.04	0.3
87	L	0.6±0.02	<0.3	1.4±0.1	0.3
90	L	0.5±0.02	<0.3	1.5±0.05	0.3
	Gl	0.8±0.05	<0.3	2.2±0.1	0.3

Abbreviations: L – liquid, Gl. – glassy, Cr. – crystalline

(R = CH_3, n-C_3H_7, i-C_3H_7) /17/. This phenomenon may indicate a cage effect. Even in this case, however, we cannot be sure that the only reason for non-linearity lies with the strong cage effect. It might well be the result of different moderator properties of the components and the energy dependence of $CCl_3{}^{38}Cl$ formation, i. e. that $k_{i,j}$ is a function of $[C_1]$.

To summarize, the results of our kinetic investigations together with the vain attempts to find any product of radical recombination seem to contradict the assumption of strong cage effect in the systems studied. In an endeavour to draw more general conclusions about the importance of this effect, this work will be continued.

Acknowledgements. The authors wish to express their sincere gratitude to Dr. R. Schiller for his substantial suggestions and critical remarks. The technical assistance of Mrs. M. Heller and Mr. G. Simó is highly appreciated.

References

/ 1/ Franck, J., Rabinowitsch, E., Disc. Faraday Soc. 30, 120 (1934).
/ 2/ Willard, J. E., Ann. Rev. Phys. Chem. 6, 141 (1955).
/ 3/ Hornig, J. F., Levey, G., Willard, J. E., J. Chem. Phys. 20, 1556 (1952).
/ 4/ Chien, J. C. W., Willard, J. E., J. Amer. Chem. Soc. 75, 6160 (1953).
/ 5/ Milman, M., Shaw, P. F. D., Chem. Soc. 1957, 130.
/ 6/ Harris, W. E., a/ Can. J. Chem. 39, 121 (1961); b/ Chemical Effects of Nuclear Transformations. IAEA, Vienna 1961, I. p. 229.
/ 7/ Milman, M., Radiochim, Acta 1, 15 (1962).
/ 8/ Vasáros, L., Machulla, H. J., Stöcklin, G., J. Phys. Chem, 76, 501 (1972).
/ 9/ Rice, W. E., Willard, J. E., J. Amer. Chem. Soc. 75, 6156 (1953).
/10/ Richardson, A. E., Wolfgang, R., J. Amer. Chem. Soc. 92, 3480 (1970).
/11/ Helton, R. W., Grauer, W. M., Rack, E. P., Radiochim, Acta 19, 44 (1973).
/12/ Machulla, H. J., Stöcklin, G., J. Phys. Chem. 78, 658 (1974).
/13/ Berg, M. E., Grauer, W. M., Helton, R. W., Rack, E. P., J. Phys. Chem. 79, 1327 (1975).
/14/ Stöcklin, G., Hot Atom Chemistry Status Report, IAEA Vienna 1975, p. 161.
/15/ Berei, K., Vasáros, L., Radiochim. Acta 21, 75 (1974).
/16/ Kardos, Zs. Berei, K., Vasáros, L., Radiochem. Radional. Letters 17, 233 (1974).
/17/ Vasáros, L., Berei, K., Kiss, I., Magy. Kém. Foly. 74, 106 (1968).

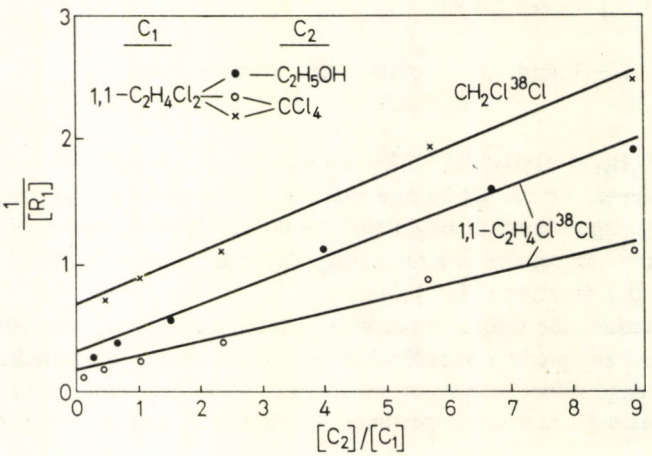

Fig. 1 Dependence of the 1,1-$C_2H_4Cl^{38}Cl$ and $CH_2Cl^{38}Cl$ formation on the composition of 1,1-$C_2H_4Cl_2$ – C_2H_5OH (•) and 1,1-$C_2H_4Cl_2$ – CCl_4 (o,x) binary mixtures

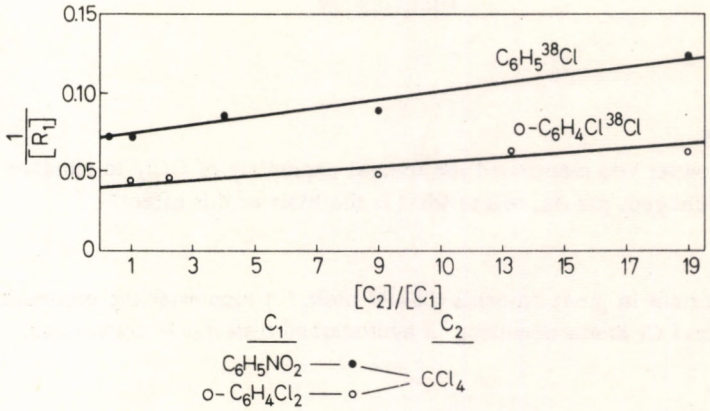

Fig. 2 Dependence of the $C_6H_5{}^{38}Cl$ and $o\text{-}C_6H_4Cl^{38}Cl$ formation on the composition of $C_6H_5NO_2$ – CCl_4 (●) an $o\text{-}C_6H_4Cl_2$ – CCl_4 (o) binary mixtures

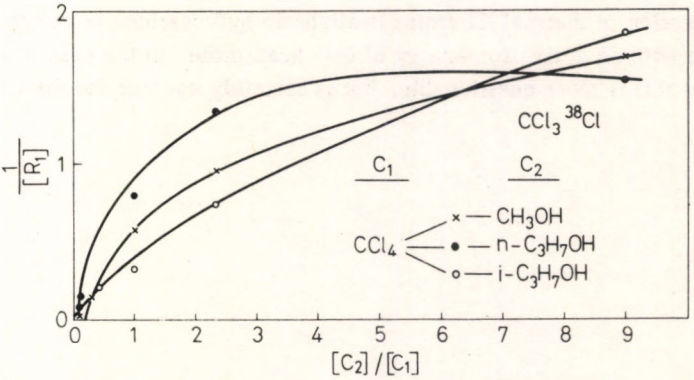

Fig. 3 Dependence of $CCl_3{}^{38}Cl$ formation on the compositon of CCl_4ROH (x-CH_3OH ●- n-C_3H_7OH o - i-C_3H_7OH) binary mixtures

H. J. ACHE

In your paper you mentioned the special capability of CCl_4 to enhance the caging process. Would you, please, tell us what is the basis of this effect?

K. BEREI

CCl_4 present in great amounts (50–90 mole %) suppresses the competing reaction of thermal Cl atoms occurring in hydrocarbon systems: H abstraction.

H. J. ACHE

If I understand your answer correctly, then you feel that the presence of CCl_4 suppresses the H abstraction by ^{38}CL because CCl_4 does not contain any H. But could not Cl_2 formation take place with Cl abstraction induced by ^{38}Cl from Cl_4?

K. BEREI

H abstraction of thermal Cl atoms in aliphatic hydrocarbons is known as a very fast reaction with an activation energy of 0–5 kcal/mole. In the case of aromatic hydrocarbons this is more questionable, but is certainly not true for the Cl abstraction from CCl_4.

NEUTRALIZATION OF IONS IN THE GAS-PHASE RADIOLYSIS OF ETHANE AND PROPANE

Janusz Gawłowski, Jan Niedzielski, Jerzy Sobkowski
Chemistry Department, The University, Zwirki i Wigury 101, 02-089 Warsaw, Poland

Introduction

The radiolysis of gaseous ethane and of propane have been studied extensively /1, 2/. However, the mechanism of ionic processes, and of neutralization of ions in particular, is far from being clearly understood. Our preliminary results concerning this problem will be presented here.

Experimental

Phillips research grade ethane, and propane, used in this study, were further purified by adsorption and distillation in vacuum. All of the above gases were checked for purity by gas chromatography. No impurities could be found in the ethane (limit of detection 10^{-5}%), propane contained less than 0.005% ethane. Hydrocarbons were dried before use by passing them through a trap containing highly activated molecular sieves 3A and then by exposing to the action of metallic sodium /3/. Sulphur hexafluoride, obtained from Matheson, was passed through a column filled with KOH, and after subsequent outgassing dried over molecular sieves 5A. Triply-distilled water was introduced into the ampoules from a potassium hydroxide solution.

Glass ampoules (volume about 140 ml) were heated at 350-400 °C first in the air and subsequently for 3-4 hours in high vacuum. In some experiments a film of metallic sodium was deposited onto the walls of a small finger attached to the ampoule.

The ethane samples were irradiated with γ-rays from a ^{60}Co 20000 Ci source at the Institute of Radiation Technique, Łódź, at a dose rate of about 0.4 Mrad hr^{-1}. The propane samples were irradiated in AECL Gammacell at a dose rate of 0.82 Mrad hr^{-1}. The nitrogen yield from nitrous oxide $G(N_2) = 10.0$ /4/ was used for dosimetry.

All hydrocarbon products were analysed by gas chromatography. Hydrogen was not determined.

Results and discussion

a) The effects of reactant purity

The yields of main hydrocarbon products originating from free radical processes in the radiolysis of ethane and propane are shown in Tables 1-3. In ethane ra-

Table 1

Yields of products in the gas–phase radiolysis of ethane, irradiated at a pressure of 200 Torr to a total dose of 0. 38 Mrad

Additives and experimental details	G molecules/100 eV			
	C_3H_8	$n-C_4H_{10}$	CH_3	C_2H_5
a)	0. 67	1. 07	0. 58	2. 4
Sodium deposited onto the walls	0. 61	1. 12	0. 49	2. 5
Ampoule not heated under vacuum	0. 57	2. 18	0. 4	4. 9
Usual purification only	0. 6	2. 06	0. 44	4. 6
H_2O – 0. 1%	0. 57	2. 35	0. 4	5. 2
O_2 – 0. 5%	0. 22	0. 21	–	–

a) experimental conditions as described in the experimental part

diolysis the main free radicals are CH_3 and C_2H_5/1c/; their yields could be calculated assuming that other routes contribute 0. 22 and 0. 21 to the yield of propane and butane, respectively (the results of the radiolysis in the presence of oxygen). The ratios for the rate constants of disproportionation and recombination were taken from the literature /5/. In the presence of SF_6 sulphur pentafluoride radical is formed /6/, its yield could be calculated assuming k_d/k_r = 0. 22 for the reaction of ethyl and sulphur pentafluoride radicals. The yield of propyl radicals in the radiolysis of propane were calculated from the yields of isomeric hexanes and other C_4 and C_5 hydrocarbons, not included in the tables. The pertinent k_d/k_r ratios were found in the literature /5/.

Comparing our data with those of other investigators ($G/n-C_4H_{10}$ = 2. 5 /1 a, c, f/ from the ethane radiolysis and G/2,3-dimethylbutane = 1. 4 /2c/ from the propane one) it is seen that our results for pure hydrocarbons are much lower. Looking for the reasons of such discrepancies we have performed experiments using hydrocarbons purified only by the usual procedures (distillation under vacuum, freeze–thaw cycles and evacuation before irradiation). The yields of hydrocarbons were found to increase–approximating those of other authors. The use of ampoules not heated under vacuum, and the introduction of water into the ampoules gave the same results.

In order to check whether our experimental procedures warrant the total removal of water traces we inserted metallic sodium into the ampoules. The results were practically the same as for sodium untreated hydrocarbons.

Thus, it may be concluded that water traces have a pronounced effect on the radiation processes in ethane and propane. We shall attempt to explain these phenomena later.

Table 2

Yield of products in the gas–phase radiolysis of ethane, irradiated in the presence of scavengers, at a pressure of 200 Torr to a total dose of 0.38 Mrad

Scavenger vol %	G molecules/100 eV						
	C_3H_8	$n-C_4H_{10}$	CH_3SF_5	$C_2H_5SF_5$	CH_3	C_2H_5	SF_5
No additives	0.67	1.07	–	–	0.58	2.4	–
0.3% SF_6	0.39	0.75	0.36	1.1	0.4	2.75	3.0
0.1% H_2O, 0.3% SF_6	0.49	1.19	0.3	1.1	0.48	3.86	2.3
0.3% N_2O	0.47	1.52	–	–	0.3	3.26	–

Table 3

Yields of hexanes and propyl radicals in the gas-phase radiolysis of propane, irradiated at a pressure of 400 Torr to a total dose of 0. 32 Mrad

Additives and experimental details	G molecules/100 eV				
	2. 3 DMB[x]	2 MP[xx]	n-C_6H_{14}	i-C_3H_7	n-C_3H_7
a)	0. 69	0. 28	0. 04	4. 5	0. 8
Sodium deposited onto the walls	0. 73	0. 29	0. 04	4. 6	0. 8
Usual purification only	1. 45	0. 38	0. 03	7. 3	0. 85
0. 04% H_2O	1. 51	0. 41	0. 03	7. 7	0. 9
0, 14% C_3H_6	0. 74	0. 34	0. 05	4. 7	0. 9
0. 05% H_2O, 1% C_3H_6	0. 7	0. 26	0. 04	4. 2	0. 66

x – 2. 3-dimethylbutane

xx – 2-methylpentane

a) experimental conditions as described in the experimental part

b) Effects of scavengers

The presence of SF_6 in irradiated ethane leads to the decrease in the yields of propane and butane and to the formation of new products: CH_3SF_5 and $C_2H_5SF_5$. However the calculated yields of ethyl radical are nearly the same as those in pure ethane (it should be stressed, however, that experimental errors are much higher in SF_6 experiments, owing to the indirect method of determining the flame ionization detector sensitivity for CH_3SF_5 and $C_2H_5SF_5$).

In ethane radiolysis, ethyl radicals are formed in primary processes and in reaction of atomic hydrogen /1d/

$$H + C_2H_6 \longrightarrow C_2H_5 + H_2 \qquad /1/$$

Thus, our results indicate that neutralization of ions does not contribute significantly to the yield of atomic hydrogen (no more than $G_H = 0.5$, if at all).

In the presence of nitrous oxide the yield of C_2H_5 was unexpectedly found to increase. Most likely some side reactions are involved: the reaction of hydroxyl radicals with the ethane and the formation of oxygenated compounds which could have the same effect as the traces of water.

The simultaneous action of water and SF_6 leads to the increase in $G_{C_2H_5}$ by 1. 4 whereas the presence of water alone increases $G_{C_2H_5}$ by 2. 7. Apparently ion-

molecule reactions, probably proton transfer from $C_2H_6^+$ or dimeric $(C_2H_6)_2^+$ ions, contribute ca. 1.3 to the yield of ethyl radicals

$$C_2H_6^+ + H_2O \longrightarrow C_2H_5 + H_3O^+ \qquad /2/$$

$$(C_2H_6)_2^+ + H_2O \longrightarrow C_2H_5 + C_2H_6 + H_3O^+ \qquad /3/$$

Reaction 2 is very fast, $k_2 = 1.3 \times 10^{-9}$ cm^3 molecule^{-1} s^{-1} /7/. Neutralization of hydronium ions yields atomic hydrogen and subsequently ethyl radicals in reaction 1. A similar mechanism has been advanced to explain the formation of HD in the radiolysis of c--C_6D_{12} and n-C_7D_{16} /8/.

In propane radiolysis we have observed the decrease in the yields of isomeric hexanes accompanied by the formation of CH_3SF_5, $C_2H_5SF_5$ and $C_3H_7SF_5$. Unfortunately RSF_5 products were not determined quantitatively which made it impossible to calculate the yield of propyl radicals in this system. Some information concerning the neutralization process may be gathered from the experiments in the presence of propylene. Bone et al. have established that neutralization does not yield atomic hydrogen in the presence of propylene /2c/. We have observed similar effects of propylene in ethylene radiolysis. In ethylene neutralization yields $G_H = 2,9$ /9/, the presence of 1% propylene totally inhibits the occurrence of such a process /10/.

Thus, the lack of the effect of propylene on the yield of isopropyl radical, may be considered as indirect evidence that the atomic hydrogen precursor of i-C_3H_7 radicals is not formed in the neutralization of ions:

$$H + C_3H_8 \longrightarrow C_3H_7 + H_2 \qquad /4/$$

The presence of water increases $G_{i-C_3H_7}$ which is probably due to the occurrence of proton transfer from $C_3H_8^+$ and $(C_3H_8)_2^+$ ions and to the neutralization of those formed in such reactions hydronium as ions as well. The presence of propylene in the system propane-water lowers $G_{i-C_3H_7}$ to the value similar to that obtained in pure propane.

This result is not surprising. Propylene, introduced in concentrations much higher than water, is expected to intercept parent propane ions. Higher order ions originating from such reactions do not form atomic hydrogen upon neutralization, as explained earlier.

Thus, in the radiolysis of both ethane and propane the neutralization of ions either does not involve the formation of atomic hydrogen at all or contributes small yields to the total yield of this product. If so, the decrease in the yield of molecular hydrogen observed by many authors in the presence of electron scavengers (ΔG_{H_2} = 2.4 /1f/ and 2.6 /2d, e/ in ethane and propane, respectively) is accounted for by the formation of molecular rather than atomic hydrogen in ion neutralization.

References

/1/ a. K. Yang, P. L. Gant, J. Phys. Chem. 65, 1861 (1961);
b. H. H. Carmichael, R. Gorden Jr., P. Ausloos, J. Chem. Phys. 42, 343 (1965);
c. C. M. Wodetzki, P. A. Mc Cusker, D. B. Peterson, J. Phys. Chem. 69, 1045 (1965);
d. C. M. Wodetzki, P. A. Mc Cusker, D. B. Peterson, J. Phys. Chem. 69, 1056 (1965);
e. M. Inoue, T. Uno, S. Sato, S. Shida, Bull. Chem. Soc. Japan 41, 2005 (1968);
f. P. T. Holland, J. A. Stone, Can. J. Chem. 52, 221 (1974).

/2/ a. J. H. Futrell, T. O. Tiernan, J. Chem. Phys. 37, 1694 (1962);
b. L. I. Bone, L. W. Sieck, J. H. Futrell, J. Chem. Phys. 44, 3667 (1966);
c. L. I. Bone, L. W. Sieck, J. H. Futrell, in The Chemistry of Ionization and Excitation. Ed. G. R. A. Johnson, G. Scholes. Taylor and Francis, London 1967;
d. N. Fujisaki, S. Shida, Y. Hatano, J. Chem. Phys. 52, 556 (1970);
e. G. R. A. Johnson, J. M. Warman, Trans. Faraday Soc. 61, 1709 (1965).

/3/ J. Gawłowski, J. Niedzielski, Roczn. Chemii 44, 685 (1970).

/4/ F. Jones, T. J. Sworski, J. Phys. Chem. 70, 156 (1966).

/5/ A. F. Trotman-Dickenson, G. S. Milne, NS RDS, NBS 9 U. S. Dept. of Commerce, Washington D. C. 1967; E. Ratajczak, A. F. Trotman-Dickenson, Supplementary Table 1970; J. A. Kerr, E. Ratajczak, Second supplement tables of bimolecular gas reactions, Univ. of Birmingham 1972.

/6/ J. Gawłowski, J. A. Herman, Can. J. Chem. 52, 3631 (1974).

/7/ L. W. Sieck, S. K. Searles, J. Phys. Chem. 53, 2601 (1970).

/8/ N. Fujisaki, T. Gaumann, Helv. Chim. Acta 57, 2091 (1974).

/9/ J. Gawłowski, J. Niedzielski, unpublished data.

/10/ J. Gawłowski, J. Niedzielski, Int. J. Radiat. Phys. Chem. 5, 419 (1973).

DISCUSSION

J. KROH

What is the mechanism of molecular hydrogen elimination? Is it abstraction of H_2 from one C-atom or reaction of hot H-atom with a neighbouring fragment of the molecule?

J. GAWLOWSKI

I do not know, but I think H_2 abstraction is more probable.

G. R. FREEMAN

Was the reaction of water proton transfer from the $C_2H_6^+$ and $C_3H_8^+$?

J. GAWLOWSKI

Yes, it was.

G. R. FREEMAN

What do you think was the reaction between $C_3H_8^+$ and C_3H_6, proton transfer, or electron transfer?

What was the effect of SF_6 on reaction products in the presence of water?

J. GAWLOWSKI

I think it may be condensation reaction or charge transfer. The yields of the products in the presence of SF_6 decreased (see Table 2).

G. CASTELLO

Are you sure that your technique of sample preparation removed all water? A long contact of sodium with hydrocarbon was found to leave some traces of water. A more efficient technique may be to bubble hydrocarbon vapour through liquid Na-K alloy during bulb-to-bulb distillation under vacuum.

What is the situation about the oxygen content? Traces of O_2 may have a stronger effect than water at a low concentration, especially during the first stage of the reaction.

In your tables are only reported the G values of some products and the results of your calculation of the radical yields. It is not possible, therefore, a complete discussion of the various yields. As an example, what are the G-values of CH_4 and C_2H_4 in the ethane radiolysis? Did you have products higher than dimers? Did you make experiments at different pressures with various dose rates on the same hydrocarbon and/or with different total doses?

J. GAWLOWSKI

We purified hydrocarbons by pressing them through a trap containing molecular sieves 3A to remove water. Traces of water and oxygen were removed efficiently by storage over highly dispersed sodium metal (Ref. /3/).

In some experiments we have determined other products than presented here. Their G-values are not concerned with the problem of ion neutralization reaction. We observed formation of higher hydrocarbons: pentanes and hexanes with G-values lower than 0.50. The effects of total dose and other parameters are presently studied.

COMPARISON BETWEEN LIQUID PHASE PHOTOLYSIS AND RADIOLYSIS OF C_3-C_4 HYDROCARBON MIXTURES

Zs. Horváth, P. Ausloos*, G. Földiák
*National Bureau of Standards, Washington, D. C. USA
Institute of Isotopes of the Hungarian Academy of Sciences,
Budapest, Hungary

Introduction

The results obtained in photolytic systems – in which specific processes can be isolated – are able to contribute a great deal to our understanding of energy deposition in radiation chemistry /1/.

In the liquid phase radiolysis of hydrocarbons the yields of excited molecules and the level of excitation cannot be predicted a priori /2/. Some singlet excited molecules will be formed by direct electron impact and perhaps also by recombination of the positive ion and electron. Although electron impact will definitely lead to the production of the singlet excited state, neutralization may also lead to an upper triplet state excited molecule. At present, very little is known about the modes of decomposition of triplet excited molecules because there is no convenient way to produce triplet excited states in the absence of the singlet excited ones /3,4/.

On the other hand, energy transfer from one molecule to the other has long been considered as a most important process in radiation chemistry /5/. Notwithstanding numerous publications concerning energy transfer there is no general consensus as to which of the following mechanism accounts for energy transfer in the liquid phase:

$$^1M^* + N \qquad M + {}^1N^*, \tag{1}$$

$$^3M^* + N \qquad M + {}^3N^*, \tag{2}$$

$$M^+ + N \qquad M + N^+. \tag{3}$$

The processes (1)–(3) are, in general, the only possible steps for energy transfer. In the liquid phase photolysis of hydrocarbon mixtures at energies below the ionization potential of molecules under study, of the three steps only step (1) occurs since the singlet states are the only activated species which are produced by absorption of high energy photons /2/.

It follows clearly from the foregoing that in order to arrive at some understanding of liquid phase radiolysis of pure hydrocarbons and of hydrocarbon mixtures we have to try to produce singlet excited states in the absence of other activated species

and then to examine their behaviour. The $n\text{-}C_4H_{10}$ – $iso\text{-}C_4H_{10}$, C_3H_8-$cyclo\text{-}C_3H_6$, $n\text{-}C_4H_{10}$-$cyclo\text{-}C_4H_8$, C_3D_8-C_3H_6 and C_3H_8-$n\text{-}C_4H_{10}$ mixtures have been photolyzed in the liquid phase at 1470 A (8.4 eV) and on the basis of these experiments we have attempted to elucidate the reaction mechanism which occurs in the liquid phase γ-radiolysis of the same hydrocarbon mixtures. In the present paper, as typical examples of alkane mixtures, only $n\text{-}C_4H_{10}$-$iso\text{-}C_4H_{10}$ and C_3H_8-$cyclo\text{-}C_3H_6$ will be discussed in detail.

Experimental

The photolysis lamp and reaction cell employed in this work were constructed and prepared at the National Bureau of Standards. The Xe-resonance lamp was operated by a microwave discharge and the resultant photons were transmitted directly into the reaction cell through a sapphire window. During the photolysis experiments the hydrocarbon liquid was thermostated to -80°C.

In the radiolysis experiments the hydrocarbons were irradiated in glass ampoules, in the liquid phase, under their own vapour pressure using the ^{60}Co irradiation facility of the Institute of Isotopes which has a nominal activity of 80 000 Ci. The temperature was 30–35°C, the integral dose was $5.9 \cdot 10^{20}$ eV g^{-1} (9.4 Mrad). The average dose rate was $9.4. \cdot 10^{19}$ eV $g^{-1}h^{-1}$ (1.5 Mrad h^{-1}).

Hydrocarbon products formed both in the photolysis and in the radiolysis were identified and determined by gas chromatography.

Results and discussion

n-butene-isobutene mixtures. From Fig. 1 it can be seen that the quantum yields of products formed in the liquid phase photolysis of $n\text{-}C_4H_{10}$-$iso\text{-}C_4H_{10}$ mixtures at 8.4 eV are linear as a function of the composition of the mixtures, the only exception being propane. The enhanced yields of C_3H_8 indicate that radical reactions occur in the system. Propyl radicals are formed in the pure $n\text{-}C_4H_{10}$ to a very minor extent, and when $iso\text{-}C_4H_{10}$ is added to $n\text{-}C_4H_{10}$ the propyl radicals also abstract H atoms from isobutane to form propane. The positive deviation in the plots shows that the reaction with isobutane is faster than with n-butane which is explained by the weak tertiary H-bonds of $iso\text{-}C_4H_{10}$.

Judging by the high yields of CH_4 and C_3H_6 and by the results obtained with $iso\text{-}C_4H_{10}$-$iso\text{-}C_4D_{10}$ 1:1 mixture, the predominant primary process in the liquid phase photolysis of $iso\text{-}C_4H_{10}$ is the molecular elimination of methane:

$$iso\text{-}C_4H_{10} \longrightarrow CH_4 + C_3H_6. \qquad (4)$$

Taking into account process (4), and the linear plot of $\phi(CH_4)$ and that of $\phi(C_3H_6)$ as a function of the composition of the mixtures, it is clearly evident that there is no apparent excitation energy transfer between n-butane and isobutane. In other words, there is no energy transfer in the system which would lead to an increased unimolecular dissociation of one compound in the mixture on account of the other.

On the basis of the photolysis studies discussed above, the CH_4, C_2H_4, C_3H_6 and C_2H_6 products in the liquid phase γ-radiolysis of n-butane, isobutane and their mixtures can be established as mainly formed via the dissociation of neutral excited molecules. Figure 2 shows that the plots of the G-values of the products mentioned above have the same characteristics as can be seen in the photolysis experiments (Fig. 1).

The C_3H_8 product does not seem to form in the same pathway in photolysis as it does in radiolysis. In photolysis the propane is a very minor product (e. g. $\phi(C_3H_6) \gg \phi(C_3H_8)$), whereas in γ-radiolysis it is one of the main products (e. g. $G(C_3H_6) \sim G(C_3H_8)$). The relatively larger yield of C_3H_8 in γ-radiolysis can be accounted for by the ionic processes:

$$(\text{iso- or n-})\ C_4H_{10}^+ \longrightarrow C_3H_7^+ + CH_3. \qquad (5)$$

Process (5) is one of the main ionic fragmentations of both n-butane and isobutane parent ion. The propyl ion formed may react with either n-butane or isobutane in a subsequent hydride transfer reaction generating propane*:

$$C_3H_7^+ + \text{n-}C_4H_{10} \xrightarrow{k_6} C_3H_8 + C_4H_9^+, \qquad (6)$$

$$C_3H_7^+ + \text{iso-}C_4H_{10} \xrightarrow{k_7} C_3H_8 + C_4H_9^+. \qquad (7)$$

On the other hand, the neutralization of iso-$C_4H_{10}^+$ which results in CH_3 and C_3H_7 radicals via the triplet state of excited isobutane can also account for the relatively high $G(C_3H_8)$ in the liquid phase radiolysis. It should be noted, however, that the above described processes do not in themselves, present any reliable explanation for the large decrease of $G(C_3H_8)$ in the mixtures (Fig. 2).

Propane-cyclopropane mixtures. The results of Table 1 show that the quantum yield of fragmentation, ϕ(molecule/absorbed photon) in propane-cyclopropane mixtures in liquid phase photolysis at 8.4 eV rises above unity. There is nothing in the literature comparable with what can be seen here.

* $k_6 = 5.6 \cdot 10^{-10}$ cc. molecule^{-1}s^{-1}, $k_7 = 4.2 \cdot 10^{-10}$ cc. molecule^{-1}s^{-1} determined by icr-spectrometer at $10^{-7} - 10^{-5}$ torr /6/.

Table 1

Liquid phase photolysis of propane-cyclopropane mixtures at 8.4 eV

C_3H_8	$\phi(C_3H_6 + C_2H_4)$
1.00:0.00	0.934
0.75:0.25	1.070
0.50:0.50	1.217
0.25:0.75	1.060
0.00:1.00	0.933

The presence of propylene and ethylene in pure cyclopropane immediately reveals two predominant primary processes occurring in the liquid phase photolysis:

$$\triangle^* \longrightarrow C_2H_4 + CH_2, \tag{8a}$$

$$\triangle^* \longrightarrow C_3H_6 \tag{8b}$$

The fact that $\phi(C_3H_6 + C_2H_4)$ in the mixtures is larger than unity can best be accounted for by the following reaction scheme:

$$C_3H_8^* \longrightarrow C_3H_6^* + H_2, \tag{9}$$

$$C_3H_6^* + \triangle \longrightarrow C_3H_6 + C_2H_4 + CH_2. \tag{10}$$

The monomolecular elimination of hydrogen represents the major mode of energy dissipation in electronically excited propane, $\phi(C_3H_6) = 0.841$. It is known that at this excitation energy a large fraction of the absorbed energy is available for partitioning between the primary decomposition products. It is very likely that in reaction (9) the propylene contains most of the energy. The propylene molecule with excess internal energy undergoes collision with cyclopropane, and according to process (10) the collision induced dissociation gives extra products, such as ethylene and a methylene radical, but the yield of propylene remains unchanged. Corresponding to this reaction scheme – as illustrated by Fig. 3 – the $\phi(C_3H_6)$ are linear and the $\phi(C_2H_4)$ show a positive deviation as a function of the composition of the mixture.

On the basis of reactions (8a) and (10) the quantum yield of methylene is expected to be equal to that of ethylene. Singlet methylene formed in the dissocia-

tion processes /7/ will insert into the propane to form n-butane and isobutane (Figure 3):

$$^1CH_2 + C_3H_8 \longrightarrow \text{iso-}C_4H_{10}, \tag{11a}$$

$$^1CH_2 + C_3H_8 \longrightarrow \text{n-}C_4H_{10}, \tag{11b}$$

or will insert into the cyclopropane to form methylcyclopropane (Fig. 3):

$$^1CH_2 + \triangle \longrightarrow \overset{CH_3}{\underset{|}{\triangle}} . \tag{12}$$

The yields of inserted methylene are calculated according to reactions (11) and (12) and are plotted in Fig. 3.

It can be seen from Fig. 3 that if the cyclopropane concentrations are higher than the equimolecular one the yields of inserted (CH_2) have a deficit compared with the yields of (C_2H_4). This deficit is enhanced by the increasing cyclopropane concentration of the mixtures. We assume, therefore, that these fractions of methylene undergo a collision induced conversion to the triplet state /8/ and this transition can be illustrated as follows:

$$^1CH_2 + \triangle \longrightarrow {}^3CH_2 + \triangle, \tag{13}$$

although it is well-known that $^3CH_2$ radicals are unreactive towards alkanes, and their fate in these systems is unknown.

The second dissociation process in the liquid phase photolysis of pure propane – as was proved by the liquid phase photolysis of C_3H_8–C_3D_8 1:1 mixture at 8.4 eV – is the CH_4 elimination, $\phi(CH_4) = 0.099$:

$$C_3H_8^* \longrightarrow CH_4 + C_2H_4. \tag{14}$$

The yields of the CH_4 exhibit a negative deviation from the linear additivity rule as a function of the composition of the propane-cyclopropane mixtures. This fact suggests that the following energy transfer may also occur in the system:

$$C_3H_8^* + \triangle \longrightarrow C_3H_8 + \triangle^*, \tag{15}$$

though judging by the small yields of (CH_4), this process is negligible compared with processes (9) and (10).

In the liquid phase γ-radiolysis of propane – cyclopropane mixtures, the plot of $G(CH_4)$ in Fig. 4 – being one of the main products in the system and also a characteristic product of C_3H_8 – can be explained by charge transfer reaction:

$$C_3H_8^+ + \Delta \longrightarrow C_3H_8 + \Delta^+. \qquad (16)$$

(The ionization potential of propane and of cyclopropane is 11.07 eV and 10.06 eV, respectively.)

The CH_4 formation of propane via ionic process can be described as follows:

$$C_3H_8^+ \longrightarrow CH_4 + C_2H_4^+, \qquad (17)$$

The shape of the plot of C_2H_4 in the γ-radiolysis (Fig. 4) is in agreement with what we have seen in the photolysis (Fig. 3). The values of $G(C_2H_4)$ in propane-cyclopropane mixtures in the liquid phase γ-radiolysis can therefore be explained both by the charge transfer process (16) and by the collision induced dissociation processes (9) and (10).

In the γ-radiolysis the yields of n-butane and of iso butane products can be explained by the CH_2 insertion processes (11) and (12).

General remarks

In the liquid phase radiolysis of hydrocarbon mixtures it is often found that there is either enhanced or reduced decomposition of one component due to the presence of the other. These observed increases or decreases are in excess of these expected from the mixture law and they are often interpreted as an indication that either charge or energy transfer occurs /9–12/. It is very difficult, however, to establish what fraction of the absorbed energy results in neutral excitation since the unimolecular fragmentation and the ion-molecule reaction often generate chemically equivalent intermediate- and end-products.

The liquid phase photolysis studies at photon energies below the ionization energy do provide a basis for interpreting those aspects of the overall decomposition in the liquid phase γ-radiolysis which cannot be associated with ion formation. In these photolysis studies the yields of the products as a function of the composition of the mixture give linear plots if all of the products are formed by molecular elimination processes (e.g. H_2, C_2H_2 elimination). The overall feature is more complex if there are hydrogen atoms or alkyl radicals formation in the primary processes. In this case the linear relationship does not necessarily hold because, e.g., radicals can react with both compounds. Furthermore in certain binary mixtures (e.g. n-alkane-cyclo-

-alkane mixtures with C-3, or similar mixture with C-4)*, it found that the quantum yield of fragmentation rises above unity. A collision induced unimolecular dissociation involving a product molecule with excess internal energy leads to the enhanced product yields resulting in non-linear plots as a function of the composition of the mixtures. In conclusion, it can be stated that even in the photolytic system where only excited molecules are formed the observed distortion of the linear plots cannot be accounted for exclusively by excitation energy transfer.

Acknowledgement. One of the authors /Zs. H/ would like to express her thanks to the International Atomic Energy Agency for supporting this research.

References

/ 1/ R.A. Holroyd, J.Y. Yang, F.M. Servedio, J. Chem. Phys. 46, 4540 (1967).
/ 2/ R.L. Platzman, Rad. Res. 1966, North-Holland Publishing Company, Amsterdam 1967.
/ 3/ B. Brocklehurst, Chem. Phys. Letters 28,357 (1974).
/ 4/ B. Brocklehurst, R.S. Dixon, E.M. Gardy, V.S. Lopata, N.J. Quinn, A. Singh, F.P. Sargent, Chem. Phys. Letters 28, 361 (1974).
/ 5/ J.P. Manion, M. Burton, J. Phys. Chem. 56, 360 (1952).
/ 6/ S.G. Lias, J.R. Eyler, P. Ausloos, Int. J. Mass Spectrometry Ion Phys. 19, 219 (1976).
/ 7/ P. Ausloos, R.E. Rebbert, S.G. Lias, J. Photochem. 2, 267 (1973/74).
/ 8/ R.D. Koob, J. Phys. Chem. 76, 9 (1972).
/ 9/ T. Kudo, S. Shida, J. Phys. Chem. 71 1971 (1967).
/10/ Zs. Horváth, G. Földiák, Radiochem. Radioanal. Letters 19, 67 (1974).
/11/ G. Földiák, Z. Horváth, Acta. Chim. (Budapest) 86, 385 (1975).
/12/ Zs. Horváth, G. Földiák, Acta. Chim. (Budapest) 86, 397 (1975).

*In the liquid phase photolysis of n-butane-cyclobutane at 8.4 eV the same effect was found. The results have not, as yet, been published

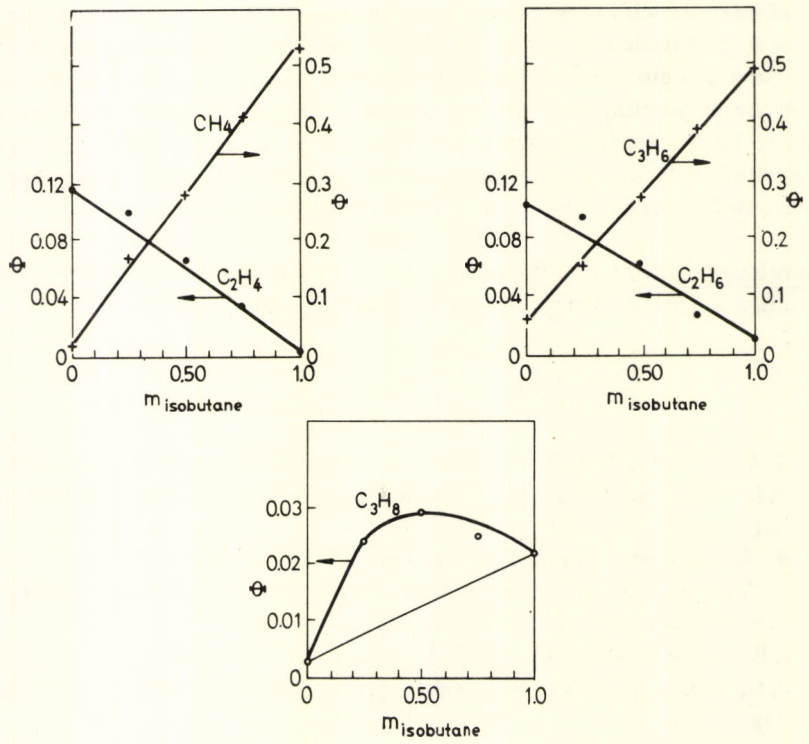

Fig. 1 Products of the liquid phase photolysis of n-butane-isobutane mixtures at 1470 A (8.4 eV)

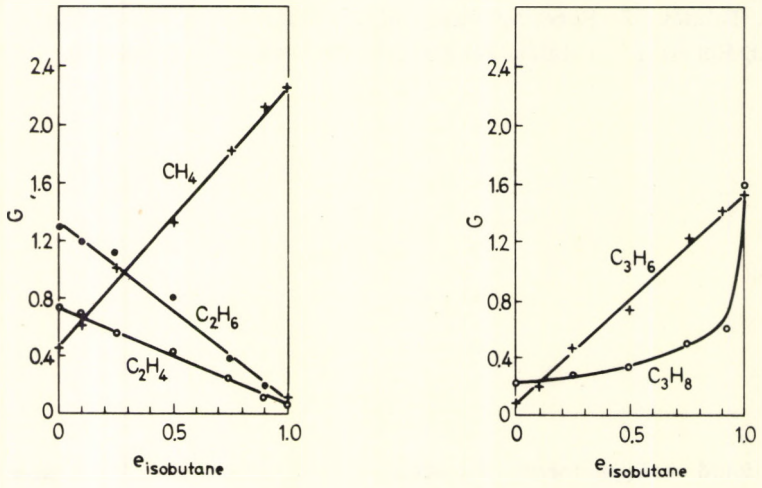

Fig. 2 Products of the liquid phase γ-radiolysis of n-butane-isobutane mixtures

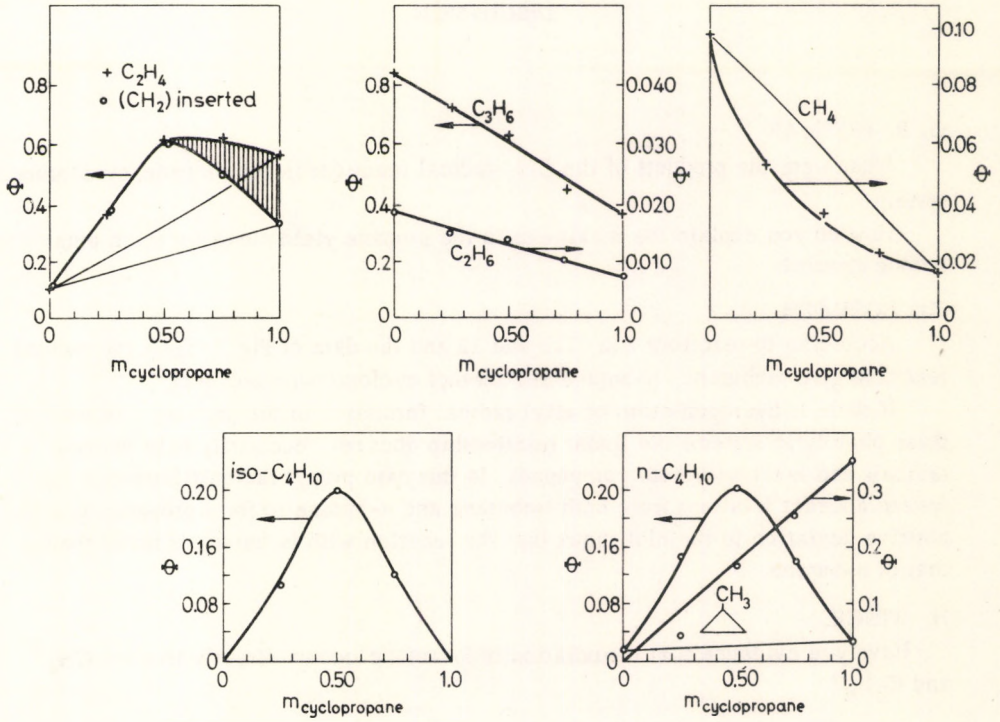

Fig. 3 Products of the liquid phase photolysis of propane-cyclopropane mixtures at 1470 Å (8.4 eV)

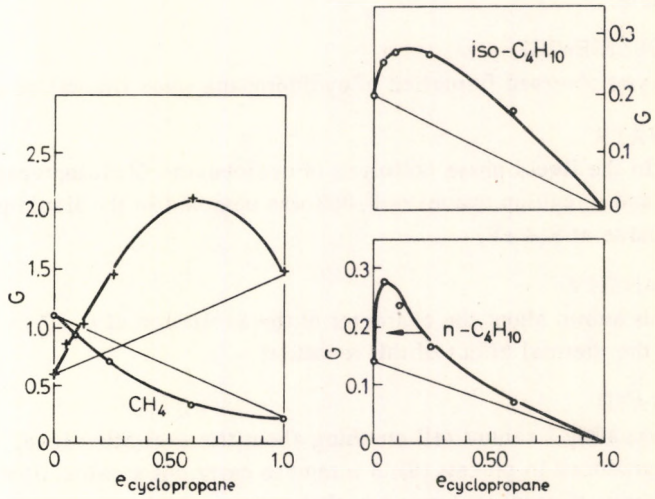

Fig. 4 Products of the liquid phase γ-radiolysis of propane-cyclopropane mixtures

G. R. FREEMAN

What were the products of the CH_2-radical reactions in the propane/cyclopropane system?

How do you explain the maximum in the propane yield curve for the n butane/iso-butane system?

Zs. HORVÁTH

According to reactions 11a, 11b and 12 and the data of Fig. 3 the CH_2-radical reactions give isobutane, n-butane and methyl cyclopropane products.

If there is hydrogen atom or alkyl radical formation in the primary processes of these photolytic systems the linear relationship does not necessarily hold because radicals can react with both compounds. In this case propyl radicals formed in the system abstract H-atoms from both isobutane and n-butane to form propane, and the positive deviation in the plot shows that the reaction with isobutane is faster than that of n-butane.

H. WINCEL

Have you evidence that dissociation of isobutane occurs directly to form CH_4 and C_3H_6?

Zs. HORVÁTH

The CH_4 elimination process was proved by liquid phase photolysis of iso-C_4H_{10}--iso-C_4D_{10} 1 : 1 mixture at 8.4 eV. CH_4 and CD_4 were found exclusively to generate in the system.

R. K. BROSZKIEWICZ

Have you observed formation of cyclopropane when irradiating cyclobutane?

Zs. HORVÁTH

Yes. In the liquid phase radiolysis of cyclobutane G(cyclopropane) = 0.15 was measured and ϕ (cyclopropane) $\sim$ 0.003 was observed in the liquid phase photolysis of cyclobutane at 8.4 eV.

B. G. DZANTIEV

What is known about the character of the excitation of $C_3H_6^*$ in the reaction (9) and about the thermal effect of this reaction?

Zs. HORVÁTH

Unfortunately I cannot tell anything about the excitation level of the propylene molecule produced in process (9). I intend to carry out a calculation to estimate the average energy of products formed in that process which may give further evidence for the occurrence of process (10).

FREE RADICAL DISTRIBUTION IN THE RADIOLYSIS OF SOLID n-PENTANE

P. Claes, B. Tilquin
University of Louvain, Department of Chemistry
CHAN - Bâtiment Lavoisier B1348, Louvain-la-Neuve, Belgium

Introduction

A post-scavenging technique was used in order to study the radical contribution to the formation of the products. If polycrystalline alkanes are annealed before irradiation, the number of radicals remain constant in the irradiated sample between a low irradiation temperature and a temperature about ten degrees under the radical recombination temperature which is determined by esr measurements. Previous work /1/ has shown that all the trapped radicals react with a scavenger during the dissolution of the irradiated solid at a dissolution temperature (T_D) lower than the one where the radicals begin to react in the solid state.

Experimental techniques

Pentane samples are successively purified, degassed, sealed under vacuum, transferred into the dissolution cell as a thin film, annealed during five hours, irradiated with γ rays at 77 K and maintained under liquid nitrogen. The end of the investigated samples is broken and propane with oxygen is introduced to the irradiated solid under vacuum. The temperature of the cell thermostat is then raised to dissolution temperature (110 K). The dissolution of irradiated pentane samples in propane lasts 4 hours. After the dissolution, the G_S values of the dimers are measured by gas chromatography. These residual G_S values are compared to the total G values obtained for molten samples. Capillary columns are used, the SE 30 stationary phase is coated directly on the inside of a glass tubing, 0.50 mm in diameter and 110 m in length. The efficiency for that capillary column is 100.000 plates in the range of the decanes. A flame ionization detector is used.

Some analytical considerations

During the radiolysis of n-pentane, the formation of the following decanes may be expected: 3,4-diethylhexane, D_{33}, 3 ethyl-4-methylpentane, D_{23}, 3-ethyloctane, D_{13}, 4,5-dimethyloctane, D_{22}, 4-methylnonane, D_{12}, n-decane, D_{11}.

Table 1
Boiling Point Method

	Dimer	Calculated B P	Experimental B P
a	–	–	156.2
b	33	163.9	160.4
c	23	163.0	161.4
d	22	162.1	161.8
e			162.1
f	–	–	163.6
g	12	165.7	165.4
h	13	166.5	166.8
i	11	174.1	174.1

The identification of these compounds can be established by direct comparison with standards.

It is possible to derive the boiling point of the radiolysis products from their retention volume, by calibration with alkanes or to determine the retention index of an alkane on the basis of its molecular structure.

Figure 1 shows a chromatogram of the heavy products of the radiolysis of n-pentane in the solid phase. The boiling points of the decanes identified by direct comparison are not available in the literature: the calculated BPs are given in Table 1 /2/ and compared to the experimental boiling points determined graphically by plotting the retention volume of known hydrocarbons vs their boiling points. In Table 2, the molecular indexes calculated by the Takács method /3/ are compared for each product to the experimental values calculated as follows /4/:

$$I_{molecular} = 0.2545\, I_{Kovats}$$

In Tables 1 and 2, the qualitative analysis is in good agreement for D_{22}, D_{12}, D_{13} and D_{11} but both indirect methods fail in the identification of D_{23} and D_{33}. Mass spectroscopy offers positive information on the saturated character of the heavy components emerging from a packed column.

Radical contribution

Table 3 shows the G values for molten samples, the residual G_S values for samples dissolved in propane containing oxygen at 110 K, and the differences ΔG between the two sets of experiments. The ΔG values, expressed in per cent $(G-G_S)100/G$, give the radical contribution to the formation of the dimers.

Table 2

Retention Index and Molecular Structure Method

	Dimer	Molecular Index	
		Calculated (Takács)	Experimental (Kovats)
a	–	–	235
b	33	240.2	239.5
c	23	238.9	240.5
d	22	242.2 (α)	241
e		242.4 (β)	241.4
f	–	–	243
g	12	245.7	244.9
h	13	246.8	246.4
i	11	254.5	254.4

Table 3

Effect of radical scavenging on the yields of decanes from irradiated solid n-pentane (4. 2Mrad)

Dimer	G	G_S	ΔG	$\Delta G\%$
33	0.03	0.02	0.01	33
23	0.19	0.13	0.06	32
22	0.23	0.11	0.12	52
12	0.24	0.09	0.15	62
13	0.06	0.03 /5/	0.02 /5/	42
11	0.09	0.05	0.04	44
Total	0.84	0.43 /5/	0.40 /5/	48
σ		0.07	0.03	

The radical contribution fluctuates from 32% to 62%, the mean value is 48%. The fact that all the dimer yields decrease in the presence of radical scavenger, indicates that trapped radicals are a mixture of primary and secondary radicals. Using G values of 0.84 and 0.43 /5/ respectively, for the total and residual dimer yields, a value of 0.40 /5/ is obtained for the yield of production of decane by recombination of pentyl radicals. Because two radicals are needed to form a dimer, the yield of radicals leading to dimer production is 0.81.

The corresponding G values calculated for each pentyl radical are:

primary radical: $1\text{-pentyl} = 2\,\Delta G_{11} + \Delta G_{12} + \Delta G_{13} = 0.25$ /5/

secondary radical: $2\text{-pentyl} = 2\,\Delta G_{22} + \Delta G_{23} + \Delta G_{12} = 0.45$

$3\text{-pentyl} = 2\,\Delta G_{33} + \Delta G_{13} + \Delta G_{23} = 0.10$ /5/

Table 4

Radical yields and contribution to the formation of dimers and olefins

Radical	G(Radical)				
	Ratio (Holroyd)	Trapped	Decanes	Pentenes	k_d/k_c
1-pentyl	1.0	0.63	0.25(5)	0.37(5)	1.5
2-pentyl	2.2	1.38	0.45	0.93	2.1
3-pentyl	1.1	0.69	0.10(5)	0.58(5)	5.6
Radical	Ratio (Cramer)				
1-pentyl	1.0	0.60	0.25(5)	0.34(5)	1.4
2-pentyl	2.5	1.50	0.45	1.05	2.3
3-pentyl	1.0	0.60	0.10(5)	0.495	4.7

A major contribution of 2-pentyl radicals in the formation of decanes is observed. A major production of that secondary radical was also proposed from esr investigations /5/.

k_d/k_c Ratio

A G value of 2.7 ($\sigma = 0.3$) for the trapped radical was calculated from the results of the post-scavenging technique /6/. If it is assumed that the trapping probability is equal for all the radicals and that the radical formation processes are phase and temperature independent, the radical distributions calculated in the liquid phase are also valid in the solid state. Experimental ratios of 1-pentyl/2-pentyl/3-pentyl are 1.0/2.2/1.1 (Holroyd, Klein) /7/ or 1.0/2.5/1.0 (Koch, Hootman, Cramer) /8/. Table 4 presents the trapped radical yields, the radical yields leading to dimer formation and the difference between these two results, which is equal to the contribution of trapped radical to the formation of pentenes.

The disproportionation-combination rate constants ratios (k_d/k_c) are related to these yields in the following way:

$$\frac{k_d}{k_c} = \frac{G_{R'(\text{pentene})}}{G_{R'(\text{decane})}}$$

The values of k_d/k_c ratio (Table 4) for secondary radicals (2 to 5) are higher than that for primary radicals (1.4). The same results are reported for all alkyl radicals /9/ studied in the liquid phase.

References

/1/ B. Tilquin, J. Allaert, A. Dautricourt, D. Mauer and P. Claes, Int. J. Radiat. Phys. Chem., 5, 343 (1973).

/2/ Carnegie Institute of Petroleum, A. P. I. research, project 44, Pittsburg (1965).

/3/ J. Takács, C. Szeta and G. Tarjan, J. Chromatogr., 56, 1 (1971).

/4/ E. Kovats, Helv. Chim. Acta, 46, 2706 (1963).

/5/ F. Thyrion. J. P. Dodelet, C. Fauquenoit and P. Claes, J. Chim. Phys., 65, 227 (1968)..

/6/ B. Tilquin, J. Allaert and P. Claes, Int. J. Radiat. Phys. Chem., (in press)

/7/ R. A. Holroyd and G. W. Klein, J. Amer. Chem. Soc., 84, 4000 (1962).

/8/ R. O. Koch, J. P. Hootman and W. A. Cramer, J. Amer. Chem. Soc., 90, 3326 (1968).

/9/ M. J. Gibian and R. C. Corley, Chem. Rev., 73, 441 (1973).

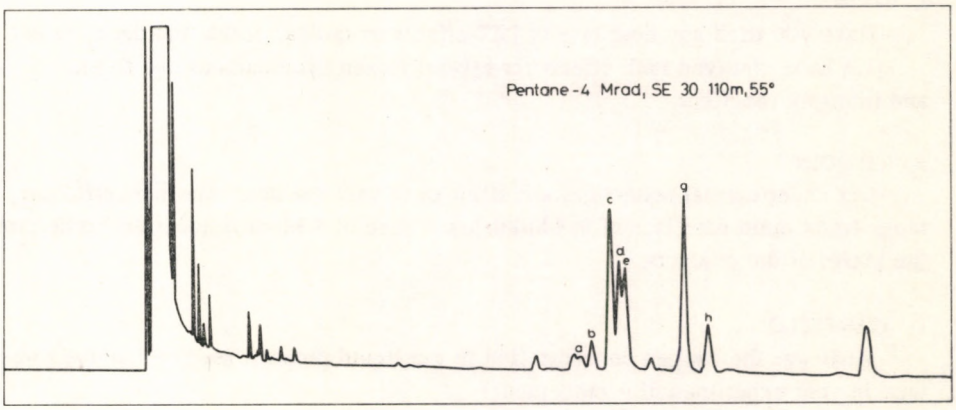

Fig. 1 Gas chromatogram of the heavy products of radiolysis of n-pentane in the solid phase.

G. R. FREEMAN

Is there a regular variation in k_d/k_c on going from the gas to the liquid and to the solid phase?

B. TILQUIN

We do not find any regular variation. In the case of cycloalkane, the cycloalkyl radical is the only paramagnetic species observed by ESR spectroscopy in solid samples irradiated with gamma rays. So using our post-irradiation scavenging technique, we can determine without any assumptions or approximations the ratio k_d/k_c in the solid state. Assuming that this ratio is equal to one in the liquid phase, we find in the solid state a lower value for the cyclohexyl radical and a higher value for the cyclopentyl radical. (B. Tilquin, J. Allaut and P. Claes, J. Phys. Chem. 78, 462 (1974).)

J. KROH

Have you tried any dose rate or LET effects on radical yields and decay rates?

We have observed such effects for several frozen hydrocarbons due to intertrack and interspur reactions.

B. TILQUIN

Our experimental setup does not allow us to vary the dose rate in a sufficient range (maximum dose rate of 0.4 Mrad/hr). A dose of 4 Mrad is necessary to determine the yields of the products.

G. CASTELLO

What was the oxygen concentration in the liquid propane used to dissolve n-pentane in your experimental arrangement?

B. TILQUIN

Propane was oxygen saturated at room temperature before being transferred into the dissolution cell, so the oxygen concentration was about 10^{-2} m/l.

THE INFLUENCE OF NH_3 AND C_2H_5OH ON THE YIELDS OF RADIOLYTIC PRODUCTS IN GAMMA-IRRADIATED LIQUID PENTANES

T. Bryl-Sandelewska, R. K. Broszkiewicz
Department of Radiation Chemistry, Institute of Nuclear Research,
Dorodna 16, Warsawa, Poland

Introduction

Ions have been found to be important intermediates in the radiolysis of liquid hydrocarbons. Yields of free ions have been determined in some of those liquids /1/ indicating that the hydrocarbon molecule structure has significant influence on the free ion yields. On the basis of positive ion scavenging /2–11/ one can deduce that the role of positive ions in the radiation-chemical decomposition of different alkanes depends on a host compound structure. However, no experiments on different isomers of a hydrocarbon have been yet reported as having been performed in one laboratory, though an importance of such an approach is self-evident in view of considerable discrepancies between results obtained by various investigators.

In the present work the effect of ammonia and ethanol applied as positive ions scavengers on some stable product yields in irradiated isopentane, n-pentane and cyclopentane has been studied.

Experimental

Koch-Light Pure Grade isopentane, n-pentane and cyclopentane were treated with concentrated sulphuric acid to remove unsaturates, then washed, dried and distilled. The purity of pentanes after that treatment was found by GC to be 99.2%, 99.5% and 99.8% for isopentane, n-pentane and cyclopentane, respectively. The only detectable impurities were: n-pentane in isopentane, isopentane in n-pentane and n-pentane in cyclopentane. P. O. CH. Gliwice Research Grade ethyl alcohol was used without further purification. Z. P. A. Chorzów Technical Grade ammonia was purified by trap-to-trap distillation and stored in a vacuum line.

All samples were degassed by the freeze–thaw technique. CO_2 was removed by additional pumping at about 0^oC. Ethyl alcohol had been added to the samples before and ammonia after the degassing. Hydrocarbon samples filled all but a small part of the irradiation vessel so that essentially all the ammonia (>95%) was dissolved. After degassing samples in glass vessels were sealed off and taken for irradiation with ^{60}Co-rays. The dose-rate was 1.53×10^{17} eV·g^{-1}·min^{-1} (Fricke dosimetry) and doses absorbed by hydrocarbons were $(5.8 + 7.1) \times 10^{19}$ eV·g^{-1}.

Gaseous products were evacuated from the irradiated samples on the vacuum line. All analysis were carried out by gas-chromatography method. C_2-C_3 products were analysed with hexadecane on Celite column (room temperature) and dimers at 75 °C using a silicone elastomer and squalane (both on Celite) column.

Results and discussion

In Fig. 1 the effect of ammonia on the yields of C_2 and C_3 products in irradiated liquid isopentane, n-pentane and cyclopentane is shown. The effect of ethanol on those product yields is shown in Fig. 2, and the effect of ethanol on dimer yields in Fig. 3.

Ammonia and ethanol have been known to be effective positive ion scavengers in irradiated liquid hydrocarbons /2,4,5,7–9,11/. As may be seen from Figs 1 and 2 the yields of the same fragmentation products in isopentane and n-pentane are strongly decreased by ammonia and ethanol so the positive ion reactions play an important role during the formation of those products.

From C_2 and C_3 product yields at zero scavenger concentration, as well as from their dependence on the increase of additive content Figs 1 and 2/, it may be seen that the C_5 alkane structure has a substantial influence on the yield of the individual product and on the role of ions in its formation too. For instance, from ethane and propylene yields in isopentane it appears, that the reaction

$$C_5H_{12}^{*} \longrightarrow C_2H_6 + C_3H_6 \qquad (1)$$

is the main fragmentation process during the radiolysis of that hydrocarbon and that appreciable portions of those products in pure isopentane arise as a result of parent ion-electron recombination reaction

$$C_5H_{12}^{+} + e^{-} \longrightarrow C_2H_6 + C_3H_6 \qquad (2)$$

In irradiated n-pentane reactions (1) and (2) seem to play a much smaller role, and they are of very little importance in the radiolytical decomposition of cyclopentane.

Propane and ethylene may be formed according to the reactions:

$$C_5H_{12}^{*} \longrightarrow C_3H_8 + C_2H_4 \qquad (3)$$

and

$$C_5H_{12}^{+} + e^{-} \longrightarrow C_3H_8 + C_2H_4 \qquad (4)$$

As may be seen from Figs 1 and 2, ethylene yields in isopentane and n-pentane are much smaller than those of propane. They do not change in the presence of the scavengers applied, whilst propane yield is strongly affected both by ammonia and by ethanol. It suggests that decomposition of the parent ions takes place before their recombination with electrons

$$C_5H_{12}^{+} \longrightarrow C_3H_7^{+} + C_2H_5 \qquad (5)$$

and it is followed by hydride ion transfer reaction

$$C_3H_7^{+} + C_5H_{12} \longrightarrow C_3H_8 + C_5H_{11}^{+} \qquad (6)$$

which may be the source of a significant part of propane.

Since the relative decrease of propane yield in the presence of ammonia and ethanol (compared with the yield in pure hydrocarbon) is larger in n-pentane than in isopentane it suggests that the role of reactions (4) and (5) is larger during the radiolysis of normal C_5 alkane than of the branched one.

The influence of the pentane molecule structure on the role of some ionic reactions is evident from dimer yields, too, and from their dependence on the ethanol concentration /Fig. 3/. The dimer yield in pure n-pentane is almost twice as large as that in isopentane, so the yield of parent radicals is much larger in the first isomer than in the second one. Ethanol much more increases the C_{10} products yield in normal alkane than in the branched one, so it means that the parent ion scavenging

$$C_5H_{12}^{+} + C_2H_5OH \longrightarrow C_5H_{11} + C_2H_5OH_2^{+} \qquad (7)$$

followed by

$$C_5H_{11} + C_5H_{11} \longrightarrow C_{10}H_{22} \qquad (8)$$

is much more important in n-pentane than in isopentane. Reaction (7) competes with ion fragmentation and recombination reactions of the type (5) and (4) and it leads to decrease of the yields of fragmentation products in both noncyclic pentanes.

It appears from our results (Figs 1 and 2) that in irradiated isopentane and n-pentane propane is the fragmentation product mostly influenced by ammonia and ethanol. In isopentane the decrease of ethane and propylene yields is comparable but smaller than that of propane. If propane ionic precursors are scavenged according to nonhomogenous kinetics described by Warman et al. /14/ the linear relationship between $(-\Delta G/C_3H_8)^{-1}$ and $(S)^{-1/2}$ (S-scavenger concentration) should be observed. As may be seen from Fig. 4, the relationship in NH_3 containing isopentane really gives a straight line and G=0. 25 for ionic precursors of propane may be

calculated. In the presence of ethanol the $(-\Delta G/C_3H_8)^{-1}$ vs. $(C_2H_5OH)^{-1/2}$ relationship is not linear (Fig. 5) so kinetics of scavenging by ethanol is more complicated and it cannot be described by Warman s equation. In n-pentane the square root relationship is not followed – neither in the presence of ammonia nor of ethanol.

Another influence of hydrocarbon structure as well as physico-chemical properties of scavenger appears if scavenging effectiveness is considered. It may be seen from our data (Figs 1 and 2) that concentrations of ammonia and ethanol at which a half of the ionic precursors of propane are scavenged differ considerably in isopentane and n-pentane. In the branched pentane two concentrations are about 0. 006 and 0. 1 mol· dm^{-3} for ammonia and ethanol, respectively, whereas in normal pentane those concentrations are equal to about 0. 015 and 0. 03 mol· dm^{-3}. On the basis of above values one can calculate relative reactivities of C_2H_5OH and NH_3 (as positive ion scavengers) as about 6×10^{-2} in isopentane and about 5×10^{-1} in n-pentane, so there exists a significant influence of both hydrocarbon molecule structure and physico-chemical properties of positive ion scavenger on the effectiveness of scavenging process. It cannot, however, be exclused that the differences in behaviour of C_2H_5OH and NH_3 may be due, in part, to the solvation of e^- by the first but not by the second additive.

In irradiated cyclopentane the most abundant ring fragmentation product is ethylene, and allene and cyclopropane appear among the C_3 products. All C_2 and C_3 product yields are small but increases of ethylene, allene and cyclopropane G values may be observed with increasing ammonia and ethanol concentrations. In isopentane and n-pentane no fragmentation product yields increased in the presence of scavengers applied. Such changes in cyclopentane may suggest that the yield of C_5 ring cleavage increases when additives are present. The same conclusion may be drawn from our observation that n-decane appears among C_{10} products in the irradiated cyclopentane-ethanol system. Half of the total dimer increase (Fig. 3) is the n-decane yield. It is not quite clear at present what kind of reactions with ethanol molecules involved may lead to such a product. It is probably not proton transfer from cyclopentane to ethanol, because of large H atoms deficit in pentenyl C_5H_9 radicals formed in that case. Possibly charge and/or excitation reactions take place as ionization potentials of ethanol and cyclopentane are quite similar (10. 47 eV /12/ and 10. 50 eV /13/, respectively) and proton transfer from parent cyclopentyl ions to ethanol may not be the most probable mechanism of reactivity transfer in the irradiated cyclopentane-ethanol system.

References

/1/ G. R. Freeman, J. P. Dodelet, Can. J. Chem. 50, 2697 /1972/.

/2/ J. W. Buchanan, F. Williams, J. Chem. Phys. 44, 4377 /1966/.

/3/ M. G. Robinson, G. R. Freeman, J. Phys. Chem. 72, 1780 /1968/.

/4/ K. Tanno, S. Shida, J. Phys. Chem. 72, 3496 /1968/.
/5/ K. Shinsaka, S. Shida, Bull. Chem. Soc. Jap. 43, 3728 /1970/.
/6/ J. A. Stone, G. Matsushita, Can. J. Chem. 49, 3287 /1971/.
/7/ K. D. Asmus, Int. J. Radiat. Phys. Chem. 3, 419 /1971/.
/8/ J. Kroh, S. Karolczak, H. Zegota, in: Advances in Radiation Research, Ed. by J. F. Duplan and A. Chapiro, New York, 1973, Vol. 2, p. 459
/9/ J. Kroh, J. Piekarska, Bull. Acad. Pol. Sci. Ser. Sci. Chim. 22, 167 /1974/.
/10/ E. L. Davids, J. M. Warman, A. Hummel, J. C. S. Faraday I, 71, 1252 /1975/.
/11/ T. Wada, S. Shida, Y. Hatano, J. Phys. Chem. 79, 561 /1975/.
/12/ K. M. A. Refaye, W. A. Chupka, J. Chem. Phys. 48, 5205 /1968/.
/13/ M. Th. Pract, J. Derwiche, Chem. Phys. Lett. 5, 546 /1970/.
/14/ M. Warman, K. D. Asmus, R. H. Schuler, J. Phys. Chem. 73, 931 /1969/.

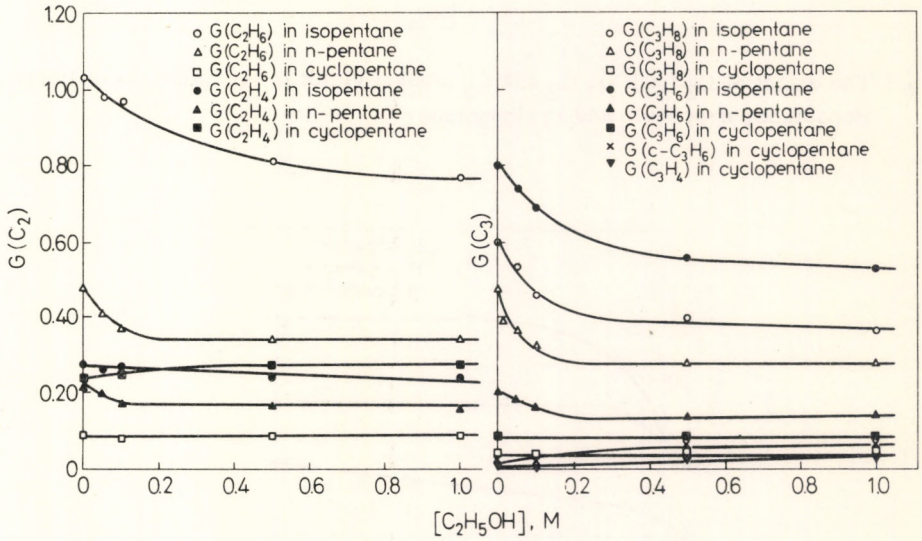

Fig. 1 The effect of NH_3 on C_2 and C_3 product yields in the radiolysis of liquid isopentane, n-pentane and cyclopentane

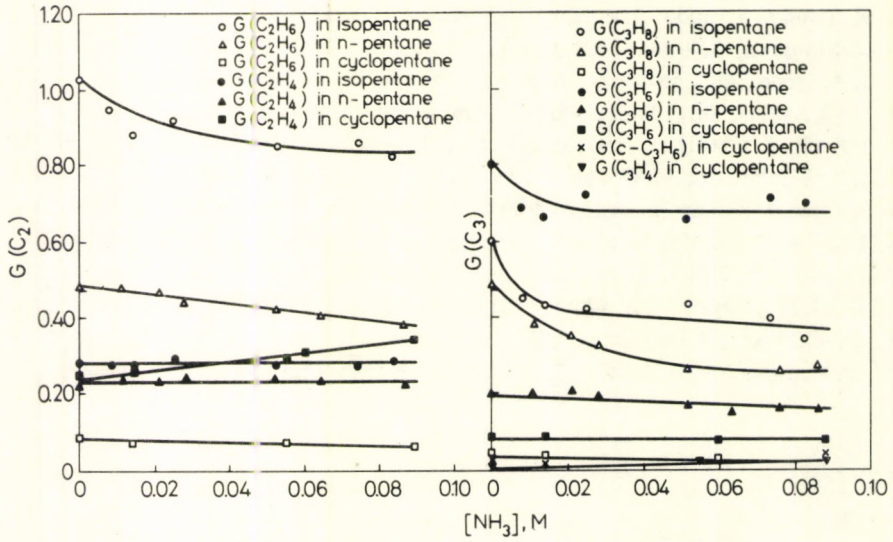

Fig. 2 The effect of C_2H_5OH on C_2 and C_3 product yields in the radiolysis of liquid isopentane, n-pentane and cyclopentane

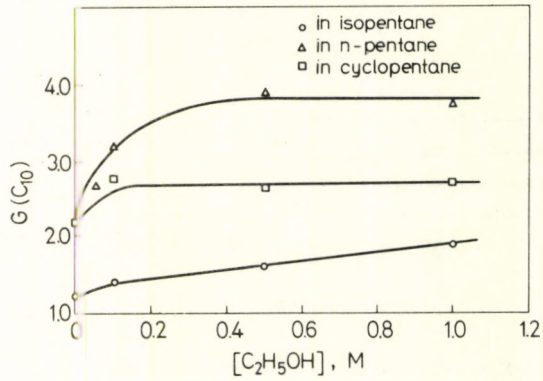

Fig. 3 The effect of C_2H_5OH on C_{10} product yields in the radiolysis of liquid isopentane, n-pentane and cyclopentane

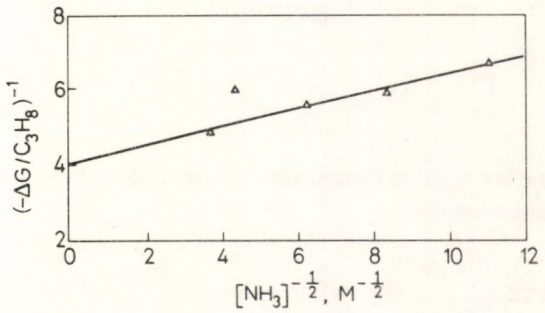

Fig. 4 Plot of $(-\Delta G/C_3H_8)^{-1}$ vs. $(NH_3)^{-1/2}$ in irradiated liquid isopentane

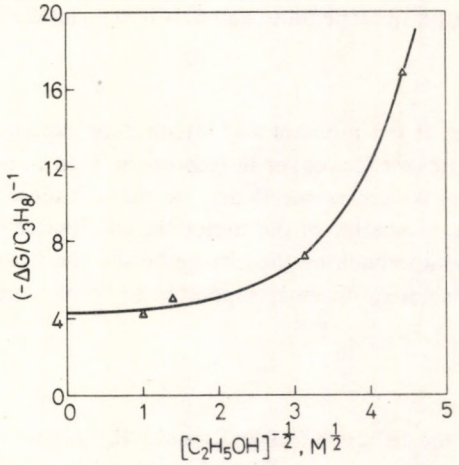

Fig. 5 Plot of $(-\Delta G/C_3H_8)^{-1}$ vs. $(C_2H_5OH)^{-1/2}$ in irradiated liquid isopentane

S. GORDON

You are using rather high concentrations of scavenger, have you accounted for direct effects of the scavenger?

R. K. BROSZKIEWICZ

The direct energy deposit in ethanol has been accounted for. It was not necessary in the case of ammonia.

G. R. FREEMAN

Would you speculate on the difference between the ratio of scavenging efficiencies $C_2H_5OH/NH_3 = 0.06$ in isopentane and 0.5 in n-pentane?

R. K. BROSZKIEWICZ

We cannot present at the moment any satisfactory explanation to that problem. Ammonia is a more efficient scavenger in isopropane than in n-propane, whereas for ethanol the situation is vice versa. It may be that all these effects depend on the localization of charge, symmetry of the molecule and finally on the probability of the scavenger molecule approaching the charge before the ion decomposes. The last hypothesis, however, is not sufficiently supported to be of more value than just a speculation.

I. MAYER

The difference in the behaviour of EtOH and NH_3 in hydrocarbons may be explained by the formation of e^-_{eth} in the hydrocarbon. This was observed by pulse radiolysis in alcohol - hydrocarbon mixtures in the similar concentration range.

R. K. BROSZKIEWICZ

I agree that this possibility cannot be excluded. Actually we put this into the printed text.

R. A. HOLROYD

I am not surprised that ethanol does not obey the square root law at high concentrations because it does form clusters and the clusters scavenge electrons. We are studying this effect at Brookhaven with methanol and it is complicated because of the formation of clusters of different size which vary in their reactivity with electron.

G. FÖLDIÁK

If the function on Fig. 5 is drawn instead of $1/-\Delta G(C_3H_8)$ versus $[C_2H_5OH]^{-1/2}$ as $\Delta G(C_3H_8)$ versus $[C_2H_5OH]^{-1/2}$, the function is nearly linear. What is the reason for this? What is the reaction mechanism?

R. K. BROSZKIEWICZ (communicated)

The coordinates on the plot in Fig. 5 are the consequence of applying the Warman et al. /14/ equation describing the non homogeneous kinetics of the scavenging reaction. They cannot be changed by simple mathematical procedure as it would change the relation between the mathematical and physical senses of the equation. In the case of the applied coordinates the overall process shows increased scavenging effect with increasing scavenger concentration. The apparent linearity obtained by changing $1/-\Delta G(C_3H_8)$ to $-\Delta G(C_3H_8)$ would reverse this effect, which is an impossible result.

Concerning the reaction mechanism we believe that the scavenger affects reactions (4) and (6).

J. KROH

The results for ethanol do not fit the square root equation for inhomogeneous kinetics. Have you tried to fit them to any other type of kinetics?

R. K. BROSZKIEWICZ

We have checked for homogeneous kinetics as well, the results were not satisfactory, however.

THE MECHANISM OF LIQUID n-HEXANE RADIOLYSIS

E. N. Avdonina

Department of Chemistry, Moscow State University
Moscow, USSR

In spite of the great advances made in recent years in the understanding of liquid n-alkanes radiolysis, many aspects have not been satisfactorily explained and our knowledge of the problem as a whole is still rather inadequate. Comparatively little studied, among others, remains the problem of hot hydrogen atom reactions, though the idea of their formation and reactions in radiolysis seems to be universally accepted. This idea was most frequently applied to explain the origin of bimolecular component of the hydrogen radiation yield not affected by thermal H atom scavengers. It was shown/1/ that in liquid n-butane radiolysis the yield of H_2, resulting from the abstraction by hot H atoms is as much as 2.1 molecules per 100 ev. The studies with charge scavengers have shown that hot H atoms can be produced from charged as well as from neutral excited species. Other types of hot H atoms reactions and their role in the formation of n-alkanes radiolysis products are not usually considered.

But at the present state of radiation chemistry of hydrocarbon the results, obtained in the studies of recoil tritium atoms reaction in n-alkanes, seem to justify an attempt to distinguish among others the sequence of processes involving hot H atom reactions and related processes in alkanes. The present communication is an attempt to evaluate the contribution of hot H atom formation and stabilization reactions in liquid n-hexane radiolysis.

The studies of recoil T atoms in liquid n-hexane show that T atoms (originally ions with the energy of 2,7 Mev) are eventually stabilized in a variety of compounds. Scavengers or the change of temperature in a wide range hardly affect tritium distribution in labelled products.

It was shown /2/, that the main recoil T atom reactions in n-hexane are:

		Yield
H atom abstraction	$T + RH = TH + R$	~50%
H atom substitution	$T + RH = RT + H$	~25%
C-C bond rupture	$T + RH = r_1T + r_2$	~10%

The composition of low molecular hydrocarbon fractions labelled by T, according Ref. /3/, is:

Methane	3.4%	Butane	1.5%	Propylene	0.3%
Ethane	1.9%	Pentane	1.0%	Butenes	0.4%
Propane	1.6%	Ethylene	0.7%	Pentenes	0.1%

All these products result from hot T reactions. Only about 5% of T atoms are found in high molecular fraction. About 10% of recoil T atoms are evidently thermalyzed, reacting further with the formation of HT.

A number of experimental techniques have permitted us to obtain information on the threshold energies for H atom reactions. It was established that for H atom abstraction it is 0.3–0.5 ev; the threshold energy of substitution is about 1.5 ev, that of C–C bond scission – about 4.5 ev. It was shown that the integral yields of these reactions grow rapidly in the interval of 2-20 ev and further change only very slowly with energy /4/. It is supposed that the majority of recoil T atoms become chemically bound, reacting in the energy range of 3-15 ev

The data on recoil T atom reactions suggest the same types of reactions for hot H atoms in radiolysis, that is, H atom abstraction, H atom substitution and C-C bond rupture. At the same time, one must consider the reactions of hot H atom formation from the irradiated parent alkane. One must also remember, that besides "hot" products analogous to tritium labelled compounds, some amount of radicals are formed – both parent and fragment ones – further participating in the usual thermal reactions.

The radiation chemistry of liquid n-alkanes can, evidently, be understood on the basis that in radiolysis some independent processes occur which could be taken as primary ones. They are followed by further reactions of unstable intermediates. A scheme of n-hexane radiolysis, including among other primary processes the reactions of hot H atom formation, is given in Table 1.

The following assumptions have been made for the primary processes of this scheme:

Reaction1. RH = H_2 + Products. It is supposed that H_2 is formed together with polyenes or biradicals, which further react giving rise to compounds with higher molecular weight than that of dimers. The yield is taken to be equal to the excess amount of hydrogen in the investigated group of products.

Reaction 2. RH = H_2 + hexene. The radiation yield is 1.3 – not affected by temperature changes and radical scavengers (iodine).

Reaction 3. RH = H_{hot} + olefine + r. This type of parent alkane decomposition, is responsible, as supposed in /5/, practically for the formation of low molec-

Table 1

Radiolysis of pure n-hexane

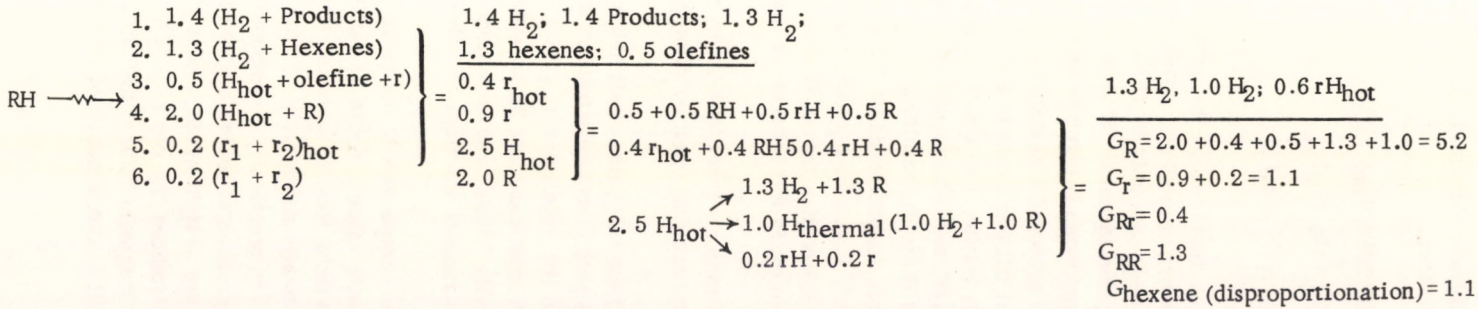

Radiation yields of products from pure n-hexane

Experimental data /6/		Values calculated from the proposed scheme
H_2	5.2	1.4 + 1.3 + 1.3 + 1.0 = 5.0
$Hexene_{(mol)}$	1.3	1.3
$Hexene_{(dispr)}$	1.2	1.1
RR	1.3	1.3
rR	0.4	0.4
rH	1.1	1.1
Olefines C_2–C_4	0.5	0.5

ular weight olefines in n-alkanes radiolysis; the yield, 0.5 molecules per 100 ev, is equal to the total amount of light olefines.

Reaction 4. C—H bond rupture, $RH = R + H_{hot}$

Reaction 5. C—C bond rupture, $RH = (r_1 + r_2)_{hot}$

Reaction 6. C—C bond rupture, $RH = (r_1 + r_2)_{thermal}$

The yields of Reactions 4–6 were evaluated using the actual yields of radical reactions in n-hexane. The radicals from reaction 5 are called "hot", because they are not sensitive to radical scavengers and react only by H atom abstraction. The same properties can be also due to reaction in tracks, H atom transfer, etc.

The total amount of hot H atoms produced is taken to be equal to the radiation yields of Reactions 3 and 4. It was supposed that stabilization of hot H atoms occurs in the same way as that of recoil tritium atoms in liquid hexane.

Instead of a product of H atom substitution reaction (labelled parent alkane in recoil T studies), being in this particular case indistinguishable from original n-hexane, one must consider only a group of H atoms, resulting from this process. As has been shown, the process of substitution is accompanied by the deposition of energy in the molecule (about 5 ev for alkanes); it can be supposed that the energy of the resulting H atoms will be considerably lower than that of H atoms, which initiate substitution. Thus, for this group of H atoms in this scheme we consider only thermal reaction of H atoms abstraction.

It was supposed also that fragment radicals react by H atom abstraction and by combination with parent radicals. Hexyl radicals react by disproportionation and combination.

It can be seen from Table 1 that the total yields of all n-hexane radiolysis products resulting, according to the scheme due to some primary and secondary reactions, are in complete agreement with the experimental values (cf. Ref. /6/). It is evident that the experimental yields in most cases can be considered as a sum of several components: the products of really "molecular" reactions (e. g. $RH = H_2$ + hexene), products of hot H atom or hot radical reactions and also the products of thermal atom and radical reactions.

The ratio of radical and molecular components in the radiation yields, according to the scheme proposed, is a definite value and can be easily demonstrated by the data on n-hexane radiolysis studies using iodine. I_2 is an effective radical scavenger, it suppresses radical reactions nearly completely. At the same time alkyl iodides are found among other products in practically corresponding amounts. The scheme of n-hexane radiolysis in the presence of iodine is given in Table 2.

From the comparison of the decrease of light hydrocarbons yields in the presence of I_2 with the yields of respective alkyl iodides one can conclude that iodine practically does not affect the processes of fragment radical formation, acting only as a scavenger: the total yield of Rr and rH in the presence of iodine is decreased by

Table 2

Radiolysis of n-hexane in the presence of iodine

$$RH \xrightarrow{\sim\sim} \left.\begin{array}{l} 1.\ 0.4\ (H_2 + \text{Products}) \\ 2.\ 1.3\ (H_2 + \text{hexene}) \\ 3.\ 0.5\ (H_{hot} + \text{olefine} + r) \\ 4.\ 2.0\ (H_{hot} + R) \\ 5.\ 0.2\ (r_1 + r_2)\ \text{hot} \\ 6.\ 0.2\ (r_1 + r_2) \end{array}\right\} = \begin{array}{l} 0.4\ H_2;\ 1.3\ H_2;\ 0.4\ \text{Products}; \\ \underline{1.3\ \text{hexene},\ 0.5\ \text{olefines}.} \end{array}$$

$$\left.\begin{array}{l} 0.4\ r_{hot} \\ 2.5\ H_{hot} \end{array}\right\} = 0.4\ r_{hot} + 0.4\ RH = 0.4\ RH = 0.4\ rH + 0.4\ R$$

$$2.5\ H_{hot} \begin{cases} \rightarrow 1.3\ H_2 + 1.3\ R \\ \rightarrow 1.0\ H_{thermal} \\ \rightarrow 0.2\ rH + 0.2\ r \end{cases}$$

$$\left.\begin{array}{l} 0.4\ rH_{hot};\ 1.3\ H_2; \\ = 0.4\ RI;\ 1.3\ RI;\ 1.0\ HI; \\ 0.2\ rH;\ 0.2\ rI \end{array}\right\}$$

$$\begin{array}{l} 2.0\ RI \\ 0.9\ rI \end{array}$$

Radiation yields of products from n-hexane in the presence of I_2

	Experimental data /6/	The values calculated from the proposed sceme
H_2	3.0	1.3 + 1.3 + 0.4 = 3.0
RI	3.58	2.0 + 0.4 + 1.3 = 3.7
rI	0.95	0.9 + 0.2 = 1.1
$rH_{unscavenged}$	0.6	0.4 + 0.2 = 0.6
Olefines $C_2 - C_4$	0.5	0.5
$Hexene_{(mol)}$	1.3	1.3

1. 07, and rI are found in the system with the yield of 0. 95 molecules per 100 ev. According to the proposed scheme, fragment radicals are produced in Reaction 3(0. 5), Reaction 6 (0. 4), and by C—C bond scission involving hot H atoms (0. 2). The total yield is 1. 1 , which agrees with the experimental value for rI.

It was found /6/ that the total yield of unscavenged by I_2 light hydrocarbons is 0. 93. According to this scheme, it is equal to 0. 5 (light olefines) + 0. 4 (abstraction by hot radicals) + 0. 2 (C—C bond scission by hot H atoms), i. e. about 1. 1, The pattern of unscavengeable by I_2 light alkanes in liquid n-hexane radiolysis is shown in Fig. 1 a and the yields of tritium labelled light alkanes in recoil atom studies for n-hexane in Fig. 1 b. It is evident that the largest possible contribution of hot H atom reactions can be represented by the cross-hatched areas of Fig. 1a. The total yield of these is 0.19 (0. 20 in the scheme). The remaining part, 0. 39 (0. 4 in the scheme) can be due to hot radical reactions, proton transfer, etc.

It is clear that the data on radical and molecular components of fragment hydrocarbon yields in n-hexane radiolysis fairly agree well with the proposed scheme.

The action of iodine as a radical scavenger is also manifested in the decrease of parent radicals and thermal H atoms reactions yields. At the same time large amounts of hexyliodides can be found; HI is unstable and difficult to estimate.

The total amount of hexyl radicals, giving the products of n-hexane radiolysis, can be calculated from the relationship:

$$\Sigma\, G_R = 2\, G_{\text{dimers}} + 2\, G_{\text{hexenes (disproportionation)}} + G_{Rr}$$

G_R from n-hexane is, according to the data of Refs /6. 7/, 5.2. The experimental value for G_{RI} is 3. 5 /8/.

Reaction 2 of the scheme under consideration (RH = H_{hot} + R) gives 2. 0 R. Hexyl radicals are produced also in abstraction by hot H atoms (1. 3), by thermal H atoms (1. 0), hot radicals (0. 4) and thermal radicals (0. 5). The total value of G_R is, therefore, 5. 2. In the presence of iodine respective amounts of R are not formed due to the reaction of iodine with thermal H atoms and thermal radicals r. The primary processes of parent radical formation are evidently not affected by iodine, since the experimental yield of RI practically corresponds to the sum of the primary processes, giving hot species (Reactions 4 and 5) yields and that of abstraction by hot H atoms (2. 0 + 0. 4 + 1. 3).

It follows, therefore, that the data on iodine scavenging are also in agreement with the proposed scheme of n-hexane radiolysis as far as the reactions involving parent radicals are concerned.

The decrease of H_2 yield in the presence of iodine is 2. 2. The formation of molecular hexenes are evidently not affected by iodine. The scavenging of thermal H atoms, according to the scheme, can account for the decrease of H_2 yield by only about 1. 0. As Reaction RH = H_{hot} + R is not affected by I_2, one can suggest that in the presence of iodine there is an inhibition of some precesses of H_2 formation together with unidentified products (Reaction 1).

This point of view is supported by the material balance considerations for the radiolysis products in the system n-hexane-I_2. It can be shown that for the same group of products (as for pure hexane) including alkyliodides, one cannot find any excess of hydrogen. But taking into account the unmeasured yield of HI (presumably about 1.0), one can suppose that the excess amount of H_2 will be about 0.5. In unscavenged hexane this value is 1.4.

This supports the idea that iodine inhibits the formation of hydrogen and some unknown products (Reaction 1) and is in complete agreement with the numerous conclusions that the effects of iodine in radiolysis are not confined to the reactions with thermal atoms and radicals.

Therefore, postulating some processes of hot H atom formation in radiolysis of alkanes and evaluating all the consequences of the primary processes and reactions of hot atoms stabilization, it is possible to explain the experimental ratio of radical and molecular components for the yields of all the products found in n-hexane. The scheme proposed agrees with the measured G-values within the limits of experimental error on the simplest assumption of complete similarity for reactions of hot H atoms in radiolysis and the processes of recoil T atoms stabilization in the same system.

If the assumptions made in this communication are true, a vast amount of experimental facts and trends in the radiolysis of n-alkanes are more or less related to the reactions of hot H atom formation and stabilization.

References

/1/ S. Shida, N. Fujisaki, Y. Hatano, J. Chem. Phys. 49, 4571 (1968).

/2/ E. N. Avdonina, Adnan Al-Dhahir, An. N. Nesmeanov, Vestnic Moscow State Univ. "Chemistry", N° 1, 42 (1970).

/3/ E. N. Avdonina, "Chimia Visokich Energii", 4, 291 (1970).

/4/ M. Menzinger, R. Wolfgang, J. Amer. Chem. Soc. 89, 5992 (1967).

/5/ E. N. Avdonina, Radiation Effects, 20, 245 (1973).

/6/ H. Widmer, Tino Gaumann, Helv. Chim. Acta, 46, 2766 (1964).

/7/ R. A. Holroyd, G. W. Klein, J. Amer. Chem. Soc. 84, 4000 (1962).

/8/ "Hydrocarbons. Aspects of radiolysis", Isdat. "Mir", Moscow, 1971, p. 235.

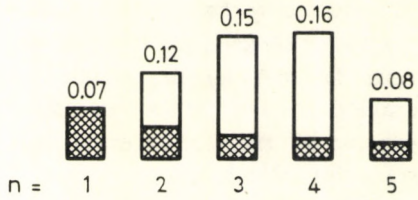

(a)

Fig. 1a Unscavengeable by iodine radiation yields of low molecular weight alkanes from n-hexane (the data of Ref. /6/). Cross-hatched areas: the largest possible contribution of hot H atom reactions

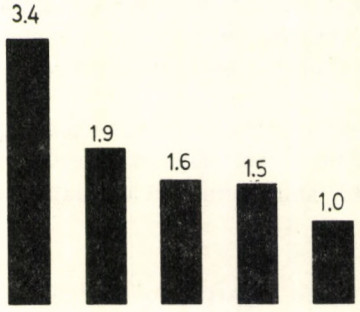

(b)

1b Relative yields of low molecular weight labelled alkanes - the products of C–C bonds rupture by recoil T atoms in n-hexane /3/. n: the number of C atoms in an alkane molecule.

V. TOLKATCHEV

H-atom may react being hot and losing its energy. What is the amount of products in γ-radiolysis of n-hexane that appear to result from hot atom reactions?

E. N. AVDONINA

It appears that all the H-atoms which are produced, and which react in the radiolysis of n-hexane are hot. As for the total amount of the radiolysis products, resulting from formation and stabilization reactions of H-atoms, I believe that it is easier to estimate the contribution of processes not involving H-atoms. According to the proposed scheme of radiolysis these are mainly reactions H_2 + products and H_2 + hexene.

G. CASTELLO

In your discussion on the general behaviour of hexane radiolysis did you use the literature values only (Widmer – Gaumann) or have you experimental results of your own? In the latter case what dose and dose rate were used, and what concentration of iodine was necessary to have constant ΔG values?

Is the sum of the total G-values in the presence of iodine plus the G of alkyl iodides and HI equal to the total G of the pure hydrocarbon? If not, how do you explain the difference?

Moreover did you find differences in H-atom abstraction and substitution in the various sites of the chain, and in the rupture of terminal C-C bonds?

E. N. AVDONINA

All the experimental data considered were taken from the paper of Widmer and Gaumann. The G-values of hexane radiolysis were obtained by these authors by means of extrapolation to zero dose. The concentration of iodine added to n-hexane was 8 mmole.

It seems that the total amount of I and HI must compensate the difference in question. Unfortunately, the data on the HI radiation yields are not as reliable as the G values of alkyl iodides.

The H atom abstraction reaction and the substitution by T atom recoil proceed practically with similar efficiency in liquid n-alkanes of different chain lengths.

The probability of T-atom reaction with C-C bond rupture does not seem to depend on its position in the n-alkane molecule.

H. WINCEL

It has been shown in several papers that in liquid hydrocarbons ionic processes occur. Why have you omitted these processes in your discussion?

Do you think that the process $T + T \rightarrow T_2$

$$T_2 \xrightarrow{\beta} T^+ + He, \quad T^+ + HR \longrightarrow RHT^+ \longrightarrow \text{decomp.}$$

should be competitive to the process presented by you?

How were the yields of the particular processes estimated? The mechanisms are not established, so that calculations based on speculative mechanisms are very problematic.

E. N. AVDONINA

The role of ions in the proposed scheme of radiolysis seems to be precursors to the excited n-hexane molecules produced by neutralization.

The concentration of T atoms in the recoil atom studies is so low that formation of T_2 cannot be competitive with the reaction of T atoms with hydrocarbon molecules.

The yields of recoil tritium atom reactions are found by measuring the radioactivity of the reaction products. At present the mechanisms of hydrogen abstraction and T atom substitution are considered established in recoil atom chemistry.

G. R. FREEMAN

How were the threshold energies measured for the H-atom abstraction, H-atom substitution and C–C bond rupture reactions?

E. N. AVDODINA

These data have obtained by Menzinger and Wolfgang in beam studies and also by photochemical methods.

H. J. ACHE

Following up on Dr. Freeman's question I would like to ask you how the threshold energies for the recoil tritium atoms leading to H abstraction, T for H substitution and C–C bond rupture were determined. I believe Menzinger's experiments were carried out with tritium ions.

E. N. AVDONINA

Menzinger and Wolfgang carried out charge exchange experiments too.

R. K. BROSZKIEWICZ

How were the recoil tritium atoms produced?

E. N. AVDONINA

They were produced by the nuclear reaction $^6Zi(n, d)^3H$.

EFFECT OF MOLECULAR STRUCTURE ON THE RADIOLYSIS OF BINARY HEXANE MIXTURES

I. György, G. Földiák
Institute of Isotopes of the Hungarian Academy of Sciences, Budapest, Hungary

Introduction

It has been known for some decades that yields of certain products formed upon the radiolysis of binary mixtures of certain hydrocarbons do not obey the rule of additivity. For example, in the case of liquid alkane-alkene and alkane-aromatic hydrocarbon mixtures, G-values of hydrogen were found to be lower, in general, than those following the simple additivity rule. These effects have usually been traced back to radical, positive charge and excitation energy acceptor properties of the unsaturated compounds. The phenomenon outlined above has been termed as radiation chemical protection.

Limited data are available on reactions taking place in binary mixtures of saturated hydrocarbons /1−4/. Experiments restricted to the determination of yields of hydrogen and some hydrocarbon fragment products support Hardwick's hypothesis, according to which violations of the additivity rule are usually brought about by a net positive charge exchange between the two components of the mixture, and the direction of the transfer process is determined by the difference in photoionization potentials of components /1/. In earlier works we presented some experimental data that support the view that apart from the photoionization potentials, a number of particular features of molecular structure, e. g. construction of carbon chain, affect the measure and types of interaction taking place between the components. In this work some new results are submitted on phenomena observed during the radiolysis of liquid hexane mixtures.

Experimental

Purum grade hydrocarbons produced by Fluka AG were used for the experiments after having been purified by gas chromatography. The impurity content was less than 0.05%. Materials, after their thorough deaeration and after their water content had been removed by a sodium mirror, were put into Rasotherm glass ampoules and sealed. For a better understanding of the role of certain intermediates during radiolysis the influence of some additives (O_2 and SO_2 as a radical acceptors as well as CCl_4 and SF_6 as electron scavengers) on the yields was studied in pure hexanes as well as in their mixtures.

Irradiations were performed at 35 ± 5°C using the 80 000 Ci nominal activity ^{60}Co source of our institute. The dose rate ($1.3 - 1.4 \times 10^{20}$ eV $g^{-1}h^{-1}$, $2.1 - 2.3$ Mrad h^{-1}) was checked regularly by alcoholic chlorobenzene dosimetry. The absorbed dose was $2.6 - 2.9 \times 10^{20}$ eV g^{-1} (4.2 – 4.6 Mrad).

Yields were determined by gas chromatography. The amount of hydrogen was measured with the thermal conductivity detector of a Chrom 31 gas chromatograph: the amounts of hydrocarbons were determined by a Becker Packard, Model 419 gas chromatograph equipped with flame ionization detector and silica, alumina, squalane and Apiezon L columns.

Results and discussion

Radiolysis of hexane–2, 2-dimethylbutane mixtures. Yields of some characteristic products formed upon the radiolysis of hexane–2, 2-dimethylbutane mixtures are presented as a function of electron fraction of the latter component in Fig. 1. It can be seen that yields of methane, ethane, isobutane and isobutene exceed, whereas G-values of hydrogen propane and butane fall well below those estimated by simple additivity. We observed the formation of the isomer of 2, 2-dimethylbutane, namely 2, 3-dimethylbutane. The yield of this product is also shown as a function of the composition of the mixture.

For a better understanding of the reaction mechanism, experiments were carried out on the radiolysis of pure hexane and 2, 2-dimethylbutane using radical and electron scavengers. Upon irradiation of the latter compound saturated with oxygen, G-values of isobutane, propane, isobutene and propene decreased by about 75, 45, 20 and 10 per cent, respectively, by comparison with the corresponding data of the pure hydrocarbon. In the presence of carbon tetrachloride, G-values of the same products varied as shown in Fig. 2. The yield of isobutene decreased drastically whereas those of isobutane, propane and propene were reduced to a lesser extent. The diminution of the G-values of propane and propene seems to run parallel within experimental error.

The results of similar experiments on hexane radiolysis are shown in Fig. 3.

On the basis of our experimental results the following schematic reaction mechanism is suggested for the radiolysis of the mixture. The differences between observed and estimated yields of the most important fragmention products can be trace back ultimately to a positive charge transfer directed from hexane parent ions to neohexane molecules:

$$n\text{-}C_6H_{12}^{+} + 2,2\text{-DMB} \longrightarrow n\text{-}C_6H_{14} + 2,2\text{-DMB}^{+}.$$

The neutralization of neohexane ions results in the formation of isobutene and ethane, for the greater part, and in that of tertiary butyl and ethyl radicals, for the smaller part:

$$2,2\text{-DMB}^{+} + e^{-} \begin{cases} \nearrow\ i\text{-}C_4H_8 + C_2H_6 \\ \searrow\ t\text{-}C_4H_9^{\cdot} + C_2H_5^{\cdot} \end{cases}$$

It was observed that upon the radiolysis of pure 2, 2-dimethylbutane, its isomer, namely 2, 3-dimethylbutane had been formed with a yield of 0. 35 molecules per 100 eV. As shown in Fig. 1, the yield of this product exceeds that calculated if the additivity rule were to be valid. As scavenger studies on the pure compound indicate, radical acceptors have no significant influence on its yield, whereas electron scavengers enhance the G-value from 0. 35 to 0. 65. On the basis of these experiments a unimolecular-type isomerization having an ionic transition state is tentatively suggested. This picture is also supported by mass spectrometry. On electron impact of 2, 2-dimethylbutane, the formation of C_3 ions in the source has been shown to proceed with a rate comparable to that of the energetically highly favourable formation of C_4 and C_2 fragments. Obviously, the formation of C_3 fragment ions cannot be the result of a simple cleavage. An ionic transient having a molecular structure similar to that of 2, 3-dimethylbutane would better account for these results.

Radiolysis of hexane–2,3-dimethylbutane mixtures. The radiolysis of hexane--2, 3-dimethylbutane mixtures was also studied. G-values vs. electron fraction of the latter compound curves are shown in Fig. 4. The shapes of the curves reveal the interactions of components or intermediates brought about by radiation. The G-values of products formed from hexane with a higher efficiency are lower, while the yields of products characteristic of 2, 3-dimethylbutane radiolysis are higher than those calculated by the additivity rule. The shapes of the curves suggest a reactivity transfer, directed from hexane to 2, 3-dimethylbutane. Diminution of yields of products characterizing hexane radiolysis appears most prominently in the case of hydrogen formation. According to the G-value vs. composition curves, fragmentation of the branched chain compound (subsequent to the transfer process) into C_3 fragments achieves a higher rate as a results of transfer.

We also irradiated systems containing oxygen and carbon tetrachloride, at the same time as radical and electron scavengers, respectively Yields are shown in Fig. 5. The observed large scale decrease in G-values indicates the important role of neutralization and radical reactions in product formation. The yields vs. composition curves for the scavenged systems show only a very slight, if any, declination from linearity The shape of propane and propene curves seems, however, to indicate a transfer process, even in this scavenged system.

$$n\text{-}C_6H_{14}^+ + 2,3\text{-DMB} \longrightarrow n\text{-}C_6H_{14} + 2\ 3\text{-DMB}^+$$

$$2.3\text{-DMB}^+ \longrightarrow C_3H_7^+ + C_3H_7$$

$$\longrightarrow C_3H_8 + C_3H_6^+$$

$$C_3H_7^+ + RH \longrightarrow C_3H_8 + R^+$$

$$C_3H_6^+ + RH \longrightarrow C_3H_8 + R^+_{-H}$$

$$C_3H_7^+ S^- \longrightarrow C_3H_6 + HS \text{ (or } H + S)$$

where S denotes a negative charge acceptor. The excess amount of 2, 3-DMB^+ ions formed as a result of charge transfer gives propyl and propene ions that can react in the scavenged system via H^--and H_2^--transfer processes. These reactions may account for the observed excess propane formation but do not explain, of course, the excess propene fields. For the interpretation of the latter phenomenon the neutralization step of $C_3H_7^+$ ions with negative ions has to be formulated.

As it was shown skeletal isomers of the 2, 2-and 2, 3-dimethylbutane were formed upon irradiation. Radical acceptors did not intercept the yields and electron scavengers enhanced the G-value of isomerisation. It should be noted that Wagner postulated a similar type of process /5/. He irradiated 3, 3-dimethyl-1-butene and observed the formation of 2, 3-dimethyl-2-butene. Considering the experimental results we suggest an ionic precursor for the isomerisation. This may proceed either directly or subsequently to the formation of 3, 3-dimethyl-1-butene as suggested by Wagner.

References

/1/ T. J. Hardwick, J. Phys. Chem. 66, 2132 (1962).
/2/ T. Kudo, S. Shida, J. Phys. Chem. 71, 1971 (1967).
/3/ P. J. Dyne, J Denhartog, Canadian J. Chem. 40, 1616 (1962).
/4/ I. György, G. Földiák, Acta Chim. (Budapest) 81, 455 (1974).
/5/ C. D. Wagner, Trans. Faraday Soc. 64, 163 (1968).

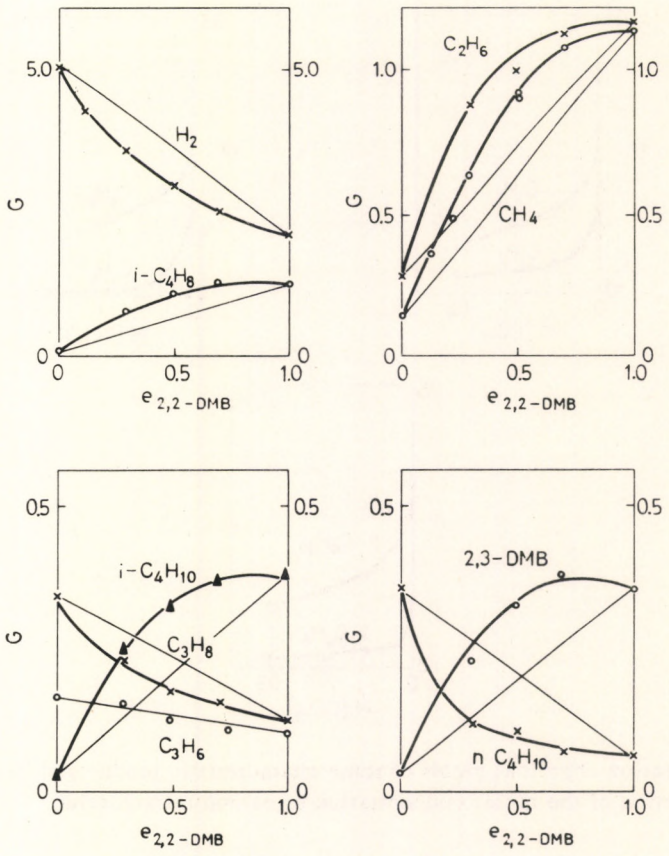

Fig. 1 G-values of certain products formed upon the radiolysis of hexane – 2,2-dimethylbutane mixtures as a function of the electron fraction of the latter component

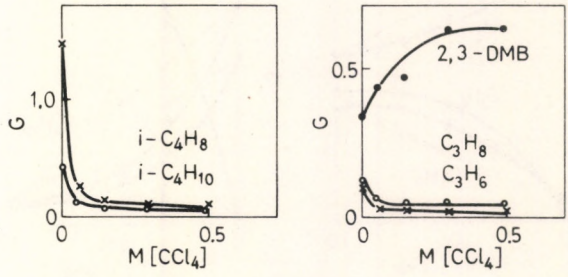

Fig. 2 Radiation chemical yields of some characteristic products of neohexene as a function of the molar concentration of carbon tetrachloride

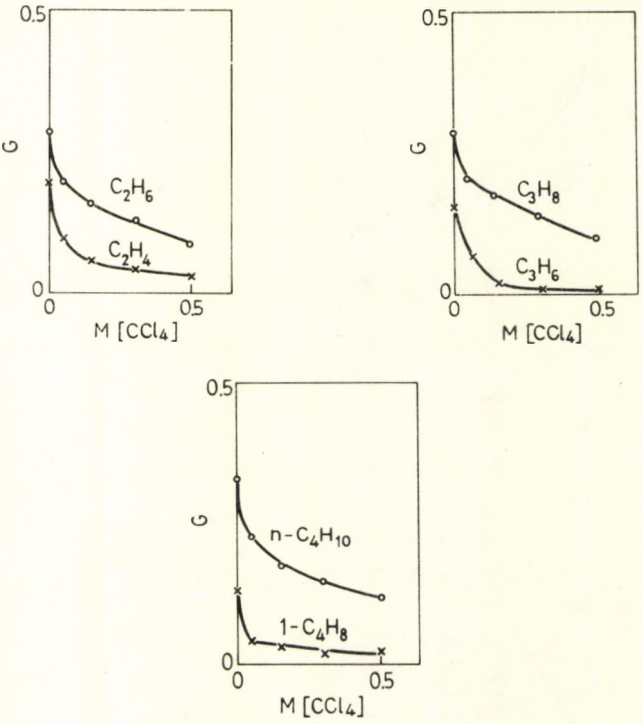

Fig. 3 Radiation chemical yields of some characteristic products of hexane as a function of the molar concentration of carbon tetrachloride

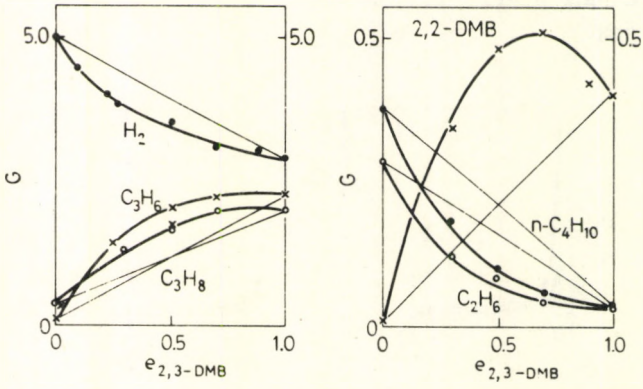

Fig. 4 G-values of certain products of irradiated hexane – 2, 3-dimethylbutane mixtures as a function of the electron fraction of the latter component

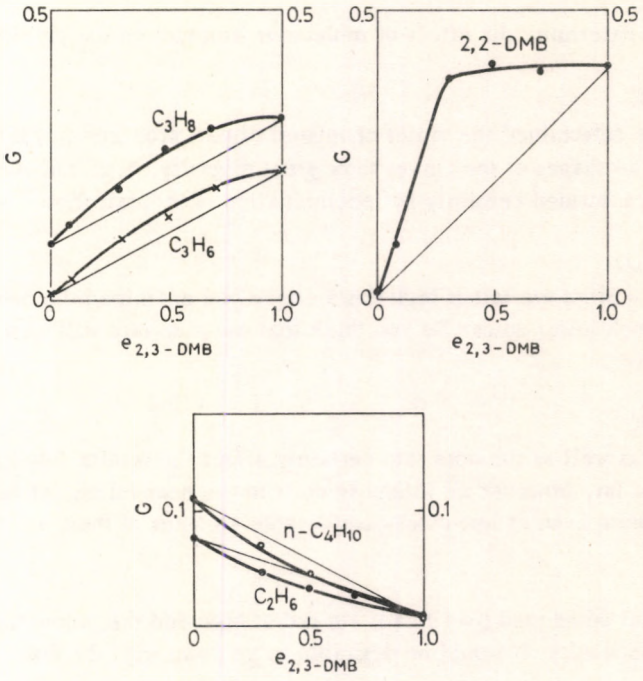

Fig. 5 Radiation chemical yields of some products formed upon the radiolysis of hexane – 2, 3-dimethylbutane mixtures containing oxygen and 0. 5 M carbon tetrachloride

DISCUSSION

G. R. FREEMAN

There was an interesting maximum in the yield of 2, 2 dimethyl butane in the n-hexane/2, 3 dimethyl butane solutions. Do you think that the maximum is mechanistically related to those in the earlier paper today by Horváth?

G. FÖLDIÁK

The maxima observed in these types of systems can be brought about by several different pathways. Fundamentally, such maxima indicate the contribution of at least two types of processes. Still more experiments are needed for a better understanding of the mechanism.

B. TILQUIN

Do you determine the effect of molecular structure on the yield of dimer?

G. FÖLDIÁK

We have determined the yields of several dimers produced in the radiolysis of solutions. The shapes of the curves show great diversity, e. g. the yields of some cross-products formed certainly by recombination of radicals show maxima.

G. CASTELLO

4. 2–4. 6 Mrad are rather high doses. Have you examined the behaviour of the system at much lower doses? Do you think that the dose rate will also have an effect on the results?

G. FÖLDIÁK

The dose as well as the dose rate certainly affect the results. We have not studied this effect so far, however we intend to do it in the near future, at least on the main products, where even at low doses considerable amounts of them are formed.

J. KROH

The total doses used ($\sim$4 Mrad) are rather high and the products of radiolysis may influence the results. It would be desirable to go down with the dose.

G. FÖLDIÁK

Thank you for the comment. It should be noted, however, that we intended to determine the yields of several products having rather low G-values. The relatively high doses applied can be explained by this fact. We are going to study dose effects on the yields of most important products.

J. DELAIRE

Do you think that excited states can contribute to the formation of final products in your mixtures?

G. FÖLDIÁK

It is very difficult to say anything about the role of excitation transfer processes in these systems. However, it might be a possible explanation to the violation of the additivity rule, e. g. in the case of propane and propene formation in irradiated n-hexane 2, 3 dimethyl butane $-O_2 - CCl_4$ systems, as shown in Fig. 5. Vacuum UV photolysis experiments would make things clearer, in our opinion.

THE ISOTHERMAL LUMINESCENCE OF γ-IRRADIATED 3-METHYLPENTANE GLASS DOPED WITH AROMATIC ADMIXTURES

J. Kroh, J. Mayer, M. Szadkowska
Institute of Applied Radiation Chemistry, 93-590 Łódź, Poland

Introduction

It has been generally assumed that a very weak delayed luminescence emitted by organic solids after irradiation at low temperature is caused by the recombination of electrons and positive ions /1-9/.

The purpose of the present work is to analyse the isothermal luminescence (ITL) in γ-irradiated 3-methylpentane glass (3 MP), containing the aromatic admixtures, in respect to fluorescence and phosphorescence of the solute. Up to now the total light emitted has been used in the kinetic treatment of the ITL phenomenon.

Experimental technique

The chemicals were purified using the methods accepted in radiation chemistry. The samples, 2.5 cm^3 by volume, were outgassed and sealed off under pressure of $\sim 10^{-4}$ mm Hg. The irradiation with γ-rays was carried out at 77 K using a ^{60}Co source at a dose rate of 6.24×10^{14} $eVg^{-1}s^{-1}$. The doses used in experiments were in the range $9.3 \times 10^{16} - 1.44 \times 10^{18}$ eVg^{-1}. After irradiation, the light emitted by the sample was examined using a specially designed, high sensitivity detection unit.

Results and discussion

The spectral distribution of ITL, observed for γ-irradiated 3 MP glass in the presence of 9,10-diphenylanthracene (DPA) exhibits a strong emission band with maximum at 435 nm which is assumed to represent the fluorescence of the added solute molecules /10/. The influence of DPA, in the range $10^{-6} - 10^{-3}$ mol^{-1} on the intensity of DPA fluorescence, measured 5 min after the end of irradiation is shown in Fig. 1.

In the presence of biphenyl (Bph) the ITL consists of fluorescence (λ = 300 - 330 nm) /6/ and phosphorescence (λ = 420 - 600 nm) /6/ of the solute.

The influence of [Bph], in the range $10^{-5} - 7.5 \times 10^{-3}$ mol l^{-1} on the intensity of both emission bands, measured 5 min after the end of irradiation is shown in Fig. 2.

The phosphorescence intensity at first increases with [Bph] and then decreases for [Bph] $\sim 2.5 \times 10^{-3}$ mol l^{-1}.

The shape of the corresponding curve is similar to that obtained for the first glow peak of methylcyclohexane glass (MCH) containing increasing amounts of Bph /8/. Moreover, the viscosity of 3 MP at 77 K is equal to 2.2×10^{12}P /11/ whereas the viscosity of MCH at 90K, when the first peak appears, is equal to 10^{11}P /11/. It is worth mentioning that the dependence of fluorescence intensity vs. [DPA] (Fig. 1) is very similar to the dependence of phosphorescence intensity vs. [Bph] in the concentration range up to 10^{-3} mol l^{-1}.

The Bph fluorescence intensity increases steadily with [Bpn] suggesting that a different mechanism may be responsible for Bph singlets formation.

In order to check the influence of annealing of 3 MP glass at 77 K /12/ on the dependence of ITL intensity vs [Bph], the samples were kept at 77 K over 20 hr., then irradiated and analysed. All the experimental points obtained for annealed matrix (Fig. 2) are placed below those found for unannealed system. Since the intensity of ITL is proportional to the rate of charge recombination it seems that the above reaction is slower in annealed glass. The influence of charge scavengers (CCl_4, $i\text{-}C_3H_7OH$) on the intensity of fluorescence and phosphorescence bands for γ-irradiated 10^{-3} mol l^{-1} Bph + 3 MP matrix is shown in Fig. 3. The scavengers influence both emission bands of Bph likewise.

The decay of ITL of γ-irradiated 3MP glass containing Bph or DPA may be expressed by linear relationship first observed by Bagdasar'yan et al. /7/.

$$I_o / I_{(t)} = 1 + \beta (t - t_o) \qquad (1)$$

where I_o, $I_{(t)}$ denote the intensity of ITL at the beginning of observation (t_o) and at time t, respectively, and β denotes a constant related to the rate of ITL decay. Figure 4 demonstrates the representation of our data for Bph by help of the Bagdasar'yan equation.

It is clearly seen that: (i) the higher [Bph], the faster is the decay of ITL, (ii) the decay of fluorescence is slower as compared with phosphorescence. For annealed matrix containing Bph the β-values are lower by ca 20% than in the cases of unannealed samples.

The production of excited states in γ-irradiated 3 MP glass in the presence of aromatic solute S may be expressed by the following scheme:

$$3\,MP \xrightarrow{G\,I_o} 3\,MP^+ + e^- \qquad (2)$$

$$e^- + 3\,MP^+ \longrightarrow 3\,MP^* \qquad (3)$$

$$e^- \longrightarrow e_t^- \qquad (4)$$

$$3\,MP^+ \longrightarrow (3\,MP^+)_t \qquad (5)$$

$$e^- + S \longrightarrow S \tag{6}$$

$$3\,MP^+ + S \dashrightarrow S^+ + 3\,MP \tag{7}$$

$$e_t^- + (3\,MP^+)_t \dashrightarrow P^* \tag{8}$$

$$e_t^- + S^+ \dashrightarrow S^* \tag{9}$$

where e^-, e_t^- denote dry and trapped electrons respectively, $3\,MP^+$, $(3\,MP^+)_t$ – dry and trapped cations of the matrix, S^-, S^+ – anion and cation of the solute, respectively, P* and S* – excited states of matrix and solute molecules (fluorescence and phosphorescence bands), respectively.

In our experiments, the solute concentration was varied over almost three orders of magnitude. The excited states of solute molecules responsible for ITL at 77 K can be produced by the electron-solute cation neutralization although for the scavenger concentration 10^{-4} mol l^{-1} such a mechanism is doubtful. Taking into account the Gallivan's and Hamill's /13/ results concerning the solute cation formation in organic matrix, the concentration of aromatic solute cations may be estimated to be at least 10-fold lower than the concentration of $(3MP^+)_t$, for 10^{-4} mol l^{-1} S in 3 MP matrix.

Possibly the energy transfer mechanism /10/ is responsible for the solute excited state formation in the solute concentration range 10^{-6} – 5×10^{-5} mol l^{-1}.

$$P^* + S \dashrightarrow S^* + P \tag{10}$$

In the concentration range $\geq 10^{-4}$ mol l^{-1} the electron-solute cation recombination is suggested to be responsible for the observed ITL. The intensity of emitted light $I_{(t)}$ can then be described by the following equation:

$$I_{(t)} = \alpha k_g [e_t^-][S^+] \tag{11}$$

where α denotes the coefficient including the luminescence efficiency, the change of units and detection system parameters. Applying a steady-state approximation to the reaction scheme the following equation can be derived:

$$I_{(t)} = \text{const} \frac{[S]}{\left(1 + \frac{k_r}{k_t} + \frac{k_s}{k_t}[S]\right)\left(\frac{k_r}{k_s} + \frac{k_t}{k_s} + [S]\right)} \tag{12}$$

where const $= \alpha k_g (G_o I t)^2$, k_r, k_t and k_s represent the rate constants of reactions (3), (4) and (5), (6) and (7) respectively. The curve representing Bph phosphorescence

vs. [Bph] for unannealed matrix shown in Fig. 2 is calculated using equation (12) and assuming $k_s/k_t = 910$, $k_r/k_t = 1$. These values are almost the same as found in our laboratory /14/ for the 3MP + Bph system at 77 K using spectrophotometric measurements. The process leading to the formation of Bph singlet excited states cannot be described by equation (12) using the above data. However, the observed influence of scavengers on intensity of ITL for Bph + 3 MP system seems to suggest that the electron-cation recombination is involved in the formation of Bph fluorescence and phosphorescence emission. Probably two types of e_t^- populations take part in ITL production. The energy released by recombination, E_R (in eV) is given by well-known equation:

$$E_R = E_i - E - P \frac{14.4}{\varepsilon R} \qquad (13)$$

where E_i is the gas phase ionization potential of S, E represents the binding energy of the electron in the trap, P is the energy of polarization of the solvent by charged species. The last term is the Coulombic energy of the ionic pair at the recombination distance, R (in Å).

If E_S and E_T are the energies of the first excited singlet and triplet states of S then the conditions for fluorescence and phosphorescence emission are $E_R > E_S$ and $E_R > E_T$. Since $E_S > E_T$/ for Bph = 4.10 eV/15/ and E_T = 2.84 eV /15/ one may conclude that the shallow trapped electrons contribute to the fluorescence whereas in phosphorescence emission the deeper trapped electrons are involved.

The slower decay of ITL fluorescence as compared with the decay of phosphorescence may be explained assuming that inter-ionic distance R for e_t^- in shallow traps is bigger than R for e_t^- in deep traps. Such an assumption is fully justified if one tries to analyse the dependence of the tunnelling decay rate constant for electrons in traps of various depth on the inter-ionic distance R /8, 16/.

It seems rather surprising that the tunnelling model can give quite a good description of the ITL phenomenon in respect to MP, which forms at 77 K rather soft glass.

In fact, a certain contribution of the thermally assisted processes should be also taken into account.

References

/ 1/ M. Burton, M. Dillon and R. Rein, J. Chem. Phys. 41, 2228 (1964).

/ 2/ F. Kieffer and M. Magat in "Actions chimiques biologiques des radiations", vol. 14. ed. M. Haissinsky, Masson, Paris 1970, p. 135.

/ 3/ P. B. Merkel, W. H. Hamill, J. Chem. Phys. 53, 3414 (1970).

/ 4/ K. Funabashi, C. Herbert and J. L. Magee, J. Phys. Chem. 75,3221 (1971).

/ 5/ T. Sawai, J. Nuclear Sci.. Techn. 8, 431 (1971).

/ 6/ C. Deniau, A. Déroulede, F. Kieffer and J. Rigaut, J. Luminescence, 3, 325 (1971).

/ 7/ Kh. L. Bagdasar'yan, R. I. Milutinskaya and Yu. V. Kovalev, Khim. Vysok. Energii 1, 127 (1967).
/ 8/ F. Kieffer, G. Lapersonne-Meyer and J. Rigaut Chem. Phys. Lett. 11, (3) 359 (1971), Int. J. Radiat. Phys. Chem. 6, 79 (1974).
/ 9/ Cardier P. Kieffer F., Lapersonne-Meyer C, and Rigaut J., Proc. Fifth Int. Congr. Radiation Research ed. by O. F. Nygzard, H. I. Adler, W. K. Sinclair, Academic Press, New York 1975, p. 426.
/10/ J. B. Berlman, Handbook of Fluorescence Spectra of Aromatic Molecules, Academic Press New York and London, 1965.
/11/ A. C. Ling and J. E. Willard, J. Phys. Chem. 72, 3349 (1968).
/12/ S. L. Hager and J. E. Willard, J. Chem. Phys. 63, 942 (1975).
/13/ J. B. Gallivan and W. H. Hamill, J. Chem. Phys. 44, 2378 (1966).
/14/ J. Kroh, J. Mayer and E. Wojciechowska, in press.
/15/ J. B. Birks, in Photophysics of Aromatic Molecules, Wiley - Interscience, London, 1970.
/16/ B. Broklehurst, Chem. Phys. 2, 6 (1973).

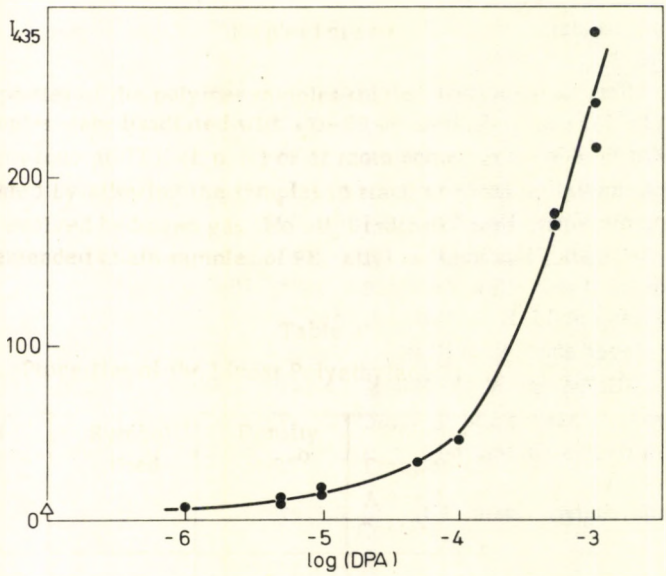

Fig. 1 The influence of DPA concentration on ITL intensity I_{DPA}, measured at 77 K, dose 1.44×10^{18} eV g^{-1}.

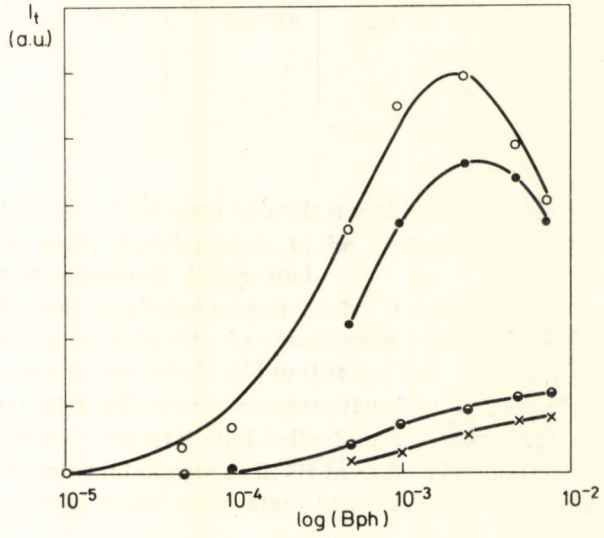

Fig. 2 The influence of Bph concentration on ITL intensity for Bph-3 MP matrix at 77 K, dose 9.3×10^{16} eVg^{-1}. Bph phosphorescence: o - unannealed matrix, the curve was calculated according to Eq. (12), Bph fluorescence: ● - annealed matrix, 20 hr. at 77 K ◒ - unannealed matrix × - annealed matrix, 20 hr at 77 K

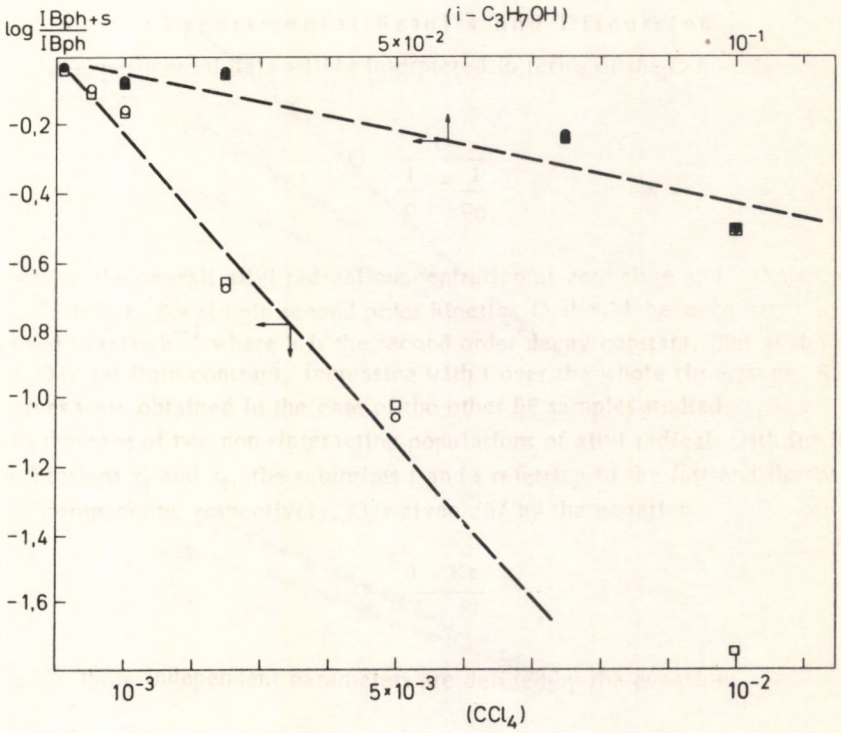

Fig. 3 Semilogarithmic plot of relative ITL intensity yield. I_{Bph+S}/I_{Bph} vs. charge scavenger concentration at 77 K, Bph = 10^{-3} mol l^{-1}, Fluorescence emission: o - CCl_4, ● - i - C_3H_7OH Phosphorescence emission: □ -CCl_4, ■ - i - C_3H_7OH

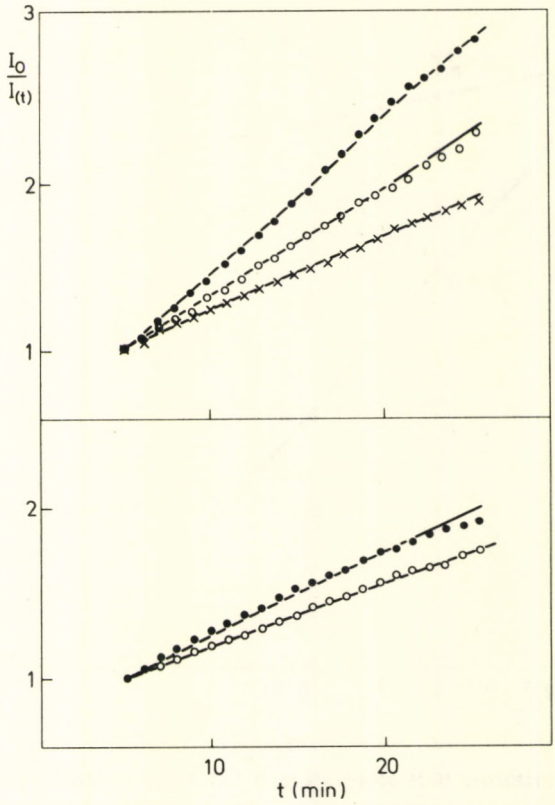

Fig. 4 The influence of [Bph] on ITL decay as expressed by Bagdasar'yan law. A - phosphorescence decay measured at 465 nm: × - 10^{-4} mol l^{-1}, o - 10^{-3} mol l^{-1} ● - 5×10^{-3} mol l^{-1}, B - fluorescence decay measured at 305 nm: o - 10^{-3} mol l^{-1}, ● - 5×10^{-3} mol l^{-1}, Dose 1.1×10^{-18} eV g^{-1}.

G. M. ZIMINA

Is transfer of excitation from the matrix to the adduct possible?

J. MAYER

There are data about this process in the liquid phase.

G. M. ZIMINA

Why not assume that such excitation energy transfer processes are effective in the solid state too?

J. MAYER

Such processes are possible in the solid state too. I talked about this in connection with DPA. Some data may be found in the photochemical works of Bolene.

R. SCHILLER

When speaking about trapped electrons you apparently always referred to traps of the matrix. Aromatics are, however, well known to be prone to transient negative ion formation by scavenging quasi-free electrons. Would the existence of such negative ion states alter the picture you gave us now?

J. MAYER

In 3MP in the presence of aromatics negative ions of the solute are formed. It is possible that the electrons may be transferred from the solute anion to the cation giving excited state of the solute molecule. Such a process may be responsible for fluorescence in Bph. This mechanism explains fluorescence even better than the interpretation given in my speech.

G. R. FREEMAN

It is surprising that in a 3-methylpentane matrix there would be a large enough number of traps deep enough to make an appreciable difference in the probability ratio triplet/singlet. What fraction of the triplets do you think were formed from electrons that were in traps too deep to form singlets?

J. MAYER

According to a recent paper of Willard, in 3MP glass there are e_t^- trapped with binding energy varied from ca. 2.5 eV down to less than 0.1 eV.

The energy E_R calculated according to the equation

$E_R = E_i - E - P - \frac{e^2}{\varepsilon R}$ - Franck Condon loss strongly depends on the numerical values put in it. These are, particularly P and the last term uncertain in the solid state at the present stage of our knowledge. Using for these the higher values than I did (P = 2.2 eV and the Franck Condon loss $\sim$0.5 eV) the boundary line of the electron

binding energy necessary to produce triplets or singlets may be shifted to the shallow trap region causing an appreciable difference in the probability ratio singlet/triplet. Therefore it is very difficult to assess at the moment the fraction of the triplets forming from electrons that were in traps too deep to form singlets.

M. MAGAT

1) You have worked at concentrations of biphenyl of the order of 10^{-2} mole. But did you take into account the fact that at concentrations above 10^{-3} mole you have an important dimer formation and only a fraction of biphenyl is in the monomer form?

2) I suppose you have considered that the a priori probability of the triplet formation is three times that of singlet formation?

3) Do you really think that an untrapped electron "remembers" if it comes from a deep or shallow trap - a condition for your thermodynamic calculations to be valid?

J. MAYER

1) Our investigation was done in the Bph concentration range 10^{-5} to 7.5×10^{-3} m/l. We are aware about the possibility of Bph dimer formation in more concentrated solutions but we have not observed the Bph excimer emission.

2) The ratio of triplet/singlet formation was not calculated in our case in absolute numbers. We can only guess about it taking into account the ratio of phosphorescence to fluorescence emissions. This ratio is a function of the Bph concentration as was shown in Fig. 2.

3) The charge recombination which leads to light emission is due to the reaction of trapped species. The trapped electrons taking part in the recombination process in addition to their binding energy distribution, are characterized by different e_t^--cation distance distribution. This parameter is included in our thermodynamic calculations.

R. KHAIRUTDINOV

What can you say about the energy transfer from the excited biphenyl molecules to CCl_4 as the second mechanism of luminescence quenching in your system?

What is the typical energy transfer distance in the case of biphenyl? What is the mechanism of the energy transfer? Did you take into account the possibility of radical recombination as a source of energy?

J. MAYER

I think that energy transfer from excited biphenyl to CCl_4 is unimportant in this system because the excitation level of CCl_4 molecules is higher than that of biphenyl.

The ITL emission observed by us is mainly due to the ionic recombination process, i. e. $e_t^- + \delta^+$. If there is some contribution of energy transfer, it may be explained by the long distance mechanism proposed by Förster. We did not calculate the distance for such a transfer in our case.

Radical recombination cannot be the source of energy because of the process of thermal energy transfer among the matrix molecules.

TRANSIENT SPECIES IN THE RADIOLYSIS OF FROZEN /77 K/ CIS-PENTENE-2

Andrzej Owczarczyk, Wacław Stachowicz
Department of Radiation Chemistry, Institute of Nuclear Research, Dorodna 16, 03-195 Warszawa, Poland

The low-temperature studies on unsaturated hydrocarbons exposed to the action of ionizing radiation lie in the centre of our scientific interests /1,2/. This article presents the results of further study on transient species produced and trapped during the radiolysis of cis-pentene-2 glassed in liquid nitrogen.

Experimental

Cis-pentene-2 (Fluka 99%) was kept over freshly heated $MgSO_4$ and doubly distilled on a column filled with helices. Gas chromatographic examination after such treatment showed no impurities. Thereafter, the reagent was successively dried over P_2O_5 and metallic sodium, degassed on a vacuum line by sixfold freeze-thaw procedure in a small vessel at 10^{-5} Torr (excluding vapour pressure of the reagent), redistilled into a 5 mm thick Spectrosil optical cell or ESR sample tube (fused silica glass) which after filling were sealed off. Diphenyl (Koch Light 99%) was purified by threefold crystallization while gaseous O_2 and SF_6 (Matheson Co. Inc. 98.7%) were only dried with silica gel and KOH before use. The samples submerged in liquid nitrogen were irradiated in a Gammacell 220 AEL ^{60}Co source with 0.09 and 0.36 Mrads and a dose rate 0.18 Mrads per hour as measured with a ferrous sulphate dosimeter.

Spectrophotometric measurements within the spectral range 250 - 1100 nm, optical bleaching and thermal annealing were carried out with measuring system composed of VSU spectrophotometer incorporating a low temperature cell box and effective cooling system which allows us to maintain a stable temperature of the cell inside a box not exceeding 78 K /2/. A similar system was also used with Unicam SP 100 ir spectrophotometer to examine the 1250 nm - 2500 nm spectral range. The ESR measuraments were carried out with JES-3X-Me JEOL spectrometer connected on line with JEC spectrum computer.

Results and conclusions

The absorption spectrum of pure cis-pentene-2 glass irradiated in liquid nitrogen and measured at 78 K exhibits three maxima: at 262 nm, 310 nm and 610 nm /Fig. 1/. The maximum at the long wave part of the spectrum was previously as-

cribed by Shida and Hamill /3/ to the parent cations /RH^+/ formed in the primary ionization process: $C_5H_{10} \xrightarrow{\gamma} C_5H_{10}^+ + e^-$. As follows from our experiments the presence of diphenyl and SF_6 scavengers in irradiated matrix markedly increases the intensity of 610 nm absorption maximum. /Figs 2 and 3/. This supports Hamill's assignment and indicates that the concurrent process of electron scavenging increases efficiently the number of cations which do not undergo neutralization. From the analysis of the spectrum of cis-pentene-2 glass with diphenyl and its comparison with the spectra of pure cis-pentene-2 and that of diphenyl anion, taking for calculations the literature values of diphenyl anion extinction coefficients at 410 nm and 610 nm ($\varepsilon\phi_2^-{}_{(410)} = 3.7 \times 10^4$ litre/mol cm /4/ and $\varepsilon\phi_2^-{}_{(610)} = 1.1 \times 10^4$ litre/mol cm /5/), the molar extinction coefficient for the absorption of cis-pentene-2 parent cations at 610 nm has been estimated: $\varepsilon_{RH^+(610)} = (1.1 \pm 0.2) \times 10^4$ litre/mol cm. On this basis the radiolytic yield of parent cation was calculated: $G_{RH^+} = 0.14 \pm 0.02$ which remain stabilized in glassy matrix. Spectral examination of cis-pentene-2 glass in near infrared (1250 – 2000 nm) did not prove any absorption within this range. The absence of trapped electrons which usually absorb in this spectral range was also confirmed by the ESR examination which showed no indication of the presence of a narrow singlet characterized for these species. Both observations allowed us to conclude that glassy cis-pentene-2 matrix does not produce trapping sites which are capable of stabilizing efficiently thermalized electrons at 77 K.

Now the following question arises: if in glassy cis-pentene-2 the parent cations are stabilized at 77 K and there is no evidence for the trapping of electrons in it, what is the form of stabilization of compensating negative charge in there? Aliphatic hydrocarbons including mono-olefines, are characterized by the negative electron affinity /6, 7/ and therefore the formation of parent anions RH^- in such matrices is less probable. On the other hand, however, free radicals which are produced with comparatively high yields in irradiated hydrocarbons usually indicate positive electron affinity and hence are capable of forming with electrons R^- diamagnetic anions: $C_5H_9^{\cdot} + e^- \rightarrow C_5H_9^-$. The presence in irradiated cis-pentene-2 10^{-3}M of SF_6 affects the remarkable decrease of the intensity of 310 nm absorption band. Similarly, oxygen caused almost complete disappearance of this absorption in the spectrum. The decrement of the intensity of 310 nm absorption in the presence of electron scavengers allowed the suggestion that it may arise from the R^- anion absorption. The evidence that supports such a view is the disappearance of 310 nm absorption in glassy cis-pentene-2 after the heating of samples from 77 K to 95 K as well as the disappearance of both 310 nm and 610 nm absorption bands after illumination of the samples with $\lambda > 280$ nm light. In both cases the accompanying luminescence light was observed. Spectral analysis of emitted light ($\lambda_{max} = 540$ nm) indicates that it originates from the phosphorescence of cis-pentene-2 molecules /8/. The mechanism of reaction which occur during the thermal annealing and optical bleaching of irradiated cis-pentene-2 glasses could therefore be as

follows:

1. Thermal annealing $R^- + RH^+ \rightarrow R^\bullet + RH^*$

$RH^* \rightarrow RH + h\nu$

2. Optical bleaching $R^- \longrightarrow R^\bullet + e^-$

$e^- + RH^+ \longrightarrow RH^*$

$RH^* \longrightarrow RH + h\nu$

Assuming like yields of both parent cations and anions (the resultant charge is equal to zero) and estimating partial superposition of 310 nm and 610 nm absorption peaks assigned to them (under assumption of the symmetry of the cation peak) it was possible to evaluate the extinction coefficient of the anion absorption at 310 nm: $\varepsilon_{R^-} = (1.2 \pm 0.4) \times 10^4$ litre/mol cm. The ESR spectra of paramagnetic species produced during the radiolysis of cis-pentene-2 glasses at 77 K are characterized by a symmetric signal composed of 9 lines with a hyperfine splitting of 14 gauss and with intensity ratios characteristic for allyl radicals /Fig. 4/. High symmetry and line intensities of the ESR signal indicate that the pentallyl radical is the predominant paramagnetic product in cis-pentene-2 radiolysis. It is known from the literature data that light allyl radicals in hydrocarbons give rise to the absorption in 230 nm – 260 nm spectral region and that the wavelength of the absorbed light increases with the increase of the length of the radical chain /9,10/. As follows from our experiments the third 262 nm absorption peak in the optical spectrum of glassy cis-pentene-2 /Fig. 1/ reveals good stability under illumination with $\lambda > 280$ nm light and disappears rapidly after heating of the sample to 95 K. Similar features exhibit the ESR signal of pentallyl radicals. In the presence of oxygen pentallyl radicals are transformed into peroxy radicals and this is accompanied by important changes in ESR and optical spectra. In ESR the spectrum becomes characterized by an asymmetric singlet of higher intensity while in the optical spectrum an increase of the 262 nm absorption takes place. Both observations allow us to interpret the 262 nm absorption peak in the optical spectrum as arising from the pentallyl radical absorption.

From the comparison of the radiolytic radical yield of pentallyl radicals estimated by the ESR method ($G_{R^\bullet} = 1.3 \pm 0.1$) with the intensity of the maximum at 262 nm, the molar extinction coefficient of this absorption could be calculated: $\varepsilon_R (262) = (3.4 \pm 0.6) \times 10^3$ litre/mol cm.

Pentallyl radicals stabilized in glassy cis-pentene-2 matrix show, at 77 K, slow isothermal decay which is ruled by second order kinetics with the rate constant k = = 0.5 litre/mol sec /Fig. 5/. The knowledge of this rate constant allowed us to calculate the viscosity of cis-pentene-2 matrix at 77 K by applying equations of Waite's theory of diffusion controlled reactions and the Stokes-Einstein relation. The viscosity calculated with the assumption that the radius of radical recombination

sphere in this matrix has a value laying between 4 and 10 angstroms /11, 12/ was found to be equal to (0. 2 – 0. 5) x 10^8 poises. The relatively low as compared with other typical organic glasses (10^{12} – 10^{18}P) viscosity of cis-pentene-2 at 77 K is probably followed by its rather high "softness" which explains the absence of stabilized electrons in this system.

References

/1/ W. Stachowicz, A. Owczarczyk, Radiochem. Radioanal. Lett. 5, 305, (1970).

/2/ W. Stachowicz, A. Owczarczyk, Radiochem. Radioanal. Lett. 15, 139 (1973).

/3/ T. Shida, W. H. Hamill, J. Am. Chem. Soc. 88, 5376 (1966).

/4/ W. H. Hamill, "Radical Ions" p. 321, Editors E. T. Kaiser, L. Keram, Interscience Publ. J. Wiley, N. Y. 1968.

/5/ T. Shida, Advances in Rad. Res. p. 469, Gordon and Brench. Sci. Publ. N. Y. 1973.

/6/ W. A. Cramer, G. J. Piet, Trans. Faraday Soc. 63. 1402 (1967)

/7/ C. F. Curtis, J. M. Francis, A. J. Swallow, J. Proc. Roy. Soc. A 287, 15. (1965).

/8/ Ju. B. Szekk, J. G. Batecha, H. W. Ałfimow, Chim. Wys. En. 4, 297 (1971).

/9/ W. H. Hamill, J. P. Guarino, M. R. Ronayne, J. A. Ward, Disc. Faraday Soc. 36, 169 (1963).

/10/ M. Dole, G. G. Böhm, Adv. in Chem. Ser. 82, 525 (1968).

/11/ S. W. Benson "The Foundations of Chemical Kinetics" s. 493, Series advanced chemistry McGraw-Hill, New York 1960.

/12/ W. Y. Wen, D. R. Johnson, M. Dole, J. Phys. Chem. 78, 1798 (1974).

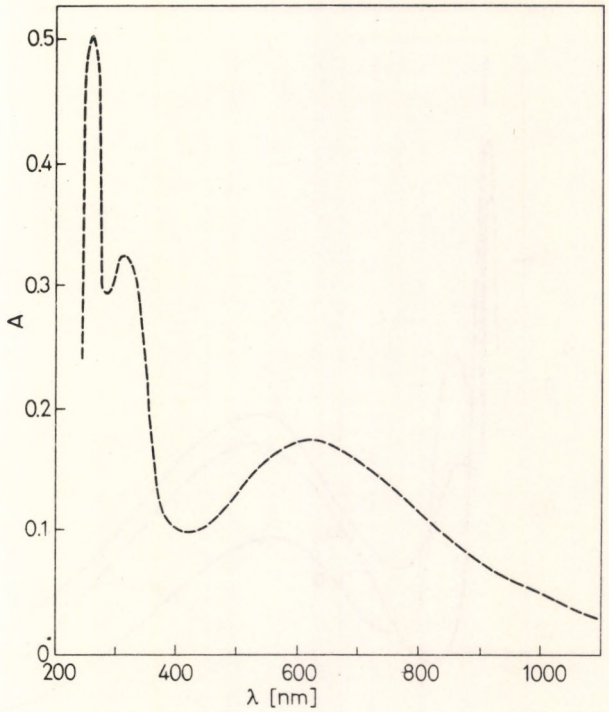

Fig. 1 Absorption spectrum of purified cis–pentene–2 glass γ–irradiated and examined at 77 – 78 K. Dose – 0. 36 Mrads; Dose rate – 0. 18 Mrads per hour; Cell thickness – 5 mm

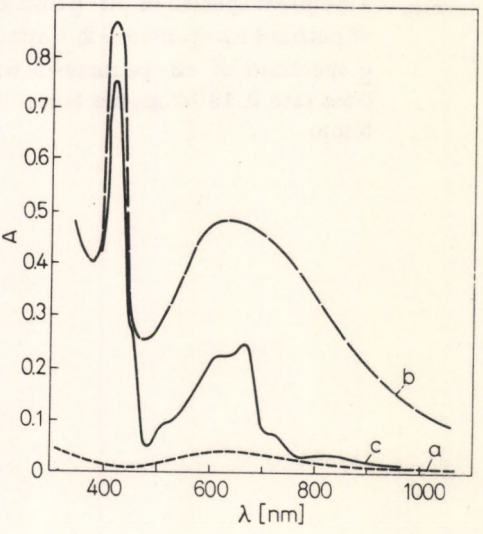

Fig. 2 Absorption spectra of cis–pentene–2 glass with diphenyl: a spectrum of purified cis–pentene–2; b spectrum of 0. 04 M diphenyl solution in cis–pentene–2; c normalized spectrum of diphenyl anion by Shida (Advances in Radiation Research, p. 469, Gordon and Breach, New York 1973). Dose – 0. 36 Mrad; Dose rate – 0. 18 Mrads per hour, Temperature – 77 – 78 K, Cell thickness – 5 mm

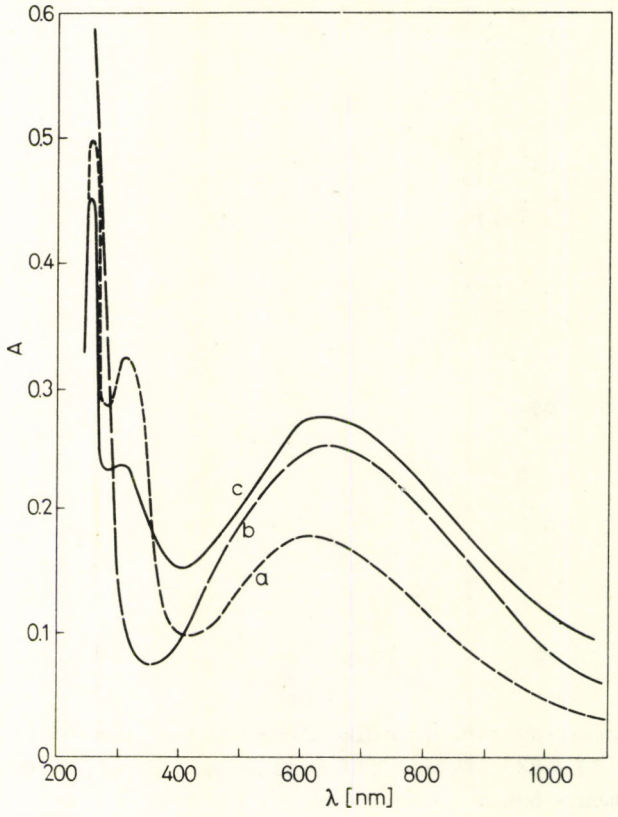

Fig. 3 Absorption spectra of cis-pentene-2 glass with oxygen and SF_6: a spectrum of purified cis-pentene-2; b spectrum of cis-pentene-2 with oxygen ($\sim 10^{-2}$M). c spectrum of cis-pentene-2 with SF_6 ($\sim 10^{-3}$M). Dose - 0.36 Mrads; Dose rate 0.18 Mrads per hour; Temperature - 77 - 78 K; Cell thickness - 5 mm

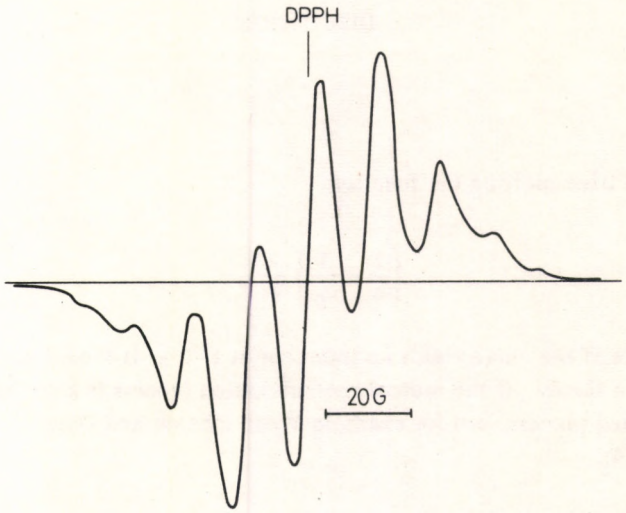

Fig. 4 ESR spectrum of purified cis-pentene-2 glass after graphical substraction of the spectrum ascribed to the irradiated sample tube. Dose - 0.36 Mrad; Dose rate - 0.18 Mrads per hour; Temperature - 77 - 78 K

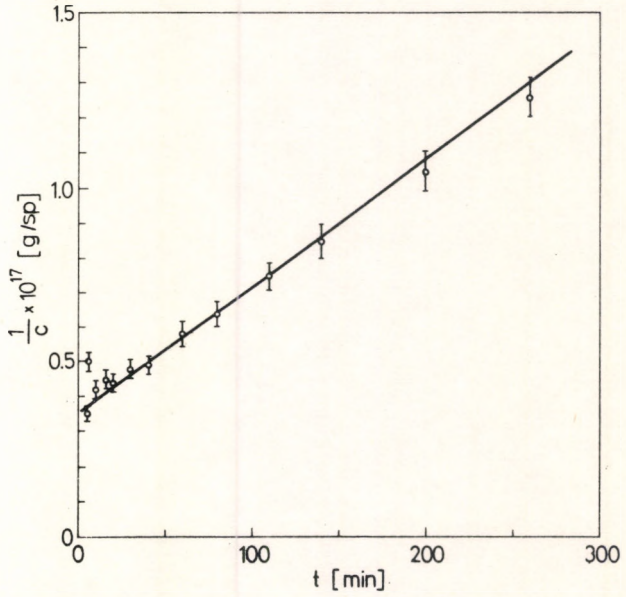

Fig. 5 Kinetics of radical decay in purified cis-pentene-2 glass. Dose - 0.36 Mrads; Dose rate - 0.18 Mrads per hour; Temperature - 77 K

M. DOLE

Have you tried plotting the function

$$\left(\frac{1}{c} - \frac{1}{c_0}\right)\frac{1}{\sqrt{t}}$$

versus $\sqrt{t}$ to see if the curve yields an intercept at $t = 0$ as it should according to the Waite diffusion theory, if the radical recombination process is a second order diffusion controlled process, see for example Wen, Johnson and Dole, J. Phys. Chem. 78, 1798 (1974).

A. OWCZARCZYK

Yes, we know your work about diffusion controlled recombination of radicals in irradiated polyethylene. We tried the test you proposed, but the intercept at $t = 0$ in our case was too small in comparison with the error limit of our ESR measurements.

DIFFERENTIAL THERMAL ANALYIS OF γ-IRRADIATED FROZEN METHYLCYCLOHEXANE

J. Kroh, E. Szajdzińska, W. Świątkowski,
Technical University of Łódź, Institute of Radiation Chemistry, Poland

Calorimetric and thermoanalytical measurements applied in radiation cryochemistry may provide valuable information as to the energetics of primary radical and ionic processes. Decay reactions of the trapped intermediates can be observed by low temperature differential thermal analysis (DTA). This method seems to offer a good completion of ESR, radioluminescence and electrical conductivity measurements.

We applied DTA for examining thermal effects which occur on heating of methylcyclohexane (MCH) matrix, γ-irradiated at 77 K. We used MCH pure grade (Koch-Light Lab. Ltd.) purified by passing through a column (ca 2 m long) of freshly activated silica gel and stored under argon.

We have constructed DTA apparatus which is schematically presented in Fig. 1. It may be operated over the temperature range from 77 to $\sim$ 275 K. Details of construction and experimental procedure were described in /1/.

MCH samples about 1 g in weight were saturated with argon and sealed in thin-wall glass ampoules (o.d. $\simeq$9.8 mm, h $\simeq$30 mm). Benzene was used as a reference material and was placed in the container B before the apparatus was put together as shown in Fig. 1. The apparatus was immersed in a Dewar vessel filled with liquid nitrogen and cooled to 77 K. The frozen sample of MCH was thrown into the container A by sleeve 8 which was then removed. After reaching the pressure $\sim 10^{-2}$ mm Hg in the apparatus the sample was heated at a rate of about 0.7 deg/min.

We examined two kinds of MCH samples: glassy and crystalline. The former were obtained by the direct immersion of the ampoules into liquid nitrogen and the latter – by slow cooling at a rate of about 2,5 deg/min. The samples were γ-irradiated at a dose rate $\sim$1 Mrad/h. The sensitivity of our detection system for measuring differential temperature limited the lowest total doses. For applied γ-doses we did not observe ESR signals of electrons trapped in the glassy matrix because as irradiation proceeds they are removed by reactions with trapped positive charges, radicals and stable radiolysis products. The concentration of free radicals, however, increases as shown in Fig. 2.

DTA results for glassy MCH are presented in Fig. 3. The upper thermogram was obtained for the unirradiated sample. One can see the base line shift due to glass

transition, the exothermic process of rapid crystallization and the endothermic peak for melting of MCH. The additional exothermic process appears as a result of γ-irradiation, it is shown on the lower thermogram in Fig. 3. This process occurs simultaneously with glass transition (extrapolated onset temperature = 95 K, peak temperature = 100 K). Similar results were obtained for crystalline MCH and they are presented in Fig. 4. The unirradiated sample exhibits only an endothermic peak due to the melting process (upper thermogram), while for the irradiated one (the lower thermogram) there is another exothermic peak just before melting (extrapolated onset temperature = 129 K, peak temperature = 141 K).

We determined heats of radiation effects by comparison of their peak areas with those for melting of unirradiated samples. The peak areas were defined according to recommendations of the Committee on Standardization ICTA (see Fig. 3 and Ref. /2/). Dependences of the heat /cal g^{-1}/ vs. γ-dose/Mrad/ are presented in Fig. 5. Plot 1 refers to glassy sample and plot 2 to the crystalline one. For the two kinds of MCH matrix the heat increases linearly with the dose in the examined range but the slope of straight line 2 is twice as small as that of straight line 1.

We suppose that the observed thermal effects are due to reactions of stabilized radiolysis products, which are realised from their traps on heating. Our DTA result prove, in a direct way, that these reactions occur at temperatures close to the phase transition points.

The nature of the reacting species is debatable. If the heat is due to combination and disproportionation reactions between radicals, the exothermicity for glassy matrix is 2.7 kcal mol^{-1} of events for the doses up to $\sim$ 5 Mrad and 7.9 kcal mol^{-1} of events in the dose range from 40 to $\sim$100 Mrad. These values are calculated on the basis of data from Fig. 2 and Fig. 3 (plot 1). On the other hand estimated heat values for reactions of methylcyclohexyl radicals in the gas phase are 64 kcal mol^{-1} for disproportionation and 79 kcal mol^{-1} for combination /5/. Thus, it seems that we did not measure the heats of radical reactions.

Alternatively, the observed DTA peaks may be ascribed to the reactions of ionic species. Temperatures of their appearance are close to those of radiothermoluminescence and thermally stimulated conductivity peaks in glassy MCH /3,4/. Recently Stanley and Willard /6/ determined the value 130 kcal mol^{-1} for the heat of reaction of radical anions with cations in 3-methylpentane. Adapting this value for our DTA results we obtain the values G_1 = 0.135 and G_2 = 0.067 for the formation of ion pairs in glassy and crystalline MCH, respectively. These radiation yields are constant up to $\sim$ 100 Mrads under the condition that no other thermal effects contribute to the observed exothermic DTA peaks.

References

/1/ J. Kroh, E. Szajdzińska, W. Świątkowski, Bull. Acad. Sci. Polon., Ser. Sci. Chim. in press.

/2/ H.G. McAdie, Thermal Analysis, 1, 591 (1971).

/3/ J. Kroh, R. Leszczyński, J. Mayer, Int. J. Radiat. Phys. Chem., 7, 999 (1975).
/4/ E. S. Freeman, D. A. Anderson, J. J. Campisi, J. Phys. Chem. 64, 1727 (1960).
/5/ Estimated from data given by: (a) Poradnik fizykochemiczny, ed. by WNT (Warsaw 1974); (b) Zbiór wielkości fizykochemicznych, ed. by PWN (Warsaw 1974).
/6/ L. H. Stanley, J. E. Willard, J. Chem. Phys., 63, 942 (1975).
/7/ C. Chachaty, J. Chim. Phys., 64, 614 (1967).

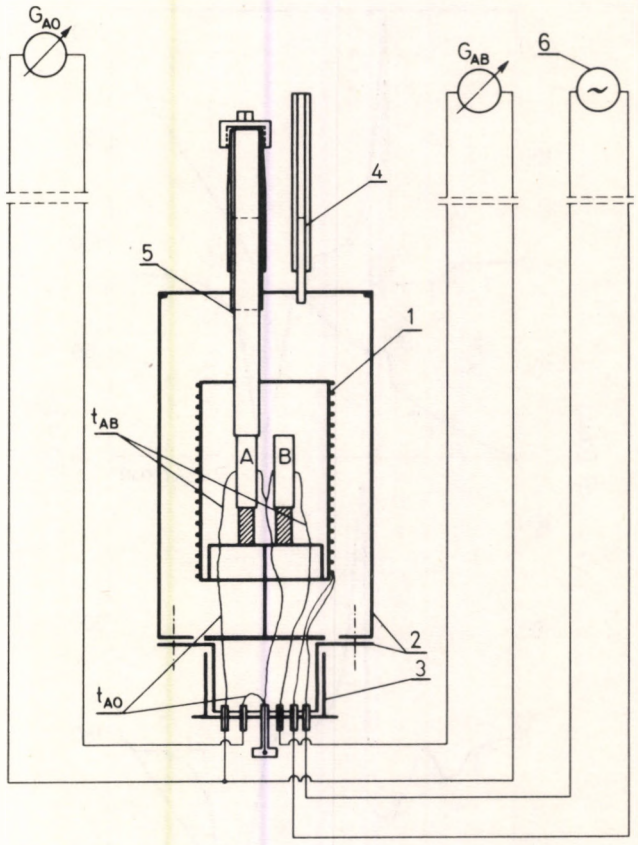

Fig. 1 The scheme of DTA apparatus. A and B – specimen containers made of copper, t_{AB} and t_{AO} – copper/constantan thermocouples, G_{AB} and G_{AO} – mirror galvanometers; 1 – electric heater, 2 – metal enclosure, 3 – Teflon cup, 4 – tube connected with a vacuum pump, 5 – removable metal sleeve, 6 – programmed voltage generator

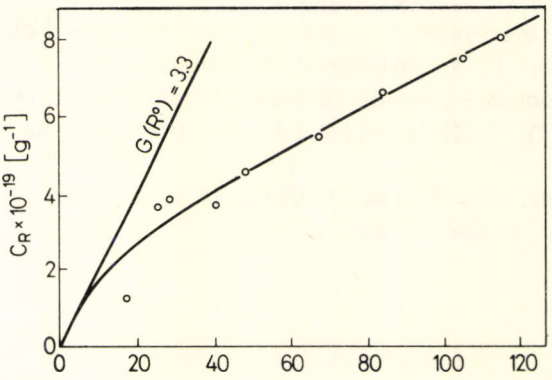
$C_R \times 10^{-19}$ [g^{-1}]
G (P°) = 3.3
D [Mrad]

Fig. 2

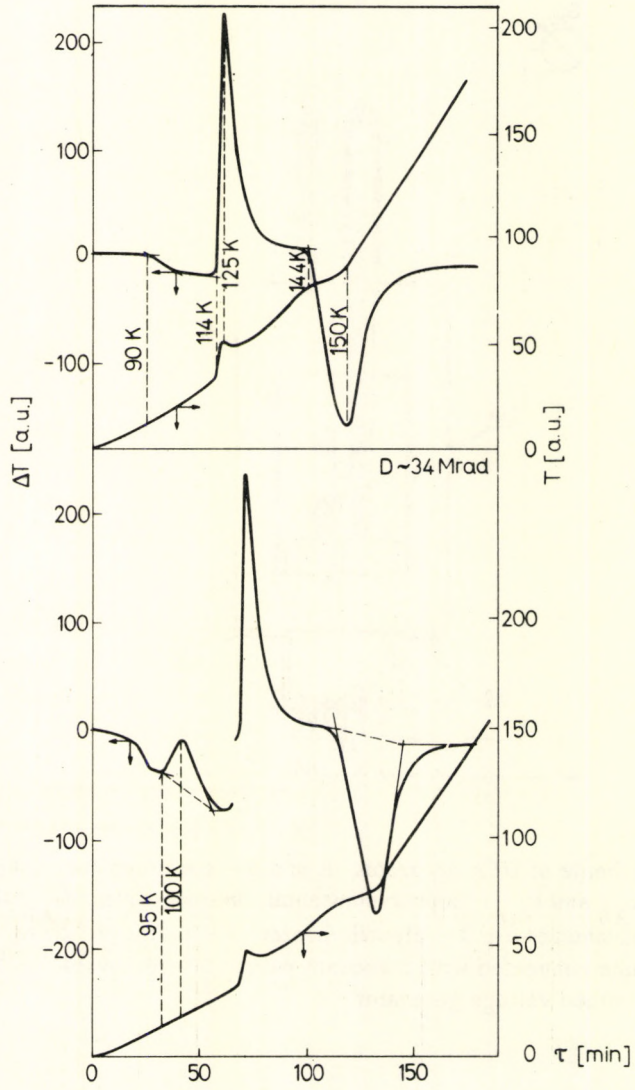
ΔT [a.u.]
T [a.u.]
90 K
114 K
125 K
144 K
150 K
D ~34 Mrad
95 K
100 K
τ [min]

Fig. 3

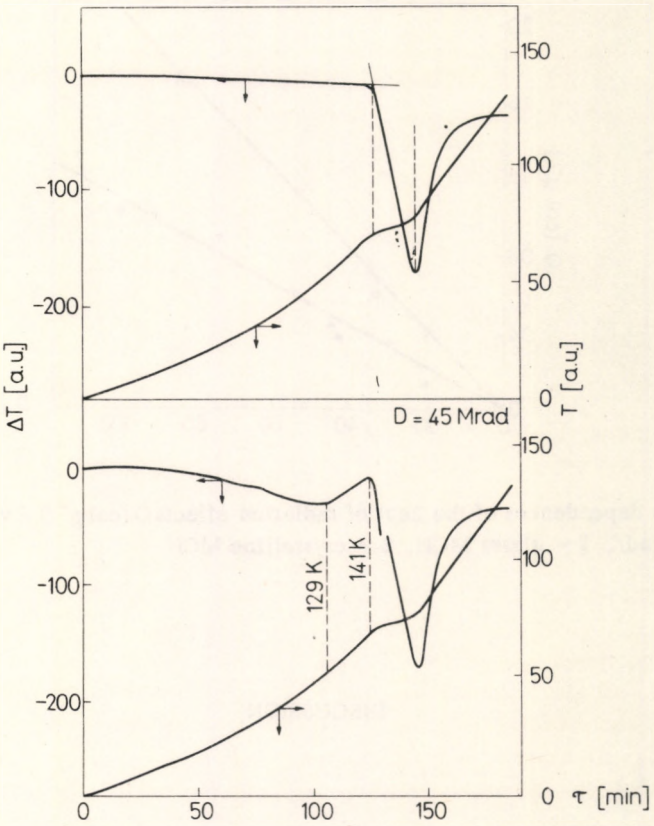

Fig. 4

Fig. 2 The dependence of radical concentration c_R /g^{-1}/vs. γ - dose D /Mrad/ for glassy MCH. The straight line was plotted on the basis of the value G = 3.3 /7/

Fig. 3 Thermoanalytical curves for glass MCH. Left-hand ordinate - differential temperature, ΔT, in arbitrary units, right-hand ordinate - sample temperature, T, in arbitrary units; abscissa - time, τ. in minutes. Upper thermogram - unirradiated sample, lower thermogram - sample γ-irradiated at 77 K with dose ~34 Mrad (4.4 times greater galvanometer sensitivity was used for the initial part of DTA curve than for the second one)

Fig. 4 Thermoanalytical curves for crystalline MCH. Upper thermogram — unirradiated sample, lower thermogram - sample γ-irradiated at 77 K with dose ~45 Mrad. (For details see Fig. 3.)

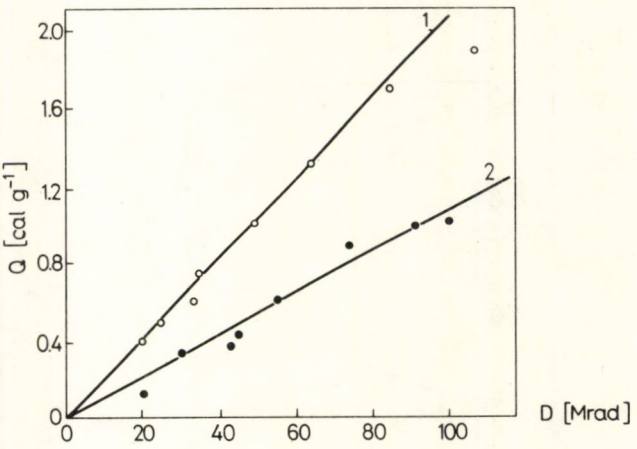

Fig. 5 The dependences of the heat of radiation effects Q (cal g^{-1}) / vs. γ-dose D /Mrad/. 1 – glassy MCH, 2 – crystalline MCH

DISCUSSION

K. KHAIRUTDINOV

How can you explain the small G-value for ion radicals in the methyl cyclohexane matrix?

E. SZAJDZINSKA

I think that these values are reasonable because only a part of primarily formed electrons react with radicals to give radical anions. Our G_1-value may be compared with that reported by Willard for glassy 3-methyl pentane (0.2 for higher doses).

RADIOLYSIS OF ALIPHATIC ALKENE-DIENE MIXTURES

A. Kovács, G. Földiák
Institute of Isotopes of the Hungarian Academy of Sciences, Budapest, Hungary

Introduction

In our institute the investigation of radiation chemistry of different hydrocarbon has been continuing for a long time.

Earlier, by studying the dose-dependence of the radiolytic decomposition of cyclohexene, it was established that the yield of conjugated dienes formed decreased exponentially with increasing dose. This effect was explained by the high reactivity of conjugated dienes /1/. By investigating the radiolysis of n-hexene isomers and cyclohexene in thé presence of radical scavengers it was found that the yield of conjugated dienes formed from the alkenes studied increased exponentially with the increase of concentration of the radical scavengers levelling off above a given concentration /2/. In order to give an adequate interpretation we assumed a competition to capture the existing radicals, i. e. between the radical scavengers added to the alkenes and the conjugated dienes formed. However, the scavenger – owing to its high concentration – captures the radical with a high probability thereby protecting the dienes formed. The consequence of this is that its yield lies very close to the amount originally formed. This effect was not found in the case of isolated dienes formed.

Only a few data are available in the literature for monoalkene–diene systems. The radiolysis of cyclohexene in the presence of 1,3- and 1,4-cyclohexadiene has been investigated by Wakeford and Freeman /3/. The effect of these two dienes on the yield of hydrogen, cyclohexane and dimers was interpreted by the existence of energy transfer and of the scavenging processes of the different radicals. No information is available in the literature concerning the radiolysis of the mixture of aliphatic alkenes and dienes.

Experimental

Hydrocarbons were supplied by Fluka with a purity of 99.97%. The cis-2, trans-4-hexadiene was produced by EGA-Chemie. All hydrocarbons underwent further purification as described elsewhere /2/. The irradiation was carried out at 25°C using a ^{60}Co γ-source with 80 000 Ci nominal activity. The dose rate was 1.4×10^{20} eV g^{-1} h^{-1} (2.2 Mrad h^{-1}) and the integral dose was (8.2 ± 0.1) 10^{20} eV g^{-1} (13.2 ± ± 0.2 Mrad). The products were analysed by gas chromatograph.

Results and discussion

Mixture of 1-hexene and cis-2, trans-4-hexadiene

A study of this system enables us to conclude that it is characteristic that the yield of the most important roducts decreases with the increase of the diene concentration – though to varying extents. For some saturated products it was observed that this drop is very significant in the small concentration range of hexadiene and the curve levels off at higher hexadiene concentration. The yields of CH_4, C_3H_8, C_4H_{10} and C_6H_{14} behave similarly to the one representing the C_2H_6 yield shown in Fig. 1. It was assumed that the intitial decrease is a result of the radical scavenger effect. This observation supports the radical mechanism suggested earlier for the 1-hexene-p-benzoquinone system /4/. At higher diene concentration, though the slope of the yield curve is less steep than at low concentration, there is still a deviation from the straight line representing the linear mixing rule. It seems to us that in this range the role of energy transfer such as excitation energy and charge transfer becomes predominant. The difference between the ionization potential of the components (1-hexene: 9.46 eV and cis-2, trans-4-hexadiene: 8.7 eV) also points to this effect. However, additional experiments are sorely needed to fully clarify these processes.

In the case of hydrogen and some unsaturated products it was observed that their yield decreases monotonously with the increase of conjugated diene (see Fig. 1: C_2H_4, C_3H_6, C_2H_2, $1\text{-}C_4H_8$ and $2\text{-}C_5H_{10}$ behave similarly). Here, it was assumed that the observed drop in the yield was caused mainly by the energy transfer processes while the role of radical capture was of minor importance.

The curve representing the yield of 1,3-butadiene passes through a sharp maximum (Fig. 2). This result is in a good agreement with those obtained by using n-hexene isomers in the presence of radical scavengers, i. e. the observed increase in the yield of 1,3-butadiene in the presence of a small amount of cis-2,trans-4-hexadiene also shows that the conjugated diene added initially to the mixture to be irradiated exerts a "protective" effect on the conjugated diene formed.

Isomerization was also observed in these processes. We succeeded in detecting the formation of trans-2,trans-4-hexadiene and cis-2,cis-4-hexadiene from cis-2, trans-4-hexadiene. It is assumed that the excited dienes of different energies produced in reactions (1) and (2) are isomerized according to 3a and 3b as follows:

$$1\text{-}C_6H_{12}^{*} + \text{cis-2, trans-4-}C_6H_{10} \longrightarrow 1\text{-}C_6H_{12} + \text{cis-2, trans-4-}C_6H_{10}^{*} \qquad (1)$$

$$\text{cis-2, trans-4-}C_6H_{10}^{+} + e^{-} \longrightarrow \text{cis-2, trans-4-}C_6H_{10}^{*} \qquad (2)$$

$$\text{cis-2, trans-4-}C_6H_{10}^{*} \longrightarrow \text{cis-2, cis-4-}C_6H_{10} \qquad (3a)$$

$$\text{cis-2, trans-4-}C_6H_{10}^{*} \longrightarrow \text{trans-2, trans-4-}C_6H_{10} \qquad (3b)$$

In Fig. 3 it is shown that both products follow the same curve as a function of concentration of the diene initially present. However, the amount of cis-2, cis-4--hexadiene is exceeded by the yield of trans-2, trans-4-hexadiene probably because of the higher stability of the trans-isomer /5/. Unfortunately no thermochemical data are available to support this statement.

1-Octene–1, 7-octadiene mixture

The study of dienes containing an isolated double bond show that the yield of a part of the products drops with the increase of diene concentration but generally the decrease is not so significant as was found in the case of the mixture containing conjugated diene (see Fig. 4: CH_4, C_4H_8 and C_8H_{18} behave similarly). Here the interaction may also be interpreted by transfer processes the details of which are not clear – though the difference between the ionization potential of the components is very small (1-octene is 9.52 eV, 1, 7-octadiene is 9.43 eV).

In some cases there is a linear relationship between the yield and the concentration (Fig. 4: 1,4-C_5H_8: the H_2, 1,3-C_4H_6 and 1-C_5H_{10} behave similarly). This linearity can be explained by the lack of interaction. Nevertheless, the existence of processes cancelling each other is not excluded. However, it is remarkable that this linearity is valid not only for the yield of the isolated dienes but also for the conjugated ones formed.

Comparison of the behaviour of isolated and conjugated dienes

Although generally similar, the radiation chemical behaviour of alkene-isolated diene and alkene–conjugated diene mixtures differs in some respects. Thus for instance, the formation of hydrogen is significantly inhibited by conjugated dienes which are known to be excellent radical scavengers. By contrast, the isolated diene has no effect on the hydrogen yield formed from 1-octene (Fig. 5).

A considerable difference was also observed in the behaviour of conjugated dienes formed during the radiolysis. A similar feature can be demonstrated by comparing the behaviour of p-benzoquinone /2/ and conjugated diene during the radiolysis of 1-hexene. In both cases the conjugated dienes formed are "protected" by the additives being in high concentration in the mixture. This is because the latter – due to its high concentration – participates with high probability in the reaction (such as radical capture) responsible for the further decomposition of dienes formed (see Fig. 6). In the case of isolated dienes this competitive effect is not operative since the yields of both isolated and conjugated dienes were proportional to the concentration.

The yield of some products, such as CH_4 (see Fig. 7), is diminished by both types of diene but the extent of the decrease was much more significant for conjugated dienes than for isolated ones. This may be explained by the different reactivities of these dienes for the radicals.

There are, of course, still many details to be clarified in the field of radiolysis of the monoalkene–diene systems and additional work is needed to fully elucidate the reaction mechanism.

References

/1/ A. Kovács, Gy. Cserép, G. Földiák, Radiochem. Radioanal. Letters, 22, 221 (1975).

/2/ A. Kovács, Gy. Cserép, G. Földiák, Acta Chim. (Budapest) in press.

/3/ B. R. Wakeford, G. R. Freeman, J. Phys. Chem. 68, 2992 (1964).

/4/ A. Kovács, Gy. Cserép, G. Földiák, Acta Chim. (Budapest) in press.

/5/ Zs. Horváth, G. Földiák, Acta Chim. (Budapest) 86, 393 (1975).

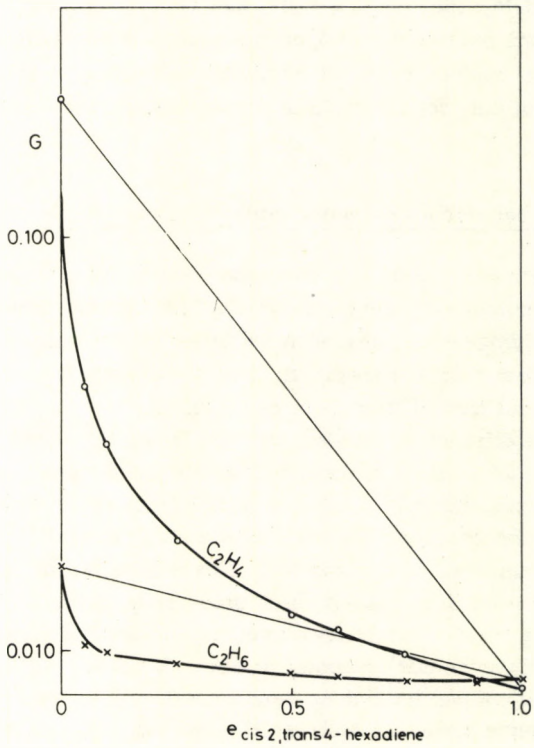

Fig. 1 G-values of ethane and ethylene produced in the radiolysis of 1-hexene-cis-2, trans-4-hexadiene mixtures

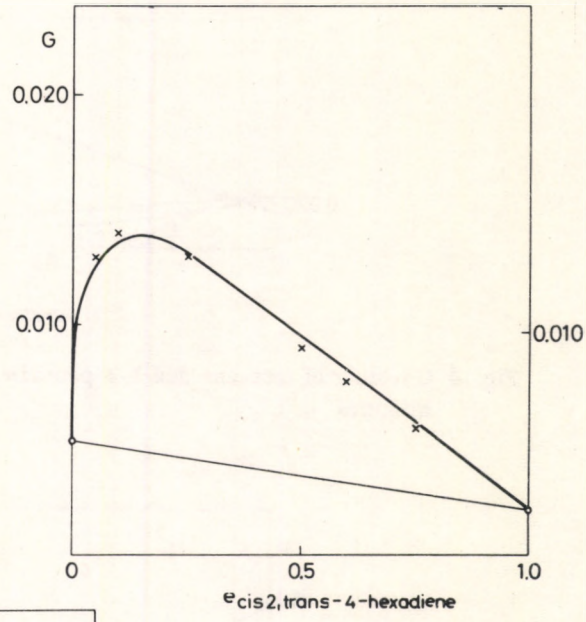

Fig. 2 G-values of 1,3-butadiene from 1-hexene-cis-2, trans-4-hexadiene mixtures

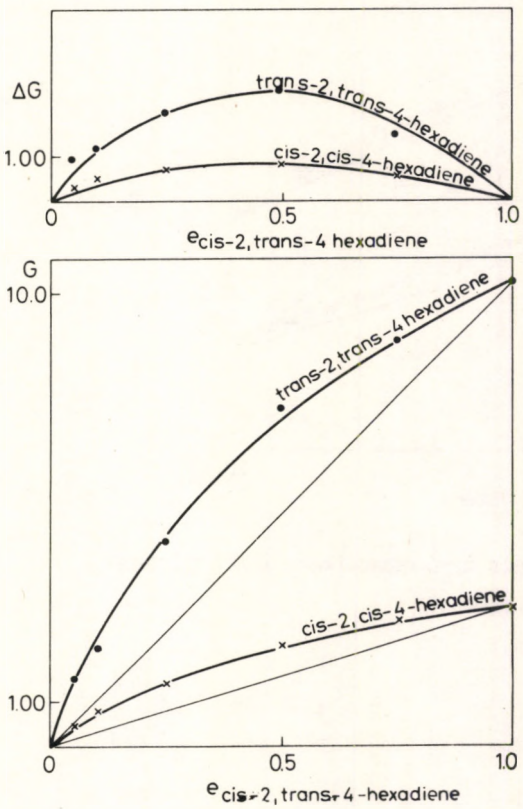

Fig. 3 G-values of trans-2, trans-4-hexadiene and cis-2. cis-4-hexadiene from 1-hexene-cis-2, trans-4-hexadiene mixtures

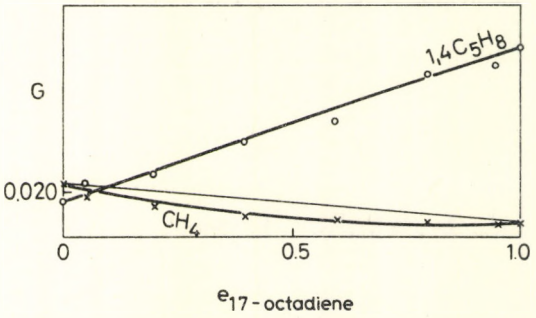

Fig. 4 G-values of methane and 1,4-pentadiene from 1-octene-1,7-octadiene mixtures

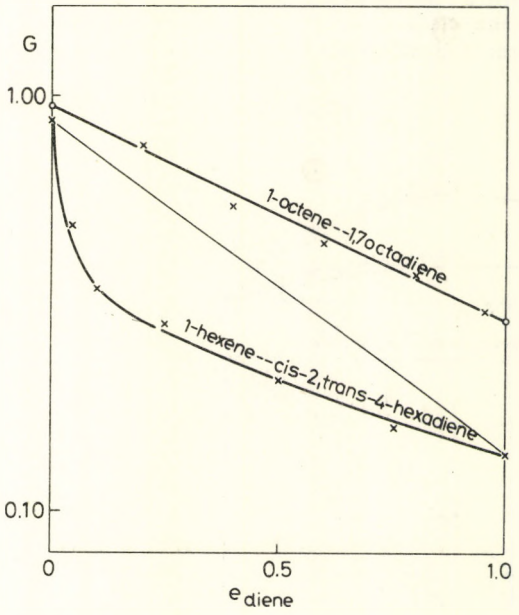

Fig. 5 G-values of hydrogen from monoalkene-diene mixtures

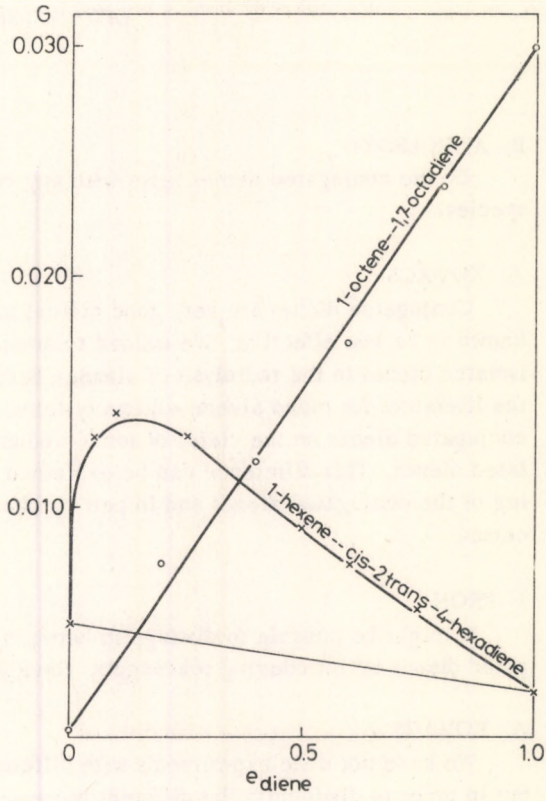

Fig. 6 G-values of 1,3-butadiene from monoalkene – diene mixtures

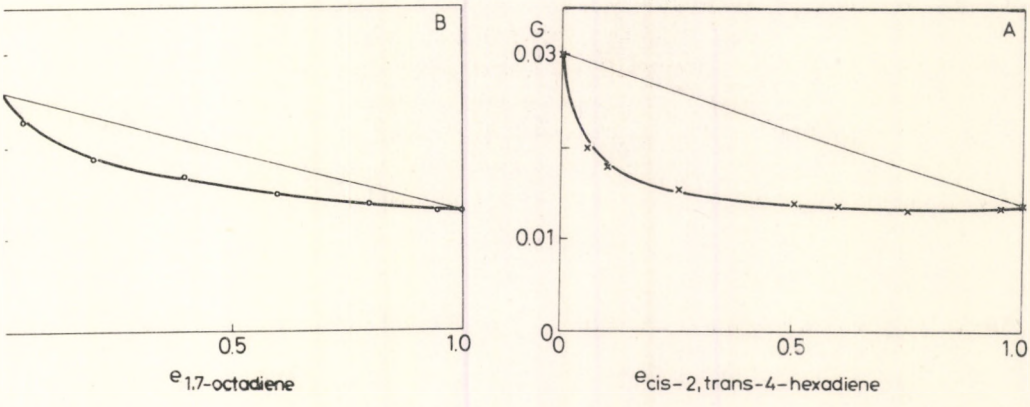

Fig. 7 G-values of methane from 1-hexene-cis-2, trans-4-hexadiene and 1-octene (A) -1,7-octadiene (B) mixtures

R. A. HOLROYD

Do the conjugated dienes react with any other intermediates like radicals or ionic species?

A. KOVÁCS

Conjugated dienes are very good radical scavengers while the isolated ones are known to be less effective. We wanted to compare the effect of the conjugated and isolated dienes in the radiolysis of alkanes, because only a few data are available in the literature for mono alkene – diene systems. We have found that the effect of the conjugated dienes on the yields of some products is more significant than that of isolated dienes. This difference can be explained in part by the effective radical scavenging of the conjugated dienes and in part by charge and excitation energy transfer processes.

J. KROH

It might be possible to distinguish between the behaviour of isolated and conjugated dienes by introducing scavengers. Have you tried any scavenging experiments?

A. KOVÁCS

We have not done experiments with different scavengers in these mixtures yet, but in order to distinguish the different processes, we want to. We have investigated the radiolysis of aliphatic hexene isomers and of cyclohexene in the presence of different scavengers.

RADIOLYSIS OF BENZENE, STYRENE AND THEIR BINARY MIXTURES

J. Kollár, G. Földiák
Institute of Isotopes of the Hungarian Academy of Sciences
Budapest, Hungary

Introduction

Most of the research concerning the radiolysis of aromatic hydrocarbons has dealt with the polymerization and with the degradation of polymers. Comparatively few works have been published in the field of the decomposition of aromatic compounds by irradiation and of these most have reported the radiolysis of benzene and alkyl substituted benzene. The present work aims to obtain more information concerning the radiolytic decomposition of aromatic compounds such as benzene, styrene and their mixtures.

In the study of radiation chemistry of aromatics both with and without side chains, usually the amount of hydrogen of the decomposition products was determined. In the γ-radiolysis of benzene in the liquid phase, different $G(H_2)$ values have been measured in the range of 0.036 to 0.044 molecule/100 eV /1–4/. These very low values were supposedly attributed to the stable delocalized π-electron structure.

It has been shown that the amount of hydrogen formed is virtually unaffected by the change of dose and dose rate and by the addition of radical- and electron-scavengers /5/, though this does depend to a great extent on the type and energy (the LET) of the irradiation /5–8/.

Several interpretations have been developed on the mechanism of the hydrogen formation. Some authors assumed that the first step is the addition of a hydrogen atom to the benzene molecule /6, 9, 10/ with the subsequent hydrogen molecule or polymer being formed in a bimolecular recombination of the radicals formed. The probability of this reaction is not very high because the amount of hydrogen is practically unaffected by iodine scavengers /11/. On the other hand authors such as Cherniak et al. /2/ assumed that the formation of hydrogen can be explained by a reaction between excited benzene and benzene in the ground state:

$$C_6H_6^{*} + C_6H_6 \longrightarrow H_2 + \text{molecule or radical.}$$

The second most important product in benzene radiolysis is acetylene. The acetylene yield determined by different authors varies between 0.007 and 0.026 molecule/100 eV /1, 2, 12/.

The acetylene yield is also independent of the dose and dose rate, and of the type of electron- and radical scavenger but, similarly to the hydrogen formation it is affected by the LET. It has been established that both the acetylene and hydrogen yields increase with increasing value of LET leaving the increment ratio unchanged. From this experimental fact the conclusion can be drawn that both the acetylene and hydrogen were formed from the same precursor /8/. Of the benzene derivatives containing a vinyl-side-chain only styrene has been investigated (and this only from the point of view of polymer formation /13, 14/), but there is no information available concerning the radiation-induced decomposition of the monomer.

In connection with the γ-radiolysis of aromatic-aromatic hydrocarbon mixtures it is worthwhile mentioning the results on the radiolysis of benzene-toluene mixture carried out by Manion and Burton /12/. As far as we know no data have been published about the radiation chemistry of the benzene-styrene mixture.

Experimental

Solutions for the experiments were prepared in an ampoule of 0.4 cm^3 volume. 0.2–0.3 g of benzene and styrene as well as their mixture in different ratios were used. Before irradiation the samples were degassed in vacuo, they were dried by using a sodium mirror and they were then sealed under vacuo. Samples were irradiated at 25°C in ^{60}Co-γ-source of nominal activity of 80 000 Ci with a dose rate of $1.5 \cdot 10^{20}$ eV g^{-1} h^{-1} (2.4 Mrad h^{-1}). The amount of dose measured by chloro-benzene dosimeter was $(2.4 \pm 0.1) \times 10^{21}$ eV g^{-1} (38.5 ± 1.6 Mrad). Of the products of radiolysis, C_1–C_4 hydrocarbons and hydrogen were analysed by gas chromatography. For the determination of hydrogen a 1.5 m column filled with silicagel with argon carrier gas and TC detector were used. For the hydrocarbons a column filled with alumina argon carrier gas and FJD detector were utilized.

Results and discussion

In Table 1 the result of radiolysis of pure benzene and styrene is summarized. The yields of hydrogen and hydrocarbons were determined from the data of 9–10 parallel experiments.

The hydrogen yield obtained from the result of benzene radiolysis is 0.039 molecule/100 eV as shown in Table 1 which is in a good agreement with the literature data. The hydrogen yield for styrene is about 25% smaller than for benzene: 0.030 molecule/100 eV. No comparison is possible since no data appear to be available in the literature. The hydrogen yield which is smaller than that of benzene cannot be satisfactorily explained. This may be due to the hyperconjugation of the benzene ring with the vinyl side chain and thus the physical interaction between the substance and the radiation can be diminished. In addition, this effect may be a consequence

Table 1

Products in γ-radiolysis of pure liquid benzene and styrene

Products	Benzene	Styrene
	G (molecule/100 eV)	
H_2	$(3.92 \pm 0.31) \cdot 10^{-2}$	$(3.03 \pm 0.41) \cdot 10^{-2}$
CH_4	$(\sim 1. 10^{-4}) < 0.001$	$(\sim 6 \cdot 10^{-4}) < 0.001$
C_2H_6	trace	trace
C_2H_4	$(\sim 3 \cdot 10^{-4}) < 0.001$	$(\sim 4 \cdot 10^{-4}) < 0.001$
C_2H_2	$(3.1 \pm 0.5) \cdot 10^{-2}$	$(0.5 \pm 0.2) \cdot 10^{-2}$
1-butane	$(4.5 \pm 1.6) \cdot 10^{-3}$	$(1.8 \pm 1.3) \cdot 10^{-3}$
1,3-butadiene	$(2.4 \pm 0.9) \cdot 10^{-3}$	$(1.0 \pm 0.7) \cdot 10^{-3}$

of a partial polymerization which occurs under irradiation or of a highly probable hydrogen-capture process. This latter may be proved by the effect of 0.1 M benzoquinone which diminishes the hydrogen yield to a value of $1.4 \cdot 10^{-2}$ molecule/100 eV.

The other main gaseous product of benzene radiolysis is acetylene with a yield in the range 0.026 – 0.036 molecule/100 eV. This value is close to those found in the literature ($G(C_2H_2) = 0.022$). The acetylene yield in the radiolysis of styrene is about 0.003 – 0.007 molecule/100 eV. There are many reasons why the acetylene yield is smaller than for benzene, among these the smaller energy transfer, polymerization processes, and the stability of the bond between the ethylene side-chain and the benzene ring, can be mentioned.

As is shown in Table 1, the butadiene and 1-butene are present at the limit of the gas chromatographic detection and the other components are only to be found in trace amounts. Since only hydrogen and acetylene among the radiolysis products can be analysed with a reasonable accuracy, only the amount of these two products is determined in the radiolysis of the mixture.

Figure 1 (line A) shows the hydrogen yield versus composition of the benzene-styrene mixture. It is characteristic that the curve passes through a minimum as a function of the concentration of styrene. The experimental error (Table 2), however, is too large to enable any unambiguous conclusion for this minimum to be drawn.

However, any of these relationships allows us to establish that between the components of the mixture it is not only one type of interaction that is operative. Among the alternatives the most probable is an energy transfer from benzene to styrene (IP for benzene is 9.24 eV /15/, IP for styrene is 8.47 eV /15/), but chemical processes may also take place.

Table 2

Hydrogen-yields in γ-radiolysis of liquid benzene and styrene mixture

Electron fraction of styrene	$G(H_2) \pm \sigma$ molecule/100 eV	Number of parallel experiments
0.00	$(3.92 \pm 0.31) \cdot 10^{-2}$	10
0.50	$(2.68 \pm 0.18) \cdot 10^{-2}$	4
0.60	$(2.55 \pm 0.21) \cdot 10^{-2}$	4
0.70	$(2.60 \pm 0.30) \cdot 10^{-2}$	4
1.00	$(3.03 \pm 0.41) \cdot 10^{-2}$	10

The hydrogen yield in the presence of 1% benzoquinone is represented by a straight line also subject to a considerable experimental error as shown in Fig. 1 (line B)*. As a possible interpretation we suggest that benzene itself is able to capture the hydrogen atoms formed and this effect can be detected together with that due to energy transfer.

In Fig. 2 the amount of acetylene formed is presented versus the concentration of the mixture. It seems that the acetylene yield is always smaller than the one we can expect on the basis of the linear mixing rule. This deviation may point to the effect of an energy transfer process from benzene to styrene. The character of the curve does not allow any other conclusion to be drawn.

Conclusions

To sum up, it has been established that in the γ-radiolysis of the mixture of benzene and styrene in the liquid phase there is an interaction between the individual components. The acetylene yield can be fully explained in the whole concentration range simply by the energy transfer while the concentration dependence of hydrogen points to a more complicated interaction, i. e. besides the energy transfer the radical scavenger effect of benzene cannot be ignored.

* The $G(H_2)$ value of pure benzene is unaffected but the hydrogen yield of styrene is decreased to the half of the original value

References

/ 1/ S. Gordon. A. R. von Dyken, T. F. Doumani, J. Phys. Chem. 62, 20 (1958).
/ 2/ G. A. Cherniak, E. Collinson, F. S. Dainton, Trans. Faraday Soc. 60, 1408 (1964)
/ 3/ B. Zimmerei, T. Gaumann, Helv. Chim. Acta 52, 764 (1969).
/ 4/ W. van Dusen, N. H. Hamill, J. Amer. Chem. Soc. 84, 3648 (1962).
/ 5/ W. G. Burns, Trans. Faraday Soc. 58, 961 (1962).
/ 6/ W. G. Burns, R. Barker, Progress in Reaction Kinetics, Pergamon Press, London 1965, Vol. 3.
/ 7/ W. G. Burns, C. R. V. Reed, Trans, Faraday Soc. 59, 101 (1963).
/ 8/ T. Gaumann, R. H. Schuler, J. Phys. Chem. 65, 703 (1961).
/ 9/ G. E. Gibson, N. Blake, M. Kalm, J. Chem. Phys. 21, 1000 (1953).
/10/ W. M. Patrick, M. Burton, J. Amer. Chem. Soc. 76, 2626 (1954).
/11/ R. H. Schuler, J. Phys. Chem. 60, 381 (1956).
/12/ J. P. Manion, M. Burton, J. Phys. Chem. 56, 560 (1952).
/13/ A. Chapiro, V. Stanett, J. Chem. Phys. 56, 830 (1959).
/14/ A. Chapiro, Radiation Chemistry of Polymeric Systems, Interscience, New York, 1962.
/15/ W. J. von Wedenejew, L. W. Gurwitsch, W. H. Kondratjev, W. A. Medwedew, Energien chemischer Bindungen, Ionizations-potentiale und Elektronen--Affinitäten, Leipzig, 1971.
/16/ M. Burton, S. Lipsky, J. Phys. Chem. 61, 1461 (1957).

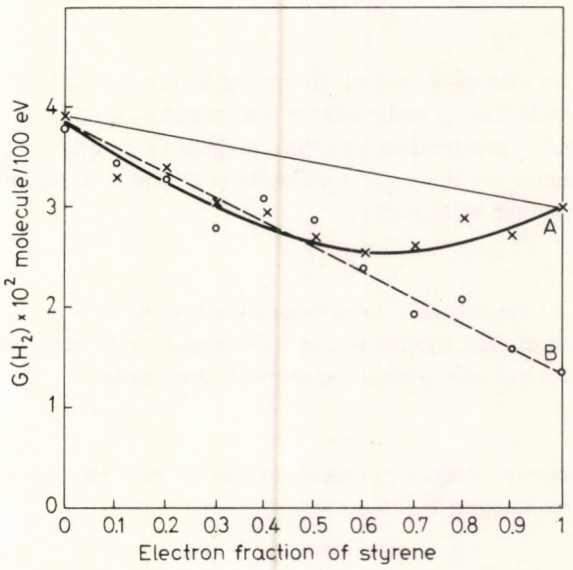

Fig. 1 $G(H_2)$ values in the radiolysis of benzene–styrene mixtures. A/x/: H_2-yields in the radiolysis of benzene-styrene mixture, B/o/: H_2-yields in the presence of 1% benzoquinone

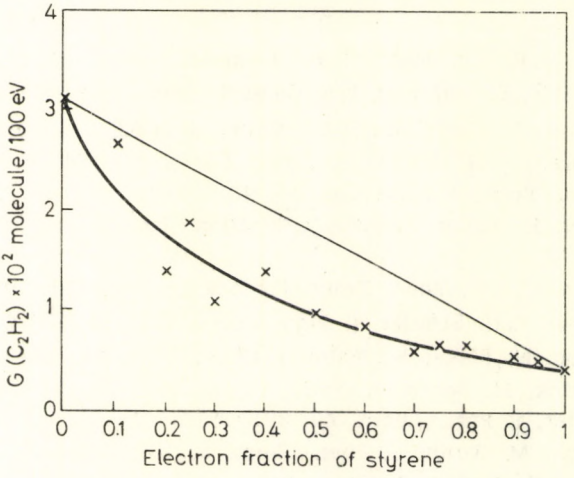

Fig. 2 C_2H_2-yields in the radiolysis of benzene–styrene mixture

DISCUSSION

A. CHARLESBY

This paper can also give useful information on the first step of polymerization of styrene. We would like to know what is the initiating species in the reaction. If it is H, for example, polymerization would perhaps be greatly reduced in the presence of benzene. Are there great differences in polymerization of styrene in the absence or presence of benzene?

J. KOLLÁR

On the basis of our previous experiments there were no great differences between polymer formation in pure styrene and in 50% mixture of styrene and benzene. In order to clarify this problem further experiments are needed.

M. ROMANCEV

Have you measured polymer products in this system? Have you studied the influence of other scavengers to $G(H_2)$?

J. KOLLÁR

We have not measured products yet, just C_1–C_4 products and hydrogen.

We have investigated only the influence of p-benzoquinone on the hydrogen yield in the mixture of benzene and styrene.

STRUCTURAL EFFECTS IN THE RADIOLYSIS OF SATURATED HYDROCARBONS

J. Kroh, A. Rucinska-Starosta, S. Karolczak
Institute of Applied Radiation Chemistry, Technical University (Politechnika)
Lodz, Poland

Introduction

Since the beginning of radiation chemistry of organic compounds much attention has been paid to establishing a correlation between the structure of molecules, their physical properties and the efficiency of radiation processes. The vast majority of data as to such correlations are available for the liquid phase.

For hydrocarbons one should point out the papers of Freeman and co-workers /1/ who determined the dependence of the yield of free ions G_{fi} and also of the most probable penetration range of electrons on the geometrical shape of molecule and related anisotropy of polarizability.

Földiák and György /2/ investigated the radiation chemical decomposition of liquid C_6 hydrocarbons and their mixtures. As to the solid state very few data are available and even these concern mainly ESR measurements for various normal and branched hydrocarbons /3/. In addition to ESR optical methods can also give useful information for solid irradiated hydrocarbons. They are commonly used for glassy samples and very rarely for polycrystalline ones. Other measurements, like isotope gas analysis, performed without melting seem to be applied in unique cases /4/.

Among emission methods radiothermoluminescence (RTL) and isothermal luminescence (ITL) are most useful, but the list of papers describing the application of these techniques and especially ITL for pure hydrocarbons seems to be surprisingly short (5–10).

Experimental technique

After degassing by the freeze-thaw technique the samples in high purity quartz (Spectrosil A) cylindrical vessels were sealed off under vacuum, placed in liquid nitrogen in a Dewar vessel and irradiated with Co^{60} γ-rays at 77 K. The dose rate was kept constant at 0.88 Mrad per hour and doses absorbed by samples varied from 0.22 to 1.76 Mrad. After irradiation, samples were transferred to a cryostat connected with scanning (Zeiss) SPM-1 monochromator via a light guide system. The intensity of luminescence was measured using EMI 9558 QB photomultiplier followed by electronic amplifier and recorder.

Hexane and dimethylbutane (Fluka AG and Koch-Light Ltd) were treated with conc. H_2SO_4, washed, dried and finally passed through silica gel. Neopentane (Fluka AG) was purified by trap to trap condensation on 5A molecular sieves. Other hydrocarbons (Chemical Samples Co.) of purity > 99% were used as received.

A Perkin-Elmer gas chromatograph model 451 was used for the determination of nitrogen and hydrogen. A 2 m long column filled with molecular sieves 5A at 40° C was applied in all analyses.

Results

Spectral distribution of ITL

All samples were polycrystalline, except 2,3 dimethylbutane which formed poor, cracked glass. Hydrocarbons investigated exhibited weak luminescence in the visible range. No UV luminescence was observed probably due to its even lower intensity. λ_{max} values were determined with an accuracy of $\pm$ 15 nm. The spectral distributions of ITL for all hydrocarbons are shown in Fig. 1.

It is seen from Fig. 1 that emission spectra are broad and exhibit two well resolved peaks which are denoted as M and P. The heights of these peaks vary for different hydrocarbons and are strongly affected by the dose absorbed. The influence of dose on the ITL spectrum is shown in Fig. 2 for neopentane and 2, 2, 5, 5-tetramethylhexane.

Kinetics of luminescence decay

The measurements of ITL intensity were started 5 minutes after the end of irradiation and then carried out for the next 30 min. At the beginning of observation I_o was at least by one order of magnitude higher than the noise level but at the end of observation this ratio was close to $\sim$ 2

The linear dependence can be obtained by plotting I_o/I_t vs $(t-t_o)$, according to the Bagdasar'yan equation /11/.

$$I_o/I_t = 1 + \beta(t-t_o) \qquad (1)$$

where I_t, I_o denote intensities at time t and t_o = 5 minutes respectively. The typical intensity against time dependence is shown in Fig. 3, where Bagdasar'yan and first order kinetics plots are presented for 2,2,3,3 tetramethylbutane. From the slope in Fig. 3 Bagdasar'yan constant β, was calculated for all investigated hydrocarbons. The values of β are listed in Table 1.

Determination of the yield of free ions G_{fi}.

The yields of free ions found by us for liquid phase are shown in Table 1. G_{fi} values were determined by using Schuler's equation /12/ for N_2O which was used as electron scavenger.

Table 1

Summary of results for all hydrocarbons investigated. Intensities of luminescence, I_o – intensity of ITL at 5 minutes after the irradiation, I_{tot} – integrated intensity of ITL over the full spectrum, β – the constant in equation (I), G_{fi} – free ions yield, r = bd penetration range of secondary electrons times liquid density

Hydrocarbon	I_o	I_{tot}	$\beta(min^{-1})$	G_{fi}	$r(10^{-8}\ qcm^{-2})$	Ref.
Neopentane	5.39	60.48	0.144	1.090	128.0	A
2,2 DMB	219.00	2888.00	0.094	0.420	59.5	B
2,3 DMB	21.90	285.00	0.134	0.225	49.4	B
n-Hexane	13.85	191.50	0.103	0.100	44.2	B
2,2,3,3 TMB	9.69	130.03	0.112	0.800*	85.0	A
2,2,3,3 TMP	11.80	149.80	0.120	0.420	74.0	A
2,2,4,4 TMP	11.50	133.30	0.150	0.830	117.0	A
3,3 DEP	5.70	52.82	0.182	0.440	–	B
2,2,5,5 TMH	16.60	178.10	0.104	0.670	102.0	B

A – J.P. Dodelet, G.R. Freeman, Can. J. Chem. 50, 2667 (1972).

B – This work

Discussion and conclusions

In contrast to the glassy samples where bulk luminescence is measured, for polycrystalline opaque medium emission is observed only from a relatively thin layer. One can argue that because of ambiguous crystalline structure of investigated compounds no meaningful conclusions can be drawn, when I_o and $I_{tot} = \int I \, dT$ are compared for various hydrocarbons, unless it is possible to introduce corrections for self-absorption, multiscattering, etc. – as proposed by Zagórski and Zimek. /13/.

Our earlier experiments show, however, that "active" layers are surprisingly similar for many hydrocarbons and thus all the interfering phenomena might be quite comparable. The crystal structure of samples should not affect spectral distribution and the kinetic parameter β related to the rate constant of luminescence decay.

The values β shown in Table 1 are rather similar for all hydrocarbons and close to values found for glassy systems /14/.

It is known that Bagdasar'yans equation (1) describe the tunnelling process and is commonly used for glasses. This equation is also fulfilled very satisfactorily for all investigated polycrystalline hydrocarbons. We believe that this observations might support the occasionally expressed opinion that micro glassy regions are responsible for trapping ITL precursors. Similar values of β for hydrocarbons of rather different geometrical structure might indicate that all these matrices exhibit the same or very similar trapping and releasing properties for charged species believed to be ITL precursors.

Spectral distribution measurements show that in irradiated hydrocarbons there are at least two species responsible for luminescence at different wavelength range. We believe that these species represent matrix cation (M^+) and product cation, probably radical cations (R^+).

A simple reaction scheme might be used for the purpose of the present discussion on the origin of luminescence:

$$RH \rightsquigarrow \begin{matrix} \bar{e}, \; M^+ = (RH^+, \; RH_2^+, \; S^+), \; R, P \text{ (stable product)} \\ \downarrow \\ \bar{e}_t \end{matrix} \qquad (1)$$

$$\bar{e}_t + M^+ \longrightarrow M + h\nu_M \qquad (2)$$

$$R + M^+ \longrightarrow R^+ + M \qquad (3)$$

$$R^+ + \bar{e}_t \longrightarrow P + h\nu_P \qquad (4)$$

Our results do not add any information on the origin of matrix luminescence for which λ_M varies from 390–490 nm. So far no one except Lewis et al. /15/ has been able

to observe low-lying excited states in pure hydrocarbons. The other peak, denoted as P which is situated at higher wavelength with λ_P in the range 600–675 nm is growing quickly with dose and it is quite reasonable to assume that it is connected with free radicals accumulating in the matrix.

Charge transfer (3) is allowed because the ionization potential for radicals IP_R is < than IP_{RH}. It was reported /16/ that alkyl radicals are charge trapping species in γ -irradiated alkanes. It is obvious that because of different IP values of RH and R, the energy released in process (2) is higher compared with the recombination energy for radical cation reaction (4). It is also interesting to notice that peak P decays faster than M, i.e. $\beta_P > \beta_M$ which corresponds to relative decay rates for biphenyl phosphorescence and fluorescence in 3 MP glasses /14/.

In spite of the reservations, analysis of I_o and I_{tot} for various compounds leads to some conclusions on the influence of structure of hydrocarbons on the ITL. If we assume that all the matrices are similar then we can discuss the differences in I_o and I_{tot} as resulting from different quantum efficiences Φ for recombination and compare our results with those presented by Rothman et al /17/, for UV induced luminescence.

Some consistent qualitative observations are as follows: luminescence of n-hexane is stronger as compared with most of the branched hydrocarbons. This conclusion seems to be more justifiable if we reject 2,3 DMB which forms glass and 2,2 DMB which exhibits anomalously high ITL. Introducing CH_3 group into molecule shifts λ_{max} of ITL toward longer wavelength as in Rothman's paper. Rothman et al. have not investigated in detail hydrocarbons with quaternal carbon atoms due to extremely low quantum efficiencies for these compounds. From our work it seems, however, that the presence of C^{IV} atoms does not drastically change the ITL level.

It is interesting to notice that the total luminescence I_{tot} as well I_o is inversely proportional to G_{fi} in liquid phase. It is clearly seen for sequence neopentane, 2,2,4,4 tetramethylpentane, 2,2,5,5 tetramethylhexane and 2,3 dimethylbutane.

In spite of these regularities we believe that in the solid state the shape of molecules: sphericity, anisotropy of polarizability, are of minor importance compared with the mutual distribution of trapped charged species and trap depths – at least for ITL process. The determination of free ion yield for 3,3 diethylpentane, i.e. for the ethyl analogue of methane shows that this molecule does not exhibit high sphericity like neopentane: for $C(CH_3)_4$ and $C(C_2H_5)_4$ the G_{fi} values for which are 1.09 and 0.44, respectively.

References

/ 1/ J.P. Dodelet, G.R. Freeman, Can. J. Chem. 50, 2667 (1972), and references cited therein.

/ 2/ G. Földiák, I. György, Acta Chim. (Budapest) 80, 385 (1974).

/ 3/ E.J. Henley, E.R. Johnson "The chemistry and physics of high energy reactions" pp. 297–333, Washington D.C., Univ. Press (1969).

/ 4/ P.J. Dyne, J. Denhartog, Can. J. Chem. 44, 461 (1966).
/ 5/ M. Burton, M. Dillon, R. Rein, J. Chem. Phys. 41, 2228 (1964).
/ 6/ F. Kieffer, M. Magat "Actions chimiques biologiques des radiations Vol. 14, ed. M. Haissinsky, Masson, Paris, 1970, p. 135.
/ 7/ M. Burton, K. Funabashi, Mol. Cryst. Liquid Cryst. 9, 153 (1969)
/ 8/ P.B. Merkel, W. H. Hamill, J. Chem. Phys 53, 3414 (1970).
/ 9/ K. Funabashi, C. Herbert, J. L. Magee, J. Phys. Chem. 75, 3221 (1971).
/10/ T. Sawai, J. Nuclear Sci. Techn. 8, 431 (1971).
/11/ Kh. Bagdasar'yan, R.J. Milutinskaya, Yu. V. Kovalev, Khim. Vysok. Energii, 1, 127, (1967).
/12/ S.J. Rzad, R.H. Schuler, J. Phys. Chem. 72, 228 (1968).
/13/ Z.P. Zagórski, Z. Zimek, Int. J. Radiat. Phys. Chem. 4, 65 (1972).
/14/ J. Mayer, M. Szadkowska, J. Kroh, in press.
/15/ D. Lewis P.B. Merkel, W.H. Hamill, J. Chem. Phys. 53, 2750 (1970).
/16/ F. Nauwelaerts, J. Ceulemans, Chem. Phys. Lett. 38, 354 (1976).
/17/ W. Rothman, F. Hirayama, S. Lipsky, J. Chem. Phys. 58, 1300, (1973).

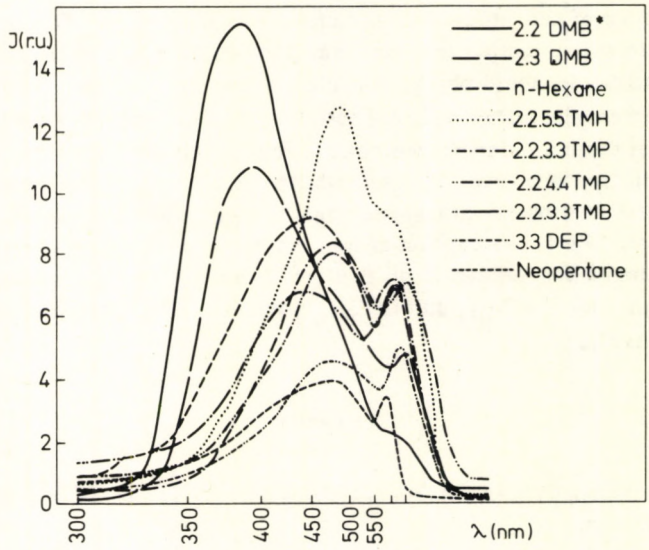

Fig. 1 The spectral distribution of ITL for all hydrocarbons investigated. The peak of 2.2 DMB is detected on sensitivity 10 times lower than the other peaks

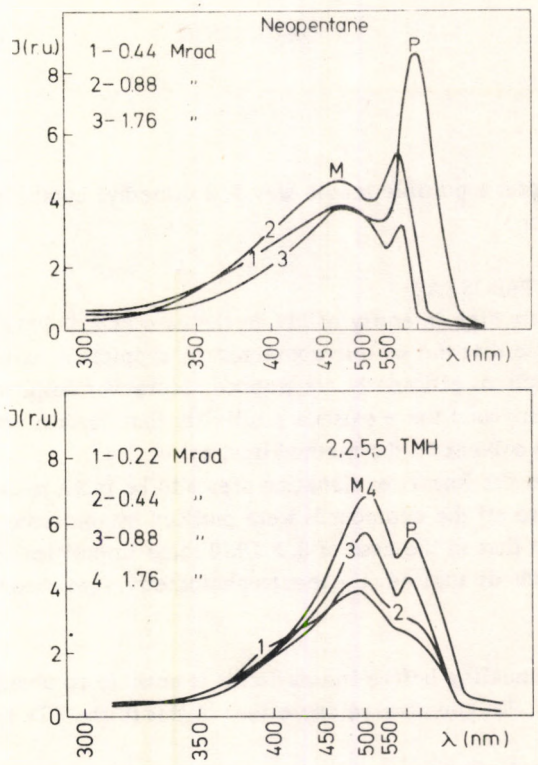

Fig. 2 The influence of dose on spectral distribution of ITL for neopentane and 2, 2, 5, 5, tetramethylhexane

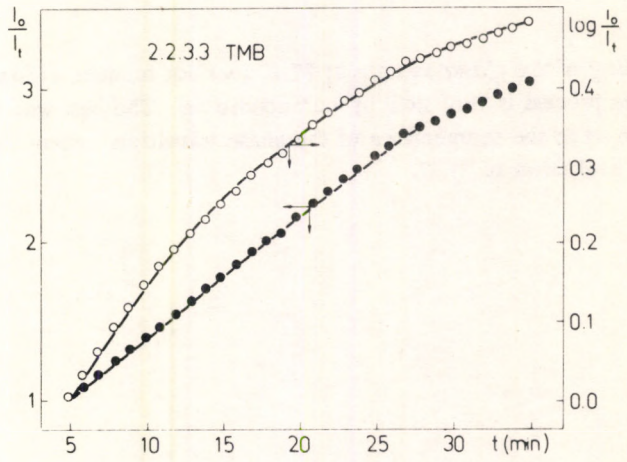

Fig. 3 The dependence of I_o/I_t and lg (I_o/I_t) as a function of time after the irradiation for 2, 2, 3, 3 TMB

Z. PAÁL

Can you suggest a possible reason why 2, 2 dimethyl butane shows anomalously high light emission?

A. RUCINSKA-STAROSTA

The anomalous high intensity of ITL in the case of 2, 2 DMB is difficult to explain. It is possible that the sample contained an appreciable amount of glassy micro-regions where electrons efficiently are trapped. Moreover despite the careful purification of the compound there exists a possibility that certain impurities were not removed from the solvent by the method used by us.

In our opinion the former explanation seems to be more reasonable than the latter one, because all the compounds were purified by the same method and it is unlikely to expect that in the case of 2, 2 DMB some impurities were not detected by the analytical methods applied (UV spectrophotometry, gas chromatography).

B. TILQUIN

By thermal annealing before irradiation it is possible to obtain a 2, 3 DM polycrystalline matrix. Do you observe any effect of this in the RTL spectrum?

A. RUCINSKA-STAROSTA

I think it is possible but I did not do it. All my samples were prepared in the same way, by rapid cooling to 77 K.

J. MAYER

Annealing of the glassy sample at 77 K does not produce crystalline structure because the process is very slow in such conditions. The best way to do it is to warm the sample up to the temperature of the phase transition, where crystallization is fast, then cool down to 77 K.

EFFECT OF MOLECULAR STRUCTURE ON THE RADIOLYSIS OF ALKENES

Gy. Cserép, G. Földiák

Institute of Isotopes of the Hungarian Academy of Sciences,
H–1525 Budapest, Hungary

Introduction

In our earlier works /1–3/ it was established that in the radiolysis of some alkenes the hydrogen yield is controlled mainly by the number and the order of C–H bonds in allylic position. On the basis of the experiments carried out by using branchless alkenes or the ones with one methyl group, it was established that this phenomenon is in correlation with the difference between the dissociation energy of C–H bonds in the molecule, i.e. there exists an inverse relationship between the specific hydrogen yield [$G(H_2)$/H increments] (Table 1) and the dissociation energies of the respective bonds. In addition, the overall $G(H_2)$ values calculated from the hydrogen increments yield are in agreement with the data measured for a number of straight chain alkenes but significant deviation can be found using cyclic hydrocarbons. The deviation depends on the carbon number of the cyclic alkene and thus on the strain energy of the ring (Figs 1 and 2). By considering the cyclic structure it is most likely that this deviation is due to the hindrance of the formation of the favourable steric position necessary for the allylic interaction of the C–H in β-position.

In earlier experiments two important data, the results of the irradiation of cyclononene and cyclopentadecene, were missing. Our recent experimental results

Table 1

Specific hydrogen yields $G(H_2)$ increments of aliphatic alkenes

$G(H_2)$/H primary allylic	0.172 ± 0.009
$G(H_2)$/H secondary allylic	0.359 ± 0.016
$G(H_2)$/H tertiary allylic	0.520 ± 0.047
$G(H_2)$/H primary non allylic	0.011 ± 0.005
$G(H_2)$/H secondary non allylic	0.026 ± 0.007
$G(H_2)$/H tertiary non allylic	0.210 ± 0.050

with these two compounds shown in Figs 1 and 2 (open triangles) support our idea described above.

As far as the steric hindrance influencing the hydrogen yield is concerned we may assume that the phenomenon found for cyclic hydrocarbons is also operative in the case of some branched chain alkenes. In this latter case a decrease in hydrogen yield is to be expected if the free rotation of carbon atom – being in the α -position with respect to the π -bond – is hindered by substitution If this assumption is true $G(H_2)$ values should be smaller than those calculated from the increment-like specific hydrogen yields mentioned above. In order to prove our idea multi-methyl substituted branched alkenes are investigated in which the effect of this phenomenon is likely to occur.

Experimental

The experimental method has been described elsewhere /4/. Alkenes, except cyclononene and cyclopentadecene, were supplied by Fluka with a purity of 98–99%. Only cyclononene and cyclopentadecene were synthesized in our institute. Before irradiation they were further purified. Irradiation was carried out at 18–20 °C using a ^{60}Co γ -source with a dose rate of 1.1×10^{20} eV $g^{-1} h^{-1}$ (1.8 Mrad h^{-1}) in the dose range $3.1-6.2 \times 10^{20}$ eV g^{-1} (5–10 Mrad). Cyclopentadecene was irradiated at 35°C in order to keep it in liquid form. The products formed were analysed volumetrically and gas chromatographically.

Results and discussion

Experimental results are shown in Table 2. In column 3, the $G(H_2)$ values calculated on the basis of specific hydrogen yield from earlier results are presented: the specific hydrogen yields [$G(H_2)$/H were obtained from the experiments carried out by using straight chain alkenes with no significant steric effect. In these molecules the direction of C–H bonds in the β-position is such that it can occupy a perpendicular position to the plane of the double bond and this is a necessary condition for the optimum allylic interaction.

By comparing the experimental and calculated data it was established that significant deviation can be found between the measured and calculated hydrogen yield $\Delta G(H_2)$ for many branched chain alkanes. In some cases, however, the measured and calculated data are in good agreement. On the basis of the molecule-model of the individual compounds, a correlation can be found between the decrement of hydrogen yield and the steric hindrance, i.e. the more the deviation of the C–H bond direction from the position most favourable for the allyl interaction, the less the hydrogen yield.

Let us consider the model of 2,3-dimethyl-2-butene (Fig. 3.) The free rotation of methyl groups on the same side of the olefinic bond is hindered by each other,

Table 2

Hydrogen and methane yields of aliphatic alkenes

	$G(H_2)$		$\Delta G(H_2)$	$G(CH_4)$
	Measured	Calculated		
-Methyl-1-butene	0.58/5/	0.61 ± 0.09	-0.03	0.07/5/
3-Dimethyl-1-butene	0.37	0.12 ± 0.06	+0.25	0.24
3,3-Trimethyl-1-butene	0.62	0.63 ± 0.08	-0.01	0.25
-Methyl-2-butene	1.10/6/	1.56 ± 0.09	-0.46	0.09/5/
3-Dimethyl-2-butene	1.22	2.06 ± 0.11	-0.86	0.17
	1.20/6/			
-Methyl-1-pentene	0.95	1.04 ± 0.13	-0.09	0.13
4-Dimethyl-1-pentene	0.75	1.55 ± 0.15	-0.80	0.16
4,4-Trimethyl-1-pentene	0.55	1.35 ± 0.12	-0.80	0.20
4-Dimethyl-2-pentene	1.03	1.62 ± 0.14	-0.59	0.30
4,4-Trimethyl-2-pentene	0.61	1.14 ± 0.11	-0.53	0.50
5-Dimethyl-2-hexene	1.17	2.06 ± 0.17	-0.89	0.20
-Hexene	1.60/3/	1.52 ± 0.10	+0.08	0.23/3/
ns-2-Methyl-3-hexene	1.30/3/	1.35 ± 0.14	-0.05	0.27/3/
ns-2,5-Dimethyl-3-hexene	1.16	1.19 ± 0.17	-0.03	0.41
2-Dimethyl-3-hexene	0.85	0.86 ± 0.10	-0.01	0.52

consequently, the probability of formation of the favourable conformation providing the allyl interaction is decreased. The effect of the rotation hindrance resulting in the decrease in hydrogen yield seems to be supported by the $G(H_2)$ value of 2-methyl-2-butene /5, 6/. This value (1.10) is higher than the one obtained from the measured $G(H_2)$ value of 2,3-dimethyl-2-butene (1.22) being diminished by the value per methyl group ($0.3: 1.10 < 1.22 - 0.3$). However, an excellent interpretation of this phenomenon can be obtained by considering the measured $G(H_2)$ value of 2-methyl-2-butene as a sum of hydrogen yield per one methyl group with free rotation (Fig. 4) (0.51) and those with hindered rotation calculated from the data concerning 2,3-dimethyl-2-butene ($0.60: 0.51 + 0.60 \approx 1.10$).

Although our results can be generally interpreted by the theory of allylic interaction and of steric hindrance, further investigation is needed because of an "exception" in the case of 3,3-dimethyl-1-butene. There the measured value is 0.37 molecule/100 eV for the hydrogen yield which is much higher than we would expect on the basis of the contribution of non-allylic hydrogens to the hydrogen yield (0.13). The specificity of this compound is that there is no C−H bond in the β-position. Although the large deviation from the $G(H_2)$ value calculated cannot be unambiguously interpreted, we suggest that owing to the non-existence of any allylic C−H bond which with its greater sensitivity would exert a "protective" effect on the other C−H bonds, the probability of the rupture of non-allylic C−H bonds must be increased.

Our present data point to more general validities of the phenomenon obtained in the case of cyclic alkenes, i.e. the hydrogen yield is decreased by the steric effect that is characteristic not only of the cyclic alkenes but is true for the straight chain alkenes if the free rotation of the C−C bond in the α-position to the π-bond is hindered by substitution.

The methane yields are presented in column 5 of Table 2. According to the first approximation the methane yield is controlled by the same effect as that of hydrogen. Nevertheless the data concerning the alkenes of same type show that the methane yield depends on the number of methyl groups, on the order of carbon connected to these methyl groups and on the relative position of methyl groups to the π-bond. As a typical example the radiolysis of 3-hexene and its derivatives substituted differently with methyl groups can be presented.

The highest methane yield can be observed with 2,2-dimethyl-3-hexene because in this molecule all methyl groups are in the β-position and three of them are bonded to a quaternary carbon atom.

A high methane yield was also measured with 2,4,4-trimethyl-2-pentene. The great number of methyl groups, three of which are in the β-position bonded to quaternary carbon, may be a good reason for a high $G(CH_4)$ value. However, the model of this molecule (Fig. 5) shows that the methyl group on the second carbon atom is located in the middle position between the methyl groups on the fourth carbon atom, consequently, twisting of the tertiary-butyl group is hindered to a great extent. It is not excluded that the strain attributed to the closely packed methyl groups may cause an ease of splitting of one methyl group from the quaternary carbon atom. Nevertheless, the isomerization of the original molecule in the transition state into 3,4,4-trimethyl-2-pentene may be considered as an other alternative. Thus the methyl groups can move into the position which is favourable for allylic interaction. This molecule is similar to the trans-2,2-dimethyl-3-hexene where the methyl groups interact with the π-bond in the same way.

The methane yield from 3,3-dimethyl-1-butene is smaller than the expected one. This also shows the exceptional behaviour of this molecule indicated by the hydrogen yield being higher than the calculated one. A lower methane yield was also found for 2,3,3-trimethyl-1-butene. This may be explained, e.g. by the fact that the addition of methyl radicals to the double bond at the chain end takes place

much easier than in the case where the double bond is located in the inner position, such as in the case of 3-hexene. This seems to be a reasonable explanation because a part of methane is formed through the methyl radical mechanism as stated in the literature and based on our own experiments.

Acknowledgement. We are indebted to Dr. F. Kling for preparing the cyclononene and cyclopentadecene.

References

/1/ Gy. Cserép, G. Földiák, Proc. 3rd Tihany Symp. Rad. Chem. Eds. J. Dobó and P. Hedvig, Akadémiai Kiadó, Budapest, 1972, Vol. 1, p. 287.
/2/ Gy. Cserép, G. Földiák, Int. J. Rad. Phys. Chem. 5, 235 (1973).
/3/ Gy. Cserép, G. Földiák, Acta Chim. (Budapest) 77, 407 (1973).
/4/ Gy. Cserép, G. Földiák, Advances in Chemistry, Ed. B. Csákvári, Akadémiai Kiadó, Budapest, 1971. Vol. 4. p. 11.
/5/ C. C. Wagner, J. Phys. Chem. 71, 3445 (1967).
/6/ J. W. F. van Ingen, W. A. Cramer, Trans. Faraday Soc. 66, 857 (1970).
/7/ F. Zuccarello, G. Bueni, G. Favini, J. Mol. Structure 18, 295 (1973).
/8/ J. D. Cox, G. Pilcher, Thermochemistry of Organic and Organometallic Compounds, Academic Press, London, 1970, p. 580.

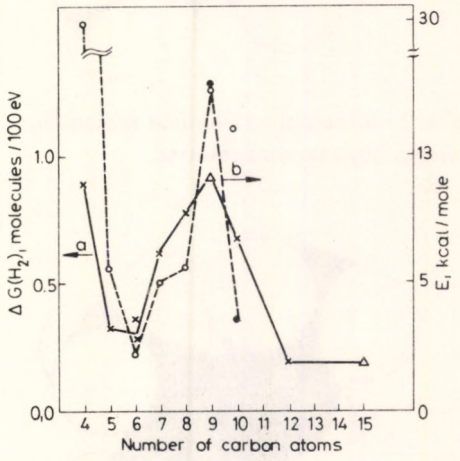

Fig. 1 (a) $\Delta G(H_2)$* values of cycloalkenes, (b) ring strain energies (E)** vs. the number of carbon atoms. + - calculated from the data of Refs /1–3/: △ - this work, ○ - data for the cis form, ● - data for the trans form.

* $\Delta G(H_2) = G(H_2)$ calculated - $G(H_2)$ measured
** The strain energy values are taken from Refs /7 and 8/

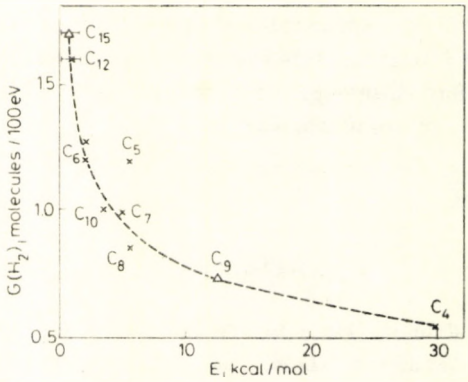

Fig. 2 $G(H_2)$ values of cyclic alkenes vs. the ring strain energies of the most stable isomers

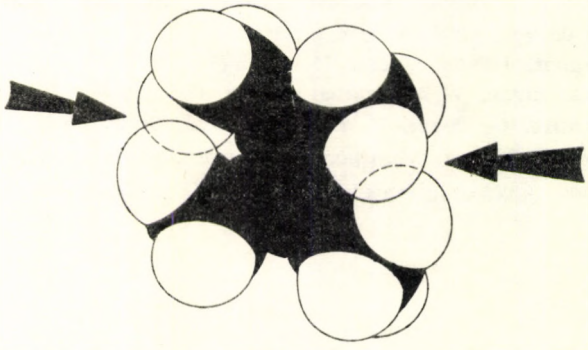

Fig. 3 The model of 2, 3 –dimethyl–2 –butene molecule. Arrows indicate the place of the steric hindrance of rotation

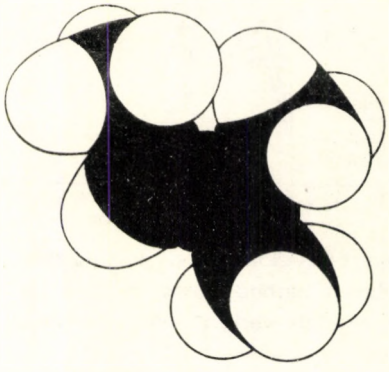

Fig. 4 The model of 2 –methyl–2 –butene molecule. The absence of steric hindrance of rotations for one methyl group is apparent

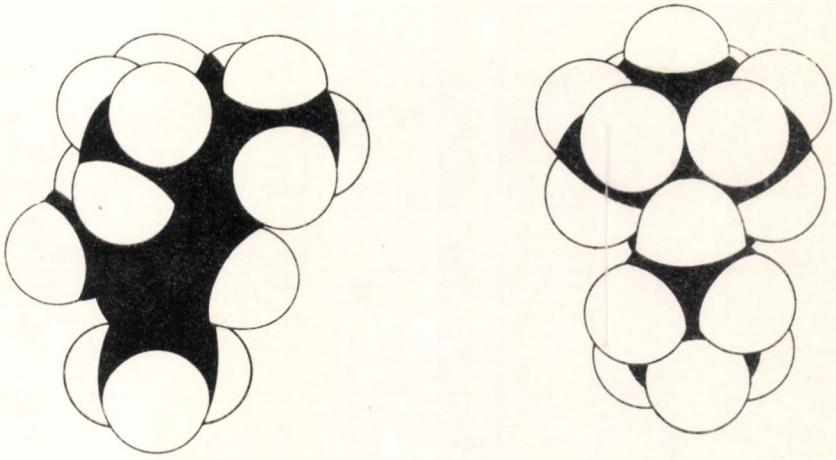

Fig. 5 Two views of the molecule-model of 2, 4, 4 −trimethyl −2 −pentene

DISCUSSION

G. CASTELLO

Do you know the relative importance of CH_4 formation with respect to other products coming from C–C bond rupture?

In other words, what is the percentage value of $G(CH_4)$ in various hydrocarbons compared with the total G of fragmentation? Are both values correlated with the structure in the same way?

Gy. CSERÉP

We have measured other decomposition products too. These data will be published in the near future. The predominant products are usually those the formation of which can be traced back to allylic bond rupture.

GAS-PHASE RADIATION CHEMISTRY of D_2 -ALKYLBENZENE MIXTURES

Giorgio Perez
Laboratorio di Chimica Nucleare, C. N. R., C. P. 10, 00016 Monterotondo Stazione (Rome), Italy

As it is well known from mass spectrometric experiments, H_3^+ ions can transfer a proton to an organic substrate. The reactions between H_3^+ ions and simpler members of the aromatic series were investigated, and proton transfer appeared the principal mode of reaction /1/. The protonated species were formed in excited states and, if not stabilized by collision, decomposed to fragment ions. Moreover, the mass spectral techniques did not permit the identification of isomeric products.

As the preparation of H_3^+ ions can be conveniently carried out by a radiolytic technique introduced by Ausloos and Lias /2/, the gas phase reactions subsequent to the protonation of an aromatic substrate can be studied.

The H_3^+ ions are produced with a $G_{H_3^+} = 2.75$, during the γ-radiolysis of H_2 and their formation occurs via the following processes /3,4/:

$$H_2 \xrightarrow{\gamma} H_2^+ + e^- \qquad /1/$$

$$H_2^+ + H_2 \longrightarrow H_3^+ + H \qquad /2/$$

In the experimental procedure 1 l ampoules were filled with few milligrams of aromatic substrate under a pressure of 2-3 torr of oxygen, and 500 torr of H_2 (or D_2), and, then, irradiated by a 7000 Ci ^{60}Co γ-source.

Blanks were performed to determine the yield of the products formed in the absence of hydrogen and the results are reported in Table 1.

The D_2-Arene system was generally preferred to the H_2-Arene system, to avoid an isotopic effect when tritium is used as tracer.

After the formation of the D_3^+ ions, the first step of the reaction is an exothermic deuteron transfer from $D3^+$ to the arene:

$$D_3^+ + ArH \longrightarrow [Ar\,HD]_{ex}^+ + D_2 \qquad /3/$$

The excited arenium ion can subsequently react in the following ways:

1) It can be collisionally stabilized and then transfer a proton to a proton acceptor present in the gaseous system:

$$[ArHD]^{+}_{ex} \xrightarrow[B]{\text{thermalization}} ArD \qquad /4/$$

2) The excited ion can undergo fragmentation or isomerization:

$$[ArHD]^{+}_{ex} \longrightarrow \text{Products} \qquad /5/$$

The first mode of reaction was studied by Cacace and his co-workers /5/. They prepared D_2T^+ ions by γ-radiolysis of D_2 containing a tracer activity of DT. The D_2T^+ ions were allowed to react with toluene and benzene and the intermolecular selectivity was determined by the activity recovered in the products:

$$D_2T^+ \xrightarrow[k_1]{\text{Toluene}} C_7H_7T \qquad /6/$$

$$D_2T^+ \xrightarrow[k_b]{\text{Benzene}} C_6H_5T \qquad /7/$$

The low value of the found ratio, $k_1/k_b = 1.3$, was ascribed to the low substrate selectivity of the protonating agent.

Table 1

Radiolysis of He–Arene mixtures: absorbed dose $1.2 \cdot 10^{21}$ eV g^{-1} of helium

Arene	Final composition (%)	
	Isomerization products	Dealkylation products
Toluene	–	0.08
o-xylene	0.12	0.40
m-xylene	0.20	0.22
p-xylene	0.25	0.24
1,2,3 trimethylbenzene	0.14	0.28
1,2,4 "	0.01	0.19
1,3,5 "	0.02	0.25
diethylbenzene	< 0.01	0.45

The intramolecular selectivity of D_2T^+ attack was deduced from the tritium distribution in the labelled toluene:

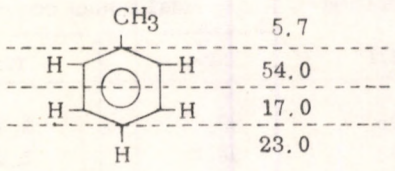

In the present work some reactions of excited arenium ions are studied. As is well known, in the liquid phase methylbenzenes undergo isomerization via the formation of an arenium ion /6/.

In the gaseous phase the first step of the arene isomerization process by D_3^+ ions is an exothermic deuteron transfer from D_3^+ to the arene, S, while the D atoms are removed by a low concentration of oxygen. The excited methylbenzenium ions, $[SD]^+_{ex}$, can subsequently undergo isomerization giving the protonated product PD^+. There is a competition between the isomerization and the collisional stabilization of a part of the arenium ions:

$$D_3^+ \xrightarrow{S} SD^+_{ex} \qquad /8/$$

$$[SD]^+_{ex} \xrightarrow{\text{isomerization}} PD^+ \xrightarrow{B} P \qquad /9/$$

$$[SD]^+_{ex} \xrightarrow{B} S \qquad /10/$$

B represents a proton acceptor, which can be the substrate itself or a base present, as impurity, in the system. Such a base can also compete with the substrate for D_3^+ ions capture.

$$D_3^+ \xrightarrow{B} D_2 \qquad /11/$$

Under steady state conditions from the suggested scheme, Eq. (12) can be developed:

$$\frac{d\,[P]}{dt} = \frac{\alpha\,[S]}{\beta+\gamma\,[S]} \qquad /12/$$

where α; β and γ are dependent on the kinetical constants, deuterium pressure, and base concentration. At a given absorbed dose, it can be written in a simpler way:

$$1/[P] = a + b/[S] \qquad /13/$$

Table 2

Xylenes isomerization data. Absorbed dose: $4.84 \cdot 10^{20}$ eV g^{-1} of deuterium

Substrate	Concentration μ mole/l	Final isomer composition (mole %)		
		o-	m-	p-
o-xylene	2.06	98.17	1.77	0.24
	8.70	98.36	1.62	0.20
	12.00	98.54	1.46	-
	55.57	99.00	1.00	-
	105.59	99.27	0.73	-
m-xylene	2.76	0.31	98.69	1.00
	10.36	0.28	98.99	0.73
	16.01	0.27	99.20	0.53
	42.38	-	99.58	0.42
	162.00	-	99.69	0.31
p-xylene	1.52	0.40	2.24	97.36
	2.83	0.29	1.88	97.83
	7.21	0.20	1.57	98.23
	21.66	-	1.15	98.85
	64.66	-	1.00	99.00

Plotting 1/ [S] against 1/ [P], the straight lines, reported in Figs 1 and 2 are obtained.

In Tables 2 and 3, the isomerization data for xylenes and trimethylbenzenes, respectively, are given.

In conclusion, according to the 1,2-methyl shift model, observed in the liquid phase, o-xylene and p-xylene isomerize to m-xylene. A second methyl shift can be observed in the isomerization of o-xylene, m-xylene undergoes isomerization to p-xylene more rapidly than to o-xylene. Hemimellitene isomerizes to pseudocumene, which, more slowly rearranges to give mesitylene. Pseudocumene gives mesitylene as the only detectable product. The absence of any measurable mesitylene isomerization can be ascribed to the relatively high stability of the mesitylenium ion.

Table 3

Trimethylbenzenes isomerization data. Absorbed dose: $6.09 \cdot 10^{20}$ eV g^{-1} of deuterium

Substrate	Concentration μmole/l	Final isomer composition (mole %)		
		1, 2, 3	1, 2, 4	1, 3, 5
1, 2, 3	4. 70	94. 2	5. 2	0. 6
	7. 07	95. 1	4. 4	0. 5
	18. 50	96. 5	3. 1	0. 4
	45. 90	98. 4	1. 4	0. 2
1, 2, 4	5. 48	–	98. 0	2. 0
	8. 35	–	98. 3	1. 7
	38. 88	–	99. 1	0. 9
	71. 21	–	99. 6	0. 6
1, 3, 5	5. 15	–	0. 3	99. 7
	17. 15	–	0. 1	99. 9
	22. 75	–	–	100. 0
	38. 28	–	–	100. 0

References

/1/ V. Aquilanti, A. Giardini-Guidoni and G. G. Volpi, Trans Faraday Soc., 64, 3283 (1968).

/2/ P. Ausloos and S. G. Lias, J. Chem. Phys., 40, 3599 (1964).

/3/ P. Ausloos, Progr. Reaction Kinetics, 5, 113 (1969).

/4/ J. Weiss and W. Bernstein, Radiation Res., 6, 603 (1957).

/5/ F. Cacace, R. Cipollini and G. Occhiucci, J. C. S. Perkin II, 1972, 84.

/6/ D. M. Brouwer, E. L. Mackor and C. MacLean, Rec. Trav. Chim., 84, 1564 (1965).

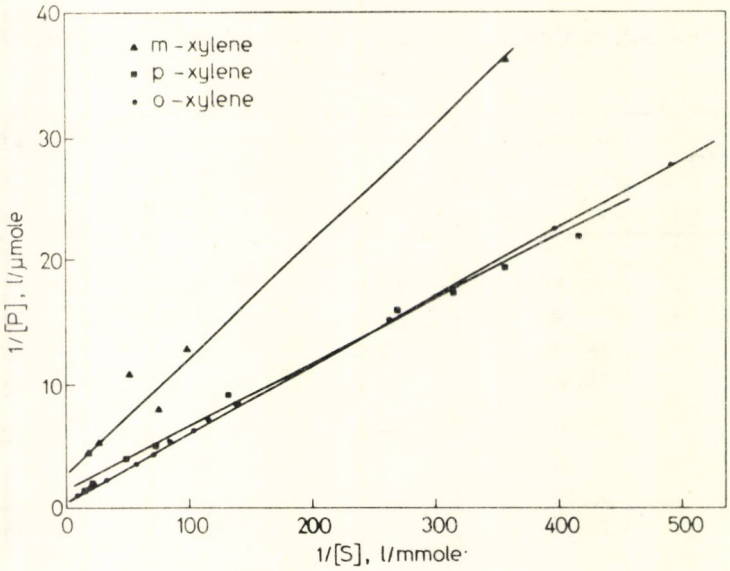

Fig. 1 Xylene isomerization: plot of 1/Product vs. 1/Substrate

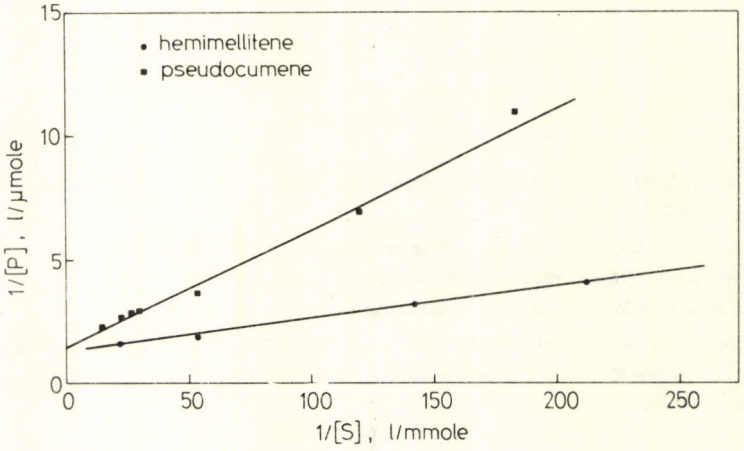

Fig. 2 Trimethylbenzene isomerization: plot of 1/Product vs. 1/Substrate

Z. PAÁL

What is the reason for the difference in the isomerization abilities of various xylene and trimethyl benzene isomers?

G. PEREZ

As determined in other experiments previously reported, the D_3^+ ions are electrophilic agents, therefore it seems that an ipso attack is less favoured in the case of m-xylene and mesitylene than in their isomers, since the methyl groups direct the attack in their para and ortho positions preferentially. Another, and probably more important, reason is that the more basic cations of m-xylene and mesitylene are more stable than the cations of their isomers, and a higher activation energy is required to get a methyl shift.

ENERGETICS AND RATES OF ELECTRON ATTACHMENT REACTIONS IN NON-POLAR LIQUIDS

R A. Holroyd
Hahm – Meitner Institute for Nuclear Research. West Berlin

Introduction

Rate constants for reactions of quasifree electrons with solutes in non-polar liquids range from less than 10^{11} to more than $10^{14} M^{-1}$ sec^{-1} and depend on solvent, temperature and the nature of the solute /2–8/. Furthermore, the rates exhibit some unusual temperature effects, for example: the temperature coefficients are negative for reactions with C_2H_5Br, N_2O, and C_2HCl_3 in $(CH_3)_4Si$, and positive for these solutes in n-hexane; the rate of electron attachment to ethylbromide goes through a maximum between −25 and −50 °C in 2, 2, 4-trimethylpentane. To correlate these data the suggestion was made that the rate constant is a function of V_0 /3/ (where V_0 is the energy of the free electron in the conduction band in the liquid). When rates measured at 20° were plotted versus V_0 maxima were observed which resemble the resonant processes observed for these molecules in the gas phase. It was further suggested that the temperature effects might also be explained by changes in V_0 with temperature.

Detailed theoretical treatments of rates of excess electrons have appeared recently in which temperature effects are considered explicitly /9. 10/. It is assumed that the quasifree electron attaches to the solute by a vertical transition. In liquids of high electron mobility the rate constant will be proportional to the density of unoccupied energy levels in the acceptor molecule at the value of V_0 for the solvent. Gas phase data may be used to determine the density of states but the acceptor levels are shifted in the liquid by the polarization energy (P^-) of the acceptor anion. The value of P^- depends on the dielectric constant and it decreases in magnitude with increasing temperature.

Thus for the reaction of an electron with an acceptor AX (reaction 1)

$$e^- + AX \longrightarrow AX^- \qquad /1/$$

the energetics in the liquid will differ from the gas phase by the heats of solution of the reactants and products. Since the polarization term (P^-) due to solution of AX^- is large, reactions which are endoergic in the gas phase may proceed readily with thermal electrons in solution. The band energy V_0 has recently been measured as a function of temperature for several non-polar liquids /11/. In general, V_0 de-

creases with increasing temperature. In this paper, some rate data are examined to elucidate the energy dependence and to show that the temperature dependence of the rate is correlated with changes in the energy terms: V_o and P^-.

Discussion

In the gas phase the rates of many electron attachment reactions pass through maxima at electron kinetic energies less than 4 eV /12/. In the liquid we assume that reaction also occurs as a vertical attachment process, with the difference that kinetic energy of the electron is replaced by the difference in total energy (E_T) between initial and final states. This energy in solution is given by

$$E_T = V_o - \chi \; P^- + \Delta H_{soln}(AX) \; + \varepsilon_k \qquad /2/$$

or, since the heat of solution of AX is generally small and changes little with temperature or solvent, by

$$E_T = V_o - \chi \; P^- + \varepsilon_k \qquad /2\,/$$

The parameter χ, which takes into account the lack of equilibrium configuration of the solvent when AX^- is first formed is taken to be 0.8 as suggested by Henglein /9/. The kinetic energy of electron (ε_k) is thermal for the molecular liquids. Values of V_o are taken from a recent photoelectric study which showed quantitatively the decrease in V_o with increasing temperature. P^- is approximated by Born's equation

$$P^- = \frac{e^2}{2a}\left(1 - 1/\varepsilon\right) \qquad /3/$$

where a is the radius of AX^- and ε the dielectric constant. Thus, the transfer of large ions into non-polar liquids will be exothermic by about 1 eV. Data on electron attachment reactions are examined below to compare the dependence on energy (E_T) in the liquid phase with the dependence on kinetic energy of the electron in the gas.

Ethyl Bromide. Data from Refs. /2 and 3/ for reaction 4:

$$e^- + C_2H_5Br \longrightarrow C_2H_5 + Br^- \qquad /4/$$

are replotted in Fig. 1 as a function of $E_T = V_o - 0.8\,P^- + \varepsilon_k$. The solid points in Fig. 1 refer to room temperature data and the open ones to points at other temperatures. The value of P^- is close to -1.1 eV and changes slightly with temperature;

for example in 2, 2, 4—trimethylpentane P^- changes from -1. 21 to -1. 09 in going from -85° to + 50° C. Over this range V_0 decreases from -0. 07 to -0. 31 eV. Thus differences in E_T mainly represent changes in V_0.

In n-hexane the rate constant increases with temperature, and since V_0 decreases with temperature these points (squares on the right side of Fig. 1) show that k decreases with E_T at high values of E_T. In $(CH_3)_4Si$ the rate constant decreases with increasing temperature and therefore these points (diamonds in Fig. 1) show that at low values of E_T the rate constant increases with E_T. Neopentane is similar to $(CH_3)_4Si$ in this respect but the rate is somewhat higher falling at a slightly higher E_T. The points for 2, 2. 4-trimethylpentane fall at intermediate values of E_T and the maximum in the rate at -50 °C is now understood in terms of a maximum in the k vs. E_T plot. The maximum rate occurs at a value of E_T = 0. 8 eV which is in good agreement with the maximum in the vertical attachment rate at 0. 75 eV for this reaction in the gas phase /13/. The half-width of the peak is slightly less in the liquid (0. 3 eV) than in the gas (0. 5 eV).

Trichloroethylene. The reaction of the electron with trichloroethylene has been studied in several solvents. In n-hexane and 2, 2, 4- trimethylpentane a positive temperature coefficient is observed. This is plotted on the right side of Fig. 2 and shows that the rate decreases with E_T. In $(CH_3)_4Si$ a negative temperature coefficient was found. Because of the large negative V_0 for this solvent these points fall at lower E_T below the peak, where k increases with E_T. The rate of reaction of electrons with C_2Cl_3H in 2, 2, 4, 4- tetramethylpentane increases with temperature to 50 °C and above this temperature the rate is approximately $8.6 \times 10^{13}\ M^{-1} sec^{-1}$ /14/. The points for this liquid are found near the maximum in Fig. 2 which accounts for the unusual temperature dependence in this liquid. Here P^- is close to -1. 05 eV and the changes in P^- with temperature and solvent are small. The differences in the values of E_T for the data shown are thus mainly due to differences in V_0.

The maximum in the rate as shown in Fig. 2 is at E_T = 0. 5 eV. This is in good agreement with gas phase data. The dissociative attachment rate has a resonant peak at 0. 39 eV and the overall attachment rate has a peak at 0. 65 eV /12/.

Sulfur hexafluoride. For SF_6 a maximum in the attachment rate is observed in the gas phase when the kinetic energy of the electrons is zero /12/. Thus a maximum is expected in the liquid when E_T = 0. The data for molecular liquids (Fig. 3) start at $\sim$ 0. 4 eV and decrease with increasing energy. Thus the data are consistent with a peak at low energy and the figure shows only the high energy tail. Also included in this figure are data in liquid argon and xenon where the rate constants at low field are 1.8×10^{14} and $4.3 \times 10^{14} M^{-1}\ sec^{-1}$, respectively /8/. In these liquids the rate decreases with increasing applied electric field, that is, with increasing average kinetic energy of the electrons. When the average kinetic energy of the electrons as given in Ref. /8/, is included in E_T, the data for liquid xenon overlap that of argon and are also consistent with the data in the molecular liquids. Further these data show that the peak must be at $E_T < 0.2$ eV. The rate in n-hexane, is very low and suggests the reaction is diffusion-limited in this solvent.

Conclusion

This analysis supports the idea that the variation in the rate of electron attachment reactions in solution is a function of the energy available. The main factor influencing changes in E_T is the solvent electron band energy (V_o). The variation in rate with energy is ascribed to changes in the density of states in the acceptor molecule with energy. The assumption that the electron reacts from the conduction band in a vertical transition seems valid for liquids of high electron mobility.

Acknowledgement. The author wishes to thank Prof. A. Henglein for many helpful suggestions.

References

/1/ U. S. Senior Scientist Awardee of Alexander von Humboldt-Stiftung 1975-76; on leave from Department of Chemistry, Brookhaven National Laboratory, Upton, N. Y. 11973

/2/ A. O. Allen and R. A. Holroyd, J. Phys. Chem. 78, 796 (1974)

/3/ A. O. Allen, T. E. Gangwer and R. A. Holroyd, J. Phys. Chem. 79, 25 (1975)

/4/ G. Beck and J. K. Thomas, J. Chem. Phys. 60, 1705 (1974); J. Chem. Phys. 57, 3649 (1972)

/5/ J. H. Baxendale and E. J. Rasburn, J. Chem. Soc. Faraday Trans. I 70, 705 (1974)

/6/ J. H. Baxendale, J. P. Keene, and E. J. Rasburn, J. Chem. Soc. Faraday Trans. I. 70, 718 (1974)

/7/ G. Bakale and W. F. Schmidt, Z. Naturforsch. 28a, 511 (1973)

/8/ U. Sowada, G. Bakale, K. Yoshino and W. F. Schmidt, Chem. Phys. Lett. 34, 466 (1975)

/9/ A. Henglein, Ber. Bunsenges. phys. Chem. 79, 129 (1975)

/10/ K. Funabashi and J. L. Magee, J. Chem. Phys. 62, 4428 (1975)

/11/ R. A. Holroyd, S. Tames and A. Kennedy, J. Phys. Chem. 79, (1975)

/12/ L. G. Cristophorou, "Atomic and Molecular Radiation Physics", Wiley-Interscience New York, N. Y. 1971

/13/ R. E. Goans and L. G. Christophorou, J. Chem. Phys. 63, 2821 (1975)

/14/ T. E. Gangwer, A. O. Allen and R. A. Holroyd, unpublished results

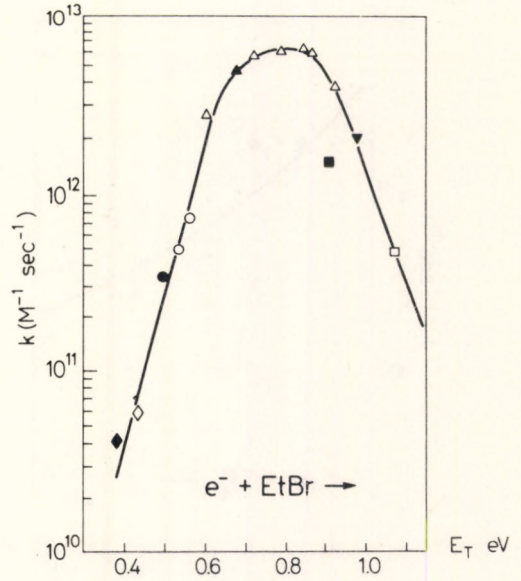

Fig. 1 Rate constant data for EtBr + e^- → at various temperatures plotted vs. E_T for different liquids: ◆ ◇ TMS, ● ○ neopentane; ▲ △ 2, 2, 4–trimethylpentane; ▼ cyclohexane, ■ □ n–hexane. Solid points are at room temperature

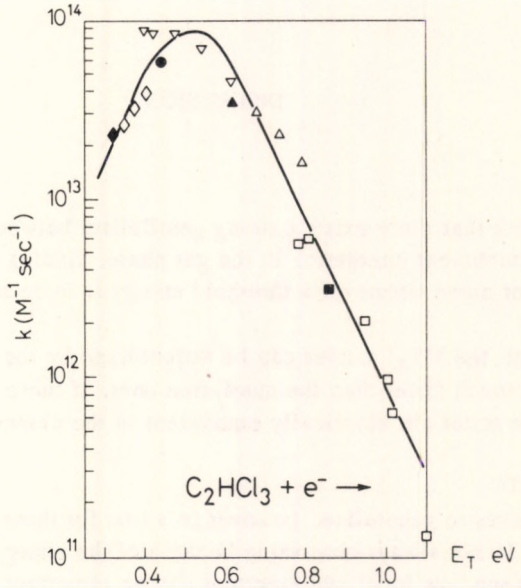

Fig. 2 Rate constant data for e^- + C_2Cl_3H → at various temperatures plotted vs. E_T for different liquids; symbols as in Fig. 1 except that ▼ ▽ represent 2, 2, 4, 4–tetramethylpentane (Ref. 14)

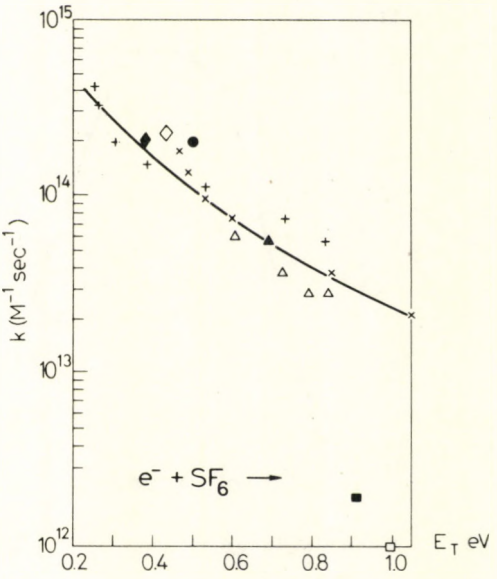

Fig 3 Rate constant data for $e^- + SF_6 \rightarrow$ under various conditions vs. E_T for different liquids; symbols as in Figs 1 and 2 and additionally: + xenon; x argon

DISCUSSION

R. SCHILLER

Do you think that there exists a strong parallelism between $k(V_0)$ curves in liquids and electron attachment energetics in the gas phase, finding always a maximum in the rate constant curve whenever a threshold energy is to be surmounted in the gas phase?

I think that the $k(V_0)$ curves can be rationalized by the assumption that localized electrons react much faster than the quasi-free ones, if there is a threshold energy, whereas the two states are kinetically equivalent in the absence of such a threshold.

R. A. HOLROYD

It is dangerous to generalize, however it is true for those reactions reported here. The maximum is not always observable because of the energy range of E_T in the liquid phase. I do not see how localized electrons can be important since electrons react with SF_6 in liquid Ar and Xe and the rate varies in a way quite similar to the dependence in molecular liquids.

W. STILLER

Christophorou compared electron attachment reaction in the dense gas phase with reactions between hydrated electrons and molecules in the liquid phase. He found correlations between the rate coefficients of both reaction types. Could you find correlations in the case of non polar solvents?

R. A. HOLROYD

Yes there is a one-to-one correlation as we have shown for these reactions, providing one replaces the kinetic energy of the electron in the gas phase by E_T, the total energy difference between initial and final states in the liquid.

Yu. A. BERLIN

What concentrations have you used in your experiment? Did you work with substances which had both signs of V_0 or only one sign?

R. A. HOLROYD

The concentrations used were between 10^{-7} and 10^{-4} M depending on the reactivity of the solute. In this work V_0 was between -0.5 and $+0.2$ eV.

G. R. FREEMAN

Whether the measured value of V_0 is positive or negative is not crucial to your argument. It is the relative values that are important. The values measured by photoinjection of electrons might be doubly affected by the scattering properties of the medium. This might make a monotonic schift in the values estimated by yourself and Schiller, but would not affect the correlations that have been made between V_0 and mobility, reaction rate constants, and so on.

L. KEVAN

How much does the absolute polarization energy change with temperature in comparison to the absolute change in V_0 with temperature in most of the alkanes?

Have you observed any electron attachment reactions in liquid alkanes which are endoergic in the gas phase?

R. A. HOLROYD

For these solutes the change in polarization energy is about 0.1 over a temperature interval in which V_0 changes by 0.24 eV.

We have studied electron attachment to CO_2 for which the electron affinity is negative (-0.4 eV) in the gas. (Ref: Holroyd, Gangwer, Allen, Chem. Phys. Lett. 31, 520 (1975).)

Currently I am studying aromatics and a fast attachment reaction is observed for styrene which has a negative electron affinity in the gas phase. Such reactions are reversible and an equilibrium can be observed.

H. J. ACHE

If the electron attachment reaction is reversible, e. g.

$$A + e^- \underset{K_2}{\overset{K_1}{\rightleftharpoons}} Ae^-$$

then would you not expect to see a negative temperature gradient at higher temperatures when the rate constant for the attachment (K_1) becomes smaller than the rate constant for the reverse reaction (K_2) and the maxima which you showed on the slides. The effect of the solvent would then be the stabilization of the complex, which would probably increase with the more polar character of the solvent.

R. A. HOLROYD

These reactions are all of the dissociative attachment type and thus equlibrium is not possible. When equilibrium occurs it is readily apparent by a marked change in the current vs. time curves as was shown in our CO_2 study (Holroyd, Gangwer, Allen, Chem. Phys. Lett. 31, 520 (1975).)

RADIATION-INDUCED CONDUCTIVITY IN SATURATED LONG CHAIN LIQUID HYDROCARBONS

I Kalinowski. J. G. Rabe, W. F. Schmidt
Bereich Strahlenchemie, Hahn-Meitner Institut für Kernforschung Berlin GmbH, West Berlin

Introduction

One of the primary processes in the interaction of high energy radiation with matter is ionization. Charge carriers are produced and in insulating materials the conductivity can increase by several orders of magnitude above the level in the absence of radiation. Investigation of this radiation induced conductivity as a function of the electric field strength and temperature can give information on ion yields and ranges of epithermal electrons. Experiments with pulsed radiation provide data on charge carrier mobilities, recombination coefficients, etc. While a lot of knowledge has been accumulated on the ionization of gases and crystalline solids much less is known about the ionization of liquids and amorphous solids.

Recent experiments with dielectric liquids have yielded a phenomenological description of the charge carrier yield and range distribution functions for epithermal electrons /1/. On the other hand, measurements of the transport properties of excess charge carriers have demonstrated electronic conduction and electron and hole mobilities were determined /2.3/.

Of the solid hydrocarbons measurements on polyethylene (PE) have attracted considerable interest since the material has great technological importance. Most of the data obtained so far, however, reflect the properties of the technological product rather than the intrinsic properties of the pure material. More could be learned from suitable model compounds which resemble the basic $-CH_2-$ structure of PE. On the other hand, new insight might be obtained from measurements on molten PE, i. e. at temperatures where no crystallinity remains.

Therefore, we investigated the radiation induced conductivity of liquid n-dodecane ($C_{12}H_{26}$), liquid n-eicosane ($C_{20}H_{42}$) and molten PE (molecular weight 2×10^5, density 0.96 g cm^{-3}) as a function of the electric field strength and the temperature. With a pulse technique we measured the mobility of excess electrons in dodecane and eicosane.

Experimental

The measurements consisted in recording the steady state ionization current generated by γ-rays in a parallel plate measurement cell as a function of the applied voltage and the temperature or in observing the decay of the electronic component

of the ionization current after a short pulse of X-rays. The cell comprised two parallel circular stainless steel electrodes of 1. 5 cm diameter enclosed by a pyrex glass tube. The electrode distance varied for different cells from 0. 025 to 0. 1 cm. The outer surface of the glass tube was coated with silver and connected to ground.

Since radiation induced conductivity effects are very sensitive to impurities a thorough purification is usually necessary. Research grade n-dodecane (Philips Petroleum Co) with a stated purity of 99. 67% was outgassed at room temperature. It was stored for one day over activated silica gel (activation of the silica gel was effected by keeping it in a vacuum at 500 °C until the pressure had dropped below 10^{-5} torr) and then transferred to the measurement cell. n-eicosane with a stated purity of 98% (Merck) was stirred vigorously with concentrated sulphuric acid at 60° C in order to remove olefines. The process was repeated with fresh acid five times within several days. After separation of the acid the material was washed with triply distilled water. Outgassing and storage over silica gel was followed by storage in contact with a sodium mirror for several days before the material was transferred to the cell. A granulate of high density PE free of additives from BASF wa used without purification. It was outgassed and molten in vacuum. The crystalline melting point of this PE was at 130 °C. The temperature of the cell was maintained by an electrical furnace.

Continuous irradiations were carried out with a ^{60}Co-γ-source. The beam was collimated by lead bricks so that only the volume of the cell was irradiated. All cables were shielded against scattered γ-rays by lead.

Bremsstrahlung X-ray pulses were obtained from a 15 MeV linear accelerator. The pulse duration was 100 nsec. The electronic circuit has been described previously /4/.

It has been observed by several authors that in very pure dielectric liquids electronic mobilities can be measured cf. /2/. Electronegative impurities reduce the lifetime of the electronic charge carries due to attachment

$$e^- + S \longrightarrow S^-$$

While in very pure liquids the decay of the electronic component $i_{el}(t)$ of the ionization current after a short pulse of X-rays is linear /4/ attachment to impurities leads to an additional loss.

$i_{el}(t)$ is then given by

$$i_{el}(t) = i_o e^{-k_s t} \left(1 - \frac{t}{t_d}\right) \qquad /1/$$

with

$$t_d = \frac{d^2}{\mu \cdot U} \qquad /2/$$

k_s is the attachment rate constant and t_d the drift time for the voltage U applied across the plate separation d, μ is the mobility.

It has been shown previously that Eq. 1 can be used to extract mobility data even in impure liquids as long as there is an influence on the decay of i_{el} by the applied voltage U /5/. The pulse dose was always so small (1–10 mrad) that volume recombination of the charge carriers produced under the present conditions could be neglected.

Measurements of the drift mobility were carried out for field strengths up to 10^5 V cm^{-1} in dodecane and 8×10^4 V cm^{-1} in eicosane.

Results

The dependence of the γ–ray induced ionization current on the electric field strength for the three compounds studied is shown in Fig. 1. n–dodecane and n–eicosane showed the behaviour of comparable dielectric liquids as n–hexane, whereas a proportionality between current and field strength was observed for molten PE. These relationships were observed in the temperature ranges studied: 25 to 142 °C for n-dodecane, 47 to 150 °C for n–eicosane, and 132 to 192 °C for PE. The ionization current increased with temperature and activation energies between 0.04 – 0.05 eV at the lower temperatures and 0.11 – 0.15 eV at the higher temperatures were estimated indicating the similary of the thermalization process for epithermal electrons in these compounds.

In liquid dodecane and eicosane the ionization current increased proportional to the dose rate whereas in molten PE a power law was obtained.

For the measurement of the electron mobility the variation of the electronic component of the ionization current after a short burst of X–rays was observed. Figure 2 shows an oscillogram. The decay occurs in the μsec time scale whereas for the positive charge carriers it takes milliseconds to reach the electrode. The decay is not linear but a nick can be noticed (arrow) when all electrons have reached the counter electrode. The mobility was obtained by fitting the decay of many traces numerically to Eq. 1 with one set of k and μ. The fidelity of the chosen values is demonstrated by the circles in Fig. 2. The value of μ agrees with a value estimated from the nick.

The values for the mobility measured as a function of the temperature are shown as an Arrhenius plot in Fig. 3.

Activation energies of 0. 22 eV for n–dodecane and 0. 19 eV for n– eicosane were estimated. In the molten PE a short lived transient after a pulse of X–rays was observed which was attributed to electrons. From the lifetime and a free ion yield of 0. 1 a mobility of 0. 25 cm^2 V^{-1} s^{-1} at 154 °C could be estimated. This mobility is in the range of mobilities determined in dodecane and eicosane.

Discussion

For radiation induced ionization currents in dielectric liquids a fairly detailed description has been developed in recent years, cf. /1/. The field dependence of the ionization currents in n–dodecane and n–eicosane is similar to that of other

hydrocarbons and with the measured dose rate free ion yields G_{fi} of 0.1 at room temperature are estimated. A more precise calculation is hampered by the fact that the sensitive volume is not very well defined since no guard ring assembly was used. It has been shown by Mozumder and Magee /6/ and by Hummel and Allen /7/ that the ion yield is correlated with the mean penetration range of the subexcitation electrons. Schmidt and Allen /8/ measured G_{fi} values at room temperature in normal alkanes from butane to n-tetradecane and found that G_{fi} remained constant as the chain length was increased beyond octane. The present results on dodecane are in agreement with these findings.

The measurements with n-eicosane were carried out at higher temperatures (melting point of eicosane t = 36.4 °C) but identical values were obtained for the ionization currents in n-dodecane and n-eicosane at the same temperature and the same field strength. Thermalization of the subexcitation electrons (= epithermal electrons) is effected by the $-CH_2-$ groups rather than by the whole molecule. Therefore it can be assumed that in polyethylene similar charge carrier yields are obtained under irradiation with γ-rays. The current-field strength characteristic is, however, completely different. The current increases proportional to the field strength up to the highest values applied.

In the liquids at higher field strengths a linear dependence of the ionization current on the field strength is observed and in this range at a certain field strength the ionization current I is directly proportional to the dose rate D

$$I \propto D^{\Delta} \qquad /3/$$

with $\Delta = 1$.

In molten PE, dependence /3/ with $\Delta = 0.87 \pm 0.02$ is observed independent of temperature. In liquids, $\Delta = 1$ is explained by the assumption that at the higher field strengths all charge carriers produced during one second are collected on the electrodes at the same time. Geminate recombination limits the magnitude of the current; however, no volume recombination occurs. If the current is limited by volume recombination, a $I \propto D^{0.5}$ dependence is observed.

Values of Δ with $0.5 < \Delta <$ have also been observed in the radiation induced conductivity of PE and other polymers at room temperature /9/. The results are interpreted on the basis of the Rose-Fowler model /10-12/. Electrons are excited into the conduction levels. They move through the material and recombine with positive charge carriers or become temporarily trapped.

The value of Δ is related to the energy distribution of the traps. For a uniform distribution $\Delta = 1$ and I is practically independent of temperature, for $\Delta = 0.5$, I increases rapidly with temperature. The corresponding activation energies between 300 and 400K are 0.05 eV and 0.3 eV. For the ionization current in the molten PE activation energies of 0.06 - 0.12 eV in the temperature range studied were obtained in agreement with the magnitude of the Δ-value.

The electron mobility in liquid n-dodecane and liquid n-eicosane show an exponential dependence on temperature with activation energies comparable to those of other alkanes. The absolute mobilities are, however, smaller if we compare the room temperature data.

Essentially two models have been proposed for the explanation of low mobilities: a) the trapping model, where the electrons exist in two states, localized and quasifree states the occupation of which is governed by Boltzmann statistics; b) the hopping model, where the electrons exist in traps and move between traps by jumps or tunnelling.

The trapping model would lead to a mobility μ_0 in the quasifree state via

$$\mu_{obs}(T) = \mu_o e^{-E_a/k_B T} \qquad /4/$$

while the hopping model would yield the mean jumping distance λ via

$$\mu_{obs}(T) = \frac{e\lambda^2 (T)\nu_0}{k_B T} e^{-E_a/k_B T} \qquad /5/$$

with ν_0 the attempt frequency, i. e. how often an electron tries to change its trap.

Both models show essentially the same temperature dependence of the mobility. Extrapolation of Eq. 4 to infinite temperatures yielded μ_0-values (133 $cm^2 V^{-1} s^{-1}$ and 33 $cm^2 V^{-1} s^{-1}$ for dodecane and eicosane, respectively) the physical significance of which is not clear.

Evaluation of the data with Eq. 5 with $\nu_0 = 10^{13} s^{-1}$/13/ gave jumping distances around 60 Å for n-dodecane and around 30 Å for n-eicosane. Values of this magnitude have been estimated also for other straight chain hydrocarbons /13, 14/.

We assume that a correlation between λ and the size of the trap exists but more information on the physical nature of the traps is necessary in order to test this hypothesis.

References

/1/ A. Hummel and W. F. Schmidt, Radiat. Res. Rev. 5, 199 (1974).

/2/ cf. e. g. W. F. Schmidt, "Electron migration in liquids and glasses", HMI-Report B 156 (1974).

/3/ M. P. de Haas, J. M. Warman and A. Hummel, Proc. 5th Int. Conf. on Conduction Breakdown in Dielectric Liquids. p. 15. Delft University Press (1975).

/4/ G. Bakale and W. F. Schmidt. Z. Naturforsch. 28a, 511 (1973).

/5/ I. Kalinowski, J. G. Rabe and W. F. Schmidt. Proc. 5th Int. Conf. on Conduction and Breakdown in Dielectric Liquids, p. 11, Delft University Press (1975).

/6/ A. Mozumder and J. L. Magee, J. Chem. Phys. 47, 939 (1967)
/7/ A. Hummel and A. O. Allen, J. Chem. Phys. 46, 1602 (1967).
/8/ W. F. Schmidt and A. O. Allen, J. Chem. Phys. 52, 2345 (1970).
/9/ e. g. S. E. Vaisberg, V. P. Sichkar, V. F. Stepanov and V. L. Karpov, Vysokomol. soed. A 11, 2577 (1969).
/10/ J. F. Fowler Proc. Roy. Soc. A 236, 464 (1956).
/11/ A. Rose RCA Rev. 12, 268 (1951).
/12/ A. Rose, Phys. Rev. 97, 322 (1955).
/13/ W. F. Schmidt, G. Bakale and U. Sowada J. Chem. Phys. 61, 5275 (1974).
/14/ U. Sowada, Thesis, Free University Berlin (1976)

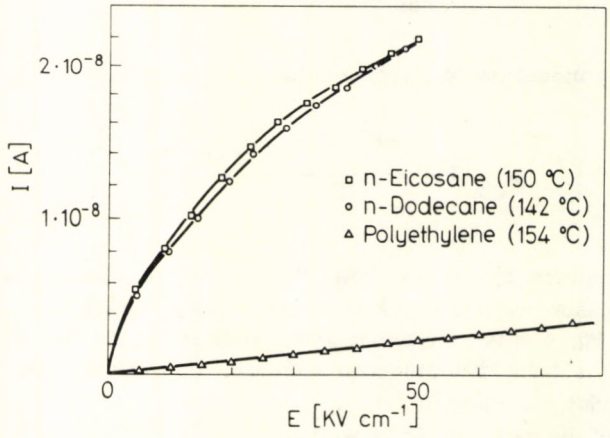

Fig. 1 Dependence of the ionization current on electric field strength in liquid n-dodecane, n-eicosane and molten high density polyethylene. γ-dose rate 3.8×10^3 rad h^{-1}. Electrode distance: n-dodecane d=0.105 cm; n-eicosane d = 0.11 cm; polyethylene d = 0.10 cm

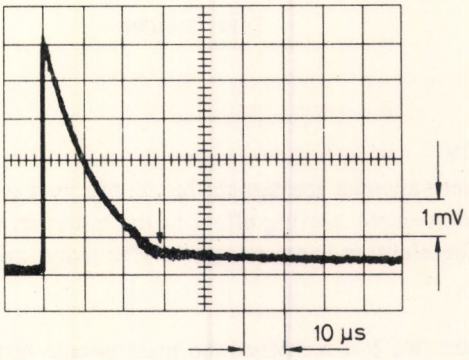

Fig. 2 Decay of the electronic component of the ionization current in n-dodecane. $E = 83.3\ KV \cdot cm^{-1}$, 0.1 µsec pulse; 23°C. Circles calculated with Eq. 1 and $k_s = 3.0 \times 10^4\ sec^{-1}$ and $\mu = 2.40 \times 10^{-2}\ cm^2 V^{-1} sec^{-1}$

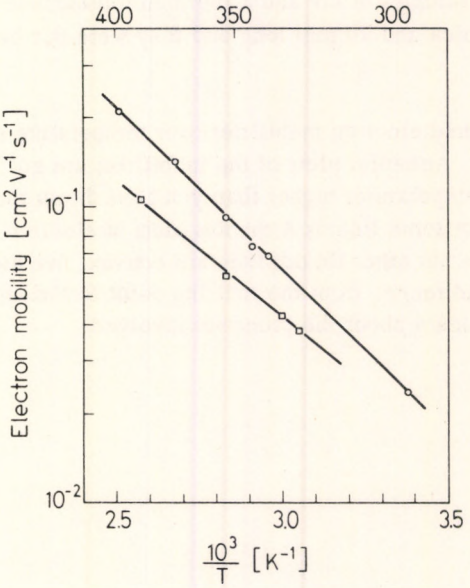

Fig. 3 Temperature dependence of the electron-mobility in: n-dodecane: O; n--eicosane: □

R. KHAIRUDTINOV

Do you take into account the sample heating in your steady state experiments? I think that the microscopic heating effect of the radiation should be taken into account because the electron beam energy in your experiments was too high.

I. KALINOWSKI

No, we did not. We just measured the macroscopic temperature. I think it is sufficient for obtaining the main features.

G. R. FREEMAN

How did you do the dosimetry in the small gap between your electrodes?

I. KALINOWSKI

We used small samples of LiF and a thermoluminescence dosimeter. The samples were about 2 mm thick and 10 mm long and they were put between the electrodes.

G. R. FREEMAN

We have measured electron mobilities over temperature ranges of several hundreds of degrees. Arrhenius plots of the mobilities are not linear. For example in n-dodecane at temperatures higher than you have shown the apparent activation energy increases. For some liquids Arrhenius plots of electron mobilities are concave towards the 1/T axis, in other liquids they are convex. We are measuring mobilities over the entire liquid range, from the melting point to the supercritical gas. We hope in this way to learn about the processes involved.

TEMPERATURE DEPENDENCE OF ELECTRON MOBILITY IN LIQUID HYDROCARBONS

L. Nyikos, E. Zádor, R. Schiller
Central Research Institute for Physics
H–1525 Budapest, P. O. Box 49, Hungary

Introduction

The mobilities of excess electrons in liquid hydrocarbons are apparently closely related to the electronic properties of the unperturbed liquids. In their most recent review-article Davis and Brown /1/ summarize the main properties of low-energy electrons in hydrocarbons stating, among other things, that: "The mobilities and work functions are correlated, increasing μ being accompanied by decreasing V_o, methane being a notable exception .... In most hydrocarbon liquids studied the electron mobilities obey an Arrhenius plot with respect to temperature." The work function or rather conduction state energy, V_o, is the interaction energy of a non-localized electron and the unperturbed liquid.

For the understanding of the transport properties of electrons three theories have been developed all the three being based on two-state models. Kestner and Jortner /2/ regarded the liquids as consisting of two types of regions differing in electron mobility. Davis, Schmidt and Minday /3/, and Schiller, Vass and Mándics /4a/ assumed the liquid to be completely homogeneous with respect to the electron transport, whereas two distinct electron states, a high-mobility localized one was thought to be present in each liquid. If P denotes the proportion of the localized electrons, μ_F and μ_L the respective mobilities of the localized and the quasi-free electrons, the observed mobility can be written as

$$\mu = \mu_F(1-P) + \mu_L P \qquad (1)$$

The two latter theories differ in the way of expressing P as a function of V_o. The comparison between experiment and theory is agreeable for all the three models, which is not surprising, since "... at this time the details of the localized state are not known, and all the three models proposed involve some parametric adjustment"/1/.

The aim of the present work is to obtain some information, partly independent of models, on the parameters involved in one of the theories mentioned above. This is being done by a detailed study of the temperature dependences and V_o dependences of the mobilities. The theory developed in our laboratory /4/ expresses P as a function

of V_o and regards the localized electron energy, E_t as a constant parameter:

$$P = (2\pi)^{-1/2} \int_{-\infty}^{(V_o - E_t)/\sigma} \exp\,[-t^2/2]\,dt \qquad (2)$$

where $\sigma = \sqrt{k}\,C_v T$ is the energy-fluctuation parameter with k being the Boltzmann constant and C_v the constant-volume heat capacity. Even if one neglects $\mu_L P$, two unknown parameters E_t and μ_F appear in the expression of μ, Eq. (1). They were previously assumed /4/ to be the same for all the open chain, saturated hydrocarbons and were found by parameter-fitting. Now an attempt is being made for the experimental determination of these two parameters along with μ_L.

Experimental

Materials

Hydrocarbons obtained from Fluka AG, Schuchardt, Merck and Koch-Light Laboratories were used, giving essentially identical results. The substances were purified by percolation through columns of activated silica gel or molecular sieve, degassing and stirring over NaK alloy in the sidearm of the mobility cell. The electrical conductivity of the purified samples was measured to be as low as about 10^{-16}ohm^{-1}cm^{-1}; typical electron lifetimes in the order of one millisecond were observed in these samples at room temperature.

Equipment and Technique

Quartz cells were used throughout the experiments with electrode distances varying between 0.2 and 0.5 cm. The measuring electrodes were surrounded by guard rings to maintain a homogeneous electric field. The temperature was measured with a thermocouple placed near to the measuring electrode. The cell was put into a double-walled copper block fitted with helical cooling tubes. The temperature was controlled by varying the flow rate of evaporated liquid nitrogen fed into the cooling spiral. The block with the mobility cell was housed in an iron shielding-box with a quartz window. Condensation of water vapour was prevented by the dry nitrogen atmosphere in the box.

Excess electrons were produced by the photoionization of TMPD (N, N, N′, N′ −−tetramethyl−paraphenylene−diamine) dissolved in the sample in a concentration of about 10^{-5} M. A nitrogen laser which produces 337.1 nm wavelengt light pulses of 5 ns duration and about 1 mJ energy was used as a light source. The laser beam illuminated almost homogeneously the volume between the electrodes. Field strengths between 1 and 24 kV/cm were applied. The current signal was fed into a Keithley

M 427 current amplifier (rise time 10 μs) and displayed on a Tektronix 466 or HP 181A storage oscilloscope.

If a sample contains no impurity except TMPD the current decays linearly in time as expected /5/, with a small exponential tail. The linear portion of the current-response was extrapolated to zero to obtain the drift time. The mobility was calculated as the ratio of the drift velocity to field strength. Electron attachment or recombination changed the decay into exponential or hyperbolical, the criterion of purity was the observation of a linear signal. All mobilities were field-independent up to the highest field applied (24 kV/cm). The mobilities at different field strengths and even in subsequent sample preparations were found to be constant within 5%.

Although the cooling apparatus permitted us to reach a temperature as low as 85K, no reliable measurements were possible below about 160K owing to the low signal-to-noise ratio.

Results

The temperature dependences of all the measured mobilities (except that in n-pentane) can be described with constant activation energies in the entire temperature range studied (see Fig. 1). The slopes of the log μ versus 1/T plots were evaluated by least-square fitting.

The measured thermal electron mobility values and activation energies are displayed in Table 1, comparing fairly well with measurements done in other laboratories.

Since a self-consistent set of V_0 values has been published /9, 12, 16/ quite recently for all but three of the compounds studied, experimental V_0 values are available. For n-heptane, n-nonane and n-dodecane V_0 was calculated from critical data using the method of Fueki, Feng and Kevan /21/ and a correlation described by Davis and Schmidt /22/ – in a slightly modified version, using van der Waals constants instead of critical volumes.

Briefly, the electron-molecule hard-core /23/ radius $\underline{a}$, was calculated from known V_0 values. The ratio of $\underline{a}$ to the cube root of $3b_0$ (van der Waals constant) was found to be $0.272 \pm 0.3\%$.

(From the van der Waals model one obtains $a_{vdW}/(3b_0)^{1/3} = 0.271$ indicating that molecule-molecule and molecule-electron hard cores practically coincide.) Using this correlation V_0 was calcuted according to the method described in Ref. /21/.

Determination of μ_L, μ_F and E_t

The obvious idea for experimental determination of μ_L, the mobility of excess electrons in the localized state, is based on the correlation between μ and V_0, i. e. on the fact that higher conduction band energies are always accompanied by lower mobility values. This, in terms of any partial localization theory, corresponds to higher probability of electron localization. For high enough V_0 values P approaches

Table 1

Measured mobility values, μ and activation energies, E_μ in saturated hydrocarbons

	μ(at 295 K) [$cm^2\ V^{-1}\ s^{-1}$]		E [eV]		V_o [eV]
	Present work	Literature	Present work	Literature	Literature
isooctane	7.0	7[a, b], 5.6[c]	0.046 ± 0.002	0.06 ± 0.01[b] 0.051[c]	- 0.24[d]
c-hexane	0.24	0.24[e], 0.35[a], 0.45[f]	- -	0.13[f], 0.16[b]	0.01[g]
3-methylpentane	0.22	0.18[h], 0.2[i], 0.22[j]	0.182 ± 0.002	0.2[i, j]	- 0.03[g] 0.01[n]
n-pentane	0.15	0.07[f], 0.14[e], 0.15[h]	0.201 ± 0.004[l]	0.183[h]	0.01[d]
n-hexane	0.093	0.07[m], 0.082[e], 0.09[a, b]	0.164 ± 0.001	0.19[b, c, e, m]	0.02[d]
n-heptane	0.046	- -	0.170 ± 0.004	- -	0.06[n]
n-octane	0.040	0.039[h]	0.183 ± 0.004	0.183[h]	0.13[k]
n-nonane	0.047	- -	0.189 ± 0.002	- -	0.15[n]
n-decane	0.038	0.025[h, o]	0.217 ± 0.006	- -	0.18[h]
n-dodecane	0.040	- -	- -	- -	0.18[n]

[a]Ref. 6., [b]Ref. 7., [c]Ref. 8., [d]Ref. 9., [e]Ref. 10., [f]Ref. 11., [g]Ref. 12., [h]Ref. 13., [i]Ref. 14., [j]Ref. 15., [k]Ref. 16., [l]around room temperature, [m]Ref. 17., [n]calculated (see text), [o]extrapolated from 344 K.

unity and one expects the mobility to become independent of V_o. In this case the quasi-free contribution to electron transport becomes negligible and the measured drift mobility coincides with μ_L.

The highest V_o values have been measured /16/ in long-chain, unbranched hydrocarbons and V_o has been found to increase in the order of normal hexane < octane< <decane < tetradecane. A systematic study of mobilities and temperature dependences in such high-V_o liquids was hoped to cast some light on the mobility of the localized state. The log μ versus V_o plot (Fig. 2) shows the expected saturation at high V_o values indicating practically total localization. The experimental value determined from the curve is $\mu_L = 0.04\ cm^2\ V^{-1}\ s^{-1}$. This is equal to the low-mobility limit obtained /4c/ by fitting the parameters of the Kestner-Jortner /2/ theory. This observed μ_L value seems to be too high for ion-like diffusion which is expected to be of the order of 10^{-3}. The explanation of this discrepancy would require a better knowledge of the nature of the localized state.

While μ_L was observed experimentally without using any particular model, E_t or μ_F cannot be determined directly. (Hall-mobility measurements might render a direct clue to μ_F; this, to the authors' best knowledge has not yet been performed on liquid hydrocarbons.) One has to express them as a function of measurable quantities by making use of an appropriate model, in this way the estimation of the parameters cannot be better than the approximations involved in the theory.

The partial localization theory /4/ was used for this purpose. (cf. Eqs 1, 2.) If $\mu_L P$ can be neglected in comparison to μ_F (i. e. if liquids with high electron mobility are investigated) the activation energy defined as $E_\mu = \underline{k}T^2 d\ln\mu/dT$ takes the form

$$E_\mu = -\frac{3\underline{k}T}{2} + \frac{\underline{k}T}{\sqrt{2\pi}}\left(\frac{V_o - E_t}{\sigma}\right)\exp\left[-\frac{(V_o - E_t)^2}{2\sigma^2}\right]\cdot\frac{1}{1-P} \qquad (3)$$

The term $-3/2\ \underline{k}T$ stems from the assumed $T^{-3/2}$ dependence /24/ of the quasi-free electron mobility. The use of the measured values of E_μ Eq. (3) enables one to calculate $(V_o - E_t)/\sigma$. By knowing V_o and σ the energy of the localized electron state, E_t can be computed (see Table 2). It can be seen to vary from liquid to liquid within the range of -0.4 ... -0.6 eV which can be compared with -0.28 eV which was obtained by fitting Eqs (1) and (2) and was thought to be the same for all the saturated, aliphatic hydrocarbons.

Further, since both P and E_μ depend only on $(V_o - E_t)/\sigma$ (cf. Eqs 2, 3), $1 - P$ can be determined from E_μ, and this leads directly to μ_F by virtue of the approximate equality $\mu = \mu_F(1-P)$. Thus, operationally speaking, μ_F is determined by E_μ and μ, two quantities which are easy to measure with reasonable accuracy, while it is independent of V_o, the accurate values of which it is generally difficult to obtain. The calculated μ_F values are summarized in Table 2. The μ_F data are in accordance with the calculations of Davis, Schmidt and Minday /3/, and suggest that the quasi-free

Table 2

Calculated quasi-free electron mobilities, μ_F and energies of the localized state, E_t

	μ(at 295 K)	E_μ	V_o	E_t	P	μ_F
	$[cm^2V^{-1}s^{-1}]$	[eV]	[eV]	[eV]		$[cm^2V^{-1}s^{-1}]$
pentane	70[a, b]	~ 0[b]	- 0.43[c]	- 0.55	0.839	440
, 4, 4-tetramethyl-pentane	24[d]	0.061[d]	- 0.36[e]	- 0.56	0.962	630
dimethylbutane	12.3[f]	0.074[f]	- 0.22[c]	- 0.45	0.972	440
, 5, 5 tetramethyl-hexane	12[a, d]	0.048[d]	–	–	0.950	240
ethylpropane	7.3[f]	0.079[f]	–	–	0.975	300
octane	7[g, h]	0.051[i]	- 0.24[e]	- 0.44	0.955	150
, 3, 3 tetramethyl-pentane	5.2[d]	0.065[d]	–	–	0.965	150

f. /18/, [b]Ref. /19/., [c]Ref. /20/., [d]Ref. /11/., [e]Ref. /9/., [f]Ref. /13/., [g]Ref. /6/., f. /7/., [i]Ref. /8/.

mobility values in hydrocarbons are in the same order of magnitude as in liquified rare gases. We would like to draw attention to the fact that in contrast to earlier conjectures a considerable fraction of electrons is localized even in neo-pentane, this high-mobility liquid.

Summary

Localized electron mobility was measured in high-V_o liquids and was found to be 0.04 V^{-1} s^{-1} indicating complex transport mechanism. The energy of the localized state, E_t, and the quasi-free electron mobility, μ_F, were calcuted using the partial localization theory and considering the temperature dependences of the measured mobilities. The data indicate that both E_t and μ_F vary from liquid to liquid, μ_F being in the order of, but always higher than, 100 cm^2 V^{-1} s^{-1} and E_t falling between -0.4 and -0.6 eV.

Acknowledgements. Sincere thanks are due to Mr. J. Balog and Mr. L. Tóth for their valuable comments regarding experimental work.

References

/ 1/ H. T. Davis, R. G. Brown, in Advances in Chemical Physics Vol. XXXI. eds. I. Prigogine and S. A. Rice. Wiley, New York 1975, p. 329.

/ 2/ N. R. Kestner, J. Jortner, J. Chem. Phys., 59, 26 (1973).

/ 3/ H. T. Davis, L. D. Schmidt, R. M. Minday, Chem. Phys. Lett., 13, 413 (1972).

/4a/ R. Schiller, Sz. Vass, J. Mándics, Int. J. Radiat. Phys. Chem., 5, 491 (1973).

/4b/ R. Schiller, J. Chem. Phys., 57, 2222 (1972).

/4c/ L. Nyikos, R. Schiller, Chem. Phys. Lett., 34, 128 (1975).

/ 5/ W. F. Schmidt, Electron migration in liquids and glasses, HMI-B 156 (1974).

/ 6/ W. F. Schmidt, A. O. Allen, J. Chem. Phys., 52, 4788 (1970).

/7a/ B. S. Yakovlev, I. A. Boriev, A. A. Balakin, Int. J. Radiat. Phys. Chem., 6, 23 (1974).

/7b/ I. A. Boriev, B. S. Yakovlev, ibid., 7, (1974).

/ 8/ A. O. Allen, T. E. Gangwer, R. A. Holroyd, J. Phys. Chem., 79, 25 (1975).

/ 9/ R. A. Holroyd, S. Tames, A. Kennedy, J. Phys. Chem., 79, 2857 (1976).

/10/ A. O. Allen, R. A. Holroyd, J. Phys. Chem., 78, 796 (1974).

/11/ J. -P. Dodelet, G. R. Freeman, Can. J. Chem., 50, 2667 (1972).

/12/ R. A. Holroyd, B. K. Dietrich, H. A. Schwartz, J. Phys. Chem., 76, 3794 (1972).

/13/ J. -P. Dodelet, K. Shinsaka, G. R. Freeman, Can. J. Chem., 54, 744 (1976).

/14/ I. Kalinowski, J. G. Raabe, W. F. Schmidt, Z. Naturforsch., 30a, 568 (1975).

/15/ J. Balog, L. Tóth, KFKI Report. 75-73 (1975).

/16/ R. A. Holroyd, L. L. Russel, J. Phys. Chem., 78, 2128 (1974).

/17/ R. M. Minday, R. D. Schmidt, H. T. Davis, J. Chem. Phys., 54, 3112 (1971).

/18/ G. Bakale, W. F. Schmidt, Chem. Phys. Lett., 22, 164 (1973).

/19/ K. Shinsaka, G. R. Freeman, Can. J. Chem., 52, 3556 (1974).

/20/ R. A. Holroyd, M. Allen, J. Chem. Phys., 54, 5014 (1971).

/21/ K. Fueki, D. -F. Feng, L. Kevan, Chem. Phys. Lett., 13, 413 (1972).

/22/ H. T. Davis, L. D. Schmidt, Can. J. Chem., 51, 3443 (1973).

/23/ B. E. Springett, J. Jortner, M. H. Cohen, J. Chem. Phys., 48, 2720 (1968).

/24/ M. Cohen, J. Lekner, Phys. Rev., 158, 305 (1967).

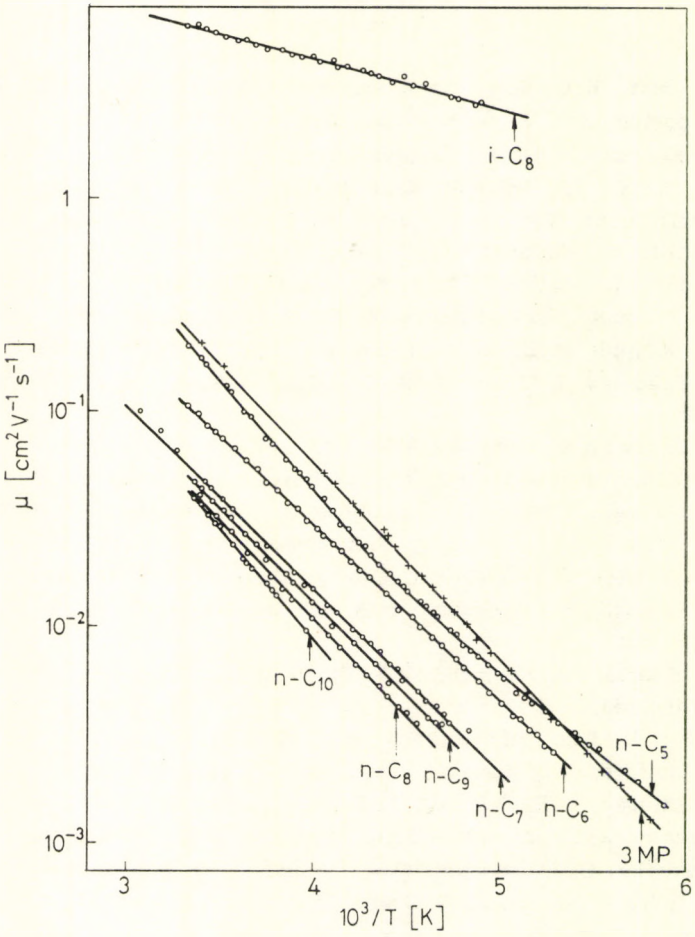

Fig. 1 Temperature dependence of electron mobilities

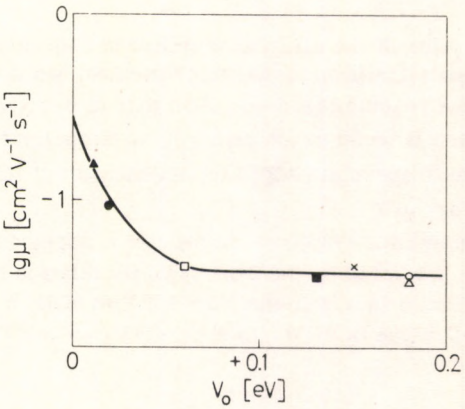

Fig. 2 Mobility values in high $-V_0$ liquids: ▲ n-pentane; ● n-hexane; □ n-heptane; ■ n-octane; x n-nonane; △ n-decane; ○ n-dodecane

DISCUSSION

R. A. HOLROYD:

Do you have E_t values for the low mobility liquids?

L. NYIKOS:

In this case the E_t and μ_F values cannot be separated in the expressions without making additional assumptions, only μ_F–E_t pairs can be obtained for any low mobility liquid.

I. KALINOWSKI

To the low mobility value: why do you take the value at room temperature as a limit for the localized state? What happens if you look at lower temperature? There the mobilities are in the order of 10^{-3}.

L. NYIKOS

The phenomenological activation energies of the mobilities lie very near to each other, thus the approximate equality of μ for high V_0 liquids holds for different temperatures, too. These liquids are, otherwise, in similar reduced state around room temperature.

G. R. FREEMAN

(1) Although our value of the electron mobility in n-decane at room temperature was obtained by extrapolation from higher temperatures, we think that the mobility of electrons in n-decane is somewhat lower than that in n-octane at the same temperature. The difference is found experimentally at temperatures above about 60 °C.

(2) Would you like to speculate about the mechanism of migration of the localized electron, represented by μ_L?

(3) The energy fluctuation dispersion parameter σ appears to be less dependent on temperature than is predicted by the heat capacity relation ($\sigma^2 = kT^2C_p$). When fitting a curve to mobilities in n-pentane from 150K to 500K it was necessary to assume a relatively small value of $d\sigma/dT$ to obtain $d(V_0 - E_t)/dT \leq 0$.

L. NYIKOS

I guess that μ_L may be understood in terms of the dynamics of energy and density fluctuations but we have not attempted any explanation yet.

The value of σ influences only E_t but not μ_F in the present approximation. The low value of $d\sigma/dT$ might indicate, among many other things, that the neglect of density fluctuations in our original treatment cannot be fully justified.

Yu. A. BERLIN

The main assumption of your theory is that the localization and delocalization of the electrons are independent events. Why is it so?

L. NYIKOS

The explanation is in the extreme dilution of the electron-solutions which renders electron-electron interaction highly improbable. This is borne out experimentally by the fact that no property of the excess electrons in liquids has ever been found to depend on the number of electrons present.

INTERACTIONS OF POSITRONS AND POSITRONIUM WITH INORGANIC COMPOUNDS IN SOLUTION*

H. J. Ache,** R. E. Wild, L. J. Bartal
Department of Chemistry, Virginia Polytechnic Institute and State University
Blacksburg, Va. 24061, USA

Introduction

The interactions of the positron which is the antiparticle of the electron with matter have been studied for some time. However, in contrast to the negatively charged electron whose importance in the various aspects of radiation chemistry has been early and widely acknowledged, the role of the positron, its reactions, and the contribution it can make to radiation chemistry have only very recently been recognized.

Thus in the following a few aspects of the interactions of the positron and its possible interrelationship with electron interactions and in turn with radiation chemistry will be demonstrated.

Especially well suited for this purpose appears to be the positronium formation process.

Positrons are most commonly emitted as a result of the radioactive decay of a neutron deficient nuclide.

They lose their high kinetic energy in collisions with the surrounding matter until they reach thermal or near thermal energies at which point the cross-section for mass annihilation with an electron assumes a maximum value.

A certain fraction of these positrons, however, may enter the bound state of the positronium (Ps) which could be formed in two ground states either in the triplet or ortho state, with parallel spin orientation and an intrinsic average annihilation lifetime of 1.4×10^{-7} s, or in the singlet or para state with antiparallel spin orientation, which has an intrinsic average lifetime of 1.4×10^{-7} s.

The most widely accepted model for Ps formation is the Ore model which assumes that the positrons slowing down from higher energies pass through an energy gap in which Ps formation is possible. The lower boundary of this "Ore gap" is defined by the expression $V - I_{Ps}$, where V is the ionization of the surrounding molecules and I_{Ps} the ionization potential of Ps, 6.8 eV. If the kinetic energy of the positrons exceeds V it is assumed that ionization of the surrounding molecules

* Work supported in part by the U. S. Energy Research and Development Agency.
** Address correspondence to this author.

($e^+ + M \rightarrow M^+ + e^- + e^+$) becomes more probable than Ps formation ($e^+ + M \rightarrow M^+ + Ps$), so that V constitutes the upper boundary of the "Ore gap." Ps atoms can be formed in the Ore gap with kinetic energies of up to 6.8 eV and react as such or after being thermalized /1 - 8/.

The experimental results, however, suggest /1/ that not all positrons form Ps and several factors have been discussed which could interfere with and inhibit this process.

The Ore model /1/ is based on the simplified assumption that all positrons whose kinetic energy lies in the Ore gap produce Ps. In practice, however, the Ps formation process in the Ore gap has to compete with all other processes that can cause moderation of the positron to energies below the lower Ore limit. The most important of these are elastic and inelastic collisions with substrate molecules, the energy transferred in the second case possibly stimulating molecular vibrations and rotations. This category also includes processes that lead to positron capture by addition of positrons to the substrate molecule AB

$$e^+ + AB \rightarrow e^+ AB \text{ or } A + e^+B.$$

If the compound formation occurs above or within the Ore gap, the captured positrons are no longer available for the formation of Ps, the yield of which is therefore decreased.

A second model for Ps formation which has been recently suggested by Morgensen et al. /9 – 13/ and Byakov et al. /14 – 15/ is the spur reaction model. They assume that Ps is formed as a result of a spur reaction between the positron and a secondary electron in the positron spur. In this model a correlation should exist between the Ps formation probability and the availability of the electrons in the spur, that is to say that Ps formation must compete with electron–ion recombination and with electron and positron scavenging by the surrounding molecules, as well as with other processes.

A model which combines certain features of both models is Tao's, "modified spur model" /16/. In this model Tao considers both the possibility of combination of a positron with an electron created in the spur as well as the "direct" formation of a positronium, similar to the mechanism discussed in the Ore model, if the total kinetic energy of the resulting electron-positron pair is less than the potential energy between them (see Fig. 1 of Ref. /16/).

Since the processes mentioned here, such as elastic scattering, stimulation of molecular vibrations and rotations in the eV range, and the addition of low-energy electrons (or positrons) to molecules or generation of electrons in the spur and their subsequent reactions with scavengers, etc., are of the greatest importance to the understanding of elementary processes in radiation chemistry, it seemed as if it would be of interest to reinvestigate some of our previously reported experimental results /5–8/ in terms of the simple and modified spur reaction model.

Experimental

The experimental procedures were essentially the same as previously described /5–8/.

A. Positron lifetime measurements

Positron lifetime measurements were carried out by the usual delayed coincidence method. /1/ The resolution of the system as measured by the prompt time distribution of ^{60}Co source and without changing the 1.27 and 0.51 MeV bias was found to be less than 0.4 nsec FWHM. Data analysis was carried out by using conventional computional methods.

B. Purity and source of reagents

Information about the purity and source of the reagents can be found in the previous reports /5–8/ to which reference is made.

C. Preparation of samples

Specially designed sample vials for the concentration studies (cylindrical glass tubes 100 mm long and 10 mm i.d.) were filled with 0.5 ml of the pure solvent or solvent mixture to which was added about 5 μCi of carrier-free ^{22}Na (obtained from ICN) as NaCl or $NaHCO_3$. These samples were subsequently brought to the appropriate solute concentrations by adding known amounts of the individual compound either as solid or in the form of a highly concentrated solution, so that only minor volume changes occurred. Before the start of the lifetime measurements each sample vial was thoroughly degassed and sealed under vacuum. In several cases a minimum amount of HCl or $HClO_4$ was used to prevent precipitation of basic forms of tin. The lifetime measurements were carried out at room temperature.

D. Assessment of rate constants

The reaction rate constants for interactions can be obtained in the usual way from the positron lifetime spectra. It has been shown that the rate constants are related to the average lifetime of the thermal Ps atoms, as represented by the lifetime of the long-lived component, τ_2, in the positron time spectra, by the following equation /5–8/

$$K = (1/\tau_2 - 1/\tau_{solv}) / [S] \qquad (1)$$

τ_{solv} is the lifetime of the long-lived component in the positron time spectra with no solute present and [S] is the solute concentration.

I_2, the intensity of the longlived component, is given by the area under this component in the positron lifetime spectra.

Results and discussion

In the previous papers /5–8/ we have interpreted our experimental results in terms of the (modified) Ore gap model /3–8/.

It was assumed that the energetic o–Ps, which is formed in the Ore gap with kinetic energies varying between 6.8 eV and thermal energies, has, as any other "hot" atom, two alternatives – namely, it may undergo chemical reactions while still hot, followed by a rapid annihilation of the positron in the resulting reaction products, or lose its excess kinetic energy in moderating collisions, becoming a thermalized Ps-atom and reacting as such.

The thermalization time of Ps is sufficiently long so that the presence and the reactions of the thermalized Ps which lead to subsequent rapid annihilation of the positron can be recognized by the appearance of a second (long–lived) component in the time spectra, and the changes of the average lifetime, τ_2, associated with this component.

On the other hand, "hot" reactions between solute and Ps-atom have to take place shortly after the birth of the Ps before it becomes thermalized. Thus, the lifetime of the positrons incorporated in positronium atoms taking part in "hot" reactions will become indistinguishable from that of the free positrons or p-Ps, i.e. it will drop out of the second component and appear as a part of the short-lived component. The only observable evidence for the occurrence of such a hot reaction is then a reduction of the number of Ps-atoms reaching thermal energies. Since this number is related to the intensity, I_2, of the second component in the time spectra, hot reaction can be detected by a decrease of I_2.

By using this approach it was found that in aqueous solutions of inorganic ions where the rate constant for the reaction between Ps and solute remains close to or below the detectable limit (10^7 1/mole · second), i.e. where reactions of thermal Ps are extremely slow, I_2 eventually assumes a lower limit (or saturation value), $I_2^{sat} \neq 0$, which is characteristic for each individual compound (Fig. 2) /5/.

This result was interpreted by assuming that $(I_2^0 - I_2^{sat})/I_2^0$ represents the fraction of all Ps-atoms formed which have sufficient energy to overcome the reaction barrier (I_2^0 = intensity in pure solvent).

By correlating the I_2^{sat} in the various systems to the free-energy changes involved in the reduction of the inorganic ion ($A_{aq}^{n+} + e^- \rightarrow A^{(n-1)+}$) (see Fig. 3) by the Ps the redox potential of the Ps atom was roughly approximated /17/.

If one wants to interpret the experimental results in terms of the simple spur reaction model one would have to consider the competition between positron and electron combination and the reaction of the electron with the scavenger (inorganic ions).

Thus in analogy with the approach used by Hamill /18, 19/ and several other authors for a simple competition for dry or solvated electrons in a solution one could derive the following correlation between the o-Ps formation probability P at

a given solute concentration [M], if the o-Ps formation probability in the pure solvent is P^o:

$$P = P^o/(1 + K[M]) \tag{1}$$

where K is the rate constant for inhibition of o-Ps formation.

If the solute is also capable of undergoing chemical reaction with thermal o-Ps (rate constant K_1) and if the thermal o-Ps annihilation with solvent is λ_p, and furthermore the annihilation rate of the free positrons in solution is λ_F, then the following expression can be obtained for the intensity I_2 and the Ps formation probability P:

$$I_2 = \frac{3}{4}P(1 + K_1[M]/(\lambda_F - \lambda_P - K_1[M])) \tag{2}$$

In a pure solvent (intensity I_2^o)

$$I_2^o = \frac{3}{4}P \tag{3}$$

Substitution of Eqs 2 and 3 into Eq. 1 results /20/ in

$$I_2 = \frac{I_2^o(\lambda_F - \lambda_P)}{\lambda_F - \lambda_P + ((\lambda_F - \lambda_P)K - K_1)[M] - KK^1[M]^2} \cdot \tag{4}$$

In water: λ_F est) $2.50 \times 10^9 x^{-1}$ $\quad I_2 = 28\%$

λ_p(obs) $0.54 \times 10^9 s^{-1}$

K_1 can be obtained from the well known correlation between the lifetime τ_2 of the longlived component in the positron lifetime spectra and the solute concentration. In dilute solutions:

$$1/\tau_2 \equiv \tau_2 = \tau_p + K_1[M] \tag{5}$$

Thus by determining I_2 at various solute concentrations [M], the rate constant K for inhibition of Ps formation can be derived.

If the solute only weakly reacts with thermal o-Ps, i.e. $K < 10^8 s^{-1}$. and if in the case of relatively small solute concentrations, i.e. [M]<1M, $K_1[M]$ and $K_1K[M]^2$ be considered as insignificant compared with $(\lambda_F - \lambda_p)$

and $(\lambda_F - \lambda_p)$ K [M] respectively, Eq. 4 can be simplified and rewritten to give

$$\frac{I_2^o}{I_2} - 1 = K\ [M] \qquad (6)$$

Plots of this function for various aqueous solutions containing solutes which exhibit only a weak reactivity towards thermal Ps are shown on Fig. 4.

The K values assessed from these plots are summarized in Table 1 and plotted in Fig. 5 on a logarithmic scale as a function of $-\Delta G^o$ for the one electron transfer process.

As can be seen from this figure a reasonable correlation exists between the free energy changes and the inhibition constants K.

Table 1

Ion	$K(M^{-1})$	$K(e^-aq)\ M^{-1}s^{-1}$ /22/
Pb^{++}	2.5	3.9×10^{10}
Sn^{++}	1.2	3.4×10^{9}
Cd^{++}	0.37	5.2×10^{10}
Ag^{+}	0.35	3.2×10^{10}
H^{+}	0.22	2.4×10^{10}
Tl^{+}	0.10	3.7×10^{10}
Zn^{++}	0.10	1.3×10^{9}
Na^{+}	0.05	$< 10^{5}$
NO_3^-	3.5	1.1×10^{10}

No apparent correlation, however, seems to exist between the inhibition constants K and the reported rate constants for the reactions of hydrated electrons (Table 1) with these compounds, which makes an interpretation of the observed inhibition in terms of a competition for solvated electrons between positron and scavenger, i.e. the inorganic ions, rather unlikely.

Another possibility would involve the combination of dry electrons and positrons, in which case scavenger and positron compete for the dry electrons. Unfortunately very little is known about the rate constants of dry electron reactions so that no satisfactory comparison can be made /23, 24/. In the cases for which the relative activities of the dry electrons toward the scavenger are known, generally a good agreement exists /16, 25, 26/. One may therefore, argue that most Ps formation and inhibition takes place within a few psec. If this assumption should prove to be correct and if indeed the positron reacts with dry electrons to form Ps, these Ps inhibition studies should reveal valuable information about the reactions of dry electrons with chemical compounds.

The correlation between the inhibition constants K and free energy for the one electron transfer process (Table 1) is interesting. It could be interpreted by assuming that the maximum of the cross section curve for electron attachment to the scavenger ions is closely related to the free energy change involved in this process:

$$A^{+}_{aq} + e^{-}_{dry} \rightarrow A^{(n-1)+}_{aq.}$$

It could however be also explained by invoking the modified spur model /16/. In this case one could argue that the cross section curve for attachment of Ps to these inorganic ions, resulting in Ps complex formation /26/ or electron transfer, shows certain maxima which coincide with the $-\Delta G$ values for the one electron transfer.

Experiments are presently carried out in our laboratory to clarify this issue.

References

/ 1/ For general references, see (a) J. Green and J. Lee, Positronium Chemistry, (Academic, New York, 1964): (b) V. I. Goldanskii, At. Energy Rev. 6, 3 (1968): (c) J. D. McGervey in Positron Annihilation, edited by A. T. Stewart and L. O. Roellig (Academic, New York, 1967), p. 143: (d) J. A. Merrigan, S. J. Tao, and J. H. Green, Physical Methods of Chemistry, edited by A. Weissberger and B. W. Rossiter (Wiley, New York, 1972), Vol. 1, Part III. D: (e) H. J. Ache, Angew. Chem., Int. Ed. Engl. 11, 179 (1972): (f) J. H. Green, MTP International Review of Science Radiochemistry Vol. 8, edited by A. G. Maddock, (Butterworth, London, 1972), p. 251: (g) V. I. Goldanskii and V. G. Virsoc, Ann. Rev. Phys. Chem. 22, 209 (1971).

/ 2/ J. E. Jackson and J. D. McGervey, J. Chem. Phys. 38, 300 (1963).

/ 3/ S. J. Tao and J. H. Green, J. Chem. Soc. 1968 A, 408.

/ 4/ S. J. Tao and J. H. Green, J. Phys. Chem. 73 (1969) 882.

/ 5/ L. J. Bartal, J. B. Nicholas and H. J. Ache, J. Phys. Chem. 76, 1124 (1972).

/ 6/ L. J. Bartal and H. J. Ache, Radiochim. Acta 17, 205 (1972).

/ 7/ L. J. Bartal and H. J. Ache, Radiochim. Acta 19, 49 (1973).

/ 8/ H. J. Ache, in "Hot Atom Chemistry Status Report" IAEA, Vienna 1975, p. 81–105.

/ 9/ O. E. Mogensen, J. Chem. Phys. 60, 998 (1974).

/10/ P. Jansen, M. Eldrup, O. E. Mogensen and P. Pagsberg, Chem. Phys. 6, 265 (1974).

/11/ M. Eldrup, V. P. Shantarovich and O. E. Mogensen, Chem. Phys. 11, 129 (1975).

/12/ P. Jansen, M. Eldrup, B. Skytte Jensen and O. E. Mogensen, Chem. Phys. 10, 303 (1975).

/13/ O. E. Mogensen, App. Phys. 6, 315 (1975).
/14/ V. M. Byakov, V. I. Goldanskii and V. P. Shantarovich, Dokl. Akad. Nauk SSSR, 219, 1090 (1974).
/15/ V. M. Byakov, Int. J. Radiat. Chem. 8, (1976) 283.
/16/ S. J. Tao, Appl. Phys. 10, (1976) 67.
/17/ L. J. Bartal and H. J. Ache, J. Inorg. Nucl. Chem., 36, 922 (1974).
/18/ W. H. Hamill, J. Phys. Chem. 73 1341 (1969).
/19/ T. Sawai and W. H. Hamill, J. Phys. Chem. 74, 3914 (1970).
/20/ This equation is identical with the formula used by A. G. Maddock et al. (Ref. /21/) to interpret their experimental results on Ps inhibition by halo-acetates.
/21/ A. G. Maddock, J. Ch. Abbee and A. Haessler, Chem. Phys. (in press).
/22/ M. Anbar and P. Neta, Int. J. Appl. Rad. Isotopes 18, 493 (1967).
/23/ For a review on dry electrons see e. g, G. Czapski and E. Peled in Proc. Fifth Int. Cong. Radiation Research ed. by O. F. Nygaard, H. I. Adler and W. K. Sinclair, Academic Press 1975, p. 356 et seq.
/24/ K. Y. Lam and J. W. Hunt, Int. J. Rad. Phys. Chem. 7, 317 (1975).
/25/ I. A. Abramenkova, L. T. Bugaenko and V. M. Byakow, Int. J. Radiat. Phys. Chem. 8, (1976) 325.
/26/ see e. g. W. J. Madia, A. L. Nichols and H. J. Ache, J. Amer. Chem. Soc. 97, (1975) 5041.

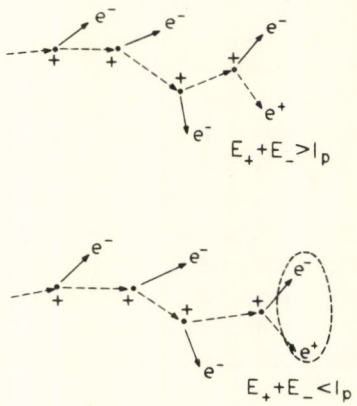

Fig. 1 Schematic pictures showing the positron in the "spur" produced by its last ionization act: upper, the combined kinetic energy of any positron-electron pair is greater than the coulombic attractive force: lower, the combined kinetic of a positron-electron pair is less than the coulombic attractive force (E_+ and E_-: total energies of positron and electron, Ip: ionization potential of positronium) (Ref. 16)

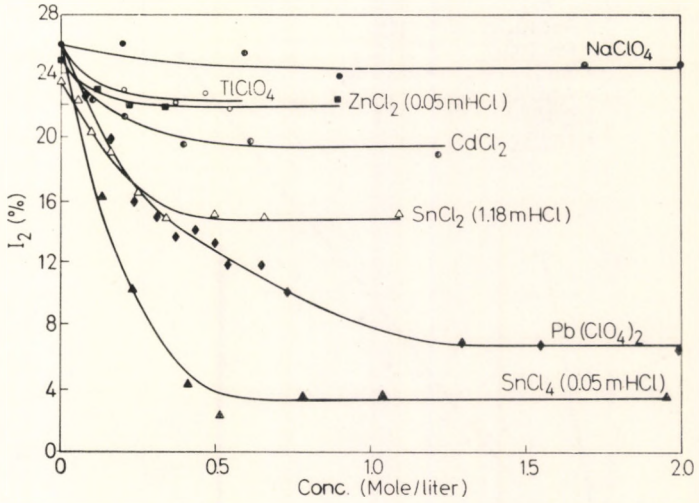

Fig. 2 I_2, the intensity of the long-lived component plotted as a function of solute concentration in aqueous solutions of inorganic ions

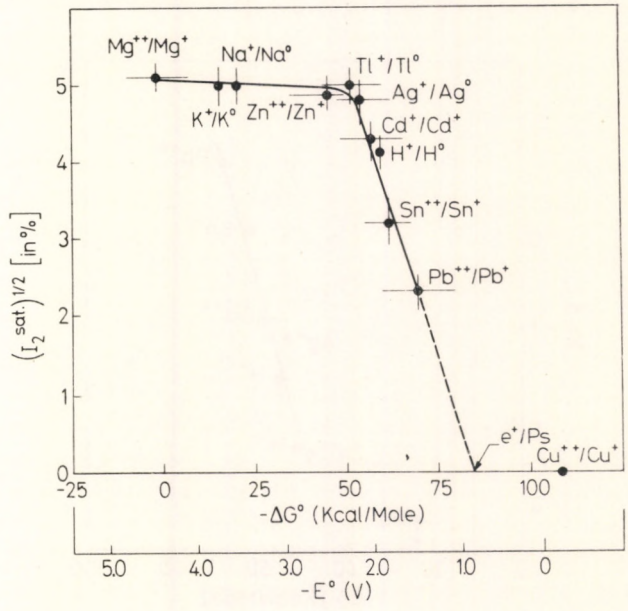

Fig. 3 I_2^{sat} vs $-\Delta G^{o}$, the change of free energy in the process $A_{aq}^{n+} + e^{-} \rightarrow A_{aq}^{(n-1)+}$

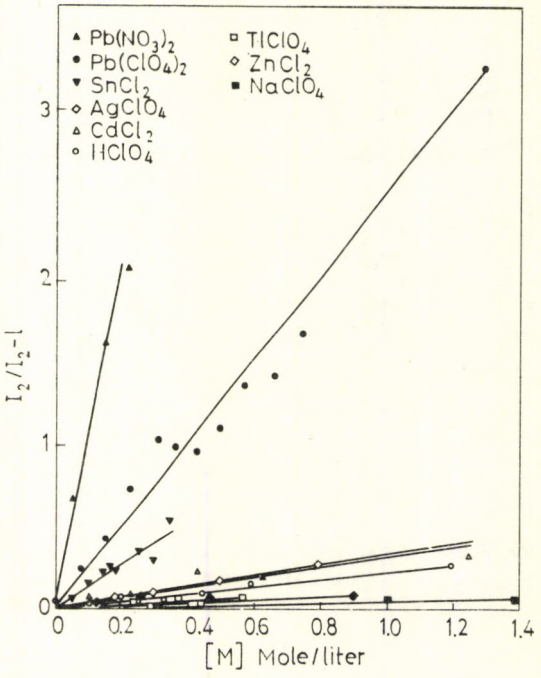

Fig. 4 $I_2/I_2^0 - 1$ vs K [M] in aqueous solutions of inorganic compounds

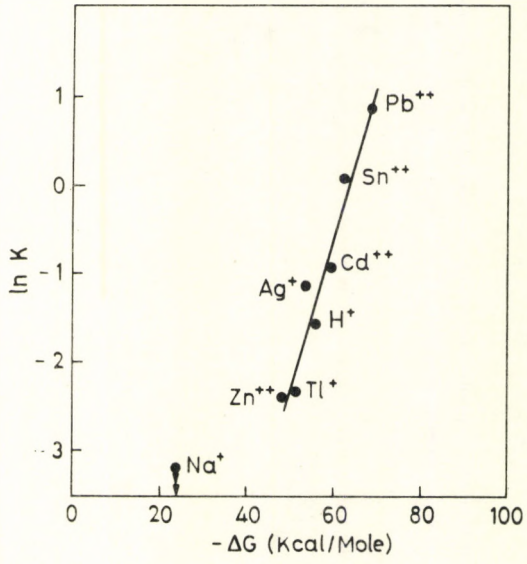

Fig. 5 ln K vs $-\Delta G$ for $A_{aq}^{n+} + e^- \rightarrow A_{aq}^{(n-1)+}$ for various ions in aqueous solutions

B. LÉVAY

Did you investigate the effect of anions on the inhibition of Ps-formation in aqueous solutions? Cl^- ions, for instance, can contribute to the inhibition of Ps-formation (see Lambrecht's recent results!).

H. J. ACHE

We investigated the effect of NO_3^- as dicussed in our paper. However, we did not include other oxyanions in our study because we tried to correlate the observed inhibition constants with the free energy for one electron transfer. While in the case of simple cations this latter mechanism is rather simple, in the case of oxyanions other processes, such as addition of the electron and secondary decomposition, etc. may occur which could obscure the primary step.

So far as the Cl^- ion is concerned, one has to use relatively highly concentrated solutions to see a significant inhibition effect. We feel that the models used in this study are better applicable to highly diluted solutions.

G. R. FREEMAN

How were the energies of the single electron transfer reactions estimated?

H. J. ACHE

Some of them, such as Na^+/Na^0, Ag^+/Ag^0 were estimated from their standard redox potentials taking into account that, because of the few atoms involved, no metallic phase is formed, i.e. to say that corrections have been made for the sublimation energy, which is not available for these reactions.

The other free energies were estimated by using Baxandale's method.

COMPARISON OF THE RADIOLYTIC AND PHOTOLYTIC PRODUCT FORMATION OF THE CT-COMPLEX BENZENE-FUMARIC-NITRILE

H. Heusinger, P. Schuler
Institute for Radiochemistry of the Technical University of Munich, Munich, FRG

Photochemical substitution and cycloaddition reactions of derivatives of maleic acid with benzene and cyclohexene are reported in the literature. In the system cyclohexene-maleic-anhydride for example, the cycloaddition product II and the substitution product cyclohexene-2-succinic-anhydride I are formed simultaneously /1/:

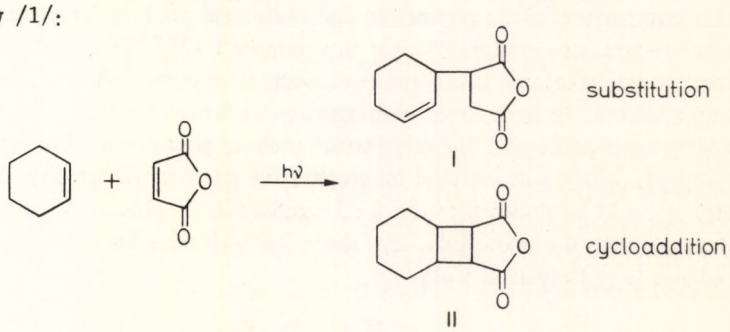

In the system benzene-maleic-anhydride the cycloaddition is followed by a Diels--Alder addition of maleic-anhydride to the diene leading to the 2:1 adduct /IV/ /2/.

The substitution product phenyl-succinic-anhydride V is only produced in the presence of a strong acid /2/:

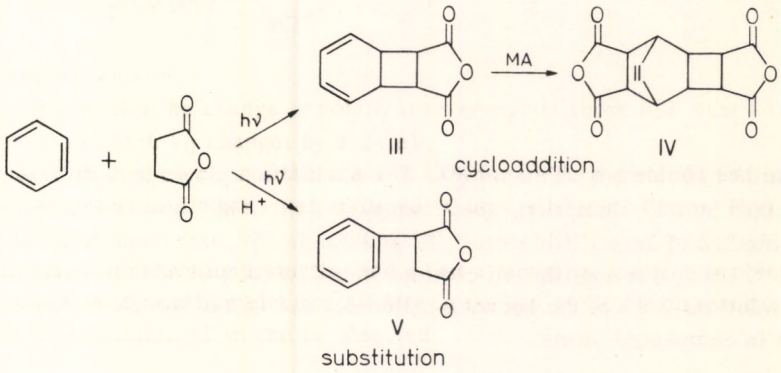

Cyclohexene and benzene form CT-complexes with maleic anhydride. By selective excitation Bryce-Smith /2/ and Barltrop /1/ showed that the product formation is due to the excitation of the CT-complex. These authors assumed that the radical ion pair, which corresponds to the excited CT-complex, forms the cycloaddition product by successive recombination of the radicals and ions. The formation of the substitution product must be due to a proton transfer reaction.

Contrary to the photochemical situation in radiation chemistry, the initial species are radical ions, electrons and highly excited states. It seems plausible, however, to presume that recombination of positive and negative radical ions, the latter being formed by electron addition to acceptors, can recombine to radical-ion pairs. These radical-ion pairs should lead to the same products as in photochemistry. In comparison to the extensive photochemical work only a few radiation chemical investigations have been performed on these systems. Some similarities in the radiolytic and photolytic product formation of the maleic anhydride-benzene system were observed by Racizewski /3/. In order to obtain more information on the mechanism of the radiation induced reactions of derivatives of maleic acid with benzene, we carried out a comparison of the photolytic and radiolytic product formation of the system benzene-fumaric-nitrile (FN). For this purpose 5×10^{-2} molar solutions of FN in benzene were irradiated using either a medium pressure mercury lamp or a Co^{60} -gamma source. In both cases isomerisation of fumaric nitrile (FN) to maleic nitrile (MN) takes place and the substitution product phenyl-succinic-dinitrile (PSDN) is formed, which was isolated by preparative gaschromatography. By mass spectrometry it could be shown that the 2 : 1 cycloaddition product VI is formed in very small amounts in the photolysis, and there was evidence for the existence of this 2 : 1 adduct in radiolysis as well:

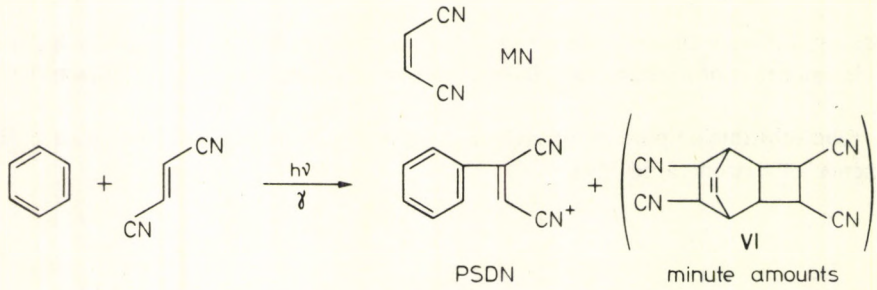

Benzene and FN form a CT-complex. The equilibrium constant of this complex, determined by UV-absorption, spectroscopy and H'-NMR spectroscopy according to the method of Benesi Hildebrand /4/ and Hanna /5/, was found to be 0.161 x x mole^{-1}. Using this equilibrium constant it can be calculated that in our 5×10^{-2} molar solutions 0.3% of the benzene molecules and 65% of the FN molecules are present in complexed form.

In the photolysis excitation of benzene, FN and excitation of the CT-complex have to be considered for product formation.

$$C_6H_6 + FN \rightleftharpoons \text{CT-complex} \xrightarrow{h\nu_{CT}} \text{complex}^* \longrightarrow \text{products (a)}$$

$$C_6H_6^* + FN \longrightarrow \text{products (b)}$$

$$FN^* + C_6H_6 \longrightarrow \text{products (c)}$$

$$FN^* + C_6H_6^* \longrightarrow \text{products (d)}$$

Due to the low concentration of FN and the position of its absorption band (λ_{max} = 233 nm) light absorption in FN can be neglected in comparison to that in benzene. This excludes product formation by reactions (c) and (d). The relative importance of reaction (a) and (b) can be obtained from the effect of filtering. Filtering was done by using ampoules of Pyrex glass instead of quartz. The u. v. spectrum of benzene, transmittance of the filter, emission characteristics of the lamp and absorbance of the complex are shown in Fig. 1.
From the data given in Fig. 1, the following can be calculated, for irradiation with unfiltered light:

$$\frac{\text{light absorbed by the CT-complex}}{\text{light absorbed by the solvent benzene}} = 0.066$$

Using pyrex glass as filter light absorption in benzene is excluded and

$$\frac{\text{light absorbed by the complex filtered experiment}}{\text{light absorbed by the complex unfiltered experiment}} = 0.039$$

The yield of products should be proportional to the light absorbed by the species responsible for product formation.
In the case that only light absorbed by the complex leads to products

$$\frac{\text{product formation filtered}}{\text{product formation unfiltered}} = 3.9 \times 10^{-2}$$

In the case that light absorbed by benzene and light absorbed by the complex leads to product formation

$$\frac{\text{product formation filtered}}{\text{product formation unfiltered}} = 3.9 \times 10^{-2} \times 6.6 \times 10^{-2} = 2.5 \times 10^{-3}$$

The experimental values (obtained from the initial slopes of the production curves) for these ratios are:

$$
\begin{aligned}
-\ \mathrm{FN} &= 2 \times 10^{-2} \\
+\ \mathrm{MN} &= 2.3 \times 10^{-2} \\
+\ \mathrm{PSDN} &= 3 \times 10^{-2}
\end{aligned}
$$

A comparison of the experimental values with the calculated values shows FN conversion as well as MN and PSDN formation to occur predominantly via excitation of the CT-complex (reaction a). Excitation transfer from the benzene triplet, which is produced by intersystemcrossing with a probability of about 0.5 /6/ from excited benzene singlet, to FN cannot contribute significantly (reaction b). Light absorbed by benzene in the unfiltered experiment leads to diphenyl and cyclohexadienes. In the filtered experiment these compounds are not produced.

The reported results can be rationalized best by assuming that excitation of the CT-complex benzene-FN is followed either by photodissociation or by product formation.

Photochemical trans-cis isomerisation reactions in aromatic solvents are usually explained by the transfer of triplet energy from the aromatic compound to the olefinic bond. This explanation does not work in our case because isomerisation of FN occurred with filtered light too, where benzene is not excited. In our case isomerisation must be due to photodissociation. In contrast to FN there is free rotation about the central C-C-bond in the FN-anion so that isomerisation can occur.

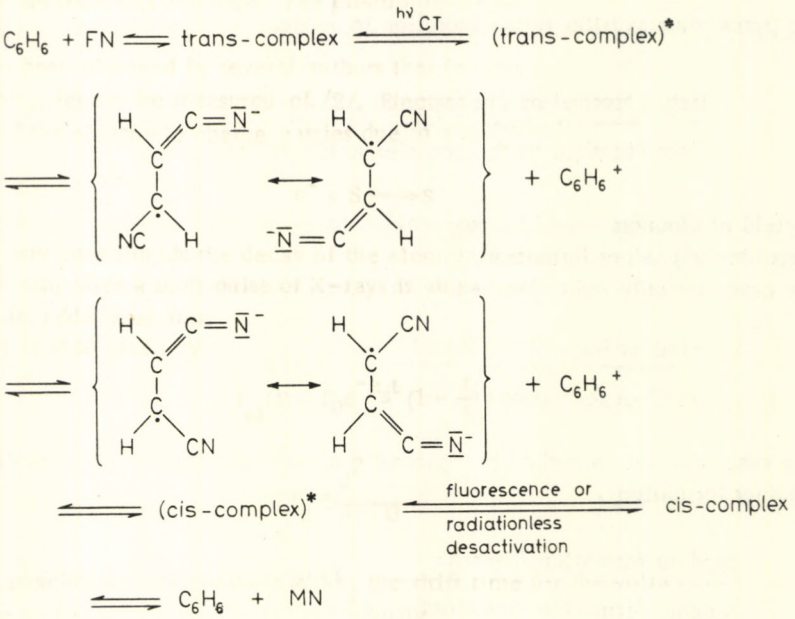

The ratio of PSDN formed using filtered and unfiltered light shows that this compound too is formed via the excited CT-complex. In this respect the system benzene-FN behaves analogous to the systems benzene-maleic anhydride but contrary to the latter system, where cycloaddition takes place, in benzene-FN substitution predominates and the cycloaddition product is found merely in minute amounts.

According to Barltrop /1/ and Bryce-Smith /2/, in the case of cyclohexene-maleic anhydride and benzene-maleic-anhydride, the excited charge transfer complex forms a zwitter ion or biradical in the first step. The second step is cycloaddition or proton transfer from the donor to the acceptor.
Proton transfer therefore should be responsible for PSDN formation.

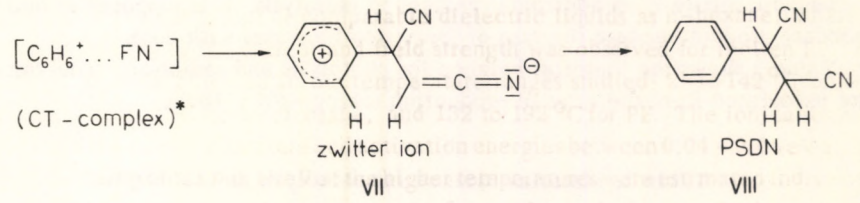



This is supported by the result that PSDN-d_6 IX is produced when benzene d_6 is used.

The results of the photolytic investigations have shown that the production of PSDN and the isomerisation of FN are typical reactions of the excited CT-complex. These products are also formed in radiolysis. Furthermore, the use of benzene-d_6 gives rise to the same sixfold deuterated PSDN molecule IX as in the photolytic process, thus indicating that in radiolysis also the postulated mechanism via the zwitter ion should be effective. Product formation by excitation transfer from triplet benzene to FN or the CT-complex is unprobable, because it was shown not to be effective in photolysis. In radiolysis the zwitter ion cannot be formed via direct excitation of the CT-complex because only 0.3% of the benzene is complexed in a 5×10^{-2} molar solution of FN. The solvent benzene will be ionised and the electrons will either recombine with the positive ions or be captured by FN. The formation of radical ion pairs by recombination of the positive radical ions of benzene with the negative radical ions of FN would explain the analogy in photo- and radiation-induced production formation.

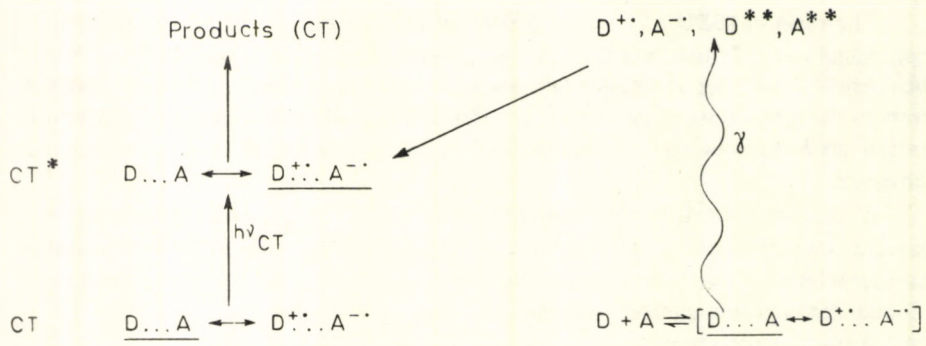

Benzoic nitrile is an additional product in radiolysis. It is supposed as being a secondary product because the rate of formation increases with dose.

Table 1 shows the material balance for photolysis and radiolysis. The values were calculated from the rates of production taking −FN = 100%.

Table 1: Material Balance for photolysis and radiolysis

Product	Photolysis unfiltered	Photolysis filtered	Radiolysis
	%	%	%
−FN	100	100	100
+MN	33.3	38.9	26.5
+PSDN	2.7	4.1	0.65
MN+PSDN	36	43	27.2
unidentified products	64	57	72.8

In the sequence photolysis filtered, photolysis unfiltered, radiolysis, there is a steady decrease in the percentage of the consumed FN which can be redetected in well defined products, the shortfall being 57%, 64% and 73% in photolysis filtered, photolysis unfiltered and radiolysis, respectively. Even by exclusive excitation of the CT−complex, another reaction channel for FN must exist which leads to unidentified products. It is supposed that this reaction channel results in some kind of polymer. It could be shown that FN reduces diphenyl formation in photolysis and both diphenyl and cyclohexadiene formation in radiolysis. This suggests that the additional shortfall in photolysis unfiltered and radiolysis in comparison to photolysis filtered is due to reactions of FN with intermediates of benzene photolysis or radiolysis. This reaction should also lead to high molecular weight compounds, because besides PSDN, the 2:1 adduct, and benzoic nitrile no other products could be detected by gaschromatography and mass spectrometry.

Conclusions

Both in photolysis and in radiolysis of the system benzene –FN isomerisation of FN to MN and production of PSDN are observed. In the case of photolysis it could be established that these reactions proceed via the excited CT–complex. There are indications that the excited CT–complex is likewise an intermediate in the radiolytic formation of these nitriles.

References

/1/ J. A. Barltrop, R. Robson, Tetrahedron Letters No. 9, 597 (1963);
R. Robson, P. W. Grubb, J. A. Barltrop, J. Chem. Soc. 2153 (1964).
/2/ D. Bryce–Smith, Pure Appl. Chem. 16, 47 (1968).
/3/ Z. Racizewski, J. Chem. Soc. (B) 1147 (1966); (B) 1253 (1967).
/4/ H. A. Benesi, J. H. Hildebrand, J. Am. Chem. Soc. 71, 2703 (1949).
/5/ M. W. Hanna, A. L. Ashbaugh; J. Phys. Chem. 86, 811 (1964).
/6/ A. Gregory, S. Lipsky, Int. Luminescence Symposium p. 160, ed. N. Riehl, H. Kallmann, München 1966.

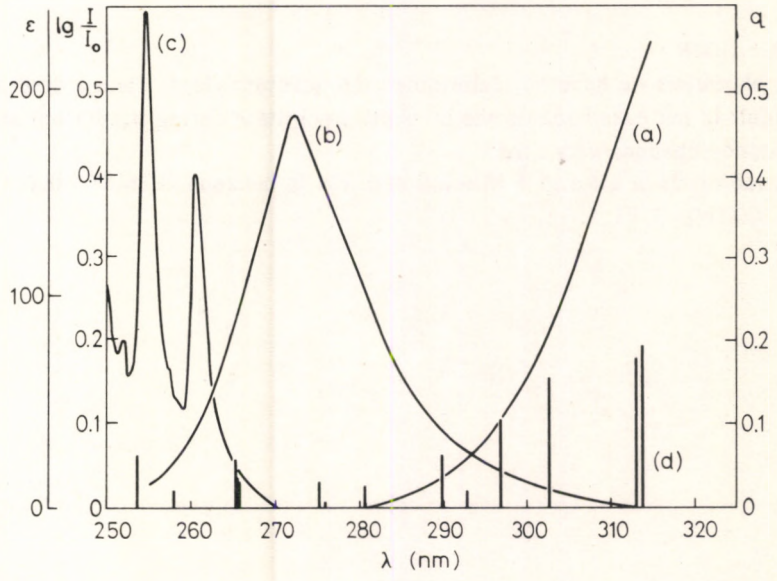

Fig. 1
a/ Transmittance of the pyrex filter (a)
b/ Absorbance of the complex benzene–FN ($\log \frac{I}{I_0}$)
c/ UV spectrum of benzene (ε)
d/ Emission characteristic of the lamp, given in arbitrary units

G. ZIMINA

Did you determine the extinction coefficient $\varepsilon(\lambda_{max})$ of the complex? What is the oscillator strength, is this a strong or a weak complex?

Does the spectrum of the cis-complex differ from that of the trans complex?

H. HEUSINGER

The extinction coefficient and the constant of the complex formation K were determined by the method of Benssi and Wildebrand: the values are published in J. Mol. Struct. 28, 23 (1975).

Benzene and FN form a CT-complex of medium strength, K = 0.7 (for comparison: benzene tetracyano ethylene K = 10.7, benzene maleic anhydride K = 2.7). λ_{max} for the cis and trans complexes are almost the same ($\sim$274)

L. GUCZI

What is the efficiency of converting molecules per energy absorbed in both cases?

H. HEUSINGER

In photolysis we have not determined the quantum yield. Such a determination is difficult in our case because the products precipitate during irradiation so that the transparency changes with time.

In radiolysis of a 5×10^{-2} M solution of FW in benzene G(PSDN) = 0.015, G(-FW) = = 2.3, G(MW) = 0.61.

GAS-PHASE REACTIVITY OF RADIOLYTICALLY FORMED BRØNSTED ACIDS TOWARD AROMATIC HALOGENATED SUBSTRATES

Maurizio Speranza, Fulvio Cacace*
Laboratorio di Chimica Nucleare, C. N. R., Monterotondo Stazione (Rome) Italy
and
*Università di Roma, Rome, Italy

In the last decade, the study of ionic reactions in the gas phase has received a considerable boost of interest due to the introduction of new experimental techniques /1-4/ that, in contrast with the classical mass-spectrometric approach, allow the isolation of the final neutral products, the determination of their structural and stereochemical features, and the extension of the kinetic methods, typical of solution chemistry, to the gas phase, where solvation, ion-pairing and other complicating factors are entirely eliminated. The substrate and positional selectivity of electrophiles, such as HeT^+ /5-7/, D_2T^+ /8, 9/, CH_4T^+ /10/, 80_{Br}^+ /11/, and several alkyl cations /12-16/, toward a number of organic molecules has been measured. Among the substrates investigated, halobenzenes have received particular attention /6, 9/ because of their peculiarity of directing the electrophilic attack toward two distinct nucleophilic centres, i. e. the π-systems of the aromatic ring and the n-electrons of the halogen(s). The present paper describes the mechanisms of the gas-phase reactions following the proton transfer from radiolytically-formed very strong Brønsted acids, as D_2T^+ and CH_5^+, to halogenated aromatic substrates.

Experimental

Evacuated bulbs, containing D_2 (DT) or CH_4 gas (760 torr), O_2 (2 torr) and the aromatic substrate (5-10 mg), were irradiated with ^{60}Co γ-rays at a dose rate of 0. 7 Mrad hour $^{-1}$. After receiving doses ranging from 1 to 10 Mrad, as determined with a Fricke dosimeter, the gaseous mixtures were analysed by gas-liquid chromatography.

Results and discussion

The gaseous Brønsted acids were obtained by techniques analogous to those introduced by Ausloos and co-workers /4/, based on the γ-radiolysis of systems containing a large excess of an appropriate gas, the aromatic compound in concentrations small enough to reduce its direct radiolysis to a negligible extent, and oth-

Table 1

Tritiated Products from the Gas-Phase Attack of D_2T^+ on Halo- and Dihalo-benzenes

Substrate	Relative yields of Tritiated Products[a]					
	Tritiodeprotonated Products			Dehalogenated Products		
M	[M+T−H]			[M+T−F]	[M+T−Cl]	[M+T−Br]
Fluorobenzene	58.9%			41.1%	–	–
Chlorobenzene	98.9%			–	1.1%	–
o-Difluorobenzene	o:53.5%	m:0.6%	p:0.1%	45.8%	–	–
m-Difluorobenzene	o: 0.2%	m:44.2%	p: 0.2%	55.4%	–	–
p-Difluorobenzene	o: 0.1%	m: 0.4%	p:61.1%	38.5%	–	–
o-Chlorofluorobenzene	o:70.7%	m: 3.6%	p: 1.6%	20.8%	3.3%	–
m-Chlorofluorobenzene	o: 0.8%	m:63.1%	p: 1.2%	27.7%	7.2%	–
p-Chlorofluorobenzene	o: 0.9%	m: 4.9%	p:71.5%	20.2%	2.4%	–
o-Bromofluorobenzene	o:61.7%	m: 7.9%	p: 9.7%	11.4%	–	9.2%
m-Bromofluorobenzene	o: 1.1%	m:64.4%	p: 1.5%	28.4%	–	4.5%
p-Bromofluorobenzene	o: 1.6%	m: 9.7%	p:63.0%	23.2%	–	2.4%
o-Dichlorobenzene	o:87.8%	m: 8.9%	p: 1.4%	–	1.9%	–
m-Dichlorobenzene	o: 0.6%	m:87.8%	p: 1.0%	–	10.6%	–

a) Referred to the combined activity of all tritiated aromatic identified. Standard deviation ca. 10%.

er additives, including a thermal radical scavenger (O_2) and a gaseous base, when required.

The radiolysis of the D_2/DT mixture produces D_2T^+ ions by the well-established /17, 18/ two-step mechanism:

$$D_2 \rightsquigarrow D_2^+ + e \qquad /1/$$

$$D_2^+ + DT \longrightarrow [D_2T^+]^{**} + D \qquad /2/$$

The excited $[D_2T^+]^{**}$ ions are thermalized by a large number of unreactive /19/ collisions with D_2 molecules:

$$[D_2T^+]^{**} \xrightarrow[\text{fast}]{+D_2} [D_2T^+]^{*} \xrightarrow[\text{slow}]{+D_2} [D_2T^2]_{\text{ground}} \qquad /3/$$

1–5 collisions 10–100 collisions

The relative yields of the tritiated final products from the gas-phase attack of the D_2T^+ ions on selected halo- and dihalo-benzenes are listed in Table 1.

The major features emerging from the experimental data can be summarized as follows:

i) tritiodeprotonation, isomerization, and dehalogenation reactions are promoted by the exothermic attack of D_2T^+ on the substrates;

ii) The extent of dehalogenation vs tritiodeprotonation is strongly dependent on the nature of the leaving halogen, increasing in the order: $Br \simeq Cl \ll F$,

iii) An opposite dependence ($F \ll Cl < Br$) of the extent of isomerization in function of the nature of the migrating halogen is observed;

iv) The nature and the position of the other halogen in the dihalobenzene systems show generally an appreciable effect both on the dehalogenation and on the isomerization reactions. It is also evident that when the influence of a given halogen substituent increases the rate of the first process, it decreases the extent of the latter, and vice versa.

Owing to the presence of two distinct nucleophilic centres in the halobenzenes, the attack of the D_2T^+ ions can promote two major processes:

(A) Attack to the π-system of the ring leading to the formation of isomeric haloarenium ions:

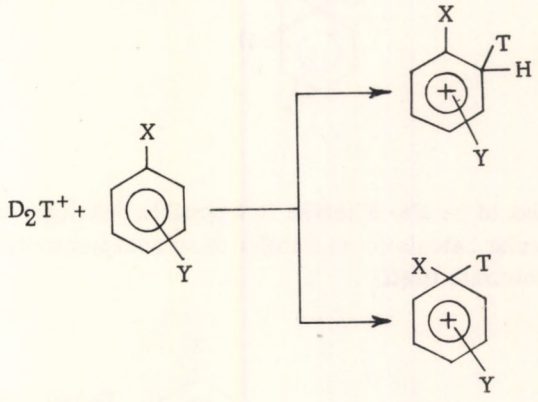

Before collisional stabilization, the excited ions are likely to undergo fast intramolecular proton shifts and, for X = Cl or Br, slower 1⟶2 intramolecular halo-

gen shifts. Eventually, the halobenzenium ions lose a proton to a gaseous base (B), either deliberately added to the system, or formed from its radiolysis:

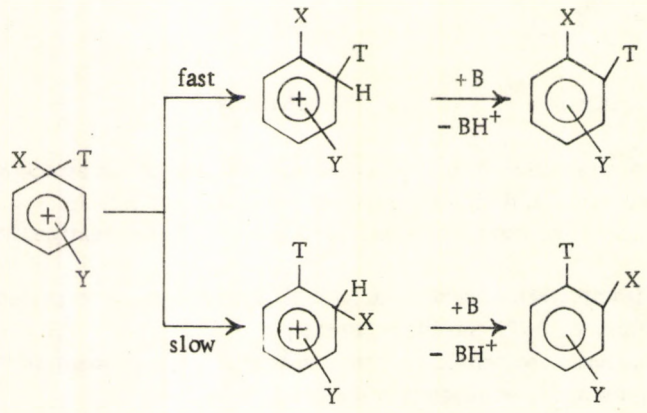

(6)

(7)

The observed migratory aptitude of the halogens, increasing in the order F≪Cl<Br, can be rationalized taking into account the nature of the suggested transition state, where the shifting halogen is necessarily characterized by a certain degree of positive polarization. Thus, the activation energy for the isomerization is expected to depend critically on the ability of the halogen to become positively polarized, which is lowest for F and increases passing to Cl and Br:

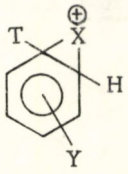

(8)

A similar trend should be also observed in a possible dehalogenation process involving an intermolecular halonium ion transfer to an acceptor molecule A, including the halogenated substrate itself:

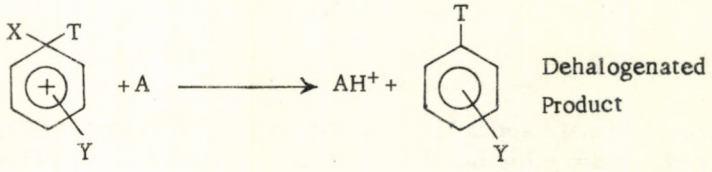

Table 2

Relative yields [a] of the dehalogenation products [M + T - X] in function of the electrophile E

Products \ Electrophile E	$E = {}^3HeT^+$	$E = D_2T^+$
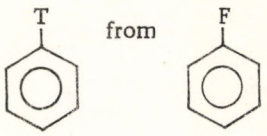	<0.3	69.8
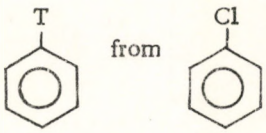	4.9	1.1
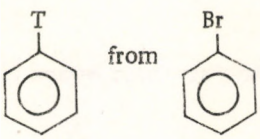	11.7	n.d.

a) Relative yields: $\dfrac{[M + T - X]}{[M + T - H]} \times 100$

As a matter of fact, as shown in Table 2, a $F \ll Cl < Br$ trend has been observed in the $^3HeT^+$ induced dehalogenation of halobenzenes /6/, which has been interpreted with a process similar to /8/. In this case, the particular reaction conditions, reported in Table 3, could not bring out any other dehalogenation mechanism, except for a direct tritiodehalogenation process analogous to the sequence /5/⟶/8/. Owing to the favourable experimental conditions, it is possible to observe in the D_2T^+ systems, a novel dehalogenation process, induced by the:

(B) Attack on the n-electrons of the halogen substituent, competitive with the attack to the ring. The reaction can proceed either via direct halide-ion abstraction,

Table 3

Experimental conditions in $^3HeT^+$, D_2T^+, and CH_5^+ induced dehalogenation reaction

	C_6H_5X [a]	T_2 [b]	D_2 [a]	O_2 [a]	CH_4 [a]
$^3HeT^+$	250	2	–	15	–
D_2T^+	ca. 1	43	758	2	–
CH_5^+	ca. 1	–	–	2	758

a) Torr

b) mCi

Table 4

$G_{(Products)}$ Values [a] of the Dehalogenated Products from the Gas-Phase Attack of RH^+ (R = CH_4, C_2H_4) on Halobenzenes

Substrates \ Products		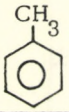
	0.6	43.5
	19.1	0.5
	25.5	1.4

a) G values x 10^2

or via the dissociation of an intermediate phenyl-halonium ion formed from the attack of the electrophile on the halogen substituent:

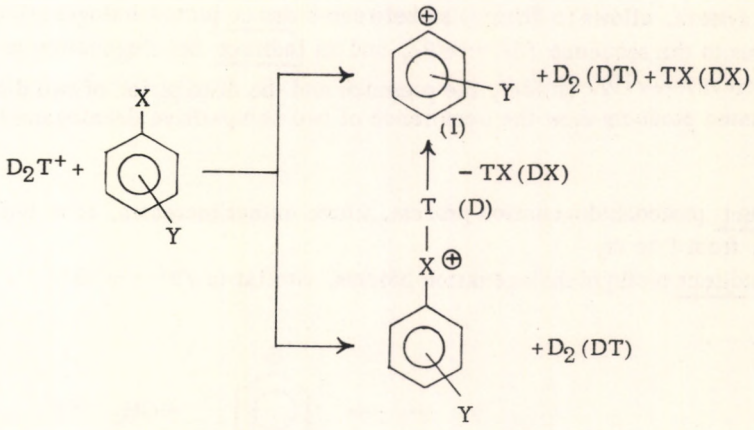

(9)

The phenyl ions (I) are suggested to efficiently attack the D_2(DT) gas, as independently verified by mass-spectrometric experiments /20/:

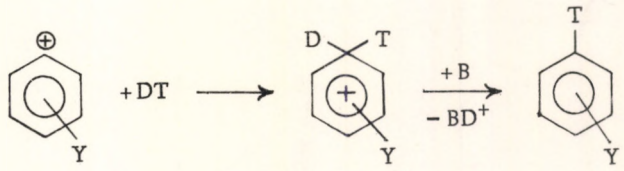

(10)

In this connection, a possible explanation of the dehalogenation trend (F ≫ Cl ≃ Br) can be based on the pronounced polarization of the C-F bond, whose individual dipole momentum in C_6H_5F exceeds that of the C-Cl bond in C_6H_5Cl by a factor greater than two, according to a recent analysis of ^{13}C chemical shifts /21/.

In the $^3HeT^+$ case, reaction /10/ does not occur because of the very large excess of the aromatic substrate, which is a nucleophile by far more efficient than DT. Consequently, the inactive phenyl ion (I), formed by the n-protonation of the substrate, is likely to react with the halobenzene, producing inactive, and therefore undetectable, products:

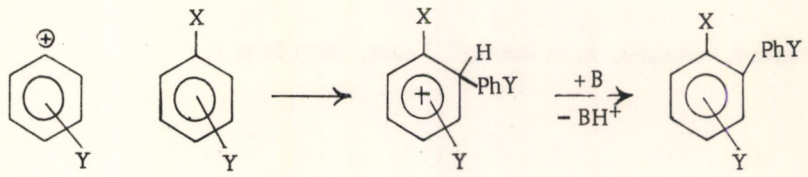

(11)

In order to verify these conclusions, further experiments were carried out using the radiolytically formed CH_5^+ ion as the gaseous electrophile. The results are reported in Table 4. The use of CH_4, as a bulk constituent of the homogeneous gaseous system, allows to distinguish between a direct protodehalogenation reaction, analogous to the sequence /5/⟶/8/, and an indirect dehalogenation process, similar to /9/⟶/10/. In fact, the presence and the distribution of two distinct dehalogenated products show the occurrence of two competitive dehalogenation reactions:

a) a direct protodehalogenation process, whose extent increases, as in the $^3HeT^+$ case, from F to Br;
b) the indirect methyldehalogenation process, similar to /9/⟶/10/:

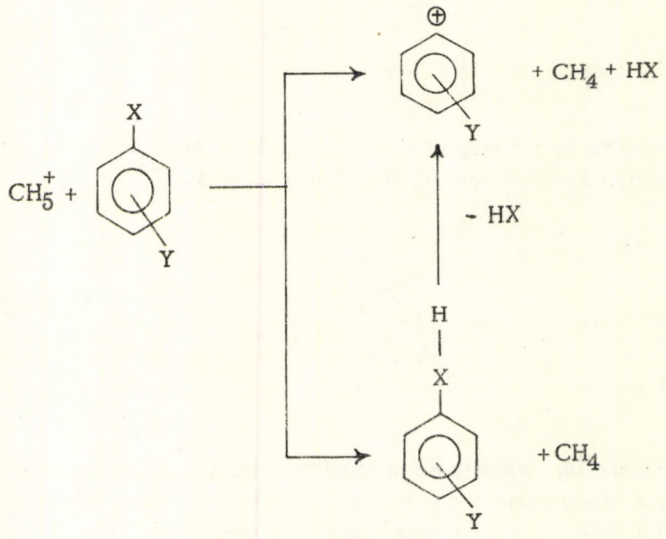

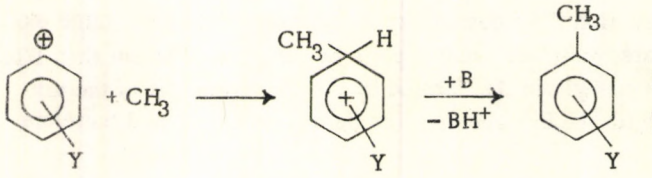

whose extent increases, as in the D_2T^+ case, from Br to F.

References

/1/ F. Cacace, "Adv. Phys. Organ. Chem.", 8, 79 (1970).
/2/ F. Cacace, in "Interactions between Ions and Molecules", P. Ausloos ed., Plenum Press, New York, 1975.
/3/ P. Ausloos, "Ann. Rev. Phys. Chem." 17, (1966).
/4/ P. Ausloos, in "Ion-Molecule Reactions", J. L. Franklin Ed., Plenum Press, New York, 1970.
/5/ F. Cacace and S. Caronna, J. Amer. Chem. Soc., 89, 6848 (1967).
/6/ F. Cacace and G. Perez, J. Chem. Soc., (B), 2086 (1971).
/7/ F. Cacace R. Cipollini and G. Ciranni, J. Chem. Soc., (B) 2089 (1971).
/8/ F. Cacace, R. Cipollini and G. Occhiucci, J. Chem. Soc., Perkin Trans. II, 84 (1972).
/9/ F. Cacace and R. Cipollini, Radiochem. Radioanal. Letters, 16, (6) 343 (1974).
/10/ F. Cacace and M. Speranza, J. Amer. Chem. Soc., 94, 4447 (1972).
/11/ F. Cacace and G. Stöcklin, J. Amer. Chem. Soc., 94, 2518 (1972).
/12/ S. Takamuku, K. Iseda, and H. Sakurai, J. Amer. Chem. Soc., 93, 2420 (1971).
/13/ F. Cacace and E. Possagno, J. Amer. Chem. Soc., 95, 3397 (1973).
/14/ F. Cacace and P. Giacomello, J. Amer. Chem. Soc., 95, 5851 (1973).
/15/ P. Giacomello and F. Cacace, Chem. Comm., 379 (1975).
/16/ P. Giacomello and F. Cacace, J. Amer. Chem. Soc., (in press, 1975).
/17/ P. Ausloos and S. G. Lias, J. Chem. Phys., 40, 3599 (1964).
/18/ P. Ausloos, "Progr. Reaction Kinetics", 5, 113 (1969).
/19/ M. T. Bowers and P. R. Kemper, J. Amer. Chem. Soc., 93, 5352 (1971).
/20/ M. Speranza, J. M. S. Henis, M. D. Sefcik, and P. P. Gaspar, to be published.
/21/ G. A. Olah, P. W. Westerman, and D. A. Forsyth, J. Amer. Chem. Soc., 97, 3419 (1975).

DISCUSSION

M. MAGAT

It is known that formation of CH_5^+ ions is possible in the condensed phase by the use of superacid systems. Could you investigate the attack of CH_5^+ ions on halobenzenes in these conditions?

M. SPERANZA

It is not possible to investigate the electrophilic attack of the CH_5^+ ion on halobenzenes in superacid systems because in such conditions formation of halobenzenium ions occurs independently from the presence of CH_5^+ ions. On the other hand, the properties of the protonated intermediates from the attack of superacids on halobenzenes have been characterized.

RADIOLYSIS OF MERCAPTO- AND THIOACIDS

G. G. Chirakadze, H. M. Nanobashvili, G. V. Katsadze
Institute of Inorganic Chemistry and Electrochemistry, Georgian SSR
Academy of Sciences, Tbilisi, USSR

A study of radiation-chemical transformations of bifunctional compounds is of considerable interest. Organic acids with the hydrogen atom of the methylene or hydroxyl groups replaced by the sulpho-hydryl group enter this class of compounds. The above compounds have a wide practical application and are of great convenience for the modelling of some important physiological processes /1/. Besides, the results obtained will contribute to the study of the mutual influence of the sulpho-hydryl and other functional groups in the irradiation field, and this, in its own turn, will lead to the generalization of the previously obtained results /2/.

The present paper deals with the study of thioacetic, mercaptoacetic and mercaptoenanthic acids in their individual states, as well as in isooctane, alcohol and aqueous solutions. γ-Irradiation has been carried out on the Co-60 unit. The dose rate, determined by the ferrosulphate method, has been varied in the range of 1×10^{14} - 1.10^{16} eV/ml sec. The technique of investigations included different methods of physico-chemical analysis: chromatographic, electrometric, spectrophotometric and others /3/. The ESR and pulse radiolysis methods were used for ascertaining the nature of the basic unstable radiolysis products. Transient species were indentified by using the U-12 accelerator. (Length of electronic pulse = 5 μ sec; cell volume=2 ml; dose=1×10^{17} eV/ml.)

Thioacetic acid under irradiation in its individual state in an inert gas atmosphere undergoes insignificant transformations. The amount of transformed acid, determined by the decrease of the sulpho-hydryl group, did not exceed 0.0013 mole at the dose of 1.6×10^{21} eV/ml. The initial radiation yield $G(-CH_3COSH)=1$ molec/100 eV. Diacetyldisulphide, the basic sulphur-containing product, was formed with a quantitative yield in calculation on the oxidized sulpho-hydryl group $G[+(CH_3COS)_2] = 0.62$. The transformation of thioacetic acid was more intensive in an oxygen atmosphere. The value of the radiation yield $G(-CH_3COSH)$ increased to 6.1 molec/100 eV. The amount of formed diacetyldisulphide, as shown in Fig. 1. passes the maximum value.

Radiation-chemical transformations and the radiation oxidation considerably increased in isooctane solutions: $G(-CH_3COSH)=9$ for 0.01M and 32-35 molec/100 eV for 0.03–0.16M solutions. As seen from Fig. 2, where chromatograms of control

Table 1

Influence of the dose rate on radiation-chemical transformations of isooctane solution of thioglycolic acid in air (1–5) and oxygen (8–11) atmospheres

N°	Dose rate $x10^{-14}$ eV/ml sec	Concentration of thioacetic acid			Radiation yield $G(-CH_3C(=O)SH)$
		Remained	Transformed		
		m/l	m/l	%	
1	control	0. 031	–	–	–
2	65	0. 029	0. 002	0. 4	15. 4
3	26	0. 026	0. 005	16. 1	36. 7
4	7. 7	0. 023	0. 008	20. 0	54. 0
5	0. 9	0. 024	0. 007	23. 0	61. 7
6	control	0. 031	–	–	–
7	65	0. 025	0. 006	19. 3	46. 3
8	26	0. 024	0. 005	22. 5	51. 3
9	18. 4	0. 020	0. 011	35. 4	30. 7
10	7. 6	0. 017	0. 014	45. 1	108. 0
11	0. 9	0. 003	0. 028	90. 3	216. 3

Note: The amount of absorbed energy corresponds to 1×10^{20} eV/ml

and irradiated 0. 15M solutions of thioacetic acids are presented, diacetyldisulphide is one of the basic sulphur-containing radiolysis products. The maximum amount of formed diacetyldisulphide does not exceed 90% in calculation on the oxidized sulpho--hydryl group and, also, passes the maximum value (Fig. 3). Gas atmosphere considerably affects the processes. The value of $G(-CH_3COSH)$ is 17. 6 in the oxygen atmosphere and 10.2 molec/100 eV in the helium one. The values of $G[+(CH_3COS)_2] = 4.6$ and $G + (CH_3COS)_2 = 2.1$ get changed in oxygen and helium atmospheres, respectively. The experiments in oxygen atmosphere were performed under constant bubbling of oxygen, as the solubility of the latter in the systems examined does not exceed 1.6×10^{-2} mole/1/4/. The results of the study of the dose rate influence on radiation-chemical transformations of the isooctane solution of thioacetic acid are summarized in Table 1. As Table 1 shows, the values of the radiation yield increase in the experiment from 46 to 216 molec/100 eV. These data indicate the occurrence of chain processes in radiolysis of thioacetic acid. The dependence of $lgG(-CH_3COSH)$ on the dose rate is shown in Fig. 4. The slope of the curve, being around 0. 5, indicates the development of the chain process with quadratic chain termination /5/.

The data on radiation-chemical transformations of thioglycolic acid in isooctane, alcohol and aqueous solutions are summarized in Table 2. In isooctane solution thioglycolic acid undergoes intensive oxidation by sulpho-hydryl group and

Table 2

Radiation-chemical transformations of thioglycolic acid in isooctane (1-4), alcohol (5-8), and aqueous (9-14) solutions

N°	Dose, x 10^{-20} eV/ml	Acid concentration by SH m/l, C	ΔC		G (-SH)	Acid concentration by (-COOH) m/l, C,	ΔC		G (COOH)
8			m/l	%			m/l	%	
1	control	0.037	—	—	—	0.040	—	—	—
2	1.0	0.010	0.027	73	16	0.019	0.021	52	13.1
3	1.9	0.004	0.037	89		0.019	0.021	52	
4	2.9	0.002	0.035	95		0.013	0.027	68	
5	control	0.070	—	—	—	0.072	—	—	—
6	1.0	0.051	0.019	26	8	0.059	0.013	18	8.1
7	1.9	0.042	0.027	38		0.059	0.013	18	
8	2.9	0.030	0.040	43		0.059	0.013	18	
9	control	0.046	—	—	—	0.046	—	—	—
10	0.5	0.035	0.011	24	12	0.046	0.000	0	0
11	1.0	0.025	0.021	47		0.046	0.000	0	0
12	2.1	0.002	0.044	96		0.046	0.000	0	0
13	2.7	0.001	0.045	97		0.046	0.000	0	
14	3.2	0.001	0.045	97		0.046	0.000	0	

dicarboxylates. The indication of the considerable influence of the carboxylic group on the sulpho-hydryl one, manifested in the increase of its radiation sensitivity as compared to other mono- and difunctional compounds /2/, is provided by the fact that up to 0.013M acid oxidizes (by the SH group) within the range of the examined doses. A similar effect is observed in aqueous and alcohol solutions of thioglycolic acid.

It is also interesting to study the "reverse" influence of the sulpho-hydryl group on the carboxylic one. With this purpose in view, alongside solutions of thioglycolic acid, solutions of acetic acid and the mixtures of acetic acid with thioalcohols have been investigated. The results obtained indicate the increase of the reaction ability of the carboxylic group in organic solvents. The increase is probably connected with the intensification of the reaction of intermolecular interaction between carboxylic and sulpho-hydryl groups in the radiation field. This reaction leads to the formation of six-membered thiolactone, occurring, according to the data of chromatographic analysis, both in alcohol and, to a larger degree, in isooctane solutions. The possible occurrence of the above reaction is also indicated by the absolute absence of hydrogen sulphide in the radiolysis products. The formation of hydrogen sulphide would point to the fact that the direction of the reaction is dif-

ferent and leads to the formation of lactone. Correspondingly disulphide, accumulating proportionally to the dose, has been the basic radiolysis product of thioglycolic acid in all solvents studied.

Unlike in other sulphur-containing polyfunctional compounds, the radiation stability increase of the carboxylic group in isooctane solution depends considerably on the concentration of thioalcohol in solution. As shown in Fig. 5 the decarboxylation reaction begins when the added amount of thioalcohol has been totally oxidized.

Similar results were obtained for the ω-mercaptoenanthic acid.

In order to establish the mechanism of the reactions the examined acids were irradiated with electron pulses and the transient absorption was measured in the 350--410 nm wavelength range.

Transient absorption is observed under irradiation of thioglycolic acid with electron pulses. On the basis of the obtained oscillograms within the range of the above wavelengths the optical absorption spectrum for thioglycolic acid was constructed (Fig. 6). This spectrum is characterized by the pronounced maximum on the 370 nm wavelength, indicating the formation of a transient species $\dot{S}CH_2COOH(RS\cdot)$ at one of the initial stages of irradiation. A similar spectrum for 2-oxyethanethiol was obtained by Swallow et al /6/. Figure 6 also presents the optical absorption spectrum for the thioacetic acid. In this case, the maximum of absorption is shifted to long wavelengths (405–410 nm). It may be expected that this absorption is caused by the $RC\leqslant^{O}_{S}$ radical.

The dependence of the change of the optical density of a transient species on time permits the construction of a kinetic curve of the decay of the transient species. As Fig. 6 shows, the species decay by two different processes of the first order. The rate constants of these species, calculated by the slope of the curve segments are 4×10^4 sec^{-1} and 0.5×10^4 sec^{-1} for thioglycolic acid and 2×10^4 sec^{-1} and 0.5×10^4 sec^{-1} for thioacetic acid.

The results obtained permit us to conclude that the sulpho-hydryl group in sulphur--containing organic acids as well as in other polyfunctional sulpho-hydryl compounds, e. g. in oxythioalcohols and organic thiocyanates /7/, is the most radiation sensitive part of the molecule and is responsible for the basic transformations of the whole molecule. The thiyl radical is one of the basic primary products here, as well as in other sulphur-containing compounds. The only exception is thioacetic acid where the oxygen-containing thiyl radical $RC\leqslant^{O}_{S\cdot}$ is formed at the first stage. The nature of the above radical is confirmed by the ESR data. The ESR spectrum of thioacetic acid represents a single line with 2 Oersted splitting. The yield of radicals is 3.2.

It can be concluded on the basis of the data obtained, that the mechanism underlying the radiation-chemical transformations of thio- and mercaptoacids is the chain one and the thiyl radical is formed at one of the initial stages. The interaction of the above radical with oxygen, with the solvent molecules, and its involvement into recombination reactions leads to the accumulation of corresponding disulphides—basic sulphur-containing radiolysis products.

References

/1/ E. E. Reid, Organic Chemistry of Bivalent Sulfur, III, New York, 1961.
/2/ H. M. Nanobashvili, G. G. Chirakadze, M. V. Panchvidze, S. E. Gvilava, G. I. Khidasheli, "Radioliz sernistykh soedineniy", II, Tbilisi, Metsniereba, 1973.
/3/ H. M. Nanobashvili, G. G. Chirakadze, M. Sh. Simonidze, L. V. Ivanitskaia, I. G. Bakhtadze, "Radioliz sernistykh soedineniy", I, Tbilisi, Metsniereba, 1967.
/4/ N. M. Emanuel, E. T. Denisov, Z. K. Mayzus, "Tsepnye reaktsii okislenia uglevodorodov v zhidkoy faze", M., Nauka, 1965.
/5/ N. P. Kostromin, V. V. Sarayeve. Khimiya vysokyh energiy, 9, 34, 1975.
/6/ G. Jayson, D. Stirling, J. Swallow, Int. J. Radiat. Biochem. 19, 143, 1971
/7/ H. M. Nanobashvili, G. G. Chirakadze, M. Sh. Simonidze, L. V. Ivanitskaia, et al., Proc. 2nd Tihany Symp. Rad. Chem., Akadémiai Kiadó, Budapest, 1967. p. 285.

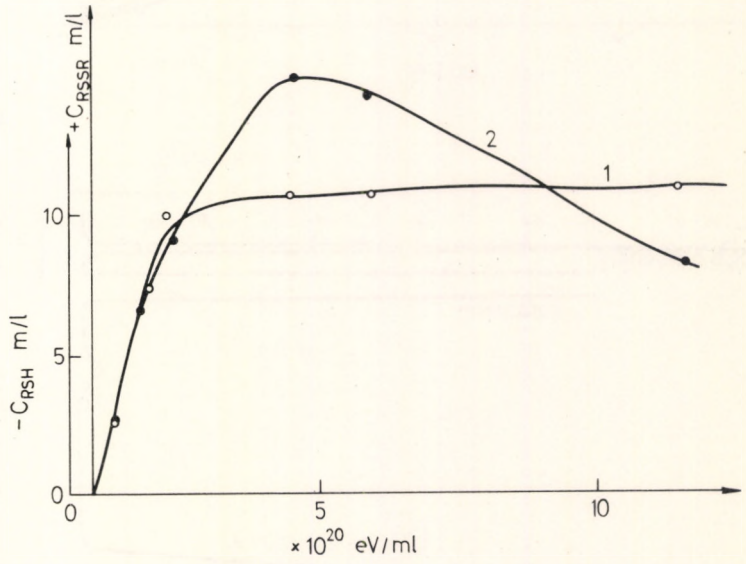

Fig. 1 Kinetic curves of radiation oxidation of thioacetic acid (1) and of diacetyldisulphide formation (2)

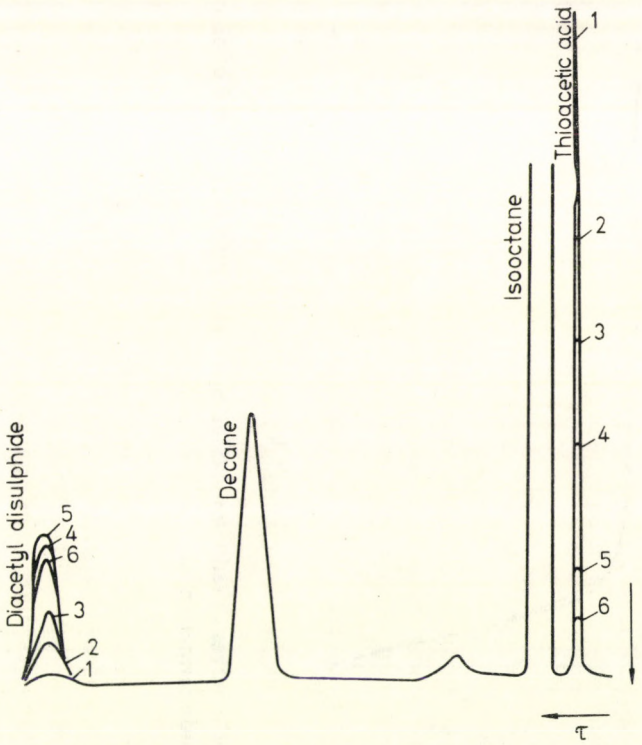

Fig. 2 Chromatogram of irradiated 0.15 M isooctane solution of thioacetic acid (1) 0.1×10^{20}, (2) 0.8×10^{20}, (3) 1.4×10^{20}, (4) 2.3×10^{20}, (5) 3.9×10^{20} and (6) 4.7×10^{20} eV/ml

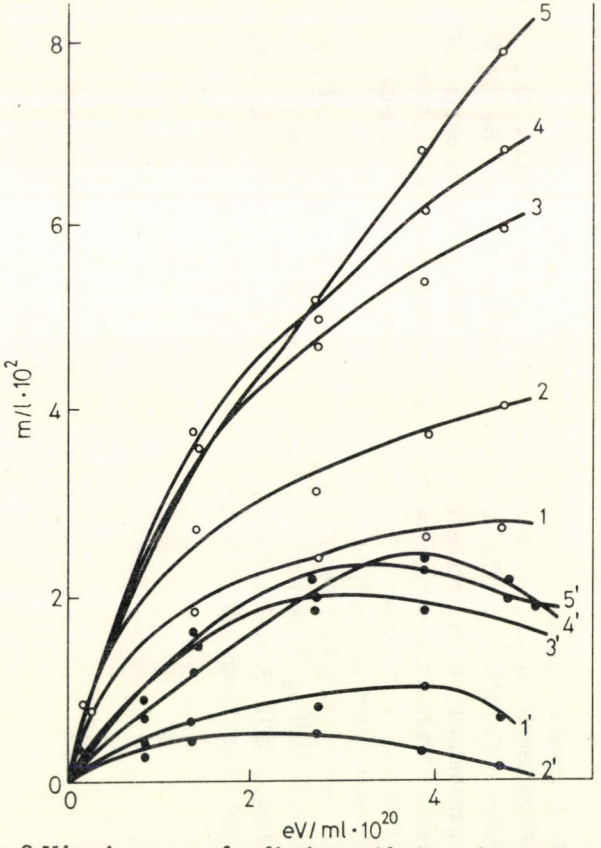

Fig. 3 Kinetic curves of radiation oxidation of thioacetic acid and of diacetyldisulphide formation (1) 0.03M, (2) 0.05M, (3) 0.08M, (4) 0.1M and (5) 0.15M solutions of thioacetic acid, ' -figures stand for disulphides

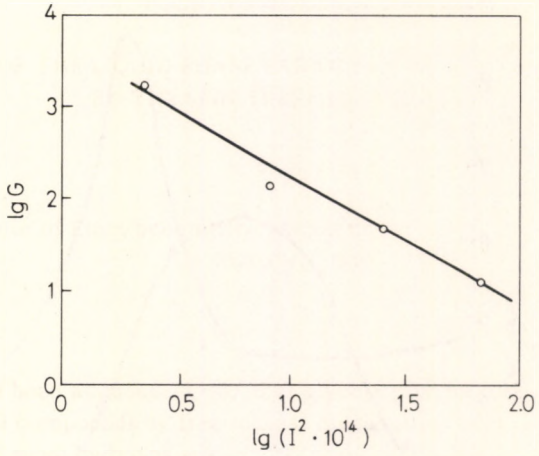

Fig. 4 Dependence lg G on I

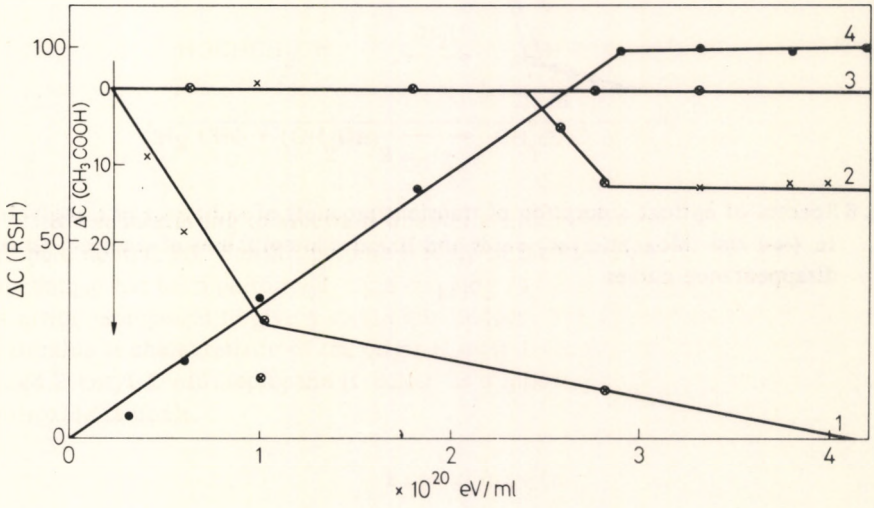

Fig. 5 Radiation-chemical transformation of acetic acid in the presence (2, 3) or absence (1) of mercaptan and oxidation of mercaptan (4)
(1) acetic acid, (2) isooctane and (3) alcohol solutions of acetic acid and mercaptan

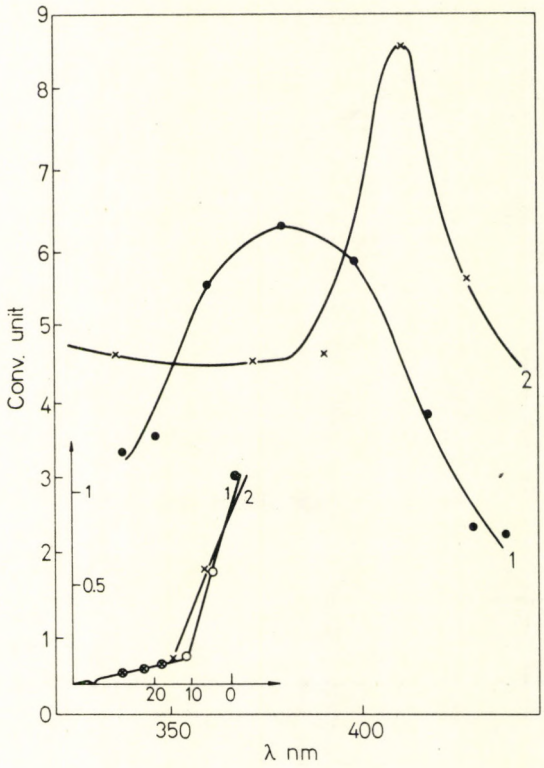

Fig. 6 Spectra of optical absorption of transient products of radiolysis of thioglycolic (-●-) and thioacetic (-×-) acids and linear anomorphoses of transient issues disappearance curves

THE RADIOLYSIS OF SOME COMPOUNDS WITH -S-, -SH, -OH FUNCTIONAL GROUPS

M. V. Panchvidze, H. M. Nanobashvili, N. Z. Dalakishvili
Institute for Inorganic Chemistry and Electrochemistry, Academy of Sciences, Tbilisi, USSR

The investigation of the radiolysis of bifunctional organic sulphur compounds is of great scientific and practical interest because of the protective nature of the organic sulphur compounds.

In this connection it was interesting to investigate the radiolysis of thio-3-pentanethiol-5 and its oxygen analogue – thio-3-pentanol-5, containing -S-, -SH, -OH functional groups. The investigation was carried out by means of various methods – EPR, pulse radiolysis, IR-spectroscopy, spectrophotometry, etc., allowing us to establish main regularities of the radiolysis.

The data obtained by the EPR method show that the main part of the EPR spectra of irradiated glassy thio-3-pentanethiol-5 presents a single line with a g-factor of 2.012 and linewidth of 30 Oe, which is probably due to ion-radicals. Besides that, an additional line is observed in the low-field with a g-factor of 2.05, which is due to the thiyl radical. This radical has an asymmetric structure with an anisotropy of the g-factor /1,2/. With increasing dose the asymmetry of the spectra sharply increases /Fig. 1a/ because of decreasing of the relative intensity of the singlet with respect to the thiyl radical-line.

The accumulation curve of the paramagnetic centres in thio-3-pentanethiol-5 has two portions: first, up to dose 5 Mrad, corresponding to the ion-radical-accumulation with a yield of $G_r = 4.5 \cdot 1/100$eV and the second, above this dose, where, essentially, thiyl radicals accumulate with a yield of $G_r = 0.9 \cdot 1/100$ eV.

Under the action of visible light the intensity of the singlet begins to decay and the lines of the thiyl radicals become clearly resolved. After 30 minutes of bleaching the spectra is completely resolved to three lines of the thiyl radical with g-values: $g_1=2.055$, $g_2=2.025$, $g_3=2000$. The total width of the spectrum is 90 Oe /Fig. 1b/. Each component of the spectrum is resolved to a doublet which indicates interaction of the unpaired electron with one of the α-protons. However, in the high field side of the spectrum other lines are observed which are due to hydrogen abstraction from the alkyl group, although the share of these radicals is very small in the total concentration of the paramagnetic centers.

In the optical spectra of thio-3-pentanethiol-5 after electron pulse irradiation two absorption bands with maxima at 410 nm and 460 nm are observed /Fig. 2/. An

absorption band at λ_{max}=410 nm is due to thiyl radicals RS$\dot{}$, while an absorption at λ_{max}=460 nm, probably, is connected with molecular cation-radicals in which the positive charge is localized on the sulphide group /3-5/.

A comparison of the data obtained by means of EPR and pulse radiolysis methods allowed us to conclude that during radiolysis of the thio-3-pentanethiol-5 molecular cation-radicals R'S^{+}R''SH and thiyl radicals RS$\dot{}$ are formed.

The data of investigation of the radiolysis of frozen solutions of thio- 3-pentanethiol-5 in isooctane is of interest. In 1% solution of thio-3-pentanethiol-5 G_r = 2.4 · 1/100 eV. With increasing thiothiol concentration the yield decreases. For the equimolar solution (50%) G_r=1.1 · 1/100 eV. At low concentrations of thiothiol the EPR spectrum essentially contains the lines of isooctane radicals while in equimolar solution a line of thiyl radical with g-factor 2.055 is clearly observed. A comparison of the radical yields in pure isooctane (G_r=2.7), in equimolar mixture: isooctane-thiothiol (G_r=1.1) and in pure thio-3-pentanethiol-5 (G_r=0.9) shows that thiothiol molecules would protect isooctane molecules /Fig. 3/.

Thio-3-pentanol-5 behaves differently. The EPR spectra of irradiated /2 Mrads/ thio-3-pentanol-5 consists of five lines with a hyperfine splitting constant of 20 Oe. At the central part of the spectrum a singlet appears which is probably due to an ion-radical. There is little change in the spectrum with increasing dose. Optical bleaching of the irradiated sample causes disappearence of the singlet. The remaining quintet is due to alcohol radicals in which an unpaired electron is localized at the α-carbon atom and unequivalently interacts with the α- and β-protons: $a^{\alpha} = a^{\beta}_1$ = 20 Oe and a^{β}_2 = 40 Oe /Fig. 4/.

The accumulation curve of radicals in thio-3-pentanol-5 has two parts: the first, up to 5 Mrad, corresponds to the ion-radical - accumulation with a yield of G_r=4.5 · 1/100 eV; the second, above this dose, to an accumulation of the alcohol radicals with a yield of G_r=1.3 · 1/100 eV. A comparison of the values of alcohol radical yields in thio-3-pentanol-5 and in normal alcohols (G_r=6 · 1/100 eV) /6/ shows that the sulphur heteroatom causes an increase of the radiation stability of the alcohol molecule.

An investigation of the short lived products of the radiolysis of thio-3-pentanol--5 by means of pulse radiolysis method shows that in the spectra of optical absorption of pulse-irradiated thio-3-pentanol-5 two absorption bands with a maximum at 460 nm and 520 nm are observed /Fig. 5/. An absorption at λ_{max}=460 nm is due to the molecular cation-radicals, in which a positive charge is localized on the sulphur atom, as in the case of aliphatic sulphides /4/. Alcohol radicals which have an absorption in the range < 300 nm, were not observed because of the strong self absorption of the thio-3-pentanol-5 in this region. Thus, molecular cation radicals and alcohol radicals are the main radical products of thio-3-pentanol-5 radiolysis. Consequently, the relative comparison of the nature of the active centers formed during radiolysis of thio-3-penthanethiol-5 and thio-3-pentanol-5 leads us to the conclusion that what is common to them is the formation of molecular cation-radicals--(R'S^{+}R''SH) and (R'S^{+}R''OH) at the first stage of the radiolysis. However, the

presence of the sulpho-hydryl and hydroxyl groups in these compounds causes an appearence of different neutral thiyl radicals in the case of thio-3-pentanethiol-5 and alcohol radicals in the case of thio-3-pentanol-5.

The main stable product of the radiation-chemical transformation of the sulpho-hydryl group of thio-3-pentanethiol-5 is the corresponding disulphide /Fig. 6/. The transformation of sulphide group leads to the formation of some oxidation products. In IR-spectra of thio-3-pentanethiol radiolysis product absorption bands of S=O and SO_2 groups are observed /Fig. 7/.

It is interesting that the rate of the radiation-chemical transformation of sulpho-hydryl group in thio-3-pentanethiol-5 is significantly less than in ethanethiol, but larger than in phenylethanethiol /Fig. 8/, which indicates the protective action of the sulphide and phenyl groups in the irradiation field.

The radiolysis of thio-3-pentanol-5 proceeds by transformation of the hydroxyl group as well as the sulphide group with a formation of the corresponding sulphoxide. It may be noted that the radiation-chemical transformation of the hydroxyl group in thio-3-pentanol-5 in definite conditions is less than in n-pentanol. It indicates the protection of the hydroxyl group by the sulphur heteroatom.

Based on the obtained results it may be concluded that each of the functional groups under investigation is characterized uniquely and contributes a definite share in the radiation-chemical transformation of the corresponding compound. By choosing definite functional groups, a directed variation of the protective nature of organic sulphur compounds in the irradiation field may be realized.

References

/1/ R. G. Barsegov, A. D. Bichiashvili, M. V. Panchvidze, H. M. Nanobashvili: Bull. Acad. Sci. of the Georg. SSR, 49, 91 (1968).

/2/ H. M. Nanobashvili, A. D. Bichiashvili: Radiolysis of Sulphur Compounds, p. III, Tbilisi, 1973.

/3/ A. Torikai, S. Sawada, K. Fueki et all: Bull. Chem. Soc., Japan, 43, 1617, (1970).

/4/ H. M. Nanobashvili, M. V. Panchvidze, R. G. Tushurashvili et al., Radiolysis of Sulphur Compounds, p. IV, Tbilisi, 1975.

/5/ W. Karmann, G. Meissner, A. Henglein: Z. Naturforsch., 22b, 273, (1967).

/6/ EPR of free Radicals in Radiation Chemistry, Moscow, "Chemistry", 1972.

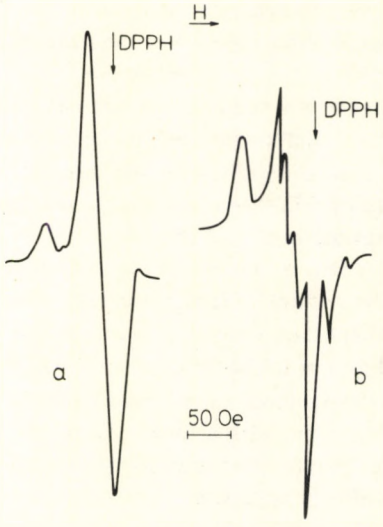

Fig. 1 EPR Spectra of thio-3-pentanethiol-5: a - Dose=15 Mrad, b - after optical bleaching

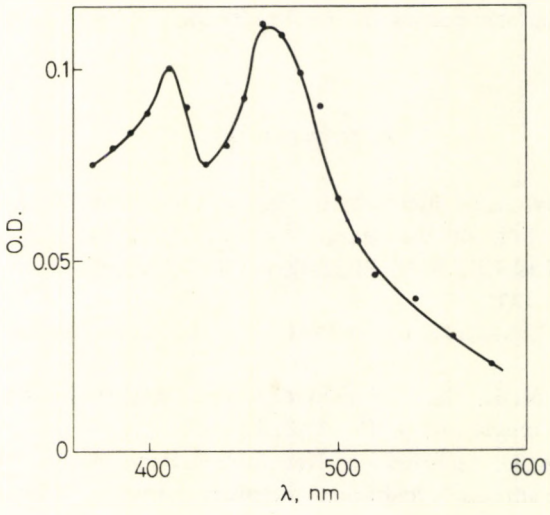

Fig. 2 Optical absorption spectrum of electron pulse irradiated thio-3-pentane-thiol-5

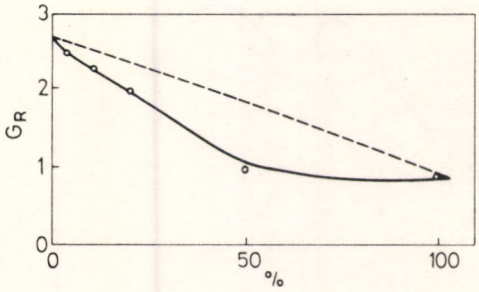

Fig. 3 Dependence of the yield of radicals on thio-3-pentanethiol-5 concentration in isooctane solutions

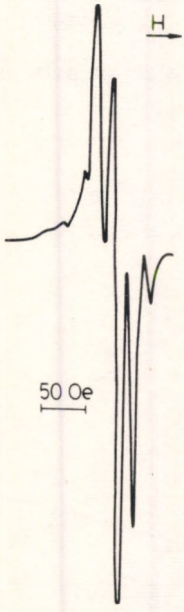

Fig. 4 EPR Spectrum of thio-3-pentanol-5 irradiated with a dose of 2 Mrad

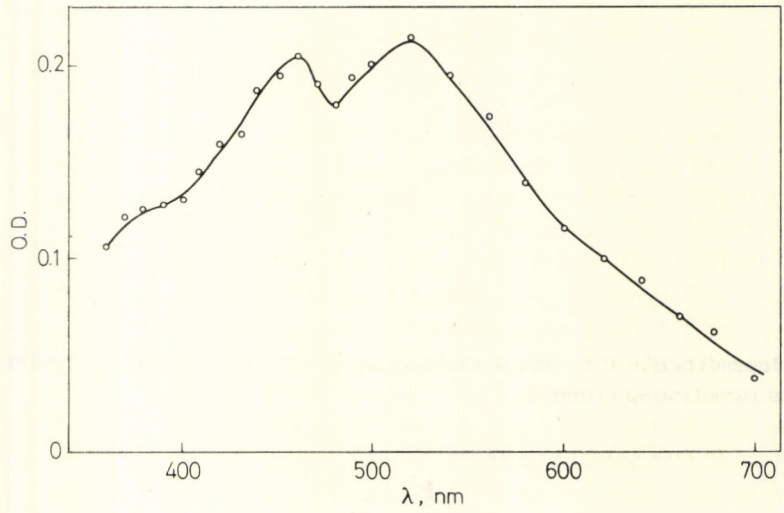

Fig. 5 Optical absorption spectrum of electron pulse irradiated thio-3-pentanol-5

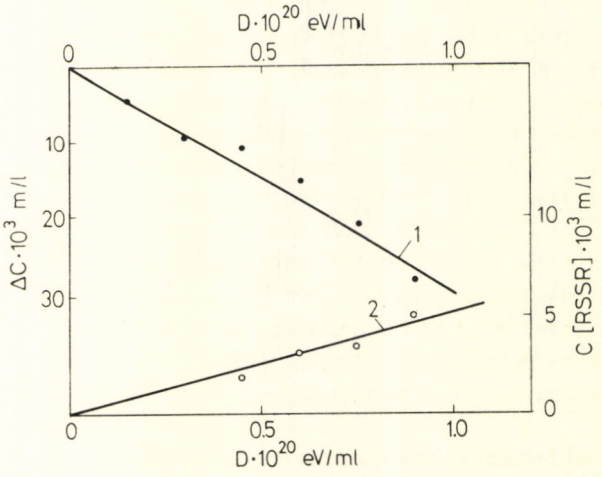

Fig. 6 Radiation-chemical transformation of 0.1 M isooctane solution of thio-3--pentanethiol-5 (1) and a formation of the corresponding disulphide (2)

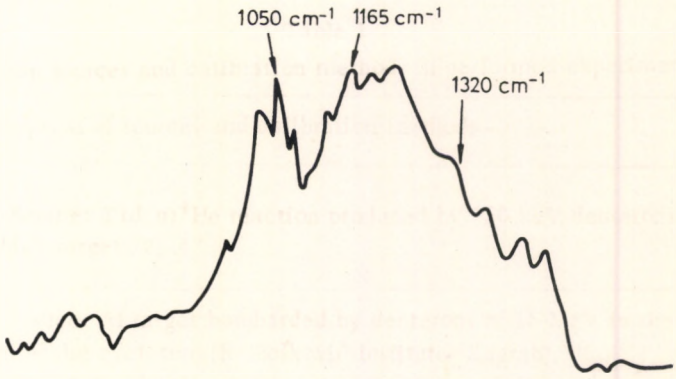

Fig. 7 IR-spectrum of thio-3-pentanethiol-5 radiolysis products: 1050 cm^{-1} - S=O, 1165 cm^{-1}- SO_2

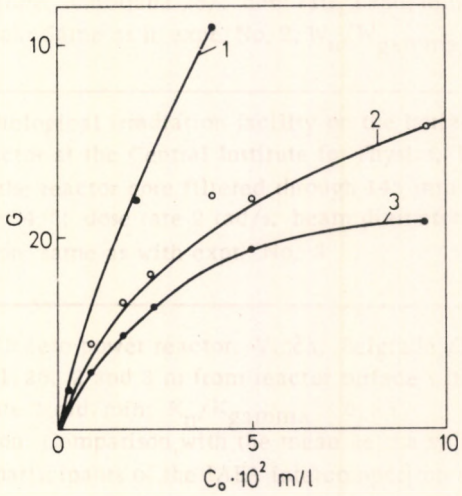

Fig. 8 Radiation-chemical transformation of isooctane solutions of ethanethiol (1), phenylethanethiol (3) and thio-3-pentanethiol-5 (2)

GAS PHASE REACTIONS OF IONS FORMED BY ELECTRON IRRADIATION OF ORGANIC COMPOUNDS

Z. Łuczyński, H. Wincel
Department of Radiation Chemistry, Institute of Nuclear Research
Warszawa, Poland

Introduction

It is well established in many radiolytic studies that a very small amount of substance added to a major compound may change the radiolytic picture significantly. It is necessary, in order to improve our understanding of radiation-chemical processes and to predict their channels, to have more information about the reactions of foreign compounds which may be present in low concentrations in the radiolytic system (as impurities or accumulated products) and which may result in significant effects on radiolytic processes – particulary on the gas–phase ion–molecule reaction mechanisms.

This paper is primarily concerned with reactions of negative ions formed by electron irradiation of a number of organic chloro-compounds containing trace amounts of different substances.

Experimental

The data on ionic reaction to be presented here were obtained with the high–pressure and low–temperature mass spectrometer which was constructed in the Department of Radiation Chemistry of the Institute of Nuclear Research (Warszawa) and designed for the investigation of ionic processes under conditions in the reaction chamber which are similar to the conditions of temperature and pressure which would prevail in gas phase radiolytic studies. The apparatus and general experimental procedure have been described previously /1, 2/. This instrument has the capacity that the pressure in the reaction chamber can be varied over the range of 0. 01 – 10 torr at temperatures 150 – 420 K; the ionization of the sample is effected by electron impact which energy can be varied between 5 and 1000 eV. The repeller and focus electrodes can be maintained at low operating potentials and under these conditions the inside of the reaction chamber is approximately field–free.

Results and discussion

The principal negative ion formed from vinyl and allyl chloride as a result of electron impact is Cl^-. At the relatively high pressures and temperatures below about 400 K this ion undergoes a stepwise solvation by parent molecules and by trace impurity molecules present in the irradiated system.

From Fig. 1, which shows a typical plot of the relative intensities of the prominent ions formed in C_2H_3Cl ionized by 800 eV electrons at a pressure of 0.8 torr as a function of temperature, it is seen that besides the relatively low yield of species $Cl^- \cdot C_2H_3Cl$ the clusters containing H_2O and HCl molecules are formed in significant quantities. A similar situation was encountered previously in methyl and ethyl chloride systems /3/ when negative ion reactions were studied, and as before we attribute the formation of the clusters containing H_2O and HCl to trace amounts of these molecules in the irradiated system.

The water molecules are assumed to originate from the walls of the apparatus and perhaps as an impurity from the starting material, while the presence of HCl could result from various processes which may follow the chloride derivatives, namely:

molecular elimination from the excited parent molecule /4/ (and positive ion):

$$C_2H_3Cl^x \longrightarrow C_2H_2 + HCl \qquad (1)$$

ion–molecule reactions /5, 6/

$$C_2H_3Cl^+ + C_2H_3Cl \longrightarrow C_4H_5Cl^+ + HCl \qquad (2)$$

$$C_3H_4Cl^+ + C_2H_3Cl \longrightarrow C_5H_6Cl^+ + HCl, \text{ etc.} \qquad (3)$$

The mole fraction of HCl present in irradiated under dynamic conditions C_2H_3Cl is of the order of magnitude 10^{-3} as estimated from the rate of production of HCl by the electron irradiation and the average rate of the gas flow through the reaction chamber. This concentration may, of course, be much higher if the system is irradiated under static conditions and the radiolytic products are accumulated.

A much more significant effect of additives on the relative abundances of ions was found in the systems containing formic and/or acetic acids. As an example, Figs 2, 3 show the relative abundances of the negative ions formed in a 5% $C_3H_5Cl–H_2$ mixture containing 0.1% HCOOH at a total pressure of 2 torr and irradiated with 1 keV electrons as a function of temperature. It can be seen that at relatively high temperatures the association of the Cl^- ion with HCOOH molecules is the most abundant species in the system even when only 0.1% HCOOH is present; at the lowest temperatures used in the experiments reported here, the $Cl^-(HCOOH)_n$ ions with $n<4$ are observed, as shown by the results given in Fig. 3.

The influence of temperature on the relative contributions of the H_2O, HCl and C_2H_5Cl molecules to the association with the Cl^- ion in the 4.5% $C_2H_5Cl–H_2$ mixture at total pressure of 1.4 torr is presented in Fig. 4. It is seen that the solvates containing C_2H_5Cl molecules disappear with lowering temperature to be replaced by those containing H_2O and HCl molecules.

Table 1.

The bond energies[a] determined from the equilibria measurements of the reaction $Cl^-A_{n-1} + A \rightleftharpoons Cl^-A_n$

$D(Cl^- - A)$		$D(Cl^- \cdot A - A)$		$D(Cl^- \cdot A_2 - A)$		$D(Cl^- \cdot A_3 - A)$	
$Cl^- - H_2O$	13.1[b]	$Cl^- \cdot H_2O - H_2O$	12.7[b]	$Cl^- (H_2O)_2 - H_2O$	11.7[b]	$Cl^- (H_2O)_3 - H_2O$	11.1[b]
$Cl^- - HCl$	23.7[c]	$Cl^- \cdot HCl - HCl$	15.2[c]	$Cl^- (HCl)_2 - HCl$	11.7[c]	$Cl^- (HCl)_3 - HCl$	10.3[c]
$Cl^- - HCOOH$	37[d]	$Cl^- \cdot HCOOH - HCOOH$	34[e]	$Cl^- (HCOOH)_2 - HCOOH$	22[e]	$Cl^- (HCOOH)_3 - HCOOH$	14[e]

a) All values in kcal/mole

b) M. Arshadi, R. Yamdagni, P. Kebarle, J. Phys. Chem., 74, 1475 (1970)

c) R. Yamdagni, P. Kebarle, Can. J. Chem., 52, 2449 (1974)

d) R. Yamdagni, P. Kebarle, J. Am. Chem. Soc., 93, 7139 (1971)

e) Z. Łuczyński, H. Wincel, unpublished data

The above observations of evolution of ionic species in the extended pressure–temperature studies of different systems may be explained as a consequence of equilibria which can generally be written, as an example for the discussion, as follows

$$Cl^-A_{n-1} + A \overset{M}{\rightleftarrows} Cl^-A_n \qquad (4)$$

$$Cl^-A_n + B \overset{M}{\rightleftarrows} Cl^-A_{n-1}B + A \qquad (5)$$

where A and B stand for ligand molecules, M for any third body.

In such reactions, the more weakly bonded ligands are replaced by those having the stronger binding energies with Cl^-. The increasing binding energies are observed between Cl^- and B = H_2O, HCl, HCOOH. The correlation of these values (Table 1) with data presented in Figs 1–3 seems to support the above interpretation. Since the association of Cl^- with HCOOH is the most strong in the systems studied, the production of the $Cl^-(HCOOH)_n$ clusters is favoured and at certain conditions (low temperatures) the Cl^- ion clustering with HCOOH occurs selectively.

Figure 5 shows the pressure dependence of the relative yields of major negative ions for the 1% HCOOH–C_3H_5Cl mixture at a temperature of 300 K estimated from the experimental equilibrium constants. It could be seen that even 1% of HCOOH present in an irradiated C_3H_5Cl will lead to a situation in which practically all produced ions are the HCOOH–containing clusters.

It should be expected that the conversion of the ions from one ion–molecule assocation to another can substantially change their chemical identity and, of course, the mechanism of ionic processes occuring in the gas phase radiolysis. Such reactions for instance as de–excitation, decomposition, neutralization may depend on the nature of ion–association.

Acknowledgement. The authors are grateful to Mr. K. Grabowski for technical assistance.

References

/1/ H. Wincel, Int. J. Mass Spectrom. Ion Phys. 9, 267 (1972).
/2/ Z. Łuczyński, H. Wincel, Int. J. Mass Spectrom. Ion Phys. 14, 29 (1974).
/3/ Z. Łuczyński, H. Wincel, Int. J. Radiat. Phys. Chem., 7, 705 (1975).
/4/ P. Ausloos, R. E. Rebbert, M. H. J. Wijnen, J. Res. Nat. Bur. Stds., 77A, 243 (1973).
/5/ J. A. Herman, J. J. Myher, A. G. Harrison, Can. J. Chem., 47, 647 (1969).
/6/ L. W. Sieck, R. Gorden Jr., S. G. Lias and P. Ausloos, Int. J. Mass Spectrom. Ion Phys. 15, 181 (1974).

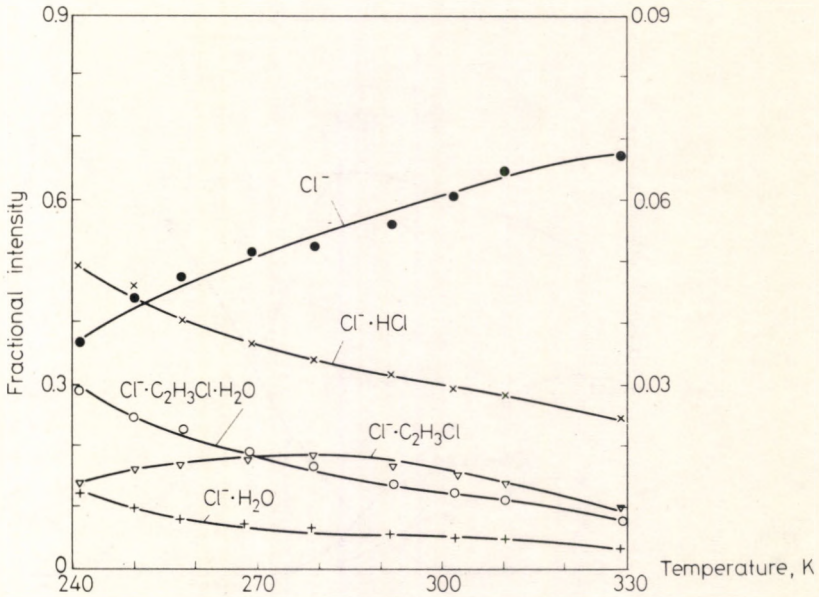

Fig. 1 Relative intensities of the major ions in C_2H_3Cl as a function of temperature at a pressure of 0.8 torr

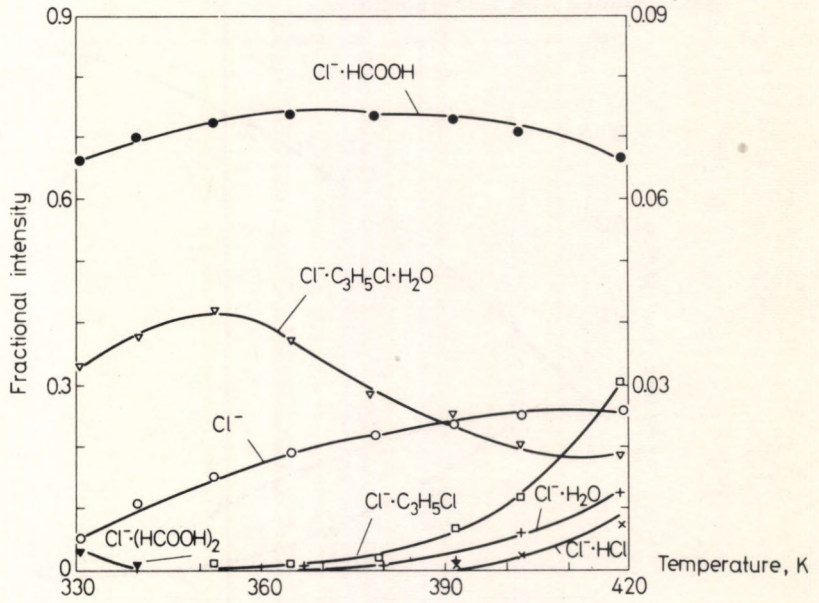

Fig. 2 Relative intensities of the major ions observed as a function of temperature in the 0.1% HCOOH – 5% C_3H_5Cl–H_2 mixture at a total pressure of 2 torr and irradiated with 1 keV electrons

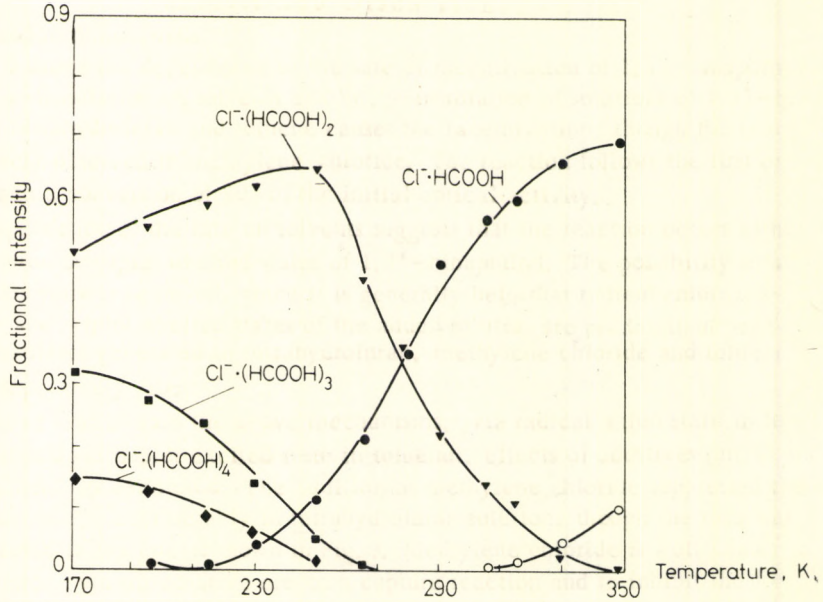

Fig. 3 Relative intensities of the major ions observed as a function of temperature in the 0.1% HCOOH – 5% C_3H_5Cl–H_2 mixture at a total pressure of 2 torr and irradiated with 1 keV electrons

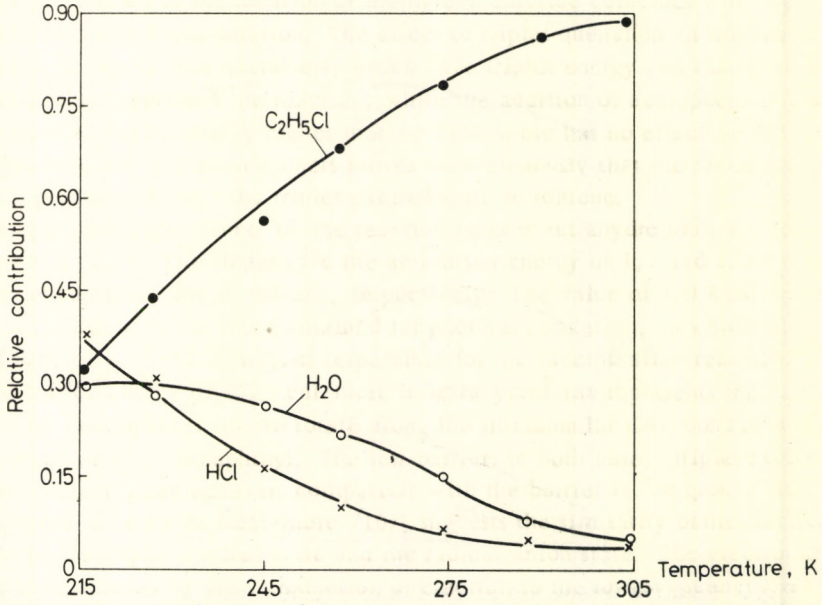

Fig. 4 Variation of the contributions of the H_2O, HCl and C_2H_5Cl molecules to the production of the solvates with Cl^- in the 4.5% C_2H_5Cl–H_2 mixture as function of temperature at total pressure 1.4 torr and irradiated with 1 keV electrons

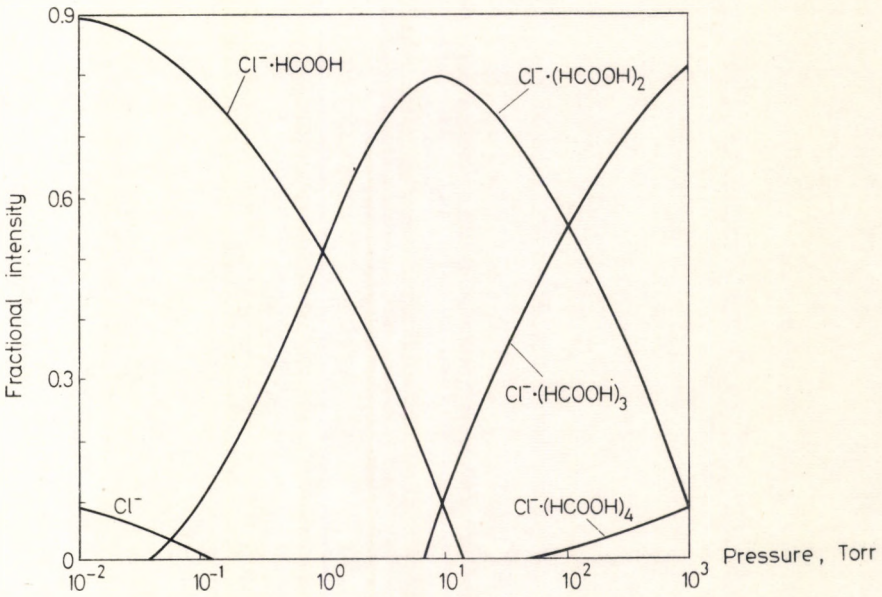

Fig. 5 Relative yields (estimated from the experimental equilibrium constants) of the major ions in the 1% HCOOH – C_3H_5Cl mixture as function of pressure at a temperature of 300 K

RADIATION PHENOMENA IN THE ETHANE-SILICON OXIDE SYSTEM IN THE REACTOR NUCLEAR RADIATION FIELD

L. Sh. Nadirashvili
Institute of Physics, Academy of Sciences of the Georgian SSR,
Tbilissi, USSR

Modern science and technology demand the solving of problems concerned with the processes in the radiation field on the surface of solids. The change of properties of a solid as a result of various defects arising in the radiation field creates new conditions for the interaction of the irradiated surface of a solid and a contacting substance /1-3/. From this point of view, solids with a large specific surface are of interest. The system "hydrocarbon-solid" presents a suitable object for observing a number of processes under irradiation.

The present paper gives the results of studies of the ethane-silica gel system in the reactor nuclear radiation field.

The silica gel used in our work had the specific surface of $600 m^2/g$, containing $7 \cdot 10^{20}$ hydroxylic groups per gram. The solid under study had previously undergone thermovacuum treatment at 573 K and 10^{-5} mm Hg, after which absorption of the hydrocarbon gas (ethane) took place. The average gas pressure in the specimen amounted to 400 mm Hg. The irradiation was carried out in a channel of the nuclear reactor at 100 kw power in the limits $10^{16}-10^{17}$ of integral flux of thermal neutrons.

The results of the studies have shown a manifold increase of relative yield of the products and a general conversion of the gas in presence of the silica gel in comparison with the homogeneous phase. The conversion of the initial hydrocarbon gas (ethane) increases proportionally to the irradiation dose reaching 70-80% at integral flux of $10^{17} n/cm^2$ (Fig. 1). Ethane concentration decrease is compensated with the formation of the gas products of the transformation system, mainly with hydrogen.

A decrease of conversion rate was observed with a simultaneous decrease of hydrogen forming rate, due to the exhaustion of the initial gas at high integral fluxes.

The analysis of the isotopic content of hydrogen in the experiments with ethane-deuterated silica gel system have shown tha a prevailing part of the processes of radiational transformation of the given system is made by the removal of the atomic hydrogen. The different character of hydrogen formation in the given case from that in the homogeneous phase at big conversions in due to the peculiarity of contribution of the solid surface in the process of radiational transformation of the system. From the rest of the gaseous products butane is the main hydrocarbon gas of the radiation transformation of the given system. The character of dependence of the relative yield

of butane on the integral flux (Fig. 2) indicates, on the one hand, the influence of a gradual exhaustion of the initial hydrocarbon gas, and, on the other hand, an increasing role of the butane proper radiation transformation at high integral fluxes. No less important here is trapping of the intermediate products: $C_2H_5^{\cdot}$ radicals or $C_2H_5^+$ ions which are fundamental sources of butane formation.

At great radiation doses trapping is realized by the surface enriched with defects of various type and also with radiation transformation products of the system, such as hydrogen and high-molecular compounds. As a result we have either regeneration of the initial molecule or transition in a bound state leading it away from the gaseous phase.

The isotopic molecule content analysis has show that after irradiation of the ethane-deuterated silica gel system with the integral flux of $8 \cdot 10^{16}$ nvt, the remaining ethane contents are: 60% C_2H_6, 25% C_2H_5D, 6% $C_2H_4D_2$ and 1% $C_2H_3D_3$. These data serve as an additional confirmation of the advantage of the decay process into ethyl radical and atomic hydrogen just as it happens at effective scattering of energy by a collision in the case of radiolysis of ethane in the gaseous phase at high pressures /4/.

The role of silica gel as an effective scatterer of ethane excited molecule energy was shown in Ref. /5/ in the case of reactions with hot hydrogen atoms.

Thus the surface of the solid, on the one hand, stimulates more intensive transformation of the adsorbed ethane, and, on the other hand, creates conditions for a more effective scattering of energy of the excited molecules and, in this way, guides the process of radiation transformation of the initial molecule mainly along the making of radicals $C_2H_5^{\cdot}$.

Isotopic analysis data have also shown an active role of hydrogen atoms constituting silica gel and essentially contributing to the processes of radiation transformation of the system /6, 7/.

The participation of radiation generated electron and hole centres of the irradiated silica gel in the radiation transformation processes of the adsorbed ethane has been studied by EPR spectrometry in different conditions of irradiating of the system /8/. The EPR spectra of silica gel, irradiated in vacuum in the channel of the nuclear reactor at 90 K and measured at 77 K, consists of the central complex signal and a symmetrically located to it hydrogen doublet (Fig. 3).

In the central signal we can distinguish the following components: a narrow one with $g = 2.0006 \pm 0.0004$, corresponding to the electrons trapped with an oxygen vacancy, and a wide one with $g = 2.0094$ and $g = 2.0150$ corresponding to the hole centres /1, 9/. The total width of the central part is 90 gauss. Oxygen inlet into the specimen irradiated in vacuum changes the spectra. There appears poorly-permissible signal of components: $g = 2.0080 \pm 0.0005$, $g = 2.0045 \pm 0.0005$, $g = 2.0015 \pm 0.0006$ that is the so called "oxygen line".

Proceeding from the interpretation of the same signal in EPR spectra of silica gel irradiated with ultraviolet light /1/, we can assume that the spectra observed by us corresponds to anion radicals O_3^-.

As has been already mentioned, the spectra also contain a doublet of atomic hydrogen, the value of the hyperfine splitting of which approaches the splitting value for a free atom of hydrogen (507.9 $\pm$ 0.7 gauss).

The doublet components are asymmetrical with different signs of asymmetry and have a structure. There is a difference in width and amplitude of high field and low field components. The concentration of hydrogen atoms at the integral flux of 10^{16} nvt makes up 10^{17} sp/g. The doublet components shape depends on the presence of various gases during the irradiation. The irradiation of SiO_2 with hydrogen containing gases leads to a more clear development of the structure (Fig. 4), whereas the presence of oxygen smoothes it over.

The study of annealed specimens has also shown a great influence of weak heating upon the structure of the doublet. Here, we can observe the vanishing of the structure and an intensity decrease in the doublet components.

A long storage of the specimens (for a year or longer) at 77 K also leads to vanishing of the structure line and a decrease of intensity of the components. Proceeding from the observed experimental data, we can suggest a possibility of the presence of two nonequivalent stabilisation centres for atomic hydrogen in the matrix of the irradiated silica gel. The present suggestion has been checked by a mathematical modelling, assuming that a complex shape of the doublet is caused by a superposition of two types of hydrogen doublets with a consideration of the anisotropy of hyperfine interactions.

The results of mathematical modelling are in satisfactory concordance with the experimental data when elementary components of a complex curve are approximated with the lines described by the Lorentz equation.

The analysis of the complex doublet shape allows us to make a conclusion that from the two types of centres of hydrogen atoms stabilisation, one provides a weak stabilisation directly on the surface of a solid, whereas the second in the surface layer.

The central part of the spectra of the irradiated SiO_2 is also considerably influenced by various radiation conditions.

The presence of hydrogen at irradiation reduces the number of hole centres. The irradiation of the ethane-silica gel system produces the central signal which is the superposition of the trapped electron and ethyl radical signals. The presence of hydrogen containing gases influences also "the oxygen line", preventing its formation. A long storage at 77 K of the specimen, irradiated together with ethane leads to vanishing of the hydrogen doublet structure.

The data of this experiment allow us to think that hydrogen atoms, stabilised in the matrix of the irradiated silica gel, possess mobility at 77 K different from zero. This causes intensity decrease of the hydrogen doublet signal of one order of magnitude at 77 K storage during a year and vanishing of the spectra of the ethyl radical.

The given variety of phenomena taking place on a solid surface in the n,γ-radiation field creates a real possibility for directed property change of materials.

The hydrocarbon gas appears to be the best indicator of the phenomena variety.

Acknowledgment. The auther would like to thank T. V. Ceckhladze for her kind guidance and useful discussions.

References

/1/ S. A. Surin, V. V. Nikisha, B. N. Shelimov, V. B. Kazanski, Khim. Vis. Ener., 8, 1, 1974.

/2/ A. G. Kotov, S. Ya. Pshezhetskii, Khim. Vis. Ener., 6, 4, 1972.

/3/ Ellison H. Taylor. Advances in Catalysis, 18, 1968.

/4/ S. G. Lias, G. I. Collin, R. E. Rebbert and P. Ausloos. J. Chem. Phys. 52, 4, 1970.

/5/ T. V. Ceckhladze, L. I. Cherkesishvili, in "Nuclear-Chemical Phenomena in Solids", Tbilissi, 1968, p. 62. (in Russian)

/6/ L. Sh. Nadirashvili, in "Nuclear-Chemical Phenomena in Solids", Tbilissi, 1973, p. 38. (in Russian)

/7/ V. V. Strelko, K. A. Suprunenko, Khim. Vis. Ener., 3, 2 (258), 1968. Theoretical and Experimental Chemistry, II, N. 5, 1966, p. 694.

/8/ T. V. Ceckhladze, L. Sh. Nadirashvili, B. G. Berulava, Ts. T. Tarkashvili, in "Nuclear-Chemical Phenomena in Solids", Izd. "Metsniereba", Tbilissi, 1973, p. 95. (in Russian)

/9/ L. Sh. Nadirashvili, B. G. Berulava, in "Nuclear-Chemical Phenomena in Solids", Izd. "Metsniereba", Tbilissi, 1972. p. 48. (in Russian)

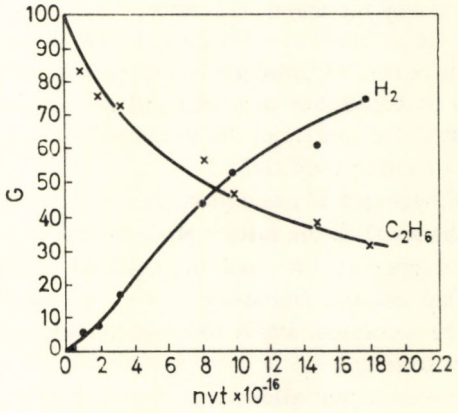

Fig. 1 Dependence of relative hydrogen and ethane molecule yields on thermal neutron integral flux

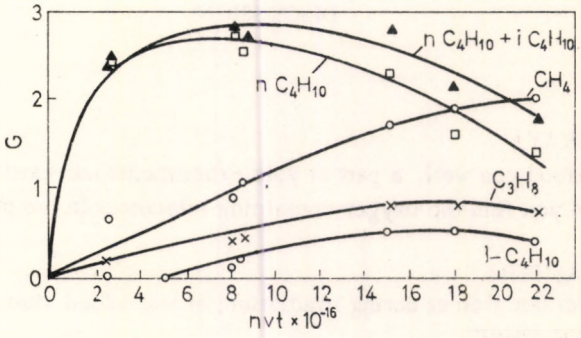

Fig. 2 Dependence of relative yield of gaseous products of the transformation system on thermal neutron integral flux

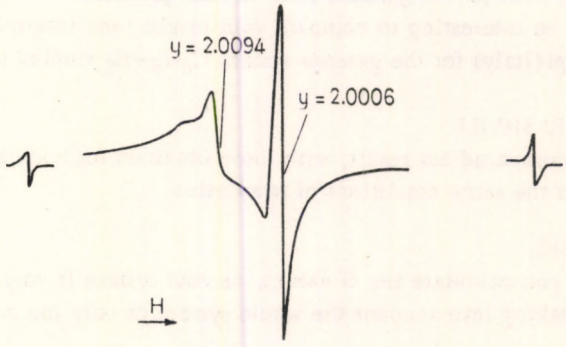

Fig. 3 EPA spectra of silica gel irradiated in vacuum in a channel of the nuclear reacto at 90K

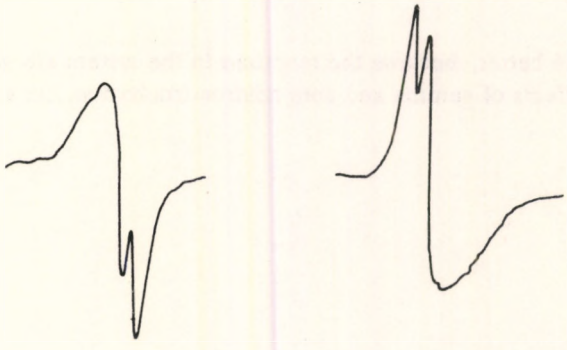

Fig. 4 Atomic hydrogen doublet conponents in EPR spectra of irradiated silica gel

G. V. PUTIRSKAYA

If I understood you well, a part of your experiments was carried out in the presence of oxygen. Did you find the oxygen containing substances in the products of radiolysis?

L. Sh. NADIRASHVILI

Oxygen was not present during irradiation, it was added after irradiation of the silica gel ethane system.

H. WINCEL

Have you estimated what part of the final products observed were formed in the gas phase and what part originated from surface processes?

It would be interesting to compare your results (and interpretation) with the data found by Volpi (Italy) for the gaseous system $C_6H_6-H_2$ studied by mass spectroscopy.

L. Sh. NADIRASHVILI

We have compared our results with those obtained for homogeneous hydrocarbon systems under the same conditions of irradiation.

J. KALECINSKI

How do you calculate the G values, as your system is very complicated. Do you calculate it taking into account the whole system or only the compounds absorbed on silica gel?

L. Sh. NADIRASHVILI

We have calculated the yields of products relatively to the initial amount of hydrocarbon gas. The total amount of the gas was taken into account.

M. MAGAT

It would be better, because the reactions in the system are very complicated, to separate the effects of gamma and pure neutron irradiation, for example by means of Bi.

GAMMA RADIOLYSIS OF PEPTIDE AND MACROLIDE ANTIBIOTICS IN THE SOLID STATE

J. O. Dzięgielewski, B. Jeżowska-Trzebiatowska, E. Kalecińska, J. Kuduk-Jaworska

Institute of Chemistry, The University, Wrocław, Poland
J. Kaleciński, J. Nawojska
Institute for Low Temperatures and Structure Research, Polish Academy of Sciences, Wrocław, Poland

In recent years increasingly more attention has been paid to the effect of ionizing radiation on antibiotics. This fact results, above all, from urgent needs for technical progress in the antibiotic sterilization processes. The results of experimental studies on the effect of ionizing radiation on antibiotics have already been discussed in some papers /1–8/. A few papers /9, 10/ concern the radiation-chemical processes occurring in irradiated antibiotics, others are confined to the studies of changes in biological activities of irradiated antibiotics or to the determination of changes in some physico-chemical properties occurring after their irradiation.

The aim of the present study is to determine the yields of radiation decomposition of the whole series of antibiotics and to elaborate the mechanism of their radiation decomposition. These results, apart from the scientific point of view, should also create the conditions for radiation sterilization of antibiotics.

Of basic significance in therapeutics are the peptide and macrolide antibiotics. Hence, in the present paper some of our results concerning these groups of antibiotics will be discussed.

The structural formulae of penicillins, viomycin sulphate and erythromycins are shown in Fig. 1.

The amount of molecules decomposed under irradiation is a linear function of the dose. The yields calculated from the slopes of the corresponding straight lines are presented in Table 1. As one can see from Table 1 the resistance of antibiotics against radiation is similar to their chemical stability, i. e. penicillin and erythromycin salts are more resistant than the corresponding acids and bases. The opposite is observed in the case of aminobenzylpenicillin, where the acid creates the intramolecular salt /17/, which leads to the higher stability, both radiation and chemical.

From the data presented in Table 1 one can see the role of the cations attached to penicillin and anions which form salts with erythromycin. The big organic cation (in procaine benzylpenicillin) or the relatively radioresistant stearic acid (in erythromycin stearate) affect the yields. In these cases the decomposition yields are less significant than in the antibiotics not having such groups. The organic cations act as protecting agents against the decarboxylation of penicillin. This was shown

Table 1

The yields of antibiotics decomposition

Antibiotics	The number of molecules per 100 eV determined by:			Decomposition after 3 Mrads in %	The number of radicals per 100 eV
	CD, ORD	iodometrically	spectrophotometrically		
1	2	3	4	5	6
6-APA	4,8 (11)	4,7 (13)	-	0.32	-
benzylpenicillin acid	28,8 (11)	-	-	-	-
benzylpenicillin K salt	7,2 (11)	-	-	0.60	0.16
procaine benzylpenicillin salt	2,2 (11)	3,5 (11)	-	0.65	0.80
phenoxymethylpenicillin acid	6,3 (11)	-	-	0.70	-
potassium phenoxymethylpenicillin salt	5,4 (11)	-	-	0.70	-
methyl phenoxymethylpenicillin ether	4,8 (11)	-	-	-	-
cloxacillin	10,4 (11)	11,7 (11)	11,5 (11)	1.60	-

Na cloxacillin salt	6,5 (11)	-	-	approx. 1	2.16
aminobenzylpenicillin x 3 H_2O	9,1 (12)	10,9 (13)	10,3 (13)	1.40	0.55
aminobenzylpenicillin x 2 H_2O	7,4 (12)	-	-	approx. 1	-
aminobenzylpenicillin	5,4 (12)	-	-	0.6	-
Na aminobenzylpenicillin salt	10,8 (12)	-	-	-	-
carboxybenzylpenicillin	8,6 (14)	11,1 (14)	11,1 (14)	1.4	0.07
sulphate viomycin	4,2 (15)	-	4,2 (15)	approx. 1	1.0
erythromycin x 2 H_2O	-	-	2,9 (16)	0.7	3.2
erythromycin	-	-	2,5 (16)	0.6	2.0
erythromycin stearate	-	-	2,3 (16)	0.7	3.3
erythromycin estolate	-	-	2,8 (16)	approx. 1	2.3

in the cases of procainebenzylpenicillin /18, 20/, N, N'-dibenzylethyldiamine penicillin G /19/ and N, N'-dibenzylethyldiamine /19/.

As one can see from Fig. 2 the EPR spectra of irradiated N, N'-dibenzylethyldiamine and benzatine penicillin are similar for both substances. The hyperfine structure of the spectra consist of two quintets (A_d = 26 Gs and A_q = 5,7 Gs). From this the radical structure presented in Fig. 3 could be concluded.

During heating of irradiated benzatine penicillin the decay of the multiplet EPR signal and the appearance of a new signal with g-anisotropy is observed. The spectrum is explained by location of an unpaired electron on the S-atom in the thiazolidine ring. It brings about the lowering of the radiation decomposition yield.

The integrated NMR signals from erythromycin and erythromycin stearate as a function of the dose are presented in Figs 4 and 5. From the decay of the signals one can conclude that the corresponding groups are protected by the organic anions /16/. These results suggest that scavenging of the H atoms by the organic anions leads to the decrease of the possibility of interaction between H atoms and CH_3, CH_2, CH and OH groups in the macrolide

$$H_3C-R + H \dashrightarrow CH_4 + R$$

The dissipation of the excitation energy by the chain anion in erythromycine salt has also played a significant role.

The data presented in Figs 4 and 5 indicate that the amount of some decomposed groups in the erythromycin base are not a linear function of the dose, hence the important role of the secondary processes in erythromycine radiolysis is suggested.

The increase of the gaseous products from 2.3 mol./100 eV for erythromycin base to 4.0 mol./100 eV for erythromycin stearate /16/ confirms the conclusion that the stearate anion can protect the erythromycin molecule against radiation.

There is evidence based on spectroscopic measurements of isolated radiolysis products of penicillins /11, 12, 21/ as well as on spectroscopic examination of penicillins /12/ themselves, that the thiazolidine-β-lactam system is the most sensitive place to radiation.

As one can see from Table 1 the yields of penicillin decomposition determined spectropolarimetrically (C. D. and ORD) are slightly lower than those determined iodometrically. The measurements based on the Cotton effect (22–24) are connected only with the electron transitions $n \dashrightarrow \pi^*$ in C = O or $n \dashrightarrow \sigma^*$ in C – S – C groups in the thiazolidine-β-lactam system. On the other hand, the iodometric method determined the change in the whole antibiotic molecule. Hence, the difference between these two methods gives the radiation decomposition occurring in other sites of the molecule. In the case of aminobenzylpenicillin one can easily calculate that 84% of the change takes place in the thiazolidine-β-lactam system and only 16% in other parts of the molecule /12/. This conclusion is supported by the fact that in the 6–APA case the decomposition yields determined by spectropolarimetric and iodometric methods are similar (Table 1).

Changes of the NMR signals obtained from viomycin sulphate irradiated with 107 Mrads and measured in D_2O at pD = 1

Proton No. according to formula	Chemical shift in non-irradiated substances*	Chemical shift in irradiated substances	Type of changes resulting from irradiation
1	2	3	4
-	-	6.61	A new signal occurs
15	6.98	-	Signal disappears
20, 24	7.87	7.87	No changes observed
31, 35	7.97	7.98	Very weak signal
9	8.10	-	Signal disappears
8, 31, 35	8.21	8, 15 and 8, 23	Very weak signal, change of multiplets structure
12	8.41	8.37	Very weak signal
37	8.35	8.55	Weak signal
6	8.68	-	Signal disappears
27	8.97	8.83	Weak signal and shift
20, 22	9.10	9.10	Weak signal
7	9.35	-	Signal disappears
13	9.75	-	Signal disappears
-	-	9.62	New signal appears
16	9.85	-	Signal disappears
-	-	9.71	New signal appears

*The chemical shifts obtained by us are in very good agreement with the data of Ref. /25/

In Table 2, some radiation changes in viomycin sulphate are presented /15/.

On the basis of the results presented in Table 2 irradiation of viomycin sulphate may be found to result in the tearing away or fragmentation of aliphatic substitutes in the polypeptide ring and in the viomycine fragment (disappearance of the NMR signals from protons 6, 7 and 8). Disappearance of the NMR signal from proton 9 indicates either polypeptide ring cleavage or proton rearrangement. The decay of the signals from protons 13 and 15 and the attenuation of the signals from proton 12 show that the chain linked to carbon atom 11 is torn away or that the bonds between atoms 12 and 13, and 14, or 14 and 15 are broken with simultaneous rearrangement of protons in the fragments formed. In the case of the bond breaking between carbon 12 and 13 it is most probable that urea is formed. In gaseous and volatile products (determined by means of an omegatron) a weak peak of M/e = 60 may be found which seems to confirm the above conclusion. The occurrence of the peak with M/e = 45 in the gaseous products also supports the probability of bond cleavage between atoms 13 and 14, which results in the formation of formamide. Hydrogen, carbon dioxide and monoxide, as well as hydrocarbons are, however, the main gaseous products evolved during the radiolysis of viomycin sulphate /15/. The chain linked to the polypeptide ring through carbon 26 is also torn away or fragmented as probably indicated by the weaker signals from protons 26 and 35.

The above presented changes are supported by I. R. study of irradiated viomycin sulphate /26/. The decrease of the vibrational intensities of the C = C bond (945 cm^{-1}), C–C and C–N bonds (880 cm^{-1}) and SO_4^{2-} group (970 cm^{-1}) has been observed. From the observation we can conclude that the most sensitive to radiation are the chemically labile fragments of viomycin sulphate.

Similar changes to those presented above have also been observed for irradiated erythromycins as has been shown in Table 3. The intensity decrease of the C–O–C vibration /27/ is evidence for bond breaks between particular rings of antibiotics.

Crystalline water brings about the increase of the radiation decomposition yields of antibiotics (Tables 1 and 3). This is caused by reactions between the radical products of water radiolysis and the thiazolidine-β-lactam ring. As a result of these reactions carboxylation of the C = O group occurs and the ring is opened /12, 19/. However, as was shown in /12/, crystalline water may cause a decrease of the decomposition yields of some groups in penicillins (NH_2 group in aminobenzyl-penicillin).

In irradiated erythromycins the influence of water on the yields is less important because of the intramolecular hydrogen bonds between water molecules and OH groups of all erythromycin rings /16/. Hence, the influence of water molecules on the whole big erythromycin molecule is weak. The radio-protection role of the hydrogen bond in the examined antibiotics seems to support the important role of the excited molecules in the mechanism of radiation decomposition of antibiotics.

The mechanism of radiation decomposition of solid antibiotics was found to exhibit a stepwise character with contribution of excited molecules and radicals /12/. The radicals have been identified /19, 20/ and some results concerning their yields

Table 3

Relative intensity changes of some frequencies, in conventional units, for dehydrated and hydrated erythromycins depending on the radiation dose

Type of group	Frequency (cm^{-1})	Intensity change in conventional units											
		Dose in Mrads											
		5.6		11.2		16.8		22.5		28.1		39.3	
		D	H	D	H	D	H	D	H	D	H	D	H
CH_3	1445	0	0	1	1	1	1	2	2	2	2	3	3
C = O	1710	0	0	1	1	1	1	2	2	2	2	2	3
C–O–C	1004	0	0	1	1	1	1	2	2	2	2	2	3
CH	2964	0	0	1	1	1	1	1	1	1	2	1	2
OH	3500	0	0	0	1	0	1	1	2	1	2	1	2

D – dehydrated substance; H – hydrate

Conventional scale of changes:

0 – no intensity change
1 – slight decrease in intensity
2 – medium decrease in intensity
3 – considerable decrease in intensity

are presented in Table 1. In irradiated penicillins the radicals are produced as a result of breaking, deprotonation or decarboxylation of the thiazolidine-β-lactam system. In the hydrates, the reactions of OH radicals and to some extent of the H-atoms of water radiolysis with the thiazolidine-β-lactam system lead to the increase of the decomposition yields of hydrates in comparison with the anhydrous penicillins.

The yields of radicals in semisynthetic penicillins consisting of $-NH_2$ or -COOH groups are higher but the radicals are unstable. Some of the primary radicals recombine, some of them give new radicals in which unpaired electrons are located on the benzene ring. The dislocation of the unpaired electron is shown in Fig. 6. As a result of this dislocation secondary radicals are produced but they further recombine with H atoms giving hexadionyl products which can bind I_2. This process can also explain why the decomposition yields determined iodometrically are slightly higher than those determined spectropolarimetrically.

Conclusions

1. The radio-sensitivity of the examined antibiotics is similar to their chemical stability, i. e. relatively high radiation decomposition yields are observed in less stable antibiotics;
2. Radiation attacks the chemically most labile fragments of the antibiotic (i. e. thiazolidine-β-lactam system in penicillin molecules);
3. The radical products of water radiolysis cause an increase of decomposition yields;
4. Intramolecular hydrogen bonds affect both the yields of decomposition and the direction of the radiation chemical processes;
5. The size and the direction of radiation changes in irradiated antibiotics suggest that there is a high possibility to sterilize by radiation some of the antibiotics.

References

/ 1/ Z. V. Ermolieva, V. I. Pochapinskij, Med. Prem. 1, SSSR, (1961).

/ 2/ Z. V. Ermolieva, V. I. Pochapinskij, A. H. Breger, Antibiotiki, 10, 904 (1961).

/ 3/ J. Holland, F. Antoni, J. Galatzenu, M. Schulman, G. J. Kozinets, (Int. At. Energy Agency, Vienna, Austria), Radiosteryl. Med. Prem. Recam. Code. Pract. Symp. Results Panel Meet. 1966–1967, 69–81, publ. 1967.

/ 4/ V. J. Pochapinskij, Z. V. Ermolieva, Antibiotiki, 9, 786 (1962).

/ 5/ V. A. Cyganov, N. S. Vasiljeva, Antibiotiki, 1, 47 (1971).

/ 6/ G. M. Eglazarova, Mied. Prem., 4, 12 (1959).

/ 7/ Ju. O. Sazykin, S. M. Chajkovskaja, V. B. Korchagin, M. A. Panina, V. N. Ivanova, V. A. Balickij, E. A. Vajner, Antibiotiki, 16, 10, 923 (1971)

/ 8/ G. Curatola, A. Addario, C. Garroni, Minerva Medice, 60, 81 3903 (1969).

/ 9/ V. V. Bochkariev, V. A. Gromov, V. V. Chrapov, V. J. Panin, N. D. Konievzkaja, T. P. Klimova, G. E. Salikova, L. A. Mołodov, A. F. Usatyj, Antibiotiki, 11, 394 (1972).

/10/ G. O. Phillips, D. M. Power, C. Robinson, J. Chem. Soc. Perkin Trans. II, 575 (1972).

/11/ J. Dzięgielewski, B. Jeżowska-Trzebiatowska, E. Kaleciński, J. Kaleciński, J. Nawojska, I. Z. Siemion, Nukleonika, 18, 513 (1973).

/12/ J. O. Dzięgielewski, Int. J. Radiat. Phys. Chem., 7, 507 (1975).

/13/ J. Dzięgielewski, J. Nawojska, Report of Institute of Chemistry, University of Wrocław, p. 39 (1973) (unpublished).

/14/ J. Dzięgielewski, J. Nawojska, Report of Institute of Chemistry, University of Wrocław, p. 5 (1974).

/15/ B. Jeżowska-Trzebiatowska, J.Dzięgielewski, J. Kuduk-Jaworska, J. Kaleciński, J. Nawojska, E. Kalecińska, Nukleonika, 20, 247 (1975).
/16/ J. Dzięgielewski, J. Kaleciński, E. Kalecińska, J. Kuduk-Jaworska, J. Nawojska, Nukleonika, in press.
/17/ J. Dzięgielewski, J. Hanuza, B. Jeżowska-Trzebiatowska, J. Kuduk-Jaworska, Bull. Acad. Polon. Sci. ser. sci. chim., 21, 657 (1973).
/18/ J. Dzięgielewski, B. Jeżowska-Trzebiatowska, Nukleonika 19, 303 (1974)
/19/ J. O. Dzięgielewski, A. Jezierski, B. Jeżowska-Trzebiatowska, H. Kozłowski, Bull. Acad. Polon. Sci. ser. sci. chim., 22, 635 (1974).
/20/ J. Dzięgielewski, B. Jeżowska-Trzebiatowska, H. Kozłowski, Bull. Acad. Polon. Sci. ser. sci. chim., 21, 605 (1973).
/21/ J. Dzięgielewski, B. Jeżowska-Trzebiatowska, I. Z. Siemion, A. Zabża, Nukleonika, 19, 291 (1974).
/22/ I. Z. Siemion, J. Lisowski, B. Tyran, J. Morawiec, Bull. Acad. Polon. Sci. ser. sci. chim., 20, 549 (1972).
/23/ J. Lisowski, I. Z. Siemion, B. Tyran, Roczniki Chemii, 47, 2035 (1973).
/24/ R. Nagarajan, L. D. Boeck, M. Gorman, R. L. Hamill, C. E. Higgens, M. M. Hoehn, W. M. Stark, J. G. Whitney. J. Am. Chem. Soc., 93, 2310 (1971).
/25/ P. Viglino, C. Franconi, A. Lai, E. Brosio, F. Centi, Organic Magnetic Resonance, 4, 237 (1972).
/26/ B. Jeżowska-Trzebiatowska, J. Dzięgielewski, J. Hanuza, J. Kuduk-Jaworska, Bull. Acad. Polon. Sci. ser. sci. chim., 22, 421 (1974).
/27/ J. Dzięgielewski, J. Hanuza, B. Jeżowska-Trzebiatowska, J. Kuduk-Jaworska, Bull. Acad. Polon. Sci, ser. sci. chim., 23, 513 (1975)

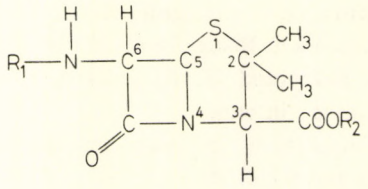

for example

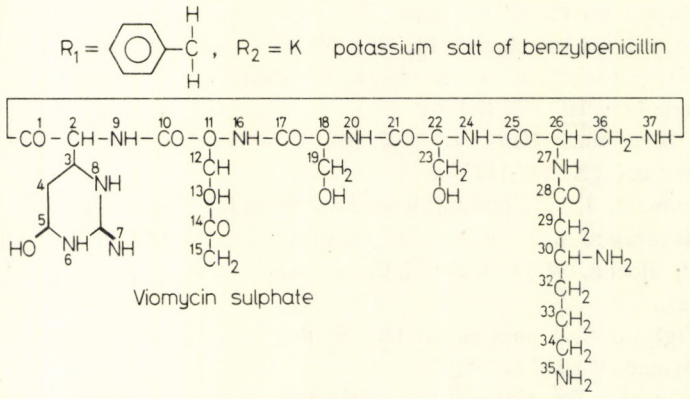

Viomycin sulphate

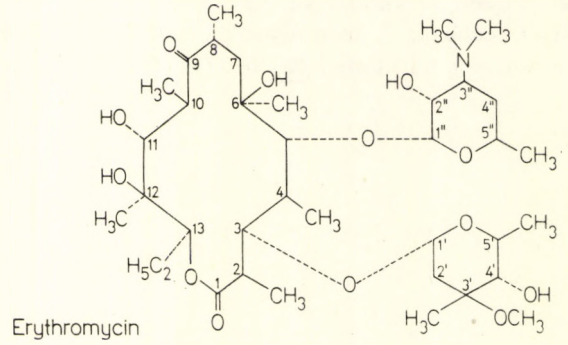

Erythromycin

Fig. 1 The formulae of penicillin, erythromycin and sulphate viomycin

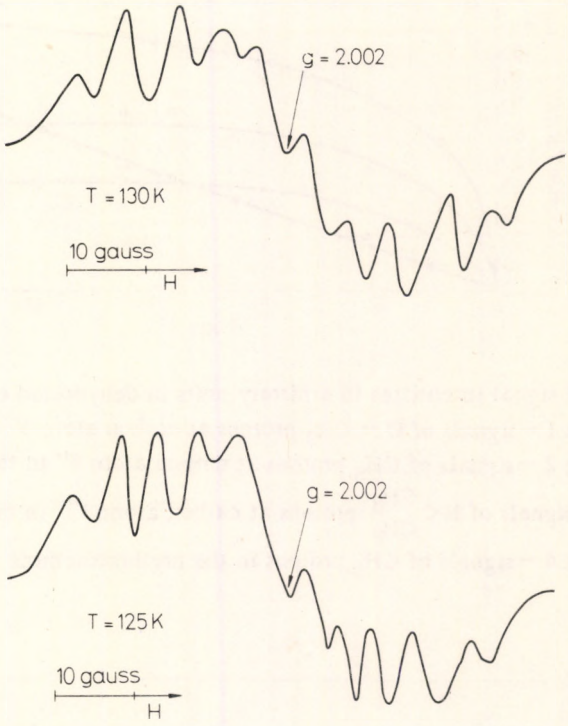

Fig. 2 EPR spectrum of N, N'-dibenzylethylenediamine and benzatine penicillin gamma-irradiated with 107 Mrads at 125 K

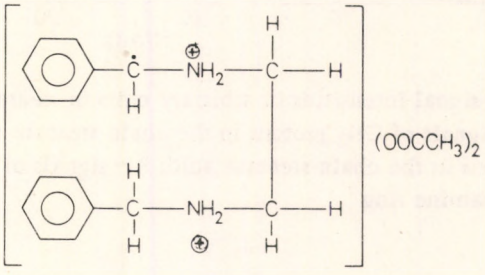

Fig. 3 Radical structure

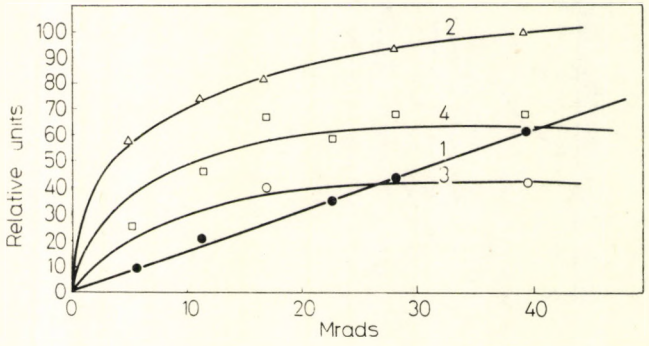

Fig. 4 NMR signal intensities in arbitrary units in dehydrated erythromycin vs. dose: 1 – signals of O – CH_3 protons at carbon atom 3′ in the cladinose ring; 2 – signals of CH_3 protons at carbon atom 5″ in the desosamine ring; 3 – signals of $N<\begin{matrix}CH_3\\CH_3\end{matrix}$ protons at carbon atom 3‴ in the desosamine ring; 4 – signals of CH_3 protons in the erythrolosamine ring.

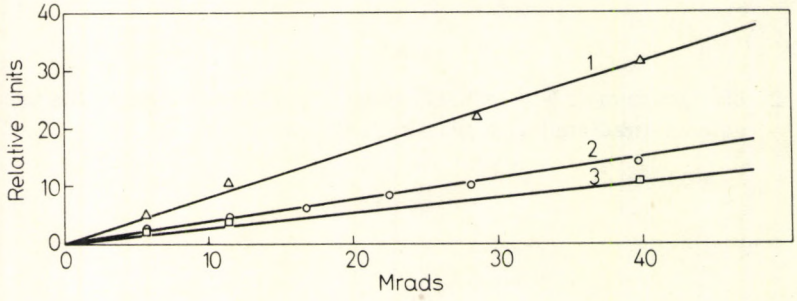

Fig. 5 NMR signal intensities in arbitrary units in stearate erythromycin vs. dose: 1 – signals of CH_3 protons in the chain stearate acid; 2 – signals of CH_2 protons in the chain stearate acid; 3 – signals of $N<\begin{matrix}CH_3\\CH_3\end{matrix}$ protons in the desosamine ring

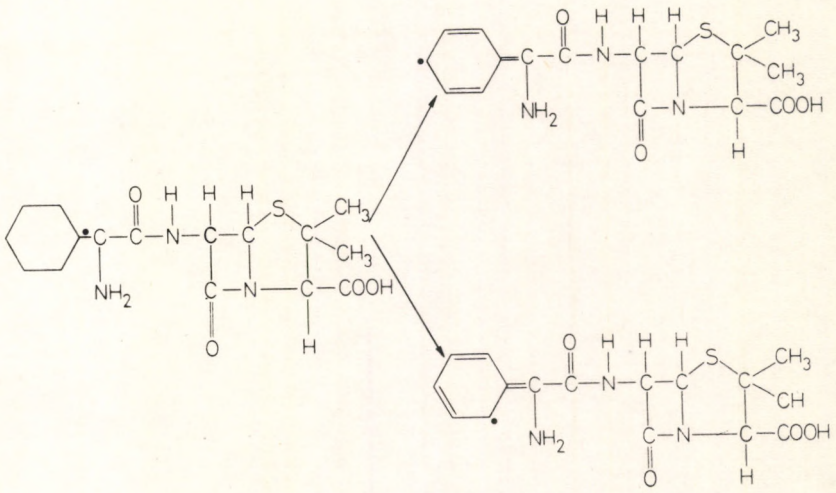

Fig. 6 The resonance structure of the radicals with a delocalized unpaired electron

DISCUSSION

I. KRALJIC

Do you have any direct evidence that OH-radicals are involved in the destruction of antibiotics?

J. O. DZIEGIELEWSKI

We have presented here only some of our results. Some of these have been published (see the references of the paper) The problem of the OH-radicals is discussed in Refs/18/ and /19/. In Ref. /19/ we reported the observation of different signals in irradiated hydrated and unhydrated aminobenzyl penicillin and concluded about the role of OH-radicals.

Unfortunately we could not give a direct evidence of this process because our ESR spectrometer could be operated only above $-150^{\circ}C$.

THE ROLE OF H ATOMS IN THE RADIOLYSIS OF HYDROGEN-CONTAINING SUBSTANCES

B. G. Dzantiev, A. N. Ermakov, V. N. Popov
Institute of Chemical Physics, Academy of Sciences of the USSR, Moscow, USSR

The radiolysis of even simple substances implies considerably complicated mechanisms. They consist of a series of elementary steps and several active species (ions, atoms, radicals, molecules) the latter ones in different energy-states.

Apparently this is the reason why the detailed mechanisms of radiation chemical transformations are not fully understood even in the case of the best known and simplest systems. A mechanism can be regarded as complete if it can describe or predict (both qualitatively and quantitatively) the dependence of the yields for each and any product as a function of the basic parameters (q), i. e. of time (t), temperature (T), pressure (p), composition of the system (ν), dose (D) and dose-rate (δ).

The practical situation is made somewhat clearer by the fact that the complicated mechanism of general validity can be simplified for certain areas of the radiolysis parameters $q = t, D, \delta, T, p, \nu$, where, as a first approximation, only a limited group of elementary reactions play a role. Under well-defined conditions one can determine the rate of one or two "critical" elementary reactions.

In the case of the important class of hydrogen-containing substances the reactions with atomic hydrogen appear often as "critical". Now we illustrate this situation by the gas phase radiolysis of two important and simple hydrogen-containing substances, ammonia and hydrogen sulphide.

Ammonia is one of the most important and at the same time a relatively simple object of radiation chemical research. Only three stable products form during its irradiation these being H_2, N_2 and N_2H_4 which makes ammonia a rather appropriate model in gas-phase radiation chemistry. Despite the apparent simplicity of the substance the present understanding of the laws of ammonia radiolysis is far from being complete. The results obtained by different research groups exhibit substantial disagreements. This refers to both the character of the dependences of yields on the radiolysis conditions and the magnitude of the product yields. Product means here either primary species (i. e. atoms and radicals) or stable molecules (i. e. hydrogen, nitrogen and hydrazine). The scatter of the results is particularly large for the latter group in that they lie in a range of several orders of magnitude. According to different

authors the limits are as follows:

$$G^{o}_{H} = 4.8 - 11.7, \qquad G^{o}_{NH_2} = 4.8 - 10.3,$$

$$G(H_2) = 2.3 - 15, \qquad G(N_2) = 0.7 - 5, \qquad G(N_2H_4) = 10^{-3} - 3.$$

The present work gives an account on the irradiation of ammonia, both in the pure state and containing scavengers, with γ-rays, fast electrons, mixed $n + \gamma$ radiation of a nuclear reactor, α-particles, fission products and multicharged accelerated ions (these last ones being C^{6+}, N^{7+}, O^{8+}, Ne^{10+}, Ar^{18+} and having an energy of 7MeV/nucleon and a total energy of E = 84−280 MeV). Both steady-state and pulse irradiations were used in static, flowing and recirculating systems. This demanded the development and construction of a series of irradiation facilities where radiolysis can be carried out thermostated, with different irradiation periods t, doses D, and dose-rates δ. At the same time several methods in dosimetry were developed and determinations of the intensity-distribution in the beams of accelerated particles were performed.

A characteristic series of the applied kinetic methods is the following: the investigation of time-dependence, detailed studies with scavengers of different active species and the application of competitive reactions. Mathematical models of the processes were developed by making use of a computer in several cases.

The product yields of ammonia radiolysis by fast electrons at p = 700 torr as a function of a number of experimental parameters are given in Figs 1. and 2. It is characteristic to all these plots that there exists a certain interval of the parameters $q = \delta$, T where the yields G_i are practically constant and at the same time one can always find an interval Δq where G_i or its first derivative $\partial G_i / \partial q_j$ changes at an experimentally significant rate. It has to be pointed out that all these rules are to be regarded as broad generalizations and the substantial scatter in the yields obtained by different laboratories is inherent in the data.

There is a wealth of ammonia radiolysis data both from our own laboratory and from different authors /1−7/ among which the names of Pshezhetskii et al. (USSR), Johns and Sworsky (USA), Gordon et al. (USA), Willis and Boyd (Canada), Belloni et al. (France) should be mentioned. These results enable one to construct a radical mechanism in the form of a system of elementary steps where the radicals R = ˙H, ˙NH, NH_2 play the central role,

$$NH_2 + NH_2 \rightarrow N_2H_4 \qquad (1)$$

$$NH_2 + NH_2 \rightarrow NH + NH_3 \qquad (1^a)$$

$$H + NH_2 \rightarrow NH_3 \qquad (2)$$

$$H + NH_2 \rightarrow NH + H_2 \qquad (2^a)$$

$$H + H + M \longrightarrow H_2 + M \qquad (3)$$

$$H + N_2H_4 \longrightarrow H_2 + N_2H_3 \qquad (4)$$

$$NH_2 + N_2H_4 \longrightarrow NH_3 + N_2H_3 \qquad (5)$$

$$H + NH_3 \longrightarrow H_2 + NH_2 \qquad (6)$$

$$N_2H_3 + N_2H_4 \longrightarrow N_2 + 2\,NH_3 \qquad (7)$$

$$NH + NH_3 \longrightarrow N_2H_4 \qquad (8^a)$$

$$NH + NH_3 \longrightarrow N_2 + 2\,H_2 \qquad (8)$$

$$NH + NH \longrightarrow NH_2 + N \qquad (9^a)$$

$$NH + NH_2 \longrightarrow NH_3 + N \qquad (9^b)$$

$$NH + H \longrightarrow H_2 + N \qquad (9^c)$$

$$N + NH \longrightarrow N_2 + H \qquad (10)$$

$$N + N + M \longrightarrow N_2 + M \qquad (11)$$

The proposed mechanism has the following special features:

(1) It is a radical mechanism. Ions and ion–molecule reactions (together with the decompositon of excited molecules) play important roles in the formation of the chemically active neutral species, they do not contribute, however, directly to the production of stable molecules (with the possible exception of a small amount of hydrogen represented by the yield $G_{H_2} \leq 0.75$).

(2) Both the strictly taken primary decomposition of NH_3 and the fast ion-molecule reactions (half-life about $10^{-9} - 10^{-10}$ sec) are counted to the primary "pre-chemical" processes during which the active species are produced.

$$NH_3 \rightsquigarrow NH_3^* \longrightarrow H + NH_2 \qquad I^a$$

$$NH_3^* \longrightarrow H_2 + NH \qquad I^b$$

$$NH_3 \rightsquigarrow NH_3^+ + e \qquad II^a$$

$$NH_3 \rightsquigarrow NH_2^+ + H + e \qquad II^b$$

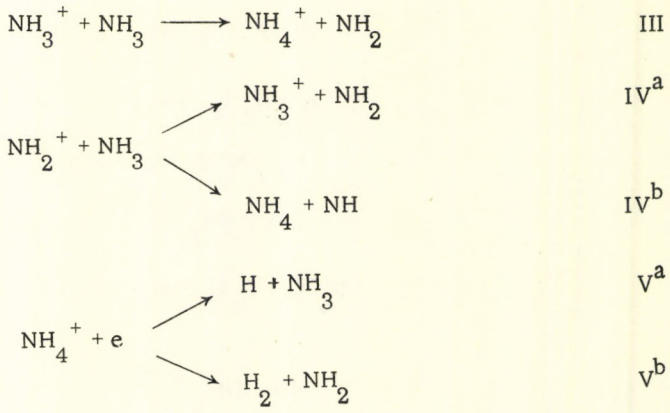

The radiation chemical yields of the ions and the rate-constants of ion-molecule reactions are known from mass-spectral data.

(3) The primary yields of the radicals ·H, ·NH and ·NH_2 were determined by special scavenger experiments where the scavenger, Ac added to ammonia was C_2H_4 or $(CH_3)_2NH$ and the parameters $q = \delta$, T, [Ac] were changed, the interval for the latter being $10^{-5} \leqslant [Ac] / [NH_3] \leqslant 5 \times 10^{-1}$. A number of products were observed (the precursors of which were one or other active species) they being hydrogen, ethane, butane and other $C_1 - C_6$ hydrocarbons, $C_2 - C_6$ aliphatic amines, hydrazine, "unscavengable" hydrogen and the decomposition products of the scavenger. By analysing the product yields as a function of irradiation parameters $G_i^{prod} = G_{i(q)}$, accounting for the side-processes and for the differences in the reactivity of the radicals using several independent methods, the following yields were found for the active precursors:

$G^o_H = 8.0 \pm 0.6$; $G^o_{NH_2} = 8.3 \pm 1.0$; $G^o_{NH} = 0.75 \pm 0.05$. The ratio $G^o_H : G^o_{NH_2} : G^o_{NH} = 1 : 1 : 10^{-1}$ can be given with reasonable accuracy.

(4) The contribution of the elementary reactions (1 – 11) of the mechanism changes with changing conditions of irradiation. Thus, for example reactions (4, 5, 7) play an important role only if t is sufficiently long to secure a steady concentration of N_2H_4, the role of reactions (6 – 8) becomes more important if T is high and δ is low, whereas second-order processes (1, 2, 3, 9) prevail at high dose rates, δ and low temperatures, T.

(5) Radicals ·H, ·NH and ·NH_2 appear both in primary and in secondary processes (6, 10, 2a, 1a). A part of ·H atoms and ·NH_2 radicals "transform" into ·NH radicals via reactions (1a, 2a), a phenomenon which increases the contribution of this highly reactive radical in the overall process of

ammonia radiolysis over the expectations based on the corresponding primary yields $G^{o}_{NH}/G^{o}_{H} \simeq 10^{-1}$. Although secondary radicals as $^{\cdot}N_2H_3$ and $^{\cdot}N$ contribute to the formation of final products (cf. reactions 7, 10, 11), this is also defined by the "weight" of the reactions of the basic radicals $^{\cdot}H$, $^{\cdot}NH_2$ and $^{\cdot}NH$ (cf. reactions 4, 5, 8).

(6) The "critical" processes in the scheme (1−11) are H atom reactions (2, 6). It is expedient to introduce a new parameter $\xi = \xi(\delta, T)$, which determines the relationship between the first-order and second-order channels of H disappearance. If the ratio $k_1 : k_2 : k_3 = 10^{-1} : 1 : 10^{-2}$ holds then for periods $t < (k_4[H] + k_5[NH_2])^{-1}$ one obtains $\xi = W_6/W_2$.

The new parameter ξ, which increases with decreasing T (E = 13.6 Kcal/M) and decreases with increasing δ, determines the rate of the secondary formation of $^{\cdot}NH$ (Eqs 2a, 1a) and $^{\cdot}NH_2$ (Eq. 6) radicals. Its magnitude indicates those particular temperature and dose-rate ranges on the [δ, T] plane, where simpler limiting laws prevail within the general mechanism (Eqs 1−11). The change from a T, δ range where $\xi > 1$ (high T and low δ) to another one where $\xi < 1$ (low T and high δ) involves a change both in the character of the $G_i = G_i(T, \delta)$ functions and in the G_i values. The introduction of the analogous parameter $\xi' = W_8/W_9$ turns out to be equally useful.

The yields of stable products of ammonia radiolysis can be expressed by independently determined radical yields and elementary reaction rates:

$$G(H_2) = G^{o}(H_2) + G^{o}_{H}\left(\varepsilon_4 + \varepsilon_6 + \varepsilon_{2a} + \frac{\varepsilon_3}{2}\right) + \left[G^{o}_{NH} + G^{o}_{H}\,\varepsilon_{2a} + G^{o}_{NH_2}(1 + \varepsilon_6)\frac{\varepsilon_{1a}}{2}\right]$$

$$\left[2\,\varepsilon_8 + \varepsilon_{10}\left(\varepsilon_{2a} + \frac{\varepsilon_3}{2} + \varepsilon_4 + \varepsilon_6\right)\right] \qquad \text{I}$$

$$G(N_2) = \frac{G^{o}_{H}\,\varepsilon_4\,\varepsilon_7}{2} + \frac{G^{o}_{NH_2}(1 + \varepsilon_6)\,\varepsilon_5\,\varepsilon_7}{2} +$$

$$+ \left[G^{o}_{NH} + G^{o}_{H}\,\varepsilon_{2a} + G^{o}_{NH_2}(1 + \varepsilon_6)\frac{\varepsilon_{1a}}{2}\right]\left[\varepsilon_8 + \varepsilon_{10} + \frac{\varepsilon_{11}}{2}(\varepsilon_{9a} + \varepsilon_{9b})\right] \qquad \text{II}$$

$$G(N_2H_4) = G^{o}_{NH_2}\,\varepsilon_1\,\alpha\,(1 + \varepsilon_6)\frac{1}{2} + \varepsilon_{8a}\left(G^{o}_{NH} + G^{o}_{H}\,\varepsilon_{2a} + G^{o}_{NH_2}\frac{(1-\alpha)}{2}\,\varepsilon_1\right) \qquad \text{III}$$

where $\varepsilon_i = \dfrac{W_{ij}}{\Sigma W_{ij}} = f(\xi)$, W_{ij} is the rate of disappearance of radical j <u>via</u> channel i and $\alpha < k_{2a}/(k_2 + k_{2a})$.

Irrespective of the analogy which exists between H_2S and NH_3, basic differences in the energy-states of H atoms and corresponding incongruencies in the two mechanisms can be observed.

There are two interrelated problems in photochemistry and radiation chemistry as branches of high energy chemistry: (a) to what extent can a certain process be described in terms of Arrhenius-type kinetics and (b) is it always possible to make use of photo- or radiation-decomposition of molecules as a method of obtaining hot atoms and radicals and of determining the rate-constants (pre-exponential factors and activation energies) for their elementary reactions.

A comparative study of the kinetics of photolysis ($\lambda = 2537$ Å) and γ-radiolysis (^{60}Co) carried out with binary $H_2S - C_2H_4$ mixtures in the gas phase is described in the present paper. The principal methods consisted of the investigation of the effect of composition, dose, temperature and addition of chemically inert moderating agents (M = He, N_2) on the yields of the main products, i.e. H_2 and C_2H_6.

Important information is rendered by the comparison of the responses of the photolyzed and radiolyzed mixtures elicited by the same effects. Photolysis unequivocally results in the formation of hot atoms due to energy and momentum conservation. The formation of hot hydrogen atoms H^+ to participate in chemical reactions can be assessed by the deviation of the rate constants of elementary reactions (bond scissions) from Arrhenius-type behaviour.

$$H + H_2S \longrightarrow H_2 + SH \qquad (12)$$

$$H + C_2H_4 \longrightarrow C_2H_5 \qquad (13)$$

In the course of mercury-lamp photolysis of the hydrogen sulphide – ethylene mixture effective energy-transfer takes apparently place from the excited ethylene molecules to hydrogen sulphide and no H atom formation proceeds via neutralization of H_3S^+ ions. This makes the kinetic schemes for radiolysis and photolysis analogous.

The concentration dependences of the hydrogen and ethane yields in the photolysis and radiolysis of the $H_2S - C_2H_4$ mixtures, discussed in terms of the accepted mechanism, enables one to evaluate the relative rate-constants of reactions (12) and (13). This relation seems to be similar for the photochemical and radiation chemical experiments and differs from that which is known for thermal atoms. This leads to the conclusions that (1) radiolysis results in hot atoms with energies similar to those of photolysis-produced atoms i.e. about 1 eV (2) fast atoms which form both in photolysis and radiolysis of H_2S react as epithermal hot atoms.

If the photolysis or radiolysis of the $H_2S - C_2H_4$ mixtures is carried out in the presence of inert H atom moderators with different concentrations the increase in the moderator concentration results in a monotonous change of the formation rate for H_2 and C_2H_6. This is in agreement both qualitatively and quantitatively with the photolytic and radiolytic processes. At a high enough moderator concentration the system attains thermal equilibrium. In this case the ratio k_{12}/k_{13} equals 0.47

for photochemical and 0.43 for radiation-chemical transformations. These figures are in harmony with each other and agree with the literature data on thermal hydrogen atom reactions.

An additional proof regarding the course of hot atom reactions in the investigated systems is rendered by the comparison of the temperature-dependences of the relative rate constants in binary (hot) and ternary (thermalized) mixtures. No temperature-dependence can be observed in the first case whereas an Arrhenius-type dependence is apparent in the second one.

Thus it can be seen that hot hydrogen atoms play an important role both in the photolysis and radiolysis of hydrogen sulphide. The description of such processes in terms of Arrhenius-type kinetics and by thermal rate constants cannot be justified.

References

/1/ Yu. Sorokin, S. Pshezhetzkii, DAN SSSR 138, 1143 (1961).

/2/ F. T. Jones, T. J. Sworski, Trans. Faraday Soc., 63, 2411 (1967).

/3/ S. Gordon, W. Mulac, P. Nangia, J. Phys. Chem., 75, 2887 (1971).

/4/ C. Willis, A. W. Boyd and O. A. Miller, Can. J. Chem., 47, 3007 (1969).

/5/ M. Cleze, M. Schmidt, J. Hagege-Temman and J. Belloni, J. Phys. Chem., 75, 19 (1971).

/6/ B. G. Dzantiev, A. N. Ermakov, T. A. Molekanova and L. T. Lomako, Izv. AN BSSR, Ser. Fiz. Energ. Nauk 2, 41 (1971).

/7/ B. G. Dzantiev, A. N. Ermakov, L. T. Lomako, and T. A. Molokanova, ibid, 3, 36 (1974).

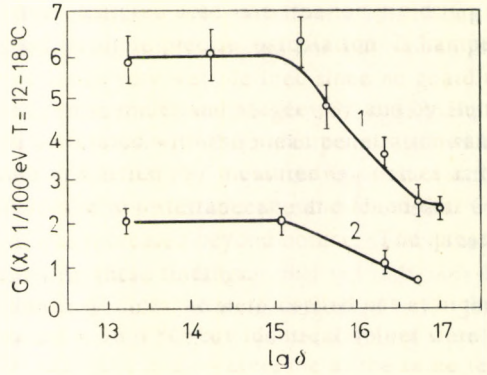

Fig. 1 The dependence of H_2 (1) and N_2 (2) yields on dose rate in ammonia radiolysis. $T = 15 \pm 3^{o}C$, $\delta = 10^{13} - 10^{17}$ eV/cm^{3}sec

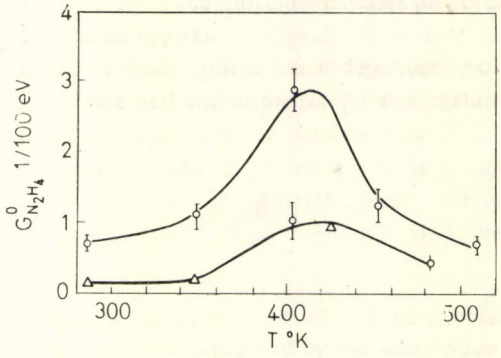

Fig. 2 The dependence of N_2H_4 yield on temperature. $\delta = 4.2 \times 10^{15}$ eV/cm^{3}sec (O), 5.5×10^{16} eV/cm^{3}sec (Δ).

RADICAL PRODUCTS OF METHANOL RADIOLYSIS. SOME DOSE RATE EFFECTS

G. M. Zimina, N. A. Bach
Institute of Electrochemistry, Academy of Sciences of the USSR,
Moscow, USSR

Solvated electrons (e_s^-) and hydroxymethyl radicals ($\dot{C}H_2$–OH) are currently admitted to be among the main transient products of methanol radiolysis, but while both the optical and ESR spectra of e_s^- are well established /1–5/, in the case of $\dot{C}H_2OH$ only the ESR characteristics are unambiguously determined /1, 6, 7/. The absorption spectrum observed in pulse radiolysis of liquid methanol and on γ-irradiation of glassy methanol comprises, besides the e_s^- band in the visible region, a poorly structured broad absorption extending into the UV which is attributed to $\dot{C}H_2$-OH /2–5/ with eventual participation of other particles. The boundaries of the band belonging to individual $\dot{C}H_2$-OH and the position of its λ_{max} are, however, not defined well enough to permit pulse radiolysis kinetic studies. This led us to reinvestigate the spectral behaviour of irradiated glassy methanol, aqueous methanol solutions and pure methanol in more detail.

Experimental

Methanol glass samples were irradiated at 77K in the dark with about 10^{16}eV/g sec dose rate and 5×10^{17} to 10^{19} doses, using Co γ-rays and Fe(II) dosimetry. Absorption spectra of glasses were measured at 77K in flat quartz cells of 2.5–3 mm thickness in a special Dewar vessel with quartz windows, fitted inside of the spectrophotometer.

Treatment of samples with light was carried out in two ways: illuminating with 15 ns pulses from a Q-switched neodymium laser (λ = 530 nm) and illuminating the samples inside the spectrophotometer with monochromatic light from its incandescent ($\lambda = 365 \pm 8$ nm) and hydrogen arc ($\lambda = 300 \pm 5$ nm) lamps.

The pulse radiolysis apparatus consisted of a linear accelerator, delivering 10 MeV electron pulses of 1 to 3 second length and 1.5×10^{17} to 1.2×10^{18} eV/ml doses, and of a conventional optical system, comprising a 1000 W xenon lamp, monochromator and phototube, the amplified output being displayed on an oscilloscope. Cylindrical quartz cells of 3.8–4 cm optical path-length were used. Dosimetry was with 0.01 $FeSO_4$ /8/ and transient $(CNS)_2^-$ spectrum /9/.

C. p. Methanol was purified with 2. 4-dinitrophenylhydrazine by the usual method and twice redistilled in helium atmosphere, the standard check being the half-life of solvated electrons to be not less than 2. 5 μsec, with 5 x 10^{16} eV/ml dose per pulse at 16°C. Doubly distilled water was checked by the value of $G(e^-_{aq}) = 2.7$. To ensure good quality of glassy-state samples, 5 mol % H_2O were added to CH_3OH.

The cells filled with liquid were thoroughly bubbled with helium and sealed off after evacuating.

Methanol in the glassy state

The absorption spectrum of methanol glass irradiated at 77K with a dose of 5 x 10^{18} eV/g and the spectra remaining after subsequent illumination with various wavelengths are presented in Fig. 1a. In accord with published data, the initial spectrum consists of a definite band with λ_{max} = 530 nm belonging to the solvated electron (e^-_s) and a broad absorption in the UV, increasing to the limit of recording at about 230 nm. With the first laser pulse (λ = 530 nm) the e^-_s absorption decreases markedly and ultimately disappears after 6–8 pulses. The vanishing spectrum retains its shape unaltered during the whole bleaching process, thus supporting its assignment to a single particle. Additional illuminating during 20 min at λ = 365 nm, followed by 15 min at λ = 300 nm causes further shifts of the long-wave edge of the residual spectra. By subtracting each spectrum from the preceeding one, five individual absorption bands with λ_{max} at 530, 460, 350, 270 and < 230 nm, shown in Fig. 1 b, were isolated in the broad unresolved spectrum of γ-irradiated methanol.

Since it has been shown by ESR that under the action of light at λ = 365 nm the $\dot{C}H_2OH$ radical remains unchanged while it dissociates at $\lambda < 300$ nm into $\dot{C}HO$ and hydrogen /10, 11/ we conclude that the absorption band 4 in Fig. 1b, which resists photolysis at λ = 365 nm and disappears at λ = 300 nm belongs to this radical. Its spectrum extends from 240 to 350 nm and is characterized at 77K by λ_{max}= 270 nm and $W_{1/2}$ = 0. 8 eV. According to Ref. /4/ the $\dot{C}HO$ band is situated in the visible region with λ_{max} = 515 nm. The absence of noticeable optical density in this range in photolysis at $\lambda \simeq 300$ nm in our experiments, as expected from ESR data, may be due to further dissociation of $\dot{C}HO$.

The absorption band 3 in Fig. 1b, with λ_{max} = 350 nm has been attributed to $\dot{C}H_2O^-$ in liquid methanol /12/. The bands with absorption maximum at λ = 460 nm and $\lambda < 230$ nm have not yet been identified.

Pulse radiolysis of aqueous methanol solutions

Transient spectra recorded during pulse radiolysis of aqueous methanol solutions saturated with N_2O should represent, according to the known reactions of H and OH with methanol, the $\dot{C}H_2OH$ absorption. However, the spectra observed in pulse radiolysis, using 0. 5 M methanol solutions with 0.02 M N_2O, and attributed to $\dot{C}H_2OH$

/11, 13/ differed from the isolated band described above and assigned to $\dot{C}H_2OH$; they were very similar to the broad absorption in pure methanol. Assuming that this discordance is due to concentration effects, we investigated solutions in the 1. 35 x x 10^{-2} to 1 M methanol range with 0. 02 M N_2O present. Spectra obtained with 4. 1 x x 10^{17} eV/ml doses in 3μsec pulses, recorded 5μsec after the end of the pulse, are shown in Fig. 2. It is seen that up to 5 x 10^{-2}M methanol the spectra consist of single bands with λ_{max} = 280 nm, similar to the $\dot{C}H_2OH$ spectrum isolated in methanol glass (Fig. 1b curve 4). For comparison the latter is drawn in Fig. 2 after correcting for the temperature difference between 77K and 300K using the coefficient $\frac{\Delta E}{\Delta T} \simeq -10^3$ eV/deg /14/ and normalizing the optical density to the liquid phase value at λ_{max} (curve 5, Fig. 1), the temperature shift of λ_{max} was found to be +13 nm. We may conclude from the good agreement between curves 5 and 2 that in dilute aqueous methanol solutions the only radical observed in pulse radiolysis is $\dot{C}H_2OH$, adequately represented by the transient spectrum.

In 0. 05 M solutions all the radicals are scavenged and G (CH_2OH) = 6. 0 was found /15/. Extrapolating the optical density recorded at t = 5μsec to the end of pulse t= 0 using $\frac{2K}{\varepsilon}$ = (4. 6 $\pm$ 0. 5) x 10^6 cm sec^{-1} (see later) we obtain GE λ_{max} = (3. 6 $\pm$ 0. 4) x x 10^3 whence the extinction coefficient of $\dot{C}H_2OH$ ε = (600 $\pm$ 100) M^{-1} cm^{-1}.

At higher concentrations the reactions become more involved and a second band appears with λ_{max} = 250 nm.

Pulse radiolysis of pure methanol

The transient UV spectrum shown in Fig. 3a was obtained in deaerated methanol using 3μsec pulses with 1. 6 x 10^{17} eV/ml doses and recorded 5μsec after the end of the pulse. Peaks are manifested at λ = 285 nm and λ = 250 nm with further absorption increase up to about 230 nm. The spectra are well reproducible, the λ_{max} values being within $\pm$ 5 nm and the optical density within $\pm$7% at (1. 3 – 1. 7) x 10^{17} eV/ml doses.

At λ = 285 nm the optical density decays following second order kinetics with $\frac{2K}{\varepsilon}$ = (4. 6 $\pm$ 0. 5) x 10^6 cm sec^{-1}. It is concluded that the absorption band with λ_{max} = 285 nm belongs to a radical which disappears in bimolecular reactions. In methanol radiolysis the main reaction of this type is recombination of $\dot{C}H_2OH$ radicals resulting in ethylene glycol $(CH_2OH)_2$ and it was natural to assign the band with λ_{max} = 285 nm to this radical. In Fig. 3a it is compared with the spectrum of $\dot{C}H_2OH$ (curve 2), transposed from the glassy state as described above. The good agreement on the long-wave side supports the liquid phase assignment. Subtracting curve 2 from curve 1 we obtain the long-wave edge of the residual spectrum (Fig. 3a, curve 3). It is seen that there is no overlapping at $\lambda \simeq$ 280–285 nm, so that the optical density at λ_{max} is a direct measure of the $\dot{C}H_2OH$ concentration.

Assuming the extinction coefficient of $\dot{C}H_2OH$ obtained in aqueous solutions to be valid in pure methanol and extrapolating to t = 0 the optical density at t = 5μsec, we obtain from the product $\varepsilon G = (4.5 \pm 0.4) \times 10^3$, neglecting the decay during the pulse, the yield of $\dot{C}H_2OH$ radicals, $G(\dot{C}H_2OH) = 7.5 \pm 1.0$. The rate constant of their recombination reaction is $K = (4.6 \pm 0.5) \times 10^6 \times \frac{\varepsilon}{2} = (1.4 \pm 0.2) \times 10^9 M^{-1} sec^{-1}$.

The absorption decay at 250 nm follows neither first nor second order kinetics, indicating a superposition of bands. The peak at 250 nm has no analogue in γ-irradiated methanol glass. This may be interpreted as a dose-rate effect, due to the relevant species originating in the interaction of two primary transient particles.

Increasing the dose per pulse leads to a more involved spectrum. Figure 3b illustrates the effect when going over from 1.6×10^{17} to 5.4×10^{17} eV/ml in 3μsec pulses (curves 1 and 2). A shoulder appears in the $\lambda > 320$ nm range. Subtracting the $\dot{C}H_2OH$ band (curve 4) as described, we isolate an additional band with $\lambda_{max} = 345 \pm 10$ nm (curve 5), also observed in the solid state spectrum. This absorption has been assigned to $\dot{C}H_2O^-$ in liquid phase investigations of the acid-base properties of $\dot{C}H_2OH$ /12/. In neutral methanol it may result from the e_s^- reaction with formaldehyde, which appears on radiolysis of methanol as CH_2O and is an efficient e_s^- acceptor since its solvation time is much longer than the microsecond range of $e_s^- + CH_2O$ reaction.

Further increase of dose per pulse and dose rate causes a decrease of optical density at λ = 250 nm and λ = 285 nm while additional transient absorption is recorded in the near UV and visible regions, thus visualizing reactions occurring at the expense of primary radicals. The interpretation of these spectra requires more extended assignment of absorption bands to identified individual particles and consideration of the main competing reactions in which they take part.

References

/ 1/ C. Chachaty, E. Hayon, J. chim. phys., 61, 1115 (1964).
/ 2/ F.S. Dainton, J.P. Keene, T.J. Kemp, G.A. Salmon, J. Teply, Proc. Chem. Soc., 1964, 265.
/ 3/ F.S. Dainton, G.A. Salmon, J. Teply, Proc. Roy. Soc. A286, 27 (1964).
/ 4/ F.S. Dainton, G.A. Salmon, P. Wardman, Proc. Roy. Soc. A313, 1 (1969).
/ 5/ A. Habersbergova, L. Josimovic, J. Teply, Trans. Far. Soc., 66, 656 (1970).
/ 6/ F.P. Sargent, E.M. Gordy, J. Phys. Chem., 78, 1977 (1974).
/ 7/ J. Moan, B Hovik, J. Phys. Chem., 79, 2220 (1975).
/ 8/ H. Fricke, E.J. Hart, Radiation Chemistry N.Y. 1966, v. 2, p. 167.
/ 9/ J.H. Baxendale, P.L.T. Bevan, D.A. Stott, Trans. Far. Soc. 64, 2389 (1968).
/10/ S.B. Milliken, R.H. Johnsen, J. Phys. Chem., 71, 2116 (1968).
/11/ B.N. Shelimob, N.N. Fok, V.V. Voevodsky, Kinetics and Catal., 4, 539 (1963) (in Russian).

/12/ K.D. Asmus, A. Henglein, A. Wigger, G. Beck, Ber. Buns. Ges. physikal. Ch., 70, 756 (1966).
/13/ M. Simic, P. Neta, E. Hayon, J. Phys. Chem. 73, 3794 (1969).
/14/ G.M. Zimina, N.A. Bach, Khim. Vys Ener., 8, 56 (1974) (in Russian).
/15/ K.M. Bansal, M. Grätzel, A. Henglein, E. Jarata, J. Phys. Chem., 77, 16 (1973).

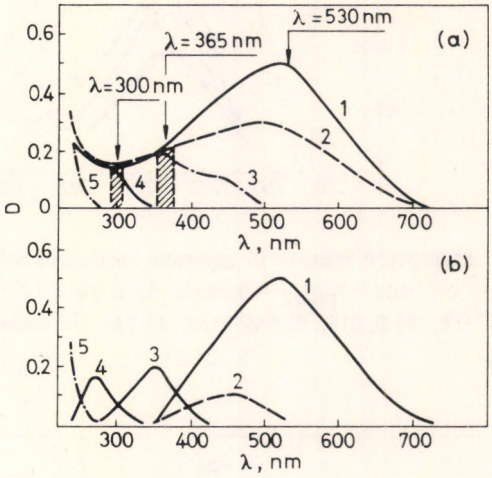

Fig. 1 Absorption spectra of γ-irradiated glassy methanol. Dose 5 x 10^{18} eV/g, 77K. (a) Spectra after illumination: 1) Initial, 2) 2 laser pulses, λ = 530 nm, 3) 6 laser pulses, λ = 530 nm, 4) 20 min photolysis, λ = 365 nm, 5) 15 min photolysis, λ = 300 nm.
(b) Individual absorption bands. 1) λ_{max} = 530 nm, e^-_{tr}, 2) λ_{max} = 460 nm, unident, 3) λ_{max} = 350 nm, $\dot{C}H_2O^-$, 4) λ_{max} = 270 nm, CH_2OH, 5) $\lambda_{max} < 230$ nm, unident

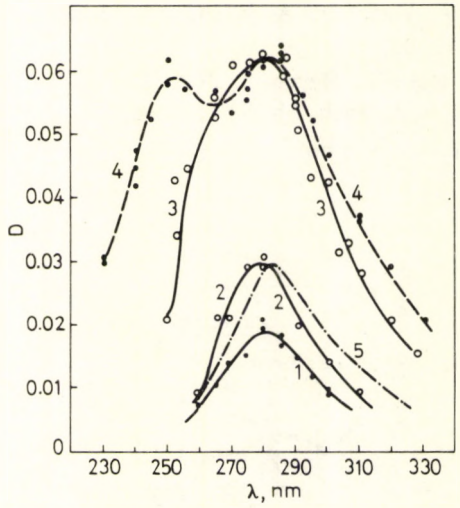

Fig. 2 Transient absorption spectra in aqueous methanol solutions. Dose per pulse 4.1×10^{17} eV/ml, $\tau_{pulse} = 3\mu$sec. 1) 1.35×10^{-2}M, 2) 2.7×10^{-2}M, 3) 5×10^{-2}M, 4) 0.3M, 0.5M, 1M, 5) $\dot{C}H_2OH$ band from glassy methanol

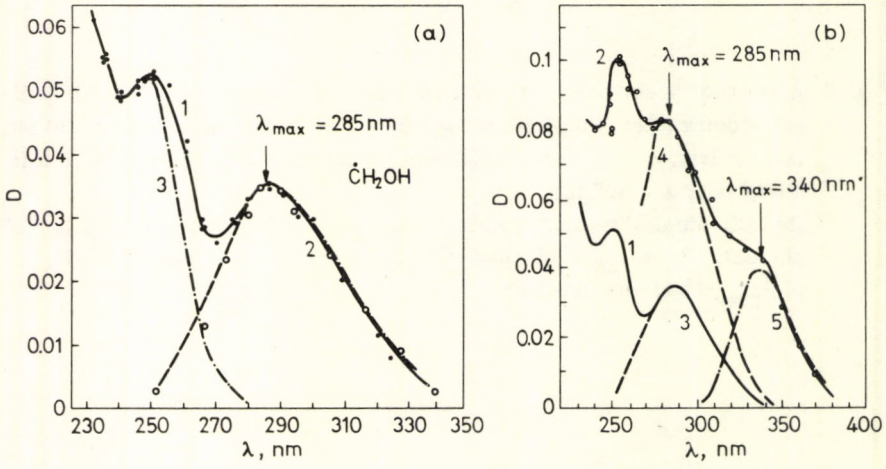

Fig. 3 Transient absorption spectra in pure deaerated methanol $\tau = 3\mu$sec.
(a) 1) Dose per pulse 1.6×10^{17} eV/ml 2) $\dot{C}H_2OH$-band from glassy methanol, 3) long-wave edge of residual spectrum,
(b) 1) Dose per pulse 1.6×10^{17} eV/ml, 2) Dose per pulse 5.4×10^{17} eV/ml, 3) $\dot{C}H_2OH$ from glassy methanol normalized to 1), 4) CH_2OH from glassy methanol normalized to 2), 5) $\dot{C}H_2O^-$

DISCUSSION

W. BELEVSKII

Did you observe in the spectra absorption due to ethylene glycol radicals?

G. ZIMINA

As it is seen on the spectra measured at small dose rates some short living species are present. One of them exhibits absorption at 285 nm, it corresponds to CH_2OH radicals. The other absorption observed at 250 nm might be assigned to the α-ethylene glycol radical. The identification of this radical is in progress in our laboratory.

Yu. D. TSVETKOV

Have you any data on the extinction coefficient for the CH_2O radicals?

What is the ratio $G(\dot{C}H_2OH)/G(\dot{C}H_2O)$ according to your measurements?

G. ZIMINA

The extinction coefficient $\varepsilon(\dot{C}H_2O) \simeq 560$ 1/M cm was taken from the literature.

The radiation chemical yield $G(\dot{C}H_2OH) = 7.5/100eV$ $G(\dot{C}H_2O)$ was also calculated but I do not remember its value correctly.

EFFECT OF ALPHA AND GAMMA IRRADIATION ON THE TRIBUTYL PHOSPHATE – CCl_4 – HNO_3 EXTRACTION SYSTEM

M. K. Abdullakhtov, G. A. Akopov, L. N. Lazarev, R. I. Lyubtsev
Atomic Energy Commission, Moscow, USSR

Introduction

Extraction methods nowadays represent the basic technique for reprocessing used fuel elements of nuclear reactors. Owing to their favourable technical and economical properties it may become possible in the future to prepare new types of fuel elements, especially for fast neutron reactors. The extraction agent mostly used is tributyl phosphate (TBP) with hydrocarbon solvents. These hydrocarbons are, however, not very favourable technologically. CCl_4 was found /1/ to be a more suitable solvent in many respects.

The effect of radiation on the extraction system TBP–CCl_4–HNO_3 has already been studied /2, 3, / but mainly the gamma radiation yield of butylphosphoric acid and that of the chlorine ion has been determined. It is known, however, that by radiolysis of this mixture other products are also formed, such as ortho-phosphoric acid which can form poorly soluble compounds with plutonium, zirconium and other elements. As a rule these mixtures would form a third phase rather easily which results in additional losses of uranium and plutonium during the course of extraction. By re-extraction, plutonium might be captured in the organic phase by forming stable, easily soluble complexes with the radiolysis products of the extraction agent. This would lower the efficiency of separation of plutonium and uranium from the fission products. This is why it is necessary not only to determine the radiolytic yields of the organic phase, but also to determine the formation and distribution of these products along the technological scheme.

The problem of differentiating between the effects of alpha and gamma radiation is not yet quite solved. According to basic assumptions used in radiation chemistry the radiation effect of different kinds of radiation with the same total dose may be different. The interaction of the intermediate products with the irradiated material should evidently be more probable in the case of low LET gamma radiation than in the case of high LET alpha radiation. Correspondingly, by using solutions having high specific alpha activities such effects may be expected to occur which cannot be observed by subjecting the system to external gamma radiation.

In the present paper the radiation resistance of the mixture 30% TBP 70% CCl_4 contacting 3 M HNO_3 is studied under the action of alpha irradiation. The radiation source was 238 plutonium introduced directly in extraction system.

Experimental

The extraction systems were irradiated in a glass vibrating extractor. The volume ratio of the organic to water phases was 3. In the aqueous phase a certain quantity of 238 plutonium was introduced. The beginning of irradiation was considered as that moment when the organic and aqueous phases were mixed. For studying radiation resistance of the mixtures the system was mixed with a frequency of 30 pulses/min followed by 10 min phase separation. The dose rate was changed by changing the amount of plutonium introduced, the integral dose by the time of irradiation. Irradiation was stopped by complete phase separation followed by a typical first cycle of extraction reprocessing technique involving acidic washing of the organic phase and then re-extraction of plutonium in solution of quadrivalent uranium. The beginning of re-extraction of plutonium was taken as the end of the irradiation.

Uranium was re-extracted in 0.08 M nitric acid solution. After this the organic phase was washed with 5% soda solution. According to preliminary experiments this was completely enough for washing the radiolysis products from the organic phase, no alkali wash was necessary.

The basic radiolytic products of TBP and CCl_4 were determined: di- and monobutyl phosphoric acids, ortho-phosphoric acid and chlorine ion. The alkyl phosphoric acids were determined by extraction separation of sulphuric and nitric acids followed by heating the mixture, the phosphoro molybdate vanadate complex was measured photometrically. Phosphoric acid was determined by photometration of the phosphoromolybdate complex after extraction with butyl alcohol. The experimental error of determination of the radiolysis products of TBP was not higher than 20—25% with a confidence coefficient of 0.95. The chlorine ion content of all products was determined nephelometrically. In uranium containing solutions the chlorine ion content was determined after separation of uranium with carbon-free ammonia. The plutonium concentration was determined radiometrically by filling analogous aqueous solutions to the mixture.

The uranium content, depending on its concentration was determined either by the volumetric ferrous phosphate vanadate method, or photometrally with arsenase S.

Results and discussion

Effect of the radiation conditions

Starting from the diffusion kinetics of radiation chemical processes /4, 5/ it can be assumed that the radiation resistance of the extraction systems would depend strongly upon the conditions of irradiation. The radiation yield of the molecular products of radiolysis depends not only on the diffusion rate from the track to the bulk of the solution, but also on the diffusion from one phase to another. Besides that the yield depends on the surrounding atmosphere too /6—8/. By irradiation of the separate

Table 1

Radiolysis product yields of the extraction system 30% tributyl phosphate – 70% CCl_4 – 3 M HNO_3 as a function of the integral dose and of the irradiation conditions

Irradiation conditions	Dose 10^{20}eV/ml	Yield, molecule/100eV			
		di-butyl acid	mono-phosphoric acid	H_3PO_4	CP^-
Separate phase system	1.8	4.3	1.8	0.19	14
	3.3	3.6	1.7	0.23	14
	7.8	2.0	1.5	0.24	11
	12	2.7	1.3	0.26	12
	18	2.5	1.2	0.24	11
Disperged system	1.6	5.6	1.2	0.25	13
	3.1	4.6	1.1	0.24	14
	7.0	3.9	1.6	0.27	14
	13	3.4	2.2	0.16	13
	19	2.7	1.9	0.15	12

phases the heavy organic phase is completely separated from the atmosphere, while in the case of the dispersion the system would intensely contact atmospheric oxygen.

Figures 1 and 2 and Table 1 show that the radiolytic yields are not strongly affected by the conditions of irradiation. The yield values obtained for dibutyl phosphoric acid /Fig. 2/ and the weak dependence of these values on the conditions of irradiation are in good agreement with the data obtained by gamma irradiation /3/. The radiolytic product formation was found to depend linearly on the integral absorbed dose. Some deviation from this linearity was found for dibutyl phosphoric acid in the disperged phase (curve 4 in Fig. 2). This can be explained by the change of the contribution of tributyl phosphate in the system as a result of evaporation of CCl_4 during irradiation /2, 3/.

The ratio of the yields of dibutyl phosphoric acid to the mono version is found to be higher by alpha irradiation than by gamma irradiation /2/. By alpha radiolysis, evidently, a deeper decomposition of tributyl phosphate to monobutyl phosphoric acid takes place with an intermediate phase of formation of dibutyl phosphoric acid.

Our data on the chlorine ion yield are significantly different from those published in Refs /2/ and /3/. At a dose of $1.6-1.8 \cdot 10^{20}$ eV/ml the chlorine ion yield obtained by us was 12–13 atoms/100 eV not depending on the irradiation conditions, while by gamma irradiation this yield was found to be /3/ 30 at a dose of $1.1 \cdot 10^{20}$ eV/ml for the separated phase and 50 for the dispersion. This difference would indicate LET effect. According to our view, however, the difference in the alpha and gamma radiolysis yields of tributyl phosphate – CCl_4 – HNO_3 is explained by the

Table

Radiolysis yields by multiple alpha irradiation of the

Cycles	Dose, 10^{19} eV/ml		Chlorine ion atoms/100 eV		Dibutyl phosphoric acid molecules/100 eV	
	per cycle	total	per cycle	total	per cycle	total
1	4.7	4.7	16.1	16.1	6.9	6.9
2	4.5	9.2	16.2	15.8	8.7	7.8
3	9.7	18.9	13.8	14.9	4.7	6.3
4	13.5	32.4	11.5	13.5	4.5	5.5
5	16.7	49.1	10.9	12.6	4.4	5.2

properties of the system itself rather than by the difference in the kind of radiation. The radiation chemical decomposition of CCl_4 is known /9/ to increase sharply in the presence of aqueous phase. As a result of this the mechanism of its radiolysis also changes. If radiolysis of dry CCl_4 in the presence of oxygen leads to formation of molecular chlorine and phosgene, in the presence of water by hydrolysis hydrochloric acid and CCl_3OH are formed /10, 11/

$$CCl_4 + H_2O \rightsquigarrow HCl + CCl_3OH$$

which decomposes subsequently as

$$CCl_3OH + H_2O \rightsquigarrow CO_2 + 3\,HCl$$

According to this mechanism the yields of the radiolysis products of CCl_4 are basically determined by the radiolysis products of water.

Evidently by irradiation of the disperged double phase system or the organic phase which has been put in equilibrium with the aqueous solution the CCl_4 radiolysis product yields will depend only the water content in the organic phase and not on the presence and composition of the aqueous phase. This assumption has been experimentally verified /2, 3/. By gamma irradiation of the double phase system (TBP–CCl_4–aqueous solution) by mixing of the phases the diffusion of the radiolysis products of water phase into the organic phase is accelerated. This increases the radiation decomposition yield of CCl_4. According to our view this explains the increase of the chlorine ion yield in the disperged phase by gamma irradiation. In the case of internal alpha irradiation, when the radiation source is in the organic phase, the radiolysis of the aqueous phase can be neglected in the case of separated phase and dispersion as well because the range of the alpha particles is very short.

2

system 30% tributyl phosphate – 70% CCl_4 – 3 N HNO_3

Monobutyl phosphoric acid molecules/100 eV		H_3PO_4 molecules/100 eV		Decomposition of tributyl phosphate molecules/100 eV	
per cycle	total	per cycle	total	per cycle	total
4.4	4.4	2.3	2.3	13.6	13.6
6.2	5.3	3.2	2.7	18.1	15.8
6.4	5.9	1.1	1.9	12.2	14.1
3.2	4.8	1.0	1.5	8.7	11.8
4.2	4.6	0.9	1.4	9.5	11.2

Correspondingly the conditions of the irradiation in this case should not affect significantly the alpha radiolysis product yields, which is indeed shown in Table 1. The small value of the total chlorine ion yield by alpha radiolysis with respect to that found by gamma radiolysis /3/ can also be explained by the effect of the radiolysis of the aqueous phase.

Effect of the dose rate

The effect of the dose rate on the product yields was studied for the system TBP–CCl_4–HNO_3 with mixing the phases. The results are shown in Figs 3 and 4. It is seen that the chlorine ion yield increases first then reaching maximum decreases (Fig. 3). This behaviour cannot be explained by a single factor, as by the effect of the concurrent reactions of recombination of the water radicals and the reaction of these radicals with acceptors /12/, in the present case with CCl_4.

The dose rate dependence of the yield of dibutyl phosphoric acid (curve 1 in Fig. 4) shows a similar character. This supports the assumption /3/ that dibutyl phosphoric acid in the TBP–CCl_4–HNO_3 system is formed by reaction of the CCl_4 radicals with TBP at the moment of the absorption of the energy.

The other radiolytic products of TBP: monobutyl phosphoric acid and H_3PO_4 are unchanged by increasing dose rate (curves 2 and 3 in Fig. 4).

Multiple irradiation of the organic phase

In all extraction technologies of processing using fuel elements the recovery of the extraction agent is considered important. In connection with this it is important to study the radiation resistivity of the extraction agent and to measure the accumulation of such reaction products which affect the extraction process unfavourably.

Table 3

Distribution of the chlorine ion content by processing of the irradiated 30% tributyl phosphate – 70% CCl_4 – 3 N HNO_3 system

Condition of irradiation	Dose, 10^{20} eV/ml	chlorine content %			
		aqueous phase	reextract plutonium	reextract uranium	soda solution
Separate phase	1.8	90.3	3.9	3.6	2.2
	3.3	90.7	2.7	2.3	4.3
	7.8	91.7	1.6	1.7	5.0
	12	90.3	1.1	1.6	7.0
	18	89.1	1.7	1.5	7.7
Dispersion	1.6	89.7	3.9	4.1	2.3
	3.1	94.8	2.2	2.1	0.9
	7.0	93.4	1.4	1.4	3.8
	13	94.4	0.7	0.5	4.4
	19	97.0	0.5	0.4	2.1

Experiments with multiple irradiation were carried out in the disperged phase in order to study radiation resistance of the extraction agent. After each irradiation cycle the organic phase was treated according to the first extraction cycle and the radiolytic yields of the agent and the solvent were determined. The results are shown in Table 2. It is seen that the chlorine ion yield decreases by increasing number of irradiation cycles. A comparison of the data of Tables 1 and 2 shows, however, that the total chlorine ion yield depends on the total absorbed dose only and not on the number of cycles. From this it can be assumed that the radiation resistivity of CCl_4 is unchanged upon multiple use of the TBP–CCl_4 extraction system.

The tributyl phosphate (TBP) yields of the radiolysis products of tributyl phosphate (TBP) show in general a tendency of decreasing by increasing number of cycles. The total yields of the decomposition products of TBP corresponding to the same total dose are significantly higher by multiple irradiation than by a single one. This is mainly due to the increase of the yields of monobutyl phosphoric acid and H_3PO_4 as a result of a post-irradiation effect.

Distribution of the radiolysis products

In order to study the effect of the radiolysis products on the technological process of extraction reprocessing of used nuclear fuel elements it is important to determine the distribution of these products along the technological scheme. This was done for the first extraction cycle, the results are shown in Tables 3 and 4. Table 3 shows that chlorine ion is mainly (90–95%) present in the aqueous phase, the rest of it

Table 4

Distribution of the radiolysis products of tributyl phosphate by processing of the 30% tributyl phosphate 70% CCl_4 – 3 N HNO_3 system

Condition of irradiation	Dose, 10^{20} eV/ml	Radiolysis product content %					
		aqueous		reextr. plutonium	soda solution		
		mono-phosph. acid	H_3PO_4	H_3PO_4	H_3PO_4	mono-butyl acid	di-phosphoric acid
Separate phase	1.8	46.6	24.5	–	75.5	53.4	100
	3.3	44.7	27.9	–	62.1	55.3	100
	7.8	46.8	44.4	–	55.6	53.7	100
	12	45.9	68.9	–	31.1	54.1	100
	18	47.2	68.9	–	31.1	52.8	100
Dispersion	1.6	53.6	18.5	28.7	52.8	46.4	100
	3.1	51.8	27.7	25.2	47.1	48.2	100
	7.0	55.3	46.3	21.7	31.4	44.7	100
	13	54.7	39.5	24.8	35.7	45.3	100
	19	56.9	37.5	33.7	29.0	43.1	100

being distributed in the re-extracted plutonium, uranium phases and in the soda washing solution. Table 3 also shows that by increasing dose the chlorine ion concentration in the soda solution increases while it decreases in the re-extraction phases. According to our view this redistribution of the chlorine ion content by increasing dose is due to increase of the yield of chloro-organic radiolytic products which would hydrolyse only in the soda solution by formation of hydrochloric acid.

Table 4 shows that dibutyl phosphoric acid remains completely in the organic phase from which it is washed out by the soda solution. Monobutyl phosphoric acid is shared between the organic and aqueous phases with a ratio of 0.35. This ratio is in good agreement with that obtained for monobutyl phosphoric acid in aqueous phase and benzene /13/ and with that obtained for water, 20% tributyl phosphate solution in dehydrated cherosine /14/.

The appearance of H_3PO_4 in the soda solution and in the plutonium re-extracted phase was somewhat unexpected (Table 4). By increasing dose H_3PO_4 is redistributed between the aqueous and soda solution phases, while its yield in the plutonium re-extract is not significantly changed. This problem needs further examination.

According to many authors (13, 15–17) butyl phosphoric acids, especially dibutyl phosphoric acid, in nitric acidic media would form complex compounds with uranium and plutonium, which are soluble in the organic phase. This results

Table 5

The uranium content in the soda washing solution as a function of the integrated dose of the alpha irradiation and of the irradiation conditions

Condition of irradiation	Dose, 10^{20} eV/ml	Uranium content, % of the mmole/l extracted		Molar ratio of dibutyl phosphoric acid to uranium	Molar ratio of the phosphorus containing products to uranium
Separate phase	1.8	3.1	0.20	2.1	2.6
	3.3	4.3	0.27	2.4	3.1
	7.8	5.5	0.47	1.9	2.6
	12	7.0	0.76	2.4	3.1
	18	9.0	0.92	2.7	3.4
Dispersion	1.6	6.3	0.40	3.1	3.4
	3.1	6.2	0.37	5.6	6.2
	7.0	11.0	0.94	4.4	5.2
	13	13.0	2.14	2.9	3.7
	19	14.8	3.48	1.8	2.3
Multiple irradiation	0.47	4.7	2.7	0.43	0.58
	0.45	4.6	2.7	0.52	0.72
	0.97	3.8	2.4	0.69	1.19
	1.35	4.5	2.6	0.83	1.16
	1.67	5.5	2.9	0.75	1.12

in a significant loss of the active elements in the case of using carbonate or alkaline washing solutions. In our experiments the plutonium content in the carbonate washing solution was not higher than 0.05% with respect to that extracted at the beginning of the irradiation. Simultaneously the uranium content in this solution is increased by increasing alpha radiation dose. This is shown in Table 5. Evidently by re-extraction of quadrivalent uranium plutonium is completely exchanged by uranium in its compounds with TBP as well as with the radiolysis products. By a subsequent re-extraction of uranium with 0.08 M nitric acid a part of uranium is retained in the organic phase and only washed out from it by carbonate washing.

It can be assumed that the increase of the uranium content in the washing solution by increasing dose is due to the accumulation of butyl phosphoric acid in the extraction system which makes uranium captured in the organic phase by re-extraction. According to Refs /15/ and /16/ monobutyl phosphoric acid forms complex compounds with uranium with a ratio of 1–1.79 depending on the initial conditions. The ratio for the dibutyl phosphoric acid – uranium complex is 2–4. From this it follows that in our experiments the sum of mono- and dibutyl phosphoric

acids to uranium ratio in the soda washing solution should always be higher than 1.79 and the ratio of dibutyl phosphoric acid to uranium should be higher than or equal to 2. Besides that, these values should be constant by increasing dose. As it is shown in Table 5 this expectation is fulfilled only at doses higher than $1.6 \cdot 10^{20}$ eV/ml. At lower doses by multiple irradiation the ratio of the phosphorous containing compounds to uranium is less than 1.

On the basis of the present data it can be assumed that the retention of uranium in the organic phase by re-extraction is not only due to the phosphorous containing radiolytic products of TBP, but due to others such as carbonic acids, intermediate compounds formed by radiation chemical oxidation and nitration of the butyl radical and also due to different chloro organic compounds. Especially significant is the role of these products in the retention of uranium in the organic phase in the case of multiple irradiation, i.e. by low irradiation doses.

References

/ 1/ Poushlenkov, M.F., Shumkov, V.G., Zemlyanouhin, V.I., Zilberman, B. Ya., Shouvalov, O.N., Voden, V.G., Shchepetilnikov, N.N., 3rd Int. Conf. Peaceful Application of Atomic Energy 10, 330 (1965) (New York).

/ 2/ Burger, L.L., Mc Clanahan, E.D., Ind. and Engin. Chemistry 50, 153 (1958).

/ 3/ Kourtenov, M.M., Poushlenkov, M.M., Zilberman, B. Ya., Graznova, A.S., Efremova, T.I., Radiokhimiya 9, 32 (1967).

/ 4/ Vereshchinsky, N.V., Pikaev, A.K., Introduction to Radiation Chemistry, Academy of Sci. USSR. 1963

/ 5/ Henley, E., Johnson, E., Radiation Chemistry Atomizdat, Moscow, 1974.

/ 6/ Barelkov, E.B., Solyanika, I.P., Atomnaya Energiya 35, 4 (1973).

/ 7/ Kertulis, V.I., Egorova, G.F., Zagoretz, P.A., Khim. Vys. Energii 4, 172 (1974).

/ 8/ Swallow, A. Radiation Chemistry of Organic Compounds, Izd. Inostr. Lit. Moscow, 1963.

/ 9/ Spurny, Z. Coll. Czech. Chem. Comm. 25, 1254 (1960).

/10/ Zimin, A.V., Egorova, Z.S., Collection of works on radiation chemistry, Ac. Sci. USSR Moscow 1955, p. 241.

/11/ Allen, A.O., Radiation chemistry of water and of aqueous solutions, Gosatomizdat, Moscow, 1963.

/12/ Shevchenko, V.B., Smelov, V.S., in "Extraction" 2nd edition, Gosatomizdat, Moscow, 1962 p. 219.

/13/ Ilozhev, A.P., Poddoubskaya, I.V., Rosen, A.M., in "Extraction" 2nd ed. Gosatomizdat, Moscow, 1962 p. 71.

/14/ Kroutikov, G.G., Solovkin, A.S., Zh. N. Khim. 15, 1610 (1970).

/15/ Solovkin, A.S., Teterin, E.G., Shesterikov, N.N., Zh. N. Khim. 18, 787 (1973).

/16/ Shevchenko, V.B., Smelov, V.S., Atomnaya Energiya, 6, 140 (1959).

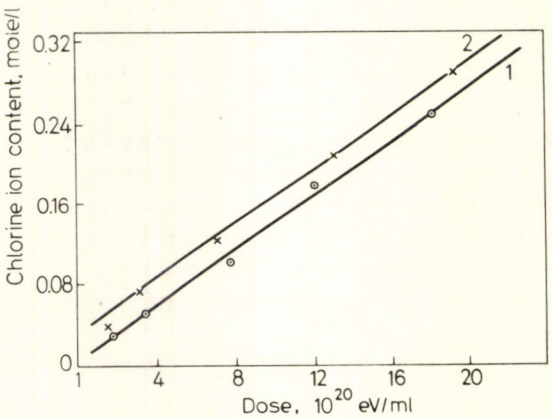

Fig. 1 Formation of chlorine ions by irradiation of the tributyl phosphate $-CCl_4-HNO_3$ system: (1) separate phase system, (2) disperged system

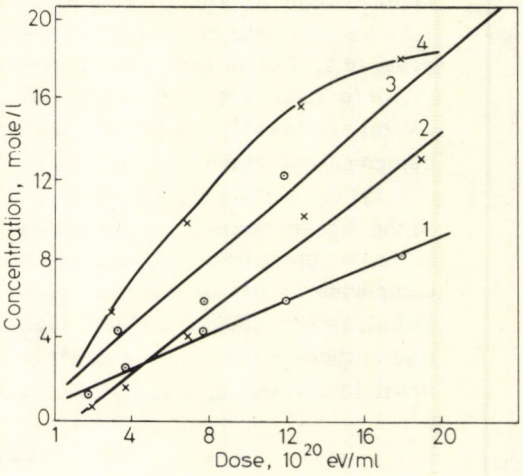

Fig. 2 Formation of butyl phosphoric acids by irradiation of the tributyl phosphate – CCl_4 – HNO_3 system: (1) monobutyl phosphoric acid, separate phase, (2) monobutyl phosphoric acid, dispersion, (3) dibutyl phosphoric acid, separate phase, (4) dibutyl phosphoric acid, dispersion

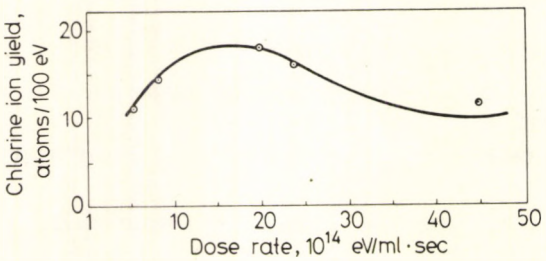

Fig. 3 The dependence of the chlorine ion yield on the alpha irradiation dose rate

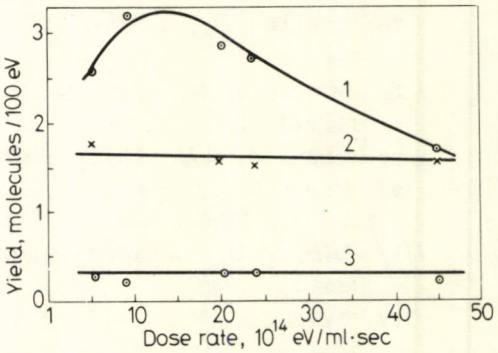

Fig. 4 The dependence of the radiolytic product yields of tributyl phosphate on the alpha irradiation dose rate: (1) dibutyl phosphoric acid, (2) monobutyl phosphoric acid, (3) H_3PO_4

STUDY OF THE LIQUID PHASE RADIOLYSIS OF ETHYLENE GLYCOL BY THE SPIN TRAPPING TECHNIQUE

A. L. Karasev

Institute of Electrochemistry, Academy of Sciences of the USSR
Moscow, USSR

Evidence has been adduced /1–3/ that glycols may be transformed to corresponding carbonyl compounds by free radical mechanisms because a free radical containing two or more hydroxyl groups undergoes dehydration to give a radical containing a carbonyl group. It was supposed in the radiolysis of aqueous solutions of ethylene glycol (EG) containing H_2O_2 or mineral acids /1/ that the chain process (1), (2) of acetaldehyde formation takes place:

$$HO\dot{C}HCH_2OH \xrightarrow{-H_2O} \dot{C}H_2CHO \qquad (1)$$

$$\dot{C}H_2CHO + (CH_2OH)_2 \longrightarrow CH_3CHO + HO\dot{C}HCH_2OH \qquad (2)$$

It was interesting to ascertain whether a similar process occurs in the radiolysis of pure neutral EG. For this purpose a study of the radiolysis of EG by the spin trapping technique has been performed. Spin trapping /4/ involves free radical accepting by a nitroso compound to give a stable spin adduct. The ESR spectrum of the resulting nitroxide is characteristic of the original short-lived radical. In this work we have used 2-butyl-2-nitrosopropane (t-BuNO) as a spin trap to produce relatively stable nitroxide radicals.

Experimental

t-BuNO was prepared using the method of Stowell /5/. Pro anal grade EG was used without further purification. Methanol-d_3 contained 98.5% of CD_3OH. Samples were evacuated at 10^{-5}torr. ESR spectra were recorded at 295K both during irradiation and after cut off the electron beam on a spectrometer coupled with an electron linear accelerator. Some experiments were conducted at several temperatures using a RE–1301 spectrometer. Samples were irradiated with series of 4.5MeV electron pulses of 2.2μsec length and dose per pulse 10^{17}eVcm^{-3}. Some samples were irradiated with Co^{60} γ-rays. The dose rate was $\sim 10^{16}$eVcm^{-3}sec^{-1}. In this case

the samples were rapidly immersed in liquid nitrogen in order to prevent the decay of less stable radical adducts. After this procedure these samples were melted in the spectrometer cavity.

Results and discussion

The ESR spectrum of a 0.03M solution of t-BuNO in EG irradiated at 295K to 10^{19}eVcm^{-3} is shown in Fig. 1a. The spectrum consists of a triplet 14.0G of doublets 1.7G (signal I) and a triplet 13.8G of triplets 4.9G (signal II). We assigned signal I to the radical adduct

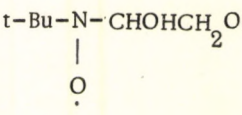

$a_N = 14.0G$

$a_H = 1.7G$

The similarity of the ESR parameters and those of adducts of t-BuNO with hydroxyalkyl radicals /6/ supports this assignment. The ESR spectrum of the 0.03M solution t-BuNO in EG irradiated to 10^{20}eVcm^{-3} shows (Fig. 1b) the presence of the additional triplet 14.7G of triplets 9.8G (signal III). The ESR parameters of this signal are very similar to those of the alkyl-t-butyl nitroxide /7/. The radical $\dot{C}H_2CH_2OH$ is the only one among those that may be formed in the radiolysis of EG which resembles alkyl radicals. The decrease of the ESR coupling constants in the case of adduct III:

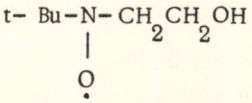

$a_N = 14.7G$, $a_H = 9.8G$ as compared with the ethyl-t-butyl nitroxide constants $a_N = 15.7G$, $a_H = 10.7G$ /7/ is accounted for by the substitution of a hydrogen atom for an electron-attracting hydroxyl group. Signal II corresponds to hyperfine interaction of the unpaired electron with the nitrogen nucleus and two protons in the adduct of acetaldehyde radical with t-BuNO:

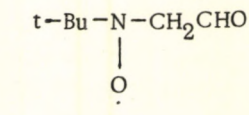

$a_N = 13.8G$

$a_H = 4.9G$

The signal II is not detected in an irradiated frozen solution of t-BuNO in EG after melting. This shows that the acetaldehyde radical does not form in the solid phase.

It is necessary to note that the ESR parameters of signal II are very similar to those of the hydroxymethyl-t-butyl nitroxide $a_N = 14.4G$ $a_H = 4.0G$ /6/. The ESR spectra of γ-irradiated solutions of t-BuNO in the mixture 3M EG$-CD_3OH$ were

examined in order to determine the origin and nature of the adduct corresponding to signal II. This signal is not observed on irradiation of this solution at 77K as well as in pure frozen EG. In this case the ESR spectrum (Fig. 2a) corresponds to the adducts of three radicals with t-BuNO: $\dot{C}D_2OH$, and $HO\dot{C}HCH_2OH$. The latter is the most stable adduct (Fig. 2b). The ESR spectrum of the solution of t-BuNO in the mixture EG – CD_3OH irradiated at 295K consists of the signals belonging to the three radical adducts: $CD_3\dot{O}$, $\dot{C}D_2OH$ and the signal II. The characteristic triplet of doublets of the $HO\dot{C}HCH_2OH$ adduct is not observed in this case. As mentioned above this very stable adduct is formed during melting of samples irradiated in the solid state. The absence of this adduct in the sample irradiated in the liquid state shows that the $HO\dot{C}HCH_2OH$ radical transforms before trapping into $\dot{C}H_2CHO$ radical which is trapped by t-BuNO. This process is possible in the liquid phase because of the low relative concentrations of EG and t-BuNO in the system. A similar result is observed in irradiated EG at low concentrations of t-BuNO (0.002M). As Fig. 1c shows, signal I is absent and signal II dominates in the spectrum. In this case the radical $HO\dot{C}HCH_2OH$ lives longer before trapping then in 0.03M t-BuNO solution so that it transforms into $\dot{C}H_2CHO$. Thus all these results support the present interpretation concerning signal II. These data show that the species corresponding to signal II originate from the decay not of the EG molecule but of the $HO\dot{C}HCH_2OH$ radical in accord with reaction (1).

A similar transformation of the glycol radical was observed in the system $Ti^{3+}-H_2O_2-EG$ in presence of acid /8, 9/. Livingston and Zeldes [10, 11] also observed it in the reaction initiated by photolysis of H_2O_2. Only the spectrum of the glycol radical was observed in pure EG but in aqueous solution in the presence of acid, the characteristic triplet of $\dot{C}H_2CHO$ was recorded instead of the spectrum of $HO\dot{C}HCH_2OH$. In the pulse radiolysis of 0.1M aqueous solutions of EG, Bansal et al. [12] found with simultaneous optical and polarographic current measurements that reaction (1) occurred only at $pH < 3$. The characteristic feature of all the mentioned systems is a homogeneous distribution of glycol radicals in bulk. It was determined experimentally that reaction (1) is acid-catalysed so that it requires the presence of protons to occur:

$$HO\dot{C}HCH_2OH_2^+ \longrightarrow \dot{C}H_2CHO + H_3O^+ \qquad (1a)$$

However in the present case reaction (1a) takes place in the radiolysis of neutral dry (0.1% of water) EG. To explain this fact it is necessary to consider the change of the acid–base state of the liquid under the action of ionizing radiation. EG is a poorly dissociating liquid (pK = 15.72). It is difficult to suppose that a considerable concentration of acid ($\sim 10^{-3}$M) may be accumulated in EG at $\sim 10^{20}$eVcm^{-3} dose. Inhomogeneous distribution of active particles formed by ionizing irradiation may be the most plausible explanation of the occurrence of reaction (1a). This involves inhomogeneity of acid–base properties of the medium. Regions of perturbation

(spurs, tracks, etc) are formed when ionizing radiation passes through the medium. Ions and primarily excited particles are localized in central zones of these regions. Thermalized electrons escape from the central zone. Thus the central zone of a spur has a high concentration of ions and excited molecules which transform into free radicals and solvated protons, so that there are certain regions with high local concentration both of radicals and Brønsted acid. These are regions in which proton-catalysed reaction (1a) takes place. The overall mechanism of the acetaldehyde radical formation in the radiolysis of neutral EG may be summarized in the following reactions:

$$(CH_2OH)_2 \longrightarrow \begin{cases} (CH_2OH)_2^+ + e^- \\ (CH_2OH)_2^* \end{cases} \qquad (3)$$

$$(CH_2OH)_2^* \longrightarrow HO\dot{C}HCH_2OH + H \qquad (4)$$

$$(CH_2OH)_2^+ + (CH_2OH)_2 \longrightarrow HO\dot{C}HCH_2OH + HOCH_2CH_2OH_2^+ \qquad (5)$$

$$HO\dot{C}HCH_2OH + HOCH_2CH_2OH_2^+ \longrightarrow HO\dot{C}HCH_2OH_2^+ + (CH_2OH)_2 \qquad (6)$$

So the radical $HO\dot{C}HCH_2OH_2^+$ takes part in reaction (1a).

References

/ 1/ C. E. Burchill, K. M. Perron, Canad. J. Chem., 49, 2382 (1971).
/ 2/ P. J. Venter, H. J. van der Linde, R. A. Basson, J. Chem. Soc., Chem. Commun, 3, 187 (1972).
/ 3/ C. V. Sonntag, E. Thoms, Z. Naturforsch., 25B, 1405 (1970).
/ 4/ E. G. Janzen, Accounts Chem. Res., 4, 31 (1971).
/ 5/ J. C. Stowell, J. Org. Chem., 36, 3055 (1971).
/ 6/ F. P. Sargent, E. M. Gardy, H. R. Fable, Canad. J. Chem., 52, 3645 (1974).
/ 7/ E. G. Janzen, Topics in Stereochemistry, New York, 6, 1971, p. 171.
/ 8/ O. L. Buley, R. O. C. Norman, R. J. Pritchett, J. Chem. Soc., B, 849 (1966).
/ 9/ B. C. Gilbert, J. P. Larkin, R. O. C. Norman, J. Chem. Soc., Perkin Trans. 794 (1972).
/10/ R. Livingston, H. Zeldes, J. Chem. Phys., 44, 1245 (1966).
/11/ R. Livingston, H. Zeldes, J. Amer. Chem. Soc., 88, 4333 (1966).
/12/ K. M. Bansal, M. G. Gratzel, A. Henglein, E. Janata, J. Phys. Chem., 77, 16 (1973).

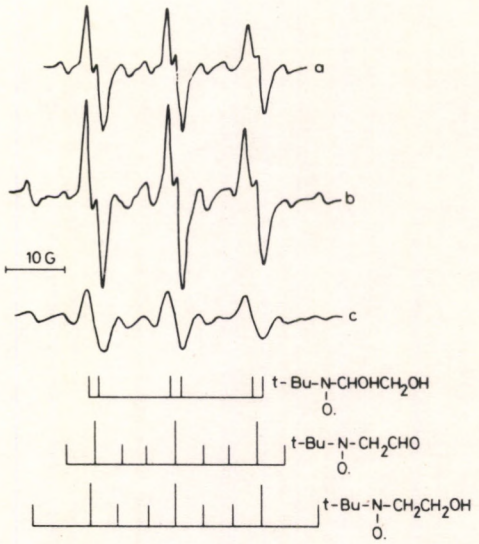

Fig. 1 ESR spectra of solutions of t-BuNO in EG irradiated by high energy electrons at 295K: a) 0.03M t-BuNO, D $\approx 10^{19}$ eVcm^{-3}; b) 0.03M t-BuNO, D $\approx 10^{20}$ eVcm^{-3}; c) 0.002M t-BuNO, D $\approx 10^{20}$ eVcm^{-3}

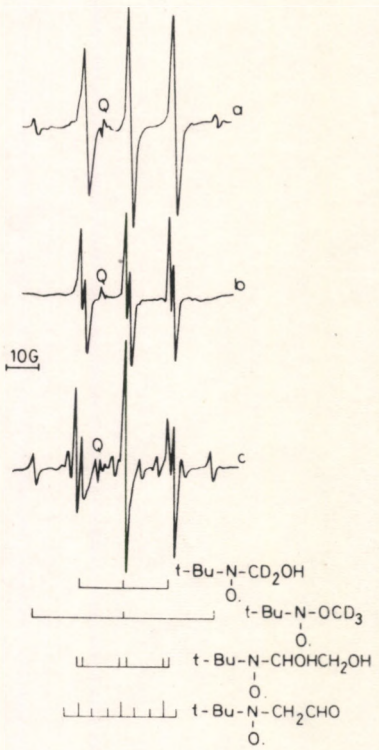

Fig. 2 ESR spectra γ-irradiated solution of t-BuNO in mixture 3M EG-CD_3OH: a) irradiation at 77K, spectrum recorded at 260K; b) irradiation at 77K, spectrum recorded at 260K; c) irradiation at 295K, spectrum recorded at 230K. Q is the signal from the silica cell

RADIATION CHEMICAL RESPONSE OF THE SYSTEM ISOOCTANE–ETHANOL–CHLOROBENZENE IRRADIATED BY NEUTRONS OF VARIOUS SPECTRA

I. Dvornik, M. Živadinović, S. Miščević, U. Zec, D. Ražem, F. Ranogajec, S. Makra*, J. Pálfalvi*

"Ruđer Bošković" Institute, Zagreb, Yugoslavia,

*Central Research Institute for Physics, Budapest, Hungary

Introduction

The system isooctane (2, 2, 4-trimethylpentane, TMP)–10% ethanol–10% chlorobenzene (CB), the TMP system, has been described in our previous publications /1–5/ as a new low level chemical dosimeter which might compete with the ferrous-sulphate dosimeter as a secondary dosimetric standard. The measured product of radiolysis is HCl formed after resonant dissociative attachment of non thermal subexcitation electrons to CB /6, 7/. Primary ionic species (Cl^- and molecular positive ions) formed in the very early stage of radiolysis are chemically stabilized by proton transfer to ethanol and solvation. This mechanism is the radiation chemical base of good dosimetric properties. It also suggests the lower effect of LET upon G(HCl), compared with the LET effect upon the yield of free radical reactions.

With high hydrogen content and low LET effect the TMP-system could be a good fast neutron dosimeter /3/. Low LET effect would give low dependence of dosimeter response upon neutron energy and the possibility of measuring the charged particle component of neutron absorbed dose. The H content being higher than in soft tissue gives higher neutron kerma in dosimeter compared to tissue. This may compensate for the effect of LET and in a favourable combination of both factors, and make the response of the dosimeter to tissue-rad equal for gammas and neutrons.

The TMP-system is currently used in practical dosimetry: as a basis for the Yugoslav accident and emergency personal dosimeter DL–M3 (produced by the "Ruđer Bošković" Institute) and for routine calibration work. Long experience in dosimetry with DL–M3 and the visual colorimeter has resulted in highest precision, accuracy and reliability obtained in a very simple way (/5/, see also below).

Experiments with neutrons described briefly in this paper were primarily designed to give as accurate as possible response data for calibration of the TNP-system for dosimetry of mixed radiation in criticality accidents. The developed experimental techniques allow further studies of the mechanism of HCl formation at high LET.

Experimental

Accurate determination of neutron kerma to better than $\pm 5\%$ is hardly possible. In our experiments different calibration methods have been used and it is probable that the systematic errors are not of the same sign.

The main features of the neutron sources used and calibration methods are listed in Table 1.

Most accurate are calibrations where the neutron kerma was measured with two different ionization chambers: one homogeneous CH equivalent with acetylene gas flow, and the other with Mg-walls and argon gas flow /15–17/. The chambers were precisely calibrated and checked with cobalt–60 gammas before and after experiments (accuracy of gamma field calibration better than 2% obtained by repeated ferrous sulphate dosimetry). To obtain K_n the W_n/W_γ values of 1.055 (expt. No. 2) and 1.065 (expts. Nos. 3 and 4) were applied after recent literature data /18–21/. The error due to smaller registration efficiency for neutrons below 0.2 MeV is negligible /22/ because of the low contribution to kerma of low energy neutrons. The correction for attenuation of kerma in chamber and dosimeter walls is performed by applying experimental and calculated data /18, 19, 23/. Conversion of kerma in CH to kerma in soft tissue or in the TMP-system is made using data about kerma to fluence ratios for corresponding neutron energies /24/. For all neutron energies the ratio of conversion factors for tissue and the TMP-system is constant and very nearly independent of neutron energy up to 13 MeV ($K_{TMPs}/K_{tissue} = 1.40 \pm 0.01$).

Except in expt. No. 1 /4/ the measurements with the TMP-system were performed with dosimeters DL–M3 and the visual colorimeters ČDL–M3 (all from normal production) described elsewhere /5/. The dosimeter DL–M3 is an ampoule 5 mm O.D. (0.5 mm wall) and 128 mm long encapsulated in a pencil 13 mm O.D. (3.5 mm wall) made of ABS plastic. Some measurements (expts. Nos. 3 and 5) with 1 cm rectangular spectrophotometric cells gave K_n values within ±2% in agreement with DL–M3 values. By applying the procedure for the elimination of systematic error /5/ and repetition of readout, the precision of the measured mean values of about ±1% was achieved in all cases for DL–M3 results. In expt. No. 4 this was checked by the obtained exact linearity of signal vs. dose plots up to 900 rad.

The separate gamma kerma (dose) measurements, in cases where ionization chambers could not be applied, were performed with thermoluminescent CaF_2 (Mn activated) pellets encapsulated in 4 mm lucite and 0.2 to 1 mm lead. The pellets were individually calibrated with cobalt-60 gammas before and after experiments. Many pellets were used with different encapsulation to obtain correction for photon energy effects, and better statistics.

The neutron sensitivity of all gamma dosimeters was accounted for using data from literature /18, 20, 25/.

From DL–M3 data neutron kerma is obtained by subtraction of gamma kerma from total kerma.

Results and discussion

The results are shown in Table 2 together with the most important data on neutron spectra used. Approximate mean neutron energies are given with respect to contribution to kerma. The G(HCl) values in column 4 are not significantly different. The

Table 1

Neutron sources and calibration methods in performed experiments

Expt. No.	Description of sources and calibration methods
1	Source: T(d, n)^{4}He reaction produced by 150 keV deuterons incident on thick target /2, 4/
2	Source: Al target bombarded by deuterons of 15 MeV in the internal beam of the cyclotron (R. Bošković Institute, Zagreb), $K_n/K_{gamma} = 6.0$; dose rate 4.0 rad/min Calibration: CH and Mg/A ionization chambers with gas flow at constant pressure /15–17/; $W_n/W_{gamma} = 1.055$
3	Source: Fission converter plate 1.5 mm thick at the TRIGA reactor, J. Stefan Institute, Ljubljana /8/, dose rate 3 rad/min, $K_n/K_{gamma} = 1.0$ Calibration: Same as in expt. No. 2, $W_n/W_{gamma} = 1.065$
4	Source: Biological irradiation facility on the horizontal channel of the WWR–SM reactor at the Central Institute for Physics, Budapest /9/. Beam coming from the reactor core filtered through 145 mm Bi and 10 mm B_4C, $K_n/K_{gamma} = 4.5$; dose rate 2 rad/s; beam diameter 150 mm Calibration: same as with expt. No. 3
5	Source: RB zero power reactor, Vinča, Belgrade /10/; irradiations performed at 1.25, 2 and 3 m from reactor surface with reactor power 4 kW, dose rate 7 rad/min; $K_n/K_{gamma} = 0.35$ Calibration: Comparison with the mean kerma values of the final results of all participants of the IAEA intercomparison after normalization to the same reactor work (kWh). Normalization performed with activation detectors. Main error source: low K_n/K_{gamma}
6	Source: Pulsed reactor VIPER /11–13/; irradiations performed 3 m from reactor core, dose rate: 10^6rad/s; $K_n/K_{gamma} = 2.0$ Calibration: Comparison of our results /14/ with the mean kerma values of preliminary and some final results of all participants. Main source of error: error of the mean and uncertainty of conversion of dose K_n in DL–M3

Table 2

Response of TMP-system to neutron kerma

Expt. No.	Neutron spectrum	Mean neutron energy MeV	G(HCl) or response with respect to neutron kerma		Response ratio c) R_n/R_{gamma}
			in TMP system	in tissue	
1	Monochromatic 14.7 MeV + scattered spectrum a)	13 ± 1	3.60 ± 0.55	5.00 ± 0.75	1.00 ± 0.15
2	Spectrum from cyclotron 15 MeV D^+ on Al target	5 ± 1	3.45 ± 0.35	4.80 ± 0.50	0.95 ± 0.10
3	Fission, uncollided	2.50	3.50 ± 0.30	4.85 ± 0.40	0.96 ± 0.08
4	Fission, H_2O moderated and filtered through Bi and B_4C	2	3.90 ± 0.30	5.45 ± 0.40	1.08 ± 0.08
5	Fission, D_2O moderated, rich in thermal and intermediate neutrons	1.70	3.75 ± 0.80	5.25 ± 1.10	1.04 ± 0.20
6	Fission, moderated and highly degraded through 20 cm Cu	0.35	3.30 ± 0.45	4.60 ± 0.65	0.92 ± 0.14
7	Fission, mean of Nos. 3–5	2	3.70 ± 0.37	5.20 ± 0.52	1.03 ± 0.10

a) Data from ref. /4/ corrected because E_n is not 14.7 MeV, but lower /27/

b) G-values defined as number of particles produced per 100 eV absorbed in the system (col. 4), response in column 5 is obtained by multiplying G-values from column 4 with the kerma ratio $K_{sist.}/K_{tissue}$; this response is equal to the hypothetical G-value which would be found if the TMP-system would absorb the same amount of energy as tissue

c) R_n are numbers from column 5; R_{gamma} = G(HCl) = 5.05 (2); the responses are for equal dose in tissue

given uncertainties are estimated values for 95% confidence. They are not exactly determined. High precision of measurement and calibration in expts. Nos. 3 and 4 justify the statement that the mean value of expts. Nos. 3 to 5 should be true within 10% absolute. Results for expts. Nos. 2 and 6 support this statement.

The G-values (col. 4) are about 30% lower than that for gammas (5.05). This is ascribed to the LET effect, which is much lower than for ferrous sulphate system. The LET effect and G is not influenced by neutron energy more than $\pm$ 20% – probably much less.

The higher energy absorption in the TMP-system ($K_{TMPs}/K_{tissue} = 1.40$) compensates for the LET effect. This means that, exposed to fluences of neutrons and gamma rays producing the same kerma in tissue, the TMP-system will give nearly equal response for neutrons and gammas, i.e. the response per tissue-rad is within about $\pm$ 10% equal for gammas and neutrons in the energy range important for accident and emergency dosimetry. In the light of trends in personal accident dosimetry /26/ this may have considerable practical importance. Thanks to other good properties of DL–M3 and the reader ČDL–M3 /5/ the same may be stated for the application of this dosimeter to personal emergency dosimetry and to calibration of irradiations in research and radiation therapy.

The LET effect found here is nevertheless appreciable and it is not easily understood in terms of the ionic mechanism /6, 7/ of HCl formation. It might be possible that some steps in solvation of primary ions are slow enough. With densely ionized tracks this may give dry and excited HCl molecules which might be lost (for detection) by addition to CB as such or after dissociation to Cl and H atoms.

Acknowledgement. Thanks are due to Mr. H. Udovč, Mr. D. Šunduković and Mrs. J. Šainović for their technical assistance, as well as to our colleagues R. Ilić, I. Mirić, P. Mirić, M. Knežević, N. Najžer and J. Kristan for some measurements and helpful discussions.

References

/ 1/ I. Dvornik, U. Zec, A. Anić, F. Ranogajec, Solid State and Chemical Radiation Dosimetry in Medicine and Biology (Proc. Symp. Vienna, 1966), IAEA, Vienna 273–280, (1967).

/ 2/ I. Dvornik, U. Zec, M. Barić, D. Ražem, Handling of Radiation Accidents (Proc. Symp. Vienna, 1969), IAEA, Vienna, 225–233, (1969).

/ 3/ I. Dvornik, Nuclear Accident Dosimetry Systems (Proc. Panel Vienna, 1969), IAEA, Vienna 131–133, (1970).

/ 4/ B. L. Gupta, I. Dvornik, U. Zec, Phys. Med. Biol. 19, 6 843–852 (1974).

/ 5/ I. Dvornik, U. Zec, D. Ražem, S. Miščević, Criteria for Radiation Protection (Proc. Third European I. R. P. A. Congress, Amsterdam, 1975) paper I 5.

/ 6/ I. Dvornik, U. Zec, Proc. Third Tihany Symp. on Radiation Chemistry (Balatonfüred, 1971), Akadémiai Kiadó, Budapest 219–222, 1972.

/ 7/ D. Ražem, I. Dvornik, ibid, 223–228.
/ 8/ N. Najžer, J. Rant, Irradiation Facilities for Research Reactors (Proc. IAEA-Sm 165), IAEA, Vienna, 161–164 (1973).
/ 9/ S. Makra, P. Zarand, Radiobiological Applications of Neutron Irradiation (Proc. IAEA Panel, Vienna 1971), IAEA, Vienna, 41–50, (1972).
/10/ I. Mirić, Ž. Ubović, Third IAEA Intercomparison Experiment of Nuclear Accident Dosimetry Systems (Vinča, May 1973), to be published by IAEA.
/11/ J. W. Weale et al., The Fast Pulsed Reactor VIPER, I: General Description, J. Brit. Nucl. Energy Soc. 7, 4 313–327, (1968).
/12/ M. H. McTaggart et al., The Fast Pulsed Reactor VIPER, II: Reactor Physics Measurements and Analysis, J. Brit. Nucl. Energy Soc. 7, 4 328–342, (1968).
/13/ H. J. Delafield et al., Preliminary Measurements of the Uniformity of Reactor Field and the Neutron Spectrum from VIPER Reactor, AERE, Harwell, and AWRE, Aldermaston, April 1975.
/14/ I. Dvornik, M. Živadinović, U. Zec, S. Miščević, 4th IAEA Intercomparison Experiment on Nuclear Accident Dosimetry (Harwell, 1975), Final Report, to be published by IAEA
/15/ G. Ahnström, A. Burtscher, J. Costa, Techn. Rep. Ser. No. 76, IAEA, Vienna, 87, (1967).
/16/ G. Ahnström, ibid No. 92, IAEA, Vienna, 111, (1968).
/17/ A. Burtscher, Instruction Manual for Twin Ionization Chambers, Reaktor-zentrum, Seibersdorf, Austria
/18/ J. J. Broerse et al., Results of the Participation in the INDI Project (Brookhaven Nat. Lab., New York, 1973), Report of the Radiobiological Institute, TNO, Netherlands, (1974).
/19/ G. Burger, E. Meier, Results of GSF-Group in the INDI Project, Report of the Radiation Protection Institute of the GSF, München-Neuherberg, (1974).
/20/ T. R. Canada et al., Radiation Research 60, 2 205, (1974).
/21/ G. Burger, F. Grünauer, E. Meier, Biomedical Dosimetry (Proc. IAEA–SM–193), IAEA, Vienna, 71–85 (1975).
/22/ R. G. Jaeger, W. Hübner (Editors), Dosimetrie und Strahlenschutz, G. Thieme Verlag, Stuttgart, 276–281, (1974).
/23/ T. D. Jones et al., Health Phys. 21 253, (1971).
/24/ R. L. Bach, R. S. Caswell, Radiation Research 35 1, (1968).
/25/ Radiation Dosimetry, Vol. III (F. H. Attix and E. Tochilin, Editors)
/26/ E. Piesch, "Trends in Calibration and Evaluation of Personnel Dosimeters", Criteria for Radiation Protection, Introductory and Review Papers (Proc. Third Eur. I. R. P. A. Congress Amsterdam, 1975) pp. 46–64.
/27/ T. Fearon, H. D. Maile, W. A. Kremer, Health Phys. 28 443, (April 1975).

Z. SPURNY

If your system is actually LET independent then how will you differentiate the RBE of gamma against neutrons and neutrons themselves in practical dosimetry?

I. DVORNIK

We have to distinguish RBE for neutrons on the cellular level from that on organism level. In addition we know now that RBE on cellular level decreases with dose, and at doses from 100 to 600 Rads for human cells has values between 1.5 and 4. On the organism level, RBE is approximately the same as for cells only in the case of even distribution of dose over the whole body. For non-even distribution of dose, RBE decreases with the ratio of maximum to minimum dose and may decrease by a factor up to five for neutrons penetrating into the body. It is characteristic that the high LET recoil component of dose falls very rapidly with depth. This is why, on the organism level, RBE is even less than 1.0 – which has been found experimentally for large animals. Because of this in practical accident or emergency dosimetry RBE for neutrons and gammas are considered to be equal. The total dose in rad units in critical organs is for most important purposes sufficient for medical treatment of irradiated persons.

For scientific analysis of an accident, separate determination of the gamma dose is necessary as well as the determination of the neutron spectrum. This is easily performed by the known methods. The advantage of our dosimeter is that it gives quick and accurate information about the total dose.

Yu. A. BERLIN

Have you an explanation about the high value of G (ionization) you reported?

I. DVORNIK

If we measure conductivity, solvated electron reactions or the same for "dry" thermal electrons, we obtain G (ionization), i.e. G of the total ions, between 3 and 5. In certain media it is possible that additional ionization takes place having definite excited states as precursors. If the energy of the excited state is low enough, it will produce electrons of comparative low energy. Electrons produced with initial energy of a few eV will be captured by parent ions immediately after thermalization because they will be very near to them. So it is possible that they cannot be detected as thermal or solvated electrons. Opposite to this such non thermal electrons should enter resonant attachment reactions with the same efficiency as all other electrons, provided that the whole cross section is the energy range of slowing down electrons. This may easily be true knowing the facts obtained for the gas phase.

RADIATION INDUCED RACEMIZATION OF 1,1'-BINAPHTHYL IN TETRAHYDROFURAN AND TOLUENE

Masahiro Irie, Takehiko Yorozu, Kikuo Yoshida, Koichiro Hayashi
The Institute of Scientific and Industrial Research, Osaka University, Suita
Osaka, Japan

Introduction

The study of the isomerization process induced by photoillumination /1/ as well as by radiation /2/ has provided invaluable information about the electronic structure of the intermediate state through which isomerization occurs/1/.

The isomerization, for example cis-trans isomerization of stilbene, is now well known as being induced by photoillumination /1/, by radiation /2/ and also by alkali metal reduction of it to radical anion /3/. The study of isomerization of enantiomers, however, is limited to a few cases, such as biphenyl derivatives /4, 5/ or sulphoxides /6/, presumably due to the difficulty of the resolution of the enantiomer. The purpose of this paper is to study the radiation-induced racemization process of 1,1'-binaphthyl having optical activity owing to molecular asymmetry as shown in Fig. 1. The effect of radiation to solution yields several kinds of reactive intermediates. The contribution of these intermediates to the racemization process of 1,1'-binaphthyl was examined in several solvents and the differences in the behaviour of the conformational change between the intermediates are discussed.

Experimental Procedures

1,1'-binaphthyl was resolved by the same method as has been used before /7/. The optical activity thus obtained has $[\alpha]_D^{20}$ of 154°. Tetrahydrofuran, methylene chloride and toluene were distilled twice over calcium hydride. Triplet quenchers were used of the same compounds as described before /7/. Each sample was degassed by the freeze-thaw cycle in a vacuum of less than 10^{-5}mmHg.

γ-irradiation was carried out by Co^{60} γ-rays with a dose rate of 9.2×10^5 rad/hr. The reaction was followed by measuring $[\alpha]_D^{20}$ with an Hitachi Polarimeter (Type PO-B). The absorption spectra of the γ-irradiated samples were measured with a conventional recording spectrometer (Hitachi EPS-3T). The temperature of the samples was controlled by the use of appropriate cooling solvents and thermocouples.

The transient absorption spectra of the irradiated samples were measured by a pulse radiolysis apparatus as described before /8/.

Results and Discussion

(I) Racemization in Solutions

Figure 2 shows the dependence of the rate of racemization of 1,1'-binaphthyl induced by γ-irradiation on solvents at 0 °C. γ-irradiation of solutions of 1,1'-binaphthyl in tetrahydrofuran and toluene causes the racemization, though the reaction is scarcely observed in methylene chloride. The reaction follows the first order kinetics to a conversion of 80% of the initial optical activity.

The dependence of the rate on solvents suggests that the reaction occurs either in radical anion or triplet excited states of 1,1'-binaphthyl. The possibility in a radical cation state is removed, since it is generally held that radical anion, radical cation and triplet excited states of the added solutes, are predominant transient intermediates generated in tetrahydrofuran, methylene chloride and toluene solutions, respectively /9/.

In order to substantiate the above mechanisms, (via radical anion state in tetrahydrofuran and via triplet excited state in toluene), effects of additives (anion and triplet quenchers) are examined. The addition of methylene chloride suppressed the rate of racemization considerably in tetrahydrofuran solution, though the rate was slightly affected in toluene as shown in Fig. 3. Methylene chloride is well known to capture electron by a dissociative electron capture reaction and to inhibit the formation of radical anions. The decrease of the rate by the addition of methylene chloride clearly proved that the racemization reaction in tetrahydrofuran proceeds through a radical anion state of 1,1'-binaphthyl.

The ineffectiveness of the addition of methylene chloride coincides with the triplet mechanism in toluene solution. The effect of triplet quenchers in toluene solution is shown in Fig. 4. The quenchers, which have triplet energy less than 55 Kcal/mole, remarkably suppressed the reaction, while the addition of acetophenone and benzophenone with triplet energy higher than 65 Kcal/mole has no effect on the reaction. The effect of triplet quenchers proves unambiguously that the racemization reaction proceeds through the triplet excited state in toluene.

The temperature dependence of the reaction rates in tetrahydrofuran and toluene are shown in Fig. 5. The slopes give the activation energy of 1.1 and 1.9 Kcal/mole in tetrahydrofuran and in toluene, respectively. The value of 1.9 Kcal/mole in toluene coincides with the value obtained for photoracemization, in which triplet excited state of 1,1'-binaphthyl is responsible for the racemization reaction.

The activation energy of 1.1 Kcal/mole in tetrahydrofuran represents the barrier necessary for the naphthyl ring to rotate along the intraannular C-C bond in radical anion state of 1,1'-binaphthyl. The low barriers in both case, (triplet excited state and radical anion state) in comparison with the barrier in the ground state, which is reported to be ca 22 Kcal/mole /10/, suggests the similarity of the electronic structure in the triplet excited state and the radical anion state. The electronic structure change induced by the introduction of electron to the lowest vacant molecular orbital is considered to be responsible for the conformational change, which gives rise to the racemization reaction.

(II) Spectroscopic study

The formation of radical anion of 1,1'-binaphthyl in tetrahydrofuran and the triplet excited state in toluene are further confirmed by the pulse radiolysis method. Figure 6 shows the absorption spectra obtained 2μsec after pulse in tetrahydrofuran (solid line) and in toluene (dotted line). The spectrum in tetrahydrofuran is similar to the spectrum of radical anion formed by sodium reduction of 1,1'-binaphthyl and is certainly attributable to radical anion of 1,1' - binaphthyl. It decayed following the second order decay kinetics. The existence of the triplet state in the spectrum is not discerned, which implies the contribution of triplet state is small.

The spectrum in toluene is similar to the spectrum obtained by laser photolysis in tetrahydrofuran and is safely attributable to triplet- triplet absorption of 1,1'-binaphthyl. The triplet state decayed according to the first order decay kinetics and the rate constant is obtained to be 7.1 x 10^4 sec^{-1}.

In order to follow directly the rotation process in a radical anion state, a spectroscopic study at low temperature was carried out. Figure 7 shows the spectrum (A) of 1,1'-binaphthyl irradiated in 2-methyltetrahydrofuran at 77 K. According to the criterion of Hamill, the spectrum is attributable to the spectrum of radical anion of 1,1'-binaphthyl. The conformation of the radical anion, however, is considered to be almost rectangular and to be different from the stable conformation of radical anion state, since at 77 K the rotation of naphthyl ring is suppressed. On raising the temperature, the spectrum changed at 100 K to that shown as B in Fig. 7. Above 100 K the spectrum did not show any noticeable change in shape but decreased. It disappeared above 118 K.

The spectrum observed above 100 K is similar to the spectrum obtained by a pulse radiolysis method at room temperature as well as that of a radical anion formed by a reduction with alkali metal. This spectrum is attributable to the radical anion of 1,1'-binaphthyl in less twisted coplanar conformation.

(III) Concentration dependence of G-Value

Figure 8 shows the dependence of G-value of racemization on the concentration of 1,1'-binaphthyl in tetrahydrofuran and toluene, respectively. In both cases the G-value increases with the increase of the concentration and shows the value as high as 10, which is much higher than the value of the yield of primary radical anion or triplet excited state (G-value of Ca 3). This fact suggests the chain reaction via radical anion as well as triplet excited state in the racemization reaction as follows,

$$S \longrightarrow S^+, e, S^* \qquad /1/$$

$$R\text{-}BN + e \longrightarrow R\text{-}BN^{\cdot -} \qquad /2/$$

$$(S\text{-}BN + e \longrightarrow S\text{-}BN^{\cdot -})$$

$$R\text{-}BN^{\cdot -} \longrightarrow S\text{-}BN^{\cdot -} \qquad /3/$$

$$(S\text{-}BN^{\cdot -} \longrightarrow R\text{-}BN^{\cdot -})$$

$$S\text{-}BN^{\cdot -} + R\text{-}BN \longrightarrow S\text{-}BN + R\text{-}BN^{\cdot -} \qquad /4/$$

$$(R\text{-}BN^{\cdot -} + S\text{-}BN \longrightarrow R\text{-}BN + S\text{-}BN^{\cdot -})$$

$$R\text{-}BN^{\cdot -} + (+) \longrightarrow R\text{-}BN \qquad /5/$$

$$(S\text{-}BN^{\cdot -} + (+) \longrightarrow S\text{-}BN)$$

$$R\text{-}BN + S^{*} \longrightarrow {}^{3}R\text{-}BN^{*} \qquad /6/$$

$$(S\text{-}BN + S^{*} \longrightarrow {}^{3}S\text{-}BN^{*})$$

$${}^{3}R\text{-}BN^{*} \longrightarrow {}^{3}S\text{-}BN^{*} \qquad /7/$$

$$({}^{3}S\text{-}BN^{*} \longrightarrow {}^{3}R\text{-}BN^{*})$$

$${}^{3}S\text{-}BN^{*} + R\text{-}BN \longrightarrow S\text{-}BN + {}^{3}R\text{-}BN^{*} \qquad /8/$$

$$({}^{3}R\text{-}BN^{*} + S\text{-}BN \longrightarrow R\text{-}BN + {}^{3}S\text{-}BN^{*})$$

$${}^{3}R\text{-}BN^{*} \longrightarrow R\text{-}BN$$

$$({}^{3}S\text{-}BN^{*} \longrightarrow S\text{-}BN) \qquad /9/$$

where S, e and (+) are solvent, electron and positive charge, respectively. R-BN and S-BN indicate the two enantiomers of 1,1'-binaphthyl. By the repetition of the processes of (3) and (4) in the case of radical anion, and (7) and (8) in the case of triplet excited state, the yield of the racemization is considered to increase. Although in the case of stilbene of appreciable energy the difference between the excited states of the two isomers prevents the chain reaction mechanism for the isomerization, the enantiomers of 1,1'-binaphthyl have no energy difference in a triplet excited state as well as in a radical anion state, and a chain reaction is expected to occur in both cases. The kinetic chain length depends only on the life time of the intermediate states. The chain reaction via triplet state observed for the racemization reaction of 1,1'-binaphthyl is, as far as the authors know, the first example of the chain reaction with a carrier of triplet excited state.

References

/1/ For example: J. Saltiel, D. W. Chang, E. D. Megarity, A. D. Rousseau, P. T. Shannon, B. Thomas and A. K. Uriarte, Pure and Appl. Chem., 41 559 (1975); S. Yamauchi and T. Azumi, J. Am. Chem. Soc., 95 2709 (1973); S. Malkin and E. Fishchn, J. Phys. Chem., 68 1153 (1964); R. H. Dyck and D. S. McClure, J. Chem. Phys., 36 2326 (1962).

/2/ H. P. Lehmann, J. Phys. Chem., 73 20 (1969); R. R. Heutz, D. B. Peterson, S. B. Srivastava, H. F. Barzynski and M. Burton, J. Phys. Chem., 70 2362 (1966); R. A. Caldwell, D. G. Whitten and G. S. Hammond, J. Am. Chem. Soc., 88 2659 (1966).

/3/ S. Sorensen, G. Levin and M. Szwarc, J. Am. Chem. Soc., 97 2341 (1975).
/4/ K. Mislow and A. J. Gordon, J. Am. Chem. Soc., 85 3521 (1963).
/5/ H. E. Zimmuman and D. S. Crumrine, J. Am. Chem. Soc., 94 498 (1972).
/6/ K. Mislow, M. Axelrod, D. R. Rayner, H. Gotthardt, L. M. Coyne and G. S. Hammond, J. Am. Chem. Soc., 87 4958 (1965).
/7/ M. Irie, K. Yoshida and K. Hayashi, to be published.
/8/ S. Fujita, H. Horii and S. Taniguchi, J. Phys. Chem., 77 2868 (1973).
/9/ A. Henglein, W. Schnabel, J. Wandenburg, Einführung in die Strahlenchemie, Verlag Chemie, GmbH-Weinhein/Bergstr. 1969 p. 247.
/10/ A. K. Colter and L. M. Clemens, J. Phys. Chem., 68 651 (1964).

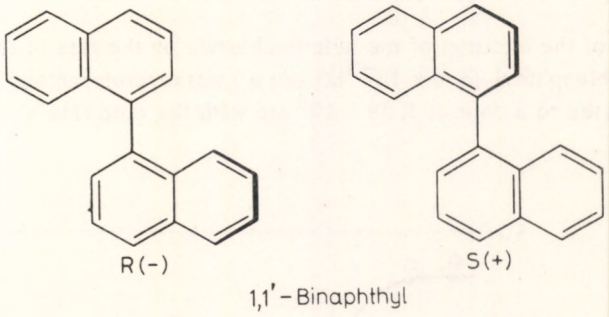

Fig. 1 S (+)-1, 1' -binaphthyl and R (-)-1, 1' -binaphthyl

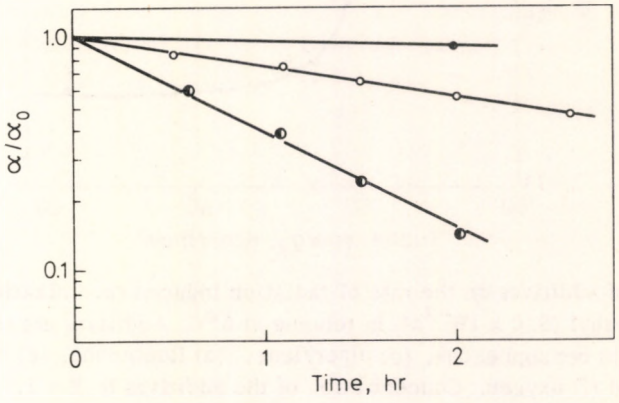

Fig. 2 Radiation induced racemization of 1, 1' -binaphthyl (8. 0 x 10^{-3}M) in (◐) toluene, (○) tetrahydrofuran and (●) methylene chloride at 0 °C. Dose rate is 9. 2 x 10^5 rad/hr

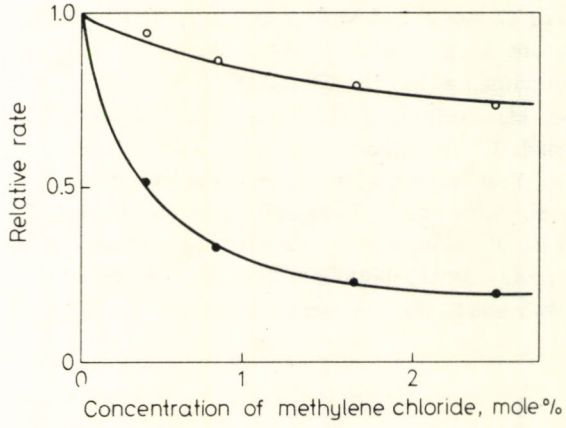

Fig. 3 Effect of the addition of methylene chloride on the rate of racemization of 1, 1′ -binaphthyl (8. 0 x 10^{-3}M) in (●) tetrahydrofuran and (○) toluene irradiated to a dose of 1. 38 x 10^{6} rad with the dose rate of 9. 2 x 10^{5} rad/hr at 0 °C.

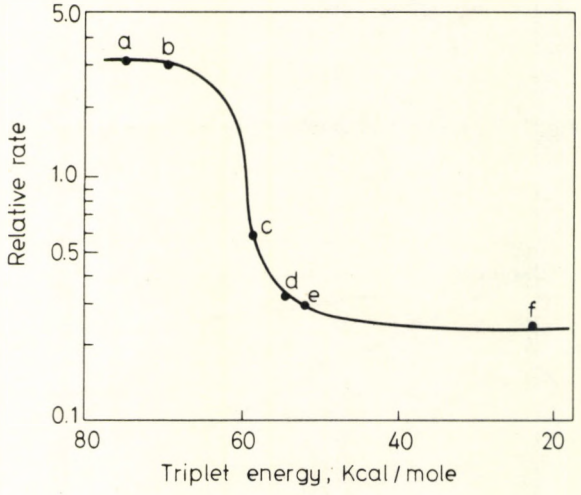

Fig. 4 Effect of additives on the rate of radiation induced racemization of 1, 1' -binaphthyl (8. 0 x 10^{-3}M) in toluene at 0 °C. Additives are (a) acetophenone, (b) benzophenone, (c) piperylene, (d) fluorenone, (e) dibenzalacetone and (f) oxygen. Concentration of the additives is 2 x 10^{-3}M.

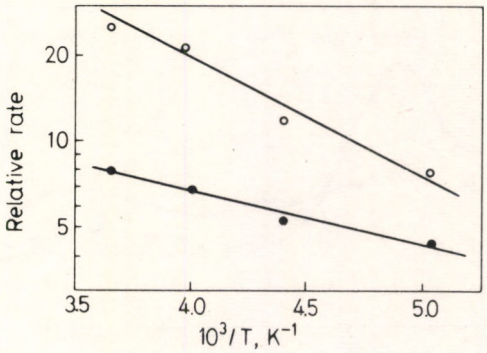

Fig. 5 Temperature dependence of the rate of radiation induced racemization of 1,1'-binaphthyl (8.0×10^{-3} M) in (●) tetrahydrofuran and (○) toluene solutions.

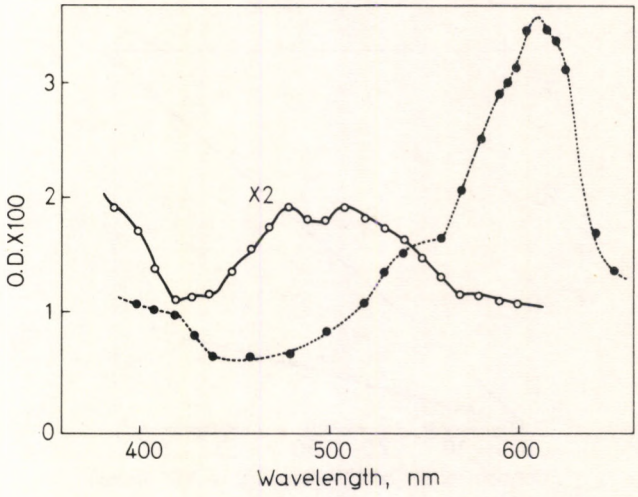

Fig. 6 Transient absorption spectra of 1,1'-binaphthyl at room temperature taken at 2μsec after the pulse in the pulse radiolysis of (○) tetrahydrofuran and (●) toluene solutions containing 4×10^{-3}M 1,1'-binaphthyl.

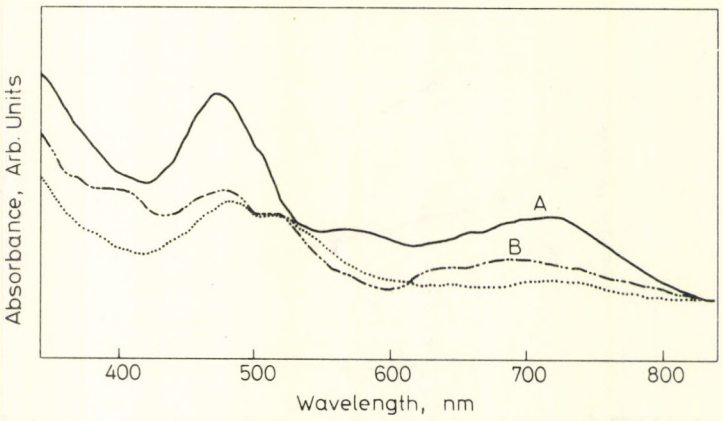

Fig. 7 Absorption spectra of 2-methyltetrahydrofuran solution containing 5×10^{-2} M 1,1' -binaphthyl at (-) 77 K (A) and (- -) 100 K (B) irradiated to a dose of 1.85×10^{5} rad at 77 K. The radical anion of 1,1'-binaphthyl obtained by sodium reduction (.....) is also shown

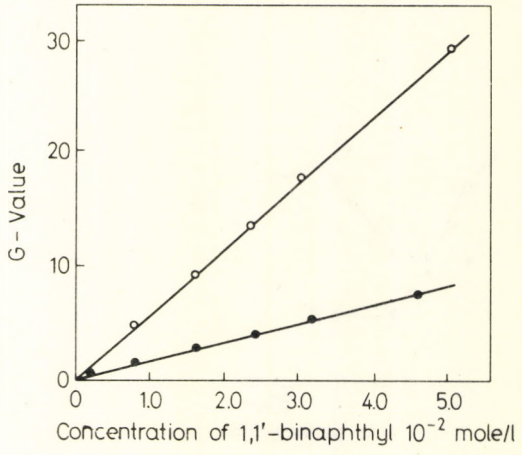

Fig. 8 Dependence of G-value of the racemization of 1,1'-binaphthyl on the concentration of 1,1' -binaphthyl in ( ) tetrahydrofuran and (o) toluene at 0°C

PART TWO

POLYMERS

KINETICS OF CHAIN ALLYL FREE RADICAL DECAY IN IRRADIATED BULK FILM, HYDROGENATED AND EXTENDED CHAIN POLYETHYLENE

Malcolm Dole, G. N. Patel, V. M. Patel, C. S. Hsu
Chemistry Department, Baylor University, Waco, U.S.A.

In studying the kinetics of free radical decay in polyethylene (PE) samples subsequent to irradiation, the possibility has to be considered that the decay rate in different locations (different zones or different phases) in the solid sample may be different. In the case of the alkyl type free radical $-CH_2\dot{C}HCH_2-$, in PE, Johnson, Wen and Dole /1/ found that the data could be quantitatively interpreted in terms of two simultaneous first-order reactions, a fast decay and a slow decay. Inasmuch as there was no evidence that the fast decay involved a different type of free radical from that of the slow decay, we assumed that the difference between the slow and fast decays was the result of two different types of environments of the radicals. The fast decay was believed to be that between radicals in the amorphous phase while it was suggested that the slow decay required first the diffusion of the radicals from the crystalline zones to the amorphous zones before reaction could occur. Kusumoto et al. /2/ have also found a fast and slow decay for alkyl radicals in single crystals of PE. Shimada and Kashiwabara /3/ proposed a two phase second-order decay of alkyl free radicals in irradiated single crystalline PE, but we suspect that their data could also be interpreted in terms of two simultaneous first order reactions as was done by Johnson et al. /1/.

The decay of chain allyl free radicals such as $-CH_2\dot{C}HCH=CH_2$ in irradiated PE follows quite different kinetics from that of the alkyl radicals. For example, molecular hydrogen has no catalytic effect on the decay of the allyl radicals in contrast to its marked effect on the alkyl radical decay. However, the decay of the allyl radicals is not simple second order. Moshkovskii et al. /4/ accordingly suggested that the allyl free radical in irradiated PE decayed at different rates in the amorphous and crystalline zones. Dole et al. /5/ developed the mathematical theory for the case of two simultaneous second-order decay reactions occurring in different zones, but under the condition that only the overall free radical concentration could be measured. Their equations are given below and applied to the interpretation of the chain allyl free radical decay in irradiated samples of bulk film, hydrogenated and extended chain PE. Before doing this it should be noted that Wen, Johnson and Dole /6/ could obtain a quantitative interpretation of the chain allyl free radical decay data in single crystals of PE in terms of a single second order decay reaction, but with diffusion control.

Experimental

The properties of the polymer samples studied are given in Table 1.

The samples were irradiated with Co-60 γ-rays at a dose rate of about 0.18 Mrad hr^{-1} in vacuo at 77 K (l. n. t.) or at room temperature (r. t.). Alkyl radicals were eliminated by allowing the samples to stand at room temperature in the presence of the evolved hydrogen gas. No allyl radicals react at r. t.; in fact in the case of the extended chain samples of PE, allyl radicals are stable up to 90°. The

Table 1

Properties of the Linear Polyethylene Samples Studied

Type of Sample	Symbol Used	Density at 25°	Volume Fraction of Amorphous Content, α_v	M_n	Vinyl Content moles $g^{-1} \times 10^4$
Marlex Film	MF	0.9595	0.272	20,000	0.80
Hydrogenated PE	HP	0.950	0.338		0.0
Extended Chain	EC	0.9938	0.036	8,900	

complete elimination of the alkyl radicals was checked by observing whether or not the outermost peak, the wing peak, in the alkyl radical electron spin resonance (esr) spectrum had completely disappeared.

The samples were irradiated in quartz tubes that fitted into our esr spectrometer. Before inserting the tube into the spectrometer, one end of the tube was annealed and then the polymer sample slid to that end before making the esr measurements. The total allyl radical spin concentrations at r. t. were obtained by taking a double integration of the total allyl radical esr spectrum, and the latter compared with that of a standard sample of DPPH in KCL. The integration was done automatically by means of a mini-computer which was interfaced with the esr spectrometer.

Kinetic studies were carried out by heating the esr cavity to the desired temperature, inserting the sample tube and adjusting the magnetic field of the esr spectrometer to the field of the highest peak of the allyl spectrum. By means of the computer, readings of peak height were taken every three minutes or at other equal time intervals as previously described /6/.

Experimental Results and Discussion

The experimental data will be interpreted in terms of the Q function defined by the equation

$$Q = \frac{t}{\frac{1}{c} - \frac{1}{c_0}} \qquad /1/$$

where c_0 is the overall allyl radical concentration at zero time and c the concentration at time t. For simple second order kinetics Q should be a constant at all times and equal to k^{-1} where k is the second order decay constant. But as shown in Fig. 1, Q is far from constant, increasing with t over the whole time range. Similar curves were obtained in the case of the other PE samples studied.

In the case of two non-interacting populations of allyl radicals with initial mole fractions x_f and x_s, the subscripts f and s referring to the fast and slowly decaying components, respectively, Q is given /5/ by the equation

$$Q = \frac{1 + Kt}{A + Bt} \qquad /2/$$

where the three independent parameters are defined by the equations

$$A = x_f^2 k_f + x_s^2 k_s \qquad /3/$$

$$B = c_0 x_f x_s k_f k_s \qquad /4/$$

$$K = c_0 x_f x_s (k_f + k_s) \qquad /5/$$

in which k_f and k_s are the second order decay constants of the fast and slowly decaying species, respectively.

In case only one species reacts at a measurable rate, e.g. $k_s = 0$, but $x_s \neq 0$,

$$Q = \frac{1}{x_f^2 k_f} + \frac{x_s}{x_f} \, t \qquad /6/$$

In this case Q should be a linear function of t.

If the two species decay with measurable rates, but the decay of each is diffusion controlled, one can apply the diffusion equation of Waite /7/, see also /6/.

The equation for Q then becomes more complicated, namely

$$Q = \frac{\sqrt{t} + a_4 t + Kt^{3/2}}{a_1 + a_2\sqrt{t} + a_3 t + Bt^{3/2}} \qquad /7/$$

where

$$a_1 = x_f^2 I_f + x_s^2 I_s \qquad /8/$$

$$a_2 = A + B\,\frac{I_f I_s}{k_f k_s} \qquad /9/$$

$$a_3 = \frac{B}{k_f k_s}\,[I_f k_s + I_s k_f] \qquad /10/$$

$$a_4 = \frac{B}{k_f k_s}\,[I_f + I_s] \qquad /11/$$

in which I_f and I_s are the intercepts at zero time of a Waite–type plot, i. e. of a plot of $\sqrt{t}/Q$ as a function of $\sqrt{t}$.

In a previous paper /5/ we have shown how the three constants A, B and K can be exactly determined by a least squares method from the data. The constants I_f and I_s are most readily estimated by approximate methods also already described /5/.

From Fig. 1 it can be seen that in all probability Q extrapolates to zero at zero time in the case illustrated. This means that either the fast or the slow or both decay reactions are diffusion controlled. Otherwise Q would extrapolate to a finite value of A^{-1} at zero time as can be seen from Eq. (2). As t goes to zero, Q must also go to zero according to Eq. (7) if both the fast and slow reactions are diffusion controlled and also if only one of them is diffusion controlled. Thus, the Q–function is a very valuable function to use in the theoretical interpretation of the data. The dashed line illustrates Q–values theoretically calculated by means of Eq. (2) using the following values of K, A and B, namely, 7.560×10^{-2} min^{-1}, 2.687×10^{-20} $cm^3\ spin^{-1}\ min^{-1}$, and 1.267×10^{-22} $cm^3\ spins^{-1}\ min^{-2}$.

Figure 2 illustrates the relationship between the x_f values for the three different types of polyethylenes studied here. The hydrogenated PE, HP, has the highest x_f value and it increases more rapidly with temperature than in the case of the Marlex film, MF, or extended chain crystalline PE, EC. It would be interesting to compare the trend of the x_f values with temperature with the fraction of sample melted at the various temperatures. In Fig. 3 the logarithm of the allyl decay constant of the slow component, $\ln k_s$, at 100° is plotted as a function of the

amorphous volume fraction, α_v, as calculated from the density at 25° by means of equation (6)

$$\alpha_v = 6.8882 - 6.8951\rho \qquad /12/$$

where ρ is the density. It is interesting to note that ln k_s is a linear function of α_v. We deduce from this fact that the slow decay process must occur in the amorphous zones. In fact, one would not expect the chain allyl free radicals to be in the crystalline zones inasmuch as shown by Waterman and Dole /8/ the allyl radicals are formed subsequent to the irradiation by the migration of alkyl free radicals to locations adjacent to double bonds. In the case of the Marlex film the decay of the alkyl free radical is markedly catalyzed by hydrogen gas which dissolves only in the amorphous zones; therefore allyl radicals must be formed in the amorphous zones. This is also probably the case with the hydrogenated PE, but we do not have hydrogen solubility or hydrogen catalytic studies on this sample. The situation with regard to the extended chain sample is somewhat more obscure, because here the catalytic effect of the hydrogen was not so pronounced.

An Arrhenius plot of k_s for the HP and MF polyethylenes is shown in Fig. 4. The slope is greatest for the HP sample; this probably signifies that the amorphous volume fraction increases more rapidly with temperature over the temperature range 60° to 110° than in the case of the Marlex film. The activation energies were 23.9 k cal mole^{-1} for the HP sample and 10.6 k cal mole^{-1} for the Marlex film. In the case of the EC polyethylene the allyl decay does not become significant until a temperature of about 100° is reached; over the temperature range 100 to 120°, the activation energy is probably related to the extent of melting over this temperature range. In fact a plot of $\Delta E^{\neq}$, the activation energy, as a function of α_v at 25° yields almost a straight line.

Conclusions

We have shown that it is possible to interpret our kinetic data for the decay of the allyl free radical in polyethylene samples of different morphology in terms of two simultaneous second order reactions of which one or both are diffusion controlled. The decay rates are highest in the sample of highest amorphous volume fraction. In the case of the single crystalline PE, data for which are not given above, the decay constant /6/ was the same order of magnitude as k_f for the HP polyethylene studied here. Apparently there were no slowly decaying chain allyl free radicals in single crystalline polyethylene. We attribute the latter to the structure of the single crystalline samples in which the allyl free radicals are all probably located in the region of the chain folds between the crystalline lamellae. It should also be noted that in our previous publication /6/ we interpreted the allyl decay data for the bulk film and in one case for the extended chain sample in terms of a single second order diffusion controlled decay reaction. However, in this paper the data

are more extensive and a better interpretation of the data is obtained by means of the two simultaneous reactions theory presented here. For example, in the case of the bulk film, all of the Waite type plots showed a maximum which is characteristic of the kinetics of two simultaneous second order decay reactions.

Acknowledgments. This research was supported by the U. S. Energy Research and Development Administration and by income from the chair in chemistry endowed at Baylor University by a gift from The Robert A. Welch Foundation. We are indebted to the Phillips Petroleum Co. for the samples of Marlex-6002 PE, and to Professor B. Wunderlich of Rensselaer Polytechnic Institute for the extended chain crystalline PE.

References

/1/ D. R. Johnson, W. Y. Wen and M. Dole, J. Phys. Chem. 77, 2174 (1973); W. Y. Wen, D. R. Johnson and M. Dole, Macromolecules, 7, 199 (1974).

/2/ N. Kusumoto, T. Yamamoto and M. Takayanagi, J. Poly. Sci. A-2, 9, 1173 (1971).

/3/ S. Shimada and H. Kashiwabara, Polym. J., 8, 448 (1974).

/4/ A. S. Moshkovskii, V. V. Panasenko, E. G. Yarmilko and A. M. Kabakchi, Sov. Prog. Chem. 37, 60 (1971).

/5/ M. Dole, C. S. Hsu, V. M. Patel, and G. N. Patel, J. Phys. Chem. 79, 2473 (1975).

/6/ W. Y. Wen, D. R. Johnson and M. Dole, J. Phys. Chem. 78, 1798 (1974).

/7/ T. R. Waite, Phys. Rev., 107, 463 (1957).

/8/ D. C. Waterman and M. Dole, J. Phys. Chem. 74, 1913 (1970).

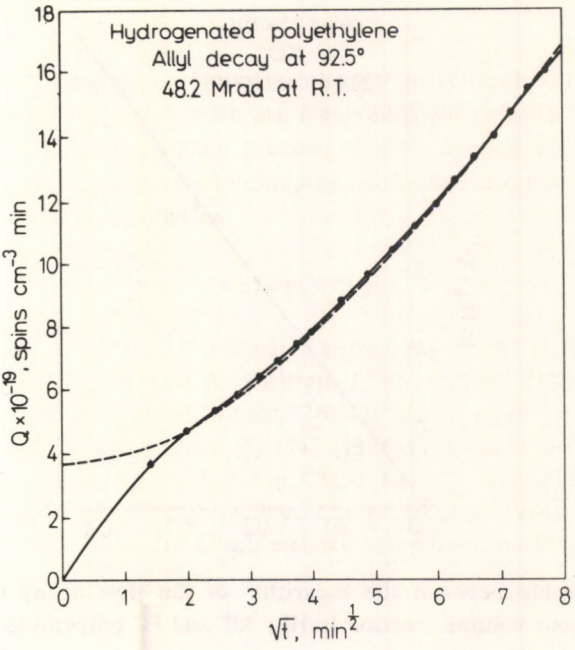

Fig. 1 Plot of the Q-function versus the square root of the time for allyl decay at 92.5° in hydrogenated polyethylene

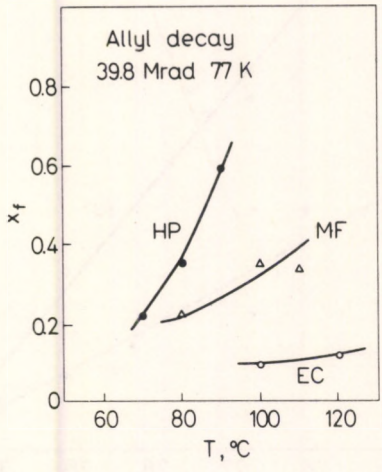

Fig. 2 Mole fraction, x_f, of the fast decaying allyl chain free radicals in hydrogenated polyethylene as a function of temperature in hydrogenated polyethylene (HP), bulk film (MF) and extended chain crystals (EC)

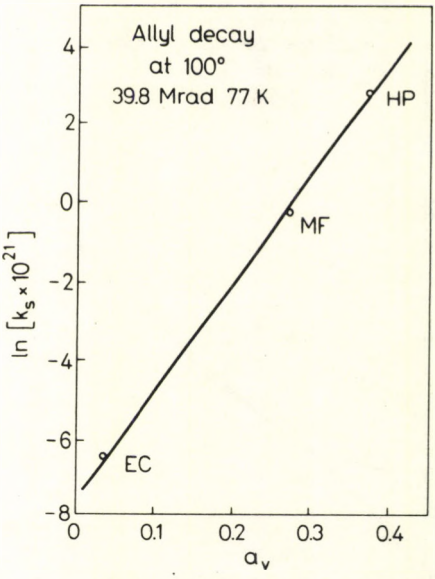

Fig. 3 Relationship between the logarithm of the slow decay constant and the amorphous volume fraction in HP, MF and EC polyethylenes

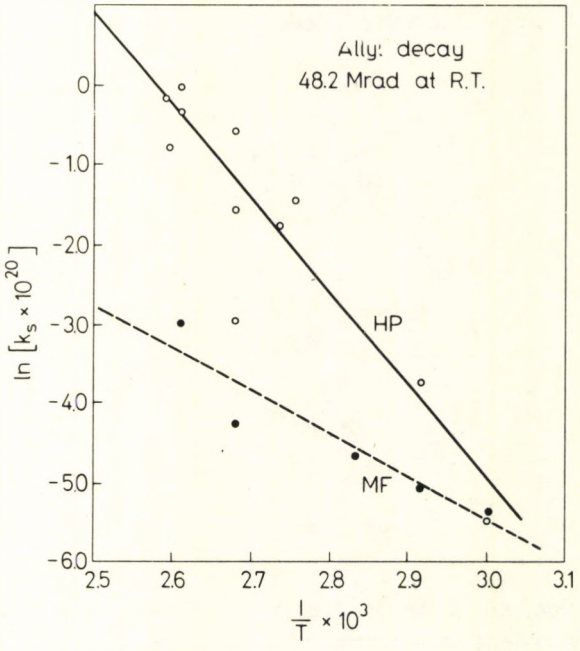

Fig. 4 Arrhenius plot of k_s values in HP and MF polyethylenes

Ya. S. LEBEDEV

If you interpret the radical decay as a diffusion controlled reaction you can find the capture radius, i.e. the distance at which radicals interact. The problem is that the distances found this way are usually too large. Did you try to calculate and interpret the values of capture distances?

M. DOLE

We have made such calculations in two recently published papers, see J. Phys. Chem. 78, 1798 (1974) and 79, 2473 (1973). In the latter paper on extended chain samples of polyethylene the capture distances were about 5×10^{-8} cm, a quite reasonable value.

P. HEDVIG

What are the species which actually diffuse? In the folded chain crystals the reaction zone is the interlamellar one, in the extended chain crystals the dislocations and defects. Diffusion should proceed from one defect to another.

M. DOLE

In the case of the chain allyl free radical, the free radicals are stabilized by a reasonance energy of about 12 kcal/mole, hence the whole segment of the chain to which the allyl free radical is attached must migrate through the solid until two allyl radicals meet and disappear by recombination. This is why allyl radicals are so stable and do not begin to react until about 90° C is reached. This is the case for extended chain samples. At 90°C and above the mobility of the chains begins to be great enough for the segments or ends containing the allyl free radical to oscillate or move about until one allyl free radical meets another and they recombine.

H. KASHIWABARA

Our paper referred to as Ref /3/ in your lecture is a study on the diffusion controlled decay process of alkyl radicals in PE, and not the simple second order reaction treatment.

You mentioned that the decay of alkyl radicals was interpreted by the first order reaction scheme with two (fast and slow) rate constants, and the decay of allyl radicals was interpreted as a diffusion controlled second order process. It looks strange to me. Since you mentioned already that the decay of the alkyl radical was affected by the hydrogen pressure, the three dimensional diffusion controlled process theory can be applied to the alkyl decay process in PE. Our paper is an example of this kind of study.

M. DOLE

We have found that alkyl radicals decay in polyethylene (PE) by a first order mechanism, not second order. If the radicals decayed by a second order process, then the relative rate of decay should depend on the initial concentration. We have found that it does not, hence it is a first order process.

The decay mechanisms of the alkyl and allyl free radicals are completely different. The alkyl radicals are resonance stabilized by about 12 kcal/mole and are much more stable than alkyl radicals. In fact in the case of extended chain PE, the PE must be heated to 90° C or higher before the allyl radicals start decaying. The slow rate determining step in the alkyl decay process is a hydrogen atom migration across chains, but allyl radicals, because of their resonance stabilization, cannot move through the solid PE by any such mechanism.

H. HEUSINGER

Do you assume that there exists only one type of allyl radical?

J. SOHMA

Concerning the question of Prof. Heusinger it seems to me that there are two types of allyl radicals: one is the end radical formed by migration of the unpaired electron to the end double bond, which is formed by a reaction like this

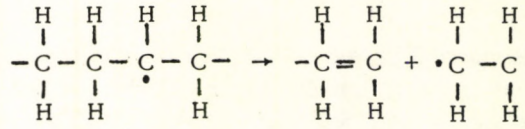

The other type is the allyl chain radical

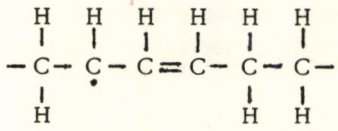

Do you think that the two radical types decay by the same reaction scheme, if the diffusion mechanism is determined by the molecular motion of the polymer, as you mentioned?

M. DOLE

From previous work we know that allyl free radicals are not formed in any significant extent when polyethylene is irradiated at 77 K. On warming to room temperature alkyl radicals migrate to positions adjacent to double bonds where allyl radicals are formed. In this process both the vinylene and vinyl double bond concentrations de-

crease, and allyl free radical formation occurs. The increase in concentration of the latter is stoichiometrically equal to the sum of the decrease in concentration of the vinylene and vinyl double bonds. Hence we know that allyl free radicals exist both at chain ends and in the chain. However in our measurements of the allyl free radical concentration by means of the ESR spectrometer, we do not distinguish between the two types of allyl radicals. We have, however, also studied allyl decay in hydrogenated polyethylene in which no vinyl groups exist before irradiation, but the decay kinetics involving two simultaneous but spatially separated second order decay reactions is also valid in this case. Hence the fast and slow decay mechanisms are not related to the two types of allyl radicals. Rather the mole fraction of the fast decaying species depends on the volume fraction of the amorphous phase.

A. CHARLESBY

There is a considerable amount of evidence to show that in single crystals cross-linking occurs at or near the surface. However, if single crystals of different sizes are irradiated, the number of crosslinks per chain length does not increase in proportion to their length. In other words if alkyl radicals move to the surface to form a cross-link there, one would expect that for the same absorbed energy per CH_2 group, more alkyl radicals will be transferred to the chain ends in the longer chains. This is not seen, and the G(crosslink) value decreases with increasing chain length. This must mean that some alkyl radicals formed within the lattice are lost by some other reaction. Could Professor Dole suggest any mechanism of radical loss within the crystal lattice?

M. DOLE

In the above comment it is implicitly assumed that the free radical yield (from which come the crosslinks by radical recombination in all probability) is independent of the crystallinity. We have found (unpublished work,) that the G value for alkyl radical formation is less in extended chain crystals than in ordinary bulk polyethylene.

One needs to work out the material balance, i.e. hydrogen, double bond and crosslink formation before one can decide whether crystallinity per se lowers crosslink formation. Also ring links or crosslinks between loops in the amorphous regions could form. Such links must be measured before drawing any conclusions regarding crosslink yield in single crystalline polyethylene.

PRIMARY PROCESSES BY RADIOLYSIS OF SOLID PARAFFINS: FORMATION OF RADICAL PAIRS AND ISOLATED RADICALS*

A.A. Dubinsky, O. Ya. Grinberg, Ya. S. Lebedev
Institute of Chemical Physics, Moscow, USSR

Introduction

Recently in the ESR spectra of many irradiated solids "forbidden" transitions at "half" fields have been observed /1-5/. The appearance of such signals indicates the presence of radical pairs in the system. The dipole — dipole doublet, characteristic to radical pairs, is in most systems not recorded by the usual single-quantum transition /$\Delta M_s = 1$/ technique because of the line broadening and because the spectrum is overlapped by the intense lines of the isolated radicals.

It will be shown in this paper that by a special analysis of the $\Delta M_s=2$ signals important information about the nature of radical pairs can be derived and thus our understanding about the mechanisms of radiolysis of solids can be improved. Typical double-quantum spectra for irradiated polymers are shown in Fig. 1.

Formation of radical pairs

There are two possibilities for radical pair formation: a/ correlated formation b/ b/ random stabilization in pairs of radicals which have been formed at different times isolated, and randomly distributed in the sample volume. In the latter case /b/ the rate of formation of pairs should be proportional to the concentration of the already formed radicals. Figure 2 shows the integrated intensities of single-quantum $\Delta M_s=1$ /I_1/ and double-quantum $\Delta M_s=2$ /I_2/ signals as a function of the radiation dose for n-decane and for polyethylene. The ratio of the intensities $I_2/I_1 = \alpha$ are also shown. This ratio is proportional to the ratio of radical pair concentration to the concentration of isolated radicals. It is seen that over the whole range of the formation curve this ratio (α) is constant. This observation led the authors of Ref. /2/ to the conclusion that a specific mechanism for radical pair formation should be effective.

Kinetic analysis shows, however, that the dose independency of α can be interpreted in terms of random formation of radical pairs as a consequence of the correlation in the radical distribution created by the radical decay processes during radiolysis.

*Preliminary results of this work have been published in Khimia Vysokih Energii 10, No 4 (1976).

This way the radical pair concentration versus dose curves does not represent uniquely the mechanism of pair formation because the effects of decay are also contained. These effects are small at small doses, though in this case the pair concentration is small too.

For studying the nature of radical pair formation a special experiment was performed. High density polyethylene having average molecular weight of 2.4×10^5 was evacuated at 350 K for 3 hrs to 10^{-3} Hg mm. This sample was irradiated at 77 K with a dose of 50 Mrad. Then the sample was heated up to that temperature where the $\Delta M_s=2$ signal vanished but the $\Delta M_s=1$ signal remained practically unchanged. This was achieved by heating up to $-10^{\circ}C$ and storing the sample there for 10 minutes. After this treatment the sample was irradiated again with a smaller dose of 5 Mrad and the double-quantum ESR signal was measured. The integrated intensity of this signal was found the same as that of the control sample, irradiated with the same dose /5Mrad/, but not subjected to previous radiation and thermal treatments (Fig. 3). Similar results were obtained for n-decane, but in this case the double quantum signal could not be made to vanish without significant decrease of the single-quantum signal intensity.

From this experiment it follows that the radical pairs, which are stabilized in these systems by gamma radiolysis, are not products of a random formation process but are rather formed at the same time as a result of reactions with the surrounding molecules of the matrix.

It is noted that by irradiation of polyethylene by accelerated electrons the α-values was found /2/ to decrease by increasing dose. The reason for this is not yet known.

Measurement of radical-radical distance in pairs

It has been shown /6,7/ that in polyethylene and n-decane single crystals where the intermolecular distances are fixed, radical pairs produce single- as well as double-quantum ESR signals because the pairs have different interspin distances.

The absence of single-quantum signals due to pairs in our not-ordered systems is explained by the inhomogeneous line broadening due to the distribution of the interspin distances. The experimentally observable parameter, which is connected with the interspin distances in pairs, is $\alpha = I_2/I_1$. The probability of the double-quantum transition is

$$\phi(r_n, \theta) = 2\left(\frac{3g\beta}{2r_n^2 H_o}\right)^2 \sin^2 2\theta \qquad (1)$$

where r_n, θ are the interspin distance and angle respectively, g is the electronic splitting factor, β is the Bohr magneton, H_o is the dc magnetic field strength.

According to Eq. (1) the α-parameter is

$$\alpha = \frac{\int_0^{\infty} \int_0^{II/2} \phi(r, \theta) \sin\theta \; P(r) \; dr d\theta}{C_R + 2 \int_0^{\infty} P(r) dr} \tag{2}$$

where P(r) dr is the concentration of radical pairs having interspin distances between r and dr; C_R is the total radical concentration.

For calculating the interspin distances, correspondingly, the P(r) function must be determined. Evidently this cannot be done simply by measuring the α-parameter. Even in the simplest case, when the double-quantum transition is due to radical pairs of the same interspin distance r^*

$$\alpha = \frac{C_p}{C_R} \phi(r^*) \tag{3}$$

where C_P is the total concentration of radical pairs, which can only be determined directly from the single-quantum spectrum.

It has been shown /8/ that additional information can be gained by saturating the ΔM_s=1 and ΔM_s=2 transitions by using high microwave power. As the transition probability of the forbidden $\Delta M_s = 2$ transition is α times less that of the allowed $\Delta M_s = 1$ transition, α times higher power is needed to saturate the double-quantum transition than the single-quantum one. Thus, the shift of the saturation curve for the double-quantum transition with respect to the single-quantum one depends on the interspin distance distribution function P(r). In n-decane, irradiated with 10 Mrad at 77 K, a 25 dB shift of the saturation curve was observed.

In Ref. /8/ the two simplest cases of interspin distance distribution were considered:

a/ all pairs have the same interspin distance r^*

$$P(r) = C_p \delta(r-r^*) \tag{4}$$

where δ is the Dirac function,

b/ pairs have been formed from randomly distributed radicals

$$P(r) = C_p \; \theta(r-r_{min}) \; f(r) \tag{5}$$

where $C_p = C_R/2$, θ is the Heaviside function,

$$f(r) = 4\pi r^2 C_R \exp\left\{-\frac{4}{3}\pi C_R (r^3 - r_{min}^3)\right\} \quad (6)$$

where r_{min} is the minimal interspin distance.

Experimentally, however, the shift of the saturation curves is found to increase by partially annealing the samples at elevated temperatures. This indicates that the interspin distance in the initial, not annealed, sample was uneven and correspondingly P(r) is different from that given in Eq. (4). On the other hand it has been shown above that the pairs stabilize not by a random process, which means that f(r) in Eq. (5) must be different from that given in Eq (6). Despite this, Eqs (4) and (6) will be used here for evaluating r_{min} by annealing. By using the experimental value /25 dB/ for the saturation shift $r^* = 5.6$ A is obtained by model a. The effective interspin distance calculated in this way is higher than that corresponding to a real distribution. By heating the sample, first the pairs having small interspin distance will disappear resulting in an increase of the r_{min} value. The increase of the "radius of metastability" with temperature corresponds to the decrease of the rate constant for the unimolecular recombination of the preformed radical pairs.

It has been shown /9/ that the effective activation energy of different molecular processes in the condensed phase can be connected with formation of free volume for paired particles depends on the distance between them, correspondingly the effective activation energy

$$E_{eff} = E(r)$$

and the rate constant for the recombination

$$k = k(r, T)$$

If, from the experimental results, it is possible to construct the temperature dependence of the minimal interspin distance $r_{min}(T)$, it becomes possible to check the structure of the rate constant because

$$k[r_{min}(T), T] = \text{const.} \quad (7)$$

The increase of the value of r_{min} by heating up leads not only to increase of the saturation shift but also to the decrease of the intensity of the double-quantum signal. This is shown in Fig. 4 for n-decane /curve I_2/. If there is a functional relation between this intensity /I_2/ and the minimum distance /r_{min}/ it is possible to con-

struct r_{min} (T) from I_2(T). Thus, by using the distribution functions given by Eqs 4 and 6, with Eq. (2) and the condition

$$\frac{4}{3}\pi r_{min}^3 C_R < 1$$

one obtains

$$\alpha \simeq 160 \frac{C_R}{r_{min}^3} \qquad (8)$$

where C_R is the radical concentration in $Å^{-3}$, r_{min} is in Å units.
The temperature dependence of the minimal interspin distance r_{min} calculated by Eq. (8) is shown in Fig. 4. Is is seen that this dependence is almost linear, which means that the effective activation energy E_{eff} and the free volume depend linearly on the interspin distance.

The problem of random pair formation in the radiolysis of hydrocarbons

By accumulation of radicals during irradiation it is evident that there is always random formation of radical pairs. The contribution of such pairs to the relative intensity of the double-quantum transitions can be calculated using Eq. (8). If it is assumed that the $r^* = 5.6$ Å interspin distance calculated above is the minimal one for random pairs, the contribution of random pairs to the parameter α at a concentration of 2×10^{-4} $Å^{-3}$ at a dose of 330 Mrad is 2×10^{-4}. Experimentally this value was found to be 5×10^{-5}. This value was found to be constant in the dose range from 5 to 330 Mrad within the limits of error /30%/ /see Fig. 2/. This means that while for pairwise formed radical pairs the interspin distance is less than 5.6 Å, independently formed radicals do not stabilize to form pairs at distances less than $r_o = 10$ Å. The presence of an already stabilized radical in a certain site of the sample looks as if it would prevent stabilization of another radical nearer than r_o.

Dicussion of the mechanism of radiolysis of solid paraffins

The spatial distribution of radicals and radical pairs is determined by the mechanism of the processes by which they are formed. There are different ways of approximation for these processes by low temperature radiolysis of organic materials /10,11/. As in the condensed phase the relaxation of the molecular excitation is

very effective, it can be assumed that the non-molecular processes are most important in radiolysis

$$RH \longrightarrow RH^+ + e^- \quad (9)$$

$$RH^+ + e^- \longrightarrow \dot{R} + \dot{H} \quad (10)$$

$$RH^+ + RH \longrightarrow \dot{R} + RH_2^+ \quad (11)$$

It has been shown /2/ that by introducing bromodecane into decane the radical pair formation yield decreases. A similar effect is observed by substituting H in n-decane with D /7/. These facts indicate the ionic mechanism of the radical pair formation

$$\begin{aligned} RH &\rightsquigarrow RH^+ + e^- \\ RH^+ + RH &\longrightarrow [\dot{R} \quad \dot{R}] + RH_2^+ \\ RH_2^+ + e^- &\longrightarrow [\dot{R} \quad \dot{R}] + H_2 \end{aligned} \quad (12)$$

The last reaction (12) might not lead to the formation of alkyl radicals, for example RH and H can be formed /11/. In this case, reaction (12) leads to the formation of isolated radicals according to (11).

The problem why radicals are not formed near to already stabilized radicals needs special consideration. The stabilization of the radical pairs $\dot{R} \ldots \dot{H}$ according to reaction (10) should precede formation of $RH^+ \ldots R^\cdot$ pairs because RH^+ appears in a given site by ionization of RH as a result of diffusion of a hole formed in another site. In this cation radical pair an electron transfer reaction is possible

$$RH^+ + R^\cdot \rightleftharpoons RH + R^+ \quad (13)$$

It is known that the ionization potential of the radicals is 2–3 times less than that of the corresponding hydrocarbons /12/. The equilibrium of reaction (13), correspondingly, is shifted in favour of the right side. Thus, when near to the cation RH^+ there is a stabilized radical, the following transformation occurs

$$\begin{aligned} RH^+ + R^\cdot &\longrightarrow RH + R^+ \\ R^+ + e^- &\longrightarrow R^\cdot \end{aligned} \quad (14)$$

This means that in this site the isolated radical is stabilized.

The data obtained in the present study show that the transfer reaction (14) proceeds faster for distances up to 10 Å than recombination of charges /10/. This hinders formation of radical pairs at distances smaller than 10 Å. "Special" radical

pairs are formed only by proton transfer according to reaction (12) – if it proceeds before neutralization occurs. It is evident that any kind of complex formation may significantly increase the yield of such pairs /see e.g. Ref. 4/. As for the homolytic dissociation of C - H bonds in excited molecules, this process, evidently, cannot lead to formation of close radical pairs because the H atoms would rapidly diffuse out of the cage.

References

/ 1/ Kurita, Y J., Chem. Soc. Japan 85, 883 (1964).

/ 2/ Iwasaki, M., Ichikawa, T. Ohmori, T. J. Chem. Phys. 50, 1984, 1991, (1969).

/ 3/ Lebedev, Ya. S., Radiation Effects 1, 213 (1969).

/ 4/ Yakimchenko, O. Ye., Lebedev, Ya.S., Int. J. Rad. Phys. Chem. 3, 17 (1971).

/ 5/ Belkova, L.P., Ya. S. Lebedev, Vysokomol. Soed. 17A, 324 (1975).

/ 6/ Fujimura, T., Hayakawa, N., Tamura, N., Chemical transformation of polymers, IUPAC Bratislava 1971.

/ 7/ Gillbro, T., Lund, A., J. Chem. Phys. 61, 1469 (1974).

/ 8/ Grinberg, O., Dubinsky Ya., Fiz. Tverd. Tela 14, 3422 (1972).

/ 9/ Lebedev, Ya. S., Burshtein, A.I., Chem. Phys. 4, 245 (1976).

/10/ Willard, J. in "Fundamental Processes in Radiation Chemistry" /P. Ausloos ed./ 1968.

/11/ Pshezetsky, S.Ya., et al., EPR of free radicals in radiation chemistry. Khimia. Moscow 1972.

/12/ Gurvich, L. V., et al., Bond energies, ionisation poetentials and electron affinities. Nauka, Moscow, 1974.

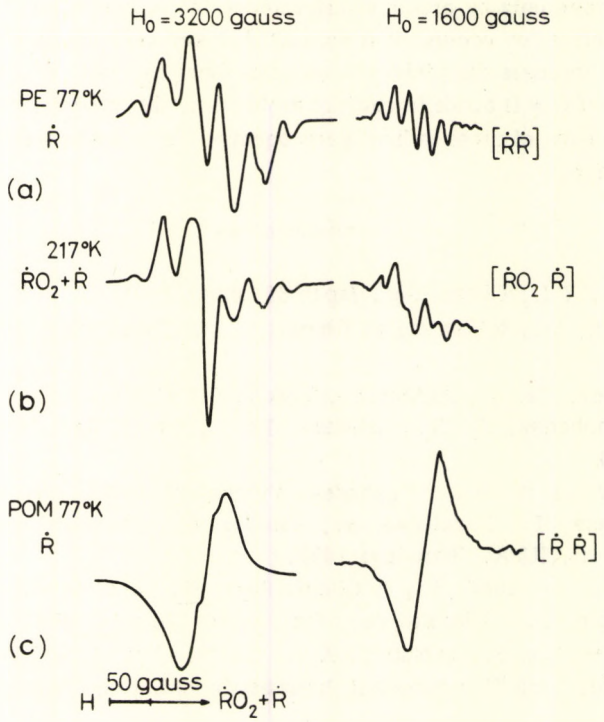

Fig. 1 Single and double quantum ESR spectra of gamma irradiated polymers: a) polyethylene in vacuum; b) polyethylene not evacuated; c) polyoxymethylene

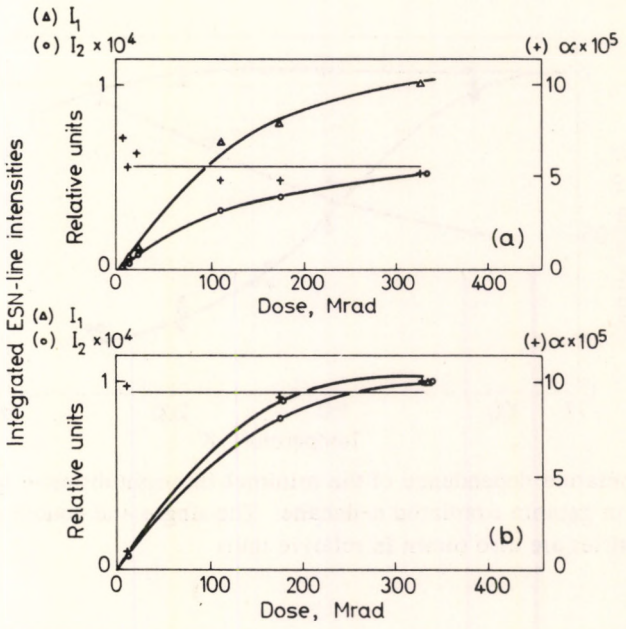

Fig. 2 Accumulation of radicals and radical pairs by gamma radiolysis. I_1, I_2 are the integrated intensities of the single and double quantum lines respectively $\alpha = I_2/I_1$. a) polyethylene 77 K; b) n-decane 77 K

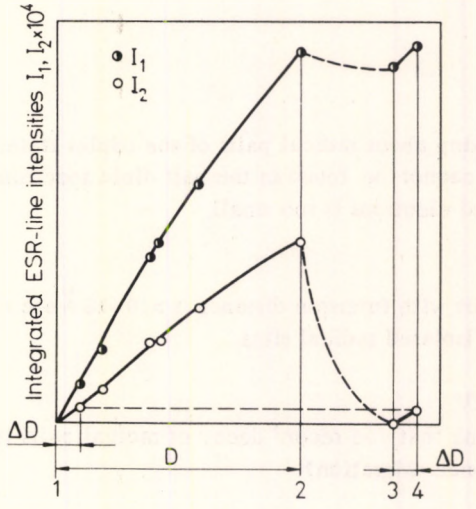

Fig. 3 Effect of preirradiation on the formation of radicals and radical pairs in gamma irradiated polyethylene. D = preirradiation dose, 50 Mrad; ΔD = = successive irradiation dose, 5 Mrad, after annealing the I_2 double quantum signal

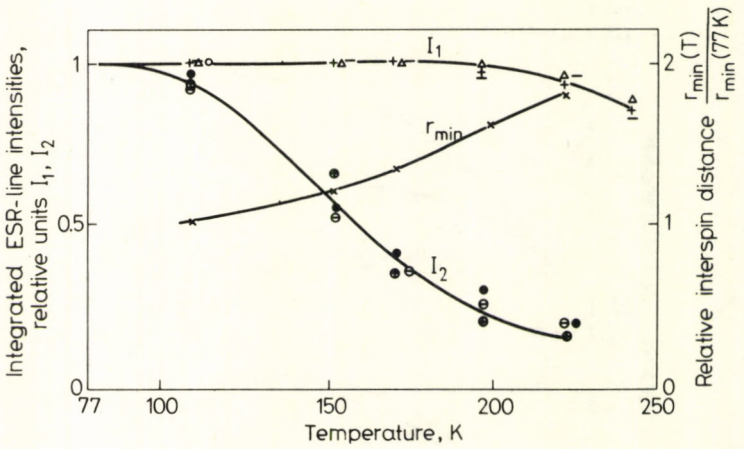

Fig. 4 Temperature dependence of the minimal interspin distance r_{min} of the radical pairs in gamma irradiated n-decane. The single and double quantum signal intensities are also shown in relative units

DISCUSSION

J. MENCZEL

You were speaking about radical pairs of the triplet state. There are, however, radical pairs which cannot be found in the half-field spectrum, if the interaction between the unpaired electrons is too small.

Ya. S. LEBEDEV

The radical pairs with interspin distance $r \geq 10-12$ Å are not, in fact, observed by ESR as pairs, but as isolated radical sites.

V. A. TOLKATCHEV

Why do you think that you record decay of radical pairs in the low temperature regions and not valence migration?

Ya. S. LEBEDEV

The strong correlation between radical – radical distance and the rate of the decay is easily explained by radical recombination in the cage. For radicals escaping from the cage one should expect an opposite dependence.

PULSED NMR STUDIES OF IRRADIATED SILICONE FLUIDS

A. Charlesby, R. Folland
Royal Military College of Science Shrivenham, Swindon, Wilts, England

Introduction

Numerous NMR measurements /1–3/ have been made on polymers and useful information can be derived. In our laboratory we have used the pulsed NMR technique to study a wide range of silicone (polydimethyl siloxane P. D. M. S.) fluids, irradiated to various extents, and have found very interesting relationships between the measured relaxation times and the molecular characteristics of the irradiated materials. These characteristics are related to the sol/gel ratio, i. e. the ratio of non-network to network material, and to the average molecular weight between crosslinks and entanglements. In many previous experiments lengthy extraction methods were used to measure the sol fraction, while the average molecular weight between crosslinked units that determines the mechanical properties of a polymer network, required measurements of swelling and elastic behaviour. If this NMR technique can be extended to other polymers, it provides a most valuable method of characterizing polymer structures, and the influence of radiation thereon. Some of these are now being studied based on the detailed analysis completed for P. D. M. S. At this stage it appears preferable to outline the main conclusions reached for P. D. M. S. polymers without elaborating the techniques used or the detailed mathematical analysis – which are being published separately. /4, 5/.

In the present paper we shall confine our attention to the behaviour of the spin-spin relaxation time, T_2. In polymer materials this relaxation time is considered to be primarily determined by the slower translatory motions of the polymer chains and as such is expected to be profoundly influenced by the presence of intermolecular couplings such as crosslinks and entanglements. In particular, as will be shown in more detail later, the spin-spin relaxation is very sensitive to the presence of a network structure whether this be of a permanent nature, produced for instance by radiation-induced crosslinking, or of a transient nature formed by the numerous chain entanglements present in high molecular weight polymers.

Unirradiated PDMS

The proton relaxation times T_1 and T_2 were measured using commercial pulsed NMR spectrometers operating at frequencies of 18 and 40MHZ (Fig. 1). The measurements were made at 11°C on samples of PDMS (about 0. 1 gm) covering a wide

molecular weight range ($\bar{M}_W \simeq 6,000$ to 100,000). The spin-lattice relaxation time, T_1, is virtually independent of molecular weight whereas the spin-spin relaxation time T_2, decreases with increasing molecular weight. Above a certain molecular weight ($\bar{M}_W \simeq 30,000$) the spin-spin relaxation exhibits a double exponential decay of the form

$$M(t)/M(o) = f_c e^{-t/T_{2L}} + (1-f)\, e^{-t/T_{2S}}$$

where T_{2L} and T_{2S} refer to the long and short T_2 components, respectively the shorter of which only appears when $\bar{M}_w > 30,000$. The fraction f represents the fraction of protons relaxing with T_{2L}. Thus $f = 1$ for $M_W < 30,000$ and $f < 1$ for $M_W > 30,000$.

It is significant that in relating viscosity to molecular weight, $\eta \propto \bar{M}_n^{1.0}$ approximately up to about 30,000, whereas $\eta \propto \bar{M}_w^{3.4}$ above this value. This change in behaviour at a critical molecular weight has been ascribed by Bueche and others to the presence of entanglements. We find that this same figure represents the point at which a T_{2S} relaxation appears.

Irradiated PDMS (below 30,000 initial molecular weight) (f values)

A range of PDMS fluids were subjected to various ^{60}Co gamma radiation doses, and their solubility measured as a function of dose. The change in soluble fraction follows that expected for a crosslinking polymer, i.e. the irradiated material is completely soluble up to a given dose (gelation dose r_g) which corresponds to an average of one crosslinked unit per weight average molecular ($f = 1$)

$$0.624 \times 10^{18}\ G\ r\ M_w = 6.02 \times 10^{23}$$
$$\text{or } r_g = 0.96 \times 10^{-6} / G\ M_w \qquad (1)$$

where r_g is measured in Mrads, and G is the number of crosslinked units per 100ev. Beyond the gel point the soluble fraction s decreases with dose and with δ (crosslinked units per weight average molecule) according to the Charlesby–Pinner /8/ relationship for an initially random distribution of molecular weight

$$s + \sqrt{s} = 2/\delta = 2r_g/r. \quad (+a) \qquad (2)$$

to which must be added a small quantity a to allow for simultaneous radiation induced degradation.

If similar irradiated specimens ($M_w << 30,000$) are examined by pulsed NMR, and the f values plotted against dose r, the same curve is obtained as the sol/dose curve derived from the solubility measurements. Thus the f values for these lower molecular weight PDMS samples appear to represent the non-network fraction of the polymer. The tentative conclusion is that the T_{2S} component arises from molecules comprising network structure, and that T_{2L} corresponds to the non-network (soluble) component.

This conclusion was verified by dissolving out the soluble fraction of the irradiated fluid, and evaporating the solvent. The sol fraction shows only a single relaxation time similar in magnitude to T_{2L} while the insoluble network-fraction has a single but much shorter T_2 similar to T_{2S}. Reintroduction of the soluble or unirradiated PDMS restores a double exponential behaviour ($T_{2S} + T_{2L}$). However the equality between f and s is only valid for $M_w << 30,000$ and a consistent difference appears as M_w approaches 30,000 as will be seen below.

f values for PDMS (initially above 30,000 molecular weight)

For these (f values) specimens, f, (which we recall represents the fraction of the total protons relaxing with the T_{2L} component) is already less than unity, although these specimens are still completely soluble. On irradiation, f decreases further and a plot of f against dose r resembles that for s against r for a system that is already in a post-gel state. In fact the two functions f and s can be superimposed if s is plotted against r/r_g ($=\delta$) and f is plotted against $r + r_e / r_g$, where r_e is a virtual dose, which in the case of a range of high molecular weight silicones measured at 11°C amounts to 6 Mrads independent of molecular weight (Fig. 2).

The explanation of this constant difference appears to be as follows. In solubility measurements of irradiated and crosslinked polymer, lengthy extraction times are needed, and only permanent crosslinks such as those provided by radiation suffice to hold molecules in the insoluble network. Pulsed NMR measurements are made in times of the order of milliseconds, and this is apparently insufficient to allow all molecules to separate. On this time scale an entanglement may therefore act as the equivalent of a crosslink, and the density of such entanglements is measured by the virtual dose of 6 Mrads – i.e. the dose which, if actually administered, would provide the same number of permanent crosslinks as the number of entanglements in fact present, even in the absence of radiation. For PDMS G (crosslinks) ~ 3.0, i.e. there are 6 crosslinked units per 100ev, and a network begins to form at a dose of 6 Mrads if

$$M_w = 0.96 \times 10^6 / G(\text{crosslinked units}) \times r_e \sim 27 \times 10^3 \qquad (3)$$

The significance of the change in viscosity/molecular weight dependence at 30,000 can now be understood. The density of entanglements, i.e. the number present per

g of polymer, is almost independent of molecular weight, except possibly for the shortest polymers, and these entanglements are distributed approximately at random throughout the fluid. At the critical molecular weight of 30,000, this density allows an average of one entangled unit per weight average molecule, just sufficient to form a three-dimensional network, albeit of temporary links. These entanglements are in dynamic equilibrium, with a given mean lifetime, as one entanglement disappears, another takes its place elsewhere. At low rates of mechanical shear, these entanglements resist the motion of molecular chains past each other, and a three-dimensional network must be broken to allow flow to proceed. At high shear rates, entanglements once broken no longer have time to reach their equilibrium value, and there is no longer a three-dimensional network resisting flow. It is in fact found that the viscosity of these fluids decreases at high shear rates, as predicted by this network model.

The variation of f value with temperature further confirms this model. For high molecular weight PDMS, with a small or zero radiation dose, most of the network will be due to entangled units, and these, being in dynamic equilibrium will vary with temperature. For such PDMS fluids, the f value does in fact vary with temperature over a wide range. For low molecular weight PDMS, with considerably less than one entangled unit per molecule, a network can only be formed by an adequate radiation dose, and the crosslinks will be of a permanent nature. In this latter case the f value is independent of temperature from the crystal melting point ($-45^{\circ}C$) to $200^{\circ}C$.

Some important conclusions emerge from these results. The nature of these entanglements is not clearly defined, but they behave as temporary crosslinks, their concentration, averaging about one per four hundred monomer units at $10^{\circ}C$, appears independent of molecular weight, but varies with T.

T_{2L} values and molecular weight

The T_{2L} relaxation relates to the non-network fraction of the specimen, which can include not only many of the original unmodified polymer molecules, but also those which comprise two or more of the original molecules linked together by temporary entanglements or permanent crosslinks. The only molecules excluded are those linked into the network fraction.

It has already been established that T_{2L} relaxation times depend on the molecular weight, decreasing as the molecular weight increases. For PDMS commercial samples, the molecular weight distribution is approximately random so that $M_w \simeq 2\ M_n$. With these specimens it is therefore impossible to determine whether T_{2L} depends on M_w or M_n. To find this out it is necessary to study a series of polymers in which the ratio M_w/M_n varies. Accordingly, a series of mixtures of a high molecular weight and a low molecular weight polymer was investigated, and the measured T_{2L} values related to the calculated values of M_w and M_n for these mixtures.

A similar set of relations is already available for the commercial samples all with $M_w \sim 2M_n$. The comparison shows that the T_{2L} values for samples of the same M_n are similar, whatever the molecular weight distribution, whereas T_{2L} values for samples with the same M_w can differ widely. It follows that T_{2L} is determined primarily by the number average molecular weight, the relation can be written

$$T_{2L} \sim 16\ M_n^{-0.5} \tag{4}$$

approximately at 11°C. The coefficient decreases as the temperature is lowered, but the same exponent of M_n has been observed in other polymers (to within a few per cent) and this may be an indication that T_{2L} is related to the mobility of the molecule as a whole. It would be interesting to determine whether T_{2L} is changed if the shape of the polymer molecules is modified, e. g. by a change in pH for suitable polymers or biopolymers.

An alternative analysis consists in measuring T_{2L} for the sol fractions of a series of irradiated polymers, and comparing these values with those obtained from a series of unirradiated molecules of known molecular weights. As the radiation dose is increased, the longer molecules are linked preferentially into the network, while the concentration of crosslinks and entanglements in the sol diminishes. The theory of random crosslinking allows one to calculate the average molecular weight of these sol molecules, as modified by crosslinks and entanglements. A comparison of T_{2L} values, based on these calculated values of M_n(sol), with T_{2L} values derived from unirradiated samples of known molecular weights leads to good agreement, confirming the validity of this method of analysis (Fig. 3).

T_{2S} and molecular weight between crosslinks and entanglements

The T_{2S} relaxation is only observed when a three-dimensional network is present, whether this be due to entanglements or permanent crosslinks. The T_{2S} relaxation time diminishes with increasing dose beyond the gel point and reflects the increasing restraints imposed on the molecular mobility as the crosslink density increases. In highly-irradiated PDMS samples of very widely differing initial molecular weights, T_{2S} tends to a common value independent of initial molecular weight, but which varies inversely as dose

$$T_{2S} \propto 1/r$$

The density of crosslinking in these polymers is proportional to dose so that the average molecular weight M_c between successive crosslinks in the same chain also varies as 1/r. (A correction is needed for finite initial molecular weight). Ultimately therefore T_{2S} measures M_c.

At lower doses T_{2S} varies from one PDMS to another, depending on their initial molecular weight. The simple relationship between T_{2S} and M_c or r no longer applies. This can be ascribed to the following causes.

1. A correction for M_c values must be applied to allow for chain ends, i. e. parts of the molecular chain linked to the network at only one point.
2. The selection of molecular sizes by the corsslinking process. On purely statistical grounds the average molecular weight of the molecules entering the network is greater than the overall initial average.
3. Similarly the average density of crosslinking on the network is greater than the average. Obviously any molecule not attracting a crosslink will appear in the sol fraction.
4. In addition to the permanent crosslinks induced by radiation, it is also necessary to include the entanglements which, as shown above, play the same role as crosslinks when measured by NMR techniques. Such entanglements do not influenced the fraction of sol or gel material, as obtained by long-term extraction.

A detailed mathematical analysis of the variation of M_{ce} with dose allowing for all these factors has been made, here M_{ce} represents the average molecular weight between crosslinks and/or entanglements. The crosslink density can be deduced from the known G value for crosslinking, and the density of entanglements immediately deduced from the virtual dose (6 Mrads at 11°C) derived independently. T_{2S} values were measured for a range of gel fractions obtained from irradiated samples of PDMS. It then appeared that T_{2S} is a direct measure of M_{ce} (Fig. 4)

$$T_{2S} \sim 0.6 \times 10^{-6} M_{ce} \text{ at } 11^{\circ}C \qquad (5)$$

where the parameter $0.6 \times 10^{-6} M_{ce}$ varies with temperature.

At first sight, it is perhaps surprising to find that the network material can be described by a single relaxation time. For instance the presence of free chain ends might be expected, because of their expected higher mobility, to give rise to an additional longer T_2 component. However, we find no evidence for this effect. This may be taken to indicate that the free chain ends serve to effect the segmental mobility of the overall network in the same way as the addition of a plasticizer.

Protons near the junction points – crosslinks or entanglements – would behave differently from those some considerable distance away from such junctions, but here again there is no evidence of any such behaviour – it is the length of the chain between junction points which determines T_{2S}.

The length of such a chain determines their mobility and elastic behaviour, and indirectly the relaxation time of protons along its length.

Thus, the observed dose dependence of T_{2S} can be empirically correlated with the molecular weight between crosslinks and/or entanglements, M_{ce}, leading to the surprisingly simple proportionality observed. However, it should be emphasised that at the present time we have no information regarding the detailed nature or correlation times of the chain motions which determine the network T_{2S} or how these are affected by the crosslink density. We may assume quite generally that $T_2 \propto \nu_{mot}$ where ν_{mot} is some average correlation frequency of the chain motions. Since T_{2S} does decrease with increasing dose, we may infer that the chain motions that determine T_2 become increasingly slower as the crosslink density increases. We are not in a position at the moment to say whether there is any corresponding significance on the molecular level to be attached to the observed simple proportionality of T_{2S} and M_{ce}.

T_{2S} in the sol fraction

Although some crosslinks can be present in the soluble fraction of an irradiated polymer, this concentration is not sufficient to form a three-dimensional network, and therefore it might appear that no T_{2S} relaxation time should be observable. In fact, for high molecular weight PDMS at doses close to the gel point, a T_{2S} relaxation time is measurable though it disappears for more highly-irradiated specimens. A detailed analysis involving residual crosslinks, reduced molecular weight of sol molecules and entanglements shows that for some specimens the combination of both crosslinked and entangled units may exceed one per weight average molecule and this is sufficient to form a temporary network, in dynamic equilibrium. Experimental values of T_{2S} for such sol fractions can be related to the calculated values of M_{ce} (Eq. 5) while the observed dose at which the T_{2S} component in the sol fraction vanishes agrees with the calculated dose for crosslinked and entangled units to equal unity.

Sol and gel mixtures

Our results for PDMS irradiated beyond the gel point show that samples which contain both gel and sol fractions together have T_{2S} and T_{2L} values which differ from those obtained for the two phases separately. This suggests that the chain motion of each phase is modified by the presence of the other. In particular the mobility of the network fraction is enhanced by the more mobile non-network material and at the same time the mobility of the latter is restricted by the surrounding network material. We have also observed increased chain mobility (longer T_2's) for crosslinked PDMS networks swollen to various degrees with solvents such as C_2Cl_4.

Other polymers

A number of polymers have been studied using this NMR technique, but the results are not yet in sufficient detail for fuller comment. One example may, however, be quoted.

Polyisobutylene is a polymer which degrades (scissions) under radiation. The number average molecular weight after a dose r, $M_n(r)$ is related to its initial value

$$1/M_n(r) = 1/M_n(o) + 1.04 \times 10^{-6} G\, r \qquad (6)$$

where G is the number of radiation-scissioned chains per 100 ev absorbed and r is the dose in Mrads.

$$\text{If } T_{2L} = C\, M_n^{-0.5} \qquad (7)$$

where C is some suitable constant, then

$$T_{2L}^2(r) = T_{2L}^2(o) + C^2.\ 1.04 \times 10^{-6} G\, r \qquad (8)$$

A plot of $T_{2L}^2(r)$ versus dose should therefore give a straight line. Figure 5 shows that this is in fact obtained for polyisobutylene measured at 150°C by NMR, after being subjected to a range of doses from 0 to 967 Mrads.

The value of C can be deduced if the initial molecular weight is known, so that the G values for scission can be directly derived. Table 1 shows that the value of the product $T_{2L}\, M_n^{0.5}$ is approximately constant for a fifty-fold decrease in M_n, with G~11 at the temperature of irradiation.

There is considerable interest in the possibility of using this pulsed NMR technique for the measurement of crosslinking in irradiated polyethylene, which is of considerable economic importance. It is already known that crosslinks do not form at random in partially crystalline polyethylene, but tend to be formed in the amorphous regions and near the surface of the crystallites. This type of behaviour is readily demonstrated in our measurements which were carried out at 150°C on polyethylene samples irradiated at about room temperature (Fig. 6). Samples which were quenched from the molten state prior to irradiation to 45 Mrads show a T_2 relaxation time approximately three times smaller than samples slowly cooled prior to their exposure to this radiation dose. For zero radiation, both samples show the same relaxation time at 150°C. This result is in conformity with the view that rapid quenching results in smaller crystallites and a somewhat higher amorphous content, both of which would enhance the degree of crosslinking.

The analysis of irradiated polyethylene by means of pulsed NMR techniques is expected to reveal a more complex situation than for PDMS. Unlike silicone fluids, polyethylene has a two-phase structure at room temperature, and the crosslinks are not distributed at random. Furthermore the molecular weight distribution is much wider, although it is not known whether this is an important factor.

Table 1

NMR values for irradiated PIB (^{60}Co gammas)

r Mrad	0	2.16	7.5	32.8	78	140	155	290	427	967
$T_{2L} \times 10^3$ observed	52	62	72	96	125	158	168	210	270	400
M_n calculated*	5200	4603	3586	1752	915	553	505	283	195	88
T_{2L} M_n0.5 (T_{2L} in sec)	3.75	4.21	4.31	4.02	3.8	3.72	3.77	3.53	3.77	3.75

*G ~11, $M_n(o)$ = 5200, NMR at 150°C

Conclusion

The use of pulsed NMR methods for the study of irradiated PDMS shows many similarities with the use of solubility and swelling techniques which have been in use for several decades. It has certain advantages: it is non-destructive and rapid, and requires small amounts of material. It can apparently be used to determine molecular weight, network structure and the density of crosslinks and entanglements. It is primarily in this last respect that it differs from the more conventional methods, and this last type of information can be of value outside the field of radiation, for the study of mechanical properties of polymers, their time dependence, creep, flow and fatigue. For this purpose it is necessary to know not only the concentration but also the lifetime of these entanglements, and their behaviour under stress.

We have not discussed the nature of these entanglements. What we can say is that they behave in the same way as permanent crosslinks as far as the NMR data are concerned. In unirradiated PDMS a change in viscosity dependence on molecular weight is observed when this concentration is sufficient to form a temporary network out of the entangled chains. In somewhat lower molecular weight PDMS this change would presumably be observable after a small radiation dose.

References

(1) J.G. Powles, Polymer 1,219 (1960).
(2) W.P. Slichter, Rubber. Chem. Technol. 34, 1574 (1961).
(3) D.W. McCall, D.C. Douglass and E.W. Anderson, J. Polym. Sci. 59, 301 (1962).
(4) R. Folland and A. Charlesby, Inst. J. Rad. Phys. Chem. (in press)
(5) A. Charlesby, R. Folland and J. H. Steven, (to be published).
(6) F. Bueche, J Chem. Phys. 20,1959 (1952).
(7) J. D. Ferry, 'Visco-elastic Properties of Polymers' (Wiley, New York, 1970).
(8) A. Charlesby and S. H. Pinner, Proc. Roy. Soc. A249, 367 (1959).

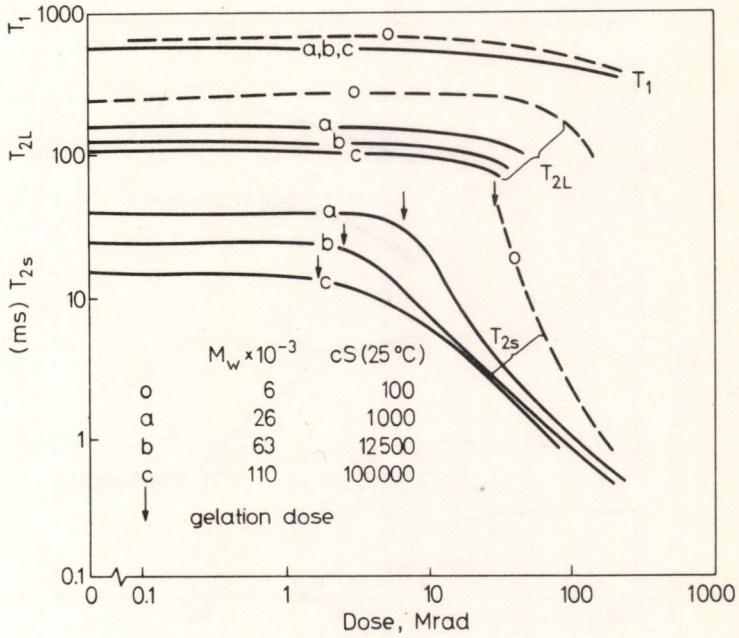

Fig. 1 Experimental data on T_1, T_{2L} and T_{2S} for PDMS fluids. O has less than one entangled unit per w. a. molecule, and T_{2S} only appears at gel point. Horizontal portions of T_{2S} are due to swelling of network by unentangled molecules of sol. Similarly for sol molecules, T_{2L} initially horizontal due to increased viscosity in the presence of network

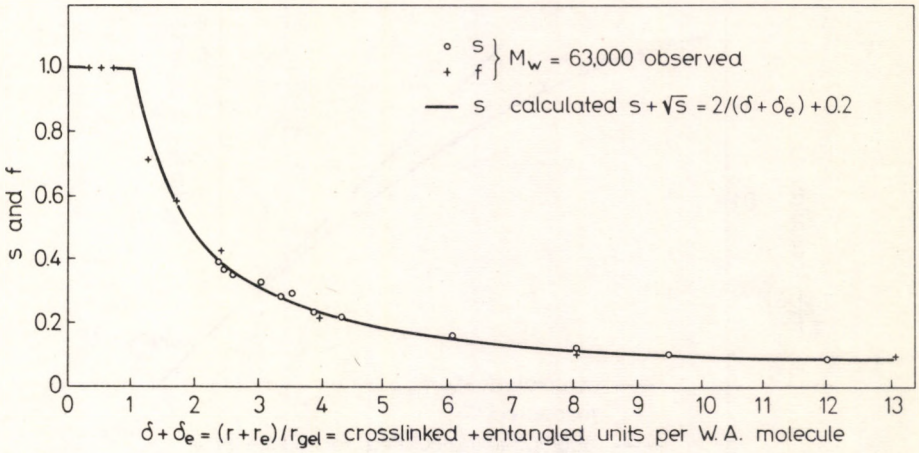

Fig. 2 Comparison of network due to permanent crosslinks (sol = s) and due to crosslinks + entanglements (f). Entanglement density is represented by a virtual radiation dose r_e

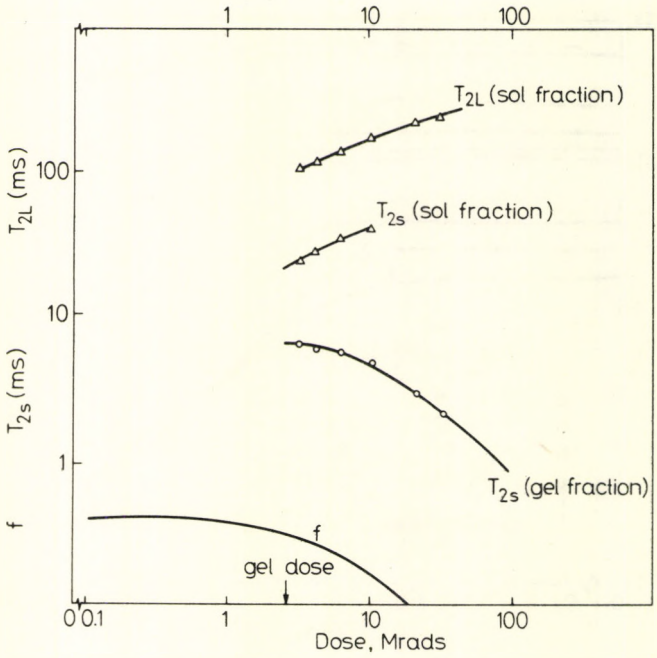
1
10
100
T_{2L} (sol fraction)
T_{2s} (sol fraction)
T_{2L} (ms)
100
10
1
T_{2s} (ms)
T_{2s} (gel fraction)
f
f
gel dose
0 0.1
1
10
100
Dose, Mrads

Fig. 3

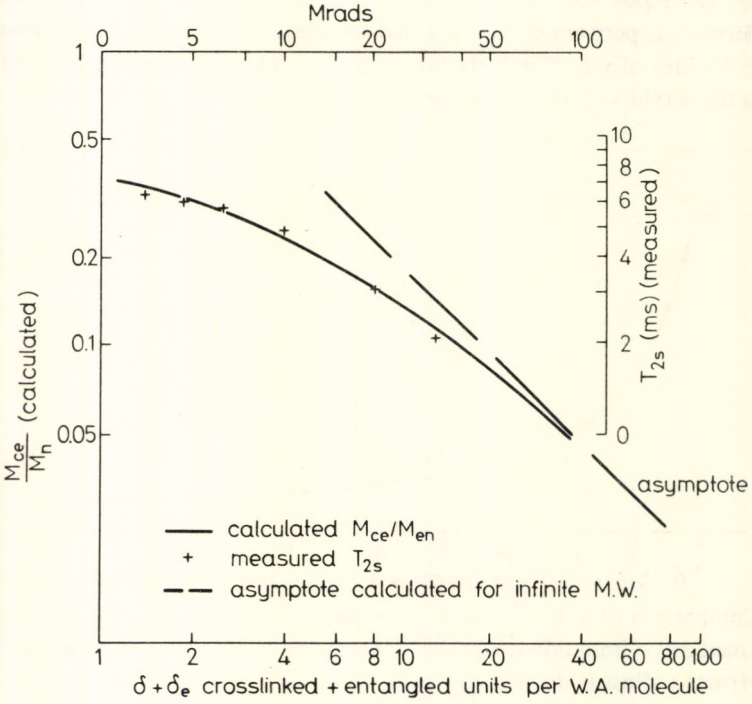
Mrads
0
5
10
20
50
100
1
0.5
0.2
0.1
0.05
$\frac{M_{ce}}{M_n}$ (calculated)
10
8
6
4
2
0
T_{2s} (ms) (measured)
asymptote
calculated M_{ce}/M_{en}
measured T_{2s}
asymptote calculated for infinite M.W.
1
2
4
6
8
10
20
40
60
80
100
$\delta + \delta_e$ crosslinked + entangled units per W.A. molecule

Fig. 4

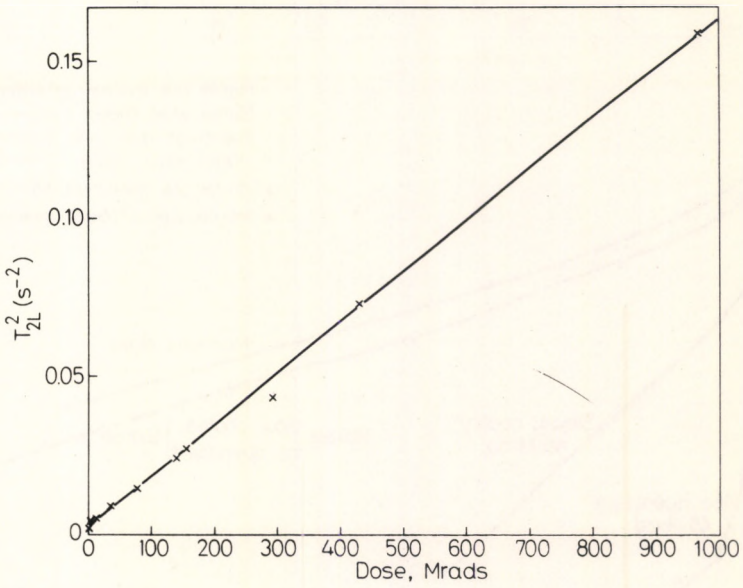

Fig. 5

Fig. 5 $T_{2L}{}^2$ values for irradiated PIB measured at 150°C

←

Fig. 3 T_{2L}, T_{2S} and f for separated sol and gel fractions of PDMS (12500 cs). Note presence of T_{2S} in sol fraction for doses up to ca. 15 Mrads

Fig. 4 Calculated average molecular weight M_{ce} between crosslinked/entangled units, allowing for molecular weight distribution, chain ends, higher crosslink density in gel, etc. Observed values of T_{2S} for gel fraction in 12500cs fluid, $T_{2S} \sim 0.05 \times 10^{-3} M_{ce}/M_n$ (ms)

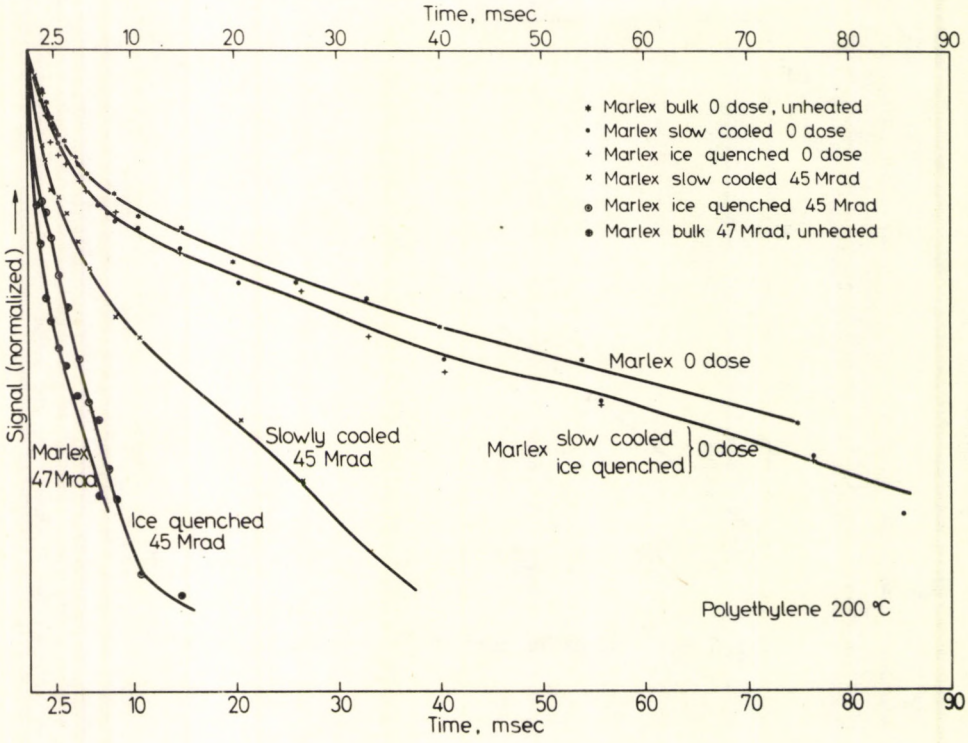

Fig. 6 Experimental values of T_2 from polyethylene samples, measured at 200°C: Irradiation at room temperature. Figure shows effect of dose and of treatment of polymer prior to irradiation.
Samples kindly provided by Professor A Keller FRS.

DISCUSSION

H. HEUSINGER

In order to take account of the entanglements before irradiation you have to add a constant virtual dose. This is taking the entanglements to be constant during irradiation. Is it not to be expected that crosslinking takes place at the entanglements, resulting in a decrease in entaglements during irradiation?

A. CHARLESBY

I would expect the density of entanglements to vary with the subsequent radiation dose. However, our results show that at any given temperature, the virtual dose is constant, independent of dose and molecular weight. At about 11°C, this density is approximately one crosslinked unit per 30 000 MW, equal to a virtual dose of about 6 Mrads. At lower temperature this virtual dose must be increased.

J. DOBÓ

Do you have, or do you expect to have a similarly good correlation in polyethylenes between solubility and swelling measurements on the one hand, and NMR on the other?

A. CHARLESBY

We have only carried out a few measurements with polyethylene produced and irradiated with different conditions. These show very considerable differences depending not only on dose but also on crystal morphology, so that the technique can certainly be used as a simple method for measuring crosslinking. However polyethylene is a much more complex system than PDMS and we have not yet found the relationships between sol fraction, crosslink density and NMR results.
crosslink density and NMR results.

J. SOHMA

The quantity f defined by you is identical to the mobile fraction, which is known to be dependent on the temperature of the NMR measurement. In your case was f found to be dependent on temperature?

If so, do you think that this temperature dependence can be attributed to the temperature dependence of the entanglement?

Do you have any experimental guarantee for that the correlation time does not change in this temperature range?

A. CHARLESBY

The quality f depends on temperature if it is due to entanglements which are temperature sensitive. For a low molecular weight PDMS (less than one entanglement per molecule) but with a high radiation dose (several crosslinked units per molecule) f does not seem to change with temperature. From these results it appears that f is determined by the total density of entanglements plus crosslinks per molecule, but not by temperature. T_{2s} and T_{21} are very dependent on temperature.

P. HEDVIG

You correlated the nuelear spin-spin relaxation time directly to molecular and structural parameters. This approximation might work in certain systems in certain temperature ranges far from a structural transition, but certainly would not be applicable generally. The structural parameters, I think, should rather be correlated

with the correlation time which is temperature, frequency, and structure dependent. By fixing the temperature and frequency, as in your case, the correlation time is swept through a range by the change of the structure. This would cause a break in the T_2 versus M_W curve. I believe that, especially when the temperature dependence of a reaction is studied, the correlation time τ_c should be used as a parameter rather than T_2.

A. CHARLESBY (communicated)

We agree that where possible it is always preferable to directly relate the physically important quantity, the motional correlation time τ_c, to the structural changes being studied rather that the measured spin–spin relaxation time. In order to obtain τ_c from T_2 requires a theoretical expression relating the two quantities, prior knowledge of the type of motion involved, and the extent to which the particular motion modulates the inter- and intramolecular dipole – dipole interactions. This is normally possible for systems composed of small molecules where straightforward rotational and translational motions can be discerned. In the case of polymer melts and networks the various chain motions are complex and possibly involve distributions rather than single correlation times and, furthermore, there is a problem of determining the extent to which the various modes of chain motion affect the dipole – dipole interactions and hence contribute to T_2.

Certainly at the present time there seems to be no straightforward way of determining values of τ_c from T_2 for such systems. Unfortunately, we are thus forced to qualitatively interpret the observed changes in T_2 in terms of, admittedly, rather loosely defined chain motions.

DIELECTRIC DEPOLARIZATION STUDY OF IRRADIATED POLYPROPYLENE

Péter Hedvig
Research Institute for Plastics, Budapest, Hungary

Dielectric depolarization spectra of non-polar polymers are known to be mainly determined by the degree of oxidation and by the multiple phase transitions of the polymer. The main source of the depolarization current peaks, when they are measured without air gap at short-circuit conditions /1/, is depolarization of the — C=O dipoles built in the chains by oxidation. This depolarization process is highly amplified by the Maxwell-Wagner-Sillars effect /2/ arising from the structural heterogeneity of the system.

The aim of the present work is to study the heterogeneous character of the radiation induced oxidation process in isotactic polypropylene by combining the dielectric depolarization method with conventional a. c., Fourier-transform /FT/ dielectric, thermomechanical and differential calorimetric /DSC/ techniques /2/.

Experimental

The facilities of the UNIRELAX device developed in our laboratory (produced by Tetrahedron ASS, Calif. USA) were used for measuring depolarization, a. c. and FT-dielectric, thermomechanical spectra and differential calorimetry. The FT-spectra were obtained by using a simplified transformation developed by Schwarzl /3/, as

$$\varepsilon'' = [3,5\ t\ \sigma(t/2) + 26,8\ t\ \sigma(2t) - 14,8\ t\ \sigma(4t)] \times 10^{12} \qquad /1/$$

$$\nu = \frac{0,113}{t} \qquad /2/$$

where ε'' is the unreal part of the complex permittivity, t is the time in sec, ν is the frequency in Hz – corresponding to time t, $\sigma(t)$ is the time dependent conductivity $\Omega^{-1}\ cm^{-1}$. For computation a Hungarian made EMG-666 computer was used.

Thermomechanical spectra were measured using extensional, torsional and compressional loads. In most cases the pulsed-load technique was used by applying stress pulses and measuring the deformation response pulses while the temperature was being swept slowly. In such cases the transitions appear as maxima of the derivative of the compliance. In some cases the forced oscillation torsional relaxometer of the UNIRELAX was used for recording mechanical spectra at fixed frequency sinusoidal load /10 Hz/

Differential calorimetry was used for measuring the crystalline melting and crystallization properties and also for studying thermal degradation. An attempt has been made to detect radiation oxidation in-source, but no thermal effect was detected at the dose-rate of the ^{60}Co source available (0. 3 Mrad/hr). Irradiations were made in an 800 Curie ^{60}Co source and by using a 60 kV 25 mA tungsten anticathode X-ray setup at a dose rate of 80 Mrad/hr. Some samples were mechanochemically degraded by multiple extrusion. The molecular weight distribution of the degraded samples were measured by gel permeation chromatography. For interpretation of the structural transitions, results previously obtained by small angle X-ray scattering /SAXS/ and small angle light scattering /SALS/ were used /4/.

Samples were prepared in a combined laboratory machine /CAMILLE, Paris/ under controlled conditions from DAPLEN-DM 55 and Hercules pro Fax and a FAX samples. Mixtures of atactic and isotactic polypropylene were used for assigning structural transitions.

Results and discussion

Figure 1 shows a typical pair of depolarization spectra obtained before and after irradiation in air. For obtaining the current-spectra the samples were polarized at 110°C at a field of 100 kV/cm, then cooled down to – 150°C at a rate of 1°C/min under field. Then after removing the field the short-circuit current was measured at a rate of heating of 1°C/min. This was the standard way of measuring the thermomechanical and DSC curves too. It is seen that the depolarization current density of the irradiated sample exhibits three characteristic peaks marked by α_c, α_a and γ respectively at +80°C, +5°C, and –50°C. The intensity of these peaks was found to depend on the degree of oxidation at different rates. The most drastic change upon irradiation was found in the temperature range between 50 and 100°C.

Figure 2 shows a typical thermomechanical spectrum measured by using a spherically tipped profile under compressional load. The logarithm of the compliance and its derivative dJ/dT is shown as a function of the temperature. These variables were calculated from the directly recorded deformation versus temperature curve. The maxima of the derivative curve directly show the multiple transition temperature of isotactic polypropylene labelled as α_a, α_a' (amorphous), α_c (crystalline) and γ. This curve is directly comparable with the depolarization current density spectrum of Fig. 1.

In Fig. 2, typical calorimetric and dilatometric curves are also shown in the melting temperature range, measured under similar conditions as the depolarization spectra shows that the α_c transition is mostly affected by the radiation induced oxidation. This transition is dependent on the crystalline structure of the polymer, it is completely absent in atactic polypropylene. The α_c transition is found to be extremely sensitive to the thermal history of the sample and is found to be connected with the inter-lamellar spacing of the chain-fold crystal structure. The thermomechanical α_c transition was found not to depend, to any great extent, on irradiation, not even at high doses. The melting-range, however, was found to change drastically by irradiation, as shown in Fig. 3 where calorimetric curves of an unirradiated and irradiated sample are shown measured by increasing and by decreasing temperature. It is seen that the melting temperature depression by irradiation is larger than the crystallization temperature depression. It is also shown that a considerable premelting zone starting from about 110°C is observed after the given thermal treatment due to recrystallization processes /5/ which become prominent at the low rate of heating of the experiment. According to gel permeation chromatographic measurements the weight average molecular weights M_w and the polydispersity /P/ values are also shown in Fig. 3.

Most changes in the mechanical spectra upon irradiation were found in the premelting zone /100°C–150°C/ where the modulus falls rapidly. At lower temperatures radiation oxidation is found to affect the rupture strain rather than the modulus.

Figure 4 shows a series of Fourier–transform curves obtained from discharge current measurements in the α_c transition region. In this experiment the sample was polarized at 110°C, then cooled at a rate of 1°C/min to 80°C, where the field was removed and the discharge current was measured as a function of time. From this decay curve, using Eqs 1 and 2, the $\varepsilon''(\nu)$ curves were computed.

It is seen that dielectric loss factor ε'' increases considerably even at low radiation doses. For samples irradiated in vacuo only a small increase in ε'' is observed.

Figure 5 compares schematically the effect of radiation oxidation on the dielectric depolarization spectrum of polypropylene (PP) with that of polyethylene (PE) studied previously /6/. Polyethylene has a transition picture similar to polypropylene, but the transition–temperatures are somewhat lower. Despite that in PE the amorphous α_a transitions are much more affected by irradiation than the crystalline α_c one. This means that in PP a much larger part of the total oxygen content is built in the interlamellar space than in PE. This is interpreted as being the consequence of the methyl side groups arranged regularly in PP at the lamellar surface ready for oxidation. In low density polyethylene the side group concentration is much lower and, as a result of their random distribution, they belong to the "amorphous" phase the transition of which appears in the temperature range between –50°C and 0°C.

The concentration of the oxide–containing (mainly carbonyl) groups calculated from the depolarization and FT–dielectric spectra appear to be much higher than that measured by infrared spectroscopy The reason for this is that oxidation

reactions proceed heterogeneously at the interlamellar space resulting in a sandwich-like structure of oxidized and unoxidized layers. Such a structure is known to exhibit an additional dielectric polarization as a result of the dipole formation at the interface of layers having different permittivities. This phenomenon is known as the Maxwell–Wagner–Sillars /MWS/ effect, it results in a large overall polarization at low frequencies depending on the permittivity gradient and on the shape–size distribution of the layers. This is why the depolarization and FT–spectra are so sensitive to oxidation. At low degrees of oxidation where the depolarization technique works well no significant change in the infrared spectra are observed.

On the other hand the sensitivity of the method to structural changes makes it necessary to combine it with structure–sensitive methods.

As in the case of polyethylene reported previously /7/ the FT–method was found useful for studying the efficiency of anti–oxidants for mechanochemical, thermal, u. v. and radiation oxidation of polypropylene compounds.

Conclusions

Depolarization current peaks corresponding to the structural transition in isotactic polypropylene were found highly affected by radiation oxidation. From this it is concluded that oxidation preferably proceeds in the interlamellar space at the lamellar surface. Fourier transform dielectric spectra measured in the α_c range (60–80°C) were found extremely sensitive to oxidative degradation and correspondingly the method is recommended as a simple tool for measuring the efficiency of anti–oxidants.

References

/1/ J. van Turnhout, Thermally stimulated discharge of polymer electrets. /Amsterdam/ Elsevier, 1975.

/2/ see in P. Hedvig, Dielectric Spectroscopy of Polymers. Adam Hilger (London), and Akadémiai Kiadó /Budapest/ 1976.

/3/ Schwarzl, Unpublished results quoted by van Turnhout in Ref. 1.

/4/ G. Bodor, Unpublished results.

/5/ R. I. Samuels, J. Polym. Sci, Polym. Phys., Ed., 13, 1417 /1975/.

/6/ P. Hedvig in P. O. Kinell, B. Rånby V. Runnstrom–Reo (eds) Nobel Symposium Series No. 22, p. 215. Almquist – Wiksell, Stockholm 1972.

/7/ P. Hedvig, Á. Somogyi, Proc. 3rd Symposium on Radiation Chemistry /eds. J. Dobó, P. Hedvig/. Vol. 1., 907, Budapest 1972.

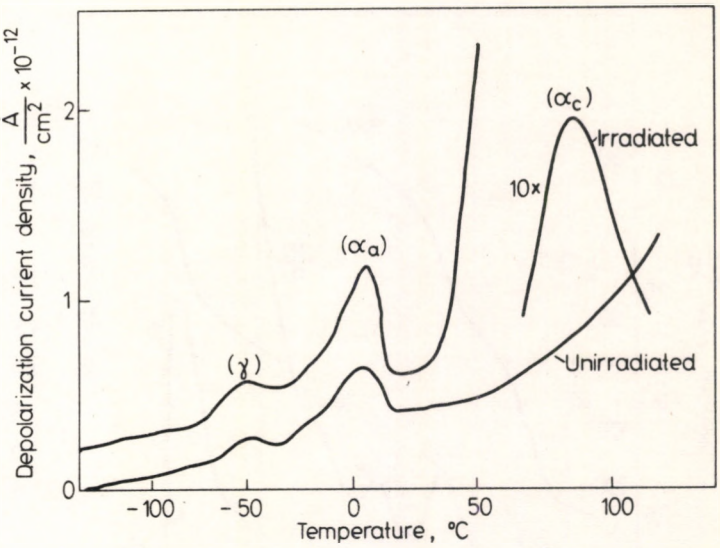

Fig. 1 **Dielectric depolarization spectra of unirradiated and irradiated isotactic polypropylene.** Daplen DM 55. Polarization: 110°C. 100 kV/cm after heating at a rate of 1°C/min. Rates of subsequent cooling and heating: 1°C/min. Irradiation: 60 kV X-rays, 20 Mrad, 25°C. Thickness: 0.2 mm

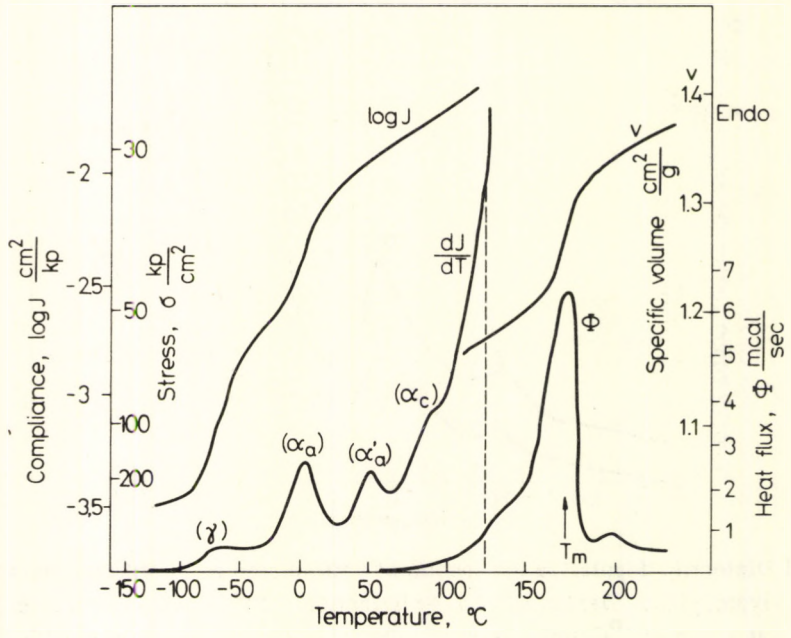

Fig. 2 Thermomechanical spectra, differential calorimetric and dilatometric curves of Daplen DM 55 type isotactic polypropylene measured after the heat treatment described under Fig. 1. J = compressional compliance, σ –stress, ϕ = heat flux, v = specific volume. Rate of heating 1°C/min for all curves. Spherically tipped profile, constant load

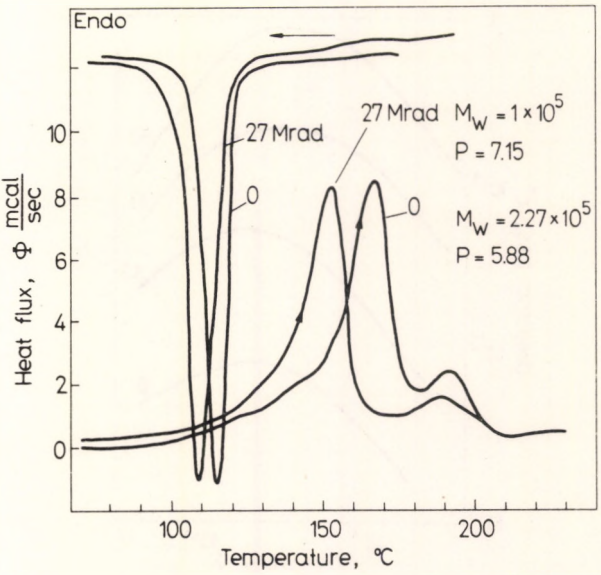

Fig. 3 Differential scanning calorimetric curves of unirradiated and irradiated Daplen DM 55 type isotactic polypropylene measured after similar heat treatment as described under Fig. 1. Irradiation ^{60}Co at a dose rate of 0. 3 Mrad/ /hr at 20°C in air. The weight average molecular weights and the polydispersity values as measured by GPC are also shown

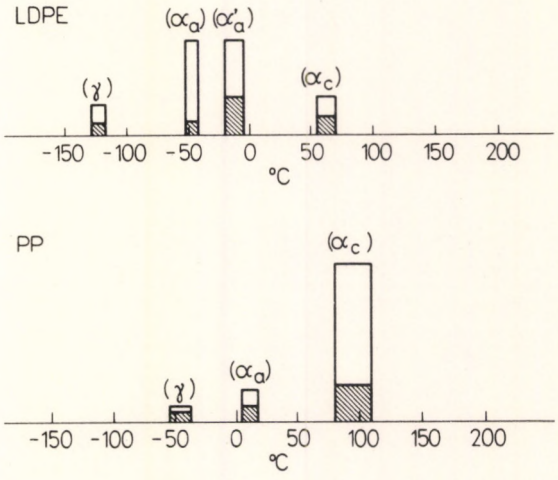

Fig. 4 Fourier transform dielectric spectra of isotactic polypropylene irradiated with different doses. Polarization: 110°C 100 kV/cm. Temperature: 80°C

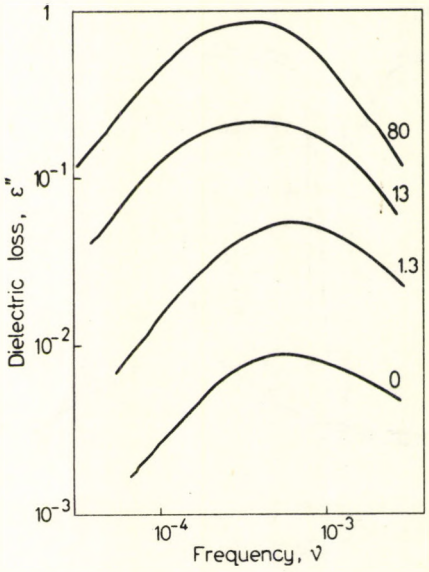

Fig. 5 Schematic comparison of the intensity of the dielectric depolarization peaks of polyethylene and isotactic polypropylene irradiated in air. Doses in Mrad

SOME PROPERTIES OF RADIATION CROSSLINKED POLYETHYLENE AND ETHYLENE – VINYL ACETATE COPOLYMER

J. Dobó, P. Forgács, Á. Somogyi, M. Rőder*
Research Institute for the Plastics Industry, Budapest Hungary
*Research Institute for the Textile Industry, Budapest, Hungary

The most important industrial process in radiation chemistry, the production of shrink materials, is based on the property of radiation crosslinked polymers, that they are stiff below and rubbery above their crystalline melting point. In the production and use of shrink materials, the slightly radiation crosslinked polymers are repeatedly heated above and cooled below their melting point. The behaviour of the shrink materials in these processes may be studied conveniently by model experiments.

For this purpose, low density polyethylene sheet of Hungarian production (Tipolen FA 2210, M.I. = 0.3, $M_n = 28.9 \times 10^3$, $M_w = 136 \times 10^3$) has been crosslinked by 15 Mrads gamma-irradiation in vacuo. The insoluble fraction in hot xylene amounted to 74.8%.

As a model experiment for the production and use of shrink materials, the sheet was heated in a commercial Instron testing apparatus to 145°C, then extended by 100%. The sample was then cooled to 50°C and heated again to 145°C (Fig. 1), with constant strain, while the stress was recorded.

During the first part of the cooling cycle, the polyethylene is in the rubbery state /1/. Correspondingly, it expands when cooled and the modulus decreases. The temperature dependence of this modulus can be seen in Fig. 2. The equation of the straight line, calculated by the method of least squares, is

$$E_{T,100} = 10^6 \quad (0.45 \pm 0.06) + (0.0074 \pm 0.0005)\, T\ (^{\circ}C) \quad \text{dyne/cm}^2.$$

The moduli in the rubbery state corresponding to this equation are of the order of 10^6 dynes/cm^2, in accordance with previous results /1/, they are approximately proportional to the dose. The corresponding stress is the shrinking force, with which the material shrinks onto the workpiece, or alternatively, with which the shrink material has to be expanded during the production process.

On further decrease of the temperature, the polyethylene begins to crystallize. The rubber elasticity changes to a steel-wire-type one, the thermal contraction exceeds expansion in the extended direction and the modulus and stress begins to

increase. Below 70°C, the increase of the stress is nearly linear. Let us take as first approximation, that the change in specific volume is independent from the extended state and that the modulus is constant between 70 and 50°C, so that the increase in stress is caused only by the thermal contraction. Then we get for the average modulus between the two temperatures:

$$E = \frac{1}{1 - \left(\frac{V_{50}}{V_{70}}\right)^{1/3}} \quad (\sigma_{50} - \sigma_{70}) = 1.1 \times 10^9 \text{ dynes/cm}^2$$

where σ means the stress and V means the specific volume taken from Fig. 3. This result seems to be reasonable. Charlesby and Hancock /2/ quote from static measurements of lightly crosslinked polyethylene about 1.3×10^9 dynes/cm^2 at 48°C. Thus, in this part of the cooling curve, the modulus is by three orders of magnitude higher than in the rubbery state but the difference in length, which has to be overcome by the stress, is much less as it equals the thermal contraction. This stress corresponds to the force by which the workpiece is enclosed by the crystalline shrink material: in contrast to the shrinking force it may be termed the holding force.

Let us consider now the heating process. With increasing temperature, the stress diminishes, but with a hysteresis: on the heating side, higher stresses correspond to the same temperature, than on the cooling side. The more perfect crystals formed at lower temperature presumably persist for a while, resulting in a lower specific volume and in a higher modulus on the heating side, both leading to higher stress. Due to the high modulus at these temperatures, small differences in dimension may result in large differences in the force.

Then, upon further increase of the temperature, the stress fails to go over smoothly into that corresponding to the rubbery state, but falls to zero or even becomes negative. This is caused through deformation and/or slow relaxation phenomena in the crystelline structure. On the other hand, no significant permanent deformation takes place in the crosslinked network: a stress exactly equal to the original one is restored as soon as it is made possible through the melting of the crystallites.

The picture is somewhat different if we repeat the same cycle with a more elastic material, e.g. with a 15 Mrad crosslinked ethylene–vinyl acetate copolymer (Miravithen D23EA, Leuna, specific weight 0.935, vinyl acetate content by weight 13%). The difference in properties of the two materials can be judged from the specific volume curves in Fig. 3. The lesser crystallinity and less perfect crystallites of the copolymer result in a broader melting range and in a smaller change of the specific volume. The specific volume measurements were made with a dilatometer similar to that described by Kovács /3/.

One may see in Fig. 4 that the initial, high temperature stress is higher for the copolymer than for the polyethylene.

The corresponding moduli in the rubbery state /see Fig. 5/ lead to the linear relationship

$$E_{T,100} = 10^6 \; [(3.33 \pm 0.16) + (0.013 \pm 0.001) \; T\,(^{o}C)] \; \text{dyne/cm}^2.$$

As the temperature-dependent part of this modulus may be related to the crosslink density, G(crosslink) for the EVA copolymer may be calculated to be almost twice as high as for polyethylene. This is in accordance with the higher insoluble fraction found for the EVA copolymer, i. e. 84. 3%.

On cooling, stress diminishes somewhat, down till 60°C, and only below 50°C can a stress increase due to stiffening be observed. Even the 45°C stress is lower than the high temperature rubbery stress and much lower than the 50°C stress in polyethylene. Thus, under the given conditions, the EVA copolymer exhibits higher shrinking force but lower holding force than does polyethylene.

Upon heating, a hysteresis may be observed here, too, but without such drastic changes of the stress as in polyethylene. In general, it may be said that the stress varies much less with the temperature than in polyethylene. A further increase in temperature brings the stress back to about the same value as before the cycle.

In conclusion, one may state, that for the crosslinked shrink materials, the shrinking force and the holding force should be distinguished. The shrinking force is operative in the rubbery state. It depends on the crosslinking density and thus on the radiation dose. On the other hand, the holding force is hardly dependent on the density of crosslinking: it is rather connected with the crystallinity and crystallization of the crosslinked material.

A more detailed discussion of the role of these two types of forces will be given in further publications.

Acknowledgement. The authors are indebted to the Hungarian Cable Works, Budapest, for permission to publish this paper.

References

/1/ A. Charlesby, Radiation effects in materials. Pergamon Press, 1960.
/2/ A. Charlesby, Hancock, N. H., Proc. Roy. Soc., A 218 (1953).
/3/ A. I. Kovács, Ind. des Plast. Mod., 7, 30 (1955).

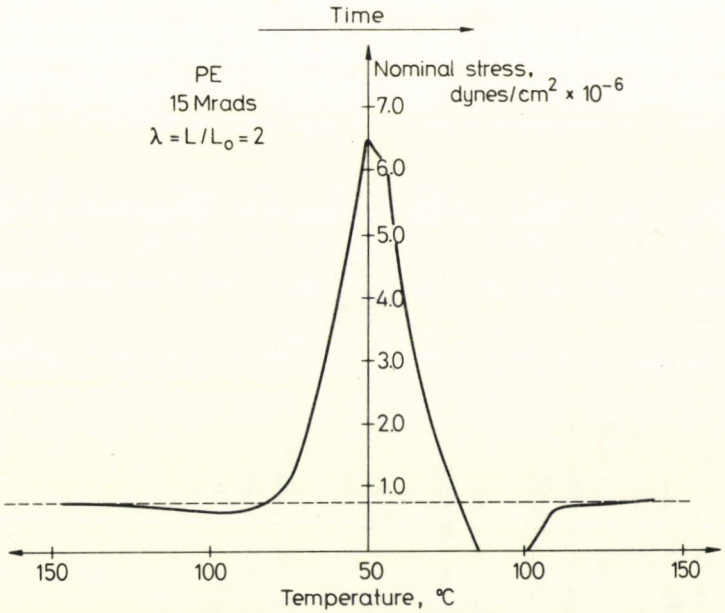

Fig. 1 Stress-temperature dependence of 15 Mrad irradiated polyethylene strained by 100 per cent.

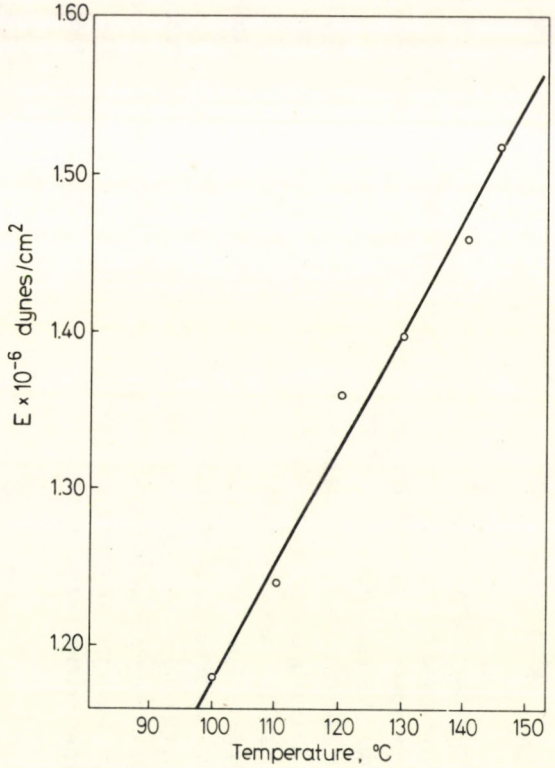

Fig. 2 High temperature modulus of 15 Mrad irradiated polyethylene, strained by 100 per cent.

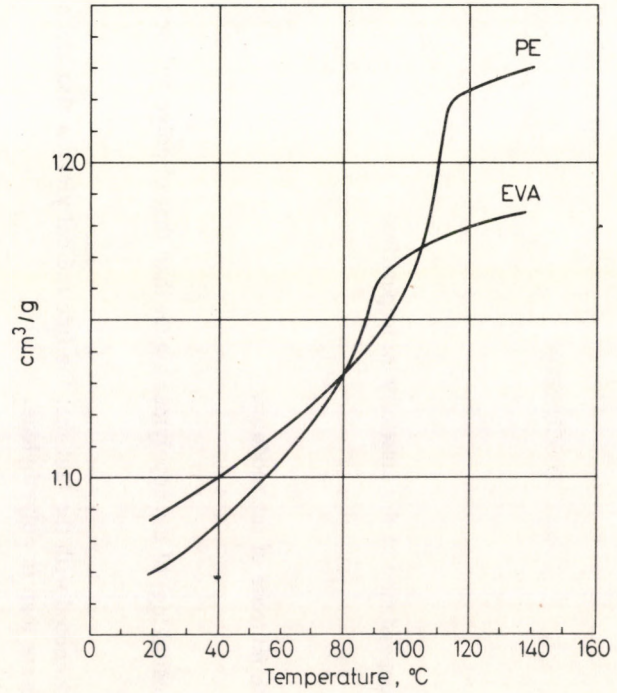

Fig. 3 Specific volume of 15 Mrad irradiated polyethylene and ethylene-vinyl acetate copolymer.

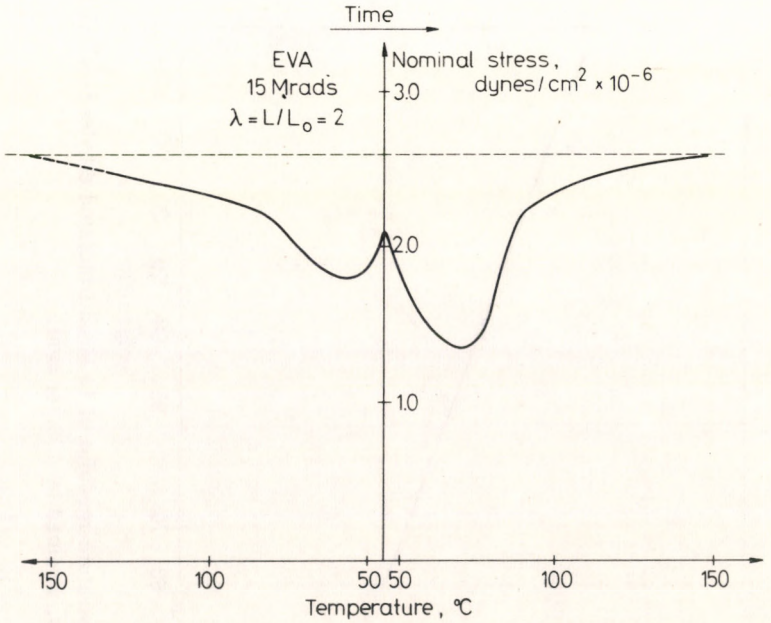

Fig. 4 Stress-temperature dependence of 15 Mrad irradiated ethylene-vinyl acetate copolymer, strained by 100 per cent. +: cooling cycle, o: heating cycle.

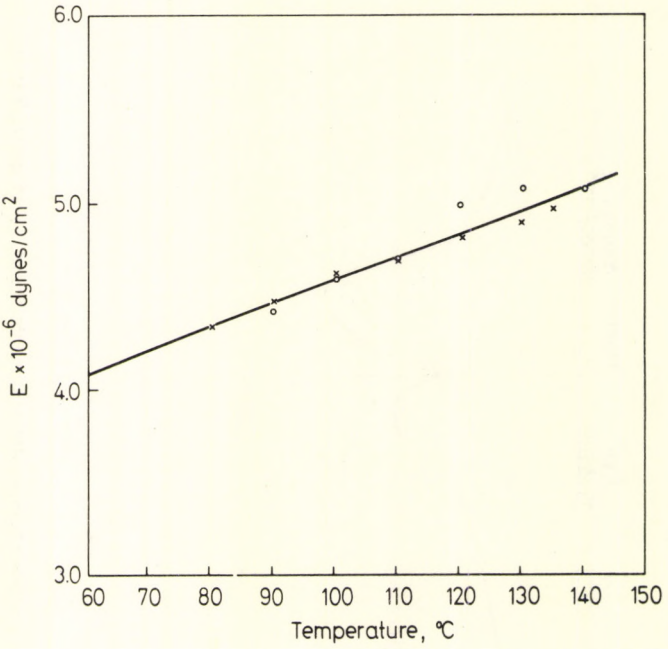

Fig. 5 High temperature modulus of 15 Mrad irradiated ethylene- vinyl acetate copolymer, strained by 100 per cent.

DISCUSSION

M. ROMANZEV

What is the dependence of the elasticity on impurities?

J. DOBÓ

There is some increase of the modulus.

M. DOLE

Why is G(crosslinking) of the copolymer higher than that of polyethylene?

J. DOBÓ

Is may be connected with the fact that the free radical yield is also higher in the polyvinyl acetate than in polyethylene.

INVESTIGATION IN THE FIELD OF SOLID STATE POLYMERIZATION XXXVIII

RADIATION-INDUCED POLYMERIZATION OF VINYL MONOMERS WITH LONG CHAIN SUBSTITUENTS

Gy. Hardy, F. Cser, K. Nyitrai, N. Fedorova
Research Institute for Plastics, Budapest, Hungary

Introduction

The discovery of stereoregular polymerization has shown that the synthetic polymers with highly regular structure have technically well applicable properties. The original aim of polymerization in the solid state was to obtain stereoregular polymers in one step utilizing the preordered array of polymerizable molecules. In some cases /1–4/ this succeeded and polymer single crystals were prepared by X-ray, γ-ray or UV irradiation of monomer single crystals.

Highly crystalline, stereo regular polymers could not be produced from crystalline vinyl monomers for commercial use at all, since the polymer formed by the irradiation in a solid state reaction interacts with the monomer crystal. Thus a phase transformation begins at a given conversion, where a non-crystalline phase develops with a quite different arrangement of monomer molecules in it /5–11/. The polymer remains isomorphous with the monomer in some cases only up to a limited conversion and later /12–15/, the crystalline lattice of the monomer is destroyed by the interactions mentioned above.

Topochemical conditions

In topochemical dimerization or polymerization processes, usually simultaneously with the reaction, a phase transformation takes place as the products form new crystalline phases. The interaction of the newly formed phase with the original one is eutectic, therefore the crystalline lattice of the monomer phase remains unchanged in the course of reaction /16–19/. This type of reaction, the so-called heterogenous-type topochemical reaction /3, 19/, was found to be very rare in the solid state polymerization of vinyl monomers /9, 19/, but the crystalline structure of the polymers obtained were different from those of the monomers. The only way to obtain polymers with regular structure is the homogenous type of topochemical polymerization. The conditions for this latter are:

(i) direct, short contact of vinyl groups along translational symmetry elements /20, 21/;

(ii) relative small change in the molecular volume /22/;
in the course of the reaction;
(iii) high binding energy in the lattice for the
monomer molecules to prevent the dissolution
of polymer and monomer molecules;
(iv) the helix periods of polymer helices coincide with
the translational periods of monomer molecules
in their lattice.

These conditions could be fulfilled by the vinyl monomers with long-chain paraffinic substituents. They have long, stiff-like geometry and therefore they are arranged in layer-like lattices.

Characteristics of long chain aliphatic structures

The crystalline polymorphism of long chain aliphatic compounds are well established /22, 23/. The lowest energy states of these molecules have triclinic or monoclinic unit cells. At higher temperatures orthorhombic and hexagonal structures develop. In long chain aliphatic compounds with polar end-groups different mesomorphic states may also appear. The latter are either smectic or nematic. In molecules with planar aliphatic side groups a twisted nematic cholesteric mesomorphous state can be detected.

We characterized these structures by means of polarization microscopy, X-ray powder photographs or diffractometry. The ratio of the longest crystallographic periods to the length of the extended molecular chains are most characteristic for the structure. When these lengths are practically the same the molecules are in rectangular layers, i.e. the chain axis of the molecules is perpendicular to the layer where they are parallelly arranged. When the longest periods greatly exceed the chain length, the layers are bilayers usually with tilted molecular axis. When this period is shorter than the molecular length the layer is a tilted one. The tilt angle /α/ can be estimated by equation /1/

$$\alpha = \arccos \frac{d_{001}}{l_{chain}} \qquad /1/$$

The inner part of the diffractogram is characteristic for the molecular arrangement in the layer. We present the different possibilities in Fig. 1.

The characteristics of smectic A (or C if the layer is tilted) are visible in Fig 1b; only a broad halo at 2– 20° can be observed. When the structure is smectic B a hexagonal layer packing is present. Hereupon a sharp ring appears /Fig. 1c/. The hexagonal cell parameters can be estimated using Eq. /2/.

$$a = \frac{2d_{110}}{\sqrt{3}} \qquad /2/$$

Figure 2. shows the (a) hexagonal and (b) orthorhombic arrangement of molecules in perpendicular layers.

In smectic E structures the molecular arrangement in the layer is orthorhombic. This is presented in Fig. 1d. In this case usually higher order reflections of (001) are also present. The two major rings correspond to (110) and (020). The a and b periods can be estimated by:

$$a = 1/\mathrm{Sqrt}[(1/2\ d_{020})^2 - (1/d_{110})^2]$$

$$b = 2 \cdot d_{020} \qquad /3/$$

The (e), (f) and (g) parts of Fig. 1 show the diffractograms of hexagonal, orthorhombic and monoclinic paraffin structure, respectively, with the same molecular length. In orthorhombic structures the two major lines coincide with the line of smectic E, but the mixed hkl reflections can also be detected. In monoclinic structures the cell parameters have to be individually analysed.

Nematic structures are very similar to smectic A in many respects, however, the inner ring characteristic of long chain periods disappears /Fig. 1a/.

Solid state polymerization data of long chain vinyl monomers

The study of solid state polymerization of these types of monomers was initiated in 1962 in our laboratory. The first monomer was cethyl-methacrylate (CMA) /24/. Later the polymerization of vinyl-laurate (VL) /25/ and allyl-palmitate (AP) /26/ were investigated. At the beginning of the liquid crystalline monomers vinyl oleate (VO) /27, 28/, cethyl-vinyl-aether (CVE) /15, 29, 30/ were investigated. Later the polymerization of N-cethyl-acrylamide (HAA) and N-cethyl-methacrylamide (HMA) /31/ were studied. Here the molecules are fixed in the layer by hydrogen bonds, too. Inter-layer hydrogen bonds fix the molecules in the crystalline lattices of β-alkyl-ithaconates /10, 32/ where allyl type functional groups exist.

The polymerization study of cholesteric monomers /35/ was initiated with cholesteryl-acrylate (KA) and cholesteryl-metacrylate (KMA) /14, 33, 34/, and followed with the study of, e.g. vinyl-esters, cholesteryl-vinylsuccinate (KVS) /13 36/.

From the radiochemical point of view the behaviour of a molecule in all condensed states should be the same /37/. Opposed to this, we obtained quite large differences in the polymerizability of one monomer in its different condensed states. This finding can only be interpreted in terms of structural conceptions. The different structures observed in our monomers are summarized in Table 1. Here we give the longest period (001), the length of the extended chain molecules /1/, the hexagonal or orthorhombic cell parameters (a, b) (if they were able to be estimated), and the nature of the struc-

Table 1
Structural data of monomers

Compound	Temperature	a'Å	bÅ	c'Å	1 Å	α	Phase
AP	10	5.12	5.12	25.57	27.5	111.5	S_B
AP	-16	4.44	7.42	?	27.5	?	S_E,/S_G/
AP	-20	5.44	7.42	24.2	27.5	118.3	C_M
CVE	6	4.50	4.50	26.0	26.30	90	S_A
CVE	-12	4.90	7.36	25.8	26.30	100.4	C_R, S_E
CVE	-50	5.74	7.97	24.66	26.30	110.5	C_M
VO	0	4.89	4.89	27.7	28.85	106	S_B
VO	-20	4.92	7.36	27.7	28.8	106	C_R
CMA	0	4.89	4.89	42.5	27.5	129.5	S_B
CMA	-12	5.80	7.68	42.4	27.5	129.6	C_M
HAA	25	4.68	7.54	24.9	27.5	115.1	C_M
HAA+POLYMER	25	5.02	5.02	31.2	27.5	90	S_B
HMA	25	12.69	8.82	21.71	27.5	127.9	C_T
HMA+POLYMER	25	5.02	5.02	31.1	27.5	90	S_B
MCIT	25	5.56	7.57	39.91	27.85	134.2	C_M
MLIT	25	10.39	7.87	33.26	22.85	133.3	C_M
MOIT	25	5.67	7.54	25.87	17.85	133.6	C_M
MBIT	25	5.64	7.14	18.73	12.85	133.3	C_M
KA	20	6.98	7.04	37.8	24.5	140.5	S_G
KMA*	25	17.88	9.73	18.28	24.5	131.8	C_M
KVS III	25	11.34	10.53	29.7	29.5	90	C_R
KVS II	25	?	9.1	20.2	29.5	137.4	C_M
KVS I	25	13.84	10.08	28.6	29.5	104.2	C_M

Notes: $a' = a \cdot \cos(\beta)$; $c' = c \cdot \cos(\beta)$; $\alpha = c'/1$; $\beta = 101.4^{\circ}$

ture. (S means smectic, C means crystalline, A, B, E and C designated the smectic structures, R, H, M respectively represent orthorhombic, hexagonal or monoclinic cells.)

Bi-layers can be observed at CMA, MCIT, MLIT, MOIT, MBIT and KA; all the others have monolayer structures. Bi-layers are all tilted; of the monolayers, only HAA shows tilted character. Orthorhombic layer structure can be found at CVE,

Table 2.

The activation energies of polymerization (ΔH) and G_M values obtained in solid (s) liquid crystalline (LQ) and liquid (L) states (x): no measured data.

Monomer	ΔH Kcal/mol			G_M		
	S	LQ	L	S	LQ	L
AP	1.67	x	5.15	5.9 (-78)	16 (0)	5.8 (50)
VL	7.32	-	7.03	1.6 (0)	-	8 (50)
CVE	1.6	0.0	-	3.8 (-10) 0.8 (-96)	8.5 (0)	0.0
VO	-0.1	0.0	5.7	6.5 (-78)	2 (-10)	10 (20)
CMA	-0.7	0.0	2.5	0.24 (-196)	0.68 (0)	0.68 (30)
HAA	x	-	x	2.3 (25)	-	x
HMA	x	-	x	0.9 (25)	-	x
MCIT	x	-	x	1.61/P(70)	-	x
MLIT	x	-	x	6.10/P (65)	-	x
MOIT	42.0	-	0.0	2500/P(50)	-	9100/P (55)
MBIT	32.0	-	0.0	7900/P (35)	-	36900/P (60)
KA	-	5.0	4.3	-	0.3 (0) 2.0 (30)	103
KMA	19.2	-	6.26	1.36 (70)	-	16.5 (50)
KVS	x	x	x	0.92 (20)	x	x

Notes: the temperature for G_M values is in brackets; P means polymers with $([\eta]) = 0.14$

CMA, VO, AP, HMA, hexagonal one at CVE /0°C/ VO /0°/, CMA /0°/. The other structures are monoclinic.

The radiochemical data calculated from the kinetic and molecular weight data of our monomers are summarized in Table 2.

In the first column the code of monomers is presented followed by the activation energies obtained in the solid, the liquid crystalline (mesomorphic) and liquid state reactions, respectively. In the next, the highest G_M values for polymer chain formation divided by P which is the average degree of polymerization are given. The values presented are calculated from kinetic data of products with the same $[\eta]$ value (0.14). Since the structure of polymers should be the same, the same $[\eta]$ means the same P.

As the values presented in Table 2 are only approximations tendencies only can be discussed.

On the basis of the activation energies the monomers can be divided into groups. The first type of monomers have lower activation energy of reaction in the solid state

than in the liquid state. These are AP, CME, VO. CVE does not polymerize in the liquid state but its ΔH in the solid state reaction is also low. VL and KA have the same values of ΔH in the liquid and in the solid (or smectic G) state. KMA and β-alkyl itaconates have high ΔH in the solid state. The first group has approximately the same G_M values both in the liquid and in the solid state. In the other groups these data for ordered state are much lower than those in the liquid one. Methacrylates have lower G values in each case than do acrylates. The G value decreases by increasing chain length in β-alkyl itaconates. The molecular weight of polymers obtained in the liquid state of allyl type monomers have been found lower than that of solid or mesomorphic state products /10, 26, 28, 32/.

These results can be compared with structural data. In the first group, the monomers have topotactic, homogeneous type polymerization in their hexagonal or orthorhombic layers with rectangular molecular chain orientation. The monomers in the third group have a tilted lattice. The polymerization here is a heterogeneous type in the solid state. The second group shows an intermediate character /34, 35/.

Let us consider the problem from the topochemical point of view. In Fig. 3 the formation of an ethylene dimer is presented. In the original situation the two molecules are closely packed in Van der Waals distance. When a reaction takes place a dimer is formed either in staggered or in trans-conformation. The centre of gravity of the molecules must be translated to each other in both cases. When we have a close packed row of ethylene molecules (as can be seen in Fig. 4) a polymer chain can be formed without translational motion only with the including of one other monomer unit (B' D') from an other row.

Both staggered and trans-conformations are illustrated. In the real lattices we have no such type of closely packed vinyl groups /see Fig. 2/. A real situation of orthorhombic CVE lattice in illustrated in Fig. 5. Figure 5a represents the lattice projected by axis c, Fig. 5b that projected in the layer plane by axis a. The projection of carbon-carbon bonds is represented by an unbroken line. The envelope of carbon atoms is presented only in Fig. 5a. The figure presents such a situation when a polymer chain has already been formed. It is visible that the chains are unchanged from the C atoms connected to 0 atoms downwards, only upwards conformation of the chains alters. The is no translation necessary along the polymer chain formation in the course of reaction, only the heads of two neighbour rows have come nearer to the reacting row. The formed polymer remained isomorphous with the orthorhombic monomer layer.

The situation is practically the same in the hexagonal case.

Figure 6 shows the X-ray powder photograph of CVE at 0°C (a) and at − 12°C (b), that for the poly CVE at 0°C (c) and at − 10°C (d). On the basis of Fig. 1, we can see that the monomer has hexagonal (S_A) layers at 0°C and orthorhombic (C_R) layers at − 12°C. The rate of polymerization at 0°C was found to be of accelerating character /15/.

The rate of reaction in the accelerated form is the same as may be measured in C_R state at − 10°C. The structure of polymer is S_B both at 0° and at −10°C. The

structure of monomer at 0°C changes from S_A to S_B and at − 10°C from C_R to S_B as an effect of polymers. This was the first example when the structure of monomer transformed in the structure of the polymer as an isomorphous component and this isomorphism remained during the whole period of polymerization.

Later the same was observed in HAA and HMA /31/. Similar effects were found in the polymerization of vinyl-stearate both in the crystalline state /38/ and in monomolecular layers /39/.

In the homogeneous topochemical process the close packing of vinyl groups remains unchanged in the course of the reaction. In this situation the collision of functional groups has the frequency of vibrational motion of individual atomic groups. This frequency is much higher than the rotational frequency of molecules in the liquid state. So the probability of favourable collision of vinyl groups is very high. Although the lifetime of ions and radical ions in the condensed state is short, the probability of ionic polymerization process is still high because of the high frequency collision of a vinyl group due to them being fixed in the vicinity. As opposed to this, the probability of the formation of protons and of hydrogen atoms, is, in the vicinity of vinyl groups, less than in the hydrocarbon tail /37/. The diffusion of these radicals to the functional groups is therefore hindered, the radical processes are retarded too. The higher molecular weight found in allyl type monomers can be explained by these effects.

The above studies allow the following conclusions. The solid state polymerization reaction of long chain vinyl compounds is determined primarily by their structural features. Favourable structures are the rectangular monolayers with either orthorhombic or hexagonal packing where polymer-monomer solid solution can be formed. The close arrangement of functional groups in layers makes the ionic radiochemical processes more probable. These are usually neglected in condensed states. The polymers formed in such a way frequently have a regular structure. This regularity is not always the result of a regular chain, but it is sometimes a consequence of side chain crystallinity.

References

/ 1/ S.E. Jamison, H.D. Noether, Polym. Lett. 1, 51, (1963).

/ 2/ J.B. Lando, V. Stannett, J. Polym. Sci. A3, 2369, (1965).

/ 3/ G. Wegner, W. Schermann, Coll. Polym. Sci. 252, 655, (1974). R.H. Baughnan, K.C. Yee, J. Polym. Sci. Chem. Ed. 12, 2467, (1974).

/ 4/ H. Naganashi, K. Ueno, M. Hasegawa, Chemistry Lett. 301, (1972).

/ 5/ Gy. Hardy, G. Kovács, Gy. Kosztersztitz, N. Fedorova, F. Cser, Proceedings Third Tihany Symposion on Radiation Chemistry. Akadémiai Kiadó, Budapest. 1972, p.601.

/ 6/ Gy. Hardy, F. Cser, G. Kovács, N. Fedorova, G. Samay, Acta Chim. (Budapest), 79, 143, (1973).

/ 7/ Gy. Hardy, F. Cser, E. Takács, J. Polym. Sci. C42, 663, (1973).

/ 8/ F. Cser, Gy. Hardy, Z. Veksli, Europ. Polym, J. 10, 1217, (1974).
/ 9/ F. Cser, Gy. Hardy, Acta Chim. (Budapest), 80, 34, (1974).
/10/ K. Nyitrai, N.L. Nguyen, F. Cser, E. Takács, Gy. Hardy, Europ. Polym. J. (1976) (in press).
/11/ F. Cser, K. Nyitrai, É. Seyfried, Gy. Hardy, Magy. Kém. Folyóirat (1976) (in press).
/12/ Gy. Hardy: Solid State Polymerization in Two-Component Systems. In "IUPAC International Symposion on Macromolecular Chemistry". Akadémiai Kiadó, Budapest, 1969, p.571.
/13/ K. Nyitrai, F. Cser. B.D. Ngoc, Gy. Hardy, Magy. Kém. Folyóirat (1976) (in press).
/14/ Gy. Hardy, F. Cser. A. Kalló, K. Nyitrai, G. Bodor, B. Lengyel, Acta Chim. (Budapest), 65, 287, (1970).
/15/ Gy. Hardy, K. Nyitra, F. Cser, Gy. Cselik, L. Nagy, Europ. Polym. J. 5, 133, (1969).
/16/ M.D. Cohen, G.M. Schmidt: J. Chem. Soc. 1996 (1964).
/17/ J. Bregman, K. Osaki, G.M.J. Schmidt, F.I. Sontag: J. Chem. Soc. 2021, (1964).
/18/ M.D. Cohen, J. Rou, G.M.J. Schmidt, J.M. Thomas: Nature 224, 167, (1969).
/19/ H. Nakanishi, M. Hasegawa, Y. Sasada: J. Polym. Sci. A2, 10, 1537, (1972).
/20/ F.L. Hirschfeld, G.M.J. Schmidt, J. Polym. Sci. A2, 2181, (1964).
/21/ F. Cser, Ph.D. Thesis, Budapest, 1973.
/22/ A.I. Kitajgorodskii, Organic Chemical Crystallography, Consultant Bureau, New York 1961.
/23/ A. Müller, Proc. Roy. Soc. London, A138, 514, (1932).
/24/ Gy. Hardy, K. Nyitrai, G. Kovács, N. Fedorova, Acta Chim. (Budapest), 43, 121, (1965).
/25/ Gy. Hardy, K. Nyitrai, J. Varga, M. Patko, Periodica Polytechnica, 9, 137, (1965).
/26/ Gy. Hardy, L. Nagy, F. Cser, Acta. Chim. (Budapest), 47, 211, (1966).
/27/ Gy. Hardy, F. Cser, N. Fedorova, M. Bátky, Magy. Kém. Folyóirat, (1976) (in press).
/28/ Gy. Hardy, N. Fedorova, G. Kovács, E. Boros-Gyevi, J. Polym. Sci. C16, 2675, (1976) (in press).
/29/ Gy. Hardy, K. Nyitrai, F. Cser, Acta Chim (Budapest), 62, 253, (1969).
/30/ Gy. Hardy, K. Nyitrai, F. Cser, Macromol, Synth. 5, 91, (1974).
/31/ F. Cser, K. Nyitrai, V. Dévényi, Gy. Hardy, Magy. Kém. Folyóirat, (1976).
/32/ K. Nyitrai, N.N. Lan, Gy. Hardy, Magy. Kém. Folyóirat, 81, 216, (1975).
/33/ Gy. Hardy, K. Nyitrai, F. Cser, Kinetics and Mechanism of Polyreactions, IUPAC Symp. Budapest, 1969. Reprint vol. IV.
/34/ Gy. Hardy, K. Nyitrai, Acta Chim. (Budapest), 65, 301, (1970).
/35/ Gy. Hardy, K. Nyitrai, F. Cser, Magy. Kém. Folyóirat, (1976) (in press).

/36/ K. Nyitrai, F. Cser, B. Lengyel, É. Seyfried, Gy. Hardy, Magy. Kém. Folyóirat, (1976). (in press).
/37/ G. Földiák, Gy. Cserép, M. Röder, L. Wojnárovics, "Chemical Reaction on the molecular structure of carbohydrogenes" (in Hungarian). Kémia legújabb eredményei, 20, Ed. B. Csákváry. Akadémiai Kiadó, Budapest, 1974.
/38/ N. Morosoff, H. Morawetz, B. Post, J. Am. Chem. Soc. 87, 3035, (1965).
/39/ M. Puterman, T. Fort, Jr., J. B. Lando, J. Coll, Int. Sci. 47, 705, (1974).

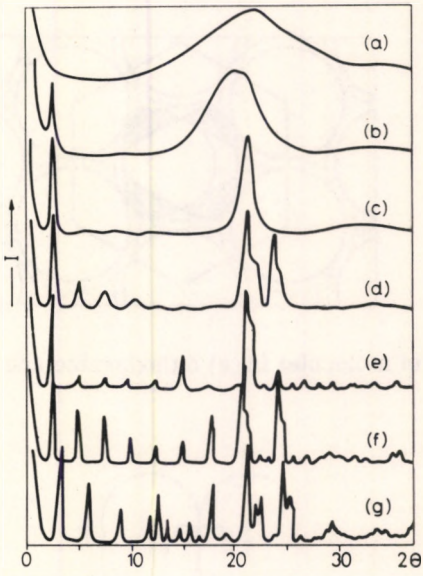

Fig. 1 X-ray diffractograms of different polymorphic modifications in paraffins

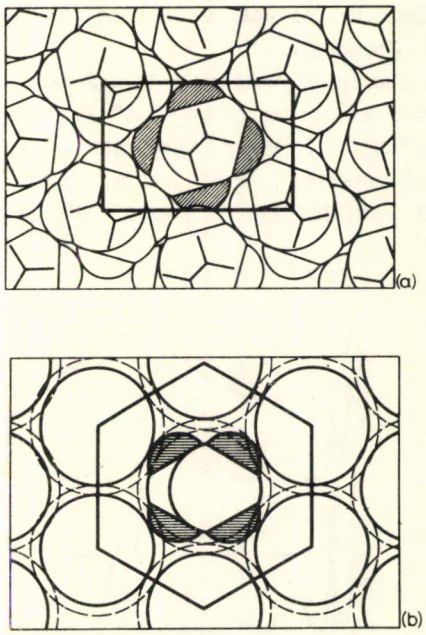

Fig. 2 Packing of molecules in (a) orthorhombic and (b) hexagonal layers.

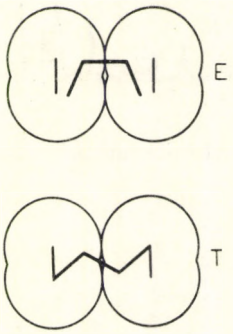

Fig. 3 Formation of ethylene dimers in eclipsed and in trans conformation

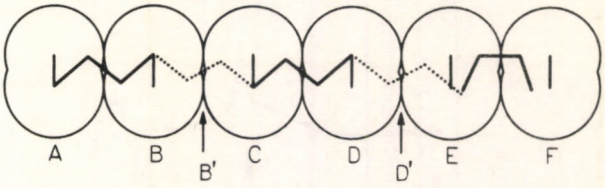

Fig. 4 Formation of a chain in a close packed vinyl layer

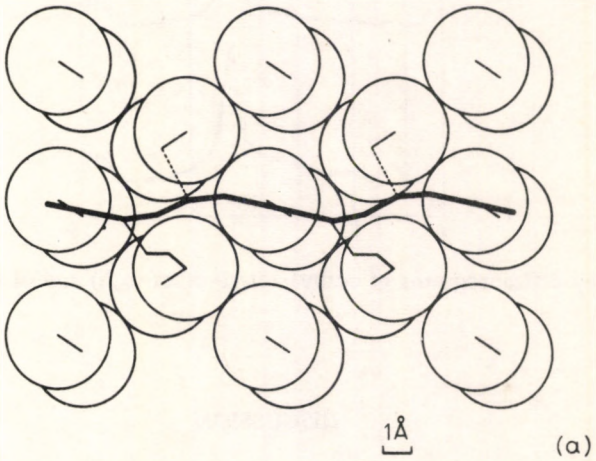

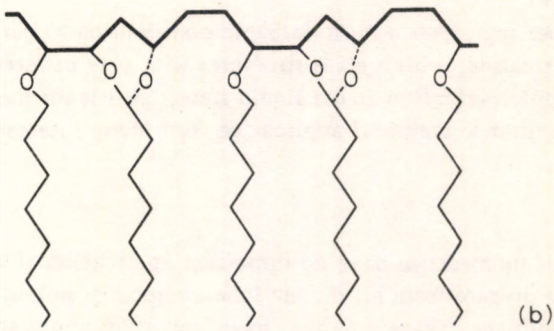

Fig. 5 Polymer chain formation in cethyl-vinyl-ether layers

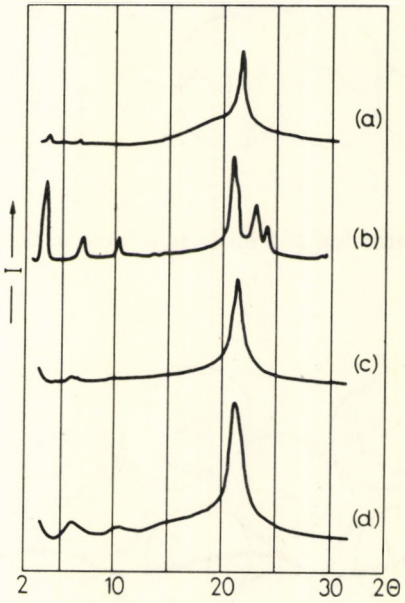

Fig. 6 X-ray diffractograms of cethyl-vinyl-ether (a,b) and of its polymers (c,d)

DISCUSSION

A. CHARLESBY

This paper represents a most valuable contribution to our understanding of solid state polymerization, which gives structures with very different properties to those obtained by polymerization in the liquid state. This leads me to ask whether we can expect to obtain new practical application from these interesting new types of material.

F. CSER

Up to this moment we have no important application of these polymers. Prof. Wegner could prepare from his diacetylene compounds polymer single crystals with very high dichroism. These polymers have important application for optical purposes. We hope our polymers will, in the future, have new applications too, e. g. poly cethyl vinyl ester films could be used as orienting spaces for nematic liquid crystals in displays.

A. CHARLESBY

That sounds most interesting.

EFFECT OF INHIBITORS ON THE GAMMA RAY INITIATED SOLID STATE POLYMERIZATION OF ACENAPHTHYLENE

L. Mahr, F. Cser, G. Kovács, Gy. Hardy
Research Institute for Plastics, 1950 Budapest, Hungary

Introduction

Chloranil (tetrachloroquinone) (KA) and bromanil (tetrabromoquinone) (BA) are effective inhibitors of radical polymerization /1/. Both of them readily form charge transfer (CT) complexes with proper electron donors like acenaphthylene (ACN) /2/. Due to their conjugated electron system KA and BA also have radiation protective properties /3/. The aim of the present work has been to investigate the effect of these inhibitors of electron donor character on the solid state polymerization of ACN. This monomer seemed to be a suitable model because its solid state polymerization behaviour has been studied in detail /4–11/. The effect of inhibitors on the kinetics of solid state initiated polymerization is also known /12–15/, but until now a solid monomer-inhibitor system of complete miscibility had not been found.

Experimental

The ACN monomer (Koch-Light product) was recrystallized from methanol and petrolether (m. p. 91.5°C). KA and BA inhibitors were applied after crystallization from methanol (m. p. 291°C and 290°C). A polarizing microscope (Zeiss Polmi A) was used for obtaining the ACN/KA and ACN/BA phase diagrams the photo current of depolarization having been measured by galvanometer at a heating rate of 2–3°C/min. The samples were prepared by melting the mixture of the two components above the m. p. of ACN. The m. p. determinations of mixtures containing more than 30 mole % of KA or BA failed because of the sublimation of ACN and the opacity of the samples. The phase conditions became unambiguous only after DTA (MOM Derivatograph) and X-ray diffractometry (Philips high-angle powder diffractograph, by Ni-filtered CuK $_\alpha$ radiation and $2\theta = 2°$/min rate of exposure). Formation of ACN–KA and ACN–BA CT complexes in solid state were proved by their diffuse-reflection-spectrum (DRS) /16/. These spectra were obtained on VSU-2P (Zeiss) spectrophotometer, having applied the insert type 45/0. Powdered $BaSO_4$ served for diluting the samples (5 g $BaSO_4$/2 × 10^{-4} mole sample).

The polymerization experiments were carried out at 40°C (this is the appropriate temperature according to the ACN/poly ACN phase diagram /7, 10, 11/. Gamma

radiation of ^{60}Co source was used for initiation at a dose rate of 4.01×10^4 rad/hr. The preparation and processing of the samples for polymerization and the viscometric molecular weight determination have been described elsewhere /4, 6, 7/.

Results

The DRS of the monomer and the haloquinones are seen in Fig. 1. The spectrum of ACN is represented by a continuous line, that of KA and BA are represented by a broken and a dotted line respectively. These spectra served as references for evaluating the spectra of the different compositions.

The DRS measured on an ACN/KA system of a composition of 1 : 1 mole ratio is shown in Fig. 2 by a continuous line. A calculated DRS by assuming the 1 : 1 mole ratio is derived from the addition of the spectra of the constituents (Fig. 1) of the aforesaid system and is represented by a broken line. The difference of these two spectra is drawn by a dotted line in the same figure. In this difference spectrum at about 500 nm there appears the CT-band of a complex that has been already proved to exist in solution /2/. During the complex formation the position of other bands of ACN are also altered as can be seen from the appearance of the absorption maxima at 220 nm and 290 nm in the difference spectrum.

The DRS of a 4 : 1 mole ratio composition ACN/BA system is presented by a continuous line in Fig. 3. The DRS that is calculated from the spectra of the components is drawn by a broken line while the difference spectrum is represented by a dotted line in Fig. 3. Similarly to the previous case, the CT-band of the complex is very intense on the difference spectrum but the bonds of ACN are only slightly modified.

The two DRS series in Figs 2 and 3 give an evidence for the existence of the same CT complexes in solid state which have been already found in 1, 2-dichloro ethane solution /2/. For KA and BA the position of the CT-bands are at 540 nm and 530 nm respectively. These values correspond to the CT-bands at 490 nm and 487 nm in liquid state.

Comparing the above presented two different spectra, it can be established that in the solid state the mode of interaction of KA and BA with ACN is not the same.

In Fig. 4 the phase diagram of the ACN/KA system is presented. At about 73–75°C a phase transition of this system in polarized light is observed, without marking it on this diagram. After the increase of temperature a eutectic melting occurs at 76°C. The corresponding eutectic composition contains 8 mole % KA.

A series of X-ray diffractograms for ACN/KA systems are shown in Fig. 5. According to these diffractograms, ACN is able to dissolve KA even in solid phase until a certain limit. However, above 50 mole % KA content the diffraction lines of KA also appear in the series. Hence, the phase transition at 73–75°C indicates most probably the decomposition of a solid solution of limited miscibility and the formation of an ideal eutectic.

The phase diagram of ACN/BA system is similar to that seen in Fig. 4. There is a eutectic formed in the system, again at 8 mole % BA content but with a m. p. of 72°C. In contrast to the ACN/KA system an intermediate phase transition in the vicinity of the eutectic temperature cannot be observed.

The X-ray diffractograms of the ACN/BA systems are shown schematically in Fig. 6. The Bragg angles and the intensities of the diffraction lines characterize an ideal eutectic /17/.

Table 1

Change of conversion, molecular weight and radiation chemical yields of polyACN formed in presence of KA after 750 hr irradiation in solid state

Composition ACN : KA	Conversion %	$\overline{M}_v$	$G_M \times 10^4$	$G_{in} \times 10^2$
1.00 : 0	42.0	31000	9.17	4.50
0.85 : 0.15	18.4	7300	4.02	8.37
0.70 : 0.30	16.5	7000	3.60	7.83
0.60 : 0.40	13.8	6300	3.01	7.28
0.50 : 0.50	8.3	5600	1.81	4.92

The conversion vs. polymerization time curves of ACN/KA systems are seen in Fig. 7. Both the rate and the limiting conversion of the polymerization decrease with the growing KA content. At the same time the accelerated character of the kinetics disappears. The increasing KA ratio depresses drastically the molecular weight ($\overline{M}_v$) of the product formed (Table 1).

It is noteworthy that by the growing ratio of KA additive the rate of polymerization changes in a similar manner as has been found in the case of a solid solution of norbornene-2, 3-dicarboxylic acid allyl and propyl ester /18/ and for the smectic solution of cholesteryl acrylate and propionate /15/.

The radiation chemical yields of polyACN in solid ACN and ACN/KA matrices are also shown in Table 1. Values of G_M and G_{in} reflect the monomer consumption and average number of chains formed per 100 eV energy absorbed by ACN (i. e. assuming that the energy absorbed by ACN is proportional to its weight fraction independently from the KA also present in the system).

For cases of ACN/BA systems, the polymerization kinetical curves are seen in Fig. 8. As opposed to the ACN/KA system, here the rate of polymerization does not depend on the BA content. It can be seen that above 20% conversion, when the rate of pure ACN is still accelerated, the limiting conversions, independently from the BA ratio, are soon reached. A similar phenomenon has been observed for the solid state polymerization of such acrylamide-bensoquinone mixtures where the quinone content exceeded that of the eutectic /13/.

Discussion

The qualitative radiation chemical properties of KA and BA are supposed as being very similar. Both of them inhibit the liquid phase polymerization of ACN very markedly without chain regeneration (i. e. no KA or BA can be built into the polymer backbone) /2/. Hence, their extraordinarily different effect on the solid state polymerization of ACN cannot be explained merely by their chemical nature.

It is assumed from indirect evidence /8, 9, 17/ that the solid state polymerization of ACN is a topotactic reaction of homogeneous character, the crystal lattice of ACN has a favourable arrangement for the chain propagation. As a result of the polymer formed, above a certain temperature, in the highly elastic or liquid state the polymerization becomes accelerated /7, 10, 11/. The autocatalytic character of such polymerizations can be well explained by the enhanced mobility of molecules in plasticized systems. The BA starts its effect only after the formation of the loosened structure, when the molecular mobility is already facilitated, but the KA displays its influence even in the period before. The different behaviour of the two inhibitors has to be attributed to the dissimilar physical structures of the ACN/KA and ACN/BA systems. It has been proved that in ACN/haloquinone/solvent systems the inhibitor acts in its complexed form /1, 2/. In the ACN/BA eutectic, those BA-containing complex sites that might be effective in the chain inhibition step, exist only at the BA/ACN interface because in the X-ray diffractograms we have not found any evidence of a crystalline complex with a separate phase. Thus, BA is unable to influence that reaction which occurs within the ACN crystals, being quite a distance from the growing chains. BA cannot inhibit sooner but only after the aforementioned polymer/monomer system has been formed. This change results in diffusion controlled processes when the BA is able to reach the reaction centres. Accordingly, on the kinetic curve the inhibition period is not at the initial stage of the irradiation.

The structural conditions are not the same for ACN/KA systems, namely, in the ACN lattice KA, as an isomorphous diluant is present. The ACN−KA complex itself is formed within the framework of the ACN lattice. This inhibitor-monomer system of molecular dispersity is the first such kind of two component system among the various other inhibitor − monomer pairs which have been studied until now from the view-point of phase conditions.

A quantitative comparison of the inhibitor efficiency of KA in the liquid and in the solid state meets difficulties. (e. g. the run of the inhibited kinetic curve in the solid state is not that typical which is usual in liquid state.) Moreover, the decrease of polymerization rate is linearly proportional with the mole ratio of KA present in the system if that is solid. There is no reaction mechanism available at present for the interpretation of an inhibition step in the crystal lattice. However, the relative efficiency of KA seems to be about the same as in the case of inert additives in solid state polymerizations /15, 18/. Because the inhibitor molecule is fixed to one point of the lattice its translation diffusion is impossible hence, the complex may interact only with (or it may be a geometric obstacle for) those growing chains which approach

its vicinity. In this aspect the inhibitor molecule in the complex is not different from those inert compounds which are unable to polymerize in the monomer lattice.

Accordingly, the different behaviour of KA and BA can be explained by their different physical structure, due to their dissimilar geometric dimensions. As the volume of ACN and KA molecules – calculated on the basis of Kitaigorodskii's data /19/ – are about the same (148.5 $Å^3$ and 149.9 $Å^3$), and the ratio of their overlapping volumes is higher than 0.95, KA easily replaces ACN in the lattice of the latter. Since the molecular volume of BA (171.0 $Å^3$) is considerably bigger than that of ACN, a mixture of substitution cannot be formed.

On the basis of the aforesaid experimental results the effect of KA and BA on the solid state initiated polymerization of ACN is considered as direct evidence of the topotactic lattice controlled mechanism of the reaction.

References

/ 1/ F. Tüdős, L. Simándi. M. Azori, MTA Kémiai Kutató Int. Közl., 7, 55 (1961).

/ 2/ L. Mahr. G. Kovács, Gy. Hardy, Magy. Kém. Foly., in press.

/ 3/ Gy. Hardy, G. Kovács, F. Cser, J. Mihály, Proc. of the Third Tihany Symp. on Radiation Chem., Ed. by J. Dobó and P. Hedvig, Akadémiai Kiadó, Budapest 1972, p. 531.

/ 4/ Gy. Hardy, G. Kovács, Gy. Koszterszitz, F. Cser, Acta Chim. (Budapest), 75, 69 (1972).

/ 5/ C. S. Chen, J. Polym. Sci., 62, 938 (1962).
J. Zurakowska-Országh, A. Gumulka, Second Tihany Symp. on Radiation Chem., Ed. by J. Dobó and P. Hedvig, Akadémiai Kiadó, Budapest 1967, p. 633,
J. C. Müller, ibid. p. 643.

/ 6/ Gy. Hardy, G. Kovács, F. Cser, Gy. Koszterszitz, Acta Chim. (Budapest), 75, 303 (1973).

/ 7/ Gy. Hardy, G. Kovács, Gy. Koszterszitz, N. Fedorova, F. Cser, Proc. of the Third Tihany Symp. on Radiation Chem., Ed. by J. Dobó and P. Hedvig, Akadémiai Kiadó, Budapest 1972, p. 601.

/ 8/ F. Cser, Acta Chim. (Budapest), 80, 317 (1974).

/ 9/ F. Cser, Gy. Hardy, ibid. 84, 297 (1975).

/10/ Gy. Hardy, F. Cser, G. Kovács, N. Fedorova, G. Samai, ibid. 79, 143 (1973).

/11/ Gy. Hardy, F. Cser, Z. Veksli, Europ. Polym. J., 10, 1217 (1974).

/12/ Gy. Hardy, J. Varga, F. Cser, E. Detrekőy, ibid. 2, 41 (1966).

/13/ Gy. Hardy, L. Nagy, F. Cser, Acta Chim. (Budapest), 47, 211 (1966).

/14/ Gy. Hardy, J. Varga, G. Nagy, E. Varga, L. Sára, ibid. 52, 219 (1967).

/15/ Gy. Hardy, K. Nyitrai, ibid. 52, 105 (1967).

/16/ H. Sato, T. Yasuniwa, Bull. Chem. Soc. Japan, 47, 368 (1974).
H. Sato, T. Yasuniwa, S. Horai, Sci. Rep. Kayoshima Univ., 23, 89 (1974).
/17/ Gy. Hardy, Solid State Polymerization in Two Component System, IUPAC Int. Symp. on Macromol. Chem. Budapest, Akadémiai Kiadó, Budapest 1969, p. 571.
/18/ Gy. Hardy, K. Nyitrai, Acta Chim. (Budapest), 65, 301 (1970).
/19/ A. I. Kitaigorodskii, Organicheskaja Kristallokhimija, Akad. Nauk. USSR, Moscow 1955.

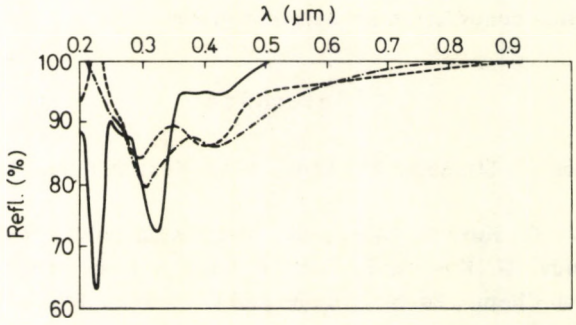

Fig. 1 Diffuse reflection spectra of the investigated compounds.
—— ACN, – – – KA, – · – · – BA

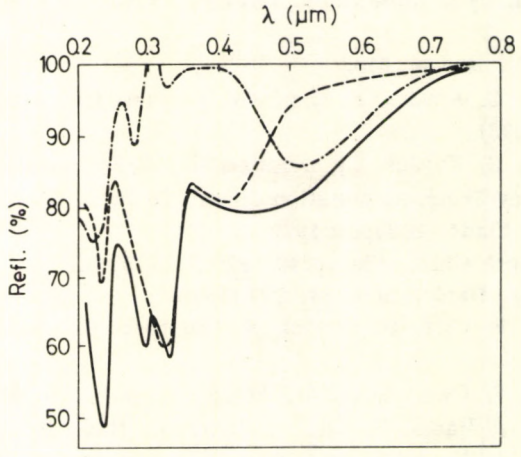

Fig. 2 Measured ——, and calculated – – – DRS of ACN/KA system of 1 : 1 mole ratio and the difference – · – · – of the two spectra

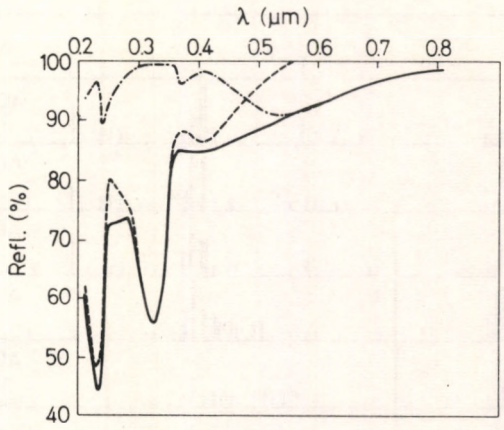

Fig. 3 Measured ———, and calculated – – – DRS of ACN/BA system of 4:1 mole ratio and the difference –·–·– of these two spectra

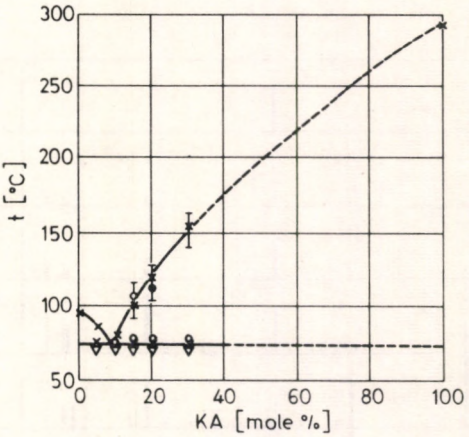

Fig. 4 Phase diagram of ACN/KA system, measured by × = polarized light, and o = DTA

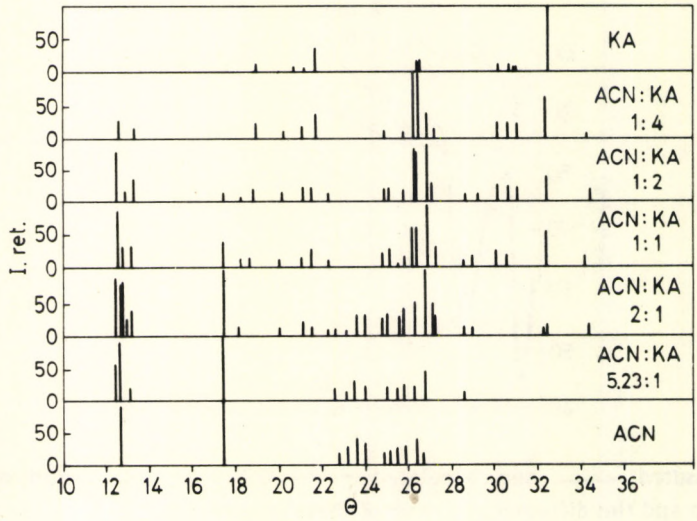

Fig. 5 X-ray diffractograms of ACN/KA systems of different composition

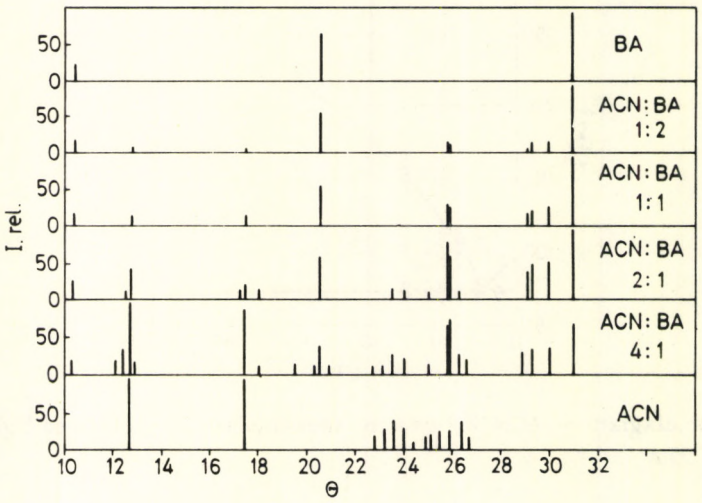

Fig. 6 X-ray diffractograms of ACN/BA systems of different composition

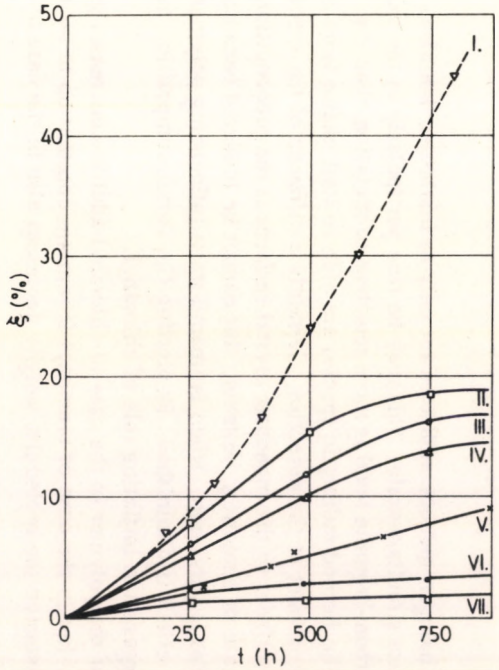

Fig. 7 Conversion vs. time of irradiation relationships for solid state polymerization of ACN (I) and in presence of KA:

II. 15 mole % KA
III. 30 mole % KA
IV. 40 mole % KA
V. 50 mole % KA
VI. 60 mole % KA

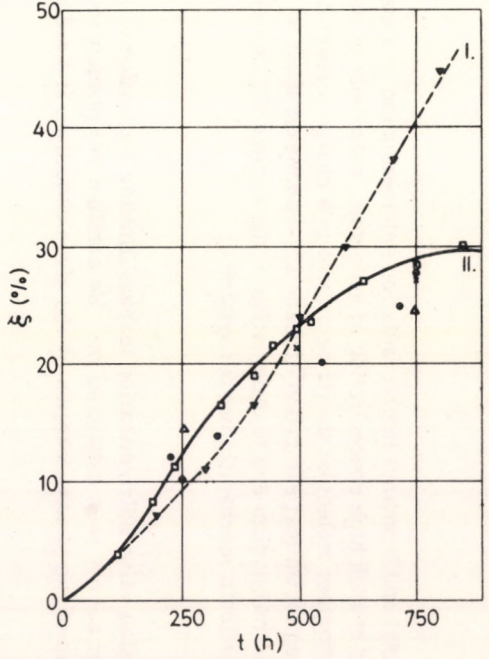

Fig. 8 Conversion vs. time of irradiation relationships for solid state polymerization of ACN (I) and in presence of BA:

II. 8, 50, 60, 80 mole % BA
□ ● o ×

H. HEUSINGER

You assume that chloranyl and bromanyl inhibit radiation polymerization of acenaphthylene. But in the presence of such high concentration of acceptors, especially in the liquid phase, most of the monomer molecules should be present in a charge transfer complex. In photochemistry it has been shown that excitation of many CT-complexes leads to polymerization by a cationic mechanism due to dissociation of the excited CT complex. Do you get evidence for a cationic mechanism in your systems?

G. KOVÁCS

Above a certain conversion value polymerization reaches limiting conversion in spite of the fact that the monomer has not been exhausted yet. We consider this phenomenon as evidence that the mechanism of the present reaction by the given conditions is a radical one.

J. ZURAKOWSKA-ORSZÁGH

Could you explain why according to the figures shown the addition of p-bromanyl seems to act at the beginning as an accelerator of the polymerization rate, besides that it does not show any inhibiting effect?

What was the molecular weight of the polymers obtained in the presence of p-chloranyl without additives?

G. KOVÁCS

It is probable that the halogen quinone additives act only as inhibitors, but also, to a less extent, as chain initiator simultaneously. This may be true particularly in the case of bromanyl, where the carbon-bromine bond is more sensitive to radiation than the carbon-chlorine bond is. The formed radiolytic species are able to start chains from the surface of the monomer component of the eutectics. Certainly a diffusion of the species from the bromanyl crystal surfaces to the monomer crystal surfaces is the precondition of such an initiation. In the case of eutectics, however, this cannot be hindered because the distance between the surfaces is very short. When bromanyl starts influencing polymerization as an inhibitor, the former effect is diminished. By plotting G_{in} versus composition the maximum obtained also suggests the initiating role of chloranyl.

The molecular weight of the polymer in the case of chloranyl additive decreases gradually with increasing conversion, but in the case of bromanyl it remains constant up to about 20% conversion. Above this conversion the molecular weight decreases also in the case of bromanyl.

THE MODELLING OF SOLID-STATE POLYMERIZATION BY MEANS OF THE MONTE CARLO METHOD

Andrzej Országh, Piotr Romiszowski
Department of Chemical Technology, University of Warsaw, Warsaw, Poland

Introduction

The problem of the modelling of polymeric chains by means of random walks was formulated more than 20 years ago/1, 2/ but only the development of computation techniques enabled numerous works in this domain to be carried out. Numerous papers (e. g. /3, 4/) were concerned with the modelling of polymeric chains by means of the Monte Carlo method. Such models were featured by the constant length of chain segments as well as constant angles between three consecutive segments. The choice of direction of the chain growth was determined by means of a pseudo-random number generator. The excluded volume effect was taken into consideration in the form of the ban of double occupancy of the same points in the lattice.

Research was undertaken for different types of two- or three-dimensional lattices. The thus formulated model of a single chain, in spite of the simplicity of assumptions enabled the examination of certain statistical features of macromolecules. The results of experiments on models correlated well with the features of real chains.

Hereunder is the description of the model of the polymerization in the post-effect, using some assumptions relating to the forming of single chains.

The model and its properties

An algorithm has been elaborated simulating the polymerization process occurring in the irradiated monomer crystal. The basic assumptions of the model are the following:

1. The crystal is represented by a chosen lattice area in the form of a cuboid.
2. The generating process of active centres in the crystal resulting from irradiation has been simulated by the random choice of coordinates of points in the chosen lattice area. The number of starting points applied for the calculation is equivalent to the radiation dose. Each of the randomly chosen points was treated as a starting point of a single chain.
3. The double occupancy of lattice points and crossing the edges of the chosen lattice area by the chains were prohibited.

4. All chains were simultaneously generated, adding successively by one segment. If the adding of a new segment to any of the growing chains led to double occupancy of the point, or caused crossing the edges of the chosen lattice area, then the segment was not added. The attempt to add a new segment was made during the next cycle of the program.
5. In order to enable the examination of the kinetics of the model process, the time parameter was introduced to the algorithm. It was assumed that the time unit is required to perform a single attempt of adding one segment to all chains.
6. The ratio of the number of lattice points occupied by all randomly chosen chains to the number of all points of the lattice was understood as a monomer in the polymer conversion degree.
7. The calculation process was terminated when the total increase of the chains length per time unit became zero.

Based on the assumptions of the model itself, as given above, equations can be deduced which describe the results of modelling experiments. The achieved agreement regarding the type of mathematical expressions of the equations with those which describe the real systems, as well as the agreement of the computed and experimental values obtained from the modelling experiments, will prove the correctness of the model assumptions. It will also enable evaluation of the conformity of the model with real systems.

While considering the modelling of single chains, the authors of this paper have come to the conclusion that geometrical properties of polymer chains can be featured, besides the mean square end-to-end distance $\bar{r}^2$, the radius of gyration $\bar{s}^2$, also by the "chain volume" V. This parameter had been defined /5/ as the number of lattice points in the smallest cuboid with its edges parallel to the lattice axis, in which the chain can be enclosed. It appeared, that the following dependency had been complied with:

$$\bar{V} = a \cdot n^b \tag{1}$$

where n is the number of chain segments, a, b are constants, dependent on the type of lattice. It was found that for self-avoiding chains in the diamond type lattice a = 0.33, b = 2.25.

While considering the polymerization model in the post-effect, it can be stated than since in the lattice of N points the I chains grow simultaneously Then each of them takes the "volume" V. where:

$$V = \frac{N}{I} \tag{2}$$

However, since the chains interrelate, each of them can grow in its effective "volume" V', where

$$V' = k \cdot V \tag{3}$$

k is the proportionality coefficient.

The maximum (limiting) conversion S_{max} (plateau on the curve conversion vs time), the existence of which results from Eq. (1), is given

$$S_{max} = \frac{I \cdot n}{N} \tag{4}$$

Using the above equation, we finally obtain:

$$S_{max} = \frac{I}{N} \cdot \left(\frac{k \cdot N}{I \cdot a} \right)^{\frac{1}{b}} \tag{5}$$

The kinetic dependencies, conversion vs time, can be deduced in the following way:

$$\frac{dS}{dt} \sim P \tag{6}$$

where P is the probability of encountering a non-occupied lattice point

Because

$$P = 1 - \frac{S}{S_{max}} \tag{7}$$

then

$$\frac{dS}{1 - \frac{S}{S_{max}}} = \frac{I}{N} dt \tag{8}$$

After integrating and transforming, we obtain:

$$S = S_{max} \cdot \left[1 - \exp \left(- \frac{I}{N \cdot S_{max}} \cdot t \right) \right] \tag{9}$$

Equation (9) is analogous to equations which describe the dependence of the monomer in a polymer conversion as a function of time applied for the real systems, known in the literature /6/.

It should be stated that in the case of the described model, the application of (5) and (9) is simple, and requires the determination of only one proportionality coefficient on the basis of knowledge of a few experimental values.

Table 1
Experimental and calculated maximum conversions for different values I

I	S_{max} (exp.)	S_{max} (calc.)
50	0.119	0.123
75	0.151	0.155
100	0.180	0.181
125	0.213	0.205
150	0.233	0.227
175	0.251	0.248

Results of experiments

Experiments have been carried out on the model with regard to a 30 unit long cube, in which $N = 28^3$ points could have been occupied (edge and wall points were inactive). In the cube were generated respectively: 50, 75, 100, 125, 150 and 175 chains in the diamond-type lattice, growing simultaneously. For each of the values of the "radiation dose" I, the experiments were carried out 10 times and the results were averaged. For each examined case the conversion S was computed. Due to multiple performance of the same experiment standard deviations of results have also been computed. These deviations did not exceed 8%, which proves correct proper repetition of the experiments. The calculations were perform ed on the digital computer CDC - CYBER 72.

In Table 1 are given the values of the maximum conversion S_{max} as a function of the applied "radiation dose" I. and also the values of the maximum conversion computed in agreement with Eg. (5). There is an evident, complete agreement between the experimental and computed values for k=6.0.

In Table 2 are given the values of experimental and calculated conversions using Eq. (9). And here, too, a good agreement appears unexpectedly between the experimental and calculated values. This agreement is much better with regard to conversions of values within the range of S_{max}, than in the initial stage of the post-polymerization. Therefore. Eq. (9) was deduced on the basis of the dependence (7), which is correct for high conversions.

Conclusions

The theoretical considerations on the model, as shown above, have in result given the kinetic dependency. conversion vs time, analogous in its mathematical form to the equations known in the literature and obligatory for real systems. This probably confirms the correctness of the model assumptions.

Table 2

Experimental and calculated conversions during the polymerization for different values of I.

I	50		75		100		125		150		175	
time	$S_{exp.}$	$S_{calc.}$	$S_{exp.}$	$S_{calc.}$	$S_{exp.}$	$S_{calc.}$	$S_{exp.}$	$S_{calc.}$	$S_{exp.}$	$S_{calc.}$	$S_{exp.}$	$S_{calc.}$
20	0.033	0.038	0.048	0.055	0.064	0.071	0.080	0.088	0.094	0.103	0.107	0.118
40	0.058	0.064	0.085	0.090	0.108	0.115	0.134	0.140	0.156	0.161	0.173	0.181
60	0.076	0.081	0.109	0.112	0.136	0.141	0.168	0.170	0.191	0.193	0.211	0.214
80	0.089	0.093	0.125	0.126	0.155	0.156	0.188	0.188	0.210	0.211	0.230	0.231
100	0.098	0.101	0.135	0.135	0.166	0.166	0.199	0.198	0.221	0.221	0.240	0.241
120	0.105	0.107	0.141	0.141	0.172	0.171	0.206	0.204	0.226	0.226	0.245	0.245
140	0.110	0.111	0.145	0.145	0.176	0.175	0.209	0.208	0.231	0.229	0.248	0.248
160	0.113	0.113	0.147	0.147	0.178	0.177	0.211	0.210	0.232	0.231	0.249	0.249
180	0.115	0.115	0.149	0.148	0.179	0.178	0.212	0.211	0.232	0.232	0.250	0.250

Also the experimental values on model examination show very good agreement with the given equations.

Therefore, the authors of the present paper can state that in spite of such simple model assumptions, it gives an image of the real course of the phenomenon of post-polymerization and can be used for further experiments on the mechanism of solid-state polymerization.

References

(1) F. T. Wall, L. A. Hiller Jr. and D. J. Wheeler. J. Chem. Phys. 22, 1036 (1954).

(2) M. N. Rosenbluth and A. W. Rosenbluth, J. Chem. Phys. 23, 356 (1955).

(3) W. Bruns, Makromolekulare Chem. 124, 91 (1969).

(4) W. Bruns, Makromolekulare Chem. 134, 193 (1970).

(5) A. Országh, A. Kolinski and P. Romiszowski, to be published.

(6) A. A. Berlin, I. M. Barkalov, V. I. Goldanski and N. S. Enikolopyan, Dokl. Akad. Nauk SSSR 161, 373 (1965).

DISCUSSION

A. ABKIN

In your Monte Carlo model where does the energy come from by which the monomer molecular approaches the active center?

A. ORSZÁGH

In these model experiments it is not possible to include the energetics in an explicit way. We could only imitate the formation of active centres by choosing coordinates of the lattice sites at random.

J. ZURAKOWSKA-ORSZÁGH

What was the average molecular weight and the distribution in these simulation experiments?

A. ORSZÁGH

The average degree of polymerization was in the range of 38–45, the distribution curve had a gaussian character. The maximal degree of polymerization was about 500.

γ-RADIATION-INDUCED COPOLYMERIZATION OF N-VINYL CARBAZOLE AND ACRYLAMIDE IN THE SOLID STATE

W. Pękala, I. Zuchowicz
Institute of Radiation Chemistry, Technical University, Łodź, Poland

There has been considerable interest in recent years in the γ-radiation-induced copolymerization of various monomer pairs in the crystalline state /1-4/. Such studies contribute to our knowledge of solid state reactions and also might lead to copolymers of unusual composition and sequence distribution.

Copolymerization might occur in solid solutions /1, 5, 6/ as well as in eutectic mixtures /3, 4, 7/. The latter seems rather puzzling when considered in conjunction with the belief that such mixtures comprise separate crystals of each monomer. It seemed interesting therefore to examine polymerization in a binary system composed of structurally highly different components, only partially miscible in the liquid state. Many monomers form such kinds of mixtures but no example of this case has been reported in relation to copolymerization.

The present investigation was concentrated on attempts to prepare copolymer from the solid system of N-vinyl carbazole /NVC, m. p.: 64°C/ and acrylamide /AA, m. p.: 84°C/.

Experimental

The purification, preparation and irradiation of monomer samples have been described previously /8/. The polymerization was followed by the gravimetric method. Immediately after irradiation at room temperature (except post-effect experiments) the samples were ground in a mortar and plunged into benzene. The polymeric products consisting the residue insoluble in benzene and the precipitate obtained from the benzene solution by addition of methanol were dried at 60°C to constant weight. The characterization of the polymers is described below.

DTA runs were made with samples heated from room temperature at a rate of 5 or 10°C/min under air in a derivatograph (F. Paulik, J. Paulik, L. Erdey system).

The polymers were examined with a Unicam SP 200G IR spectrometer in the form of KBr pellets and with an X-ray diffractometer type DRON-1, employing nickel filtered CuK_α radiation in the angular range of 2 - 35° (powdered samples).

The determination of polymer composition was carried out by elemental analysis.

Results and discussion

A solid AA–NVC mixture comprises separate crystals of each monomer. In the liquid state the components are only partially miscible. Miscibility of monomers over a range of monomer feed ratio 0. 5–1. 0 M NVC depends on the temperature of the system. AA–rich mixtures (> 0. 5 M AA) form two liquid phases (Fig. 1). It is probable that the system forms a eutectic mixture containing 90 mole per cent NVC, although we cannot exclude that at the beginning of crystallization of the second component, the first one is fully crystallized. In the latter case the presence of a finely dispersed crystal mixture is improbable /9/.

The kinetic curves of the solid state polymerization of the AA–NVC system for various monomer feed ratios are given in Fig. 2. The highest conversion has been obtained with pure acrylamide. N–vinyl carbazole is much more resistant to irradiation than AA. At the dose and temperature of the experiments NVC conversion does not exceed a few per cent. To our knowledge N–vinyl carbazole polymerizes according to accelerated kinetics but at much higher doses of irradiation /10, 11/. The total conversion depends on the dose rate and on the monomer feed ratio (Fig. 3). The copolymer yield increases continuously with increasing AA content in the mixture. This trend is in contrast to a majority of previously studied systems in which a maximum conversion has been reported to occur at the eutectic mixture /4, 7/ but is similar to the results obtained by Hardy and Boros–Gyevi with vinyl chloroacetate-vinyl laurate system /9/.

Polymeric products were separated with solvents into three fractions as follows: The polymers dried to constant weight were extracted with benzene to yield Fraction I (soluble) and Fraction II (insoluble). Precipitate obtained from the extract (Fraction I) by addition of methyl alcohol was found to consist of poly–NVC. Dried to constant weight Fraction II, insoluble in benzene, was extracted with water to yield Fraction IIa (soluble) and Fraction IIb (insoluble). Poly–AA was obtained from water extract (Fraction IIa) by addition of methyl alcohol.

The characterization of poly–AA and poly–NVC has been described previously /8/.

Fraction IIb (insoluble in water) was shown by elemental and infra–red (Fig. 4) analyses to contain comparable amounts of NVC and AA. The absorption bands characteristic of C–H bonds in aromatic compounds (720 cm^{-1}) and of the N–H bond of the amide group (1650 cm^{-1}) are clearly recognizable. Repeated extraction with benzene and with water did not affect the infra-red band intensities. However, to minimize the possibility that insoluble Fraction IIb might consist of a mixture of degraded and crosslinked homopolymers, postpolymerization was carried out. Under these conditions water insoluble polymer was also obtained. It seems to indicate that Fraction IIb consists of copolymer. Some other investigations have been made in order to differentiate between copolymers and a mixture of homopolymers. Figure 5 shows the X–ray diffraction diagrams of AA and NVC polymers. There is a marked difference between curve 1 and 2. The copolymer nature of

Fraction IIb was also proved by derivatographic test (Fig. 6). The copolymer yield depends on the monomer feed ratio, as seen in Fig. 7. Assuming that the monomer pair used in the present work forms a system in which the two components crystallize separately it is probable that AA might form a copolymer with NVC only at the interfaces rather than in the eutectic system and that after the reaction at the crystal interfaces only homopolymerization occurs.

In all experiments the amount of copolymer does not exceed 10% of the total polymers. The proportion of NVC in the copolymer seems to vary according to its proportion in the monomer mixture. The present observation is in contrast to previously studied systems in which the copolymer composition approximated the eutectic composition irrespective of the monomer feed ratio /7/. However, Kearney et al. have reported that the NPhA proportion in the NVC–NPhA copolymer varies also according to its proportion in the initial monomer mixture /3/.

The small NVC content (< 20 mole per cent) in the AA–NVC copolymer might be explained by the relatively low radiation yield of the NVC radicals.

References

/1/ M. Nishii, H. Tsukamoto, K. Hayashi, S. Okamura, J. Appl. Polymer Sci., 11, 1171 (1967).

/2/ J. E Herz, V. T. Stanett, Macromol. Rev., 3, 1 (1968).

/3/ J. J. Kearney, J. H. Herz, V. T. Stanett, Mol. Cryst. Liq. Cryst., 9, 485 /1969/.

/4/ A. Chapiro, P. Lesaulnier, Eur. Polymer J., 10, 171 (1974).

/5/ J. Zurakowska –Országh, 2nd Symposium on Radiation Chemistry, Tihany, 1966.

/6/ C. S. Chen, D. Grabar, J. Polymer Sci., C4, 869 (1964).

/7/ Gy. Hardy, J. Varga, G. Nagy, Makromol. Chem., 85, 58 (1965).

/8/ W. Pękala, I. Zuchowicz, Nukleonika, in press.

/9/ Gy. Hardy, E. Boros–Gyevi, Acta Chimica Hung., 50, 319 (1966).

/10/ A. Chapiro, Gy. Hardy, J. Chem. Phys., 59, 993 (1962).

/11/ J. Kroh, W. Pękala, Bull. Acad. Polon. Sci., Ser. Sci. Chem., 12, 419 (1964).

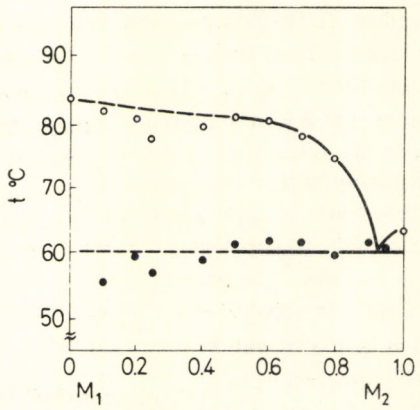

Fig. 1 Phase diagram of the system N-vinyl carbazole (M_2)-acrylamide (M_1)

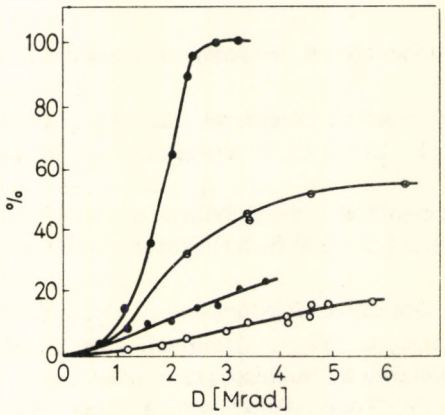

Fig. 2 Total conversion of the NVC-AA system versus γ-radiation dose. Dose rate: 0.576 Mrad/h. ⊗-Pure acrylamide, ⊖- 0.75 M AA, ○-0.25 M AA

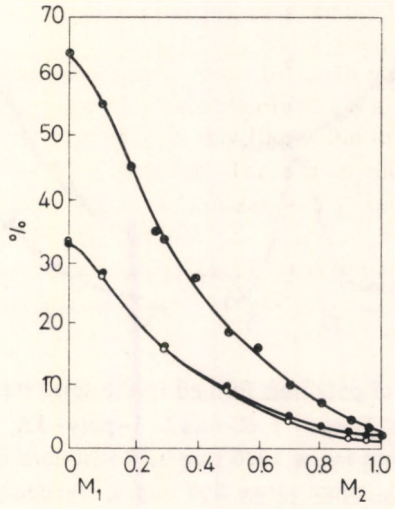

Fig. 3 Effect of monomer composition on the total conversion of the system N-viny carbazole (M_2)- acrylamide (M_1) at various dose rates

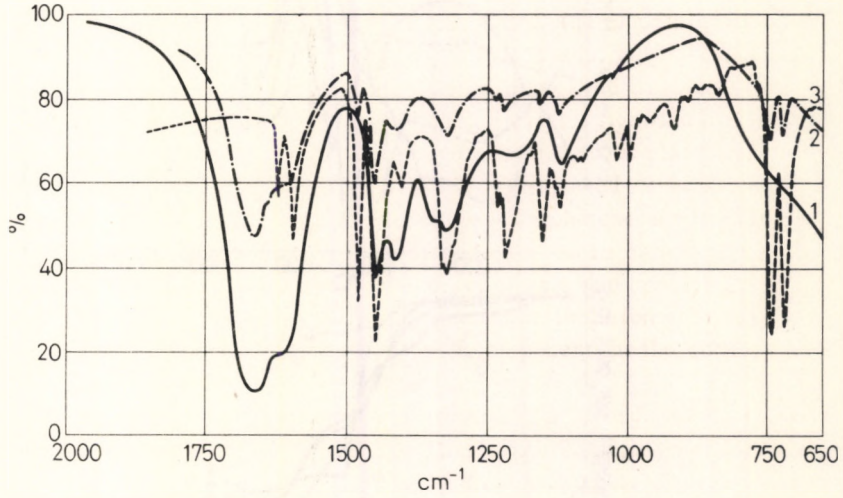

Fig. 4 Infra-red spectra of polymers formed in the solid state polymerization of the NVC-AA system. Dose - 1.63 Mrad. 1-poly-AA, 2-copolymer (30% NVC, by weight), 3-poly-NVC

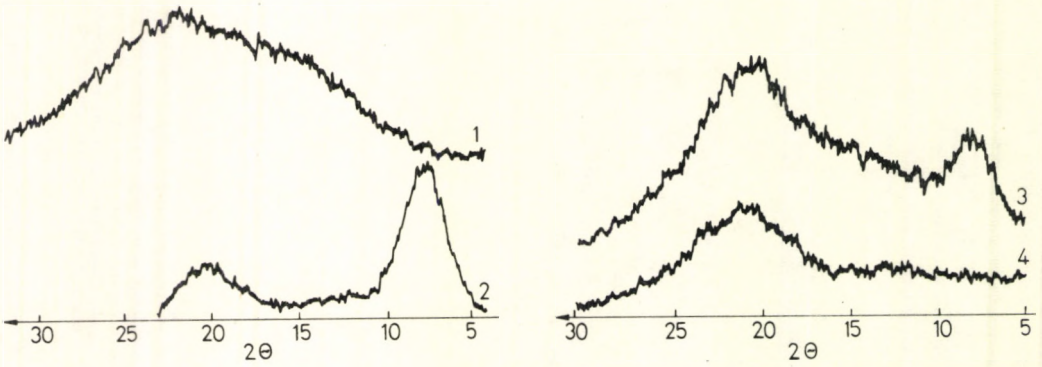

Fig. 5 X-ray diagrams of polymers formed in the solid state polymerization of the NVC-AA system. Dose - 1. 63 Mrad. 1-poly-AA, count range 500 imp/s, 2-poly-NVC count range 1000 imp/s, 3-mixture of homopolymers (50% NVC, by weight), count range 500 imp/s, 4-copolymer (50 % NVC, by weight), count range 500 imp/s

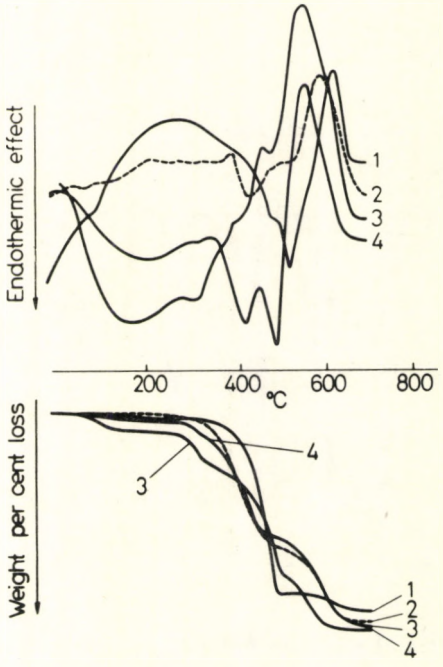

Fig. 6 DTA and TG curves of polymers formed in the solid state polymerization of the NVC-AA system. Dose - 1. 63 Mrad. 1-poly-NVC, 2-copolymer (50% NVC, by weight), 3-poly-AA, 4--mixture of homopolymers (50% NVC, by weight)

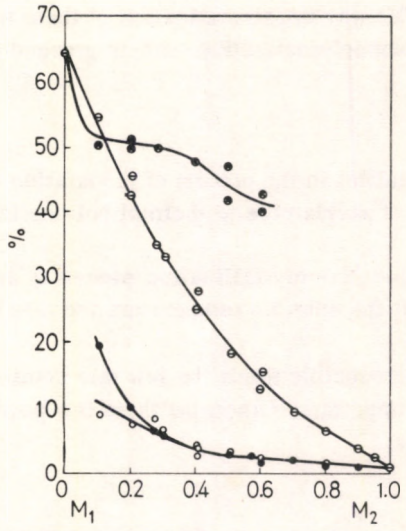

Fig. 7 Effect of the monomer composition on the polymer yields in the solid state polymerization of the system N-vinyl carbazole M_2 - acrylamide (M_1). Dose - 1. 63 Mrad. ⊖- total polymer products, ●-poly NVC, O- copolymer, ⊗- pAA.

DISCUSSION

J. ZURAKOWSKA-ORSZÁGH

If copolymerization proceeds only in the interphase, the copolymers might have the structure of block copolymers.

W. PEKALA

It is very probable, but at present we do not have enough evidence on that.

H. HEUSINGER

Do you assume that homopolymerization and copolymerization proceed by the same mechanism?

W. PEKALA

All our experiments were done at room temperature in the presence of air. As I know, in these conditions both monomers: AA and NVC, polymerize with the free

radical mechanism. This way copolymerization of these monomers, which proceeds simultaneously with homopolymerization, should proceed by the free radical mechanism too.

Gy. HARDY

Do you have difficulties in the process of preparation of your eutectic mixture, e. g. very high ability of acrylamide to thermal polymerization in these circumstances?

I think that a consecutive crystallization process is impossible in the eutectic system. As you know, at the eutectic temperature the rate of crystalization of both components is equal.

For obtaining a reproducible result the low rate cooling procedure of mixture crystallization is very important. Otherwise there is a possibility of formation of a quasi-eutectic structure.

W. PEKALA

Yes, at the beginning of our work with the NVC–AA system we had difficulties in preparation. In order to obtain reproducible results the conditions of preparation of the mixtures and those of irradiation had to be carefully fixed. We did not observe any thermal polymerization of AA below 100°C.

F. CSER

By formation of the eutectic structure the crystal sizes of the components are very small. Upon quenching with liquid nitrogen also very small crystals are formed. This is most important for solid state polymerization.

Another problem is that you have two monomers, two homopolymers and the copolymer in the system during irradiation. This is a five-component system having possibly very complicated phase behaviour. We always find a small amount of polymer in N–vinyl carbazol after melting, this polymer phase is plasticized by the monomer. On the other hand acrylamide does not solve its polymer. Correspondingly in your irradiated system these phases should be present too, where copolymerization can take place. I think that this phase is more convenient for copolymerization than the interphase between NVC and AA.

W. PEKALA

NVC and AA do not mix in the liquid phase in all feed ratios and the components crystallize separately. Under these conditions the dimensions and distribution of the macro-crystals in the matrix may be quite different from that of the eutectic mixture.

I agree that radiation polymerization of some pairs of monomers in the solid state results in a complicated system. In our case to exclude the influence of radiation on the polymeric products, postpolymerization was carried out. The polymeric products obtained this way were quite similar to those obtained in source.

EFFECT OF TEMPERATURE ON KINETICS OF RADIATION INDUCED SOLID-STATE POLYMERIZATION OF SUBSTITUTED ACRYLAMIDES

J. Żurakowska-Országh, A. Gumułka
University of Warsaw, Department of Chemical Technology, Poland

Introduction

Our previous investigation on the solid state polymerization of the series of N-substituted acrylamides and methacrylamides were carried out mainly at room temperature /1–4/ especially in the case of polymerization induced by simultaneous irradiation.

The effect of temperature was studied only for few monomers of the acrylamide series in order to establish the influence of polymerization temperature on the properties of the polymer obtained /5, 6/.

The main purpose of the present paper is a study of the effect of the changes in structure of the particular monomers of the homologous series of substituted acrylamides on their reactivity at various temperature and the activation energy of the solid state polymerization.

Experimental

Monomers selected for investigation include: a series of N-tert-alkylacrylamides from N-tert-butylacrylamide up to N-tert-heptylacrylamide with various isomers and pairs of monomers of the acrylamide and methacrylamide series with identical aliphatic, aromatic and alicyclic substituents.

Both series of monomers with their chemical formulae and melting points are presented in Tables 1 and 2 respectively.

All these monomers with exception of acrylamide and methacrylamide were prepared in our laboratory as described in our previous publications /1–4/.

In order to obtain reproducible results the standard method of purification and sample preparation was adapted. Particular monomers from several syntheses were collected together, dissolved in methanol and recrystallized several times from methanol and afterwards from ethanol in order to obtain a sharp melting point. Finally the monomer was precipitated from ethanol solution by the addition of water. This technique enabled us to obtain crystals of comparatively homogeneous size. The crystals were dried at room temperature under vacuum to remove excess of solvent and finally in a desiccator over P_2O_5 to constant weight.

Table 1

List of monomers of N-tert-alkylacrylamide series

No.	Monomer	Chemical formula	Melting point (K)
1	N-tert-butylacrylamide	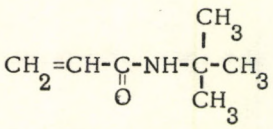	403.1
2	N-tert-amylacrylamide	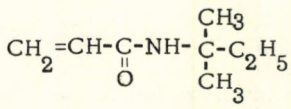	367.0
3	N-1, 1-dimethybutylacryl-amide	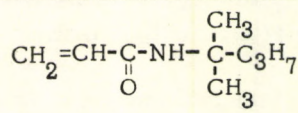	337.4
4	N-1-methyl-1-ethylpropyl-acrylamide	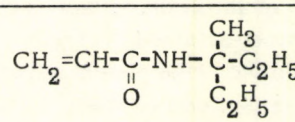	345.6
5	N-1, 1, 2-trimethylpropyl-acrylamide	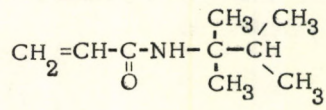	373.2
6	N-1,1-dimethylamylacryl-amide	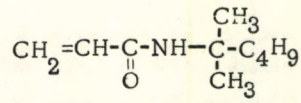	334.3
7	N-1-methyl-1-ethylbutyl-acrylamide	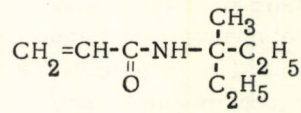	355.2
8	N-1,1-diethylpropyl-acrylamide	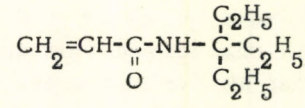	387.0
9	N-1,1,3-trimethylbutyl-acrylamide	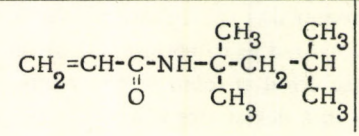	331.7

Table 2.

List of monomers of acrylamide and methacrylamide series

No.	Monomer	Chemical formula	Melting point (K)
1	Acrylamide	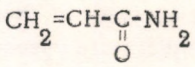	357.2
2	N-tert-butyl-acrylamide	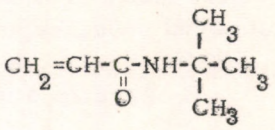	403.1
3	N-cyclohexyl-acrylamide	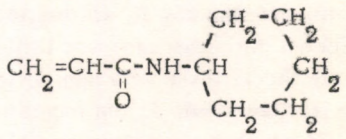	386.2
4	N-phenyl-acrylamide	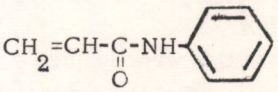	380.2
5	Methacrylamide	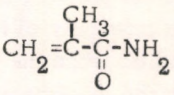	368.2
6	N-tert-butyl-methacrylamide	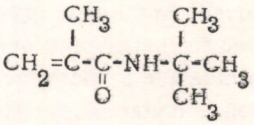	327.6
7	N-cyclohexyl-methacrylamide	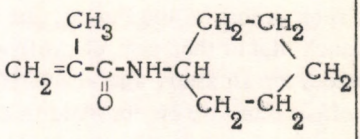	381.0
8	N-phenyl-methacrylamide	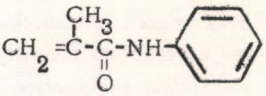	359.7

For each experiment 2 grams samples were used. They were sealed in "Thermisil" glass tubes filled with pure dry nitrogen. The procedure of nitrogen purification as well as sample preparation was the same as described in our previous publications /1–4/.

Irradiations were carried out in a ^{60}Co- γ -rays source "Gammacell-220" at dose rate of 81888 rad/hr. Special thermostatic equipment was constructed as previously described /5/ assuring the accuracy of about $\pm$ 0.1 ^{o}C.

After irradiation, samples were opened and the monomer separated by extraction in a 1:1 methanol-water solution. In the case of acrylamide pure methanol was used for extraction. After careful drying the polymer content was determined gravimetrically.

Results and discussion

Polymerization was carried out at various temperatures, namely: 300, 310, 320, 330, 340, 350 and 360 K. Of course, the whole temperature range could not be applied for all the series as it was limited by the melting point of particular monomers. For all the series a very regular increase of polymerization rate with temperature rise was observed. As the experimental material is very large, kinetic curves for three selected monomers, namely: N-1,1-diethylpropylacrylamide in Fig. 1, N-cyclohexylacrylamide in Fig. 2 and N-cyclohexylmethacrylamide in Fig. 3 are presented.

Times of irradiation were adapted according to the reactivity of particular monomers in order to obtain a degree of conversion up to about 10%. The results obtained show that some of our previous observations on the effect of various alkyl and aryl substituents on the reactivity of respective monomers at room temperature occurs in a similar manner also when the polymerization was performed at higher temperatures, namely with the increase of the length of one of the substituents from N-1,1-dimethylethylacrylamide up to N-1, 1-dimethylamylacrylamide an increase of reactivity is observed. In the case of N-hexyl and N-heptyl isomers the lowest conversion is obtained for substituents of symmetric structure, as for instance, N-cyclohexylacrylamide and N-diethylpropylacrylamide with three ethyl substituents on the tertiary carbon. Acrylamide for the whole range of temperatures is more reactive than methacrylamide. However in certain cases some deviation occurs, namely as seen in Fig. 2 and Fig. 3, the polymerization rate of N-cyclohexylacrylamide is much higher than that of cyclohexylmethacrylamide up to 340 K, at 350 K, the differences are smaller, and at 360°K a change in relative reactivity takes place. A similar effect can also be observed in the case of N-phenylacrylamide and phenylmethacrylamide as seen in Fig. 4.

To get some more systematic aspect of this relation the activation energies of the whole series of monomers were calculated.

Calculations were carried out for very low degree of conversion (1–3%) where the influence of the presence of the polymer on the polymerization rate can be ignored.

In order to determine with accuracy the course of curve S = f(t) for a low degree of conversion, experimental curves of conversion vs time were described by

corresponding equations that best fit the relationship. Usually the function $S = at^n + bt$ was applied, the coefficients were determined by the least squares method. Calculations were performed with the aid of a computer.

The polymerization rate is equal to $v = dS/dt$. However, the determination of v by direct differentiation may lead to serious errors as the values of the derivatives of curve S(t) can have different values from those of the real curve. Usually in the range $1\% < S < 3\%$ there are only 2-3 experimental points. Using the function S(t) a further 8 values of t can be calculated corresponding to assumed S values. It appeared that in this range the relation of conversion agains the time of irradiation can be approximated linearly by the equation $S = a_1 t + b_1$. The coefficients a_1 and b_1 were calculated using the least squares method with the aid of a computer. At the same time calculation results were checked by comparison with values obtained from experimental data.

The polymerization rate v was easily calculated as it was equal to the coefficient a_1. Activation energy was calculated from the equation:

$$\ln v = \frac{-E_a}{RT} + \ln A$$

Having a series of values of ln v for corresponding 1/T values the coefficient E_a/R was calculated in a similar way by the least squares method with the aid of a computer. These relations enable the calculation of the activation energies E_a.

Activation energies for the series of N-tert-alkylacrylamides are presented in Table 3, those of the series of N-substituted acrylamides and methacrylamides in Table 4. From these data some general observations can be made:

a) The introduction of N-substituent in the acrylamide as well as the methacrylamide series causes an increase in the activation energy. The lowest activation energy was obtained for pure acrylamide.

b) The presence of the methyl substituent of the α-carbon of the vinyl group increases the activation energy. Values obtained for monomers of the acrylamide series are always lower than those of the methacrylamide series with identical substituents. Especially high differences were obtained between N-cyclohexylacrylamide and N-cyclohexylmethacrylamide.

c) The comparison of the activation energy of N-hexylacrylamide isomers shows that highest values were obtained for N-1, 1-dimethylbutylacrylamide with the comparatively long butyl group, the lowest for N-cyclohexylacrylamide with the symmetric substituent.

Similar relations were obtained also for the N-tert-heptylacrylamide series, namely: the highest activation energy was attained by N-1, 1-dimethylamylacrylamide with the long pentyl group, the lowest by N-1,1-diethylpropylacrylamide with three symmetric ethyl groups.

The comparison of these results with kinetic data shows that isomers of highest reactivity in the solid state polymerization process have the lowest activation energies and those with very low reactivity - the highest activation energy.

Table 3.

Activation energy of the N-tert-acrylamide series

No.	Monomer	E_a, Kcal/mol	E_a, $J \cdot 10^{-3}$/mol
1	N-tert-butylacrylamide	12.0	50.2
2	N-tert-amylacrylamide	11.5	48.1
3	N-1,1-dimethylbutylacrylamide	26.2	109.7
4	N-1-methyl-1-ethylpropylacrylamide	16.4	68.5
5	N-1,1,2-trimethylpropylacrylamide	11.9	49.7
6	N-1- 1-dimethylamylacrylamide	19.2	80.3
7	N-1-methyl-1-ethylbutylacrylamide	15.4	64.4
8	N-1,1-diethylpropylacrylamide	15.0	62.9
9	N-1,1,3-trimethylbutylacrylamide	14.2	59.6

Table 4

Activation energy of the N-substituted acrylamide and methacrylamide series

No.	Monomer	E_a, Kcal/mol	E_a, $J \cdot 10^{-3}$/mol
1	Acrylamide	8.9	37.2
2	N-tert-butylacrylamide	12 0	50.2
3	N-cyclohexylacrylamide	10.2	42.8
4	N-phenylacrylamide	22.2	92.8
5	Methacrylamide	10.4	43.5
6	N-tert-butylmethacrylamide	12.8	53.5
7	N-cyclohexylmethacrylamide	31 8	133 1
8	N-phenylmethacrylamide	26.1	109.3

References

/1/ J. Żurakowska-Országh, Chim. Ind., 93, 405 (1965).

/2/ J. Żurakowska-Országh, J. Polym. Sci., C, 16, 1931 (1968).

/3/ A. Országh, J. Żurakowska-Országh, Proc. Tihany Symp. Radiat. Chem., 583, (1967).

/4/ J. Żurakowska-Országh, IUPAC Budapest, 4, 61 (1969).

/5/ J. Żurakowska-Országh, B. Zaleski, A. Gumułka, W. Busz, J. Polym. Sci., 42, 115 (1973).

/6/ A. Országh, J. Żurakowska-Országh, B. Zaleski, IUPAC Madrid, Prep., 1, 1-16, (1975).

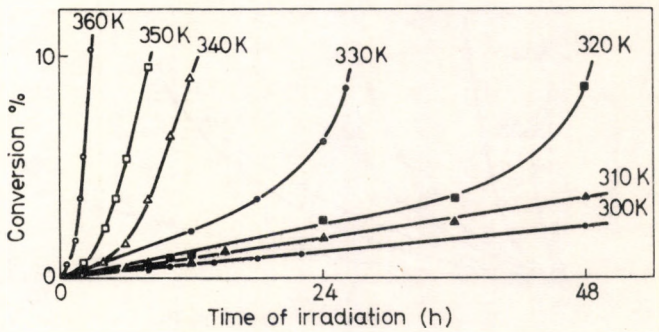

Fig. 1 Effect of temperature on solid state polymerization of N-1,1-diethylpropylacrylamide

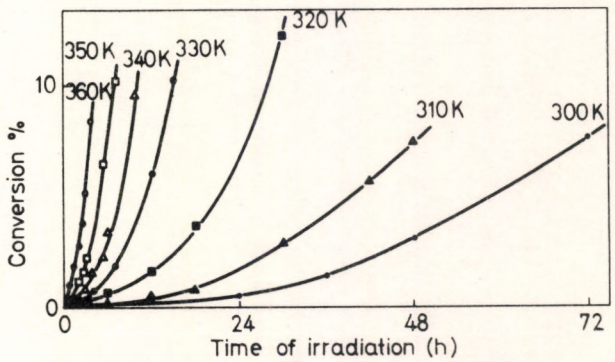

Fig. 2 Effect of temperature on solid state polymerization of N-cyclohexylacrylamide

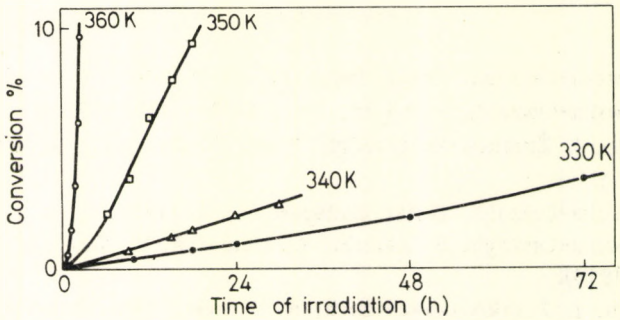

Fig. 3 Effect of temperature on solid state polymerization of N-cyclohexylmethacrylamide

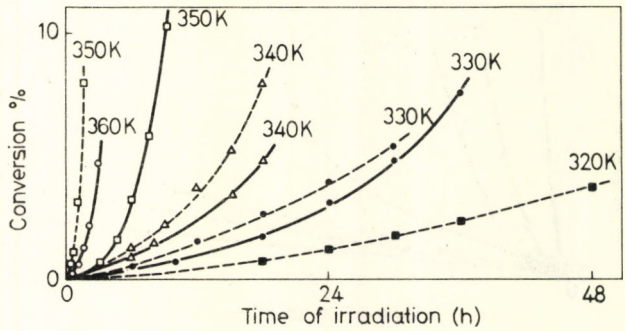

Fig. 4 Polymerization of N-phenylacrylamide and N-phenylmethacrylamide at various temperatures: N-phenylacrylamide ● - 330 K, △ - 340 K, □ - 350 K, ○ —360 K, N-phenylmethacrylamide ■ -- 320 K, ● -- 330 K, △ -- 340 K, □ -- 350 K,

F. CSER

Did you investigate the interaction of the polymer formed in the reaction with the monomer and the effect of this on the reaction scheme?

J. ZURAKOWSKA-ORSZÁGH

We studied the activation energy using data for conversion up to 3% just to avoid the necessity for studying the reactions of the polymer with the monomer.

A. ABKIN

Did you study the post polymerization? How does the activation energy of the process of polymerization performed during irradiation differ from that of post polymerization?

Are there any X-ray structural analysis data for the crystalline monomers you studied (acrylamide compounds)? If so, how do they correlate with the kinetic data?

J. ZURAKOWSKA-ORSZÁGH

Some investigations on the post polymerization of all these monomers have been carried out. The results and their comparison with the in source data will be presented in a separate publication.

We did some X-ray investigation on the structure of N - tert alkyl acrylamide monomers, but these are not finished yet. We shall publish the results later.

RADIATION INDUCED POLYMERIZATION AND COPOLYMERIZATION OF ISOBUTENE AND ISOBUTENE-VINYLIDENE CHLORIDE IN THIOUREA CANAL COMPLEXES

H. P. Bohlmann, Ch. Schneider,
Institute of Physical Chemistry, University of Cologne, FRG

Introduction

The first detailed investigations on polymerization in canal complexes were carried out by Brown and White /1,2/. They studied a large number of very different types of monomers with regard to their ability to form complexes with urea or thiourea which might be used for stereospecific polymerization reactions. In addition, a few copolymerizations, especially with butadiene derivatives, were carried out. Later on, Kawasaki et al. /3,4/ and Kiss /5/ and Polgar et al. /6/, studied in detail the polymerization of acrylonitrile in urea canal complexes and reported on the copolymerization of acrylonitrile with ethylacrylate /4/ and with acrolein /6/. An excellent structural study on the polymerization of 1,3-disubstituted dienes in thiourea canal complexes was carried out by Chatani et al /7,8/. Nevertheless, a lot of problems are still unsolved and the amount of experimental data is small.

In connection with work on the copolymerization behaviour of isobutene with halogenated monomers we were interested to get some knowledge about the possibility to homo- and copolymerize isobutene in a thiourea canal complex.

Experimental

Thiourea (TH) was recrystallized twice from distilled methanol and dried at about 80°C in vacuo for 24 h. It was then finely ground and stored at 50°C under reduced pressure. Isobutene (IB) (Philips Petroleum Corporation, 99 %) was passed over CaH_2, vinylidene chloride (VDC) (Merck) was distilled twice under nitrogen. Solvents and inhibitors were used without further purification. Thiourea, solvent, and inhibitor were mixed in glass ampoules and connected to a high vacuum line. Isobutene and vinylidene chloride were condensed into the ampoules and the mixture was carefully freed from impurities, especially oxygen, by successive freezing and thawing cycles. No speeial precautions were taken to remove traces of water. To improve the reproducibility of feed composition the monomer quantities were determined by measuring the pressure of a constant gas volume. The ampoules were sealed off and stored at low temperatures to complete the formation of adducts.

The γ-ray-initiated polymerization was carried out at different temperatures and at dose rates in the range from $4,0 \cdot 10^4$ to $2,9 \cdot 10^5$ rad/h.

After irradiation the ampoules without thiourea were opened so that isobutene and vinylidene chloride could evaporate. In the case of the thiourea samples the polymer adduct was ground and washed several times with warm water or methanol to remove thiourea and residual monomer. It was then dried under reduced pressure. The composition of the copolymer was obtained by elementary analysis of the chlorine content.

Results and Discussion

A. Polymerization of Isobutene in Thiourea Canal Complex

A few polymerization experiments were carried out to learn about the reaction conditions necessary for the polymerization of IB in TH canal complexes. It turned out that addition of merely TH to isobutene did not affect the polymerization rate of the free isobutene at all. However, when adding small amounts of acetone to the IB/TH mixture and allowing it to stand for a few days, the polymerization rate increased by a factor of 2-3. When triethylamine (TEA) was added as an inhibitor the polymerization of the free isobutene as well as that of the IB/TH mixture was completely suppressed while in the case of the system IB/TH/Acetone no effect on the polymerization rate was observed. We therefore conclude that firstly, addition of acetone is necessary for canal complex formation and, secondly, triethylamine is able to suppress the free cationic polymerization of isobutene outside the canal but is too large a molecule to enter the canal and to affect the polymerization inside the thiourea inclusion complex. If acetone is replaced by methanol, conversion strongly decreases. Therefore, all further experiments were carried out with a mixture of TH/IB/Acetone/TEA.

Figure 1 shows the relation between the conversion of isobutene and the formation time of adducts. It can be seen that at $-30^{\circ}C$ formation is complete after about 4 to 5 days of aging. Conversion further depends on the molar ratio of IB:TH and on the amount of acetone necessary for the crystallization of the adducts. Experiments showed that maximum conversion is obtained for a molar ratio IB/TH of about 1:3 and for addition of about 16 % mole acetone, referred to TH.

Figure 2 shows the dependence of conversion on the irradiation time for the polymerization of the IB/TH canal complex in comparison to the free isobutene polymerization. Canal complex polymerization depends linearly on irradiation time and is 2 to 3 times faster than the free polymerization. Since the radiation induced free polymerization of isobutene is known to proceed cationically at low temperatures the question arises whether polymerization in canal complexes follows a cationic or a radical mechanism. Experiments on the temperature dependence of the conversion show that the conversion increases with increasing temperature up to about $15^{\circ}C$ followed by a sudden decrease (Fig. 3). At about $20^{\circ}C$ the conversion obtained is

almost zero. In comparison, it could be shown by a simple thermal measurement that the IB/TH monomer complex is surprisingly stable even above the boiling point of IB, decomposition does not take place before 18°C. In the range from -20°C to +10°C an activation energy of about 6,6 kcal/mole (27,8 kJ/mole) is obtained. The increase of conversion with temperature is very likely due to an increasing mobility of the isobutene units in the thiourea matrix. There is an additional change in the conversion-temperature curve in the range between -30°C and -20°C which we are not able to explain at the moment.

The inclusion polymer of isobutene is sticky, it is soluble in the usual nonpolar solvents and has a molecular weight of about $8 \cdot 10^3$.

B. Copolymerization of Isobutene with Vinylidene Chloride in a Thiourea Canal Complex

From literature data it has been suggested /8/ that inclusion copolymerization is favoured if the two monomers form the same type of crystal lattice with the host. We assumed that vinylidene chloride might be an ideal copolymerization partner for isobutene since the two monomers are very similar in size and symmetry. Vinylidene chloride is known to form a thiourea canal complex which is isomorphic in structure with the cyclohexane /TH inclusion complex /8/.

The free copolymerization of isobutene and vinylidene chloride has been investigated by several authors at different temperatures using photoinitiation, γ-rays, or chemical initiators. At temperatures of about -78°C and especially in the presence of solid additives a polymer product consisting almost exclusively of isobutene was obtained /9,10/ due to a cationic homopolymerization of the isobutene. With increasing temperature the cationic process no longer plays a significant role and at room temperature and above, a radical copolymerization takes place for which reactivity ratios of $r_{IB} \approx 0,05$ and $3,3 > r_{VDC} > 1,3$ are reported /9-12/.

We were interested to see if copolymerization of isobutene and vinylidene chloride in a thiourea canal complex would yield different results compared to the free copolymerization, especially with regard to reaction rate and copolymer composition. It has been assumed before /6/ that copolymerization in inclusion complexes generally leads to copolymers with the same ratio of components as the corresponding initial monomer mixture.

Preliminary polymerization experiments showed that 2,6-di-tert-butyl-4-methylphenol is an appropriate inhibitor since it suppresses the homopolymerization of IB and of VDC as well as the copolymerization of these monomers. On the other hand, it does not affect the homo- and copolymerization of IB and VDC in TH canal complexes. Obviously, the inhibitor molecule has too large a diameter to enter the thiourea canal.

In Fig. 4 the composition of the copolymer is plotted versus the composition of the monomer mixture for thiourea complex copolymerization at different temperatures, dose rates and doses as well as for the free copolymerization. It can be seen that no

significant differences exist. In all cases VDC is incorporated into the copolymer to a higher extent than IB as is usual for the free radical copolymerization. In addition, the IR spectra of the inclusion copolymers with varying mole % of VDC are very similar to the corresponding IR spectra of the free copolymerization. The simplest explanation of this surprising result would be that no copolymerization in the thiourea canals but only the usual free copolymerization has taken place. However, we know that the presence of DTMBPh does suppress the free copolymerization. Furthermore, the reaction rate in the IB/TH complex copolymerization is more than one order of magnitude higher than in the case of the free copolymerization as is shown in Fig. 5 where the dependence of the reaction rate on the composition of the monomer mixture is plotted. Furthermore, at -78 °C where the yield is negligible in the case of the free radical copolymerization, we get a considerable amount of copolymer in the case of complex copolymerization. Further work is in progress especially to get deeper insight into the composition and structure of the monomer canal complexes in copolymerization reactions.

Acknowledgement. The authors gratefully acknowledge the financial support of this work by the Bundesministerium für Forschung und Technologie.

References

/1/ D. M. White, J. Ámer. Chem. Soc. 82 5678 (1960)
/2/ J. F. Brown, D. M. White, J. Amer. Chem. Soc. 82 5671 (1960)
/3/ M. Kawasaki, T. Maekawa, K. Hayashi, S. Okamura, J. Macromol. Chem. 1 (3), 489 (1966)
/4/ M. Kawasaki, T. Maekawa, K Hayashi, S. Okamura, J. Macromol. Chem. 1 (3), 507 (1966)
/5/ L. Kiss, Magy. Kém. Foly. (Ung. Z. Chem.) 74 (3), 125 (1968)
/6/ S. Polgár, L. Kiss, B. Kaplan, M. Barkalov: Proceedings of the Third Tihany Symposium on Radiation Chemistry, Akadémiai Kiadó, Budapest 513 (1972)
/7/ Y. Chatani, S. Nakatani, H. Tadoroko, Macromolecules 3 (5), 481 (1970)
/8/ Y. Chatani, S. Nakatani, Macromolecules 5 (5), 597 (1972)
/9/ A. P. Sheinker, A. D. Abkin et al., Doklady Akad. Nauk S. S. S. R. 124 632 (1959)
/10/ E. V. Kristal'nyi, S. S. Medvedev, Vysokomolekol. Soedin. 7 1377 (1965)
/11/ K. H. Hellwege, U. Johnsen, K. Kolbe, Kolloid-Z-Z. Polymere 214 45 (1966)
/12/ T. Fischer, J. B. Kinsinger, C. W. Wirsen, J. Polym. Sci. B, 4 379 (1966)

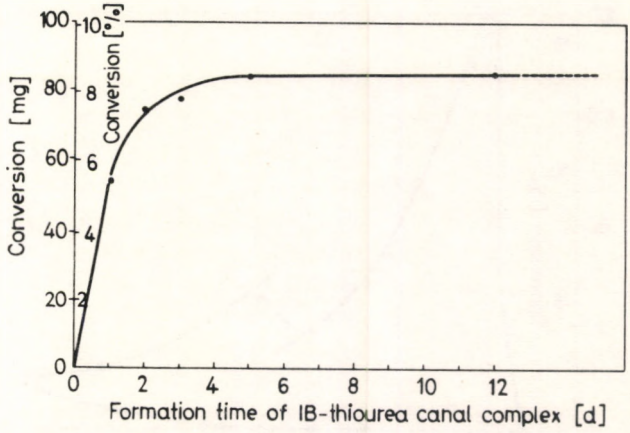

Fig. 1 Plot of conversion versus formation time of adducts. Molar ratio IB/TH = 1:3; aging temp. : -30°C, polym. temp. : -78°C; dose rate: $2.9 \cdot 10^5$ rad/h, irrad. time: 20 h

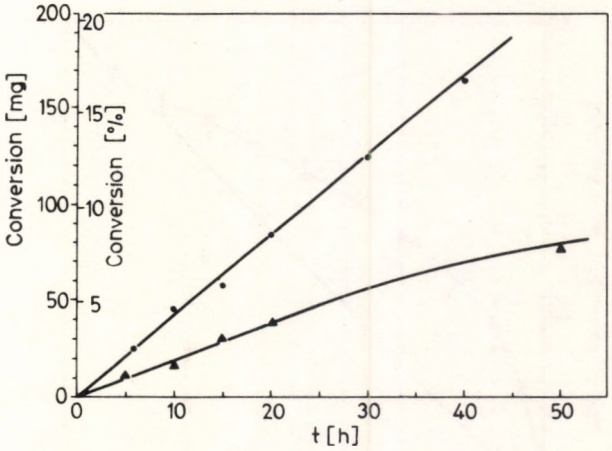

Fig. 2 Dependence of conversion on irradiation time. Polym. temp. : -78°C; dose rate: $2.9 \cdot 10^5$ rad/h. ▲ polymerization of isobutene in bulk; ● polymerization of isobutene-thiourea canal complex molar ratio: IB/TH = 1:3

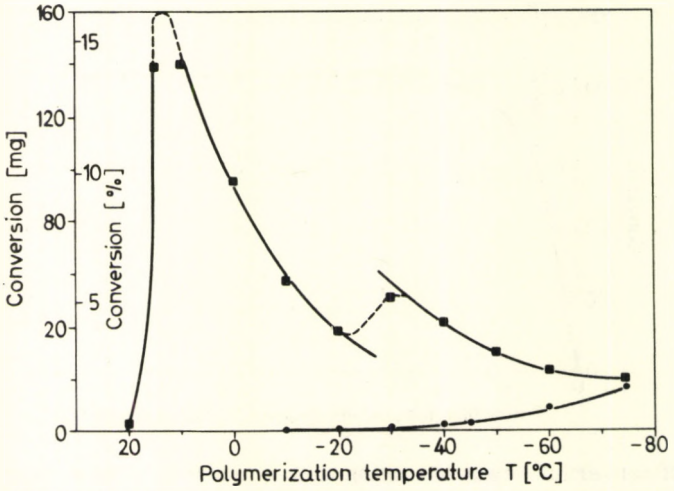

Fig. 3 Dependence of conversion on polymerization temperature. Dose rate: $4.0 \cdot 10^4$ rad/h; irrad. time: 20 h. ● free polymerization; ■ inclusion polymerization, molar ratio IB/TH = 1:3; aging temp.: $-30^{\circ}C$

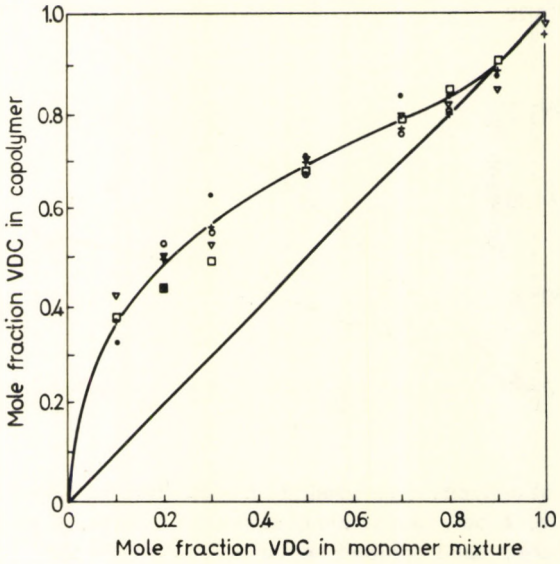

Fig. 4 Plot of copolymer composition versus composition of monomer feed. Free copolymerization: ● temp.: $-30^{\circ}C$; dose rate: $6.6 \cdot 10^4$ rad/h; irrad. time: 30 h inclusion copolymerization: + temp.: $-30^{\circ}C$; dose rate: $6.6 \cdot 10^4$ rad/h; irrad. time: 30 h; □ temp.: $-78^{\circ}C$; dose rate: $2,9 \cdot 10^5$ rad/h; irrad. time: 10 h; ▽ temp.: $-78^{\circ}C$; dose rate: $4.0 \cdot 10^4$ rad/h; irrad. time: 2 h; ○ temp.: $-30^{\circ}C$; dose rate: $4.5 \cdot 10^4$ rad/h; irrad. time: 2 h.

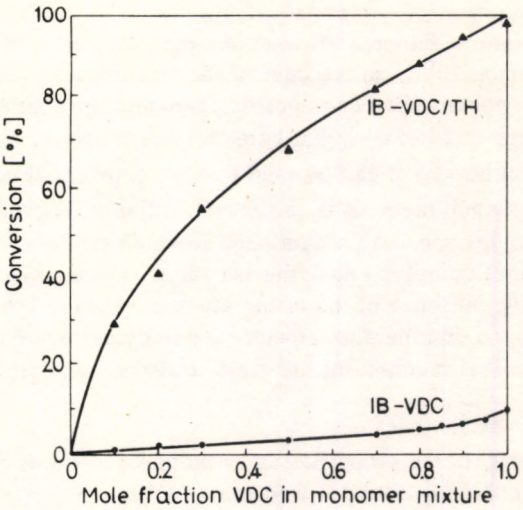

Fig. 5 Dependence of reaction rate on the composition of the monomer feed for the free copolymerization and the copolymerization in thiourea canal complexes. Polym. temp.: -30°C; dose rate: $6,6 \cdot 10^4$ rad/h; irrad. time: 30 h

DISCUSSION

A. ORSZÁGH

On the curve presenting copolymerization versus time at temperature of about -30°C a break is observed. Is it possible that at this temperature some isomorphic transition occurs?

Ch. SCHNEIDER

It is possible, but we do not have any evidence.

P. HEDVIG

In there any DSC signal observed in the temperature range between -80°C and +18°C?

Ch. SCHNEIDER

We did not do any DSC measurements.

L. KISS

What is the decomposition temperature of the isobutene and isobutene -vinylidene chloride - thiourea channel complex?

What evidence do you have that the mixture studied is a real channel complex and not just a mixture of the components?

Ch. SCHNEIDER

For the isobutene – thiourea channel complex we obtained a decomposition temperature of about +18°C. In the case of the isobutene – vinylidene chloride – thiourea channel complex the decomposition temperature seems to be still higher, may be in the range of 24 –29°C, but here the results are not quite unequivocal.

From IR measurements it can be seen that we obtain real copolymer and not a mixture of two homopolymers. It is, however, rather difficult to distinguish between a channel complex reaction and a catalyzed reaction on the surface of thiourea. Our evidence for channel complex copolymerization is : (1) the much higher rate of the reaction even in the presence of inhibitors which suppress polymerization outside the channel, (2) we get a considerable amount of copolymer even at –78°C where in the case of free radical mechanism the yield is almost negligible.

J. ZURAKOWSKA-ORSZÁGH

Did you investigate the properties and structure as well as the molecular weight of the copolymer obtained? Did you find some difference between this structure and that of copolymers obtained by conventional methods?

Ch. SCHNEIDER

We have just started to investigate the molecular weight and its distribution. From infrared spectra we could not observe any difference between the conventional and inclusion copolymers.

F. CSER

In your experiments the ageing temperature was the same as the temperature where the activation energy curve exhibits a break. Did you try to age samples at different temperatures?

Is it probable that the polymerization mechanism is different below –30°C than above it, e. g. changes from ionic to radical?

Ch. SCHNEIDER

We did experiments in which the samples were aged at the same temperature at which polymerization was carried out, e. g. between –78°C and +10°C. The shape of the conversion–temperature curve was always the same with the break always at about –30°C.

Unfortunately we do not know anything about the mechanism in the case of homopolymerization of isobutene in the channels.

V. S. IVANOV

The results of this work show direct evidence about the sensitizing effect of the channel complex in radiation polymerization. Although some examples of these effects have been mentioned earlier in the literature, it is essential to emphasise the importance of certain kinetic effects observed by Dr. Schneider by comparing the cationic polymerization of pure isobutene with that in the channel complex. The monomer selected here polymerizes exclusively with the cationic mechanism.

STUDY OF THE γ-RAY PRODUCED PARAMAGNETIC SPECIES IN THE UREA-ACRYLONITRILE CHANNEL COMPLEX AT LOW TEMPERATURE

L. Kiss, M. Irie*, K. Hayashi*
Research Institute for Plastics, Hungary
*Industrial and Scientific Research Institute of Osaka University, Osaka, Japan

Introduction

It is known that various vinyl and diene monomers are able to form so-called channel complexes with urea and thiourea, and that in these complexes the included monomers can polymerize under the influence of ionizing radiation resulting in stereoregular polymers.

The kinetics of in-source polymerization as well as postpolymerization of the urea-acrylonitrile channel complex have been studied before /1–8/. The kinetic study of the polymerization of this complex, however, did not give any unambiguous answer to the question which kind of active centres are able to initiate the polymerization in this system. In this paper we attempted to clarify the nature of these paramagnetic centers by the ESR method.

Experimental

Urea was purified by recrystallization twice, from a saturated solution of dried urea in methanol, and subsequently by drying at 80°C under reduced pressure. After drying it was powdered finely and dried again under reduced pressure at 80°C for 24 hours. Acrylonitrile was purified and distilled by the technique described in Ref. /1/.

The complex was formed in sealed "suprasil" ESR-tubes under atmospheric pressure the same way, as reported earlier /1/. However, in some cases before mixing of the components in the ESR-tube they were degassed. After degassing the components the monomer was redistilled into the ESR-tube containing degassed urea, and finally sealed under high vacuum (10^{-5} torr). The samples were irradiated by a 60–Co gamma source, of the Industrial and Scientific Research Institute of Osaka University having a nominal activity of 7000 Ci. The dose rate was usually 0.06 Mrad/hr, sometimes we used 2 Mrad/hr with a total dose up to 4 Mrad. For the ESR-measurements a "Varian E–6" model ESR-spectrometer was used.

Samples were usually irradiated in a "suprasil" tube. The "suprasil" sample tube, however, was found to give a significant signal after irradiation with a total dose 0.36 Mrad. In order to avoid this in some cases, we prepared the complex under vacuum in common "pyrex" capillary tubes and after irradiation, from this tube, under

liquid nitrogen in darkness we removed the irradiated complex and transferred it into an unirradiated ESR-tube. After this operation the quartz sample tube was degassed again under high vacuum at 77 K, and sealed at this temperature. It is necessary to emphasize that the samples were irradiated in darkness at 77 K, and the spectra were recorded at the same temperature.

The gamma irradiated samples were illuminated in the cavity resonator of the ESR spectrometer, using a super-high pressure mercury lamp type SP−500. The infrared-component of the light was filtered out with water. For selection of the necessary wave-lenghts we used "Toshiba" filters: VR−60 (600 nm), VY−50 (500 nm) and UV−31 (310 nm).

Results

Effect of the mole ratio of the components in the initial mixture

The mole percent of urea in the initial mixture was changed from 2 to 92.6 mole%. The results are shown in Fig 1. Curves 1 and 2 represent the dependence of the relative concentration of the paramagnetic centres ($R^{\cdot}$) as a function of the urea content in moles per cent of the initial mixture. In the case of curve 1 ($R^{\cdot}$) was calculated with respect to the acrylonitrile content of the mixture. As it is seen, in this case ($R^{\cdot}$) permanently increases. In this case the initial mixture contained only a very small amount of monomer, i.e. channel complex and a big amount of tetragonal urea. By plotting ($R^{\cdot}$) against the weight per cent of the total mixture a maximum approximately at 50 mole% of urea content is shown. This is the real ratio of urea to acrylonitrile in the complex /11, 12/.

Oxygen effect

In the present work most of the samples were prepared under atmospheric pressure. In most of the present experiments air saturated monomer was used. In the ESR-spectra of the irradiated samples were found to be asymmetrical even at 77 K (Fig 2, spectrum 1). After storage at 195 K and after cooling down to 77 K, at the middle of spectrum a very strong asymmetrical peak appeared (Fig. 3) which was identified as being due to $RO_2^{\cdot}$ radicals. At 195 K the relative concentration of the $RO_2^{\cdot}$ radicals was found to depend on the storage time. The time dependence of the relative concentration of the $RO_2^{\cdot}$ radicals are shown in Table 1. It can be seen that their concentration grows during one hour storage time, reaching a maximum, then decreases. After 16 hours storage at 195 K the $RO_2^{\cdot}$ concentration decreases to its initial value. The observed $RO_2^{\cdot}$ radicals in the complex are assigned to acrylonitrile molecules because in the ESR-spectrum of pure finely powdered urea irradiated and stored at the same experimental conditions as the channel complex no peroxy-signal is found (Fig 2, spectrum 3). Bensasson et al. /15/ found similar ESR signals when they studied the radiation polymerization of acrylonitrile in the solid phase in the presence of air.

For samples prepared in vacuum no $RO_2^{\cdot}$ signal appeared (Fig 2, spectrum 2).

Effect of visible light on the transformation of the paramagnetic centres after gamma irradiation at 77 K

First of all we would like to emphasize that after irradiation in the gamma source the samples became yellow and their shade of colour depended on the total dose. This colour could be photobleached by illumination with 310, 500 and 600 nm light. ESR-spectra were recorded after gamma irradiation, and during photobleaching in the cavity resonator with 310 nm (time of exposure 180 sec) represented in Figs 4 and 5. It may be seen that after photobleaching a peak of the middle of the spectrum disappeared (Fig 4). This peak is indicated on Fig 4 by an arrow, the width of this peak is 3.6 G (peak to peak) (cf. Fig. 5). The total area under the spectrum (Fig. 4) was found to increase by 50% during photobleaching.

Table 2 shows the influence of photobleaching, with different wavelengths on ($R^{\cdot}$), in the gamma irradiated urea-acrylonitrile channel complex. In this case the

Table 1

Depedence of the $RO_2^{\cdot}$ radical concentration on storage time at 195 °K in the urea acrylonitrile channel complex

Storage time hours	RO_2 concentration %
0.083	100
1.000	209
16.000	95

Table 2

Effect of photobleaching on the relative radical concentration induced by gamma rays at 77 K in urea acrylinitrile channel compex. Dose-rate: 0.06 Mrad/hr; total dose: 0.36 Mrad

Time of illumination, min	Relative radical conc., %	λ nm
–	100	600
5	172	600
10	167	600
–	100	500
5	156	500
10	131	500
–	100	310
6	112.4	310
18	87.6	310

time of light-exposure was relatively long. It is clear that changing the wavelength ($R^{\cdot}$) at first increases, and subsequently decreases, to its initial value.

The kinetics of the photobleaching is shown in Fig. 6. For the samples irradiated by a dose rate of 0.06 Mrad/hr, with a total dose 0.36 Mrad it may be seen that the radical concentration increases strongly reaching a limiting value in 15 sec. At a dose rate of 2 Mrad/hr (total dose 4 Mrad) no change of the radical concentration upon illumination was observed. When the sample was irradiated with a high dose rate, 2 Mrad/hr, but the total dose was only 0.36 Mrad, approximately 10% increase of ($R^{\cdot}$) by illumination was found.

When the monomer contained 10^{-2} mole/l methyl-ethyl-ketone under the same experimental conditions, a 20% increase of the radical concentration upon illumination was found.

Discussion

According to Fig. 1 curve 1 extremely large relative concentration for the paramagnetic centres in the complex are found at low AN- concentrations. This has also been observed by Karasef and Larin /9/ and Tabata /10/ and explained by assuming energy transfer from U to AN. In these experiments, however, the total radical concentration was related to the AN-content. As the AN-radicals cannot be separated quantitatively from the U radicals, at low AN concentrations it seems more reasonable to relate the total radical concentration to the total weight. In this case the maximum value is observed at about 50% AN-concentration, curve 2.

As for the oxygen effect it was assumed earlier /2/ that the oxygen molecules are unable to build into the hexagonal cavity of the urea channel. Figure 2 shows, however, the appearance of a typical peroxy signal in the complexes prepared by using non-deareated monomer while no such signal appears in the case when oxygen is completely removed.

It was also shown /2/, that the kinetics of the polymerization reaction was not influenced by the presence of oxygen.

In the present work we have shown that the yellow colour of the irradiated sample could be photobleached and simultaneously the ESR spectrum was changed. Moreover, the radical concentration increased by 50% upon photobleaching. In a previous work /6/ we reported that a visible light induced postpolymerization in this system proceeded even at 77 K, and by heating up the sample irradiated at 77 K to between 77 and 123 K a very strong luminescence effect was observed. This is considered as evidence of the presence of some charged species, such as electrons and holes, in the irradiated system.

Cramer /13/ considers that the cavity of an inclusion complex is to be regarded as a region of high electron density, so the cavity behaves as an electron donor, that is as a "base" in the Brönsted–Lewis sense. On the basis of this we can assume that in the acrylonitrile molecules embedded in urea cavities electron excess centres: anion radicals are stabilized.

On the basis of presented experimental results we supposed that during irradiation at 77 K in urea-acrylonitrile channel complex at least three kinds of paramagnetic species are formed:

$R^{\cdot}$ – a neutral free radical
$R^{\bar{\cdot}}$ – a charge excess anion radical type centres and
$e^{\cdot}$ – trapped electrons.

At small dose rate (0.06 Mrad/hr) and dose (0.36 Mrad) levels the concentration of these species linearly increased in time. At high dose rates (2 Mrad/hr) and high total dose (4 Mrad) the concentration of neutral free radikals increased linearly but the concentration of electron excess centres quickly saturated.

By photobleaching, the electron excess centres can dissociate giving a neutral free radical and another charged paramagnetic centre

$$R^{-} \longrightarrow R_1^{\cdot} + X^{-}$$

At lower dose rates the ratio of $\frac{(R^{\bar{\cdot}})}{(R^{\cdot})}$ is higher than at higher dose rate. By photobleaching the trapped electrons can either recombine with positive holes or produce an anion with acrylonitrile.

Karasef /14/ showed that within the cavity, on the influence of gamma irradiation from methyl-ethyl-ketone, some cation and anion radicals were formed. Perhaps this reaction is able to compete with the formation of charge excess paramagnetic species of the included acrylonitrile. Therefore the initial concentration of these species in the presence of this ketone is less than in the case of their absence.

It seems that this is a probable mechanism of the described phenomenon.

Acknowledgements. The authors are grateful to the Japanese International Cooperation Agency and to the International Atomic Energy Agency for the financial support of the research.

The authors wish to thank to Dr. K. Tamura, Dr. H. Hatada, and Dr. P. Hedvig for their helpful discussions concerning this work.

References

/ 1/ L. Kiss, IUPAC International Symposium on Macromolecular Chemistry, Prague. Preprint p. 374.

/ 2/ L. Kiss, M. Kém. Folyóirat 74/3, 125 (1968).

/ 3/ M. Kawasaki, T. Maekava, K. Hayashi, S. Okamura, J. Polym. Sci. 1/3, 489 (1966).

/ 4/ S. Polgár, L. Kiss, A. M. Kaplan, I. M. Barkalov, Proc. of the Third Tihany Symposium on Radiation Chemistry. Akadémiai Kiadó 1971. p. 513.

/ 5/ L. Kiss, Sz. Bálint, M. Kém. Folyóirat 74/3, 128 (1968).
/ 6/ L. Kiss, S. Polgár, IUPAC International Symposium on Macromolecular Chemistry. Akadémiai Kiadó, Budapest. Vol. IV, 1969 p. 45.
/ 7/ L. Kiss, S. Polgár, IAEA–SM 123/40, 523, Munich (1969).
/ 8/ L. Kiss, IUPAC International Symposium on Macromolecular Chemistry, Helsinki. 1–23, 133 (1972).
/ 9/ A. L. Karasef, V. A. Larin, Khimija Vysokyh Energii 4/1, 56 (1972), 6, 5. 444 (1972).
/10/ Y. Tabata, (private communication).
/11/ L. Kiss, J. Polym. Sci. (in press).
/12/ F. Yoshii, T. Abe, N. Hayakawa, N. Tamura, Kobuushi Ronbunshu 32/7, 406 (1975).
/13/ V. F. Cramer, Einschluss-Verbindungen. (Transl. from Germán to Russian) Izd. Innost. Lit. p. 121, (Moscow, 1958).
/14/ A. L. Karasef, Khimija Vysokyh Energii 6/6, 519 (1972).
/15/ R. Bensasson, A. Bernas, M. Bdard, R. Marx, J. Chem. Phys. 60, 950 (1963).

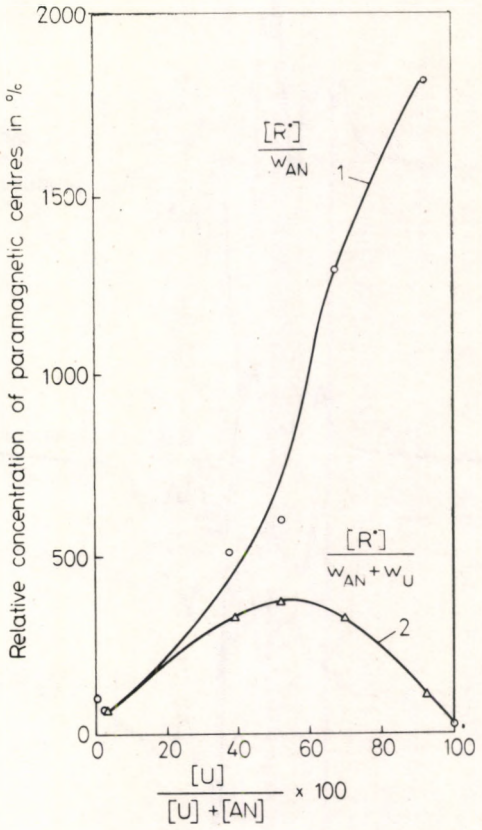

Fig. 1 Dependence of the relative concentration of the paramagnetic centres on the mole% of urea content in the reaction mixture. Ageing time at 195 K is 72 hr; Dose-rate: 0.06 Mrad/hr; total dose: 0.36 Mrad. Temperature of the irradiation: 77 K. Curve 1: calculated with respect to the acrylonitrile content of channel complex; Curve 2: calculated with respect to the weight of the reaction mixture

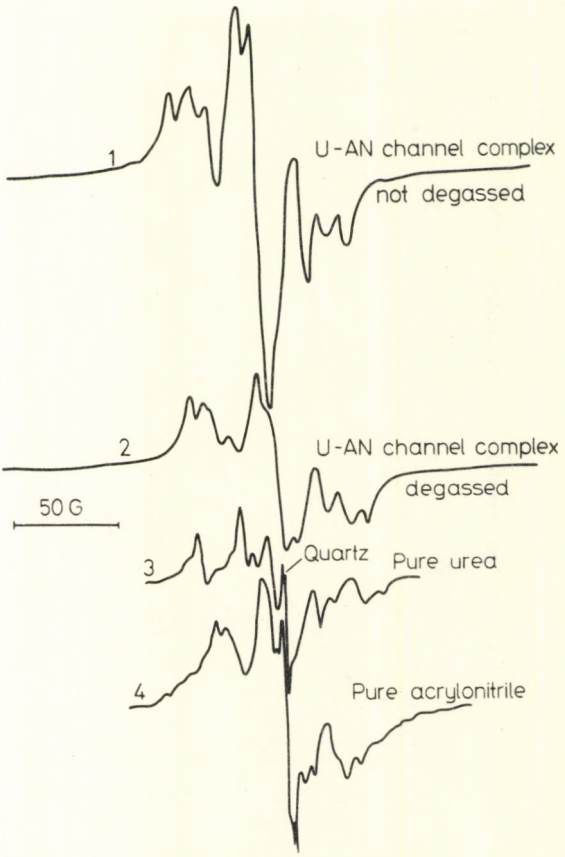

Fig. 2 ESR-spectra of not degassed (1), degassed (2) acrylonitrile channel complexes in comparison with that of pure urea (3) and pure acrylonitrile (4). Temperature of the irradiation 77 K; Dose-rate: 0.06 Mrad/hr; total dose: 0.36 Mrad

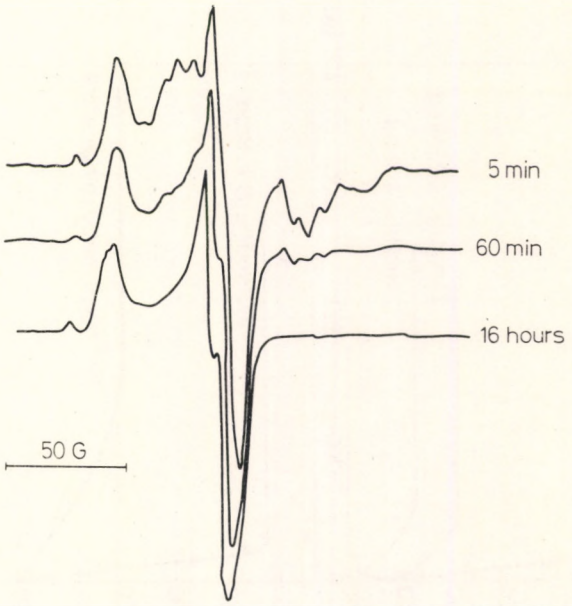

Fig. 3 ESR-spectra of gamma irradiated urea-acrylonitrile channel complex, aged at 195 K for different periods of time. Temperature of the the irradiation: 77 K; Dose rate: 0.06 Mrad/hr; total dose: 0.36 Mrad

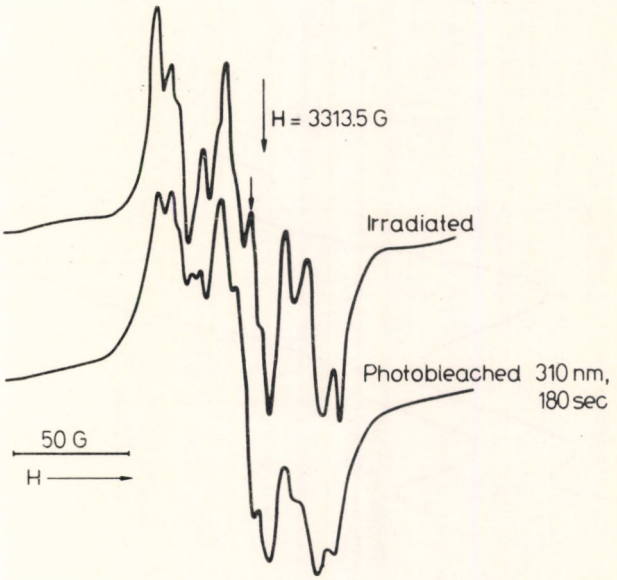

Fig. 4 Photobleaching of the ESR-spectrum of the gamma irradiated urea-acrylonitrile channel complex. The sample was irradiated at 77 K. Dose-rate: 0.06 Mrad/hr; total dose: 0.36 Mrad

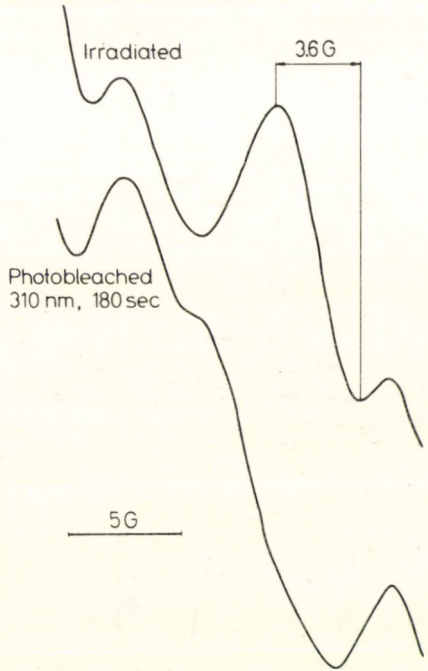

Fig. 5 The middle part of the spectrum, shown in Fig. 4

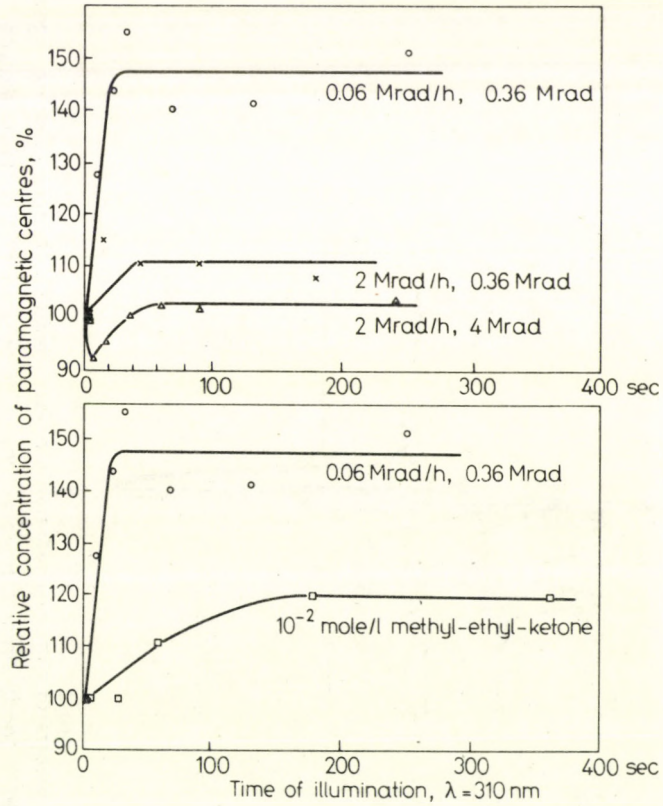

Fig. 6 Dependence of the relative radical concentration on the time of photobleaching. (λ = 310 nm)

H. HEUSINGER

You detect trapped electrons and radical anions. Where is the positive charge located?

L. KISS

In the hexagonal urea matrix.

A. KARASEV

Did you observe the signal of the urea radicals in the inclusion compound? Are the urea molecules damaged by radiation?

What was the urea content you used for generation of the peroxy radical? Is this radical observed with all composition of the mixture?

L. KISS

The spin concentration in urea is much less than that in the included acrylonitrile. I think that the urea lattice is not appreciably damaged.

Peroxy radicals were observed for all mixture compositions including the 48 mol % acrylonitrile 52 mol % urea one which is the composition of the complex. This was proved by us using differential scanning calorimetry and also by Japanese researchers using NMR technique. No peroxy signal could be detected in the polycrystalline tetragonal urea.

Y. TABATA

Where is the trapping site of the ions? It is difficult to get a perfect crystal of the urea complex. Don't you think that electrons and ions may be trapped in disordered regions?

Did you assign the initiating and propagating species? Did you observe any transformation of radicals by elevation of the temperature or by photobleaching?

L. KISS

I think that electrons and ions are stabilized in the defect sites inside the channel while the positive charges in the urea matrix.

We tried to assign the paramagnetic species. The structure of the anion radical is considered to be following

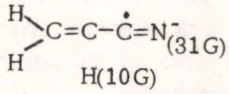

(a)

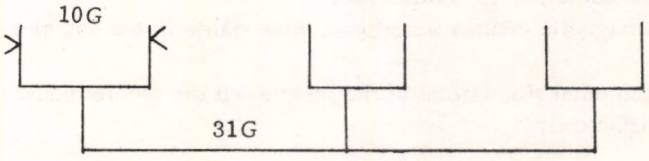

Besides that an octet is found in the spectrum corresponding to

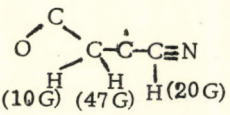

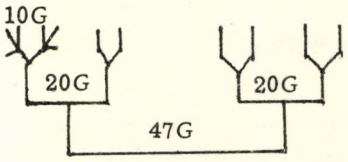

I think that these radicals are formed by irradiation of the polymer chains.

In the spectrum two doublets of separation of 168 and 280 gauss are also observed. The corresponding species have not yet been identified.

By increasing the temperature the spectrum changes appreciably, the transformed radical structures have not been identified yet. The character of the spectra are similar to those observed by you, Ref. /10/. Photobleaching effect is shown in Fig. 4 of the paper.

H. KASHIWABARA

According to your Fig. 1 it seems that you show energy transfer being effective in the complex system. Is that correct?

Concerning the decay behaviour of the paramagnetic centres in the complex did you observe any difference between the decay behaviour in pure acrylonitrile and that in the complex?

You showed an identification diagram of the radicals. Did you make computer simulation in order to identifity the spectra observed?

L. KISS

Curve 1 of Fig. 1 indeed seems to indicate energy transfer. In this case the relative concentration of the paramagnetic centres was calculated with respect to the acrylonitrile content. When, however, this concentration is related to the total weight (curve 2), a maximum is exhibited at about equimolar ratio of the components. This ratio was found to correspond to the composition of the complex. As the yield of the paramagnetic centres in the free tetragonal urea is by a factor of 500 less than that in the complex I think that it is not needed to assume energy transfer here.

The paramagnetic centres were found more stable in the complex than in pure polyacrylonitrile.

We did computer simulations of the spectra but the species could not be separated and identified satisfactorily.

TEMPERATURE DEPENDENCE OF THE IRRADIATION EFFECTS IN POLYTETRAFLUOROETHYLENE

H. Kashiwabara, S. Shimada, H. Hori, H. Imamura, J. Itoh
Nagoya Institute of Technology, Showa-ku, Nagoya 466, Japan

Polytetrafluoroethylene (PTFE) is a well known material as a typical fluorinated polymer and its irradiation effects have been studied by many authors since the investigation of the irradiation effect in polymers started more than twenty years ago. Main chain scission and the increase of the crystallinity are the well known facts in respect of the irradiation effect of PTFE. On the other hand, PTFE is interesting with respect to the study of the molecular motion in the solid phase. With respect to these characteristics the temperature dependence of the irradiation effects of PTFE presents an interesting problem. In the present paper, data on the temperature dependence of the change of molecular weight and that of crystallinity will be reported and related considerations in connection with the knowledge of molecular motion will also be presented.

Molecular weight was estimated by the measurement of the enthalpy of fusion which was determined from the the DSC curve. Molecular weight, M_n, is known to be correlated with the enthalpy of fusion, ΔH_c, by the following equation /1/

$$M_n = 2.1 \times 10^{10} \Delta H_c^{-5.16} \qquad (1)$$

Reduction of the molecular weight of PTFE by the irradiation was reconfirmed using the above equation and molecular weights estimated were plotted against the dose of γ-irradiation at room temperature in Fig. 1. The materials were also subjected to γ-irradiation up to the total dose of 1 Mrad at liquid nitrogen temperature and at various temperatures ranging from 0 to 200°C. Molecular weights after irradiation at various temperatures were also estimated according to Eq. (1) and they are plotted against the temperature of the irradiation. Table 1 shows the effect of temperature of irradiation to the change of the molecular weight. Figure 1 indicates that reduction of the molecular weight after the irradiation has a kind of saturation character at a dose of 2 Mrad and no drastic reduction of the molecular weight appears for much larger doses than 2 Mrad. This must be a reflection of competition between main chain scission and recombination of the degraded portions. Since the cage effect cannot be so strong in the amorphous region, degraded molecules in the

same region can be arranged into the crystalline part. Thus, the molecules, which can escape from recombination after degradation, must be reduced with increasing dose, and the degradation process should be saturated at a certain dose. This kind of consideration is supported by the data presented Table 1, i.e. it shows a rather drastic decrease of the molecular weight after the irradiation at higher temperatures than the temperature ranges in which the relaxation processes in the amorphous phase start. From Table 1, Fig. 2 can be drawn and this shows schematically the situation mentioned above.

The change of the crystallinity due to the irradiation was also affected by the post-irradiation heat treatment. IR spectrometry was applied to the study of crystallinity. Film-shaped specimen with thickness of 67 was irradiated at room temperature up to the various doses (dose rate of 2.5×10^5 r/hr). Post-irradiation heat treatment was also carried out at various temperatures ranging from room temperature to 300°C for 2 hours and absorbances were measured at the wave numbers of 778 cm and 2368 cm, respectively, by an IR spectrometer. These measurements give us the percent concentration of the trans $-CF_2-$group. According to a simple assumption of two phases, crystalline and amorphous, the following relation between extinctions for amorphous and crystalline parts can easily be obtained,

$$E_c^i = \frac{E_c^o}{C_c^o} - \frac{E_c^o}{E_a^o}\frac{C_a^o}{C_c^o} E_a^i \qquad (2)$$

where E means extinction, C means concentration, subscripts a and c correspond to amorphous and crystalline, superscript i means state of the actual measurement, and superscript o stands for a standard state.

Practically, $\frac{E_c^o}{C_c^o}$, $\frac{E_c^o}{E_a^o}$ and $\frac{C_a^o}{C_c^o}$ must be constant quantities, and these quantities can be determined experimentally by the following procedure: Plots of E_o^i against E_a^i and determination of the factors, A and B, in the equation of the type,

$$E_c^i = A + B \cdot E_a^i \qquad (2)$$

by use of the method of least squares. Thus the crystallinity C_c^i can be estimated from the relation

$$C_c^i = E_c^i / A \ , \ (A = E_i^o / C_c^o) \qquad (3)$$

Table 1
Effect of Temperature of Irradiation on Molecular Weight

Temperature (°C)	Mn (x10^4)	Temperature (°C)	Mn (x10^4)	Temperature (°C)	Mn (x10^4)
-196	7.4	73	3.0	140	1.9
0	3.9	80	2.8	150	1.9
9	4.4	90	2.5	160	1.7
31	3.2	100	1.9	170	1.9
40	3.3	110	1.6	180	2.1
50	3.5	120	1.9	190	1.7
60	3.2	130	1.4	200	1.6

Figure 3 shows the data arranged in this way. The abscissa of Fig. 3 indicates the extinction of the amorphous-band and the ordinate means that of the crystalline-band. Values of A and B in Fig. 2' were obtained by the use of the method of least squares, and they were 0.213 and −0.050, respectively, as shown in the figure. Figure 4 indicates the variation of the crystallinity due to post-irradiation heat treatment, and the values were estimated by the use of Eq. (3). We can say that crystallinity increases drastically after the post-irradiation heat treatments at higher temperatures than the temperature range in which the molecules in the paracrystalline phase are set to the motion. According to the viscoelastic study by McCrum it is called glass I transition, /2/ and according to the MMR study by Iwayanagi and Sakuraki it is called transition in the paracrystalline phase /3/. Degraded molecules in the paracrystalline phase can easily be rearranged to the regular crystal when they are set to the motion. This is a cause of the remarkable increase of the crystallinity due to the post-irradiation heating mentioned in the above part of the present paper /4/. Crystallinity change due to the irradiation can also be arranged from the same data of extinction measurements. The relation between crystallinity and dose of irradiation is shown in Fig. 5 and it indicates that the increase of crystallinity due to the irradiation saturates at the dose of ca. 2 Mrad and this can also be a reflection of the competition between degradation and recombination of the degraded molecules as mentioned in the case of the molecular weight change due to the irradiation.

References

/1/ T. Suwa, M. Takehisa, S. Machi, J. Appl. Polym. Sci. 17, 3253 (1973).
/2/ N. G. McCrum, Macromol. Chem. 34, 50 (1959).
/3/ S. Iwayanagi, I. Sakuraki, J. Polym. Sci. C. No. 14, 29 (1966).
/4/ Similar phenomenon can also be observed in broad line NMR study of PTFE, M. Tutiya, Japan. J. Appl. Phys. 7, 440 (1968).

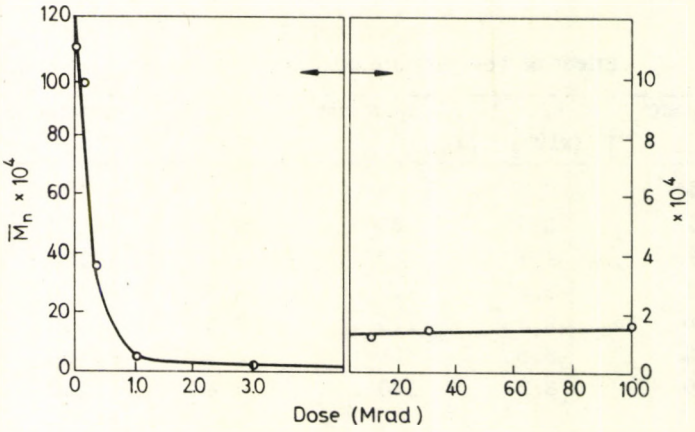

Fig. 1 Relation between molecular weight and dose of irradiation

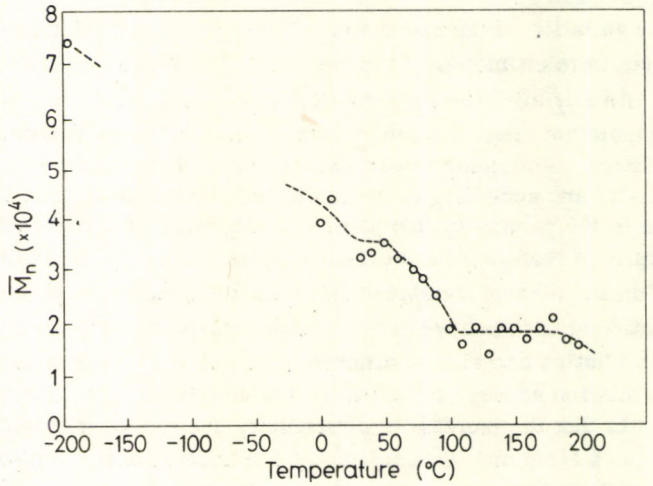

Fig. 2 Relation between molecular weight and irradiation temperature

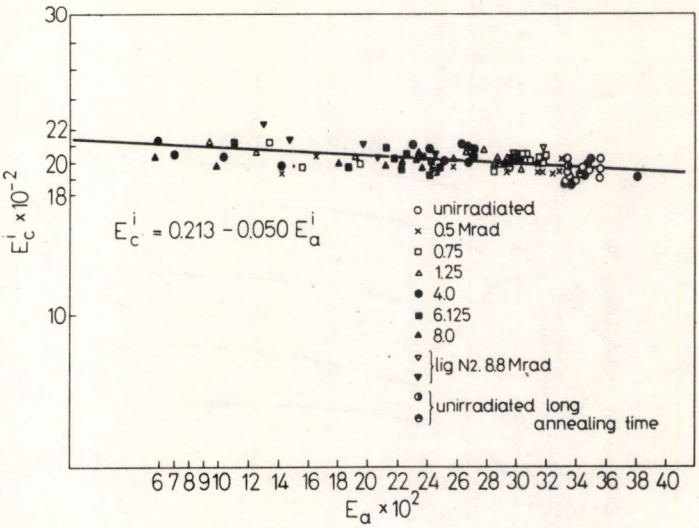

Fig. 3 Arrangement of the data of extinction measurement in connection with Eq. (3). Descriptions in the figure indicate dose of irradiation and other irradiation conditions

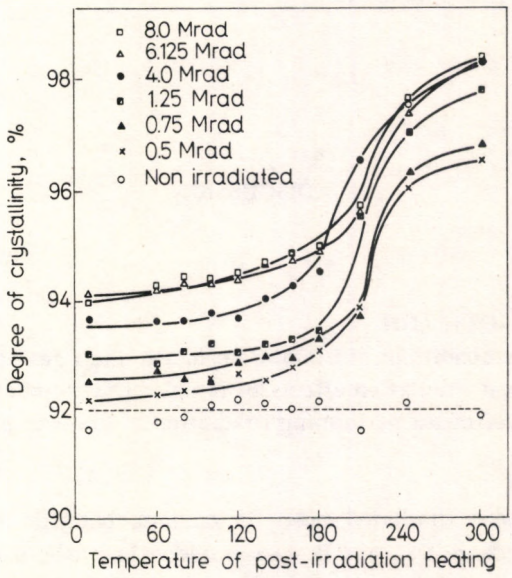

Fig. 4 Relation between crystallinity and temperature by post-irradiation heating

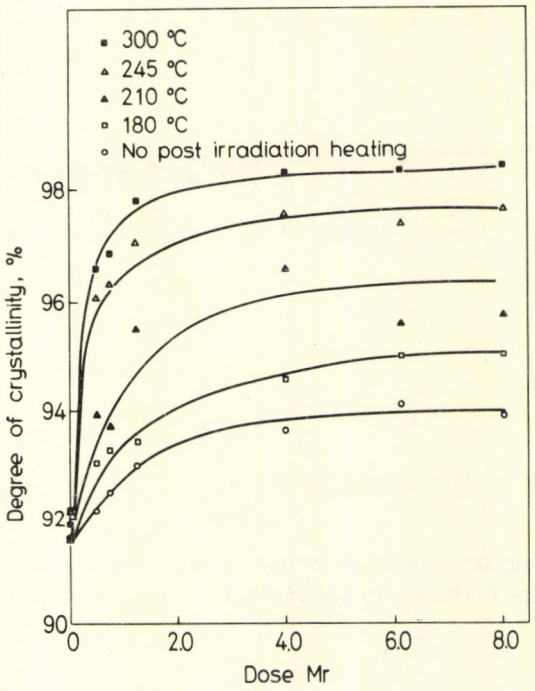

Fig. 5 Relation between crystallinity and dose of irradiation, post-irradiation heating temperatures are indicated

DISCUSSION

J. ZURAKOWSKA-ORSZÁGH

What were the conditions of irradiation: in air, inert gas or vacuum?

You studied post irradiation effects for samples irradiated at room temperature. Did you do similar experiments performing irradiation at lower temperatures?

H. KASHIWABARA

The samples were irradiated mostly in vacuum, but after irradiation they had to be subjected to air because DSC and IR measurements had to be made in air.

If irradiation at very low temperature were made the results could be much clearer. In our experiments just one example of irradiation at liquid nitrogen temperature was

obtained. In this case crystallinity was also remarkably increased by post irradiation heating to 180°C and 300°C.

A. CHARLESBY

Could you provide any information on the remarkably high sensitivity of PTFE to radiation induced degradation which leads to very poor mechanical properties at small doses?

H. KASHIWABARA

It should be interpreted in terms of free radical process. Well, according to my experience irradiated PTE was very brittle; dynamic mechanical measurements were impossible to perform, but IR measurements could be made.

P. HEDVIG

I think I can answer Professor Charlesby's question. I studied radiation degradation of PTFE by different conditions of irradiation and could follow the process step by step by ESR and by measuring the mechanical properties (see J. Polymer Sci. A1, 1145 (1969)). The reaction scheme is the following:

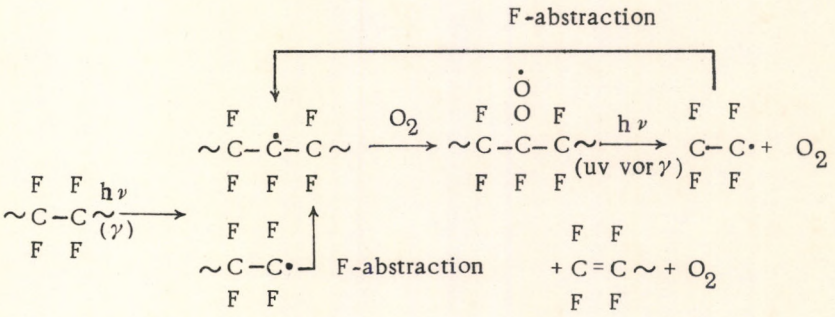

From this scheme it follows that PTFE is degraded by radiation only in the presence of oxygen. Indeed the rupture strain of well deoxygenated samples does not change significantly in the dose range of 1 to 10 Mrad ^{60}Co when they are irradiated in vacuum and oxidized afterwards, while an abrupt fall in the rupture strain is observed for samples irradiated in air.

These results seem to contradict Dr. Kashiwabara's measurements, namely that the number average molecular weight of PTFE irradiated in vacuum drops abruptly at a dose of about 1 Mrad (Fig. 1). In this region the mechanical properties of the polymer irradiate in vacuum are quite stable, but for those irradiated in air a similar dose dependence of the rupture strain is observed – as seen in Fig. 1 of Dr. Kashiwabara's paper for the molec

ular weight. Therefore I think that some oxygen might have been present in these experiments during irradiation.

H. KASHIWABARA

I did not talk about the change of the mechanical properties of PTFE due to irradiat but I would like to emphasize that physical properties (relaxation process in solid PTFE) close correlation with the increase of crystallinity.

Your comment on the mechanism of the degradation is very reasonable, this mecha nism of yours is well known, but I wanted to show that the saturation character of the ir- radiation effect (say Fig. 1) must be an indication for a competition between degradatio and recombination due to the cage effect in the crystalline phase.

SOME ASPECTS OF RADIATION-INDUCED TRANSFORMATIONS OF CELLULOSE

W. M. Dziedziela, J. Rosiak
Institute of Applied Radiation Chemistry, Wróblewskiego 15, Łódź, Poland

The radiation modification of cellulosic materials has reached the industrial applications stage /1,2/. For this reason as full as possible investigations of the influence of ionizing radiation on cellulose are necessary. Irradiation considerably changes the structure, reactivity and physicochemical and mechanical properties of cellulose. The magnitude of these alteration depends on the conditions of irradiation and the alteration depends on the conditions of irradiation and the nature of cellulose substrate and its morphology /2,3/.

The main object of the present investigations was linen cellulose. To our knowledge no data on the radiolysis of this material has been reported. Radiation effects in linen and cotton cellulose were compared. In particular, the influence of air and radiation dose from ^{60}Co on radical yields, carbonyl and carboxyl contents and polymerization degree of cellulose chains were investigated.

Experimental

Desized, bleached and mercerized commercial linen (170 g/m^2) and cotton (142 g/m^2) fabrics were used as sources of cellulose. Defibred fabrics were purified by conventional procedure /4/, air dried and conditioned (21°C, 65% RH) to moisture content 6.5% in cotton and 7.8% in linen fibre.

The initial number average degrees of polymerization of linen and cotton cellulose were 500 and 670, respectively. The samples placed in glass ampoules were irradiated with ^{60}Co γ-rays at room temperature. Some of the samples before sealing were degassed to 10^{-4} mm Hg. The dose rate estimated with modified Fricke dosimeter was 0.54 Mrad/h.

For ESR experiments samples were irradiated in scaled quartz ampoules at 77 K. ESR spectra were taken with a SE-X/2 spectrometer at temperature of liquid nitrogen. Free radical concentrations were calculated by double integration of ESR spectra of the samples and the standard (DPPH).

The carbonyl content in irradiated cellulose was determined by the method described in /5/, the carboxyl groups by Davidson and Nevell method /6/.

In order to determine the molecular weights of cellulose, samples were converted into their trinitrates by using the undegradable method described by Alexander and Mitchel /7/ Nitrogen content in the products (ca. 13.6%) was estimated by using nitron reagent /8/. Cellulose nitrates were dissolved in ethyl acetate (0.5–4g/l) and intrinsic viscosities were measured at 25°C with a Ubbelohde viscometer. Parallel determinations of number average molecular weights were carried out by a Hewlett - Packard 501 osmometer. The determined intrinsic viscosities as well as molecular weights were adjusted for nitrogen content /8/. The ampoules with the samples for determination of molecular weights, CO and COOH groups were opened 10 and 45 days after irradiation and the appropriate measurements were carried out.

Results and discussion

Formation of free radicals. ESR spectra of linen cellulose irradiated at liquid nitrogen temperature with dose 2.5 Mrad are shown in Fig. 1. On comparing the spectra of degassed and aerated samples one can find that oxygen does not change the shape of the ESR signals. Heating of irradiated samples to 303 K is followed by irreversible changes of shape and decreasing of signal intensity, especially in the case of aerated samples (see Fig. 2). This latter effect can be assigned to the effect of moisture contained in the air above the sample /9/.

The obtained spectra of linen cellulose are practically identical with those recorded in the case of cotton cellulose II /10/. It is noteworthy to mention that samples irradiated in liquid nitrogen show after heating the same spectra as those irradiated at room temperature /11,12/. Assuming that analysis of hyperfine structure of ESR spectrum for cotton cellulose irradiated at 77 K /10/ is valid also for linen cellulose, one can conclude that the above presented spectrum is the superposition of several kinds of radicals with the highest fraction of the radical localized on C_5.

In Fig. 2 the concentration of free radicals in linen cellulose is plotted against radiation dose. At 77 K the presence of oxygen does not influence the yield of free radicals (curve 1). For doses above 2 Mrad the dose dependence of concentration of free radicals is not linear. Similar effect of "saturation" has also been observed in the case of partially hydrolized cellulose irradiated at 77 K /13/. This phenomenon can be explained by the low thermal stability of that part of radicals at liquid nitrogen temperature which are disappearing during irradiation.

It has been supposed /10/ that this decay is connected with recombination of radicals which form radical pairs. After heating of the samples to 303 K a further fraction of radicals disappears especially in aerated samples, but the residual concentration is proportional to the dose (curves 2 and 3).

Formation of carbonyl and carboxyl groups. Like for cotton cellulose /5/ and wood pulp /14/ irradiation of linen cellulose results in increase of the concentration of oxidized (carbonyl and carboxyl) groups. Results for linen and cotton celluloses are shown in Fig. 3.

The concentration of carboxyl and carbonyl groups increases with absorbed dose, the changes being more evident for the latter. No difference between yields of these groups in both kinds of cellulose has been observed. The concentration of carbonyl groups in the samples irradiated in air is only slightly higher than in vacuum. This indicates that the majority of these groups form as a result of internal transformation of the anhydroglucose units. Some of these transformations lead to scission of the cellulose chain /15/. Results of determinations carried out 10 days and 45 days after irradiation were the same, within the range of experimental error.

Degradation of cellulose. Scission of the chains is the main effect in irradiated cellulose and it results in decrease of the polymerization degree. DP values are usually calculated from viscosity measurements of cellulose solutions in suitable solvent (e.g. Cuam, Cuen, Cadoxen) /16-18/. These solvents are strongly alkaline and the dissolved cellulose can undergo oxidative degradation /19/, as well as degradation connected with the presence of carbonyl groups in irradiated cellulose /5/.

For these reasons such a procedure has been chosen which consists in conversion of cellulose into its trinitrate, determination of molecular weights of this derivative by osmometry in ethyl acetate solution, and calculation of number average degrees of polymerization. Calculations were corrected for nitrogen content in nitrated samples. To our knowledge no procedure of this kind has been applied in relation to irradiated cellulose. Results are shown in Table 1.

Data in Table 1 support the conclusion /17/ that the presence of air during irradiation practically does not influence the degradation of cellulose. In contrast to earlier suggestions /20/, for air-dried cellulose post-irradiation degradation has not been observed.

In order to calculate G (scission) of cellulose chains it was necessary to check the correctness of the procedure used. For this reason parallel osmometric and viscometric measurements of nitrated celluloses were carried out. In Fig. 4 intrinsic viscosities are plotted as a function of number average molecular weights in a logarithmic scale. The experimental results may be represented by a straight line, which can be expressed with the equation

$$[\eta] = 5.0 \times 10^{-5} \bar{M}_n^{1.03} \qquad (1)$$

A very similar equation (2) was obtained earlier /21/ for various kinds of celluloses which were not radiation degraded

$$[\eta] = 3.8 \times 10^{-5} \bar{M}_n^{1.03} \qquad (2)$$

Neglecting the small difference due to the lack of nitrogen content one can state almost perfect agreement with the experimental results.

This proves that a correct method has been used in the present work and also shows that the decay of radicals during nitration of irradiated cellulose /22/ does not cause further degradation of cellulose.

Table 1

Number average degree of polymerization of linen and cotton celluloses irradiated with ^{60}Co gamma rays under various conditions

Dose (Mrad)	Degree of polymerization							
	linen				cotton			
	air		vacuum		air		vacuum	
	after		after		after		after	
	10 days	45 days	10 days	45 days	10 days	45 days	10 days	45 days
0	500	–	500	–	670	–	670	–
0.5	–	385	–	365	401	401	404	399
1.1	287	339	316	313	322	346	342	364
2.2	260	234	266	240	313	306	280	282
5.9	173	164	171	171	196	–	234	–
9.7	155	158	151	143	159	–	153	150

The number average molecular weights of cellulose calculated from values given in Table 1 allowed us to make the graph shown in Fig. 5.

Practically no difference exists between the points for linen and for cotton. According to Charlesby's theory of degradation /23/ one can calculate yields of radiation degradation of cellulose

$$G_{/sc/} = 0.965 \times 10^{6} \times D^{-1} [\bar{M}_{n}^{-1} - \bar{M}_{no}^{-1}] \qquad (3)$$

where $\bar{M}_{no}$ and $\bar{M}_{n}$ are number average molecular weights before and after irradiation, respectively, and D is the dose (Mrad). Using the least squares method $G_{/sc/} = 2.9$ was obtained. In spite of many reports on radiation degradation of cellulose only in a few of them are the $G_{/sc/}$ values given. They range from 2 to 25 /15, 17, 18/.

We believe that such considerable differences can be ascribed to the various methods of viscosity measurements used and to the application of various relationships between molecular weight and intrinsic viscosity as well as to making an assumption on random distribution of molecular weights of cellulose irradiated even with small doses. In several reports there is a suggestion of dose dependence of $G_{/sc/}$ /15-17/. The radiation degradation yield obtained in the present work calculated from direct measurements is close to the yields of degradation and crosslinking for the majority of synthetic polymers /24/ as well as to the yield of cleavage of the glycosidic bonds irradiated in the solid state methyl α-D-glucopyranoside (G(glycose) = 2.33) /25/.

References

/ 1/ A.S. Hoffman, in Proc. Symp. Utilization of Large Radiation Source and Accelerators in Industrial Processing, Munich, 1969.

/ 2/ J.T. Guthrie, Polymer, 16, 134 (1975).

/ 3/ Cr. Simionescu, R. Butnaru, and Gh. Rozmarin, Cellulose Chem. Technol. 7, 153 (1973).

/ 4/ J.H. Kattering, and C.M. Conrad, Ind. Eng. Chem., Anal. Ed. 14, 432 (1942).

/ 5/ J.C. Arthur, F.A. Blouin, and R.J. Demint, Amer. Dyestuff Reptr., 49, no 11, 383 (1960).

/ 6/ G.F. Davidson, and T.P. Nevell, J. Text. Inst. 39, T 102 (1948).

/ 7/ W.T. Alexander, and R.L. Mitchel, Anal. Chem., 21, 1497 (1949).

/ 8/ C.H. Lindsley and M.B. Frank, Ind. Eng. Chem. 45, 2491 (1953).

/ 9/ O. Hinojosa, Y. Nakamura and J.C. Arthur, J. Polymer Sci., Pt. C, No. 37, 27 (1972).

/10/ D.S. Khamidov, U.A. Azizov, N.K. Milinchuk, and Kh.U. Usmanov, Vysokomol. Sojedin. 14, No. 4, 838 (1972).

/11/ S. Dilli, J.T. Ernst and J.L. Garnett, Aust. J. Chem. 20, 911 (1967).

/12/ M. Shimada, Y. Nakamura, Y. Kusama, O. Matsuda, N. Tamura, and E. Kageyama, J. Appl. Polymer Sci., 18, 3387 (1974).
/13/ Kh. Usmanov, U.A. Azizov, V.K. Milinchuk, and D.S. Khamidov, J. Polymer Sci., Symp. No 42, 1607 (1973).
/14/ R. Imamura, T. Ueno, and K. Murakami, Bull. Inst. Chem. Res., Kyoto Univ., 50, No. 1, 51 (1972).
/15/ P.K. Christensen, and B.M. Tolbert, Norsk Skogindustri, 19, No. 1, 12 (1965).
/16/ A.U. Ahmed, and W.H. Rapson. Nucl. Sc. Appl., 5 A, No. 4, 33 (1969).
/17/ A. Sakurada, T. Okada, and K. Kaji, J. Polymer Sci., Pl, C, No. 37, 1 (1972).
/18/ J.T. Guthrie, M.B. Huglin, and G.O. Phillips, J. Polymer Sci., Pl. C., No. 37, 205 (1972).
/19/ S.N. Danilov, T.J. Samsonova, and L.S. Bolotnikova, Usp. Khimii, 39, No 2, 336 (1970).
/20/ Kh. U. Usmano, and N. Vakhidov, Vysokomol. Sojedin., 11, No. 7, 1501 (1969).
/21/ E.H. Immergut, B.G. Ranby, and H.F. Mark, Ind. Eng. Chem., 45, No. 11, 2483 (1953).
/22/ W.M. Dziedziela, J. Rosiak (unpublished results)
/23/ A. Charlesby, M. Ross, and P. Alexander, Proc. Roy. Soc. A 223, 392 (1954).
/24/ "The radiation chemistry of macromolecules", ed. M. Dole, Academic Press, New York, London 1973, vol. II.
/25/ G.O. Phillips, F.A. Blouin, and J.C. Arthur, jr., Radiat. Res. 23, 527 (1964)

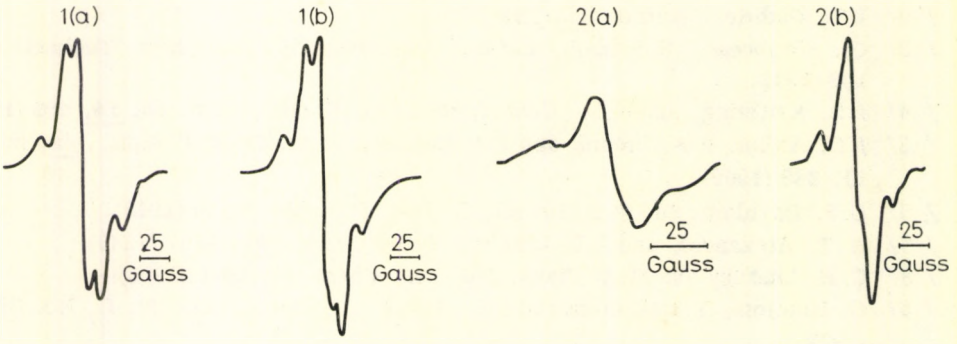

Fig. 1 ESR spectra of linen cellulose irradiated at 77 K in air /1a/ and in vacuum /1b/ 2a and 2b – the same samples after heating to 330 K for 5 min. Dose 2.5 Mrad, temperature of measurement 77 K.

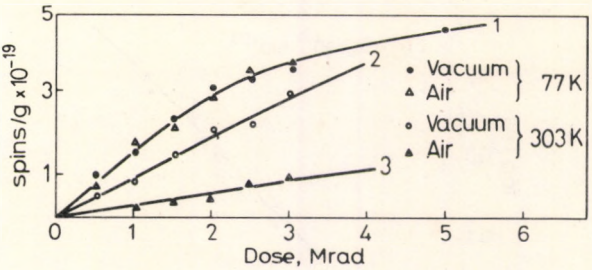

Fig. 2 Radical formation in linen cellulose. Curve: 1 - irradiation at 77 K, 2 - irradiation at 77 K and heating to 303 K for 5 min (vacuum), 3 - irradiation at 77 K and heating to 303 K (air). Temperature of measurement 77 K, standard - DPPH

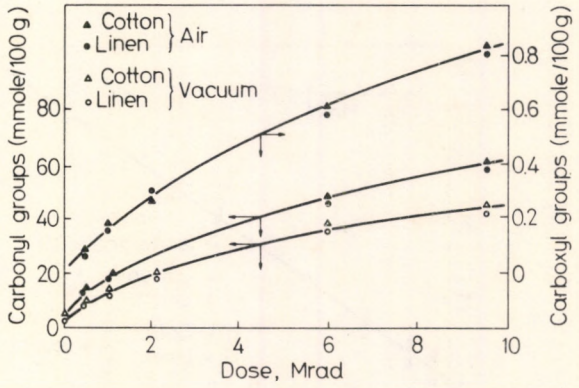

Fig. 3 Concentration of carbonyl and carboxyl groups formed in irradiated linen and cotton celluloses

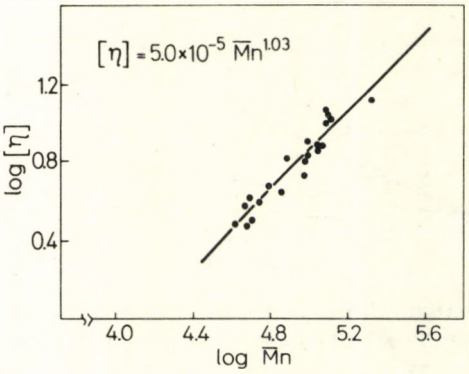

Fig. 4 Intrinsic viscosities versus number average molecular weights of cellulose nitrate in ethyl acetate at 25°C.

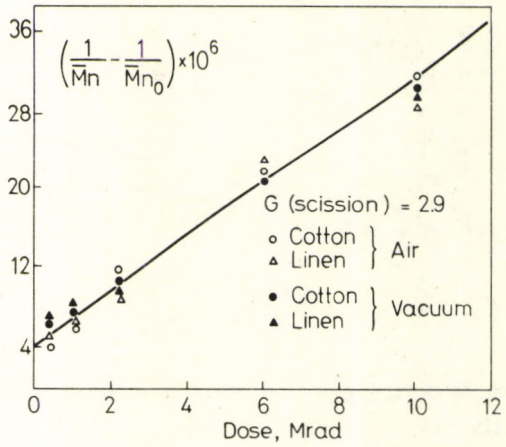

Fig. 5 Influence of radiation dose on yield of scission of linen and cotton cellulose chains

J. PUIG

Did you try to investigate the effect of water content of the cellulose samples during irradiation? In other words: do you think that the ratio of scission to crosslinking in cellulose is influenced by water?

W. M. DZIEDZIELA

Cellulose belongs to those polymers which only degrade by irradiation. Up to now there is no direct evidence for radiation induced formation of crosslinks in cellulose. We did not study the influence of water content of cellulose on radiation degradation of cellulose, but it has been done earlier by Arthur et al. (Amer. Dyestuff Rep. 49, 383 (1969)) and by Glegg and Kertész (J. Polym. Sci. 26, 289 (1957)). No significant effect has been observed.

L. WUCKEL

I wonder why you found no peroxy radicals under irradiation in air. This is of interest because polymers can undergo a chain peroxidation process. The question is: is that the case in cellulose too?

W. M. DZIEDZIELA

There is no common view on the formation and stability of peroxide groups in air-irradiated cellulose (Sakurada et al. J. Polymer Sci., (C) No. 37, 1 (1972)). We believe that in cellulose, as opposed to some synthetic polymers, a chain peroxidation process does not take place because the shapes of the ESR spectra of the samples irradiated in air and in vacuum are very similar. This is true for the case of irradiation at room temperature (Sakurada) and at the temperature of liquid nitrogen (this report).

A. CHARLESBY

This work provides a most useful value for G(scission). Was this for air or vacuum irradiation, and can you find any difference between degradation in the amorphous and crystalline regions? This could perhaps be done by dissolving and recrystallizing the same material before repeating the radiation treatment and measurements.

W. M. DZIEDZIELA

Within the range of experimental error no difference between G(scission) for air and vacuum irradiation has been observed (see Fig. 5). The investigation of the influence of crystallinity was beyond the scope of this work. Undoubtedly there is some difference in the crystallinity of the linen and cotton celluloses used in our experiments. The G(scission) values, however, are the same for both types of cellulose.

Your suggestion is very interesting, we shall try to check it.

KINETIC STUDIES OF THE DEGRADATION OF POLYMERS IN SOLUTION

D. Lindenau, G. Beck, U. Hagen,* W. Schnabel
Hahn-Meitner-Institut für Kernforschung Berlin GmbH, Bereich Strahlenchemie, D 1000 West Berlin

Introduction

Recently a device has been developed in our laboratory which serves to monitor the change of the intensity of scattered light after irradiating a system with a short pulse of ionizing radiation or with a flash of UV light /1–7/. The time resolution is about one μs. In conjunction with pulse radiolysis or laser flash photolysis the following reactions can be investigated: (a) growth of macromolecules (polymerization), (b) crosslinking of macromolecules, (c) main chain degradation of macromolecules. In the latter case the observed lifetime of the LSI change can be correlated with an intermediate leading to main chain rupture or to the diffusion time of the fragments generated by main chain scission. If the time to accomplish a bond rupture is sufficiently short the diffusion of the fragments is the rate determining step with respect to the observed change of LSI. This kind of behaviour was at first found with dilute solutions of polyphenylvinylketone /1/, where the disentanglement of coiled macromolecules could be directly observed. Recently evidence for the preferential solvation of macromolecules could be obtained by our method /6/.

In this paper results are reported which were obtained during the electron irradiation of polyisobutene (PIB), polymethylmethacrylate (PMMA), polymethylvinylketone (PMVK) and native calf thymus deoxyribonucleic acid (DNA).

Experimental

The apparatus used is shown schematically in Fig. 1. It has been described in detail before /1–3/. The cell with the polymer solution is irradiated with 2 μs pulses of 15 MeV electrons from an L-band linear accelerator (Vickers). The analysing light was provided by an argon-ion laser (Spectra-Physics, model 165–00) with a nominal output of 2 W. The light passed the cell at right angles with respect to the electron beam. The scattered light was directed over a light guide to the photomultiplier. The signal was displayed on a storage oscilloscope.

*Nuclear Research Centre, Karlsruhe, Institute for Radiation Biology

The polymers PMVK and PMMA were polymerized by ^{60}Co-γ-rays. PIB samples were obtained by courtesy of BASF AG. The calf thymus DNA was isolated in the laboratory of Prof. U. Hagen in the Kernforschungszentrum Karlsruhe (Institut für Strahlenbiologie).

The solvents were of highest commercial purity and were fractionally distilled before use. Polymer solutions were freed from oxygen by bubbling with argon which was purified beforehand by Oxisorb (Messer-Griesheim).

Results and Discussion

(a) Polyisobutene. Polyisobutene (PIB) undergoes only main-chain scission without simultaneous crosslinking upon irradiation with ionizing radiation.

Figure 2a shows the decrease of LSI caused by the decrease of the average molecular weight observed in solutions of pentane, decane and hexadecane as a function of time. The decay of LSI follows first order kinetics according to Fig. 2b. The halflife $\tau_{1/2}$ (LSI) of the decrease of LSI was not influenced by the addition of cyclohexene, which on the other hand drastically reduced the extent of degradation. It is thus concluded that the time of establishing scissions of bonds in the main chain is much shorter than $\tau_{1/2}$ (LSI) and that the latter corresponds to disentanglement diffusion. This is furthermore evidenced by the following findings: $\tau_{1/2}$ (LSI) increases with decreasing PIB concentration, i. e. with decreasing macroviscosity. However, $\tau_{1/2}$ (LSI) increases linearly with increasing microviscosity as shown in Fig. 3, where $\tau_{1/2}$ (LSI) is plotted as a function of solvent viscosity. Measurements with PIB samples of different average molecular weight $\bar{M}_w$ yielded $\tau_{1/2}$ (LSI) $\propto \bar{M}_w^{0.34}$. This is a significantly weaker dependence on $\bar{M}_w$ than expected for translational diffusion. From this result it is inferred that disentanglement and translatory diffusion can be distinguished.

This reasoning was affirmed by experiments using mixtures of n-propanol and n-hexane as solvents. As shown in Fig. 4, $\tau_{1/2}$ (LSI) increases with increasing n-propanol content. The dependence of $\tau_{1/2}$ (LSI) resembles fairly well the respective dependence of the mean square end-to-end distance indicating that the disentanglement diffusion is easier for loosely ([C_3H_7OH] : 0–10 vol. %) than for tightly ([C_3H_7OH] : 10–20 vol. %) coiled macromolecules.

(b) Polymethylmethacrylate. The oscilloscope traces obtained with PMMA in acetone solution (see Fig. 5) yield evidence for two different intermediates both resulting in main chain degradation: one decaying rapidly with $\tau_{1/2}$ (LSI, fast) $\approx 20\mu s$, the other decaying slowly with $\tau_{1/2}$ (LSI, slow) = 4. 0 ms. Oxygen reacts with the slowly decaying species thus inhibiting the degradation partially (see lower trace in Fig. 5). $\tau_{1/2}$ (LSI, slow) decreases with increasing oxygen concentration indicating that the slowly decaying portion of the LSI change corresponds to the lifetime of an intermediate whose decay leads to main chain scission. It is assumed that this intermediate is a side group radical (P·). From the dependence of the degree of degradation and of

$\tau_{1,2}$ (LSI, slow) on the oxygen concentration the rate constant $k_{O_2 + P\cdot} = 1.4 \pm 0.2 \times 10^6\ M^{-1}\ s^{-1}$ was evaluated.

(c) Polymethylvinylketone. As shown in Fig. 6 the LSI of a PMVK solution irradiated in an oxygen-free acetone solution decreases immediately after the electron pulse with a halflife of about 15 μs indicating a decrease of the molecular weight, i. e. main chain degradation. At a later stage an increase of the LSI is observed caused by intermolecular crosslinking. This case corresponds to the often observed phenomenon of "simultaneous degradation and crosslinking". It appears that we were at the first time able to discriminate kinetically by a relatively high time-resolution of the detection method the two different steps of a so-called" simultaneous process".

Obviously upon radiation of the polymer two different kind of intermediates are formed, one of which causes main chain rupture and is short-lived. It pertains presumably to an excited state. The other one responsible for crosslinking is rather long-lived and probably a lateral macroradical. As is shown by trace (b) in Fig. 6 oxygen decreases the extent of main chain cleavage and prevents crosslinking completely.

(d) Deoxyribonucleic Acid. Recent studies concern the degradation of DNA /7/. Calf thymus DNA was irradiated in oxygen-saturated 0. 01M NaCl solution at a DNA concentration of 0. 07 g/l. Typical results are shown in Fig. 7.

By monitoring the decrease of the LSI after a pulse with an absorbed dose greater than ca. 50 krad a fast decrease in the ms-range was observed which was followed by a slow decrease with $\tau_{1/2}$ (LSI)$\approx$8s. Irradiation with pulses of an absorbed dose smaller than about 10 krad yielded no decrease after the first pulse, but after the second pulse the rapid decay followed by the slow decrease was observed. The results are explained in the following way: fragmentation of the double strands requires scissions of bonds on the single strands. If these scissions are placed at sites directly opposite to each other, the fragments can separate immediately after the pulse. This case is schematically depicted in Fig. 8a. The fast LSI decay is assigned to the diffusion of DNA fragments generated by double strand breaks of this kind. The cleavage process itself must be faster than the shortest value of $\tau_{1/2}$ (fast)$\approx$ lms since $\tau_{1/2}$ (fast) decreases with increasing degree of degradation.

$\tau_{1/2}$ (slow) is attributed to the detachment of segments generated by single strand breaks of the type described in Fig. 8(b). In this case the melting of the segments between the breaking points is necessary before the separation of the fragments can occur. If the length of the segments passes a critical length the melting process becomes rate determining with respect to the decay of LSI and is therefore observable by our method.

Conclusion

The results reported above demonstrate that the time resolved light scattering detection method in combination with pulse radiolysis is capable of investigating a variety of problems concerning chemical reactions as well as the dynamic behaviour

of macromolecules in dilute solution. In a similar way interesting results have been obtained by crosslinking the light scattering detection method with laser flash photolysis /1, 4–6/.

References

/1/ G. Beck, J. Kiwi, D. Lindenau, W. Schnabel, Europ. Polymer Journal 10, 1069 (1974).

/2/ G. Beck, G. Dobrowolski, J. Kiwi, W. Schnabel, Macromolecules 8, 9 (1975).

/3/ G. Beck, D. Lindenau, W. Schnabel, Eur. Pol. J. 11, 761 (1975).

/4/ G. Beck, J. Kiwi, D. Lindenau, W. Schnabel, Colloid and Polymer Science, 254, 162 (1976).

/5/ G. Beck, G. Dobrowolski, J. Kiwi, W. Schnabel in: Lasers in Physical Chemistry and Biophysics, Elsevier Scientific Publishing Company, Amsterdam (1975), p. 283.

/6/ G. Dobrowolski, W. Schnabel, Z. Naturforsch. 31a, 109 (1976).

/7/ D. Lindenau, U. Hagen, W. Schnabel, Z. Naturforsch. 31c (in press).

/8/ A. Henglein, C. Schneider, Z. phys. Chem. NF 19, 367 (1959).

/9/ E. D. Kunst, Recl. Trav. chim. Pays Bas Belg. 69, 125 (1950).

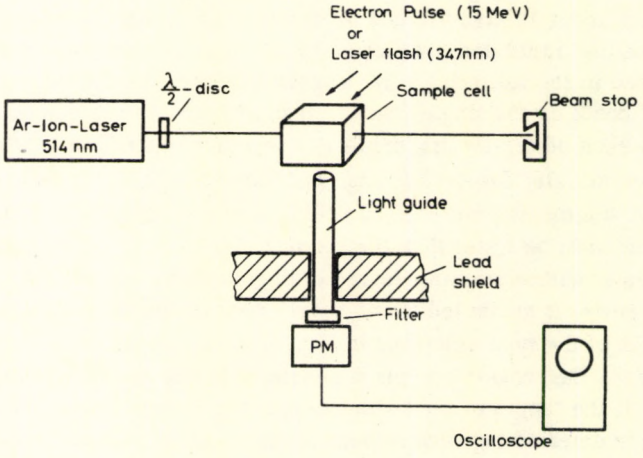

Fig. 1 Schematic diagram of the apparatus

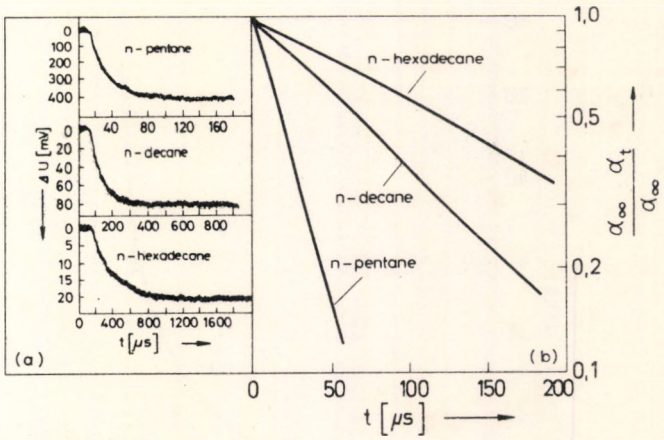

Fig. 2 (a) Oscilloscope traces obtained by monitoring the change of LS intensity after irradiation with a pulse of 15 MeV electrons in different solvents. [PIB]: 0. 027 base mole l^{-1}, $\bar{M}_w$ = 2. 1 × 10^6, absorbed dose 4 × 10^4[rad], pulse length 2 μs
(b) First order plots of data of Fig. 1

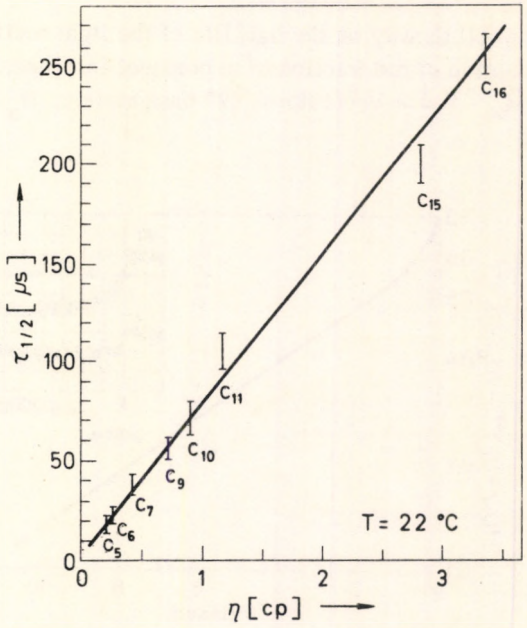

Fig. 3 Influence of microviscosity on the half life of the light scattering signal. $\tau_{1/2}$ (LS) as a function of solvent viscosity. Solvents: n-hydrocarbons from n-pentane to n-hexadecane, $\bar{M}_w$ = 2. 1 × 10^6, [PIB] = 0. 027 base mol/l, D_a = 4 × 10^4 [rad], pulse length 2 μs

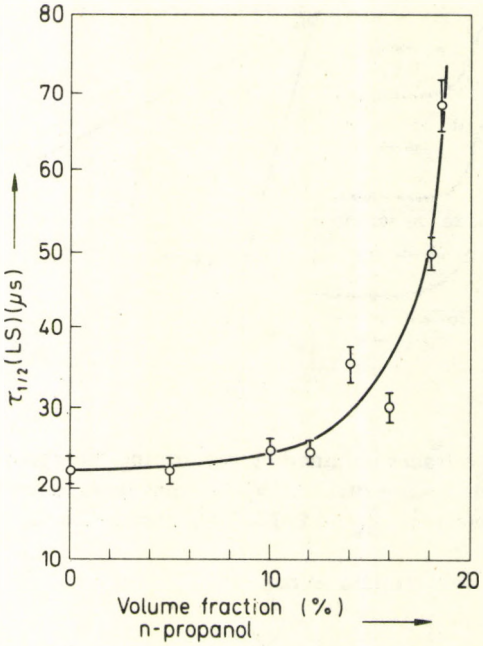

Fig. 4 Influence of coil density on the half life of the light scattering signal. $\tau_{1/2}$ (LS) as a function of the fraction of n-propanol in n-hexane-n-propanol mixtures. $\bar{M}_w = 2.1 \times 10^6$ [PIB]: 0.027 base mole/l. $D_a = 4 \times 10^4$ [rad], pulse length 2 μs

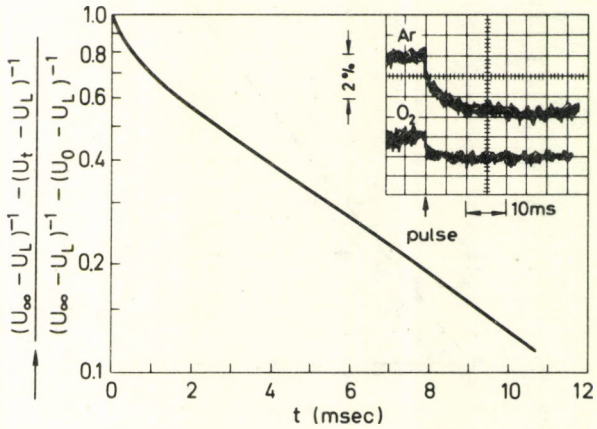

Fig. 5 The decay of the light scattering signal after a 2 μsec-pulse of 15 MeV electrons. PMMA in acetone at 25°. Ar-saturated solution, c: 5×10^{-4} g/ml. $\bar{M}_{w,o} = 9.25 \times 10^6$. Insert: typical oscilloscope traces observed in the presence and absence of oxygen

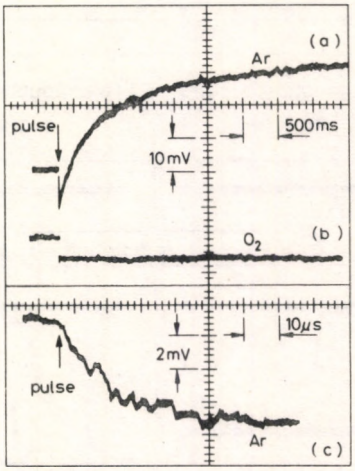

Fig. 6 Pulse irradiation of polymethylvinylketone in acetone solution (2.0 g/1). Dose per pulse: 2×10^4 rad. Oscilloscope traces demonstrating changes of light scattering intensity after the electron pulse (a) in Ar-saturated solution, (b) in oxygen saturated solution, (c) time resolved decay of LSI before the increase (compare (a))

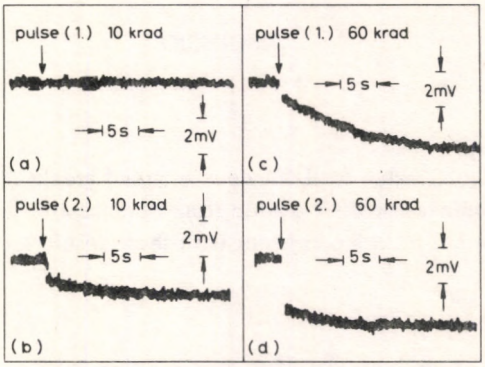

Fig. 7 Oscilloscope traces demonstrating the change of the light scattering intensity after irradiation of a DNA solution (7.5×10^{-2}g/1) at room temperature. The initial LSI corresponding to 23 mV

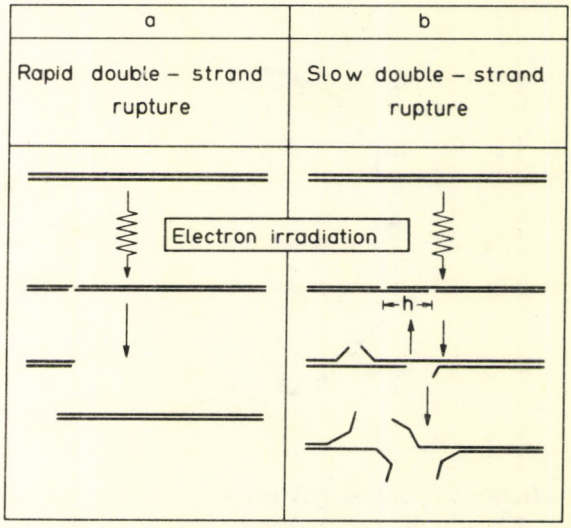

Fig. 8 Schematic description of the generation of double strand breaks in DNA

DISCUSSION

C. L. GREENSTOCK

At low doses the G value for DNA double strand breaks (~ 0.1) is much lower than single strand breaks but DNA double strand breaks are $(\text{dose})^2$ dependent. Are your multiple pulse LSI results consistent with these results?

D. LINDENAU

We plotted the degree of degradation at the first pulse as a function of the absorbed dose and found a linear dependence at doses greater than 10 Mrad within the error-limit, In contrast, for denaturated, single stranded DNA no limiting dose is needed for degradation.

FUNDAMENTALS OF A RADIATION-INDUCED PROCESS FOR PVC CHLORINATION

M. Bär, K. Friese, H. Rehor, J. Reinhardt
Zentralinstitut für Isotopen- und Strahlenforschung Leipzig
der Akademie der Wissenschaften der DDR

Introduction

Experiments for PVC chlorination were made as early as in the thirties, soon after the large-scale production of PVC had begun. They resulted in the first process of chlorinating PVC, namely PVC chlorination in solution /1/, which is still used on a technical scale today. In this process PVC is chlorinated in organic solvents, mostly halogen hydrocarbons, using UV irradiation or radical catalysts and is completely dissolved in the course of the reaction. The PVC thus obtained has a chlorine content of 62 to 64%. Due to its considerably increased solubility in the usual solvents it can be used for lacquers and adhesives. It is also used in the production of synthetic fibres.

Research work on the chlorination of PVC along new lines began in the USA and the Federal Republic of Germany in the early sixties /2/. PVC is chlorinated not in solution but in suspension. Its chlorine content ranges from 66 to 69%. The substance is boiling resistant and can be treated thermoplastically. The process consists in dispersing PVC in hydrochloric acid, swelling it by the addition of halogen hydrocarbons and chlorinating in the presence of radical catalysts or with UV irradiation. During chlorination the polymer is not dissolved. It is then recovered by distilling the halogen hydrocarbons, neutralizing, washing and drying.

In Table 1 the most important properties of boiling-resistant PVC as compared with some other competing polymers are listed /3/.

Table 1
Properties of chlorinated PVC as compared with other thermoplastics

	PVC chlorinated	PVC	PE	PP	ABS
density (g/cm^3)	1.52	1.40	0.95	0.91	1.06
tensile strenght (kg/cm^2)	650	550	110-400	300-400	390
elongation (%)	25	15	450-800	100-650	30
vicat softening point at 5 kg (^oC)	120	84	65	85	–

PVC chlorination by γ-irradiation

Chlorination in suspension and some other conventional processes have disadvantages, such as working in aqueous, strongly acid suspension in the presence of organic solvents and the related problem of corrosion; the problems of removing the solvents, neutralizing and drying; the use of circulating processes because of the short range of UV radiation or the application of pressure to shorten the relatively long reaction times. Therefore we made experiments on the chlorination of PVC powder without solvents in the presence of γ-radiation.

Initiating chemical reactions by γ-irradiation is a technique which is now used in a number of industrial processes, such as the sulpho-chlorination and the sulpho-oxidation of hydrocarbons. The prerequisites for such processes are a radical mechanism for the reaction and a sufficiently high G-value of at least 10^3 mol/100 eV. An important problem in the direct chlorination of PVC powder is to eliminate the heat of reaction of about 27 kcal/mol of reacted chlorine in order to prevent the PVC from being baked or decomposed above 70°C. The experiments were therefore carried out in a cooled fluidized-solid reactor. The temperature was controlled so as not to exceed the softening point of the polymer.

The fluid process requires a special PVC powder. It must be readily fluidized as well as chlorinated. These two requirements are incompatible. Compact pellets of uniform size are best suited for the fluid process, whereas spongy powder having a large surface area reacts most readily with chlorine. Compact pellets virtually do not react in the fluid process. It should be added that with spongy powder a stable fluid bed can only be maintained for a longer period because due to the radiation no electrostatic charging occurs. Under the conditions of γ-irradiation the reaction proceeds so violently, especially in the initial phase, that the reactor has to be cooled and an inert gas added to the chlorine. The inert gas used in our experiments was nitrogen. The initial nitrogen concentration can be 20–50 vol %. For continuous chlorination the hydrochloric acid formed in the reaction could well be used as the inert gas in a gas cycle.

The experiments on the γ-irradiated chlorination of PVC were made using a Soviet radiation unit of the RCH-γ-30 type (12 kCi, D_L = 0.9 × 10^6 or 1.5 × 10^5 rad/h) and an open unit designed at our institute of the GB 77 type (about 4.5 kCi). The design of the latter unit makes possible a greater variation of activity.

Dependence of the reaction rate on reaction parameters

The direct chlorination of PVC powder in the fluid process is a heterogeneous reaction which is dependent on many parameters: the spongy state of the powder, the reaction temperature and the ratio of chlorine to inert gas have already been mentioned. Besides these, the dose rate and the total dose as well as the oxygen content in the gas are of importance for the course of the reaction. The γ-irradiated chlorina-

tion of PVC, like every radical reaction, is influenced by oxygen. The effect of oxygen is twofold. On the one hand it obviously reduces the reaction rate drastically, and on the other the thermal stability of the CPVC is considerably lowered due to the insertion of oxygen groups in the polymer. For these reasons the oxygen concentration in the gas should be lower than 200 ppm. Studies of the dependence of the reaction on the dose rate have shown that the chlorination proceeds most favourably at 25,000 rad/h. The course of the reaction at 70°C and 25 krad/h can be seen from Fig. 1.

Under the above-mentioned conditions the destruction of the polymer as measured viscometrically and osmometrically is so small that the thermal stability of the CPVC is not appreciably affected. The chain length decreases as the dose rate increases. Above 100 krad/h the chains are affected so strongly that even with short reaction times this can be seen from the discolouring of the polymer. Depending on the reaction conditions some PVC particles remain unreacted in the powder. In Fig. 2 the relation between the chlorine content of CPVC, reaction time and unreacted PVC is shown for 25 krad/h and 70°C.

A scheme of the pilot plant for the batch reaction is given in Fig. 3.

Comparison between the properties of γ-irradiated and conventionally chlorinated CPVC

Besides a comparison of the mechanical properties it is of particular interest to see whether

- the homogeneity of the polymers with respect to the chlorine content is approximately the same in the dry and the wet state,

γ-irradiation results in a change of the ratio between the $-CHCL$, $-CCL_2$ and $-CH_2$ groups,

- with the same chlorine content the glass transition temperature, T_G, is the same as in the conventional process.

Investigations of the structure by means of fractionation, NMR measurements, the determination of T_G, etc. have shown that there are no significant differences between the polymers produced by γ-irradiation and in the wet-state process /4/. In both polymers the ratio of the $-CH_2$, $-CH_4Cl$ and $-CCl_2$ groups is 17:66:17. As can be seen from Fig. 4 the T_G-values for CPVC of varying chlorine content lie along the same curve in both cases. The mechanical properties as for example, the tensile strength, which is about 700 kg/cm^2 (measured for 1 mm sheet thickness), are approximately equal.

Experimental work has advanced so far that kg quantities of CPVC can be produced by γ-irradiation in our pilot plant in a continuous process. The product has the same properties as conventional CPVC and can even be better extruded. Thus, the chlorination of PVC with γ-irradiation in the dry state turns out to be a process whose advantages over conventional processes lie in the short reaction times and a considerably simplified mode of operation.

References

/1/ DRP 596911, Ruebenssaal, C.R., Kunststoffe 39, 51 (1949).
/2/ USP 2996489, DAS 1232749.
/3/ G. Czehovsky, Kunststoffe 60, Nr. 6, pp. 354-355 (1970).
/4/ F. Keller, H. Opitz, B. Hösselbarth, D. Beckert, W. Reicherdt, Faserforschung und Textilchemie 26, 7, pp. 329-339 (1975).
/5/ B. Hösselbarth, F. Keller, H. Rehor, W. Reicherdt, Charakterisierung von strahlenchemisch chloriertem PVC mittels Differentialkalorimetrie, submitted to "Plaste und Kautschuk".

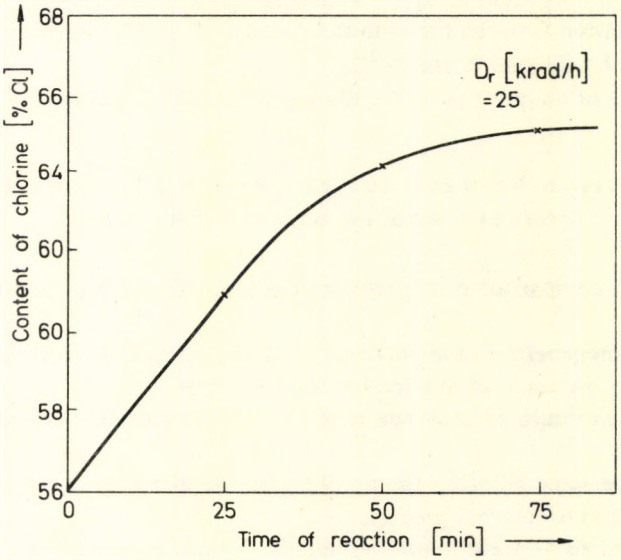

Fig. 1 Radiation chlorination of PVC at 70 °C at a dose rate of 25 krad/hr

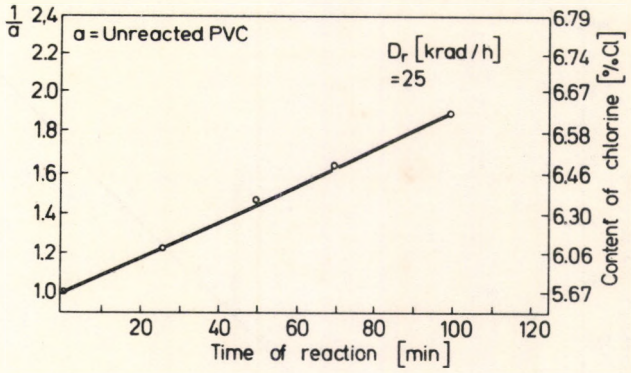

Fig. 2 Kinetic plot for radiation chlorination of PVC at 70 °C

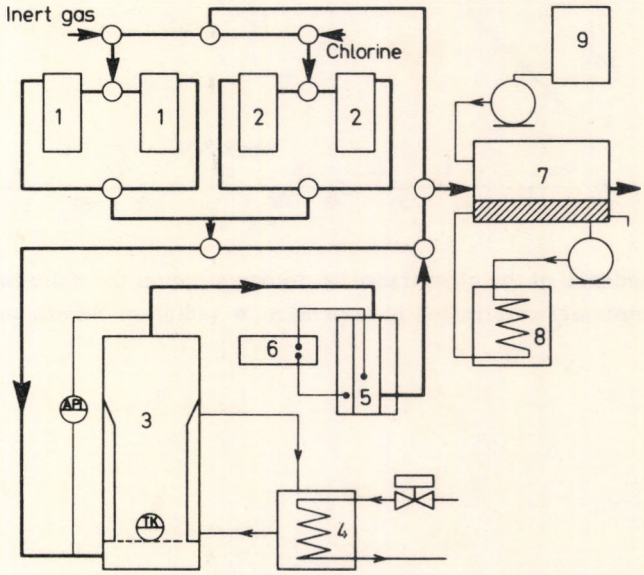

Fig. 3 Scheme for pilot plant (batch reactor) for the γ-irradiated PVC chlorination in the fluid process: 1. flow rate for inert gas, 2. flow rate for chlorine, 3. fluidized reactor, 4. thermostat, 5. separator for dust, 6. electrostatic separator, 7. scrubber for chlorine, 8. cooling apparatus, 9. container for alkalis

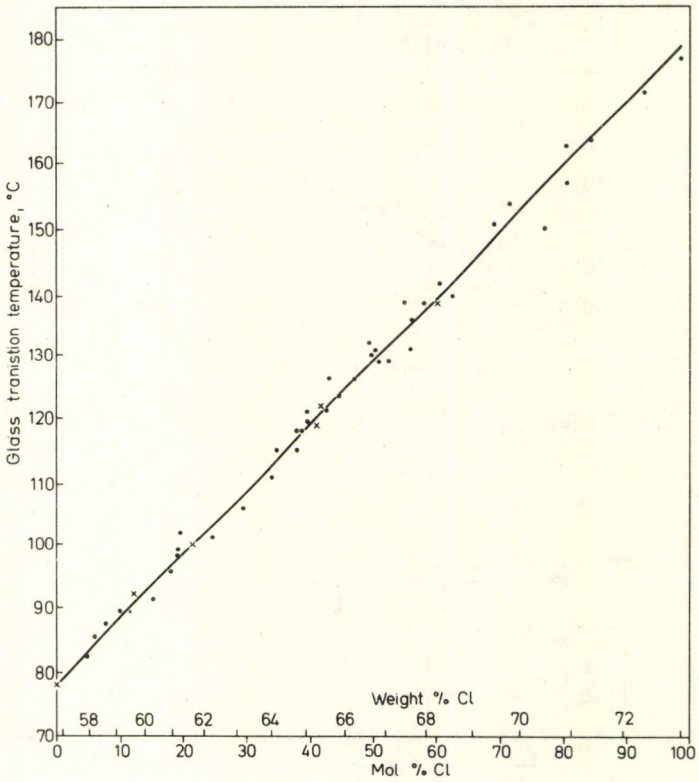

Fig. 4 Dependence of the glass transition temperature on the chlorination of PVC: x chemically chlorinated in suspension, ● radiation chlorinated

J. ZURAKOWSKA-ORSZÁGH

Did you start the production of radiation chlorinated PVC?

What is the production per year?

What was the difference in the molecular weight distribution after chlorination in comparison with that of the original PVC?

M. BÄR

At present we do not have any semi-industrial setup in our institute. The industrial scale experiments are planned to be completed by 1978 in cooperation with a factory. A pilot plant will be built there of capacity of some thousands of tons of PVC. Construction of a large scale plant will be decided later.

The K-value of the PVC used was about 70, it decreased to 68 upon radiation chlorination similarly as by conventional chlorination.

L. WUCKEL

Can you tell something about the ageing behaviour of your PVC? I think one has to pay attention to the fact that double bonds are formed by irradiation of PVC which would affect its weathering stability.

M. BÄR

The total dose by radiation chlorination was such that degradation and elimination of hydrogen chloride accompanied by double bond formation did not significantly influence the properties of the product. We do not have data about the long term (years) ageing properties of our product.

A. CHARLESBY

If the product is identical with that obtained by conventional chemical techniques why should one use radiation, and why is the product, with such useful properties, not already used on a large scale when it has been available chemically for some considerable time?

M. BÄR

The product obtained by radiation chlorination will be by about 500 DM/ton less expensive than conventionally chlorinated PVC because instead of a 6-step process a single-step process is used.

J. DOBÓ

The cheap, solventless method of PVC chlorination in fluidized bed with conventional catalysts is not made on industrial scale. The main reason is that this

is a chain process with a high activation energy in which much heat is evolved. Without solvent there is a great danger of the running away of the reaction. With radiation initiation, however, the overall activation energy is much less, and thus there is less danger of runaway and of overheating. I do not know whether the solventless fluidized bed chlorination method will ever become an industrial process, but if so, there is a big chance that it will be initiated by radiation.

Overheating, however, remains a danger even by radiation initiation which should not be neglected. The discolouration at high dose rates mentioned in the paper is probably a consequence of local overheating.

M. BÄR

Radiation chlorination of PVC will become an industrial process in GDR by 1978, on a pilot scale at the beginning. As to the discolouration at high dose rates it is a consequence of the increased radiation chemical degradation and not of local overheating as the problem of heat transfer is solved in our process.

RADIOLYSIS AND POLYAMIDES, PROTECTION FROM IONIZING RADIATION

V.M. Goryaev, G.G. Ryabchikova, A.E. Chalykh, G.M. Plavnik
Institute of Physical Chemistry, Academy of Sciences of the USSR
Moscow, USSR

A great number of papers devoted to the study of radiation-chemical processes in polyamides have been published /1-4/. However, the problem localization of the degradation and cross-linking processes at certain phases of the amorphous-crystalline polymer was not considered and a priori they were assumed to proceed in the whole polymer bulk. Yet, such a study is essential for understanding the effect of the polymer matrix phase state on the radiolysis processes as well as for searching effective methods of protection of polyamide from radiation damage. An experimental study of the site location with the predominance of degradation and structural processes to proceed in polyamide radiolysis is the subject to be examined in this paper.

The objects for examination were 23 μm thick oriented nylon-6 fibres of the 14-K type. They were Co-irradiated at a dose rate of 1 Mrad/hr with a dose range from 1 to 3000 Mrad.

Structural changes of the samples at wide angles of scattering were studied by an X-ray apparatus Dron-I. The X-ray record of the samples at small angles was conducted in a four-slit chamber with an ionization recording detector /5/. X-rays of Cu k_α was used. The swelling of samples was investigated by the weight technique in aqueous phenolic solutions of 1% to 6%. The end amino- and carboxyl-groups were determined potentiometrically. The densities were measured in gradient tubes to an accuracy of $\pm$ 0.001 g/cm^3.

Aromatic compounds: α — naphthol, pyrogallol, phenothiazine, quinhydrone incorporated into the fibres from solution were used as protection from the radiation effect. Modification of the fibres by radiation vapour-phase graft-polymerization of styrene and acrylonitrile was realized by means of an electron accelerator, (E = 1-5 Mev).

Figure 1 shows the results obtained on the intensity changes of the small-angle reflex maximum (I_{max}) of concentrations of end groups (N) and of the polymer density (ρ), being a function of the absorbed dose (R). In the dose range of about 5 Mrad all the curves are observed to be extremal. The changes in I_{max}-R and N-R correspond to the curves with a maximum, and those in ρ-R to the curves with a minimum.

Figure 2 illustrates the maximum swelling function (Q) of the irradiated fibres in 1.5 and 6% aqueous phenolic solutions. Earlier measurements /6/ have shown that swelling proceeds at the expense of the amorphous part of the polymer in 1.5% phenol solutions, the crystalline part remaining unchanged, whereas the crystallites melt and uniphase solutions are formed in 6% phenolic solutions. Thus, swelling intensification in 1.5% and reduction in 6% pehnolic solutions is related to a change in the sample crystallinity (Table 1) in the first case and to formation of a uniform spatial network in the second. The sample crystallinity was calculated using the following equation /6/:

$$\phi_{cr} = 1 - \left\{ \frac{Q(R_2)}{Q(R_1)} \quad \frac{Q'(R_1)}{Q'(R_2)} \right\} \left[1 - \phi_{cr}(R_1) \right]$$

where $Q(R_1)$ and $Q(R_2)$ stand for the degree of fibre swelling in 1.5% solution, $Q'(R_1)$ and $Q'(R_2)$ for that in a 6% solution, R_1 and R_2 are absorbed doses. The same figure shows the dependence of a number of chains within the network calculated from the changes in the swelling maximum in a 6% solution as a function of the dose. The curve M_c^{-1}-R is seen to be S-shaped with a marked plateau in the 100-500 Mrad range. X-ray patterns of irradiated polyamide samples swollen in 6% aqueous-phenolic solutions were observed after the solvent was extracted from the samples. Two rings are visible in the pattern of the sample irradiated at 500 Mrad. With an increase in the dose rate to 1000 Mrad the X-ray pattern shows clearly-defined diffraction semi-rings with considerable intensity at the meridian.

The entity of experimental data obtained permits stating that degradation and cross-linking are localized at different phases.

With low doses up to the gelation point (25 Mrad) the crystalline structure of the sample remains virtually the same. Thus, it can be suggested that the radiation-chemical processes in the polymer over this dose range are localized preferably in the amorphous phase. At the same time the complicated character of changes in I_{max}-R, N-R, and ϱ-R shows that the radiation-chemical processes are two-stage. At first, up to 5 Mrad, degradation is dominant. This can be seen from an abrupt increase in the concentration of the end groups evidencing a break of peptide bonds, in reduction of polymer density and intensity rise of the small-angle reflex. Cross-linking, along with degradation, becomes apparent starting from 5 Mrad, and its contribution increases with the absorbed dose. A specific feature of this stage is the formation of ensembles of cross-linked branched macromolecules, preceding the formation of a complete spatial polymer network.

Above the gelation point cross-linking becomes dominant. This is seen from the swelling maximum reduction in the 6% solution and from the polymer density increase. A specific feature of this stage is that the cross-linking to 500 Mrad also proceeds mostly in the amorphous phase. The dose range of 100-500 Mrad will be particularly noted. It corresponds to a marked slowing down of the rate – a plateau on the depen-

Table 1
Degree of crystallinity of irradiated fibres

$D \cdot 10^{-2}$ Mrad	ϕ_{cr}, %	
	by swelling	by X-ray patterns
0	-	56
5	42	47
10	31	37
20	18	20
30	8	8-10

dence of M_c^{-1} of R. Apparently, the reason is that the amorphous phase is already cross-linked, whereas to form the spatial network in the crystalline phase a certain degree of disturbance of the network is required. It can be conceived that a gradual accumulation of defects violating the order of chain positions in crystallites occurs within this dose range. These defects can be called latent since they have an indifferent effect on the diffraction pattern and the extent of crystallinity. A chain breaking, resulting in local disturbed sites and also ter- and tetrafunctional nodes seems to be the primary contribution from emergence of defects. At a dose of 500 Mrad this defect concentration becomes sufficient to initiate the network formation in the crystal phase with its gradual decomposition, finally resulting in the formation of an amorphous structure (Table 1).

A characteristic feature of cross-linking is that a spatial structure process within the crystalline bulk phase occurs under conditions of an already formed spatial network embracing both the disordered sites inside the fibrils and the interfibrillar layers. As a result the whole polymer matrix becomes cross-linked after the emergence of a network structure in the crystalline bulk phase. The data of wide-angle X-ray structural analysis on the swollen samples in the 6% phenolic solution indicate the conservation of the former orientation in a sample irradiated with 1000 Mrad, whereas those irradiated with 500 Mrad under similar conditions appear to be completely unoriented. The stable orientation of the crystallites in the swollen polymer (at a dose of 1000 Mrad) seems to be due to a partial conservation of the crystalline structure as a result of intra- and intermolecular chain cross-linking in the bulk.

Due to great changes in structure, in physico-chemical and mechanical properties of irradiated polyamides it is required to rise their radiation stability. Two methods of protection were used in this research: the traditional antirad method by means of aromatic compounds, and that first used by us /7/ for modification of the fibre surface by radiation vapour-phase graft polymerization of styrene and acrylonitrile. It was determined in earlier experiments that the structure and the physico-mechanical properties of fibres: the tensile strengh and the relative elongation upon rupture, are retained on the level of the initial ones in the presence of both additives and graft-copolymers in an amount up to 8-10%. It should be mentioned that the mono-

mers were grafted mostly at the surface since the process was accomplished under conditions with the rate of polymerization being much higher than that of the monomer diffusion through the matrix.

A comparative investigation of the protective action of additives and graft copolymers proved that protection wes efficient in both cases. The protection provided by graft copolymers is expressed in a higher stability of the crystalline structure /8/, slight alteration in intensity of the small-angle reflex /5/, higher values of tensile strength and elongation /7/ as illustrated by Fig. 3, the lower yield of paramagnetic centres. The greatest protective action of the aromatic compounds is observed with pyrogallol and with α-naphthol. This is probably due to their interaction with free radicals, to healing of defects, and to incorporation of molecules into the site of broken chains.

The protective action of graft copolymers seems to stem from two factors. First, the shielding action of the component grafted on the surface: about 60% of the energy incident onto the sample is known to be absorbed by its surface and to be dissipated in intensive chemical reactions occurring in the amorphous regions of the near-to-surface layer. Second, the existence of strong chemical bonds: matrix–graft component, favour more efficient energy transfer from the substrate polymer to the graft-polymer.

Thus, the data supplied permitted us to distinguish definitely between processes of degradation and cross-linking implemented at small dose rates, to localize the range of intensive operation of these processes, and to realize effective protection of polyamides.

References

/1/ A. Charlesby, "Atomic Radiation and Polymers". Moscow, "JL", 1962.

/2/ R. Bolt, J. Carrol, "Radiation effects on organic materials", Moscow, "AI", 1965.

/3/ A.S. Fomenko, E.P. Abramova, T.M. Daryeva, A.A. Beloded, E.P. Furman, A.I. Brodskii, Vysokomol. Soed., 10A, 507, 1968.

/4/ M. Dole, "Radiation Chemistry of Macromolecules", N.Y.-L., 1973.

/5/ G.M. Plavnik, V.M. Goryaev, V.I. Spitsyn, G.G. Ryabchikova, Dokl. Akad. Nauk SSSR, 202, 878 (1972).

/6/ V.M. Goryaev, A.E. Chalykh, G.M. Plavnik, G.G. Ryabchikova, V.I. Spitsyn, Vysokomol. Soed., A16, 1554 (1974).

/7/ V.M. Goryaev, G.G. Ryabchikova, Z.N. Tarasova, L.G. Tokareva, "Radiation Chemistry of Polymers", Moscow, "Nauka", 1966.

/8/ V.I. Spitsyn, V.M. Goryaev, G.M. Plavnik, G.G. Ryabchikova, P.Ya. Glazunov, V.A. Bersenev, Khimiya vysokikh energii, 4, 477 (1970).

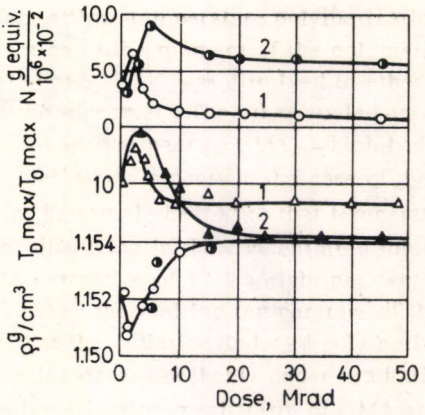

Fig. 1 Dependence of the maximum of the small-angle x-reflex: of the concentration of end-groups, and polymer density, on the dose
1 - vacuum, 2 - air

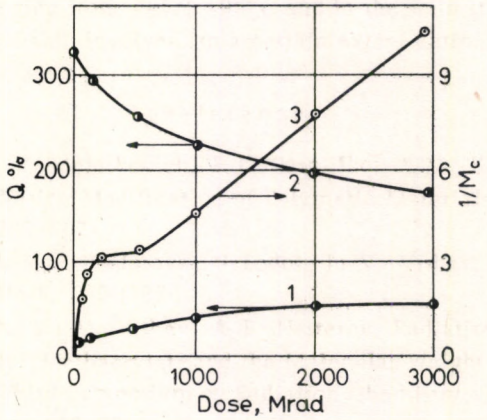

Fig. 2 Dependence of the maximum of swelling on the dose in (1) 1.5% (2) 6.0% aqueous phenolic solutions and M_c^{-1} (3)

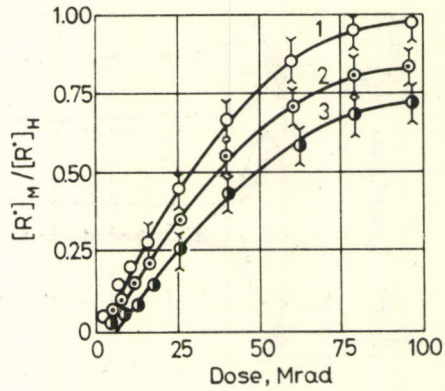

Fig. 3 Dependence of the concentration of free radicals on the dose 1) nylon-6 without addition, 2) with the addition of α-naphthol, 3) with graft polystyrene

INFLUENCE OF γ-IRRADIATION ON AROMATIC POLYIMIDES

M. Pietrzak, M. Wojciechowska
Institute of Applied Radiation Chemistry, Technical University, Łódź, Poland

Experimental

The following polyimides were investigated:

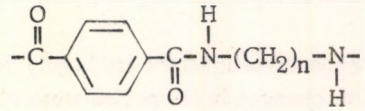

within the range $2 \div 10$.

They were prepared from chloride of terephthalic acid and proper diamines. Powdered samples of polymers were γ-irradiated to the total dose $10 \div 3000$ Mrad, at the dose rate equal to 0.5 Mrad/hr, in the presence of air and after degasing to the pressure equal to 10^{-5} Torr. Irradiations were usually performed at room temperature. For ESR measurements at 77 K, however, the irradiations were also done at 77 K. The IR determinations were executed in KBr.

Results and discussion

The intrinsic viscosity of unirradiated polyimides, determined in concentrated sulphuric acid, depends markedly on whether the number of methylene groups in the aliphatic part of the chain is even or odd (Fig. 1).

For polyimides irradiated in the absence of air the intrinsic viscosity increases linearly with the absorbed dose (Fig. 2). For polyimides irradiated in the presence of air the intrinsic viscosity decreased with the absorbed dose, rapidly at first then more slowly. Both these effects depend on whether the number of methylene groups between the aminogroups is even or odd (Fig. 3). Polyimides with an even number of methylene groups are more easily cross-linked in the absence of air while polyamides with odd number of methylene groups are more easily degraded in the presence of air. It seems that this effect is due to the fact that polyimides with an even number of methylene groups crystallize more easily, the adjacent chains are in closer contact, and there is a diminution of the diffusion of oxygen which accelerates the degradation.

The ESR spectra of the irradiated polyimides depend on the number of methylene groups in the aliphatic change. For small numbers only singlets were observed, for higher numbers a poorly resolved multiplet structure was evident (Fig. 4). Polyamides irradiated at room temperature in the presence of air contained about 10^{16} spin/g (Fig. 5), while polyimides irradiated in the absence of air contained about 10^{17} spin/g. At the total dose about 50 Mrad the effect of saturation was observed. At 77 K there was no effect of oxygen on free radical concentration which was 10 to 100 times that observed at room temperature. There was no saturation effect at that temperature.

The concentration of free radicals depends significantly on the length of the aliphatic part of chain (Fig. 6). The concentration of the free radicals increases with the increase of the number of methylene groups and is always higher for the even numbers than for the odd ones. This phenomenon is connected with the decrease of the protective action of aromatic ring with length increase and change in crystal structure.

All polyimides under the investigations are highly resistant to the action of the ionizing radiation. The changes in IR spectra were observed only for the highest total doses equal to about 3000 Mrad (Fig. 7a and 7b). Irradiation of polyamides increases the IR background and extends the absorption band. In the presence of air the new absorption bands are observed, which were indentified as due to peroxides (1175 cm^{-1}), hydroperoxides (3120 cm^{-1}), epoxy rings (1260 cm^{-1}), aldehyde (1400 cm^{-1}) and carboxy (1720 cm^{-1}) groups.

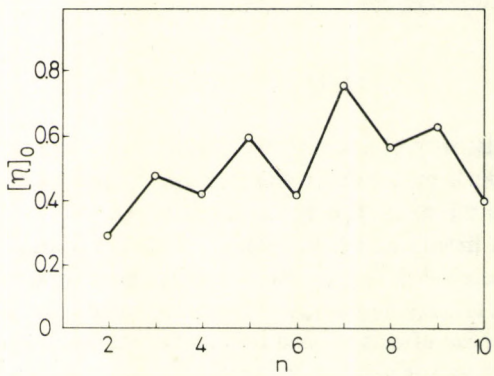

Fig. 1 Intrinsic viscosity of polyamides with varying number of methylene groups

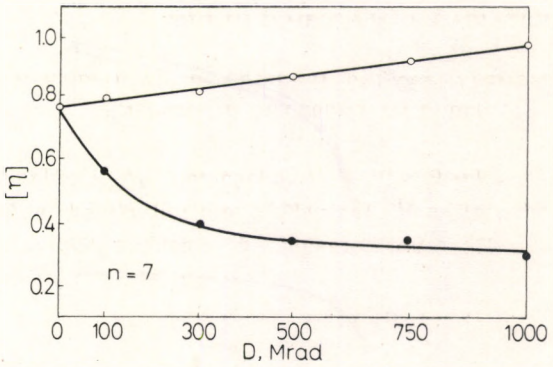

Fig. 2 Dependence of polyimide (n=7) intrinsic viscosity on absorbed dose: irradiation in the presence of air ●, irradiation in the absence of air ○

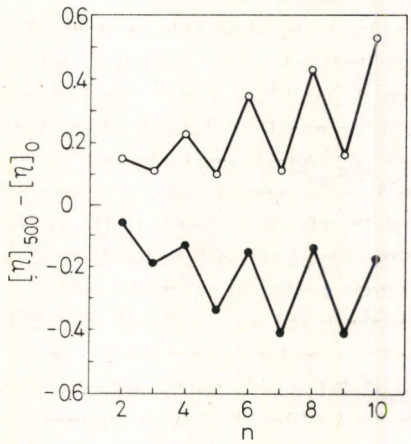

Fig. 3 Change of polyimide intrinsic viscosity after γ-irradiation to total dose of 500 Mrad: in the presence of air ●, in the absence of air ○.

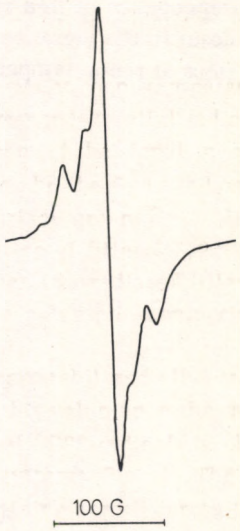

Fig. 4 ESR spectrum of polyimide (n=9) irradiated at 77 K in the absence of air

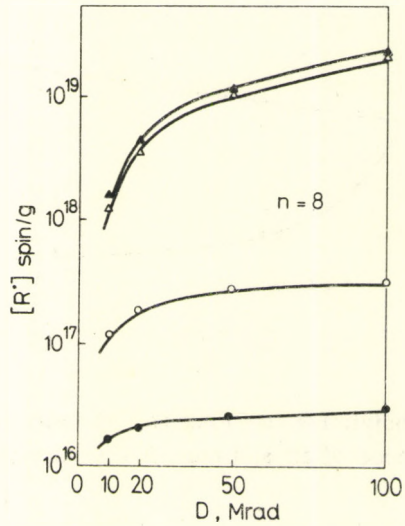

Fig. 5 Dependence of free radical concentration in polyimide (n=8) on absorbed dose: in the presence of air ● and ▲, in the absence of air ○ and △, irradiations at room temperature ● and ○, irradiations at 77 K ▲ and △

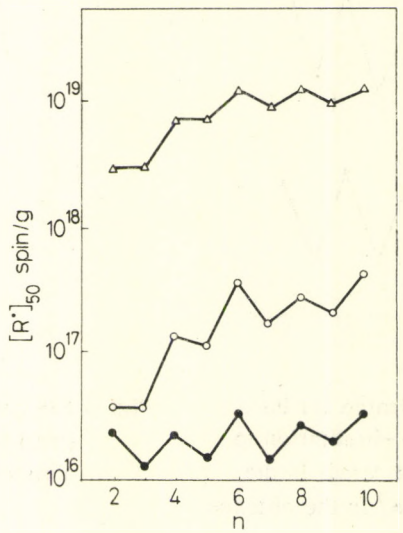

Fig. 6 Concentration of free radicals in polyimides irradiated to the total dose of 50 Mrad. For details see Fig. 5

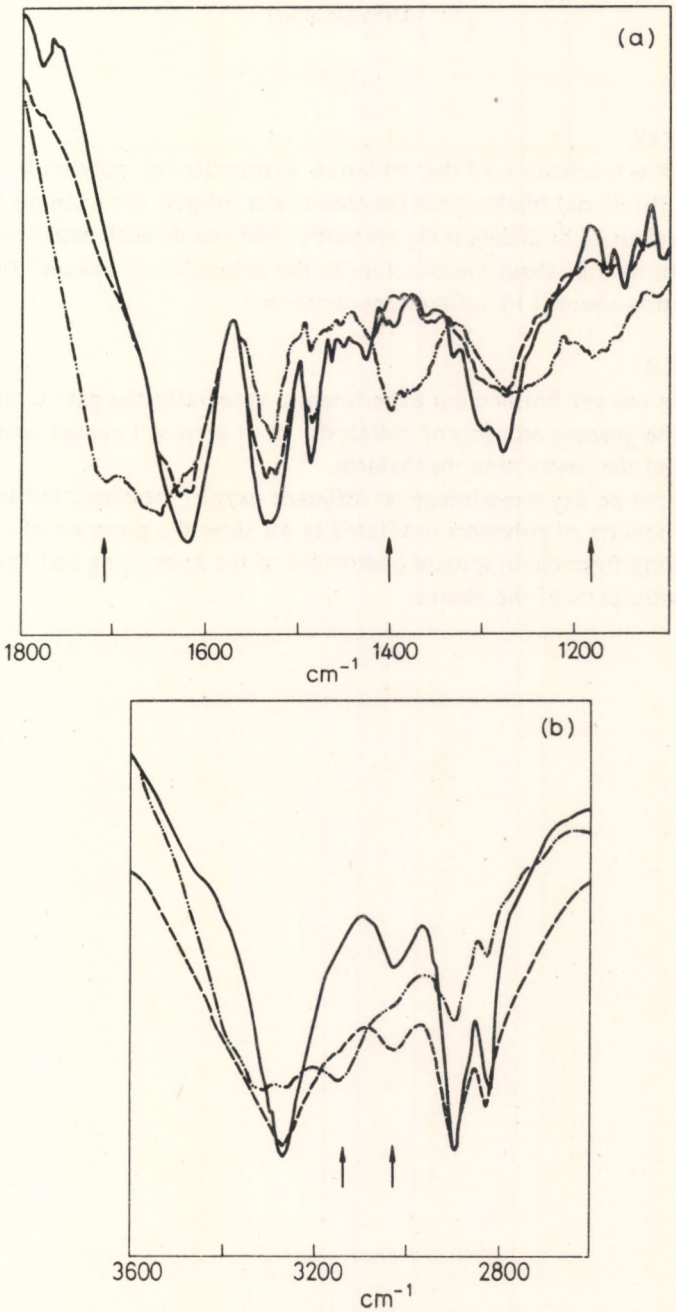

Fig. 7 IR spectrum of polyimide (n=8): unirradiated sample ———, sample irradiated to total dose 3000 Mrad in the presence of air — ·· — and in the absence of air -----

M. ROMANZEV

What is the mechanism of the oxidative destruction of polyimides? In order to prove the diffusional hindrance in the presence of oxygen. for example. experiments should be performed at different O_2 pressures. Did you do such experiments?

What can be told about the structure of the peroxide compounds? Do you have any information about it by infrared spectroscopy?

M. PIETRZAK

We have not yet finished our experiments, especially the gas chromatographic analysis of the gaseous products of radiolysis, so at present I cannot answer your question about the destruction mechanism.

We did not do any experiments at different oxygen pressures, but we plan to.

Infared spectra of polymers irradiated in air show the presence of carboxyl groups resulting from chain scissions, peroxides of the epoxy ring and hydroperoxides of the aliphatic parts of the chains.

THE INFLUENCE OF THE DOSE RATE ON THE ISOMERIZATION OF CIS-1,4-POLYISOPRENE IN NATURAL RUBBER LATEX

E. Jaworska, L. Stolarczyk
Institute of Nuclear Research, Department of Radiation Chemistry, Dorodna, Warszawa, Poland

The study of radiation induced cross-linking of the natural rubber latex was published in many papers /1–4/ and was concluded by the description of the technology of prevulcanization /5–7/ on an industrial scale.

The radiation sources used in the process were ^{60}Co γ-source and linear electron accelerator. It was found that the properties of rubber films prepared from latex irradiated by the same dose depended on the radiation source used. This was observed independently by French researchers /6/ as well as in our Laboratory, but the reasons for it have not, as yet, been cleared up. The papers published on the differences of the action of γ- and electron irradiation on polyisoprene chains have dealt, with the irradiation of polymer in the solid state or in the form of organic solutions /8/. The doses used were hundreds of megarads in a nitrogen atmosphere or in a vacuum.

These conditions are greatly different from those used in technologies of prevulcanization of natural rubber latex which result in optimal product properties. For that reason the aim of the present paper is to evaluate the influence of the dose rate on the changes involved in a polyisoprene chain irradiated the same way as in technology. This means irradiation of the polymer in the latex form by doses up to 10 megarads in air.

Experimental

Prevulcanization of the latex (Hevea-Exceltex DC) was performed with the addition of 1.8% (by weight) of CCl_4 as sensitizer.

The radiation sources used were ^{60}Co γ-source with a dose rate of 19.3 rad/sec and a linear electron accelerator (energy 10 MeV, average current 0.6 mA) with an average dose rate of about 10^5 rad/s. The temperature of the latex in the γ source was about 25 ^{o}C and in the accelerator it was related to the absorbed dose, but did not exceed 50 ^{o}C for the maximal dose of 10 Mrad. The conclusions related to radiation induced changes of the polymer chains were based on the following experiments performed for rubber films:

a) Equilibrium swelling in benzene and toluene. The calculation of the degree of cross-linking and the coarse evaluation of the cis-trans isomerization are based on the analysis using the Flory-Rehner's equation. It is assumed /9/ that the Huggins parameter (μ) values of cis-polyisoprene were, in benzene and toluene respectively, $\mu_B = 0.44$ and $\mu_T = 0.43$. For trans-polyisoprene the respective values $\mu_B = 0.52$ and $\mu_T = 0.36$ were used.

b) Mechanical properties of the rubber films:
- tensile strength R_r, kG/cm^2
- elongation at break $_r$, %
- permanent set ε_t, %
- modulus at 500% elongation δ_{500}, kG/cm^2

c) Thermal ageing in air at 70°C by 96 hours
(without any antioxidants added)

d) Infrared absorption spectra

Results and discussion

The properties of rubber films prepared from the latex irradiated in the ^{60}Co γ source and in the linear electron accelerator are shown in Tables 1 and 2. Figure 1 shows the relation between the dose and the degree of cross-linking as calculated from the equilibrium swelling in benzene and in toluene not considering the change of the Huggins parameter. (μ was taken, in these calculations, to be equal to that of pure cis-polyisoprene).

The calculation of the degree of cross-linking ν was performed by means of Flory-Rehner's equation /10/ in the form

$$\nu = - \frac{V_r + \ln (1-V_r) + \mu V_r^2}{V_o \rho_r \left(V_r^{\frac{1}{3}} - \frac{V_r}{2} \right)} \qquad (1)$$

It should be noted that calculation of ν by Eq. (1) is connected with serious cumulation of errors. The value of ν in Eq. (1) is 50–150 times smaller than the values of its particular components (one component is negative, two components are positive). The accuracy of the calculation changes from about $\pm$ 25% to about $\pm$10% for ν values 0.4×10^{-4} and 1×10^{-4}, respectively. Nevertheless ν-values obtained for the same sample were always higher when calculated from benzene swelling than when calculated from toluene swelling. This systematic difference can be explained by the assumption of the influence of cis-trans polyisoprene isomerization initiated by irradiation in cis-polyisoprene.

When some amount of trans-polyisoprene appears the Huggins parameter μ has to be changed. The μ value of cis-polyisoprene in benzene is higher than in toluene

Table 1

Mechanical properties of rubber films prepared from latex irradiated in ^{60}Co source and in electron accelerator R_r tensile strength, kg/cm^2 ε_r - elongation at break %, ε_t - permanent set, % S_{500} modulus at 500 % elongation

Mechanical properties / Source	2 Mrad				5 Mrad				10 Mrad			
	R_r	ε_r	ε_t	δ	R_r	ε_r	ε_t	δ	R_r	ε_r	ε_t	δ
γ	220	990	13	13,6	280	910	7	20.0	219	720	4	29.6
$\bar{e}$	190	1020	19	11.9	250	1010	10	15.6	279	840	8	21.7

Table 2

Thermal ageing of rubber films prepared from latex irradiated (dose 5 Mrad) in ^{60}Co source and electron accelerator. The mechanical properties are given in per cents of the initial values

Change of mechanical properties% / Source	tensile strength	elongation at break	permanent set	modulus
	ΔR_r	$\Delta \varepsilon_r$	$\Delta \varepsilon_t$	$\Delta \delta_{500}$
γ	85	98	110	90
$\bar{e}$	68	102	120	83

and for μ-values of trans-polyisoprene the relation to the kind of solvent is opposite. So neglecting the trans-polyisoprene content results in too high values when calculated from toluene-swelling. The above mentioned cumulation of errors does not permit one to calculate accurately the radiation induced cis-trans isomerization; just a coarse evaluation can be performed. In this coarse evaluation the assumption is made that the μ parameter of the cis-trans mixture is linearly dependent on the composition according to

$$\mu = X \cdot \mu_{cis} + (1-X)\mu_{trans} \qquad /2/$$

where X is the concentration of the cis form.

Introduction of the above mentioned μ_{cis} and μ_{trans} values in Eq. (2) for benzene and toluene-swelling and successive introduction of Eq. (2) to Eq. (1) gives for each solvent the degree of cross-linking expressed as the function of the composition X and the experimental parameters (V_r, V_o and ρ_r). By equating the ν-values obtained from benzene (ν_B) and toluene (ν_T) swelling of the same sample it is possible to calculate X. In the case of highest doses used the evaluated X values are about 0.89 and 0.84 for γ-source and for linear electron accelerator, respectively.

The above mentioned errors cumulated in Eq. (1) do not permit the use of these numbers as the proper values for evaluation of the degree of cis-trans isomerization, but it can be assumed that the degree of isomerization induced by electron irradiation is greater than that induced by γ-irradiation. Probably the degree of isomerization evaluated in the described manner is too high. The real degree seems not to exceed 10% (see below) for linear electron accelerator at the maximal used dose. Similar direction of changes (smaller isomerization involved by γ-irradiation) was observed by Golub and Danoon /8/ in solid unvulcanized rubber.

The results of infrared absorption spectra correlate with the above given analysis of the changes of the Huggins parameter. The comparison of spectra of rubber films prepared from electron irradiated latex with the spectra of films from γ-irradiated latex gives small, but significant shifts towards higher frequency in the 1315, 1130 and 840 cm^{-1} bands. According to Binder /11/ about 10% trans-C/CH_3/ = CH- is required for the 1325 cm^{-1} band to appear definitely in the spectrum. So it has to be assumed that the degree of cis-trans isomerization, even at high dose rates and at maximal doses used, does not exceed 10%. The G_{isom} values in this case are of the order of ten. Along with cis-trans isomerization other changes in the polymer chain are also possible. For instance in rubber films prepared from electron irradiated latex the absorption in the 1645 cm^{-1} band is greater and in 1380 cm^{-1} or 1450 cm^{-1} bands smaller than in films prepared from γ-irradiated latex. Absorption in this range is attributed, according to Saunders and Smith /12/, to vibrations of $=CH_2$ and $-CH_3$ groups, respectively. Probably the increase of the probability of the reaction /8/

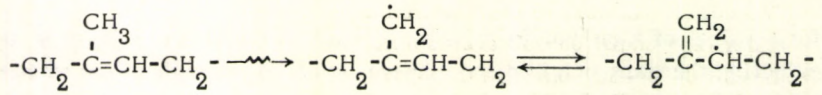

As a result of this the number of vinylidene groups is enhanced and that of the methyl groups is diminished.

In addition to all these conclusions the possibility of double-bond migration cannot be eliminated. The result of this migration, especially at the polymer chain-ends, would be the appearance of some 1,2 or 3,4 isomers. According to Garmonow /13/ even a small content of these isomers in polyisoprene 1,4 strongly influences the mechanical properties of cross-linked rubber.

The observed differences between the properties of rubber films prepared from latexes prevulcanized by the same dose but at different dose rates are probably connected with various causes and depend not only on the differences of the yield of cross-linking. If all the differences were connected with the degree of cross-linking only, then all the points in Figs 2 and 3 would lie on the same curve irrespective of the dose rate in the prevulcanization process. In the ν-source the processes of diffusion including cross-linking seems to dominate. In the electron accelerator,

as the effect of the apparent LET increases, the domination of trace processes is more probable. In the last case the greater parts of the polymer chain are excited and probably isomerization is increased. The probability of the reaction between the excited polymer and the products of water radiolysis seems to be enhanced too. Among others, the yield of peroxides is probably increased by electron irradiation resulting in diminished resistance to thermal ageing (see Table 2).

The difference in the composition of non-rubber-like products of radiolyis /14/ seems not to influence the observed properties of the rubber films. The influence of non-rubber-like substances on the mechanical properties of rubber was observed by Gregg and Makej /15/. he latex used in our work was double centrifuged and so the content of these substances in the samples ought to be of minor importance.

References

/ 1/ Minoura Y., Asac M., J. Polym. Sci. 5, 233, 401 (1961).
/ 2/ Karpow W.L., Industrial Use of Large Radiation Sources /IAEA/ Conf. Proc. Salzburg, 1, 363 (1963).
/ 3/ Lamm A., C., Rev. Gen. Caoutch., 39, 217 (1962).
/ 4/ Ambroz H., Zieliński W., Polimery 13, 112, 145, 194 (1968).
/ 5/ Puig J., Atomic Energy Rev. (IAEA), 9, /2/, 373-397 (1971).
/ 6/ Laizier J.', Rev. Gen. Caoutch. Plast., 11, 897-899 (1973).
/ 7/ Jaworska E., Ambroz H., Kowalski J., Oprac. wewn. IBJ Nr 74/XVII (1974).
/ 8/ Golub M.A., Danoon J., Can. J. Chem., 43, 2772-2785 (1965).
/ 9/ Weissberger A., Physical methods of organic chemistry, 1, 493 (1949).
/10/ Flory P.J., Rehner J., J. Chem. Phys. 11, 512 (1943).
/11/ Binder J.L., J. Polym. Sci. Part A, 1, 37-46 (1963).
/12/ Saunders R.A., Smith D.C., J. Appl. Phys., 20, 953 (1949).
/13/ Garmonow J.B., Kauč i Rez., 32 /5/, 6, (1973).
/14/ Jaworska E., Hoffmann J., Chmielińska M., Oprac. wewn. IBJ Nr 11/XVII (1974).
/15/ Gregg E.S., Makej D.H., Kauč. i Rez., 32/6/, 3, (1973).

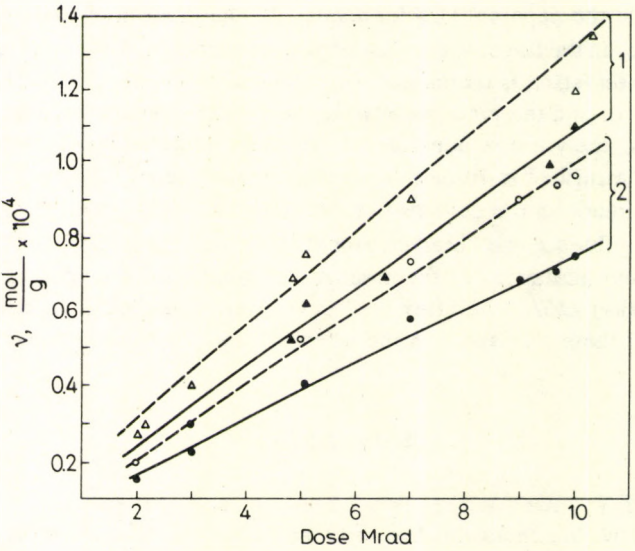

Fig. 1 Plots of degree of crosslinking against dose for samples irradiated in ^{60}Co sources (1) and electron accelerator (2). Equilibrium swelling was performed in toluene (●▲) and in benzene (○△)

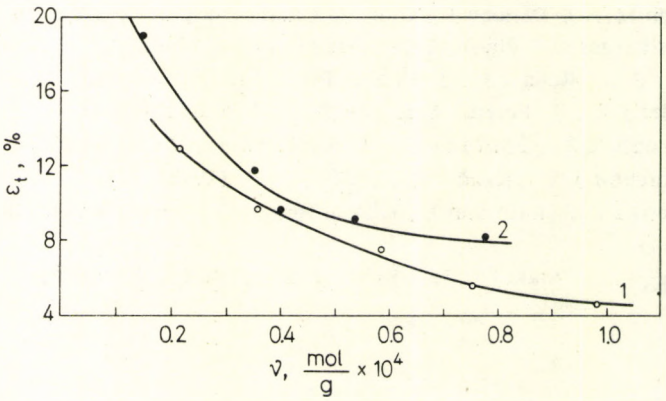

Fig. 2 Plots of tensile strength R_r against degree of crosslinking ν for samples irradiated in ^{60}Co sources (1) and electron accelerator (2)

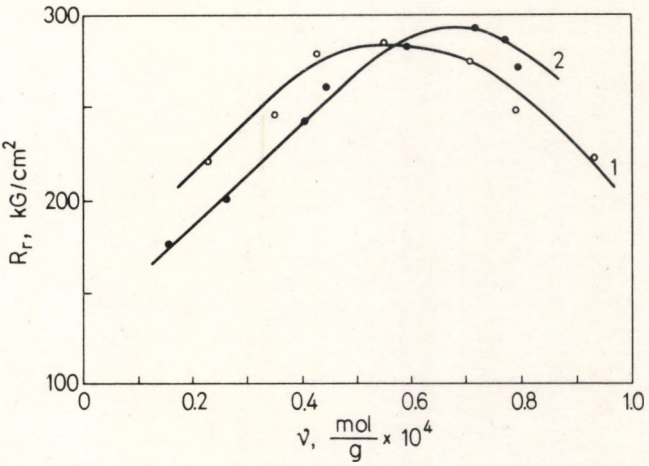

Fig. 3 Plots of permanent set ε_t against degree of crosslinking ν for samples irradiated in ^{60}Co sources (1) and electron accelerator (2)

THERMOLUMINESCENCE IN IRRADIATED POLYMERS

A. Charlesby
Royal Military College of Science, Shrivenham, Swindon, Wilts, U. K.

Many materials show luminescence on irradiation and subsequent heating. This behaviour is also found in many polymers. A study of the conditions under which this luminescence arises can be expected to produce information on the behaviour of electrons in these insulating materials, whereas the more usual method of injecting the electrons from electrodes by means of electrical fields complicates the situation by the introduction of space charge effects. Thermoluminescence also permits the study of the behaviour of electrons following ionization, when they are thermalized and either recaptured or trapped close to or away from their parent ion.

Thermoluminescence

A basic observation is that many polymers show a small leakage current on warming above room temperature at which they were standing for long periods. However if the same polymer had previously been irradiated at a lower temperature a much higher current is observed when the temperature is raised, even well below room temperature. The explanation is that radiation liberates electrons many of which then become trapped. On subsequent warming, these electrons are liberated and provide the charge carriers. A related effect is the light emitted during this warming period /1/. This light emission occurs as a series of peaks in the neighbourhood of one or more temperatures depending both on chemical structure and polymer morphology. Thus polyethylenes of different degrees of crystallinity show similar peaks but of widely different magnitude. Furthermore the presence of oxygen which is an efficient electron trap introduces an extra peak but in this case oxygen must be present as a distinct molecule and not combined with a polymer chain /2,3/.

The light emission/temperature curve is referred to as the glow curve. The individual peaks are usually broad and this could be explained as due to the finite time needed for an electron to become untrapped. However, several arguments point to the view that not all traps within the same glow peak are of identical depth. Thus the width of individual peaks is not greatly altered if the temperature is raised

more slowly. Furthermore if a heating cycle is used in which the polymer is raised to that corresponding to the maximum of a glow peak, and the specimen is then cooled and reheated, the new peak is displaced towards higher temperature. If all traps corresponding to one peak had been of identical depth the effect of this cycling would have been to reduce the overall height within the peak but not its shape. It must however be stated that neither the depth nor even the nature of these traps is as yet well defined, although the apparent coincidence of some of these peaks with mechanical transition temperatures would indicate that they occur primarily at defects or irregularities within the polymer structure. As the temperature is raised these defects can disappear locally thereby releasing the electron.

The spectrum of light emission is a further point for discussion. This spectrum does not usually relate to that of the polymer but is more characteristic of the fluorescence and phosphorescence of certain impurities present in very low concentration and usually of aromatic character. These impurities can be removed by washing in a suitable solvent and replaced by other compounds or additives which then provide a change in spectrum but not in the position of the glow peaks. Thus if P is the polymer matrix and A the additive (in very low concentration) then the location of the glow peak corresponding to electron release depends on P while the emission spectrum is due primarily to the excited molecule A*. If the formation of A* occurs due to electrons becoming mobile then there are several possible explanations:

a. Before electron release the additive is in the form of A*. One must then explain why the hole produced by ionization at the same time as the electron reaches the additive first whereas the electron is trapped.

b. Both hole and electron are trapped within the polymer and when the electron or hole is released they both recombine within the matrix. The energy thus made available migrates to the additive by some form of energy transfer and is then emitted in the form of light. Experiments to decide between these and other theories are now being carried out.

Preglow (Isothermal Luminescence: ITL)

If radiation is carried out at a temperature of 77K or even much lower and the polymer is maintained at this temperature, light is nevertheless emitted for long periods. This preglow (ITL) follows an unusual relation in that light intensity does not decrease exponentially with time but as 1/t. To account for this time dependence one may envisage an appropriate distribution of trap depths. It can then be shown that a relatively small variation in trap depth can account for this time dependence. However light emitted should still be very dependent on temperature and it is in fact observed that even at 4K there is no significant drop in light intensity /4/.

An alternative theory is that electrons trapped in the vicinity of a cation can tunnel to it with little or no temperature dependence /5/. Allowing for the Coulombic potential of the cation, the inverse time dependence can then be explained on the basis of a single trap depth with electrons at various distances from their respective

cations. However this theory does not provide any information on either the depth of the trap or on the mean distance of the electron from the cation. As time progresses, tunnelling will occur from electrons situated at greater distances from the cation, but for a reasonable range of observation times this variation in distance will be small.

Electrical Field Stimulated Luminescence

Luminescence observed in an irradiated polymer film can be greatly enhanced if an electrical field is applied between semi-transparent electrodes on the film. This electrically stimulated luminescence shows very interesting features which can best be seen during preglow when the temperature can be maintained constant. When the field is applied during luminescence decay there is a sudden increase in its intensity but this decays rapidly to little more than the original glow density. When the field is removed the light intensity sinks back to approximately the continuation of the original glow curve. A second or third application of the field then produces only a small increase in luminescence /6, 8/. However if the field is reversed and re-applied, luminescent enhancement can again be very large (Figs 1, 2). This observation clearly shows that a directional effect is involved in the enhanced rate of untrapping which ultimately accounts for the luminescence. The model to consider is a series of electrons (probably geminate electrons) distributed at various distances from their respective cations and in random directions relative to the external field. Thus with one field direction electrons lying on one side of their cations will be encouraged to re-combine with them, whereas the electrons lying on the other side will find their untrapping inhibited until the field is reversed.

Let us now consider two methods of electron release — by thermal untrapping and by tunnelling. In its simplest formulation the former method implies that once an electron is untrapped it can wander through the polymer matrix until it reaches the vicinity of a cation with which it combines. The distance over which it can travel can be quite large and this is shown by the conductivity observed on warming. The thermal untrapping of electrons can be stimulated by an electric field but there is not any necessary pairing of electron and cation to explain the directional effect. In one direction the activation energy for thermal release from a trap is reduced by the external field E_e by an amount $aeE_e(k)T$ where a is the effective radius of the trap and e the electron charge. In the opposite direction the activation energy is increased by the same amount, but this is of minor importance since the electron will preferentially escape in the direction of the field and once released can wander towards any positive charge. This situation will not apply if the electron is trapped in the vicinity of a positive charge but this is not an essential requirement for thermal release as it is for tunnelling. Here the rate of release depends on the dimensions of the barrier between electron and positive charge, i. e. on trap depth and radial distance. This barrier will be affected both in magnitude and direction by the external field and if the Coulombic field is involved its effects can be com-

puted using the quantum theory. The necessary calculations have been carried out by the author /7/ but is would not be appropriate to present the somewhat detailed mathematical analyses in this context. Only the main lines of argument will be mentioned.

The quantum theory states that the rate of tunnelling involves the integral of $(U - E)^{\frac{1}{2}}$ across the barrier and with an external field this becomes $(U - E - E_e)^{\frac{1}{2}}$. This integral has been computed for a number of trap depths and external fields and it then transpired that these computed values can be represented very adequately by simple algebraic expressions. These can then be integrated for all directions of the external field and the net result is a series of equations giving (a) the immediate enhancement of luminescence at the time t_o after radiation exposure when the field is applied suddenly, and (b) the subsequent decay of luminescence at an additional time t_d. Both these depend on a single parameter y fixed by trap depth and external field E_e. The only quantity assumed is the pre-exponential which was taken as 10^{13} sec^{-1} but the results are very insensitive to this value. Figures 3, 4 and 5 show how the parameter y influences the immediate light enhancement and subsequent decay.

In the experiments the degree of enhancement at the time when the field is applied has been measured for a series of external fields and at various times t_o. This gives one set of values of y. With the field applied the the further time t_d needed for the light intensity L (E_e) to sink back to the value L(O) measured immediately before application of field was determined, from t_d/t_o a second set of values of y was derived. From these values of y the trap depth in polyethylene could be immediately deduced. For fields of between 1.32×10^7 to 5.15×10^7 Vm^{-1} the first method leads to a trap depth of 1.2 ± 0.1 e. v while the second method leads to a trap depth of 1.5 ± 0.1 e. v. /8/. The difference may be due to the assumption that all traps are of equal depth. In any case these values agree reasonably well with the trap depths deduced by an entirely different method, i. e. activation energy for mobility using a surface charge technique /9/ which leads to trap depths of between 0.99 and 1.45 e. v. Although this field stimulated luminescence has only been applied to thin polyethylene films there seems no obvious reasons why it cannot be extended to thin films of other insulating materials provided that a sufficiently high electrical field can be applied.

We may now discuss the difference between the traps involved in preglow luminescence and those involved during thermal untrapping. My present view is that the former traps are deeper but are located closer (~60A) to their parent ions, electrons which fill them are primarily geminate electrons and their release by tunnelling does not involve any thermal process. The remaining traps are located at random within the specimen, they are more shallow than the traps involved in preglow. These traps can be filled at random by more mobile (i. e. non-geminate) electrons distributed throughout the specimen, recombination following release can then occur with any ion encountered during subsequent wandering of these electron within the specimen. No directional effect is therefore involved, although some of the

electrons released on warming may be recaptured in one of the deeper traps near a cation and thus provide an additional contribution to tunnelling when the temperature is reduced. The fact that preglow is still observed if a polyethylene specimen is heated to a much higher temperature and then cooled would support the view that two different mechanisms of untrapping are involved. The highest temperature peak in the glow curve from polyethylene may possibly correspond to these deep traps.

Luminescence from Organic Scintillators

Organic scintillators are frequently used as radiation dose-rate meters, the intensity of light emitted serving as a measure of absorbed energy, for this purpose the time lag between absorbed energy and light emission must be extremely small. One can then ask whether the phenomenon of thermoluminescence which requires an increase in temperature for light emission from a low temperature is in any way related to the behaviour of these organic scintillators. It could be argued that electrons are trapped at low temperatures so that the light emitted on warming is a measure of the total absorbed dose, whereas in the same material irradiated above the glow peak temperature these electrons can no longer be trapped and there is almost an immediate response, so that the scintillator acts as a dose-rate meter.

In our experiments a commercial scintillator was used, the matrix polymer being polyvinyl toluene (PVT) incorporating 3% p terphenyl and 0.1% POPOP as wavelength shifter, etc. Comparable experiments were carried out with samples of the matrix of PVT alone. These were subjected to high doses from a 10,000 Curie Co 60 source at 77K and their preglow and glow curves and light emission spectra obtained. In addition measurements were made on light emitted during radiation with a low intensity Co source, (to minimise interference with the measuring equipment), with Sr 90 betas and with filtered UV. The main conclusions /10/ are as follows:

Both the commercial scintillator and the PVT matrix itself show the 1/t intensity dependence of preglow, following absorption of high energy gamma doses from 0.1 to 0.5 Mrads, and for periods up to hours after irradiation. On warming a single peak is seen in the glow curve at approximately 109K for PVT alone and 114K for the scintillator. The warming rate was 2°C/min and the half breadth of each peak was approximately 15°. The emission spectrum of PVT thermoluminescence shows one major peak at about 310nm and a smaller peak at about 430nm. On the other hand the scintillator emission consists primarily of a single peak at about 420nm due to the wavelength shifter. These wavelengths do not correspond to the emission spectrum of p terphenyl or POPOP irradiated alone. With beta radiation the main peaks occur at about 320 and 420 nm respectively for emission during irradiation at room temperature.

The total light emission following irradiation consists of the preglow and the glow peak. The former can be integrated over a period from ns to hours using the

reciprocal time dependence but the integrated preglow + glow peak light emitted is lower by at least two orders of magnitude than the light emitted for the same dose delivered at room temperature. Thus the simple model of light emission as being due to either release of electrons following or during radiation (depending on temperature) cannot be sustained. One must envisage an additional mechanism of light emission which is almost instantaneous at room temperature and does not contribute to delayed emission on warming from a low temperature. It is of interest to note that no extra peaks are observed with gamma radiation as compared with UV photons. It is also worthy of note that the efficiency of photon creation in irradiated PVT + aromatic additives is relatively high in spite of the fact that these same materials are very resistant to radiation-chemical changes because of the sponge effect.

The conclusion that the trapped electrons involved in preglow and thermoluminescence are not a major factor in light emission at room temperature is confirmed by the fact the intensity of the immediate light emission at room temperature is similar to that observed during irradiation at low temperatures, well below the glow peaks.

References

/ 1/ Blake, A.E., Charlesby, A. Randle, K.J., J. Appl. Phys. D 7, 759 (1974).

/ 2/ Charlesby, A., Partridge, R.H., Proc. Roy. Soc. A 271, 170, 188 (1963), ibid. A 283, 329 (1965), J. Polymer Sci. B1 439 (1963).

/ 3/ Boustead, I., Charlesby, A., Europ. Polym. J. 3, 459 (1967), Proc. Roy. Soc. A 316, 219 (1970).

/ 4/ Kieffer, F., Lapersonne, M.C., Regant, J., Int. J. Radiat, Phys. Chem. 6, 79 (1974).

/ 5/ Mikhailov, A.I., Doklady, A.N., Phys. Chem. SSSR 197, 136, 223 (1971).

/ 6/ Charlesby, A., Proc. 10th Conf. Radioisotopes, Japan Atomic Ind. Forum 304 (1971).

/ 7/ Charlesby, A., to be published.

/ 8/ Charlesby, A., Owen, G.P., Int. J. Radiat. Phys. Chem. 8, 343 (1976).

/ 9/ Davies, D.K., Lock, P.J., J. Electrochem. Soc. 120, 266 (1973).

/10/ Charlesby, A., Carter, A.C., Martyn, N.P.W., to be published.

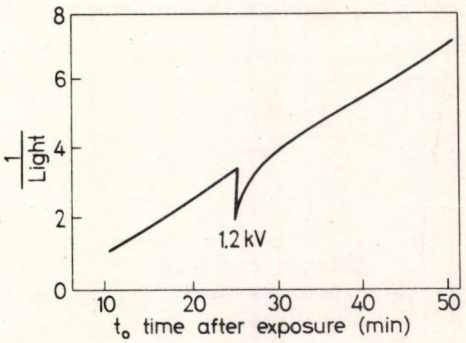

Fig. 1. Reciprocal dependence of preglow intensity emission on time and recovery after field-enhanced luminescence – polyethylene

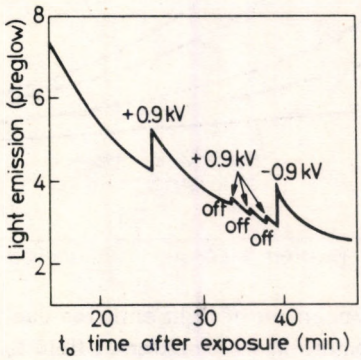

Fig. 2. Directional effect of electrical field
+ 0. 9KV on – off 4 times
– 0. 9KV recovery of effect

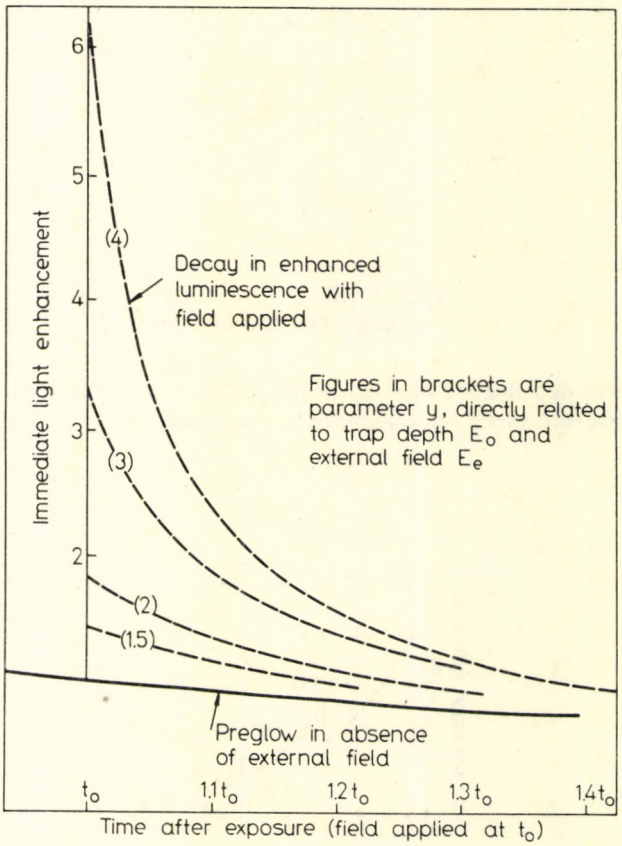

Fig. 3. Theoretical enhancement of light emission due to field-enhanced tunnelling, t_o time after exposure at which external field E_e is applied. Immediate enhancement at t_o, subsequent reduction at $1.1t_o$ . . . . Bottom curve shows extrapolated preglow intensity in absence of external field (1/t)

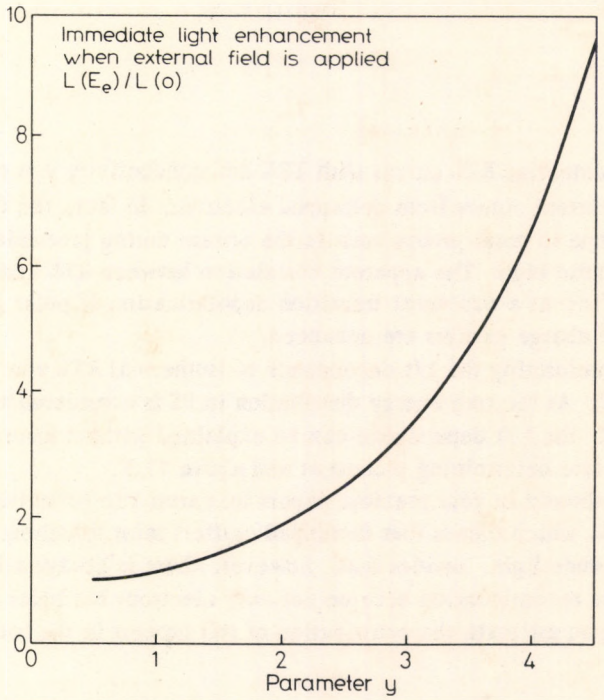

Fig. 4. Immediate enhancement from L (O) to L (E_e) when external field is applied

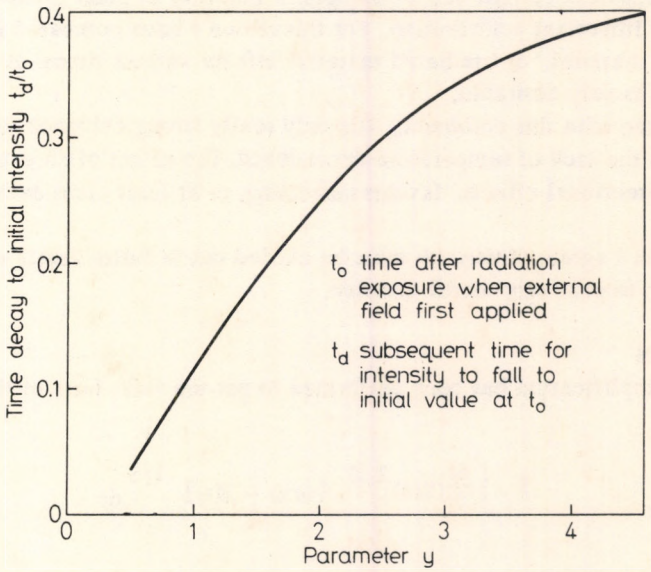

Fig. 5. Time (t_d) for enhance intensity L_e (t_o + t_d) to decay to value L_o (t_o) immediately prior to application of field

P. HEDVIG

(1) By comparing RTL curves with TSC and conductivity you seem to consider that all the current comes from detrapped electrons. In fact, the dipole depolarization current due to polar groups built in the system during processing and during irradiation is quite high. The apparent correlation between RTL and TSC is due to a structural effect: at a structural transition depolarization of polar groups as well as detrapping of charge carriers are enhanced.

(2) By interpreting the 1/t dependence of isothermal RTL you used the tunnel effect approach. As the trap energy distribution in PE is considered to be approximately experimental, the 1/t dependence can be explained without assuming tunnel effect as being the rate determining process at and above 77 K.

(3) You showed in your previous papers that aromatic impurities had a significant effect on RTL, which means that detrapped carriers must somehow reach the impurity centre to produce light. Besides that, however, there is always a high probability of electron-hole recombination because not only electrons but holes are detrapped. What would you estimate the contribution of this process in the total light emission to be?

A. CHARLESBY

(1) An apparent current due to changes in mobility of polar groups is - as you say - a very important contribution. For this reason I have compared irradiated with unirradiated material, or irradiated material left for various times. A more detailed examination is very desirable.

(2) I agree with this comment. The only really strong evidence in favour of tunnelling is the lack of temperature dependence. The effect of an external field, leading to directional effects, favours tunnelling, or at least close association of charge pairs.

(3) Again I agree. This work must be carried out in fuller detail so that an answer can be given to your very useful question.

A. ORSZÁGH

What simplification has been performed to get the final form of the equation-

$$P = \int \frac{2r}{\hbar}(2m)^{1/2} \left[h(x) - E(r)\right]^{1/2} dr$$

taking into consideration that integration is to be performed as a double integral $\iint F(r\Theta)\, dr\, d\Theta$?

A. CHARLESBY

The equation for P must be extended to take into account an external field E_e. This leads to

$$\int (u-E-E_e)^{1/2} dr$$

The computer is used to calculate this integral for various values of trap depth E_0 and external field E_e.

It is then found that P can be expressed approximately as a linear function of parameters simply related to E_0 and E_e. This is a great simplification and the integral for all directions can then be obtained very easily. Full details will be given in the paper when published.

Ya. S. LEBEDEV

The 1/t kinetic law is quite usual for solid state reactions. Annealing and some other low temperature radical reactions almost always exhibit stepwise character and obey the kinetic law

$$[R] = [R_0] - C \ln t$$

Thus for the reaction rate

$$\frac{d[R]}{dt} \propto \frac{1}{t}$$

This comes from the wide range dispersion of the kinetic constant in a solid matrix and from the dispersion of the tunnelling distances. Charge recombination may be considered as a particular example of such dispersion.

THE KINETICS AND MECHANISM OF RADIATION-INDUCED IONIC GRAFT POLYMERIZATION

V. Ya. Kabanov, L. P. Sidorova, R. E. Aliev, V. I. Rudneva
Institute of Physical Chemistry of the Academy of Sciences of the USSR,
Moscow, USSR

Formerly it was shown /1, 2/ that radiation-induced graft polymerization in the liquid phase can take place under thoroughly dry conditions by the ionic mechanism by means of ionic centres formed in polymers under irradiation which initiate grafting. Thus, radiation-induced grafting of some monomers polymerized only ionically (α-methylstyrene, vinyl-n-butyl ether, isobutylene) has been performed.

It is of interest to perform radiation-induced grafting of monomers polymerized both radically and ionically (for example, styrene, acrylonitrile, 4-vinyl-pyridine, 2-methyl-5-vinylpyridine, phenylacetylene etc.). The radiation-induced polymerization and grafting of these monomers by the radical mechanism has been published in detail /3, 4/ but in the literature, information about their radiation-induced liquid ionic grafting is absent. Formerly the radiation-induced ionic grafting of some of these monomers was performed in frozen systems /5, 6/ The realization of the radiation-induced ionic grafting of the above mentioned monomers allows one to obtain modified polymers with new properties. The kinetics and mechanism of radiation-induced ionic grafting of these monomers have not been studied either.

In this work radiation-induced grafting of "raw" (dried by $CaCl_2$ or CaH_2) and extremely dried monomers has been performed under similar conditions (temperature, dose rate, dose) in the liquid phase.

Styrene, acrylonitrile, 4-vinylpyridine, 2-methyl-5-vinylpyridine, phenyl acetylene, propylene oxide, acrolein have been used as monomers. Grafting onto low (LDPE) and high (HDPE) density polyethylene (100 and 170 μm thick) and polytetrafluorethylene (PTFE) (10 μm thick) films has been performed. The drying technique of monomers, their grafting in the liquid phase, the determination of grafting value and radiation yield $G_{(-m)}$ have been published /1, 2/. The molecular weights of homopolymers in the liquid phase have been determined by viscometry and ebulliometry. According to the first approach one can consider these molecular weights to be equal to the grafting chain molecular weights.

The comparative data on the radiation-induced grafting polymerization of some, monomers are shown in Table 1. As it is seen the grafting rate of extremely dried monomers is considerably high. So it is increased by 5. 5 times for styrene and by

Table 1

Radiation-induced graft polymerization from the liquid phase

Polymer	Monomer	Drying degree of monomer	Temperature °C	Dose rate (rad/sec)	Dose (rad)	Grafting, %	$G_{(-m)}$ (mole/100 eV)	Molecular weight
HDPE	Styrene	"raw"	0°	1.7	$8 \cdot 10^3$	4.3	$4.9 \cdot 10^4$	$6.6 \cdot 10^5$
		"dry"	0°	1.7	$8 \cdot 10^3$	23.4	$2.2 \cdot 10^5$	$1.4 \cdot 10^6$
LDPE	Acrylo-nitrile	"raw"	20°C	1.2	$2.1 \cdot 10^4$	5	$4 \cdot 10^4$	$5.2 \cdot 10^5$
		"dry"	20°C	1.2	$2.1 \cdot 10^4$	15	10^5	$6.4 \cdot 10^5$
LDPE	4-vinyl-pyridine	"raw"	20°C	1.2	$7.8 \cdot 10^4$	52	$4 \cdot 10^4$	$1.5 \cdot 10^6$
		"dry"	20°C	1.2	$7.8 \cdot 10^4$	162	$7 \cdot 10^4$	$5.6 \cdot 10^6$
PTFE	4-vinyl-pyridine	"raw"	20°C	1.2	$7.8 \cdot 10^4$	1.5	$7 \cdot 10^4$	$0.8 \cdot 10^3$
		"dry"	20°C	1.2	$7.8 \cdot 10^4$	2.5	$7 \cdot 10^4$	10^4
LDPE	2-methyl-5-vinyl-pyridine	"raw"	20°C	9	$2.5 \cdot 10^4$	19	$4.7 \cdot 10^4$	$3 \cdot 10^5$
		"dry"	20°C	9	$2.5 \cdot 10^4$	35	$8 \cdot 10^4$	$4 \cdot 10^5$
LDPE	phenyl acetylene	"raw"	20°C	44	$8 \cdot 10^7$	7.0	6.0	$9 \cdot 10^3$
		"dry"	20°C	44	$8 \cdot 10^7$	10.0	8.0	$11 \cdot 10^3$
HDPE	propylene oxide	"raw"	0°C	365	$1 \cdot 10^8$	4.0	6.0	-
		"dry"	0°C	365	$1 \cdot 10^8$	4.5	7.0	-
LDPE	propylene oxide	"raw"	0°C	365	$1 \cdot 10^8$	2.5	4.0	-
		"dry"	0°C	365	$1 \cdot 10^8$	3.8	6.0	-
LDPE	acrolein	"raw"	0°C	4	$9 \cdot 10^4$	25.0	$4.8 \cdot 10^5$	-
		"dry"	0°C	4	$9 \cdot 10^4$	34.5	$6.7 \cdot 10^5$	-

3 times for acrylonitrile and 4-vinylpiridine. This is accounted for as the contribution of the ionic mechanism to the grafting process.

The grafting rate for the overall mechanism (radical + ionic) is given by Eq. (2) if the transfer rate constant is equal to zero.

$$V_{gr.} = \left\{ \left(\frac{K_p}{2K_t} \right)^{1/2} \left(\frac{G_r \cdot \rho}{100 \cdot N_a} \right)^{1/2} \cdot I^{1/2} + \frac{I \cdot \rho}{100 \cdot N_a [X]} \left(\frac{K_{1p} G_r^+}{K_{1t}} + \frac{K_{2p} G_r^-}{K_{2t}} \right) \right\} [M] \quad (1)$$

where K_p, K_{1p} and K_{2p} are propagation rate constants of the radical, cationic and anionic reactions, respectively, K_t, K_{1t} and K_{2t} are the corresponding termination rate constants, [X] is the concentration of inhibiting impurities (water in particular), I is the dose rate (eV $g^{-1}sec^{-1}$), N_A is the Avogadro number, G_R^+, G_R, and G_R^- are the radiation yields of radical, cationic and anionic centres, respectively, ρ is the concentration of polyethylene(gl^{-1}) of swollen film, M is a monomer concentration (mole l^{-1}).

According to this equation a contribution of the ionic mechanism increases when the concentration of inhibiting impurity [X] (water in the present case) decreases. Perhaps the grafting rates of monomers in Table 1 will be higher if the water concentration decreases still more.

The curve in Fig. 1 concerning kinetic studies of the system "dry" styrene - HDPE is an experimental confirmation of the ionic grafting because

$$\frac{V_{gr.}}{V_{rad}} - 1 \sim \sqrt{I} \quad (2)$$

As we can see in Table 1 the molecular weights of the polymers increase if the water concentration decreases. For example, the molecular weight increases twice for polystyrene and at about 4 times for poly-4-vinyl-pyridine.

The molecular weight of the polymer obtained both radically and ionically may be expressed (4) by

$$M_n = 1000d \; a \left\{ \frac{K_p}{K_f[M] + \left(K_t G_r I \frac{\rho}{100 \cdot N_a} \right)^{1/2}} + \right.$$

$$\left. + (1-a) \left(\frac{K_{1p}}{K_{1f}[M] + K_{1t}[X]} + \frac{K_{2p}}{K_{2f}[M] + K_{2t}[X]} \right) \right\} \quad (3)$$

where d is a monomer density, a is the fractional contribution of the radical mechanism to the overall process, K_f, K_{1f} and K_{2f} are transfer rate constants of radical, cationic and anionic mechanism, respectively.

This equation points out the independence of the molecular weight upon the concentration of the inhibiting impurity [X] under the radical mechanism and the growth of the molecular weight by decreasing [X] under the ionic mechanism.

Theoretical curves for the dependence of the molecular weights on the concentration of inhibiting impurity [X] for the different dose rates (according to Eq. (3)) show (Fig. 2) that the molecular weight of the polymer increases if the concentration of [X] decreases and the transfer rate constant is zero.

At present we have practically no experimental data on the transfer rate constants for the polymer chain propagation by the free ionic mechanism. Perhaps the transfer rate constant is small for 4-vinyl-pyridine and therefore this is the highest increasing of the molecular weight.

In recent years polymerization studies of monomers with triple bonds have been carried out. As a result polymers with double bonds exhibiting semiconductor properties have been obtained /7, 8/. However there is no information in the literature about the radiation-induced ionic polymerization and grafting of these monomers. Therefore grafting of phenyl acetylene (PA) under extremely dried conditions is of interest.

Analysis of ultra-violet spectra of polyphenylacetylene (PPA) homopolymers in benzene solution has shown the displacement of the absorption band at 325 cm^{-1} by about 15 cm^{-1} to a long wave region for PPA obtained from "dry" PA. It is explained by increasing the length of the conjugate sequences. Besides the number of paramagnetic centres (p. m. c.) is at 2. 5 times more in such homopolymers than in the homopolymer obtained from "raw" PA ($4.2 \cdot 10^{17}$ and $1.6 \cdot 10^{17}$ p. m. c. respectively). ERS-spectra are single symmetric singlets with g-factor of 2. 003 which is close to the g-factor of the free electron.

There is an increase of the grafting rate of "dry" propylene oxide as compared to "raw" ones. Infra-red spectra show difference of the grafted chain structure. The optical densities for the C-O-C and C=O bonds are different for "dry" and "raw" systems. They are equal to 3. 1-3. 6 and 2. 0-2. 2 respectively, so the polymer has 1. 5 times more C-O-C bonds under grafting of "dry" propylene oxide.

The radiation-induced ionic grafting of acrolein onto polyethylene has been performed with much higher radiation yield than radical ones and besides the homopolymer formation is small. Grafted acrolein polymers have C-O-C bonds together with aldehyde groups.

Irradiated swollen systems (polymer+monomer, polymer+monomer+solvent) have been investigated by low temperature ultra-violet-spectroscopy method for the explanation of elementary acts of the radiation-induced ionic grafting polymerization. Active centres of radical and ionic nature have been formed under irradiation in the systems close to the conditions of performing radiation-induced grafting when a monomer has been introduced in the polymer by means of swelling. Ultra-violet spectra of LDPE and PVC swollen in styrene (St) and α-methylstyrene (α-MeSt) are shown in Figs 3 and 4. As we can see PVC-radicals (250 cm^{-1} absorption band), St-radicals and α-MeSt-radicals (305-310 cm^{-1} and 320-325 cm^{-1} absorption

bands respectively), St- and α-MeSt-cation-radicals (340 and 345 cm^{-1} absorption bands), dimer St- and α-MeSt-cation-radicals (460 and 470 cm^{-1} absorption bands) are formed under irradiation of such systems (Fig. 3, curves 3, see also Fig. 4). The data on low temperature ultra-violet-spectroscopy are in accordance with the data obtained by ESR-spectroscopy and pulse radiolysis (9-11).

This is the reason to suppose that anion-radicals, active centres of anionic polymerization, form according to the interaction of monomer molecules with "dry" (quasi free) electron. The extremely high reactivity of the latter ($k \sim 10^{12}$ l/mole sec.) has been established (12-14). The formation of anion-radicals of different monomers has been established by ESR-spectroscopy method in glass hydrocarbon matrices (15-17).

According to the literature data and the results of this study we can postulate the following elementary acts of radiation-induced ionic grafting:

Cationic mechanism

$$C_6H_5CH = CH_2 \longrightarrow (C_6H_5CH = CH)_2^{+} + \bar{e} \qquad (1)$$

$$(C_6H_5CH = CH)^{+\cdot} + C_6H_5CH = CH_2 \longrightarrow CHC_6H_5(CH_2)_2\overset{+}{C}HC_6H_5 \qquad (2)$$

$$P^{\cdot} + (C_6H_5CH = CH_2)^{+\cdot} \longrightarrow P\text{-}CH_2\text{-}\overset{+}{C}HC_6H_5 \qquad (3)$$

$$P^{\cdot} + \overset{+}{C}HC_6H_5(CH_2)_2\overset{+}{C}HC_6H_5 \longrightarrow P\text{-}CHC_6H_5(CH_2)_2\overset{+}{C}HC_6H_5 \qquad (4)$$

$$R - \overset{CH_2}{\overset{|}{\underset{CH_2}{\overset{|}{C^{+}}}}} + CH_2 = CHC_6H_5 \longrightarrow R - \overset{CH_2}{\overset{|}{\underset{CH_2}{\overset{|}{C}}}} - CH_2\text{-}\overset{+}{C}HC_6H_5 \qquad (5)$$

$$\overset{CH_2}{\overset{|}{\underset{CH_2}{\overset{|}{CH^{+\cdot}}}}} + \dot{C}H = CHC_6H_5 \longrightarrow \overset{CH_2}{\overset{|}{\underset{CH_2}{\overset{|}{CH}}}} - CH_2 - \overset{+}{C}HC_6H_5 \qquad (6)$$

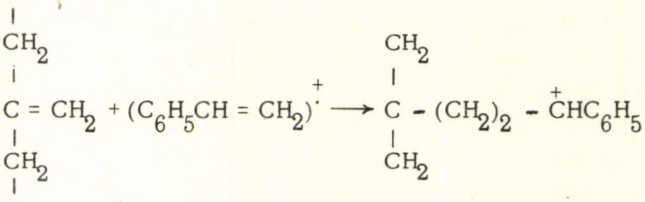

(7)

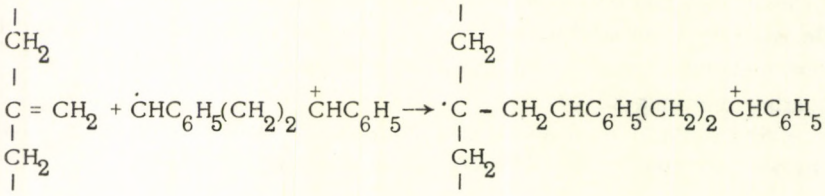

(8)

Anionic mechanism

$$CH_2 = CH - CN + e \longrightarrow (CH_2 = CH - CN)^{\cdot -} \quad (9)$$

$$(CH_2 = CH - CN)^{\cdot -} + CH_2 = CH - CN \longrightarrow \dot{C}HCN(CH_2)_2\,\bar{C}HCN \quad (10)$$

$$P^{\cdot} + (CH_2 = CH - CN)^{\cdot -} \longrightarrow P - CH_2 - \bar{C}HCN \quad (11)$$

$$P^{\cdot} + CHCN(CH_2)_2\,\bar{C}HCN \longrightarrow P - CHCN(CH_2)_2\,\bar{C}HCN \quad (12)$$

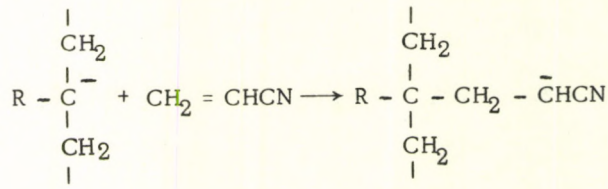

(13)

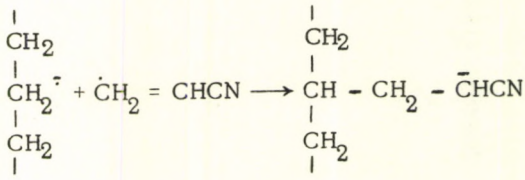

(14)

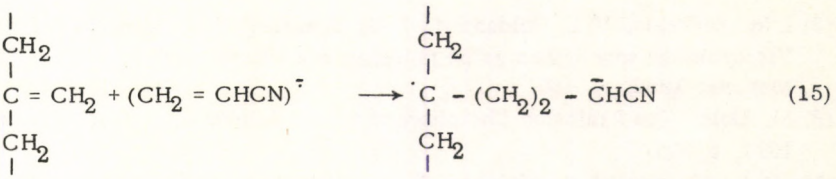

(15)

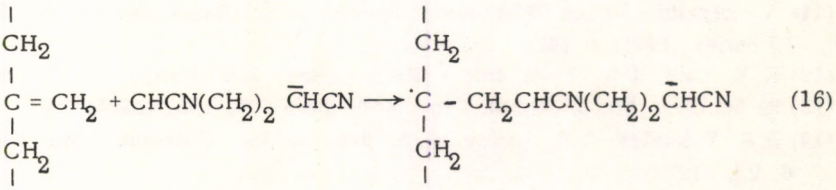

(16)

So ion-radicals as first intermediates (reactions 1 and 9) are generated under irradiation of the "dry" system "monomer-polymer" in the liquid phase. The second step of the initiating process in the liquid phase is formation of dimer ion-radicals (reactions 2 and 10) since the dimer-formation is characteristic for many irradiated olefins. Ion-radicals and dimeric ion-radicals can combine by their radical ends with radicals generated in the polymer according to reactions 3, 4, 11 and 12. Ionic centres (ions and ion-radicals) generated under irradiation in the polymer combine with monomer molecules and radicals (reactions 5, 6, 13; 14). The combination of ion-radicals and dimer ion-radicals with the residual or formed double bonds can also facilitate the ionic grafting according to reactions 7, 8, 15, 16. An initial event of radiation-induced ionic grafting can be either radical or ionic. The relationship between the number of these events depends on the conditions, perhaps. In all the above mentioned reactions an ionic centre is generated which is the beginning of the polymer chain propagation by the free-ionic mechanism.

References

(1) V. Ya. Kabanov, L. P. Sidorova, Vysokomolek. Soedin., 14A, 2091, (1971).

(2) V. Ya. Kabanov, L. P. Sidorova, V. I. Spitsyn, Europ. Polym. J., 10, 1153, (1974).

(3) A. Chapiro, Radiation Chemistry of Polymeric Systems, New York–London, 1962.

(4) B. L. Tsetlin, A. V. Vlasov, I. Yu. Babkin. "Radiation Chemistry of Polymers", "Nauka", Moscow, 1973, p. 198.

(5) A. M. Jendrychowska-Bonamour. Europ. Polym. J., 6, 1491, (1970).

(6) A. Chapiro, A. -M. Jendrychowska-Bonamour. Compt. Rend. Acad. Sci., C265, 484, (1967).

(7) A. A. Berlin et al. Chimiya polisoprjazhennych sistem, "Chimiya", Moscow, 1972.

(8) I. M. Barkalov, V. I. Goldanskii, B. G. Dzantiev, S. S. Kuzmina. Trudy II Vsesoyusnogo soveshchaniya po radiatsionnoi chimii, Izdatelstvo AN SSSR, Moscow, 1962. p. 455.
(9) M. Dole. The Radiation Chemistry of Macromolecules, v. 1, N. Y. –London, 1974, p. 335.
(10) V. P. Khimov, G. S. Zhdanov, V. K. Milinchuk. Tesisy dokladov II Vsesoyusnoi konferentsii molodych uchenych po radiatsionnoi chimii, Obninsk, 1975.
(11) K. Hayashi. Action Chimique et Biologique des Radiations, ed. M. Haissinsky, 15 Series, 1971, p. 145.
(12) K. Y. Lam, J. W. Hunt. Int. J. Radiat. Phys. and Chem., 7, 317, (1975).
(13) R. Schiller. Int. J. Radiat. Phys. and Chem., 7, 193, (1975).
(14) B. S. Yakovlev, I. A. Boriev, A. A. Balakin. Int. J. Radiat. Phys. and Chem., 6, 23, (1974).
(15) T. Gillbro, J. Polym. Sci., Lett. Ed., 11, N5, 309, (1973).
(16) M. Iwasaki, M. Fukaya, S. Fusii, H. Muto. J. Phys. Chem., 77, 2739, (1973).
(17) A. D. Abkin, A. P. Sheinker, G. N. Gerasimov. "Radiation Chemistry of Polymers", "Nauka", Moscow, 1973, p. 7.

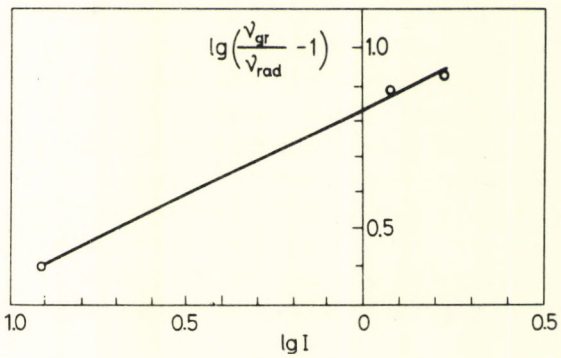

Fig. 1 ($V_{gr}/V_{rad} - 1$) as a function of $I^{1/2}$ for grafting of styrene onto high density polyethylene

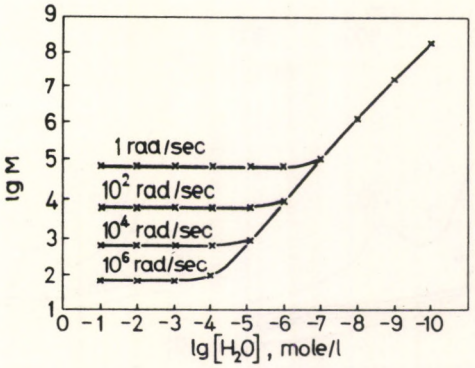

Fig. 2 Molecular weight of the polymer as a function of water concentration in the system for different dose rates (theoretical curves)

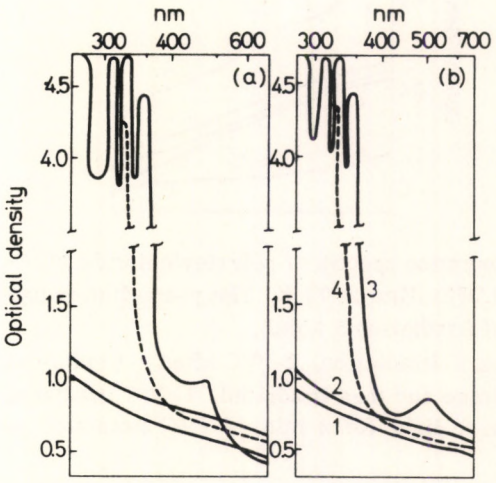

Fig. 3 Ultra-violet absorption spectra of polyvinylchloride (PVC) films irradiated at 77 K (dose of radiation 5 Mrad). The spectra were recorded at 77°K.
a) 1-PVC, 2-PVC swollen in 1.2-dichloroethane, 3-PVC swollen in a mixture of α-methylstyrene (6.8 mole), 4-same as in 3 but prior to taking the spectrum samples were kept for 15 min at 195°K,
b) same as in a) but styrene (7.8 mole) was used instead of α-methylstyrene

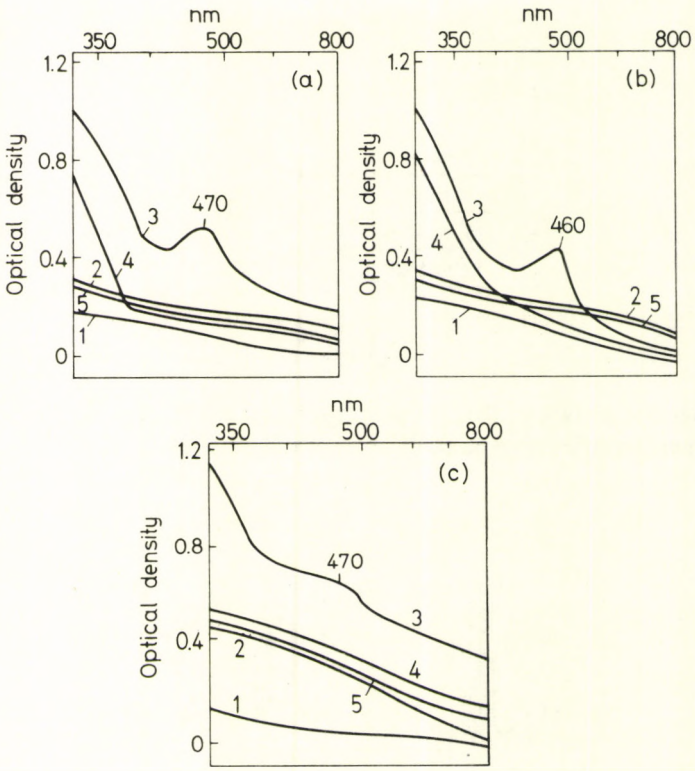

Fig. 4 Ultra-violet absorption spectra of polyvinylchloride (PVC) and high density polyethylene (LDPE) films at 77 K. The γ -irradiation had been performed at 77 K (dose of irradiation 5 Mrad).

a) 1-PVC before γ -irradiation, 2-PVC after γ -irradiation, 3-PVC swollen in α -methylstyrene and then irradiated, 4-PVC irradiated and then photo-bleanched by u. v. light for 2 min, 5 PVC irradiated and then kept at 195 K for 15 min,

b) same as in a) but styrene was used instead of α -methyl-styrene

c) 1-LDPE before γ -irradiation, 2-LDPE after γ -irradiation 3-HDPE swollen in α -methylstyrene and irradiated, 4-HDPE irradiated and then photo-bleached by u. v. light for 2 min, 5 LDPE irradiated and then kept for 15 min at 195 K.

MODIFICATION OF INORGANIC MATERIALS WITH POLYMERS BY IONIZING RADIATION

M. Pešek, J. Jarkovský, F. Pultar
Institute for Research, Production and Application of Radioisotopes, Prague, Czechoslovakia

Somewhat later than in the case of wood-plastic combinations, a similar technique of impregnation and curing has begun to be applied to other materials, too. Approximately ten years ago, experiments started with the modification of concrete and other inorganic materials /1-6/. Nowadays, this is one of the areas of greatest interest in applied radiation chemistry.

I will not go into all the technologic processes which can be used for the preparation of combinations of inorganic materials with polymers. After all, similar combinations have been known already before, e. g. polymer mortars and polymer concrete. These materials, however, are prepared by other techniques, e. g. by mixing of mortar with PVAc, PVC or other dispersions and they have different properties and applications.

Our attention was paid to systems where inorganic semi-products are impregnated with the impregnation mixture and in the second step the monomers incorporated in the inorganic semi-product are cured by the effect of ionizing radiation.

Using the impregnation and curing by ionizing radiation, a number of materials can be modified, as for instance bricks, unglazed ceramics, various products of cement or asbestos cement, semi-products of plaster or Sorel cement, sandstone, marl, various kinds of limestone, granite sediments, pyrite and aluminium plant wastes, flotation sludges and a number of other inorganic materials. Polymerizable monomers alone or their mixtures can be used as impregnation mixtures, e. g. methyl methacrylate and other acrylates and methacrylates, unsaturated polyester resins and their mixtures with monomers, e. g. with styrene, methyl methacrylate or with other polymerizable compounds.

When using trichloroethyl or tetrachloroethyl acrylates and methacrylates, non-flammable combinations of inorganic materials with polymers or combinations containing a non-flammable organic component can be prepared. In this case low viscosity materials which penetrate readily into the fine pores of the inorganic material are used. These monomers are low volatile and polymerize at lower radiation doses than other monomers.

The unsaturated polyester resins alone are at normal temperatures too viscous for the impregnation of most inorganic materials. It is advantageous to use them

either diluted with other less viscous monomers or it is preferable to heat the impregnation mixture before use. Using adequate viscosities of the impregnation mixture, we can, in addition, control the impregnation depth and thus the consumption of the impregnation mixture and the properties of the product.

The monomers incorporated in the inorganic semi-product are preferably polymerized by ionizing radiation. The curing may be also accomplished with the use of chemical initiators but this method has a number of disadvantages. First, there is the danger of polymerization of the impregnation mixture in the storage tank or in the impregnation vessel, and second, the impregnated articles require a a relatively long heating which leads to the loss of the volatile components of the impregnation mixture from the surface of the impregnated articles, the viscosity of the impregnation mixture increases gradually, the impregnation mixture cannot be heated during impregnation, and so we could continue enumerating further drawbacks.

The radiation method is therefore preferable, namely in industrial applications. On the other hand, it requires higher costs for the construction of the irradiation unit. The radiation doses required for the curing of the incorporated impregnation mixture differ according to the type of the used monomer dose rate and irradiation conditions. For impregnation mixtures based on unsaturated polyester resins which contain up to 50% styrene, the radiation doses necessary for the curing of the incorporated impregnation mixture amount to about 1 Mrad. For methyl methacrylate and gamma radiation this value is about 2 Mrad.

By this technique it is possible to modify a number of materials, semi-products and products. This treatment reduces the absorptivity of the so stabilized materials, increases the resistance to temperature variations and corrosive environment, improves the mechanical properties, appearance and some other properties, as for instance polishability.

We will not discuss all application possibilities of this method, the greatest part of which are described in the literature. We shall concentrate on one prospective area, namely on lining materials made of inorganic-polymer combinations.

Marble, travertine and similar lining materials are extensively used in the building industry but they are in rather short supply.

High quality lining materials can be, however, prepared by impregnation of inorganic semi-products with a polymerizable impregnation mixture and successive curing by ionizing radiation. The basic inorganic semi-products, blocks for instance, can be prepared from ground or crushed limestone, flotation sludges, ground marl, power plant ashes or other materials and from cement or plaster or other hydraulic binders. We have tested a relatively great number of combinations of various inorganic materials with different compositions of the basic inorganic components. To obtain good results with plaster as binder, however, it is necessary to use a relatively large quantity of the impregnation mixture (40 to 50% related to the mass of the starting semi-product) which is uneconomical. With plaster as binder and and impregnation mixture containing 80% CHS Polyester 115 and 20% styrene-acrylonitrile /50:60/ the samples showed a compression strength of 500-1500 kp/cm^2.

The properties may be further improved by addition of fibrous materials like glass, basalt or even metal fibres and by the use of cement as binder of the inorganic semi-product. These semi-products accept less polymer than materials prepared with plaster as principal binder. In dependence on the impregnation conditions, thickness and on the composition of the impregnation mixture, these materials contain from 5 to 25% polymer.

The following procedure was employed for the preparation of construction materials like panel boards and for testing samples:

1. A block was cast from the basic components and allowed to set.
2. The block was cut into plates of required thickness, usually 2—2. 5 cm.
3. The plates were dried first in air and then in a drier at about 80°C.
4. The plates were impregnated using vacuum and overpressure of the mixture of 80% CHS Polyester 115 and 20% styrene-acrylonitrile.
5. The incorporated impregnation mixture was polymerized in sealed containers by ^{60}Co-gamma radiation at an average dose rate of 0.06 Mrad/h.
6. The samples were ground and polished.

By this procedure both the samples for performance tests and panel boards 60 x 25 x 2,5 cm were prepared. The samples of test cubes and balks were checked for the following properties:

- Compression strength, where the material was tested in dry state, soaked with water, frozen and heated.
- Tensile bending strength (dry, soaked, frozen, heated).
- Mechanical coefficients.
- Thermal expansivity and swelling capacity.
- Grindability.
- Machinability and polishability.
- Weathering resistance (sodium sulphate test).

In addition, the cutting properties of the untreated blocks of the starting inorganic material were determined and it was found in all cases that the inorganic semi-product can be cut very well on circular and frame saws generally used in quarries. The inorganic semi-product can be also well cut, milled, ground or otherwise machined. The overall machinability was estimated as "easy". According to performance standards used in the Czechoslovak stone industry, the samples were listed in the first category of difficulty among the Carara marble, Spiš travertine and others, or even better.

To enable a comparison we are presenting the values of these new materials and those of two types of Czechoslovak marbles:

1. Marble Supíkovice (Moravia - Jeseník), this is a marble of fair quality
2. Marble Nezdice, medium quality marble.

Simple compression strength. /ČSN 721157/ cube 5 cm.

Dry. Modified samples ..... 640 kp/cm^2
Marble Supíkovice ..... 700–1000 kp/cm^2
Marble Nezdice ..... 500–650 kp/cm^2

After freezing (25 cycles) to −20°C.

Modified samples ..... 430 kp/cm^2
Marble Supíkovice ..... 660–850 kp/cm^2
Marble Nezdice ..... 500–750 kp/cm^2

After heating (25-fold heating of the soaked material to +70°C and 25-fold cooling to +20°C in water bath, 1 cycle, duration 1 day).

Modified samples ..... 520 kp/cm^2
Marble Supíkovice ..... 700–900 kp/cm^2
Marble Nezdice ..... 460–700 kp/cm^2

Tensile bending strength. (ČSN 721157) balks 2x5x15cm. The samples were tested dry, soaked, frozen and heated.

Dry. Modified samples ..... 80–150 kp/cm^2
Marble Supíkovice ..... 64–140 kp/cm^2
Marble Nezdice ..... 40–73 kp/cm^2

In addition, the fragility, softening, freezing and heating coefficients were determined. All results lie within the marble values.

Grindability. (ČSN 721158) The tests were performed on the Amsler testing machine.

Modified samples ... 0.224, 0.315, 0.244 cm^3/cm^2
Marble Supíkovice .. 0.344, 0.337, 0.298 cm^3/cm^2
Marble Nezdice ... 0.454, 0.410, 0.437 cm^3/cm^2

The results indicate that the values are very favourable. The grindability is a property which is important for the possible use as floor coverings and also for the general evaluation of machinability.

Thermal expansivity. It was determined on balks 20x30x150 mm and is comparable with marbles.

Linear swelling is also comparable with marbles.

Machinability is very good, all tested samples were listed in the first group with Carara marble, travertine from Spiš, Tušín, etc.

Gloss was estimated as dull, incoherent, which is quite acceptable.

Weathering resistance. (Sodium sulphate test – ČSN 721176). Samples 5x2x15cm were used for these tests. The samples were soaked with a saturated solution of sodium sulphate and put in the drier where they were heated overnight to 105°C and this procedure was repeated. After a few cycles the samples were examined for weight loss. Generally it can be said that materials which exhibit after 10 cycles a weight loss of less than 12% are suited for outside use. This test is rather deleterious and the materials often decompose completely. With marbles the loss is usually up to 5%. In the tested cured samples practically no weight losses were observed. It

should be noted, however, that the tests were preformed on a smaller number of samples than is prescribed by the standard.

These tests indicate that the materials are very well suited both for indoor and outdoor applications and for floor building industry nowadays which are of a considerably inferior quality.

Although these results appear very favourable, there are nevertheless still problems to be solved. In some samples for instance, the impregnation of the whole mass is not complete and even on the surface of the plates small areas can sometimes be observed which are not sufficiently impregnated. These problems remain to be solved.

Lining materials based on this principle may be prepared also as lightweight by preparing e. g. the basic inorganic material in porous form like travertine, or by adding porous foamy materials to the inorganic mixture when preparing the basic inorganic semi-product.

Moreover, various additives can be added to the impregnation mixture, both soluble or dispersed. So we can add for example dispersed dyes, bronze, aluminium powder or else, which partly fill the cavities in the impregnated boards and after grinding display interesting decorative effects. By adding dyes to the basic inorganic materials, different colour shades, marbling and colour combinations can be obtained.

This method can be used also for a number of natural materials, like limestones, sandstones, marls, etc. We have reached good results for instance with this method of impregnation and successive radiation curing with limestones from Vrača (Bulgaria). We have obtained a material with improved physico-mechanical properties which is easily polishable, with a marked grain and in various color shades. Limestone itself is not polishable, which considerably reduces its value.

We have shown only one of the application possibilities of such materials and we have demonstrated that this new technique has a much wider field of application. However, the floor coverings and lining materials prepared by this method could be the beginning of a widespread assertion of these new inorganic-polymer combinations.

References

/1/ U. S. pat. 3 567 496.
/2/ Brit. pat. 1 143 898.
/3/ Czech. pat. 146 178.
/4/ French pat. 2 035 979.
/5/ USSR pat. 346 276.
/6/ Singer, K., Paper presented at the Third Symposium on Radiation Chemistry, Tihany, 10-15 May 1971. Paper B/59.

T. CZVIKOVSZKY

Concerning the weatherability of your product what is the time scale of the mentioned sodium test?

Did you measure the long term properties of your product and did you confer the sodium test with some classical methods, as xenotest or natural ageing?

Did you compare the properties of your composite material with chemically hardened polyester marble or epoxy mortar composites?

M. PESEK

The duration of one cycle of the sodium test is one day and the test is composed of 10 cycles. The long term properties have not been measured yet.

The properties of the composite are generally dependent on the amount of polymer present. Composites with epoxy resins have generally better properties, but the epoxy systems are more expensive than the polyester ones.

I. BABKIN

Did you observe any effect of heat treatment, I mean by heating the system above the melting point, on the properties, while dealing with non crosslinked polymers?

M. PESEK

We have dealt with crosslinked polymers only.

J. ZURAKOWSKA-ORSZÁGH

Did you consider the economic aspects of the industrial process?

M. PESEK

Yes we did. The economic aspects are the most important in the complex problem of inorganic - polymer composites. In the Czechoslovak building industry marble is imported from Bulgaria mainly. From this point of view it is possible to consider the economic success of this product.

DIFFUSION OF LOW MOLECULAR WEIGHT SUBSTANCES INTO RADIATION-GRAFTED POLYMER FILMS

I. Yu. Babkin, A. I. Krasnogorov, K. N. Kitaev, G. V. Solovyeva
The Branch of the Karpov Institute of Physical Chemistry, Obninsk, USSR

The formation of a near-surface layer grafted on polymer films and fibres from the gaseous phase is a complicated process as far as kinetics and structure of the forming polymer and captured substrate layer are concerned. An approximate description of this process assuming its stationary character /1/ allows us to determine only the type of the grafted polymer distribution in the bulk of the film. Meanwhile structural features of the grafted layer formed under condition of diffusion kinetics are of interest from the point of view of peculiar conditions of its formation (rather low and variable monomer concentration, radiation cross-linking, retardation of structural relaxations). Moreover, these structural features can improve barrier (insulating) properties of polymer films by decreasing their structural and technological defects, free volume and diffusion ways, etc.

Experimental

Polytetrafluoroethylene (PTFE) and high pressure polyethylene (PE) films were used in this work, the film thickness being from 50 to 100 μm. Grafted polyacrylonitrile (PAN) and polystyrene layers were obtained by γ and electron irradiation (0.8 Mev) of the films in monomer vapours at 28°C and relative pressure $P/P_s = 0.9$. To obtain clearly expressed heterophase systems the conditions of polymerization were chosen in accordance with the characteristic parameter of the grafted polymer distribution /1/

$$\alpha = \left[\left(\frac{K_p^2}{K_o} G \right)^{1/2} \frac{I}{D^*}^{1/2} \right]^{1/2} \frac{L}{2} \qquad (1)$$

where K_p and K_o are the propagation and termination constants respectively: G is the radiation radical yield in the film, I is the dose-rate, D^* is the diffusion coefficient of the monomer. The α values varied from 1 to 5.

Structural modifications of the grafted layers were obtained in different ways: by removing the corresponding solvents to which the samples were exposed: by rapid

substitution of dimethylformamide by methanol, or by liophylization (porous structure or B - structure) and by removing the solvent slowly (packed H structure). Visual observation of a rough surface relief was made by a JSH-2 type scanning electron microscope. Experimental values of vapour adsorption on the surface A_o were determined from the initial diffusion fluxes, measured by the device described in /2/. The distribution of the grafted polymer in the bulk of the film was controlled by microinterferometry of cuts by method /3/. The permeability was determined by the Gardner method /4/.

For studying the microrelief of the grafted film surface in terms of specific surface S_a we used the idea of "net" isotherms of adsorption /5/. These isotherms, obtained from the sorption kinetics data by extrapolation to zero-time adsorption equilibrium namely at the surface of polymer $a_o\,(P/P_o)$. The amount of a low molecular weight substance in the adsorption layer is connected with the average concentration of it in the bulk $\bar{c}\,(t)$ at the time t and the limit equilibrium concentration c_m by means of the equation

$$a_o = \frac{Ac_m - \bar{c}\,(t)}{1-A}$$

where

$$A = 1 - \frac{8}{\pi^2} \sum_{n=1}^{\infty} \frac{1}{(2n-1)^2} \exp\left[-(2n-1)^2 \frac{\pi^2 Dt}{L^2}\right] \qquad (2)$$

where D is the diffusion coefficient, L is the film thickness.

Considering the adsorbate on the polymer film as a real two-dimensional gas, "net" isotherms were described by the equation of non-localized adsorption /6/

$$\frac{\Theta}{1-\Theta} + \ln\frac{\Theta}{1-\Theta} - \ln\frac{P}{P_s} = \ln K, P_s - K_2\Theta \qquad (3)$$

where

$\Theta = \frac{a}{a_m} = \frac{a_o \omega N}{Sa}$, a_o is the same as in Eq. (2) a_m is the capacity of the monolayer, ω is the area occupied by the adsorbate molecule in the packed monolayer, N is Avogadro's number, K, and K_2 are constants taking into account adsorbate-adsorbent and adsorbate-adsorbate interaction respectively, P/P_s is the relative pressure, S_a is a specific surface considered as the characteristics of the surface microrelief.

Results and discussion

The formation of the heterophase system in the course of grafting from the gaseous phase is expressed in the typical shape of the kinetic curves. The characteristic results for one of the studied systems (PE-PAN) are given in Fig. 1. At low dose rate (curve 1) the curve has an S- form showing acceleration of the process in the middle part, caused by "purification" of the system from inhibiting contaminations as well as by the stimulating influence of gel-effect. In this case the grafted polymer is comparatively uniformly distributed through the film thickness and a high degree of grafting can be achieved at relatively low doses.

At higher dose rates (curves 2 and 3) two stages of the process are observed: rapid formation of a "stop" layer /7/ (stage 1) and sharp decrease of the rate (stage II) the rate of the process being constant up to high doses in stage II. The latter is due to the fact that in this stage monomer is grafted on the layer of its own polymer. This agrees with the data of grafting rate of acrylonitryle on pure PAN film of the same thickness (curve 4) under similar conditions. It is also confirmed by the character of the PE+PAN film thickness change in the course of grafting (Fig. 2). While forming a "stop" layer the thickness is practically unchanged then its uniform proportional growth under stationary conditions of outer layer formation is observed.

The most essential structural changes occur in the film in stage I. In this connection a significant change of the value of "true" outer surface area perunit of visible geometrical area which is due to the microrelief evolution should be noted. Such increase of the "roughness" owing to the appearance of supermolecular PAN structures on the film surface and their formation in stage I gradually results in packing this layer. This follows from the decrease of the S value (Fig. 3) at high doses before the beginning of stage (II).

(Special experiments showed that only irradiation of the films in the absence of monomer did not give great changes of S.)

This dependence has a somewhat different character for the PTFE-PAN system (curve 2), but its correct interpretation is complicated by the destruction of the substrate at high doses.

The analysis of the grafted polymer distribution and film properties shows that three characteristic zones can be selected in the grafted layer (Fig. 4):

I: diffusion zone with little content of grafted polymer,

II: a "stop" layer.

III: a pure grafted polymer layer in the mixture with homopolymer.

Relative changes of the permeability of vapours through PE films after PAN grafting under different conditions are given in Fig. 5. Comparatively uniform distribution of PAN throught the film bulk ($\alpha \leqslant 1$) is seen to result in a moderate drop of relative permeability even at high content of PAN. In this case a continuous PAN phase or a tight enough contact between PAN microphase and PE matrix does not appear to be formed and the structure is not packed by the grafted polymer. This results in a practically linear dependence of $\lg P/P_0$ on PAN fraction. On the contrary,

in the case of formation of layers II and III (curves 2 and 3) the relative drop of permeability is very sharp: PE+PAN film containing 19% of PAN is less permeable than pure PAN.

Let us consider how directed structuring of the grafted layer influences the permeability of the film to the vapours of lov molecular weight substances. Previously it was shown /5/ that in suitable solution swelling the grafted polymer layer may give it the most porous (high values of C_0 by adsorption of alcohols and hydrocarbons) and the most densely packed (low values of a_0) structures by either rapid substitution of the solvent for the insolvent or by removing the solvent by slow evacuation. Such modification of the structure always results on increase in the permeability (black points and points 4, 5 in Fig. 5) the greatest effect (a shift of $\lg P/P_0$ values) being observed for the samples with a well formed stop layer. It is significant that despite the large difference of a_0 and S values for structures H and B /5/ their permeabilities are nearly the same. Parallel with the structural modification of layer III easily detected by adsorption methods, the separation of microphase of the grafted polymer on layer II appears to take place in addition of the solvent this being accompanied by the appearance of additional diffusion ways. It is based on the supposition that the polymer layers formed at high dose-rates are anomally packed non-relaxed systems, having higher barrier properties and the main diffusion resistance being in layer II.

References

/1/ G. Odian, R.L. Kruse, J. Polym. Sci., 691 (1969).

/2/ J.Yu. Babkin, A.J. Krasnogorov, M.M. Mitin, Zavodsk. Lab. 39, 113 (1973).

/3/ H. Matsuo, K. Iino, M. Kondo, J. Appl. Polym. Sci., 7, 1833 (1963).

/4/ H.F. Payne, W.M. Gardner, Ind. and Eng. Chem., 29, N8, 893 (1937).

/5/ J.Yu. Babkin, A.J. Krasnogorov, K.N. Kitaev, Vysokomol. soed. A 17, No 8, 1835 (1975).

/6/ T. Hill, J. Chem. Phys., 14, 144 (1946).

/7/ J. Dobo, Magyar. Kem. Lapja, 25, N7, 368 (1970).

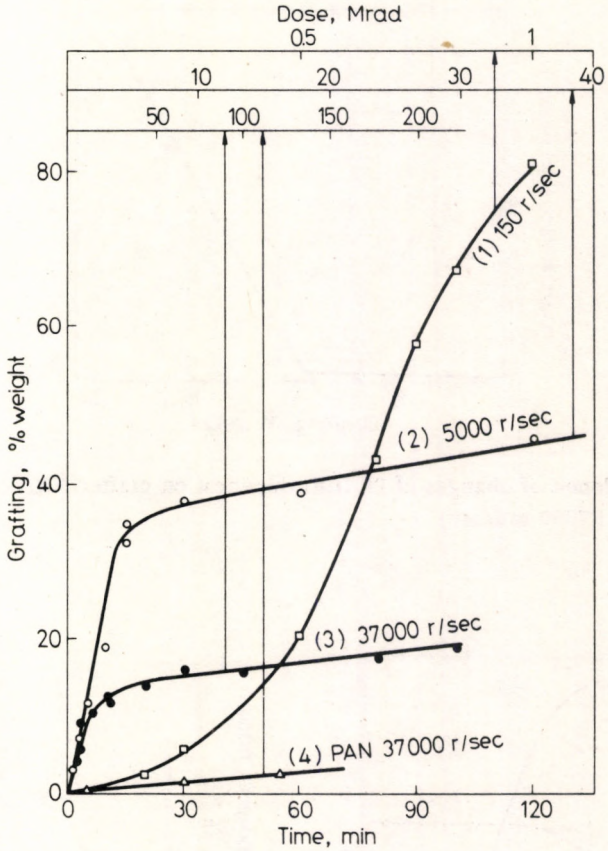

Fig. 1 Kinetics of (PAN) accumulation on (PE) and polyacrylonitrile films

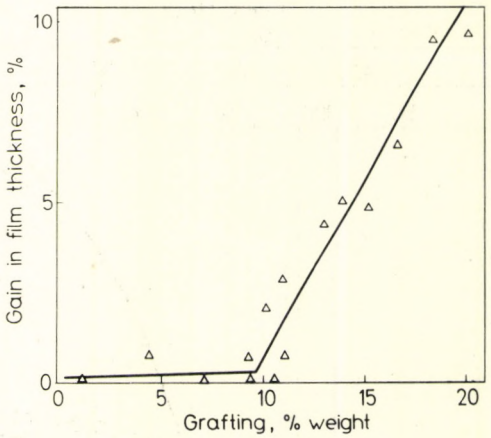

Fig. 2 Dependence of changes of PE film thickness on grafted PAN content (dose rate -- 37000 rad/sec)

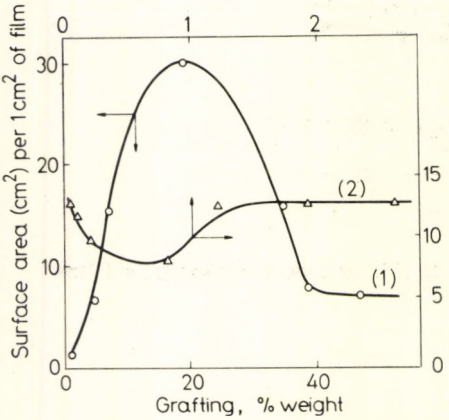

Fig. 3 Dependence of true surface area on the content of grafted PAN. 1 - PE+PAN, 2 - PTFE+PAN (dose rate 5000 rad/sec)

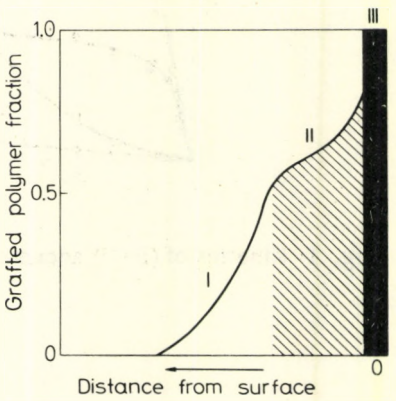

Fig. 4 Scheme of zones formed by grafting

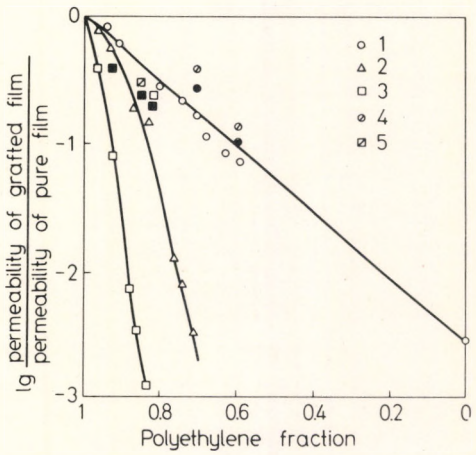

Fig. 5 Changes of the relative permeability of hexane vapour through PE films modified by grafting with acrylonitrile at dose rates: 1 - 150, 2 - 5000, 3 - 37000 rad/sec. Black points and points 4, 5 after formation of structures H and B, respectively

DISCUSSION

J. ZURAKOWSKA-ORSZÁGH

Do you have some information on the average molecular weight of the grafted copolymers? Did you get a few long, or many short branches?

J. BABKIN

We have no reliable data on the molecular weights because it is not easy to separate the grafted polymer from polyethylene. The other complication is that the grafted layers are crosslinked.

EFFECT OF HIGH PRESSURE ON THE FORMATION OF FREE RADICALS IN RADIOLYSIS OF POLYMERS

V. K. Milinchuk, V. P. Kirjuhin, E. R. Klinshpont
The Branch of the Karpov Institute of Physical Chemistry, Obninsk, USSR

Introduction

The rate and the way of chemical reactions in the gaseous, liquid and solid phases are known to depend greatly on high pressures /1/. However, no data about high pressure effect on the radiolysis of polymers are available. The investigations of high pressure effect on the radiochemical processes in the solid state are of great importance for establishing the elementary stages of the radiolytic mechanism and for the elucidation of the possibility of action on the efficiency and direction of radiation conversions of substances by means of high pressures.

In the present work a study was carried out to find the regularity of free radical formation in polytetrafluoroethylene (PTFE), polypropylene (PP) and polyethylene (PE) irradiated by γ–ray at pressures from 1 to 27 kbars.

Experimental

The experiments were carried out with commercial polymers. The samples of polymers were irradiated at 77 and 300 K by ^{60}Co γ–rays at a dose–rate of 700 rad/sec. The high pressures at 77 K were obtained in a thick–walled brass cylinder which was filled with water. It was then closed and cooled slowly to 77 K. Due to the water–ice phase transition a pressure of 1. 5 kbar built up inside the cylinder /2/. A control sample was irradiated in the opened cylinder. Irradiated samples were taken out of the cylinders under the layer of liquid nitrogen. Pressures from 1 to 27 kbars at 300 K were obtained in a "plunger–cylinder" chamber (Fig. 1), made of steel Y 8A hardened up to 56–58 HRc. The pressure in the chamber was determined by the force acting on the area of the sample. The radical concentration was determined by ESR study.

Results and discussion

The results of measuring concentration of the free radicals in polymers γ–irradiated at normal and high pressures are given in Table 1. One can see in PTFE and PP the free radical vs concentration decreases 1. 3–1. 5 times at 1. 5 kbar. The high

Table 1

The effect of high pressure on the formation of free radicals in radiolysis of polymers at 77 K

Sample	Dose, Mrad	Radical concentration 10^{18} cm^{-3}		
		at P_1 = 1 bar	at P_2=1.5 kbar	$[R]_{P_1} / [R]_{P_2}$
Polytetrafluoroethylene	30	1.3	0.85	1.5
Polypropylene	9	22	16.5	1.3
Polyethylene	7	21.0	22.0	1

pressure effect on the generation of radicals under γ-irradiation in PE has not been observed. The obtained results show the decrease of the radical yield in some polymers at high pressures.

The yield of free radicals (G_R) is one of the main values allowing one to evaluate the efficiency of radiochemical transformations in the polymers. It is usually determined by the linear part of a dose curve. Initial parts of the curve of accumulation of peroxide radicals in PTFE at 300 K at normal and high pressures are given in Fig. 2. The high pressure is seen to decrease greatly the G_R in PTFE. At 5 kbar, G_R is twofold less and at 14 kbar is fourfold less compared with the G_R in the polymers γ-irradiated at normal pressure. The effect of pressure on G_R in PTFE in a region of 1 to 27 kbars is shown in Fig. 3a. Increasing pressure from normal to 1 kbar decreases G_R twofold and keeps this value at a pressure up to 7 kbar. The G_R value decreases again at a pressure of more than 7 kbar.

The dependence of G_R on pressure may be connected with phase transitions of PTFE. PTFE under high pressures is well known to undergo polymorphous transitions [3,4] and at a pressure from 1 to 27 kbar it may be in three different phases (Fig 3,b). The first and the second phases are less dense and more compressible. High pressures in these phases result in a twofold decrease in the same efficiency. G_R is, to a large extent, influenced by the pressure in the third phase which is more dense and less compressible. Thus, the mechanism of high pressure effect on G_R appears to be different in different phases.

The high pressure may influence the scission of chemical bonds and free radical reactions as well. It is probable that the high pressure in PTFE in the first and the second phases influences the secondary processes occurring in the irradiated polymer, i.e. the free radical reactions which occur as a result of the break-up of C-C-bonds, which are initially as radical pairs in a "cage".

That the high pressure decreases the process of radical generation due to the break-up of C-C bonds is confirmed with the dependence of the radical concentra-

tion upon the temperature (Fig. 4). In PTFE γ-irradiated at normal pressure and containing "middle" ($\sim CF_2CF(O\dot{O})CF_2\sim$) and "terminal" ($\sim CF_2CF_2\dot{O}_2$) peroxide radicals in approximately equal ratio, the radical concentration begins to decrease at temperatures higher than 310 K. In the sample γ-irradiated at 1.5 kbar the radical decay begins at temperatures higher than 370 K. This is due to the fact that PTFE samples γ-irradiated at high pressure contain mainly "middle" peroxide radicals which have higher thermostability compared with "terminal" ones /5/. In PTFE containing only "terminal" peroxide radicals, the radical decay begins at the same temperature as in the sample γ-irradiated at normal pressure. Increasing the radical thermostability and decreasing G_R (about twofold) in the samples, γ-irradiated at a pressure up to 7 kbar proves the suppression of the break-up of C-C-bonds. The pressure up to 7 kbar in PTFE appears to increase the rate constant of radical recombination in the "cage".

The great decrease of G_R in the third phase shows that the pressure more than 7 kbar acts on the scission of C-F bonds. It might be supposed that in the third phase due the to high density of the polymer, the formation of radicals decreased owing to the "cage" effect. However, the polymer density is little changed and cannot greatly affect the rate constant of F-atom leaving the "cage".

It is quite probable that the high pressure affects the stages preceding the radical generation, for instance, the processes of transfer and dissipation of the absorbed energy. It is known that at high pressures a shift of electron levels of the molecules occurs, triplet states being changed to a smaller extent than singlet ones [6]. According to Ref. /7/, the generation of free radicals in hydrocarbons occurs over triplet states by predissociation. If it is supposed that in PTFE the generation of radicals occurs over the triplet states, the decrease of radical yield with increasing pressure, observed in the third phase may be connected with the decrease of singlet-triplet separation. The diagram of singlet-triplet levels at normal and high pressures is given in Fig. 5. The scheme shows the possibility of decreasing intersystem crossing at high pressure. This results in the decrease of the generation of radicals in PTFE due to scission C-F bonds from triplet states. It is the shift of the singlet-triplet states. It is the shift of the singlet-triplet states under pressure that explains the decrease of the efficiency of photochromic processes occurring over the triplet states /8/.

Thus the decrease of the radical yield at high pressures shows great depression of radiochemical processes in polymers. It is clear that the efficiency and the way of radiochemical processes in both polymers and other substances may be affected by high pressure. Additionally, the application of high pressure is sure to open new possibilities of studying the elementary stages of processes occurring in a substance under high energy radiation.

References

/1/ A. Ya. Kalashnikov, Zh. Vsesoyusn. Kim. Obshch. im. D. I. Mendeleeva 18, 61 (1963).

/2/ B. G. Lasarev, L. S. Kan, Zh. Eksp. Teor. Fis., 14, 439 (1944).

/3/ L. D. Lifshitz, Yu. S. Genshaft, V. K. Markov, Yu. N. Ryabinin, Vysokomolek. Soed., 3, 624 (1961).

/4/ C. Pistorius, Polymer, 5, 315 (1964).

/5/ H. Tanaka, A. Matsumoto, N. Goto, Bull. Chem. Soc. Japan, 37, 1128 (1964).

/6/ S. Arnold, W. B. Whitten, A. S. Damask, J. Chem. Phys., 61, 5162 (1974).

/7/ V. G. Plotnikov, Opt. Spectrosc., 26, 928 (1969).

/8/ D. G. Wilson, H. G. Drickamer, J. Chem. Phys., 63, 3649 (1975).

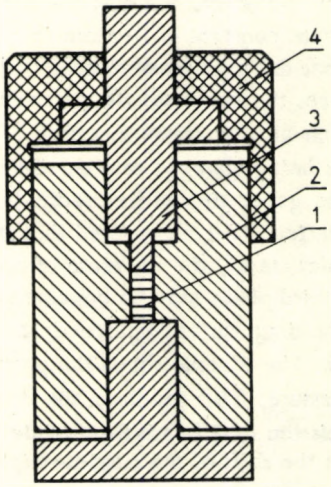

Fig. 1 High pressure chamber 1 – sample; 2 – cylinder; 3 – plunger; 4 – screw-nut

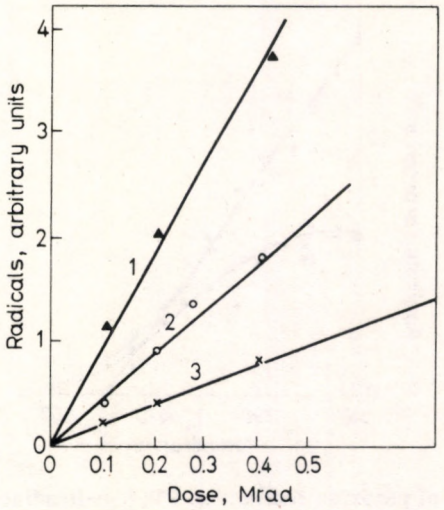

Fig. 2 Concentration of peroxide radicals in PTFE at 300 K vs dose. 1 – at 1 bar, 2 – at 5 kbar; 3 – at 14 kbar

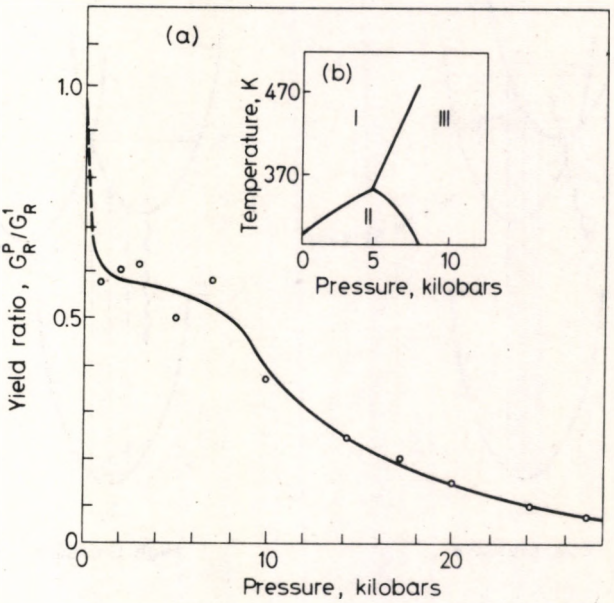

Fig. 3 a) Free radicals yield vs pressure in PTFE at 300 K.
b) Phase diagram of PTFE

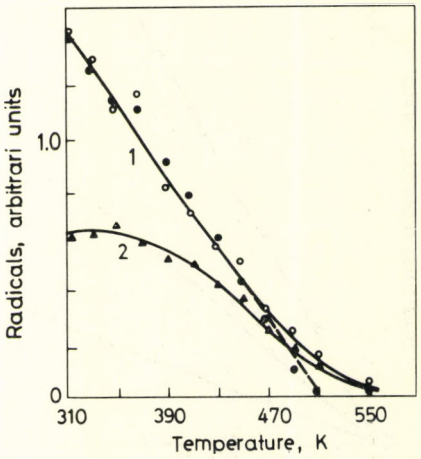

Fig. 4 Concentration of peroxide radicals in PTFE γ-irradiated at normal pressure (1) and at 1,5 kbar pressure (2) vs temperature. Black points – the sample, containing only "terminal" peroxide radicals

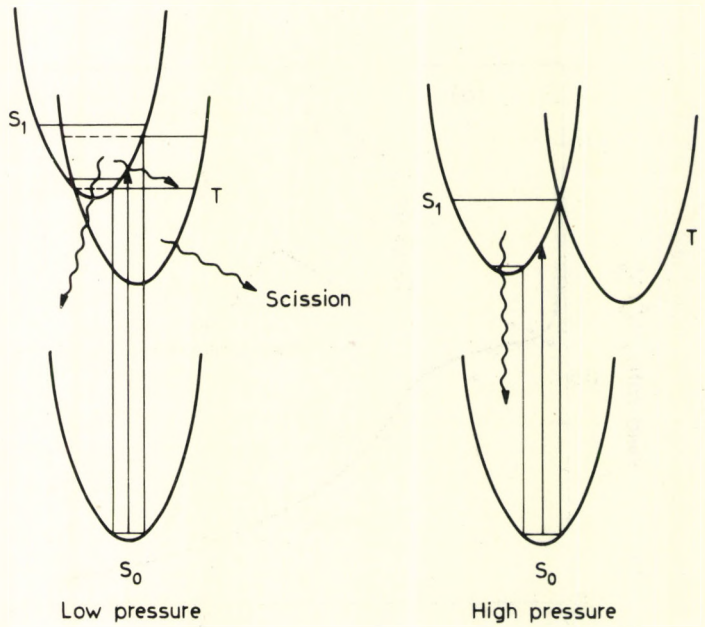

Fig. 5 A scheme of potential energy curves of ground and exited states, showing a possible mechanism of pressure effects on the efficiency exited molecule destruction into radicals

RADIATION GRAFT-POLYMERIZATION OF POLYFUNCTIONAL SUBSTANCES IN ELASTIC MATRIX

A. S. Kuzminskii, T. S. Fedoseeva
Scientific Research Institute of the Rubber Industry, Moscow, USSR

To obtain an efficient radiation vulcanization process of carbon-chain elastomers the optimum dose value for cross-linking should be reduced from 20-25 Mrad to 3-5 Mrad.

In the carbon-chain rubbers the value of the radiation-chemical yield of cross-links is low and consists of several units per 100 eV. To increase the radiation yield of cross links some sensitizing additives containing chlorine atoms, transition metals, their salts and oxides were used/1/. The attempts of practical application of these compounds have not proved to be of noticeable success.

Changing a cross-linking process into a radical chain one was found to be a more fruitful approach to solving the problem. For this purpose polyfunctional substances(PFS) of different unsaturated acids and their derivatives were used (such as acrylates, methacrylates, isocyanurates, maleinates, etc). However, these substances are not widely used because of their volatility, toxicity and high cost. Oligomeric compounds with methacrylate end-groups we have proposed, effectively reduce the vulcanization dose, at the same time being free of the above mentioned deficiencies, i. e. the oligomers are non-volatile, have relatively low cost and show good compatibility with rubbers.

Being subjected to ionizing radiation these compounds are easily polymerized within an elastic matrix, therefore the process changes into a chain one and the optimum vulcanization dose value are reduced.

The objective of the present work was to determine a mechanism of the radiation cross-linking of elastomers in the presence of polymerizable substances.

Experimental

Commercial rubbers EPR(ethylene-propylene copolymer), EPDM(ethylene-propylene terpolymer), SKN-26 (butadiene-acrylonitrile), SKMS-30(butadiene-methylstyrene) were mixed with PFS on mills. TMGF-II(tetra-methyl methacrylate-bisglycerol phthalate) and ODUA(oligodiene-urethane methacrylate) whose content was adopted to be 20 phr were used as PFS, as well as a monofunctional trimethyl-oxy disilane methacrylate(10phr).

Compounds in the form of 0, 5 mm thick plates moulded in a press at 80°C were irradiated on a Co^{60} radiation source (in vacuum, dose rate 1 Mrad/h) and on "U-10" and "Electron" electron accelerators (exposed to air, beam current and energy values for the "U-IO" and "Electron" being 250μ A and 4mA, and 2 and 0, 7 MeV respectively).

The cross-linking rate and three-dimensional cross-linking density were evaluated by IR and sol-gel techniques. The structure of graft-polymers was investigated by small angle X-ray diffraction with a "Geigerflex" instrument.

The physico-mechanical properties were investigated by standard tensile strength, relative and set elongation test.

Results and Discussion

When IR spectra of the compatible systems, containing rubber and PFS, were investigated, the decreasing of the 1645 and 810cm^{-1} band intensity was found, related to the methacrylate end double bonds of PFS/2/, which indicates their taking part in the polymerization process. The decrease of the end double bond-content is accompanied by an increase of the elastomer cross link-density. (Figs 1 and 2), i. e. that polymerization of PFS end groups occurs and the polymerized rigid block is linked to two rubber molecules, resulting in elastomer cross-linking by rigid polymer bonds.

The efficiency of the elastomer cross-linking depends on their chemical structure in such a way that the higher is the cross-linking rate, the less is the increase in the cross-linking density due to PFS.

It should be proposed that elastic chain cross-linking reactions with and without PFS take place simultaneously but the rate constants are different:

$$\text{Met} - R_1 - \text{Met} + 2R_2H \xrightarrow{K_1} R_2 - \text{Met} - R_1 - \text{Met} - R_2 \qquad (1)$$

$$R_2H + R_2H \xrightarrow{K_2} R_2 - R_2 \qquad (2)$$

where R_2H represents rubber molecules, Met $- R_1 -$ Met an oligomer with end methacrylate groups.

If $K_1 \gg K_2$, then the cross links are predominantly formed with PFS, otherwise if $K_1 < K_2$ carbon-carbon cross links between polymer chains are formed with greater probability.

The polymerized oligomer PFS molecules form rigid blocks in the elastic matrix which not only increases the cross-linking density but leads to increase of the tensile strength of unfilled vulcanizates (Fig. 3), in a similar way as peroxide initiated graft-polymerization of oligo ester acrylates described earlier/3/.

Table 1
The radiation chemical yield values
of cross-linking and degradation processes

		EPR		EPDM		SKN-26	
	Radiation type	Control	Modified	Control	Modified	Control	Modified
G cross-linking	Co^{60}	-	6.0	2.3	9.2	-	20
links/100eV	U-10	1.2	3.5	3.7	13.0	18	45
G degradation	Co^{60}	-	-	-	-	-	-
	U-10	0.4	2.4	0.8	1.7	0.08	0.13
Cross-linking coefficient $K=\frac{G_{mod.}}{G_{contr.}}$	Co^{60}						
	U-10	7.5		3.5		2.5	

As is shown in Fig. 3 (curve 6), reinforcement takes place even in the case when the grafted oligomer has elastic chains (grafting of oligo diene urethane methacrylate), as well as in the case of grafting the monomer, which contains one methacrylic group (see curve 7). It means that the strength of the unfilled elastomers increases as a result of graft polymerization of any compounds forming heterogenous blocks. The efficiency of the inforcement of the PFS elastomers depends on the nature of the rubber and PFS as well. In this case the reinforcement coefficients for different rubbers expressed as a ratio of the strength of the modified sample to that of the reference one at the same radiation dose varies from 2.5 to 6.

Small angle X-ray diffraction study of grafted samples revealed the presence of heterogenous inclusions (see Fig. 4). The slope of the diffraction curve for EPR samples is seen more clearly and shifted towards the direction of smaller angles. Qualitatively this fact may be connected with the presence of larger heterogeneous blocks in EPR than in EPDM. Taking into consideration that both polymers are similar in chemical nature the observed difference in the size of blocks may be connected with side unsaturated groups in EPDM molecules, these groups may affect the initiation rate of graft polymerization process. This fact indicates the important role of initiation during the formation of the graft polymer morphological structure. The validity of this supposition is confirmed by the dependence of the graft polymer properties upon radiation type. As is seen from the data given in Fig. 5, maximum strength values of vulcanizates, irradiated by accelerated electrons and γ-quanta, are different and can be obtained at different network densities.

Summary

1. It has been shown that the radiation-chemical yield of cross links in the rubbers is increased in the presence of PFS,
2. Heterogenous blocks, which increase the strength of material, are formed as a result of radiation-initiated PFS graft polymerization within an elastic matrix,
3. Reinforcement effect of unfilled vulcanizates is observed in the case of grafting monofunctional compounds and oligomers, containing elastic chains,
4. It has been found, that irradiation with accelerated electrons and γ-quanta gives materials of various strengths.

References

(1) V. G. Kozlov, M. Ya. Kaplunov, Z. N. Tarasova and B. A. Dogadkin, Vysokomolecul. soedin., AIO, 987-88, (1968).

(2) Z. S. Egorova, I. A. Slovokhotova, V. L. Karpov and B. A. Kiselev, Plastmassy, N6.., 18-23, (1965).

(3) A. S. Kuzminskii, A. A. Berlin and S. N. Arkina, Uspekhi chimii i phyziki polymerov, Moscow, Khimia, 1973., 239-258.

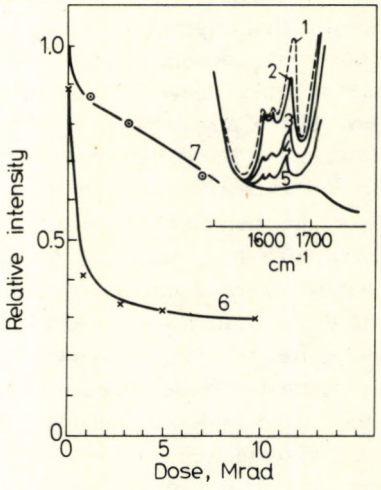

Fig. 1 Influence of the dose on the decrease of the relative double-bond content in PFS (1645cm^{-1}) (Radiation with Co^{60}, room temperature); 1 – nonirradiated EPR with 20phr PFS (tetra-methacrylate-bis-glycerol-phthalate), 2 – the same, irradiated by 1 Mrad; 3 – 5 Mrad; 4 – 15 Mrad; 5 – nonirradiated EPR; 6 – intensity variation of 1645 cm^{-1} in EPDM with 20phr PFS, 7 – the same in EPR

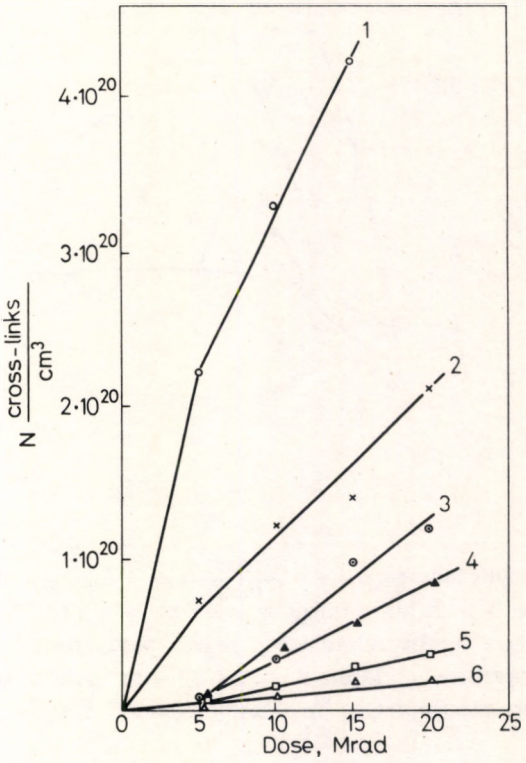

Fig. 2 Crosslinking number as a function of dose: 1 – SKN-26 with 20phr PFS, 2 – SKN-26; 3 – EPDM with PFS; 4 – EPR with PFS; 5 – EPDM; 6 – EPR

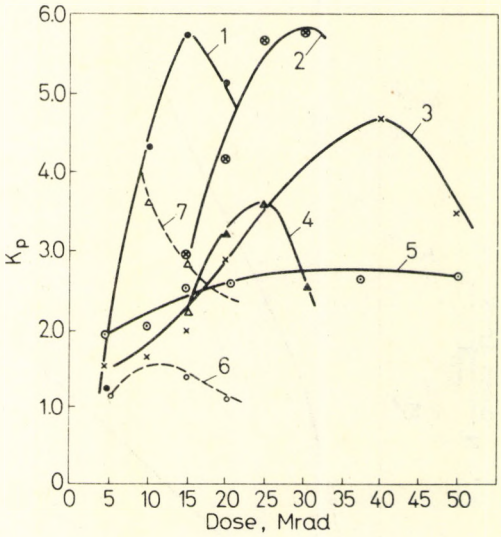

Fig. 3 Tensile strength factor Kp ($Kp = \frac{P\ mod.}{P\ contr.}$) as a function of dose for rubbers: 1 – SKN-26; 2 – SKMS-30ARK; 3 – EPDM, 4 – SKS-30, 5 – EPR (as PFS were used tetra-methacrylate-bis-glycerol-phthalate), 6 – EPDM with ODUA (oligodieneurethaneacrylate), 7 – SKF-26 with 10phr of tri-methyl-oxydisilanemethacrylate (radiation by electron beam U-10)

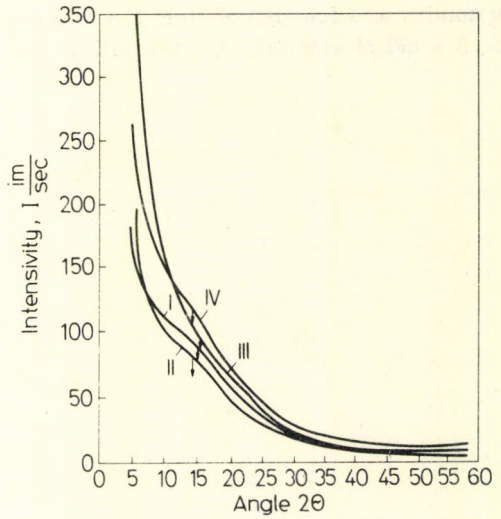

Fig. 4 Small angle X-ray diffraction curves: I, II – EPR with 20 and 50phr PFS; III, IV – EPDM with 20 and 50phr of PFS

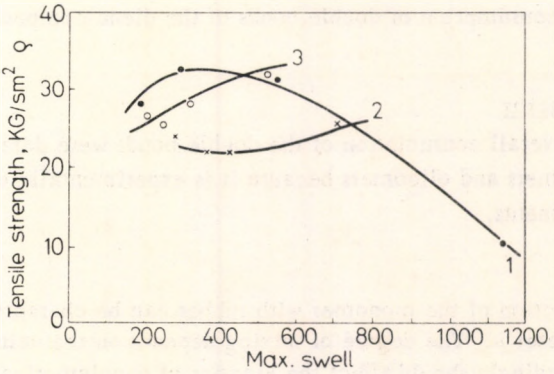

Fig. 5 Tensile strength of modified unfilled EPDM vulcanizates as a function of crosslinking density for different types of radiation: 1 - Co^{60}; 2 - electron accelerator "Electron"; 3 - electron accelerator "U-10"

DISCUSSION

J. DOBÓ

Were the doses corresponding to the same swelling different when cobalt source and accelerators were used (see Fig. 5)?

A. S. KUZMINSKII

For obtaining optimal resin properties different doses were needed by cobalt irradiation than by using accelerators.

J. ZURAKOWSKA-ORSZÁGH

What were the ageing properties of the vulcanisates obtained according to the method described in the paper in comparison with the properties of the same rubbers vulcanised by the conventional method?

A. S. KUZMINSKII

By thermal ageing outdoors and indoors, a gain of a factor of 2-10 was observed.

H. HEUSINGER

You compared the consumption of the double bonds of the polyfunctional additives in ethylene copolymer and in ethylene propylene diene terpolymer. Could you

determine the consumption of double bonds of the diene component of the terpolymer too?

A. S. KUZMINSKII

Only the overall consumption of the double bonds were determined for the irradiated elastomers and oligomers because it is experimentally difficult to differentiate between components.

A. ORSZÁGH

The interaction of the monomer with rubber can be characterized by the Flory-Huggins parameter μ. The degree of mixing depends on the value of this parameter which correspondingly should affect the kinetics of copolymerization and the physico-chemical properties of the copolymers. Did you calculate this parameter for the rubber monomer systems?

A. S. KUZMINSKII

We did not determine the Flory-Huggins parameter. All the oligomers studied were well miscible with the rubbers. During the process of vulcanisation, however, microheterogeneities are formed in the system which have a considerable effect on the physico-chemical properties.

P. KOURIM

Is there a sharp decrease of the elongation of the radiation cured rubbers in the presence of PFS?

A. S. KUZMINSKII

The elastic properties of the grafted vulcanisates are very good, the elongation at break reaches the value of 300–400%.

INVESTIGATION OF ELECTRON BEAM CURED UNSATURATED POLYESTER RESINS

Gisela Zeppenfeld, Renate Kiessig

Akademie der Wissenschaften der DDR, Institut für Technologie der Fasern, Dresden

and

VEB Kombinat Chemische Werke Buna-Schkopau, Deutsche Demokratische Republik

Introduction

Unsaturated polyester resins are cured by the influence of ionizing radiation with high effectivity. They form crosslinked products suitable for many applications, for instance to finish wood, wood products, plastics, metals and to produce glass fibre laminates, wood plastic combinations and concrete materials /1/. The technical realization of such processes already has gone on very well. By means of special electron beam accelerators with high intensity it is possible to produce the products in a profitable way /2/.

Up to now we have only little knowledge about the reaction mechanism of the radiation curing under such conditions. First investigations about the kinetics by low radiation intensity led to the conclusion that radiation curing – similar to peroxidic curing – is a simple copolymerization reaction between unsaturated polyester and monomer /3/. Under technical conditions such a mechanism is surely not correct, because it was found that the properties of the radiation products may be changed by increasing the radiation dose, though the monomer completely reacted by a small dose /4–6/.

This report is a contribution to clearing up the reaction mechanism of radiation curing of unsaturated polyester resins under technical conditions, i.e. high intensity, presence of air and high yield.

Method

Under technical conditions it is not possible to use usual kinetic methods. Therefore we have chosen the following method: We cured the resins in the form of films of about 0.5 mm thickness by means of the electron beam accelerator type ELT-1.5 and examined the stress–strain behaviour and the sol fraction of the radiation products. We used special unsaturated polyester resins on the base of longer chain diols and diacids producing soft polymers with rubber–like behaviour. In this way we have prevented the stopping of the reaction by "freezing" the radicals, noticed by Demmler in polymers below their glass transition temperature /7/. It was also possible to neglect stress relaxation processes. The results were stress strain curves in accordance

with the relationship:

$$\sigma/(\alpha - \alpha^{-2}) = \text{constant}$$

This corresponds with the "New Hooke" equation:

$$E = 3\sigma/(\alpha - \alpha^{-2})$$

and we could calculate a value for crosslinking density ν' using the well known equation /8/:

$$\nu' = E/3\,RT = \sigma/(\alpha - \alpha^{-2})\,RT$$

or expressed in terms of the G-value of crosslinking (the number of units crosslinked per 100 eV absorbed):

$$G_v' = 0.48 \cdot 10^6\, \nu'/\rho \cdot r = 0.48 \cdot 10^6\, q/wr$$

This G_v'-value is the result from simultaneously proceeding processes of crosslinking and degradation. To prove the degree of degradation and to determine the origin G-value of crosslinking the values of sol fraction were applied. The sol fractions as a function of the radiation dose r were:

$$s + \sqrt{s} = a + b(r + c)r^2$$

between the limits of 2 to 50 Mrad. The c-values being below 5 it was possible tc neglect the third number in the function above 10 Mrad. In this case the function is identical with the relationship by Charlesby /8/

$$s + \sqrt{s} = p_o(q_o + 1)\, u_1 q_o r$$

which was developed by him for radiation crosslinking and degradation of a polymer with random distribution and which is also valid without random distribution above 10 Mrd. The value a corresponds to the ratio of fracture density p_o to crosslinking density q_o and the value b corresponds to the inverse product of crosslinking density q_o and numerical average degree of polymerization u_1.

Moreover we have taken into consideration that two fractures are necessary to crack one crosslinking:

$$q = q' + p/2$$

and that fracture density and crosslinking density increase proportional to the radiation dose accordingly to

$$p = p_o \cdot r; \qquad q = q_o \cdot r$$

This was proved by Charlesby /8/ and confirmed by our own experiments. Under such conditions we could derive the following relations for the G-value of degradation G_A and the origin G-value of crosslinking G_v using of the G-value of crosslinking G_v' received by the stress-strain-curves and the value a by the sol fraction results:

$$G_A = 4 \cdot a \cdot G_v' / (2 - a)$$

$$G_v = 2 \cdot G_v' / (2 - a)$$

By means of the value b and considering the stoichiometric composition of the resin we were able to calculate a value for the numerical average degree of polymerization of the monomer u_M:

$$u_M = \frac{(0.48 \cdot 10^6 / w \cdot b \cdot G_v) - u_{PE}\,(1 - M)}{M}$$

Results

The G-values of crosslinking are independent from the dose rate in the range which we have researched of 10^5 to 10^6 rad/s. They are a constant for a polyester resin mixture of a certain composition.

With regard to the influence of the chemical composition we have found:

1. The G-values of crosslinking depend on the type of monomer. High values of about 100 and more were received with vinyl acetate. Butyl acrylate has given the lowest G_v-values up to about 10. The G_v-values have increased proportional with the ratio of ethyl acrylate to butyl acrylate, when the monomer butyl acrylate was substituted by ethyl acrylate in some resin types. But the influence of the monomer is different and seems to be dependent on the type of the polyester. /Fig. 1/.
2. In every case there is a significant influence on the G-values of crosslinking by the unsaturated double bond in the polyester. For an unsaturated polyester resin on the base of isophthalic acid in combination of butyl acrylate, allowing to produce soft films in a large range, the G_v-values were increasing directly proportional to the content of maleic acid from 0 to 0.8 mol. /Fig. 2/
3. Furthermore the G-values of crosslinking are influenced by tertiary CH-groups for instance introduced by means of propane-1,2-diol and by amino-groups, for instance introduced by means of toluene diisocyanate. Both of them increase the G_v-values, but the effect seems to be especially high in the case of a polyester containing longer aliphatic chains, for instance introduced by butane-1,4-diol (Figs 3 and 4).

4. The monomer content in the usual range from 15 to 50% and the acid number of the polyester (a standard for the degree of the polycondensation) in the usual range from 25 to 60 does not significantly influence the G-values of crosslinking (Figs 5. and 6).

The change of the sol fraction from the monomer content and the acid number, also observed by other authors /4,8/, simply results from the changed stoichiometric composition of the polyester resin. This follows from the calculation of the numerical average degree of polymerization of the monomer u_M. This value was found to be about 30 in the range of higher G-values of crosslinking, increasing up to 200 below $G_V^* = 50$. It seems to be dependent from the type of monomer as well as from the polyester, but independent from monomer content and acid number. (Fig. 7).

The G-values of degradation were determined to be about 20. Within the tolerance of the method we could not find any significant influence by the polyester resin composition. We therefore assume the degradation to be the result of an oxygen dissolved in the resin.

Only the polyester resins on the base of HET-acid have shown higher values of about 30 to 35. In this case it is possible that there is an additional effect of a direct chain decomposition by steric hindered radical structures.

Conclusions

Thus the radiation curing of unsaturated polyester resins within the said conditions represents a random crosslinking process of a mixture of the polyester and the monomer, respectively its homopolymer, accompanied by a random degradation process.

Contrary to the usual peroxidic curing process of unsaturated polyester resins there were following deviations:

– The initiation does not take place by a thermal decomposition of special initiators and by transfer of the radical function to the polyester, but by a direct effect of the radiation to the resin.

In this case the radicals arise from the polyester (P) as well as from the monomer (M) and their reaction products (P_xM_y).

$$P \rightsquigarrow P^{\cdot} \qquad (1)$$

$$M \rightsquigarrow M^{\cdot} \qquad (2)$$

$$P_xM_y \rightsquigarrow (P_xM_y)^{\cdot} \qquad (3)$$

It depends on the radiation sensitivity of the components which of these reactions is preferred. Tertiary CH-groups and amino-groups seems to play an important role for the formation of the primary radicals because of their low linkage energy.

– The propagation reaction does not run down like an alternative addition of the polyester radicals to the double bonds of the unsaturated polyester and to the monomer. The presence of different types of radicals in high density sooner leads to a more random addition in the following way:

$$P^{\cdot} + M \longrightarrow PM^{\cdot} \quad (4)$$

$$P^{\cdot} + P \longrightarrow P_2^{\cdot} \quad (5)$$

$$M^{\cdot} + M \longrightarrow M_2^{\cdot} \quad (6)$$

$$M^{\cdot} + P \longrightarrow MP^{\cdot} \quad (7)$$

$$PM_n^{\cdot} + M \longrightarrow PM_{n+1}^{\cdot} \quad (8)$$

$$PM_n^{\cdot} + P \longrightarrow PM_nP^{\cdot} \quad (9)$$

$$(M)P_m^{\cdot} + M \longrightarrow (M)P_mM^{\cdot} \quad (10)$$

$$(M)P_m^{\cdot} + P \longrightarrow (M)P_{m+1} \quad (11)$$

$$M_n^{\cdot} + M \longrightarrow M_{n+1}^{\cdot} \quad (12)$$

$$M_n^{\cdot} + P \longrightarrow M_nP^{\cdot} \quad (13)$$

The reactions 8, 10 and 12 take place in the beginning of the reaction in competition with the reactions 9, 11 and 13. They lead to the formation of homopolymer and branchings. Corresponding with the experimental results the chains are the longer the higher the reaction velocity of the reactions 8, 10 and 12 compared with the reactions 9, 11 and 13. Especially important for crosslinkings are the reactions 9 and 11. They explain the direct proportionality between the G-value of crosslinking and the content of maleic acid in the polyester.

– Because of the independence of the dose rate the termination does not consist of a recombination of growing radicals, but of a privileged recombination of the growing radicals $(P_xM_y)_g^{\cdot}$ with primary radicals $P^{\cdot}$, $M^{\cdot}$ and $(P_xM_y)^{\cdot}$. Combination reactions lead to further crosslinking, as for instance

$$(P_xM_y)_g^{\cdot} + P^{\cdot} \longrightarrow P_{x+1}M_y \quad (14)$$

Disproportion reactions lead to the formation of double bonds, for instance according

$$(P_xM_y)_g^{\cdot} + P^{\cdot} \longrightarrow P_{x1}M_{y1} + (P_{x2}M_{y2}) = CH_2 \quad (15)$$

– We have furthermore an addition of oxygen to different radicals and a stabilization of the resulting peroxi-radicals by means of chain decomposition, as

$$(P_x M_y)^{\cdot} + O_2 \longrightarrow /(P_x M_y)\text{-}oo^{\cdot}/ \longrightarrow (P_{x1} M_{y1})CHO + (P_{x2} M_{y2})CO^{\cdot} \quad (16)$$

and by direct chain decomposition of steric hindered radical structures, as

$$(P_x M_y)^{\cdot} \longrightarrow (P_{x1} M_{y1}) = CH_2 + (P_{x2} M_{y2})^{\cdot} \quad (17)$$

The result of such a reaction process is a cubic network with three different types of crosslinked units. Besides the usual crosslinking between polyester and monomer there are crosslinkings between monomer units and between polyester units.

The properties of such systems will differ from the properties of unsaturated polyester resins obtained by peroxidic curing. This is confirmed by first investigations in this direction. We have received polymers with a higher stability against solvents, higher tensile strength, but with an extensibility which is lower than in usual rubberlike materials.

References

/1/ Zeppenfeld, Gü., Zeppenfeld, Gi., Ebert, W., Holztechnologie 11 1, pp 13–20 (1970)

/2/ Zeppenfeld, Gü., Kiessig, R., Holztechnologie 13 1, pp. 50-55 (1972).

/3/ Burlant, W., Hinsch, J., J. Polymer Sci. Pt. A pp. 2135-49 (1964).

/4/ Hoffman, A. S. Smith, D.E., Modern plastics 6, pp. 43/111 (1966).

/5/ Schuh, K., Strukturuntersuchungen an strahlenvernetzten Polyesterharzen. Thesis Univ. Stuttgart 1972.

/6/ Ahmed, T., Funke,W., Angew. makrom. Chemie 37 566, pp. 125–133 (1974)

/7/ Demmler, K., Kunststoffe 57 7, pp. 566–572 (1967).

/8/ Charlesby, A., Atomic radiation and polymers. Pergamon Press Oxford 1966.

Explanation of the used symbols

σ	external force
α	length in the stressed direction of unit length in the origin specimen
E	elastic modulus
ν	crosslinking density in mol/cm^3
q	crosslinking density in mol/substance unit, $q = \nu \cdot w/\rho$
r	radiation dose, expressed in Megarad (Mrad)
R	gas constant

T	absolute temperature, measured in degrees Kelvin
w	molecular weight of the substance unit = $(1-M)w_{PE}+Mw_M$
ρ	density in g/cm^3
G_v'	G-value of crosslinking, determined from stress-strain-curves
G_v	the origin G-value of crosslinking
G_A	G-value of degradation
s	sol fraction
p	fracture density in mol/substance unit
u_1	numerical average degree of polymerization = $(1-M)u_{PE} + M \cdot u_M$
u_n	numerical average degree of polymerization of the monomer content in the polyester resin
w_{PE}	molecular weight of the polyester condensation unit
M	monomer content of the polyester resin
w_M	molecular weight of the monomer unit
u_{PE}	degree of polycondensation of the polyester

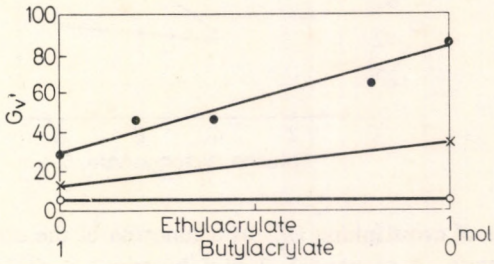

Fig. 1 G-value of crosslinking as a function of the ratio of ethyl acrylate to butyl acrylate. ● polyester on the base of adipic acid, ○ polyester on the base of isophthalic acid, x polyester on the base of HET-acid

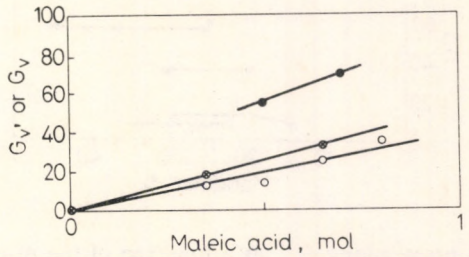

Fig. 2 G-values of crosslinking G_v' and G_v as a function of the content of maleic acid. ● polyester on the base of adipic acid/monomer ethyl acrylate-G_v', ○ polyester on the base of isophthalic acid/monomer butyl acrylate-G_v', ⊕ polyester on the base of isophthalic acid/monomer butyl acrylate-G_v

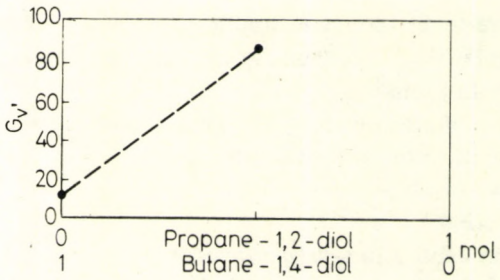

Fig. 3 G-values of crosslinking G_v' as a function of the ratio of propane-1,2-diol to butane-1,4-diol

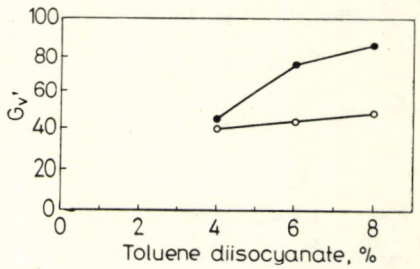

Fig. 4 G-values of crosslinking G_v' as a function of the content of toluene diisocyanate. ● propane-1,2-diol/butane-1,4-diol mixture, ○ propane--1,2-diol/butane-1,3-diol mixture

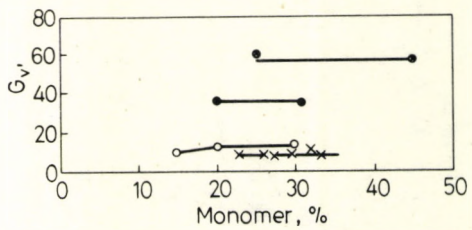

Fig. 5 G-value of crosslinking G_v' as a function of the monomer content. ● polyester on the base of adipic acid/monomer butyl acrylate, ○ polyester on the base of isophthalic acid/monomer butyl acrylate, x polyester on the base of HET-acid/monomer butyl acrylate, ⊕ polyester on the base of adipic acid/monomer ethyl acrylate

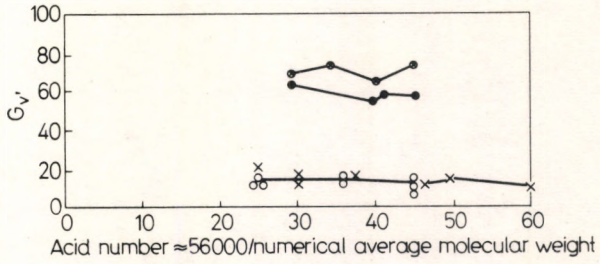

Fig. 6 G-values of crosslinking G_v' as a function of the acid number (signs as in Fig. 5)

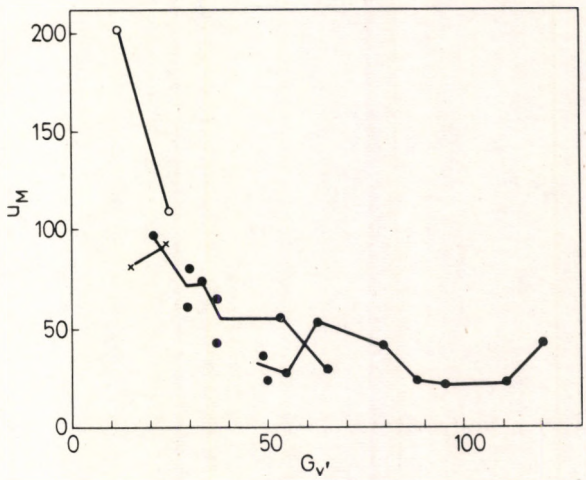

Fig. 7 Numerical average degree of polymerization of the monomer u_M as a function of the G-value of crosslinking G_v' (signs as in Fig. 5)

BEHAVIOUR OF FREE RADICALS IN CURED POLYESTER RESINS

G. V. Shiryaeva, K. G. Glashkova, E. R. Klinshpont
Branch of the Karpov Institute of Physical Chemistry, Obninsk, USSR

It is known that the radiation method of curing polyester coatings has a number of advantages over a thermochemical process: rates of the process increase, less plant space is needed, the coating is cured in practically no time at room temperature, this fact permits one to apply thermosensitive materials as substrate.

It may be supposed, however, /1, 2/ that radiation cured coatings will undergo the process of ageing to a larger extent than thermocured ones due to the trapping of great number of free radicals.

Under service conditions, under the action of ambient air, moisture, temperature, sun radiation these radicals or their recombination products will promote the acceleration of the oxidation destruction process.

The aim of our work was to study the processes of formation and decay of free radicals in curing, under service conditions and accelerated ageing coatings cured by radiation and thermochemical methods.

The composition consisting of polyester PE-232 and three ethyleneglycol dimethacrylate TGM-3 as monomer in the ratio of 1:1 was chosen for studying. The regime of the radiation curing of this composition was studied by us before /3/. Thermochemical curing was carried out by the usual method /4/. It should be noted, that it differed by longer curing time (3. 5 hours) by the presence of oxygen and by the higher temperature (+60°C). The degree of curing was controlled by gel-content (90-95%) and surface hardness (0. 7-0. 8).

ESR spectra were studied at 77 K by using a RE-1301 radiospectrometer /5/. The accelerated ageing of the coatings was carried out in a I. P. -1-3 chamber at 40°C in dry conditions. The changes of hardness, gel-fraction weight glance and the outward appearance of the coatings were measured during ageing. The accelerated ageing of the films for ESR studying was made under UV-light by means of a mercury lamp (UPK-4). The intensity of 365 nm line was $3 \cdot 10^{16}$ quanta/cm^2/sec.

The dependence of the free radical concentration on dose is given in Fig. 1a – at 77 K, Fig. 1b – at room temperature. The free radical yield was calculated from curve a, its value being 0. 5. The concentration of free radicals trapped in the coating film at the total curing dose was determined from curve b, its value being $\sim 10^{19} g^{-1}$. In the process of the thermocuring this concentration was

small compared with radiation curing, its value being not higher than $5 \cdot 10^{16} g^{-1}$.

ESR spectra for different curing methods were shown in Fig. 2 a - at 77°K using Co^{60} γ-ray, b - at room temperature using an accelerator, c - thermochemical curing. It should be noted that all the spectra were practically the same 5 line 23 $\pm$ 1 Oe and singlet. The pattern of 5 line spectrum and its temperature dependence showed that it was related to the radicals

$$-CH_2-\overset{R}{\underset{CH_3}{C.}}$$

The free radicals trapped in the radiation cured samples are rather unstable. The decay time of the free radicals at room temperature in air is 100-150 hours. At room temperature in vacuum the radicals decay is 2-3 times slower. This fact shows that the oxidation processes affect the decay of the free radicals. In the presence of O_2 the decay of free radicals is connected with the formation of peroxy radicals, followed by the reaction with a polymer matrix, a regeneration of alkyl radicals, and so on. These processes result in the formation of hydroperoxides, peroxide and carbonyl groups /6/ in the polymers. This is indicated by the sharp increase of the decay rate and by closing the decay curves in vacuum and in air with increasing temperature because the free radical decay in air depends on temperature to a smaller extent than the recombination and disproportion processes determined by the molecular mobility of the polymer matrix.

The kinetics of free radical decay in air is described with a second order equation (Fig. 3) and the calculated effective activation energy is 25$\pm$5 kcal/mol (Fig. 4) above room temperature. This value is the same as the activation energy of PMMA, it characterises molecular mobility of the polymer matrix /7/. The radical decay activation energy in vacuum at temperatures from 40° to 100° is practically the same as mentioned above, but it is $\simeq$10 kcal/mol in air /8/.

To study the ageing of radiation and thermocured coatings, an investigation was performed of the formation of free radicals at 77 K under UV-light in the films, in which the free radicals trapped in the curing process decayed under different conditions. ESR spectra of the free radicals proved to be the same irrespective of the curing methods and to be a singlet (Fig. 5), but not 5 lines as detected in the cured samples. The dependence of the concentration on UV-illumination time for thermo- and radiation cured samples in which the radicals have been decayed at room temperature is given in Fig. 6. It may be seen that limiting concentration of the free radicals is several times higher in the thermocured samples than in the radiation cured ones.

To explain this fact the formation of free radicals under UV-light in some components of uncured composition was studied. The free radicals proved to be formed generally in pure TGM-3 (5 lines ESR spectrum) and in the initiator (peroxide radicals). They are not formed under UV-light in cobalt naphthenate styrene

solution. In uncured PE-232 + TGM-3 (1:1) composition the free radicals are formed with a 5 lines spectrum. In cured compositions the free radicals are formed in a greather amount than in uncured ones and ESR spectrum is a singlet. In PE-232 resin itself, the ESR spectrum of the free radicals formed under UV-light is singlet too.

Additionally, the radiation and thermocuring of samples under the same conditions in vacuum has been carried out. The concentration of the free radicals formed under UV-light in these samples is given in Fig. 7. It may be seen that the curves are more close than those in Fig. 6, and the limit concentration in both cases is approximated to that in the radiation cured film.

On the basis of this fact it may be supposed that the reason for the higher concentration of the free radicals formed during ageing thermocured films as compared with the radiation cured ones is their long thermocuring in air. It is likely to result in the accumulation of photosensitive oxygen containing groups, in the samples.

Investigations carried out in the I. P.-1-3 chamber have shown that the changes of hardness, gel-content, glance etc. are practically the same for thermo- and radiation-cured samples. The service properties of the radiation-cured films are not worse than those of the thermocured ones.

Summary

1. A great number of free radicals are stabilized in the radiation-cured coatings - their concentration being 2-3 orders higher than in thermocured films. However, they decay quickly even at room temperature.

2. The free radicals formed during ageing are different from radicals formed during curing. Their concentration is 2-3 times higher in the thermocured samples than in the radiation cured ones. This difference is due to their long thermocuring in air.

References

/1/ X. Demmler, J. Schlag, Farbe und Lack 77, No. 3, 224-231 (1971).
/2/ R. S. Astakhova, E. L. Malachevskaya, O. Kh. Aveskina, N. G. Shtan'ko, Lakokrasochnye materialy i ikh primenenie No. 5, No. 6. (1973).
/3/ G. V. Shiryaeva, L. G. Lapa, Lakokrasochnye materialy i ikh primenenie No. 3, 39-42 (1974).
/4/ K. P. Belyaeva, T. V. Todorova, N. G. Shtan'ko, "Lakokrasochnye materialy dlya otdelki izdelii iz dereva" Moscow, Khimiya, 1971.
/5/ S. Ya. Pshezhetskii, A. G. Kotov, V. K. Milinchuk, V. A. Roginskii, V. I. Tupikov, EPR svobodnyh radikalov v radiatsionnoj khimii, Moscow, "Khimiya", 1972.
/6/ S. Ohnishi, S. Sugimoto, I. Nitta, J. Polym. Sci. A-1, 605-625 (1963).
/7/ V. V. Voevodskii, Fizika i khimiya elementarnyh khimicheskih protfessov, Moscow, "Nauka", 1969.
/8/ J. C. W. Chien, C. R. Boss, J. Polym. Sci., 5, A-1, 3091-3103 (1967).

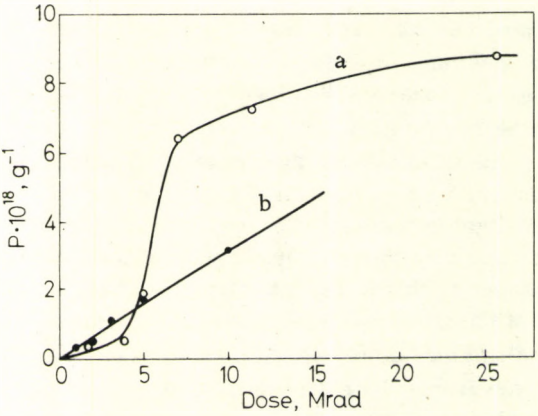

Fig. 1 Free radical concentration VS the dose: (a) – at 77 K; (b) – at room temperature

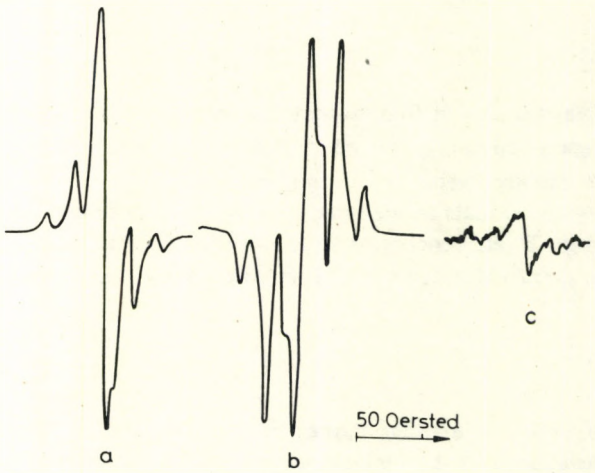

Fig. 2 ESR free radical spectra in samples cured; (a) – at 77 K; (b) – at room temperature; (c) – thermochemically

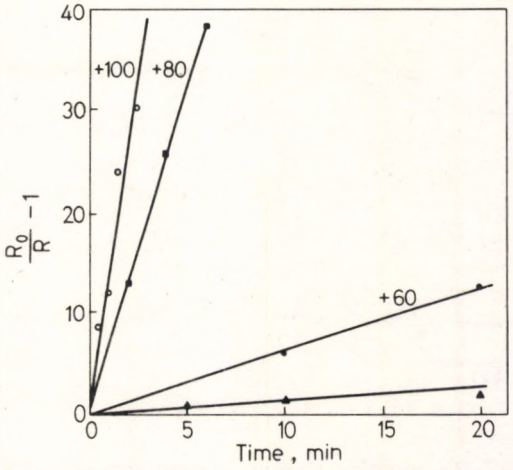

Fig. 3 Kinetic free radical decay curves at different temperatures in 1/2-t coordinates

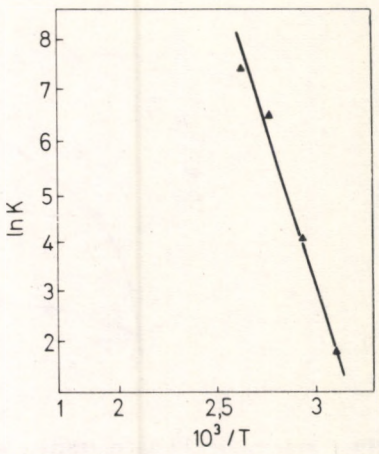

Fig. 4 Temperature dependence of the free radical decay constant

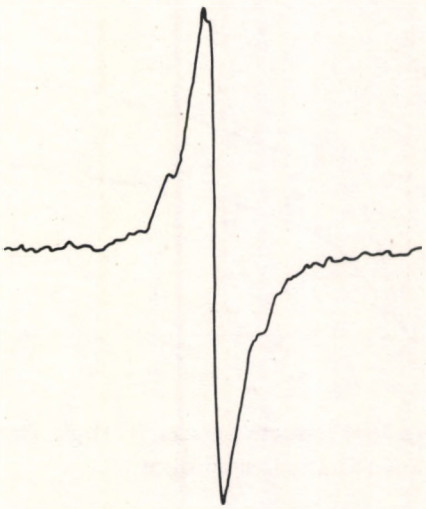

Fig. 5 ESR spectrum of free radicals formed under UV-light at 77 K

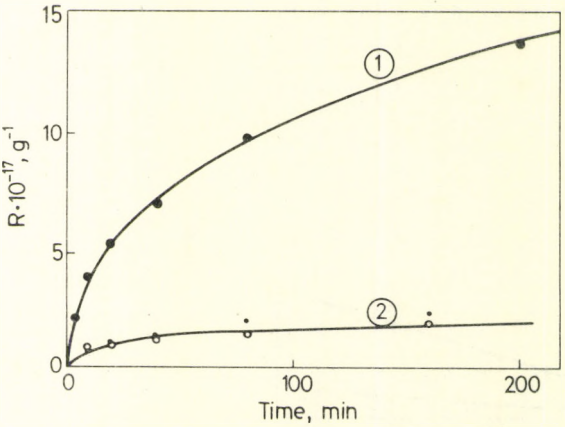

Fig. 6 Free radical concentration versus UV-illumination time: 1 – thermochemically cured films, 2 – radiation cured films

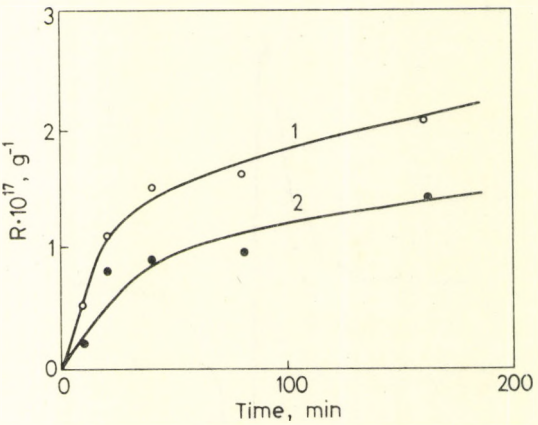

Fig. 7 Kinetics of free radical formation under UV-light cured in vacuum: 1 – thermocured films; 2 – radiation cured films

PILOT - SCALE EXPERIMENTS ON RADIATION PROCESSING OF WOOD-PLASTIC COMPOSITES

T. Czvikovszky
Research Institute for Plastics, H-1950 Budapest, Hungary

There are only few groups in the world publishing details of pilot-scale experiments on radiation chemical processing. One of the reasons for this could be that nowadays the "know-how" is sometimes more interesting than the original patent itself. Some recent examples show, however the growing interest in the radiation chemical technology /1-5/ and in particular on the radiation processing of wood-plastic composites /WPC/ /6-10/. The International Atomic Energy Agency has always made special efforts to apply radiation research inthe chemical processing. The present study of preparation of WPC out of tropical woods of Venezuela was such an effort.

The project – also sponsored by the United Nations Development Program – had three distinct steps. In the first step the main question to answer was whether the tropical woods of South America, containing special resinous aromatics and being of extremely porous structure, are suitable for the radical polymerization of vinyl monomers or not. Among the hundreds of publications on WPC /11/, there is only little information about the application of tropical woods /12/. Having a positive answer to the question, six selected but abundant Venezuelan wood species were combined with four monomer systems, and the physical and mechanical properties of the twenty-four WPC variants were determined. The detailed results of this screening are described elsewhere /13/.

The second step of the three-year project was a technological modelling of the impregnation and of the under-water irradiation process. On that basis was finally developed in the third step a pilot-scale processing line of 50 ton/year WPC capacity, using 50,000 Ci Co-60. In the followings some excerpts of these three steps are presented.

Radiation chemistry of vinyl polymerization in tropical woods

A rapid method was needed for the evaluation of the inhibition effect and of curing dose. The dielectric method of monitoring the conversion /14/ was not applicable here. Measuring the temperature of the polymerizing system is well known, e.g. in the polyester technique, and was applied for WPC system as well /15/.

Small blocks (5x5x5 cm^3) of Saman wood (Pithecellobium Jupumba, - a dark brown tropical wood of the Venezuelan forest) was impregnated with methyl methacrylate (MMA) and irradiated with different dose-rates at room temperature. On the curves of Fig. 1 it is easy to determine the point where the exothermic process begins. An example: the inhibition period at 0.045 Mrad/hour is more than 4 hours long. The pure, twice distilled and deaerated MMA in block has no inhibition, but even the technical grade, stabilized MMA without Saman starts to polymerize at 0.045 Mrad/hour within 40 minutes. Another significant point on the curves is where the acceleration - the gel-effect - begins. The main question is where to place the last point on the cooling curve considered as the end of the polymerization.

The complete mathematical evalution has been described elsewhere /16/. The final relationship between the monomer conversion (ΔM) and the temperature difference between the sample and the ambiance (ΔT) is the following:

$$\Delta M = \frac{c_1}{c_2} \int_0^t \left(\frac{\Delta T}{dt} + c_3 \Delta T \, dt \right)$$

where c_1, c_2 and c_3 are constants depending on the polymerization heat of the monomer, the specific heat of the system and the heat-dissipation conditions of the sample, respectively. A good approximation is to determine the final point of polymerization on the cooling part of the curve with the same ΔT which is valid at the moment when the acceleration begins. Another method is to form the first (and second) derivative of the curve: an exponential cooling curve has purely exponential derivatives. Fortunately not all tropical woods inhibit the vinyl polymerization so much. The curves of polymerization of MMA in Sangre de Drago wood (Pterocarpus Vernalis) - which served finally for the pilot-scale production - is shown in Fig. 2.

The curves 1 to 6 correspond to 300, 150, 78, 45, 30 and 21 krad/hour respectively.

The curing dose in function of the dose rate, calculated from such experiments, is seen in Fig. 3 in logarithmic scale. As expected, nearly 0.5 slope is valid for pure MMA, and the same is for crude (technical grade, stabilized) MMA. Interestingly enough, a parallel is obtained for the polymerization of technical MMA in Sangre de Drago wood, but the slope is much lower for Saman, where significant inhibition is obtained.

Table 1. shows the parameters of the $D = A\ I^B$ relationship (where D is the curing dose in Mrads and I is the dose-rate in krad/hour) for the following investigated monomer systems:

MMA	:	Methyl methacrylate
ST.AN	:	Mixture of styrene, and acrylonitrile, 60/40 by volume.
MMA.AR	:	Mixture of MMA and AROPOL unsaturated polyester, 80/20 by volume
ST.AN.AR	:	Mixture of styrene, acrylonitrile and AROPOL unsaturated polyester, 48/32/20 by volume

Table 1
Parameters of the radiation polymerization of different monomers in block and in tropical woods

	A pre-exponential factor	B dose-rate exponent
MMA pure	0.050	0.54
MMA (stabilized)	0.060	0.54
MMA-Saman wood	0.265	0.29
MMA-S. Drago wood	0.100	0.51
MMA.AR	0.053	0.65
MMA.AR - S. Drago wood	0.160	0.44
ST.AN	0.137	0.55
ST.AN - S. Drago wood	0.215	0.43
ST.AN.AR	0.029	0.68
ST.AN.AR - S. Drago wood	0.070	0.53

It is seen that the last, three-component system, which gives a tough cross-linked polymer, is the most favourable for the radiation polymerization among the systems under consideration. It can be cured with very low doses, especially at low dose-rates.

Technological modelling of radiation processing of wood-plastic composites

The facility for the impregnation of wood with vinyl monomer mixtures is seen in Fig. 4. This arrangement was used in the first step of the project. The wood samples were placed in a steel impregnator tank, and were evacuated during 1 hour or more. Subsequently the monomer was added. Afterwards the pressure tank and the impregnator were pressurized with nitrogen at a pressure of 800 Hgmm during 6 hours or more. Finally the non-absorbed monomer was collected. In the first step of the present project the irradiation of the impregnated wood samples was performed in aluminium foils. In the next step – to try the technological possibilities – an irradiation tank was made out of aluminium. However the rectangular tank (130x500x500 mm) of 4 mm wall thickness could not resist the pressure which developed during the exothermic polymerization of about 25 kg of impregnated wood. Thus, we have chosen the underwater irradiation method which gave effective cooling.

The main component of the reduced model was a stainless steel tank of 300x300x x150 mm inner dimensions which served for the impregnation and for the irradiation as well. The tank was attached to the same impregnation line as that of Fig. 4. After

the impregnation cycle, the same tank, containing the impregnated wood was transferred and irradiated.

The irradiation was performed in the water (in the depth of 5 metre) irradiating from both sides with two Co-60 slabs of 290x25x5 mm dimensions and of 7000 Ci total activity. The average dose rate in the filled tank was 99 krad/hours. With this arrangement not only the processing parameters of the selected WPC system were determined – such as: impregnation rate and time, heat and pressure effect of polymerization, curing dose under technical conditions – but also a series of very important other questions like the position and type of valves, introduction of temperature- and pressure-sensors in the tank, precautions of avoiding the polymer deposition on the inner wall and bottom of the tank, fittings and gaskets, etc.

Pilot plant experiments

On the basis of the successful experiments with the reduced model the construction of a pilot scale plant was decided for the radiation processing of impregnated wood in larger dimensions and quantities. The under-water irradiation plant 50,000 Ci Co-60 as well as the impregnation line was constructed and installed by the Atomic Energy of of Canada Ltd. The system itself was very similar to that of published by Green /17/, however, it was adapted to the local conditions and modified according to experience.

A typical working cycle of the pilot plant was the following. The stainless steel impregnator-irradiator tank of 200x1000x1030 mm^3 dimensions was filled with 36 boards of Sangre de Drago wood of the following dimensions: 29x148x1020 mm^3. Then the tank was closed using neopren gaskets, and attached to the impregnation line. This line consists of a mixer drum, a pneumatic mixer, a monomer dispensing cylinder with sight glass, followed by the impregnator itself. On the other side two vacuum pumps (for rough and fine vacuum), a trap, two manometers and a nitrogen dispensing system were attached. Because of the safety prescriptions all electric installations (lamps, motors, pumps, etc.) were located outside the impregnation room. A vacuum better than 20 Hgmm was applied during 1.0 hour. Subsequently about 100 kg ST.AN.AR monomer mixture was introduced. (The composition is mentioned above.) After 8.0 hours of impregnation at normal pressure 35 kg of monomer was absorbed. Then the rest of monomer was drained off and recycled. Afterwards the tank was attached to the irradiation line: lowered in the pool between two panels of Co-60 pencils distributed on about 1 m^2 surface.

The 50,000 curies gave a quite homogeneous dose-rate distribution in the tank, the average being 70 krad/hours. The exothermic polymerization process reached the maximum temperature in the centre, about 80 ^{o}C, in about the 10th hour. After 14 hours of irradiation (0.98 Mrad) the polymerization could be considered as finished. After opening the tank the plastic impregnated boards were stored for some days before machining with standard woodworking machines. The monomer conversion was about 94%, the monomer content of WPC being about 240 kg/m^3. The monomer distribu-

tion was completely homogeneous in the wood. The tank was prepared within 1 hour for the next impregnation, thus, a complete cycle was finished in 24 hours. The above mentioned process is naturally only one particular case – but is weil reproducible. More than 2 tons of WPC were produced from this variant during the experimental runs for parquet flooring. Other wood-plastic combinations need other processing parameters. Manufacturing more than 2 tons in repeated experimental runs the feasibility of radiation processing of plastic-impregnated tropical woods has been demonstrated. The installed parquet flooring is under test in various public institutions of Venezuela.

A preliminary technical design using the same 50,000 Ci irradiator panels, but six impregnator-irradiator tank showed a potential annual capacity of over 200 tons of WPC.

References

/ 1/ "Large Radiation Sources for Industrial Processes" Symp. Int. Atomic Energy Agency, Munich, 18–22. August 1969.

/ 2/ Spencer, P.C. .... and others in the Conference "Process Radiation in the Plastics Industry" Pullman, Washington 11 June 1969.

/ 3/ Hummel, R.W. Rep. Progr. Appl. Chem. 57, 683–686 (1972).

/ 4/ Singer, K. .. and others in the Proceedings of "Peaceful Uses of Atomic Energy" UN-IAEA New-York-Vienna 1972. Vol. 14.

/ 5/ Puig, J. and others CEA Bulletin d'Information Sci. Techn. 171. June 1972.

/ 6/ Shiryaeva, G. V. Karpov, V.L.... Radiats. Khim. N° 2. 316–320 (1972).

/ 7/ Taylor, G.B., Dietz, G.R.... Nuclear Technology 13, /1. 72–77 (1972).

/ 8/ Glukhov, V.I., Matveev, V.K.: Plast. Massy N° 5. 25–27 (1973).

/ 9/ Spindler, M.W., Pateman, R. Hills, P.R.: Composites 4 N° 6. 246–253 (1973).

/10/ Proksch, E.: Allg. Prakt. Chem. 24, 14–16 (1973).

/11/ Czvikovszky T: Atomic En. Rew. 6, N° 3, 3–99 (1968).

/12/ Miettinen, J.K., Autio, T.: Proc. Jap. Conf. Radioisotop. Tokyo (1969).

/13/ Czvikovszky T: Project documents of the IAEA-UNDP common project VEN 02/71. Nov. 1971 – Nov. 1974. IAEA, Vienna

/14/ Hedvig, P., Czvikovszky T.: Angew. Makromol. Chemie 21, 79–85 (1972).

/15/ Rayavee, E.L., Kalninsh, A.J.: Proc. Third Tihany Symposium on Rad. Chem., Akad. Kiadó, Budapest, 1972. pp. 853–858.

/16/ Czvikovszky T: Perez-Alarcon J.: Latinoamerican Conf. Use of Large Radiation Sources, Santiago de Chile 18–22 June 1973.

/17/ Green, W.R.: Paper presented at Conf., Radiation and Isotope Techniques in Building Industry, Brussels, 28-29. Oct. 1970.

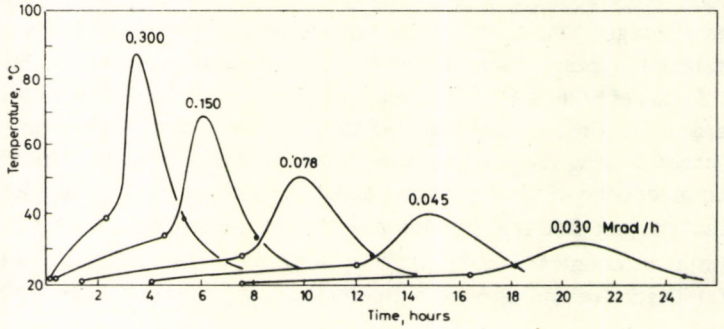

Fig. 1 Temperature of samples of Saman wood impregnated with methyl methacrylate, during radiation polymerization

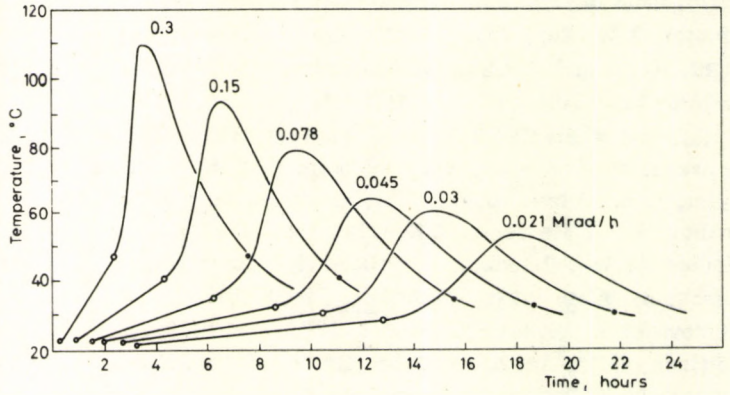

Fig. 2 Temperature of samples of Sangre de Drago wood impregnated with methyl methacrylate, during radiation polymerization

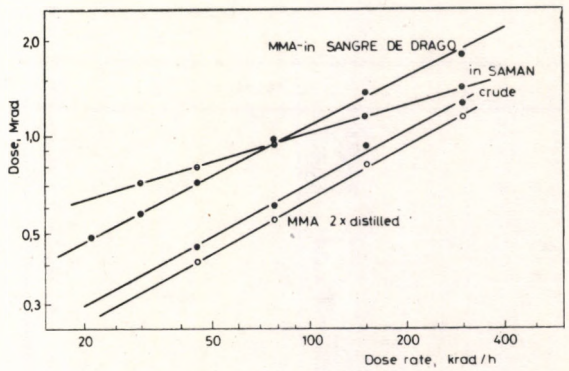

Fig. 3 Curing dose as a function of dose rate for methyl methacrylate wood composites

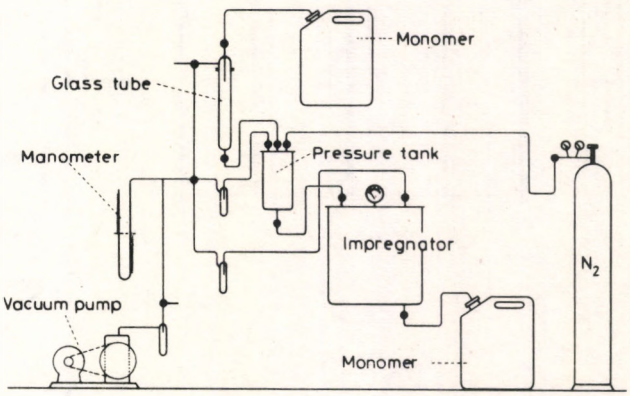

Fig. 4 Impregnation facility

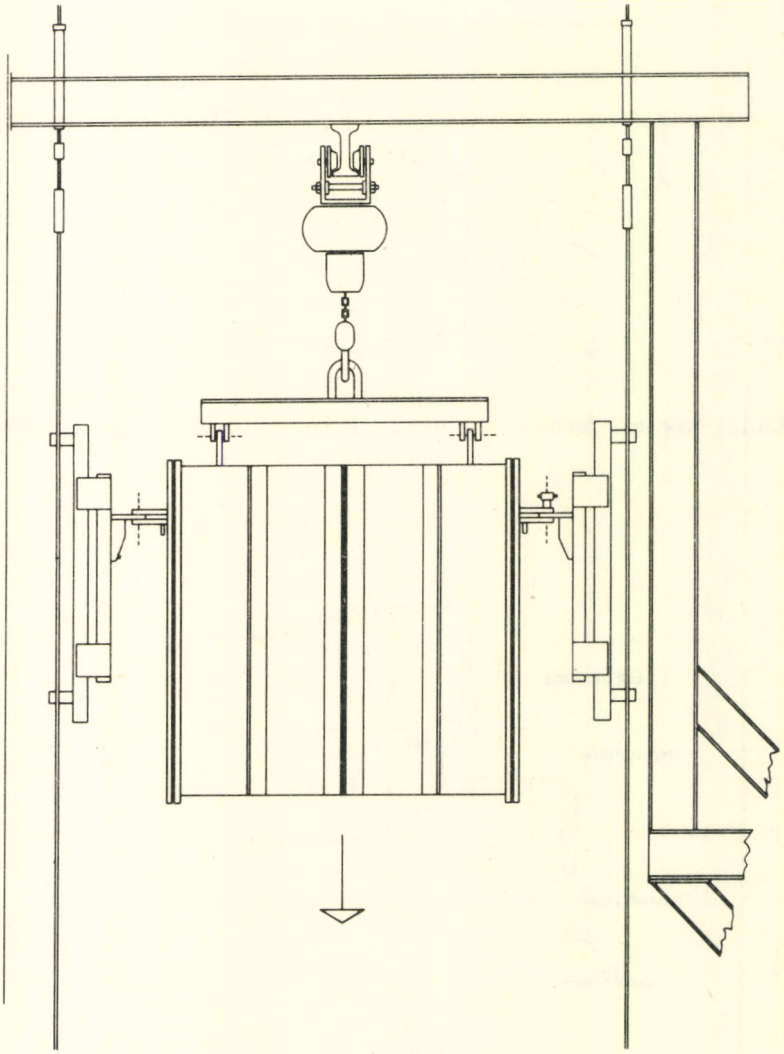

Fig. 5 The impregnator irradiation tank of the pilot plant attached to the lifting system

I. BABKIN

Did you have any trouble in connection with deformation of thin plates and planks because of the non uniform distribution of stress in the samples after polymerization?

T. CZVIKOVSZKY

Impregnated wood may deform during swelling in the monomer but practically not after radiation curing. Wood plastic composites of thin (2–3 mm thick) veneers were prepared by us in a special frame without any warping. WPC plated chipboard panels of good quality were prepared with these veneers. Certainly all the phenomena of deformation and warping are dependent on the quality of the wood.

A. CHARLESBY

One has to pursue of the economics of the process. What are the relative costs of polyester and wood? Can we coat only the surface, which is the part we want to improve.

T. CZVIKOVSZKY

In the project presented an economic study has been made as well. It came out that not the radiation treatment was expensive but the monomer-polyester mixture, which, in fact, was found to be too expensive for the potential market of WPC flooring in Venezuela. In our case approximately 250 kg of monomer mixture was used for impregnation of one cubic metre of wood. At the time of the oil crisis (1974) the price of this amount of mixture was over 200 US dollars. At the same time the price of the wood used was below 100 US dollars/cubic metre. The solution of this problem can be what Prof. Charlesby has proposed: partial impregnation as applied for WPC by A. Bormester in West Berlin.

J. R. PUIG

Wood plastic composites are quite well known nowadays. Work carried out in laboratories all over the world has established that this product is very good from a technical standpoint.

The commercial success, however, depends very much on the market conditions which vary from one country to another and, of course, on the additional cost imposed on the original wood. This original cost for a large part is due to the resin

loading. Whether curing is done by radiation or by catalyst is perhaps a secondary problem according to my opinion.

It is known that WPC is commercialized in such countries as the USA, but it has not been commercialized in France so far. I would like to mention a special application of this process which is studied in France not in industry but in the field of preservation of old wooden pieces of art. In this case, because of the high value of the object, the additional cost of the resin has not the same importance as for marketable goods which have to find their consumers. It can be expected that a highly decayed wooden statue, for instance, might be preserved by this technique for a number of years.

ON THE GRAFTING OF POLYETHYLENE INITIATED BY PRE-IRRADIATION IN AIR

A. Bartl and L. Wuckel
Akademie der Wissenschaften der DDR, Zentralinstitut für Festkörperphysik und Werkstofforschung, Dresden, GDR

Polyethylene (PE) is one of the most suitable polymers for investigations concerning the radiation peroxidation grafting because it is readily peroxidized under irradiation in the presence of air. In the peroxidation grafting only the first stage involves a radiation treatment, namely, the irradiation of the polymer in presence of air at very low dose rates. With respect to the grafting initiated by the peroxidized polymer the question arises whether diperoxides or hydroperoxides are formed. It was Chapiro /1/ who studied in detail the kinetics of peroxidation grafting of acrylonitrile on PE. He concluded that graft copolymerization is mainly induced by diperoxides. In contrast, Dolgowa et al. /2/ reported that hydroperoxides are mainly formed by pre-irradiation of PE in air. Chapiro, and Dolgowa et al. used acrylonitrile as the monomer to be grafted.

In this work we have investigated the peroxidation of PE by pre-irradiation with low dose rates of cobalt-60-γ-radiation as well as the grafting of styrene onto PE films peroxidized under the same conditions. In contrast to acrylonitrile, styrene is a fairly good swelling agent for PE and the polymer formed is soluble in its monomer. Therefore we believe that the system PE/styrene is very suitable for kinetic investigations. Furthermore, we used EPR-measurements to provide some information on the kind of peroxides formed in PE.

Experimental

Use was made of low density PE films (ρ = 0.920 g·cm^{-3}). Films of the polymer 0.1 mm thick were subjected to different doses of gamma-rays (cobalt-60) in the presence of air using low dose rates (0.007 MR/h) at room temperature. The films were then heated in an excess of styrene at temperatures ranging from 20 to 70°C. The grafting yield was determined gravimetrically. The peroxide content was obtained by titrating the iodine eliminated after boiling the films in a mixture of toluene and acetic acid with added KI.

EPR measurements have been conducted after low dose rate irradiation as well as on films irradiated with extremely high dose rates (500 Mrd/h). High dose rate

irradiation was performed with 2 MeV electrons of a Van de Graaff type accelerator. The EPR measurements were made with a Varian V-4502 spectrometer the dual sample cavity of which contains an oriented ruby single crystal in one of the two channels. That line of the ruby, which is useful for concentration measurements, was calibrated with the Varian standard "strong pitch sample".

Results and discussion

Figure 1 shows the peroxide yield of a PE-film as a function of dose irradiated at the low dose rate of 0.007 MR/h. It can be seen that the peroxide concentration is built up linearly with dose up to a limiting value. From the linear portion of the curve we obtain a G-value of about 30.

The grafting after irradiation at low dose rate in air is shown in Fig. 2. As can be seen, the conversion time curves are nearly linear up to high conversions. The slope rises with increasing temperature indicating that the reaction is initiated by peroxides: the linear portion corresponds to a steady rate of initiation by the thermal decomposition of peroxides. Figure 3 demonstrates the well known fact that the rate of polymerization is directly proportional to the square root of the peroxide concentration and hence to the square root of dose.

The overall activation energy of the grafting reaction is 15 kcal/mole. Usually it was assumed that the activation energy for propagation is the same as in homogeneous low viscous media, i.e. 7.2 kcal/mole. Taking this value we get for the activation energy of initiation $E_i = 30$ kcal/mole. It is known that the activation energy for decomposition of diperoxides lies about this value. In contrast to this high activation energy the grafting proceeds already at 20 and 40°C with a considerable rate (see Fig. 2) although diperoxides should be stable at these temperatures.

The results in Fig. 2 lead to the assumption that the grafting is initiated by hydroperoxides. Thus the problem is to find out whether diperoxides or hydroperoxides are formed in PE under irradiation in air. Only a few experimental data are available in this field. Results on radiation peroxidation pertain to polypropylene in which hydroperoxides are formed by chain reaction /1,3,4/.

The radiation peroxidation of PE is presumably a result of the following reactions /1,4/:

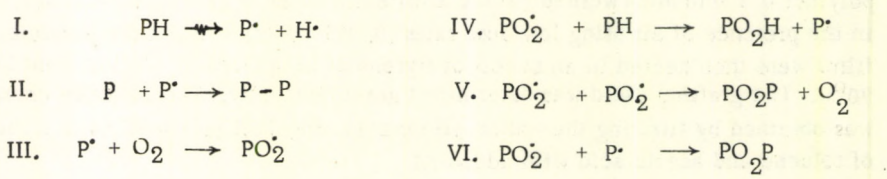

(The formation of carbonyl groups is not taken into consideration.)

The peroxy radicals formed under irradiation in air can be detected easily using the EPR technique owing to the differences in the saturation behaviour of the $PO_2^{\bullet}$ -radicals compared with that of hydrocarbon radicals (Fig. 4). In order to clarify the problem mentioned above we examined the time and temperature dependence of the peroxy radicals. Figure 5 demonstrates the decay of $PO_2^{\bullet}$-radicals in PE after irradiation at low dose rate in air. The $PO_2^{\bullet}$-radicals which are mobile within the matrix decay by a first order reaction. Another part is trapped in certain sites and reacts only if temperature is raised. Figure 6 shows the radical decay after high dose rate irradiation obtained by pre-irradiation with electrons. The higher dose rate affects the decay mechanism only in that way that (owing to the high initial concentration) the component which in Fig. 5 seems to be constant shows here a first order decay too though of course with a lower rate. We can therefore conclude that the two different decay rates are caused by the existence of two different regions (the crystalline and the amorphous) wherein the radicals reside.

The activation energy of the $PO_2^{\bullet}$-radical decay in the amorphous phase is 4 kcal/mole. For the decay in the crystalline phase we found a value of 18 kcal/ /mole (Fig. 7).

The shapes of the decay curves as well as the value of the activation energy found for the decay within the amorphous phase can be accounted for by Reaction IV precluding the formation of diperoxides via Reactions V and VI. Steps V and VI should be diffusion controlled processes which are second and first order with respect to the $PO_2^{\bullet}$ --concentration change. These processes do not follow the simple shape of the curves shown in Figs 5 and 6. The EPR results thus confirm that irradiation leads to hydroperoxides. These results are confirmed by the G-value for peroxidation which was found to be about 30. Since the G-value of the peroxy radicals G_{PO_2} is only in the order of 1 we conclude that hydroperoxides are formed by a chain reaction assumed by Neudörfl /3/ in the case of polypropylene oxidation and more generally by Chapiro /4/:

$$\left.\begin{array}{lcl} P^{\bullet} + O_2 & \longrightarrow & PO_2^{\bullet} \\ PO_2^{\bullet} + PH & \longrightarrow & PO_2H + P^{\bullet} \end{array}\right\} \text{n times}$$

It follows from the above conclusion that the graft copolymerization of pre-irradiated low density polyethylene is primarily a result of initiation by hydroperoxides. The results can be explained by the assumption that Reaction IV can proceed in low density polyethylene even at room temperature because of the presence of tertiary hydrogen.

References

/1/ A. Chapiro, Radiation Chemistry of Polymeric Systems, Interscience, New York, 1962, Chapter XII.

/2/ [illegible]

... Z. u. Z. Polymere, 224 2, S. 132 (1968).

/4/ A. Chapiro, IUPAC International Symposium on Macromolecular Chemistry, Budapest, 1969, pp. 593 – 605.

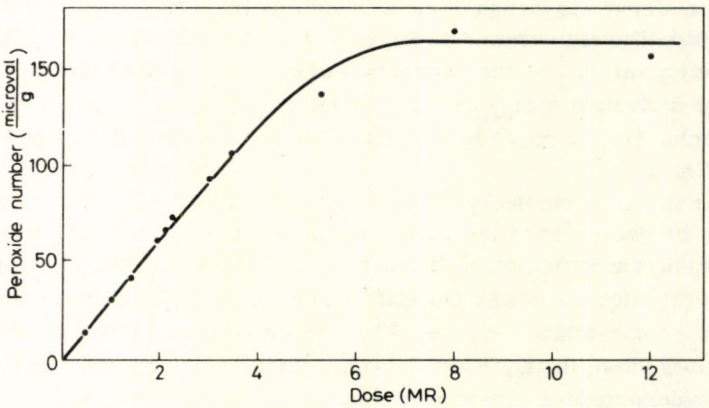

Fig. 1 Concentration of peroxides as a function of irradiation dose (d=0. 1 mm; D_L= = 0. 007 MR/h; T_B = 20°C)

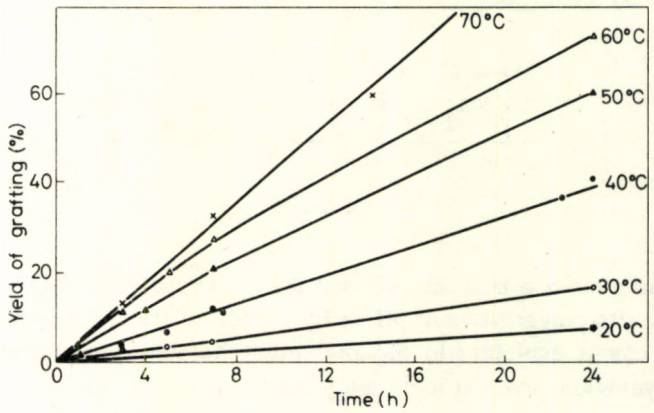

Fig. 2 Yield of grafting as a function of time and temperature (d=0. 1 mm; D_L = =0. 007 MR/h; D = 1 Mrd)

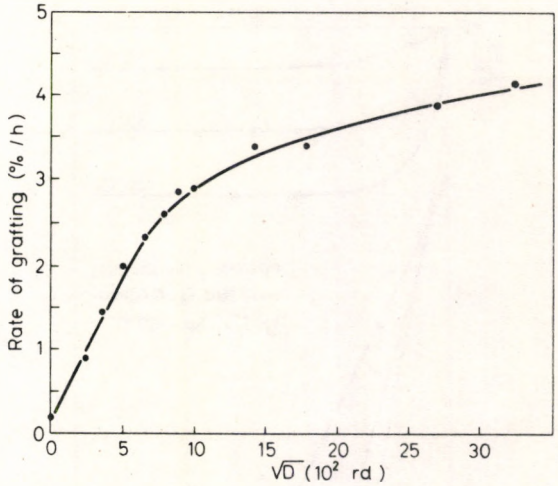

Fig. 3 Initial rate of grafting as a function of the square root of irradiation dose
(d = 0. 1 mm; D_L= 0. 007 MR/h; $T_B = 20^oC$; $T_p = 50^oC$)

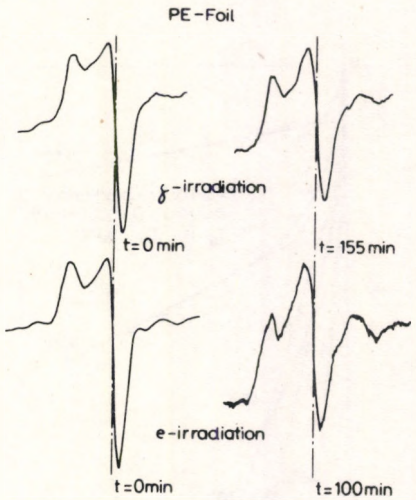

Fig. 4 EPR spectra of PE after irradiation in air at 30°C

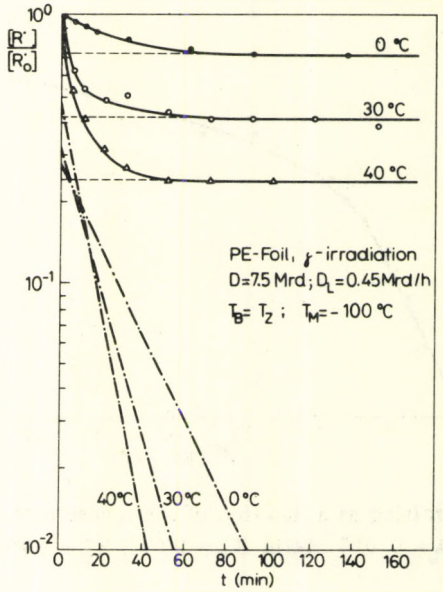

Fig. 5 Peroxy radical decay of gamma-irradiated PE at various temperatures

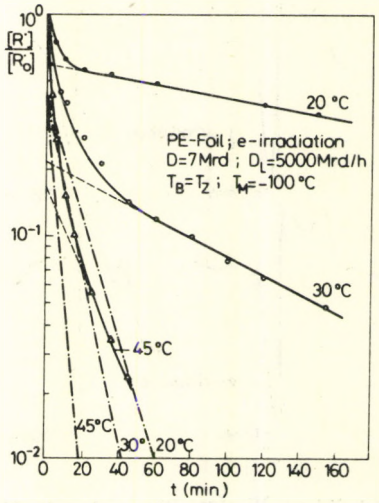

Fig. 6 Peroxy radical decay of electron-irradiated PE at various temperatures

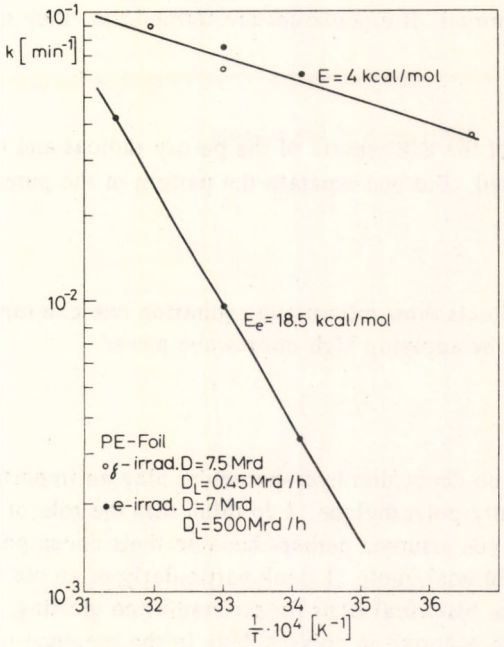

Fig. 7 Arrhenius plots of the peroxy radical decay in the amorphous and crystalline regions

DISCUSSION

J. DOBÓ

I do not completely agree with your arguments against diperoxide formation. Even chain oxidation does not exclude formation of diperoxides. Neither would an activation energy of 30 kcal/mole for the initiation exclude a reaction running at a measurable rate around 40°C as the rate of termination is very low too.

At present the best way to differentiate between peroxide and hyperoxide initiations is that the latter yields high amounts of homopolymer. This is particularly true for monomers exhibiting no thermal homopolymerization, as acrylonitrile, for example.

L. WUCKEL

The propagation steps for a chain reaction can only be the steps III and IV in our paper. They lead to hydroperoxides and not to diperoxides. In our opinion mainly

hydroperoxides are formed. If diperoxides are formed too, they should be formed by another mechanism.

H. KASHIWABARA

A superposition of the ESR spectra of the peroxy radical and the carbon radical can usually be observed. Did you separate the pattern of the pure peroxy radicals?

L. WUCKEL

Since peroxy radicals show microwave saturation one can separate the signal of the peroxy radical by applying high microwave power.

M. MAGAT

Although I have no doubt that hydroperoxides play an important role in peroxidation of low density polyethylene, I do think that the role of diperoxides is more important than you assume, perhaps because their decomposition energy is probably lower than 30 kcal/mole. I think particularly of an old paper (1954) by Chapiro which was the historical basis for preirradiation grafting. Chapiro observed that more crosslinking occurred in polyethylene in the presence of oxygen than in its absence, but these crosslinks broke at a relatively low temperature. In addition the amount of homopolymer is small and can be reduced by the use of OH scavengers. This last observation shows, however, that hydroperoxides are not absent.

The hydroperoxide formation in the case of polypropylene is not a strong argument in favour of their presence in the case of low density polyethylene since in this last polymer the amount of mobile H atoms is much smaller than in polypropylene.

L. WUCKEL

We think that the concentration of the H atoms is not the only condition for the formation of hydroperoxides in polymers. For instance as Neudorf showed some years ago a chain hydroperoxidation takes place in polypropylene as well as in polyethylene oxide.

APPARENT AND TRUE GRAFTS IN POLYETHYLENE-STYRENE SYSTEM GRAFTED BY PREIRRADIATION IN VACUO AND IN AIR

M. Barić. I. Dvornik, F. Ranogajec, J. Dobó*
Institute "Ruđer Bošković", Zagreb, Yugoslavia
*Research Institute for Plastics, Budapest, Hungary

When a grafting reaction is carried out onto a preformed polymeric base, the weight gain does not necessarily mean covalently bound grafts: it may come as well from inextractably occluded homopolymer. To distinguish between the two possibilities, dissolution of the grafted polymer followed by fractional precipitation as well as turbidimetric titration /1,2/ has been proposed. Hoffman et al. suggested slicing of the polyethylene foils before extraction /3/. By a modification of this method we investigated low density polyethylene-styrene grafted foils prepared by simultaneous irradiation and by chemical initiators /4/. It could be established that the grafted foils prepared both by simultaneous irradiation as well as by chemical initiators contain a rather high percentage of occluded homo-polystyrene. This homopolymer cannot be eliminated by simple soaking and extraction. A much more effective elimination of the homopolymer can be achieved by extraction following the slicing of the grafted foils.

Recently we determined covalently bound grafts obtained by simultaneous technique by dissolution of grafted polymer and fractional precipitation and found that this method is in quantitative agreement with the slicing method if higher grafting yields (>200%) are concerned. In such cases covalent graft determined by both methods was about 30% of the extent of apparent grafts.

In the present paper we will discuss the results for the true graft yield obtained by applying the slicing method on grafts prepared by preirradiation in vacuo and in air.

Experimental

Low density and high density polyethylene foils in the form of approximately 10 × 40 mm samples were used. Styrene was three times distilled in vacuo before use. The foils were preirradiated in ^{60}Co source of 7000 Ci. For further details of experimental procedure see elsewhere /4, 6/.

After grafting the foils were soaked in benzene for 24 hours at room temperature, vacuum dried and weighed. In accordance with our previous nomenclature

/4/ the per cent weight increase

$$\left(\frac{\text{weight of grafted foil}}{\text{weight of ungrafted foil}} - 1\right) \times 100$$

is referred to as apparent graft Y_1. The foils were then sliced at intervals of 1 mm and extracted with benzene for an additional 45 hours at 40 or 75 °C. The percentage weight increase against the ungrafted foils is referred to as Y_3. The majority of samples worked up in the present investigation were prepared in grafting experiments reported earlier /5, 6/.

Results

The results obtained by extraction of the sliced, vacuum-preirradiation grafted foils are shown in Table 1. (The incompleteness of experimental data is due to the disintegration of some foils which were extracted at 75 °C.) The difference against the grafted foils prepared by simultaneous irradiation and by chemical methods is striking: whereas all foils grafted over about 30% showed a very substantial weight loss after slicing and extraction, here the highest weight loss is only 4% and about half of the foils lost 1% or less of their weight. The small differences in the weight loss are not related either with the type of the base polymer or with the experimental conditions. The absence of weight loss after slicing and extraction may thus be considered as being specific for the grafting method. This is remarkable in view of the following circumstances:

(1) It applies equally to very different foil materials, LD polyethylenes (two grades), HD polyethylene, polypropylene, polytetrafluorethylene,

(2) It applies even to very high degrees of grafting (over 300%),

(3) It applies also to grafted foils with visibly inhomogeneous structure, similar to those shown in an earlier publication /6/, i. e. to foils containing some bubbles, dents, more or less opaque parts. These inhomogeneities are thus not necessarily connected with homopolymer content. In the case of grafting by simultaneous irradiation and by chemical initiators, even seemingly homogeneous foils contained high fraction of extractable homopolymer.

Our results confirm the view that the homopolymer found in the foils grafted by other methods is not produced by degradation during the extraction, otherwise homopolymer should also be found in the samples preirradiated in vacuo.

The results of slicing and extraction of air preirradiated polyethylene-styrene grafts are shown in Table 2. This method of grafting gives more homopolymer than the preirradiation in vacuo, but much less than simultaneous irradiation or grafting by chemical initiators. In Fig. 1 a comparison of the grafting efficiency (onto low density polyethylene) of four different methods is presented. The quantities of homopolymer as determined in styrene solution were in no case (of both

Table 1
Extraction results

Preirradiation dose	2.5 Mrad				13 Mrad				30 Mrad			
Grafting temperature	20 °C*		60 °C*		20 °C*		60 °C*		20 °C*		60 °C	
	Y_1	Y_3/Y_1	Y_1	Y_3/Y_1	Y_1	Y_3/Y_1	Y_1	Y_3/Y_1	Y_1	Y_3/Y_1	Y_1	Y_3/Y_1
FERTENE [a]	65.2	0.997							90.2	0.997		
0.15 mm	100.0	0.992							166.0	0.993		
									220.1	0.988		
									271.0	0.988		
OKITEN [b]	64.0	0.992							106.5	0.995		
0.15 mm	98.0	0.988							195.5	0.990		
	121.0	0.989							250.8	0.986		
									302.0	0.981		
HOSTALEN GC [c]			56.1	0.976					15.5	1.000	152.7	1.000
0.07 mm			99.5	0.960					32.8	1.000	286.0	0.980
HOSTALEN GC [c]	193.2		55.4	0.970			197.3	0.963	10.0	1.000	157.0	0.970
0.1 mm	335.3		125.5	0.990					103.0	0.990	296.3	0.987
HOSTALEN GC [c]	20.1	0.985	58.1	0.994			158.0	0.980	14.5	0.972		
0.3 mm			111.1	0.991			253.4	0.970				
POLYPROPYLENE	115.9		66.6		195.2	0.995	140.5	0.996				
0.06 mm	226.5		117.3		298.0	0.983	152.3	0.972				
	285.3		121.5		384.0	0.997	173.2	0.961				

Table 1 (cont.)

Preirradiation dose	2.5 Mrad				13 Mrad				30 Mrad			
Grafting temperature	20 °C*		60 °C*		20 °C*		60 °C*		20 °C*		60 °C*	
	Y_1	Y_3/Y_1	Y_1	Y_3/Y_1	Y_1	Y_3/Y_1	Y_1	Y_3/Y_1	Y_1	Y_3/Y_1	Y_1	Y_3/Y_1
POLYPROPYLENE	158.0		49.5		145.2	0.993	126.5	1.000	160.0	0.970	101.5	1.000
0.12 mm	215.0		57.3		275.3	0.998	143.2	0.986	265.0	0.975	139.3	0.980
	243.0		98.0		352.3	0.986			330.0	0.967	163.9	0.961
TEFLON					10.7	0.962	23.6	0.996			20.3	0.990
0.12 mm					51.7	0.992	32.3	0.970				
					64.4	0.986						

a, b = low density polyethylene
c = high density polyethylene

* The extraction with benzene was performed at 75 °C, in the other experiments at 40 °C, for 45 hours

Table 2:
Preirradiation in air. The Y_3/Y_1 ratio as a function of Y_1; preirradiation dose 1.4 Mrad

	40 °C		60 °C	
	Y_1	Y_3/Y_1	Y_1	Y_3/Y_1
LUPOLEN 1810 H[a] 0.05 mm	14.2	0.975	111.5	0.960
			46.9	0.965
			4.5	0.985
LUPOLEN 1810 H[a] 0.1 mm	29.6	0.980	110.5	0.950
	59.0	0.980	46.3	0.950
			4.1	0.985
			438.0	0.850
LUPOLEN 2400 E[b] 0.1 mm	30.4	0.980	114.5	0.970
	53.2	0.985	60.0	0.965
			8.0	0.975
LUPOLEN 5041 D[c] 0.05 mm	51.7	0.985	78.2	0.950
	39.0	0.980	45.5	0.965
			8.6	0.970
LUPOLEN 5041 D[c] 0.1 mm	47.6	0.975	8.5	0.975
			128.0	0.980

a, b, = low density polyethylene

c = high density polyethylene

preirradiation grafting methods) higher than could be predicted from the thermal polymerization rate of styrene. The extraction before slicing gave in no case measurable amount of homopolymer except air preirradiated 438% grafted foil. With other foil types similar trends have been observed.

Discussion

1. The length of the grafted chains

The average degree of polymerization of the grafted chains is the ratio of the number of molecules polymerized to the number of free radicals initiating grafting. The G value of the initiating radicals is obviously lower than the free radical yield in polyethylene as

– the alkyl radicals decay practically completely on heating to room temperature,

– part of the allyl radicals also decays before contacting styrene,

– this decay may be accelerated by the increased chain mobility through grafting and swelling,

– a part of the free radicals (grossly 50%) remains trapped in the crystalline parts of polyethylene inaccessible for grafting.

According to a recent survey of Dole /7/, the G value for allyl radicals in high density polyethylene may be 0.2–0.3. Thus, a G value of 0.1 for the trapped free radicals capable of initiation of grafting may well be the highest reasonable estimate. Jones /8/ on the other hand, derived from kinetic measurements for the initiating trapped radicals G = 0.002, let us take it for the lowest estimate. At a preirradiation dose of 2.5 Mrads, this corresponds to 1.5×10^{17} and 3×10^{15} radicals per gram of polyethylene, respectively. The total yield of styrene polymerized onto 1 g polyethylene at 20 °C amounts to 3 g = 1.8×10^{22} molecules of styrene per gram of polyethylene. This gives for the degree of polymerization of the grafted chains (for the two estimates of the initiating free radicals concentration) 10^5 and 6×10^6, respectively. The accepted chain transfer constant for styrene monomer would limit the degree of polymerization at 20 °C to about 3×10^4 /9/. Thus, the greater part of the polystyrene formed should be found in the form of homopolymer extractable after slicing, clearly in contrast with our findings. Disagreement can be explained by taking into account the chain transfer to polystyrene. A support for this explanation are the results of Henrici-Olivé and Olivé /10/ who reported for branching as high a value as one side chain of polystyrene per 5000 styrene monomer units.

2. The formation of homopolymer in grafting by other methods than by preirradiation in vacuo

There may now be given a more complete picture of the formation of homopolymer found in polyethylene foils grafted by simultaneous irradiation and by chemical initiators. Two questions are to be answered:

(1) How the homopolystyrene is formed?

(2) Why the homopolystyrene cannot diffuse out of the undamaged foil?

At the beginning of the grafting reaction styrene monomer penetrates the amorphous parts of the foils. At this instant the actual concentration of monomer near the grafting sites may be quite low. The rest is made up from polyethylene. Thus, at this stage of the reaction, the concentration of the polyethylene chains relative to that of the monomer is very high. This means that in the case of simultaneous irradiation the initiation process takes place predominantly on the polyethylene chains while in the case of chemical initiators the primary radicals may abstract with high probability hydrogen atoms from the polyethylene backbone, thus giving rise to the formation of true graft copolymers.

As the reaction proceeds, the concentration of monomer inside the foil becomes higher and higher, as the equilibrium swelling grows quite steeply with the degree of grafting /11/. As the diffusing styrene molecules are transformed to polymer two processes occur:

Firstly, the concentration difference of styrene in polystyrene inside and outside the foil becomes regenerated, this difference being the driving force of futher monomer supply,

Secondly, according to the thermodynamics of the two polymers in a common solvent, the polystyrene will tend to separate from the polyethylene. Thus, a microphase separation occurs, at the beginning on the molecular level. Those parts of the foil, which are richer in polystyrene, will now preferentially be swollen by styrene. One may estimate that at this stage of reaction these sites of the foil may consist of up to 50% or more of styrene monomer. The rest is made up mainly of polystyrene (grafted or not grafted). But, these are exactly those domains of the foil, where the greater part of the reaction takes place.

Thus, conditions favourable for homopolymerization and unfavourable for grafting are established. A substantial part of the radiation initiation takes now place in the styrene-polystyrene phase and the primary radicals formed in the monomer phase undergo predominantly to a chain growth reaction and not to a chain transfer to polyethylene. It may be also remembered that according to previous results /12/ only primary radicals are capable of chain transfer to polyethylene, while the growing styryl radicals are not.

The homopolystyrene formed will continue to move in this microheterogeneous environment towards higher concentrations of styrene (or, during the soaking of the foils, of benzene) and towards lower concentrations of polyethylene, the relatively ungrafted parts of polyethylene constituting barriers for this movement. Thus, only a minor part of the homopolymer will diffuse out of the foil no matter how long the soaking time and how high the extraction temperature may be. The greater part accumulates in bubbles, where more and more styrene (or benzene) accumulates as well, leading to the growth of the bubbles.

When, however, the grafting is performed by preirradiation methods, no initiation takes place in the monomer phase. Because of the comparatively low temperatures and short reaction times used in the vacuum preirradiation grafting, the thermal polymerization does not yield significant quantities of homopolymer. If, now, chain transfer to monomer is negligible, the high yield of true graft in samples prepared by this method is understandable.

References

/ 1/ T. Matsuda, K. Hayakawa, B. Eda, K. Kawase, Chem. High Polymer 10, 634 (1961).

/ 2/ T. Matsuda, K. Hayakawa, B. Eda, K. Kawase, Chem. High Polymer 10, 639 (1961).

/ 3/ A.S. Hoffman, E.R. Gilliland, E.W. Merrill, W.H. Stockmayer, J. Polym. Sci. 34, 461 (1959)
/ 4/ M. Baric, I. Dvornik, J. Dobó, Proc. Third Tihany Symp. Radiation Chemistry, 1971, Akadémiai Kiadó, Budapest, 1972. p. 1001.
/ 5/ F. Ranogajec, I. Dvornik, J. Dobó, Eur. Polym. J. 6, 1169 (1970)
/ 6/ J. Dobó, F. Ranogajec, I. Dvornik, Croat. Chem. Acta 42, 551 (1970).
/ 7/ M. Dole, The Radiation Chemistry of Macromolecules, Vol. 1, Academic Press, New York and London, 1972, p. 339.
/ 8/ T.T. Jones, British Plastics 33, 525 (1960).
/ 9/ G. Henrici-Olivé, S. Olivé, Fortschritte der Hochpolymerenforschung 2, 538 (1961).
/10/ G. Henrici-Olivé, S. Olivé, Polymerisation. Katalyse-Kinetik-Mechanismen, W. Foerst, H. Grünewald (Eds), Verlag Chemie, Weinheim, 1969, p. 31.
/11/ M. Fels, R.Y.M. Huang, J. Appl. Polym. Sci. 14, 537 (1961).
/12/ T. Czvikovszky, J. Dobó, J. Polym. Sci., C 16, 2973 (1967).

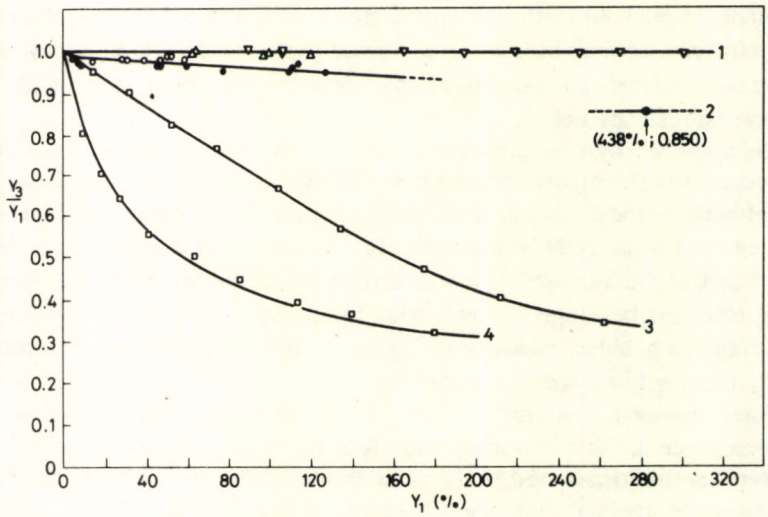

Fig. 1 Comparison of the grafting efficiency (of styrene onto low density polyethylene) of four different grafting methods. 1) Preirradiation in vacuo: △ – 2.5 Mrad, ▽ - 30 Mrad, 2) Preirradiation in air (1.4 Mrad): o - 40 °C, ● - 60 °C, 3) Simultaneous grafting: 3000 rad/h, 40 °C, 4) Chemical initiator, 0.06% AIBN, 40 °C

SOME PROBLEMS OF MODIFICATION OF FABRICS BY MEANS OF VAPOUR PHASE RADIATION GRAFTING

G. G. Ryabchikova, G. V. Zdolnikova*, P. Ya. Glazunov,
P. V. Vlasov*, V. I. Spitsyn
Institute of Physical Chemistry of the Academy of Sciences of the USSR,
Moscow, USSR
*Moscow Textile Institute, Moscow, USSR

Half-woollen fabrics containing up to 50% of viscose fibres find a wide practical use. These fibres are extremely hygienic. However, these fabrics are characterized by low resistance to wear due to viscose fibres in their content.

The latest investigations give us a reason to believe that the process of radiation graft copolymerization can play a notable part in solving one of the urgent problems – obtaining materials with desired properties. Modification of fabrics by the grafting of small quantities of polymers essentially improves their physico-chemical and mechanical properties /1–3, 7/.

To increase resistance to wear of half-woollen fabrics we used the direct method of radiation graft copolymerization from saturated vapour of styrene. Under our working conditions, there was practically no homopolymerization. Grafting was carried out in an enlarged laboratory set-up, with the use of an electron accelerator (the energy of electrons was about 0.8–1 MeV) /4/.

Under the condition of the enlarged synthesis we found the dependence of the output of graft polystyrene on the absorbed dose and dose rate (Fig. 1) to be similar to the dependence reported in Ref. /5/.

The physico-mechanical properties of the modified fabric samples containing from 5 to 25% of graft polystyrene have also been investigated (Fig. 2). The optimum weight gain has been found to be 5%. The fabric obtained is characterized by higher resistance to wear (by 2–2.5 times), while the other physico-mechanical parameters – rupture stress, hardness to fraction and the weight of 1 linear metre being practical unchanged. Therefore the optimal amount of 5% of graft polystyrene was chosen to obtain half-woolen fabric with increased resistance to wear.

The properties of graft fabrics depend very much on the distribution of the polymer in the modified samples, whether it is located only on the surface forming an outer coating or distributed evenly in its volume, or if it forms a layer with certain diffusion into the depth of the sample. In order to solve various problems of modifying materials it is necessary to ensure the desired distribution of the graft polymer.

Cross-sections of viscose, polyamide and woollen fabrics composing the half-woollen fabric and containing graft polystyrene were investigated by means of optical microscopy. To reveal the distribution of graft polystyrene through the cross-sections

of fibres the latter was treated by chlorine-zinc-iodine solution /6/. Each component of the graft fabric is dyed by this solution to definite colour: viscose – brownish-violet, polyamide – orange, wool – light-yellow. Polystyrene is not coloured by this reactant. The distribution of coloured regions shows the places of grafting.

The investigation of the cross-sections of modified viscose filaments showed that for low graft polystyrene contents (5%) the latter is distributed in the oriented texture of the filament. With the increase of the polystyrene content up to 23%, grafting extends inside the filament but the surface distribution predominates. For this quantity of polymer we already see uneven grafting. The higher the content of polystyrene the less uniform the grafting. Modified viscose filaments with 75% polystyrene are grafted either in some parts of the surface, or in a continuous layer on the surface in the whole volume. The uneven distribution of the polymer through the sections of filaments can be explained by the fact that diffusion of the monomer in the filament was made difficult by twisting and in entanglement of filaments in the fabric.

Graft polymerization of polystyrene on polyamide fibres takes place in the volume under different quantities of polymer. There is no grafting on the surface layer of the fibres due to the oxidation of polyamide. This is proved by the orange ring around the polystyrene grafted in the volume (76%).

The analysis of the cross-sections of modified woollen fibres shows that under the conditions used there is practically no radiation graft polymerization on wool.

So far as the purpose of modification of the half-woolen fabric is to increase its resistance to wear, special attention should be paid to the distribution of grafted polystyrene on the sections of viscose fibres since these have the lowest resistance to wear compared with polyamide and woollen fibres. When the content of grafted polymer is low (5%) grafted polystyrene distributed in the orientated texture of fibres prevents the nucleus from destruction by wear.

To get fabrics with improved properties the optimum conditions of radiation graft-copolymerization have been determined by the method of rotable central composition planning of the second order /8/. The choice of the model of the second order is explained by a small range of changes of variables. Besides it was found that there is a non-linear dependence between the optimization parameter (the quantity of graft polymer) and one of the factors (dose rate) (Fig. 1).

Dose, dose rate and the temperature were considered as main factors determining the radiation graft polymerization. The above-mentioned independent variables, levels and intervals of their variation are given in Table 1. The values of factors at zero level and the interval of their variation are based on the data obtained from the preliminary study of the process of radiation graft polymerization. On the base of Table 1 we worked out the matrix of planning tests, its realization enabled us to calculate the coefficients of the regression equation for the dependencies under study. The equation we got is

$$y = 6.68 + 1.58X_1 - 2.05X_2 + 2.87X_3 + 0.44X_1X_3 - 1.22X_2X_3 + 0.98X_2^2 \quad (1)$$

$$G = -15.92 - 12.03D + 4.59P + 0.35t + 0.34Dt - 0.23Pt + 3.59P^2 \quad (2)$$

Table 1

Factors	Levels of variations					Intervals of variations
	-1.682	-1.00	0	+1.00	+1.682	
ζ_1 – dose, Mrad	0.30	0.39	0.52	0.65	0.74	0.13
ζ_2 – dose rate, Mrad/hour	0.17	0.52	1.04	1.56	1.91	0.52
ζ_3 – temperature, ^{o}C	53	60	70	80	87	10

Table 2

Name	Fabric	
	Modified and dyed	Ready
Density of 10 cm		
Warp	281	288
Weft	258	254
Rupture load. kgf		
Warp	63.1	68.8
Weft	38.2	39.9
Rupture elongation, mm		
Warp	47.0	46.5
Weft	45.8	44.0
Thickness of fabric, mm	0.654	0.670
Mass of fabric $\frac{g}{m^2}$	238.0	237.0
Air permeability, m^3	7.72	8.38
Hardness to fraction, $\frac{mgf}{cm}$		
Warp	348	328
Weft	232	219
Capillarity, cm	13.5	14.5
Resistance to abrasion, circle	29068	18119

Equations (1) and (2) may be interpreted as the equation of a certain surface in a three-dimensional space. In order to find the optimal conditions for the grafting thus to obtain the half-woollen fabric with 5% of polystyrene, the surface of response (geometric image of the responce function) in the range of optimum was investigated with the help of two-dimensional sections, which give us a clear idea of the possible changes of the optimization parameter under variation of independent variables. We obtained 2-dimensional sections for each pair of factors provided that the values of the third were fixed. The values of factors at zero level – in the centre of the experiment – were taken as fixed values.

To obtain the section of the surface of response given in Fig. 3 we substitute $X_3 = 0$ (the temperature 70°C) into the initial equation (1). As a result we have the equation of the given section (3). The contour curves corresponding to the 3, 5, 7, 10 and 15% of graft polystyrene are shown in the section. The analysis of the contour curve corresponding to 5% content of polystyrene made it possible to establish the optimal conditions for the process of radiation graft polymerization to obtain the fabric with the desired properties. In order to find these optimal conditions we proceeded from the minimal time of reaction: the absorbed dose was 0.43 Mrad, dose rate was 1.91 Mrad/hour, the temperature was 70°C.

The initial fabric modified by radiation graft polymerization under the optimal conditions was finished by standard methods. Physical and mechanical properties of the modified and non-modified fabrics after the process of technological finishing are given in Table 2. The physical and mechanical properties of the modified and non-modified fabrics do not differ much, except in resistance to wear.

Air permeability of the modified fabric is a little lower than that of the standard fabrics. Evidently it results from the more dense structure of filaments owing to the grafting of polystyrene. Practically speaking, the hygroscopic properties (which were evaluated by capillarity) of the modified and standard fabrics do not differ, this means that the presence of 5% graft polystyrene in the fabric does not affect its hygroscopic property.

References

/1/ Rutherford H. A., Armstrong A. A., Text. Res. J., 30, No. 7. 546, (1960).

/2/ H. U. Usmanov, A. Azizov, M. U. Sadykov. "Radiation Chemistry of Polymers", Moscow, "Nauka", 153, (1966).

/3/ Dille S., Garnett J. L. Austral. J. Chem., 21, No. 2, 397 (1968).

/4/ P. V. Vlasov, G. G. Ryabchikova, G. V. Zdolnikova, P. Ya. Glazunov, Trudy Moskovskogo tekstilnogo instituta. Vyp. 2, 70, (1971).

/5/ U. A. Arifov, G. A. Klein et al. Izv. AN UzSSR, Seriya fiz.-mat. nauk, No. 4, (1960).

/6/ T. V. Melik-Bezhbeut et al. Krasheniye i otdelka, No. 10, 1973.

/7/ B. L. Tsetlin, I. Yu. Babkin. "Radiation Chemistry of Polymers", Moscow, "Nauka", (19

/8/ V. B. Tikhomirov. Matematicheskiye metody planirovaniya experimenta pri isuchenii netkannykh materialov. M., 1963.

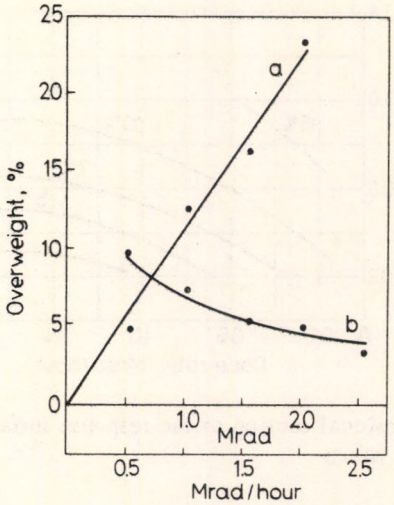

a) $g = 11.06\,D$ (1)

b) $g = 13.12 - 7.84\,M + 1.73\,M^2$ (2)

Fig. 1 Dependence of the amount of grafted polystyrene:
a) on the dose absorbed (1.04 Mrad/hour 70°C),
b) on the dose rate (0.52 Mrad, 70°C)

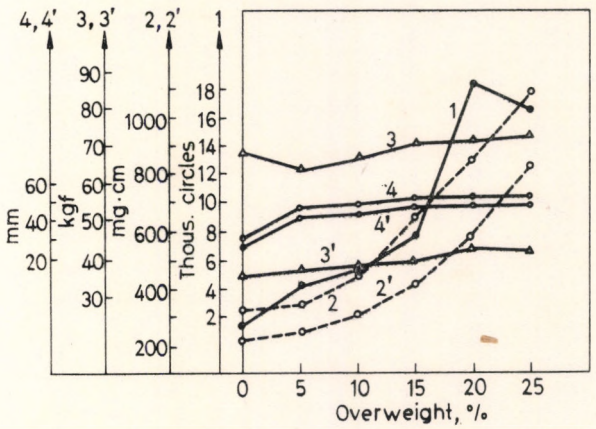

Fig. 2 The influence of the quantity of grafted polystyrene on the physical and mechanical properties of the fabric:

1) resistance to wear,
2) warp hardness to fraction,
2') weft hardness to fraction,
3) warp rupture stress,
3') weft rupture stress,
4) warp rupture strain,
4') weft rupture strain

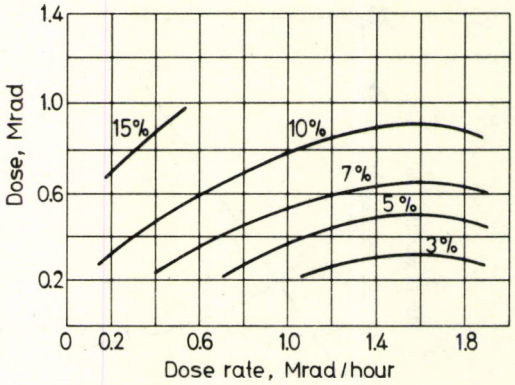

Fig. 3 The 2-dimensional section of the response surface where $X_3 = 0$ (the temperature 70°C)

THE INTENSIFICATION OF RADIATION-INDUCED POLYMERIZATION THROUGH COMPLEXATION OF MONOMERS

V. S. Ivanov, E. N. Konstantinova, I. I. Migunova, E. S. Oparina,
V. K. Smirnova, E. E. Kever
Leningrad State University, Leningrad, USSR

We know various ways of performing intensification, i.e., sensitification, of the radiation-induced polymerization (SRP) based on phenomena of physical or chemical character /1/. The SRP method is associated with the increasing of the efficiency of the process and maintains constant such kinetic parameters as temperature, pressure, dose rate and total dose. Commonly used for the SRP method are additive-sensitizers although the influence of some definite physical factors, for instance, electric field, is in some cases found to be substantial /2/. The mechanism of the sensitizers' reaction varies.

The physical character of the sensitification shows itself during solid-state polymerization when sensitizers, acting as unpolymerized additives, form eutetic systems with a monomer /3,4/. The heterogeneous polymerization in binary systems is intensified in the same manner /5/. The formation of glass-forming systems via addition of a monomer to the long-chain molecule matrix also stimulates the polymerization by changing the rigidity of the system during glass softening /6/.

In other cases, when chemical phenomena lie at the root of the observed kinetic effect, the sensitizer acts as an additive which produces additional initiation centres or provides energy exchange with the monomer, when various methods of radiation-induced polymerization are used /1,7,8/. Related to this type of sensitizer are the additives providing an increase of the polymerization efficiency at the cost of energy gains through the complexation of monomers. The SRP method, using the introduction of inorganic /9,10/ or element-organic /II/ additives forming complexes with a monomer, is described in the literature.

The present report deals with the problem of intensification of radiation-induced (co)polymerization via selection of a comonomer pair of organic character, which forms charge-transfer complexes (CTC). In addition to the expected kinetic effect this formation may lead to the development of pure polymers not contaminated with mineral impurities, which in some cases deteriorate their serviceability. The formation of CTC is typical for the monomers distinguished by their donor-acceptor properties. Alternating copolymers are formed during copolymerization of these monomers. However, the mechanism of this process still remains debatable.

Some comonomers forming CTCs have been chosen and investigated. These were styrene (St), a typical electron-donating monomer and N-2,4-dimethylphenylmaleimide (DMPhMI) possessing electron-acceptor properties. The influence of CTC on the copolymerization with heptylacrylate (HA) has been investigated. The addition of HA increases elasticity of the formed terpolymer due to internal plastification.

In order to obtain evidence for CTC, St and DMPhMI spectra (Fig. 1) have been used and recorded with a SPECORD spectrophotometer in the range of 34000–22000 cm^{-1} (294–455 nm), toluene (dielectric constant = 2.4) serving as a solvent. The acceptor concentration was equal to $1.0 \cdot 10^{-3}$ mole/l and the donor concentration varied in the range of 0.26–8.7 mole/l. With the DMPhMI and St bands (curves 1,2, respectively) overlapping the peak of the charge-transfer band, we were able to detect only a part of this band (curve 3) from the point of 32000 cm^{-1} (312 nm).

The equilibrium constant (K) of the complex and the extinction coefficient (ε) have been determined with 32000, 31500 and 31000 cm^{-1} frequencies and calculated according to Ketelaar's equation /12/. The value of $K = 0.025 \pm 0.010$ l/mole and that of $\varepsilon = 1970$ $l.mole^{-1}.cm^{-1}$ allow us to characterize the complex as a weak one. The mentioned value of K is agreement with the data available in the literature for the following systems: divinylether-maleimide (K=0.037 l/mole) /13/ and 4-dimethylaminostilbene-N-ethylmaleimide (K = 0.064 l/mole) /14/.

The constant for the formation of weak CTCs is known to decrease with an increase of the permittivity of the solvent, whereas the scission constant increases /15/. This would increase the concentration of the initiating radicals and the polymerization rate and decrease the molecular weight of polymers during radical initiation. It was for this reason that we considered it to be reasonable to investigate the kinetic effect of radiation-induced polymerization of St-DMPhMI system in benzene (dielectric constant = 2.3) and DMF (37.6), i.e., in solvents possessing different values of permittivity. Initiation was carried out with γ-rays of Co^{60}. Figure 2 shows the extreme dependence of the copolymer yield (curves 1,2) on the monomer feed composition. The maximum point corresponds to the equimolecular composition. The observed effect appears to be associated with a weak CTC, whose scission would increase the number of radicals giving rise to constants of cross propagation of chain, especially in DMF (Fig. 2, curve 2).

Curve 3, representing the dependence of intrinsic viscosity on the monomer feed composition, shows the minimum point at the equimolecular composition. However, the curve climbs monotonically from St to DMPhMI except for minimum point. The observed effect allows us to assume that at the minimum point a striking increase of propagation and termination constants takes place leading to the maximum yield of a copolymer with more short chains. This results in a lowering of the copolymer intrinsic viscosity.

Figure 3 illustrates the dependence of the copolymer composition on the monomer feed composition for the St-DMPhMI system. The copolymer composition

Table 1.
Radiation-induced copolymerization of HA-St-DMPhMI systems and thermostability of obtained terpolymer, (1 Mrad/hr, 3 Mrad)

Monomer feed composition, mole %			T °C	% Nonpolymerized monomers	Loss weight at 280°C, %
HA	St	DMPhMI			
90	10	0	25	1.3	8.1
90	5	5	25	1.3	2.3
90	2	8	25	2.9	3.1
80	20	0	25	1.7	7.2
80	10	10	25	1.2	2.6
80	8	12	25	2.1	3.8
60	40	0	60	19.9	7.0
60	20	20	60	0.5	0.9
60	10	30	60	1.5	1.6

depends little on the monomer feed composition within the broad range (30—70% St). This indicates that an alternating copolymer may be developed. We have obtained the following values of the copolymerization constants: $r_1 = 0.022 \pm 0.002$ for DMPhMI and $r_2 = 0.003 \pm 0.001$ for St. The calculations were performed on a computer using the versatile method /16/. That the product of these constants approximates zero is characteristic for formation of an alternating copolymer. Finally, using the obtained values we have calculated the run number (R) /17/. Its value ($R_{50} = 0.98$) taken at equimolecular relation of comonomers also proves the formation of an alternating copolymer.

One of the present concepts on the mechanism of alternation is given in Ref. /11/. The ESR investigations of the butylmethacrylate-2,3-dimethylbutadiene system in the presence of complexing agents and maleic anhydride-dimethylbutadiene system have shown monoradicals to take part in this process. The formation of a copolymer with the monomer units alternating regularly should be associated with the relative increase of the cross propagation constants as compared with homopolymerization constants of this monomer. The data given in the present report are in agreement with the above-mentioned concept of the mechanism of formation of an alternating copolymer.

The discussed St and DMPhMI binary system is a model fragment providing support for the hypothesis of sensitizing influence of the CTC. The validity of the SRP hypothesis has been tested in HA-St-DMPhMI sytem. As shown in Fig. 4, the maximum yield of the terpolymer corresponds to the equimolecular relation of St-DMPhMI in ternary system. The terpolymer obtained under conditions of maxi-

Table 2.

Destruction temperatures of terpolymers (rate of temperature rise 4°C/min, in air); radiation conditions: 1 Mrad/hr; 3 Mrad; 25°C

Monomer feed composition, mole %			Destruction temperatures, °C
HA	St	DMPhMI	
70	30	0	308
70	20	10	310
70	15	15	355
70	10	20	328

mum conversion has at the same time increased thermostability which is estimated upon losing volatile products in vacuum during two hours under conditions of isothermality (Table 1).

In order to obtain the complete characteristics of the terpolymer a combined thermoanalysis has been performed using a MOM derivatograph (Hungary). For the investigation some polymers with HA=70% have been taken, with St and DMPhMI contents varying in them. Table 2 gives destruction temperatures and shows that the thermostability of the terpolymer reaches its maximum at the equimolecular relation of St and DMPhMI. The obtained data on the terpolymer thermostability reveal the important function of the alternating fragment in the macromolecular chain. Similar observational data on other St copolymers are given in paper /18/.

Hence, the proposed SRP method through usage of CTC not only enhances the procedure but also enables us to get pure modified polymers with increased thermostability.

Acknowledgement. The authors acknowledge the assistance of Dr. K. K. Kalninsh in detecting CTC with the spectrophotometer.

References

/ 1/ V.S. Ivanov, I.I. Migunova, Kinetics and Mechanism Polyreactions, vol.4, Akadémiai Kiadó, Budapest, 1969, p. 57.

/ 2/ H. Roth, F. Keller, G. Fleischer, Faserforsch. und Textiltechnik, 25, 539 (1974).

/ 3/ Gy. Hardy, J. Varga, G. Nagy, F. Cser, J. Erö, J. Polym. Sci., C16, 2583 (1967).

/ 4/ V.S. Ivanov, L.A. Petrukhno, L.F. Musienko, Europ. Polym. J., 6, 1539 (1970).

/ 5/ L.A. Petrukhno, V.S. Ivanov, Vysokomolek. soed., A16, 1469 (1974).

/ 6/ A. Chapiro, D. Roussel, J. Polym. Sci., C16, 3011 (1967).

/ 7/ V.S. Ivanov, Radiation Polymerization, Publishing House "Chemistry", Leningrad, 1967, p.68.
/ 8/ A.D. Abkin, A.P. Sheinker, G.N. Gerasimov, in "Radiation Chemistry of Polymers", Publishing House "Nauka", Moscow, 1973, p. 7.
/ 9/ V.F. Kulikova, I.V. Savinova, V.P. Zubov, V.A. Kabanov, L.S. Polak, V.A. Kargin, Proc. Second Tihany Symp. Radiation Chemistry, Akadémiai Kiadó, Budapest, 1967, p.493.
/10/ I. Kaetsu, A. Ito, K. Hayashi, Kobunshi Kagaku, 28, 230 (1971).
/11/ V.A. Kabanov, Acta Chim. Sci. Hung., 81, 129 (1974).
/12/ J.A.A. Ketelaar, C. Van de Stolpe, A. Goudsmit, W. Dzacubas, Rec. Trav. Chim, 71, 1104 (1952), ibid., 70, 499 (1951).
/13/ G.B. Butler, G.C. Corfield, Progress in Polymer Science, edit. A.D. Jenkins, Pergamon Press, vol. 4, 1975, p.135.
/14/ H. Yamakita, K. Hayakawa, J. Polym. Sci., A-1, 10, 2223 (1972).
/15/ G. Briegleb, J. Czekalla, Angew. Chem., 72, 401 (1960).
/16/ K.A. Makarov, G.M. Tomashevskaja, E.M. Dynkin, A.F. Nikolaev, Vysokomolek. Soed., A13, 2739 (1971).
/17/ N.A. Plate, A.D. Litmanovitsch, Vysokomolek. soed., A14, 2503 (1972).
/18/ A.P. Andreev, V.V. Zaitzeva, R.V. Kutscher, Ju.S. Zaitzev, Plast. massy, N 2, 54 (1975).

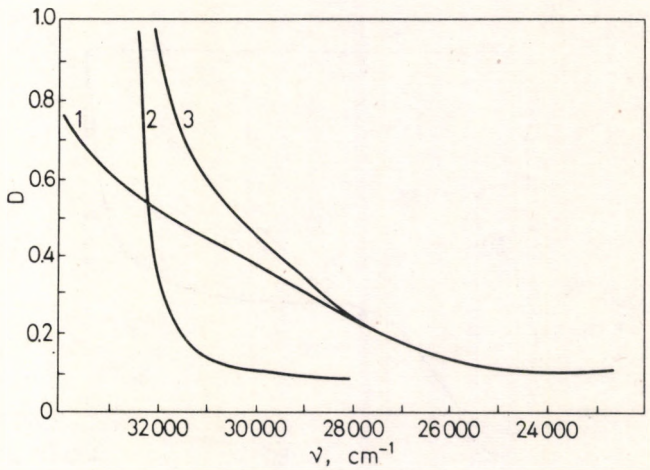

Fig. 1 UV-spectra of DMPhMI and St solutions in toluene: (1) DMPhMI ($1.0 \cdot 10^{-3}$ mole/l; (2) St (3.13 mole/l; (3) DMPhMI ($1.0 \cdot 10^{-3}$ mole/l) + St (3,13 mole/l). Path length = 1 cm

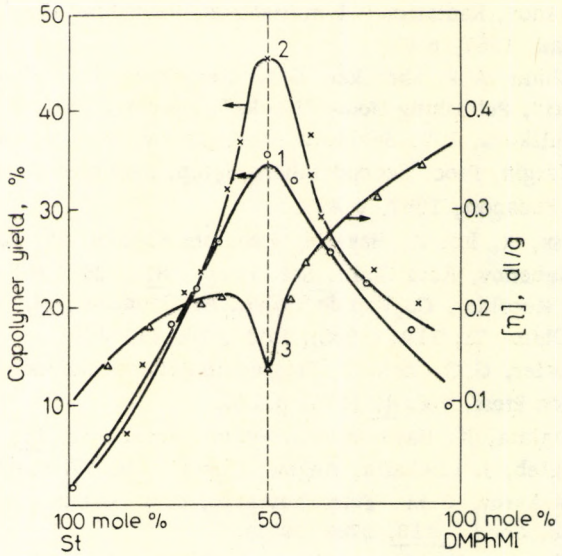

Fig. 2 The dependence of yields of copolymers St-DMPhMI (curves 1 and 2) and its intrinsic viscosity (curve 3) on monomer feed composition (1 Mrad/hr, 1,5 Mrad, 25°C, a concentration 2 mole/l). (1) benzene; (2,3)DMF

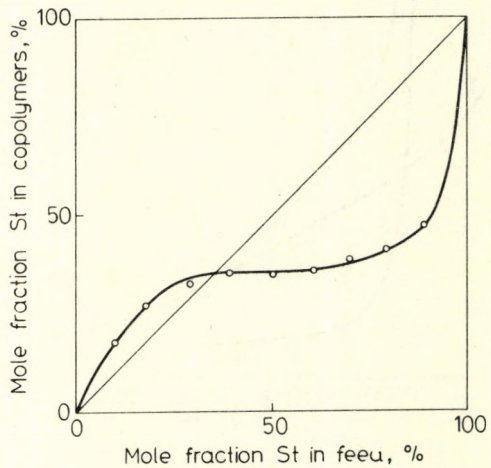

Fig. 3 The dependence of copolymer composition on monomer feed composition (I Mrad/hr; 1.5 Mrad; 25°C; concentration 2 mole/l in benzene)

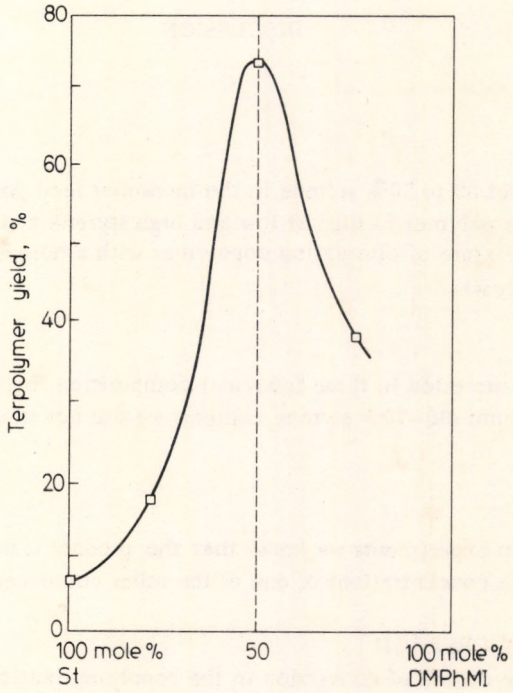

Fig. 4 The effect of CTC sensitization at its radiation-induced copolymerization with HA (1 Mrad/hr; 0.25 Mrad; 60^0C; in bulk; 60% HA)

H. HEUSINGER

In the range of 30 to 70% styrene in the monomer feed you get an alternating copolymer. Is the polymer formed at low and high styrene concentrations a statistical copolymer or a mixture of alternating copolymer with a homopolymer of the monomer component in excess?

V. S. IVANOV

As we were interested in those monomer composition regions where the kinetic effect was maximum (30–70% styrene content) we did not study in detail other compositions.

Ch. SCHNEIDER

From our own experiments we know that the product is not a mixture of homo- and copolymer at high concentrations of one or the other component, but a real copolymer.

J. ZURAKOWSKA-ORSZÁGH

What was the degree of conversion in the copolymerization process shown in your Figure 3?

V. S. IVANOV

The data represented in Fig. 3. correspond to small, up to 8%, conversions.

CATIONIC POLYMERIZATION OF STYRENE BY MEANS OF PULSE RADIOLYSIS

S. Egusa, S. Arai,* A. Kira,* M. Imamura*, Y. Tabata
Nuclear Engineering Research Laboratory, The University of Tokyo, Tokai-mura, Ibaraki 319-11, Japan
and
*The Institute of Physical and Chemical Research, Wako-shi, Saitama 351, Japan

Introduction

The radiation-induced polymerization of bulk styrene /1, 2/is known to proceed predominantly via a cationic mechanism under extreme conditions of purity and dryness even at room temperature. It is also well known that styrene in alkyl halides polymerizes when irradiated at low temperatures via both free-radical and cationic mechanisms concurrently, and the lower the temperature, the more favourable a cationic mechanism becomes even under normal conditions of purity and dryness /3-5/.

Several pulse radiolysis studies have been made with a view to elucidating the nature of ions responsible for the initiation and propagation reactions. Yoshida et al. /6/ attempted a pulse radiolysis study of styrene in n-butyl chloride at room temperature. However, tne result is not necessarily definitive because they failed to observe the 630-nm band of a styrene monomer cation radical which Shida and Hamill /7/ had found in a γ-irradiated glassy solution. Irie et al. /8/ made a laser photolysis study of cationic polymerization of α-methylstyrene in the presence of electron acceptors. The result is interesting in connection with radiation-induced cationic polymerization of styrene.

We have carried out a microsecond pulse radiolysis study on styrene in solution at low temperatures. We found that a styrene monomer cation radical is so reactive that it decays within a pulse duration of 1 μsec above -150°C. We were able to observe five cationic species by lowering the temperature to -165°C. In order to identify these species, a matrix isolation study has also been carried out. The present paper mainly describes the absorption spectra, the assignment and the kinetic behavior of species which may be responsible for radiation-induced cationic polymerization, especially for the initiation processes.

Experimental

All chemicals were obtained from Tokyo Kasei. n-Butyl chloride (BuCl) and styrene (St) were distilled and dried with $CaSO_4$ and CaH_2, respectively.

Isopentane (iP) and 3-methylpentane were passed through a silica gel column and dried with CaH_2. The purified chemicals were stored in vacuo, and dried fur-

ther with silica gel baked at 250°C for a few hours before the distillation into irradiation cells. 1,2-Dihydronaphthalene was used without further purification.

The pulse radiolysis apparatus and experimental procedures were essentially the same as described in the previous paper /9/. The energy of electron pulses from a Van de Graaff accelerator was 2.7 MeV, and the pulse duration was 1 μsec. Samples were cooled by blowing cold nitrogen gas, and the temperature of samples was monitored with a thermocouple attached to the sample holder.

Results and discussion

The temperature must be lowered below −160°C in order to measure absorptions of a styrene monomer cation radical by means of microsecond pulse radiolysis. A transparent liquid solution of styrene is obtained in a mixture of isopentane and n-butyl chloride (4:1 in volume) at −165°C.

The absorption spectra obtained on the pulse radiolysis of a 0.15 M styrene solution at −165°C are shown in Fig. 1. The spectrum immediately after a 1 sec pulse is composed of five absorption bands, namely, A_1 in the near i.r. region M_1 at 630 nm, A_2 at 590 nm, B at 460 nm and C at 420 nm. Although there is another intense absorption band below 380 nm, it is not shown in Fig. 1. It is difficult to obtain precise spectra in this region because the transmission of analysing light is reduced.

Monomer Cation Radical. The absorption maximum of M_1 is in good agreement with that of the monomer cation radical ($St^{+}\cdot$) observed in a γ-irradiated glassy solution at −196°C by Shida and Hamill /7/. The decay of M_1 is more rapid than that of any other band. Moreover, the pulse radiolysis of a dilute (0.02 M) styrene solution gave rise to the same spectrum as that of $St^{+}\cdot$. These facts lead to the conclusion that M_1 is due to $St^{+}\cdot$.

Associated Dimer Cation Radical. In order to identify absorption bands other than M_1, glassy solutions of 0.1 M styrene and 0.05 M 1,2-dihydronaphthalene in a mixture of 3-methylpentane and n-butyl chloride (4:1) were irradiated with ^{60}Co γ-rays (3×10^{18} eV g^{-1} min^{-1}) at −196°C. The absorption spectra are shown in Fig. 2. The spectra (1) were obtained from the samples irradiated at −196°C. The spectra (2) were measured at −196°C after the samples were slightly warmed in the air, and the spectra (3) after further warming. These glassy solutions scarcely cracked when warmed. In Fig. 2a, another band of $St^{+}\cdot$ is seen at 350 nm (M_2), and the broad-band around 1600 nm is the same as A_1 in Fig. 1 where only a part of A_1 below 1000 nm is shown because of an upper limit of the detector. The bands, M_1, A_1, A_2 and B, appear in both Fig. 1 and Fig. 2a, but C appears only in Fig. 1.

1,2-Dihydronaphthalene has a similar structure to that of styrene, but the cationic polymerizability is small because of the steric hindrance /10/. In Fig. 2b, the monomer cation radical is considered to have its absorption bands at 593 and 403 nm (M_1' and M_2'), which correspond to M_1 and M_2 in styrene, respectively. Upon warm-

ing the glass these two bands disappear, and new bands appear instead at 1350, 575 and 405 nm (A'_1. A'_2 and A'_3). The new bands are ascribed to a single species judging from the similarity between their decays, as is shown in the spectra /2/ and /3/.

Badger and Brocklehurst /11/ reported that an associated dimer cation radical of aromatic compounds has an intermolecular charge-resonance band in the near i. r. region and a band in the vicinity of each band of the monomer cation radical. Therefore, the bands, A'_1, A'_2 and A'_3, are reasonably ascribed to an associated dimer cation radical of 1, 2-dihydronaphthalene. In Fig. 2a, the bands, A_1 and A_2, seem to correspond to A'_1 and A'_2, respectively, and consequently are due to an associated dimer cation radical of styrene ($St_2^{+\cdot}$).

Bonded Dimer Cation Radical and other species. In Fig. 1, the band B grows parallel with the decay of $St^{+\cdot}$. This behaviour suggests that B is also due to a cationic dimer species which is formed by the reaction of $St^{+\cdot}$ with St. The behaviour of B, however, differs from that of $St_2^{+\cdot}$ under some experimental conditions. For instance, the pulse radiolysis of a 0. 004 M styrene solution in a mixture of 1, 1--dichloroethane and n-butyl chloride (1:1) at $-155^{\circ}C$ gave rise to a spectrum composed of the intense band, B, and the very weak bands of $St_2^{+\cdot}$. Furthermore, the band corresponding to B does not appear in 1, 2-dihydronaphthalene. These facts indicate that B is due to a species different from $St_2^{+\cdot}$, though both of them are cationic dimer species. The band B is considered to be a species responsible for polymerization, i. e. , a kind of initiating species, because it does not appear in 1, 2--dihydronaphthalene. The band B, therefore, may be ascribed to a bonded dimer cation radical ($\cdot St-St^+$), which initiates propagation reactions by reacting with styrene.

The band B is considered to disappear mainly by the reaction with styrene when the concentration of styrene is high enough for the propagation reactions. The broad band around 460 nm in the spectrum at 160 μsec after pulse in Fig. 1 may be due largely to another species than $\cdot St-St^+$. The bottom curve in Fig. 1 shows the spectrum observed at 50 μsec after pulse on the pulse radiolysis of a 0. 3 M styrene solution in the iP-BuCl mixture at $-150^{\circ}C$. The spectrum decayed slowly without changing its shape, though A_2, B and C disapeared within about 12 μsec after pulse. The spectrum seems to be composed of three absorption bands, namely, P_1 around 540 nm, P_2 around 450 nm and P_3 in the u. v. region. The fact that traces of polymer were really obtained in this case leads to the possibility that the main parts of the spectrum are attributable to a growing polymer carbonium ion ($\sim\sim\sim St-St^+$).

The band C in Fig. 1 was observed only by pulse radiolysis. Only C was scavenged when 0. 05 M methanol (: scavenger of carbonium ions) was added to a 0. 03 M styrene solution at $-165^{\circ}C$. From these facts, the band C is tentatively assigned to an α-methyl benzyl carbonium ion, i. e. , the monomer carbonium ion (StH^+), which may be formed by proton transfer from a solvent cation radical to styrene.

Behaviour of Transient Species. At least five cationic species were observed in the low-temperature pulse radiolysis. The solid curves in Fig. 3 show the observed change in the optical density at each peak with time. The curves, except the curve

at 980 nm, do not necessarily represent the kinetic behaviour of each species because of the overlap of bands. Only St_2^+ actually absorbs at 980 nm. The large amount of St_2^+ at the end of pulse and the small increase after the pulse indicate that a large part of St_2^+ is formed almost within 1 μsec pulse, as is shown by the curve at 980 nm. The tendency was more remarkable at a higher concentration of styrene. At a lower concentration, the smaller amount of St_2^+ at the end of pulse and the increase corresponding to the decay at 630 nm were observed. These facts can be explained if we assume an auto-associated neutral dimer of styrene (St_2) which is in equilibrium with styrene under the present experimental conditions. The rapid formation of St_2^+ within 1μsec pulse is considered due to the positive charge transfer from a solvent cation radical to St_2, and the slow formation of St_2^+ is considered due to the reaction of St^+ with St.

In order to see the kinetic behaviour of species other than St_2^+, it is necessary to decompose the observed spectrum into its component bands at each time after pulse. This procedure is practicable using a computer simulation method, if the spectral shape of each species is available. The spectral shape of St^+ was measured in a γ-irradiated glassy solution of 0.05 M styrene in n-butyl chloride at -196^oC. The crude spectral shape of A_2 was obtained from the result of pulse radiolysis of 0.14 M styrene solution in an iP-BuCl (9:1) mixture at -165^oC, and modified further on the assumption of a Gaussian shape. The spectral shape of P_1 was used without modification because it includes neither M_1 nor A_2. The result for the spectra of 0.15 M styrene solution in Fig. 1 is shown by the broken curves in Fig. 3. The decay of St^+ corresponds to the growth of St_2^+ and $\cdot St-St^+$. The kinetic behaviour of a species at 590 nm agrees with that of St_2^+ at 980 nm. The agreement confirms the assignment that A_2 is also due to St_2^+. The broken curve at 540 nm shows that the species of P_1 grows parallel with the slow decay of St_2^+ and $\cdot St-St^+$.

On the basis of the above assignment and the kinetic behavior of each species, we propose the following reaction scheme for the radiation-induced cationic polymerization of styrene.

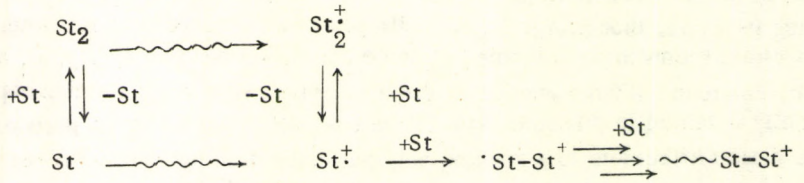

A solvent cation radical transfers its positive charge to St and St_2 to form St^+ and St_2^+, respectively. The reaction of St^+ with St forms St_2^+ and $\cdot St-St^+$ concurrently. The dissociation of St_2^+ produces St^+, which reacts with St to form St_2^+ or $\cdot St-St^+$. The propagation reactions are initiated by the reaction of $\cdot St-St^+$ with St.

The monomer carbonium ion, StH^+, to which the band C may correspond, also initiates propagation reactions.

References

/1/ K. Ueno, K. Hayashi and S. Okamura, Polymer, 4, 431 (1966).

/2/ R. C. Potter and D. J. Metz, J. Polymer Sci., A-1, 9, 441 (1971).

/3/ S. Okamura, T. Higashimura and S. Futami, Isotopes & Rad., 1, 216 (1958).

/4/ A. Shapiro and V. Stannet, J. Chem. Phys., 56, 830 (1959).

/5/ C. S. H. Chen and R. F. Stamm, J. Polymer Sci., 58, 369 (1962).

/6/ H. Yoshida, M. Noda and M. Irie, Polymer J., 2, 359 (1971).

/7/ T. Shida and W. H. Hamill, J. Chem. Phys., 44, 4372 (1966).

/8/ M. Irie, H. Masuhara, K. Hayashi and N. Mataga, J. Phys. Chem., 78, 341 (1974).

/9/ S. Arai, A. Kira and M. Imamura, J. Chem. Phys., 54, 5073 (1971).

/10/ A. Mizote, T. Tanaka, T. Higashimura and S. Okamura, J. Polymer Sci., A-1, 4, 869 (1966).

/11/ B. Badger and B. Brocklehurst, Trans. Faraday Soc., 65, 252 (1969).

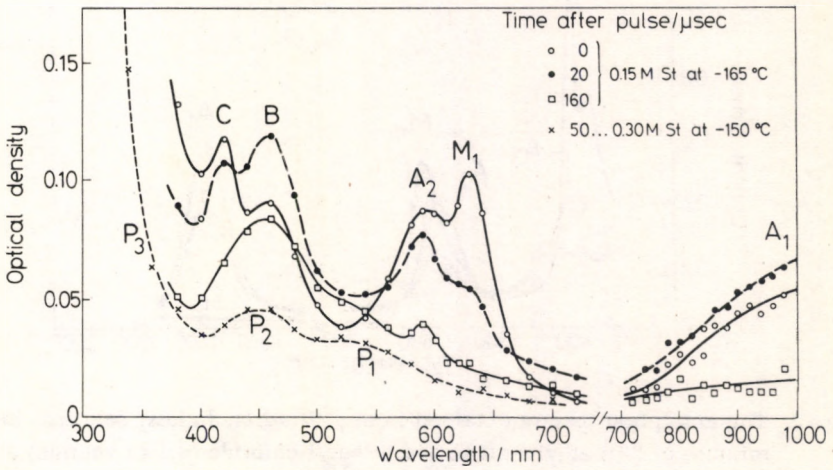

Fig. 1. The absorption spectra obtained on the pulse radiolysis of styrene solutions in a mixture of isopentane and n-butyl chloride (4:1 in volume)

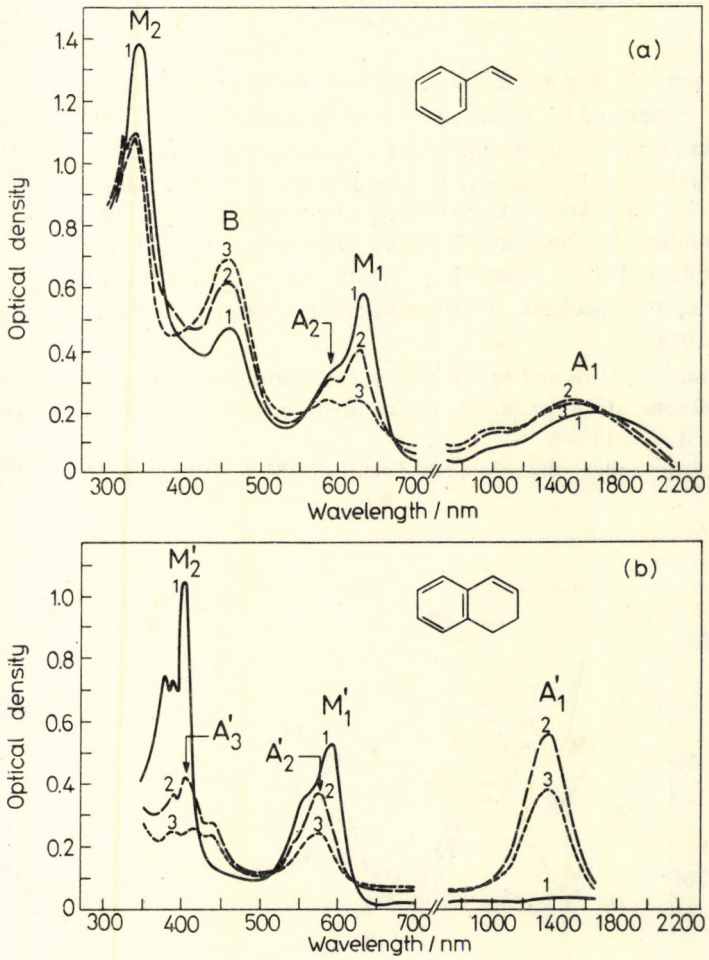

Fig. 2. The absorption spectra obtained from γ-irradiated glassy solutions in a mixture of 3-methylpentane and n-butyl chloride (4:1 in volume) at -196°C. (a) 0.1 M styrene, 4.5×10^{19} eV g^{-1}. (b) 0.05 M 1,2-dihydronaphthalene, 3×10^{19} eV g^{-1}. (1) after γ-irradiation, (2) after slight warming, (3) after further warming

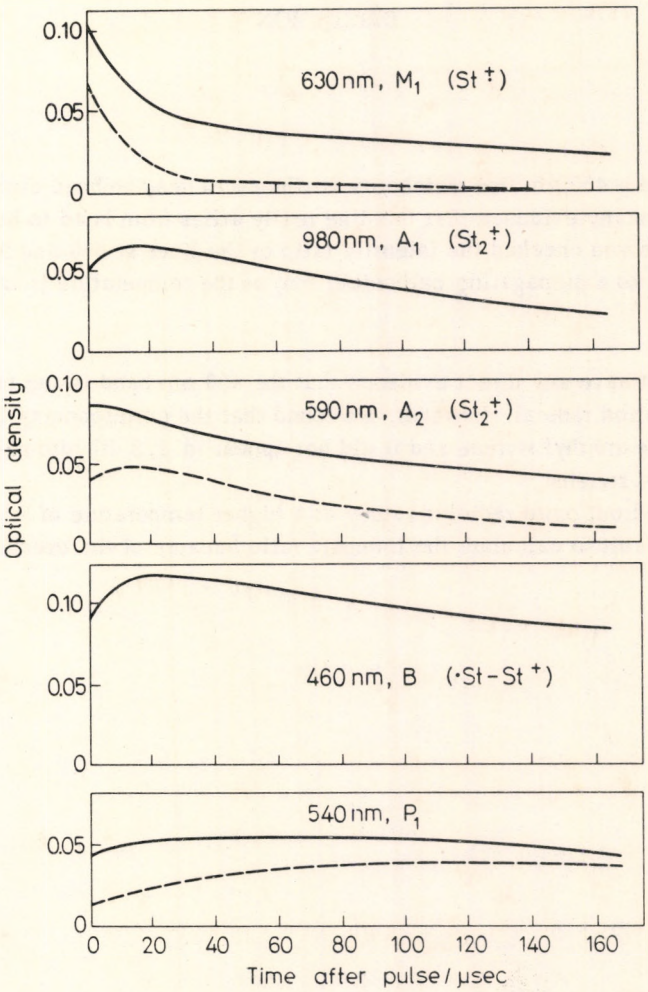

Fig. 3 The solid curves show the observed change in the optical density at wavelengths of the characteristic bands with time. The broken curves show the kinetic behaviour of each species obtained by decomposing the observed spectra (see text)

J. MENCZEL

You found a 450 nm line which you attributed to head to head dimer cation radicals. Have you any evidence that this line really arises from head to head cation radicals? Have you checked the intensity ratio of the lines at 450 and 340 nm (which you attributed to a propagating carbonium ion) as the temperature is raised?

Sh. EGUSA

We do not have any direct evidence that the 450 nm band is due to the head to head dimer cation radical. However, we found that the corresponding band appeared at 480 nm in α-methyl styrene and it did not appear in 1, 2 dihydro naphthalene and trans β-methyl styrene.

We carried out pulse radiolysis study at a higher temperature of $-155^{\circ}C$. It is, however, difficult to calculate the intensity ratio because of the overlap of the bands.

CATIONIC POLYMERIZATION OF N-VINYLCARBAZOLE BY MEANS OF PULSE RADIOLYSIS

Akira Sugawara, Seiichi Tagawa, Yoneho Tabata *
Nuclear Engineering Research Laboratory, University of Tokyo, Tokai, Ibaraki, Japan

Introduction

It is well known that N-vinylcarbazole can be polymerized via radical or ionic mechanism, depending on the polymerization condition.

Formation of the cyclodimer of N-vinylcarbazole (trans-1, 2-dicarbazylcyclobutane) /1/ was reported by Ellinger /2/, and Breitenbach et al. /3/, independently. It has been now made clear that the cyclodimer of N-vinylcarbazole can be produced by various methods, such as thermal (metal catalyzed) /4/, electrochemical /3, 5/, photochemical /6, 7/ and radiation-induced reactions /8–10/, resulting in the formation of an N-vinylcarbazole cation radical in the presence of excess N-vinylcarbazole in certain aerated solvent conditions.

Both polymerization and cyclodimerization proceed via the cation radical, and they are greatly influenced by oxygen and solvents /11, 12/. Direct observation of the formation of vinylcarbazole cation radical was carried out independently by using pulse radiolysis, /8–10/ laser photolysis /13/, and flash photolysis /14, 15/. These effects on the polymerization and dimerization have been recently investigated in our laboratory. These results are summarized in Table 1.

The mechanism of the chain reaction, the solvent and oxygen effects have been investigated by several authors through product analysis /11, 16, 17/ and both product analysis and pulse radiolysis /10/. However, the true picture is difficult to obtain from those studies because of a lack of the direct observation and information as to the initiating and propagating species. The pulse radiolysis technique is known to be very effective and powerful for the study of the early stage of radiation-induced reaction. However, few attempts /8, 9, 10, 18/ have been made using the pulse radiolysis technique for studying behaviour of reactive intermediates involved in radiation-induced polymerization.

To make clear the role of solvent and oxygen in the polymerization, mixtures of two different solvents were used as the polymerizing media. It has been reported in our previous paper /10/ that benzonitrile and nitrobenzene behave in different ways in the dimerization and polymerization as the solvent. That is, the dimeriza-

* To whom correspondence should be addressed.

Table 1

Solvent and oxygen effects on final products /10/

	Product			
	Aerated		Deaerated	
	DMA		DMA	
ϕCN	D	x	P	x
Acetone	D	x	P	x
Methylethylketone	D	x	P	x
Diethylketone	D	x	P	x
Acetophenone	D	x	P	x
ϕNO_2	P	x	P	x
Benzene	P	x	P	x
Tetralin	P	x	P	x
Toluene	P	x	P	x

Table 2

Solvent and oxygen effects on radiation-induced reactive intermediates and final products /10/

Solvents	Deaerated	Aerated
Nitrobenzene	ϕNO_2^-, M^+, P^+, P	ϕNO_2^-, M^+, P^+, P
Benzonitrile	ϕCN^-, M^+, (P^+), P	$O_2^-(?)$, M^+, D^+, D

M^+: monomer cation of vinylcarbazole
D^+: dimer cation
D: cyclodimer
P^+: propagating cation
P: polymer

tion occurs in aerated benzonitrile, while polymerization in aerated and deaerated nitrobenzene. In our present experiments, both the solvent and oxygen effects on the transient spectra as well as the final products are clearly shown to be significant in the radiation-induced reactions.

Both the direct observation of the reactive intermediates and the product analysis in the same solutions are considered to be necessary to elucidate the detailed mechanism of complicated reactions such as dimerization and polymerization. The reactive intermediates and final products in irradiated benzonitrile and nitrobenzene are summarized in Table 2 /10/.

Experimental

Materials

N-Vinylcarbazole was recrystallized six times: three times from n-hexane and then three times from methanol solutions. Benzonitrile and nitrobenzene from Wako were fractionally distilled in an atmosphere of nitrogen. Further purification of DPPH and triethylamine as scavengers was not carried out.

Pulse radiolysis system

The n-second pulse radiolysis system has been described elsewhere /19/. Only an outline of the equipment relevant to this work is presented here. The schematic representation of an experimental setup of this system which is being used at Nuclear Engineering Research Laboratory is shown in Fig. 1. An electron beam of about 1.6 MeV from a Febetron 707 was used throughout. The duration of pulse was 50 nsec. Light from a Ushio 150-W xenon lamp was focussed through the cell by a Suprasil quartz lens system. Grating monochromator, photomultiplier, and amplifier were placed behind blocks of lead for their protection against radiation. Rectangular irradiation cells made of Suprasil were used. Internal light path length was 1 cm. Time resolution of the system was less than 20 nsec by using 10 nsec optical pulse.

Measurement of the molecular weight distribution

The distribution of the molecular weight was measured by using a high-speed liquid chromatograph with the column of GPC.

Results and Discussion

Measurement of the reactive Intermediates

Initial yield of vinylcarbazole cation radical. The spectrum of vinylcarbazole cation radical measured by using the pulse radiolysis technique is shown in Fig. 2. Figure 3 shows the initial yield of vinylcarbazole cation radical measured at 620 nm as a function of volume % of nitrobenzene in the binary mixtures with benzonitrile. The initial yield decreases with increasing the volume % of benzonitrile. The initial yield in nitrobenzene solution is about three times greater than that in benzonitrile solution. The lifetime of the vinylcarbazole cation radical does not change irrespective of the change of volume ratio of solvents.

Initial yield of nitrobenzene anion radical. Figure 4 shows the absorption spectra in the shorter wavelength region observed in aerated nitrobenzene solution of 20 mM vinylcarbazole, in pure aerated nitrobenzene solution, and in aerated benzonitrile solution of 20 mM vinylcarbazole at 2 μsec after pulses. The absorption peak observed around 440 nm is similar to the spectrum of nitrobenzene anion

radical observed in glassy state at 77 K, except for small shift to a shorter wavelength. Therefore, the band is ascribed to nitrobenzene anion radical.

Figure 5 shows the initial yield of nitrobenzene anion radical observed at 450 nm as a function of volume % of nitrobenzene in the binary mixtures with benzonitrile. Fig. 5a and 5b show the initial yields of nitrobenzene anion radical in the binary mixtures with and without vinylcarbazole, respectively. Although the absorption of benzonitrile anion was observed in deaerated benzonitrile solutions, it was not observed in aerated benzonitrile solution. Therefore, an anion radical of oxygen molecule is considered to be the main negative species in aerated benzonitrile solutions. These anion formations can be explained by competitive electron capture among oxygen, nitrobenzene and benzonitrile.

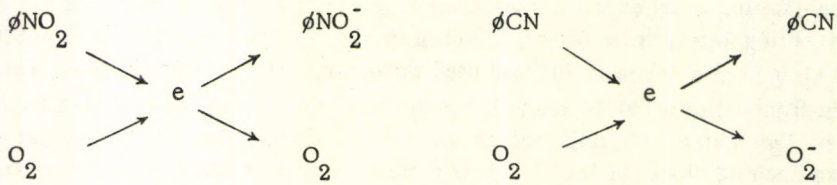

The absorption was not observed for 100 volume % benzonitrile solution in Fig. 5b, but was just apparent in Fig. 5a in the presence of monomers. The long-lived species, except for anion radicals of nitrobenzene and benzonitrile, is considered to exist. But this absorption is negligibly small compared with the initial yield of nitrobenzene anion.

The yields of monomer cation in Fig. 3 and those of solvent anion in Fig. 5 have a very similar dependence on the concentration of nitrobenzene in the binary mixtures above about 5 volume % nitrobenzene. However, no nitrobenzene anion radical was observed at higher concentration of benzonitrile above about 95 volume %. In this region, the anion radical of oxygen molecule should exist as the gegen ion of vinylcarbazole cation radical.

Product analysis

Figure 6 shows the yield of the final products produced in irradiated monomer solution in air as a function of volume % of nitrobenzene. The cyclodimer was only obtained at higher concentrations of benzonitrile above about 95 volume %, while polymer was obtained below the 95 volume % of benzonitrile.

It is interesting to note that in the concentration region of benzonitrile above 95 volume %, the cyclodimer is produced, and the O_2^- ion is formed in the same concentration region. From these experimental facts, the anion radical of oxygen molecule is considered to play an important role in the formation of the cyclodimer.

Figure 7 shows the yields of final products both in the presence and in the absence of air as a function of volume % of nitrobenzene. The yields of the polymer

decreases with decreasing volume % of nitrobenzene. A minimum in the yield was observed around 3−6 volume % of ϕNO_2 both in the presence and in the absence of air. After the minimum, the yield of the cyclodimer increases rapidly with decreasing volume % of nitrobenzene in the presence of air and the polymer yield increases in the absence of air. Attention should be drawn to the facts that there is a minimum of the yield in deaerated solutions and that the yield of polymer is greater in aerated solutions than in deaerated ones. Figure 8 shows the molecular weight and the degree of dispersion of polymers calculated from the measured distribution of molecular weight as a function of volume % of nitrobenzene in the binary mixtures. The molecular weight of the polymer is smaller in aerated solutions than in deaerated solutions. The molecular weight decreases with decreasing volume % of nitrobenzene both in aerated and deaerated solutions.

Effect of chemical inhibitors

The scavenger effects are shown in Table 3.

Table 3
Effects of inhibitors on dimerization and polymerization

Inhibitor / Solvent	DPPH	Triethylamine, Dimethylaniline Aniline
ϕNO_2	not inhibited (Polymerization)	inhibited (Polymerization)
ϕCN	inhibited (Cyclodimerization)	inhibited (Cyclodimerization)

Effect of oxygen on the polymerization

As is mentioned above, it is strongly suggested that oxygen plays a very important role in the cyclodimerization of vinylcarbazole as a negative ion O_2^-. The scheme of the ionic chain cyclization reaction of vinylcarbazole is proposed as follows

$$S \longrightarrow S^{+\cdot} + e$$

$$S^{+\cdot} + M \longrightarrow S + M^{+\cdot}$$

$$O_2 + e \longrightarrow O_2^-$$

$$M^{+\cdot} + O_2^- \longrightarrow [M^{+\cdot} \cdots O_2^-]$$

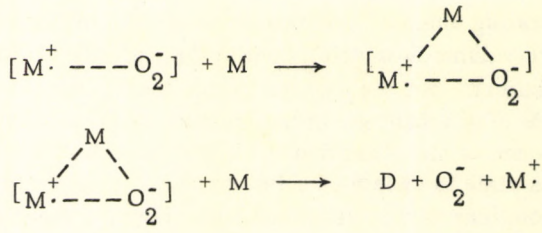

where S is a solvent molecule.

The yield of the polymer is greater in aerated solutions than in deaerated solutions. However, the molecular weight of the polymer is smaller in aerated solutions than in deaerated solutions as mentioned above. Therefore it is indicated that molecular oxygen promotes the chain transfer reaction in the higher concentration region of nitrobenzene. Molecular oxygen may act as a chain transfer agent, as is expressed by following scheme.

Propagation:

$$M_n^+ + M \longrightarrow M_{n+1}^+$$

Chain transfer:

$$M_n^+ + O_2 \longrightarrow [M_n^+ - - - O_2]$$

$$[M_n^+ - - - O_2] + M \longrightarrow [M_n - - O_2 - - M]^+$$

$$[M_n - - O_2 - - M]^+ \longrightarrow M_n + [O_2 - - M^+]$$

$$[O_2 - - M^+] \longrightarrow O_2 + M^+$$

$$M^+ + M \longrightarrow M_2^+$$

Effect of oxygen on the polymer yield may be due to the retardation of the termination reaction by stabilization of gegen negative ions based upon the presence of molecular oxygen in the polymerizing media, though the lifetime of cationic species observed by using pulse radiolysis is not very different either in the presence or in the absence of air. In other words, the retardation of the termination reaction is considered to be due to the interaction between oxygen molecule and cationic species. The interactions of oxygen molecule and negative species with cationic species compete with each other. The steady state concentration of negative species depends on dose rates, whereas the concentration of oxygen molecules is constant irrespective of dose rates. Dose rates in the case of pulse radiolysis are very high compared with γ-irradiation in the case of product analysis. As the result, the

oxygen effect on the polymer yield is expected to be greater at lower dose rates. Therefore, the effect of molecular oxygen on the polymerization can be explained without any contradiction between γ- and pulse experiments, even if the lifetime of cationic species observed by using pulse radiolysis is not different in the absence and presence of air.

Effect of solvent on the polymerization

In the higher concentration of benzonitrile above about 95 volume %, only the cyclodimerization occurs and the spectra of cationic species can be observed in the presence of air. The cyclodimerization is inhibited by both radical and cation scavengers. This suggests that for the cyclodimerization, two reactive sites in the linear bonded dimer cation radical – radical and cationic – are needed. Therefore, if either the radical site or the ionic site is scavenged, the cyclodimerization is considered to be completely inhibited.

On the other hand, the polymerization occurs in the absence of air. The polymerization is inhibited not only by radical scavengers, but also by cation scavengers.

These experimental results strongly indicate that the initiating species is the cation-radical and the propagation reaction takes place via a radical mechanism.

The sharp decrease in the product yield by the increase of nitrobenzene can be explained by strong action of nitrobenzene as an effective radical inhibitor.

In the higher concentration of nitrobenzene, only polymerization takes place both in absence and in presence of air and the polymerization is inhibited completely by cation scavengers, not by radical scavengers. As the growing polymer cation species can be detected spectrophotometrically by the pulse radiolysis method, it is quite certain that the polymerization takes place via cationic mechanism.

On the other hand, the initial yields of monomer cation radical and its lifetime depend a little upon the contents of nitrobenzene in the binary mixture above 5 volume % nitrobenzene. Therefore, the large dependence of the polymerization rate on the concentration of one component in the binary mixtures should be based upon the propagation process. This may be explained in terms of dielectric constant, solvation power of media and stabilizing tendency of cation species in the binary mixtures. They are depending on the relative concentration of both solvents.

Acknowledgment. The authors are grateful to Dr. K. Hamanoue, Kyoto Institute of Technology for his cooperation through this research. The authors wish to express their sincere thanks to Dr. S. Machi and Mr. T. Watanabe of JAERI in Takasaki for their help in measuring the distribution of molecular weight.

References

/ 1/ L. P. Ellinger, J. Feeney, and A. Ledwith, Monatsh. Chem., 96, 131 (1965).

/ 2/ L. P. Ellinger, Chem. Ind. (London), 1982 (1963), Polymer, 5, 559 (1964).

/ 3/ J. W. Breitenbach, O. F. Olaj, and F. Wehrmann, Monatsh. Chem., 95, 1007 (1964).

/ 4/ F. A. Bell, R. A. Crellin, H. Fujii, and A. Ledwith, Chem. Commun., 251 (1969).

/ 5/ D. H. Davies, D. C. Phillips, and J. D. B. Smith, J. Org. Chem., 38, 2562 (1973).

/ 6/ R. A. Carruthers, R. A. Crellin, and A. Ledwith, Chem. Commun., 252 (1969).

/ 7/ J. W. Breitenbach, F. Sommer, and G. Unger, Monatsh Chem, 101, 32 (1970).

/ 8/ S. Tagawa, S. Arai, A. Kira, M. Imamura, Y. Tabata, and K. Oshima J. Polym. Sci. B10, 295 (1972).

/ 9/ S. Tagawa, S. Arai, M. Imamura, Y. Tabata, and K. Oshima, Macromolecules, 7, 262 (1974).

/10/ S. Tagawa, Y. Tabata, S. Arai, and M. Imamura, J. Polym. Sci. B12, 545 (1974).

/11/ K. Tada, Y. Shirota, and H. Mikawa, J. Polym. Sci., Chem. Ed. 11, 2961 (1973).

/12/ H. F. Kaufman, J. W. Breitenbach, and O. F. Olaj, J. Polym. Sci., Polym. Chem. Ed., 11, 737 (1973).

/13/ Y. Taniguchi, Y. Nishina, and N. Mataga, Bull. Chem. Soc. Jap., 46, 1646 (1973).

/14/ Y. Shirota, K. Kawai, N. Yamamoto, K. Tada, T. Shida, H. Mikawa, and H. Tsubomura, Bull. Chem. Soc. Jap., 45, 2683 (1973).

/15/ M. Yamamoto, K. Kitagawa, S. Nishimoto, and Y. Nishijima, Chem. Lett., 745 (1973).

/16/ K. Tada, Y. Shirota, and H. Mikawa, Macromolecules, 6, 9 (1973).

/17/ A. Ledwith, Accounts Chem. Res. 5, 133 (1972).

/18/ M. Katayama, M. Hatada, K. Hirota, Y. Yamazaki, and Y. Ozawa, Bull. Chem. Soc. Jap., 38, 851 (1965), C. Schneider, A. J. Swallow, Makromol. Chem., 114, 155 (1968), J. Polym. Sci. B4, 277 (1966), C. Schneider, Adv. Chem. Series. (Am. Chem. Soc., Washington) 91, 219 (1969). R. C. Potter, and D. J. Metz, J. Polym. Sci., A−1, 9, 441 (1971). H. Yoshida, M. Noda, and M. Irie, Polymer J. 2, 359, (1971), Sangster, Discussion Meeting on Radiation Chemistry, 1974 Argonne N. L.

/19/ S. Tagawa, A. Sugawara, Y. Tabata, S. Takada, and T. Ueda, Symp. Radiation Chem., Oct. 1975. Tokyo.

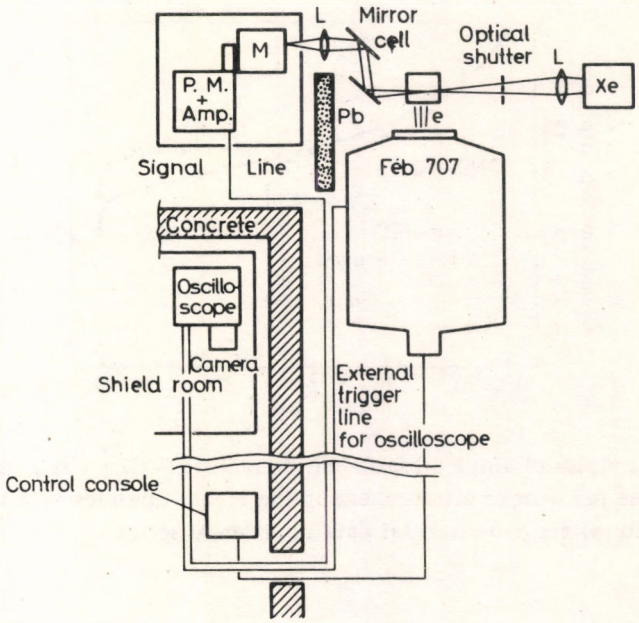

Fig. 1 Schematic representation of an experimental setup of nsec pulse radiolysis system used at Nuclear Engineering Research Laboratory in Tokai. Febetron 707 is used as the pulse generator

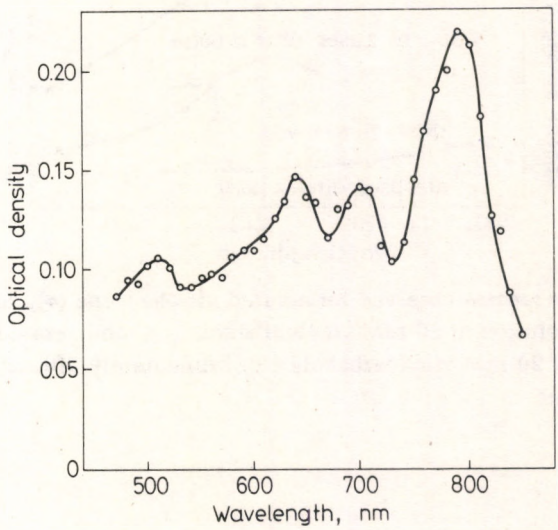

Fig. 2 Absorption spectrum observed for aerated benzonitrile solution of 3 mM vinylcarbazole immediately after a pulse at room temperature

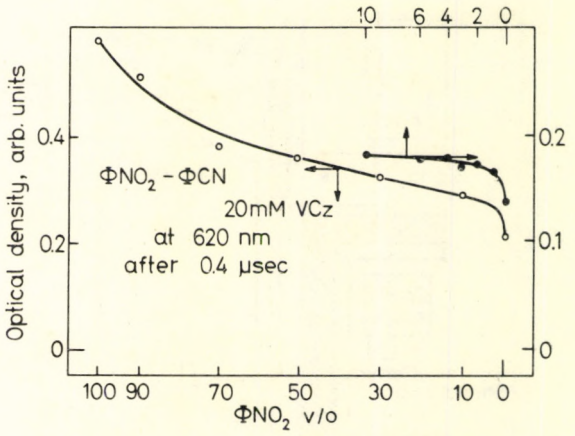

Fig. 3 Initial yields of vinylcarbazole cation radical ($VCZ^{+\cdot}$) as a function of volume per cent of nitrobenzene in the binary mixtures with benzonitrile. (o) and (•) are experimental data in different series

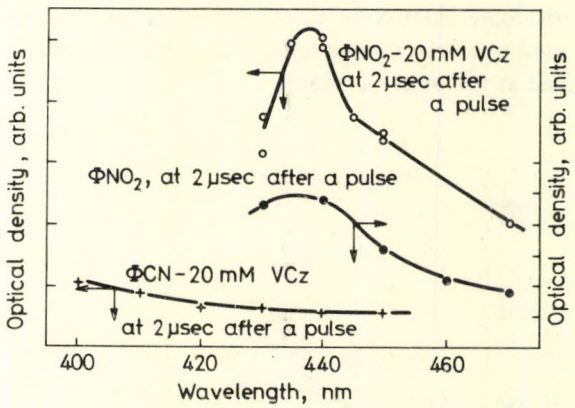

Fig. 4 Absorption spectra observed for aerated nitrobenzene (•), aerated nitrobenzene solution of 20 mM vinylcarbazole (o), and aerated benzonitrile solution of 20 mM vinylcarbazole (+) immediately after a pulse at room temperature

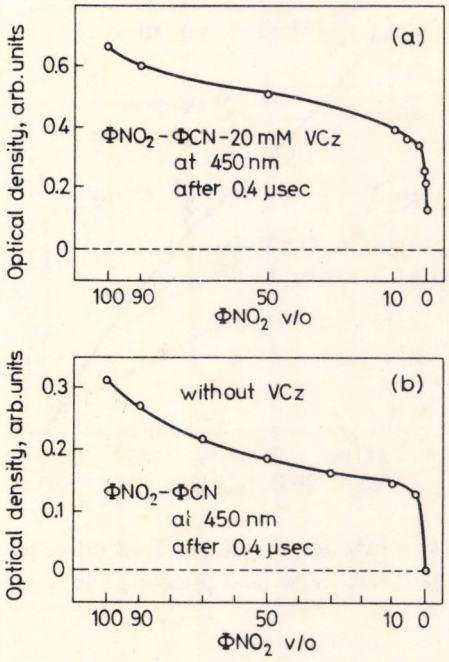

Fig. 5 Initial yields of ϕNO_2^- as a function of nitrobenzene volume % in the binary mixtures with benzonitrile in presence (a) and absence (b) of vinylcarbazole

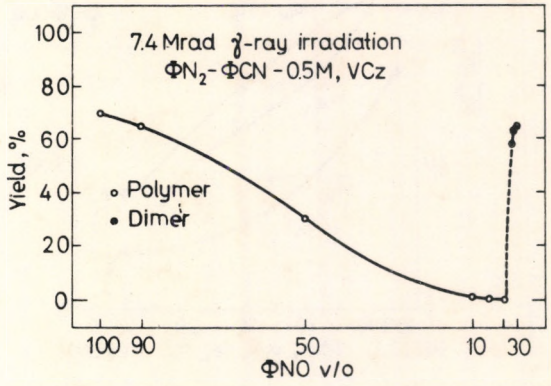

Fig. 6 Polymer and cyclodimer yields as a function of volume % of nitrobenzene in the binary mixtures with benzonitrile in presence of air

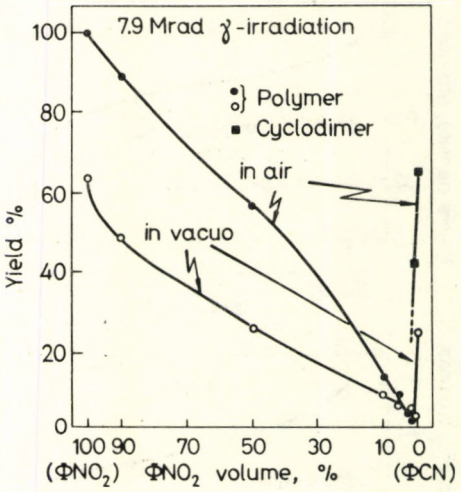

Fig. 7 Product yields as a function of volume % of nitrobenzene in the binary mixtures with benzonitrile in both presence and absence of air

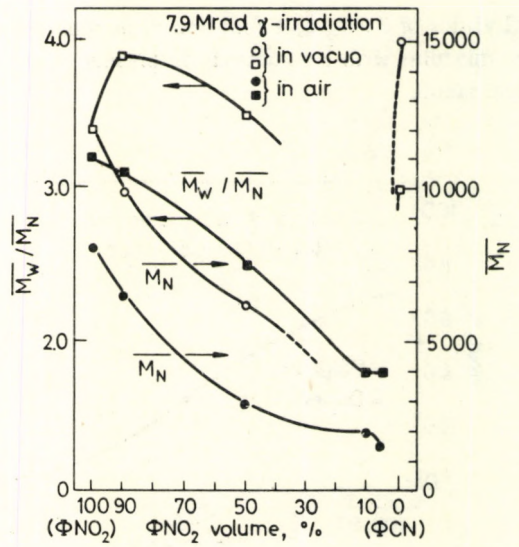

Fig. 8 Number average molecular weight ($\overline{M}_N$) and polydispersity ($\overline{M}_W/\overline{M}_N$) as a function of volume % of nitrobenzene in the binary mixtures with benzonitrile

J. ZURAKOWSKA-ORSZÁGH

In your paper you used the expression "aerated" and "deareated" product. Does it mean that a special aeration of the samples was carried out, or they were just irradiated in the presence of air?

Y. TABATA

We irradiated the samples under atmospheric pressure without water.

RADIATION INDUCED POLYMERISATION OF THE SYSTEM CYCLOHEXENE-N-ETHYLMALEIMIDE

H. Heusinger, E. Wipfelder, J. Heinzl, H. Zott
Institute for Radiation Chemistry, Technical University, Munich, FRG

The photolysis of donor-acceptor pairs has been investigated by several authors. Robson, Grubb and Barltrop (1) showed that in the unsensitized photolysis of the system cyclohexene – maleic anhydride, 1:1-cycloaddition and substitution take place.

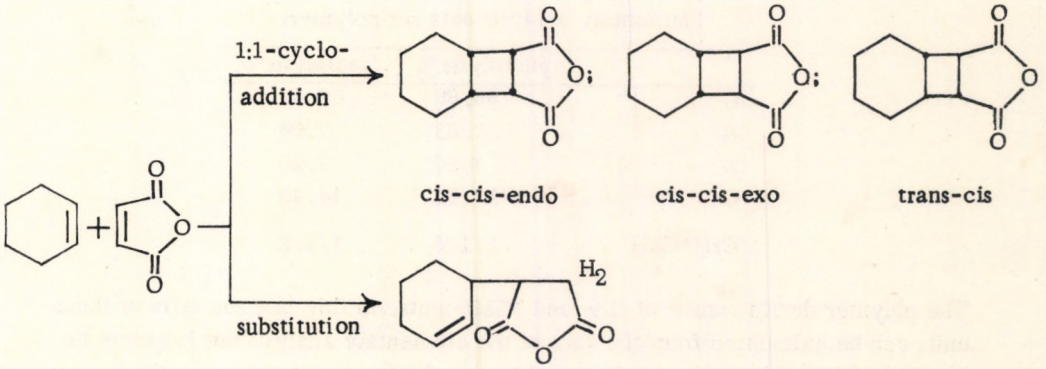

By selective excitation they established that an excited charge-transfer complex is the intermediate of this product formation. In the photolysis of the same system, sensitized by benzophenone, Schenck, Hartmann and Steinmetz /2/ obtained copolymers and only at low temperatures (-80°) was cycloaddition observed. Schuler, Thamm and Heusinger /3,4/ showed for the photolysis and radiolysis of the systems benzene--fumaric nitrile and benzene-di-chloro-maleic anhydride that cycloaddition, substitution and polymerisation reactions can take place. They observed analogies in the photo- and radiation-induced product formation.

In order to get more insight in the reactions of such donor-acceptor pairs we investigated the radiolytic and the photolytic product formation of the system cyclohexene-N-ethyl-maleimide (CH-NEMI). In photolysis the degassed samples (0.1 mole/l NEMI in CH) in glass ampoules were irradiated by a high pressure mercury lamp. Radiolysis was performed by ^{60}Co-γ-rays. In both cases the same products were observed, but in photolysis the 1:1-cycloaddition predominates whereas in radiolysis the polymerisation predominates.

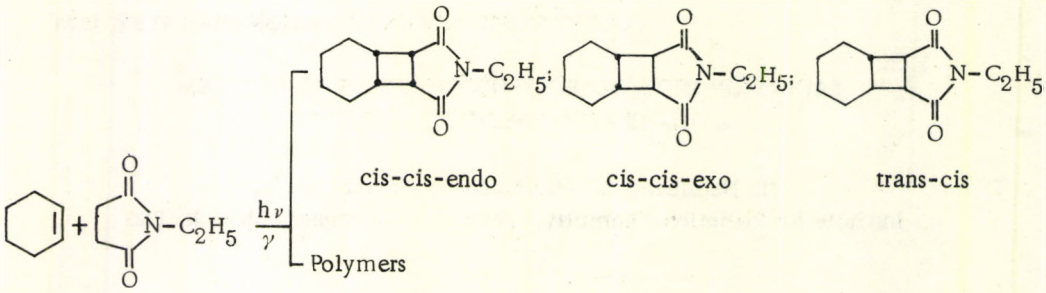

The conformations of the three isomeric structures of the cycloaddition products were determined by ^{1}H-NMR-spectroscopy and mass spectrometry. In this report we shall concentrate on the structure and the mechanism of polymer formation. The molecular weight M_n of the polymer obtained by photolysis and radiolysis is about 1000.

Table 1
Elementary analysis data for polymers

	photolysis %	radiolysis %
C	66.60	68.41
H	7.63	7.96
N	7.96	7.20
O	17.81	16.43
CH/NEMI	1/1.5	1/1.2

The polymer should consist of CH- and NEMI-units. In this case the ratio of these units can be calculated from the data of the elementary analysis but it cannot be decided if a copolymer or a mixture of homopolymers is present.

IR- and NMR-investigations

The IR- and NMR-spectra of the polymer obtained by photolysis and radiolysis are almost identical.

The IR-spectrum of the polymer (Fig. 1) shows no absorption bands of the original C=C-double bonds of the monomers CH and NEMI (CH stretch: 3062 cm^{-1}; 3020 cm^{-1}; $\nu_{C=C}$: 1650 cm^{-1}; $CH_{out\ of\ plane}$: δ = 715 cm^{-1}; δ = 696 cm^{-1}, C=O-band is moved from 1715 cm^{-1} in the monomer NEMI to 1695 cm^{-1} in the polymer due to elimination of the conjugation with C=C). The five-membered ring of NEMI is conserved in the polymer (C=O: 1770 cm^{-1}; 1695 cm^{-1}). These results show that polymerisation takes place via the C=C-double bonds of the monomers. This is supported by the ^{1}H-NMR and ^{13}C-NMR spectra (Fig. 2).

The existence of a minute amount of $-\overset{H}{\underset{|}{C}}=\overset{H}{\underset{|}{C}}-$ bonds is indicated by the band at $\delta = 6.03$ ppm. Due to polymerisation of the monomers via the C=C-double bonds two kinds of methin protons are observed (NEMI: $\delta = 3.55$, CH: $\delta = 2.87$). The large chemical shift of the methin proton of CH must be due to adjacent NEMI-groups, revealing that CH is incorporated in a copolymer. An evaluation of the band integrals (Photolysis: CH-protons: 6, NEMI-protons: 7, radiolysis: CH-protons: 8, NEMI-protons: 7) results in ratios of CH/NEMI in photolysis 1/1.6 and in radiolysis 1/1.25 which are in reasonable agreement with the results of the elementary analysis. The ratio of the band integrals of CH_2/CH_3 is found to be exactly 2:3. Evidently no reactions at the ethyl group takes place. The ^{13}C-NMR-spectra lead to the same conclusions. The fact that only one kind of CO-group ($\delta = 177.64$ ppm) is detected in C^{13}-NMR proves that polymerisation does not lead to a rupture of the NEMI-ring. This reaction was shown by Nakayama and Smets /5/, to occur in the anionic polymerisation of N-n-butyl-maleimide.

In order to distinguish between a mixture of homopolymers and copolymers the samples were analysed by liquid chromatography (LC), Fig. 3. Both the radiolytic and the photolytic polymer contains one main component and traces of a second one. The two components were collected and identified by mass spectrometry (Fig. 4).

The component present in small amounts comes out to be the homopolymer of NEMI. Its spectrum is characterized by peak groups which differ by $\frac{m}{e} = 125$, corresponding to NEMI units. The copolymer is characterized by masses $\frac{m}{e} = (n \cdot 82 + m \cdot 125)$ $(CH)_n(NEMI)_m$ with $n < m$ (CH:82, NEMI: 125). Spectra taken at reduced electron energy show that parent ions and fragment ions obtained by elimination of CH or NEMI units are responsible for the observed peaks. The existence of a copolymer is also evident from pyrolysis-GC-MS investigations of the polymer (homo-and copolymer not separated by LC). The dimeric fragments CH-NEMI and NEMI-NEMI were detected whereas CH-CH is not observed, revealing that no CH-homopolymer or CH-NEMI-copolymer with CH-diades is present.

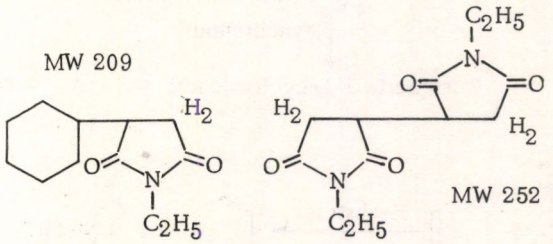

The homopolymer fraction was determined quantitatively using an authentical homopolymer as standard. The copolymer fraction was obtained subtracting the weight of the homopolymer from the weight of the original sample. It comes out that in

radiolysis as well as in photolysis the produced polymer consists of about 2% homopolymer and 98% copolymer. Correction of the values obtained by elementary analysis (Table 1) for homo-polymerisation results in a ratio $\left(\frac{CH}{NEMI}\right)_{h\nu} = 1{:}1.4$ and $\left(\frac{CH}{NEMI}\right)_{\gamma} = 1.15$ in the copolymer, corresponding to an alternating copolymer.

UV-absorption and NMR-spectroscopy give no evidence for the existence of a CT-complex between CH and NEMI. The influence of the type of irradiation on cycloaddition and polymerisation is shown in Table 2.

In solutions saturated with air the photolytic cycloadduct formation was found to be almost unchanged whereas polymerisation is fully suppressed.

The 1:1-cycloadduct formation has a maximum at a NEMI-concentration range of $4 \cdot 10^{-2}$ mole/l in photolysis and of 10^{-2} mole/l in radiolysis whereas the rate of polymerisation increases steadily with NEMI-concentration in both cases (Fig. 5).

The primary photolytic reaction is the selective excitation of the acceptor NEMI, shown in Eq. (III)

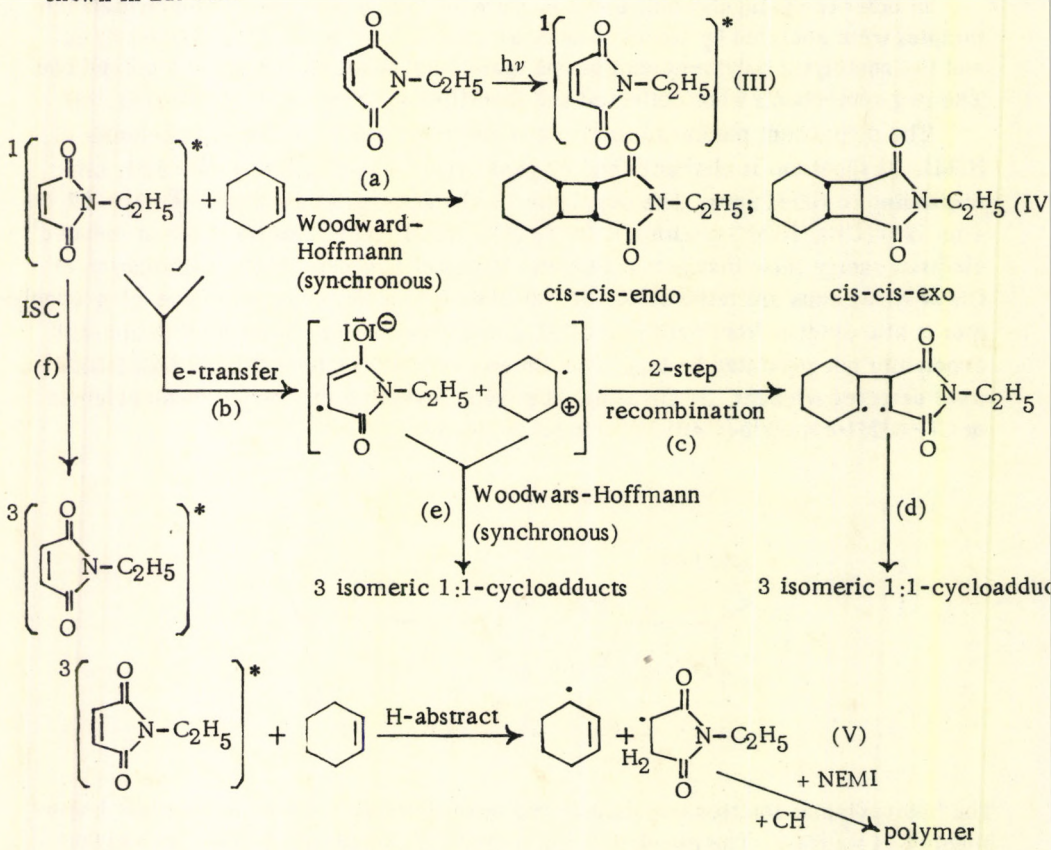

The excited singlet state of NEMI should be able to give with CH the two cis-cis-1:1-cycloadducts via a concerted Woodward-Hoffmann reaction (Eq. IVa). The formation of the trans-cis-cycloadduct could not occur via a concerted reaction. The fact, that all three cycloadducts show no O_2-influence, excludes this concerted cycloadditon. Because of the increased electron affinity of the singlet excited NEMI, compared with that of the NEMI ground state, electron transfer from CH to ^{1}(NEMI)* should be possible (Eq. IVb). A two-step mechanism, as proposed by

Table 2
Product balance, based on NEMI-consumption

photolysis	NEMI %	cycloaddition products %	polymer %
O_2-free	50	40	5
O_2-saturated	50	42	-
radiolysis	50	7	40

Robson et al. (1) in the system CH-MAH could explain the 1:1- cycloadduct formation (Eq. IVc-d). On the other hand, a concerted reaction starting from the radical-ion-pair (Eq. IVe), which can be allowed by the Woodward-Hoffmann selection rules, may result in the three isomeric 1:1-cycloadducts too.

Nakayama and Smets /5/ succeeded in polymerizing N-n-butyl-maleimide by anionic initiation. But the lack of formation of any anionic copolymer with MMA and AN shows that copolymerisation affords strong electrophilic double bonds. These results make an anionic copolymerisation mechanism between CH and NEMI rather unfavourable. Otherwise a cationic copolymerisation starting from the free cyclohexenyl-radical seems to be rather unreasonable too. Concerning the higher nucleophily and the much higher concentration of CH instead of NEMI, it may be assumed that cyclo-hexene-diades should be found in the copolymers. But neither mass spectrometry nor pyrolyse-GC-MS-coupling indicate those diades. In addition the results of elementary analysis, which show a minor or at most an equal content of CH compared with NEMI, contradicts a cationic copolymerisation mechanism. These observations show that different intermediates are included in the 1:1-cycloadduct and in the polymer-formation. The influence of O_2 on the polymer yield suggests that a triplet excited state of NEMI should be responsible for copolymerisation. In competition with the cycloaddition via the excited ^{1}(NEMI)* intersystem-crossing to the excited ^{3}(NEMI)* -triplet should be discussed (Eq. IVf). The attack of ^{3}(NEMI)* on a cyclohexene-molecule may result in a hydrogen-abstraction, which will induce the formation of an almost alternating CH-NEMI-copolymer without CH-diades (Eq. V). The absence of CH-diades in the copolymer shows that the endgroup of the propagating radical decides what kind of monomer will be added. A cyclohexenyl-endgroup only allows the NEMI-addition.

Comparing the photoexcitation of the system CH-NEMI with the radiation induced excitation the primary radiolytic reaction will be the ionization of the solvent CH.

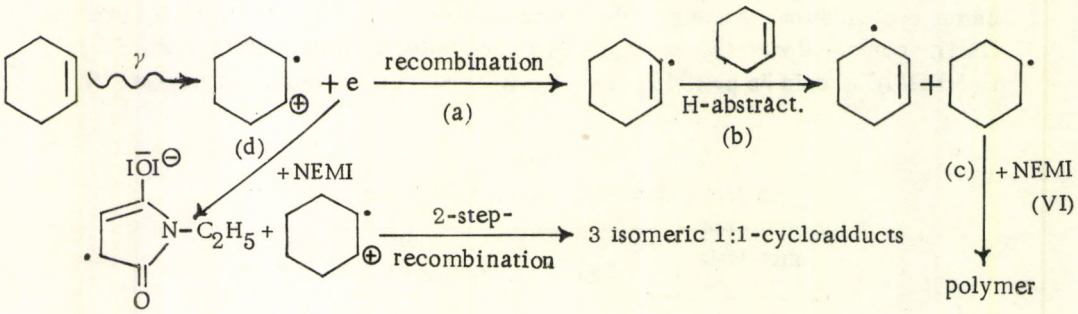

In competition with the very effective recombination of $(CH)^+$ and e^- (Eq. VIb), which will lead via reaction (Eq. VIc, d), analogously to the photolytic copolymerisation, to a radical copolymerisation of CH and NEMI, the electron scavenging character of NEMI results in the formation of $(NEMI)^-$ (Eq. VIe). The rather low stationary concentration of $(CH)^+$ and $(NEMI)^-$ makes a meeting of the two radical ions very unfafourable (Eq. VIf). It will be expected that in the γ-irradiated CH-NEMI-system the polymerisation dominates over the cycloaddition. The small amount of cycloaddition product and the high quantities of copolymers in the radiolysis of CH-NEMI confirm these assumptions. An additional point to support these statements is the lowering of cycloadduct formation if a strong electron acceptor like TCNE is added /6/.

References

/1/ R. Robson, P.W. Grubb, J.A. Barltrop, J. Chem. Soc. 2153 (1964).
/2/ G.O. Schenck, W. Hartmann, R. Steinmetz, Chem. Ber. 96, 498 (1963).
/3/ P. Schuler, Dissertation, Technische Universität München 1973. P. Schuler, H. Heusinger, Photochemistry and Photobiology, to be published.
/4/ H. Thamm, Dissertation, Technische Universität München 1975.
/5/ Y. Nakayama, G. Smets, J. Polym. Sci. A-1, Vol. 5, 1619–1633 (1967).
/6/ J. Heinzl, Diplomarbeit, Technische Universität München 1974.

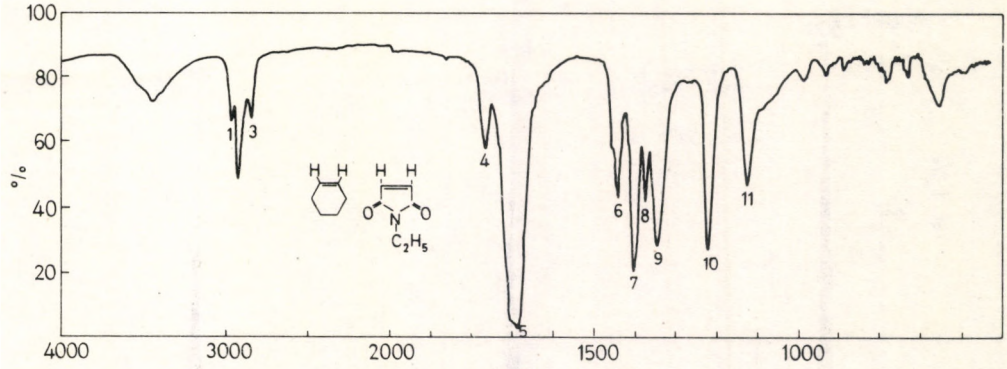

Fig. 1 IR spectrum of the polymer

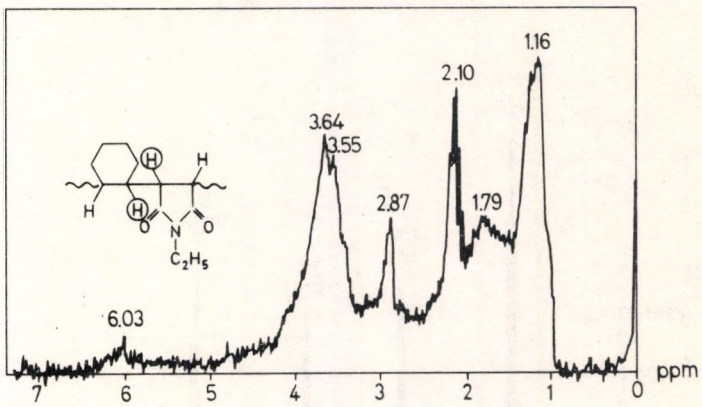

Fig. 2 ^{1}H NMR spectrum of the polymer

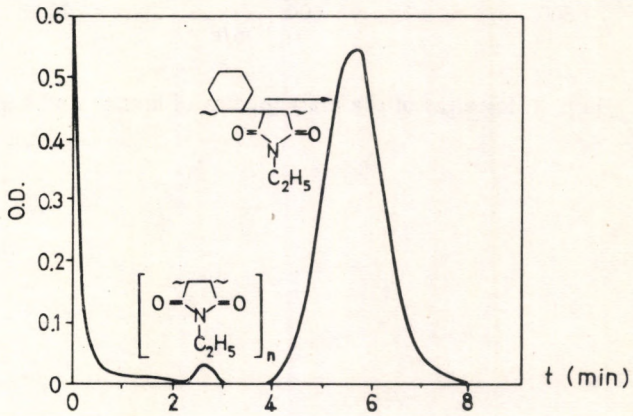

Fig. 3 LC spectrum of the polymer. Experimental: Column: ϕ_i = 4 mm; length: 50 cm; packing material: n-octyl parasil C; temperature: 25 ^{o}C; solvent: EtOH/ cyclohexane; flow: 0.6 ml/min, detection: UV 245 nm

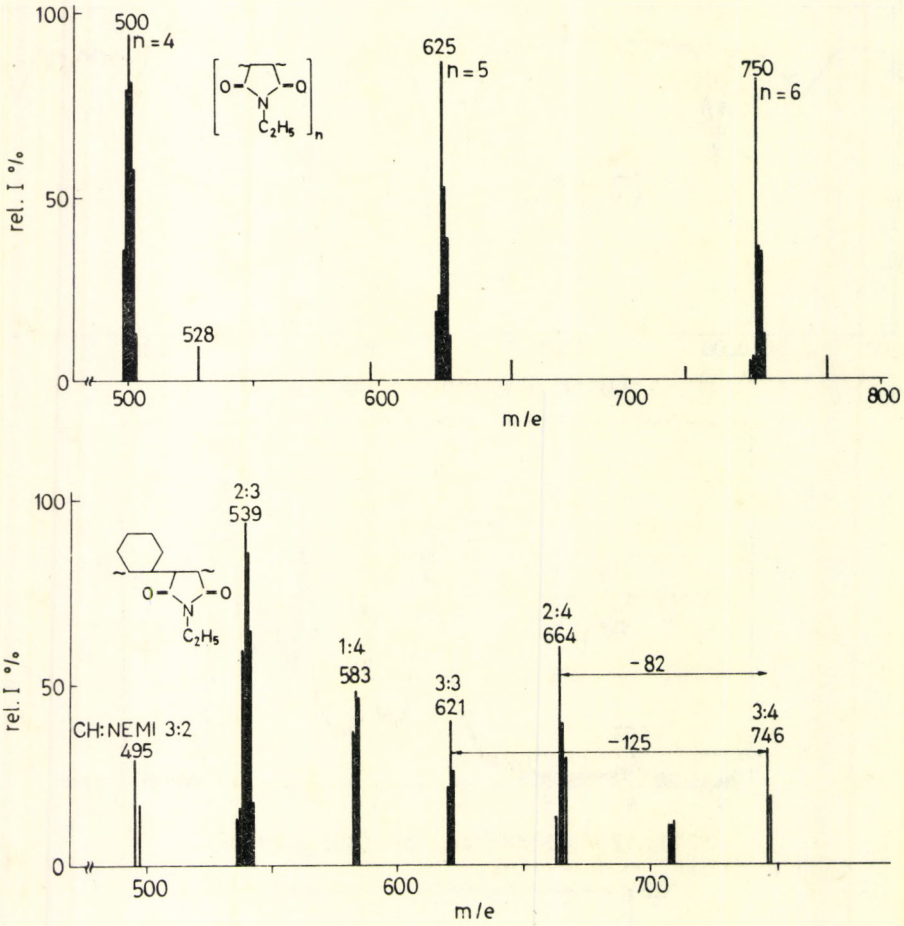

Fig. 4 Excerpts of the mass spectra of homo- and copolymer

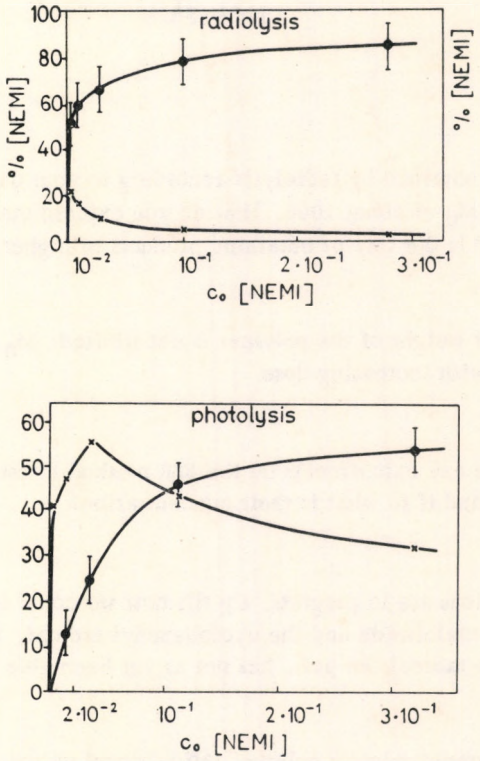

Fig. 5 Product formation dependent on c_o /NEMI/ ·
—— x —— NEMI consumption for 1:1 cycloaddition
—— ● —— NEMI consumption for polymerisation calculated from LC-data and product balance

V. IVANOV

The polymers obtained by radiolysis according to your data have number average molecular weights M_n of about 1000. How do you explain that the molecular weight is limited and what is the way of obtaining products of higher M_n?

E. WIPFELDER

The molecular weight of the polymer is not limited. M_n depends on the absorbed dose, it increases with increasing dose.

J. MENCZEL

Have you done any experiments by the ESR method to establish the existence of radical-ion pairs, and if so what is their concentration?

E. WIPFELDER

ESR investigations are in progress. Up till now we could identifity the propagating radical of N-ethyl maleimide and the cyclohexenyl radical. A spectrum, which can be attributed to the radical ion pair, has not as yet been able to be detected.

Ch. SCHNEIDER

How does the cycloadduct : polymer ratio depend on the temperature?

E. WIPFELDER

The formation of the cycloadducts increases with temperature. The ratio of cycloadduct : polymer was not determined as a function of the temperature.

RADIATION-INDUCED POLYMERIZATION OF β-NITROSTYRENE

Binh Dinh-Ngoc, Wolfram Schnabel
Hahn-Meitner-Institut für Kernforschung Berlin GmbH, Bereich Strahlenchemie, West Berlin

Introduction

Intense research work has been devoted during the past decade to the capability of ionizing radiation to induce the ionic polymerization of various monomers. It was found that monomers such as styrene and isobutylvinylether polymerize readily by a free cationic mechanism upon irradiation with γ-rays if they had been purified sufficiently beforehand /1-3/. Only relatively sparse information was obtained, however; so far on radiation-induced anionic polymerizations. Most of the relevant investigations were carried out with acrylonitrile or with nitroethylene.

Several authors reported that the copolymerization of acrylonitrile (AN) with styrene (St) in solution at -78°C proceeds by an anionic mechanism or that both an anionic mechanism and a radical mechanism coexist /4-7/. Recently /8/ it was reported that during the irradiation of AN/St mixtures in dimethylformamide (DMF) solution radical anions are formed which grow simultaneously in two directions adding AN units by an anionic mechanism on one end and forming a random copolymer at the other end.

Evidence for the radiation induced anionic polymerization was obtained from irradiations of glassy systems containing AN. Solvents were dimethylformamide, triethylamine or methyltetrahydrofuran /10, 11/. The radiation induced polymerization of rigorously purified bulk AN at -78°C was shown to proceed by an anionic mechanism /12, 13/.

Nitroethylene was found to polymerize under the influence of γ-irradiation by Sokolov et al. /14/. Indications for a radical polymerization mechanism were obtained. Later Ymaoka et al, investigated the radiation-induced polymerization of nitroethylene in tetrahydrofuran solution at low temperature /15/, and the polymerization of bulk nitroethylene at 10°C /16/. From the results of scavenger experiments it was inferred that the polymerization proceeds via an anionic mechanism.

It was reported that bulk 1-nitropropene-1 does not polymerize under the influence of γ-irradiation and that copolymers obtained by irradiating mixtures of AN and 1-nitropropen-1 in solution (DMF, THF, toluene) were formed by a radical mechanism /17/.

The aim of this paper was to extend the research to other nitrocompounds. It appeared that β-nitrostyrene (βNS) could serve as a further model compound to substantiate a radiation-induced anionic polymerization mechanism. β-nitrostyrene is

known to undergo anionic polymerization initiated by weak bases such as methoxide ions but fails to undergo radical and cationic polymerization /18–21/. It has also been reported that β-nitrostyrene may serve as an inhibitor or a retarder for free radical polymerizations /22, 23/.

Experimental Part

(a) Materials. β-nitrostyrene (Aldrich, 97%) was recrystallized three times from n-hexane solution and dried under high vacuum. The melting point was 57.5–58.0°C.

Methacrylonitrile (Merck-Schuchardt, p.a. 99%) was freed from stabilizer by washing with saturated $NaHSO_3$ solution, and an aqueous solution 1% in NaOH and saturated with NaCl. After washing with saturated NaCl solution it was dried over $CaCl_2$ and twice distilled under reduced pressure.

α-methylstyrene (Ferak, Berlin, 99%) was washed with aqueous NaOH solution (20%) and with distilled water. It was dried with $CaCl_2$ and CaH_2. After having passed columns with activated Al_2O_3 and silicagel (Woelm) it was distilled from CaH_2 over a Vigreux column. The middle fraction was used.

Hexamethylphosphotriamide (Merck, Schuchardt, p.a. 99%) was distilled from a flask containing metallic sodium over a Vigreux column into a flask containing molecular sieve (Merck, 5Å and 10 Å). After two days it was distilled under reduced pressure (b.p. 85°C at 2.3 Torr).

b) Preparation and Irradiation of Samples. In most cases samples were prepared by a high vacuum technique. Cells containing βNS were attached to a high vacuum line, to which flasks containing monomers and in some cases HMPT were connected. The liquid compounds were degassed by several freeze, thaw and pump cycles and then condensed into the cells with βNS. Finally, the cells were separated from the vacuum line by sealing.

During the scavenger experiments HMPT solutions containing βNS were saturated with SF_6 (Kalichemie AG), N_2O (Linde AG, 99,5%) or O_2 (Linde AG, 99,99%) by bubbling with one of the gases for about 30 minutes.

For the irradiation a ^{60}Co-γ-source (ca. 16 000 Ci) was used. The absorbed dose rate determined by Fricke-dosimetry ($G(Fe^{3+}) = 15.5$) amounted to 0.2 to 0.4 Mrad/h.

(c) Analytical Procedures. Elemental analyses were carried out with a Hewlett-Packard CHN Analyzer, model 185.

For IR measurements a Perkin Elmer apparatus, model 421 was used. UV absorption measurements were performed with a Carl Zeiss RPQ20AV spectrophotometer.

Results

(a) Irradiation of Bulk β-nitrostyrene. Several samples of βNS were irradiated in the solid state at room temperature and at -80°C with doses up to 40 Mrad. Polymer was not formed. Also thermal post-irradiation treatment at a temperature slightly below the melting point of 58°C did not yield polymer.

(b) Irradiation of β-nitrostyrene in Solution. No polymer was formed upon room temperature irradiation of βNS in THF solution at concentrations between 10 and 20 mol%. In HMPT solutions, however, polymer was obtained, which precipitated during the irradiation. Its properties are similar to the properties of poly (β-nitrostyrene) generated by sodium methoxide initiation. The melting point under decomposition is about 285°C. The polymer did not dissolve. A great variety of solvents was tested. Swelling was observed with 1-chloronaphthalene and 2-chlorobenzothiazol. Piperidine and N-methylmorpholine decomposed the polymer totally at room temperature yielding coloured solutions. A soluble fraction containing telomers could be extracted with methylethylketone at room temperature indicating the polymeric nature of the reaction product.

Figure 1 shows the dependence of the rate of polymerization on the concentration of βNS in HMPT solution at room temperature. The rate possesses a maximum at about 4 mol% indicating autoinhibition of βNS. A similar effect has been observed recently by Chapiro et al. during the polymerization of acrylonitrile in DMF /9/.

In order to elucidate the polymerization mechanism several experiments were carried out in the presence of scavengers. The results are shown in Fig. 2, where the conversion of monomer is plotted vs. the time of irradiation. Solutions containing 3.64 mol%, βNS were saturated with either N_2O or SF_6 or O_2 at a pressure of 1 atmosphere. For comparison a series of runs was carried out with Ar saturated solutions. As is demonstrated in Fig. 2, the polymerization is retarded by N_2O, SF_6, and O_2. The relative rates of polymerization evaluated from the slopes of the straight lines are 1.00 (Ar) : 0.55 (N_2O) : 0.10 (SF_6) : 0.025 (O_2). SF_6 and N_2O are known to scavenge electrons. O_2 may react both with electrons and carbanions. Since SF_6 and N_2O retard effectively the polymerization it is assumed that during the initiation step electrons are attached to βNS thus forming radical anions which react with intact βNS molecules.

$$e^-_{solv} + \beta NS \longrightarrow \cdot\beta NS^-$$

$$\cdot\beta NS + \beta NS \longrightarrow \cdot NS\text{-}\beta NS^-$$

(c) Copolymerization experiments.

(c-1) β-nitrostyrene – α-methylstyrene (αMS)

αMS forms long chain polymers only by ionic mechanism. Radical initiation leads only to oligomers. Therefore, αMS was selected as a monomer suitable for ionic copolymerization studies.

Irradiation of a monomer mixture containing 10 mol% βNS at 25°C with a dose of about 10 Mrad yielded no polymer. In HMPT solution containing 35 mol% monomer, however, polymer was formed. Figure 3 shows the copolymer composition as a function of monomer composition. The shape of the curve is typical for an ionic copolymerization. The rate of monomer conversion was about one order of magnitude lower than in HMPT solutions containing no αMS. All copolymers were insoluble.

(c-2) β-nitrostyrene - methacrylonitrile (MAN).

The irradiation of mixtures of βNS and MAN in bulk at -20°C yielded copolymers. As shown in Fig. 4(a) copolymers formed in mixtures with only small portions of NS contain high fractions of βNS units indicating an ionic polymerization mechanism. The addition of βNS to MAN reduced the conversion of monomer appreciably as shown in Fig. 4(b). The polymerization of bulk MAN proceeds presumably via a radical mechanism, which is completely suppressed by the addition of βNS.

Upon irradiation of monomer mixtures dissolved in HMPT at room temperature copolymers were formed whose composition corresponded exactly to the curve in Fig. 4(a) for copolymers formed by irradiation of the bulk monomer mixture at 20°C. However, the conversion was about five times higher than in that case indicating that the ionic copolymerization is favoured in HMPT solutions.

Discussion

From the results obtained during the experiments with electron scavengers it is inferred that the polymerization of βNS observed in HMPT solutions proceeds via an anionic mechanism. If electrons are prevented from being attached to β NS molecules formation of the initiating species - presumably an anion radical - is inhibited. Further evidence for the occurrence of an ionic mechanism was obtained from the copolymerization experiments. The shape of the polymer-monomer composition curves strongly indicates an ionic mechanism. The significant capability of HMPT to promote the polymerization of βNS may be due to several reasons. HMPT is a solvent which has the property to stabilize transient ionic species produced under the influence of ionizing radiation. It has been reported /24, 25/ that solvated electrons are formed by irradiating HMPT with γ-rays or fast electrons. Furthermore, HMPT acts certainly as a stabilizer for positively charged intermediates as do similar solvents such as triethylamine or DMF. Thus the rapid recombination of ion pairs is relatively improbable in HMPT, i.e. there is a good chance for ionic species to undergo reactions with solutes. Therefore, it appears to be feasible that HMPT exerts a promoting influence on the start reaction. On the other hand, it is possible that also the propagation step is strongly affected by this solvent, e.g. by complex formation between HMPT and the propagating ion.

Acknowledgement. The authors are grateful to Dr. U. Faass, Institut für Organische Chemie der Technischen Universitat Berlin, for giving them the opportunity to use that institute' equipment for carrying out the elemental analyses.

References

/ 1/ K. Hayashi, "Radiation-induced polymerization by free ions", in Actions Chimiques et Biologiques des Radiations", M. Haissinsky (ed.), Quinziéme série, Masson et Cie., Paris 1971.

/ 2/ T.F. Williams, "Radiation-induced polymerization", in P. Ausloos (ed.) "Fundamental Processes in Radiation Chemistry"

/ 3/ R.C. Potter and D.J. Metz, "γ-Radiation-induced ionic polymerization of pure liquid styrene", J.Polym. Sci. A-1, 9, 441 (1971).

/ 4/ L.P. Mezhirova, Z. Smigaseivich, A.P. Sheinker and A.D. Abkin, Vysokomol. Soedin. 5, 473 (1963).

/ 5/ L.P. Mezhirova, A.P. Sheinker and A.D. Abkin, Vysokomol. Soedin, 3, 99 (1961).

/ 6/ V. Tsuda, J. Polym. Sci. 54, 193 (1961), ibidem 58, 289 (1962).

/ 7/ K. Hayashi, M. Nishii and S. Okamura, Isot. Radiat. Japan, 3, 344 (1960).

/ 8/ A.-M. Jendrychowska-Bonamour, J. Chim. Phys. 63, 855 (1966).

/ 9/ A. Chapiro, F. Jaberg and L. Perec-Spritzer, Eur. Polym.J. 11, 637 (1975).

/10/ L. Perec, J. Chim. Phys. 66, 1742 (1969).

/11/ M. Bodard-Gauthier and R. Marx, J.Polym. Sci. C 16, 4241 (1968).

/12/ S. Iiyama, S. Abe and K. Namba, Nippon Kagaka Kaishi 2428 (1974), J.Polym. Sci., Polym. Lett. 11, 81 (1973).

/13/ L.P. Toltaukhova, N.V. Bayantseva and A.P. Sheinker, Vysokomol. Soedin. B14, 567 (1972).

/14/ V.N. Sokolov, I.Ya. Puddubuyi, V.V. Perekalin and F. Evdokimov, Dokl. Akad. Nauk 138, 619 (1961).

/15/ H. Yamaoka, R. Uchida, K. Hayashi and S. Okamura, Kobunshi Kagaku 24, 29 (1967).

/16/ H. Yamaoka, F. Williams and K. Hayashi, Trans. Farad. Soc. 63, 376 (1967).

/17/ W.P. Alanija, E.G. Gorlow and N.G. Kusnetzow, Izv. Vyssh. Ucheb. Zaved., Khim. Khim. Tekhnol.

/18/ D. Vorlander and P. Herrmann, Chem. Zentralbl. 1, 730 (1899).

/19/ D.E. Worral, J. Amer. Chem. Soc. 49, 1598 (1927).

/20/ A.V. Topchiev, V.P. Alaniya and I.S. Mazel, Doklad. Akad. Nauk, SSSR 125, 1048 (1959).

/21/ R.W.H. Berry and R.J. Mazza, Polymer 14, 172 (1973).

/22/ G.R. Barret, U.S. Patent 2537015 (1951) and 2537018 (1951), Chem. Abstr. 45, 3195, 3170 (1951).

/23/ M. Kreisel, U. Garbatski and D.H. Kohn, J. Polym. Sci., Polym. Lett. 2, 81 (1964).

/24/ E.I. Maltsev and A.V. Vannikov, Khim. Vysok. Energ. 8, 328 (1974).

/25/ H. Nauta and C. van Huis, J. Chem. Soc., Farad. Trans. 1, 68, 647 (1972).

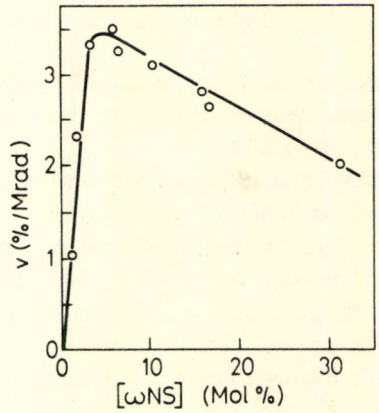

Fig. 1 Polymerization of βNS in deaerated hexamethylphosphotriamide at room temperature. The rate of polymerization vs. the monomer concentration. Absorbed dose rate 0.5 Mrad/h. Absorbed dose: 8 Mrad

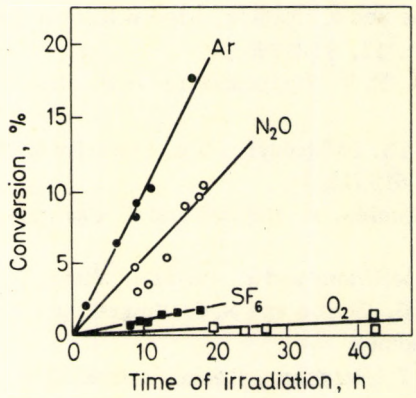

Fig. 2 Influence of scavengers on the polymerization of βNS (3.64 mol%) in hexamethylphosphotriamide solution at room temperature. Conversion vs. time of irradiation. Absorbed dose rate: 0.5 Mrad/h. The solutions were saturated with the gases indicated in the figure prior to irradiation at a pressure of 1 atmosphere

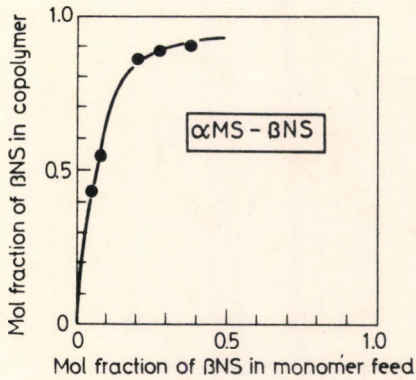

Fig. 3 Copolymerization of α-methylstyrene and β-nitrostyrene in HMPT at room temperature. Copolymer composition vs. composition of monomer mixture. Concentration of monomers: 35 mol%. Absorbed dose rate: 0.5 Mrad/h. Absorbed dose: 10 Mrad

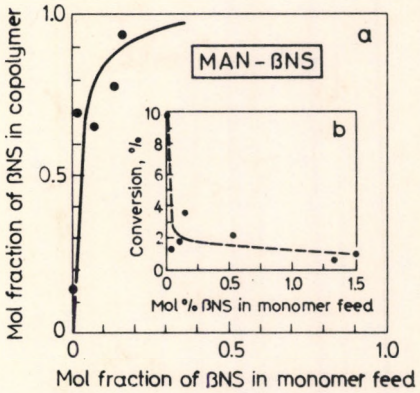

Fig. 4 Copolymerization of methacrylonitrile and β-nitrostyrene at $-20^{\circ}C$ in bulk. (a) Copolymer composition vs. composition of monomer feed (b) Monomer conversion vs. composition of monomer feed. Absorbed dose: 10 Mrad

SOLID STATE POLYMERIZATION OF N-VINYLPHTHALIMIDE

M. Kerekes, J. Varga
Department of Plastics and Rubber, Technical University, Budapest, Hungary

In addition to the chemical nature of the monomer, crystallochemical factors have a significant effect on the kinetics of solid state polymerization and the structure of the polymer formed /1/. Investigations of polymerization processes of monomers having polymorphous modifications, are of considerable interest, since the role of crystallographic factors can be determined. Indirect and direct data can be found in the literature on the role of polymorphism in solid state polymerization /1/. The role of polymorphism has been studied in the case of solid state polymerization of acrylonitrile /2,3/, tributyl-vinylphosphonium bromide /4/, methacrylic acid /5/, and N-vinylphthalimide (NVPI). In these papers differrent reactivites of polymorphous modifications have been pointed out.

The aim of this study was to give a report on the γ-radiation induced solid state polymerization of polymorphous modifications of NVPI.

Experimental

NVPI was prepared by means of a method described in /7/ and was recrystallized three times from isopropyl alcohol solution.

The polymorphism of NVPI was studied by X-ray, thermoanalytical and polarization optical methods. Polymerization kinetics were followed by gravimetric measurements. ESR spectra of radicals formed during γ-irradiation were performed on a JEOL-ME-3X spectrometer.

The description of these experimental methods has been reported in detail in our earlier papers.

Results and Discussion

Three polymorphous modifications of NVPI have been prepared. The melting points of individual modifications are: NVPI-186°C, NVPI-II 75°C and NVPI-III 82°C. It has been established that the the first two of these are enantiotropic, so they can mutually be transformed into each other in the solid state. Their equilib-

rium transition point determined by Kofler's solvent method /8/ is 40.5°C. The II → I transition has been studied by differential scanning calorimetry. It was found to be between 50 and 75°C. This is an endothermic transition with enthalpy change of 1.04 kcal/mole. NVPI-I is stable in the temperature range between 40.5 and 86°C, NVPI-II. is stable below 40.5°C. The NVPI-III modification is unstable in all conditions (it is monotropic). The existence of these three modifications is proved by X-ray diffractograms given in Fig. 1.

The second modification, NVPI-II was obtained as diamond-shaped crystal plates by crystallization at room temperature from isopropyl alcohol solution. NVPI-I is fomed by solidification of the melted NVPI or by crystallization from solutions at higher temperatures (they have the shape of acicular crystals). NVPI-III, which is instable, can be prepared, with difficulty, from NVPI-II at about 60°C. Due to the hindered feature of solid state transitions, individual modifications can be supercooled and, in some cases, can be slightly overheated. Thus, all the three modifications may be stored for a long time at room temperature, therefore, it is possible to make a comparison between their solid state polymerization processes at the same conditions (temperature, dose rate, pressure).

The solid state polymerization of the three modifications is of an accelerated character, but their polymerization rates are strongly different. The highest rate of polymerization has been observed for NVPI-I and the lowest one for NVPI-II (Fig. 2). Similar results were obtained for other temperatures, except above 60°C, where NVPI-II changed into NVPI-I. The activation energy calculated from the temperature dependence of the solid state polymerization rate, is 5.7 ± 0.5 kcal/mole for NVPI-I, and 11.0 ± 0.5 kcal/mole for NVPI-II and III (these values differ from those previously reported /6/, however that evaluation was made on the basis of rather few experimental data).

We have determined the dependence of the solid state polymerization rate on the dose rate for the I and II modifications. It has been found that the rate of polymerization process is a linear function of the dose rate in both cases.

The mechanism of the solid state polymerization has been determined by the inhibitor method employed in our earlier studies /10/. Benzoquinone (BQ) and 8-hydroxy-quinoline (HQ) were used as inhibitors. BQ and HQ form simple eutectic systems with the modifications of NVPI. The characteristics of these systems are summarized in Table 1. Like the mentioned inhibitors an inert additive, such as succinicimide (SI) forms a simple eutectic with different modifications of NVPI (Table 1).

BQ and HQ retard significantly the solid state polymerization of modifications of NVPI (Fig. 3). On increasing the BQ concentration up to the eutectic composition the retarding effect is increased. If the BQ concentration is further increased the retarding effect is not changed considerably. HQ retards the polymerization to a lesser degree, its retarding effect increases monotonously in the examined interval as its concentration is increased. The inert additive (SI) (Fig. 3) either slightly raises the polymerization rate (for NVPI-I and NVPI-II) or it has no effect on that (within the experimental error limits.)

Table 1.
Characteristics of binary systems of NVPI with different additives

Monomer		Additive		Eutectic melting temperature	Eutectic composition
–	melting temperature °C	–	melting temperature °C	°C	NVPI mole %
NVPI-I	86	BQ	115.7	57.5	63.0
NVPI-II	75	BQ	115.7	53.0	67.0
NVPI-III	82	BQ	115.7	55.0	65.0
NVPI-I	86	HQ	74.0	43.0	46.0
NVPI-II	75	HQ	74.0	40.5	47.0
NVPI-I	86	SI	125.0	72.0	18.0
NVPI-II	75	SI	125.0	62.0	15.0
NVPI-III	82	SI	125.0	68.0	17.0

A comparison of the effects produced by radical scavengers and the inert additive on the polymerization rate makes it possible to establish without doubt that solid state polymerization of NVPI proceeds according to the radical mechanism.

The absence of complete inhibition in the two-component solid systems forming eutectic mixtures was expectable on the basis of our earlier studies since in heterogeneous crystalline mixtures the inhibitor can make its radical scavenger action first of all on the monomer-inhibitor boundary surface /9,10/. Accordingly, the inhibiting effect is increased till the eutectic composition is reached. In the case of HQ we have found a deviation from this rule. It can be explained by the assumption that a small quantity of the inhibitor may be inserted as inclusion in the defects of the monomer crystals. Thus, the inhibitor can act as a radical scavenger not only on the monomer-inhibitor boundary surface but within the monomer phase as well.

In addition to these studies there is another observation proving the radical mechanism of the NVPI polymerization: in the solid state the polymerization may be initiated by azo-bis-isobutyronitrile (ABIN). ABIN and the first modification of NVPI form a single eutectic system. Kinetic plots at different initiator concentrations measured below the temperatures of the solidus line (60°C) are given in Fig. 4.

The structure and concentration of radicals formed during irradiation of NVPI were studied by electron spin resonance (ESR). In conditions of solid state polymerization in NVPI-I and NVPI-II radicals of the same structure are formed. The ESR spectrum of these radicals is a triplet with the distribution of 1:2:1 as shown in Fig. 5.

The triplet arises from the growing radicals having the following probable structure /11/:

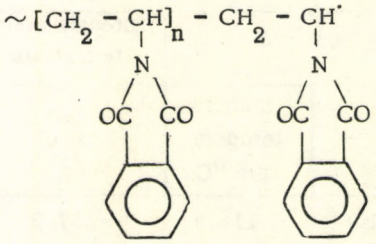

We have studied the radical concentration as a function of the total irradiation dose. A surprising result has been obtained: the concentration of radicals formed in NVPI-I is about ten times more than that found in NVPI-II (Fig. 6). In the case of low temperature irradiation at -196°C, when no polymers are formed, the concentration of radicals formed under the influence of 0.9 Mrad total dose, is 8.3×10^{17} spin/g in NVPI-I and 4×10^{15} spin/g in NVPI-II. Radicals formed during irradiation at low temperature gave a singlet ESR spectrum (see Fig. 5), which is changed into a triplet as the temperature is raised.

The different inclinations of the polymorphous monomers to polymerize in the solid state are usually attributed to the fact that the mutual orientations of vinyl groups are not the same as those having an effect on the chain propagation. Nevertheless, our studies show unanimously that the crystalline structure of the monomer may have a significant effect on the initiation step (radical formation) of solid state polymerization. A similar conclusion can be drawn comparing the results of ESR measurements with the kinetic studies of post-polymerization of NVPI-I and II.

Post-polymerization kinetic plots of NVPI-I and II. are given on Fig. 7. These curves are of a decelerated character, they approximate limiting values. The post-polymerization rate of NVP-I is substantially greater than that of NVPI-II. The post-polymerization rates and the limiting conversions are increased with increasing temperature, the value of the apparent activation energy is 11.0 kcal/mole.

The temperature dependence of the post-polymerization of NVPI-II is not so definite, since it is changed into NVPI-I at about 50°C, as it was proved by polarization microscopy, DTA and DSC investigations.

At the NVPI II $\longrightarrow$ NVPI I phase transition the mobility of monomer molecules as well as of the active centres is suddenly increased. However, the simultaneous change of the mobility and order does not result in sudden increase in the post-polymerization rate, in spite of the earlier reported observations made at fusion of numerous monomers /12/. The reason for this is that the recombination rate of radicals is greater than the post-polymerization rate during the phase transition.

The above mentioned assumption and the greater post-polymerization rate for NVPI-I are unanimously confirmed by ESR measurements. In Fig. 8 it can be seen that the radical concentration in NVPI-II is much less than in NVPI-I. Due to the

phase transition taking place above 40°C, the radical concentration is rapidly decreased.

The development of the post-polymerization rate is in good agreement with the development of the radical concentration.

At present further investigations are in progress in our laboratory, namely:

ESR-measurements of irradiated at −196°C monocrystals of NVPI, in order to determine the radical structure,

DSC-measurements for measuring the phase diagram of polymer-monomer systems,

gas-chromatographic analysis of products formed under the influence of the γ-irradiation,

investigations on the structure of the polymer formed and measurements on its thermal properties.

Acknowledgments. The authors wish to thank Dr. A. Rockenbauer and Dr. A. Kálmán for their help in ESR and X-ray measurements, as well as Miss K. Fekete, Miss Zs. Fekete, Mr. G. Molnár and Mr. B. Orbán for taking part in the experimental work.

References

/ 1/ Chapiro, A., in Encyclopedia of Polymer Science and Technology, Vol. 11 Interscience Publ. 1969, p. 702.

/ 2/ Bensasson, R., Dworkin, A. Marx, R., J. Polymer Sci. C4, 881 (1964), Kaplan, A.M., Kirjukin, D.P., Barkalov, I.M., Goldanszkij, V.J., Kinetics and Mechanism of Polyreactions. Vol. III. Akadémiai Kiadó, Budapest, 1969, Barkalov, J.M., Kinetics and Mechanism of Polyreactions. Plenary and Main Lectures, Akadémiai Kiadó, Budapest, 1971, pp. 555-570.

/ 3/ Finkel'stein, E.I., Abkin, A.D., Vysokomol. Soed., B11, 340 (1969).

/ 4/ Chen, C.S.H., Grabar, D.G., J. Polymer Sci., C4, 849 (1964).

/ 5/ Sakai, I., Iwasaki, M., J. Polymer Sci., A1, 3143, 3177, 3191 (1969).

/ 6/ Hardy, G., Varga, J., Nagy, G., Cser, F., Jobbágy, M., Kinetics and Mechanism of Polyreactions, Vol. IV., 69, Akadémiai Kiadó, Budapest, 1969.

/ 7/ Nikolaev, A.F., Usakov, S.N., Izvestia Akad. Nauk, Otd. Him. Nauk, 1235 (1957)

/ 8/ Kofler, L., Kofler, A., Thermo-Mikro-Methoden. Chemie Verl. Weinheim, 1954.

/ 9/ Hardy, G., Kinetics and Mechanism of Polyreactions. Plenary and Main Lectures, Akadémiai Kiadó, Budapest, 1971, pp. 571.

/10/ Hardy, G., Varga. J., Cser, F., Detreköy, E., Europ. Polym. J., 5, 133 (1969).

/11/ Fischer, H., in Advances in Polymer Science, 5. Band. Springer-Verlag, Berlin-Heidelberg-New York, 1967/1968, pp. 463-530.

/12/ Kargin, V.A., Kabanov., V.A., Papiszov, I.M. J. Polymer Sci., C4, 767 (1964).

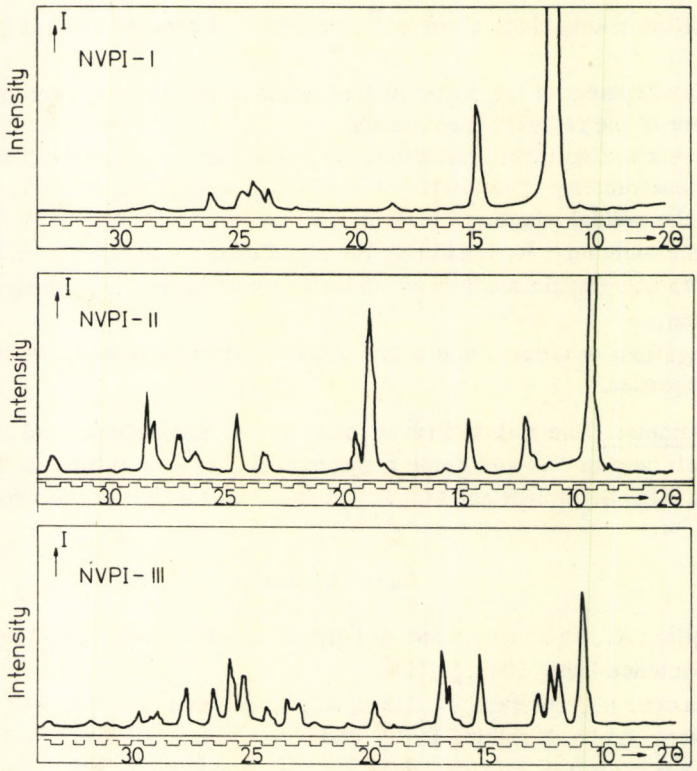

Fig. 1 X-ray diffractograms of the modifications of N-vinylphthalimide

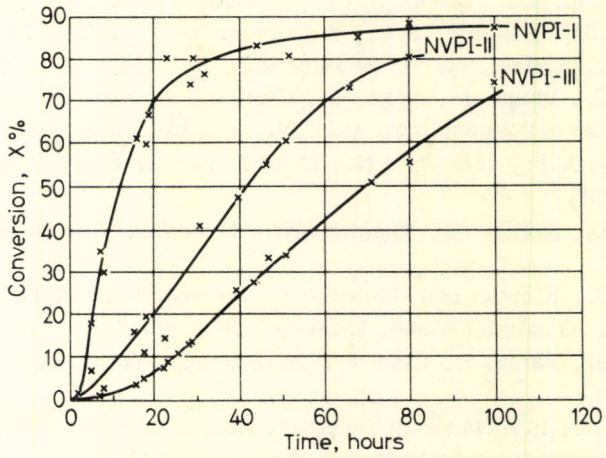

Fig. 2 Polymerization kinetic plots of the modifications of N-vinylphthalimide. Temperature: 30°C, dose rate: $1.84 \cdot 10^5$ rad/hr

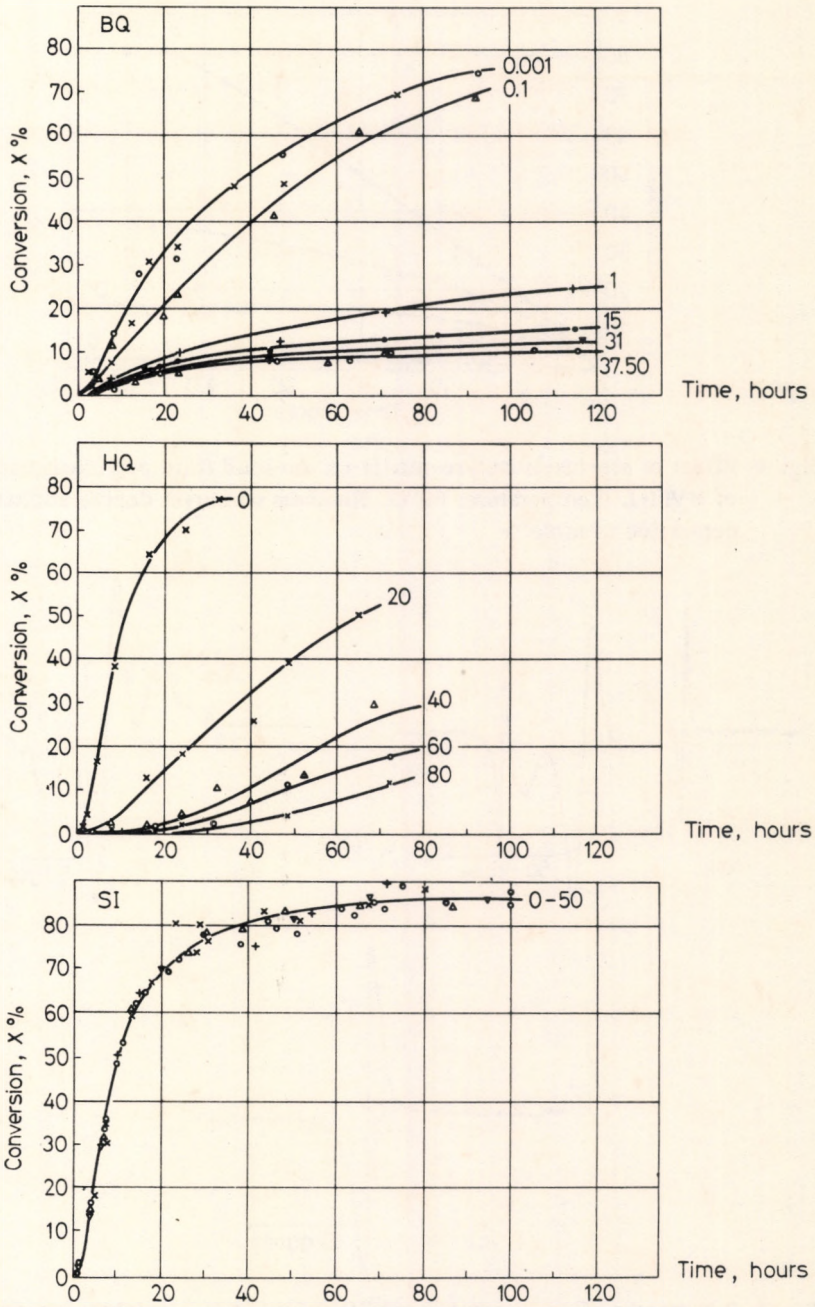

Fig. 3 Effect of additives on the polymerization kinetics of NVPI-I. BQ benzoquinone, 50°C, $1.99 \cdot 10^5$ rad/hr, HQ 8- hydroxy quinoline, 35°C, $1.508 \cdot 10^5$ rad/hr, SI inert adduct: succinimide, 30°C, $1.04 \cdot 10^5$ rad/hr. Numbers on curves indicate additive concentrations in mole %

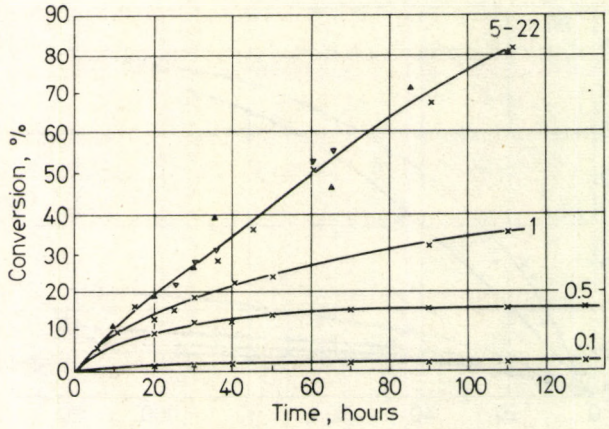

Fig. 4 Effect of aso-bis-isobutyro-nitrile on the solid state polymerization kinetics of NVPI-I. Temperature: 60°C. Numbers on curves denote additive concentration in mole %

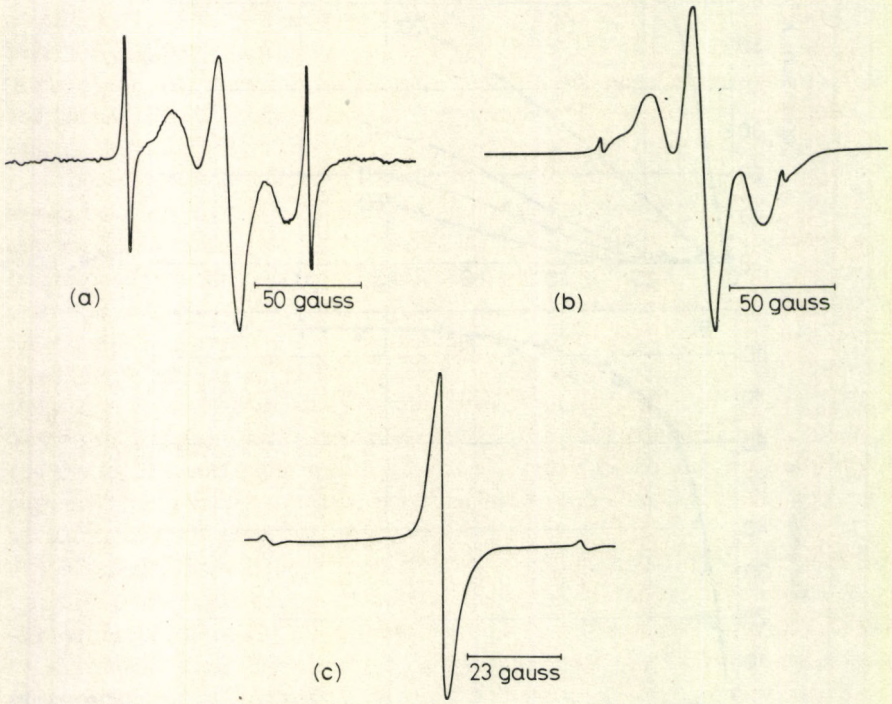

Fig. 5 ESR spectra of the irradiated modifications of N-vinylphthalimide: a) NVPI-I, 20°C, 9.75 Mrad, b) NVPI-II, 20°C, 9.75 Mrad, c) NVPI-I, -196°C, 9.75 Mrad

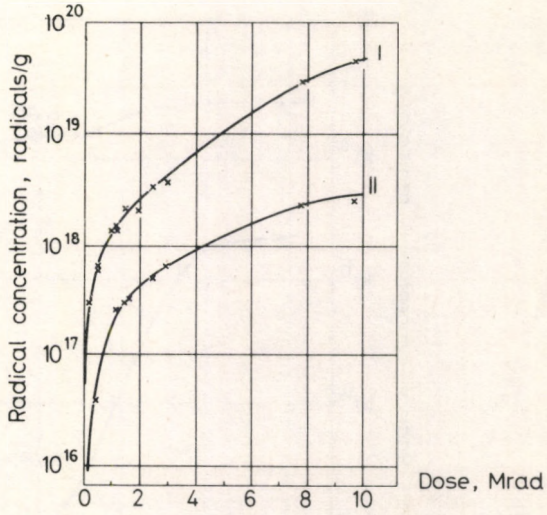

Fig. 6 Accumulation of radicals in two modifications of N-vinylphthalimide as function of irradiation dose. Temperature: 20°C

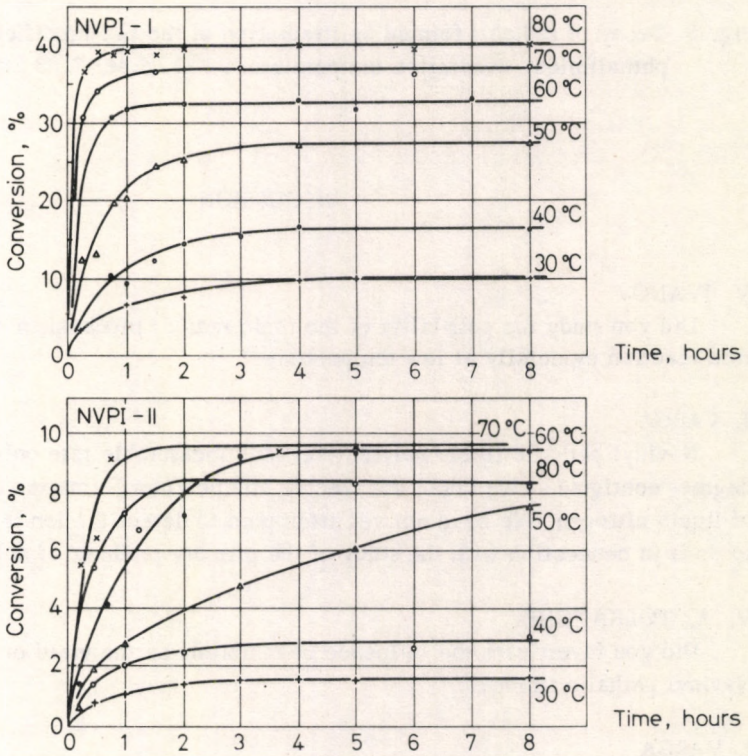

Fig. 7 Post polymerization kinetical curves of N-vinylphthalimide modifications. Irradiation temperature: 20°C, dose: 2.07 Mrad

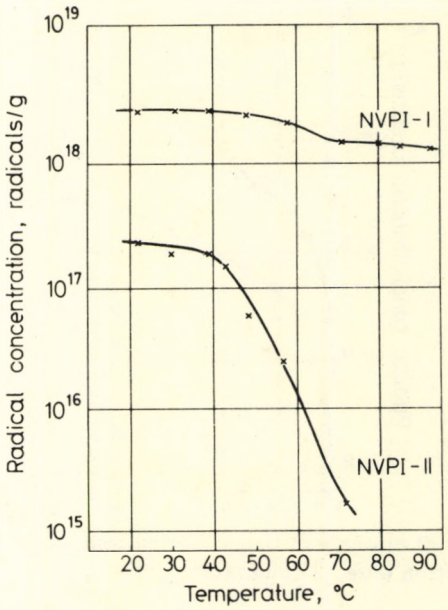

Fig. 8 Decay of radicals formed by irradiation of the two modifications of N-vinyl-phthalimide. Irradiation temperature: 20°C, dose: 7.83 Mrad

DISCUSSION

V. IVANOV

Did you study the possibility of the ionic radical mechanism of the polymerization reaction especially at low temperatures?

J. VARGA

N-vinyl phthalic imide polymerizes with measurable rate only above zero degrees centigrade. We could not observe any polymer formation at the temperature of liquid nitrogen. We have not yet attempted to detect the ion radical but we plan to do it in connection with the study of the primary products of radiolysis.

V. A. TOLKATCHEV

Did you investigate the influence of inhibitors on the yield of the free radicals in N-vinyl phthalic imide?

J. VARGA

Only the pure monomer (single component system) was studied by ESR.

RADIATION-INDUCED POLYMERIZATION OF GLYCIDYL METHACRYLATE AT LOW TEMPERATURES

A. P. Meleshevich, Yu. V. Vishev, A. E. Nesterov
Pisarzhevsky Institute of Physical Chemistry,
Ukrainian Academy of Sciences, Kiev, USSR

The radiation-induced polymerization of glycidyl methacrylate (GMA) at positive temperatures has been studied and described earlier (1-4). The polymerization of GMA at temperatures ranging from 0 to 70°C goes through the chain radical mechanism and involves double bonds. The effective activation energy was found to be 3.3 Kcal/mole. The number-average molecular weight of the forming polymer ranges from 0.6×10^6 to 1.2×10^6 and the ratio M_w/M_n - from 1.5 to 2.0 The radiation chemical yield of the monomer consumption is $6 \times 10^3 + 2 \times 10^4$ molecules/100eV in the mentioned conditions.

In the present work the process of the radiation-induced polymerization of GMA at low temperatures is studied.

Experimental

The preparation of the monomer and the irradiation procedure were those described earlier (2. 3). The monomer was irradiated in the temperature range between -60°C and -196°C with doses ranging from 15 Krad to 45 Mrad at dose rates from 12.5 to 1500 rad/sec. The molecular weight of poly-glycidyl methacrylate (PGMA) and the molecular weight distribution (MWD) for PGMA were obtained using a G-120 ultracentrifuge (produced by MOM, Hungary).

The analysis of epoxy groups was carried out according to OCT (State standard) 12497-67 and that of double bonds by titration with ClBr.

Results and Discussion

Figure 1 shows the polymer yield curve for the polymerization of GMA depending on temperature (15 Krad, 60 rad/sec). One can see that the decrease of radiation temperatures leads to a sharp increase of polymer yield. So, the latter is 0.2 weight per cent at -65°C and increases to 6.5 weight per cent at -92°C. Such an increase in the mentioned temperature range equals 0.25 weight per cent/grade, which is 6 times that obtained at temperatures ranging from 0°C to 70°C.

Usually the sharp change of polymerization rate for a monomer is connected with the change of its aggregate state like liquid-solid state. The temperature determination for the phase transition of GMA makes it possible to establish that on cooling the substance, its freezing temperature is $-95^{\circ}C$, and on heating the sample, preliminarily frozen in liquid nitrogen, the melting temperature of GMA is $-65^{\circ}C$. Therefore the monomer was found to be supercooled at temperature from -65° to $-95^{\circ}C$.

The radiation-induced polymerization kinetics of GMA at temperatures ranging from -65° to $-95^{\circ}C$ (Fig. 2) differs from that obtained at positive temperatures. As has been described /1, 2/, the kinetic curve for the dependence of the polymer yield on the dose has an S-like nature. Linear dependence of the polymer yield on dose is observed to high degrees of monomer conversions in the temperature range from $-65^{\circ}C$ to $-95^{\circ}C$.

The radiation-induced polymerization of GMA under radiation the monomer in the solid state differs from that of GMA in the liquid state at temperatures ranging from $-95^{\circ}C$ to $-70^{\circ}C$. So, a linear dependence of the polymer yield on dose is observed at the initial stage of the polymerization of GMA irradiated at $-196^{\circ}C$. Conversion of the monomer reaches 11-12 weight per cent at 0.6 Mrad. Then the polymerization rate decreases noticeably and within the following 3 Mrad the increase of the polymer yield is only 3 weight per cent. It should be added that under conditions of liquid-phase polymerization gel-fraction appears at doses of 15-50 Krad and degrees of conversion of 5-10 weight per cent, but at temperature $-196^{\circ}C$ it does not form, as far as the dose is 45.5 Mrad, though the polymer yield reaches 35.1 weight per cent.

The radiation yield of the polymer is 2.9×10^4 molecules/100eV and the effective activation energy for the polymerization process at the temperature ranging from $-65^{\circ}C$ to $-95^{\circ}C$, determined from the Arrhenius diagram, is -6.8 Kcal/mole.

The dose rate raised to the 0.89 power in the equation $U = KJ^n$, the value and the sign of the effective activation energy and increasing the reaction rate with decreasing temperature are characteristic of the ionic mechanism of the radiation-induced polymerization of GMA in the supercooled state. At the same time a further decrease in temperature leads to a sharp drop of the polymerization rate, which accounts for a change of the monomer aggregate state. By irradiation of the monomer in the temperature range between $-98^{\circ}C$ and $-196^{\circ}C$ a small decrease in the polymer yield was observed from 1.2 weight per cent at $-98^{\circ}C$ to 0.4 weight per cent at $-196^{\circ}C$ (Fig. 2, curve 4) and decrease in radiation yield of the polymer from 5.5×10^3 molecules/100eV at $-98^{\circ}C$ to 1.6×10^3 molecules/100eV at $-196^{\circ}C$. The ionic process of the polymerization seems to remain at this temperature range since the value $E_{eff} = 1.0$ Kcal/mole and $n = 1.0$.

The present characteristics are important but not sufficient to estimate the mechanism of radiation-induced polymerization. It is the results of molecular weight distribution (MWD) study that characterize it.

Table 1

Average molecular weight and polydispersity of PGMA obtained in liquid state (15 Krad*, vacuum, $-83^{o}C$)

Dose rate, rad/sec	$\bar{M}_n \times 10^{-5}$	$\bar{M}_w \times 10^{-5}$	$\bar{M}_z \times 10^{-5}$	$\bar{M}_w/\bar{M}_n$	$\bar{M}_z/\bar{M}_w$
12.5	2.6	2.7	2.8	1.04	1.04
240.0	7.2	7.4	7.5	1.02	1.02
1 500.0	8.4	8.5	8.6	1.01	1.01

* The soluble part of the polymer was investigated

Table 2

Average molecular weight and polydispersity of PGMA (vacuum, $-196^{o}C$)

Dose, Krad	Dose rate, rad/sec	$\bar{M}_n \times 10^{-5}$	$\bar{M}_w \times 10^{-5}$	$\bar{M}_z \times 10^{-5}$	$\bar{M}_w/\bar{M}_n$	$\bar{M}_z/\bar{M}_w$
100	62	4.5	8.0	11.1	1.78	1.39
200	62	1.5	2.8	4.0	1.84	1.46
400	62	1.2	2.1	3.1	1.75	1.48
150	100	1.4	2.5	3.4	1.80	1.38
150	200	2.0	3.5	5.2	1.78	1.38
150	370	2.6	4.9	7.1	1.87	1.45

MWD data have been determined for PGMA samples obtained in liquid state ($-83^{o}C$) and for the monomer radiated in solid state at $-196^{o}C$. The results of MWD investigation and that of the effect of dose rate on molecular weight of the polymer obtained at $-83^{o}C$ are presented in Fig. 3 and Table 1. One can see in Fig. 3 and Table 1, that MWD for PGMA obtained in the given conditions is narrow and the ratio M_w/M_n equals approximately 1.0. The latter hardly changes with dose rate. The radiation-induced polymerization of GMA is identified as ionic by the ratio M_w/M_n. It is important to point out that the molecular weight of the polymer increases with increasing dose rate, and in the case of radical process, as has been shown in /3/, the molecular weight of the polymer decreases with increasing dose rate.

MWD investigation for PGMA obtained by radiation depending on the dose shows that the differential MWD curves for such polymer are bimodal (Fig. 4). The shape of the curves and the polydispersivities for all the samples remains the same in spite of the changes of radiation parameters (dose, dose rate) (Table 2). Moreover the dependence of radiation-induced polymerization rate on dose rate is peculiar to ionic processes, as has been mentioned, and the polymer dispersion is characteristic

Table 3

Experimental and calculated values of average molecular weights and polydispersity of PGMA (150 Krad, 100 rad/sec, vacuum, -196°C)

MWD	$\bar{M}_n \times 10^{-5}$	$\bar{M}_w \times 10^{-5}$	$\bar{M}_z \times 10^{-5}$	$\bar{M}_w/\bar{M}_n$	$\bar{M}_z/\bar{M}_w$
I by Tung	0.4	0.5	0.6	1.30	1.20
II by Tung	2.3	3.1	4.2	1.40	1.30
Σ by Tung	1.4	2.5	3.6	1.80	1.40
experiment	1.4	2.5	3.4	1.80	1.40

of radical processes, as can be seen from Table 2. That is why we had to interpret bimodal MWD curves to elucidate the polymerization mechanism.

The interpretation of bimodal distribution was carried out by means of the linear diagram method of Tung /5, 6/. The results calculated from MWD differential curves, average molecular weights of PGMA and polydispersity obtained by the Tung method are presented in Fig. 4 and Table 3.

The analysis of the differential MWD curves I and II and the data listed in Table 3 show the MWD of both polymers to be narrow. It is known /7, 8/, that polydispersity $M_w/M_n < 1.5$ specifies the polymers obtained by ionic mechanism. Therefore, in the case of polymerization of GMA irradiated at -196°C both polymers are formed by the ionic mechanism.

The bimodality of MWD can be caused by the fact that the reaction of the radiation-induced polymerization of GMA irradiated in the solid state at -196°C proceeds through active centres of two types, i. e. it may be double bonds and epoxy groups. The chemical analyses of both functional groups of the irradiated monomer and PGMA have been carried out to clear up this supposition. These analyses show that the polymerization reaction involves both double bonds and epoxy groups. Consumption rate of epoxy groups under γ -radiation is almost constant up to the dose of 45 Mrad and that of double bonds is constant in a narrow dose range and decreases sharply at 0.5-0.7 Mrad. The decrease of the polymer yield at the dose range mentioned above might be explained by that fact (see Fig. 2, curve 4).

It is of interest that the polymerization of supercooled GMA involves double bonds mainly at the stage of the soluble polymer formation, while epoxy groups do not participate in the polymerization reactions.

It is possible that in the course of radiolysis of the monomer in the solid state the polymerization goes not at the moment of radiation but as a result of the post-effect at the melting temperature of the monomer. Usually such reactions are initiated by the frozen radicals. The study of the influence of quinol (4.7 weight per cent) on the polymerization of GMA radiated at -196°C by the dose of 2 Mrad shows the yield of PGMA to be of 14.9 weight per cent, while after irradiation the pure monomer it equals 17.8 weight per cent. Since quinol had

shown an inhibiting effect at low-temperature polymerization of the monomer, it was used for determination of the moment of the polymerization reaction. For this purpose GMA radiated at $-196^{o}C$ was dissolved in ether cooled below the melting temperature of the monomer. The ether cooled at $-78^{o}C$ had contained 6 weight per cent of quinol with respect to GMA, which had to suppress the development of the post-polymerization process in the case of the polymer formation by radical mechanism in the sample heated to that temperature. However, the frozen irradiated system dissolving in the concentrated solution of quinol in ether at $-78^{o}C$ leads to PGMA extraction of 17.9 weight per cent. This fact indicates polymer formation well below the melting temperature of the monomer ($-65^{o}C$). The stated data suggest that the radiation-induced polymerization of GMA at deep cooling proceeds in the solid state - probably under irradiation.

When studying the polymerization mechanism of GMA at low temperatures the influence of the reactive additives on the process rate has been tested. It has been found that acetone and to a smaller extent quinol and DFPH inhibit the polymerization while chlorine methylene increases noticeably the polymer yield. These facts indicate the cationic mechanism of the process.

The data presented above allow us to consider that the low-temperature radiation-induced polymerization of GMA proceeds by ionic mechanism in both the super-cooled state ranging from $-65 \div -95^{o}C$ and in the solid state ranging from $-98 \div -196^{o}C$ and probably involves, to a certain extent cation, radicals.

References

/1/ G. N. Pjankov, A. P. Meleshevich, E. G. Jarmilko, A. M. Kabakchi, Sz. I. Omelchenko, Radiation Modification of Polymeric Materials, Izd "Technika", Kiev, 1969, pp. 202-207.

/2/ A. P. Meleshevich, I. P. Fedorova, H. Lodos, Ju. V. Vishev, Khim. Promyshlennost Ukraini, No 6, 7-9 (1970).

/3/ A. P. Meleshevich, Yu. V. Vishev, A. E. Nesterov, Radiation-Induced Polymerization of Glycidyl Methacrylate and the Molecular Weight Distribution of its Polymers, Proc. Third Symposium on Radiation Chemistry, Akadémiai Kiadó, Budapest, 1971, pp. 659-667.

/4/ A. E. Fajnerman, A. P. Meleshevich, Ju. V. Vishev, L. N. Vologina, "Synthesis and Physical Chemistry of Polymers", Izd. "Naukova dumka", Kiev, 1975. 15. pp, 26-30.

/5/ Fractionation of Polymers, (ed. M. Kantova,) Izd. "Mir", Moscow, 1971, pp. 335-362.

/6/ Ju. S. Lipatov, A. E. Nyestyerov, T. M. Grischenko, R. A. Veselovski, Textbook of Polymer Chemistry, Izd. "Naukova dumka", Kiev, 1971.

/7/ V. N. Cvetkov, V. E. Eskin, Sz. Ja. Frenkel, Struktura makromolekul v rastvorah, Izd. "Nauka", Moscow, 1964. 719.

/8/ Sz. Ja. Frenkel, Introduction to the statistical theory of polymerization, Izd. "Nauka", Moscow and Leningrad, 1965.

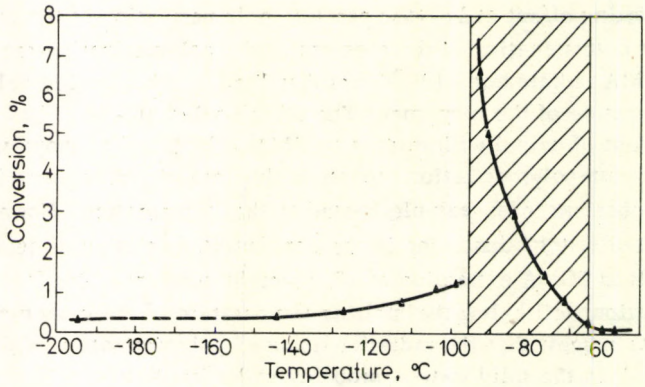

Fig. 1 Dependence of the yield of polyglycidyl methacrylate on temperature (15 Krad, 60 rad/sec, vacuum)

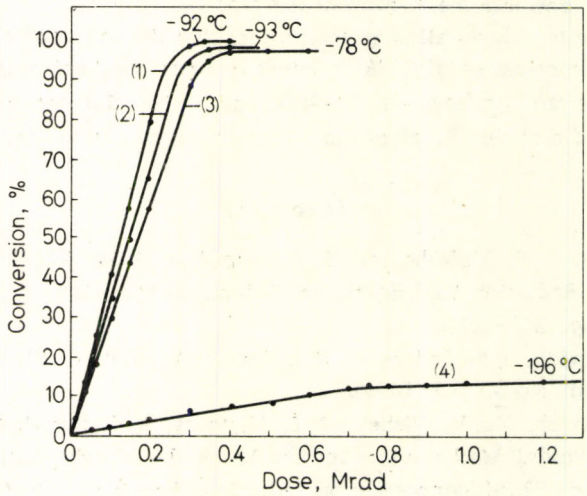

Fig. 2 Dependence of the yield of polyglycidyl methacrylate on dose at different temperatures (60 rad/sec, vacuum, (1) $-92^{\circ}C$: (2) $-93^{\circ}C$: (3) $-78^{\circ}C$: (4) $-196^{\circ}C$)

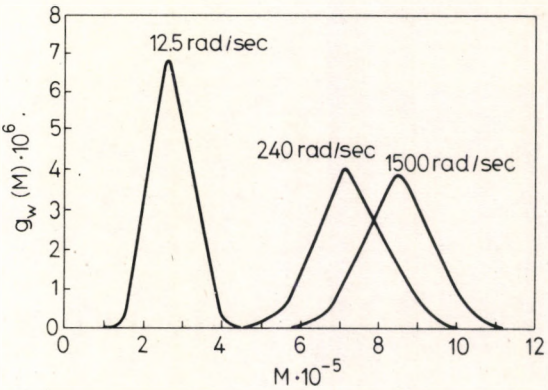

Fig. 3 Differential molecular weight distribution curves of polyglycidyl methacrylate in the dependence on dose rate of radiation (vacuum, $-83^{\circ}C$)

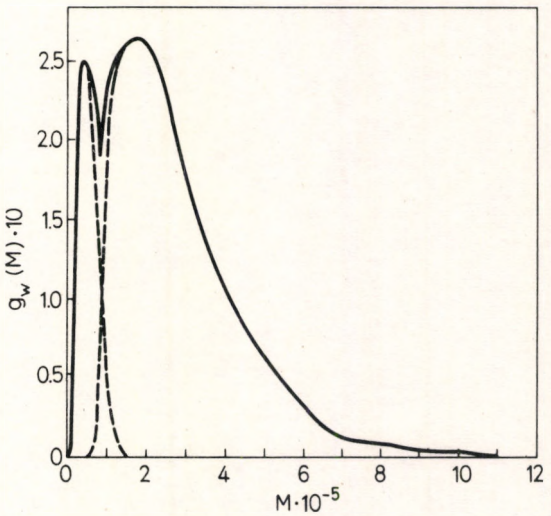

Fig. 4 Differential molecular weight distribution curves of polyglycidyl methacrylate (150 Krad, 100 rad/sec, vacuum, $-196^{\circ}C$, ——— = experimental curve: – – – = calculated according to Tung)

RADIATION-CHEMICAL PROCESSES IN POLYETHYLENE CONTAINING FILLERS OF DIFFERENT NATURE

V. P. Gordienko, K. A. Suprunenko, V. N. Doroshenko, A. M. Kabakchi
L. V. Pisarzhevsky Institute of Physical Chemistry, the Ukrainian SSR Academy of Sciences, Kiev, USSR

Studies on the effect of ionizing radiation upon crystallizable polymers containing fillers of different nature are promising as to the possibility of controlling polymer radiolysis.

This paper considers the effects of high energy electrons on radiation chemical conversions in both low (LDPE) and high density polyethylene (HDPE) containing dispersed SiO_2 (S_d = 175 m^2/g) and TiO_2 (S_d = 5–7 m^2/g) in quantities ranging from 0.1 to 18 vol.%.

Samples for ESR measurements were irradiated in air at room temperature. The ESR spectrum obtained consists of seven lines and corresponds to allyl radicals (ΔH = 14.5 gauss) /1/. However, the central component of the signal involves radiation induced defects in fillers. In particular, these may be the $\equiv SiO\cdot$ radicals generated in the homolytic decomposition of the aerosil surface groups $\equiv SiO-H$; positive holes, free electrons, trapped by vacancies in the lattice of fillers /1,2/. It should be noted that the concentration of paramagnetic centres in irradiated fillers is too low to affect significantly the mode of ESR signal for a polymeric composition even at high absorbed doses and great amount of fillers.

The determination of concentration of polyethylene stabilized allyl radicals at different absorbed doses has shown the dependence of this value upon the quantity of fillers and the type of polymer. The greatest number of LDPE radicals is observed either for low filled (0.2 vol % SiO_2) or highly filled systems (Fig. 1). The radical concentration for both unfilled polymer and that containing aerosil (up to 10 vol.%) is higher in HDPE than in LDPE (Fig. 1). The same regularity of allyl radical stabilization in irradiated systems was found for LDPE and HDPE containing TiO_2. It is known that the best radical traps are defects within the polymer crystalline structure /3/ and the fillers capable of changing the extent of these defects /4/. The highest concentration of polymer stabilized radicals is observed for those quantities of fillers which correspond to the maximum defect within a crystalline structure.

The difference in the concentration of stabilized radicals in filled system may be also due to the participation of active fragments in the homolytic decomposition of filler surface groups, an increase in the absorbed dose in polymer boundary layers at the expense of energy exchange between components and also the effect of air

oxygen /5/. To eliminate the latter stabilized radicals are thermally deactivated immediately after the polymer has been irradiated /6, 7/. The study on thermal stability of radicals in irradiated filled LDPE at temperatures higher than 293 K has indicated that the radical decay in such systems is more accelerated compared to an unfilled polymer (Fig. 2). The accelerated decay of stabilized radicals of the irradiated polymer in the presence of fillers was observed at higher temperature even for HDPE containing SiO_2 and TiO_2. This phenomenon seems to be related to the accelerated decay of stabilized radicals in the polymer boundary layers which have high defects within the structure and the incompact packing of polymer chains /8, 9/. In the extreme case, the polymer layers adjacent to the filler surface possess an amorphous structure /9/. Such a state of polymer boundary layers, on the one hand, should favour the increased radical stabilization in them at temperatures not higher than 293 K, on the other hand, accelerate their decay at temperatures higher than 293 K – which has been proved by our experiment. Besides, the possibility of thermal deactivation of polymer radicals in the reaction with stabilized radicals of fillers was not ruled out which also should result in accelerated decay of radicals.

IR spectroscopy data obtained allow us to suggest the possibility of direct interaction of polymer molecules with the fillers surface during irradiation. During irradiation of polyethylene containing aerosil it has been found that the absorption bands appear at 1020 and 1270 cm^{-1} and their intensity is increased on increasing the absorbed dose (Fig. 3). This is due to the presence of $\geqslant$Si-O-R and $\geqslant$Si-R groups /10–12/. Therefore, the irradiation of filled systems on the polyethylene basis favours the inoculation of macromolecules to the aerosil surface. This process is likely to proceed via the scheme:

$$RH \rightsquigarrow R^{\cdot} + H \qquad (1)$$

$$\geqslant SiOH \rightsquigarrow \geqslant SiO^{\cdot} + H \qquad (2)$$

$$-Si\overset{O}{\diagup\diagdown}Si\leqslant \rightsquigarrow \geqslant SiO^{\cdot} + \geqslant Si^{\cdot} \qquad (3)$$

$$\geqslant SiO^{\cdot} + R^{\cdot} \longrightarrow \geqslant Si-O-R \qquad (4)$$

$$\geqslant Si^{\cdot} + R^{\cdot} \longrightarrow \geqslant Si-R \qquad (5)$$

Increasing the absorbed dose for polyethylene – TiO_2 systems results in the increase of the absorption intensity at 1200-1400 cm^{-1} and also the band occurrence and the increase in its intensity at 1430 cm^{-1} (Fig. 3), which should correspond to the appearance of the structures of the type – $CH_2-COO^-Ti^+\leqslant$ $\geqslant$Ti-O-C$\leqslant$ /13/ and $\geqslant$Ti-C$\leqslant$ /14/. The polymer-filler bond may seem to be also formed according to the reactions in (1) – (5).

The higher stabilization of polyethylene radicals, a decrease in their thermal stability in irradiated filled polymer and, also, the formation of chemical bonds between polyethylene macromolecules and filler surface should favour changing the extent of radiation crosslinking in systems. Actually, the maximum gel-fraction indicating the extent of polymer intermolecular crosslinking is observed either for a system containing a small amount of fillers (Fig. 4), i.e. for the regions with high stabilization of polyethylene radicals. With 1–5 volt % of fillers for LDPE and 2–5 vol % of fillers for HDPE during irradiation the intramolecular crosslinking is likely to be predominant – which corresponds to the best polymer ordering /4/.

In the formation of cross-links within the irradiated crystallizable polymer the distances between the molecular chain sites are decreased from 4.54 A (intermolecular distances) to 1.53 Å (C-C valence bond distance). Therefore, the chain sites adjacent to the crosslinks proved to be out of the ordered regions which should lead to a decrease in the polymer ordering of the whole irradiated system. The decrease in the cross dimensions of LDPE crystallites with increasing absorbed dose is observed for all systems studied (Fig. 5). However, it is evident that fillers taken in small amounts (0.5–1 vol%) inhibit the decay of polymer crystalline structures while great quantities of fillers sensitize it. Analogous changes take place in studying general ordering and secondary supermolecular polyethylene forms in irradiated systems. Different stability of polyethylene crystalline structures during irradiation is likely to be accounted for by differences in the polymer initial structure and the nature of radiation induced conversions in heterogeneous systems.

The changes in the polyethylene structure included by ionizing irradiation should affect polyethylene properties. Composition materials containing small amounts of fillers irradiated by doses of 30–60 Mrads have the best strength compared to the initial polymer (Fig. 6). Thus, small amounts of dispersed fillers increasing the extent of polyethylene intermolecular crosslinking together with the stability obtained during irradiation of a crystalline structure result in polymer strengthening. Thus, the concentration of stabilized radicals, their thermal stability, the ratio of the extent of intermolecular and intramolecular crosslinking, the number of inoculated molecules, the extent of defect within a crystalline structure and physico-mechanical characteristics may be changed in a crystallizable polymer containing fillers of different nature under irradiation.

References

/ 1/ S. Ya. Psezhecki, "ESR of free radicals in radiation chemistry", Izd. Khimia1972.

/ 2/ P.O. Kinell, A. Lund, T. Vanngard, Acta Chem. Scand., 19, 2113 (1965).

/ 3/ N. Kusumoto, T. Jamamoto, M. Takajanagi, J. Polymer Sci., A-2, 9, 1173 (1971).

/ 4/ V.P. Gordenko et al. Vysokomol. Soed. A17, No 8, 1737 (1975).

/ 5/ M. Doul, "Crystalline polyolefins", "Khimija", 2, 386 (1970).

/ 6/ D.T. Turner, J. Polymer Sci., B1, 2, 101 (1963).
/ 7/ H.V. Kang, O. Saito, M. Dole, J. Am. Chem. Soc., 89, 9 (1967)
/ 8/ Yu. S. Lipatov, Physical chemistry of loaded polymers "Naukova dumka", 1967.
/ 9/ Yu. M. Malinski, Uspehi Khimii, 39, 1511 (1970)
/10/ L. Bellami, Infrared Spectra of Complex Molecules, IL., 1963.
/11/ A.G. Lizogub, Spectral Analysis in Organic chemistry. "Tekhnika", 1964.
/12/ A.I. Akiskin et al. Khim. Vysok. Energii, 7, No.5, (1973).
/13/ M.S. Akutyin, G.M. Ozerov, Vysokomol. Soed. 1, 713 (1959), 8, 2195 (1966).
/14/ N.A. Tsumayevski, Uspekhi Khimii, 32, 1152 (1963).

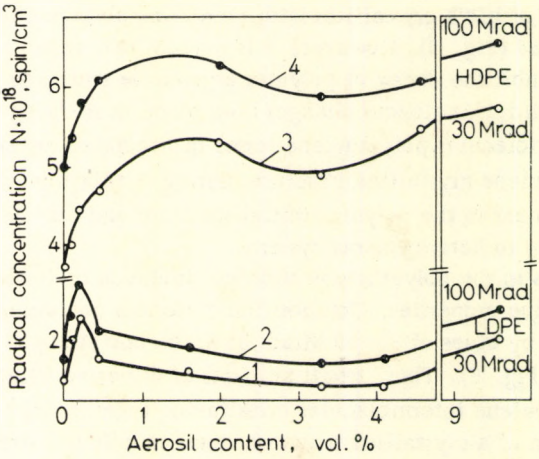

Fig. 1 Dependence of concentration of low density LDPE and high density HDPF polyethylene radicals stabilized at 293 K upon the aerosil content at absorbed doses of 30 and 100 Mrads

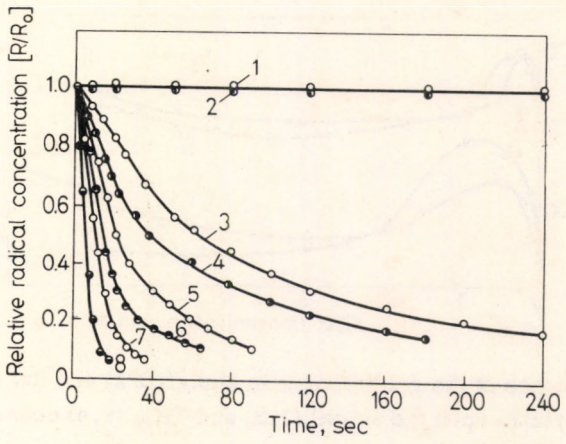

Fig. 2 Dependence of the relative concentration of stabilized radicals in LDPE (1, 3, 5, 7) and compositions with 2% TiO_2 (2, 4, 6, 8) upon time at 293 (1, 2); 348 (3, 4), 368 (5, 6), 388 K (7, 8); absorbed dose = 30 Mrad

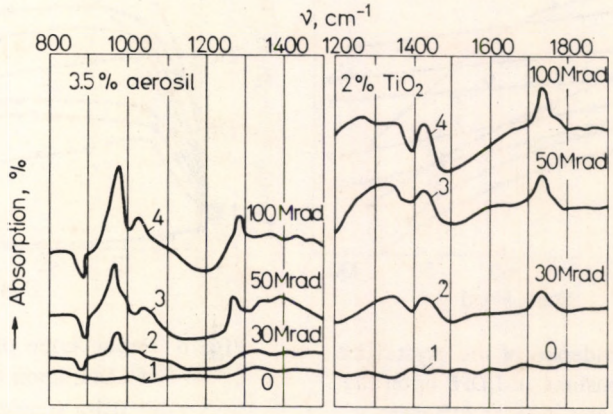

Fig. 3 IR spectra of LDPE containing 3. 5% aerosil and 2% TiO_2 at different absorbed doses in differential recording relative to nonirradiated compositons

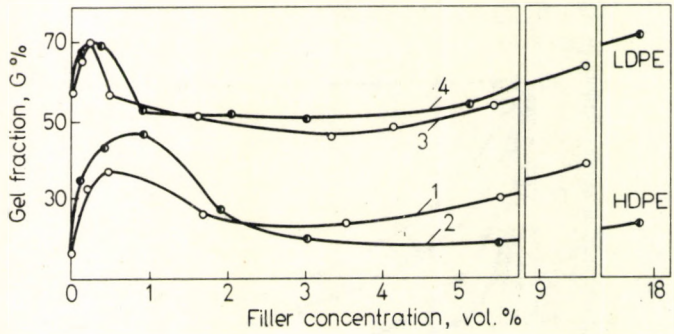

Fig. 4 Dependence of the gel-fractions in high (HDPE) and low (LDPE) density polyethylenes upon the aerosil (1, 3) and TiO_2 (2, 4) concentrations; absorbed dose 10 Mrad

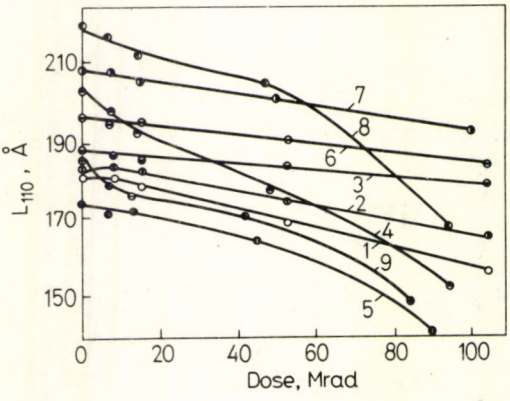

Fig. 5 Dependence of the crystallite dimensions in LDPE upon the absorbed dose at different filler-concentrations: 1) 0; 2) 0.2; 3) 0.5; 4) 4.1; 5) 9.6% aerosil; 6) 0.4; 7) 0.9; 8) 3.0; 9) 5.1% TiO_2

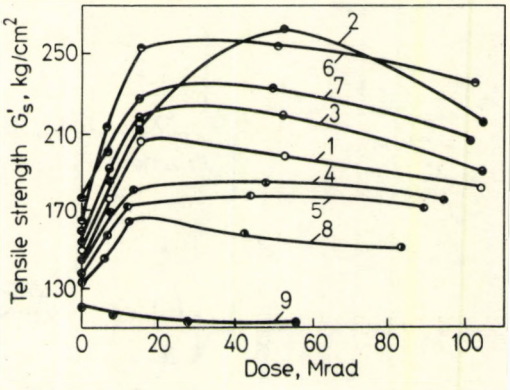

Fig. 6 Dependence of tensile strength of LDPE upon the absorbed dose at filler concentrations, 1) 0; 2) 0.2; 3) 0.5; 4) 4.1; 5) 9.6% aerosil; 6) 0.4; 7) 0.9; 8) 5.1; 9) 17.8% TiO_2

LET EFFECT ON FORMATION AND STABILIZATION OF RADICALS IN POLYMERS

B. K. Pasalsky, Ja. I. Lavrentovich, V. A. Vonsyatzki, A. M. Kabakchi
L. V. Pisarzhevsky Institute of Physical Chemistry, Kiev, USSR

The investigation of the chemical nature of formation and stabilization of primary and intermediate products of radiolysis is of great importance in the radiation chemistry of polymers. Interesting data may be obtained if polymers are exposed to radiation of different linear energy transfer (LET) at low temperatures. The conditions for the stability of primary active particles are created at low temperatures, this favours separating the stages of their creation and following chemical transformation. The use of radiation with different LET has allowed us to change the concentration of the primary particles at the moment of their formation.

In this article the results of kinetical investigation of radical formation, as well as peculiarities of their stabilization, character of radical space distribution and thermal stability in polymers are reported.

The effect of Co^{60} gamma-radiation, protons (7 Mev), deuterons (14 Mev) and alpha-particles (28 Mev) upon polyethylene (PE), polypropylene (PP), polyisobutylene (PIB), polymethylmethacrylate (PMMA), polycaprolactam (PCA) and polyethylene-terephtalate (PETP) has been investigated. Polymer films of different thicknesses have been irradiated in vacuo ($10^{-4}-10^{-5}$ torr) at the temperature of boiling of nitrogen. The methods of irradiation and dosimetry have been described in /1, 2/. ESR spectra have been recorded with the radiospectrometer RE 1301, electronic relaxation characteristics have been determined with a modified device of similar type /3/.

The performed experiments have shown that LET change from 0.2 to 50 Kev/mc does not effect the ESR parameters of polymers irradiated at 77 K (see Table 1). It may be a proof that the observed radicals are primary or intermediate particles arising during physico-chemical stage of radiolysis. Analysis of the ESR spectra has shown the presence of stabilized radicals in many polymers under irradiation formed by the breaking of hydrogen atoms from the main polymer chain. It may be supposed that hydrogen atom formation is a predominant primary effect of polymer irradiation as it takes place in the case of irradiation of individual organic substances.

The kinetic investigation of the radical formation has shown that the mean concentration (C_{av}) of these particles grows linearly with the increase of the absorbed dose in a wide interval. As an example, in Fig. 1 the data for irradiated PE and PCA are shown. On the basis of analogous data obtained for other polymers the radiation

Table 1

ESR spectral parameters of radicals in polymers irradiated by radiation with different LET at 77 K

Polymer	Radical	Number of lines	Width of the spectrum ΔH gauss
Polyethylene	$\sim CH_2-\dot{C}H-CH_2\sim$	6	162
Polypropylene	$\sim C\dot{H}_2-CH(\dot{C}H_2)-CH_2\sim$	4	88
Polyisobutylene	$\sim CH(CH_3)-\dot{C}H-(CH_3)\sim$		
	$\sim C(CH_3)_2-\dot{C}H-C(CH_3)_2\sim$	2	44
Polymethyl-methacrylate	$\sim \dot{C}(COOCH_3)(CH_3)CH_2\sim$	9	92
Polycaprolactam	$\sim CH_2-CO-NH-\dot{C}H-CH_2\sim$	5	80
Polyethylene-terephtalate	ion-radical	1	8

Table 2

Radiation yields at stabilized radicals in polymers

Polymer	Radiation yield of radicals, 1/100 eV	
	Gamma-rays Co-60 LET = 0.2 Kev/mc	Alpha-particles LET = 50 Kev/mc
Polyethylene	2.56	0.56
Polypropylene	2.90	1.60
Polyisobutylene	2.10	0.45
Polymethylmethacrylate	2.20	1.20
Polycaprolactam	0.48	0.48
Polyethyleneterephtalate	0.03	0.02

yields of stabilized radicals were calculated. The results are summarized in Table 2. It may be seen that in many polymers the radiation yield of radicals decreases with the LET rise. But the effect of the LET change is not really apparent if PCA or PETP is irradiated. It may be supposed that in PETP and PCA, the radiation energy undergoes migration from tracks to the bulk before radical formation. According to the data /4, 5/ the energy migration may occur at significant distances, up to 1000 Å. In other polymers the radicals are probably stabilized in the spurs and tracks of charged particles reaching higher concentration in these places than in the bulk. Thus the

Table 3

The spatial distribution of radicals in polymers

Polymer	Gamma-rays Co-60				Alpha-particles			
	Dose Mrad	C_{av}, 10^{-17}	C_{loc}, 10^{-17}	$\frac{C_{loc}}{C_{av}}$	Dose, Mrad	C_{av}, 10^{-17}	C_{loc}, 10^{-17}	$\frac{C_{loc}}{C_{av}}$
Polyethylene	3	500	-	1	22	110	550	5
					174	600	685	1.1
Polyisobu-	1.5	17	74	4.3	50	135	520	3.8
tylene	10	120	150	1.2	210	500	550	1.1
Polymethyl-	6.1	8.6	70.4	8.2	48	27.3	87	3.2
methacrylate	48.8	65	70.4	1.1	160	79	87	1.1
Polycapro-lactam	5	28.3	-	1	15.4	57	-	1
Polyethylene-terephthalate	16	3.85	-	1	41	5.7	-	1

conditions for pairwise interactions of radicals are created. The decrease in radiation yield of radicals with the LET rise may be explained by their partial decay in tracks.

To confirm the foregoing assumption the character of space distribution of the stabilized radicals has been investigated by the concentration broadening and the continuous saturation of the ESR signal.

The ESR spectral line widths in irradiated polymers were found to increase with the increase of absorbed dose or C_{av} of radicals. The broadening of the ESR spectra of irradiated PIB and the dependence of individual line width on C_{av} of radicals are given in Fig. 2. The obtained dependence is described well by the equation

$$\Delta H_1 = \Delta H_0 + A \cdot C_{av},$$

where H_i is the width of the individual ESR line at C_{av}, ΔH_0 – width of the individual ESR line at $C_{av} = 0$. The value of coefficient is 7.0×10^{-20} e · cm^3, it shows that the local concentration (C_{loc}) of radicals is near to the average one /6/. The effect of broadening of the ESR spectral line in PIB becomes distinguishable at the gamma-ray doses above 10 Mrad and the alpha-particle doses above 100–150 Mrad. This may be due to the different space distributions of radicals at low doses.

For the determination of the character of space distribution of radicals the continuous ESR signal saturation method has been employed. As an example, the ESR spectra of the irradiated PIB recorded at different powers of microwave field are shown in Fig. 3. The form of the ESR spectra is evidently independent of the microwave field power, the reduction of the absorption intensity of signals indicates their saturation. Similar effects are observed for ESR signals recorded in other polymers. Thus the use of the continuous saturation method for the determination of relaxation parameters is possible, the spin-lattice relaxation time (T_1) and the spin-packet width (ΔH_s). These parameters were determined form the saturation curves (see Fig. 3) For the determination of C_{loc} of radicals according to the formula $\Delta H_d = 5.4 \times 10^{-20} C_{loc}$ the dependence ΔH_s on C_{av} in the wide interval of concentrations was investigated since $\Delta H_s = \Delta H_0 + \Delta H_d$ where H_0 is a component of ΔH_s which may involve electron–nuclear interactions. Typical ΔH_s versus C_{av} curves are shown in Fig. 4. For PCA, the dependence ΔH_s and C_{av} has a linear character, but for PIB the regions of independence of ΔH_s an C_{av} are observed on the curve. It may be due to stabilization of radicals in microregion (spurs and tracks). The summarized results of the character of the space distribution of radicals in polymers are shown in Table 3. For PE, PIB and PMMA C_{loc} in alpha-particle tracks is higher than the C_{av} in the bulk of the polymer. For PIB and PMMA C_{loc} has been detected under gamma-irradiation. With the growth of dose C_{av} approaches gradually to C_{loc} and at some or dose values $C_{av} = C_{loc}$. One may also see that such concentration levelling occurs more quickly under gamma-irradiation than under alpha-irradiation. The spurs seem to overlap at considerable lower doses than the alpha-particle tracks. On the basis of the data about C_{loc} and according to formula $R = (G \cdot LET/\pi \cdot C_{loc} \cdot 100)^{1/2}$ the radius of the alpha-particle track has been estimated to be 15–20 Å in PIB.

Table 4
Kinetic parameters of thermal decay of radicals in polymers

Polymer	lg Ko		E(eff)., kcal/mol.		Temperature interval, °C
	Gamma-rays	Alpha-particles	Gamma-rays	Alpha-particles	
Polyethylene	-	-	5.0	5.0	223–243
Polypropylene	-	-	5.0	5.0	193–223
Polyisobutylene	-4.3	-3.4	18.0	18.0	203–223
Polymethyl-methacrylate	-7.0	-6.6	20.0	20.0	289–306
Polycaprolactam	-2.0	-2.0	26.0	26.0	293–318

The information of the character of the radical distribution may be obtained from the investigation of the dependence of spin-lattice relaxation time (T_1) on C_{av}. As one may see from Fig. 5, similar change $1/T_1$ with C_{av} is observed for alpha- and gamma-irradiated PCA. But in PE this dependence is essentially different, it may be connected with the irregular radical distribution and a different change of the surrounding matrix, for example, due to crosslinking of polymers.

To confirm the grade of irregularity of the stabilized radical distribution, their thermal decay was examined. As one may see in Fig. 6, the radical decay rate in alpha-irradiated samples is higher than in gamma-irradiated ones for polymers where $C_{loc} = C_{av}$ as well as for PE and PP. For many polymers the radical decay process fits the kinetic equation of second order. The summarized kinetic data of radical thermal decay in polymers are listed in Table 4. One may see that the radical stabilization in tracks changes mostly the value of a pre-exponential factor and has no effect on the effective activation energy.

Thus, one may suppose that in PE, PP, PIB and PMMA at 77 K the energy of radiation is realized for chemical reactions locally in spurs and tracks. In these polymers the formed tracks are stable in time. In other polymers the tracks erode as a result of migration processes at the physico-chemical stage of radiolysis. The data on the character of space radical distribution and thermal decay of radicals presented in the report confirm the results obtained about the LET effect on radiation yields of final products of radiolysis of polymers /7/ and may be interesting for the elucidation of the features of the kinetics and the reaction mechanism in a solid state when the real distribution of radicals should be taken into account.

References

/1/ Ya. I. Lavrentovich et al., Khim. Vys. Energ., 3, 147 (1969).

/2/ B. K. Pasalsky et al., Vysokomolek. soed., 16A, N12, 2762 (1974).

/3/ O. M. Taranucha et al., Teor. and Exper. chimia, N 1, 131 (1968).

/4/ F. Deuton, The report to the XX Congress, IUPAC. Moscow, 12–18 July, (1965).

/5/ H. S. Andreeva et al., Vodorodnaja svjaz, M., "Nauka", (1964), p. 290.

/6/ S. Wyard, Proc. Phys. Soc., 86, 587 (1965).

/7/ Ya. I. Lavrentovich et al., Proc. Third Tihany Symp. Radiation Chemistry, vol. 1, Akadémiai Kiadó, Budapest 1972, p. 871.

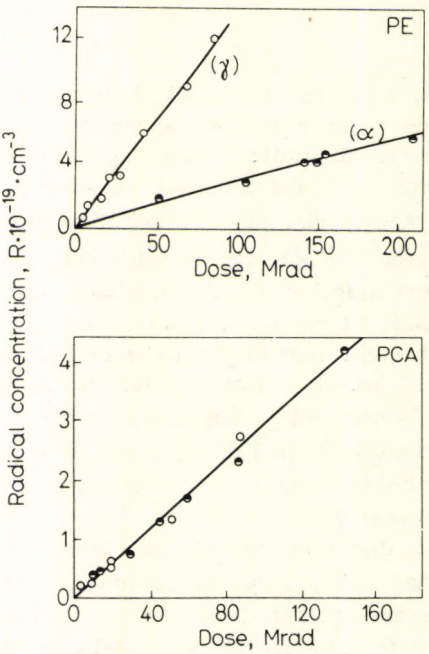

Fig. 1. Dependence of the concentration of stabilized radicals in polyethylene (PE) and polycaprolactam (PCA) on the absorbed dose under irradiation: 0 – gamma-rays Co–60, ◒ – alpha-particles

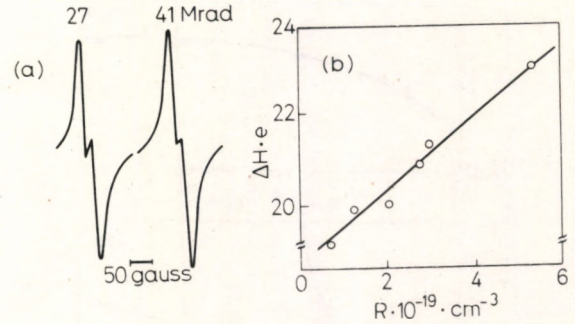

Fig. 2 ESR spectra of radicals (a) and dependence of their individual line width on concentration (b) for polyisobutylene (PIB)

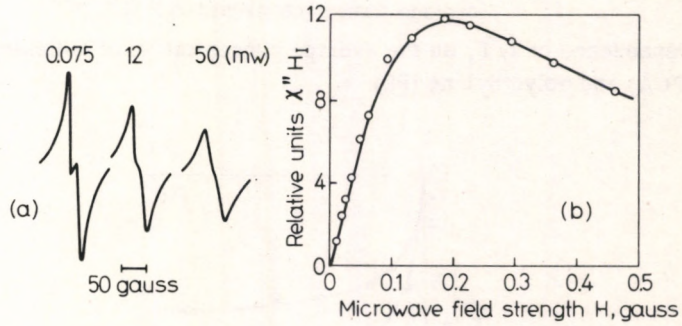

Fig. 3 Change of ESR spectra for polyisobutylene with power of microwave field (a) and the course of ESR signal saturation (b)

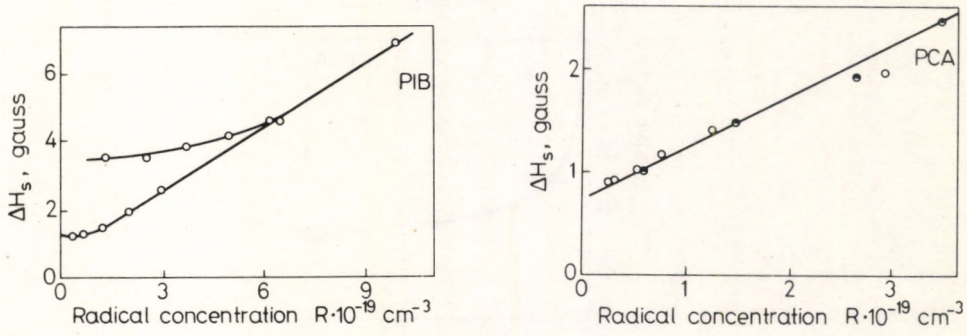

Fig. 4 Dependence of spin-package width of average concentration of radicals in polyisobutylene (PIB) and polycaprolactam (PCA) irradiated by Co-60 gamma-rays (○) and alpha-particles (◒)

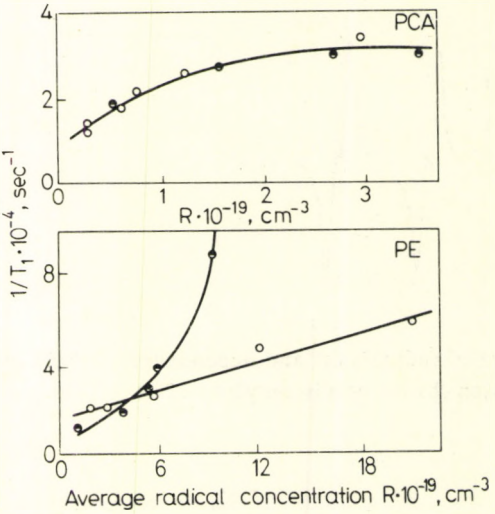

Fig. 5 Dependence of $1/T_1$ on the average concentration of radicals in polycaprolactam (PCA) and polyethylene (PE)

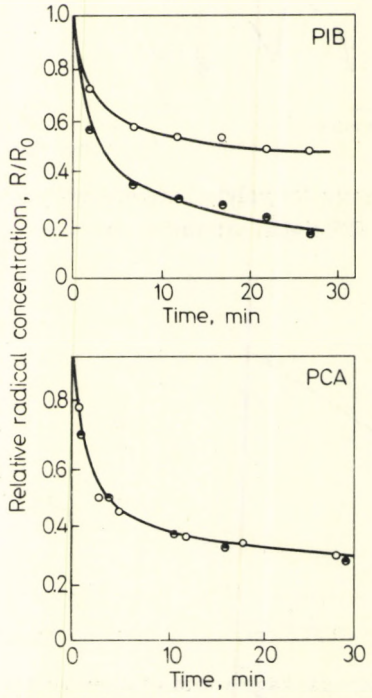

Fig. 6 Kinetic curves of radical decay in polyisobutylene, (PIB) and polycaprolactam (PCA) under irradiation: ○ – gamma-rays Co-60, ● – alpha-particles

RADIATION POLYMERIZATION OF VINYL FLUORIDE AND VINYLIDENE FLUORIDE AND THEIR GRAFTING TO SOME FIBRES AND FILMS

M. K. Asamov, Kh. U. Usmanov, A. A. Yulchibaev, T. S. Syrlybaev,
S. G. Yulchibaeva, A. Valiev
State University, Taskent, USSR

The investigation of the polymerization of fluorine-containing monomers and their grafting to natural and synthetic polymers is of scientific and practical interest due to the valuable physico-chemical properties and applications of fluorine-containing polymers. Thé current work is aimed at investigating radiation polymerization of vinyl fluoride (VF) in emulsion and suspension as well as graft polymerization of VF and vinylidene fluoride (VF_2) to cellulose and its derivatives, natural silk (NS), polyethylene (PE) and polyvinyl chloride (PVC). Polyvinyl fluoride (PVF) obtained by polymerization of VF in suspension and emulsion under Co^{60} gamma irradiation. In contrast to PVF obtained in bulk this product dissolves well at increased temperature in dimethyl formamide, dimethyl sulphoxide and cyclohexanone which enables the determination of its molecular weight, which according to the polymerization conditions, ranges from 132,000 to 440,000. The density of PVF obtained in suspension and emulsion varies from 1.3506 to 1.3856 g/cm^3 whereas for PVF obtained by radiation polymerization in bulk this constitutes 1.3961 g/cm^3.

As seen from Fig. 1 thermomechanical curves of PVF obtained with water of 1:1 ratio are of peculiar form. At 202°C the sample flows and above 240°C there is a decrease in deformation due to splitting hydrogen fluoride from it. The thermomechanical curves of samples obtained with water ratios 1:3 and 1:4 are somewhat different, these do not show a decrease in deformation. As the water ratio decreases the flow temperature tends to increase from 180 to 220°C which is due to raise of the molecular weight of PVF. The thermostability of PVF samples decrease by increasing water content. For samples, for instance, obtained with (VF: water) ratio 1:1, 1:2, 1:3, 1:4, 1:8 and 1:10 the weight losses are 0.7, 1.7, 2.0, 2.8, 3.1, 16.0 and 20.2% respectively (Fig. 2). Graft polymerization of VF and VF to fibres and films was carried out in the gaseous phase at dose rates from 10 to 100 rad/s in wide dose intervals.

Study of the kinetics of grafting VF to various samples of cotton cellulose (CC) shows (Fig. 3) that grafting to mercerized and solvent treated samples proceeds with greater rate than to the initial CC. This seems to be due to the increase of the reactivity of CC with mercerization and solvent treatment. This phenomenon is particularly seen in the case of CC solvent treatment by isoamyl alcohol. In this

case the maximum PVF content in the graft copolymer amounts to 11.9%, whereas for the interval CC it comes to 5.1%.

The data of Fig. 3 show that grafting of VF to CC in the presence of vapours of includating reagents leads to greater increase in the graft copolymer yield. For instance, in the presence of vapours of isoamyl alcohol the maximum PVF content in the graft copolymer is 13.5%. This is due to the fact that on the one hand solvent vapours evoke swelling of fibres which facilitate diffusion of the monomer molecules in them, on the other, radiolysis products of the solvent molecules react through chain transfer to CC macromolecules.

Grafting of VF and VF_2 to NS was also investigated in the present work. Data of Fig. 4 show that at a dose of 90 rad/s and a radiation duration of 16 hours, the average rate of grafting of VF and VF_2 is 0.94 and 0.33%/hr, respectively, i.e. VF grafting efficiency is higher than that of VF_2.

Grafting of VF was performed to diacetate cellulose (DAC) and triacetate cellulose (TAC) at doses of 2, 68 and 100 rad/s. The data obtained show that under similar conditions the greater gain is observed with grafting to TAC (Fig. 5). This is evidently due to the TAC chain rigidity leading to life-span increase of free radicals at the expense of hindering the process of their recombination.

Study of VF grafting to PVC plasticized by mixture of platicizers composed of top alcohol phthalates and tricresyl phosphate (PVC–I) and PVC containing dibutyl phthalate (PVC–II) show that VF is best grafted to PVC–I (Fig. 6).

Study of the kinetics of graft polymerization of VF and VF_2 to fibres and films have thus made it possible to assess the rate of grafting depending upon irradiation dose, polymer nature, monomer and solvent.

The rate of graft polymerization for all systems studied depends upon the dose rate to the power of less than one indicating bimolecular rupture of the growing chains which is peculiar to radical chain-processes. Of certain interest was the investigation of some physico-chemical properties of the synthesized graft co-polymers.

Data of sorption of water vapours by graft copolymers show that grafting of fluorine-containing monomers to CC and its derivatives gives rise to a distinct fall of their sorption capacity as compared with the initial samples (Fig. 7). The sorption capacity decreases with PVF content in the graft copolymers.

The higher hydrophobic effect revealing water-repellent properties is one of the distinctive features of modified fluorine-containing graft copolymers. Waterproof properties may be assessed by the angle of wetting. Data given in Fig. 8 show the change in the boundary angle of wetting depending upon the nature and content of graft PVF. Figure 8 also shows that with increase in the content of graft fluorine-containing polymer the angle of wetting rises. An increase in the hydrophobic properties depends upon the nature of the grafted monomer as well. With similar content of graft PVF and polyvinylidene fluoride (PVF_2) it is a graft copolymer PVF_2 that exhibits greater waterproof properties. Hydrophobic effect, which is due to the presence of graft chains of fluorine polymers with higher light stability, is retained

on ultraviolet illumination during more than 100 hours and when washed over a long period as well. Grafting of VF and VF_2 to CC, its derivatives and to NS leads to their increased resistivity to mineral acids. For instance, graft copolymers with 11.0% and 19.0% of PVF dissolve in 50% HNO_3, 260 and 420 times slower respectively, as compared with initial samples.

Data on rot-resistance of synthesized graft copolymers show that with copolymer content of not less than 8–10% of PVF and 6–7% of PVF_2 no growth of micro-organism is observed on them, whereas micro-organisms grow well on initial and irradiated fibres.

The electron microscopy method was used to study the structure of graft copolymers CC and its derivatives. The study of replicas of the surface and of the inner fibrillar parts of graft copolymers show that as a result of grafting of VF and VF_2 the structure of the surface layer of cellulose fibres smoothes off largely, but there are folds on it in between which globular particles are seen, a factor peculiar to graft chains located mainly in places of fibre-folds. The study of the fragment structure of fibrillar parts of graft copolymers shows that on grafting of VF and VF_2 to CC there occurs some inter-separation of structural elements (fibrils and microfibrils).

The thermal destruction of modified PVC samples in the range of 170–260°C was studied to find the effect of graft fluorine-containing chains on thermostability of graft copolymers. The comparative study of the thermal destruction of the initial PVC and its graft copolymers with PVF shows that thermal decomposition of graft copolymers takes place by 20°C higher (190°C) as compared with the initial one (170°C). At 260°C in vacuum the weight loss of graft copolymers containing 9.4 and 13.2% of PVF constitutes 40.0 and 44.0% respectively, whereas for the initial PVC it is 78% (Fig. 9).

The rise in thermostability is one of the key factors in grafting fluorine-containing polymers. This is particularly valuable for PE. Graft copolymers of PE are characterized by maintaining form at temperatures above crystalline melting. This is also revealed with thermomechanical testing. As seen from thermomechanical curves of the initial, irradiated PE and its graft copolymers given in Fig. 10, the graft copolymers containing 8.0 and 18.1% of PVF are characterized by yield temperatures of 140° and 170°C respectively whereas for the initial PE it is 125°C.

Conclusions

1. The radiation polymerization of vinyl fluoride in emulsion and suspension and also the graft polymerization of vinyl fluoride and vinylidene fluoride to cellulose and its derivatives, natural silk, polyethylene and polyvinylchloride in a dose interval from 10 to 100 r/s was studied. It was found that radiation dose rates and integral doses, nature of polymer, monomer and solvent affect the yield of graft copolymers.

2. It was found that the graft copolymers feature higher thermal, heat, chemostability, waterproof properties and stability to ultraviolet rays and micro-organisms.

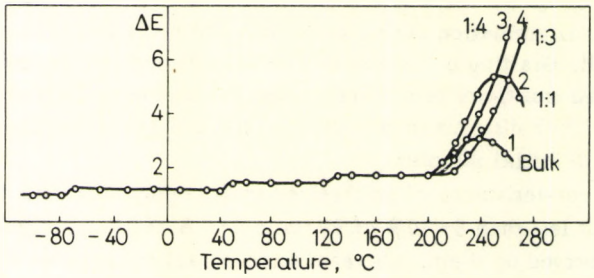

Fig. 1 Thermomechanical curves of polyvinyl fluoride (PVF) samples

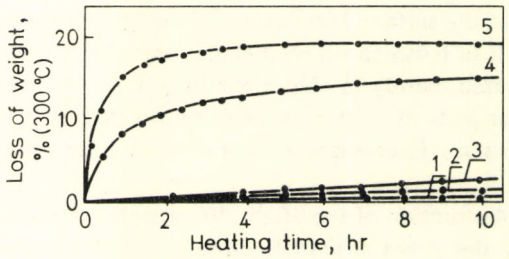

Fig. 2 Kinetics of weight loss of polyvinyl fluoride (PVF) samples at 300°C

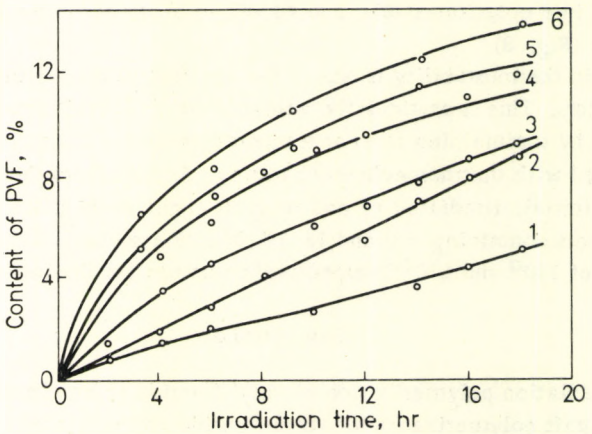

Fig. 3 Kinetics of grafting of vinyl fluoride to various cotton cellulose (CC) samples. (1) The initial CC, (2) mercerized CC, (3) CC solvent treated with dimethylformamide, (4) grafting in the presence of dimethyl formamide vapours, (5) CC solvent treated with isoamyl alcohol, (6) grafting in the presence of isoamyl alcohol vapours

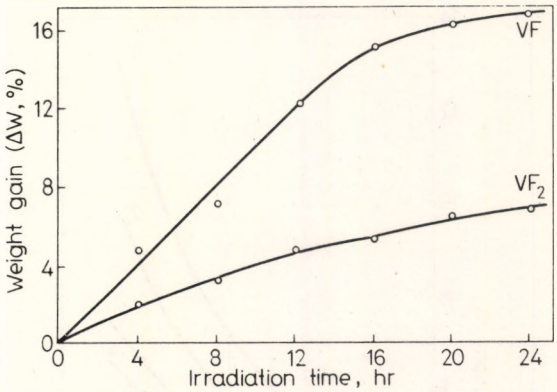

Fig. 4 Kinetics of vinyl fluoride (VF) and vinylidene fluoride (VF_2) grafting to natural silk (NS) in the presence of water vapours at an irradiation dose of 90 rad/s

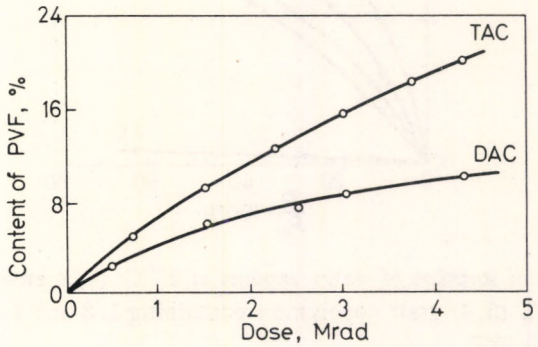

Fig. 5 Kinetics of vinyl fluoride (VF) grafting to diacetate cellulose (DAC) and triacetate cellulose (TAC) at an irradiation dose of 68 rad/s

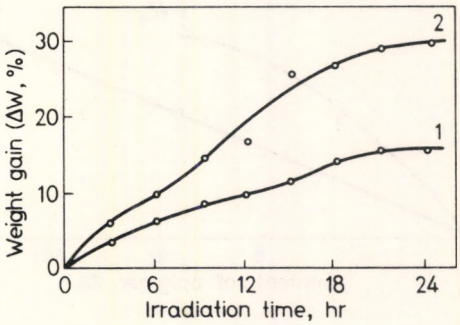

Fig. 6 Dependence of weight gain upon the time of irradiation during graft polymerization of PVC–II(1) and PVC–I(2) to VF at an irradiation dose of 70 rad/s

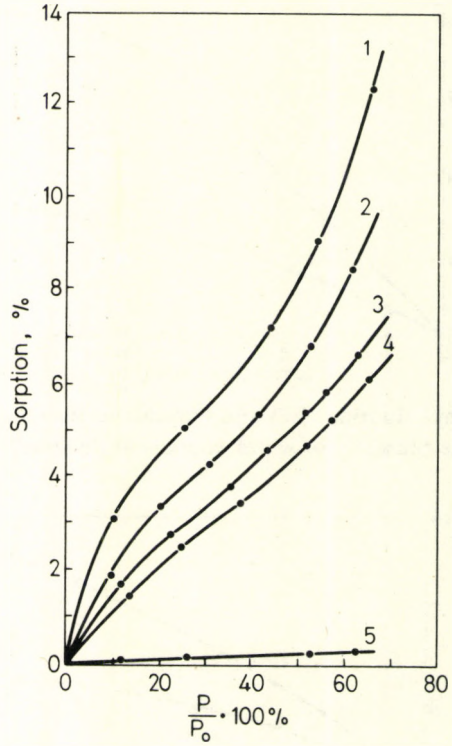

Fig. 7 Isotherms of sorption of water vapours at 25°C: (1) mercerized CC, (2) the initial CC, (3, 4) graft copolymers containing 1.3 and 3.7% of PVF respectively, (5) PVF

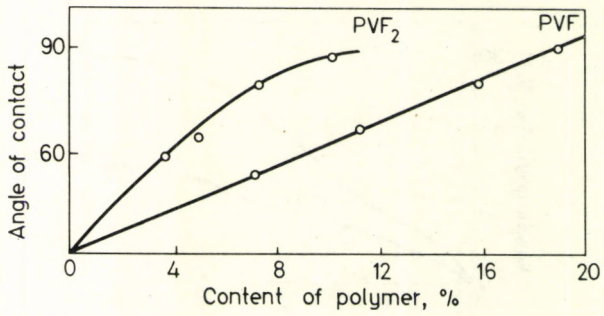

Fig. 8 Dependence of the boundary angle of wetting upon the content of graft polyvinyl fluoride (PVF) and polyvinylidene fluoride (PVF_2)

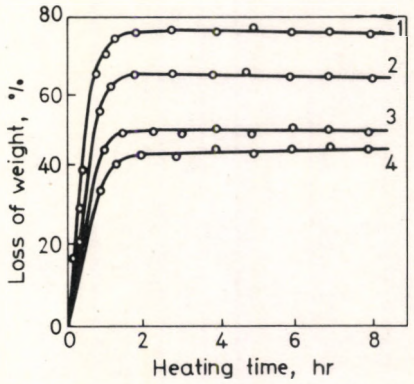

Fig. 9 Kinetics of weight loss of graft copolymers PVC–I to PVF at 260°C in vacuum: (1) PVC–II, (2) irrad. PVC–II, (3, 4) graft copolymers containing 9.4 and 13.2% PVF respectively

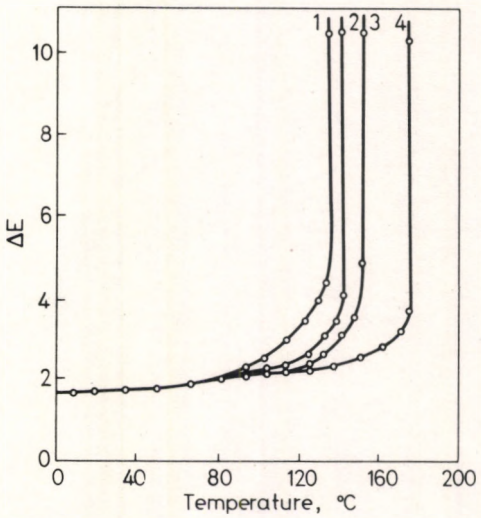

Fig. 10 Thermomechanical curves of graft copolymers PE to PVF: (1) the initial PE, (2) irradiated PE (irradiation dose = 68 rad/s, irradiation time = 18 hrs), (3, 4) graft copolymers containing 8.0 and 18.1% of graft PVF, respectively

PART THREE

AQUEOUS SOLUTIONS

QUANTUM EFFECTS IN RADIOLYSIS AT CRYOGENIC TEMPERATURES

Jerzy Kroh, Andrzej Płonka

Technical University /Politechnika/, Institute of Applied Radiation Chemistry, Łódź, Wróblewskiego, Poland

To estimate the significance of quantum effects in the radiolysis at cryogenic temperatures the decay of trapped electrons, e_t^-, in the γ-irradiated 8 M NaOH glasses was followed in the temperature range 20 - 173 K. Thermal decay of e_t^- in the samples irradiated at 77 K begins at about 113 K and proceeds up to about 173 K with a very small value of the apparent activation energy /1/. Above that temperature a rapid decay of e_t with significant activation energy was observed /2/. This decrease of the apparent activation energy for e_t^- decay with temperature decrease could be taken as the evidence of increasing contribution of electron tunnelling at low temperatures if there was no evidence that going from room temperature to about 170 K the opposite changes are observed /3/. The Arrhenius plot of the rate constant is always concave to the origin.

Trying to understand these phenomena let us look at the DTA results for 8 M NaOH glass/4/ (Fig. 1).

The experimentally observed glass transition temperature, T_g, is equal to about 166 K. It was evidenced /5/ that all glasses show the presence of one secondary relaxation (β process) between 77 K and their respective T_g around which the main relaxation occurs (α process). The secondary relaxation was always seen at a temperature 30 - 50 K below T_g (cf. the onset of thermal decay at 113 K). The intensity of the β relaxation was generally about an order of magnitude smaller than the intensity of the α relaxation and, moreover, the apparent activation energy for β process was 5 - 10 times smaller than that for the α process. Besides, recent dielectric relaxation study /6/ of glass-forming liquids revealed the presence of two relaxation regions at temperatures above T_g. The low frequency relaxation was attributed to the cooperative rearrangement of molecules. The high frequency relaxation, which continues to exist in the glassy state, was suggested to be due to the hindered rearrangement of the molecules encaged by large regions which have been made relatively immobile by the stringency of a cooperative motion. The hindered reorientation of dipoles in liquids at low viscosity has about the same Arrhenius energy as the β process seen in glasses.

Thus it seems that thermal decay of e_t^- is entirely controlled by the relaxation processes proceeding in the matrix. The same processes are likely to determine e_t^- decay upon photobleaching.

Recently we have reported /7/ that in the same range of temperatures one can obtain either negative or positive values of the apparent activation energy for trapped electron decay in the alkaline ice upon photobleaching. Trapped electrons produced by γ-irradiation at 77 K decay upon photobleaching in the temperature range 77 – 173 K, with the negative value of the apparent activation energy are represented in Fig. 2. Trapped electrons produced by γ-irradiation at 173 K decay upon photobleaching, in the same temperature range and under similar experimental conditions, with the positive value of the apparent activation energy are represented in Fig. 3.

To explain these results it is sufficient, in our opinion, to assume that the matrix becomes more relaxed upon warming. A part of e_t^- decays but the majority of it is redistributed into more stable traps upon photobleaching. On the other hand, upon cooling the relaxation processes are stopped and because of this e_t^- decay is slowed down.

This explanation is consistent with very low quantum efficiency of photobleaching reported recently /8/. "Slow delayed" bleaching, pertinent to our conditions, was assumed to be a consequence of thermal relaxation of the medium in response to the fact that each trapped electron to be bleached absorbed, on average, about 100 photons of nearly 2 eV. This energy is dissipated mainly as heat in the vicinity of the traps and local "hot-spots" produced in that way could cause bulk structural changes at which time the reaction of electrons may occur. To support this point of view we have performed some photobleaching experiments below 77 K. In the temperature range between 20 and 60 K the 8 M NaOH glass is virtually rigid but the same phenomena are observed Figure 4 represents trapped electrons produced by γ-irradiation at 20 K decay upon photobleaching with the negative value of the apparent activation energy, while those produced by γ-irradiation at 60 K decay under the same experimental conditions, with the positive value of the apparent activation energy are illustrated in Fig. 5.

Thus in contrast to the results reported by Hamlet and Kevan /9/ for temperature independent photobleaching rate between 4 and 77 K, we have observed the same phenomena as for the previously explored temperature range, i. e. above 77 K. In the temperature range under the present investigations, however, there is no possibility for thermally induced matrix relaxation and this was, according to our opinion, the origin of the observed phenomena. Because of that we believe that matrix relaxation below 77 K, as well as trapped electron redistribution into more stable traps, accompanies the induced optical transitions during which reorientation of water molecules proceeds.

References

/1/ J. Kroh and A. Płonka, Int. J. Radiat. Phys. Chem. 6, 211 (1974).
/2/ J. Kroh and C. Stradowski, Radiochem. Radioanal. Letters 4, 265 (1970).
/3/ G. V. Buxton, F. C. R. Cattel and F. S. Dainton, Trans. Faraday Soc. 67, 687 (1971).
/4/ J. Kroh, A. Płonka and E. Szajdzińska - in press.
/5/ G. P. Johari and M. Goldstein, J. Chem. Phys. 53, 2372 (1970).
/6/ G. P. Johari, J. Chem. Phys. 58(4), 1766 (1973).
/7/ J. Kroh and A. Plonka, Chem. Phys. Letters 28, 186 (1974).
/8/ D. C. Walker and R. May, Int. J. Radiat. Phys. Chem. 6, 345 (1974).
/9/ P. Hamlet and L. Kevan, J. Am. Chem. Soc. 93, 1102 (1971).

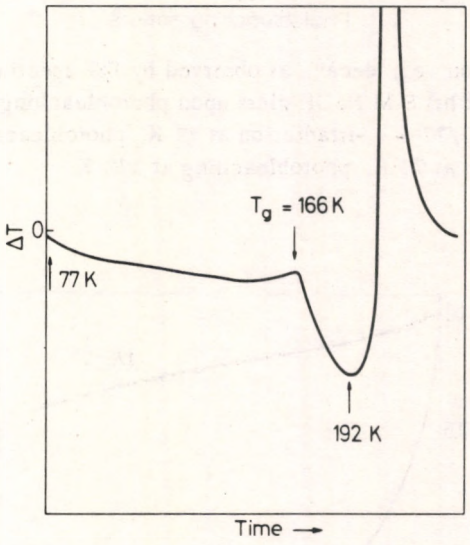

Fig. 1 DTA for 8 M NaOH glass

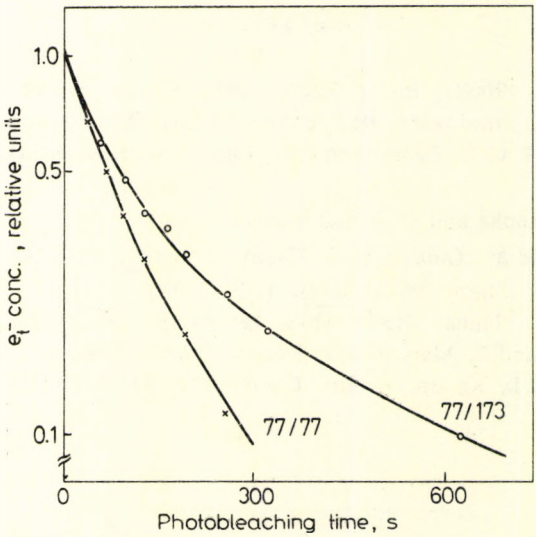

Fig. 2 Trapped electron, e_t^-, decay, as observed by ESR spectra, in γ-irradiated (1.3 Mrad/hr, 1 hr) 8 M NaOH glass upon photobleaching with broad band visible light: 77/77 – γ -irradiation at 77 K, photobleaching at 77 K, 77/173 – γ -irradiation at 77 K, photobleaching at 173 K

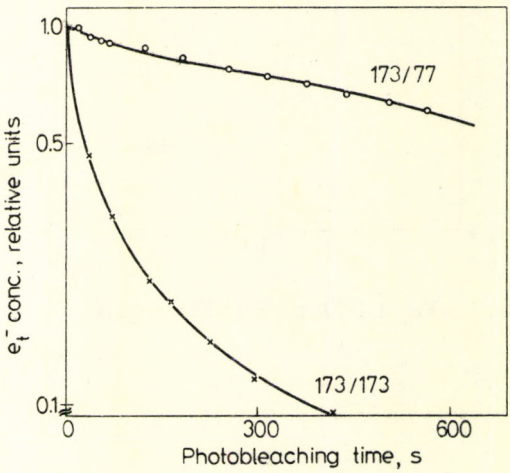

Fig. 3 Trapped electron, e_t^-, decay, as observed by ESR spectra, in γ-irradiated (1.3 Mrad/hr, 1 hr) 8 M NaOH glass upon photobleaching with broad band visible light: 173/173 – γ -irradiation at 173 K, photobleaching at 173 K, 173/77 – γ -irradiation at 173 K, photobleaching at 77 K

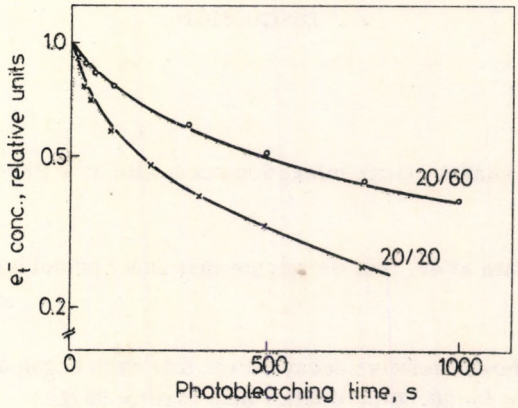

Fig. 4 Trapped electron, e_t^-, decay, as observed by ESR spectra, in γ-irradiated (0, 3 Mrad/hr, 1 hr) 8 M NaOH glass upon photobleaching with broad band visible light: 20/20 – γ -irradiation at 20 K, photobleaching at 20 K, 20/60 – γ -irradiation at 20 K, photobleaching at 60 K

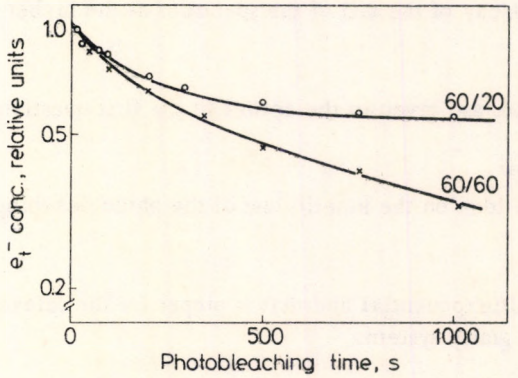

Fig. 5 Trapped electron, e_t^-, decay, as observed by ESR spectra, in γ-irradiated (0, 3 Mrad/hr, 1 hr) 8 M NaOH glass upon photobleaching with broad band visible light: 60/60 – γ -irradiation at 60 K, photobleaching at 60 K, 60/20 – γ -irradiation at 60 K, photobleaching at 20 K.

M. MAGAT

Does in your opinion matrix relaxation occur also at 4.2K?

J. KROH

We have no data at 4K, but we assume that under photobleaching it is possible.

G.R. FREEMAN

Your graphs showed relative decay curves that each began at unity. Would the absolute decay rate for 20/60 be smaller than that for 20/20?

J. KROH

Yes, it starts from the lower value and it ends at the higher value during the same period of time as with the 20/20 curve.

G.R. FREEMAN

If part of the electrons decayed upon warming from 20 K to 60 K, you might be observing the decay of the tail of the spectrum at the higher temperature.

J. KROH

No, the reasons are given in the answer to the first question.

Yu. D. TSVETKOV

Have you any idea on the kinetic law of the photobleaching curves?

J. KROH

Yes, it is multiexponential and that is proper for the relaxation processes proceeding in the glassy systems.

R. KHAIRUTDINOV

Why do you think that the decrease of the apparent activation energy is the evidence of the tunnelling mechanism? I think that there is no relationship between apparent activation energy and mechanism, because apparent activation energy depends on many factors, which can change with temperature.

J. KROH

We do not explain our results by tunnelling mechanism. We quoted that the decrease of the apparent activation energy for e_t^- decay with temperature decrease could be, and really was, taken as the evidence of increasing contribution of electron tunnelling at low temperatures.

THE ELECTRON TRANSFER PROCESSES IN X-IRRADIATED ALKALINE ICE AT 77 K

J. Kroh, J. Mayer, P. Polewoj*
The Institute of Applied Radiation Chemistry 93-590 Łódź, Poland

Introduction

Alkaline ice is well known for its efficiency in trapping electrons generated by ionizing radiation at 77K. The trapped electrons e_t^- have been observed in this glassy matrix over a wide NaOH concentration range i.e. from 5M to 20M /1/. The G-values of e_t^- in glassy alkaline ice are dependent on the previous history of the sample. The glassy matrix represents the thermodynamically unstable state which tends to the stable, crystalline structure /2/. It is worth mentioning that the sodium hydroxide solutions form several crystalline hydrates NaOH x nH_2O where n = 0, 5 - 7 /3/. The $G(e_t^-)$ values increase with rising OH^- concentration up to 10 M (4-6) whereas for more concentrated solution the literature data are inconsistent /1a/.

The aim of the present work is to check the influence of the matrix composition on the yield of the trapped electrons and on the position of wavelength maximum, λ_{max} of their optical absorption spectra. Some preliminary results concerning the e_t^- decay in alkaline ice with varying NaOH concentration in the presence of scavenger are presented too.

Experimental

Sodium hydroxide solutions were prepared either by using Analar NaOH and doubly distilled water or by dissolving Na (analytical grade, Merck) in double-distilled water placed in Ni coated brass vessel /7/. The preparation of the samples was performed in an atmosphere of pure, dry nitrogen. The decay of e_t^- was examined in the presence of $NaNO_3$ (puriss. grade) as a scavenger.

Disc-shaped ice samples of about 2 mm thickness and 14 mm in diameter were prepared at 77K using the method described previously /8/.

The irradiations were carried out with X-rays (60 keV) at a dose rate of about 0,4 Mrad/hr. The optical absorption spectra were recorded using a specially designed low temperature cryostat and Beckman DK-2A spectrophotometer. All the operations with irradiated samples were carried out at 77K in the darkness.

*Permanent address: The Mendeleev Institute of Chemical Technology, Moscow, USSR

Results and discussion

The dependence of e_t^- yield, as expressed by d (O. D.)/dt on NaOH concentration, [NaOH] is shown in Fig. 1. The e_t^- yield for each concentration of NaOH was found from the slope of the plot of e_t^- optical density, O. D. at λ_{max} vs. time of irradiation. It is worth mentioning that the e_t^- -yield is dependent on the storage time of the NaOH solution in glassware at room temperature. Probably the SiO_2 dissolved in alkaline solution /9/ decreases the yield of e_t^-. For example for 20 M NaOH the yield of e_t^- decreases by about 20% after the 8 days of storage in glass vessel as compared with the sample prepared from fresh solution.

The shape of the curve shown in Fig. 1 is almost the same as obtained by Kevan /5/ using the EPR method. The e_t^- optical absorption spectra for various NaOH concentrations are shown in Fig. 2. It is evident that λ_{max} shifts towards longer wavelengths with increasing [NaOH] and also the spectrum becomes broader. The dependence of λ_{max} on [NaOH] is shown in Fig. 3. The minimum value of λ_{max} = 571. 6 $\pm$ 1. 3 nm was found for [NaOH] $\simeq$ 8 M. The λ_{max} of e_t^- absorption in pure ice is also shown for comparison.

The electrons trapped in concentrated NaOH solutions ([NaOH] = 18. 8 M) are unstable at 77 K even in pure matrix. The storage of such irradiated glassy samples at 77 K in dark causes the original absorption (measured 4 min. after irradiation) to disappear at long wavelength side (Fig. 4). This is accompanied by the blue shift of the λ_{max}. This process is faster for less concentrated NaOH solution, i. e. 17. 2 M and 15. 3 M. The e_t^- are stable in 8 M NaOH at 77 K over about 8 hours. In this matrix similar shift of e_t^- band was observed in the ms time scale using pulse radiolysis technique /10/.

In the presence of scavenger the e_t^- decay in alkaline matrix at 77 K is commonly attributed to quantum-mechanical tunnelling /10-17/. The e_t^- decay curves in the presence of 0. 05 M $NaNO_3$ for X-irradiated 8 M and 17. 5 M NaOH are shown in Fig. 5. The initial e_t^- is lower and the observed decay faster for higher concentration of NaOH. In contrast to previous results /12, 13/ the λ_{max} value does not change appreciably during the e_t^- decay in 8 M NaOH. The evidence has been found that the photobleaching of the sample by the light of spectrophotometric lamp can accelerate the e_t^- decay in the presence of a scavenger.

The properties of e_t^- depend on the composition of the alkaline matrix. The rough analysis of the results presented strongly suggests that the electrons stabilized in less concentrated solutions, [NaOH] $<$ 8-10 M, and in more concentrated ones, [NaOH] $>$ 10 M, behave in a different way. There seems to be a transition concentration range i. e. 8-10 M where a minimum value of λ_{max} is observed (Fig. 3) and the dependence of e_t^- yield vs. [NaOH] changes its slope (Fig. 1). The e_t^- optical absorption spectrum for concentrated solution shifts towards shorter wavelength during the storage at 77 K. In addition the electrons in such a matrix are very reactive towards scavengers. The observed results are very difficult to explain as based on the currently accepted model of electron traps in aqueous systems /1, 18/. According to this model the electron trap in alkaline

ice consists of water molecules. The analysis of certain physical properties (vapour pressure, compressibility) and thermodynamic data (integral and differential heat of solution) of the aqueous NaOH solutions at 293K /3/ strongly suggests that in the NaOH concentration range 8-10 M the microstructure of the liquid undergoes substantial changes. It may be important even at 77K if one takes into account that the alkaline glass is produced by rapid cooling of liquid sample. In the presence of an electrolyte the water molecules are compressed /19/ causing the "water walled" trap to become smaller, due to the loss of free volume. Hence λ_{max} decreases as compared with pure ice. The red shift of λ_{max} for concentrated NaOH solution, ([NaOH]>10 M, may be explained assuming the formation of new kind of traps probably involving NaOH molecules, eg. via hydrated pairs $[Na^{+}\ddot{-}e^{-}]_{aq}$ as suggested by Shubin et al. /20/ in order to explain the results of pulse radiolysis of concentrated alkaline solutions at room temperature.

References

/1/ (a) A. K. Pikajev, "Solvated electron in radiation chemistry" ed. by "Nauka", Moscow, 1969 (in Russian)

(b) D. Schulte-Frohlinde and K. Vacek, "Radiation Chemistry of Aqueous Frozen Solutions" in Current Topics in Radiation Research ed. by M. Ebert, A. Howard, North-Holland, London, 1969.

/2/ P. P. Kabeko, Amorphous materials (in Russian), Publishing House of the Acad. Sci. USSR, Moscow, 1952.

/3/ Gmelins Handbuch der Anorganischen Chemie, System nr 21, Erd. Bd. Lfg. 2, 1965, pp. 847-875.

/4/ P. N. Moorthy, L. J. Weiss, Adv. in Chem. Series 50, 180 (1965).

/5/ L. Kevan, J. Phys. Chem. 69, 1081 (1965).

/6/ K. Eiben and D. Schulte-Frohlinde. Z. Phys. Chem., Neue Folge, 45, 20 (1965).

/7/ C. A. Brusilovskii, Zavodskayn Laboratoriy a 24, 1203 (1958).

/8/ J. Kroh, Cz. Stradowski, J. Mayer, Radiochem. Radioanal. Lett. 2(4), 209 (1969).

/9/ S. K. Drubova, Glass for chemical laboratories (in Russian), Nauka, Moscow, 1965.

/10/ J. Kroh Cz. Stradowski, Proceedings of the Fifth International Congress of Radiation Research, ed. by O. F. Nygard, H. I. Adler, W. K. Scinclair. Academic Press N. Y., 1975.

/11/ B. G. Ershov and E. L. Tseitlin, Khim. Vys. Energ. 4, 186 (1970).

/12/ K. I. Zamaraev, R. F. Khairoutdinov, Chem. Phys. 4, 181 (1974).

/13/ J. Kroh, Cz. Stradowski, Int. J. Radiat. Phys. Chem. 5, 243 (1973), 7, 23 (1975).

/14/ J. R. Miller, Chem. Phys. Lett, 22; 180 (1973), J. Phys. Chem., 79, 1070 (1975).

/15/ F. S. Dainton, M. J. Pilling and S. A. Rice, Faraday Trans. II, 71, 1311 (1975).

/16/ E. J. Marshall, M. J. Pilling and S. A. Rice, Faraday Trans. II, 71, 1555 (1975).

/17/ M. J. Pilling, S. A. Rice, Faraday Trans. 71, 1563 (1975).

/18/ F. S. Dainton Berichte der Bunsen Gesellschaft, 75, 608 (1971).

/19/ U. A. Dibrov, V. P. Masozec, R. P. Matveeva, Zh. Prikl. Khim. 37, 29 (1964)

/20/ (a) W. N. Shubin, L. F. Slepnova, W. D. Majboroda, Int. J. Radiat. Phys. Chem. 7,371 (1975).

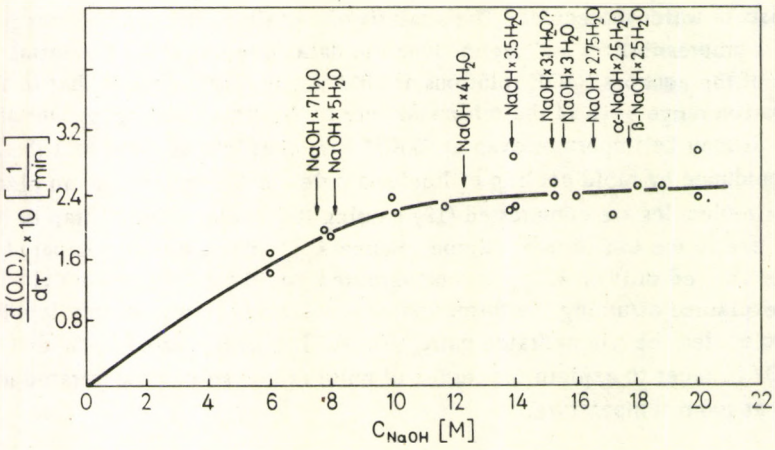

Fig. 1 The dependence of d (O. D.)/dt vs. [NaOH]. The optical density O. D. of e_t^- was measured 4 min. after the end of irradiation at λ_{max} of optical absorption spectrum. The arrows indicate the [NaOH] corresponding to sodium hydroxide hydrates

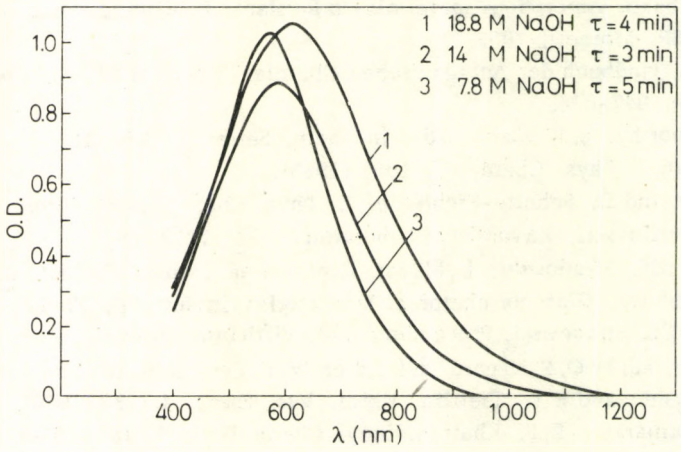

Fig. 2 The e_t^- optical absorption spectra for various NaOH concentrations

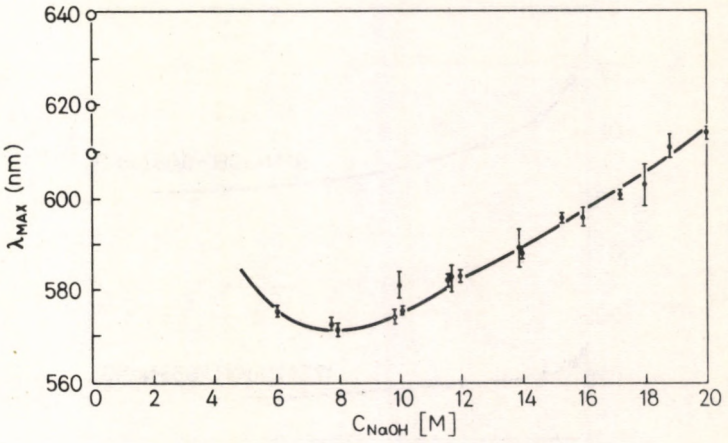

Fig. 3 The dependence of λ_{max} of e_t^- absorption spectrum vs. NaOH. The spectra were measured 4 min after the end of irradiation. The level of confidence 0.9. o indicates the λ_{max} of e_t^- optical spectrum for pure ice /1/

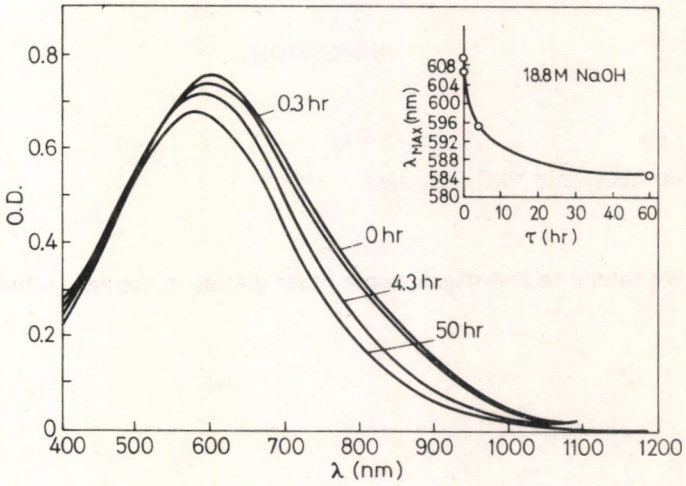

Fig. 4 The influence of storage time of the sample at 77K on the position of e_t^- absorption spectrum for 18.8 M NaOH matrix. Inset: The dependence of λ_{max} of e_t^- optical spectrum on storage time of the sample at 77K, [NaOH] = 18.8 M.

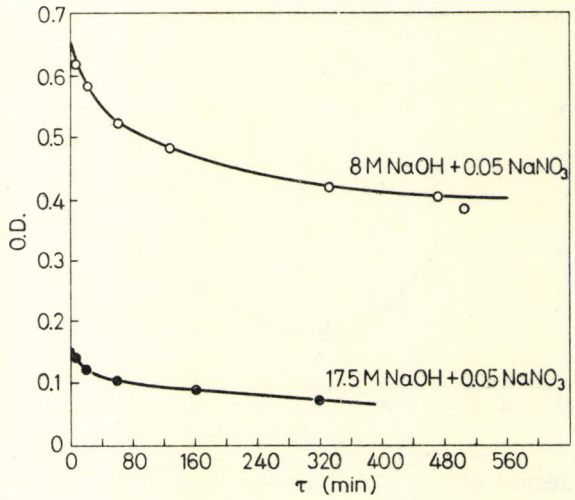

Fig. 5 The $e_{\tilde{t}}$ decay in the presence of 0.05 M $NaNO_3$ in alkaline matrices of different composition at 77 K

DISCUSSION

A. K. PIKAEV

Did you study only NaOH glasses?

J. KROH

Yes. We intend to investigate some other glasses in the near future.

SPECTRAL SENSITIVITY OF PHOTOCONDUCTIVITY EFFECT IN FROZEN ALKALINE SOLUTIONS

Jan Grodkowski, Zbigniew Paweł Zagórski
Department of Radiation Chemistry, Institute of Nuclear Nesearch, Warsaw, Poland

Introduction

The motivation of this paper consisted of the attempt to explain energy levels of trapped electrons in a polycrystalline matrix of 2N NaOH. We have found previously /1, 2/ that trapped electrons may be transferred by illumination to the conductivity band giving rise to a measurable electric current. Spectral response of the photoconductivity seemed to be close to the absorption spectrum of trapped electrons, as was found in glassy 10M NaOH /3/. This paper presents more precisely the character of this relationship for 2N NaOH, after normalization of illumination conditions, in particular the wavelength of the bleaching light.

Experimental

The principal part of the measuring apparatus was described previously /1/. Spectral investigations were performed with the set of interference filters IF (Carl Zeiss, Jena, GDR). Particular filters were checked on the spectrophotometer SP-1800 (Unicam, England). The source of bleaching light here was a tungsten lamp 750 W (Narva, GDR). This lamp was calibrated against a standard light source of known energy distribution. All experimental points are therefore referred to a constant number of quanta.

Results

Figure 1 presents the spectral dependence of photocurrent in arbitrary units for 2M NaOH after irradiation with a dose of electric field: 4 and 6 kV/cm.

Figure 2 shows the same dependence for the sample which was partially, in succession bleached. As before, 2M NaOH was used, the radiation dose was 2 krad, the field gradient 4 kV/cm.

Figure 3 shows that electron irradiation (10 MeV from the linear electron accelerator LAE 13/9 in our Institute) gives similar effects – qualitatively identical (the same λ_{max}) and quantitatively almost the same. Doses were 2 krad and 100 krad (50 pulses delivered in 30 seconds). As in previous measurement after γ irradiation

/2/, there was no linear dependence of the integrated current on the irradiation dose, As a matter of comparison, Fig. 4 shows results on glassy 15 M NaOH on the same bleaching facility, after 10 krad. One has to note the very low level of the effect. (Arbitrary units of current are the same in all figures.)

These results show that there are substantial differences between the positions of maxima in both media: for a glassy one ca 600 nm and for a crystalline one ca 500 nm.

Even larger differences occur in the intensity of the effect. The question arose to what extent a higher internal absorptivity of the polycrystalline sample (in comparison to the glassy one) is responsible for these differences, An investigation of self-absorption of polycrystalline samples made in this laboratory /4/ by the thermoluminescent method indicates that the real optical path in such media may be by one order of magnitude or more larger than the one expected from the geometrical shape and size of the sample.

A study was performed on the attenuation of light in frozen 2M NaOH. The photocurrent is related linearly to the intensity of bleaching light in the whole 400-800 nm spectrum. An equivalent of absorption spectrum of trapped electrons was obtained by changing the thickness of the sample over electrodes. As the reference, a sample was taken in which the thickness of the layer over the level of electrodes was practically nil. The absorption effect was particularly clear for layers of 3-5 mm thickness and doses over 15 krad. Results are shown in Fig. 5, in which O. D.'s are plotted.

Discussion and conclusions

2M frozen NaOH solution at 77 K is a matrix of complex structure and texture which is less known than the so called glassy one. Dissipation of light in 2M NaOH is different from that in the 5M NaOH sample. The paper /4/ mentioned above, concerning the increase of the light path suggests a factor of 10. Taking the yield of trapped electrons in 2 M NaOH to be equal to G = 0.4 /5, 6/ and using the molar absorption coefficient $\varepsilon = 2 \times 10^4\ M^{-1}\ cm^{-1}$ /7/, the results in Fig. 5 give also the factor of 10 as the increase of the real light path.

Spectra published in the literature characterize e_t^- in glassy 10 M NaOH /7/ with a maximum at 585-590 nm and in crystalline pure ice /8/ with a maximum at 640 mm.

The shape of our spectrum in Fig. 5 is qualitatively similar to the spectrum of e_t^- trapped in a glassy sample, but it does not explain the different character of spectral dependence of photoconductivity in polycrystalline and glassy /3/ samples. The most probable explanation seems to be the different structure of energy levels of electrons trapped in a glassy and crystalline alkaline matrix. Similar dependence of photocurrent maximum shift was observed in other glassy frozen aqueous systems /9/. A coincidence between spectral response of photocurrent with the spectrum of

trapped electrons was found only in 10 M NaOH and the effect was explained by a strong polarization of water molecules by OH^- ions.

The situation in the 2 M NaOH solution seems to be an intermediate case between pure ice where an existence of the bound excited state of trapped electrons was found /8/ and a glassy alkaline matrix where direct transition of electrons from the ground state to free state in the conduction band /3/ occurs. The existence of photoconductivity in the whole investigated spectrum suggests that the excited state of trapped electrons is located close to the conduction band and may autoionize, or that the observed effect results from the distribution of different types of traps which have the possibility of bound-bound or bound-free optical excitation.

References

/1/ Z. P. Zagórski, J. Grodkowski, Z. Zimek, Radiochem. Radioanal. Letters 1, 305 (1969).

/2/ Z. P. Zagórski, J. Grodkowski, Proc. Third Tihany Symp. Rad. Chem., Akadémiai Kiadó, Budapest, pp 1413-1420, 1972.

/3/ I. Eiselc, L. Kevan, J. Chem. Phys. 53, 1867 (1970).

/4/ Z. P. Zagórski, Z. Zimek, S. Sitkowska, Int. J. Radiat. Phys. Chem. 4, 65 (1972)

/5/ P. N. Moorthy, J. J. Weiss, Phil. Mag. 10, 659 (1964).

/6/ L. Kevan, J. Phys. Chem. 69, 1081 (1965).

/7/ H. Hase, L. Kevan, J. Chem. Phys. 54, 908 (1970).

/8/ Keisuke Kavabata, J. Chem. Phys. 55, 3672 (1971).

/9/ Shoji Noda, L. Kevan, J. Phys. Chem. 78, 2454 (1974).

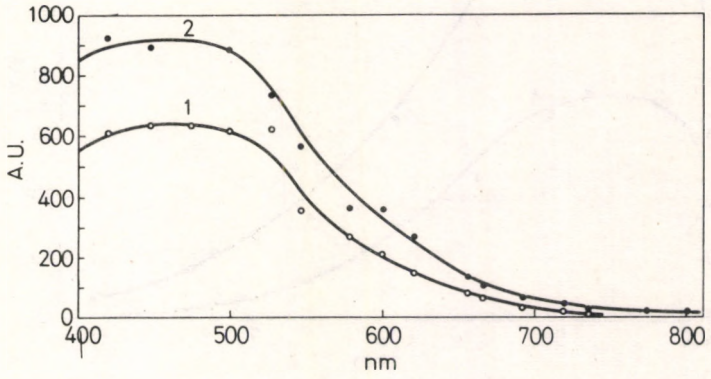

Fig. 1 The dependence of photocurrent on the wavelength of bleaching light in γ irradiated (2 krad) 2 M NaOh. Electric field 1) 4 kV/cm, 2) 6 kV/cm

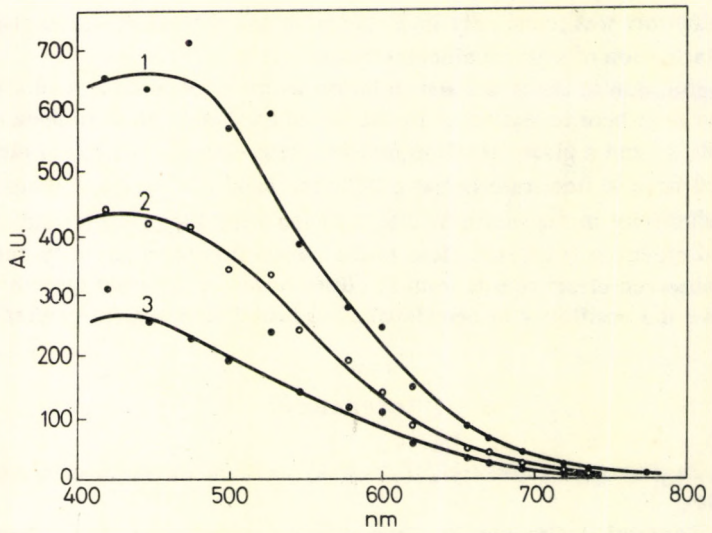

Fig. 2 The dependence of photocurrent on the wavelength of bleaching light in γ irradiated (2 krad) 2 M NaOH subsequently partially bleached (Field 4 kV/cm)

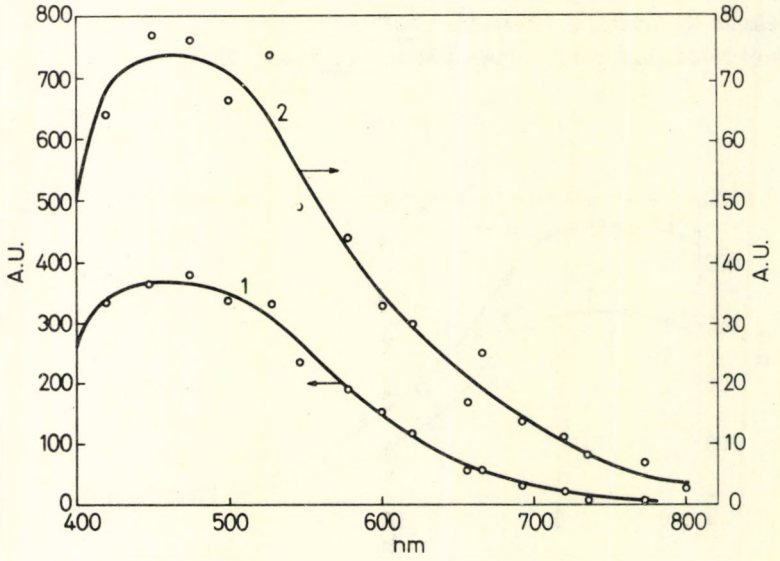

Fig. 3 The dependence of photocurrent on the wavelength of bleaching light in electron beam irradiated 2M NaOH 1) 2 krad 2) 100 krad (Field 4kV/cm)

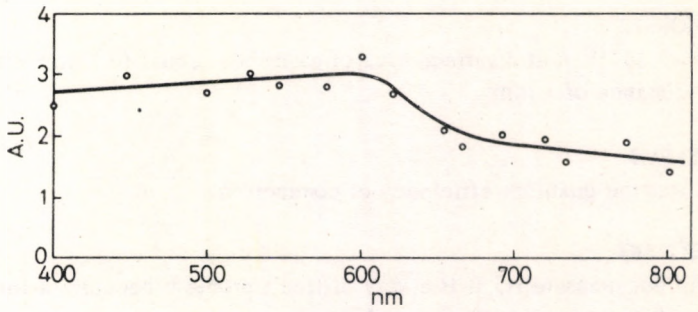

Fig. 4 The dependence of photocurrent on the wavelength of bleaching light in 15 M NaOH – (2 krad, 4 kV/cm)

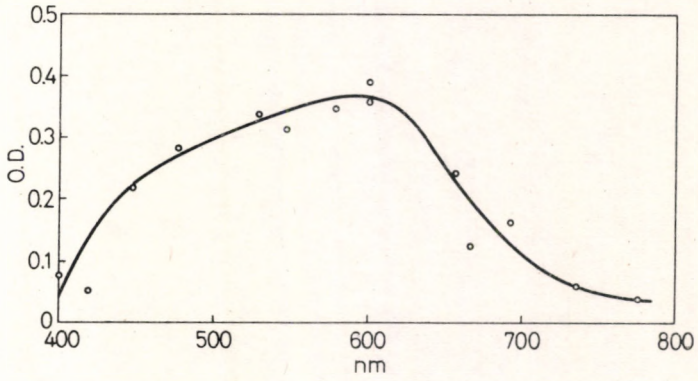

Fig. 5 Absorption spectrum of γ irradiated (18 krad) 2 M NaOH, 3 mm thick layer of the sample, field 4kV/cm

DISCUSSION

A. K. PIKAEV

Have you any data on the structure of your so called polycrystalline samples?

Z. P. ZAGÓRSKI

No, we have not. No direct measurements have been done on the structure of those samples.

G. R. FREEMAN

What were the magnitudes of the photocurrents?

Z. P. ZAGÓRSKI

10^{-13} to 10^{-10} A at a surface area of electrodes equal to 1 cm^2 and with the electrode-distance of 1 mm.

G. R. FREEMAN

What was the quantum efficiency of conduction?

Z. P. ZAGÓRSKI

We did not measure it. It is a very difficult problem because of the internal reflections of the polycrystalline sample.

SPATIAL DISTRIBUTION OF TRAPPED ELECTRONS AND O^- IN β- AND γ-IRRADIATED NaOH GLASSES AT 77K

A. M. Raitsimring, R. I. Samoilova, V. M. Moralev, Yu. D. Tsvetkov

Institute of Chemical Kinetics and Combustion, Institute of Inorganic Chemistry, Siberian Branch of the Soviet Academy of Sciences, Novosibirsk, USSR

In irradiated alkaline glasses electrons and radical-ions are observed to become trapped at 77K. According to the data presented in Ref. /1/ the generation mechanism for these particles can be described by the reactions:

$$H_2O \longrightarrow e_m + H_2O^+ \quad (1)$$

$$H_2O^+ + H_2O \longrightarrow H_2O + H_2O^+ \quad (2)$$

$$H_2O^+ + OH^- \longrightarrow H_2O + OH \quad (3)$$

$$OH \longrightarrow O^- + H^+ \quad (4)$$

$$e_m + T \longrightarrow e_{tr} \quad (5)$$

It follows from the scheme that the spatial distribution of trapped electrons is to be determined by their path lengths before trapping, and that of the O^- radical-ions by the number of charge transfer acts from H_2O^+ to H_2O. There are no data available on the spatial distribution of O^-, and only contradictory ones for that of e_{tr} in the literature. In Refs /2, 3/ the local concentrations of e_{tr} being equal to $10^{19} cm^{-3}$ were determined in γ-irradiated alkaline ice by the stationary saturation method.

The comparison of decay reactions for e_{tr} generated by UV-source and γ-rays has enabled the investigators to infer a uniform spatial distribution /4/. An indirect estimation of local concentration values for e_{tr} in these systems can also be carried out using the data of photocurrent measured as a function of the thickness of the layer frozen on a photocathode /5/. It gives $C^1 \sim 10^{16}$ cm^{-3}.

In the present work the electron spin echo method (ESE), sensitive to dipole-dipole interactions of paramagnetic particles, was employed to study the spatial distribution of paramagnetic centres in irradiated substances. Local concentrations are possible to be determined by the ESE method, analysing the laws of phase relaxation caused either by the spectral /7/ or instantaneous /8/ diffusion mechanisms. The latter, possessing a number of advantages, was employed in the present work.

Experimental and results

9M frozen aqueous solutions of NaOH were studied. T_2O was introduced into the solutions to emit β-particles, the dose rate being 0.16×10^{20} eV cm^{-3} hr^{-1}. Other samples were subjected to Co^{60} γ-rays at 77K, the dose rate being 0.4×10^{20} eV cm^{-3}hr^{-1}. To determine the absolute concentrations of e_{tr} the ESR technique and low temperature spectrophotometry /9/ were used. Ditches for optical measurements were 1 mm long, the extinction coefficient for e_{tr} was assumed to be 1.4×10^{4}l mol cm^{-1} at $\lambda = 585$ nm /1/. The absolute concentrations of O^- were measured by the ESR technique. The ESR spectra were registered by an X-band spectrometer at microwave power received by a cavity of ~ 0.4 μ M.

The phase relaxation rate of trapped electrons was measured by the two-pulse ESE technique at 77K. At this temperature O^- radical-ions have too short spin-lattice relaxation time ($T_1 \sim 10^{-7}$ sec) to be measured by an ESE-spectrometer used in the experiments /6/. At 4.2K T_1 time for O^- increases up to about 10^{-3} sec, which makes possible to study the phase relaxation of the paramagnetic centres. The design of a helium cryostat used for ESE measurements was described in Ref. /10/.

The e_{tr} accumulation kinetics for β-irradiated samples are given in Fig. 1. The accumulation curve is seen from Fig. 1 to be distinctively bell-shaped /11/. Similar curves have been obtained for γ-irradiated samples. A maximum e_{tr} concentration in β-irradiated samples is $\simeq 1.5 \times 10^{18}$ cm^{-3} at the absorbed dose being $\simeq 2 \times 10^{20}$ eV cm^{-3} and that of in γ-irradiated samples reaches 2.9×10^{18} cm^{-3} at the same absorbed dose. G values of O^- (in 1/100eV) in β-irradiated samples estimated from the initial parts of the accumulation curves are 2.7 ± 0.3 and 3.7 ± 1.2, respectively. The value of G_e obtained spectrophotometrically is 2.9 ± 0.3. It is consistent with the measurements performed by the ESR technique.

Simultaneously with the measurements of average e_{tr} and O^- concentrations a dipolar broadening of the ESR line for these paramagnetic centres for different average concentrations was defined by the ESE technique. The method of dipolar broadening measurements is given below.

The kinetics of phase relaxation for trapped electrons is described by the relation

$$v(2\tau) = v(0) \exp(-2b_m\tau - m\tau^2) \qquad (1)$$

In this equation the quadratic term ($-m\tau^2$) depends on electron-nuclear interaction /12/, and m is independent of concentration of the paramagnetic centres. A linear plot of two-pulses ESE signal decay is given in Fig. 2. In these coordinates the tangent of the slope gives the value of $m = 2.9 \times 10^{-11}$ sec^{-2}, and the intersection of the Y-axis gives the value of the phase relaxation rate, $2b_m$.

Phase relaxation caused by the instantaneous diffusion mechanism is determined by a dipole-dipole interaction only between the spins excited by microwave

pulses. Thus, for example, in the case of e_{tr} phase relaxation the dipole-dipole interaction between a trapped electron and O^- does not contribute to the e_{tr} ESE signal decay. This is so since due to their different g-factors, the lines of the ESR spectrum for these paramagnetic centres are separated by 70 Oe, whereas the amplitudes of the microwave pulses are in the range of 5 to 0.5 Oe. This excludes the possibility of their simultaneous excitation. We have shown /13/ that the dependence of the phase relaxation rate (b_m) observed upon the dipolar broadening Δ for the spin flip-flop process rates $W < 10^5 sec^{-1}$ is

$$b_m = \Delta \cdot \langle \sin^2 \frac{\Theta}{2} \rangle_{g(\omega)} \qquad (2)$$

where $\Theta = \gamma H_1 t_u$. Here t_u and H_1 denote duration and amplitude of the microwave pulses, respectively, and $g(\omega)$ is the line shape of the trapped electrons /14/,

$$g(\Delta\omega) = \frac{1}{\sqrt{\pi}\cdot\delta} \exp\left\{ - \frac{\Delta\omega^2}{2\delta^2} \right\} \qquad (3)$$

where δ is the Gaussian line shape parameter equal to 5 Oe.

The procedure of finding out a portion of the spins being excited, $\left\langle \sin^2 \frac{\Theta}{2} \right\rangle_{g(\omega)}$, is reduced to calculation of the integral

$$\left\langle \sin^2 \frac{\Theta}{2} \right\rangle_{g(\omega)} = \int_{-\infty}^{+\infty} \frac{\sin^2 \left[1/2\, t_u \sqrt{\Delta\omega^2 + (\gamma H_1)^2}\right]}{\Delta\omega^2 + (\gamma H_1)^2} \cdot g(\omega)\, d(\Delta\omega) \qquad (4)$$

The characteristic dependence of the decay rate upon a portion of the spins being excited (i.e. upon amplitude of the microwave pulses) is the particular feature of the phase relaxation caused by the instantaneous spectral diffusion mechanism as compared with other phase relaxation mechanisms. Figure 2 shows this dependence.

Thus, the calculation procedure for the dipolar broadening is reduced to the following. Study is made of the dependence of the decay rate b_m upon H_1. From Eq. (4) the values of $\left\langle \sin^2 \frac{\Theta}{2} \right\rangle$ for data of H_1 are calculated, and the dependence of b_m upon $\left\langle \sin^2 \frac{\Theta}{2} \right\rangle$ is obtained. The tangent of the slope of this curve gives the dipolar broadening value.

Figure 3 shows the dependence of the dipolar broadening, Δ for trapped electrons upon the average concentration of e_{tr} for γ- and β-irradiated samples (in the concentration range of $2 \times 10^{17}\ cm^{-3} < C_e < 1.3 \times 10^{18} cm^{-3}$). Δ is

described by the following expression

$$\Delta = K C_e = (6 \pm 2) \times 10^{-13} C_e . \quad (5)$$

A theoretical calculation of K_t performed in Ref. /8/ gives the value of $K_t = 8.1 \times 10^{-13} cm^{-3} sec^{-1}$ which is in good agreement with the value observed. The lower limit of the average concentrations which is possible to measure depends on the sensitivity of the ESE instrument, whereas the upper one is determined by the maximum of possible e_{tr} concentration in an irradiated sample.

The dipolar broadenings of e_{tr} should be noted as being similar at equal average concentrations corresponding to different parts of the accumulation curve (Fig. 3).

The kinetics of O^- phase relaxation is described by the relation

$$v(2\tau) = v(O) \exp \{-2b_m \tau - a\tau^3\} \quad (6)$$

Interaction of the electron spins with the matrix nuclei results in a third power time dependence for the ESE signal decay with $a = 4.6 \times 10^{16} sec^{-3}$. The difference between e_{tr} and O^- phase relaxation kinetics may be indicative of different environments of both paramagnetic centres. Besides, the exponential decay of the ESE signal for O^- is modulated at 20 kHz which corresponds to the nuclear Larmour frequency for Na^{23} in the field of 3300 Oe. Analysis of these modulation effects makes it possible to define parameters of O^- trap /15/.

The dipolar broadening occurred due to interaction of O^- radical-ions with one another is estimated by Eqs (2), where

$$g(\omega) = \int_0^{\Delta\omega_0/2} \frac{e^{-(x-t)^2}}{\sqrt{t}} dt \Big/ \int_0^{\Delta\omega_0/2} dt \int \frac{e^{-(x-t)^2}}{\sqrt{t}} dx \quad (7)$$

where $x = (\omega - \Delta\omega_0)/\Delta\omega_0$. Here $\Delta\omega_0$ is the individual component broadening of O^- being equal to 12 Oe. Relation (7) was obtained by simulating the experimental spectrum by means of an electronic computer.

Figure 4 shows the dependence of O^- dipolar broadening upon the average concentration in γ- and β-irradiated samples while accumulating under irradiation. As shown in Fig. 4, in γ-irradiated samples

$$\Delta = K \times C_{O^-} = 7.2 \times 10^{-13} C_{O^-} \quad (8)$$

in the concentration range of $10^{17} cm^{-3} < C_{O^-} < 2 \times 10^{19} cm^{-3}$.

In β -irradiated samples the dipolar broadening is independent of the average concentration (or dose) up to $C_{O^-} \simeq 1.5 \times 10^{18} cm^{-3}$, and is described by Eq. (8) starting from $C_{O^-} \simeq 2.5 \times 10^{18} cm^{-3}$.

Discussion

The absence of dependence of O^- dipolar broadening upon the average concentration up to $C_{O^-} = 1.5 \times 10^{18} cm^{-3}$ is indicative of the fact that trapping of these radicals occurs in spatially restricted regions, i.e. in ionizing particle tracks. The subsequent accumulation of the radicals results in overlapping of the tracks: the distribution approaches uniformity. As a result of this, there appears a linear dependence of Δ upon C_{O^-} starting from $2.5 \times 10^{18} cm^{-3}$. The local concentration of O^- radical-ions in a track can be calculated as

$$C^L_{O^-} = \frac{\Delta}{K} = 2 \times 10^{18} cm^{-3} \qquad (9)$$

where Δ' is O^- dipolar broadening for the region where Δ is independent of C_{O^-}. Having assumed the tracks to be cylinder-shaped, and distribution of the radicals to be uniform inside the tracks, we have for radii of the radical track

$$R = \sqrt{\frac{G \cdot LET}{100\pi \cdot C^1_{O^-}}} \qquad (10)$$

where LET is the linear energy transfer of a β-particle being equal to 1eV Å^{-1}. The radical track radius for O^- calculated from Eq. (10) is 75 Å. Close values (65 and 85 Å) should be noted to be obtained for sizes of the tracks for SO_4^- and PO_4^{2-} radical-ions in β -irradiated glassy solutions of sulphuric and phosphoric acids at 77K /16/. As in γ-irradiated samples Δ depends linearily upon the average concentration throughout the region of measurements it is possible (issuing from the error of the experiment) to show only the upper possible limit of $C^1_{O^-} \leq 3 \times 10^{17} cm^{-3}$.

The dipolar broadening for e_{tr} is also linearily connected with the average concentration of electrons both in γ - and β -irradiated samples throughout the region of measurements. Estimation of e_{tr} local concentrations gives the value of $C^1_e \leq 2 \times 10^{17}$ cm^{-3}, a track radius for e_{tr} must be not less than 200 Å.

Thus, the spatial distributions of trapped electrons and O^- radical-ions are shown by the data obtained to be different. This is due to different spatial scales for the reaction of charge transfer and for electron thermalization.

Since the average distance between O^- radical-ions in a track equals to 70 Å, it can be inferred that before O^- would form from H_2O^+ there occur at least 15 charge transfer acts. Distances as long as that are probably due to the Coulomb field influence on reaction (2) in a track.

Studying spatial distribution of H atoms, SO_4^- and PO_4^{2-} radical-ions in α-and β-irradiated solutions of sulphuric and phosphoric acids we have found a nonuniform mutual spatial distribution of radiolysis products, M^+ and e_m being their precursors /16/. This phenomenon might be seen to be a rule for systems where the radiolysis mechanism is predominantly ionic in character.

References

/1/ Pikaev, A. K., Solvatirovannyi electron v radiatsionnoi khimii, M., "Nauka", 1969, p. 289.

/2/ Chernova, G. P., Ershov, B. G., Grinberg, O. Ya., Lebedev, Ya. S., Izv. AN SSR, ser. khim., 2439, (1968).

/3/ Zimbrick, J., Kevan, L., J. Am. Chem. Soc., 88, 3678 (1966).

/4/ Moan, J., Kaalhus, O., Int. J. Radiat. Phys. Chem. 5, 441 (1973).

/5/ Berry, W. B., J. Chem. Phys. 54, 1837 (1971).

/6/ Semenov, A. G., Khmelinskii, V. E., PTE, 5, 197 (1967).

/7/ Milov, A. D., Salikhov, K. M., Tsvetkov, Yu. D., Zh. Exp. Theor. Fiz. 63, 2329 (1973).

/8/ Raitsimring, A. M., Umanskii, B. A., Salikhov, K. M., Tsvetkov, Yu. D., J. Phys. Tv. T. 16, 756 (1974).

/9/ Koralev, V. V., Plusnin, V. F., Bashin, N. M., Zh. Phys. Chem. (USSR) 49, 2440 (1975).

/10/ Raitsimring, A. M., Salikhov, K. M., Bychkov, S. F., Tsvetkov, Yu. D., J. Ph. T. T., 17, 484 (1975).

/11/ Zimbrick, J., Kevan, L., J. Am. Chem. Soc. 89, 2483 (1967).

/12/ Milov, A. D., Salikhov, K. M., Tsvetkov Yu. D., J. Ph. T. T. 15, 1187 (1973).

/13/ Raitsimring, A. M., Salikhov, K. M., Dikanov, S. A., Tsvetkov Yu. D., J. Ph. T. T. 17, 3174 (1975).

/14/ Zimbrick, J., Kevan, L., J. Chem. Phys., 47, 2364 (1967).

/15/ Yudanov, V. F., Raitsimring, A. M., Dikanov, S. A., Tsvetkov, Yu. D., J. Struct. Chemistry, (in press)

/16/ Raitsimring, A. M., Moralev, V. M., Tsvetkov, Yu. D., J. Chem. High Energy 9, 517 (1975).

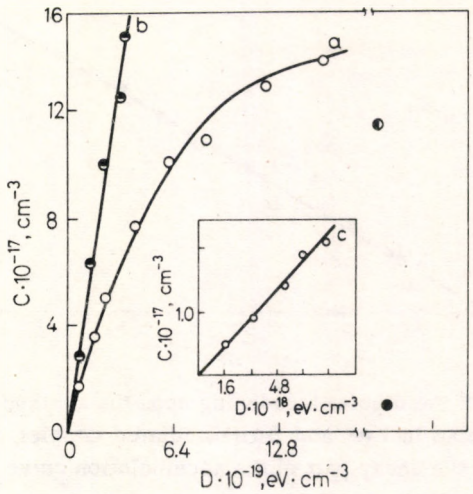

Fig. 1 Dependence of e_{tr} (a) and O^-(b) concentration upon the absorbed dose in β-irradiated samples. (◐) - 3.7×10^{20} eV cm^{-3}: (●) - 15.2×10^{20} eV cm^{-3}. The straight line (c) corresponds to the initial part of curve (a)

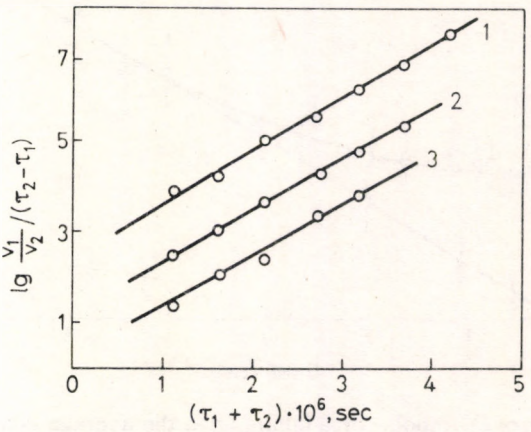

Fig. 2 Linear plot of the ESE signal amplitude decay for trapped electrons at various values of $\Theta = \gamma H_1 t_u$: 1 - 148°, 2 - 85°, 3 - 45°. v_1 and v_2 are values of the ESE signal amplitude at times τ_1 and τ_2, respectively

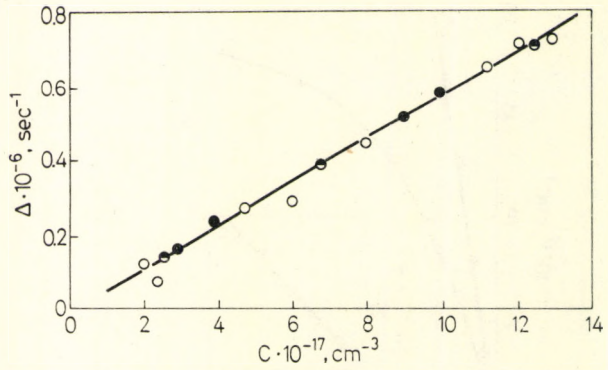

Fig. 3 Dependence of the dipolar broadening upon the average concentration of trapped electrons in γ (●) and β (○)-irradiated samples. Blackened dots correspond to the decay part of the accumulation curve

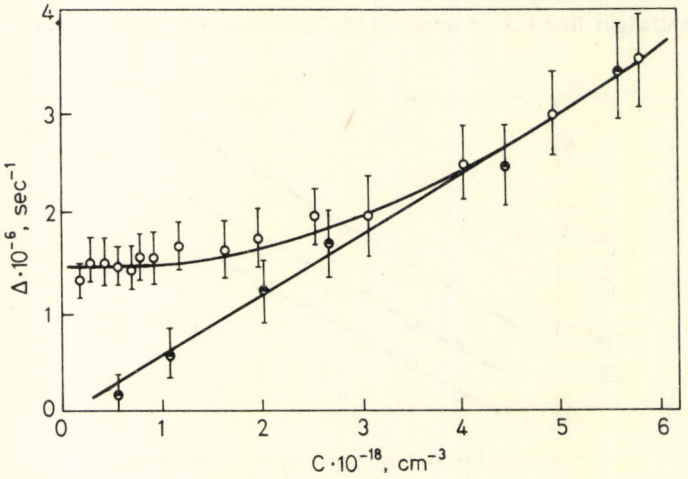

Fig. 4 Dependence of O^- dipolar broadening upon the average concentration in β (○) and γ (●)-irradiated samples

M. MAGAT

I would like to report very briefly about some work done in our laboratory by Dr. Kieffer and Mrs. Lapersonne-Mayer in collaboration with Dr. Klein from C. N. R. Strasbourg and pertaining to the electron distribution very short time (a few nanoseconds) after the passage of the ionizing particle, before the memory of the track has disappeared.

These authors have shown previously that in the case of doped methylcyclohexane (MCH) the rate of isothermal luminescence (ITL) was temperature independent between 4.2 and 77K, which is consistent with a tunnelling process and could be described by a simple hyperbolic law $I(t) = \frac{A}{t}$, where A is a constant, and I(t) the fluorescence intensity at time t, the equation being valid between $t = 2\mu$ sec and several hours.

The validity of this equation over such a long period of time shows that, as could be expected, the memory of the primary track was lost and that measurements beginning a shorter time than 2μ sec after the passage of the particle were necessary. This could be achieved using the technique of "photon counting" using a multichannel analyser and a time-to-amplitude converter analysing coincidences between two photo-multipliers, a technique well known in nuclear physics. Very weak microcurie sources of β and α particles (90-Sr and 210-Po) were used. The decay observed consists of two components, the one faster than the resolution time (5×10^{-10} sec) was due to the fluorescence of the "dope" used, the other "slow" due to the electron-cation recombination. For α particles the decay of this component could be described for $t \geq 10 \times 10^{-9}$ sec by a Debye-Edwards relation

$$I(t) \propto t^{-1.3}$$

while for β particles the curve has a different, complicated shape. Obviously under these conditions the memory of the track was not yet lost. More and better reproducible results are necessary before a theoretical interpretation can be attempted. This required a very careful selection of the "dope" or "scintillator", which has to have a very short fluorescence time, a good fluorescence yield and have no tendency to form dimers at concentrations at which the contribution of the "spurs" is important. Experiments have shown that a concentration of 3×10^{-5} is necessary if the spur observation over about 200 nsec is required. This subsidiary work is now completed and more quantitative experiments will begin shortly.

M. V. VLADIMIROVA

Do you have data about α-radiolysis?

D. TSVETKOV

Yes, they are presented in the last figure of the paper.

M. MAGAT

For how long after the passage of the ionizing particle are you investigating the track?

D. TSVETKOV

We studied the radical distribution after irradiation, our results refer to trapped radicals. This means that the time is practically infinity.

A. K. PIKAEV

Does the value of track radius 75 Å, which has been measured from O^- spatial distribution, mean that in alkaline ice there is a hole migration?

A. M. RAITSIMRING

Yes, this means that 15 acts of proton transfer [reaction (II)] take place before the O^- appears by reaction (IV).

G. R. FREEMAN

What was the average energy of the β particles?

A. M. RAITSIMRING

Tritium β -particles were used.

G. R. FREEMAN

I am interested that the average radius is estimated to be $\geq$ 200 Å. Does your method emphasize the short radii, or the long radii in the distribution?

A. M. RAITSIMRING

The ESE-method in experiments under discussion can give information only on the mean value of $\langle 1/r_{ik}^3 \rangle$. This value does not contain any information on the distribution function. But we can compare this value with a statistically uniform distribution (solutions of stable radicals, for example) and with that of the radicals in irradiated solids. This comparison can give information about radical track parameters.

J. KALECINSKI

What is the relationship between your results and the results of Bugaenko et al. concerning the spatial distribution of radicals? If I remember correctly, the results of Bugaenko concerning the chlorate acids have given the evidence on the ESR data that there is a similar spatial distribution for H radicals.

A. M. RAITSIMRING

I know a number of results on spatial distribution obtained by means of stationary saturation ESR method. But the truth is that the interpretation of these results strongly depends upon the theory of this method which has not been developed properly yet. We discussed some common errors in the interpretation of the experimental results in terms of this method in J. Theor. and Exp. Chem. (ZhETF, in Russian) 7, 848 (1971).

ONE-ELECTRON REACTIONS IN FROZEN AQUEOUS SOLUTIONS OF CYSTINE-CONTAINING BIOCHEMICAL SYSTEMS

Z. Gasyna, S. Bachman, S. Galant, S. Witkowski
Institute of Applied Radiation Chemistry, Technical University, Łódź, Poland

Introduction

The disulphide groups play an important role in the radiation chemistry of proteins. A great number of investigations has therefore been carried out to elucidate the radiation-induced reactions of these groups and their relation to the degradation of proteins and enzyme inactivation /1/. It has been found that in an aqueous solution of the cystine-containing protein the attachment of an electron or hydrogen atom to the disulphide group is an important primary process which provides fast consecutive intramolecular radical chain reactions /2,3/. Since the primary adduct products are short-lived species it is not easy to observe them under usual experimental conditions.

The present study was carried out to obtain further information on the nature of the primary species produced in the protein moiety using X or γ irradiation of glassy solutions frozen at 77K.

Experimental

Solutes in glass-forming solvents, frozen at 77 K can capture electrons upon irradiation and produce their anions if the concentrations of the solute are sufficiently high. In such a system the optical measurements in the near UV and visible regions provide spectral information on the solute anion alone. However, part of the electrons remains trapped by the solvent which can be eliminated by bleaching with visible light. The chemicals, all of analytical grade, were used as received. Triply distilled water was used. The solvents, mixtures of equal volumes of water and ethylene glycol (EG/H_2O), 40% (V/V) ethylene glycol in water, 8 mol dm^{-3} NaOH, all made transparent glasses when frozen to 77 K under our experimental conditions. Human serum albumin (HSA) and γ-globulin (IγG) were purchased from Riomed. Ribonuclease was obtained from Koch Light Laboratories Ltd. Oxidized glutathione (GSSG) was prepared from reduced glutathione (Schuchard) by oxidation with oxygen. The sample solutions were degassed to exclude oxygen. In the optical absorption experiments disc-shaped ice samples, about 1 mm thick and 10 mm in diameter, were prepared at 77 K. The samples were supported in washer-like rings without optical windows. For the ESR experiments, solid transparent pellets were made by allowing drops of the solution to fall into liquid nitrogen. The irradiation was carried out by ^{60}Co -rays at a dose rate of Mrad h^{-1} or with X-

rays at a dose rate of 2.4 Mrad h^{-1}. The X-ray source was a Machlett OEG-60 type machine operated at 40 keV.

Optical spectra were observed using a Beckman DK-2A Spectrophotometer. ESR spectra were recorded on a Polish-made X-band, SE/X-20 spectrometer, with a 100 kHz field modulation. The preparation, irradiation, optical and ESR measurements of sample solutions were carried out at 77 K in the dark.

Results

When the solution of a cystine-containing peptide or protein in ethylene glycol-water is exposed to X or γ -rays at 77 K, absorptions of both trapped electrons (e_t^-) and reaction products of the solute with the electrons appear. The optical spectrum of a 2.5×10^{-2} mol dm^{-3} frozen solution of oxidized glutathione in EG/H_2O irradiated at 77 K is shown in Fig. 1A.

A considerable part of this spectrum is due to e_t^- (λ_{max} = 570 nm). However, when a 40% EG water system containing 10^{-2} mol dm^{-3} HCl, was used as a host matrix for GSSG, the optical spectrum showed a weak absorption band of the trapped electrons (Fig. 1B). If the electrons are eliminated either by bleaching with visible light ($\lambda > 450$ nm) or annealing at 145 K, the spectra B and C in Fig. 2 are obtained, respectively. All these spectra indicate an absorption peak around 400 nm. We attribute it to $RSSR^-$ radical anion. The position of the peak and its intensity depend largely on the pH (Fig. 3).

An X-irradiated sample of serum albumin (10^{-2} mol dm^{-3} disuphide) in EG/H_2O has an optical spectrum that is almost identical with that of GSSG (Fig. 4A). When the irradiated frozen solution of HSA in EG/H_2O was photolysed with $\lambda > 320$ nm, the spectrum in Fig. 4A changed to 4B and 4C, where an increase in the absorption in the range of 300 to 350 nm and a corresponding decrease at 400 nm are seen. When the solution was warmed from 77 K the spectrum changed to 4D. The absorption spectrum closely resembles that obtained on the photobleaching of the irradiated solution of HSA. This is a striking difference from the system of GSSG in EG/H_2O, where the photolysis of the irradiated system with $\lambda > 320$ nm caused the band at 400 nm to dissapear without giving a new absorption in the investigated wavelength region. Correspondingly, the band around 400 nm does not become more intense on annealing of the system.

When an X-irradiated sample of the cystine protein (10^{-2} mol dm^{-3} disulphide) was annealed in the temperature region where e_t^- decayed, it gave rise to an optical absorption spectrum (Fig. 5) almost identical for all the proteins investigated (HSA, I γ G, ribonuclease). Accordingly, on optical bleaching with $\lambda > 450$ nm, the spectrum of the irradiated sample undergoes a similar change, i.e. an absorption peak around 400 nm is left.

The solutes HSA, ribonuclease, and I γ G (all 10^{-2} mol dm^{-3} in disulphide) reduce the X-ray-induced yield of e_t^- in EG/H_2O by around 66%, 30% and 10%,

respectively. Assuming an extinction coefficient of 10^4 dm^3 mol^{-1} cm^{-1} of the $RSSR^-$ radical anion at the absorption maximum /4, 5, 6/ radiation yields of the order of 1 were found for the investigated proteins.

It has been suggested /7/ that a greater availability of disulphide bridges towards hydrated electrons can account for the increase in absorption around 400 nm. Assuming that the changes in the availability of disulphide bridges in protein could be induced by a denaturing agent, we examined the effects of 4 mol dm^{-3} urea and of 1% sodium dodecyl sulphate and measured the yield of $RSSR^-$ radical anion in HSA.

It was found that the values varied less than 25% with respect to unmodified HSA. The ESR spectrum of NaOH glass exposed to X-rays at 77 K is well known /8/. When 2.5×10^{-2} mol dm^{-3} GSSG in 8 mol dm^{-3} NaOH is irradiated at 77 K, a spectrum is obtained which is slightly different from the spectrum attributed to the trapped electrons and O^- radicals (Fig. 6A). When the sample was bleached with visible light ($\lambda > 450$ nm) the e_t^- signal disappeared and the other singlet, exhibiting an anisotropy, increased by around 20% (Fig. 6B). Annealing of an X-irradiated sample containing GSSG showed that the singlet remained in the temperature region where the O^- radicals decayed (Fig. 6C). ESR spectra were also measured at 77 K for the solutions showing the optical spectra in Fig. 1B. When 2.5×10^{-2} mol dm^{-3} GSSG was introduced to acid 40% ethylene glycol water, it gave rise to a spectrum superimposed on the solvent radicals spectrum.

The X-ray-induced spectrum changed to the spectrum that was almost identical with this in 8 mol dm^{-3} NaOH, when annealed at the temperature where the solvent radicals decayed (Fig. 7). In all cases, annealing of the samples at higher temperature caused the anisotropic singlet to disappear without giving rise to new detectable ESR centres (Fig. 7B).

Discussion

The disulphide radical anion $RSSR^-$ formed in peptide or protein molecules has an optical absorption band around 400 nm and is seen both in 8 mol dm^{-3} NaOH and EG/H_2O glasses. The ESR spectrum of the radical anion is a broad singlet with a linewidth of 20-25 G and a g-factor of about 2.010 in the case of $GSSG^-$ in acid EG/H_2O. The disulphide radical anion is produced by the reaction of disulphide group with X-ray-produced electrons.

Experimental data similar to those here have been found by others. The characteristics of the optical spectra of $RSSR^-$ are very similar to those found by Shida /9/ for organic disulphides in alcoholic and ethereal solvents at 77 K. It has been reported /10,11/ that the ESR spectrum of the disulphide anion is a broad singlet with g-value for the derivative crossover ranging from 2.012 to 2.017. The optical spectra obtained by Hoffman and Hayon /12/ in the pulse radiolysis of alkaline solutions of GSSG also closely resemble the spectra of $G\dot{S}SG^-$ in frozen glasses, while the spectra in acid solutions showed a band with $\lambda_{max} \simeq 330$ nm. The latter was attributed by these authors to thiyl $RS^{\cdot}$ radicals. The reason that in irradiated samples of GSSG in

acid/H_2O, we only see a band around 400 nm is probably that the $G\dot{S}SG^-$ radical anion is not subjected to protonation at 77 K. The difference between spectra in acid and neutral or alkaline glasses possibly reflects only a difference in a state of protonation of the electron adduct to disulphide but may also be a result of a change in the configuration of $G\dot{S}SG^-$ on softening of the rigid glass. Lichtin et al. /2,3/ have found transient absorption spectra generated by the action on aqueous solutions of ribonuclease of hydrated electrons and of H atoms, with a band centred around 400 nm. However, this band is more diffuse as a result of consecutive reactions within ribonuclease molecules. If one considers the yields of $R\dot{S}SR^-$ observed for proteins in frozen glasses one can assume that at least part of the electrons reacts with the protein moiety and that the formation of $R\dot{S}SR^-$ radical anions involves electron relocalization. This would probably explain why a conformational change induced in protein has little effect on the yield of the anion at 77 K. The difference between spectra of $R\dot{S}SR^-$ formed in various proteins may be explained in terms of the dihedral angle of the disulphide bond, β, since both the λ_{max} and the intensity of the absorption can be sensitive functions of the angle /14/. The disulphide anion is stable only in the low-temperature rigid matrix. Reactions of the type

$$R\dot{S}SR^- \longrightarrow RS^{\cdot} + RS^- \qquad (1)$$

and

$$R\dot{S}SR^- \longrightarrow RSH + \dot{R}S^- \qquad (2)$$

may be responsible for the disappearence of the disulphide anion on softening of the rigid glass /15/. Although, it has been shown /12/ that the decay of $R\dot{S}SR^-$ in solution is directly dependent upon the H^+ concentration and thus involves the stage of protonation to form $R\dot{S}SHR$ radicals. Moreover, it has been suggested /16/ that radicals previously identified as $RS^{\cdot}$ are better described as $R\dot{S}SHR$ radicals. The present results indicate that the secondary sulphur radicals are not formed on annealing of irradiated glasses containing disulphides, since the thiyl radical (or even $R\dot{S}SHR$) has a characteristic ESR spectrum, not seen presently. Softening of the rigid glass can, however, mobilize protons and result in the charge neutralization. Thus, the fate of the disulphide anion upon warming is probably protonation followed by a bond fission without giving rise to $RS^{\cdot}$ radicals.

Photoexcitation of the disulphide radical anion may also result in the bond splitting reactions (1) or (2) /9,11/. If the absorption in the 330 nm region is in fact due to $RS^{\cdot}$ radical then it follows that reaction (1) occurs on photoexcitation of $R\dot{S}SR^-$ derived from cystine units of HSA (Fig. 4). In the case of the disulphide group in a protein molecule the fragments are caged. They may recombine on softening of the matrix, thus reproducing $R\dot{S}SR^-$ radical anion.

The relatively strong absorption around 300 nm can be assigned to radicals derived from aromatic groups of protein /17/. These radicals are probably formed in the reac-

tion involving RŜSR radical anion. However, further experiments on irradiated solutions of cystine peptides containing aromatic residues are needed to clarify whether the aromatic groups are involved in the secondary radical transfer reactions.

References

/ 1/ T. Sanner, A. Pihl, Scand J. clin Lab. Invest. Suppl. 106, 53 (1969).
/ 2/ N.N. Lichtin, J. Ogdan, G. Stein, B.B.A. 263, 14 (1972).
/ 3/ N.N. Lichtin, J. Ogdan, G. Stein, B.B.A. 276, 124 (1972).
/ 4/ G.E. Adams, G.S. Mc Naughton, B.D. Michael, Trans. Faraday Soc. 64, 902 (1968).
/ 5/ G.E. Adams, R. Armstrong, A. Charlesby, B.D. Michael, R.L. Willson, Trans. Faraday Soc. 65, 732 (1969).
/ 6/ G.E. Adams, R.L. Willson, J.E. Aldrich, R.B. Cundall, Int. J. Radiat. Biol. 16, 333 (1969).
/ 7/ G.O. Phillips, D.M. Power, C. Robinson, J.V. Davies, B.B.A. 295, 8 (1973).
/ 8/ T. Henriksen, Radiat. Res., 23, 63 (1964).
/ 9/ T. Shida, J. Phys. Chem. 72, 2597, (1968); 74, 3055 (1970).
/10/ F.K. Truby, D.C. Wallace, J.E. Hesse, J. Chem. Phys. 42, 3845 (1965).
/11/ S.B. Milliken, K. Morgan, R.J. Johnsen, J. Phys. Chem. 71, 3238 (1967).
/12/ M.Z. Hoffman, E. Hayon, J. Am. Chem. Soc. 94, 7950 (1972).
/13/ R. Braams, Radiat. Res. 31, 8 (1967).
/14/ H.E. Van Wart, A. Lewis, H.E. Scheraga, F.D. Saeva, Proc. Nat. Acad. Sci. U.S.A. 70, 2619 (1973).
/15/ K. Jaeger, A. Henglein, Z. Naturforsch A 21, 1251 (1966).
/16/ M.C.R. Symons, J. Chem. Soc, Perkin Trans. II 1618 (1974).
/17/ E.J. Fendler, J.H. Fendler, Progress in Physical Organic Chemistry, eds. A. Streitwieser Jr. R.W. Taft, Interscience, New York, 1970 p. 260.

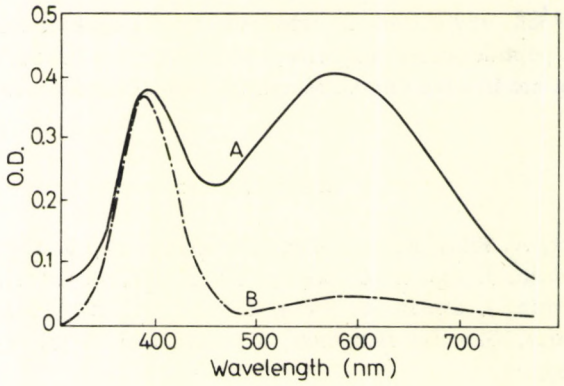

Fig. 1 Optical absorption spectra of A: 2.5×10^{-2} mol dm^{-3} GSSG in EG/H_2O exposed to X rays at 77 K dose 400 krad, B: 2.5×10^{-2}, mol dm^{-3} GSSG 40% EG 10^{-2} mol dm^{-3} HCl exposed to X rays at 77 K dose 400 krad

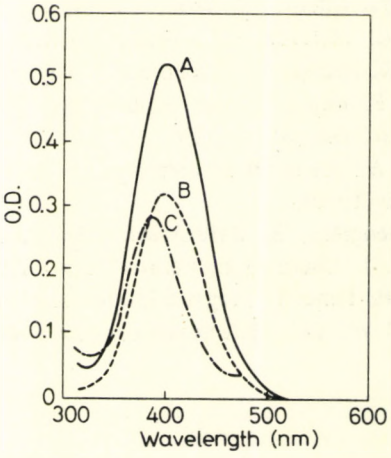

Fig. 2 Optical absorption spectra of A: 1.5×10^{-2} mol dm^{-3} GSSG in EG/H_2O irradiated to a dose of 400 krad at 77 K. B: sample A after bleaching for 10 min by $\lambda > 450$ nm, CG... sample B heated to 145 K

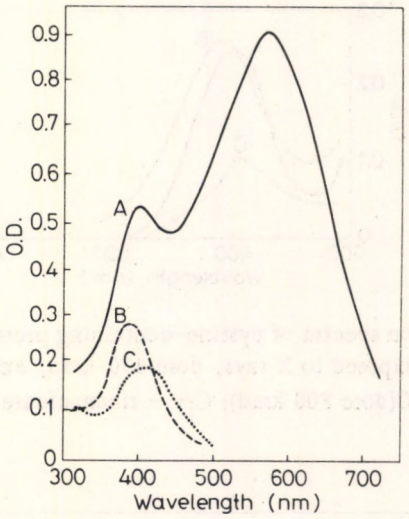

Fig. 3 Optical absorption spectra of 2.5×10^{-2} mol dm^{-3} GSSG in EG/G_2O matrices irradiated to a dose of 400 krad, and annealed at 145 K. A: 0.1 N NaOH in EG/H_2O matrix, B:--- neutral EG/H_2O, C: -.- 0.1 N HCl in EG/H_2O matrix

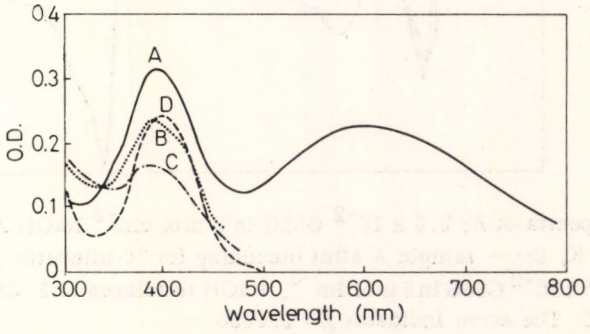

Fig. 4 Optical absorption spectra of A:-- HSA(10^{-2} mol dm^{-3} in SS) in EG/H_2O irradiated to a dose of 400 krad, B:... HSA in EG/H_2O irradiated 400 krad, photobleached with $\lambda > 450$ nm and subsequently exposed for 5 mm to $\lambda > 320$ nm light at 77 K, C:-·-·-sample B exposed for additional 5 min to $\lambda > 320$ nm light. D: --- sample G annealed at 145 K

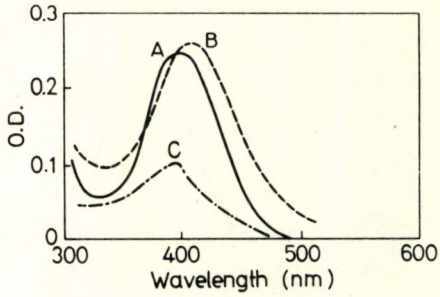

Fig. 5 Optical absorption spectra of cystine-containing proteins (10^{-2} mol dm^{-3} in SS) in EG/H_2O exposed to X rays, dose 400 krad, and annealed at 145 K. A:-HSA, B:--1λ G(dose 800 krad): C:-.- ribonuclease

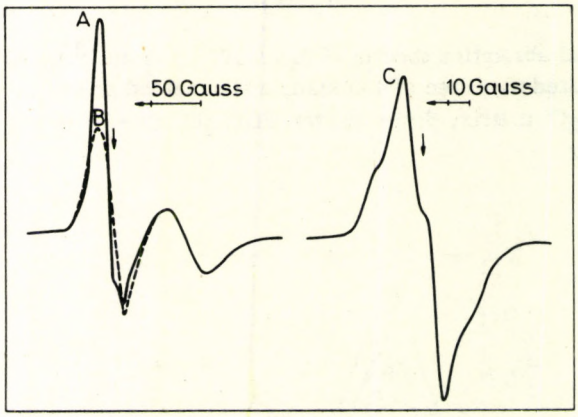

Fig. 6 ESR spectra of A: 2.5×10^{-2} GSSG in 8 mol dm^{-3} NaOH X irradiated to 1 Mrad at 77 K, B:--- sample A after bleaching for 10 min with $\lambda > 450$ nm, C: 2.5×10^{-2} GSSG in 8 mol dm^{-3}. NaOH irradiated to 1 Mrad and annealed at 150 K. The arrow indicates g = 2.0036

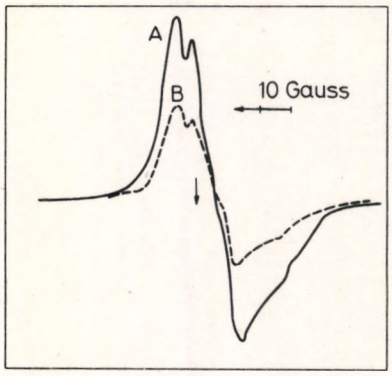

Fig. 7

DISCUSSION

G. CHIRAKADZE

Did you study the influence of the oxygen on the nature of optical absorption spectra of the proteins?

Z. GASYNA

No, we did not.

I. KRALJIC

Did you compare the absorption spectra of peptides and proteins in folded and unfolded (denatured) state?

Z. GASYNA

We only compared the absorption spectra of modified and unmodified human serum albumen. The values obtained varied by less than 25% with respect to unmodified protein.

GAMMA RADIOLYSIS OF ALKALI AND ALKALINE EARTH NITRATES IN CONCENTRATED AQUEOUS SOLUTIONS IN FROZEN AND LIQUID STATES

J. Kaleciński
Institute for Low Temperatures and Structure Research, Polish Academy of Sciences, Wrocław, Poland

Nitrates are good model systems for radiation research. This is why they were examined many times in aqueous solutions /1,2,3/, as well as in solids /4,5/ and melts /6,7/. In the last systems it was shown that there is a close relationship between the kind of cations and the decomposition yields. This relationship was correlated with the free volume factor for both the solids /5/ and the melts /7/.

It is very interesting to know how the yields of nitrate decomposition change in the presence of different cations when the NO_3^- ions are in the matrix of water molecules, both in frozen and liquid states. Therefore, the aim of the present paper is to determine the yields of direct and indirect effects of radiation and to settle what agents affect the direct and indirect effects.

The general relationship between the measured yield and the direct and indirect effects for nitrate solutions is given by Eq. (1).

$$G(NO_2^-) = f_{ind}\, G(NO_2^-)_{ind} + f_d\, G(NO_2^-)_d \qquad (1)$$

where f_d and f_{ind} are the electron fractions of nitrate and the matrix, respectively.

In Figs 1 and 2 some experimental results for solutions of nitrates frozen at 77 K are presented. As one can see from Figs 1 and 2, the yields of nitrate decomposition are the linear functions of nitrate, in agreement with Eq. (1). On the basis of the experimental results and Eq. (1), the yields have been calculated and presented in Table 1. Average yields of hydrogen peroxide, also presented in Table 1, are very low and are nearly independent of the cations used as well as of the electron fraction of nitrate ions. The contrary is observed for the yields of direct effect of nitrate decomposition. A pronounced relationship between the yield and the size of the cations exists here (Table 1). This suggests that the free volume factor may play an important role in the radiation decomposition of nitrate ions in aqueous matrices. The conclusion is supported by the fact that the mechanism of nitrate radiation decomposition is the same in the presence of different cations as it is shown by EPR spectra (Fig. 3). The spectra consist of $\cdot NO_3$ singlets and NO_2 and NO_3^{2-} triplets for all examined nitrate solutions. Moreover, the intensity rate of the $\cdot NO_3$ peak to the $\cdot NO_2$ peak is 3 : 1 for the examined systems. We

believe, therefore, that the only factor affecting the yields in the frozen solutions is the free volume factor. The numerical value of the free volume is equal to the difference between the volume of the void obtained by removing two neighbouring water molecules in the alkali nitrate solutions (40 cm^3 per mole) or three neighbouring water molecules in the alkaline earth nitrate solutions (66.5 cm^3 per mole) and the own volume of the corresponding ions /8/. The free volumes calculated in that way are presented in Table 1.

According to /7, 8/ the probability of dissociation (β) of radiation activated nitrate ions depends on the free volume (V_f). The main process responsible for the direct effect are illustrated by Eqs (2), (3) and (4):

$$NO_3^- \longrightarrow NO_3^{-*} \begin{cases} \xrightarrow{k_{2a}} NO_2^- + O \\ \xrightarrow{k_{2b}} \text{deactivation by dissipation} \\ \xrightarrow{k_{2c}} \text{other deactivation} \end{cases} \qquad (2)$$

$$k_{2a} = k^o_{2a}\beta$$

$$k_{2b} = k^o_{2b}(1-\beta) \qquad (3)$$

$$\beta = \exp(\gamma V_c/V_f)$$

$$NO_3^{-*} + O \longrightarrow NO_2^- + O_2 \qquad (4)$$

where k^o_{2a}, k^o_{2b} and k_{2c} are the rate constants of the respective processes when the free volume (V_f) is very large, β is the dissociation probability, γ numerical factor assumed here as equal to 1, and V_c is the critical volume equal to the volume of the dissociated fragments, i.e. the volume of an oxygen atom equal to 7 cm^3 per mole.

The above set of equations leads to Eq. (5) which connects the yield of direct effect and the free volume of the system.

$$\frac{2}{G(NO_2^-)_d} + \frac{k^o_{2a} - k^o_{2b}}{G^* k^o_{2a}} + \frac{k^o_{2b} + k_{2c}}{G^* k^o_{2a}} \exp(7/V_f) \qquad (5)$$

where G^* is the primary yield of radiation activated nitrate ions.

The agreement between the experimental data (Table 1) and Eq. (5) is very good, as one can see in Fig. 4.

Some experimental results concerning the liquid nitrate solutions are shown in Figs 5 through 8. The data presented in Figs 5 through 8 confirm the validity of Eq. (1).

Table 1

The yields and the free volumes in the frozen systems of nitrates

system	temperature K	the cation radius Å	$G(NO_2^-)_d$ ions/100 eV	$G(H_2O_2)^{*)}$ molec/100 eV	the free volume cm^3/mole
$LiNO_3$	77	0.60	5.1 ± 0.15	0.13	12.8
$NaNO_3$	77	0.97	4.1 ± 0.2	0.09	10.9
KNO_3	77	1.33	2.8 ± 0.1	0.08	7.4
	195		2.6 ± 0.1	-	
$Mg(NO_3)_2$	77	0.65	5.1 ± 0.15	0.10	12.4
	195		5.0 ± 0.15	0.09	
$Sr(NO_3)_2$	77	1.12	3.7 ± 0.15	0.09	9.5

*) the standard error is equal to 0.015

Hence on the basis of Eq. (1) and the experimental data, the yields of direct and indirect effects have been calculated (Table 2). These data demonstrate the following:

- the yields of indirect effects are many times higher than those for corresponding frozen solutions (see also Figs 1 and 2);
- the kind of cation affects the yields of indirect and first of all the direct effects;
- the yields are higher in the systems where formate or ethanol are present.

The high yields of indirect effect observed in the liquid systems are probably caused by diffusion processes which can easily proceed in liquids and are hindered in the frozen systems.

The increase of the yields of indirect effect in the presence of ethanol or formate are consistent with the following scheme:

$$NO_3^- + 2\, e_{aq}^-(H) \longrightarrow NO_2^- \qquad (6)$$

$$NO_2^- + 2\, OH \longrightarrow NO_3^- + H_2O \qquad (7)$$

$$COOH^- + OH \longrightarrow COO^- + H_2O \qquad (8a)$$

$$C_2H_5OH + OH \longrightarrow R + H_2O \qquad (8b)$$

$$NO_3^- + 2COO^- \longrightarrow NO_2^- \qquad (9a)$$

$$NO_3^- + 2\, R \longrightarrow NO_2^- \qquad (9b)$$

Table 2
The yields in the liquid systems of nitrates

system	$G(NO_2^-)^{*}_{ind}$ ions/100 eV	$G(NO_2^-)^{**}_{d}$ ions/100 eV	$G(H_2O_2)^{*}_{extr}$ molec/100 eV	$G^{***)}_{red}$ radic/100 eV	$G^{***)}_{OH}$ radic/100 eV	$G(-H_2O)^{***)}$ molec/100 eV
KNO_3	0.68	5.5	0.60	3.92	2.56	3.76
$KNO_3 + C_2H_5OH$	3.24	6.3	1.05			
$NaNO_3$	0.78	4.4	0.80	3.86	2.30	3.90
$NaNO_3 + HCOONa$	3.08	7.1	1.20			
$LiNO_3$	0.69	6.3	0.60	3.33	1.95	2.75
$LiNO_3 + C_2H_5OH$	2.64	6.1	1.45			
$Mg(NO_3)_2$	0.76	5.2	0.80	4.04	2.52	4.12
$Mg(NO_3)_2 + HCOONa$	3.28	6.3	1.45			

*) the standard error is equal to 0.03

**) the standard error is equal to 0.1

***) the standard error is equal to 0.06

On the basis of the above set of equations and the yields of indirect effects, the radical yields of water radiolysis have been calculated and presented in Table 2. These yields for all the examined systems, excepting $LiNO_3$, are similar and are in good agreement with commonly accepted values for acid solutions /9/. The radical yields calculated from the $LiNO_3$ system are significantly lower and correspond rather to the yields accepted for neutral solutions /9/.

The yields of hydrogen peroxide slightly decrease with the increase of the electron fraction of nitrate ions (Figs 5 through 8). The yields of hydrogen peroxide extrapolated to zero nitrate concentration have also been presented in Table 2. On the basis of these extrapolated values and the corresponding yields of OH radicals, the yields of water decomposition have been calculated and also presented in Table 2. $G(-H_2O)$ is equal to about 4 molecules per 100 eV for the majority of the systems, in agreement with the commonly accepted value, but for the $LiNO_3$ system the obtained value is again too low.

The interesting feature is the influence of ethanol or formate on the yields of direct effect. The yields reach the limiting value of 6.3 ions per 100 eV and are higher than those for the corresponding solutions without the scavengers of OH radicals. There are, however, two exceptions: a) in the $LiNO_3$ system, the yields are nearly the same for both solutions (i.e. in the presence and in the absence of ethanol), b) in the $NaNO_3$ system, the yield is higher than 6.3 ions per 100 eV. The above features may suggest that the radiolysis products of ethanol or formate are involved in some degree into the processes of direct radiation decomposition of the NO_3^- ions.

It is worth noting that the value of $G(NO_2^-)_d$ being equal to 4.4 ions per 100 eV for the $NaNO_3$ solutions is in agreement with the values obtained in Ref. /1, 10/, but is lower than expected if one takes into account the size of Na^+ cations and the free volume factor. Therefore, in liquid solutions in addition to the free volume some other processes like solvation of ions may play a significant role.

There is no doubt that the structure of the matrix is also very important. The influence of the matrix structure on the yields is clearly demonstrated in Fig. 9 where the data for 9 M KOH solutions at 195 K are shown. For the polycrystalline solutions the yields of nitrate decomposition are very low: 0.07 and 0.09 ions per 100 eV for 0.02 M and 0.1 M KNO_3, respectively, whereas for the glassy solutions the yields are many times higher: 0.38 and 0.51 ions per 100 eV for the same concentrations of KNO_3.

The comparison of the yields of direct effect for polycrystalline and glassy or liquid solutions show that in the last systems the yields are significantly higher —which is also evidence that the matrix structure affects the yields.

References

/ 1/ a. M. Daniels in: Adv. Chem. Ser., 81, 153 (1968),
b. M. Daniels, E. E. Wigg, J. Phys. Chem., 73, 3703 (1969)

/ 2/ T. Sworski, R. W. Matthews, H. A. Mahlman, in: Adv. Chem. Ser., 81, 164 (1968)

/ 3/ a. B. G. Ershov, A. K. Pikaev, Rad. Research Rev., 2, 1 (1969),
b. L. Kevan, in: Action chimiques et biologiques des radiations, Vol. 13, Masson et Cie, Paris, 1969, p. 57–117

/ 4/ J. Cunningham. J. Phys. Chem., 70, 30 (1966)

/ 5/ W. W. Boldyrev, Intern. J. Radiat. Phys. Chem., 3, 155 (1971)

/ 6/ J. Kaleciński, ibid, 4, 171 (1972)

/ 7/ J. Kaleciński, ibid, 4, 181 (1972)

/ 8/ J. Kaleciński, Bull. Acad. Polon. Sci., Ser. sci. chim., 22, 21 (1974)

/ 9/ G. V. Buxton, in: Radiation Research, G. Silini Ed., North-Holland Publ. Comp., 1967, p. 235–249

/10/ V. M. Vladimirova, Khim. Vys. Energ., 9, 452 (1975)

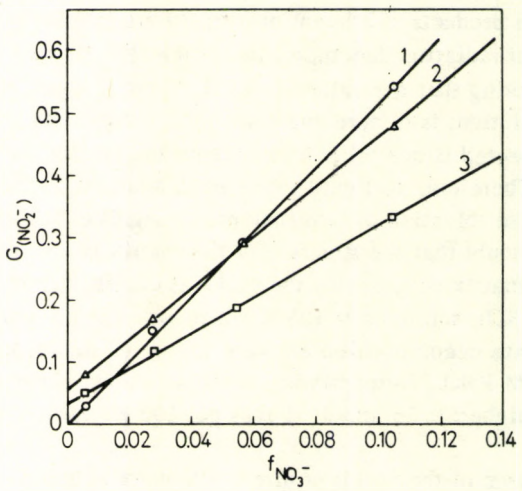

Fig. 1 Nitrite yields vs. the electron fraction of nitrate ions in solutions frozen at 77 K 1 – $LiNO_3$, 2 – $NaNO_3$, 3 – KNO_3

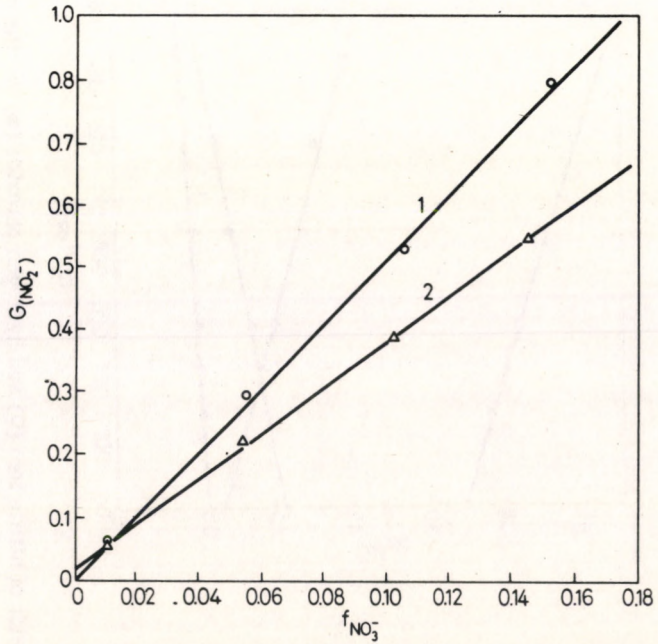

Fig. 2 Nitrite yields vs. the electron fraction of nitrate ions in solutions frozen at 77 K: 1 – $Mg(NO_3)_2$, 2 – $Sr(NO_3)_2$

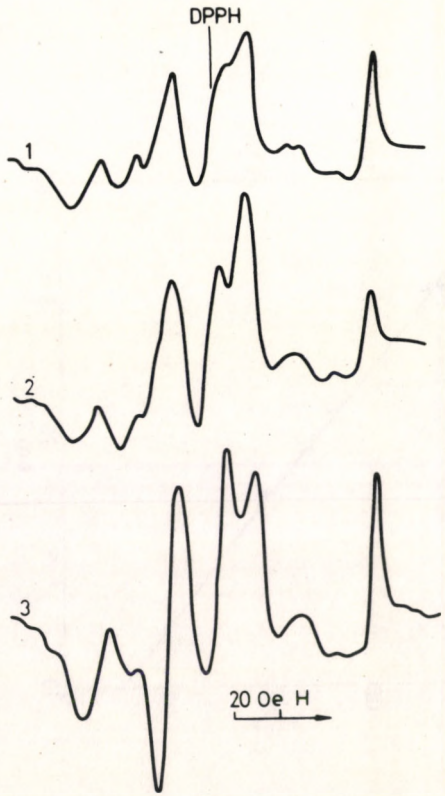

Fig. 3 The EPR spectra of irradiated frozen nitrate solutions: 1 – 1 M $LiNO_3$, 2 – 1 M $Sr(NO_3)_2$, 3 – 1 M $Mg(NO_3)_2$

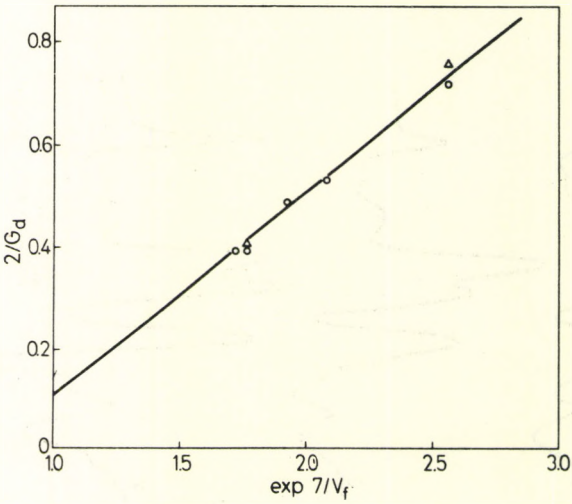

Fig. 4 Plot of $2/G\ (NO_{2d}^-)$ vs. $\exp(7/V_f)$, Eq. (5): circles – nitrate solutions at 77 K, triangles – nitrate solutions at 195 K

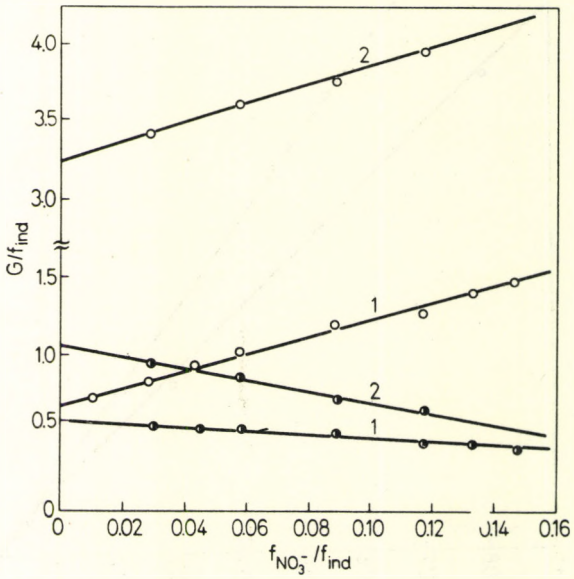

Fig. 5 Yields of nitrite ions (○) and hydrogen peroxide (◑) vs. the electron fraction of nitrate ions in solutions at 20°C: 1 – KNO_3, 2 – KNO_3 + 0.35 M C_2H_5OH

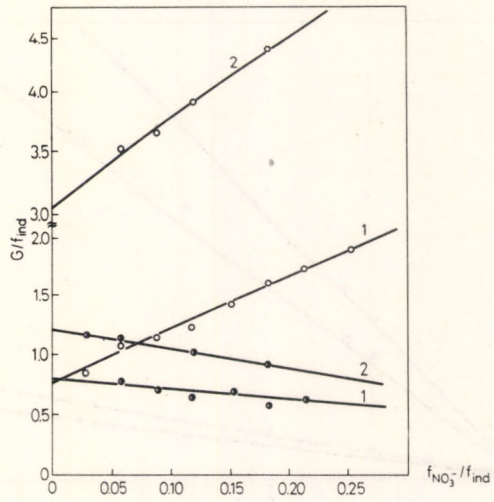

Fig. 6 Yields of nitrite ions (○) and hydrogen peroxide (◑) vs. the electron fraction of nitrate ions in solutions at 20°C: 1 – $NaNO_3$, 2 – $NaNO_3$ + 0.1 M HCOONa

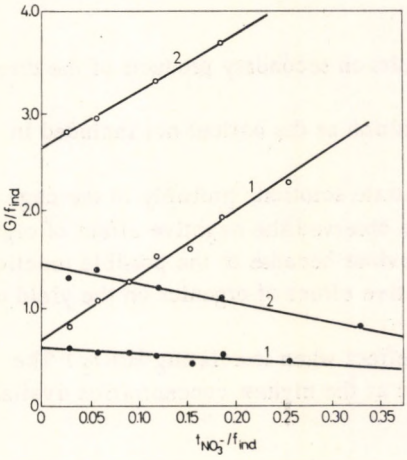

Fig. 7 Yields of nitrite ions (○) and hydrogen peroxide (◑) vs. the electron fraction of nitrate ions in solutions at 20°C: 1 – $LiNO_3$, 2 – $LiNO_3$ + + 0.35 M C_2H_5OH

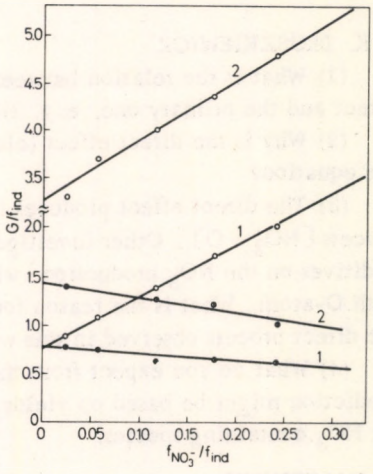

Fig. 8 Yields of nitrite ions (○) and hydrogen peroxide (◐) vs. the electron fraction of nitrate ions in solutions at 20°C: 1 – $Mg(NO_3)_2$, 2 – $Mg(NO_3)_2$ + 0.1 M HCOONa

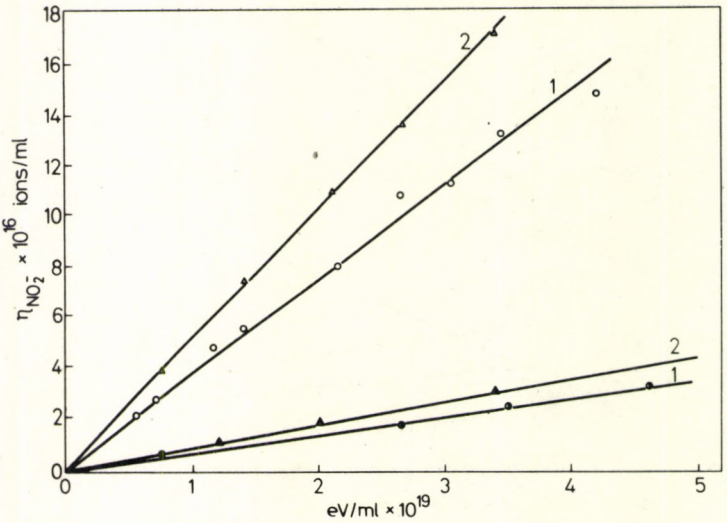

Fig. 9 Plots of nitrite ions vs. dose in 9 M KOH glassy (upper lines) and polycrystalline (lower lines) solutions frozen at 195 K: 1 – 0.02 M KNO_3, 2 – 0.1 M KNO_3

DISCUSSION

R. K. BROSZKIEWICZ

(1) What is the relation between the results on secondary products of the direct effect and the primary one, e. g. NO_3 ?

(2) Why is the direct effect (electron fraction at the cation) not included in the equation?

(3) The direct effect produces NO_3 in nitrate solution, probably in the cage process $[NO_2 + O]$. Other investigators have observed the negative effect of organic additives on the NO_3 production, which is obvious because of the possible reaction with O-atom. What is the reason for the positive effect of organics on the yield of the direct process observed in this work?

(4) What do you expect from the direct effect when irradiating HNO_3 ? The prediction might be based on yields measured at the highest concentration available for NO_3 containing species.

J. KALECINSKI

(1) I have measured mainly the yields of nitrite, hence I can only suppose that the primary products, e. g. NO_3, undergo some reactions like disproportionation, dissociation or the reaction with water molecules which lead to the end products. My simple mechanism summarizes the process by reactions (2)–(4).

(2) The electron fractions of the cations are included in Eq. (1) together with the electron fraction of H_2O and are denoted as $f_{indirect}$.

(3) The NO_3 radicals are not the only primary products at nitrate decomposition. Hence I believe that formates and ethanol, or their radiolysis products, are involved somehow in the mechanism of the direct effect, i. e., by reactions with other primary products of nitrate decomposition (e. g. NO_3^{2-}, NO_2, O^-).

(4) The mechanism of the HNO_3 radiolysis is rather complicated. But I suppose on the basis of the size of the HNO_3 molecule that the yield of direct effect should be higher than that of other nitrates. Vladimirova et al. in their paper presented at this Symposium give the value $G(-HNO_3)_{direct}$ equal to 7 molec/100eV, which is in agreement with my expectation.

R. SCHILLER

This question may have some bearing on all the papers of this session. The effect of dielectric properties, i. e. dielectric constant and dispersion is well known to play a decisive role in ionic processes. They define ionic yields and solvated electron spectra and may also influence reaction rates. I would like to know if any detailed dielectric study on high-concentration, low-temperature aqueous glasses has been carried out and if so, have the results been compared with radiation chemical observations.

L. KEVAN (Session Chairman)

Dielectric constant studies of concentrated aqueous solutions have been carried out, but I do not believe analogous measurements of frozen aqueous matrices have been done. However, there is a general correlation, which has exception though, between matrix polarity measured by either the dielectric constant or molecular dipole moments, and trapped electron optical and magnetic spectral properties for a series of organic glasses. In aqueous glasses containing high solute concentrations there are similar rough correlations with the matrix polarity or estimated by the size and change of the dissolved ions which serve to polarize the water molecules in addition to the water-water interaction. For example, see S. Noda and L. Kevan, J. Phys. Chem., 1974.

I. KRALJIC

I would like to know how big is the increase in direct effect in the presence of formates and how do you explain it, what is the role of free volume factor in this effect?

J. KALECINSKI

The increase of the yields at direct effect in the presence of formates is about 2 molec/100 eV, as we can see in Table 2. The formates are involved somehow in the mechanism of the direct decomposition of nitrates. Their influence on the free volume is rather insignificant because of the low concentration of formates (0.1 M) used. Hence we prefer the former possibility.

A. K. PIKAEV

(1) Did you measure the yields of oxygen for the solutions of different nitrates?

(2) How do you define free volume in the case of aqueous solutions?

I. KALECINSKI

(1) In a few experiments we measured oxygen and obtained the stoichiometric amount with nitrates. We did not measure it systematically.

(2) The free volume of the solution is the difference between the volume at the void obtained by removing the water molecules and the volumes of the ions (H^+ and NO_3^-) occupied the void. The volumes of the ions I have taken according to the known values of the ionic radii.

G. R. FREEMAN

Can you estimate the difference in the free volume of the glassy and polycrystalline samples in your last slide?

J. KALECINSKI

The difference in the free volume of the glassy and polycrystalline samples is not a big one. I think that the difference in the yields presented in Fig. 9 is caused not by the difference in the free volume, but by other agents similar to that in the case of the frozen and liquid neutral nitrate solutions.

G. R. FREEMAN

How do you estimate the free volume? Ions are compressible, so their effective volumes might be different in crystals and in solution.

J. KALECINSKI

As I said, the volumes of the ions were calculated from the known ionic radii. If they are slightly different in aqueous solutions having the additional constant value which we should add to the values calculated previously, then we change the expression: $\exp \frac{\gamma V_c}{V_t}$, which is the same thing as if we changed the numerical value of γ. This, however, affects mainly the slope of the straight line but not the validity of Eq. (5), as has been demonstrated in Fig. 4 of Ref. /7/ cited here.

KINETIC PECULIARITY OF H-ATOM ABSTRACTION BY METHYL RADICALS IN SOLID STATE

B. V. Bol'shakov, M. P. Fuks, V. A. Tolkatchev, A. I. Burstein

Institute of Chemical Kinetics and Combustion, Siberian Branch of the Soviet Academy of Sciences, Novosibirsk, 630090, USSR

The hydrogen atom abstraction is a process which plays a significant role in radiation chemistry. In this paper we shall deal with the reaction kinetics of methyl radicals with matrix molecules. Such processes have been investigated in several papers /1–3/. The kinetics of the reaction $\dot{R}+R'H \longrightarrow RH+\dot{R}'$ has been shown in some cases to be non-exponential /1, 3/. In Ref. /3/ this question has been examined in methanol glass, and the methyl radical concentration has been shown to obey the law

$$C = C_0 \exp(-k\sqrt{t}) \qquad (1)$$

where t denotes reaction time.

To test if "$\sqrt{t}$ law" is specific for methanol matrix properties we carried out investigation of the methyl radical reaction in crystalline sodium acetate hydrate. Methyl radicals were produced by γ-irradiation of sodium acetate hydrate. Kinetic measurements were made by an ESR spectrometer. The experimental procedure and preliminary results were reported in Ref. /4. / The present paper gives a dependence of the methyl radical reaction kinetics upon temperature and matrix isotopic composition. It should be noted that in contrast to Ref. /4/, if the kinetic rate was high enough, measurements were carried out directly in a dewar tube in the nitrogen gas flow. The dewar tube was placed in a cavity. Accuracy of the temperature stability was placed in a cavity. Accuracy of the temperature stability was of $\pm 0,3$K.

In Fig. 1 a decay curve of $\dot{C}H_3$ radicals in $CH_3COONa \times 3H_2O$ is plotted in the coordinates $\lg(C/C_0)$ versus $\sqrt{t}$ at several temperatures. In these coordinates a straight line was obtained. Similar results were obtained for mixtures $(CH_3COONa + CD_3COONa) \times 3H_2O$ as well as for $(CH_3COONa + CD_3COONa) \times 3D_2O$. Isotopic composition of the sodium acetate was varied from 0% to 90% of CD_3COONa, Figure 1b shows the precision of law (1). For this purpose one of the kinetic curves is plotted in the coordinates $\lg(C/C_0)$ vs t^n, where n=0. 35; 0. 5; 0. 65. One may see from Fig. 1 that if n=0. 35 or 0. 65, the dependence of $\lg(C/C_0)$ vs t^n is non-linear and deviation from linearity is out of error limits. If n=0. 4 or 0. 6 the deviation is within the error limits, i. e. the determination accuracy of n is of ± 0.1.

An intense decrease in the reaction rate should be noted to be a peculiarity of the H-atom abstraction reactions if in the reactive molecules H-atoms are replaced by D-atoms. In sodium acetate, as one can see from Fig. 2, this effect also takes place. However, Fig. 2 shows that the same effect occurs if H_2O is replaced by D_2O. Usually one associates the isotopic effect in the H-atom abstraction reactions with a tunnelling probability lower for D-atoms than for H-atoms /2/. Our experiments show that in any case this is not the only reason for the reaction rate decrease.

The experiments mentioned above also show that the theoretical approach to the H-atom tunnelling reactions /5/ is too rough. Actually it cannot explain law (1) and besides, the H_2O - D_2O effect is difficult to explain with this approach because variation of k in this case is close to the magnitude of k itself. From our point of view the intense effect of isotopic composition of unreactive cage components can be understood if one supposes that the constant k is affected by intermolecular cage motions, their spectrum depending on the matrix isotopic composition.

Now we will discuss the models to explain the experimental results. The methyl radicals are supposed to react with "singled out" matrix molecules rather than with any other ones and the rate constant for the reaction is controlled by diffusion. In this case the rate constant is as follows /6/:

$$k = 4\pi\ rD\ (1 + r/\sqrt{\pi Dt})\ M$$

where r is the reaction radius, D is the diffusion coefficient, M is the concentration of the "singled out" matrix molecules, which are reactive relatively to methyl radicals. This equation makes it possible to explain the "$\sqrt{t}$ law", but in the papers cited in Ref. /7/ it has been noted that $\lg(C/C_0)$ is proportional to $\sqrt{t}$ up to $(C/C_0) \ll 1$ if $Mr^3 \sim 1$. In our case this criterion means that M is in close agreement with the concentration of the matrix molecules and that in the "in-cage" reaction its rate is limited by diffusion. Therefore, we believe that diffusion cannot play any role in the reaction discussed.

According to the classical ideas the cage reaction would be expected to follow Eq. (2)

$$C = C_0 \exp(-kt) \qquad (2)$$

but not Eq. (1). Thus, to explain the experimental results one may suppose that the "$\sqrt{t}$ law" is valid due to averaging some cage properties. Exponent expansion (making use of the Laplace transformation) gives

$$\frac{C(t)}{C_0} = \exp(-k\ \sqrt{t}) = \int_0^\infty \frac{k}{2\sqrt{\pi \nu^3}} \exp\left(-\frac{k^2}{4\nu}\right) \exp(-\nu t)\, d\nu \qquad (3)$$

Distribution (3) is difficult to interpret. After the substitution: $\nu = \frac{A}{\omega^2}$ $k = (\frac{2A}{\langle \omega^2 \rangle})^{1/2}$ expression (3) takes the form

$$C(t) = C_0 \int_0^\infty \sqrt{\frac{2}{\pi \langle \omega^2 \rangle}} \exp(-\frac{\omega^2}{2\langle \omega^2 \rangle}) \exp(-\frac{A}{\omega^2} t)\, d\omega \qquad (4)$$

which can be interpreted.

Let us suppose that the reaction of a methyl radical with its partners in the system consisting of the methyl radical and the neighbouring matrix molecules may be described as the transition in a three-level system (Fig. 4) Level 1 is associated with the initial state: 3 - with the final one, when the partners are CH_4 and $\dot{C}H_2COO^-$ radical, level 2 corresponds to the intermediate cage state resulting just after H-atom transition. From level 2 the system relaxes to level 3 accompanied by the release of the bonding energy difference.

Let us assume that probability of the "in cage" reaction is constant, but there is a probability distribution among cages. If transition probability of $1 \longrightarrow 2$ (W_{12}) is equal to A/ω^2, where $\omega = (E_1 - E_2)/\hbar$, A is a a proportionality factor and distribution is a Gaussian function, the time dependence of concentration dependence vill be of the form of equation (4).

The transition probability W_{12} may be proportional to $1/\omega^2$ in many cases. The existing experimental data do not allow us to select among various assumptions but to make the problem more clear the following variant is possible to examine.

The transition probability W_{12} is to be expected to result from modulation of the potential barrier transparency by the thermal noise with a correlation time τ_1 and from a random modulation of deviation from resonance of 1 and 2 states (ω) with a correlation time τ_2.

The system Hamiltonian is as follows

$$H = \begin{Vmatrix} H_{11} + V_{11}(t) & V_{12}(t) + b \\ V_{21}(t) + b^* & H_{22} + V_{22}(t) \end{Vmatrix}$$

where H_{11}, H_{22} are the matrix elements of unperturbed system Hamiltonian, $V_{ij}(t)$ is a random time function, b is a time average value of the non-diagonal matrix element.

Solution of this problem for the limiting conditions, i.e. at $V_{ij} = 0$ or $b = 0$ is known /8/. For our case, if the correlation functions are exponential, one may demonstrate by the perturbation method that

$$W_{12} = \frac{1}{\hbar^2} \frac{V_{12}(0)^2 \tau_c}{1 + \omega^2 \tau_c^2} + \frac{1}{\hbar^2} \frac{b^2 \tau_2}{1 + \omega^2 \tau_2^2} \qquad (5)$$

where $\frac{1}{\tau_c} = \frac{1}{\tau_1} + \frac{1}{\tau_2}$

If ω distribution function is wide enough the situations close to resonance can be neglected. So it is possible to neglect 1 in Eq. (5) and shall have the necessary form for transition probability.

If state 1 is an excited state rather than a ground state the above arguments do not change. In this case k must be multiplied by factor $\exp(-\omega/2kT)$, where U is the difference between the energies $E_1 - E_0$.

In the model described above the " γ t law" appears due to deviation from resonance distribution of states 1 and 2. This distribution may be associated with a minute random change of the matrix structure.

The approach presented shows that the structure of the constant k may be rather complicated. It is a combination of the transition matrix element and correlation time. These magnitudes depend not only on reactant properties but also on the spectra of intermolecular cage motions. We hope that further experiments will clarify this problem.

References

/1/ B. N. Shelimov, N. V. Fok, V. V. Voevodskii, Kinetika i Kataliz, 4, 539 (1963); E. L. Zhuzhgov, N. N. Bubnov, V. V. Voevodskii, Kinetika i Kataliz, 6, 56 (1963); W. G. French, J. E. Willard, J. Phys. Chem., 72, 4604 (1968); M. A. Neiss, J. E. Willard, J. Phys. Chem., 79, 783 (1975).

/2/ A. Campion, F. Williams, J. Amer. Chem. Soc., 94, 7633 (1972); J. Wang, F. Williams, J. Amer. Chem. Soc., 94, 2930 (1972); E. D. Spraque, F. Williams, J. Amer. Chem. Soc., 93, 787 (1971).

/3/ B. V. Bol'shakov, V. A. Tolkatchev, Chem. Phys. Lett. (in press).

/4/ M. P. Fuks, B. V. Bol'shakov, V. A. Tolkatchev, Reaction Kinetics and Catalysis Letters, 4, No. 4 (1975).

/5/ J. Le Roy, F. Williams, J. Phys. Chem., 76, 546 (1972); R. B. Bell, Trans. Faraday Soc., 55, 1 (1959); V. I. Gol'danskii, Dokladi Akademii Nauk USSR, 124, 1261 (1959).

/6/ S. Chandrasekar, Rev. Mod. Phys., 15, 1 (1943); T. R. Waite, J. Chem. Phys., 28, 103 (1958).

/7/ I. D. Campbell, F. D. Looney, Austral. J. Chem., 15, 642 (1962); A. I. Burstein, Yu. D. Tsvetkov, Dokladi Akademii Nauk USSR, 214, 369 (1974).

/8/ Carrington, A. D. McLachlan, Introduction to Magnetic Resonance, Harper and Row, New York and London, 1967; H. M. McConnel, J. Chem. Phys., 35, 508 (1961); A. I. Burstein, G. M. Zhidomirov, Teor. I exper khimia (in Russian) 4, 719 (1968).

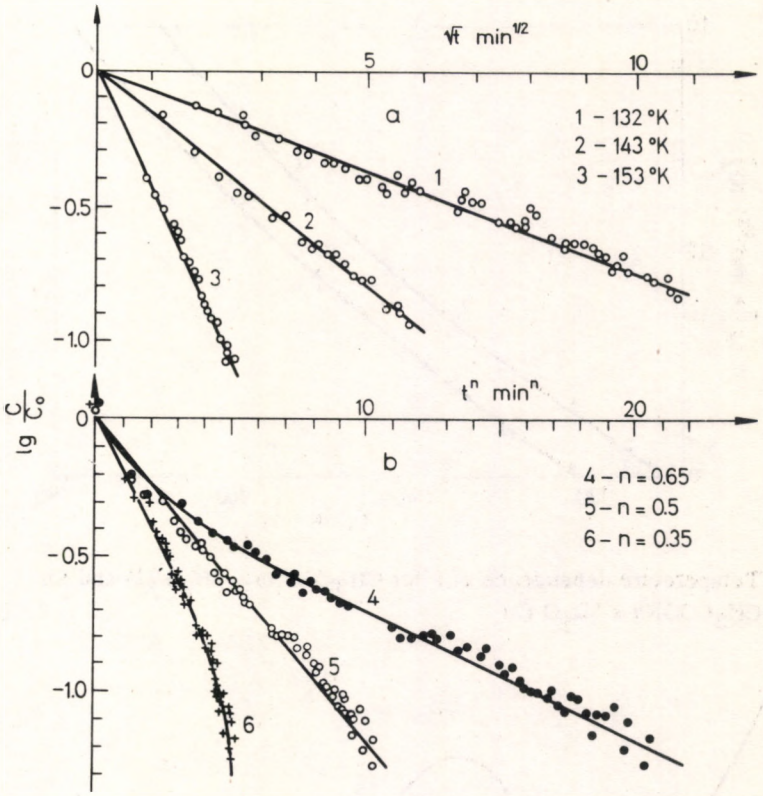

Fig. 1 Decay kinetics of the CH_3 radicals in $CH_3COONa \times 3H_2O$ at several temperatures (a) and in $CH_3COONa \times 3D_2O$ at 145K (b)

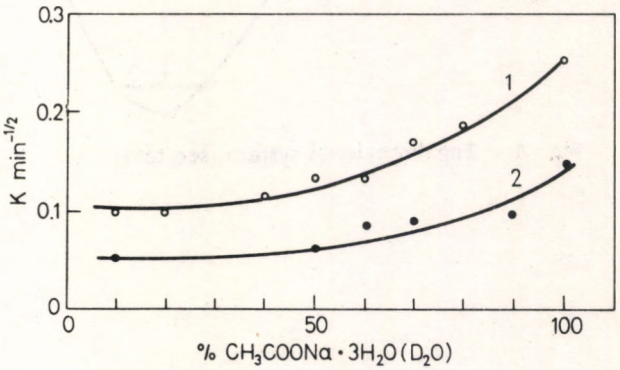

Fig. 2 Isotopic composition dependence of k at 137K. Isotopic composition of water: (1) H_2O, (2) D_2O

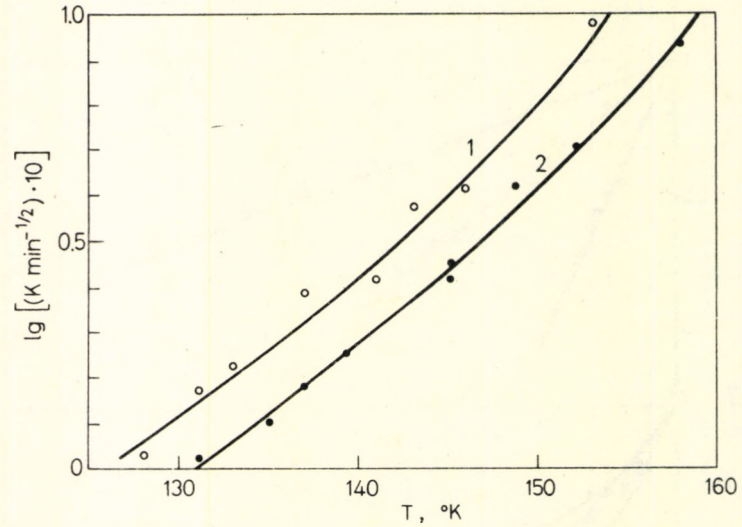

Fig. 3 Temperature dependence of k for $CH_3COONa \times 3H_2O$ (1) and for $CH_3COONa \times 3D_2O$ (2)

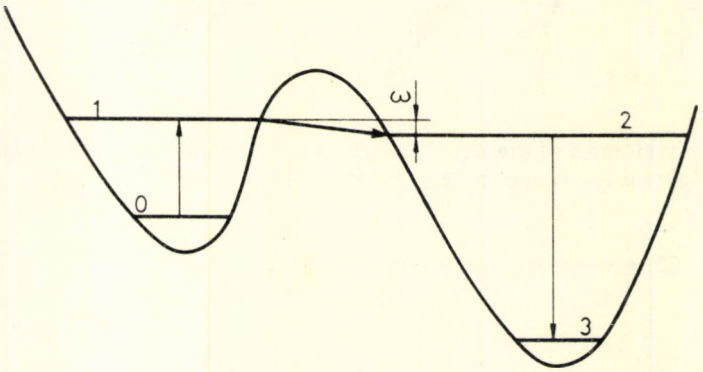

Fig. 4 The three-level system (see text)

I. SOHMA

Is your model different from the quantum tunnelling of an adjacent hydrogen to a methyl radical?

B. V. BOLSHAKOV

Absence of level resonance and the matrix motions come into play through the barrier modulation by the thermal noise.

Yu. BERLIN

(1) It is possible to explain the square-root kinetical law by the diffusion model. Why is it necessary to use the tunnelling model?

(2) Of what size is your barrier?

B. V. BOLSHAKOV

(1) The diffusion model cannot explain the validity of the "$\sqrt{t}$ law" up to 95%.

(2) At present, the form and size of barrier are not known, but one may think that it does not differ from the usually supposed barrier size in tunnelling H-atom reaction (about 10 Kcal/mol; 0.5 Å).

H. WINCEL

Did you determine the isotope effect of the reaction studied and how do these data correlate with those for gas phase?

B. V. BOLSHAKOV

The isotope effect can be seen in Fig. 2. The value is close to the gas phase value.

POSSIBLE REACTIONS OF H_2O^+ IONS AND "DRY" ELECTRONS IN THE RADIOLYSIS OF AQUEOUS SOLUTIONS

O. P. Stepanova, F. G. Nichiporov
Institute of Physics, Moscow, USSR

Chemical reactions brought about by the primary products of water radiolysis – H_2O^+ ion and nonsolvated electron – presently attract more and more attention in view of the radiation transformations at early stages of radiolysis.

The picosecond pulse radiolysis data /1/ demonstrate that at low concentrations of acceptors, electrons are solvated before they take part in chemical reactions, but at concentrations $\geqslant$ 0.1M electrons effectively interact with solutes:

$$e^- + A \longrightarrow A^-. \qquad (1)$$

As to H_2O^+ ions they transform into H_3O^+ ions and OH-radicals during a period of time $< 10^{-12}$ s:

$$H_2O^+ + H_3O \longrightarrow H_3O^+ + OH \qquad (2)$$

in analogy to their behaviour in the gas phase /2/. A question arises whether one can suppress reaction (2) by adding some solute which competes with H_2O for H_2O^+. We can expect that side by side with reaction (2) reactions (3, 4) would take place in sufficiently concentrated solution of acceptors:

$$H_2O^+ + A \rightarrow A^+ + H_2O \qquad (3)$$

$$H_2O^+ + A \rightarrow AH^+ + OH \qquad (4)$$

We have tried to ascertain reactions (3) and (4) investigating the luminescence of aqueous acetone solutions under the action of a proton beam.

As the formation of the exited state of acetone besides direct excitation is connected with ion recombination one may expect that the investigation of this system may give information on the chemical reactions of primary products of water radiolysis.

The usual optical pulse radiolysis system was used with some obvious modifications in order to observe emission spectra. A linear accelerator proton beam of energy of 24 MeV was used by us as source of ionizing radiation. Radiation was never ac-

companied by Cherenkov radiation. Dose per pulse was about 100 krad. The observed luminosity did not change during subsequent 10 – 15 pulses. This shows that luminescence is not connected with the accumulation of any radiolytic products. The shape of luminescence spectrum does not change noticeably with acetone concentration and is in agreement with literature data about the emission spectra of triplet excited acetone molecules /3–5/. From the time dependence of luminescence signal and from the length (20 μs) of the proton pulse we may conclude that the lifetime of observed excited state is $\leq 10^{-5}$ s. This estimation does not contradict the lifetime value $1/\lambda = 20\,\mu$s of triplet acetone /6/. So it is probable that luminosity observed by us is related to the formation of triplet acetone molecules.

The formation of excited states of pure acetone during its irradiation may take place by direct excitation as well as by recombination of acetone ions. It is possible in aqueous solutions that the "direct" action of radiation on acetone which leads to its excitation proceeds at the expense of the energy absorbed by water.

We propose the following mechanism of such action:

$$H_2O^+ + H_2O \xrightarrow{k_2} H_3O^+ + OH \qquad (2)$$

$$H_2O^+ + (CH_3)_2CO \xrightarrow{k_3} \begin{cases} H_2O + (CH_3)_2CO^+ & (3') \\ OH + (CH_3)_2COH^+ & (4') \end{cases}$$

$$e^- + (CH_3)_2CO \longrightarrow (CH_3)_2CO^- \qquad (1')$$

$$(CH_3)_2CO^+ + e^- \longrightarrow (CH_3)_2CO^* \qquad (5)$$

$$(CH_3)_2CO^+ + (CH_3)_2CO^- \longrightarrow (CH_3)_2CO^* + (CH_3)_2CO \qquad (6)$$

Figure 2 shows the dependence of emission intensity L (square of the area under the curve of spectrum) on acetone mole fraction (μ). The form of this dependence supports the assumption on the presence of "indirect" action of radiation in formation of excited acetone: $d^2L/d\mu^2 < 0$ at low μ. At higher μ values the change of the curve is determined by radiationless decay of triplet acetone in water. The value of the rate constant in our case is $k_q \simeq 10^4\ M^{-1}s^{-1}$ in agreement with that estimated in Ref. /6/. Taking into consideration the "indirect" action for L (μ) we may write, in terms of ionic reactions, the following expressions:

$$\frac{L}{L_o} = \left[\frac{G_1}{G_2} (1-x) \frac{1}{1+\dfrac{k_2[H_2O]}{k_3[(CH_3)_2CO]}} + x \right] \cdot \frac{1}{1+\dfrac{k_q}{\lambda}[H_2O]} \qquad (7)$$

Here G_1 and G_2 are yields of the primary active particles in water and acetone respectively and x is the electron fraction of acetone. As we can see from Fig. 2 this mechanism describes the experimental dependence satisfactorily.

In support of reaction (3') competing with (2) we may note that the gas phase ionization potentials of acetone and water are 8.27 eV and 12.6 eV, respectively. Therefore reaction (3') is exothermic (at least if solvation energy can be neglected).

In order to elucidate the role of nonsolvated electrons in the formation of excited acetone mulecules one has to discuss the results of this work in conjunction with the data on positronium formation probability in liquids.

According to the ideas developed in Refs. /7–11/ positronium in liquids is formed by intratrack recombination of nonsolvated electron and positron.

$$e^+ + e^- \dashrightarrow Ps$$

competing with recombination

$$H_2O^+ + e^- \dashrightarrow H_2O^*$$

Figures 3 and 4 show the action of electron acceptors on emission intensity of aqueous acetone solutions and on positronium formation probability, respectively. It should be pointed out that quenching action of solutes on luminosity correlates with inhibiting action on positronium formation. From this it follows that the positronium and excited molecules are formed by similar mechanisms: the precursor of both products is nonsolvated electron*.

To confirm that the oxidizing agent is H_2O^+ ion we have investigated the influence of halide ions on the luminescence of 0.86M acetone aqueous solution. Figure 5 shows that the quenching action of halide ions increases with decrease of their electron affinity. The rate constants of halide ions reactions with PR (PR-excited acetone or its precursor) correspond to the following relations:

$$K_{PR+I^-} : K_{PR+Br^-} : K_{PR+Cl^-} = 100 : 10 : 1 \qquad (8)$$

(K_{PR+Cl^-} denotes rate constant of $PR+Cl^-$ for acid medium, it depends weakly on pH, see Fig. 5).

*The extremely strong quenching action of NO_2^- ions should be noticed. It seems that they act not only as electron scavengers but mainly as positive ions acceptors (being electron donors). It leads to the weakening of the inhibiting action on positronium formation and to the increase of quenching action on luminosity of aqueous acetone solutions.

It is interesting to note that a high reactivity of NO_2^- to trapped electrons in frozen glasses was found in Ref. /14/ and to H_2O^+ ion in Ref. /15/.

It is possible that halide ions (x^-) are donors of electrons to the excited acetone or to its precursors – $(CH_3)_2CO^+$ and H_2O^+:

$$(CH_3)_2CO^* + X^- \dashrightarrow (CH_3)_2CO + +e^-_{solv}$$

$$(CH_3)_2CO^+ + X^- \dashrightarrow (CH_3)_2CO + X.$$

$$H_2O^+ + X^- \dashrightarrow H_2O + X.$$

The relative rate constants of H_2O^+ with X^- in glassy solutions at 77K are given in Ref. /15/:

$$k_{H_2O^+ + I^-} : k_{H_2O^+ + Br^-} : k_{H_2O^+ + Cl^-} = 20 : 4 : 1 \qquad (9)$$

independently of pH*.

From Eqs (8) and (9) and the pH-independence of k_{PR+Cl^-} we can see that identification of PR as H_2O^+ ions is quite likely and does not contradict experimental data. So it appears to be established that the H_2O^+ ions take part in energy transfer from water to acetone.

Thus the conclusion can be drawn that the idea about chemical reactions of primary products of water radiolysis – H_2O^+ ions and "dry" electrons – enables one to understand such phenomena as positronium formation in water and primary radiation chemical yields of water radiolysis products from a unified picture.

References

/ 1/ K.Y. Lam and J.W. Hunt, Int. J. Radiat. Phys. Chem., 7, 317 (1975).
/ 2/ W.L. Tal'roze, E.L. Frankevich, Proceedings of 1st Soviet Symposium on Radiation Chemistry, "Akademiya Nauk", Moscow, 1958, p. 13 (in Russian).
/ 3/ S. Arai, A. Kira, M. Imamura, J. Chem. Phys. 54, 5073 (1971).
/ 4/ G.E. Rences and F.S. Wettack. J. Am. Chem. Soc. 91, 7514 (1969).
/ 5/ R.F. Borkman and D.R. Kearns. J. Chem. Phys., 44, 945 (1966).

* The following are the relations between rate constants of halide ions with OH-radicals /16/:

$$k_{OH+Cl^-} : k_{OH+Br^-} : k_{OH+I^-} = 1 : 0.1 : 1$$

(k_{OH+Cl^-} also refers to acid medium but strongly depends on pH)

/ 6/ G. Porter, R.W. Yip, J.M. Dunston, A.J. Cessno and S.E. Sugamory. Trans. Faraday Soc. 67, 3149 (1971).
/ 7/ L.T. Bugaenko, V.M. Byakov and E.P. Kaljazin. Symposium on Radiation Chemistry of Aqueous Systems (Abstracts), "Nauka", Moscow, 1973, p. 5.
/ 8/ V.M. Byakov, V.I. Goldanskyi, and V.P. Shantarovich, Doklady AN USSR, 219, 633 (1974).
/ 9/ V.M. Byakov, V.I. Grafutin, E.V. Minaichev, F.G. Nitchiporov, Yu. V. Obuchov and O.P. Stepanova. Himiya Vysokich Energii, 10, 3 (1976).
/10/ O.A. Anisimov, Yu.N. Molin. Himija Vysokich Energii, 9, 541 (1975).
/11/ Y.M. Byakov. Intern. J. Radiat. Phys. Chem. 8, 657 (1976).
/12/ S.J. Tao and J.H. Greek, J. Phys. Chem., 73, 882 (1969).
/13/ Bartal, I.B. Nicholas and H.I. Ache, J. Phys. Chem., 76, 1124 (1972).
/14/ J.R. Millu. J. Phys. Chem., 79, II, 1070 (1975).
/15/ W.N. Belevskiy, S.I. Belapushkin, and L.T. Bugaenko, Himiya Vysokich Energii, 9, 252 (1975).
/16/M. Anbar and P. Neta, Intern. J. Appl. Radiation and Isot. 18, 577 (1967).

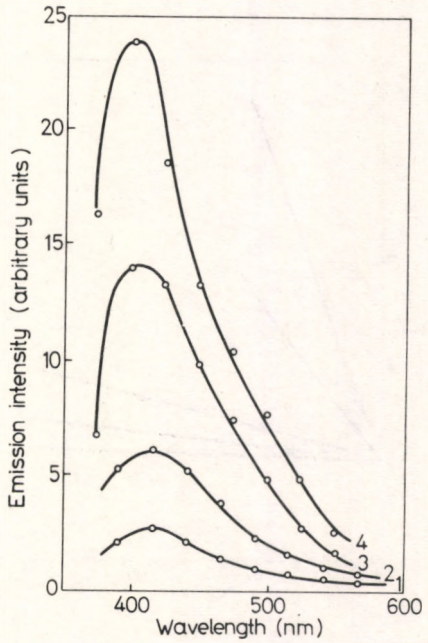

Fig. 1 Emission spectrum from acetone aqueous solutions: (1) 0.86 M acetone, (2) 5.2 M acetone, (3) 8.6 acetone, (4) 13 M acetone

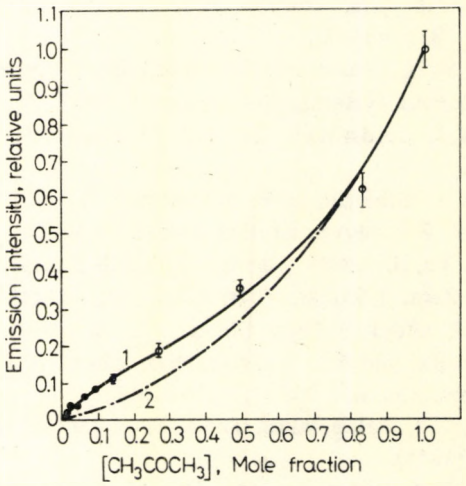

Fig. 2 Emission intensity as function of acetone mole fraction. Curve 1 was calculated from (7), Curve 2 was calculated taking into consideration the direct action of irradiation on acetone only

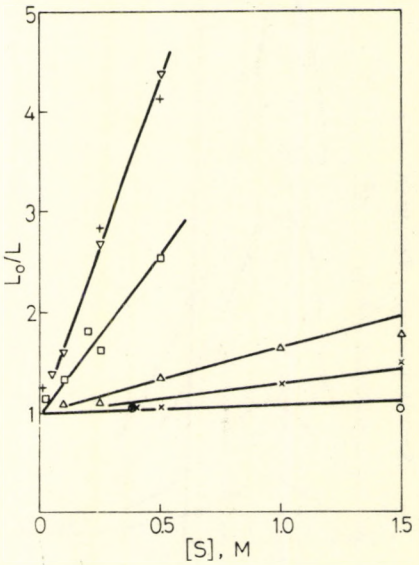

Fig. 3 Inverse emission intensity from 0.86 M aqueous acetone solution as function of concentration of electron acceptors ⊙ – $ZnSO_4$, ⊗ – H_2SO_4, x – $CH_2ClCOOH$, △ – $CdCl_2$, (⊡ – HIO_3, + – $NaNO_2$, ▽ – $Cu(NO_3)_2$

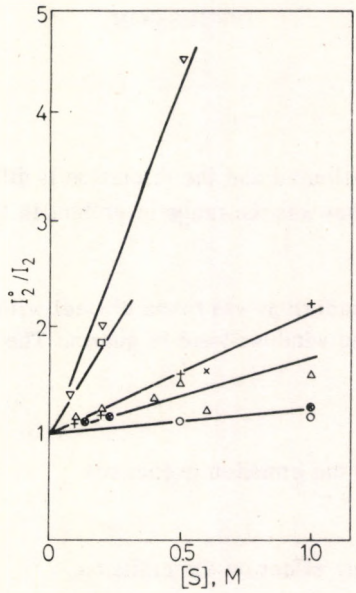

Fig. 4 Inverse probability of positronium formation against the concentration of electron acceptors. ⊙– $ZnSO_4$ /9/, ⊗– H_2SO_4 /12/, x – $CH_2ClCOOH$ /9/, △– $CdCl_2$ /9, 13/, + – $NaNO_2$ /9/, ▽–$CuCl_2$ /10/ ⊡– KIO_3/9/

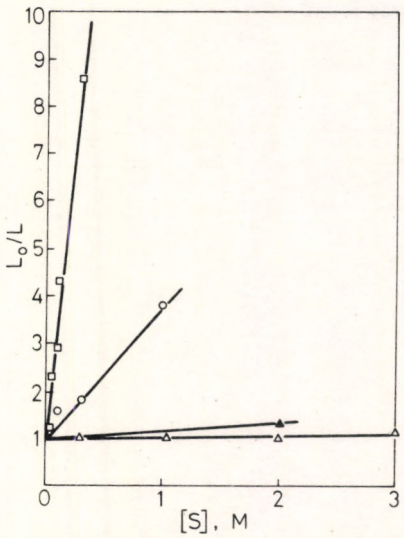

Fig. 5 Inverse emission intensity from 0.86 M aqueous acetone solution against the the halide ions concentration. ⊡– KI, ⊙– KBr, △– KCl, ▲– KCl + 0.4 M H_2SO_4

Z. P. ZAGÓRSKI

The paper was not distributed and the discussion is difficult. However, how was the cell constructed and what was the range of protons in the solution?

O. P. STEPANOVA

The cell for proton-irradiation was made of steel with a wall-thickness of about 0.05 mm. The torus-shaped windows were of quartz. The proton path-length was about 3–4 mm.

C. L. GREENSTOCK

At what pH (acid) was the emission quenched?

O. P. STEPANOVA

H^+ ions do not have any effect on the emission.

C. L. GREENSTOCK

What is the lifetime of the excited state and is it affected by acid?

O. P. STEPANOVA

$\tau_{1/2} \leqslant 10^{-5}$ sec. was found.

SOME REGULARITIES IN OH RATE CONSTANTS

I. Kraljić
Laboratoire de Physico-Chimie des Rayonnements,* Université de Paris-Sud 91405 Orsay, France

Introduction

A considerable number of OH rate constants has thus far been determined by various techniques /1/. The comparison of data obtained with most frequently used methods has shown that they give comparable results and thus the standardization of OH rate constants has been achieved /2/. In view of the important role OH radicals play in radiobiology, it would be of interest to find some correlations and eventually to establish some regularities concerning the reactivity of this strongly oxidizing intermediate. It would be a very complex if not an impossible task to find a rule which would be valid for different systems since OH radicals react with most organic compounds, reducing agents etc. However, it is to be expected that similar systems (compounds) reacting with OH radicals via the same mechanism (in a kind of elementary reaction) would and could show some regular pattern or correlation. Thus; the electron transfer process in reactions between oxidizable anions and OH radicals should depend in some way on the oxidation potential of anions. Another type of regularity may be observed in the reactions of certain classes of organic and biological compounds including bio-polymers. For the success of finding such regularities one needs rather precise results related to the same conditions of pH, etc. The p-nitrosodimethylaniline(RNO) competition method gives precise and reproducible results (when working at low concentrations, etc. /2,4/). Thus, by using such results it has been possible to find some correlations between OH rate constants and several classes of systems which are described in this paper.

Experimental

The radiolytic competition method using RNO for the determination of OH rate constants has been described previously /3, 4/. Doubly or triply distilled water has been used in preparing all solutions. Enzymes, nucleic acid bases and other compounds have been Calbiochem, Merck or Fluka products. Bacteriophage T-2 was isolated in the Laboratori di Fisica, Istituto Superiore di Sanità in Rome. All

*associé au C. N. R. S.

measurements of optical density (O. D.) were performed on a Zeiss PMQ II spectrophotometer, the competition between RNO and T-2 for OH radicals being followed on a Cary 15 spectrophotometer. The pH of all solutions (pH 9.0 or 7.0) was adjusted with a sodium tetraborate or phosphate buffer, the solutions were irradiated in 200-c. or 10000-c. cobalt-60 γ-sources.

Results and discussion

For an elementary reaction between one oxidizing un-charged intermediate, such as the OH radical, and various (reducing) anions occurring via the same mechanism one would expect that easily oxidizable anions would react faster than those which are difficult to oxidize. In order to see what kind of relationship this can give, the oxidation potential of anions vs. their OH rate constants was plotted (Fig. 1). For halides, pseudohalides and some other anions the dependence obtained is not a simple one, but most anions presented in Fig. 1 are on or close to the drawn curve. If one assumes as a first approximation that this dependence is valid, it would then be possible to evaluate the oxidation potential of an anion if one knows the rate constant of its reaction with OH radicals. For reaction 1:

$$N_3^- \longleftrightarrow \frac{1}{2}(N_3)_2 + e^- \qquad (1)$$

the oxidation potential cannot be measured since $(N_3)_2$ is not stable enough to make the process really reversible. From the plot in Fig. 1 and using the easily determined rate constant of the reaction N_3^- + OH one can evaluate the oxidation potential of reaction (1) to be around -0.2 V.

The curve in Fig. 1 shows a maximum at the oxidation potential around $\pm$ 0 V. This is rather difficult to understand. It may mean that the mechanism of electron transfer from anions to OH radicals is not a simple process, i.e. that it may occur via two somewhat different pathways. It is also possible that another parameter, besides the oxidation potential, plays an important role in these electron transfer reactions.

If a group of similar compounds (e.g. nucleic acid bases) reacts via the same mechanism with some other species, one would expect that the reactivity of addition (condensation) products should in some way depend on the reactivity of both reacting partners. In such a case the competition for OH radicals between the two moieties can take place and may lead to an intermediate rate constant for the addition product. By looking into the data on OH rate constants of nucleic acid bases, nucleosides and nucleotides shown in Table 1 it can be seen that the nucleosides (or nucleotides) have the rate constants which are in between the rate constants of the base and of the sugar. These results obey rather closely the

simple expression:

$$k_n = \frac{k_b + k_s}{2} \qquad (2)$$

In the case of nucleotide, one takes for k_s the rate constant of the sugar phosphate. Using this equation, the calculated rate constants of nucleosides and two nucleotides agree well ($\pm$ 10% error) with the measured values. For the base guanine, which is sparingly soluble, we did not measure its OH rate constant. The calculated value based on Eq. (2) indicates that this base reacts very rapidly with OH radicals, i. e. faster than other nucleic acid bases. It can be mentioned that such an expression can be valid if the measurements pertain to the same conditions of pH and if the reactive sites of the two reacting moieties in the condensation product are not too much influenced by the bond formed between them.

An extension of Eq. (2) to halogenated uracils (bromo- and iodo-derivatives) seems also to be valid, but in this case it is more difficult to explain such a behaviour:

$$k_{Hal\text{-}U} = \frac{k_U + k_{Hal^-}}{2} \qquad (3)$$

$k_{Hal\text{-}U}$ = OH rate constant of halogenated uracil, k_{Hal^-} = OH rate constant of halide ion, k_U = OH rate constant of the uracil. In order to explain the validity of Eq. (3) one can assume that the halogen atom in Hal-U would have a partial reactivity which is observed for the halide ion (Br^-, I^-), which may be a reasonable assumption for reactions with an uncharged radical (OH). In the case of 5-bromouracil (5-BU) this expression gives an error of about 10% for the calculated rate constant, for idio-derivatives the error may be larger (Table 1).

The competition method using RNO can be applied to the determination of OH rate constants of bio-polymers, such as enzymes /4/ and even bacteriophages. The results on OH rate constants of several enzymes plotted vs. their molecular weight (MW) give a roughly linear relationship (Fig. 2). The active volume or the surface of the enzyme which is open to the OH radical attack depends on the molecular weight of such a polymer, thus one may expect as a first approximation that larger enzymes would have higher rate constants than the smaller ones. However, it is possible that the enzymes or proteins having relatively high proportion of rapidly or slowly reacting amino acids would not obey this linear relationship.

The native bacteriophage has a protein coat around the nucleic acid core. On the surface of it the amino acids of coat proteins can react with OH radicals which diffuse towards the phage particle. Again, one can expect in the first approximation that the larger the phage the higher the OH rate constant could be observed. The rate constant for the reaction of the phage T-2, obtained in competition experiments with RNO, is $2,9 \times 10^{14} M^{-1}s^{-1}$. By extrapolation of the linear plot

Table 1

Rate constants for OH radical reactions with components of nucleic acids (in units of $10^9 M^{-1}s^{-1}$)

Base	$k_{base + OH}$	$k_{nucleoside + OH}$	$k_{nucleotide + OH}$
T	6.2[+]	4.7 4.3[a]	
U	6.8[x]	4.1 4.4[a]	
C	6.5	4.2 4.3[a]	3.9 4.2[a]
A	6.1	4.5 4.1[a]	4.1[+] 4.1[a]
G	13.0[a]	7.6[+]	
5-BU	4.2[+] 3.9[a]		
5-IU	>6.2 10.0[a]		
5-IUdR	>6.2 9.1[a]		

Sugar	Ribose	Ribose-monophosphate	Desoxy-ribose
$k_{s + OH}$	2.14[+]	2.05	2.42

a: Calculated values obtained by means of Eq. (2) or (3).
x: Reference /3/
+: Reference /4/

in Fig. 2 one obtains somewhat lower value for this rate constant but the agreement is still rather good ($1.6 \times 10^{14} M^{-1}s^{-1}$). In the absence of some further rate constants for the phages or viruses it is premature to consider that the linear relationship should be valid. In these experiments with T-2 it was also found that RNO, which is a specific OH radical scavenger in dilute aerated solutions, protects the phage very well, confirming thus that the major damaging agent in the radio-biology of aerated systems is the OH radical /7/.

Acknowledgements. The author wishes to express his thanks to Dr. Clara Frontali and to Dr. M. Ageno for their kindness and hospitality during the work on phage T-2 in the Laboratori di Fisica, Istituto Superiore di Sanità, in Rome. Thanks are also due to Dr. C. N. Trumbore for helpful discussions and comments.

References

/1/ M. Anbar and P. Neta, Int. J. Appl. Radiat. Isotopes, 18, 493 (1967).
/2/ R. L. Willson, C. L. Greenstock, G. E. Adams, R. Wageman and L. M. Dorfman, Int. J. Radiat. Phys. Chem., 3, 211 (1971).
/3/ I. Kraljić and C. N. Trumbore, J. Am. Chem. Soc., 87, 2547 (1965).
/4/ I. Kraljić, The Chemistry of Ionization and Excitation, Eds, G. R. A. Johnson and G. Scholes, Taylor and Francis Ltd, London 1967, p. 303.
/5/ Handbook of Chemistry and Physics, D-111, Chemical Rubber Co., Cleveland, Ohio 1972-1973.
/6/ K. R. Lynn and G. Orpen, Int. J. Radiat. Biol., 14, 363 (1968.
/7/ I. Kraljić, Third Int. Congress of Radiation Research, Cortina d'Ampezzo, 1966, Book of Abstracts, No. 525 p. 133.

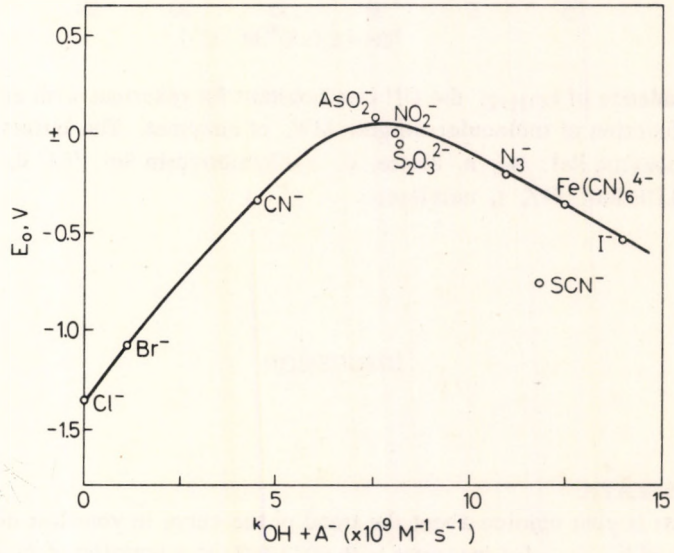

Fig. 1 Dependence of k_{OH+A^-}, the OH rate constant for reactions with anions, on the E_o, the redox potential of anions. The data on OH rate constants are from Refs /3/ and /4/, the redox potentias are from Ref. /5/

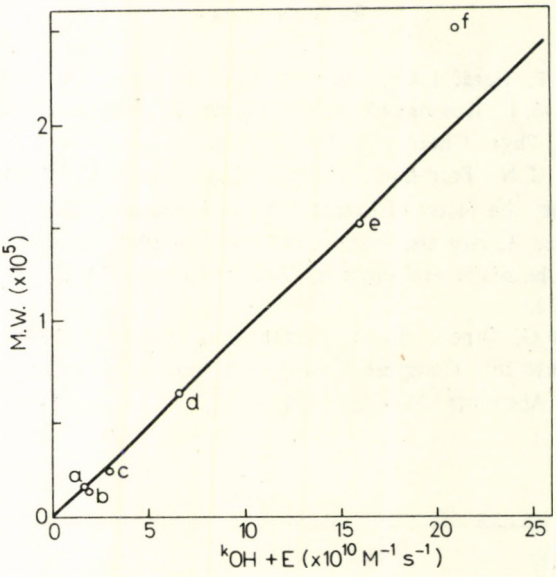

Fig. 2 Dependence of k_{OH+E}, the OH rate constant for reactions with enzymes, as a function of molecular weight, MW, of enzymes. The letters are: a, lysozyme Ref. /4/, b, RNase, c, α-chymotrypsin Ref. /6/, d, DNase I, e, ALDH Ref. /4/, f, catalase.

DISCUSSION

G. V. PUTIRSKAYA

(1) What is your opinion about the trend of the curve in your last diagrams (the dependence of $k_{OH + E}$ for reactions with enzymes, as a function of molecular weight) with the further increase of molecular weight? Will it have a saturating character or not?

(2) I do not understand, how you have a linear dependence of $k_{OH + E}$ versus M. W. if the increase of M. W. of molecules is not a linear function of their surface.

I. KRALJIC

(1) I should like to point out that this dependence is roughly linear and may serve in predicting the approximate value for OH rate constant of enzymes and proteins having molecular weight in the limit of the diagram (Fig. 3). With enzymes

of higher molecular weight one expects to obtain higher absolute values for OH rate constants owing to a larger volume and surface which may react with OH radicals diffusing toward the polypeptide. The very high OH rate constant for phage T-2 may mean that there would be no saturation or levelling off. How far the roughly linear relationship would go is difficult to tell without making more experiments.

(2) The native enzymes and proteins have secondary and tertiary structure (with many hydrogen bonds) and may not show the linear relationship between M. W. and the surface. The roughly linear dependence between M. W. of enzymes and their OH rate constants is based on experimental results, moreover, this linear relationship seems to be in agreement with the results by Dale on protection experiments in which the protection effect obtained by various proteins did not depend on M. W. but only on their weight amount. Such a behaviour indicates linear relationship between M. W. and the rate constant for reaction with reacting radical (OH radical). At this time I do not know how to explain theoretically the roughly linear relationship in Fig. 3.

I. KALECINSKI

(1) Can you explain the non-linear dependence between the rate constants and the redox potentials?

(2) I would like to inform you that some years ago we (B. J. Trzebintowska, E. Kalecinski, I. Kalecinski) measured the rate constants of the reaction between the complex ions of the type: $M(CN)_5NO^{n-}$ and the OH radicals and e^-_{aq}. We obtained a good correlation between the rate constants and the infrared frequency at the NO group. The last one is to some extent the measure of the electron-activity of the NO group.

I. KRALJIC

(1) There are two possibilities which could cause such a dependence (a) it may be that the mechanism of electron transfer from these anions occurs via two different pathways (with and without formation of intermediate OH adduct), and (b) some other parameter than E_o is more important in these reactions.

(2) Your work on nitroso-pentacyano-complexes indicates that it is the NO-group which is the major reactive site in reactions with OH radicals and e^-_{aq}.

C. L. GREENSTOCK

(1) Electron transfer oxidations of donors by OH are in equilibrium and for poor donors there will be a considerable back reaction which will reduce the effectiveness of A^- in competing with RNA for OH radicals, thus changing the estimated rate constants. Could this account for the non-linear relationship between redox potential and rate constant?

(2) When DNA is degraded chemically or enzymically the reactivity increases with decreasing MW.

(1) In the determination of these OH rate constants (Fig. 1) simple competition kinetics were always valid indicating that back reactions were not important. The non-linear relationship may indicate that the oxidation potential of anions is not the major parameter influencing the OH rate constants. Another parameter, such as the free energy, may be decisive for such reactions.

(2) Degraded DNA has an overall reactivity which is higher than that of non-degraded DNA, but at the same time the molar concentration is increased. On the other hand, the absolute value of OH rate constant for longer DNA molecules will be higher than for shorter ones (supposing otherwise the same base composition).

RADIATION INDUCED PRECIPITATION OF FERRIC COMPOUNDS FROM NEUTRAL AQUEOUS FERROUS SALTS SOLUTIONS

Zofia Stuglik, Zbigniew Paweł Zagórski
Department of Radiation Chemistry, Institute of Nuclear Research, Warsaw, Poland

Introduction

The system of Fe(II) (SO_4^{2-}, or ClO_4^-) in neutral aqueous solution (pH 6−8), being currently the subject of our research in the field of pulse radiolysis, offers interesting new observations in radiation chemistry of iron salts. Iron (II) ions, weakly or not coordinated, are stable up to the pH of 7−8 whereas iron(III) precipitates in the same medium already over pH 4. Irradiation of neutral iron(II) solution results in the formation of yellowish brown precipitate. The solution must be oxygen free from the initial stage of preparation, because traces of O_2 cause irreversible precipitation. Some phenomena observed in the system are already published /1/: the present paper concentrates on the phenomenon of precipitation of Fe(III) hydroxides.

Experimental

As the source of radiation the ~ 1.5 A electron (10 MeV) beam from our linac LAE13/9 was applied. Pulse duration was 2.5 or 5.5 μs.

Pulse radiolysis arrangement for transient absorption measurement was using some parts from our "Stand No 1 for Pulse Radiolysis" /2/ but contained new elements from the "Stand No 2" (not yet published). The single light path was 2 cm long. The system of syringes was specially adapted for the oxygen free preparation, analysis and processing of solutions.

The arrangement for the measurement of scattered light was a new one. The scheme of it is shown in Fig. 1. In the construction of this stand, we used experience gained during the investigation of a faint emitted light in the Čerenkov Light Selfabsorption Method /3/. After several attempts to measure scattered light from a laser beam we have found the xenon arc lamp to be superior to the laser, due to the free choice of wavelengths. The optimum wavelength was 400 nm. Preparation of reagents is due to be published in the complete paper on the Fe(II)-neutral radiation chemistry.

Results

The motivation for this particular investigation was

i) to find out to what extent the precipitation influences the measurement of transient spectra in neutral Fe(II) solutions,

ii) to collect information on the reactivity of Fe(III) during the course of polymerization,

iii) to find out the kinetics of final precipitation, i. e. the formation of a sol.

The first measurements have shown that the process of precipitation is a slow one thus it does not interfere with the measurement of spectra after the pulse. Figure 2 shows the spectrum identified as $FeOH^{2+}$ in $Fe(ClO_4)_2$ + $NaClO_4$ solution (pH 6). It is identical with the spectrum obtained in $FeSO_4$ + Na_2SO_4 solution (pH 7. 5) published in an earlier paper /1/. The comparison of both spectra proves that sulphates do not play any substantial role in this stage of reactions.

It is surprising that the full precipitation process lasts for several seconds. We have taken every care to exclude the possibility of photochemical effects at such prolonged illumination of the system. For this purpose each sample was checked: illumination was periodically interrupted by the action of the shutter. No substantial photochemical effects were found, therefore we present only continuous measurements.

Figure 3 shows the process of precipitation as observed through scattered light after the application of 10 pulses (totalling krads), denoted by the bar. The system was composed of 2×10^{-2} M $FeSO_4$, 0. 1 M Na_2SO_4, pH 7. 0, N_2O saturated.

Figure 4 shows the different influence of subsequent pulses on the system. The first pulse (arrow) does not contribute much to the process of precipitate formation, the next ones (arrows), applied to the same sample cause more precipitate to form. The system, a little faster one in precipitation, was composed of 10^{-2}M in $FeSO_4$, 0. 1 M Na_2SO_4, Ar saturated.

The $FeOH^{2+}$ is not reactive towards products of water radiolysis, as was proved by the application of different dose rates and by administering a train of pulses to the system. Some phenomena expected from colloid chemistry were also observed. For example, an excess of $FeSO_4$ exhibits a protective effect on the sol formed and makes the precipitation process longer.

Discussion

The measurements on precipitating systems show, that the first pulse connected with the delivery of ca 5–10 krads is not very effective in producing Fe(III) precipitate which scatter light. $FeOH^{2+}$ polymerizes very slowly i. e. the process takes a few seconds. Subsequent pulses, creating new $FeOH^{2+}$ are more effective in this respect. The new $FeOH^{2+}$ formed probably attaches to the already existing, larger aggregates thereby contributing to the increase in dissipated light.

REFERENCES

/1/ Z. Stuglik, Z. P. Zagórski, Radiochem. Radioanal. Letters 22, 257 (1975).

/2/ Z. P. Zagórski, J. Grodkowski, Z. Zimek, W. Roszczynko, Institute of Nuclear Research Report, IBJ – Report 1564/XVII/C/B, 1975.

/3/ Z. P. Zagórski, Z. Zimek, Int. J. Radiat. Phys. Chem. 7, 529 (1975).

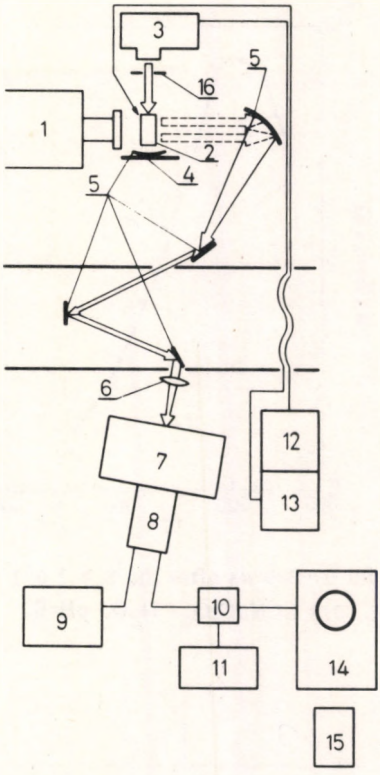

Fig. 1 Pulse radiolysis arrangement for the measurement of kinetics of scattered light after the pulse irradiation.

1 – window part of the linear electron accelerator
2 – suprasil cell with two optically perfect windows (facing white arrow and dotted arrows)
3 – Xenon lamp with housing and filters
4 – A screen with mirror opposite the cell
5 – Mirrors collecting scattered light and forming the periscope system
6 – Quartz lens
7 – Monochromator
8 – Photomultiplier
9 – High voltage supply
10 – Set of damping and filtering electronics
11 – Light level measurement
12 – Panel for steering of solution exchange
13 – Panel for xenon lamp operation
14 – Oscilloscope Tektronix 556
15 – Hewlett Packard, Polaroid Camera
16 – Shutter operated from outside the accelerator room

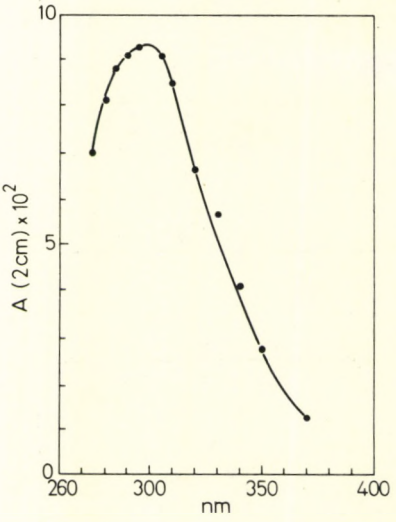

Fig. 2 Spectrum lasting for 0 −200 μs after the 3.7 $\pm$ 0.1 krad pulse, applied to 10^{-2} M $Fe(ClO_4)_2$, 0.1 M $NaClO_4$, N_2O, pH=6

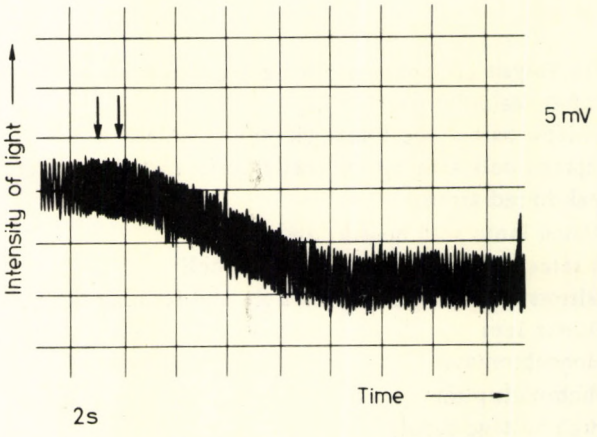

Fig. 3 Scattered xenon arc light at 400 nm from pulsed solution of 2 x 10^{-2} $FeSO_4$, 0.1 M Na_2SO_4, NO_2 saturated pH7.0. 10 pulses (7 Krad each) applied between arrows

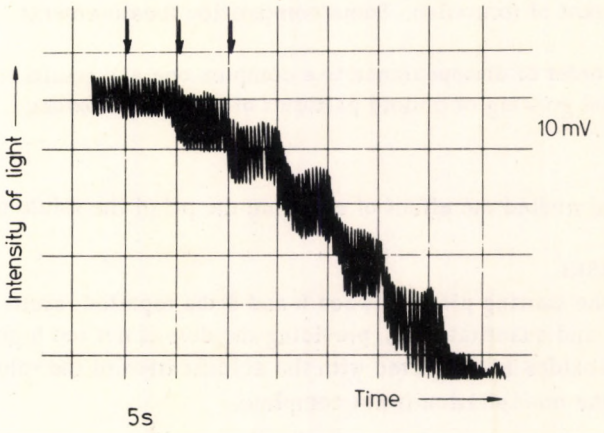

Fig. 4 Scattered xenon arc light at 550 nm from solution 10^{-2} M $FeSO_4$, 0.1 M Na_2SO_4, Ar saturated pH 7.0. Pulses of 7 krads repeated every 5 seconds

DISCUSSION

R. SCHILLER

Did you record the absorption during nephelometry and if so what was the spectral behaviour like on this very long time scale?

Z. P. ZAGORSKI

Yes, in the absorption measuring regime one sees gradually lowering level of analysing light, due to the scattering of light by growing particles. However, in this long time scale there are no new intermediates, and the important, early one is measured during, and just after the pulse when there is no colloid present yet.

I. KRALJIC

(1) On what basis can you consider the intermediate $Fe(OH)^{2+}$ as a primary product of Fe^{2+} + OH reaction? Does the rate constant of this reaction correspond to the rate of formation of the intermediate $Fe(OH)^{2+}$?

(2) What is the order of disappearance of the intermediate $Fe(OH)^{2+}$?

Z. P. ZAGORSKI

(1) Yes, from the ČLS Method we know that $FeOH^{2+}$ is the first product observed on the nanosecond time scale. At the moment we cannot give the precise value of

the rate constant of formation. Some competition measurements are still being performed.

(2) The order of disappearance is a complex one and results from the slow nucleation and growing of colloid particles of Fe(III) hydroxides.

R. MAY

Have you studied the effect of changing the pH of the solution?

Z. P. ZAGORSKI

Yes. If the starting pH is between 6 and 8 the reported results are the same, both qualitatively and quantitatively, providing the dose is not too high. The precipitation of Fe(III) hydroxides is connected with the acidification of the solution. If the dose is too high, the precipitation is not complete.

R. BUITENHUIS

By which method do you remove oxygen: by deaeration before preparation of the samples and handling later on under an oxygen-free atmosphere?

Z. P. ZAGORSKI

Preparation of the sample is performed in the special apparatus, where the solution containing at first only Na_2SO_4 or $NaClO_4$ is deaerated or saturated with N_2O. Next a pre-weighed small crystal of $FeSO_4 \cdot 7H_2O$ (or perchlorate) is added under air-free conditions, pH controlled and the solution pumped into a syringe.

M. COLOSIMO

Have you any effect due to the concentration of iron (II) ?

Z. P. ZAGORSKI

Yes: (1) There is an influence of [Fe(II)] on the final $G_{Fe^{3+}}$ value (cf. Ref. /1/)

(2) There is no influence on the intermediate spectrum of $FeOH^{2+}$ after the pulse.

(3) There is a slight influence of Fe^{2+} concentration on the kinetics of Fe(III) hydroxides polymerisation, and sol formation.

PULSE RADIOLYSIS OF THE LANTHANIDE AND ACTINIDE ELEMENTS

S. Gordon, J. C. Sullivan, W. A. Mulac, D. Cohen, K. H. Schmidt
Chemistry Division, Argonne National Laboratory, Argonne, Illinois 60439. U. S. A.

Introduction

The focus in fundamental studies of the solution chemistry of lanthanide and actinide ions lies in describing the role of the 4f and 5f electrons of the respective series in chemical reactions and providing a basis for developing models for the interaction of these electrons with their chemical environment.

Pulse radiolysis is a powerful tool for probing these roles using the e^-_{aq} and OH radical to study the redox properties of these ions in various valence states. The rate constants for the reaction of e^-_{aq} with most of the lanthanide +3 ions have been reported /1−4/, as well as some of the properties of the resulting +2 ions resulting from a few of these reactions /4, 5/. In addition, some rate constants have been reported for Pu and Np ions under various conditions /6, 7/.

Although there is reasonable agreement on the e^-_{aq} rate constants for many of the lanthanides, serious discrepancies remain in the values reported for a number of the members of this series /8/.

We have reexamined in greater detail the rate constants for the reaction of e^-_{aq} with all the lanthanides and have obtained spectra of the resulting product +2 ions for several which have been as yet unreported.

In addition, we have determined rate constants for e^-_{aq} with a number of actinides and have determined the spectra of transients and stable species resulting from a number of these reactions.

Experimental

The perchlorates of the actinides were prepared as previously described /9−11/. The lanthanide perchlorate solutions were prepared from the solid perchlorates (purity 99.99%), or obtained from the oxide (99.99%) by fuming the oxide with $HClO_4$, evaporating the solution to dryness, fumed a second time, evaporating to dryness again and then diluted with H_2O to the desired concentration and the pH adjusted with carbonate-free NaOH.

The lanthanide solutions were degassed by the syringe technique. Radioactivity associated with the actinides precluded using the syringe technique for degassing and a bubbling technique was used in which the irradiation cells were filled directly from

the degassing unit. The oxygen content of the degassed solution was determined on a Van Slyke-gas chromatograph combination /12/ and was found to be of the order of 0.1 μM/l in all cases.

Spectra of the transient species produced by single electron pulses were obtained using a streak camera-TV scanning method described in previous publications /13, 14/. The rate data were obtained by conventional photomultiplier techniques /15/.

The kinetic data were scanned from a smoothed trace of the Polaroid film by using an automatic line follower (Hewlett Packard, Type F3B), converted to digital form in a 400 channel analyzer and processed by a Xerox Sigma V computer. Some data were obtained by digitizing the PMT output in a Biomation 8100 transient recorder in conjunction with a backoff circuit and processed by the Sigma V computer. The unweighted data were processed by a nonlinear least squares program with parameters k, I_0 and I, where k is the pseudo first order rate constant, I_0 is the initial light intensity and I is the light intensity at time t. Standard deviations were calculated and are given in the text. The pseudo first order rate constants were plotted as a function of concentration of the ion involved and the second order rate constant obtained from the slope obtained by a least squares linear regression analysis of the data.

Results and discussion

Lanthanide series.

The rate constants for the reaction of e^-_{aq} with the lanthanide series of elements are summarized in Table 1.

The rate constants in this study reported in Table 1 were determined over a wider concentration range than previous studies. In addition, Baxendale et al. /2/ have pointed out the importance of using fresh solutions due to slow coagulation of the hydrolyzed lanthanides. In addition, the salts used in this study were perchlorates rather than sulfates.

The data in Table 1 can be roughly divided into three groups: (a) the group with rate constants in the range of 10^{10} M^{-1} sec^{-1} comprising Eu, Yb, and Sm, (b) an intermediate group with rate constants ($10^7 - 10^8$) comprising Gd, Ho, Er, and Tm, and (c) a relatively unreactive group with rate constants (10^6 and less) consisting of Pr, Nd, Dy, Tb, and Lu. The suggestion has been made that the $4f^0$, $4f^7$ and $4f^{14}$ shell configuration lead to relative ion stability. The rate constant data for Eu and Yb are in agreement with this concept but it fails when applied to Gd, Ho, Er, and Tm.

Faraggi et al. /4/ have studied the effect of ionic strength on the reactions of e^-_{aq} with Eu(III), Sm(III), and Yb(III). They found that a plot of ionic strength against rate constant for all three of these reactions resulted in a slope of -5.9. They interpreted this as evidence for dimerization of these trivalent ions in solution. We have studied the effect of ionic strength on the rate constant of e^-_{aq} with Eu(III) using $Li(ClO_4)$ to vary the ionic strength. Using the same impact parameter as Faraggi, et al., we observed in sharp contrast to their results a slope of -1.5. The slope of -5.9 indicating

Table 1
pH 6.0, T = 23 °C

Lanthanide	Conc range ($M \times 10^3$)	This study	Ref. 1	Ref. 2	Ref. 3
Eu^{+++}	0.057 − 0.285	$(6.50 \pm 0.03) \times 10^{10}$	6.10×10^{10}		$(6.1 \pm 0.3) \times 10^{10}$
Yb^{+++}	0.0219 − 0.226	$(4.30 \pm 0.2) \times 10^{10}$	4.3×10^{10}	3.7×10^{10}	$(4.7 \pm 0.3) \times 10^{10}$
Sm^{+++}	0.05 − 0.107	$(1.96 \pm 0.10) \times 10^{10}$	2.5×10^{10}		$(2.3 \pm 0.3) \times 10^{10}$
Tm^{+++}	0.105 − 0.158	$(3.29 \pm 0.24) \times 10^{8}$	3×10^{9}		
Gd^{+++}	3.0 − 60.0	$(9.12 \pm 0.72) \times 10^{7}$	5.5×10^{8}		
Ho^{+++}	7.31 − 146.0	$(1.44 \pm 0.02) \times 10^{7}$	2.4×10^{9}	6.6×10^{7}	
Er^{+++}	6.0 − 150	$(1.01 \pm 0.04) \times 10^{7}$	7.7×10^{7}		
Pr^{+++}	6.9 − 115.0	$(2.33 \pm 0.1) \times 10^{6}$	2.9×10^{8}	1×10^{7}	
Nd^{+++}	3.7 − 61.9	$(3.18 \pm 1.2) \times 10^{6}$	5.9×10^{8}		
Tb^{+++}	7.2 − 121.0	$\ll 10^{6}$	3.7×10^{8}	1.7×10^{7}	
Dy^{+++}	3.0 − 226.0	$(3.51 \pm 0.32) \times 10^{6}$			
Lu^{+++}	22.0 − 114.0	$(4.86 \pm 0.13) \times 10^{6}$			

a charged ion of +6 does not seem reasonable to us. In fact if the Eu(III), Yb(III), and Sm(III) existed as dimers in solution, the rate constants for e^-_{aq} with these ions as calculated from the pseudo first order constants would be double the values reported by them. This would lead to a value for the rate constant of e^-_{aq} reacting with Eu(III) of greater than 10^{11} which is rather unlikely. Furthermore, the existence of a $(Eu)_2^{+6}$ as a noncoordinated ion is not very probable and is further inconsistent with the impact parameter of 1.33 used in their ionic strength plot. A further inconsistency is their use of a radius of 5 Å for Eu(III) reacting with Sm(II) to calculate the rate constant for this reaction using the Debye equation. This value of 5 Å would lead to an impact parameter of 2.5 for the ionic strength plot instead of the value of 1.33 which they used. Figure 1 shows our ionic strength plot for the dependence of $k[e^-_{aq} + Eu(III)]$ using 2.5 as the impact parameter. Each point on this figure represents a value of the logarithm of the second order rate constant obtained from the dependence of the pseudo first order rate constant on Eu(III) concentration at different values of ionic strength. The slope of this plot is -2.05 ± 0.05. A possible explanation for this value is the hydrolysis of the Eu(III), Eq. (1):

$$Eu^{3+} + nH_2O \rightleftharpoons Eu(OH)^{2+}(H_2O)_{n-1} + H^+ \qquad (1)$$

Using our streak camera technique we have determined spectra for divalent Eu, Sm, Yb, Tm, Gd, and Ho. Our spectrum for Sm(III) agrees fairly well with that reported by Pikaev et al. /5/. Figure 2 shows the divalent spectra which we obtained by using a single 3 μsec pulse on (a) 0.1 M $Tm(ClO_4)_3$ at pH 6.0 under 100 atmospheres pressure of H_2, (b) 0.1 M $Gd(ClO_4)_3$ at pH 6.0 under 100 atmospheres of H_2 and, (c) 0.13 M $Ho(ClO_4)_3$ at pH 6.0 containing 0.1 M tertiary butanol.

The H_2 converts the OH radical to an e^-_{aq} by

$$OH + H_2 \longrightarrow H_2O + H \qquad (2)$$

$$H + OH^- \rightleftharpoons e^-_{aq} \qquad (3)$$

The tertiary butanol scavenges the OH radical and the spectrum of a pulsed blank tertiary butanol solution has been subtracted from the spectrum produced in solution (c) to give the spectrum C. Pulsing a solution of $Ho(ClO_4)_3$ under 100 atmospheres of H_2 gave the same spectra as shown in Fig. 2C.

Actinide series. It is interesting to compare the reactivity of the actinide series (5f) with e^-_{aq} with the lanthanide series (4f). Table 2 lists rate constants for a number of transuranic elements. Pikaev et al. /6, 7/ have studied reactions of e^-_{aq} with Np in various oxidation states in highly alkaline solutions. The data reported in Table 2 were obtained at pH's of 5.3–6.8 where the structures of the ions investigated are more firmly established.

Table 2
Rate constants for e^-_{aq} + An[a]

	pH	[M] ($\times 10^{-4}$)	k(10^{10} M^{-1} sec^{-1})	E^o, v[b]
Am(VI)	5.3	0.104 – 0.833	3.11 $\pm$ 0.08	
Am(VI)	6.0	0.12 – 1.20	3.95 $\pm$ 0.87	
Am(V)	5.2	0.14 – 2.80	2.68 $\pm$ 0.01	
Pu(VI)	5.6	0.12 – 1.00	6.44 $\pm$ 0.37	-0.916
Pu(VI)	6.1	0.09 – 1.08	5.76 $\pm$ 0.27	
Np(VI)	5.3	0.20 – 2.00	6.32 $\pm$ 0.05	-1.137
Np(V)	5.8	0.202 – 3.03	5.43 $\pm$ 0.18	
Np(V)	5.3	0.21 – 2.10	1.97 $\pm$ 0.04	-0.739
Np(V)	6.1	0.208 – 1.08	2.13 $\pm$ 0.03	
U(VI)	5.3	0.50 – 10.0	1.73 $\pm$ 0.01	-0.063
U(VI)	6.8	0.10 – 1.00	1.25 $\pm$ 0.02	

[a] 24°C, $I = 1 \times 10^{-3}$

[b] For the reactions, $AnO_2^+ + H^+ = AnO_2^{++} + 1/2H_2$.

It should be noted that all the rate constants for the An(VI) and An(V) elements listed in Table 2 appear to be diffusion controlled and except for Eu(III), Sm(III), and Yb(III), are much higher than the corresponding trivalent lanthanide series.

The data in Table 2 also indicate that for the reduction of Np(V) there is no evidence for a hydrogen-ion dependence of the rate constants. There is a small increase in the values of the apparent rate constant with decreasing pH for the Pu(VI), Np(VI) and U(VI) ions although the variations in the case of Pu(VI) is not statistically significant. Am(VI) shows an increase of rate constant with increasing pH. In addition, there is no apparent correlation between the rate constants and the oxidation potential of the oxidants.

It is rather surprising that the rate constants for the reactions

$$e^-_{aq} + An(VI) \longrightarrow An(V) \qquad (4)$$

and

$$e^-_{aq} + An(V) \longrightarrow An(IV) \qquad (5)$$

do not differ by a greater amount than is actually observed. Reaction (4) does not require any structural changes in the ions involved whereas reaction (5) requires a reorientation of the six coordinating water molecules.

The lack of correlation between oxidation potentials of the An(V) and An(VI) ions and with structural changes may be the results of the fact that all the reactions appear to be diffusion controlled. Another possible explanation is that these reactions proceed by a tunnelling mechanism, also suggested by Pikaev et al. /6/.

In addition to these rate constants, we have obtained transient spectra for Am(IV) both by reduction of Am(V) with e^-_{aq} and oxidation of Am(III) with OH. We have also observed a transient spectrum presumably Cm(IV) from the oxidation of Cm(III) with the OH radical.

References

/ 1/ J. K. Thomas, S. Gordon, and E. J. Hart, J. Phys. Chem., 68, 1524 (1964).

/ 2/ J. H. Baxendale, E. M. Fielden, and J. P. Keene, Proc. Roy. Soc. (London) Ser. A286, 320 (1965).

/ 3/ S. Gordon in "Pulse Radiolysis", M. Ebert, J. P. Koene, A. J. Swallow, and J. H. Baxendale, eds., Academic Press, London, 1965, p. 285.

/ 4/ M. Faraggi and Y. Tendler, J. Chem. Phys. 56, 3287 (1972).

/ 5/ A. K. Pikaev, G. K. Sibirskaya, and V. I. Spitsyn, Dokl. Akad. Nauk SSSR 209, 1154 (1973).

/ 6/ A. K. Pikaev, M. P. Mefod'eva, N. Krot, and V. I. Spitsyn, Khim. Vys. Energ. 1, 505 (1973).

/ 7/ A. K. Pikaev, M. P. Mefod'eva, N. Krot, and V. I. Spitsyn, Izv. Akad. Nauk SSSR, Ser. Khim. 12, 2847 (1974).

/ 8/ M. Anbar, M. Bambenek, and A. B. Ross, NSRDS – NBS Circular 43, May 1973, pp. 59.

/ 9/ J. C. Sullivan, A. J. Zielen, and E. Deutsch, Inorg. Chem. 82, 5288 (1960).

/10/ C. J. Wechsler, J. C. Sullivan, and E. Deutsch, Inorg. Chem. 13, 2360 (1974).

/11/ T. W. Newton, J. Phys. Chem. 74, 1661 (1970).

/12/ E. J. Hart and J. K. Thomas, Argonne National Laboratory Rept. ANL–7856, Sept. 1971.

/13/ S. Gordon, K. H. Schmidt, and J. E. Martin, Rev. Sci. Instr. 45(4), 552 (1974).

/14/ K. H. Schmidt, S. Gordon, and W. A. Mulac, Rev. Sci. Instr. 47(3), 356 (1976).

/15/ M. S. Matheson and L. M. Dorfman, "Pulse Radiolysis", M. I. T. Press, Cambridge, Mass., 1969.

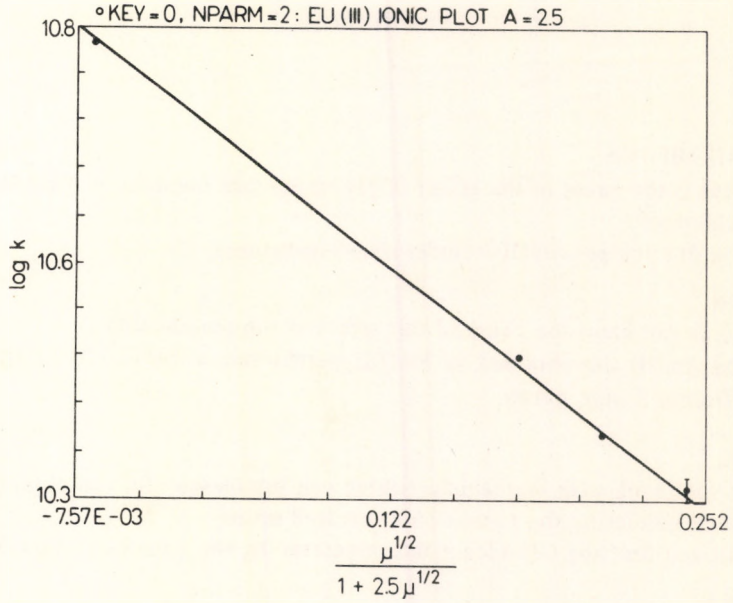

Fig. 1 Ionic strength plot for Eu(III) + e^-_{aq}

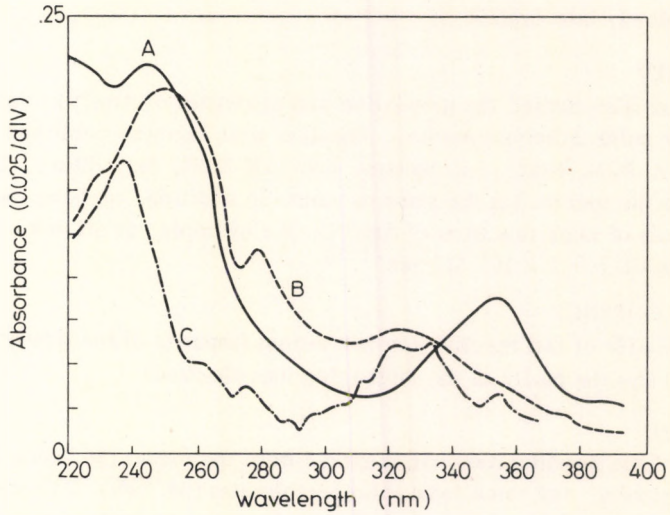

Fig. 2 Spectra of Tm^{+2}(A), Gd^{+2}(B) and Ho^{+2}(C)

M. V. VLADIMIROVA

(1) What is the cause of the effect of pH on the rate constant of Am(VI) + e^-_{aq} (solvated electron) ?

(2) How did you get Am(II)? Under what conditions?

S. GORDON

(1) We do not know the cause of this effect at the present time.

(2) The Am(II) was obtained by Am(III)-perchlorate at pH 5.8 by reduction with e^-_{aq} (from a 3 μsec pulse).

I. KRALJIC

(1) In your work with lanthanides (which can luminesce) did you observe any luminescence indicating the formation of excited states?

(2) Did you find any OH adduct intermediates in the experiments on OH reactions?

S. GORDON

(1) We did not observe any luminescence, only Cerenkov radiation.

(2) We did find an absorption which may be ascribed to an intermediate in the case of reduction of Am(V) by e^-_{aq} and in the case of oxidation of Am(III) to Am(IV) by OH. These formed very rapidly, i.e. faster than 10 nanoseconds and then grew relatively slowly into Am(IV).

A. K. PIKAEV

We have also studied the production and properties of Am(IV) ions in aqueous solutions by pulse radiolysis method. The data were recently published (A. K. Pikaev, V. P. Shilov, N. N. Krat, V. I. Spitsyn, Izv. AN SSSR, Ser. Khim., No. 4 (1976).) Our data on the spectra are the same as yours. In addition, we have measured the rate constants of some reactions of Am(IV). For example, at pH ~4
$k[OH + Am(III)] = 3 \times 10^8\ M^{-1}sec^{-1}$.

R. K. BROSZKIEWICZ

Even 0.01% of fast reacting ion is a serious impurity of the slowly reacting one. How, then, was the purity of the lanthanide ions checked?

S. GORDON

Most of the perchlorates were prepared from the oxides (99.999%), checked spectroscopically, and some from solid perchlorates (99.99%). All rate constants were obtained by plotting the pseudo first-order rate constants at varying lanthanide or actinide perchlorate concentrations and the second order rate constant was calculated from the slope of this straight line (processed by a least squares program, described). This procedure takes care of the effect of any impurity (highly unlikely).

RADIATION-CHEMICAL TRANSFORMATION OF ARSENIC IONS

H. M. Nanobashvili, M. V. Mamaladze
Institute of Inorganic Chemistry and Electrochemistry, Tbilisi, 380093, USSR

Recently attention has been drawn to the study of radiation chemical transformation of complicated anions, such as oxy-anions of manganese, chlorine, sulfur, antimony, arsenic and others, in view of their considerable scientific and practical interest /1, 2/.

Although a certain amount of data on the above anions is currently available, a number of problems connected with the effect of radiation on these ions has not been sufficiently studied. This is particularly true for the radiation chemical behaviour of arsenic compounds which are of considerable interest for the practical application of high energy radiations. We have therefore undertaken a study of the radiation chemical transformation of arsenites and arsenates under different conditions and established the general regularities of the occurring processes in order to work out a directed performance of radiolysis in corresponding systems.

In this paper considerable attention is focused on the study of transient and stable radiolysis products of the investigated systems by means of different physico-chemical and chemical methods (electrochemical, spectrophotometric, ESR) and, also, the determination of the gradual change of the oxidation degree of arsenic ions in the radiation field is attempted. On the basis of the results obtained a radiolysis mechanism for arsenites and arsenates is suggested.

A Co−60000 unit was used as radiation source, dosimetry was carried out by the ferrosulphate method. The dose rate varied in the 10^{15}–10^{16} eV/ml. sec range by changing the distance between the radiation source and the sample. Irradiation of samples was carried out in molybdenic and quartz glass cells of different types. Different arsenic compounds, variously substituted arsenites and arsenates (h. p.) were investigated. Alcohols, acetone, sodium hypophosphite, N_2O and others were used as acceptors after purification by means of the accepted technique.

Different methods were used for the study of radiolysis processes of arsenic ions. Arsenic was determined by amperometric titration and chemical methods.

The experimental data were processed by the method of the least squares. An estimated error in the values of radiation-chemical yields did not exceed $\pm$ 10%.

The study of radical products was performed by the ESR method. The samples were irradiated on the Co−60000 at 77 K. The range of absorbed energy was 1−5

Mrad. The dose rate was 1 −1.25 Mrad/h. ESR spectra were recorded on the radiospectrometer EPR-2M at 77 K /3/.

The ESR spectra of dilute aqueous solutions (10^{-4} m-10^{-1}M) of variously substituted arsenites NaH_2AsO_3, Na_2HAsO_3, Na_3AsO_3, irradiated with a dose of 2 Mrad, consist of the assymetric doublet with 40 Oe splitting, belonging to the OH radical (Fig. 1a).

The ESR spectra of frozen saturated (2-3M) solutions of the above compounds (polycrystals), irradiated with a dose of 3 Mrad, represent basically the superposition of the two species: OH radicals and the paramagnetic centres, belonging to arsenic (Fig. 1b, 1c).

The ESR spectra of 1.65M H_3AsO_4, irradiated with the dose of 1 Mrad, basically consist of the OH radicals (Fig. 2b). The lines related to the As(IV)-containing radical are also seen in the spectrum. The ESR spectra of saturated aqueous solutions of H_3AsO_4, H_3AsO_4 in 10M KOH are the radicals, belonging to As(IV) (Fig. 2a, 2d). Heating of the irradiated samples permits one to single out the pure spectrum of the radical, belonging to As(IV) (Fig. 2c). The spectrum consists of the quartet with $\sim$32 Oe splitting with $\sim$120 Oe general width. The ESR spectra of saturated aqueous solutions of NaH_2AsO_4 and Na_2HAsO_4 under γ irradiation with the dose of 1.9 Mrad are similar to the spectrum presented in Fig. 3a.

Paramagnetic centres (PMC), formed in 2.9 M NaH_2AsO_3 and 2 M Na_3AsO_3 in 10M KOH under γ irradiation with a dose up to 3.5 Mrad, basically consists of the singlet with g-factor 2.001, belonging to e^-_{tr} and of the lines, belonging to the arsenic (II)-containing radical. A similar spectrum was obtained in the case of 2 M Na_2HAsO_3 in 10 M KOH.

The ESR spectra of saturated H_3AsO_4 and Na_2HAsO_4 solutions in 1 M C_2H_5OH or in pure C_2H_5OH irradiated with the dose of 0.6 −4.2 Mrad apart from the ethanol radicals $CH_3\dot{C}HOH$ and the electron, formed during irradiation of C_2H_5OH (characterized by the correlation of the hyperfine structure line intensivities 1 : 4 : 6 : 4 : 1 and by 21.5 Oe splitting between the components), also contain a quartet belonging to the arsenic (IV) radicals, with 32 −38 Oe splitting (Fig. 3).

The spectrum presented in Fig. 3d seems to belong to the adducts $H_4AsO_4 \cdot C_2H_4OH$.

Besides the radicals belonging to C_2H_5OH, the signals of the arsenic (II)-containing radicals were observed in the spectra of irradiated (dose = 0.6 −2.5 Mrad) 2 −3 M H_3AsO_4 and Na_2HAsO_4.

Thus, the use of the ESR method has enabled us to identify transient arsenic radicals − As (II) and As(IV) the further transformation of which in aqueous solutions under γ-radiation proceeds with the formation of a number of stable products.

The dependence of radiation chemical transformation of arsenite ions on different factors (the amount of absorbed energy, concentration, pH, the nature of acceptors and others) has been studied.

The data obtained indicate that radiation chemical transformation of 10^{-3} M H_3AsO_3 (pH $\sim$ 1 −4) proceeds with the formation of arsenate with the yield G_0 [As(V)] = 3.18 and hydrogen peroxide with the yield $G_0(H_2O_2)$ = 4.35. In the

Table 1

Dependence of radiation chemical transformation of 5×10^{-2}M Ma_2HAsO_3 + 10^{-2}M $(CH_3)_2$ CO + H_2O system on absorbed energy.

Dose rate = 1.55×10^{16} eV/ml. sec

Absorbed energy 10^{20}eV/ml	Concentration of As(III)mole/1 $\times 10^{-2}$	Concentration of As(V)mole/1 $\times 10^{-3}$
-	4.63	-
0.13	4.54	1.10
0.28	4.47	1.70
0.56	4.46	1.95
1.10	4.39	2.60
1.63	4.32	3.40
2.20	4.26	4.00
2.80	4.17	4.75

G_o [-As(III)] = 5.6 G_o [As(V)] = 5.6

pH range between 8 and 11 transformation of arsenites into arsenates occurs with yields ranging from G_o [As(V)] = 5.62 to G_o [As(V)] = 12.74, respectively, and in 10^{-2} M Na_2HAsO_3(pH ~ 11) G_o [(As(V)] = 20 thus the arsenite oxidation process develops in accordance with the chain mechanism.

The radiation chemical transformation of arsenite ions with the formation of arsenate ions occurs under irradiation of $2 \cdot 10^{-2}$M Na_2HAsO_3 (pH ~ 9.8).

In a $2 \cdot 10^{-2}$M Na_2HAsO_3 solution the initial yields of transformation of As(III) ions and formation of As (V) ions are G_o [-As(III)] = 2.95 and G_o [As(V)] = 2.57, respectively.

The radiation chemical reduction of As(III) ions to As(II), in alkaline medium proceeds with the participation of hydrated electrons. An addition of electron acceptors, N_2O or acetone leads to the depression of the arsenites reduction process (Table 1).

The radiation chemical transformation of arsenite ions could be represented as follows:

$$H_2AsO_3^- + OH \longrightarrow H_2AsO_3 + OH^- \quad (1)$$

$$AsO(OH)_2 + O_2^- \longrightarrow AsO(OH)_2 \cdot O_2^- \quad (2)$$

$$2H^+ + H_2AsO_3^- + AsO(OH)_2 \cdot O_2^- \longrightarrow 2H_2AsO_4 \rightleftharpoons 2H^+ + 2HAsO_4^{2-} \quad (3)$$

$$AsO(OH)_2 + H_2AsO_3^- \longrightarrow AsO(OH)_2 \cdot O_2^- + H_2AsO_3 \quad (4)$$

$$H_2AsO_3^- + e_{aq}^- \longrightarrow H_2AsO_3^{2-} (\longrightarrow OH^- + HA_sO_2^-) \quad (5)$$

Thus, radiation chemical transformation of arsenites depends on different factors. In acid and neutral media only the ions from As(III) get oxidized to As(V), whereas in alkaline medium, alongside the oxidation of arsenite-ions into arsenates, their reduction may also occur.

It should be mentioned that under definite conditions the radiation chemical oxidation of arsenites with formation of arsenates proceeds in accordance with the chain mechanism.

Radiolysis of arsenate aqueous solutions has been studied in a wide range of absorbed energy, pH solute concentration and in the presence of acceptors.

According to the data obtained, transformation of As(V) ions with formation of As(III) occurs under introduction of the acceptors of the OH radicals of ethanol and sodium hypophosphite.

For instance, the radiation chemical reduction of ions As(V) with formation of As(III) (yields: $G[As(V)] = 3.98$, $G[-As(III)] = 3.54$) occurs in the system $10^{-2}M\ H_3AsO_4 + 5 \cdot 10^{-2}M\ C_2H_5OH$ in H_2O.

Radiation-chemical transformation of As (V) ions in acid medium can be represented by the following scheme:

$$OH + C_2H_5OH \longrightarrow H_2O + \dot{C}_2H_4OH$$

$$H + H_3AsO_4 \longrightarrow H_4AsO_4$$

$$2H_4AsO_4 \xrightarrow{-HOH} H_3AsO_3 + H_3AsO_4$$

$$H_3AsO_3 + H_2O_2 \longrightarrow H_3AsO_4 + H_2O$$

$$H_3AsO_3 + \dot{C}_2H_4OH \longrightarrow H_2O + H_2\dot{A}sO_2 + CH_3COH$$

Thus, the radiation chemical transformation of arsenite and arsenate ions proceeds through intermediate states As(IV) and As (II), which are observed by means of pulse radiolysis /4/ and electron paramagnetic resonance methods.

References

/1/ M. Haissinsky and M. Lefort, J. Chem. Phys. 48, 429 (1951).

/2/ M. Daniels and I. Weiss, J. Chem. Soc., 7, (1958).

/3/ M. V. Mamaladze, G. R. Natroshvili, H. M. Nanobashvili, Bull. Acad. Sci. of the Georg. SSR, 81, 3, (1976).

/4/ G. A. Adams, J. W. Boag, B. D. Michael. Trans. Faraday, Soc., 61, 1964 (1965).

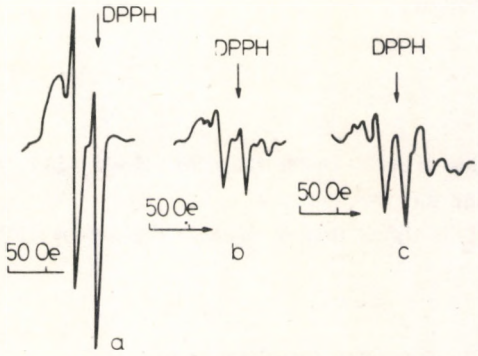

Fig. 1. ESR spectra of γ-irradiated arsenites: (a) 10^{-4} - 10^{-2} M MaH_2AsO_3, Na_2HAsO_3. Na_3AsO_3 (D≈2Mrad) (b) 2 - 3 M Na_2HAsO_3 (D≈3Mrad) (c) 2 - 3 M $Na\ H_2AsO_3$, $NaAsO_3$ (D≈3Mrad)

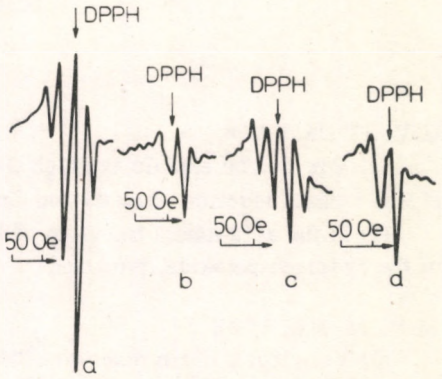

Fig. 2. ESR spectra γ-irradiated 1. 65 M H_3AsO_3: (a) in water D = 1Mrad. (b) in water D = 4. 3Mrad. (c) in water D = 4. 3Mrad after heating (d) in 10 M KOH at 77 K

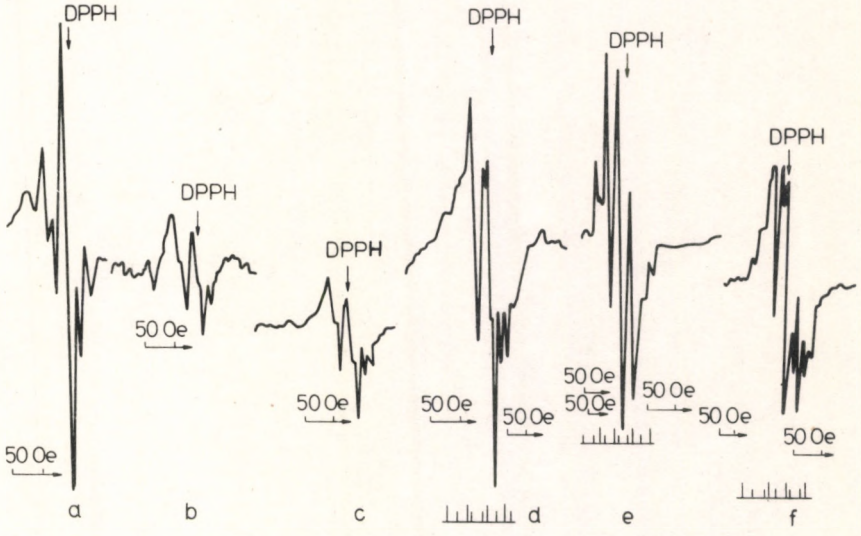

Fig. 3. ESR spectra of γ-irradiated arsenates in 1 M C_2H_4OH: (a) 1M C_2H_5OH, (b) 2M H_3AsO_4 (D≈0. 6 Mrad) (c) 2M H_3AsO_4 (D≈1 9Mrad), (d) 2M H_3AsO_4 (D≈4.2Mrad) (e) 2. 5M NaH_2AsO_4 (D≈3 4Mrad), (f) 2M H_3AsO_4 (D = 2. 5 Mrad), after heating

G. V. PUTIRSKAYA

(1) How do you explain the high G-value of As(V) in the range of pH= 8 −11? If it is a chain reaction, how do you describe this mechanism?

(2) In the acid media the yield of H_2O_2 is higher than 4. What is the mechanism of the hydrogen peroxide formation?

M. V. MAMALADZE

(1) Yes, it is a chain reaction. OH radicals oxidise As(III) ions and then O_2 reacts with As(IV) produced giving rise to As(V).

(2) The mechanism is as follows:

$$H + O_2 \longrightarrow HO_2$$

$$HO_2 + As(III) \longrightarrow HO_2^- + As(IV)$$

$$HO_2^- + H^+ \rightleftharpoons H_2O_2$$

RADIATION CHEMISTRY OF THE CHLOROCOMPLEXES OF THE PLATINUM GROUP METALS

R. K. Broszkiewicz
Institute of Nuclear Research, Department of Radiation Chemistry,
Warsawa, Poland

Irradiation of dilute aqueous solutions produces highly reactive species in processes of the radiolysis of water. These species subsequently oxidize or reduce the solute, which is virtually unchanged by the direct action of ionizing radiation. This is contrary to the situation occurring on illumination of such a solution, when the energy of light is absorbed by solute rather than by solvent. In consequence, the methods of radiation chemistry, mainly pulse radiolysis, present to a chemist unique opportunities in studying the redox reactions of inorganic compounds.

In order to follow the mechanisms of those reactions we have selected chlorocomplexes of platinum metals. They had been fairly well investigated already and, parallelly with complexes of Co(III), were used as examples in the description of relations between the structure of a complex and its chemical properties.

This presentation summarizes the information obtained in our works hitherto performed, i. e. on complexes of Rh, Pd, Ir and Pt.

The experimental technique has been described elsewhere /1, 2/.

Chlorocomplexes of the Platinum Metals

The following stable compounds belong to this group: planar $PdCl_4^{2-}$ and $PtCl_4^{2-}$, octahedral $RuCl_6^{3-}$, $RuCl_6^{2-}$, $RhCl_6^{3-}$, $PdCl_6^{2-}$, $OsCl_6^{3-}$, $OsCl_6^{2-}$, $IrCl_6^{3-}$, $IrCl_6^{2-}$, and $PtCl_6^{2-}$. In this work a compound is considered to be stable if it does not change appreciably within the period of the pulse radiolysis experiment. Stability of the palladium complexes had, however, to be obtained by addition of a considerable excess of chloride or hydrochloric acid and the Rh(III) complexes were investigated in their aquated form.

The absorption spectra of the octahedral complexes as determined by Jørgensen /3/ and of the planar one obtained in this work are shown in Fig. 1. It should be noted that in case of ruthenium, osmium and iridium it is possible to transform one stable complex into another by one electron-transfer reaction without changing the symmetry. A similar process in the case of palladium and platinum requires the

change of symmetry, and formation of a transient trivalent ion. Rhodium complexes are not stable at valencies other than three.

Consequently, the following possible reactions may be considered:

1. Oxidation of Ru(III), Os(III) and Ir(III) and reduction of Ru(IV), Os(IV) and Ir(IV) should produce a stable product;
2. Reduction of all bi- and trivalent complexes should produce unstable mono- or bivalent transients;
3. Oxidation of Pd(II) and Pt(II) or reduction of Pd(IV) and Pt(IV) should produce an unstable trivalent transient;
4. Oxidation or reduction of Rh(III) should produce unstable transients, respectively, Rh(IV) and Rh(II);
5. Oxidation of tetravalent complexes to a higher valency level cannot be ruled out by principle, though is not very likely on the basis of known difficulties in obtaining this result when applying most powerful oxidizing agents in thermal reactions.

The evidence obtained on these assumed processes is presented later, it has not, as yet, covered complexes of ruthenium and osmium.

Results and Discussion

Reduction of complexes by e^-_{aq} or H is very fast. The data are shown in Table 1.

Apart from Rh(II) complex, which does not exhibit any transient absorption observable within the available 300 −750 nm range all remaining ions produce the expected stable or transient species.

Oxidation of those complexes is rapid as well, OH being a stronger agent than Cl_2^- or Br_2^-. The data are shown in Table 2.

It deserves mentioning that in neither case did we observe formation of any species attributable to an unusually high valency level, exceeding that of four, which confirms the doubt expressed earlier.

In our hitherto finished studies the case of a simple single electron transfer between stable octahedral complexes is represented by Ir(III) and Ir(IV). Oxidation of Ir(III) to Ir(IV) is shown in Fig. 2 and the $IrCl_6^{2-}$ ion formed is stable for at least 500 μs indicating that no ligand exchange follows immediately the transfer of an electron.

Reduction of Ir(III) produces transient Ir(II)-complex, probably octahedral, with absorption maximum at 280 nm /4/. High-dose gamma-irradiation produced an aquochlorodimer of Ir(IV) with G-value of about. 0.3, i.e. ionizing radiation initiates redox processes and ligand exchange in a ratio of about 10:1.

In the study on Rh(III) complexes we dealt with a case when neither the product of reduction nor that of oxidation is stable. As mentioned earlier we failed to

Table 1
Reduction of the chlorocomplexes of platinum metals

Parent complex	Reducing agent	Reduced complex	Rate constant $M^{-1}s^{-1}$	Absorption maximum of reduced transient complex nm	Extinction coefficient of the transient complex $M^{-1}cm^{-1}$
$Rh(H_2O)Cl_5^{2-}$(III)	e_{aq}^-	$Rh(H_2O)Cl_5^{3-}$(II)	4.4×10^{10}	?	?
$Rh(H_2O)_5Cl^{2+}$(III)	e_{aq}^-	$Rh(H_2O)_5Cl^{+}$(II)	5.5×10^{10}	?	?
$PdCl_6^{4-}$ (II)	e_{aq}^-	$PdCl_6^{5-}$(I)	1.1×10^{10}	340	2250
$IrCl_6^{3-}$(III)	e_{aq}^-	$IrCl_6^{4-}$(II)	6.4×10^{9}	280	1740
$IrCl_6^{2-}$(IV)	e_{aq}^-	$IrCl_6^{3-}$(III)	9.6×10^{9}	stable complex	stable complex
$IrCl_6^{2-}$(IV)	H	$IrCl_6^{3-}$(III)	9.2×10^{9}	stable complex	stable complex
$PtCl_4^{2-}$(II)	e_{aq}^-	$PtCl_4^{3-}$(I)	9.3×10^{9}	310	2930
$PtCl_6^{2-}$(IV)	e_{aq}^-	$PtCl_5^{2-}$(III)	2.0×10^{10}	410	3700

Data in part published in Refs /4, 8, 9, 13, 15/

Table 2

Oxidation of the chlorocomplexes of platinum metals

Parent complex	Oxidizing agent	Oxidized complex	Rate constant $M^{-1}s^{-1}$	Absorption maximum of oxidized transient complex, nm	Extinction coefficient of the transient complex, $M^{-1}cm^{-1}$
$RhCl_6^{3-}$(III)	Cl_2^-	$RhCl_6^{2-}$(IV)	-	600	600
$Rh(H_2O)Cl_5^{2-}$(III)	OH	$Rh(H_2O)Cl_5^-$(IV)	2.6×10^9	560	1100
$Rh(H_2O)Cl^{2+}$(III)	OH	$Rh(H_2O)_5Cl^{3+}$(IV)	2.8×10^9	550	770
$PdCl_6^{4-}$(II)	OH	$PdCl_6^{3-}$(III)	6.3×10^9	320	4700
$IrCl_6^{3-}$(III)	OH	$IrCl_6^{2-}$(IV)	8.9×10^9	stable complex	stable complex
$PtCl_4^{2-}$(II)	OH	$Pt(OH)Cl_4^{2-}$(III)	8.0×10^9	450	2830
$PtCl_4^{2-}$(II)	Cl_2^-	$PtCl_6^{3-}$(III)	1.3×10^9	290	7000
$PtCl_4^{2-}$(II)	Br_2^{1-}	$PtCl_4Br_2^{3-}$(III)	2.8×10^8	310	8400

Data in part published in Refs /4, 8, 9, 11, 13, 15/

observe the spectrum of Rh(II), whose maximum, by analogy to Ir(II), may be expected to occur in the UV region and was probably screened by the very large self absorption of Rh(III). Rh(IV) has been found to be produced by action of OH or Cl_2^- and decays with a half-life of about 1 ms. The absorption spectra of various complexes of Rh(IV) are shown in Fig. 3.

Similar spectra of a highly unstable species were previously attributed to Rh(IV) by authors who oxidized Rh(III) with very strong agents /5, 6/.

As $RhCl_6^{3-}$ is stable in HCl solution only and aquates rapidly in water, we have established the actual structure of Rh(III) aquochlorocomplex using the ionic strength effect on the rate constant of the reaction between e_{aq}^- and the particular complex. It seems that this method can be very useful in the analysis of complexes which exchange charged for uncharged (or vice versa) ligands within a few minutes.

It may be of some interest to point out that our results on Rh(IV) seem to confirm a generalization expressed by Jørgensen /7/ that octahedral d^3, d^4 and d^5 but not d^6 complexes have bands at long wavelengths. Clearly the absorption of $4d^5$ Rh(IV) at 550 – 600 nm, resembling that of $5d^5$ Ir(IV), and exceeding by a factor of about 100 that of $4d^6$ Rh(III) meets the case.

Another item arising from the study of redox reactions of octahedral Rh(III) aquochlorocomplexes is the relative effectiveness of different ligands as electron conductors. Apparently H_2O is a better conductor than Cl^- in the reduction than in the oxidation reactions, though in either case it should follow similar outer-sphere mechanism. This inconsistency obviously merits a deeper investigation.

In respect to reactions of the planar Pt(II) complex, we expressed earlier /8/ an idea that the oxidizing OH radical produces with the chloroplatinite plane an inner-sphere activated complex absorbing at 450 nm which is subsequently transformed into more stable trigonal bipyramid, absorbing at 410 nm – the same band at which Pt(III) produced by reduction of Pt(IV) absorbs. This idea was checked and discussed later by other authors /9, 10/. Some of them proposed an alternative mechanism postulating formation of the planar $PtCl_4^-$ structure /10/.

To verify our hypothesis we have tested oxidation of Pt(II) with Cl_2^- and Br_2^- The results obtained with Cl_2^- are shown in Fig. 4. They indicate that in HCl solution, when OH is quantitatively transformed into Cl_2^-, the absorptions at 450 and 410 nm disappear and another one, at 290 nm is produced.

An analogous experiment on neutral Br^- solutions, where the ionic strength effect on reaction between Br_2^- and $PtCl_4^{2-}$ may be followed, gave similar results, however the absorption peak was at 310 nm. The calculated product of the reacting charges was about +2.

The latter results indicate that the oxidizing species is incorporated into a transient structure together with the oxidized $PtCl_4^{2-}$ excluding the mentioned hypothesis of $PrCl_4^-$ formation. Very similar results have been recently obtained by Stover et al /12/.

Though, by virtue of a very considerable structural similarity, palladium chlorocomplexes might be expected to react in the same manner as the platinum

ones this is not the case. In particular, we failed to observe formation of any intermediate structures which could be ascribed to transient inner-sphere complexes /13/. An explanation to this fact has been found in the ability of Pd(II) to produce quasi-octahedral structures which do not allow an inner-sphere mechanism. This ability had been proposed by Harris et al /14/, objected to later by Jørgensen /7/ and confirmed recently by Volchenshova and Yatsimirskii /16/. Our result gives to it an independent proof.

Conclusions

The results described in this work are presented in order to exemplify the usefulness of the radiation chemical methods in studies on inorganic chemistry. Having selected a group of complexes which had already been very well investigated by inorganic chemists we were able to obtain a further insight into their properties and mechanisms of reactions. In particular it proved to be possible to observe directly the spectra of activated complexes, establish kinetic parameters of rapid processes, check the fast ligand exchange and verify the actual co-ordination number of a complex. They indicate the problem of how an electron is actually transferred in a redox process, though to solve it nano- or subnanosecond impulses should probably be used.

Literature

/ 1/ G. E. Adams, J. W. Boag and B. D. Michael, Trans. Faraday Soc. 61, 492 (1965)

/ 2/ E. Kozlowska-Milner, R. Broszkiewicz and J. Stanikowski, Radiochem. Radioanal. Letters, 22, 269 (1975)

/ 3/ C. K. Jørgensen, Mol. Phys. 2, 309 (1959).

/ 4/ R. K. Broszkiewicz, J. chem. Soc. Dalton 1973, 1799.

/ 5/ G. H. Ayres, Anal. Chem. 25, 1622 (1953).

/ 6/ F. P. J. Dwyer and R. S. Nyholm, Nature 160, 502 (1947).

/ 7/ C. K. Jørgensen, Absorption Spectra and Chemical Bonding in Complexes, Pergamon Press, 1962.

/ 8/ G. E. Adams, R. K. Broszkiewicz and B. D. Michael, Trans. Faraday Soc. 64, 1256 (1967).

/ 9/ A. S. Ghosh-Mazumdar and E. J. Hart, Int. J. Radiat. Phys. Chem. 1, 165 (1969).

/10/ R. C. Wright and G. S. Laurence, J. Chem. Soc. Chem. Comm. 1972, 132.

/11/ R. K. Broszkiewicz and J. Grodkowski, Int. J. Radiat. Phys. Chem. (in press).

/12/ D. K. Stover et al, Int. J. Radiat. Phys. Chem. 7, 693 (1975).

/13/ R. K. Broszkiewicz, Int. J. Radiat. Phys. Chem. 6, 249 (1974).

/14/ C. M. Harris, S. E. Livingstone and I. H. Reese, J. chem. Soc. 1959, 1505.

/15/ M. Anbar and P. Neta, Int. J. appl. Radiat. Isot. 18, 493 (1967).

/16/ I. I. Volchenshova and K. B. Yatsimirskii, Zh. neorg. Khim. 18, 1875 (1973).

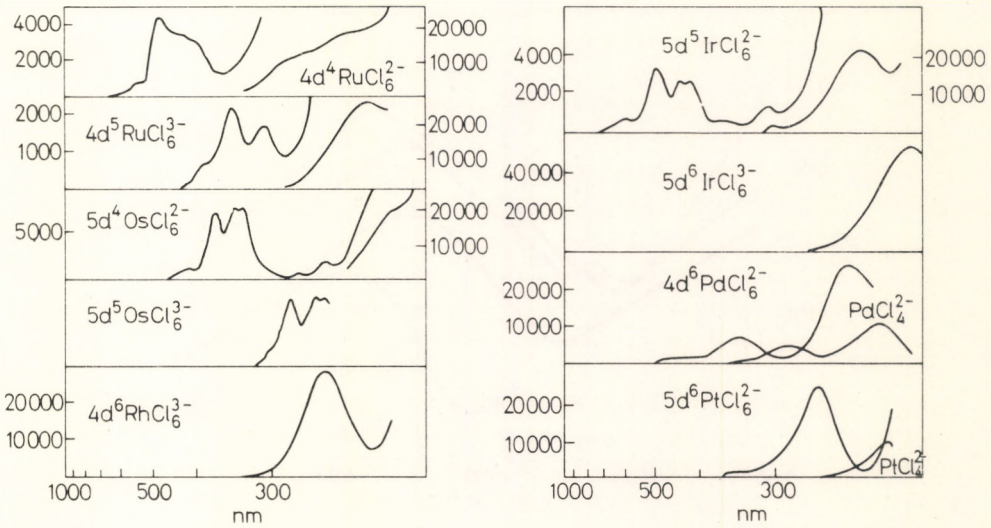

Fig. 1 Absorption spectra of stable complexes of the platinum group metals

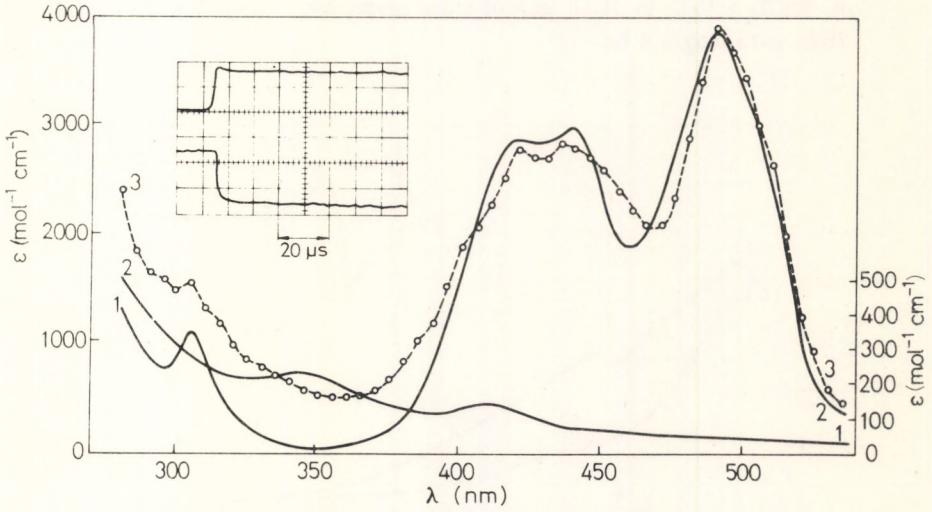

Fig. 2 Absorption spectra of $IrCl_6^{3-}$ and $IrCl_6^{2-}$ in aqueous solution: 1. unirradiated $IrCl_6^{2-}$. 2. unirradiated $IrCl_6^{3-}$. 3. end of pulse absorption of N_2-saturated 0.3 mM $IrCl_6^{3-}$ (1 and 3, left hand scale: 2. right-hand scale).
Inset: oscilloscope traces of absorption recorded at 435 nm in N_2-saturated solution of $IrCl_6^{3-}$ (upper trace) and $IrCl_6^{2-}$ (lower trace) /4/

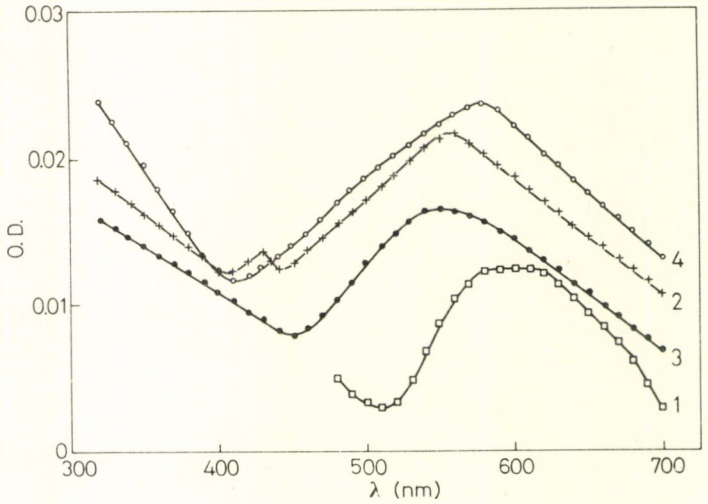

Fig. 3 Transient absorption spectra of Rh(IV) complexes: 1. $RhCl_6^{3-}$ in 5M HCl, 20 μs after pulse absorption: 2. $Rh(H_2O)Cl_5^{2-}$ in H_2O, end of pulse absorption: 3. $Rh(H_2O)_5Cl^{2+}$ in H_2O, and of pulse absorption: 4. $RhCl_3 \times H_2O$ in H_2O, and of pulse absorption. Dose: 1×10^{17} eV/ml: light path length 4 cm

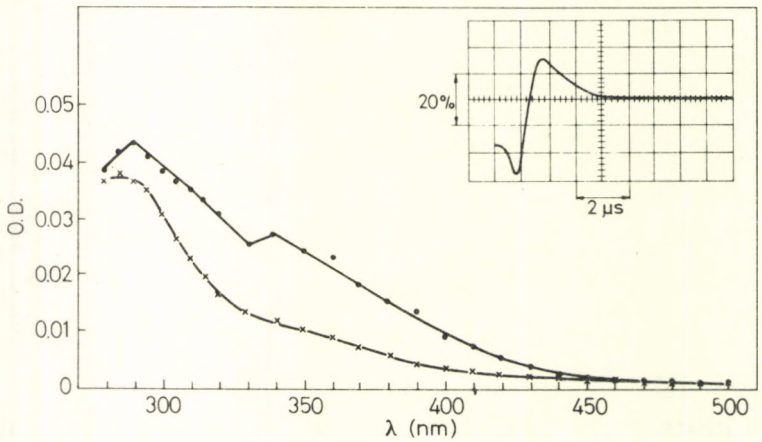

Fig. 4 Transient absorption spectra of pulse irradiated $PrCl_4^{2-}$ in 0.1M HCl: 1. End of pulse absorption, 2. 40 μs after the pulse absorption. Inset: oscilloscope trace of absorption at 340 nm. Dose: 1×10^{17} eV/ml. Light path length 1 cm /11/.

J. KALECINSKI

Are the rate constants presented in the Table apparent or chemical (i. e. calculated by taking into account the diffusion controlled rate constants)?

R. K. BROSZKIEWICZ

The rate constants are chemical.

I. KRALJIC

I should like to point out that the rate constants in your work with OH, Br_2^- and Cl_2^- depend on the redox potential of these oxidizing intermediates. If one attempts to make a correlation between these rate constants and oxidation potentials one may take as a first approximation the values for Cl^-/Cl_2 and Br^-/Br_2 couples.

R. K. BROSZKIEWICZ

In this work no attempt was made to correlate rate constants of OH, Cl_2^- and Br_2^-. The aim of using Cl_2^- and Br_2^- was solely to apply them as oxidizing agents different from OH.

RADIATION-CHEMICAL REDUCTION OF METAL IONS IN HNO_3 SOLUTIONS BY γ- AND, α -RADIOLYSIS

M. V. Vladimirova. I. A. Kulikov, A. A. Ryabova, A. S. Milovanova
State Committee on the Peaceful Utilization of Atomic Energy,
USSR

In the present work the yields of Ce^{3+} and O_2 have been determined both in the presence and in the absence of Tl ions in HNO_3 solutions at Ce^{4+} concentrations of 10^{-4} – 10^{-2}M and γ-radiation dose rate, between 2 x 10^{15} and 5 x 10^{17} eV/ml. min. The results are illustrated in Figs 1–3. On α- radiolysis $G(Ce^{+3})$ and $G(O_2)$ were determined at $[Ce^{4+}] = 10^{-4}$M and I = 5 x 10^{15} – 5 x 10^{16} eV/ml. min. The results are shown in Fig. 1. The results obtained are compared with data available in the literature on radiation reduction of various metal ions. Figures 1–3 show complex dependences of $G(Ce^{3+})$, $G(O_2)$ and $G(Ce^{3+})_{Tl^+}$ on $[HNO_3]$, $[Ce^{4+}]$ and I. At $[Ce^{4+}] = 10^{-4}$M (Fig 1) in the $[HNO_3]$ range of 0.1 - 1.0 M, $G(Ce^{3+})$ grows, in the $[HNO_3]$ range of 1.0 - 5.0 M the yield of Ce^{3+} is essentially constant, at $[HNO_3] > 5.0$ M $G(Ce^{3+})$ lowers. The absolute value of the Ce^{3+} yield increases with decreasing the dose rate.

At $[Ce^{4+}] = 10^{-2}$ M (Fig. 1, curve 5) with an increase of $[HNO_3]$ from 1.0 to 10 M $G(Ce^{3+})$ grows. In the $[HNO_3]$ range 1.0 – 6.0 $G(Ce^{3+})$ is lower than at $[Ce^{4+}] = 10^{-4}$M, at $[HNO_3] = 10$M $G(Ce^{3+})$ is higher in this case.

As Fig. 2 shows, $G(O_2)$ in cerium solutions is also dependent on $[Ce^{4+}]$, $[HNO_3]$ and I. The yield of Ce^{3+} in the presence of Tl^+ ions does not depend on experimental conditions in the $[HNO_3]$ range of 1.0 – 5.0 M, in 10M $[HNO_3]$ $G(Ce^{3+})_{Tl^+}$ depends on $[Ce^{4+}]$. The results shown in Fig. 1 differ from the data in Ref. /1/. In Ref. /1/ $G(Ce^{+3})$ is equal to 5.5 – 5.8 ion/100 eV, in the $[HNO_3]$ range 1.0 – 10M, $[Ce^{4+}] = 10^{-4}$M and I = 3 x 10^{18} eV/ml. min. It is seen from Fig. 1 that in α-radiolysis, the mode of $G(Ce^{3+})$ dependence on $[HNO_3]$ is the same as that in γ-radiolysis. However, in the former case the yields of Ce^{3+} are substantially higher. It is interesting to compare the results obtained in the reduction of Ce^{4+} with the data on the reduction of other metal ions (Figs 3, 4). The results of Figs 3 and 4 have been taken from Refs /2, 3, 4/. It follows from Fig. 3 that on γ-radiolysis in the HNO_3 solution of 10^{-3} – 5 x 10^{-2}M $G(-NpO_2^{2+})$ and $G(-PuO_2^{2+})$ are higher than $G(Ce^{3+})$ which is supposed to be equal to the standard value 2.3 ion/100 ev.

In Ref. /4/ it is shown that large yields of Np and Pu ion reduction are due to an additional formation of H_2O_2 in the solution by the reaction OH + OH that competes with the reaction of radical on oxidation of PuO_2^+ and NpO_2^+ ions. However, in Pu

solutions a considerable part is played by reactions $HO_2 + OH$ and $H_2O_2 + OH$ that lower the yield of H_2O_2 formed in the solution. This results in lowering $G(-PuO_2^{2+})$ with the growth of acidity. On α-radiolysis (Fig. 4) in the $[HNO_3]$ range of $10^{-3} - 10^{-1}$ M $G(Ce^{3+})$ is supposed to be just the same as $G(-NpO_2^{2+})$, in solutions of a higher concentration $G(Ce^{3+}) \gg G(-NpO_2^{2+})$ and $G(-PuO_2^{2+})$ the yields being the same as on γ-radiolysis.

To account for the results obtained let us consider radiation-chemical reactions that take place in nitric acid solutions of Ce^{4+}.

The action of radiation on the molecules of H_2O, HNO_3 and NO_3 ions brings about the following transformations:

$$H_2O \xrightarrow{\sim} H,\ OH,\ H_2,\ H_2O_2 \qquad (A)$$

$$HNO_3 \xrightarrow{\sim} NO_2,\ OH \qquad (B)$$

$$NO_3 \xrightarrow{\sim} NO_3, e^- (H) \qquad (C)$$

The NO_3 radical recombination in spurs and tracks results in NO_2 and O_2 formation.

$$NO_3 + NO_3 \longrightarrow 2\,NO_2 + O_2 \qquad (1)$$

The direct action of radiation on HNO_3 and NO_3^- plays a prominent part in HNO_3 solutions with the concentration higher than 1.0M. In dilute solutions HNO_2 and NO_3 are mainly formed by the mechanism of the indirect action of radiation.

$$NO_3^- + H \longrightarrow NO_2 + OH^- \qquad (2)$$

$$2NO_2 + H_2O \longrightarrow NO_2^- + NO_3^- + 2H^+ \qquad (3)$$

$$NO_3^- + OH + H^+ \longrightarrow NO_3 + H_2O \qquad (4)$$

$$NO_3 + H_2O \longrightarrow NO_2 + H_2O_2 \qquad (5)$$

$$NO_2^- + OH(NO_3) \longrightarrow NO_2 + OH^- (NO_3^-) \qquad (6)$$

Ce^{4+} reduction and Ce^{3+} oxidation take place according to the reactions:

$$2Ce^{4+} + H_2O_2 \longrightarrow 2Ce^{3+} + 2H^+ + O_2 \qquad (7)$$

$$Ce^{4+} + HO_2 \longrightarrow Ce^{3+} + H^+ + O_2 \qquad (8)$$

$$2Ce^{4+} + HNO_2 + H_2O \longrightarrow 2Ce^{3+} + 3H^+ + NO_3^- \quad (9)$$

$$Ce^{3+} + OH \longrightarrow Ce^{4+} + OH^- \quad (10)$$

$$Ce^{3+} + NO_3 \longrightarrow Ce^{4+} + NO_3^- \quad (11)$$

Reaction (8) takes place on γ-radiolysis in aerated solutions and at $[NO_3^-] < 0.5$M. At higher $[NO_3^-]$ all H atoms are used for the NO_2^- formation /5/.

In the presence of Tl^+ ions the following reactions take place:

$$Tl^+ + OH \longrightarrow Tl^{2+} + OH^- \quad (12)$$

$$Tl^+ + NO_3 \longrightarrow Tl^{2+} + NO_3^- \quad (13)$$

$$Tl^{2+} + Ce^{4+} \longrightarrow Ce^{3+} + Ti^{3+} \quad (14)$$

In nitric acid solutions the part played by reaction (15) is important:

$$H_2O_2 + HNO_2 \longrightarrow (H^+ + NO_3^-) + H_2O \quad (15)$$

From the scheme presented here it can be seen that there are a number of competing reactions. Mathematical calculations were made that showed that the rate of reaction (9) was 10^3 times higher than that of reaction (6), i. e. in the presence of Ce^{4+}, reaction (6) is suppressed. In this case $G(HNO_2) = 1/2[G(H) + G^{d.a.}](HNO_2)$ (d. a. and i. a. stand for direct and indirect actions of radiation respectively.)

As is shown by calculations and experimental results obtained for acid solutions of $NaNO_3$ at a concentration of $[NO_3^-] \geq 0.5$ M essentially all the OH radicals transform into NO_3. It is a significant fact since the latter in accordance with reaction (5), may give an additional amount of reducing agents in a solutions. The experimental results show that NO_3 hydrolysis takes place at $[HNO_3] \leq 5.0$M and $[Ce^{4+}] \leq \leq 10^{-4}$M. At $[Ce^{4+}] = 10^{-2}$M the absence of hydrolysis is likely to be associated with an increase of the initial Ce^{3+} concentration in the solution. The absence of hydrolysis in HNO_3 if the concentration is higher than 5. 0M is possible to be accounted for by an increase of reaction (11) rate constant with acidity /6/. The presence of a hydrolysis reaction is demonstrated by large yields of oxygen found in cerium solutions (curve 1, Fig. 2). According to reaction (7) $G(O_2)$ is a measure of the Ce^{4+} and H_2O_2 interaction. In the absence of NO_3 hydrolysis, i. e. in solutions containing Tl^+ ions, scavenging NO_3 radicals, the yield of O_2 (curve 3. Fig. 2) is lower.

By considering the competition of reactions (5) and (11) it is shown that their rate is dependent on the dose rate to various extents being $V_{11} = \phi(I^2)$, $V_5 = \phi(I)$.

The calculation shows that the ratio V_{11}/V_5 diminishes with decreasing I. This means that the extent of NO_3 hydrolysis and, hence, the yield of Ce^{4+} ion reduction is the higher the less is I, all other things being equal.

The kinetic calculations showed reaction (15) to proceed in HNO_3 (>5. 0M) at $[Ce^{4+}] = 10^{-4}$M. The extent to which it proceeds is the larger the higher is I.

The effect of the dose rate on reaction (15) is well seen from the results of Fig. 4. In solutions of PuO_2^{2+} (with considerably lower rate constants for the H_2O_2- - HNO_2 interaction than Ce^{4+}) the yields are lowered at the expense of reaction (15) in a weakly acidic region. In the case of a more active isotope (Pu-238) the reduction yield is lower than in the case of less active Pu-239. On γ-radiolysis ($I = 2 \times 10^{15}$ ev/ml. min.) the role of reaction (15) in a PuO_2^{2+} solution also manifests itself at $HNO_3 \geqslant 10^{-1}$M. For NpO_2^{2+} ions the yields are lowered at $HNO_3 >$ (0. 1–0. 5M).

Thus, at $[Ce^{4+}] = 10^{-4}$M reactions (5), (7), (9), (11), (15) proceed in solutions. Reactions (5) and (15) take place at $[HNO_3] <$ 5. 0M and > 5. 0M, respectively. At $[Ce^{4+}] = 10^{-2}$M reactions (7), (9) and (11) take place.

In this case:

$$G(Ce^{3+}) = 2G_{H_2O_2} + 2G_{HNO_2} - G_{NO_3} \quad (19)$$

$$G(Ce^{3+})Tl^{+} = 2G_{H_2O_2} + 2G_{HNO_2} + G_{NO_3} \quad (20)$$

$$G_{H_2O_2} = G_{O_2}$$

$G(O_2)$ is equal to the O_2 yield in cerium solutions minus G_{O_2} in pure HNO_3 of the corresponding concentration. By rearranging expressions (19) and (20) one obtains:

$$G_{NO_3} = \frac{G(Ce^{3+})Tl^{+} - G(Ce^{3})}{2} \quad (21)$$

The values of GNO_3 and $GHNO_2$ found from expressions (21) and (19) (for deaerated solutions) are given in Fig. 5.

By substituting the yields in the case of 1. 0M HNO_3 into expression (21) (γ-radiolysis) one finds that $G_{NO_3^-} = 3.8$ radical/100 ev. Since in 1. 0 M HNO_3 only 5% of energy is taken up by NO_3^- ions the formation of NO_2^- and NO_3 may be believed to occur by the mechanism of the indirect action of radiation. The obtained value of G_{NO_3} is larger than G_{OH} on γ-radiolysis of 0. 4M H_2SO_4 (3. 0 radical/100 ev). The authors came to the conclusion that this is due to an increase in the water decomposition yield in HNO_3 solutions. In Ref. /5/ it is shown that on γ-radiolysis with an increase of $[NO_3^-]$ from 0. 001 to 0. 1 M in neutral $NaNO_3$ solutions G_{-H_2O} increases

from 3. 8 to 4. 5 molecule/100 ev. By substituting the values of G_{NO_3} and $G_{H_2O_2} = G_{O_2}$ into expression (19) one finds that in 1. 0 M HNO_3 the HNO_2 yield is equal to 3. 0 molecule/100 ev. The yield of water decomposition may be calculated from the following expressions:

$$G_{(HNO_2)} = 1/2\, G_{-H_2O} - G_{H_2} \qquad (22)$$

$$G_{NO_3} = G_{-H_2O} - 2G_{H_2O_2} \qquad (23)$$

$$G(Ce^{3+})_{Tl^+} = 2G_{-H_2O} - G_{H_2} \qquad (24)$$

The calculation showed that in 1. 0 M HNO_3 G_{-H_2O} is equal to 6. 0 $\pm$ 0. 25 molecule/100 eV. The H_2O_2 yield, equal to $G(O_2)$ in 1. 0M HNO_3 in the presence of Ce^{4+} and Tl^+ is found to be equal to 0. 9 $\pm$ 0. 1 molecule/100 eV. This H_2O_2 yield at an OH radical recombination in a spur equal to 0. 3 also complies with the yield of water decomposition of 6. 0 molecule/100 eV. The experimental data on the yield of O_2 (H_2O_2) in 5. 0M and 10M HNO_3 show that in these solutions $G(-H_2O)$ is also equal to 6. 0 molecule/100 eV.

The calculations of the authors based on the data used to determine $G(O_2)$ in nitric acid solutions of NpO_2^{2+} and HNO_3 solutions /7/ showed that on α-radiolysis $G(-H_2O)$ is equal to 3. 5 – 4. 5 ion/100 eV in the HNO_3 concentration range 10^{-3} – – 0. 3M. The authors believe that in HNO_3 solutions more concentrated than 1. 0M as on γ-radiolysis G_{-H_2O} is equal to 6. 0 molecule/100 eV.

This yield G_{-H_2O} along with the low yields of OH-radicals results in high reduction yields in HNO_3 solutions on α-radiolysis. In H_2SO_4 (10^{-3} – 0. 5M) the reduction yield is equal to 3. 0 ion/100 eV /4/.

Based on the available experimental data an attempt is made to find the yields of HNO_2 and NO_3 formation and the yields of NO_3^- and HNO_3 decomposition by the mechanism of the direct action of radiation. Then on the basis of the experimental data OH radicals originating in accordance with scheme B are assumed to convert to NO_3 radical.

According to the schemes B and C one can write the following:

$$G^{d.a.}_{HNO_2} = \frac{1}{2} G_{-HNO_3}, \qquad G^{d.a.}_{HNO_2} = \frac{1}{2} G_{-HNO_3^-} + \frac{1}{2} XG_{-NO_3^-}$$

$$G^{d.a.}_{NO_3} = G_{-HNO_3}, \qquad G^{d.a.}_{NO_3} = G_{-NO_3^-} - XG_{-NO_3^-}$$

(X is the degree of NO_3 radical recombination in spurs, tracks).

Considering the degree of HNO_3 dissociation the expressions for $G^{d.a.}_{HNO_2}$ and $G^{d.a.}_{NO_3}$ take the form of:

$$G^{d.a.}_{HNO_2} = A\frac{1}{2} C_{-NO_3^-}(1+X) + (1-A)\frac{1}{2} G_{-HNO_3} \quad (25)$$

$$G^{d.a.}_{NO_3} = AG_{-NO_3^-}(1-X) + (1-A)\, G_{-HNO_3} \quad (26)$$

(A is a fraction of the overall energy, absorbed by NO_3^- and HNO_3 that is the share of the NO_3^- ions.

Using the expression

$$G_{HNO_2} = f\, G^{i.a.}_{HNO_2} + (1-f)\, G^{d.a.}_{HNO_2}$$

$$G_{NO_3} = f\, G^{i.a.}_{NO_3} + (1-f)\, G^{d.a.}_{NO_3}$$

(f is a fraction of the overall energy absorbed by water), the yields were found of the direct action of radiation at different HNO_3 concentrations. It turned out that with an accuracy of $\pm$ 20% in the HNO_3 range of 2-10 M $G^{d.a.}_{NO_3} = 4.0 \pm 0.8$ radic. / 100 eV, $G^{d.a.}_{HNO_2} = 5.0 \pm 1.0$ molec/100 eV on γ-radiolysis. Using these values and specifying the various degrees of HNO_3 dissociation one obtains the following expression in accordance with (25) and (26):

$$G_{-NO_3^-}(1+X) = 10, \quad G_{-NO_3^-}(1-X) = 4.0$$

Rearranging these expressions one finds $G_{-NO_3^-} = 7.0 \pm 1.0$ ion/100 ev.

Table 1

Yields of product formation and decomposition by mechanism of direct action of radiation (per 100 eV absorbed by NO_3^- + HNO_3)

$[HNO_3]$, M	G_{NO_3}		G_{HNO_2}		$G_{-NO_3^-}$	G_{-HNO_3}
	γ-	α-	γ-	α-		
0.1	3.0	0.0	5.5	7.0	7.0	7.0
0.5	3.0	0.15	5.5	7.0	7.0	7.0
1.0	3.2	0.35	5.3	6.8	7.0	7.0
5.0	4.0	1.75	5.0	6.2	7.0	7.0
10.0	4.7	2,8	4.7	5.6		

Some data are available in the literature according to which $G_{-NO_3^-}$ is equal to 7.0 /1/. 10.0 /8/ and 8 – 17 ion/100 ev /9,10/. In compliance with reaction /1/

$$2\,G\,(O_2) = G\,(NO_3 + NO_3) = XG_{-NO_3^-}$$

The treatment of the data on O_2 yields in HNO_3 solutions with consideration for the degree of HNO_3 dissociation results in $G\,(O_2) = 2.0$ molecule/100 eV absorbed by NO_3^- ions. Using this value one finds $X = 0.55$, $G_{-HNO_3} = 7.0 \pm 3.0$ molecule/100 ev. Table 1 tabulates the yields of radiolysis products, formed by the case of α-radiolysis the degree of NO_3 radical recombination in tracks is assumed to be equal to unity. It follows from the Table that there is a significant difference in the yields of NO_3 and HNO_2 formed according to the mechanism of the direct action of radiation in the case of γ-and α-radiolyis.

References

/ 1/ Bugaenko, L. T., Roshchentaev, B. M. Khimya vysokich energi 5, 472 (1971).
/ 2/ Kulikov, I. A., Vladimirova, M. V., Khimya vysokich energii 6, 75 (1972).
/ 3/ Vladimirova, M. V., Kulikov, I. A., Ryabova, A. A., Radiokhimya 17, 327 (1975).
/ 4/ Vladimirova, M. V. Kulikov, I. A., Ryabova, A. A., Milovanova, A. S., Radiokhimya, 18, 172 (1976).
/ 5/ Kulikov, I. A. Vladimirova, M. V., Khimya vysokich energii 9, 288 (1975).
/ 6/ Matthews, R., Mahlman, H., Sworsky, T., J. Phys. Chem. 76, 2680 (1972).
/ 7/ Saveliev, Y. I., Ershova, Z. V., Vladimirova, M. V., Radiokhimya 9, 225 (1967).
/ 8/ Pikaev, A. K., Sibirskaya, G. K., Doklady A. N. SSSR, 215, 645 (1974).
/ 9/ Sworski, T., Matthews, R., Mahlman, H., Adv. Chem. Series 81, 164 (1968).
/10/ Daniels, M., Adv. Chem. Series 81, 15 (1968).

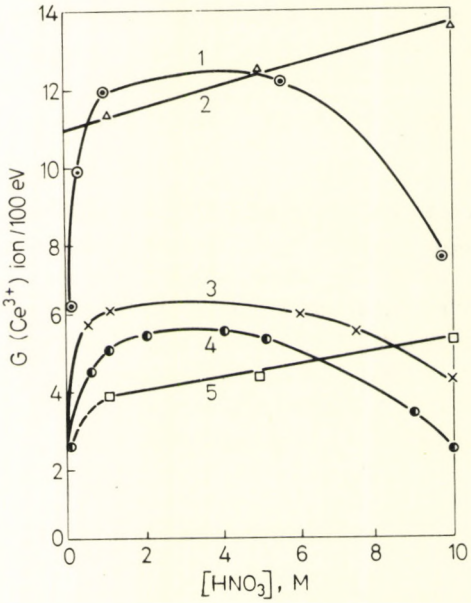

Fig. 1 Relationship between G(Ce^{3+}) and [HNO_3]. 1 G(Ce^{3+}) α-radiolysis; 2 G(Ce^{3+}) $Te^{+}\gamma$-radiolysis; 3, 4, 5 G(Ce^{3+}) γ-radiolysis; X[Ce^{4+}] = 10^{-4} M; I = $2 \cdot 10^{15}$ ev/ml min; ◐ [Ce^{4+}] = 10^{-4} M; I = $5 \cdot 10^{17}$ ev/ml·m ; ⊡ [Ce^{4+}] = 10^{-2} M; I = $2 \cdot 10^{15} - 5 \cdot 10^{17}$ ev/ml · min

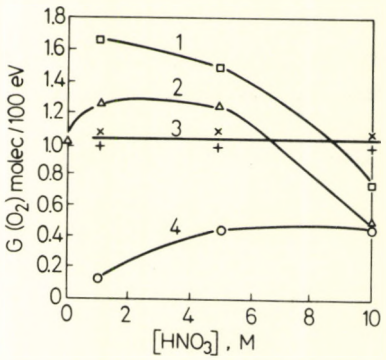

Fig. 2 Relationship between G(O_2) and [HNO_3] on γ-radiolysis. 1□ [Ce^{4+}] = 10^{-4} M; I = $2 \cdot 10^{15}$ ev/ml · min; 2 Δ [Ce^{4+}] = 10^{-4} M; I = $5 \cdot 10^{17}$ ev/ml · min; 3 +[Ce^{4+}] = $10^{-4} - 10^{-2}$M [Tl^{+}] = 10^{-3}M, I = $2 \cdot 10^{15}$ ev/ml·min; x[Ce^{4+}] = 10^{-2} M; I = $2\ 10^{15} - 5 \times 10^{17}$ ev/ml·min 4 G(O_2) in HNO_3

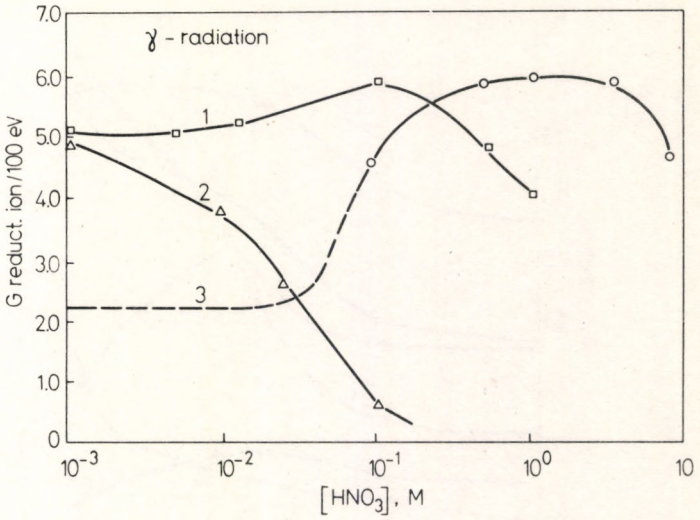

Fig. 3 Relationship between $G(Ce^{3+})$ ○, $G(-NpO_2^{2+})$ □, $G(-PuO_2^{2+})$ △ and $[HNO_3]$ at $I_\gamma = 2 \cdot 10^{15}$ ev/ml. min

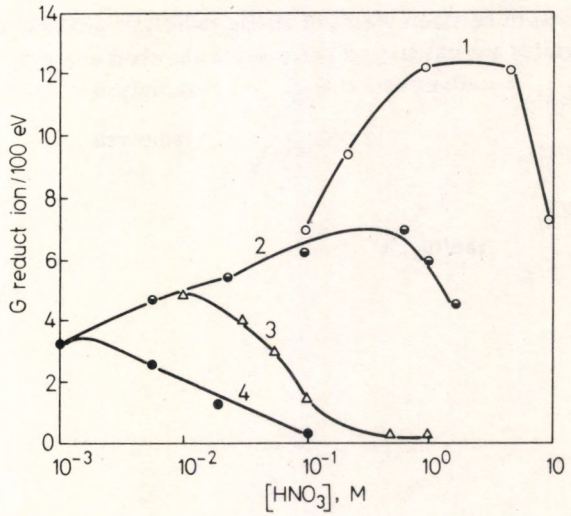

Fig. 4 Relationship between $G(Ce^{3+})$ ○, $G(-NpO_2^{2+})$ ◒, $G(-PuO_2^{2+})$ (△ Pu-239, ● Pu-238) and $[HNO_3]$ on α-radiolysis.

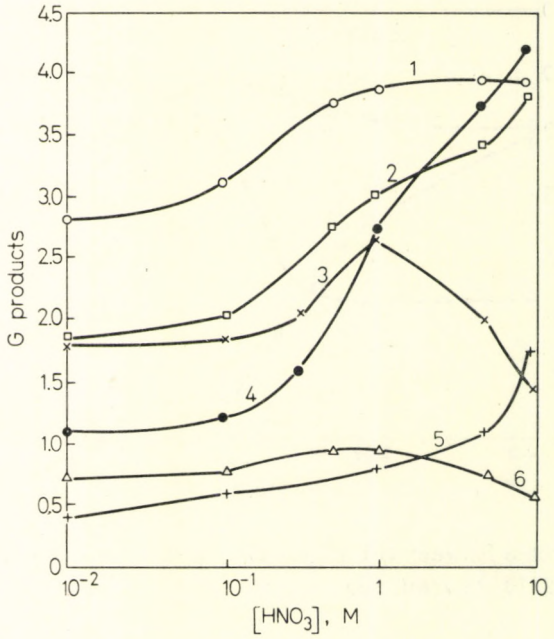

Fig. 5 Relationship between yields of HNO_3 radiolysis products and [HNO_3] (The yields are calculated per overall absorbed energy)

3 x $G_{H_2O_2}$ α-radiolysis 1 o G_{NO_3} γ-radiolysis

4 o G_{HNO_2} -"- 2 □ G_{HNO_2} γ-radiolysis

5 + G_{NO_3} -"-

6 Δ $G_{H_2O_2}$ γ-radiolysis

PULSE RADIOLYSIS OF HYDRATES: RELATION TO THE RADIATION CHEMISTRY OF AQUEOUS SOLUTIONS

Z. P. Zagórski, J. Grodkowski, Z. Zimek, K. Bobrowski
Department of Radiation Chemistry, Institute of Nuclear Research, 03-195 Warsaw, Poland

Certain aspects of aqueous radiation chemistry suggested the consideration of the pulse radiolysis of hydrates as the field which contributes to the better understanding of radiation chemistry in both liquid and frozen aqueous solutions.

The idea of performing conventional pulse radiolysis on solid polycrystalline hydrates could not be realized for a long time because the technique was limited to completely clear samples, preferably monocrystals. There is only a limited number of compounds which can be grown as single crystals and thus the collection of a rich material adequate to the high number of varieties of hydrates was impossible.

The development of a version of pulse radiolysis, consisting of the measurement of Čerenkov light self-absorption /1/ made possible the investigation of opaque samples. Samples for the investigation may be as opaque as the familiar pellets of sodium or potassium hydroxide.

Experimental

Linear electron accelerator LAE 13/9 was used as radiation source. According to our technique /1/ the longest single pulses possible were used (5.5 μs). Current in the pulse was adjusted between 0.3 and 1.0 A, according to the dose needed /2/. Energy of electrons was 10 or 13 MeV. The measuring circuit was as described in Ref. /1/, except that different photomultipliers were used (EMI and RCA) and the oscilloscope used was Tektronix Type 556.

The extreme tolerance of the method towards the transmission of light by the sample made practically every kind of preparation possible. Except putting simply the crystals into a proper vessel, we used pellets of polycrystalline material obtained in a press used for the preparation of samples for infrared studies. Some samples were prepared by melting. All auxiliary holders, etc. exposed to radiation were made from a non-emitting material or the spectrum of emitted background was carefully measured and taken into account in calculations. Experiments were done at room temperature.

Figure 1 shows the typical record of the Čerenkov light self-absorption in hydrates. The lowering of the intensity of emitted light is very distinct and easy to

measure. At the same time it is possible to check if there is no isothermal fluorescence after the pulse. If there is no absorption at the chosen wavelength, the plateau of the signal does not change its level and represents at the same time the contour of the pulse (dotted line).

The changes of kinetics obtained from solids are even better expressed than was reported in Ref. /1/ for liquids. That is due to the fact that the actual light path emitted from the bulk of the solution is not a straight line corresponding to geometry, but is much longer than that. The effect was described earlier /3/ in connection with radiothermoluminescence studies on polycrystalline, frozen material. Methods of interpretation described there are applied to the present investigation as well.

Results and discussion

The brevity of this paper prevents us from quoting all the results in full. Only conclusions will be presented with the attempt to provide a preliminary general picture. which is not a complete one at this stage of research.

Table 1

Intermediate absorption spectra of the hydrated electror in hydrates during the electron pulse

A. Absorption identified as e^- stabilized by one or a small number of H_2O molecules

$KOH \cdot 1/2H_2O$, $2K_2CO_3 \cdot 3H_2O$, $Na_2B_4O_7 \cdot 10H_2O$, $Na_2SO_3 \cdot 7H_2O$,

$Na_2S_2O_3 \cdot 5H_2O$, $K_3PO_4 \cdot 3H_2O$, $(CH_3)_4NOH \cdot 5H_2O$, $LiOH \cdot H_2O$

B. No intermediate spectrum

$Li_2SO_4 \cdot H_2O$, $LiBr \cdot H_2O$, $Na_2CO_3 \cdot 10H_2O$, $LiClO_4 \cdot 3H_2O$

$NaCH_3COO \cdot 3H_2O$, $NaH_2PO_2 \cdot H_2O$, Na - citrate $\cdot 3H_2O$,

$Na_2HPO_4 \cdot 2H_2O$, $CaSO_4 \cdot 2H_2O$, $FeSO_4 \cdot (NH_4)_2SO_4 \cdot 7H_2O$,

$FeSO_4 \cdot 7H_2O$, $Ce(SO_4)_2 \cdot 5H_2O$, $Ce(NO_3)_3 \cdot 6H_2O$.

Table 1 summarizes the behaviour of investigated hydrates.

One may state generally that some hydrates show at room temperature the intermediate absorption ascribed to the stabilized electron. The phenomenon lasts more or less during the pulse only and decays rapidly after it. There is no afterglow and no permament coloration. On the contrary, practically all corresponding "dry" salts show phenomena resembling F-centre formation, accompanied often by fluorescence. As it is the case with F-centres, the lattice parameters impose the frequency of oscillations of trapped electrons, therefore every dry compound has a different absorption spectrum after irradiation. The case of hydrates is different: the dominating, characteristic wavelength of absorption (basically ca 520 nm) is independent of the very different composition of the crystal which indicates strongly that only water molecule – one or a small group – is involved in the temporary stabilization of the electron.

The "no signal" group of hydrates demands some comment. The absence of e^- spectrum may be due to impurities scavenging electron. Also in hydrates which have a lot of "lattice water" of ice-like structure there is a possibility for oxygen to be present in comparatively large concentrations as the crystals are in equilibrium with air. It is possible that new criteria of purity applied to hydrates may change the position of a compound in this Table. Changes in the mode of hydration may also turn the position. For example, slightly weathered crystals of $Na_2CO_3 \times 10H_2O$ exhibit a weak but clear spectrum of stabilized electron. Obviously not all H_2O molecules are the same: some are more strongly coordinated and promote e^- stabilization better.

There is a separate class of hydrates which obviously do not belong to the compounds listed. There are, e.g. $ZnSO_4 \times 7H_2O$, $3CdSO_4 \times 8H_2O$, $LaCl_3 \times 6H_2O$, $Na_2HPO_4 \times 2H_2O$ in which intermediates other than electron are visible or quite new phenomena appear, like in $CeCl_3 \times 6H_2O$ in which Ce^4 present is temporarily bleached.

The published knowledge on hydrates is presently rather modest. Some compounds are investigated thoroughly, but these are not of a great importance to our problem. Four major monographs /4–7/ on the subject quote helpful data but they are not sufficient to discuss phenomena in terms of radiation chemistry.

It seems that the first condition for a high yield of an electron in hydrates is a strong, dominating coordination of water at the cation.

Particular cases will be treated in separate publications. In these publications a comparison will be made with frozen hydrates.

References

/1/ Z. P. Zagórski, Z. Zimek, Int. J. Radiat. Phys. Chem. 7, 529 (1975).

/2/ K. Bobrowski, J. Grodkowski, Z. P. Zagórski, Nukleonika 21, (1976). in press.

/3/ Z. P. Zagórski, Z. Zimek, E. Sitkowska, Int. J. Radiat. Phys. Chem. 4, 65 (1972).

/4/ M. B. Ormerod, "The Architecture and Properties of Matter, An Approach through Models", Edward Arnold, London 1970, (transl. from German, Verlag Chemie.)
/5/ M. Falk, O. Knop, "Water in Stoichiometric Hydrates" in F. Franks (ed.) Water, Vol 1–4, Plenum Press New York 1973, Vol. 2, pp. 55–113
/6/ P. Schuster, W. Jakubetz, W. Marius, "Structure of Liquids" in Topics in Current Chemistry 1975, p. 60.
/7/ J. E. Gordon, "The Organic Chemistry of Electrolyte Solution" John Wiley & Sons, New York 1975, Chapter 2. Ion Solvation.

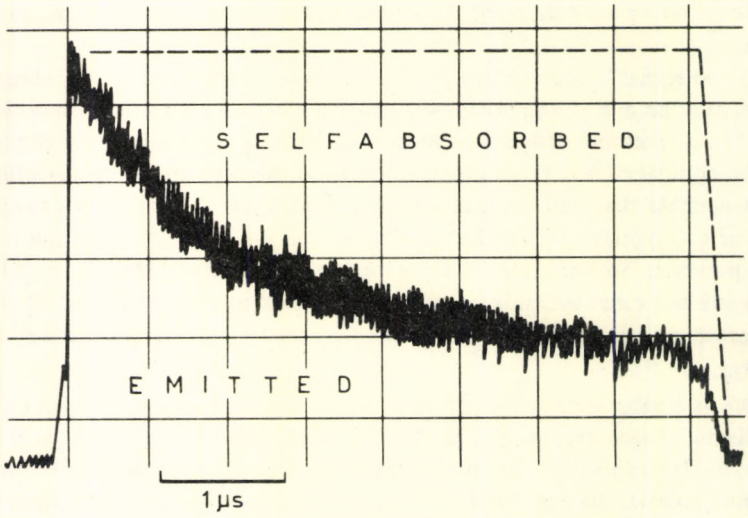

Fig. 1 Intensity of light versus time

J. DELAIRE

As vou know Dr. Hart and coworkers reexamined the spectrum of the solvated electron and found an absorption in the near U. V. At Orsay, in our laboratory Drs. Belloni and Saito just found such an absorption for the solvated electron in liquid ammonia. Did you try to examine the absorption in this region in the case of hydrates?

Z-P. ZAGÓRSKI

We have looked into the near U. V. region, because the original Čerenkov-spectrum secures even more light at U. V. than in the visible region. We did not observe transient selfabsorbtion comparable in intensity to the one at the 520 mm region. The next, more refined version of our apparatus will make possible a measurement with higher sensitivity.

G. ZIMINA

To what species can you ascribe the absorption in the KOH + 1/2 H_2O system at λ = 520 nm?

Z. P. ZAGÓRSKI

To the stabilized electron.

G. ZIMINA

Are the radiation chemical yields (G-values) determined for the observed short-lived species?

Z. P. ZAGÓRSKI

Not yet, because the real optical path length and molar absorptivity are not known.

G. ZIMINA

What dose and optical path length do correspond to the optical density $D > 3$?

Z. P. ZAGÓRSKI

The optical density > 3 was determined for the dose of 10 krad. The true optical path length was substantially longer than the geometrical one. It is evident from the diagram in Fig. 5 in Ref. /1/ that the optical density of 3 is well measurable by our method, whereas in conventional absorption spectrometry the measurement is not possible in this range.

POLARIZATION INTERACTIONS IN DIFFUSION-CONTROLLED REACTIONS OF HYDRATED ELECTRONS WITH MOLECULES

Wolfgang Stiller, Rainer Schmidt
Zentralinstitut für Isotopen- und Strahlenforschung der AdW der DDR,
705 Leipzig, GDR

Introduction

The aim of the present paper is the theoretical assessment of the ion-molecule interactions with diffusion-controlled reactions in dilute solutions. Comparisons with pulse radiolytic studies are made concerning reactions between hydrated electrons and molecules in aqueous solutions.

Theory

I. Basic relations

The starting point of the considerations is the expression for the rate coefficient /1. 2/

$$k = \frac{4\pi}{10^3} N_a \; D_{AB} \cdot r_{AB} \cdot f \equiv k_{sm} \; f \qquad (1)$$

of diffusion-controlled reactions between particles A and B producing a potential U(r) (r being the distance between two particles A and B) the action of which can be described by the correction factor f in the form (2):

$$f = \left[r_{AB} \int_{r_{AB}}^{\infty} e^{U(r)/KT} \, r^{-2} \, dr \right]^{-1} \qquad (2)$$

In Eqs (1) and (2) the symbols have the following meaning:

k_{sm} Smoluchowski's rate coefficient /1/ in 1 mole^{-1} s^{-1} for neutral reactants,

N_A Avogadro's number

K Boltzmann's constant

D_{AB} effective diffusion coefficient in cm^2 s^{-1}.

r_{AB} effective reaction radius in cm

T absolute temperature

In the derivation of Eqs (1) and (2) the following important assumptions were made:

(i) Reaction condition:

$$n_B(r_{AB}) = 0 \qquad n_B \text{ is the concentration of particles B,} \tag{3}$$

that is the touching of a particle A and a particle B immediately leads to a reaction.

(ii) Boundary value condition:

$$\lim_{r \longrightarrow \infty} n_B(r) = \bar{n}_B \qquad \bar{n}_B \text{ is the mean concentration of the particles B} \tag{4}$$

(iii) Spherical symmetry of the diffusion problem to be solved:

$$n_B = n_B(r) \tag{5}$$

We are especially interested in a theoretical treatment of diffusion-controlled ion-molecule reactions, this is to be discussed in the following pages. In such a case the charge-dipole interactions have to be considered. In order to get a realistic interaction potential U_f for the liquid state also the screening action of the nearest neighbour particles on a reactive ion-molecule pair has to be taken into consideration. Now we simplify the problem by using a gas phase potential U_g for the description of the ion-molecule interactions. In reality the potential U_g will be reduced by the screening effects. Employing the potential U_g instead of the realistic potential U_f we assess the maximum effects of the ion-molecule interactions in solutions.

Two cases of interactions will be considered:

1. Interactions between ions and polarized molecules:

$$U \simeq U_g = U_p(r) = -\frac{1}{2}\,\frac{\alpha e^2}{\bar{\varepsilon}^2 r^4} \tag{6}$$

where e is the ionic charge, α the polarizability of the molecule and $\bar{\varepsilon}$ the relative dielectric constant

2. Interactions between ions and molecules with permanent dipole moments μ :

$$U \simeq U_g = U_d(r) = -\frac{e\,\mu}{\bar{\varepsilon} r^2}\cos\theta \tag{7}$$

θ is the angle between the dipole axis and the connection line between ion and dipole; $\theta = 180^\circ$ is assumed for the sake of simplicity

II. Results

Case 1: Combination of Eq. (2) with (6) gives

$$f = f_p(\rho_p) = \frac{\rho_p}{\int_0^{\rho_p} e^{-x^4}\,dx} \qquad \rho_p = r_p/r_{AB} \tag{8}$$

with

$$r_p = \left(\frac{1}{2}\,\frac{\alpha e^2}{\bar{\varepsilon}^2\, KT}\right)^{1/4} \tag{9}$$

It is remarkable that the polarization energy (6) is equal to the thermal energy KT if the distance r between ion and molecule is equal to the "range of the polarization force" r_p. In this respect the quantity r_p is the parallel to the Onsager length in the case of charged particles A and B with Coulombic interaction The correction quantity $f_p(\rho_p)$ is a monotonically increasing function of ρ_p. The following typical values (ρ_p/f_p) are given for illustration of the numerically obtained results: (0.0/1.00000), (0.1/1.00002). (0.2/1.00032). (0.3/1.00162). (0.4/1.00511), (0.5/1.013).

Case 2: Eq. (2) gives in connection with Eq. (7):

$$f = f_d(\rho_d) = \frac{d}{\int_0^{f_d} e^{-x^2}\,dx} \qquad \rho_d = r_d/r_{AB} \tag{10}$$

with

$$r_d = \left(\frac{e\,\mu}{\bar{\varepsilon}\ KT}\right)^{1/2} \tag{11}$$

The quantity r_d represents, in a way analogous to r_p, the "equilibrium distance", here with respect to the equality of charge–dipole interaction energy and the thermal energy KT. The correction factor f_d monotonically increases with the ratio of the radii r_d/r_{AB} which is demonstrated by the following characteristic values (ρ_d/f_d): (0.0/1.00), (0.5/1.08), (0.8/1.22), (1.0/1.34).

If the ion–molecule interactions disappear ($\alpha \to 0$ $\mu \to 0$), the corresponding quantities r_p and r_d and therefore also ρ_p and ρ_d tend to zero. Then f_p and f_d are exactly equal to one, that is $k = k_{sm}$ in Eq. (1) and the expression for neutral non-interacting reactive particles A and B are obtained /1/.

Table 1
Diffusion-controlled ion-molecule-reactions in H_2O at 20-25°C C

1.1 Polarization model

B	r_B(Å)	$D_B(10^{-5} cm^2 \cdot s^{-1})$	$\alpha(10^{-24} cm^3)$	$k_{th} = k_{sm} \cdot f_p(10^{10} l \cdot Mol^{-1} \cdot s^{-1})$	k_{exp}
I_2	2.5 ± 20% /4/	1.2 ± 15% /4/	11 /6/	2.27 ± 0.70	5.2 ± 0.3 /7/
CS_2	2.2 ± 20%	1.2 ± 15%	8.74	2 13 ± 0.65	3.1 ± 0.3 /8/
CCI_4	2.9 ± 20%	1.0 ± 15%	10.5	2.14 ± 0.65	3.1 ± 0.3 /9/
CO_2	2.0 ± 20%	1.6 ± 15%	2.65	2.18 ± 0.65	2.7 ± 0.3 /10/

Table 2
Dipole model

B	r_{AB}(Å)	$D_{AB}(10^{-5} cm^2 \cdot s^{-1})$	μ (D)	$k_{th} = k_{sm} \cdot f_d(10^{10} l \cdot Mole^{-1} \cdot s^{-1})$	k_{exp}
$CHCI_3$	5.4 ± 20% /3, 4/	5.6 ± 15% /3, 5/	1.18 /11/	2.34 = 2.29 · 1.02	2.0...3.0 /12-14/
NH_3*	4.0 ± 20% /15/	13 ± 15% /15/	1.46 /11	4.14 = 3.94 · 1.05	4.3

* Here the reaction partner A is H^+

Comparison with experiments

In the final section we wish to compare our results with experimental work concerning preferably rate coefficient measurements of diffusion-controlled ion–molecule reactions in dilute aqueous solutions (see Tables 1 and 2).

Table 1 includes some measured rate coefficients k_{exp} of reactions between hydrated electrons e^-_{aq} ($r_A = r_{aq} \approx 2.7$ Å, $D_A \approx 4.5 \cdot 10^{-5}$ $cm^2 s^{-1}$ /3/) and molecules B of different polarizability in dilute aqueous solutions at 25°C. The comparison between k_{exp} and k_{th} shows the qualitative correctness of the calculated factor f_p. Because of the low values of $\rho_p = r_p/r_{AB}$ ($C \leq \rho_p \leq 0.5$) as a consequence of the high dielectric constant of water, however, the factor f_p does not exceed 1.01. This means that the contribution of the polarization effects in k_{th} is no more than about 1% compared with k_{sm}.

Table 2 provides two examples for reactions discussed on the basis of a charge-(permanent) dipole model. The correction factor f_d is higher than f_p for equivalent ratios of the radii, but the increase of k_{th} above k_{sm} is less than about 5%.

Summary

Under the assumptions made, the evaluation of polarization and dipole interaction effects with diffusion-controlled ion-molecule reactions gives correction factors which modify Smoluchowski's rate coefficient in the right direction (increase) towards to experimental data. In aqueous solutions, however, these effects are very small being about 1% for reactions with polarizable molecules and about 5% for reactions with molecules having permanent dipole moments. More important effects should be expected for ion–molecule reactions in dilute solutions of solvents with low dielectricity constants.

References

/ 1/ M. Smoluchowski, Physik. Z. 17, 557, 585 (1916).
/ 2/ P. Debye, Trans. Electrochem. Soc. 82, 265 (1942).
/ 3/ M. S. Matheson, Adv. Chem. Ser. 50, 45 (1965).
/ 4/ Landolt-Börnstein: Zahlenw. u. Funkt. Springer-Verl. Berlin 1950.
/ 5/ K. A. Reddy, L. Doraiswamy, Ind. Eng. Chem. Fund. 6, 77 (1967).
/ 6/ H. Staude, Phys.-Chem-Taschenbuch, Bd. 1, Akad. Verlagsges. Leipzig 1945.
/ 7/ J. K. Thomas, J. Phys. Chem. 68, 1524 (1964).
/ 8/ L. M. Dorfman, M. S. Matheson, Proger. React. Kin. Vol. III Pergamon Press, Oxford 1965.
/9/ L. M. Dorfman, M. S. Matheson, Progr. React. Kin. Vol. III Pergamon Press, Oxford 1965.

10/ K. Eiben, Angew. Chem. 82, 652 (1970).
/11/ D'Ans/Lax: Taschenb. f. Chem. u. Physiker, Vol. 3 Springer Verlag, Berlin 1970.
/12/ S. Gordon, E. J. Hart, M. S Matheson, J. Rabani, J. K. Thomas, Disc Faraday Soc. 36, 193 (1963).
/13/ E. J. Hart, J. K. Thomas, S. Gordon, Rad. Res. (Suppl.) 4, 74 (1964).
/14/ E. J. Hart, S. Gordon, J. K. Thomas, J. Phys. Chem. 68, 1271 (1964).
/15/ R. Weston, H. A. Schwarz: Chemical Kinetics, Prentice Hall Inc. Englewood Cliffs, New Jersey 1972.

DISCUSSION

Yu. A. BERLIN

What boundary conditions have you used in your calculations?

W. STILLER

We used:

$$n_B(r_{Reaction}) = 0$$

$$\lim_{r \to \infty} n_B(r) = \bar{n}_B$$

(n_B is the number density of reactant B, $\bar{n}_B$ is its average.)

R. KHAIRUTDINOV

What kind of polarization coefficient did you use in your calculations – microscopic or average one?

W. STILLER

In order to compare our results with Debye's coulomb case we applied macroscopic values for α and static ones for ε.

R. KHAIRUTDINOV

The effect for real value of ε will be larger, I expect.

W. STILLER

Yes, this is so.

J. SOBKOWSKI

What value of dielectric constant has been accepted in your calculation? It is well known that the dielectric constant changes markedly with the strength of the electric field.

W. STILLER

I agree with Prof. Freeman s arguments regarding the application of the static value of ε.

G.R. FREEMAN

The dielectric constant reaches the static value of the bulk solvent at a relatively short distance from an ion. The distance is only 2 or 3 molecular diameters, so your use of the static value is a good approximation.

W. STILLER

I agree with you.

ACTIVATION ENERGY FOR THE RECOMBINATION OF HYDRATED ELECTRONS IN H_2O AND D_2O

B. Hickel
DRA/SRIMa, Cen, Saclay B. P. N° 2, 91190 Gif Sur Yvette, France

Introduction

The reaction between two hydrated electrons to give hydrogen is nearly diffusion controlled and an activation energy of 5.2 ± 0.3 Kcal/mole was determined by Gottschall and Hart using a steady state method /1/. This value was higher than most of the activation energies for the reactions of hydrated electrons and two explanations were given /2/.

1) There is an equilibrium between hydrated electrons and an intermediary species such as the dielectron

$$2\,e_s^- \rightleftharpoons (e_s^-)_2 \xrightarrow{H_2O} H_2 + 2OH^-$$

The activation energy measured pertains to the decomposition of dielectrons to give hydrogen.

2) There is a side reaction at elevated temperature which decreases the steady state concentration of hydrated electron and increases the apparent rate of recombination.

We have studied by pulse radiolysis the recombination of hydrated electrons. This method, in principle, overcomes the two difficulties met by steady state radiolysis. First, it is possible to follow the initial decay of hydrated electrons before the establishment of any equilibrium with dielectrons. Secondly, if there is a side reaction with an impurity it is possible to check it by examination of the kinetics. Moreover, in pulse radiolysis the concentration of hydrated electrons is at least three orders of magnitude higher than in steady state radiolysis and, correspondingly, a reaction with an impurity would be less important compared to the bimolecular recombination of hydrated electrons.

Experimental

Most of the experiments were carried out with a linear accelerator at Risø (Denmark). The duration of the 10MeV electron pulse can be varied between 0.4 and 4 μsec giving a dose range from 0.2 to 3.5 Kilorads. Experimental details on the pulse radiolysis system are given elsewhere /3/. The decay of hydrated electrons was

monitored at 600 nm using a spectrophotometric detection system. Owing to the low solubility of hydrogen in water, a pressure cell which can withstand a pressure of 30 atmospheres of hydrogen above the solution was used. The concentration of hydrogen in the solution varied from 2.7×10^{-2}M at 5°C to 2.1×10^{-2} M at 65°C. The irradiation cell was cooled or heated in a thermostated bath and the time between the removing of the cell and the experiment was recorded. The temperature inside the cell was then corrected. For that the change of temperature in the solution under a pressure of 29 atmospheres of hydrogen after heating was determined by interferometric measurement /4/. It was found that the decay of temperature is exponential and follows Newton's law of cooling.

Figure 1 gives the logarithmic plot of $\frac{T_o - T_r}{T_c - T_r}$ as a function of time where T_o is the temperature of the thermostated bath, T_r and T_c the temperature of irradiation room and the temperature of the solution inside the cell, respectively. The time t is in minutes. In most of the experiments t was less than five minutes.

Results

After the electron pulse, the following reactions take place:

$$H_2O \longrightarrow e_s^-, H_3O^+, H, OH, H_2 H_2O_2 \quad (1)$$

$$OH^- + H_3O^+ \longrightarrow 2H_2O \quad k_2 = 1.3 \times 10^{11}\ M^{-1}s^{-1} \quad (2)$$

$$OH + H_2 \longrightarrow H + H_2O \quad k_3 = 5 \times 10^{7}\ M^{-1}s^{-1} \quad (3)$$

$$H + OH^- \longrightarrow e_s^- \quad k_4 = 2 \times 10^{7}\ M^{-1}s^{-1} \quad (4)$$

$$e_s^- + H_2O_2 \longrightarrow OH + OH^- \quad k_5 = 1.2 \times 10^{10}\ M^{-1}s^{-1} \quad (5)$$

$$e_s^- + e_s^- \longrightarrow H_2 + 2OH^- \quad k_6 = 5 \times 10^{9}\ M^{-1}s^{-1} \quad (6)$$

Under our experimental conditions reactions (1) to (4) are finished 10 μsec after the end of the pulse and there are only hydrated electrons and molecular hydrogen peroxide in the solution. But H_2O_2 does not contribute to the decay of hydrated electrons because reaction 5 gives an OH radical and then a few microseconds later, an H atom and another hydrated electron by reactions (3) and (4) /5/. If there is no side reaction, the kinetics for the decay of the hydrated electrons should be second order. Experimentally this was obtained by preirradiating the solution by pulse irradiation with a dose of about 40 Kilorads. The lifetime of the hydrated electrons increases until it reaches a plateau. Probably the main effect of preirradiation is to destroy the last traces of oxyger

in the solution by the overall reaction /6/

$$H_2 + 1/2\ O_2 \longrightarrow H_2O$$

The second order plot for the decay of e_s^- at room temperature in H_2O and D_2O is shown in Fig. 2. The dose is about three Krads and the concentrations of e_s^- were calculated using ε = 12 400 and 13 500 at 600 nm in H_2O and D_2O, respectively. The decay follows second order kinetics over more than three half times and the rate is slower in D_2O by 20%. From the slope we found $(k_6)_{H_2O} = 5.0 \pm 0.3 \times 10^9\ M^{-1}s^{-1}$ and $(k_6)_{D_2O} = 4.0 \pm 0.3 \times 10^9\ M^{-1}s^{-1}$. To check further the absence of side reactions, the dose was decreased by a factor of fifteen. Figure 3 gives the decay of e_s^- in D_2O at low dose. From the slope equal to $2k_6/\varepsilon l$ where l is the length of the cell (l = 7.1 cm) a rate constant $(k_6)_{D_2O} = 4.2 \pm 0.3 \times 10^9 M^{-1}s^{-1}$ was calculated, in good agreement with the value at high dose.

The effect of temperature on the rate of reaction (6) was studied between 5°C and 65°C. The absorption coefficient ε of e_s^- at different temperatures was calculated from the product $G(e_s^-) \times \varepsilon$ which is known in H_2O from pulse radiolysis experiments /7/ and from the variation of $G(e_s^-)$ with temperature in H_2O and D_2O /8/. In D_2O the product $G(e_s^-) \times \varepsilon$ is known only at 25°C /9/ and we have made the assumption that the small variation of the product $G \times \varepsilon$ with the temperature is the same in D_2O as in H_2O.

The Arrhenius plots for the recombination of hydrated electrons are given in Figs 4 and 5. In H_2O the activation energy is independant of the pH of the solution between pH 11.6 and 13 and is equal to 4.2 ± 0.5 Kcal mol^{-1}. In D_2O $E = 4.8 \pm 0.5$ Kcal mol^{-1}. These values seem at the first sight to be lower than the value of 5.2 ± 0.3 Kcal mol^{-1} determined earlier by steady state radiolysis /1/. But in Ref. /1/ the yield of e_s^- was considered as constant. Taking into consideration the increase of $G(e_s^-)$ with temperature /8/ the value decreases by 0.5 Kcal mol^{-4} giving $E = 4.7 \pm 0.3$ Kcal mol^{-1} in good agreement with our results.

These values are close to the activation energy for the diffusion of hydrated electron in H_2O which is 4.8 ± 0.5 Kcal mol^{-1} /10/ and 4.2 ± 0.4 Kcal mol^{-1} /11/ determined by pulse radiolysis conductivity and flash photolysis conductivity, respectively (the latter being independent of the yield of e_s^-). This suggests that the activation energy for the diffusion of e_s^- represents the main contribution to the activation energy of reaction (6). At room temperature the rate in D_2O is lower than in H_2O and

the ratio $\dfrac{k_6(H_2O)}{k_6(D_2O)} = 1.25 \pm 0.1$ is close to the ratio of the viscosities $\dfrac{\eta(D_2O)}{\eta(H_2O)} =$

$= 1.23$ suggesting that the diffusion coefficient of e_s^- is slower in D_2O than in H_2O. To check this assumption further we have recently, at Saclay, studied both in H_2O and D_2O the very rapid reaction between e_s^- and $C_6H_5NO_2$ which is truely diffusion

controlled. Application of the Smoluchowski equation

$$k_{diffusion} = \frac{4\pi N}{1000} (r_{e_s^-} + r_{C_6H_5NO_2}) (D_{e_s^-} + D_{C_6H_5No_2})$$

shows that the ratio $\frac{(D_{e_s^-})_{H_2O}}{(D_{e_s^-})_{D_2O}}$ is close to 1.3.

It would be interesting to test this hypothesis by direct measurement of the mobility of hydrated electrons in D_2O.

Acknowledgments. The author wishes to thank A. Miller for the interferometric measurement of cell temperature, J. Eriksen, P. Genske and the staff of the accelerator department at Risø for technical assistance. The author also thanks the Danish Atomic Energy Commission for financial support during the course of this work.

References

/ 1/ W.C. Gottschall and E.J. Hart, J. Phys. Chem. 71, 2102 (1967).
/ 2/ E.J. Hart and M. Anbar, The hydrated electon, Wiley-Interscience, New York, NY, 1970, p. 174.
/ 3/ P. Pagsberg, H. Christensen, J. Rabani, G. Nilsson, J. Ferger and S.O. Nielsen. J. Phys. Chem. 73, 1029 (1969).
/ 4/ A. Miller, E.K. Hussmann and W.L. Mc Laughlin, Rev. Sci. Instrum. Vol. 46, N°. 12, 1635 (1975).
/ 5/ B. Hickel and K.H. Schmidt. J. Phys. Chem. 74, 2470 (1970).
/ 6/ E.J. Hart and E.M. Fielden. Advan. Chem. Ser. 50, 253 (1965).
/ 7/ B.D. Michael, E.J. Hart and K.H. Schmidt. J. Phys. Chem. 75, 2798 (1971).
/ 8/ K.N. Jha, T.G. Ryan, G.R. Freeman J. Phys. Chem. 79, 868 (1975).
/ 9/ E.M. Fielden and E.J. Hart, Radiation Research 33, 426 (1968).
/10/ G.C. Barker, P. Fornles, D.C. Sammon and B. Stringer, Trans. Faraday Soc. 66, 1498 (1970).
/11/ K.H. Schmidt, Int. J. Radiat. Phys: Chem. 4, 439 (1972).

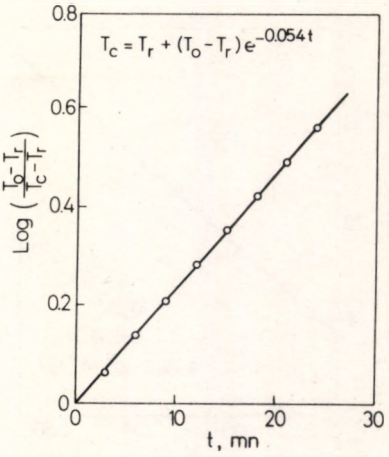

Fig. 1 Temperature change of the solution inside the pressure cell

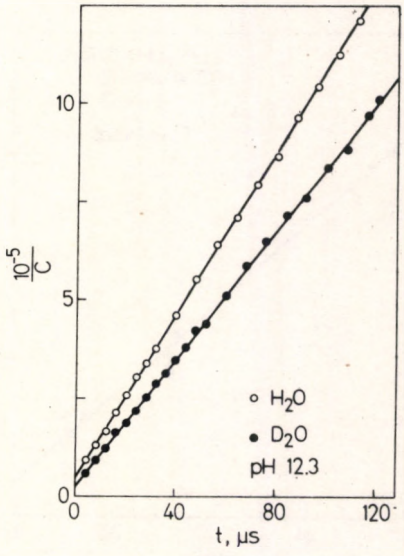

Fig. 2 Second order plot for the decay of hydrated electron in H_2O and D_2O at 23°C. Dose ≃ 3. 5 Krads

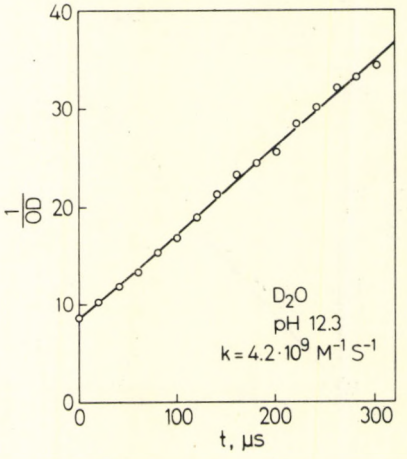

Fig. 3 Plot of the reciprocal of optical density against time in D_2O. Dose $\simeq$ 200 rads. λ = 600 nm

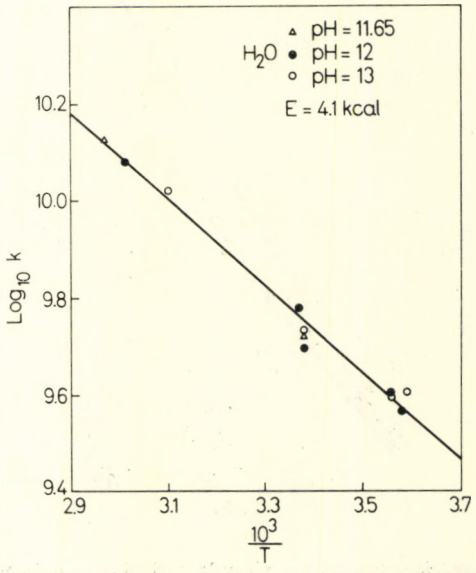

Fig. 4 Arrhenius plot for the recombination of hydrated electrons in H_2O

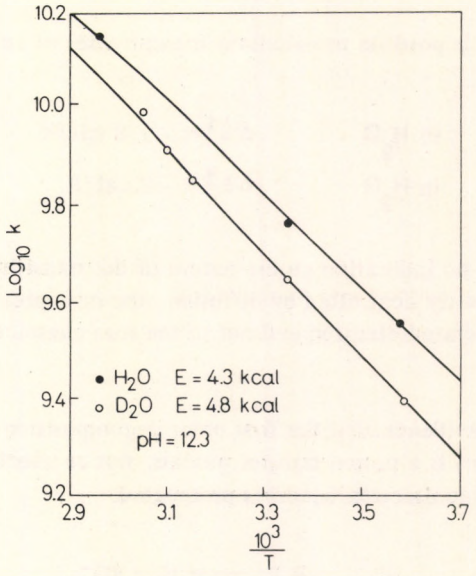

Fig. 5 Arrhenius plot for the recombination of hydrated electrons in H_2O and D_2O at pH 12.3

DISCUSSION

Z. P. ZAGÓRSKI

What was added to the solution to adjust the pH, and in what concentration?

B. HICKEL

The solution was first deaerated by bubbling with argon, then sodium hydroxide from a saturated solution was added and the pH of the solution was measured. After that the solution was saturated with hydrogen. The purpose of this procedure was to avoid possibly any contamination of carbonate.

G. R. FREEMAN

Would you speculate about the structure of the transition state for

$$e^-_{aq} + e^-_{aq} \longrightarrow 2H_2 + 2OH^-_{aq} \; ?$$

B. HICKEL

From the data it is possible to calculate the entropies of activation ΔS^{+} for reaction (6):

$$\text{in } H_2O \qquad \Delta S^{\ddagger} = -1.9 \text{ cal/K}$$

$$\text{in } H_2O \qquad \Delta S^{\ddagger} = -3 \text{ cal/K.}$$

But these values give no indication on the nature of the transition state because the reaction being mostly controlled by diffusion, the entropies of activation refer to the diffusion of hydrated electron and not to the true chemical rate.

G. R. FREEMAN

There is recent evidence that the first order decomposition of solvated electrons in alcohols (and water) is a proton transfer process, not an electron transfer process. The site of the solvated electron becomes protonated.

$$e^-_{solv} + ROH \longrightarrow H + RO^-_{solv}$$

A similar mechanism could apply to the reaction between two solvated electrons. The protonation of two adjacent solvated electrons would form H_2. This reaction would be less endoergic than the first order decomposition, because of the energy gained from formation of the H-H bond. The rate constant of $e^-_{aq} + e^-_{aq}$ is therefore relatively large with an activation energy similar to that of diffusion.

TRANSIENT ION-PAIRS IN PULSE IRRADIATED ALKYL IODIDES

Hch. Büchler, R. E. Bühler
Laboratory for Physical Chemistry, Swiss Federal Institute of Technology,
8092 Zürich, Switzerland

Introduction

In previous studies /1/ of aqueous solutions of alkyl iodides we were able to prove that the OH-radical is reacting by the way of an equilibrium between an outer charge-transfer (CT)-complex $(RI, OH)_{solv}$ and an inner CT-complex $(R^+ \cdot IOH^-)_{solv}$. Radical-molecule reactions in polar systems may therefore change over to ionic process. In an attempt to find more examples for such inner-outer complex equilibria, studies of pure liquid alkyl iodides were started. The polarity of these liquids (e. g. at 20°C: $\varepsilon(CH_3I) = 7.0$, $\varepsilon(C_2H_5I) = 7.8$) is high enough to expect formation of such solvated ion pairs (inner complexes). The CT-band of the outer complexes (I, RI) are known from the literature /2, 3/, although several inconsistent spectral assignments do exist /3, 4, 5/. We expected that some of the published discrepancies have to do with the formation of inner-CT-complexes.

The present paper is a preliminary report about the test for the occurrence of transient inner-outer complex equilibria.

Experimental

The pulse radiolysis technique for liquid samples (temperature range ca. 80 – 330 K) was as previously described /6/. The dosimetry was carried out by Al-calorimetry with suitable corrections for the dose-depth distribution. The samples were studied in many different cells; all-quartz, stainless steel, alumina and others. Unless specifically mentioned, the results given in this paper are from stainless steel cells. The compounds studied were: methyl iodide, ethyl iodide, i-propyl iodide, ethyl bromide and i-propyl bromide. They were all carefully freed from halogen, dried, and purified by distillation (ca. 40 theoretical plates). Due to extreme sensitivity to photolysis, all purifications were carried out in the dark. Furthermore, the analysing light beam in pulse radiolysis was blocked from the cell up to about 2 ms in advance to the radiation pulse by a very fast shutter system.

Reaction model

Based on the previously published results from flash photolysis /2, 3/, pulse radiolysis /4, 5/ and theoretical considerations /3, 7/ (Fig. 1), the following reaction mechanism, shown in its most simple form, has to be tested:

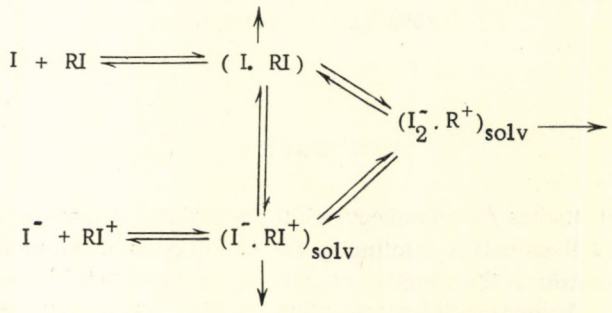

There are one outer CT-complex and two inner CT-complexes. The latter two correspond to the known partial dissociation of RI^+. The outer complex should be detectable by its CT-band in the range 470 – 500 nm (see Fig. 1E). The inner complex $(I_2^-.R^+)_{solv}$ should be observed by the I_2^- absorption at 390 nm. The I_2^- cannot be produced otherwise, except for a small contribution from the free ion yield. The second inner complex $(I^-.RI^+)_{solv}$ should be detectable by the RI^+ absorption at 440 nm, or, if present as a dimer cation, a^+ 540 nm and 760 nm /8/.

Results and discussion

In reproducing the known transient spectra in ethyl iodide at room temperature /4/ a fast build up process at 390 nm was discovered. To slow down this process, the spectra for methyl iodide, ethyl iodide and i-propyl iodide were all measured at -60°C: Figs 2, 3 and 4.
The following spectra can be distinguished:

A. An initial transient spectrum (typically 1 – 1.5 μs after pulse end): It shows two absorption bands, centred at 480 – 500 nm and at about 380 nm. The spectrum decays rapidly within a few μs, as is easily measured in the visible band. The decay reaction is of mixed order, but tends to be close to second order. The initial decay at 380 – 400 nm is identical to the decay at 480 nm, however it is rapidly covered up by the appearance of a new transient:

B. This secondary transient absorbs strongly at 370 – 380 nm and reaches its maximum concentration at about 80 μs (CH_3I), 1100 μs (EtI) and 600 μs

(i-PropI). For EtI and i-PropI the build up is slower than the decay of the initial spectrum and its decay kinetics is of first order with a half life of 3.9 ms (EtI) or 2.3 ms (i-PropI). (The corresponding decay in CH_3I was not measured.)

C. A weak absorption at about 720 nm can be detected. It disappears virtually simultaneously with the initial spectrum.

D. The final spectrum (best seen in Fig. 3) with a peak at 460–480 nm and a strong increase at $\lambda < 400$ nm is clearly due to iodine as a radiolysis product.

The absorbance of the initial and of the secondary species differ substantially for the three alkyl iodides, particularly the spectra for CH_3I are much weaker throughout.

By comparing the results with the reaction mechanism to be tested, we assign the initial transient spectrum to the outer CT-complex (I, RI) and the inner CT-complex $(I_2^-, R^+)_{solv}$ in equilibrium: the 480–500 nm band is the outer CT-transition and the 380 nm band the I_2^- absorption. This assignment is supported by the following observations:

a) If the temperature is increased the ratio of the initial 480 nm band to the 380 nm band (ratio of outer complex to inner complex) is increasing:

T(°C)	EtI	i-PropI
-60	0.66	0.53
+20	0.85	0.60
+40	-	0.74

(The time of comparison is chosen to compensate roughly for viscosity changes.) This ratio-increase corresponds to the expected shift of the complex equilibrium with temperature, due to a decrease in solvent polarity (e.g. for EtI: $\varepsilon(-60°C) = 10.6$, $\varepsilon(+30°C) = 7.56$).

b) For identical dose (6.4 krad) and -60°C the absorbances of the initial transient absorption (as measured at 480 nm or 380 nm) do correlate roughly with the known yields of iodine atoms [calculated from $G(I_2)$]

	$D_{initial}$(480 nm)	$D_{initial}$(380 nm)	G(I)
CH_3I	0.12	0.19	2.6
EtI	0.26	0.46	4.1
i-PropI	0.28	0.52	5.8

Some uncertainties for this comparison stem from the assumptions that the calculated yield of I-atoms can be taken from Co-source irradiations, and that the absorption coefficients are the same in all three systems.

c) The comparison of the initial spectrum with flash photolysis results /2, 3/ in Fig. 3 reveals a surprising correspondence. Here again, the ratio D_{480}/D_{380} is larger at room temperature (flash photolysis result) than at -60°C (pulse radiolysis result).

d) Analogous studies in pure ethyl bromide and i-propyl bromide do yield quite different transient spectra, indicating that no transient CT-complexes are formed. This is analogous to the results in aqueous solutions, where OH-radicals form complexes with alkyl iodides, but not with alkyl bromides (probably due to the higher ionization potentials).

The weak absorption at about 720 nm can either be due to the I_2^- from the inner complex, or to the dimer cation $(RI)_2^+$. In the latter case the complexed monomer cation should also absorb at about 540 nm. This band might be hidden by the long wavelength tail of the CT-band at 480 nm.

The secondary transient absorbing at 370 −380 nm has the following characteristics:

a) For ethyl iodide and i-propyl iodide it is not a direct product from the complex decay: the build up process is slower (for CH_3I a direct formation is possible).

b) The following table indicates that the maximum absorbance correlates roughly with the known G(HI)-yields from Co-irradiations:

	D_{max}	G(HI) /4/
CH_3I	0.25 − 0.30	0.5
EtI	0.95	2.0
i-PropI	$\geqslant$ 1.4	5.8

(Again the same assumptions are made as in section b) for the initial transient spectrum.) Since a substantial part of the HI-yield is expected to derive from unimolecular ejection ($RI^{**} \longrightarrow HI$ + alkene) a similar correlation is expected with the yield of alkene (except for the CH_3I-system).

c) The decay in EtI- and i-PropI-solution is of first-order at low temperature (-60°C), however of second-order at higher temperature (-10°C to + 50°C). It seems that two competing decay reactions exist, one of first order and one of second order. At low temperature the second-order process in substantially slowed down.

Although proposals can be made for the assignment, further experiments are needed to assign this secondary absorption.

The room temperature spectra were studied in various types of cells, as there was a strong increase in transient absorption by changing from an all-quartz to an all stainless steel cell. The differences are explained by the photolysis effect of the internally produced Čerenkov-radiation /9/. This Čerenkov radiation is emitted into a forward cone along the electron beam. With a metal rear this Čerenkov radiation is reflected back into the cell. The result of this effect is shown in Fig. 5 for i-propyl iodide at room temperature. The spectra are almost identical. However, the Čerenkov effect increases the absorbance for the spectrum at 2 μs by a factor of 4 and at 180 μs by a factor of 7. The latter corresponds to the increase in I_2-yield. The 380 nm absorption at 2 μs corresponds to the secondary species, which we found to correlate with G(HI) (The D_{max} was passed at about 1 μs). We conclude therefore, that due to the Čerenkov effect the HI-yield is increased by a factor of 4, and the I-atom yield by a factor of 7. This is reasonable, as it can be expected that photochemistry (low photon energy) relative to radiation chemistry produces a lower HI/I yield-ratio.

Conclusions

The outer CT-band for I. RI with all three alkyl iodides is located at 480-500 nm as expected from flash photolysis /2, 3/ and theoretical studies /3, 7/.

The iodine atom CT-complex is in equilibrium with the corresponding inner CT-complex $(I_2^- . R^+)_{solv}$, due to the polarity of the solvent.

There is no proof that the second inner complex $(I^- . RI^+)_{solv}$ is actually formed.

After the decay of the inner-outer complex equilibrium, a new transient appears, which correlates with the known yield of HI (or possibly with the corresponding yield of the alkene). For EtI and i-PropI the new transient is not directly a product from the complex decay.

For detailed interpretation more work is in progress.

Acknowledgment

This work was supported by the "Schweizerischer Nationalfonds zur Förderung der wissenschaftlichen Forschung".

References

/1/ U. Brühlmann, H. Büchler, F. Marchetti, R. E. Bühler, Chem. Phys. Letters 21, 412 (1973), details to be published.

/2/ T. A. Gover, G. Porter, Proc. Roy. Soc. A 262, 476 (1961).

/3/ R. E. Bühler, Radiat. Res. Review 4, 233–258 (1972).

/4/ C. Capellos, A. J. Swallow, J. Phys. Chem. 73, 1077 (1969).
/5/ M. Ebert, J. P. Keene, E. J. Land, A. J. Swallow, Proc. Roy. Soc. A287, 1 (1965).
/6/ B. Hurni, U. Brühlmann, R. E. Bühler, Int. J. Radiat. Phys. Chem. 7, 499 (1975).
/7/ R. E. Bühler, J. Phys. Chem. 76, 3220 (1972).
/8/ A. Habersbergerova, I. Janovsky, P. Kourim, Radiat. Res. Rev. 4, 123 (1972).
/9/ H. Büchler, R. E. Bühler, unpublished results (1976). The proof for this effect will be published elsewhere.

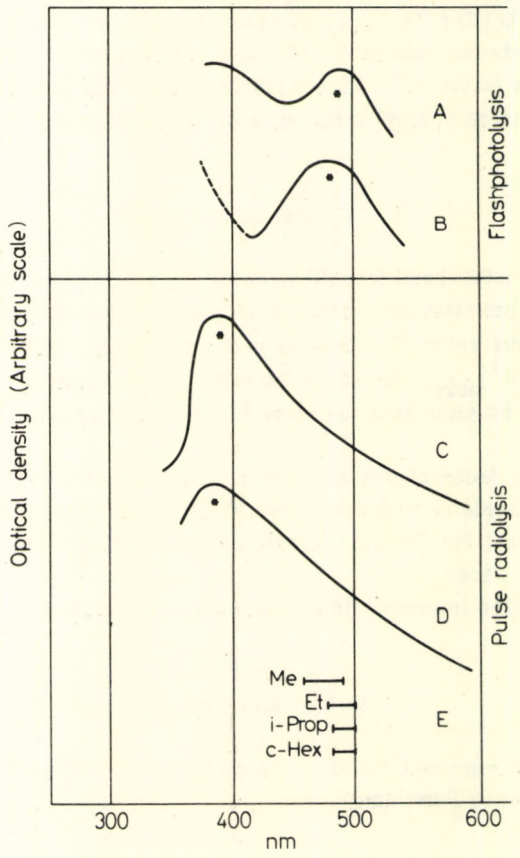

Fig. 1 Transient spectra (room temperature) redrawn from the literature:
A: I_2 in ethyl iodide /2/,
B: I_2 in methyl iodide (Bühler unpublished),
C: pure cyclohexyl iodide /5/,
D: pure methyl, ethyl and i-propyl iodide /4/,
E: predicted position of the CT-band /7/

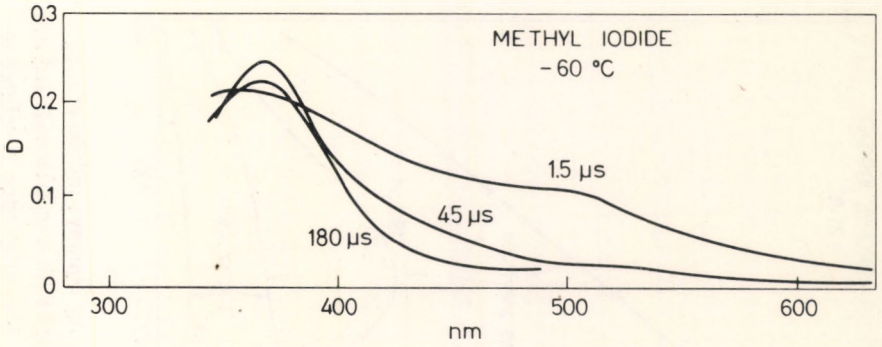

Fig. 2 Transient spectra of pure methyl iodide at -60°C. Dose = 5.9 krad

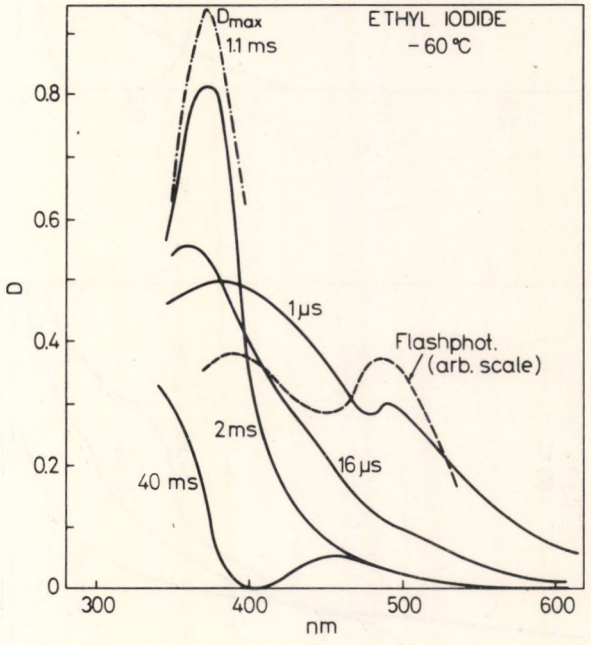

Fig. 3 Transient spectra of pure ethyl iodide at -60°C. Dose = 6.4 krad

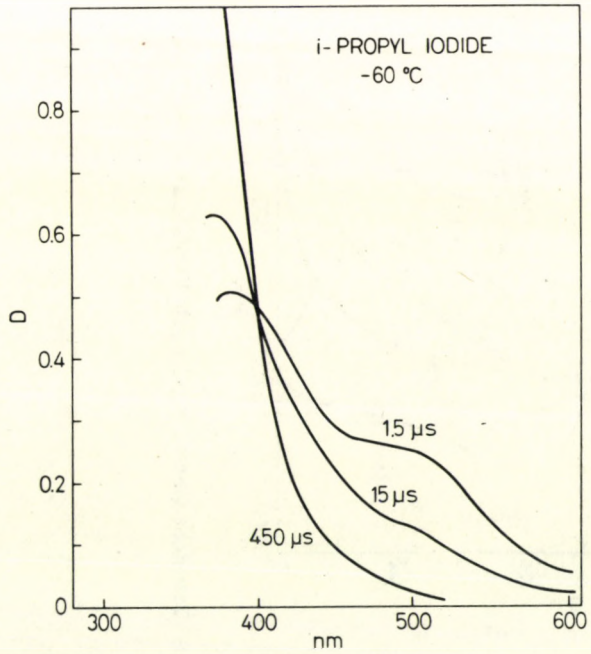

Fig. 4 Transient spectra of pure isopropyl iodide at -60°C. Dose = 6.3 krad

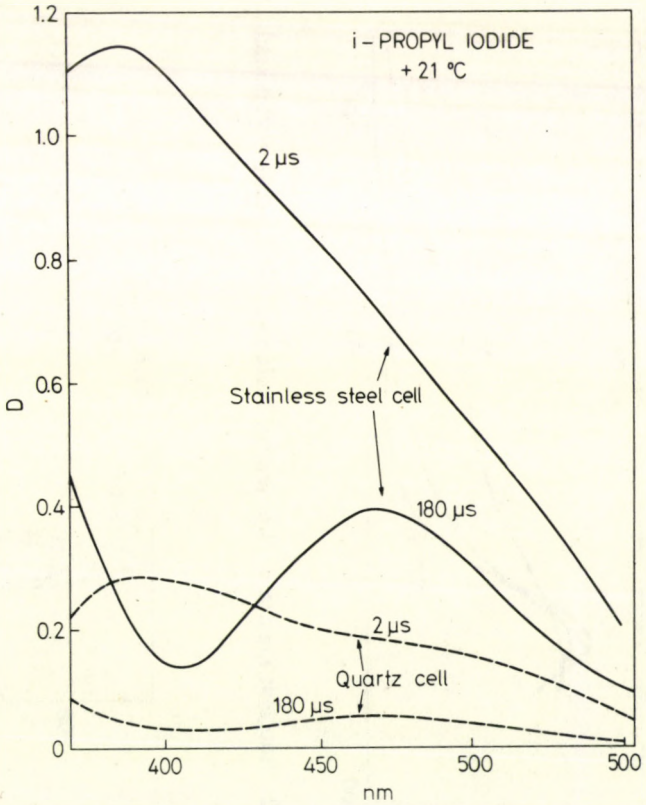

Fig. 5 The transient spectra for i-propyl iodide at room temperature as recorded with a quartz cell and with a stainless steel cell. The difference is related to the Čerenkov-photolysis.

R. F. KHAIRUTDINOV

I know from the gas reaction kinetics that in a similar reaction between iodine and potassium atom electron transfer preceeds the complex formation. What do you think about the possibility of such a mechanism of complex formation in the case of your processes?

H. BÜHLER

If I understand your question properly, you ask whether the I-atom reacts by process (1) or by process (2) + (3) in the following reaction model:

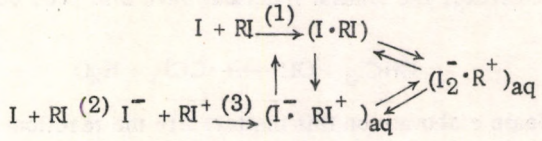

We cannot distinguish between these processes, since whatever complex you form first, the equilibrium is established faster than the experimental time resolution. Furthermore, process (3) is already occurring from the radiolytically produced ions. In general, it seems to me unlikely that process (2) is effective in liquid systems.

E. ZÁDOR

Could you see some transient conductivity in your system? What is the lifetime of the ion pairs? Would you expect similar ion pairs of alkyl iodides in hydrocarbons?

H. BÜHLER

We did not measure conductivity, however it is not to be expected that ion contribute to conductivity.

The lifetimes are in the order of a few μs. In hydrocarbons the polarity of the solvent is so low that any inner–outer complex equilibrium will be shifted almost entirely to the outer complex.

Z. P. ZAGÓRSKI

Working myself with Čerenkov radiation I am surprised by the very large photochemical effect ascribed to this source of photochemically active light.

Would you mind giving semi-quantitative data from which Čerenkov light intensity may be estimated (energy of electrons, current of the beam, n coefficient of the solution)?

H. BÜHLER

We also were puzzled by the laziness of the increase in absorbance by going from quartz to metal alloys. The effect is related to the extreme photosensitivity

of the alkyl iodides. The electron beam data are: max. 2 MeV, a few Å, 50 ns pulse (Febetron 705).

T. SÖYLEMEZ

Your suggestion of OH radical addition to the alkyl iodide seems rather peculiar

$$RI + OH \rightleftarrows (RI \cdot OH) \rightleftarrows (R^+ \cdot HOI^-)_{aq}$$

In the case of alkyl chlorides (RHCl) and alkyl fluorides (RHF) we have, on the other hand, observed hydrogen abstraction reactions of OH radicals:

$$RHCl + OH \longrightarrow \cdot RCl + H_2O$$

In the case of $CHCl_3$, the similar reactions have also been observed by Rezansoff et al.

$$CHCl_3 + OH \longrightarrow \cdot CCl_3 + H_2O$$

Would you please elaborate on this matter? Are the reactions of alkyl iodides very much different from those of alkyl chlorides and alkyl fluorides?

H. BÜHLER

Your question concerns the aqueous solutions of alkyl iodides. As this has not been the subject of my contribution, and as the proof of the mechanism is based on very elaborate work I must refer to a letter we published in Chem. Phys. Letters (1973) or to the forthcoming paper in Chem. Physics.

However, as I already pointed out in this contribution, the complexes and the corresponding mechanism is only found with alkyl iodides, not with alkyl bromides. This is probably due to the higher ionization potentials.

G. CASTELLO

You compare your results with the G values of iodine and hydrogen iodide obtained by gamma irradiation. At what dose, dose rate and temperature were these G values obtained?

Do you think that they can be readily compared with pulse radiolysis results, taking into account the possible effects of different experimental conditions on HI/I yield ratio?

Furthermore, do you have any value of alkene yield that can confirm your results?

H. BÜHLER

I already pointed out in the paper that the comparison of pulse radiolysis data with Co-source irradiations has some weakness and we will add pulse radiolysis-yield data as soon as possible. However, we used the comparison in a semiquantitative way only. Furthermore, we feel that the order of magnitude (particularly for relative use) still holds, as we can measure the $G(I_2)$ at 40 ms and as the HI is dominantly the product of a unimolecular ejection process. There have been no alkene-yield measurements made yet.

PICOSECOND PULSE RADIOLYSIS STUDIES OF HYDRATED ELECTRON REACTIONS

Max S. Matheson, J. R. Miller, C. D. Jonah
Chemistry Division, Argonne National Laboratory, Argonne, Illinois 60439, USA

Introduction

Several factors may cause rate constants observed in concentrated solutions to vary from those found in dilute solutions. If hydrated electrons are suddenly introduced into a solution, the diffusion-controlled reaction of the hydrated electrons with a neutral solute should decrease with time, since, if the initial positions of solute and hydrated electron are random, the fraction of surviving e^-_{aq} having close solute neighbors will decrease with time until a steady state is attained /1, 2/. We /3, 4/ and others /5, 6/ have recently shown that the time dependence for a number of reactions fits the Noyes' equation within experimental error. Other factors enter if the solute is charged. For example, Coulombic interaction between solute and e^-_{aq} will decrease as the solute concentration is increased, and for very fast reactions e^-_{aq} may react before an equilibrium ionic atmosphere can ba formed around it.

Having established these effects on rate constants in concentrated solutions, we have examined these factors in several additional interesting systems.

Experimental section

Stroboscopic Pulse Radiolysis System. The stroboscopic pulse radiolysis apparatus has been described elsewhere /3, 7/. The technique was developed by Hunt and co-workers /8/ and has been modified to take advantage of the intense single fine-structure pulse available from the Argonne Linac. As seen in Fig. 1 the beam is spread horizontally and the center portion is intercepted by the Čerenkov generator, while the rest of the beam is passed around the 270° magnet to delay it by a fixed time and focussed in the reaction cell. The central portion of the beam generates Čerenkov light in the 1 atm of xenon gas in the generator, and this light is delayed a variable amount by mirrors moving at a constant speed. The accelerator is pulsed 60 times per second and the moving mirrors cause the Čerenkov light pulse to scan cell absorption from a time 500 psec before the electron pulse enters the cell to 3500 psec after. This relatively wide time range enables reaction rates to be measured over a wider concentration range. The electron and light pulses have approximately the same width (30 psec FWHM) and this width determines the time re-

solution. The hydrated electron absorption was followed at 600 nm. The optical transmission data were stored and subsequently manipulated in the Chemistry Division Sigma 5 computer /9/. Since solutions are repetitively pulse-irradiated, a flow system was used to minimize buildup of products.

Materials. Solutions were made with water purified by deionization and filtration using Continental Water Co. equipment. The conductivity was equivalent to that of triply-distilled water. Reagent grade solutes were used, although trace impurities would not affect rates on the experimental time scale.

Rate Constants. A non-linear least squares fitting of the experimental data was used to determine the rate constant k, for a given solute concentration. A correction was made for the small amount of "spur" decay observed for the hydrated electron. The finite pulsed width or resolution time does not decrease the measured rate constant.

Results and discussion

Neutral Reactants. According to Noyes /2/ the time dependence of the rate constant for reaction of two kinds of molecules, A and B, is given by

$$k_t = k_\infty \left[1 + \frac{k_\infty}{4\pi r_{AB} D_{AB} (N/10^3)} \frac{r_{AB}}{(\pi D_{AB} t)^{1/2}} \right]$$

where k_t is the rate constant at time t, k_∞ is the rate constant at long times, r_{AB} is the reaction radius, D_{AB} is the coefficient for relative diffusion of A and B, and N is Avogadro's number. The diffusion-controlled encounter rate is $4\pi r_{AB} D_{AB} N/10^3$ in units, $\underline{M}^{-1}$ sec^{-1}. It is assumed that A and B are randomly distributed. In our work we assume the A-B distances are randomly distributed, and also calculations by Naleway (described in ref. /3/) indicate solute depletion effects in spurs are small.

We have already reported on the reactions of e^-_{aq} with nitromethane and with acetone /3/. The first of these is diffusion-controlled ($k_\infty/(4\pi r_{AB} D_{AB} N/10^3) \simeq 1$) and shows time dependence in agreement with eq. 1. However, for acetone k_∞ is about one third the diffusion-controlled value ($k_\infty/(4\pi r_{AB} D_{AB} N/10^3) = 0.35$), and the predicted time dependence is small. In agreement the observed k shows no time-dependence within experimental error.

Mercuric chloride is essentially undissociated in polar solvents and Nazhat and Asmus /10/ have shown by microsecond pulse radiolysis that $k_a = (4.0 \pm 0.3) \times 10^{10}$ $\underline{M}^{-1}$ sec^{-1}.

$$e^-_{aq} + HgCl_2 \rightarrow HgCl + Cl^- \qquad (a)$$

Using $D_{HgCl_2} = 1.18 \times 10^{-5}$ cm^2 sec^{-1} /11/ and $D_{e^-_{aq}} = 4.96 \times 10^{-5}$ cm^2 sec^{-1} /12/ requires $r_{AB} = 8.6 \times 10^{-8}$ cm, if k_a is equal to the diffusion-controlled en-

counter rate, $4\pi r_{AB}D_{AB}N/10^3$. This is larger than the reaction radius 5.7 Å estimated from r_e = 3.0 Å and r_{HgCl_2} = 2.7 Å (the latter from physical volume). Thus, e^-_{aq} + $HgCl_2$ is an interesting reaction which should show time-dependence at high concentrations of $HgCl_2$. The time-dependence found (Fig. 2) is in good agreement with the Noyes' theory. To fit our data in Fig. 2 we used $k_\infty = 3.6 \times 10^{10}$ $\underline{M}^{-1}$ sec^{-1} (just outside the error given by Nazhat and Asmus), which reduces r_{AB} to 7.8 Å. This value of r_{AB} still indicates electron tunneling in the reaction.

Charged Reactants. Debye /13/ has evaluated the effect of Coulombic interaction on reactions between charged species, and for a diffusion-controlled reaction between ions A and B gives

$$k_{diff} = \frac{4\pi r_{AB} D_{AB} N}{10^3} \left\{ \frac{Z_A Z_B r_O}{r_{AB}} / \left(\exp\left[\frac{Z_A Z_B r_O}{r_{AB}}\right] - 1\right)\right\} \qquad (2)$$

in dilute solution. r_{AB}, D_{AB} and N are as defined in eq. 1, Z_A and Z_B are the units of electronic charge on ions A and B, and $r_O = e^2/\underline{D}kT = 7.1 \times 10^{-8}$ cm in water at 25°C, where e = charge on electron, $\underline{D}$ = dielectric constant, $\underline{k}$ = Boltzmann constant, and T = °K. The term in braces shows the effect of the Coulombic interaction on the diffusion-controlled rate. If A reacts with B in a solution containing an excess of inert salt, the ionic atmospheres around A and B will reduce the Coulombic interaction. If A (in our case e^-_{aq}) is suddenly introduced into a concentrated solution of pure reactive salt, one of whose constituents is ion B, it may react before it acquires an ionic atmosphere and this will affect the rate constant. In our earlier paper we showed that it is reasonable to take $k_1 = \sqrt{k_2 \times k_0}$, even at high concentrations, where k_1 is the rate constant when e^-_{aq} reacts without an ionic atmosphere, k_2 is the rate constant where both e^-_{aq} and ion B have ionic atmospheres and k_0 is the rate constant one would find in a given concentration of salt if both e^-_{aq} and ion B reacted without ionic atmospheres. For k_0 it is assumed the principal effect would be due to the effect of salt concentration on the diffusion of e^-_{aq} and so k_0 is assumed to vary with salt concentration in proportion as $k(e^-_{aq} + CH_3NO_2)$ varies with salt concentration.

The reaction of e^-_{aq} + Ag^+ is interpreted in terms of effects discussed above (see Fig. 3). The rate constant for k_b was measured for

$$e^-_{aq} + Ag^+ \rightarrow Ag^o \qquad (b)$$

dilute $AgClO_4$ with or without added $NaClO_4$. This gave $k_b = 4.5 \times 10^{10}$ $\underline{M}^{-1}$ sec^{-1} at ionic strength, μ = 0 (in agreement with some literature values) /14/, and the lower dashed line for k_2 in Fig. 3. Using $D_{Ag^+} = 1.75 \times 10^{-5}$ cm^2 sec^{-1} from mobility /15/ and $r_{Ag^+} = 1.3 \times 10^{-8}$ cm from crystal radius, eq. 2 gives $k_{diff} = 4.46 \times \times 10^{-10}$ $\underline{M}^{-1}$ sec^{-1}, essentially identical with the measured k_b. Variation of $k(e^-_{aq}$ +

+ CH_3NO_2) had been measured for 0.05 M CH_3NO_2 in $LiClO_4$ (not $NaClO_4$) and this was used to determine k_0. The dependence of k_0 (not shown) on salt concentration is small, and k_1 calculated from $\sqrt{k_2 \times k_0}$ is shown as the middle curve.

To apply eq. 1 to $e^-_{aq} + Ag^+$ in concentrated $AgClO_4$ solutions we replace D^*_{AB} by D^*_{AB} where D^*_{AB} varies with salt concentration as $e^-_{aq} + CH_3NO_2$, i.e., as k_0. We replace r_{AB} by r^*_{AB} where r^*_{AB} at $\mu = 0$ is r_{AB} times the term in braces in eq. 2 or 8.85×10^{-8} cm, and r_{AB} varies as $k_1/(4\pi N D^*_{AB}/10^3)$, since the reaction is diffusion-controlled and e^-_{aq} reacts without an ionic atmosphere. Further, we assume that at each concentration $AgClO_4$ one uses the corresponding value of k_1 as the effective k_∞ in eq. 1. The variations in r^*_{AB} and D^*_{AB} partially compensate and the maximum effect is to reduce the calculated k_t by 15% at 0.25 M $AgClO_4$. The upper (solid) line in Fig. 3 was calculated on the basis of these assumptions, and is in reasonable agreement with the experimental points. The $e^-_{aq} + Ag^+$ system was very difficult experimentally, since Ag^0 precipitates and coats the windows gradually reducing the cell transmission.

We conclude that the reaction of e^-_{aq} with Ag^+ is diffusion-controlled and the rate constant shows the expected time dependence. This result contrasts with earlier measured rate constants /3/ for reaction of e^-_{aq} with two other positive ions, Cd^{2+} and Cu^{2+}, which are about 3/4 and 1/2 the diffusion-controlled values. For these latter two reactions the rate constants are close to the estimated k_1's at high concentration and show little time dependence.

Acknowledgement. We thank Don Ficht, Joseph Becker, Benno Nadere, and Lee Rawson for consistently producing a fine electron beam for our experiments. We are also grateful for the invaluable assistance of Robert Clarke. Special thanks are due to Barbara Saunders and William Mulac for rate constant measurements in dilute solutions of $AgClO_4$.

References

/ 1/ F. C. Collins and G. E. Kimball, J. Colloid. Sci., 4, 425 (1949).
/ 2/ R. M. Noyes, Prog. React. Kinet., 1, 129 (1961).
/ 3/ C. D. Jonah, J. R. Miller, E. J. Hart and M. S. Matheson, J. Phys. Chem., 79, 2705 (1975).
/ 4/ M. S. Matheson, E. J. Hart, J. R. Miller, and C. D. Jonah, Radiat. Res., 59, 110 (1974), Abstract B-20-4.
/ 5/ G. V. Buxton, F. C. R. Cattell, and F. S. Dainton, J. Chem. Soc. Faraday Trans. 1, 71, 115 (1975).
/ 6/ T. J. Chuang and K. B. Eisenthal, J. Chem. Phys., 62, 2213 (1975).
/ 7/ C. D. Jonah, Rev. Sci. Instrum., 46, 62 (1975).
/ 8/ M. J. Bronskill and J. W. Hunt, J. Phys. Chem., 72, 3762 (1968), M. J. Bronskill, W. B. Taylor, R. K. Wolff, and J. W. Hunt, Rev. Sci. Instrum., 41, 333 (1970).

/ 9/ P. Day and J. Hines, Oper. Systems Rev., 7, No. 4, 28 (1973).
/10/ N. B. Nazhat and K. D. Asmus, J. Phys. Chem., 77, 614 (1973).
/11/ Extrapolated from data Int. Crit. Tables, Vol. V, p. 65.
/12/ K. H. Schmidt, Int. J. Radiat. Phys. Chem., 4, 439 (1972).
/13/ (a) P. Debye, Trans. Electrochem. Soc., 82, 265 (1942), (b) S. R. Logan (Trans. Faraday Soc., 63, 1712 (1967)) has refined the treatment, but for p = 1 (reaction on every collision) the estimated correction to (2) is less than 1%.
/14/ "Selected Specific Rates of Reactions of Transients from Water in Aqueous Solution. 1. Hydrated Electron", M. Anbar, M. Bambenek, and A. B. Ross, NSRDS-NBS, U. S. Gov't. Printing Office, Washington, D. C. 20402 (1973).
/15/ Electrochemistry, G. Milazzo, Elsevier Publ. Co., New York (1963), p. 60.

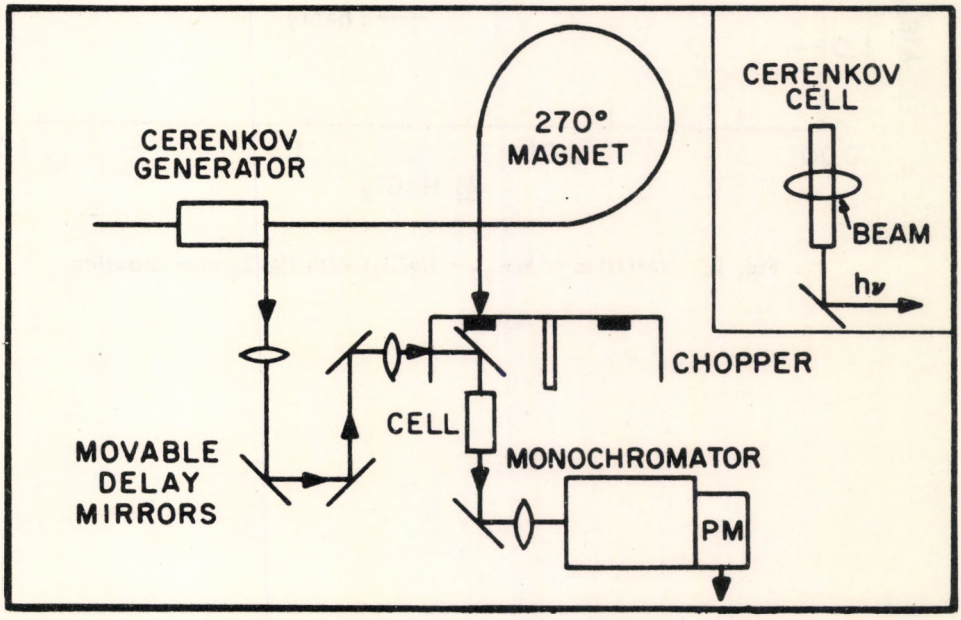

Fig. 1. Stroboscopic pulse radiolysis apparatus: PM = photomultipler. Chopper enables correction for Cerenkov generated in cell. Upper right shows center of beam is intercepted by Cerenkov cell

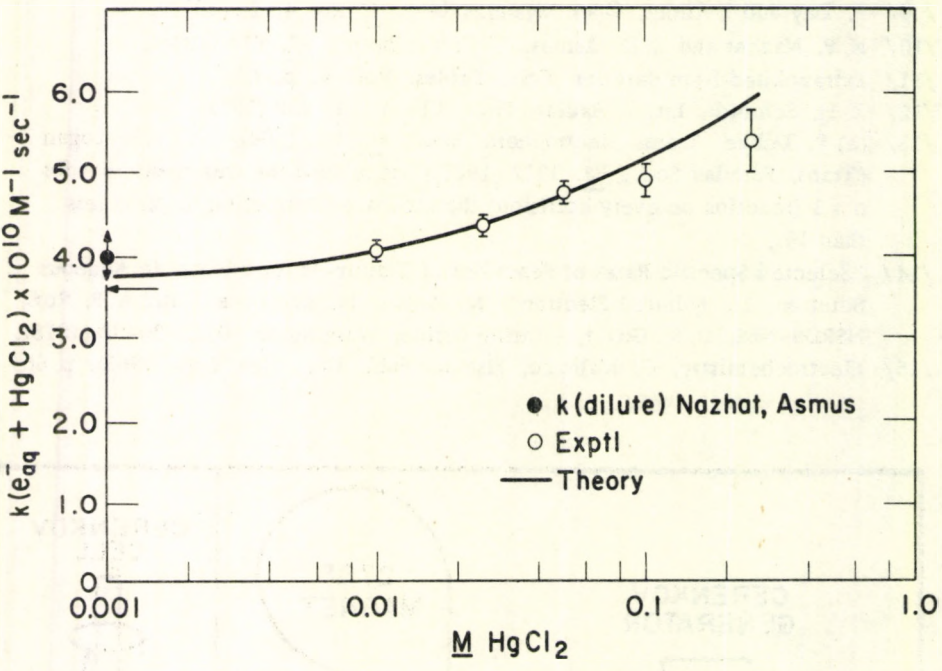

Fig. 2. Variation of $k(e^-_{aq} + HgCl_2)$ with $HgCl_2$ concentration

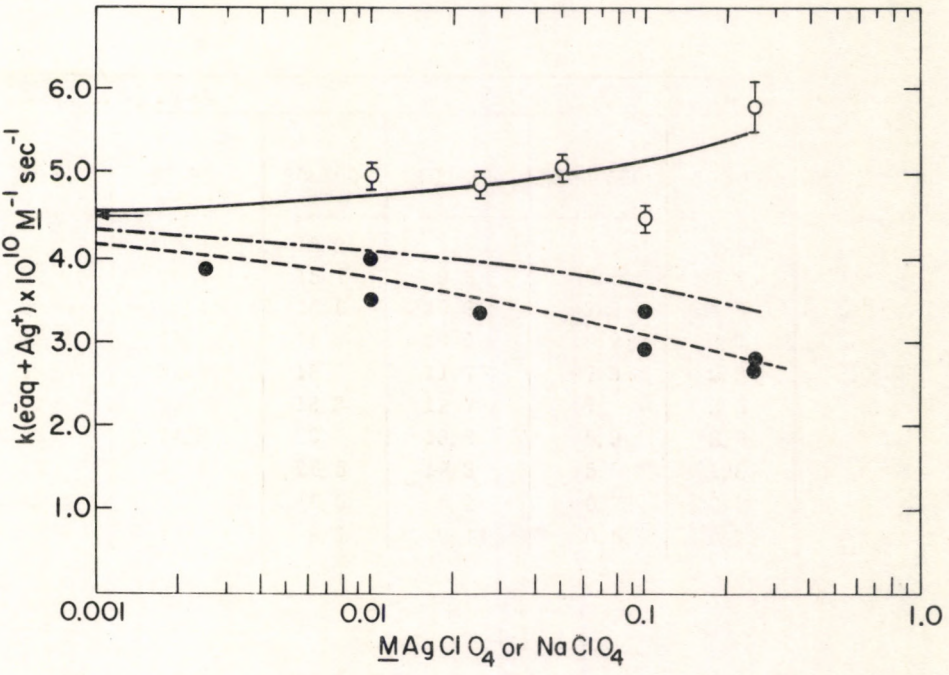

Fig. 3. Variation of $k(e^-_{aq} + Ag^+)$ with concentration: - - - k_2; - . - . k_1; —— k_t or time-dependent rate constant. Circles, exptl. points: ○, pure $AgClO_4$; ●, dil $AgClO_4$ in $NaClO_4$

RADIOLYSIS OF AQUEOUS SOLUTIONS OF MONO- AND DIPHOSPHATES OF FRUCTOSE

Henryk Żegota, Stefania Bachman
Institute of Applied Radiation Chemistry. Technical University of Łódź, Poland

Introduction

The radiation chemistry of phosphate esters has received considerable attention with a view to understanding the mechanism of radiation damage of DNA /2,3,7,8/. Furthermore, their role in metabolic pathways of carbohydrates has prompted the investigation of radiation effects induced in aqueous solution of sugar phosphates /1-6/.

Although much is known about the mechanism of radiation damage of ribose and glucose phosphates, very little is known on the mechanism of radiolysis of fructose phosphates. Fructose-1, 6-phosphate (Harden-Young ester), fructose-6-phosphate (Neuberg ester) and fructose-1-phosphate (Robinson-Tanko ester) take an important part in the enzymatic breakdown and synthesis of carbohydrates.

First reports on radiolysis of aqueous solutions of glucose phosphates were published by Kochetkov et al. /1,9/. Irradiation leads to a decomposition of sugar esters and to a release of inorganic phosphate. The formation of phosphate-free products is accompanied by the release of p_i.

In the present investigations we made an attempt to determine the radiation yields of dephosphorylation of fructose phosphates and decomposition of the sugar residue. The results of kinetic experiments as well as the ESR measurements of free radicals indicate that fructose mono- and diphosphates behave differently during irradiation.

Materials and methods

Aqueous solutions (10^{-2}M) of fructose phosphates (sodium salts, Calbiochom A grade) were saturated with highly purified argon by bubbling for 30 min. before irradiation. When it was desired to examine the reaction of e^-_{aq}, samples containing 0.1 or 0.5 M tert-butyl alcohol were prepared. The reaction of OH radicals were studied for samples saturated with N_2O which converts e^-_{aq} to OH radicals.

Samples of 10 ml volume were irradiated in a ^{60}Co source with a dose rate of 4×10^{17} eV ml^{-1} min^{-1}. Dosimetry was carried out with standard Fricke solution.

The concentration of inorganic phosphate was estimated by the modified Bartlett and Lewis method /10/, sugar residue was determined by resorcinol reaction /11/.

Determinations of reactive carbonyl groups were made using the micro method described by Fields and Dixon /12/.

Determinations of rate constant of OH radical reaction with fructose phosphate were based on the competitive PNDA method /13/. Samples for competition measurements were γ irradiated in a Gammacell 200 source at a dose rate of 5.2×10^{16} eV ml^{-1}.

For ESR measurements samples were prepared by dropping 1 M solutions into liquid nitrogen. Frozen spheres of about 3 mm in diameter were selected. After irradiation with a dose equal to 5×10^{19} eV g^{-1} (dose rate 8×10^{17} eV g^{-1} min^{-1}) samples were stored in the dark at 77K. ESR spectra were recorded on a SE/X-20 spectrometer working at 100 kHz field modulation. Liquid nitrogen Dewar vessel and variable temperature attachment enabled us to carry out ESR measurements between 77K and 210K. Photobleaching of the samples was carried out inside the ESR cavity with white light of a tungsten lamp. To calculate the absolute G values of radicals for frozen sugar solutions parallel measurements were done with standard neutral ice samples at 77K. For ice sample the G(OH) value was taken to be equal to 0.7 /15/.

Results and discussion

Yield of inorganic phosphate release

Plots of the yield of P_i against dose are approximately linear for all phosphates in the dose range studied /Fig. 1/. G values calculated are presented in Table 1.

The yield of P_i released depends on the phosphate content in fructose-phosphate molecule.

The influence of N_2O which converts solvated electrons into OH radicals and tert-butyl alcohol which is a selective and efficient OH radical scavenger ($k = 5.2 \times 10^8$ M^{-1} sec^{-1}) /16/ on the yields of P_i is shown in Table 1.

$G(P_i)$ values for F-1-P, F-6-P and F-1, 6-P increased from 1.0, 1.1 and 1.8 measured in the presence of argon to 1.6, 1.7 and 2.8, respectively in deoxygenated and N_2O saturated solutions.

Table 1

G values of inorganic phosphate release in aqueous solution of fructose phosphates (10^{-2}M) in the absence and presence of scavengers

	IF-1-P	F-6P	F-1, 6-P
Argon	1.0 ± 0.2	1.1 ± 0.2	1.8 ± 0.2
N_2O (saturated)	1.6 ± 0.2	1.7 ± 0.2	2.8 ± 0.3
0.1 M t-butanol			0.9 ± 0.2
0.5 M t-butanol			0.4 ± 0.2

When 0.1 N t-butanol was used to scavenge OH radicals the P_i yield for F-1, 6-P dropped to 0.9, whereas in 0.5 M t-butanol G(P_i) dropped to 0.4. The fact that even at very high tert-butanol concentration the phosphate release proceeds with relatively high yield might indicate some contribution of H atoms in this process.

From the results of scavenger experiments it is clear that OH radicals are the main reactive species responsible for the inorganic phosphate release during radiolysis of water solution of sugar-phosphates.

Yield of radiolytic decomposition of sugar residues

The yields of radiation induced decomposition of sugar residue were determined from the results of resorcinol reaction known as Seliwanoff test for fructose /11/. This method provides the accurate values for fructose esters. The concentration of fructose residues decreases linearly in the dose range studied and the decrement is greater for monophosphates than for diphosphate esters (Fig. 2). G values for decomposition of the sugar residue of phosphates in the presence of scavengers as measured from the slopes of the yield -dose dependence are presented in Table 2.

Scavenging of electrons with N_2O causes significant increase of G values for all phosphates, moreover for F-1,6-P the yield in N_2O saturated solutions is twice as high as the G values for experiments without scavenger.

In the experiments with t-butanol as a competitive OH scavenger it has been found that progressive increase of t-butanol concentration suppresses the decomposition of phosphate esters.

Results of the scavenging experiments confirmed the predominant role of OH radicals both in the ester bond scission and in sugar residue decomposition.

The yield of release of inorganic phosphate for fructose monophosphates was found always to be lower than the G values of the disappearance of sugar residue. Fructose-diphosphate behaved in the opposite way, i.e. the yield of P_i release was higher than the yield of decomposition of the sugar residue.

The total yields of the P_i release and decomposition of the fructose residue were found in the range G(total) = 4.8 – 5.3. These values are lower than the G = 6 which corresponds to the sum of OH radicals and H atoms in the radiolysis of water saturated with N_2O /17/.

Table 2

Yields of decomposition of sugar residue of fructose phosphates in aqueous solution (10^{-2}M) in the presence and absence of radical scavengers

	F-1, 6-P	F-1-P	F-1, 6-P
Argon	2.0 ± 0.3	2.2 ± 0.2	1.2 ± 0.2
N_2O (saturated)	3.2 ± 0.3	3.5 ± 0.3	2.5 ± 0.3
0.1 M t-butanol			0.7 ± 0.1
0.5 M t-butanol			0.3 ± 0.1

Reaction of hydroxyl radicals; rate constants

The relative rates of OH reactions were determined by the competition method in the presence of N,N-dimethyl-p-nitrosoaniline (PNDA) /13/. The results of some earlier investigations /18-20/ showed that PNDA method requires technical and analytical care if confident results are to be obtained. Willson et al. /14/ compared data from steady-state competition method and pulse radiolysis results and found that both methods gave consistent values of the rate constants when the rate constant for the reaction of OH radicals with PNDA was taken as 1.25×10^{10} M^{-1} sec^{-1}. Figure 3 shows typical competition plots of mono- and diphosphate of fructose in PNDA solutions. Separate set of experiments was carried out for D-glucose in the presence of PNDA. The relative rates obtained in this experiment showed good agreement with literature data /21/. The rate constants for the reaction of OH radicals with fructose phosphates are sumarized in Table 3.

Recently Greenstock and Shierman /6/ determined the yield of inorganic phosphate release to establish the overall OH reactivity towards the phosphate esters. These authors reported a comprehensive list of OH rate constants with nucleotides, coenzymes, sugar-phosphates and phospholipid components. These determinations, however, give rate constant values for reaction of OH with fructose-phosphates higher than in the case of PNDA method.

ESR measurements

ESR spectra. Figure 4 shows the ESR spectra of 1 M neutral frozen aqueous solution recorded at 77K immediately after irradiation. The dose was constant for all samples and equal to 5×10^{19} eV g^{-1}.

The spectra of fructose and F-1,6-P ices consist of the superimposed signals of OH radical, trapped electron (e_t^-) and sugar radicals ($R^{\cdot}$). The portion of the spectrum

Table 3
Rate constants for reaction of hydroxyl radicals with fructose phosphates estimated by the PNDA competitive method

Compound	$\frac{k_{s + OH}}{k_{PNDA + OH}}$	$k_{s + OH}$ ($M^{-1}sec^{-1}$)
F-1, 6-P	0.12 ± 0.2	1.5×10^9
F-1-P	0.16 ± 0.3	2.0×10^9
F-6-P	0.17 ± 0.3	2.1×10^9
Glucose	0.19 ± 0.3	2.3×10^9
Glucose	-	$1.9 \times 10^{9*}$

*Thymine competitive reaction /21/

due to the trapped electron can be eliminated by exposing the sample to visible light. The remaining spectrum is due to OH and carbohydrate radicals. Subtraction of these two spectra gives a singlet line, which has ESR parameters similar to e_t^- in irradiated glucose and saccharose ices /22/. The peak-to-peak linewidth of the e_t^- singlet is about 12.5 gauss, and does not vary in the fructose and F-1,6-P ices. The linewidths of e_t^- and the sugar radicals are independent of the radiation dose up to 9×10^{19} eV g^{-1}. Unlike fructose and F-1,6-P ices, frozen 1 M aqueous solutions of F-1-P and F-6-P do not trap electrons efficiently after irradiation. ESR spectra of F-1-P and F-6-P ices recorded at 77K consist of the absorptions of OH and sugar radicals only (Fig. 4). When the irradiated fructose monophosphate ices are illuminated with visible light only slight change is observed in the spectrum. No hydrogen atom spectra are recorded at this molarity and it indicates that the H˙ reacts efficiently with sugar-phosphate molecules or with other species present during radiolysis at 77K.

The comparison of the intensities of the low-field lines for fructose and fructose-phosphate ices provided the direct evidence that OH radicals contribute only to a small extent to the ESR spectrum of F-1,6-P. This observation and the ability to stabilize the electrons in 1 M (44% w/v) F-1,6-P ice indicate that the matrix frozen at 77K contains numerous glassy regions. Fructose-monophosphate ices (about 30% w/v) have predominantly polycrystalline structure. One can expect that geometry of investigated solute molecules affects the structure of solids at 77K. Fructose-monophosphate molecules are highly unsymmetrical because a large terminal phosphate group protrudes over the sugar plane. Fructose-diphoshate due to its two phosphate groups is more symmetrical thus more suitable for building up glassy regions.

Thermal annealing of irradiated samples in the temperature range 77–140K removes both e_t^- and OH radicals. Near 190K the remaining absorption is entirely due to sugar phosphate radicals. The spectra obtained in this way are poorly resolved (Fig. 4b).

The ESR spectra of fructose and fructose-1-phosphate exhibit mainly a broad doublet with the splitting constant equal to 17.5 gauss which could be due to radicals arising after proton abstraction from the primary alcohol group at C_1. Elimination of the proton from C_3 can also give doublet by interaction of the unpaired electron with axial proton at C_4. The hyperfine constant about 11 gauss would be expected

Table 4
Yields of trapped electrons and sugar free radicals in M ices of fructose and its phosphates at 77K

	Fructose	F-1-P	F-6-P	F-1,6-P
G (radicals)	1.4	1.2	2.4	2.0
G (radicals photobleaching)	1.2			1.7
$G(e_t)$	0.2	–	–	0.3

for H_β proton splitting /23/, i.e. much lower than the experimental value. The other radicals are probably produced with a much lower yield.

The spectrum due to F-1,6-P radicals produced on irradiation of neutral ices consists of lines of at least two radicals, a poorly resolved doublet splitted by about 20 gauss is superimposed on a triplet splitted by about 30 gauss.

Yield of e_t^- and sugar free radicals in 1 M frozen aqueous ices of fructose-phosphates. Figure 5 shows the dose dependence of total spin concentration and trapped electrons for fructose and its phosphate esters ices. Table 4 summarizes the results of ESR measurements and photobleaching experiments. The value $G(e_t^-) = 0.20$ for 1 M ice of fructose is significantly lower than $G(e_t^-) = 1.3$ for 4.5 M glassy ice of fructose reported by Zimbrick and Myers /24/.

It should be noticed that the yields of e_t^- and $R^\cdot$ are not the same in fructose, fructose-monophosphate and fructose-diphosphate ices studied at the same molarity. Among all matrices investigated in this work fructose-1,6-phosphate ice is obviously the most efficient for trapping electrons. The differences in the yield of stable e_t^- among fructose and its phosphates ices can be caused by differences in the H bonding of H_2O molecules to the sugar molecules. In turn, these differences can cause changes in the concentration of suitable traps for radiation produced mobile electrons.

References

/ 1/ N.K. Kochetkov, L.I. Kudriashov, N.A. Chlenov and L.P. Grineva, Zh. Obshch. Khim., 41, 2071 (1971).

/ 2/ L. Stelter, C. von Sonntag and D. Schulte-Frohlinde, Int. J. Radiat. Biol., 25, 515 (1974).

/ 3/ L. Stelter, C. von Sonntag and D. Schulte-Frohlinde, Z. Naturforsch., 30b, 609 (1975).

/ 4/ V.A. Sharpatyi, Proc. Third Tihany Symp. on Radiat. Chem., Eds. J. Dobo and P. Hedvig, Akadémiai Kiadó, Budapest, 1972, p. 1345.

/ 5/ N.S. Fel., L.A. Zaczerskaya, M.A. Chlenov, L.P. Grineva, L.I. Kudriashov, P.I. Dolin and N.K. Kochetkov, Abstr. IVth Int. Biophys. Congress. Moscow, 1972, p. 190.

/ 6/ C.L. Greenstock and Z. Shierman, Int. J. Radiat. Biol., 28, 1 (1975).

/ 7/ N.K. Kochetkov, L.I. Kudriashov, N.A. Chlenov, and L.I. Grireva, Carbohydrates Res., 35, 235 (1974).

/ 8/ S. Bachman and H. Zegota, Nukleonika, 20, 439 (1975).

/ 9/ N.K. Kochetkov, L.I. Kudriashov, M.A. Chlenov, and L.P. Grineva, Dokl. Akad. Nauk SSSR, 202, 847 (1972).

/10/ E.M. Bartlett, and D.H. Lewis, Anal. Biochem., 36, 159 (1970).

/11/ R.G. Kulka, Anal. Chem., 63, 542 (1956).

/12/ R. Fields and H. Dixon, Biochem. J., 121, 587 (1971).

/13/ I.J. Kraljic and C.N. Trumbore, J. Amer. Chem. Soc., 87, 2547 (1965).

/14/ R.L. Willson, C.L. Greenstock, G.E. Adams, R. Wageman, and L.M. Dorfman, Int. J. Radiat. Phys. Chem., 3, 211 (1971).
/15/ P.J. Baugh, K. Kershaw and G.O. Phillips, J. Chem. Soc., B, 1482 (1970)
/16/ L.M. Dorfman and O.E. Adams, Reactivity of the Hydroxyl Radical in Aqueous Solutions, NSRDS - NDS 46, June 1973.
/17/ Adams G.E., Boag J.W. Michael B.D., Trans Faraday Soc., 61, 492 (1965).
/18/ F.S. Dainton and B. Wisall, Trans. Faraday Soc., 64, 694 (1968).
/19/ J.H. Baxendale and A.H. Khan, Int. J. Radiat. Phys. Chem., 1, 11 (1968).
/20/ T. Masuda, S. Makano and M. Kondo, J. Radiat. Res., 14, 339 (1973).
/21/ G. Scholes and R.L. Willsen, Trans. Faraday Soc., 63, 2983 (1967).
/22/ J. Bardsley, P.J. Baugh and G.O. Phillips, J. Chem. Soc. Perkin II, (1975) 614.
/23/ A. Samuni and P. Neta, J. Phys. Chem., 77, 2425 (1973).
/24/ J.D. Zimbrick and L.S. Myers, J. Chem. Phys., 54, 2890 (1971).
/25/ M. Dizdareglu, D. Henneberg, G. Schomburg and C. von Sonntag, Z. Naturforsch., 30b, 416 (1975).

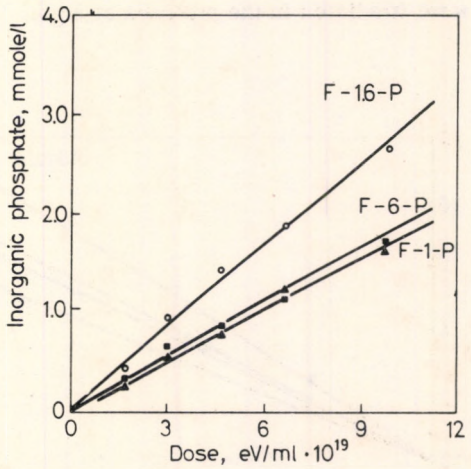

Fig. 1 Release of inorganic phosphate from neutral solutions of fructose phosphates irradiated in the presence of argon

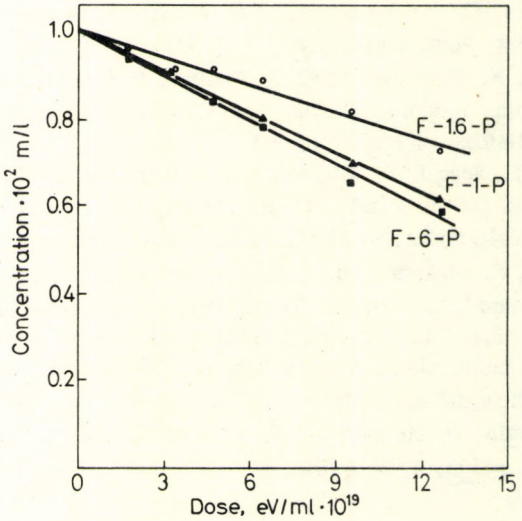

Fig. 2 Decomposition of sugar residue of fructose phosphates in aqueous solution. Samples were irradiated in the presence of argon

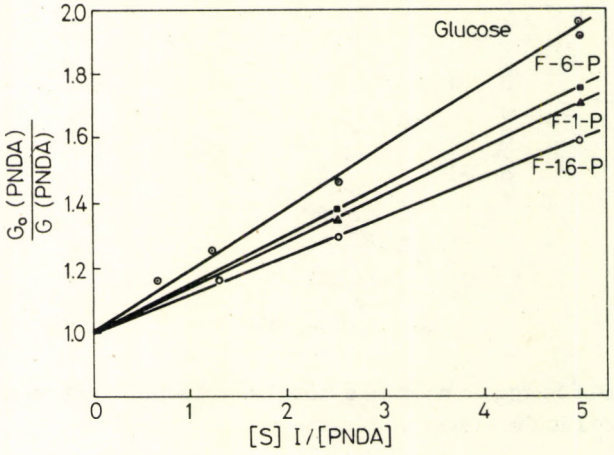

Fig. 3 Typical competition plots for the reaction of OH radicals with fructose phosphates by using the PNDA method /13/

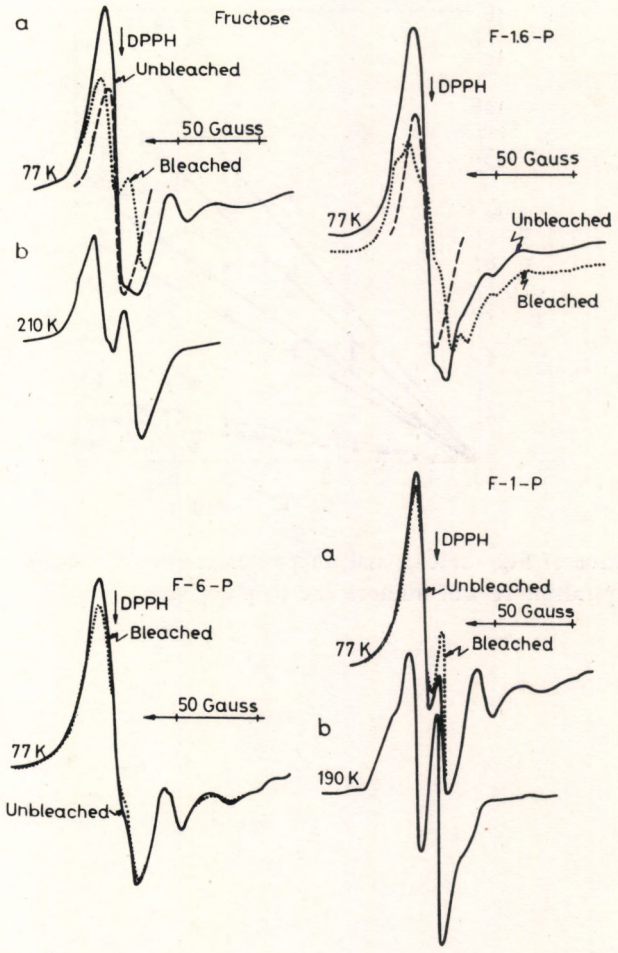

Fig. 4 ESR spectra of 1 M neutral ices of fructose and its phosphates recorded at 77K before and after photobleaching /a/ and after thermal annealing /b/. Dashed curves are due to the difference spectrum of e_t^-. The dose was constant and equal to 5×10^{19}eV g^{-1}

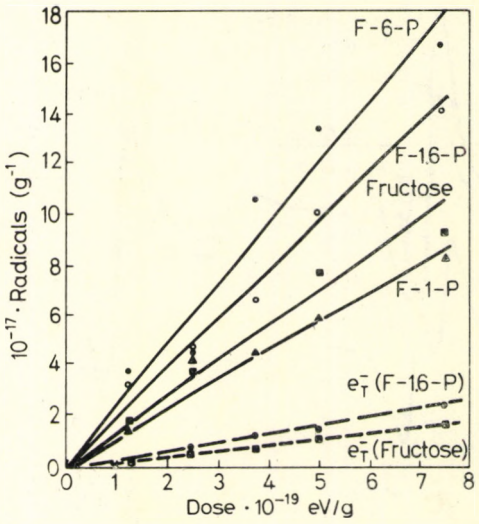

Fig. 5 Formation of free radicals and trapped electrons /e_t^-/ during γ-irradiation of polycrystalline ices of fructose and its phosphates

THE RADIOLYSIS OF A SURFACTANT IN THE FOAM USING IONIZING RADIATION

Yu. A. Panin, S. P. Buslaeva, R. V. Dzhagatspanyan, N. G. Konkov,
L. M. Makarochkina, L. B. Upadyshev, M. T. Filippov
All-Union Scientific Research Institute of Radiation Engineering, Moscov, USSR

Studies of the gamma-radiolysis of solutions and waste waters containing surfactants showed that when irradiating the solutions of non-biodegradable surfactants the latter converted into biodegradable products which can be removed with conventional methods.

The main shortcoming of the gamma-radiation is its high cost which is unacceptable for waste processing in the case of scaled-up industrial application. Recently, electron accelerators have become widely used in industrial radiation-chemical processes. They are specified by high power and low cost of the radiation energy as compared with a radioisotope source. However, when irradiating condensed systems with accelerated electrons the beam energy is transferred to a thin layer of the substance which prevents the carrying out of homogeneous irradiation of the system and decreases the efficiency of the beam.

The authors of this report proposed the use of an electron accelerator for irradiating the foam obtained from waste waters which contain surfactants or other pollutants that can cause foaming /1/. When irradiating the foam the conditions for transferring the beam energy to the liquid become better and the liquid has an easier access to the oxygen present in the gas phase. Besides, through enriching the foam with the surfactant it becomes possible, in principle, to enhance the radiation-chemical yield of the surfactant degradation.

The radiation destruction of the foam obtained from the solutions of alkyl-benzene sulphonate (ABS), alkylnaphthalene sulphonate (Nekal) and OC-20 type hydroxy-ethyl-substituted alcohols in the cycling and continuous systems was studied. An ELIT-1 type accelerator with an effective electron energy of about 0.6 MeV and an effective beam power of about 0.17 kW was used as a radiation source. The results of some experiments are given in Table 1.

Experiments on irradiation OC-20 type solutions (500 mg/litre or about 5×10^{-4} M) in the running-solution system showed that the treatment degree increased with increasing the V_a/V_l ratio of air flow rate to liquid flow rate other conditions being equal (Fig. 1).

On the basis of the above described experiments the following principle of radiation-floatation treatment is suggested. The surfactant is removed from the liquid

Table 1

Experiment No.	Irradiation time, min	Surfactant concentration mg/litre		
		Initial, according to UVS method*	Final, according to UVS method*	Final, according to methylene blue method
			Nekal	
1	10	100	2.7	-
2	10	100	5.0	0.9
3	10	100	23.5**	-
4	15	500	26.4	1.6
			alkylbenzene sulphonate	
5	10	200	34***	1.0
6	10	400	57***	-
7	10	800	120***	-
8	10	100	16.6	0.5

Cycling mode, accelerated electron current – 250 μ A

*Ultraviolet spectrum absorption analysis at 224 nm,

**foaming with argon in this experiment and with air in all other experiments,

***air flow rate 5.8 litre/min and 1.1 litre/min in other experiments

with the fractionated foaming method and the obtained foam is irradiated with the electron beam in the same or in another apparatus (Fig. 2).

The efficiency of the treatment which may be obtained by this method is determined by

$$\frac{C_k}{C_r} = 1 + \frac{V_k}{V_1}\left(1 - \frac{C_k}{C_r}\right) + \frac{V_f}{V_1} A \frac{\Gamma_A}{C_r} \qquad (1)$$

It differs from the equation for the conventional foaming floatation apparatus which is of the following form:

$$\frac{C_1}{C_r} = 1 \frac{V_k}{V_1} A \frac{\Gamma A}{C_r}$$

where C_1 – surfactant concentration in the liquid to be decontaminated,

C_r – surfactant concentration in the treated liquid (raffinate),

C_k – surfactant concentration in the foam condensate to be fed back into the apparatus,

Γ_A – dynamic surface excess, mol/cm^2,

A – specific foam surface, cm^2/cm^3,

V_l, V_k, V_f – flow rates of the liquid to be treated, of the condensate and of the foam, respectively.

When $C_k < C_r$ the second term of Eq. (1) is positive. Consequently, the efficiency of the treatment will be higher than in the case of simple foaming fractionation.

In order to make clear some details in the processes which occur when irradiating the foam, the gamma-radiolysis of the foam obtained from the solutions of alkylbenzene sulphate and Nekal with the help of oxygen and argon was studied. In Fig. 3 the kinetic curves of the surfactant degradation in the foam and solution are plotted. In the case of Nekal the curves are similar to those in Fig. 3 but they are smoother and do not reveal sharp change at the beginning of the irradiation. G-values of the surfactant degradation are listed in Table 2.

Table 2

Experimental conditions	G_{surf}				G_{O2}	
	Methylene blue		Ultraviolet spectrum		I	II
	I	II	I	II		
ABS, 1500 mg/l, foam, O_2, P = 36 rad/s	44	1.5	28	1.2	930	12
ABS, 1500 mg/l, solution, O_2, P = 36 rad/s	3.3	3.2	3.2	3.2	12	12
ABS, 1500 mg/l, foam, O_2, P = 4 rad/s	35	-	35	-	970	-
ABS, 100 mg/l, foam, O_2, P = 36 rad/s	1.2	-	0.9	-	11	-
ABS, 1500 mg/l, foam, A, P = 36 rad/s	1.5	-	1.25	-	7.2	-
Nekal, 1500 mg/l, foam, O_2, P = 36 rad/s	30.0	3.6	2.1	4.0	300	19
Nekal, 1500 mg/l, solution, O_2, P = 36 rad/s	4.0	4.0	3.6	3.6	6.0	6.0

High G_{-surf}- and G_{-O_2}-values in the initial part of the graphs (G_{-surf} = 30–45, G_{-O_2} = 300 – 1000 molecules/100 eV) demonstrate the presence of the chain processes. When irradiating solutions under analogous conditions the yields do not exceed the values that are specific for the non-chain processes.

The yield differences are supposed to be accounted for by the foam features. As to such features, one must know first of all that at the surface of the foam film there is a layer of oriented, slightly movable molecules of the surfactant having a concentration in the order of 10^{-10} mole/cm^2, for example 3.55×10^{-10} mole/cm^2 in the case of the alkylbenzene sulphonate /3/. If the surface layer thickness is taken to be equal to 10–30 Å, the surface volume concentration of the surfactant is about 1 M which is high enough for chain processes to occur. As high yields cannot be observed in the solutions having the same molar concentration as the average concentration in the foam, one must assume that, when irradiating the foam formed with oxygen, the chain process of the surfactant oxidation takes place in the surface film layer. High surfactant concentration in the layer as well as good contact of the layer with oxygen in the gas phase may promote the chain process.

The approximate evaluation of the foam surface in our experiments ($V_a \approx 640$ cm^3/s, $A \approx 100$ cm^2/cm^3, $\Gamma \approx 3.55 \times 10^{-10}$ mole/cm^2) showed that at the foam surface there might be not more than 2.2×10^{-5} mole ABS while during 15 minutes from the beginning of the irradiation about 14×10^{-5} mole reacted, i.e., 7 times more than the initial amount. So, during that time the foam surface had to become renewed at least 7 times.

Such surface renewal may occur in two ways: a) by destroying the old surface under the influence of the radiation and forming a new one (during the irradiation the air was fed to the system), b) by means of the desorption of "damaged" molecules of the surfactant from the surface layer and the adsorption of the intact molecules from the interstitial liquid. The obtained results do not permit us to name the perdominant mechanism of the surface layer renewal. One may only suppose that to some degree both mechanisms may take place.

Two experimental facts are of interest:

1. The large oxygen flow rate per one oxidized molecule of the surfactant $G_{-O_2} : G_{-surf} \approx 20$. As 1.5 molecules of O_2 are needed for the complete oxidation of the $-CH_2-$ group it corresponds to the oxidation of all the side chains of the ABS molecule consisting on the average of 10 to 12 groups of $-CH_2$,
2. Independence of G_{-surf} on the dose rate showing the linear chain termination.

The alkylbenzene sulphonate molecules are on the interface as a dense layer, the aliphatic radicals being oriented toward the gas phase forming a compact hydrocarbon film in which the oxidation chain process can occur.

Of great interest is the fact itself that the chain process occurs in the surface layer and stops after some time has elapsed. This phenomenon may be explained in several ways:

1. By slow oxygen diffusion from the gas phase into the surface layer.
2. By reduction of the total foam surface with time.

3. By the decrease of the concentration of the reactive surfactant molecules in the surface layer.
4. By the gathering of the inhibitors of the chain process in the surface layer or in the interstitial liquid.

According to some considerations which are not presented here the third and fourth factors are the most propable ones. It is difficult to consider the effect of concentration decrease because of the lack of experimental data and the lack of knowledge of the mechanisms which take place when the foam is irradiated.

It was mentioned above that during the chain process termination (15 min,) the foam surface was renewed not less than 7 times, i.e. the renewal time $\tau \leqslant 100$ s. The approximate consideration of mechanisms of renewal of the surface layer by means of molecular adsorption – desorption or film destruction-formation shows that the time for setting the stationary surface concentration is much less than 100 s and consequently the chain process termination was due to some other reason.

Such reason seems to be the pile-up of the inhibitors. It is known that during radiation oxidation of aromatic compounds phenols and polyatomic alcohols being inhibitors of the chain processes, are formed. When piling up in the surface layer and in the interstitial liquid these compounds might inhibit the chain oxidation process.

The possibility of the occurrence of the surfactant radiolysis chain process while irradiating the foam is of considerable interest both from practical and from theoretical points of view. One may suppose that the chain process in the monomolecular and essentially two-dimensional layer of the oriented molecules must differ from processes taking place in the liquid phase.

On the other hand, the reproduction of the oxidative chain radiolysis in a continuously operating apparatus may be used for the increase of the output and decrease of the costs of the radiation treatment of waste waters containing surfactants.

So, the study of the radiolysis of the surfactants in foams and particularly when using a beam of accelerated electrons is worthy of further through examination.

References

/1/ Patent applied for, SSSR, 1971.

/2/ M. T. Filippov, Yu. A. Panin et al.: Waste water purification by irradiation of foams (in Russian), Khim. promyshlennost, (in press).

/3/ B. I. Newsen, J. Appl. Chem. 16, 43 (1966).

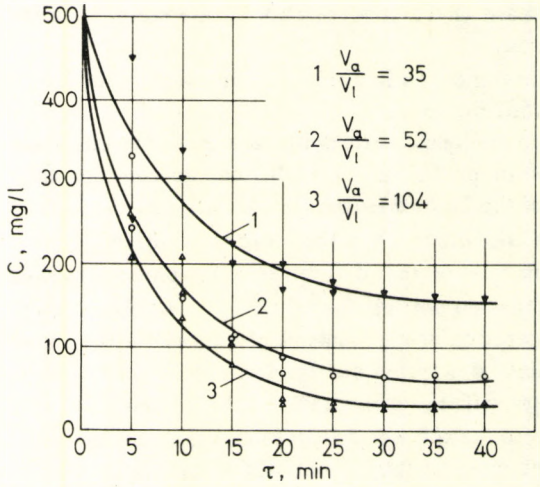

Fig. 1 Dependence of OC-20 concentration on the velocity of the solution feeding

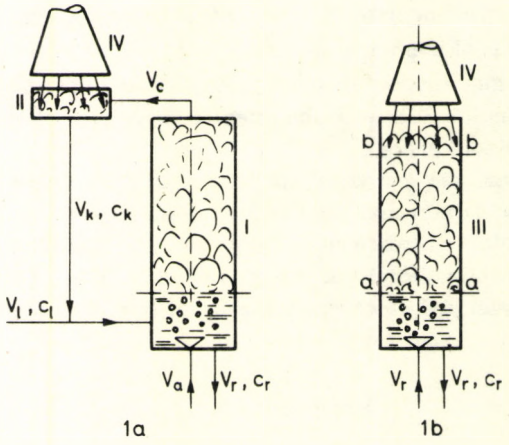

Fig. 2 Radiation-floatation apparatuses. a) Irradiating the foam in the off-system destruction facility, b) Irradiating the foam in the volume in which it is formed

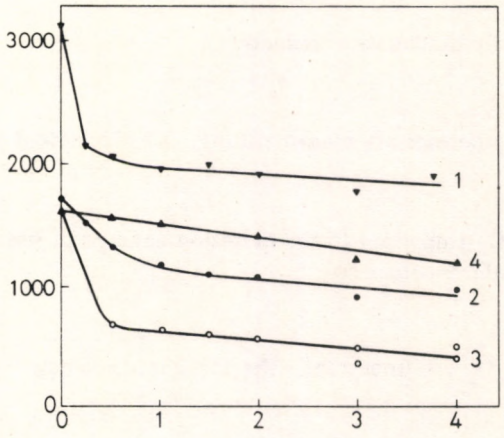

Fig. 3 Radiolysis of alkylbenzene sulphonate in the foam and in the solution:
1. Concentration change according to the ultraviolet spectrum method,
2. COD change in the foam, 3. Concentration change in the foam according to the methylene blue method, 4. Concentration change in the solution

DISCUSSION

R. K. BROSZKIEWICZ

What were the energy and dose-rate of the electrons used?

Yu. PANIN

We used an accelerator of electrons of the type ELNT-1 with electron energy E = 0.65 MeV, power 170 watt dose-rate 10 kRad/s.

R. K. BROSZKIEWICZ

How was the dose, absorbed by the foam measured? How was the calibration of a plastic film dosimeter done to simulate the situation in a heterogenic foam?

Yu. PANIN

We used PMMA foils for dosimetry. Evaluation of the data was based on average volume and Z_{eff}. The accuracy of a dosimetric process of this type is about 40%. The dosimetric equivalent of foams is not available at present.

C. L. GREENSTOCK

Is damage mainly oxidative or reductive?

Yu. PANIN

The oxidative processes are overwhelming. But pH decides everything.

C. L. GREENSTOCK

Are O_2^- and H_2O_2 important in the radiation damage of surfactants, and what do you speculate is the mechanism?

Yu. PANIN

Both O_2^- and H_2O_2 are important. The mechanism is now under study.

C. L. GREENSTOCK

Under best conditions, are the neutral surfactants like OC-20 damaged more or less than the charged surfactants like ABS?

Yu. PANIN

The damage of OC-20 and ABS proceeds with about the same rate of radio-oxidation at the same absorbed dose.

REACTIONS OF PYRIMIDINE RADICALS IN IRRADIATED AQUEOUS SYSTEMS: INTERMEDIATE ROLE OF CARBOCATIONS

K. Y. Al-Yamoor, A. Garner, K. M. Idriss Ali, G. Scholes
Radiation and Biophysical Chemistry Laboratory,
University of Newcastle Upon Tyne,
Newcastle, England

Introduction

We have previously reported /1/ that in the γ-radiolysis of solutions of dihydropyrimidines (PyH_2) the radicals produced by dehydrogenation at the C(5)—C(6) bonds can be oxidized to carbocations which can then lead to production of both parent pyrimidine (Py) and the corresponding hydrohydroxypyrimidine (PyH(OH)):

$$PyH_2 + OH \longrightarrow PyH\cdot + H_2O \qquad (1)$$

$$PyH\cdot + Ox \longrightarrow [PyH]^+ + Ox^- \qquad (2)$$

$$PyH(OH) + H_3O^+ \underset{(b)}{\overset{H_2O}{\longleftarrow}} PyH^+ \xrightarrow[(a)]{H_2O} Py + H_3O^+ \qquad (3)$$

Reactions (3a) and (3b) represent solvolytic elimination and substitution, respectively, of the intermediate carbocation. In the case of dihydrouracil (DHU) and dihydrothymine (5-Me-DHU) solutions, the relative extents of 3a and 3b involving the carbocations produced from the 6-yl radicals were pH-dependent, more substitution occurring under acidic conditions. Since a similar pH variation was noted in irradiated solutions containing no oxidant it was suggested that some carbocations can also arise by a dismutation process of the type:

$$PyH\cdot + PyH\cdot \longrightarrow [PyH]^+ + [PyH]^+ \qquad (4)$$

Subsequent pulse-radiolysis studies of these (PyH_2 + oxidant) systems showed /2/ that the elimination reaction (3a) proceeds via an intermediate which decays by a first-order mechanism ($t_{1/2} \approx 150\mu s$). Further experiments which indicate the nature of this intermediate, are reported below.

In the radiolysis of Py solutions, the OH adducts, PyOH· produced by OH radical addition at the C(5)—C(6) double bond, should, by analogy with reactions (2) and (4), produce the carbocation, $[PyOH]^+$. Solvolytic elimination and substitution should then lead to the formation of isobarbituric/barbituric acid derivatives (from

6-yl or 5-yl radicals) and pyrimidine glycols respectively (reaction 5)

$$PyOH(OH) + H_3O^+ \underset{(b)}{\overset{H_2O}{\leftarrow}} [PyOH]^+ \underset{(a)}{\overset{H_2O}{\rightarrow}} PyOH + H_3O^+ \qquad (5)$$

In this paper we present evidence for the involvement of $[PyOH]^+$ and show that the elimination process (5a) has an intermediate similar to that in the PyH_2 system.

Results and discussion

Radiolysis experiments were carried out in the presence of N_2O to convert the solvated electrons into OH radicals, the primary reactions with the solutes, therefore, predominantly involve OH. Structures of the various solutes used are indicated in Fig. 1.

1. Dihydropyrimidines

(a) γ-Radiolysis

Table 1 gives the yields of parent Py and of the corresponding 5-hydro-6-hydroxypyrimidines in γ-irradiated solutions of several dihydropyrimidines, both in the presence and absence of ferricyanide ions as oxidant, and also as a function of pH.

G(Py) was obtained directly by spectrophotometry and G[PyH(OH)], again by spectrophotometry, after dehydration to the parent Py on treatment with acid. The identities of the acid-labile products in the irradiated solutions of DHU, 5-Me-DHU and 1,3-diMe-DHU solutions were confirmed by comparison of their rates of dehydration with those of the photohydrates of the corresponding Py which are known to be 5-hydro-6-hydroxy-pyrimidines; the identity of the hydrolyzable product in the irradiated 6-Me-DHU solutions has not been definitely established. The presence of oxidant enhances the observed yields, as would be expected if more carbocations are produced under these conditions. Decreasing the pH of the DHU and 5-Me-DHU solutions results in an increase in G[PyH(OH)] and decreases in G(Py), detailed experiments over the pH range 2–6 show that the results follow a dissociation-type curve with apparent pK's between 3 and 4. With 1.3-diMe-DHU, however, there is no pH-dependence and it seems that solvolytic substitution is the predominant reaction of the carbocation produced from the 6-yl radical. On the other hand, solvolytic elimination is the predominant process in the irradiated 6-Me-DHU solutions.

(b) Pulse Radiolysis

The PyH· radicals exhibit broad absorption bands around 400 nm /3–5/ and their decay at this wavelength follows second-order kinetics ($k_{(PyH\cdot + PyH\cdot)} \simeq$

Table 1

Effects of pH and $Fe(CN)_6^{3-}$ ions on the yields of parent pyrimidine (Py) and 5-hydro-6-hydroxypyrimidine [PyH(OH), hydrolyzable material] in the γ-radiolysis of aqueous N_2O-saturated solutions of dihydropyrimidines ($[PyH_2]$ = 1 mM).

pH	2				5–6			
$[Fe(CN)_6^{3-}]$	0		0.1 mM		0		0.1 mM	
PyH_2 \ yield (G)	Py	PyH(OH)	Py	PyH(OH)	Py	PyH(OH)	Py	PyH(OH)
DHU	1.2	0.9	0.2	2.9	1.6	0	3.7	0
5-Me-DHU	0.7	0.7	0.5	2.4	1.4	0	3.6	0
6-Me-DHU	2.6	0.4	3.4	0.5	2.7	0.6	4.2	0.6
1,3-diMe-DHU	0.5	0.7	0.3	2.8	0.6	0.7	0.5	3.1

$\simeq 10^9\ M^{-1}\ s^{-1}$). Reaction of PyH· with ferricyanide ions can also be followed at 400 nm, $k_{(PyH\cdot + Fe(CN)_6^{3-})} \simeq 10^9\ M^{-1}\ s^{-1}$). Both these processes (particularly the latter) lead to the formation of an intermediate, which has no discernible absorption at wavelengths > 260 nm, and which is the precursor of the parent Py. The formation of Py, followed at 260 nm, is kinetically first-order and values for the rate constants have been studied in some detail (Table 2A). The experiments were carried out using a Febetron (Model 706) 600 keV pulsed electron generator. With this apparatus the high initial [OH] due to rapid electron beam attenuation is actually an advantage in these PyH_2 systems (in the absence of oxidant) since there is a clearer kinetic separation between the initial bimolecular decay of PyH· radicals and the subsequent first-order build-up of parent Py.

The results (Table 2A) show that in pulsed solutions of DHU, 3-Me-DHU, 5-Me-DHU and 6-Me-DHU the parent Py precursors can be formed as a results of reactions (2) and (4) followed by (3a). The observed rate constants (k) increase with increasing acidity, with apparent pK's matching those obtained from the determination of product yields, plots of k versus $[H^+]$ were found to be linear. Activation parameters were obtained from studies of the effect of temperature on the first-order rate constants, there was little spread, typical values for DHU solutions being $\Delta H^{\ddagger}$ = 24.5 kJ mol^{-1} and $\Delta S^{\ddagger}$ = − 91 $JK^{-1}\ mol^{-1}$. In pulsed solutions of those dihydropyrimidines where the N(1) position is substituted, viz. 1,3-diMe-DHU and dihydrouridine, no comparable build-up of parent Py was observed, if a Py precursor is present, it must decay faster than the experimental limit quoted in Table 2A. These observations underline once more the significance of chemical substitution at the N(1)-C(6) bond in determining the relative extents of solvolytic

Table 2

Effects of pH and $Fe(CN)_6^{3-}$ ions on the rate constants k, for the formation of: A. parent pyrimidines from dihydropyrimidines ($[PyH_2]$= 1 mM); B. substituted isobarbituric acids from parent pyrimidines ([Py] = 1 mM), in the pulse radiolysis of aqueous N_2O-saturated solutions at 24 ± 1°C

		Rate constants, $k/10^3$ s^{-1}			
	pH	5–6		3	
PyH_2 or Py	$[Fe(CN)_6^{3-}]$	0	1 mM	1 mM	pK* (app)
	DHU	5.0	5.3	28**	3.7
	3-Me-DHU	4.3	4.6	14**	3.7
	5-Me-DHU	5.7	6.2	> 35	–
A	6-Me-DHU	2.2	2.2	8.1	3.2
	1,3-diMe-DHU	> 35	35	> 35	none
	Dihydrouridine	> 35	35	> 35	none
	U	5.0**	5.3	19**	3.5
	3-MeU	3.0**	3.1	21**	3.7
B	6-MeU	2.9**	3.4	8.9	3.3
	1,3-diMeU	> 35	> 35	> 35	none

*Apparent pK from plots of half life against pH (these values essentially coincide with those obtained from plots of yield against pH), errors ± 0.1.

**Errors are ± 20% (the errors for the other values of k are less than ± 10%.).

substitution and elimination, and in particular, would suggest that the presence of an H atom at N(1) is a necessary condition for the formation of the Py precursor. The small yield of Py observed in γ-irradiated 1,3-diMe-DHU solutions (Table 1), and seen in the pulse experiments as an initial absorption at 260 nm, may arise from other processes which are referred to below.

2. Pyrimidines

(a) γ-Radiolysis

To test whether carbocations resulting from the oxidation of Py OH-adducts can undergo the competitive processes (5a) and (5b), product yields were determined. Some results for uracil are given in Table 3. In solutions containing ferricyanide

Table 3

Effects of pH $Fe(CN)_6^{3-}$ ions on the product yields in the γ-irradiation of aqueous solutions of uracil (10 mM) containing N_2O (125 mM).

	G-values			
pH	3–4		5–6	
Product \ $[Fe(CN)_6^{3-}]$	0	1 mM	0	1 mM
Dimers	3.3	0.2	4.4	0.2
Hydrohydroxy-uracil	0.4	0.2	0.3	0.6
Uracil glycols	0.3	4.0	0.3	2.2
Isobarbituric acid	0.1(2)	0.8	0.5	1.9
Other products	0.0(3)	0.3	0.0(2)	0.5
G(-uracil)	4.2	5.6	5.5	5.4
% material balance	98	98	100	100

ions, uracil glycols and isobarbituric acid are the major products, and their pH-dependence parallels those of PyH(OH) and of Py in the corresponding irradiated DHU solutions. Thus the fate of $[PyOH]^+$ is similar to that of $[PyH]^+$. In the absence of oxidant the main products are dimers $[(PyOH)_2]$ and it is clear, as observed, that their production should be suppressed by ferricyanide ions.

(b) Pulse Radiolysis

Since the optical absorption maxima of isobarbituric acid derivatives are at slightly longer wavelengths than the corresponding Py, it is possible to monitor the kinetics of their formation in pulse-radiolysis experiments at wavelengths around 285 nm, where there is little interference from the tail of the Py absorption. Isobarbituric acid and its derivatives are produced in a first-order manner and the similarity of the kinetic parameters to those for PyH_2 are evident from the data in Table 2A. No isobarbituric acid derivative can arise from the C(5) OH-adduct of thymine, and, accordingly, no first-order process was observed.

(c) Flash Photolysis

It has been suggested /6/ that a possible mechanism for the formation of Py photohydrates (the corresponding 5-hydro-6-hydroxypyrimidines) proceeds via protonation of singlet excited states. One form of the protonated Py could then be identical to $[PyH]^+$ and, it is of interest in this respect that the apparent pK for pho-

tohydration of uracil /6/ and for the formation of hydrolyzable material in the radiolysis of DHU solutions are essentially identical. There should also be a solvolytic elimination process in photolyzed Py solutions, leading to the return of parent Py. Using a conventional flash-photolysis apparatus (time resolution $\sim 20\,\mu s$), it was found that photobleaching was, in fact, followed by some return of the parent Py, in a first-order process with rate constants and apparent pK's essentially identical to those in the corresponding pulsed PyH_2 solutions. Identical kinetics were observed in the photolysis whether the solutions were aerated, deaerated or saturated with N_2O, as expected if the return does not involve excited states or free radicals.

3. Fate of the Carbocations

The lifetimes of these carbocations in a hydroxylic solvent such as water should be very short; it is rather unlikely, therefore, that the measured values of k correspond to reactions (3a) and (5a). This view has been confirmed by preliminary studies of conductivity changes in pulsed (DHU + oxidant) solutions where it has been found that proton release follows immediately upon oxidation of the PyH radical /7/. Reactions (3a) and (5a), therefore, involve an intermediate step.

One possibility is that the intermediate is an unstable hydrate. Given the correlation between the radiation and photochemical effects it is relevant to point out that Wang and Nnadi /8/ have already suggested that the low quantum yields of photohydrates in various Py solutions is a consequence of the production of a gem-diol at C(4) [-HN - $C(OH)_2$ - CH =] which subsequently dehydrates. One of the difficulties in supposing that such a diol is produced in the radiolysis of solutions of PyH_2 and Py is that charge delocalization from C(6) to C(4), which is a necessary prerequisite for production of a gem-diol by solvolysis, must involve prior enolization between C(5) and C(4), one would expect that carbocation-solvent interaction is too fast to allow such a rearrangement.

An alternative possibility is that the intermediate is an "isopyrimidine" which subsequently isomerizes, and a reaction scheme involving this is given in Fig. 2 for the case of a carbocation (azacarbonium ion) resulting from the oxidation of the 6-yl radical of DHU. The isomerization of the isopyrimidine proceeds by water and base-catalyzed deprotonation at C(5), followed by rapid reprotonation at N(1). The scheme predicts that the observed rate constant for the formation of Py, k, is equal to $k_0 + [k_1 k_2/(k_{-1} + k_2)][H^+]$, where $k_2 = k_2^S + k_2^E$, a linear dependence of k with $[H^+]$ was observed experimentally. It is obvious that no isopyrimidine can be produced from N(1) substituted carbocations, and here, C(5)-elimination will account for the formation of some parent Py. The effects of substituents at N(3) and C(5) are consistent with the scheme. The C(5) OH-adduct of thymine is a special case where no isomerization of the intermediate can occur, indeed, Hahn and Wang /9/ have reported the isolation of the expected radiolysis intermediate by dehydration of thymine glycol. The C(6) methyl group may exert a steric effect which favours elimination, although the lack of an effect of pH on the hydrolyzable material ap-

pears anomalous. If the scheme of Fig. 2 is correct it would imply that the mechanism of photohydration of pyrimidines involves azocarbonium ions fomed by proton abstraction from water by singlet excited states.

Acknowledgement. This work has been supported by the North of England Cancer Research Campaign to whom thanks are due

References

/1/ Haysom H. R., Phillips J. M. and Scholes G., J. Chem. Soc. Commun., 1082, (1972).

/2/ Haysom H. R., Phillips J. M., Richards J. T., Scholes G. and Willson R. L., "Fast processes in radiation chemistry and biology". The Institute of Physics, John Wiley and Son, 241 (1975).

/3/ Myers L. S. and Theard L. M., J. Amer. Chem. Soc., 92, 28 (1970)

/4/ Scholes G., Israel J. Chem., 10, 1107 (1972).

/5/ Barszcz D. and Fielden E. M., Int. J. Rad. Biol., 25, 539 (1974).

/6/ Burr J. G., Park E. H. and Chan A., J. Amer. Chem. Soc., 94, 5866 (1972).

/7/ In collaboration with K-D. Asmus and R. L. Willson.

/8/ Wang S. Y. and Nnadi J. C., J. Chem. Soc. Chem. Commun., 1160 (1968).

/9/ Hahn B-S and Wang S. Y. J. Amer. Chem. Soc., 94, 4764 (1972)

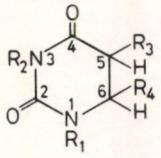

Fig. 1 Dihydropyrimidines. Parent pyrimidines are unsaturated between C(5) and C(6).

DHU	R_1, R_2, R_3, R_4 = H
3-Me-DHU	R_1, R_3, R_4 = H, R_2 = Me
5-Me-DHU	R_1, R_2, R_4 = H, R_3 = Me
6-Me-DHU	R_1, R_2, R_3 = H, R_4 = Me
1,3-diMe-DHU	R_1, R_2 = Me, R_3, R_4 = H
Dihydrouridine	R_1 = ribosyl, R_2, R_3, R_4 = H

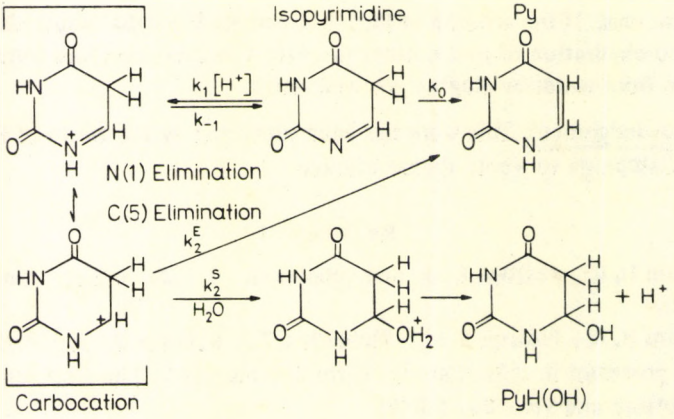

Fig. 2 Carbocation reactions (Py = Uracil)

STUDIES ON THE REACTIONS BETWEEN ALIPHATIC HYDROCARBON RADICALS AND RADIOLYTICALLY FORMED HYDROGEN PEROXIDE

Turan Söylemez, Turgut I. Balkaş
Middle East Technical University, Ankara, Turkey

Introduction

Even though hydrogen peroxide is present as a primary molecular product in the radiolysis of every aqueous solution and it is known to be a very reactive oxidizing reagent its reactions with the organic radicals produced during radiolysis have not been studied extensively. This was due to the general belief that these reactions would be rather slow as compared with the other, diffusion controlled reactions, of organic radicals, e. g. dimerization reactions /1/. The results obtained in the radiolysis of aqueous methane solutions, however, have shown that the methyl radicals undergo a very fast reaction with hydrogen peroxide. /2/

$$CH_3 + H_2O_2 \longrightarrow CH_3OH + OH \qquad /1/$$

The rate constant of reaction /1/ is 3.5×10^7 M^{-1} sec^{-1}. The aim of this work is to investigate the possible reactions of aliphatic hydrocarbon radicals with the radiolytically produced hydrogen peroxide. For this purpose cyclopentane, cyclopentene and n-pentane have been chosen as the representative solutes for cycloalkanes, cycloalkenes and alkanes, respectively.

Experimental

Materials. Cyclopentane, cyclopentene and n-pentane were obtained from Fluka and used without further purification. Fisher certified potassium iodide, sodium chloride, potassium phthalate, and ammonium molybdate were used in solutions. Matheson certified nitrous oxide was purified by trap-to-trap distillation on the vacuum line.

Sample Preparation and Irradiation. A 9 cc sample of triply distilled water was outgassed on a vacuum line and transferred into a Pyrex irradiation cell 6. 0 cm long and 1. 0 cm i. d. The desired amounts of aliphatic hydrocarbons and nitrous oxide were metered out on the vacuum line and transferred to the irradiation cell,

and the cell was sealed off. The fraction of hydrocarbon in the solution phase was calculated by the method described by Söylemez and Schuler /1/. The irradiation cell was shaken vigorously for half an hour and kept still for two hours before irradiation.

γ-irradiations were carried out inside Co-60 source (Gamma cell 220) at dose rates determined by Fricke dosimetry to be 4.2×10^{16} eV $g^{-1}min^{-1}$, 1.3×10^{17} eV $g^{-1}min^{-1}$ and 4.1×10^{17} eV g^{-1} min^{-1}.

Analysis. Radiolytically produced hydrogen peroxide was measured by the tri-iodide method described previously /3/. A Unicam SP-500 series 2 spectrophotometer was used in these experiments

Results and discussion

Hydrogen Peroxide Production. From the radiolysis point of view one of the simplest cycloalkanes to work with is certainly cyclopentane where rate constants of reactions with primary radicals are well known /1/. The production of hydrogen peroxide with dose is illustrated in Fig. 1 for 2.5×10^{-3}M cyclopentane solutions containing 10^{-2} M nitrous oxide. The initial hydrogen peroxide yields calculated at low doses for three different dose rates are identical to each other and equal to 0.68 which agrees quite well with the initial hydrogen peroxide yield (0.7) reported in the literature /4/. The gradual decrease observed in the hydrogen peroxide production at doses greater than 2×10^{18} eV g^{-1} reaches plateau values. As can be seen from Fig. 1, these plateau values increase with increasing dose rates.

Cyclopentene, an unsaturated analogue for cyclopentane, was chosen as a representative of cycloalkenes. The radiolysis of aqueous solutions of cyclopentene has been investigated in detail previously /1/. The production of hydrogen peroxide with dose is illustrated in Fig. 2 for 8.2×10^{-3}M cyclopentene solution containing 10^{-2}M nitrous oxide. The initial hydrogen peroxide yield calculated at low doses is 0.66 ± 0.05 which is also quite close to the value reported in literature /4/. Similar decrease in hydrogen peroxide production to that of cyclopentane solutions is observed in this case also at doses greater than 2×10^{18} eV g^{-1} and the plateau values increase with increasing dose rates.

n-Pentane, a noncyclic aliphatic hydrocarbon, has been investigated. The similar build up in hydrogen peroxide production as described for cyclopentane and cyclopentene solutions has also been observed in the radiolysis of aqueous solutions containing 10^{-2} M nitrous oxide and 5.0×10^{-3} M n-pentane (shown in Fig. 3). The initial hydrogen peroxide yield calculated is 0.62 ± 0.05 which is a little lower than the expected value /4/.

These results indicate that at high doses the radiolytically produced hydrogen peroxide undergoes certain reactions with species produced during radiolysis. Among the primary radicals, the hydrated electron is the most reactive one

against hydrogen peroxide

$$H_2O_2 + e^-_{aq} \longrightarrow OH + OH^- \qquad /2/$$

Even though the rate constant of reaction /2/ is very high, $k_2 = 1.3 \times 10^{10}\ M^{-1} sec^{-1}$ the radiolytically produced hydrogen peroxide will be protected by the presence of 10^{-2} M N_2O in these systems. The reactions of hydrogen atoms and hydroxyl radicals with hydrogen peroxide can be neglected because their reaction rates are much smaller than that of hydrated electrons /5/. One can, thus, conclude that the decrease in hydrogen peroxide yield can be due to the reaction of hydrogen peroxide with the aliphatic hydrocarbon radicals (R·) produced during radiolysis.

$$R\cdot + H_2O_2 \longrightarrow ROH + OH \qquad /3/$$

Reaction /3/ takes place particularly at high doses where the concentration of hydrogen peroxide is high enough to react with R· which would otherwise undergo dimerization reactions.

Rate Constants for Reactions Between Aliphatic Hydrocarbon Radicals and Hydrogen Peroxide. Since the hydrolysis reactions of cyclopentyl radicals have not been observed /1/ and the concentration of hydrogen atoms is only a tenth of the concentration of hydroxyl radicals, only the following reactions are considered for kinetic treatment:

$$c\text{-}C_5H_{10} + OH \xrightarrow{k_{OH}} c\text{-}C_5H_9 \qquad /4/$$

$$2\text{-}C_5H_9 \xrightarrow{k_R} C_{10}H_{18} + c\text{-}C_5H_8 + c\text{-}C_5H_{10} \qquad /5/$$

$$c\text{-}C_5H_9 + H_2O_2 \xrightarrow{k_{H_2O_2}} c\text{-}C_5H_9OH + OH \qquad /6/$$

Cyclopentanol is an expected product of reaction /6/ because methanol has been detected in similar reactions of hydrogen peroxide with methyl radicals /2/.

Taking into account the steady-state radical concentrations, the differential equation describing the production of hydrogen peroxide becomes

$$\frac{d\,[H_2O_2]}{dt} = \frac{10\, G_{H_2O_2}\, d\, D}{N} - K_{H_2O_2}\left(\frac{5\, G_{OH}\, d\, D}{N\, k_R}\right)^{1/2} [H_2O_2] \qquad /7/$$

where $G_{H_2O_2}$ is the initial yield of hydrogen peroxide, G_{OH} is the total hydroxyl radical yield, d is the density of the solution in gcm^{-3}, D is the dose rate in $eV\ g^{-1}\ sec^{-1}$ and N is the Avogadro's number.

Equation /7/ can be directly integrated in order to obtain the expression for hydrogen peroxide production which can be evaluated for $t = \infty$

$$[H_2O_2]_\infty = \lim_{t\to\infty}[H_2O_2] = \frac{10\, G_{H_2O_2}}{k_{H_2O_2}} \left(\frac{d\, D\, k_R}{5\, N\, G_{OH}} \right)^{1/2} \qquad /8/$$

where $[H_2O_2]_\infty$ corresponds to the plateau concentrations of hydrogen peroxide.

Substituting the reported value of $k_R = 2.0 \times 10^9\ M^{-1}\ sec^{-1}$ /1/, $G_{OH} = 6.0$ (for nitrous oxide solutions) and $d = 1.0\ g\ cm^{-3}$ and the experimentally observed D, $G_{H_2O_2}$ and (H_2O_2) values into Eq. (8), $k_{H_2O_2}$ values have been calculated (shown in Table 1). As can be seen from Table 1, the agreement among the values calculated for three different dose rates is very good. The average rate constant, $4.6 \times 10^4\ M^{-1}\ sec^{-1}$, is much smaller than the value reported for the rate constant of reactions between methyl radicals and hydrogen peroxide /2/. This difference is probably due to the different sizes of the radicals. The smaller methyl radicals should be much more reactive against hydrogen peroxide than the cyclopentyl radicals.

Since the reaction of hydroxyl radicals and cyclopentene produces two different radicals /1/, namely 23% cyclopentenyl and 73% cyclopentanol radicals, it is not very straightforward to calculate the rate constant of the reaction between each radical and hydrogen peroxide. Assuming these radicals behave in similar ways the total rate constant can be estimated by the same procedure described above. Substituting the reported value of the rate constant of dimerization reaction of cyclopentenyl radicals, $k_R = 1.5 \times 10^9\ M^{-1}\ sec^{-1}$ /1/ and the experimentally observed D, $G_{H_2O_2}$ and $[H_2O_2]_\infty$ values into Eq. (8), $k_{H_2O_2}$ have been estimated and these values are also shown in Table 1. The average rate constant obtained, $3.7 \times 10^4\ M^{-1}\ sec^{-1}$, is quite close to the value calculated for cyclopentyl radicals. This is expected because of the similarities in the character of these cyclic radicals.

Because the radiolysis of aqueous solution of n-pentane has not been studied previously, the determination of the rate constant of reactions between n-pentyl radicals and hydrogen peroxide is not possible at this stage. However, using the rate constant for dimerization reactions of cyclopentyl radicals in this case also, the rate constant for the reaction between n-pentyl radicals and hydrogen peroxide can be estimated. The values estimated are shown in Table 1. The average rate constant obtained is $3.4 \times 10^4\ M^{-1}\ sec^{-1}$ which is again very close to the value calculated for cyclopentane and cyclopentene cases.

All of the above results clearly indicate that the reactions of hydrogen peroxide and hydrocarbon radicals have to be taken into account in radiolysis studies particularly at doses higher than $2 \times 10^{18}\ eV\ g^{-1}$.

Table 1.

Determination of H_2O_2 and $k_{H_2O_2}$ in solutions containing various aliphatic hydrocarbons

System	Cyclopentane–N_2O		Cyclopentene–N_2O		n–Pentane–N_2O	
D ($eV\ g^{-1}\ min^{-1}$)	H_2O_2 (M)	$k_{H_2O_2}$ ($M^{-1}\ sec^{-1}$)	H_2O_2 (M)	$k_{H_2O_2}$ ($M^{-1}\ sec^{-1}$)	H_2O_2 (M)	$k_{H_2O_2}$ ($M^{-1}\ sec^{-1}$)
4.2×10^{16}	4.5×10^{-5}	4.2×10^{4}	6.3×10^{-5}	2.5×10^{4}	7.8×10^{-5}	2.2×10^{4}
1.3×10^{17}	7.8×10^{-5}	4.3×10^{4}	8.2×10^{-5}	3.4×10^{4}	8.7×10^{-5}	3.5×10^{4}
4.1×10^{17}	1.1×10^{-4}	5.4×10^{4}	9.5×10^{-5}	5.2×10^{4}	1.2×10^{-4}	4.5×10^{4}

References

/1/ Turan Söylemez and R. H. Schuler, J. Phys. Chem., 78, 1052 (1974).

/2/ G. C. Stevens, R. H. Clarke and E. J. Hart, J. Phys. Chem., 76, 3863 (1972).

/3/ A. O. Allen, C. J. Hochanadel and A. Ghormley, J. Phys. Chem., 56, 575 (1952).

/4/ A. O. Allen and R. A. Holroyd, J. Ama. Chem. Soc., 77, 5852 (1955).

/5/ M. Anbar and P. Heta, Int. J. Appl. Radiat. Isotopes, 18, 493 (1967).

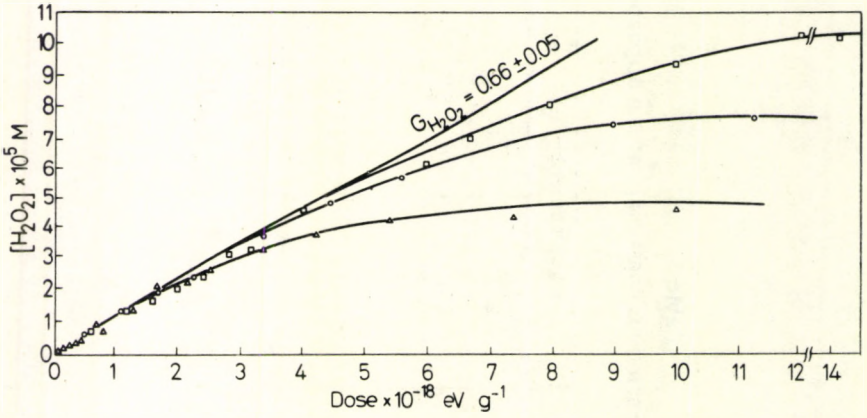

Fig. 1. Formation of hydrogen peroxide in aqueous solutions containing 2.5 mM cyclopentane and 10 mM nitrous oxide for dose rates of (□) 4.1×10^{17} eV g^{-1} min^{-1}. (○) 1.3×10^{17} eV g^{-1} min^{-1} (△) 4.2×10^{16} eV g^{-1} min^{-1}.

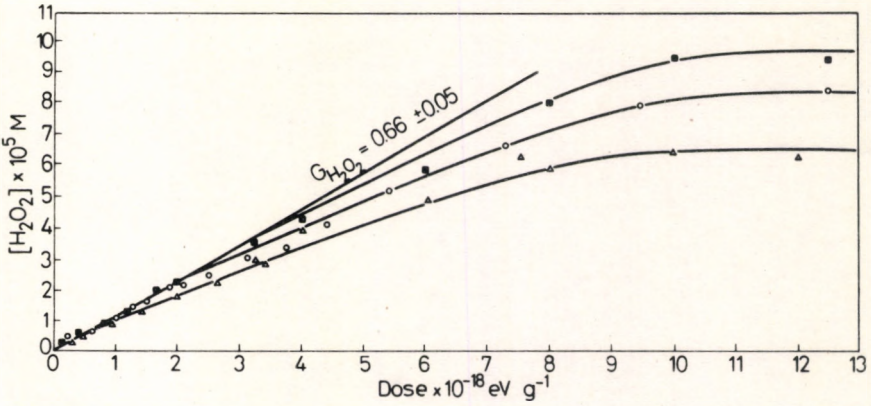

Fig. 2. Formation of hydrogen peroxide in solutions containing 8.2 mM cyclopentene and 10 mM nitrous oxide for dose rates of (■) 4.1 x 10^{17} eV g^{-1} min^{-1}, (○) 1.3 x 10^{17} eV g^{-1} min^{-1} (△) 4.2 x 10^{16} eV g^{-1} min^{-1}

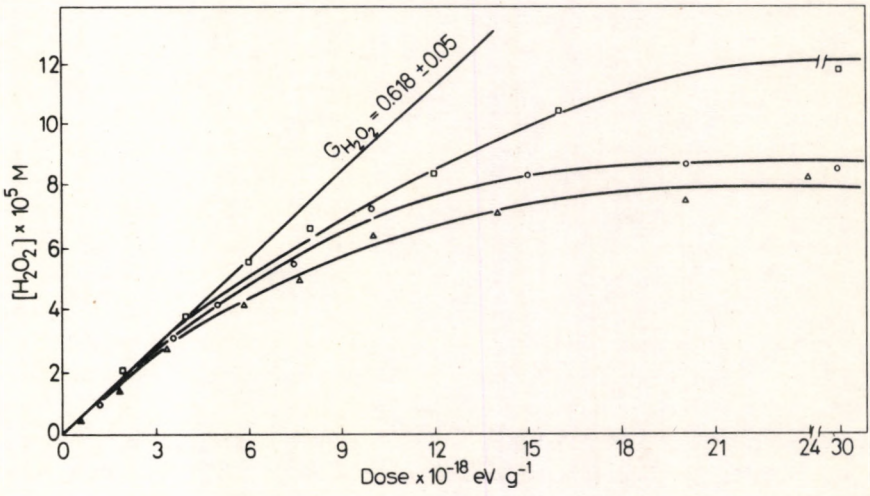

Fig. 3. Formation of hydrogen peroxide in aqueous solutions containing 5 mM n-pentane and 10 mM nitrous oxide for dose rates of (⊡) 4.1 x 10^{17} eV g^{-1} min^{-1} (○) 1.3 x 10^{17} eV g^{-1} min^{-1} (△) 4.2 x 10^{16} eV g^{-1} min^{-1}

PULSE RADIOLYSIS OF AQUEOUS SOLUTIONS OF SODIUM o-IODHIPPURATE

L. I. Kartasheva,* Z. M. Potapova,** A. K. Pikaev,* V. T. Kharlamov**

*Institute of Physical Chemistry of the Academy of Sciences of the USSR, Moscow, USSR

**Institute of Biophysics of the Ministry of Public Health of the USSR, Moscow, USSR

During the study of γ-radiolysis of aqueous solutions of sodium o-iodhippurate, ^{131}I, performed in connection with the problem of radiation sterilisation of radiopharmaceutical preparations /1-3/, it was found that the main products of radiolytic transformation of this compound are iodide, o-hydroxyhippurate and hippurate ions. In order to elucidate the mechanism of the formation of these products we investigated in detail the pulse radiolysis of these solutions under various conditions.

A linear electron accelerator U-12 (electron energy 5 MeV, pulse duration 2.3 μsec) was used: Optical detection of short-lived species was achieved by means of the pulse radiolysis apparatus /4, 5/. In Refs /4, 5/ the methods of irradation and dosimetry were also described. Lightfilters which eliminated the light with wavelengths below 300 nm were used to prevent photolysis due to the analysing light.

In deaerated 10^{-3} M aqueous solution of sodium o-iodhippurate (pH $\sim$ 7) a transient optical absorption with the maximum at 330–340 nm was observed (Fig. 1, curve 1). In the case of the same solution saturated with N_2O the intensity of absorption is higher by a factor of approximately 2 (Fig. 1, curve 2), the shape of the optical band is slightly changed because of the relative decrease of the absorption in the short wavelength region. In the presence of OH scavengers (tert.-butyl alcohol or ethylene glycol) the intensity of this absorption is decreased and in the presence of 0.2 M tert.-butyl alcohol completely disappears. On the basis of these data it is possible to conclude that the precursor of the species with the optical absorption having a maximum at 330-340 nm in the solutions saturated with N_2O is the OH radical. By analogy with benzene and its derivatives for which the formation of hydroxycyclohexadienyl radicals is characteristic (see, for example, Refs /6–9/) it may be supposed that the absorption under consideration is due to the product of OH addition to the benzene ring of the o-iodhippurate molecule, i.e. the radical RC_6H_4IOH where R is $CONHCH_2COO^-$. Molar extinction coefficient ε of this radical was evaluated in the case of the solution saturated with N_2O. For this solution $G(RC_6H_4IOH) = G_{OH} + G_{e^-_{aq}} = 5.7$. If we neglect the small contribution of the absorption of the product of H addition to benzene ring, i.e. the radical RC_6H_4IH, then $\varepsilon_{max} = 3.4 \times 10^3\ M^{-1}\ cm^{-1}$ ($\pm$ 15%).

The rate constant of OH reaction with o-iodhippurate was determined by means of the study of the competition of the reaction of OH with this compound and thiocyanate or carbonate ions (the absorption of $(CNS)_2^-$ or CO_3^- was observed. Neutral solutions saturated with air were used to eliminate the absorption of hydrated electron (e_{aq}^-). The value of the rate constant obtained is shown in Table 1.

The decay of the radicals RC_6H_4IOH was monitored at 350 nm. It was found that the decay rate in neutral solutions saturated with N_2O depends on the dose per pulse (the dose was changed from 2.5×10^{13} to 6×10^{17} eV/ml). Therefore the decay curves were treated by the method of normalized concentrations /10,11/, which gives the possibility of the determination of rate constant of the first- (or pseudo-first) order and second-order reactions. The values of rate constants obtained by such a method are presented in Table 1.

Table 1.

Rate constants of reactions at radiolysis of aqueous solutions of sodium o-iodhippurate

Reaction	pH	Rate Constant
$OH + RC_6H_4I$	~7	$5.4 \times 10^9 M^{-1}sec^{-1}$
$e_{aq}^- + RC_6H_4I$	~7	$5.5 \times 10^9 M^{-1}sec^{-1}$
$H + RC_6H_4I$	2	$1.9 \times 10^9 M^{-1}sec^{-1}$
$RC_6H_4IOH + O_2$	~6.5	$6 \times 10^6 M^{-1}sec^{-1}$ *
		$1 \times 10^7 M^{-1}sec^{-1}$ **
$RC_6H_4IOH + RC_6H_4IOH$	~7	$2k = 3 \times 10^8 M^{-1}sec^{-1}$
	~3.5	$2k = 9.6 \times 10^8 M^{-1}sec^{-1}$
Decay of RC_6H_4IOH in first order reaction	~7	$4.8 \times 10^3 sec^{-1}$
	3.5	$10^4 sec^{-1}$
Decay of RC_6H_4	~7	$1.1 \times 10^4 sec^{-1}$
$RC_6H_4O + RC_6H_4O$	3.5	$2k = 2.6 \times 10^9 M^{-1}sec^{-1}$
Decay of RC_6H_4O in first order reaction	3.5	$2.6 \times 10^4 sec^{-1}$
$RC_6H_4IH + RC_6H_4IH$	3	$2k \sim 7 \times 10^9 M^{-1}sec^{-1}$

*Rate constant was measured from the rate of decay of RC_6H_4IOH in the presence of oxygen.

**Rate constant was measured from the rate of formation of peroxide radical.

One of the main products of γ-radiolysis of neutral aqueous solutions of o-iodhippurate is o-hydroxyhippurate /2/. Moreover, it is known /9/ that, for example, in the case of C_6H_5F the OH radical in a slightly acid medium (pH $\sim$ 5) either undergoes addition to carbon atom in ortho-position or attacks the carbon bound to fluorine. On this basis it may be suggested that in neutral solutions of o-iodhippurate the OH radical is mainly added to carbon atom which is bound to be iodine atom. Earlier /1/ it was proposed that during γ-radiolysis of aqueous solutions of o-iodhippurate iodide ions are formed both via the reaction of this compound with e^-_{aq} and via the reaction with OH. Apparently I^- ions are formed as a result of decomposition of RC_6H_4IOH radicals and as a result of recombination and disproportionation of these radicals.

The rate constant of the reaction of e^-_{aq} with sodium o-iodhippurate was measured in deaerated solution (pH $\sim$ 7). The rate constant was determined from the rate of the decay of e^-_{aq} optical absorption at 720 nm in the presence of different concentrations of o-iodhippurate. The value obtained is given in Table 1.

The deaerated neutral solutions in the presence of tert.-butyl alcohol which is an effective scavenger of OH radicals were studied for obtaining the optical absorption belonging to the product of the reaction between e^-_{aq} and o-iodhippurate. In this system the transient optical absorption with maximum at about 310 nm is formed (Fig. 2, curve 1). Its intensity is considerably decreased in the presence of oxygen or N_2O. Obviously this absorption is mainly due to the product of dissociative addition of e^-_{aq} to o-iodhippurate, namely to radical RC_6H_4.

The determination of the exact value of ε for radical RC_6H_4 is complicated by the reaction of o-iodhippurate with an H atom. As it follows from the experiments with the acid solutions (see below) in this reaction an H atom is added to the benzene ring of the o-iodhippurate molecule and abstracts iodide ion. By accounting for the contribution of the absorption belonging to the products of the reactions of H atoms with o-iodhippurate in neutral medium it became possible to calculate the value of ε for RC_6H_4. The optical absorption spectrum of RC_6H_4 obtained after the subtraction of the absorption under consideration is shown in Fig. 2 (curve 2). In the calculation of ε it was accepted that $G_{e^-_{aq}} = 2.8$ and $G_H = 0.55$. Deaerated 6×10^{-4} M solution of o-iodhippurate containing 0.2M tert.-butyl alcohol was used for the determination of ε. In this solution all the OH radicals and all the H atoms react with alcohol and o-iodhippurate, respectively. It was calculated that ε for RC_6H_4 at 310 nm is equal to 700 $M^{-1}cm^{-1}$ ($\pm$ 20%).

The decay of RC_6H_4 is a first-order process (the rate constant is presented in Table 1). The rate of this process does not depend on the dose per pulse within the investigated range (from 1.5×10^{17} to 6×10^{17} eV/ml). This process is certainly not the reaction of RC_6H_4 with organic compounds being present in the solutions. Obviously RC_6H_4 is the precursor of hippurate ion which is observed among the products of γ-radiolysis of neutral aqueous solutions of sodium o-iodhippurate.

In acid medium the spectra of short-lived species are different from the spectra in neutral solution. Figure 3 (curve 1) shows the spectrum of optical absorption of

10^{-3} M solution of o-iodhippurate saturated with N_2O (pH ~ 3.5) immediately after the pulse. For comparison the spectrum of the same solution at pH ~ 7 observed under other conditions being equal is shown in this Figure (see curve 2). These spectra exhibit the following differences. First, at pH ~ 3.5 in addition to the maximum at 330–340 nm there are the maxima at 360 and 410 nm. Second, in acid medium the absorption in ultraviolet region is less intense than in neutral solution. The bands with maxima at 330–340 and 360 nm may be assigned to the products of the addition of OH and H to benzene ring, respectively. More clear "development" of the band of H adduct (λ_{max} = 360 nm) in acid medium is explained by lower intensity of the band of OH adduct (λ_{max} = 330–340 nm) in this medium and by higher yield of H atoms (under our experimental conditions ca. 6% of e^-_{aq} react with H_3O^+ but not with N_2O).

Obviously the band with maximum at 410 nm belongs to the radical of phenoxyl type, i.e. to RC_6H_4O. This assignment is confirmed by the following facts. First, in aqueous solutions of other aromatic compounds (phenol, cresol, etc.) /12/ phenoxyl radicals absorb the light in the same region of the spectrum. Second, the formation of phenoxyl radicals is favoured by H_3O^+ ions /9/. We observed that at equal doses per pulse the ratio of optical densities of the solution at 330 and 410 nm immediately after the pulse decrease with decreasing pH. It was found that for the above-mentioned solution this ratio is equal to 8.9, 2.6 and 1.2 (after taking into account the absorption of the products of the reactions of H and e^-_{aq} with o-iodhippurate) at pH ~ 7, 3.5 and 1.1, respectively (at pH 1.1 the ratio is given for optical densities at 360 and 410 nm because at this pH these are the absorption maxima of the OH adduct and phenoxyl radical, respectively). Third, the kinetics of the decay of the bands with maxima at 330–340 and 410 nm are different.

The value of ε for RC_6H_4O was determined on the basis of the suggestion that ε for OH adduct does not depend on pH. In this determination the yields of OH adduct and phenoxyl radical (from the values of doses per pulse, initial optical densities at 330 and 410 nm and yield of OH radicals) were calculated at first. It was found that ε_{410} for RC_6H_4O is 2.6×10^3 $M^{-1}cm^{-1}$. The spectrum of this radical obtained after the abstraction of the absorption of RC_6H_4IOH, RC_6H_4IH and RC_6H_4 from the overall spectrum (Fig. 3, curve 1) is curve 3 in Fig. 3.

The kinetics of the decay of OH adduct and phenoxyl radical depends on the dose per pulse. Hence the kinetic curves were treated by the method of normalized concentration /10,11/. The rate constants of the first-order and second-order reactions obtained by such a method are listed in Table 1. It is seen that in acid medium the reaction of second order is noticeably faster than in neutral solution. It may be explained by the transformation of OH adduct (and, obviously, H adduct) in acid medium into electroneutral molecule, i.e. into $C_6H_4(I)(OH)CONHCH_2COOH$. This transformation is confirmed by the shift of λ_{max} of optical absorption band of this radical in acid medium. For example, at pH 1.1 λ_{max} = 360 nm.

As it is seen from Table 1, the value of rate constant of RC_6H_4IOH decay in first-order process is comparatively low. At the same time in acid medium

phenoxyl radical is formed in relatively large amount during the pulse. On this basis it is possible to conclude that phenoxyl radical is not a product of the decay of RC_6H_4IOH. Apparently RC_6H_4IOH and RC_6H_4O are formed directly in the reaction of RC_6H_4I with OH:

$$RC_6H_4I + OH \longrightarrow RC_6H_4IOH \quad (1)$$

$$RC_6H_4I + OH \longrightarrow RC_6H_4O + HI \quad (2)$$

Obviously the ratio of rate constants k_1/k_2 decreases with decreasing pH.

The band with λ_{max} = 310–320 nm which belongs to RC_6H_4 is distinctly "developed" in the spectrum of irradiated 10^{-3}M solution of o-iodhippurate saturated with N_2O at pH 1.1. In this solution almost all of the hydrated electrons react with H_3O^+ but not with N_2O they being transformed into H atoms. Hence the yield of H atoms in this system at pH~1 is much more higher than in neutral medium and solution at pH. 3. 5. Obviously H atoms can react with o-iodhippurate in two ways: by addition to benzene ring and by abstraction of iodine forming RC_6H_4.

The products of the reaction between H atoms and o-iodhippurate were studied in more detail using the solutions containing tert.-butyl alcohol which is an effective scavenger of OH radicals. Figure 4 (curve 1) shows an example of the optical absorption spectrum of 6 x 10^{-4}M solution of o-iodhippurate (pH 3) saturated with argon and containing 0.2M tert.-butyl alcohol immediately after the pulse. In this solution all the OH radicals react with alcohol. Almost all the hydrated electrons (ca. 90%) react with H_3O^+ ions and are transformed into H atoms (ca. 10% of e_{aq}^- react directly with o-iodhippurate). It is seen that the maximum of intense optical absorption band is at 360–370 nm. Besides, the second band with the maximum at about 320 nm is seen in the spectrum. Obviously the band with λ_{max} = 360–370 nm belongs to H adduct and the band with $\lambda_{max} \sim 320$ nm is due to RC_6H_4. The optical absorption spectrum of the solution at pH 2 has similar shape (Fig. 4, curve 2). Curve 3 in Fig. 4 is the spectrum of H adduct in the solution at pH 2. This spectrum was obtained by the subtraction of the RC_6H_4 spectrum from the overall spectrum (Fig. 4, curve 2). The subtraction was based on the suggestion that the absorption spectrum of RC_6H_4 is the same both in neutral solution and in acid medium. For comparison the spectrum of H adduct in neutral medium (curve 4) is also shown in this Figure. It is seen that in acid solution λ_{max} is slightly shifted to longer wavelengths. Obviously like in the case of OH adduct the shift of the maximum is due to the transformation of the radical under consideration in the acid medium into the electroneutral species.

The rate constant of the reaction of H atoms with o-iodhippurate was determined. It was obtained by means of the study of the competition of the reaction of H atoms with o-iodhippurate and ethylene gylcol. 10^{-3}M solution of o-iodhippurate (pH 2) saturated with argon and containing 0.2M tert.-butyl alcohol was used in these experiments. The optical density of the solutions at 360 nm was measured. The value of this rate constant is given in Table 1.

The radicals RC_6H_4IH disappear in the reaction of the second order (the kinetics was measured at doses per pulse from 1×10^{17} to 9.8×10^{17} eV/ml). The value of the rate constant of this reaction is shown in Table 1. However, it is not excluded that at even lower doses per pulse this radical can decay also via the reaction of the first order.

In the presence of oxygen the origin of transient optical absorption is changed. The spectrum of oxygenated 6×10^{-4}M solution of o-iodhippurate (pH 6.5) measured immediately after the pulse coincides practically with the spectrum of OH adduct (i.e. radical RC_6H_4IOH) in neutral solutions saturated with N_2O (Fig. 5, curve 1). This coincidence was expected because almost all the atoms in this solution react with oxygen. However, in the absence of oxygen the OH adduct decays rapidly, but in the presence of oxygen the new short-lived species is formed during this process. The new species has the optical absorption spectrum with maxima at 320, 400 and 430 nm (Fig. 5, curves 2 and 3). Obviously this species is the product of the interaction between RC_6H_4IOH and oxygen, i.e. peroxide radical $RC_6H_4IOHO_2$.

The rate constant of the reaction between RC_6H_4IOH and oxygen was obtained both from the rate of decay of OH adduct and from the rate of formation of peroxide radical. In the first case the correction for the decay of RC_6H_4IOH in other processes was done. In the second case the value obtained is the approximate upper limit because OH adduct disappears not only in the reaction with oxygen. The data on the rate constants are listed in Table 1.

The kinetics of the decay of peroxide radical depends on the dose per pulse. At the lowest dose used (1.5×10^{17} eV/ml) this radical decays mainly in a first order process. The rate constant is ca. $(4-5) \times 10^2$ sec^{-1}. At the highest dose used (9×10^{17} eV/ml) the decay occurs mainly in a second-order process. The rate constant 2k is equal to $(3-4) \times 10^4$ $\varepsilon_{420} M^{-1}$ sec^{-1}.

Thus, this study shows that in neutral deaerated solutions of o-iodhippurate the main short-lived intermediate products of the radiolysis are the radicals RC_6H_4IOH and RC_6H_4 appearing as a result of the reactions with OH and e^-_{aq}, respectively. In acid medium the mechanism of radiolytic transformations is different. The difference consists mainly in the formation of a radical of the phenoxyl type. The H atoms reacting with o-iodhippurate give phenyl and cyclohexadienyl radicals. In oxygen-containing solutions peroxide radicals play an important role in radiolytic transformations.

REFERENCES

/1/ Z.M. Potapova, V.T. Kharlamov, A.K. Pikaev and A.F. Gus'kov. Khimiya vysokikh energii, 7, 509 (1973).

/2/ Z.M. Potapova, V.T. Kharlamov, A.K. Pikaev and A.F. Gus'kov. Khimiya vysokikh energii, 9, 442 (1975).

/3/ V.V. Bochkarev, V.T. Kharlamov, A.K. Pikaev, V.V. Sedov, E.P. Pavlov, Z.M. Potapova, L.P. Shubnyakova, A.F. Gus'kov and E.G. Tushov. Med. radiol., 1976 (in press).

/4/ A. K. Pikaev, G. K. Sibirskaya, E. M. Shirshov, P. Ya. Glazunov and V. I. Spitsyn. Doklady AN SSSR, 200, 383 (1971).
/5/ A. K. Pikaev, G. K. Sibirskaya, E. M. Shirshov, P. Ya. Glazunov and V. I. Spitsyn. Doklady AN SSSR, 215, 645 (1974).
/6/ L. I. Kartasheva, Z. S. Bulanovskaya, E. V. Barelko, Ya. M. Varshavskii and M. A. Proskurnin. Doklady AN SSSR, 136, 143 (1961).
/7/ L. M. Dorfman, I. A. Taub and R. E. Bühler. J. Chem. Phys., 36, 3051 (1962).
/8/ B. Chutny and A. J. Swallow. Trans. Faraday Soc., 66, 2847 (1970).
/9/ N. A. Vysotskaya. Uspekhi khimii, 42, 1843 (1973).
/10/ T. E. Pernikova, S. A. Kabakchi, V. N. Shubin and P. I. Dolin. Radiation Effects, 5, 133 (1970).
/11/ A. K. Pikaev, T. P. Zhestkova and G. K. Sibirskaya. J. Phys. Chem., 76, 3765 (1972).
/12/ E. J. Land and M. Ebert. Trans. Faraday Soc., 63, 1181 (1973).

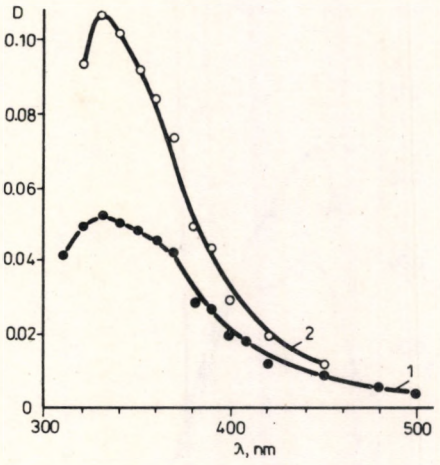

Fig. 1 Spectra of optical absorption of 10^{-3}M aqueous solutions of sodium o-iodhippurate saturated with argon (1) or N_2O (2) (pH ~ 7) immediately after pulse (dose per pulse 1.7×10^{17} eV/ml, optical path length, 1 is 2 cm)

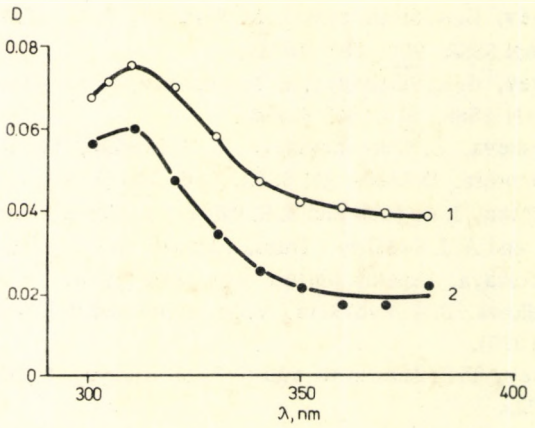

Fig. 2 Spectrum of optical absorption of deaerated 4 x 10^{-4}M aqueous solution of sodium o-iodhippurate containing.0.2M tert.-butyl alcohol (pH ~7) immediately after pulse (dose per pulse 3 x 10^{17} eV/ml, l = 5.8 cm) (1) and spectrum of optical absorption of radical RC_6H_4 (2)

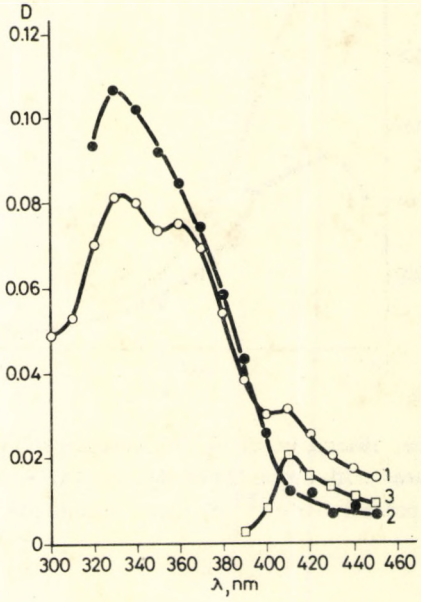

Fig. 3 Spectra of optical absorption of 10^{-4}M solution of sodium o-iodhippurate saturated with N_2O at different pH immediately after pulse (dose per pulse 1.7 x 10^{17} eV/ml, l = 2 cm): 1 – pH 3.5, 2 – pH ~7, 3 – spectrum of phenoxyl radical

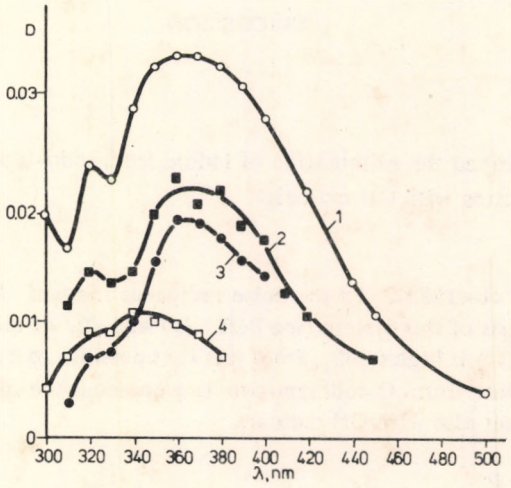

Fig. 4 Spectra of optical absorption of sodium o-iodhippurate solutions in the presence of tert.-butyl alcohol saturated with argon at different pH immediately after pulse (l = 2 cm): 1 – 6 x 10^{-4}M solution of o-iodhippurate containing 0.2M tert.-butyl alcohol at pH 3 (dose per pulse 4 x 10^{17} eV/ml), 2 – 10^{-3}M solution of o-iodhippurate containing 0.2M tert.-butyl alcohol at pH 2 (dose per pulse 2 x 10^{17} eV/ml), 3 – spectrum of cyclohexadienyl radical at pH 2, 4 – spectrum of cyclohexadienyl radical at pH 7

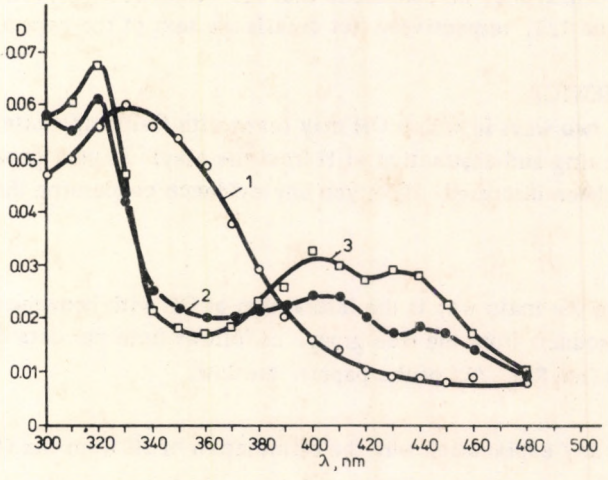

Fig. 5 Spectra of optical absorption of neutral 6 x 10^{-4} M solution of sodium o-iodhippurate saturated with oxygen: 1 – immediately after pulse, 2 – 100 μ sec after pulse, 3 – 250 μ sec after pulse (dose per pulse 2.5 x 10^{17} eV/ml, l = 2 cm).

I. KRALJIC

Have you observed the elimination of iodine from iodo-hippurate as a consequence of the reaction with OH radicals?

A. K. PIKAEV

We could not observe this by the pulse radiolysis method. However, during the study of γ-radiolysis of this system (see Refs. /1/ and /2/ of the paper) we found that initial value of $G(I^-)$ is high ($\sim$6). From this it is possible to conclude that the elimination of iodine from O-iodhippurate is a consequence of the reactions not only with e^-_{aq} and H, but also with OH radicals.

C. L. GREENSTOCK

What are the rate constants for the two reactions of OH with O-iodhippurate:

$$RC_6H_4I + OH \longrightarrow RC_6H_4IOH \quad (1)$$

$$RC_6H_4I + OH \longrightarrow RC_6H_4O + HI \quad (2)$$

A. K. PIKAEV

The ratio of k_1/k_2 is decreased with decreasing pH. From initial optical densities at 330 and 410 nm it may be concluded that the values of k_1/k_2 are 8.9, 2.6 and 1.2 at pH 7, 3.5 and 1.1, respectively (for details see text of the paper).

R. K. BROSZKIEWICZ

There are two ways in which OH may react with O-iodhippurate, i.e. addition to the benzene ring and abstraction of H from the alkyl. In your paper only the first possibility has been discussed. Have you any evidence concerning the second way of reaction?

A. K. PIKAEV

In our case the main way is the interaction of OH with benzene ring, because the yields of products from the side group, as follows from our data on γ-radiolysis of this systems (see Ref. /2/ of the paper), are low.

G. SCHOLES

Have you any explanation why the elimination of HI from the OH adduct is pH-dependent?

A. K. PIKAEV

The possible explanation is given in the literature (see, for example, Ref. /9/ of the paper).

INTERACTIONS OF DRUGS WITH BIOLOGICAL MACROMOLECULES AS STUDIED BY PULSE RADIOLYSIS

C. L. Greenstock, C. Banerjee, G. W. Ruddock
Medical Biophysics Branch, Atomic Energy of Canada Limited,
Whiteshell Nuclear Research Establishment, Pinawa, Manitoba, Canada

The rate of reaction of the primary reactive species (e^-_{aq}, H, OH) formed in aqueous solution with a solute is dependent upon temperature (T), solvent dielectric constant (ε), and upon the charges (Q_1, Q_2), encounter radii (r_1, r_2) and diffusion constants (D_1, D_2) of the reactive species and solute respectively, and can be calculated on the basis of diffusion theory /1, 2/:

$$k_D = 4\pi(r_1 + r_2)(D_1 + D_2)\,N \cdot 10^{-3}\{[Q_1Q_2e^2/\varepsilon kT(r_1 + r_2)]/\exp[Q_1Q_2e^2/\varepsilon kT(r_1 + r_2)]\} =$$

$$= 4\pi(r_1 + r_2)(D_1 + D_2)N \cdot 10^{-3} \text{ if } Q_1 \text{ and/or } Q_2 = 0$$

For e^-_{aq}, where $D_1 = 4.5 \times 10^{-5} cm^2 s^{-1}$ /3/ and $r_1 = 3\,\text{Å}$ /4/, the calculated rate constants for diffusion controlled reactions with most reactive small molecules $k_D \sim 2-4 \times 10^{10}\ M^{-1}s^{-1}$, are in good agreement with experiment.

When a small molecule becomes incorporated into a polymer as a repeating subunit, such as a nucleotide moiety in DNA or an amino acid residue within a protein, or becomes associated in some way with such a polymer, its reactivity drops dramatically because of its loss of mobility, shielding by neighbouring sites within the ordered structure of the polymer, and, in the case of charged polyanions (DNA, RNA, phospholipids), because of inter-molecular ionic strength effects. Pulse radiolysis, in exploiting this change in reactivity, provides a kinetic application to the study of small molecule binding to polymers /5, 6/. Such chemical effects of small molecules interacting with biopolymers may have important implications with respect to their biological activity. Many drugs and antibiotics including proflavin, acridine orange, actinomycins and ethidium bromide are known to inhibit nucleic acid synthesis /7/. In addition, many mutagens, carcinogens and antitumour agents are known to associate with DNA, RNA or proteins. The interaction of radiosensitizers with key target biopolymers within the cell could be important in enhancing their effectiveness /8/, by increasing the efficiency of the underlying fast free radical reactions between target radicals and radiation modifiers /9, 10, 11/.

Experimental

The ethidium bromide analogue 3,8-dinitro-5-methyl-6-phenyl-phenanthridium bromide (nitroEB) was a kind gift from Dr. M. Cory of Stanford Research Institute. Bleomycin was generously provided by Bristol Laboratories. Bovine serum albumin, myoglobin, the sodium salt of calf thymus DNA type 1, and the sodium salts of stearic and oleic acid were from Sigma Chemical Company. The biopolymers were prepared in triply distilled water, stored in a cool dark place, and solutions deoxygenated by careful bubbling with high-purity argon for 30 minutes. The pH was adjusted to neutrality with $HClO_4$ or KOH, and hydrated electron reactions were studied using 0.1 M t-butanol as OH scavenger. The pseudo-first order rate constants for e^-_{aq} reactions with the various small molecules in the presence and absence of biopolymers were obtained kinetically by monitoring the decay of e^-_{aq} absorption at 650 nm and were corrected for the finite e^-_{aq} lifetime in the matrices containing no small molecules. The corrected rates were used to quantitate the degree and extent of binding using a kinetic binding parameter. The experimental details of the pulse radiolysis apparatus have been described previously /12/. A 3 MeV Van de Graaf generator was used to deliver 0.1−1 krad doses to the sample within a single 50 ns pulse. Ultraviolet cut-off filters were used to prevent photolysis of the solutions by the 150 W pulsed Xenon analysing lamp.

Results and discussion

Figure 1 shows a diagrammatical representation of the kinetic binding assay employed in these pulse radiolysis studies. In the absence of binding – the overall reaction rate $k'(s^{-1}) = 0.693/t_{1/2}$, measured from the decay of the e^-_{aq} absorption, will be equal to the sum of the e^-_{aq} reactivities of the biopolymer (P) and the solute(s), $k_p[P] + k_s[s]$. In the presence of binding, the observed reaction rate k'_{obs} drops to $k_p[P\ \text{unbound}] + k_{s\ \text{bound}}[P\ \text{bound}] + k_s[s\ \text{unbound}] \simeq k_p[P] + k_s[s\ \text{unbound}]$. Under these conditions, the concentration of free s is $(k'_{obs} - k_p[P])/k_s$ or $f[s]$ where f is the fractional change in the rate of reaction of e^-_{aq} with s, as measured experimentally. In order to quantitate the binding process, we have defined a kinetic binding parameter $B = (k'_p + k'_s - k'_{obs})/k_s[P]$ which represents the molar fraction of small molecules bound to biopolymer. In all the experiments to be described, the biopolymer concentration is expressed in terms of the effective concentration of subunits (DNA nucleotides, protein amino acids, micelle monomers) and hence B refers to the molar fraction of small molecules bound to each biopolymer subunit. In the absence of binding B becomes zero, and for complete association it becomes [s bound]/[P]. This kinetic expression can be used in a modified Scatchard expression /6, 13/,

$$B/[s\ \text{unbound}] = K(n-B) \qquad (1)$$

to determine the association constant K, and the number of binding sites per biopolymer subunit n.

The intercalation of an ethidium bromide analogue nitroEB to highly polymerised DNA was studied in detail using pulse radiolysis. The e^-_{aq} reactivity of a fixed (10^{-4}M) concentration of nitroEB was measured in the absence and presence of DNA at different concentrations. From Fig. 2 it can be observed that the apparent dye reactivity decreases by an order of magnitude with increasing DNA concentration up to 0.05%. In all cases the e^-_{aq} decays are exponential. In experiments performed at different nitroEB concentrations (Fig. 3), for a particular DNA concentration, the rate of e^-_{aq} reaction with unbound nitroEB increases linearly with the total nitroEB concentration. From the slopes of these lines, the pseudo-first order rate constants for the reaction of e^-_{aq} with the freely diffusing nitroEB remaining unbound in aqueous solution in the presence of DNA can be determined. The measured rate constants are shown plotted against the DNA nucleotide concentration in Fig. 4. The rate constant for the reaction of e^-_{aq} with nitroEB drops precipitously at low DNA concentrations ($\leq$0.2 mM) where intercalation of nitroEB, present in concentrations ranging from 0.1 to 1×10^{-4} M, is most effective. This qualitative estimate of binding can be further refined by the use of the kinetic binding parameter B, in the modified Scatchard expression. A plot of B/ [nitroEB unbound] against B, shown in Fig. 5, yields a two-component curve whose negative slopes are a measure of K and whose intercepts on the abscissa are n. A comparison of these binding parameters with those for ethidium bromide published previously (6) in Table 1 shows that both the degree of binding (as measured by K) and the extent of intercalation (as measured by n) are lower for the dinitroderivative, which is not unexpected in view of the fact that the two amino groups of ethidium bromide have been replaced by bulky nitrosubstituents. The difference is most noticeable in the strong primary binding which presumably represents the true intercalation within the grooves of the DNA double helix. The steric hindrance of the nitro groups militates against the close association of the dye and the biopolymer necessary to fully develop the short-range hydrophobic interaction. There is only a 2–3 fold difference in the weaker secondary binding observed at high dye/DNA ratios, between the two dyes. This binding is probably determined more by the electrostatic attraction between the polyanionic phosphodiester backbone of DNA and the positive charge on the dye molecules or the stacking forces exerted by the pi system between adjacent or closely packed dye molecules, and would be expected to be less affected by dye substituent effects.

Table 1

A quantitative comparison of the two-component binding to DNA of ethidium bromide and the dinitro-derivative

Parameter	EB		NitroEB	
	Strong binding	Weak binding	Strong binding	Weak binding
$K(10^4M^{-1})$	160	1.8	19	0.8
n	0.12	0.37	0.014	0.13

Although the nitroEB is less effective in intercalating into DNA, nevertheless, it is strongly associated with the genetic material of the cell, and such effects could have marked biological consequences. The dinitroderivative was tested, because of its high electron-affinity, for its possible practical application /8/ as a radiosensitizer of hypoxic tumour cells in radiotherapy. The chemical mechanism for radiosensitization of electron-affinic nitro-compounds /9, 10, 11/ is believed to involve their interception of free radicals formed in important cellular targets, producing enhanced, potentially lethal radiation-chemical damage to these targets. Such processes involving either direct or indirect effects of radiation would become more efficient if the radiosensitizer were intimately associated with the target macromolecule. These pulse radiolysis studies have established that such compounds as nitroEB of high electron-affinity can be selectively incorporated into such key target macromolecules as DNA. Testing of the biological effects of such intercalating radiosensitizers will be important in evaluating the pharmacological utility of such potential chemotherapeutic agents.

An important application of binding studies is in the selection of dyes whose interactions are specific to a particular biopolymer and pulse radiolysis has been used to probe such binding specificity. Table 2 contains data for ethidium bromide binding to different model biopolymers. It is clear that some binding to protein, carbohydrate and lipid components does occur, but DNA intercalation is the major interaction. In the search for specific probes, several reagents have been screened for their binding properties with protein, nucleic acid, carbohydrate and lipid components (Table 3). Besides the specificity of ethidium bromide binding to DNA, quite specific reactions of the sulfhydryl reagent diamide with bovine serum albumin and of the fluorescent hydrophobic probe 8-anilino-1-naphthalene sulfonate (ANS) with oleate micelles and to a lesser extent with BSA are observed.

Besides its usefulness in the study of the interactions of selective reagents with biopolymers, the pulse radiolysis assay can be used to study the underlying physicochemical mechanisms of action of biologically active agents including drugs, antibiotics, antitumour agents, carcinogens and radiation modifiers. Table 4 shows how

Table 2
Ethidium bromide binding to model biopolymers

Biopolymers	$k_{e^-_{aq}}$ ($M^{-1}s^{-1} \times 10^{10}$	Binding
Control	4.0	
BSA	3.5	-
Myoglobin	1.3	+
Chondroitin sulfate	0.8	+
DNA	0.2	++
Stearate	1.0	+
Oleate	1.0	+

Table 3

Specificity of small molecule binding to model biopolymers

Small molecule	$k_{e^-_{aq}}$ ($M^{-1}s^{-1} \times 10^{10}$)				
	Alone	with protein[1]	with DNA[2]	with carbohydrate[3]	with lipid[4]
Ethidium bromide	4.0	3.5	0.2*	0.8	1.0
Diamide	2.8	1.8*	2.8	2.7	2.8
ANS	4.0	2.6	4.0	3.5	1.0*

[1] BSA

[2] Calf thymus DNA

[3] Chondroitin sulfate

[4] Oleate micelles

* Strong binding

Table 4

Kinetic parameters for screening the potential binding of various small molecules to DNA

Class	$k_{e^-_{aq}}$ ($M^{-1}s^{-1} \times 10^{10}$			
	Small molecule	Alone	with 0.1% DNA	Binding
Dyes	Acridine orange	2.3	0.1	++
	Proflavin	2.8	0.2	++
Metal ions	Cu	3.1	0.4	++
	Fe	6.0	0.6	++
Sensitizers	Nitrofurazone	2.8	1.5	+
	TAN	2.0	< 0.1	++
	Menadione	5.0	2.1	+
Protectors	Cysteine	1.0	1.0	-
Antibiotics	Actinomycin D	3.3	2.4	+
Antitumour agents	Adriamycin	6.0	< 0.1	++
	Bleomycin	5.0	< 0.1	++
Carcinogens	Acetylaminofluorene	1.6	0.6	+
	Benzo (a) pyrene	0.6	0.2	+
	Methyl cholanthrene	0.6	0.4	+
	β Naphthylamine	1.8	1.4	+

the kinetic binding assay reveals the strong binding to DNA of the mutagenic dyes acridine orange and proflavin, the metal ions Cu^{2+} and Fe^{3+}, the antitumour agents adriamycin and bleomycin and also the stable free radical triacetonamine-N-oxyl (TAN) which is an electronaffinic radiosensitizer.

These studies show that pulse radiolysis has the potential for studying a wide range of interactions between small molecules and biopolymers. The experiments are performed in situ, are not limited to fluorescent, coloured or radioactively labelled substrates, and do not necessitate the use of separatory techniques which may perturb some forms of binding.

References

/ 1/ M. Smoluchowski, Zeit. Physik. Chem., 92, 192 (1917)

/ 2/ P. Debye, Trans. Electrochem. Soc., 82, 265 (1942)

/ 3/ K. Schmidt, W. L. Buck, Science, 151, 70 (1966)

/ 4/ J. Jortner, Radiat. Res. Suppl., 4, 24 (1964)

/ 5/ G. O. Phillips, D. M. Power, C. Robinson, J. V. Davies, Biochim. Biophys. Acta., 295, 8 (1973)

/ 6/ C. L. Greenstock, G. W. Ruddock, Chem. -Biol. Interactions, 11, 441 (1975)

/ 7/ E. F. Gale, E. Cundliffe, P. E. Reynolds, M. H. Richmond, M. J. Waring "The Molecular Basis of Antibiotic Action" Ch. 5, J. Wiley and Sons, London, New York (1972)

/ 8/ C. L. Greenstock, G. W. Ruddock, Biochim. Biophys. Acta, 383, 464 (1975)

/ 9/ C. E. Adams, M. S. Cooke, Int. J. Radiat. Biol., 15, 457 (1969)

/10/ R. L. Willson, P. T. Emmerson in "Radiation Protection and Sensitization", ed. H. L. Moroson, M. Quintiliani, Taylor and Francis, London (1970)

/11/ C. L. Greenstock, I. Dunlop, Radiat. Res. 56, 428 (1973)

/12/ J. W. Hunt, C. L. Greenstock and M. J. Bronskill, Int. J. Radiat. Phys. Chem., 4, 87 (1972)

/13/ A. Scatchard, Ann. N. Y. Acad. Sci., 51, 660 (1949)

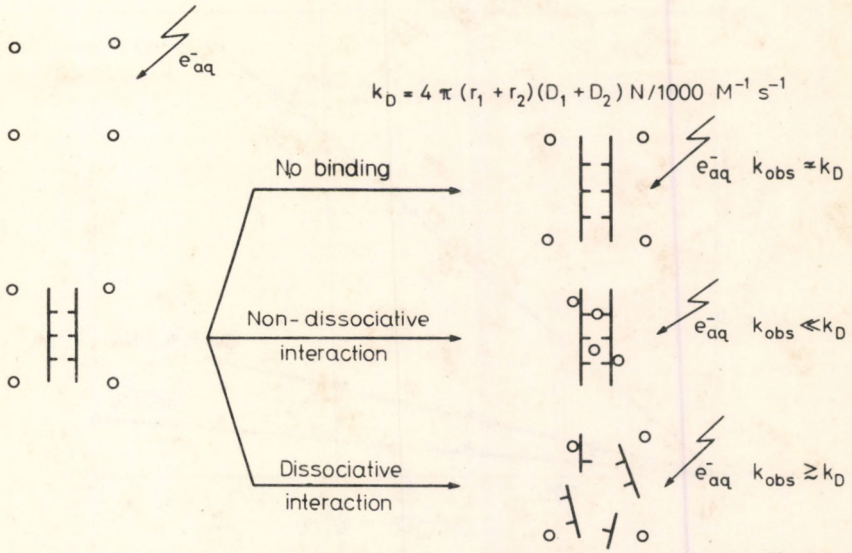

Fig. 1. Interaction of small molecules with biopolymers and the effect on small molecule reactivity.

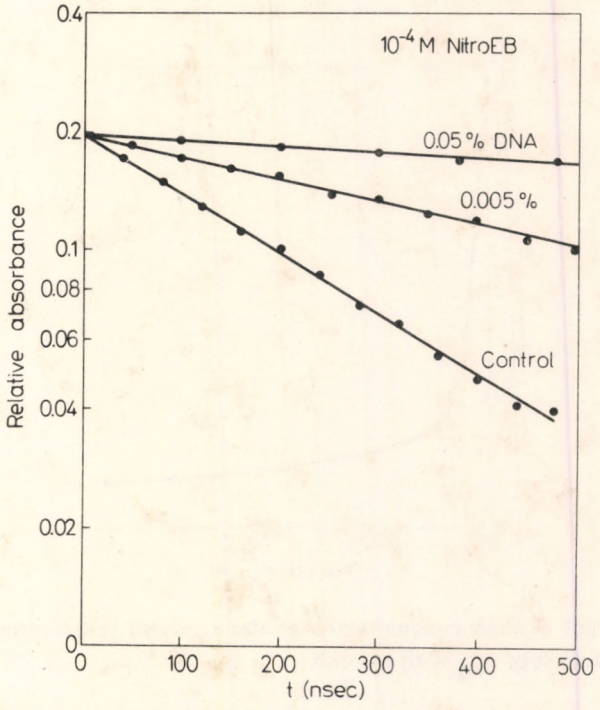

Fig. 2. Effect of DNA concentration on the rate of the reaction of e^-_{aq} with nitroEB

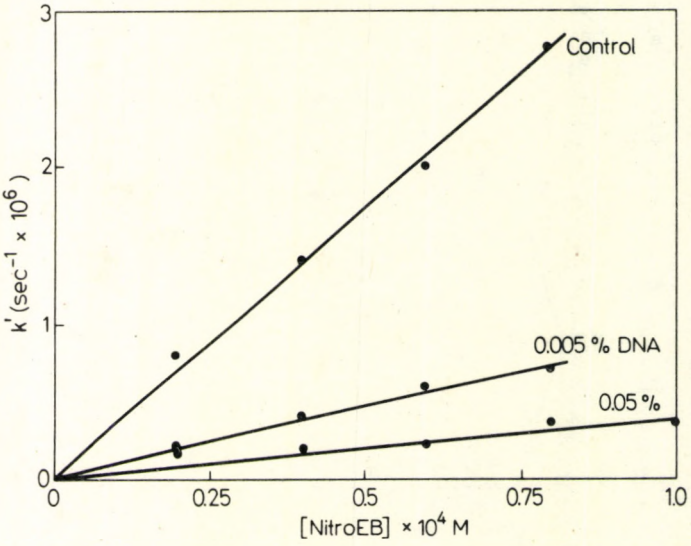

Fig 3. Variation in nitroEB reactivity towards e^-_{aq} as a function of nitroEB concentration, for solutions containing different DNA concentrations

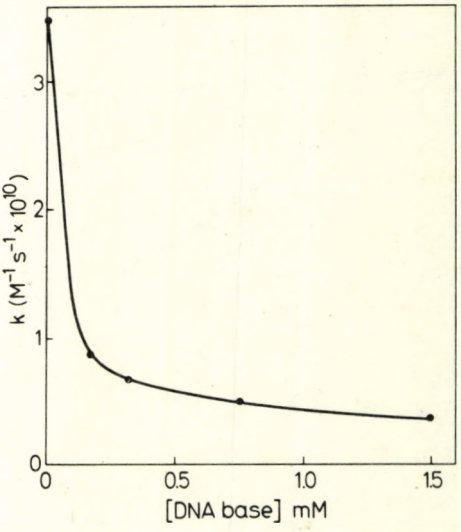

Fig. 4. Effect of DNA concentration on the apparent rate constant for the reaction of e^-_{aq} with nitroEB

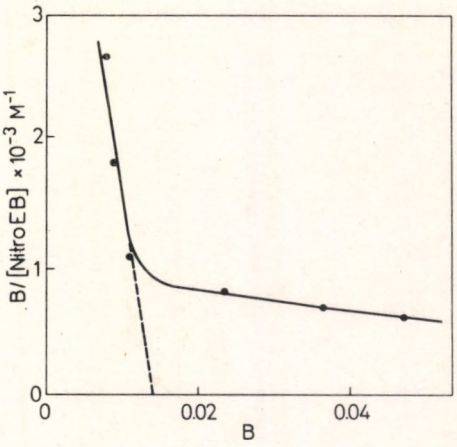

Fig. 5. Modified Scatchard plot for the binding of nitroEB to DNA

DISCUSSION

L. KEVAN

Can you postulate a structural model for the binding of ethidinium bromide to DNA with respect to making the Br less accessible to e^-_{aq} ?

C. L. GREENSTOCK

The ethidium bromide is intercalated in the wide grooves of DNA and the drop in e^-_{aq} reactivity is partly due to a decrease in diffusion following binding and also because it is partially buried. The use of different drug derivatives may help quantitate the structural aspects of the decreased reactivity. We are looking at different drug substitutes binding to different DNA conformational forms in order to understand the details of this binding.

APPLICATION OF PULSE RADIOLYSIS AND LASER PHOTOLYSIS TECHNIQUE IN STUDIES OF RADIATION INDUCED PROCESSES IN LIQUID PHASE

J. Bös, O. Brede, W. Helmstreit, R. Mehnert
Zentralinstitut für Isotopen- und Strahlenforschung der AdW der DDR, Leipzig, DDR

1. Apparatus

The application of pulse radiolysis together with the laser photolysis technique allows, in many cases, a better understanding of radiation induced processes. The main parameters of devices we used to study the mechanism and kinetics of radiation induced reactions in the liquid phase are given in Fig. 1 /1/.

Reactive species are generated by pulse radiolysis, laser photolysis or by a combination of both. Electron pulses from a Soviet-made pulse transformer accelerator of type ELIT-1A are absorbed in the sample contained in a quartz cell. The dose per pulse is 10 krad corresponding to an intermediary concentration of about 10^{-5} M at a G-value of one. The N_2-lasers used emit 10^{15} and 10^{16} quanta per pulse. If pulse radiolysis and laser photolysis are combined, the electron pulse is started first and the laser pulse is synchronized with a preset time delay /2/. It is thus possible to excite short-lived intermediaries and to observe their decay as a result of fluorescence or of other reactions.

The transients produced in the sample by irradiation are monitored by optical spectroscopy or conductivity measurements.

The equipment for the time-resolved optical spectroscopy consists of pulsed XBO 450 or XBO 900 lamp as the analysing light source, a usual quartz lens system, a monochromator SMP 2 from Carl Zeiss Jena, photomultipliers RCA 1 P 28, RCA 7102, EMI 9558 Q and a semiconductor photodiode SP 101 from VEB WF Berlin. The output from these detectors is fed into an oscilloscope of the type HP 183 A and the trace photographed.

The ions produced in the sample by electron or light pulses are detected by conductivity measurement. The conductivity changes are followed by the voltage-divider method which is schematically shown in Fig. 2. Voltage pulses on resistance R were recorded by the oscilloscope HP 183 A. The electrodes in the conductivity cell for pulse radiolysis are spaced with a variable distance from 0 to 3 mm, their area being 1 cm^2. Under the conditions: voltage U = 1 kV, resistance R = 50 Ω, electron mobility μ = 0.35 cm^2/Vsec and measurable voltage change of 20 mV one gets, for the minimum of the concentration to be detected, about 10^{-9} M. The time resolution of the device is defined by the length of the electron pulse and can be assumed to be longer than 10 nsec. The correspondent parameters of the cell for laser

photolysis are 2 mm and 0.54 cm^2. The detectable electron concentration is of the same order of magnitude. For the detection of the intermediates produced by the combination of pulse radiolysis and laser photolysis the equipment for optical spectrosocpy is used.

The fields investigated by the described methods are presented in the third column of Fig 1.

2. Results of experimental studies

2.1. Solvated electrons in hydrocarbons

In pulse radiolysis experiments with optical spectroscopy using semiconductor photodiode SP 101, amplifier and oscilloscope at room temperature and $\lambda = 1000$ nm the absorption of solvated electron was measured in n-hexane, cyclohexane and n-heptane. The time dependence of the absorption is shown in Fig. 3. Under the same conditions no absorption could be detected in isooctane. This fact is in accordance with the higher electron mobility in isooctane and the higher rate constant k_1 of the electron-cation-recombination reaction

$$RH^+ + e_s^- \longrightarrow \text{products} \qquad (1)$$

The recorded curves are similar to those of other authors /3,4/. From the decay kinetics the following values of the rate constant k_1 are calculated:

n-heptane:	4×10^{13} M^{-1} sec^{-1}
n-hexane:	6×10^{13} "
cyclohexane:	2×10^{14} "

The last two rate constants are in agreement with the values in /3,4/.

2.2 Detection of 3-methyl-cyclohexene cation

With the same equipment used in 2.1, the absorption spectrum of the 3-methyl--cyclohexene cation (Fig. 4) probably the dimer /5/ has been observed in a solution of 10^{-1} M 3-methyl-cyclohexene and 2×10^{-3} M CCl_4 in isooctane. The formation of cation is assigned to the transfer of positive charge from the solvent.

Here, we wish to thank Dr. Gy. Cserép of the Institute of Isotopes of the Hungarian Academy of Sciences for preparing the 3-methyl-cyclohexene samples.

2.3 Fast electron and photon-induced reaction in styrene solutions

a) Formation of styrene anion. 3 MW laser pulses with a wavelength of 337.1 nm generate electrons in a 10^{-4} M solution of N, N, N', N' -tetramethyl-paraphenylene-

diamine in cyclohexane by a two photon process

$$TMPD \underset{}{\overset{h\nu}{\rightleftharpoons}} TMPD^* \qquad (2)$$

$$TMPD^* \xrightarrow{h\nu} TMPD^+ + e^- \qquad (3)$$

The time dependence of electron concentration was determined by conductivity measurement and is given in Fig. 5a. In the presence of 10^{-5} M styrene appears a more rapid decrease of electron concentration (Fig. 5b) which may be assigned to the electron attachment reaction

$$St + e^- \longrightarrow St^- \qquad (4)$$

with the rate constant $k_4 = 4.5 \times 10^{12}$ M^{-1} sec^{-1}. For the electron attachment reaction to 1-methylstyrene and 1.1'-diphenylethylene the values 2.8×10^{12} M^{-1} sec^{-1} and 1.3×10^{12} M^{-1} sec^{-1}, respectively, are obtained.

b) Formation of styrene cation. The styrene dimer cation was observed in the pulse radiolysis of N_2O-saturated solution of styrene in cyclohexane by charge transfer from the solvent and subsequent ion-molecule reaction. The growth in absorption is shown in Fig. 6: styrene concentration is 1×10^{-3} M (curve 1) and 4×10^{-3} M (curve 2).

c) Fluorescence of styrene. The fluorescence of styrene was observed at 320 nm after exciting the solvent molecules by electron pulse irradiation

$$(C_6H_6)_2^S + St \longrightarrow 2\,C_6H_6 + St^S \qquad (5)$$

$$St^S \longrightarrow St + h\nu_f \qquad (6)$$

For a comparison Figs 7a and 7b show the Čerenkov emission of a 10^{-1} M solution of CCl_4 in benzene and the fluorescence of benzene at the same wavelength. The rate constant of the energy transfer reaction is $k_5 = (8.3 \pm 3.0) \times 10^9$ M^{-1} sec^{-1} and the lifetime τ_6 of styrene singlet is < 8 nsec.

2.4 Fluorescence of the excited ketyl radical

Electron pulses produce in a solution of 10^{-2} M benzophenone in cyclohexane the benzophenone triplet which forms ketyl radical by H abstraction from the solvent /6,7/

$$Ph_2CO^T + C_6H_{12} \longrightarrow Ph_2\dot{C}OH + \dot{C}_6H_{11} \qquad (7)$$

Spectrum and time dependence of the absorption at 540 nm of the ketyl radical are given in the Fig. 8a and 8b. Under the experimental conditions used the half-life of the ketyl radical and its extinction coefficient are $> 1\,\mu$sec and 3×10^4 M^{-1} cm^{-1},

respectively. The synchronized 0.2 MW laser pulse with a wavelength of $\lambda = 337.1$ nm was efficiently absorbed by ketyl radicals and caused their excitation. The fluorescence of ketyl radicals was observed at 570 nm (Fig. 8c)

$$Ph_2\dot{C}OH + h\nu_1 \longrightarrow Ph_2\dot{C}OH^S \quad (8)$$

$$Ph_2\dot{C}OH^S \longrightarrow Ph_2\dot{C}OH + h\nu_f \quad (9)$$

A calculation taking into account the final pulse length gives the fluorescence lifetime $\tau_9 = (2.0 \pm 0.3)$ nsec. The assumption that excited ketyl radicals are produced by this way is confirmed by the following facts: without electron pulses no fluorescence was detected at this wavelength, the intensity of the fluorescence is proportional to the dose of the electron pulse absorbed in the sample, and using different delay times the intensity of fluorescence is proportional to the time dependence of the absorption of the radical decay (Fig. 8d). The effectivity of the method can be increased if tunable pulsed lasers of the MW range are used.

References

/1/ D. Bertram, O. Brede, W. Helmstreit, R. Mehnert, Z. Chemie 15, 125 (1975).
/2/ R. Mehnert, O. Brede, W. Helmstreit, Z. Chemie 15, 447 (1975).
/3/ J. H. Baxendale, C. Bell, P. Wardman, Chem. Phys. Letters 12, 347 (1971).
/4/ J. H. Baxendale, C. Bell, P. Wardman, Faraday Transactions I, 69, 776 (1973).
/5/ B. Badger, B. Brocklehurst, Trans. Faraday Soc. 65, 2582 (1969)
/6/ E. Hayon, T. Ibata, N. N. Lichtin, S. Simic, J. Phys. Chem. 76, 2072 (1972).
/7/ O. Brede, W. Helmstreit, R. Mehnert, Z. physik. Chemie (Leipzig) 256, 505 (1975).

Initiating method	Detection method	Field of investigation
Pulse radiolysis	Optical spectroscopy	
electron accelerator ELIT-1A	photomultipliers	
-pulse length: 15 ns	- time resolution: 2-100 Msec	
-energy: 1 MeV	- spectral range: 230-1200 nm	
-pulse current: 20A	-sensitivity: >1% absorption change	primary reactions of aliphatic and aromatic olefines
	semiconductor photodiode:	
	-time resolution: 10 nsec	
	-spectral range: 500-1300 nm	charge transfer reactions
	-sensitivity: >0.1% absorption change	in hydrocarbons
	pulse oscilloscope:	
	-bandwidth: 250 MHz	
	-sensitivity: 10 mV/cm	
	Conductivity measurement.	
	-time resolution:>10 nsec	
	-detection threshold: 20 mV	
Laser photolysis	Optical spectroscopy	
-pulse length: 2;4 ns		
-wavelength: 337.1 nm		
-pulse power: 0.2; 3 Mw		
	Conductivity measurement	electron attachment
	-time resolution:≤2 nsec	reactions
	-detection threshold:≤2 mv	
Combination of pulse radiolysis and laser photolysis	Optical spectroscopy	fluorescence of the ketyl radical

Fig. 1. Apparatus for investigation of radiation induced reactions

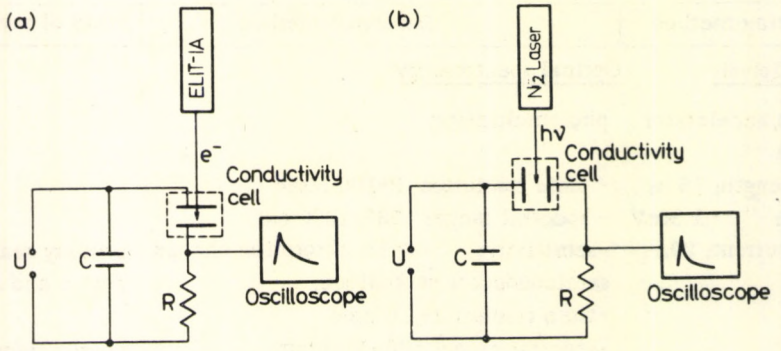

Fig. 2. Experimental arrangements for conductivity measurements: a) pulse radiolysis, b) laser photolysis

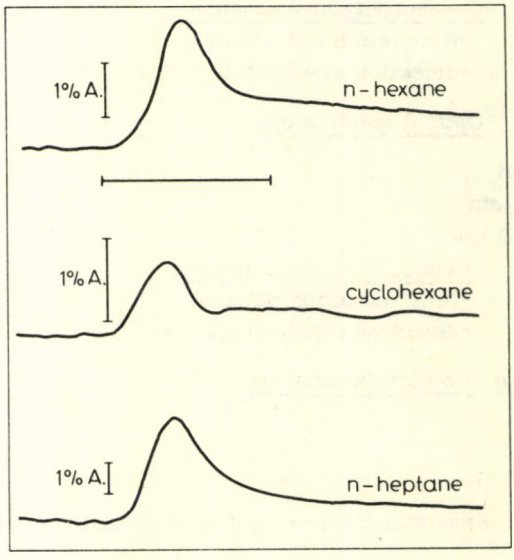

Fig. 3. Optical absorption of e_s^- as a function of time (λ=1000nm)

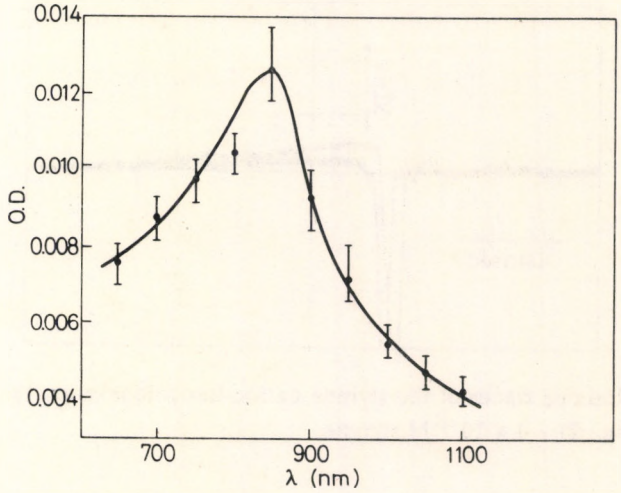

Fig. 4. Optical absorption spectrum of the 3-methyl-cyclohexene cation in isooctane

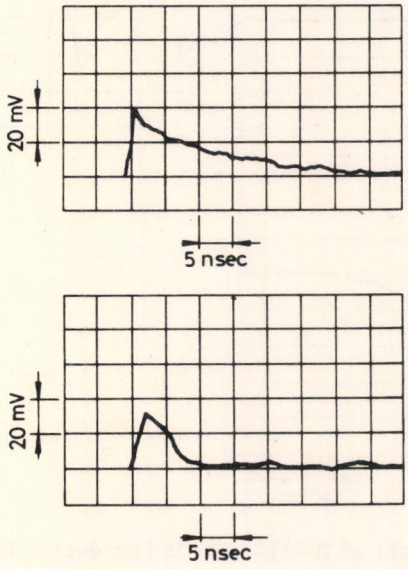

Fig. 5. Oscilloscope traces of e_s^-: a) in 10^{-4} M TMPD solution in cyclohexane, b) in 10^{-4} M TMPD solution in cyclohexane with 10^{-5} M styrene

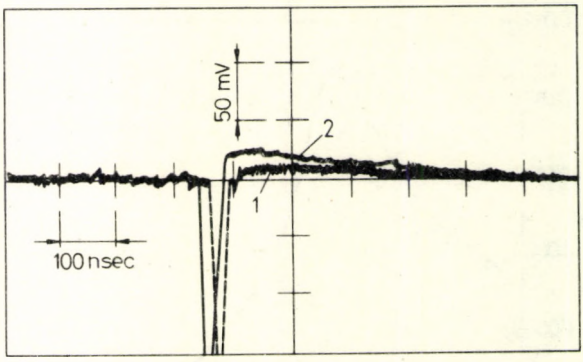

Fig. 6. Oscilloscope traces of the styrene cation in cyclohexane. 1) - 1 x 10^{-3}M styrene, 2) - 4 x 10^{-3} M styrene

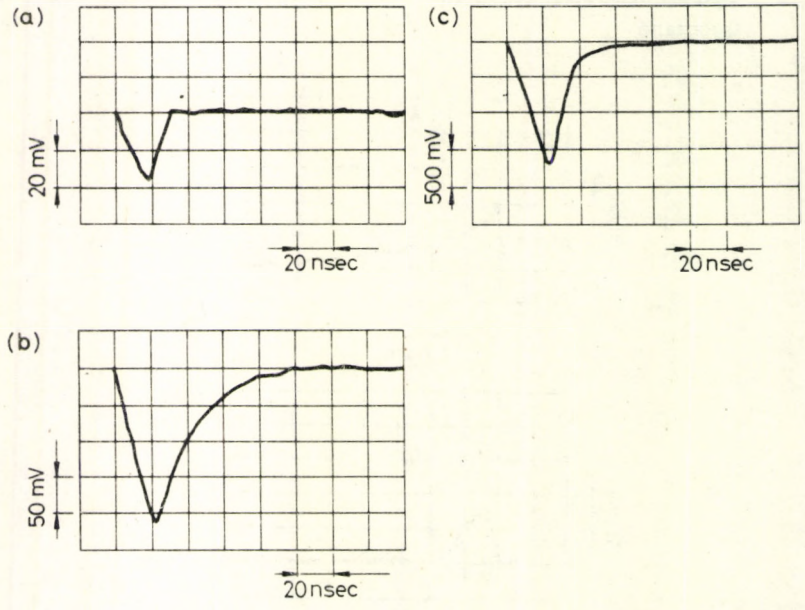

Fig. 7. a) Čerenkov light of 10^{-1} M CCl_4 in benzene: b) Fluorescence of benzene, c) Fluorescence of 10^{-2} M styrene in benzene (λ=320nm)

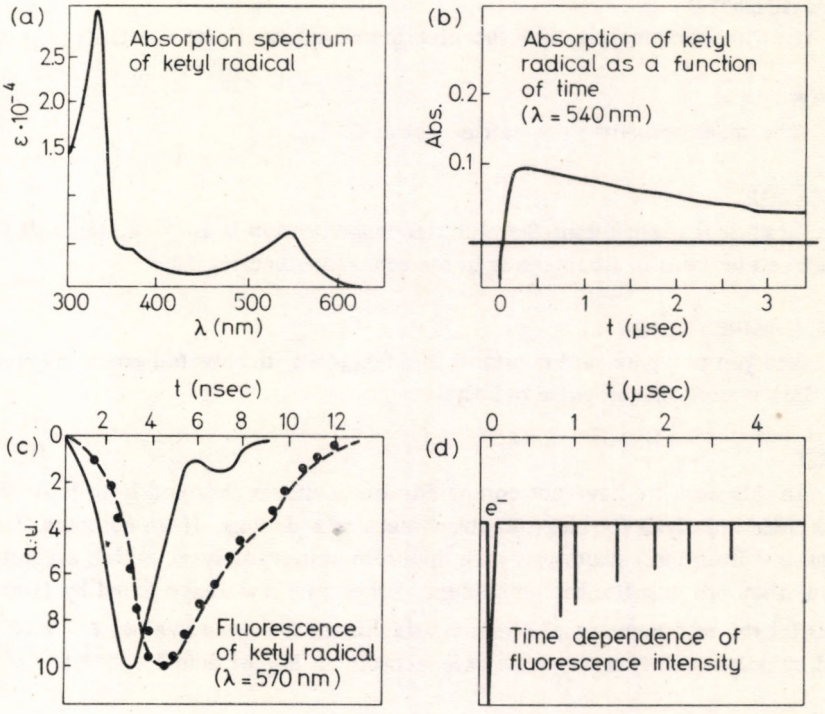

Fig. 8

DISCUSSION

R. SCHILLER

The electron-yield in iso-octane is higher than in normal hexane. Why does higher mobility prevent you from observing this higher concentration optically?

J. BÖS

The higher electron mobility in iso-octane leads to a rate constant of recombination which is much higher than that in h-hexane. If we assume a calculated value of 4×10^{15} $M^{-1}sec^{-1}$ for the rate constant of electron–cation recombination in iso-octane and an electron concentration of 10^{-6} M^{-1} the half life of the electrons is of the order of magnitude of 10^{-10} sec. The time resolution of our equipment is in the nanosecond range.

R. A. HOLROYD

At what temperature was the electron attachment rate constants (k_4) measured?

J. BÖS

The measurements were carried out at 20°C.

E. ZÁDOR

In optical experiments the electron concentration is 10^{-6} M, the half life of the free electrons in isooctane is in the subnanosecond region.

R. F. KHAIRUTDINOV

Did you compare rate constants of acceptors with solvated electrons produced by flash photolysis and pulse radiolysis?

J. BÖS

In this work we have not compared rate constants obtained from laser photolysis and pulse radiolysis for electron attachment to acceptors. If we compare the rate constants from laser photolysis with this from pulse radiolysis, which are not given here, they are in sufficient agreement. For example we have found by laser photolysis for the rate constant of electron attachment to pyrene a value, 4.5×10^{12} $M^{-1}s^{-1}$ and by pulse radiolysis the same rate-constant is higher than 1×10^{12} $M^{-1}s^{-1}$.

Z. P. ZAGORSKI

(1) From Fig. 8c it is visible that the pulse used has two peaks. What is the procedure of calculating the fluorescence of short duration?

(2) What was the length of laser beam path from the cell to the detector? If long, were any effects observed due to vibrations?

J. BÖS

(1) For calculating the fluorescence of short duration we applied the relation

$$a(T) = \int_0^T L(T - t) \exp(-t/\tau) dt$$

where T is the time, τ the lifetime of fluorescence, a(T) the measured time dependence of fluorescence, L(t) the shape of initiating laser pulse. Numerical calculation and comparison of measured and calculated curves has given the best value of τ.

(2) In these experiments the laser beam was not observed by the detector after passing the cell. The detector observed the analysing light from the XBO 450 lamp.

A COMPARATIVE STUDY OF RADIATION INDUCED OXIDATION OF HEPTENE-1 IN THE PURE ORGANIC PHASE AND AQUEOUS EMULSION

E. Kroó, L. Kovács, G. V. Putirskaya
Central Research Institute for Chemistry of the Hungarian Academy of Sciences,
1525 Budapest, Hungary

Early literature data on the oxidation of hydrocarbons in emulsion /1-4/ show that emulsification can accelerate the oxidation of organic compounds. Using emulsion polymerization as an analogy for emulsion-oxidation, one might expect that emulsification should cause rate enhancement. Briefly, the theory of emulsion polymerization /5-6/ has utilized the concept of isolation of the chain carriers in the soap micelle, thereby preventing termination. As has been demonstrated in the literature /7/, the initiation by γ-irradiation has distinct advantages in emulsion polymerization over chemical initiation realizing a steady and easily attenuated source of initiation and a lack of chemical contamination. By using irradiation technique and comparing emulsion and bulk oxidation of some organic materials, Saraeva and Yui-tai /8/, Hyde and Verdin /9/, Van Sickle et al. /10/ obtained data which contradict earlier literature observations and theoretical predictions, showing no significant difference between the two types of oxidation. Gebicki and Allen/11/ however, observed acceleration of the radiation induced oxidation of Na-linoleate when its concentration was higher than the critical micelle concentration.

It is obvious that one of the main complicating factors is the inhomogenity of the emulsion systems since reactions might occur in the dispersed oil phase, in the micellar phase, at the solute-solvent interfaces and in the bulk solvent. Unfortunately, topological considerations, that is, investigations on radiation induced oxidation processes in the distinct phases, are inadequate with the exception of aqueous solutions containing relatively readily soluble organic materials, mainly alcohols. Our present report deals with the radiation induced oxidation of heptene-1 in the pure organic phase (A), in aqueous solution (B) and in aqueous emulsion at relatively low concentration of the organic phase (C) containing no emulsifying agent.

Experimental

The irradiation of closed systems was carried out in neutral media at room temperature under atmospheric pressure at a continuous mixing of the system but allowing the organic layer above the aqueous phase not to break into droplets. Simulta-

neously, systems under oxygen pressure of 20 atm. were also irradiated in order to examine the effect of oxygen concentration expectedly having no influence on the oxidation process. Experimental data justified this assumption. A thin layer of heptene-1 above the aqueous phase was applied in order to maintain equilibrium concentration of heptene-1 in both the gaseous phase and the aqueous phase during oxidation. As analyses of this phase indicated, oxidation processes within this layer as well as transition of any oxidation product from the aqueous phase to the layer or in the opposite direction could be neglected. The γ-ray dose rate from ^{60}Co source was $4.2\text{-}15.7 \times 10^{16}$ eV/ml sec determined by ferrous ion dosimetry. Heptene-1 was purified by distillation and kept on metallic sodium.

Figure 1 demonstrates the concentration of heptene-1 vs time after switching off the emulsifying device (Type Biomix) producing polydisperse system (C). The dotted line represents the solubility of heptene-1 in water, that is, system B. Irradiation in case C was applied 15-20 minutes after having completed the emulsification when the concentration of the oil phase no longer decreased considerably.

Product analyses

System A: Oxidation products were measured by gas chromatography on Apieson L and Carbowax 4000 columns. In addition, hydroperoxide was also determined by polarography /12/.

Systems B and C: With the exception of hydrogen peroxide, no volatile products could be observed in this case as supported by gas chromatography. This enabled us to isolate the products by low temperature vacuum distillation. Part of the residue was dissolved in isopropanol separating the residue into two parts. After desiccation of the two fractions elementary composition and infrared spectra were measured. Hydrogen peroxide was determined by Ghormley's method /13/ with the modification that — in case C — isopropanol was added to the reagents in 1:4 ratio in order to dissolve the emulsion droplets. Isopropanol offers several advantages for the literature /14/. Hydrogen peroxide reacts very fast with iodine, but the organic peroxide reacts more slowly, thus hydrogen peroxide can be determined separately. In the presence of oxygen and heptene-1, however, the formation of iodine did not stop until the iodide had been consumed preventing the determination of organic peroxides.

Results and discussion

System A: With the exception of epoxy compounds we have observed the same compounds as Saraeva et al /15/. Figure 2 illustrates the accumulation of products while G values are demonstrated in Table 1. In the presence of an inhibitor (10^{-4}M jonol) only hydrogen peroxide formation can be observed, thus the rate of consumption of the inhibitor corresponds to the rate of initiation being $G = 1.29$. The G values for the products in Table 1 therefore indicate the occurrence of a chain process with a short chain length.

Table 1
G values of different oxidation products
of heptene-1 rad. ind. ox. in case A.

compound	G
hydroperoxide	3.21
heptene-1-on-3	2.51
*heptene-2-ol-1	1.49
heptene-2-al	0.36
heptene-1-ol-3	0.29

*not identified unambiguously

Results in aqueous environment (systems B and C): Two interesting results were found: (i) no difference was detected between oxidation processes in systems B and C, that is, in the presence or absence of oil droplets in the aqueous solution of heptene-1 and (ii) none of the oxidation products of case A (Table 1) could be observed. This means that reactions take place merely in the aqueous phase, a result which is in conflict with literature data /8/.

In our system, where the wall has a profound effect on the oxidation processes (see later) it can be excluded that radicals terminate before colliding with an oil droplet. A feasible explanation is that the hydrated oxy-radical cannot react with hydrophobic organic molecules. The fact, that – contrary to the oxidation in case A – no chain reaction occurs in aqueous phases supports this assumption. An amphiphile molecule on the surface of the oil droplet (an emulsifier agent) might possibly facilitate chemical reactions with the hydrated radical, e.g. by a transfer mechanism /10/.

Radicals which initiate chemical reactions, emerge only from water and scavenging from the spur by the solute molecules can be excluded by taking into account that chemical reactions do not take place in the oil droplets and the concentration of the dissolved heptene-1 is low enough ($< 10^{-3}$ M). e^-_{aq} and H$^\cdot$ will not be disttinguished and oxygen transforms them instantly to O_2^- and $HO_2^\cdot$. In the presence of N_2O, which transforms e^-_{aq} (H) to OH$^\cdot$, no surplus hydrogen peroxide formation could be observed, that is heptene-1 scavenges all the OH$^\cdot$ radicals. This is a result of the diffusion controlled OH$^\cdot$ addition to the double bond. Hydrogen abstraction is much slower and was not be taken into consideration. Addition and hydrogen abstraction by the $HO_2^\cdot$ (O_2^-) is also slow, these radicals therefore terminate or recombine yielding organic peroxide or hydrogenperoxide, respectively. One of the two end products in the residue after vacuum distillation of the reaction mixture was identified as a large molecular weight ketone-polyperoxide. The structure of the other product is unknown but elementary analyses showed a large inorganic content, mainly of potassium. It was reasonable to consider this fraction as a product of radical terminations

on the wall. G values for these two end products G(I) and G(II) have been calculated for C_7 carbon skeleton among the products indicating the number of heptene-1 transformed. Assuming no "carbon" loss during oxidation and distillation, the rate of the consumption of heptene-1 is:

$$-G(\text{heptene-1}) = G(I) + G(II)$$

We propose the following mechanism for the radiation induced oxidation of heptene-1 in aqueous solution:

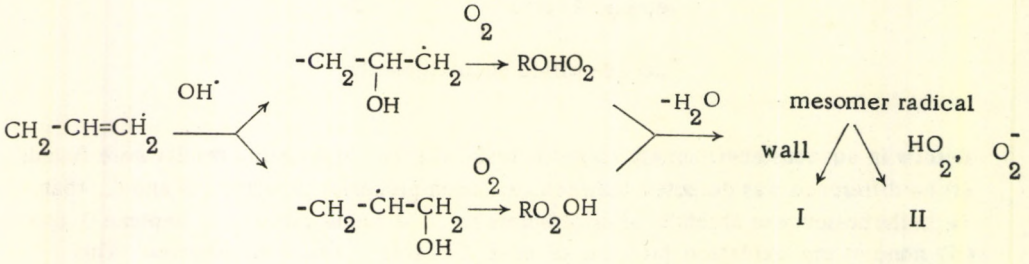

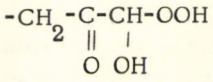

II. condensation polyperoxide

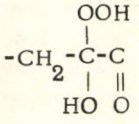

Water elimination step:

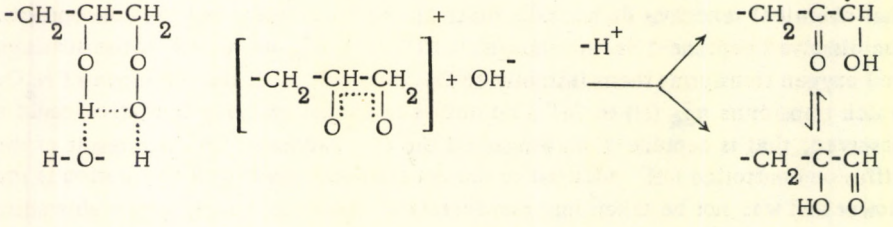

OH· addition to the α or β position is the first step of the oxidation and the radicals react with oxygen to form peroxy radicals. This is followed by a water elimination step. Similar kind of eliminations are well known in the literature /16, 17/. The formation of the mesomer radical can be interpreted by a tautomer rearrangement. This radical can either react on the wall giving the end product I or combine with

$HO_2^{\cdot}$ (O_2^-) radicals forming keto-hydroxy-hydroperoxide. We succeeded in isolating however, only one product of polycondensation of these compounds, a polyperoxide (end product II). As ether bonds could not be observed by i.r., condensation of the following type

$$-C-O-H + H-O-O-C- \longrightarrow -C-O-O-C- + H_2O$$

must be supposed.

This mechanism enables us to deduce the balance equations for the initiating radicals and molecular products:

$$G_{(HO_2+O_2^-)} - 2[G(H_2O_2) - G_{H_2O_2}] = G(II)$$

$$-G(\text{heptene-I}) = G(I) + G(II) = G_{OH}$$

which can be fulfilled by substituting our experimental values of $G(H_2O_2)=1,4$, $G(I)\sim$ ~ 0.8, $G(II)=1.5$ and literature data $G_{(HO_2^{\cdot}+O_2^-)} = 2.9$, $G_{OH}=2.3$, $G_{H_2O_2}=0.7$.

References

/ 1/ E.G.E. Hawkins, J.Chem. Soc. 2076 (1949).

/ 2/ G.P. Armstrong, R.H. Hall, D.C. Quin, J. Chem. Soc. 666 (1950).

/3,4/ R.V. Kucher, S.D. Kaz'min, Kinetics and Catalysis 2, 263 (1961), 3, 422 (1961).

/ 5/ F.A. Bovey, I.M. Kolthoff, A.I. Medelia, E.J. Mechon. "Emulsion Polymerization". Interscience Publishers, New York 1955.

/ 6/ C.P. Roe, Ind. Eng. Chem., 60, 30 (1969)

/ 7/ V.Stannett, J.A. Gervasi, J.J. Kearney, K. Araki, Division of Isotopes Development, AEC Document TID 24281, 1967.

/ 8/ V.V. Saraeva, T.Yui-tai, Kinetics and Catalyses 4, 725 (1963).

/ 9/ S.M. Hyde, D. Verdin, Trans. Faraday Soc., 64, 144, 155 (1968).

/10/ D.E. Van Sickle, D.G. Hendry, J.K. Castleman, C.W. Gould J.Org. Chem. 36, 3423 (1970).

/11/ J.M. Gebicki, A.O. Allen, J. Phys. Chem., 73, 2443 (1969).

/12/ M.F. Romantsev, D.S. Sydykova, V.V. Saraeva, Zh. Anal. Khim. 22, 1574 (1967)

/13/ C.J. Hochanadel, J.Phys.Chem., 56, 588 (1952).

/14/ V.R. Kokatnur, M. Jelling, J. Am. Chem. Soc., 63, 1432 (1941).

/15/ D.S. Sydykova, V.V. Saraeva, H.A. Bach, Khim. Vys. Energ., 8, 65 (1969).

/16/ C.E. Burchill, K.M. Perron, Can.J.Chem., 49, 2382 (1971).

/17/ K.M. Bansal, M. Cratzel, A. Henglein, E. Jonata, J. Phys. Chem., 77, 16 (1973).

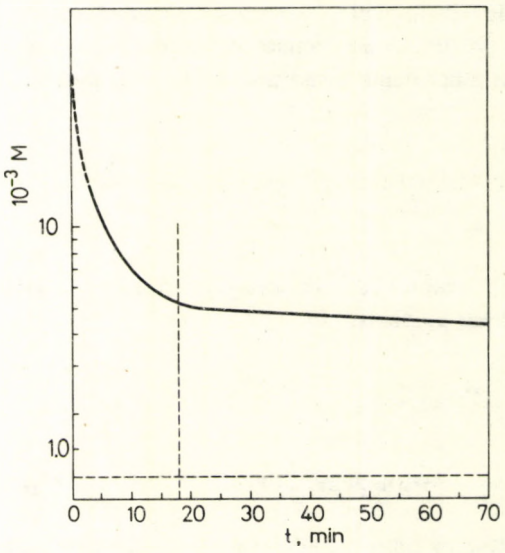

Fig. 1 Concentration of heptene-1: in --- system B and ——— system C

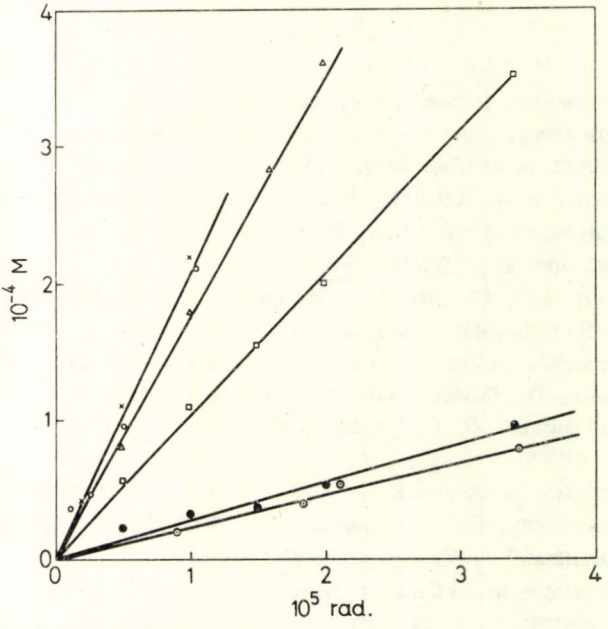

Fig. 2 Product accumulation in case A, ○ hydroperoxide by gas chromatography, × hydroperoxide by polarography, △ heptene-1-on-3, □ heptene-2-ol-1, ⊕ heptene-2-al, ⊙ heptene-1-ol-3

RADIOLYSIS OF ORGANIC COMPOUNDS IN DEAERATED AQUEOUS SOLUTIONS. 2-PROPANOL AND ACETONE IN THE PRESENCE OF FERROUS AND FERRIC IONS

Marcello Colosimo
Laboratorio di Chimica Nucleare, C.N.R., C.P. 10. 00016 Monterotondo Stazione, Rome, Italy

Introduction

The reactions between metal cations and organic radicals in aqueous solutions receive great attention from radiation chemists. On the contrary, little information is still available on the same subject, when iron ions are used at neutral pH. Because of the instability of iron ions in the aqueous medium in the presence of oxygen, radiation chemistry works are carried out either at acidic pH, or iron in the complexed state is used. Moreover, extensive studies are carried out regarding the problems of Fricke dosimetry. Thus, very little is known about the radiation chemistry of iron cations in aqueous solution at neutral pH, and, obviously, about their influence on the decay reactions of organic radicals under such conditions. In fact, after interval of several years only a brief communication has recently appeared, dealing with the radiolysis of iron (II) and iron (III) in aqueous solutions at neutral pH /1,2/. (It is, however, known from the programs that this topic will also be treated by other researchers during this symposium).

Results and discussion

In the following section some results are reported which were obtained from a study on the effects of adding iron(II) and iron (III) during the radiolysis of acetone and 2-propanol in a aqueous solution, free of oxygen, at neutral pH.

During all the experiments the mixtures were made up with triple distilled water under nitrogen stream and freshly prepared. The samples were irradiated in pyrex ampoules, sealed under the reduced pressure of 5×10^{-2} torr. The dose rate of the Cobalt gamma-source was 0.40 Mrad/h at about 300K.

Figure 1 shows that ferric sulphate solutions obey the Lambert-Beer's law, also in the absence of oxygen and in the presence of nitrogen at 304 nm within the range of the concentrations used during the following irradiations.

The irradiation of 1.00×10^{-4} M ferric sulphate results in the absence of any absorbance at 304 nm. On the ground of Stuglik and Zagórski's conclusions it is assumed that iron (III) is still present in the irradiated solutions, though in unknown concentrations. No guess can be made either about the concentration of iron (II), which forms at a diffusion-controlled-rate.

Figure 2 shows that during the irradiation of 1.01×10^{-4} M ferrous sulphate, ferric ions are produced and their build-up increases linearly with the irradiation time. Figure 3 presents the radiolysis of 7.83×10^{-3} M 2-propanol. The yields are reported as percentages.

Inverted triangles refer to the recovered 2-propanol in the pure 2-propanol solutions, squares and circles refer to the recovered 2-propanol and the acetone formed, when 0.98×10^{-4} M ferrous ions are added, triangles and crosses refer to the recovered 2-propanol and the acetone formed, when 2.00×10^{-4} M ferric ions are added. As it is shown, the presence of iron cations strongly effects the disappearance of 2-propanol and induces the formation of acetone. No great difference can be noticed after adding either ferrous or ferric ions. In both cases mass balance is obtained between acetone formed and 2-propanol disappeared. Figure 4 shows the radiolysis of 8.00×10^{-3} M acetone presented in the same way as 2-propanol in the previous figure. Crosses refer to the recovered acetone in the pure acetone solutions. Triangles refer to the recovered acetone, when 0.98×10^{-4} M ferrous ions are added; circles refer to the recovered acetone, when 2.00×10^{-4} M ferric ions are added. Also in this case, adding either of iron ions causes the same effect: it reduces the disappearence of acetone. No 2-propanol is found as a product of the radiolysis in all the experiments.

The processes in the reaction scheme given in Fig. 5 are those which occur during the radiolysis of 2-propanol and acetone in water, as established by a wide number of investigations /4-12/. One can see, that the α-2-propylalcohol-radical, also called acetone ketyl-radical, is the main organic intermediary.

Concluding remarks

From the present results some conclusions can be drawn:

(1) ferrous and ferric ions seem to be suitable to radiation chemistry works, even at neutral pH, provided that the presence of oxygen is avoided.

(2) the addition of either type of iron cations in the reported systems: a) the decomposition of the organic substrates is reduced, b) the formation of acetone from 2-propanol is induced, c) the formation of the other organic products is reduced.

Thus, it is suggested, that ferric ions oxidize α-2-propylalcohol-radical to acetone, also at neutral pH, and in the absence of oxygen.

The present results do not enable us to clarify the drastic protective action of iron ions and the disappearance of organic molecules other than 2-propanol and acetone. More experiments are in progress to gain further information of these effects.

References

/ 1/ H.A. Dewhurst, Disc. Faraday Soc. 1952, 225.
/ 2/ Z. Stuglik and Z.P. Zagorski, Radiochem. Radional. Letters, 22, 257 (1975).
/ 3/ R.C. Turner and K.E. Miles, Can.J. Chem., 35, 1002 (1957).

/ 4/ I. D. Draganic and Z. D. Draganic, The Radiation Chemistry of Water, Academic Press, New York and London, 1971.
/ 5/ G.E. Adams, Quad. Ric. Sci., CNR, Italy 68, 27 (1970).
/ 6/ K.-D. Asmus, A. Henglein, A. Wigger und G. Beck, Ber Bunsenges physik Chemie, 70, 756 (1966).
/ 7/ K. Eiben and R.W. Fessenden, J. Phys. Chem., 75, 1186 (1971).
/ 8/ N.B. Nazhat and K.-D. Asmus, J. Phys. Chem., 77, 614 (1973).
/ 9/ K.-D. Asmus, H. Möckel, and A. Henglein, J. Phys. Chem., 77, 1218 (1973).
/10/ W. Fessenden, J. Phys. Chem., 77, 2055 (1973).
/11/ B.C. Gilbert, R.O.C. Norman, and R.C. Sealy, J.C.S. Perkin II, 1973, 2174.
/12/ C. Walling and S. Kato, J. Amer. Chem. Soc., 93, 4275 (1971).

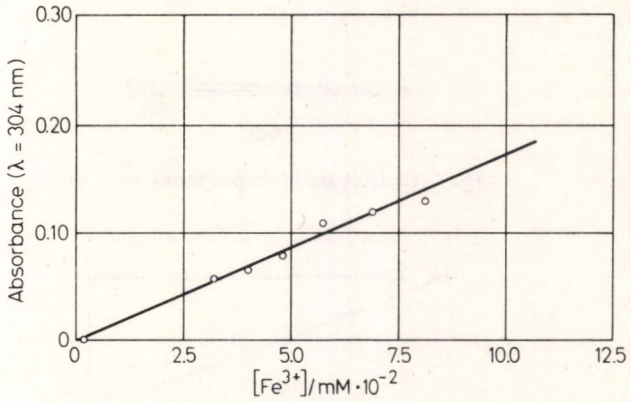

Fig. 1 Optical absorption vs. concentration plot for Fe (III) solutions

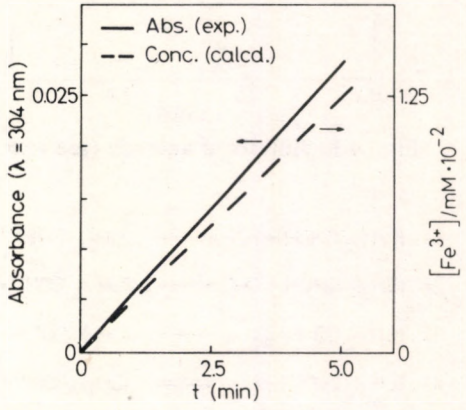

Fig. 2 Production of Fe (III) during irradiation

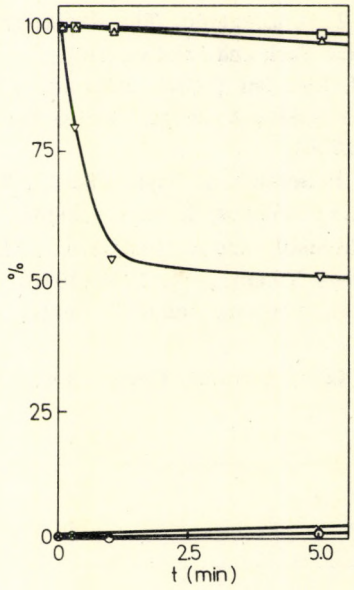

Fig. 3 Radiolysis of 2-propanol (see text)

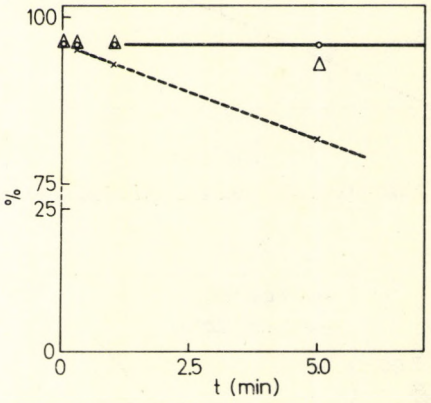

Fig. 4 Radiolysis of acetone (see text)

1) $(CH_3)_2CHOH + H^{\bullet} \longrightarrow (CH_3)_2COH^{\bullet} + H_2$

2) $(CH_3)_2CHOH + OH^{\bullet} \longrightarrow (CH_3)_2COH^{\bullet} + H_2O$

3) $(CH_3)_2CO + e^-_{aq} \longrightarrow (CH_3)_2CO^{\bullet -} + xH_2O$

4) $(CH_3)_2CO^{\bullet -} + H_2O \rightleftharpoons (CH_3)_2COH^{\bullet} + OH^-$

Fig. 5

Z. P. ZAGORSKI

(1) What was the pH of the solution after the irradiation? If Fe(III) was present at the beginning, did you observe the increase of pH?

(2) What were the final products of oxidation? Was the oxidation going as deep as to produce organic acids, which may change the pH?

M. COLOSIMO

(1) The pH of the solutions was not measured after irradiation. At the ion conversions used it was assumed that no significant pH change took place.

(2) During the radiolysis, the mass balance of organic compounds (2-propanol and acetone) was obtained in 2-propanol solutions, in the presence of iron ions. In the acetone solution, only in one case did the presence of iron ions cause a decrease in the acetone destruction. So it was assumed that in the presence of iron ions no carbon containing compounds other than acetone and 2-propanol played important roles, also because of the low conversions used during this work.

G. R. FREEMAN

Did you measure the G-values of Fe^{2+} and acetone?

M. COLOSIMO

No, I did not. I reported only the yields of the organic materials as a percentage. Anyway, the G-value for acetone is about 1.2×10^{-2}, calculated at the higher conversion (Fig. 3) and in the presence of added ferrous ions.

RADIOLYTIC OXIDATION OF p-XYLENE IN WATER-EMULSION

I. Matus, G. V. Putirskaja
Central Research Institute for Chemistry of the Hungarian Academy of Sciences,
Budapest, Hungary

As is known, the radiation-initiated oxidation of hydrocarbons shows increased efficiency and selectivity in polar media /1–5/. Owing to the low solubility of these compounds in polar solvents, attention has been focused on emulsions in the hope of finding chain reactions in the oxidation of hydrocarbons similar to those observed in the polymerization of some monomers, Since the oxidation of hydrocarbons also proceeds by a free-radical mechanism, the chain mechanism may be attributed to a decrease in the probability of chain termination due to the recombination of radicals in the droplets of the emulsion. The use of alkyl aromatic compounds seemed to be advantageous because of the low amount of byproducts formed. The advantage of the initiation of oxidation by radiation is that no formation of by-products and decrease in their concentration needs to be taken into consideration.

Para-xylene water emulsions were prepared for the experiments by the use of ultrasonic vibrations. The concentration of p-xylene was between $2 \cdot 10^{-2} - 5 \cdot 10^{-2}$ M without any coalescence. Because of the low concentration of p-xylene no direct effect of radiation, only the reactions of primary particles formed in the water had to be taken into consideration:

$$H_2O \longrightarrow H,\ e^-_{aq},\ OH,\ H_2,\ H_2O_2$$

The oxidation of p-xylene was studied under two different conditions:

1. oxidation by $OH^{\cdot}$ radicals
2. oxidation by $HO_2^{\cdot}$ and $OH^{\cdot}$ radicals

In the first case the primary reducing particles were transformed into $OH^{\cdot}$ radicals by N_2O /6, 7/.

$$e^-_{aq} + N_2O \xrightarrow{H_2O} OH^{\cdot} + OH^- + N_2$$

$$(k = 8.67 \times 10^9 M^{-1} s^{-1})$$

$$H + N_2O \longrightarrow N_2 + OH^{\cdot}$$

$$(k = 1.25 \times 10^{4} M^{-1}s^{-1})$$

$$G(OH) = 6 \text{ molecules/100 eV}$$

In the second case, the emulsions were saturated with 20 atm O_2. In neutral solution the reactions are as follows /8, 9/:

$$e^-_{aq} + O_2 \longrightarrow O_2^- \overset{H_2O}{\rightleftharpoons} HO_2^{\cdot}$$

$$(k = 1.9 \times 10^{10} M^{-1}s^{-1})$$

$$H + O_2 \longrightarrow HO_2^{\cdot} \rightleftharpoons O_2^-$$

$$(k = 2.1 \times 10^{10} M^{-1}s^{-1})$$

A pressure vessel was used for the experiments, the saturations were accomplished by N_2O at 4 atm (0.1M) /10/, or with O_2 at 20 atm (2.6×10^{-2}M). The samples were irradiated with ^{60}Co γ-rays at a dose rate of 1.56×10^{17} eV/ml × min. The hydrogen peroxide was determined by the modified method of Ghormley /11/, and the organic products were analysed on a gas chromatograph. The products of oxidation by $OH^{\cdot}$ radicals are shown in Fig. 1. During oxidation, the accumulation of H_2O_2 can be seen with the same yield as the molecular quantities: $G(H_2O_2) = 0.70$ molecules/100 eV. The G-values of the p-tolubenzyl alcohol and p-tolualdehyde are almost the same, their accumulation at the beginning of irradiation is followed by a decrease in their concentration at a higher dose. The rate of p-toluic acid accumulation is constant with a value of G = 5.51 molecules/100 eV. p-Toluic acid is a product of the further oxidation of intermediates and seems to be formed by a chain mechanism. To ascertain the reaction-mechanism, two types of acceptors for OH radicals have been used: isopropanol and stable iminoxyl radical ($VR^{\cdot}$): 2, 2, 5, 5-tetramethyl-4-phenyl-3-imidazolin-3-oxid-1-oxyl /12/. Although the concentration of isopropanol was changed between 10^{-4} and 10^{-2} M, the yields were strongly reduced only at 10^{-2} M to a value of $G(H_2O_2) = 0.18$ molecules/100 eV. The yields of p-tolubenzyl alcohol and p-tolualdehyde decreased by a factor of two in solutions containing no isopropanol, and the yield of p-toluic acid isopropyl ester found instead of p-toluic acid was: G = 3.21 molecules/100 eV.

The stable iminoxyl radical in 10^{-3} M concentration had no effect on the formation of H_2O_2, but the yield of p-toluic acid decreased by a factor of three in emulsion containing no acceptor: G = 1.80 molecules/100 eV. Fig. 2. shows the products of oxidation obtained in the emulsion saturated with 20 atm oxygen. Comparison of the two processes has been made in Table 1. Linear accumulation of peroxides can be

Table 1

G values from radiolysis of p-xylene in water-emulsion

Products	t, (h)	N_2O, 4 atm	O_2, 20 atm	10^{-3} M i-propanol		10^{-3} M VR'	
				N_2O, 4 atm	O_2, 20 atm	N_2O, 4 atm	O_2, 20 atm
H_2O_2	2	0.7	1.60	0.66	1.60	0.70	1.28
	15	0.6					
p-tolubenzyl alcohol	2	0.23 − 0.13	0	0.20	0.05	0.06	0
	15	0.1					
p-tolualdehyde	2	0.25 − 0.15	1.54 − 0.3	0.23	0.20	0.12	0.1 − 0.22
	15	0.1					
p-toluic acid	2	5.51	4.54	0	0	1.80	1.33
	15	4.28					
p-toluic acid isopropylester	2	0	0	2.57 − 5.63	0	0	0

seen with a value of $G = 1.60$ molecules/100 eV which, according to analytical results, is mostly H_2O_2. The decomposition of alkyl-aromatic hydroperoxide compounds in aqueous solution is probably very fast. The quantity of p-tolubenzyl alcohol is hardly detectable. The formation of p-tolualdehyde is considerable at the beginning of the reaction: $G(RHO) = 1.54$ molecules/100 eV, but its concentration on further irradiation gives a constant value. The yield of p-toluic acid is somewhat smaller than was found in an N_2O atmosphere: $G(ROOH) = 4.54$ molecules/100 eV. Isopropanol at a concentration of $10^{-4} - 10^{-3}$ M has no effect on the yield of H_2O_2, but reduces the formation of carbonyl compounds to half of its value, while no formation of p-toluic acid (ester) could be observed at all.

The presence of iminoxyl radicals (which do not react with $HO_2^{\cdot}$ radicals) /13/ does not give rise to alcohols, changes the accumulation of p-tolualdehyde and decreases the amounts of p-toluic acid by a factor of three.

Comparison of p-xylene oxidation in water emulsion with different radicals, leads to surprising results. In the emulsion saturated with N_2O, the formation of one molecule p-toluic acid requires 6 $OH^{\cdot}$ radicals, according to the usual mechanism:

$$RH_3 + OH^{\cdot} \longrightarrow RH_2 + H_2O$$

$$\dot{R}H_2 + OH^{\cdot} \longrightarrow RH_2OH$$

$$RH_2OH + OH^{\cdot} \longrightarrow \dot{R}HOH + H_2O$$

$$RHOH + OH^{\cdot} \longrightarrow RHO + H_2O$$

$$RHO + OH^{\cdot} \longrightarrow RO^{\cdot} + H_2O$$

$$RO^{\cdot} + OH^{\cdot} \longrightarrow R{=}O{-}OH$$

With a yield of p-toluic acid as high as 5.51 molecules/100 eV, this mechanism would require a value $G(OH^{\cdot}) = 33$. In the case of a complete transformation of radicals formed in water into $OH^{\cdot}$, we have only a sixth part of the above value. This shows that in the case of a large amount of N_2O, the mechanism of oxidation is something different from that described above. The H_2O_2 does not take part in the chain reaction, as can be seen from its constant G-value. The oxidation mechanism in the presence of large amount of N_2O is not clear yet (e. g. in the case of toluene). In our opinion the N_2O molecules also take part in the mechanism. Dainton and coworkers /14/ investigated the reaction of the $H^{\cdot}$ atom with N_2O, in which the O atom is split off the N_2O by the $H^{\cdot}$ atom ($k = 2.7 \times 10^7 M^{-1}s^{-1}$). By

analogy, the next reaction may be supposed (cf. Ref /15/):

$$H^{\cdot} + N_2O \longrightarrow N_2 + OH^{\cdot} \qquad Q = 55 \text{ kcal/mol}$$

$$RH_3 + OH^{\cdot} \longrightarrow \dot{R}H_2 + H_2O$$

$$\dot{R}H_2 + N_2O \longrightarrow \dot{R}H_2O + N_2 \qquad Q = 35 \text{ kcal/mol}$$

$$E^x = 2.75 \text{ kcal/mol}$$

$$\dot{R}H_2O + RH_3 \longrightarrow RH_2OH + \dot{R}H_2$$

$$R = C\,C_6H_4CH_3$$

The reaction in the emulsion may also proceed inside the p-xylene droplets, where the concentration of N_2O is high compared to that of p-xylene.

The iminoxyl radical (unlike isopropanol) not only competes with $OH^{\cdot}$ radicals, but also accepts the alkyl radicals, which can be seen from the decrease in the p-toluic acid yield.

The oxidation of p-xylene in the presence of oxygen may occur by initiation with $OH^{\cdot}$ and $HO_2^{\cdot}$ radicals as shown in the following scheme:

$$RH_3 + \begin{cases} HO_2^{\cdot} \\ OH^{\cdot} \end{cases} \longrightarrow \begin{matrix} H_2O_2 \\ H_2O \end{matrix} + RH_2$$

$$\dot{R}H_2 + O_2 \longrightarrow RH_2OO^{\cdot}$$

$$RH_2OO^{\cdot} + RH_3 \longrightarrow RH_2OOH + \dot{R}H_2$$

$$2\,RH_2OO^{\cdot} \longrightarrow RH_2OH + RHO + O_2$$

$$RH_2OOH \longrightarrow \dot{R}H_2O + OH^{\cdot}$$

$$\dot{R}H/OH/ + HO_2^{\cdot} \longrightarrow RH\begin{matrix} OOH \\ OH \end{matrix} \xrightarrow{+RHO} 2R{=}\begin{matrix} O \\ OH \end{matrix}$$

Detection of the transient hydroperoxides may be hindered by their fast decomposition in water. In the oxygen-saturated emulsion the two types of acceptors applied have different effects on the yield of products.

Isopropanol accepts both the $OH^{\cdot}$ and $HO_2^{\cdot}$ radicals, decreases the yield of aldehyde by half and prevents the formation of p-toluic acid.

In the case of the iminoxyl radical as a good $OH^{\cdot}$ acceptor, the formation of p-toluic acid may occur by the initiation of $HO_2^{\cdot}$ radicals not only through $H^{\cdot}$

atom abstraction but via the combination with R radicals as well:

$$R^{\cdot} + HO_2^{\cdot} \longrightarrow ROOH$$

$$\dot{R}HOH + HO_2^{\cdot} \longrightarrow RH\begin{matrix}OOH\\OH\end{matrix} \xrightarrow{+RHO} 2\,ROOH + H_2$$

Comparing our results with the oxidation of toluene in aqueous solution /4/, we may draw the following conclusion: in the case of the xylene molecule the second CH_3 group blocks the oxidation of the benzene ring. In the case of toluene benzoic acid was obtained in the O_2 saturated solution with a yield as low as $G = 1.1$ molecules/100 eV, with N_2O in the solution neither acid nor aldehyde could be measured,

Compared with the pure organic phase /16/, the main advantage of p-xylene oxidation in water emulsion is that p-toluic acid is formed at room temperature, whereas in organic phase only hydroperoxide, alcohol and aldehyde are formed. This supports the assumption that the oxidation of p-xylene is more advantageous in water emulsion than in the pure organic phase.

References

/ 1/ I. N. Komarov, N. M. Baranova, Zh. fiz. khim., 202, 629 (1972)
/ 2/ V. V. Sarayeva, Tscin-Yuy Tay, Kinetika i kataliz 4, 823 (1963).
/ 3/ V. V. Sarayeva, T. V. Onopko, N. P. Kostromin, Report on 3rd All-union Conference on Liquid Phase Oxidation of Organic Compounds, Minsk, 1975.
/ 4/ H. C. Christensen, R. Gustafsson Acta Chemica Scand. 26, 937 (1972).
/ 5/ Dale E. Van Sickle, Dale G. Hendry, Jane K. Castleman, Constance W. Gould, J. Org. Chem., 36, 3423 (1971).
/ 6/ S. Gordon, E. J. Hart, M. S. Matheson, J. Rabani, J. K. Thomas, Disc. Faraday Soc., 36, 193 (1963).
/ 7/ F. S. Dainton, S. A. Sills, Prog. Chem. Soc., 223, (1962).
/ 8/ S. Gordon, E. J. Hart, M. S. Matheson, J. Rabani, J. K. Thomas, J. Am. Chem. Soc., 85, 1375 (1963).
/ 9/ S. Gordon, E. J. Hart, J. K. Thomas, J. Phys. Chem., 68, 1262 (1964).
/10/ E. Hayon, "Radiation Chemistry of Aqueous Solutions" ed. G. Stein, Jerusalem 1967. p. 157.
/11/ G. J. Hochanadel, J. Phys. Chem., 56, 588 (1952).
/12/ L. V. Bolodarskiy, G. A. Kutikova, Izv. A. N. SSSR, Ser. Khim. No 5, 937 (1971).
/13/ Putirskaja G. V., Matus I., Muratbekov M. B., Rockenbauer A., Acta Chim. in press.
/14/ F. S. Dainton, D. C. Walker, Proc. Roy. Soc., A285, 339 (1965).
/15/ N. M. Emanuel, D. G. Knorre, Chemical Kinetics (in Russian) 1974, p. 128.
/16/ P. N. Komarov. Zh. Fiz. Khim. 40, 243 (1966).

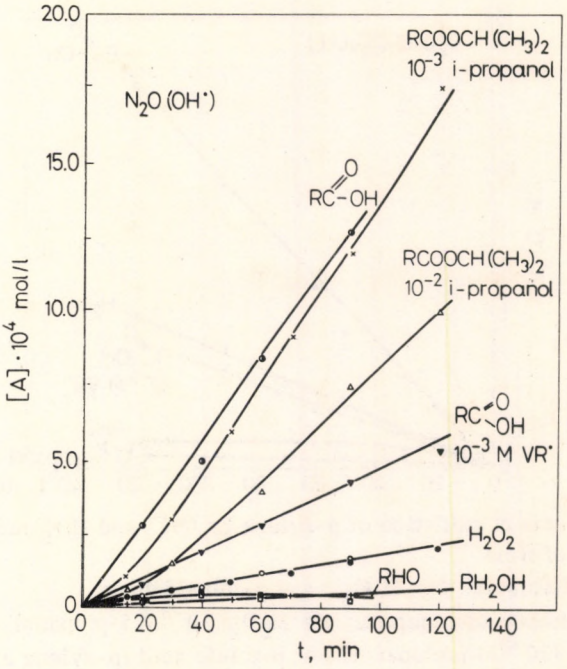

Fig. 1 The products of oxidation of p-xylene by OH· radicals as a function of time. Without acceptors: ● = p-toluic acid, ○ = H_2O_2, + = p-tolubenzyl alcohol, □ = p-tolualdehyde.
In the presence of acceptors: × = p-toluic acid isopropylester (10^{-3}M i-propanol) △ = p-toluic acid isopropylester (10^{-2}M i-propanol) ▼ = p-toluic acid (10^{-3}M iminoxyl radical) ● = H_2O_2 (10^{-3} iminoxyl radical)

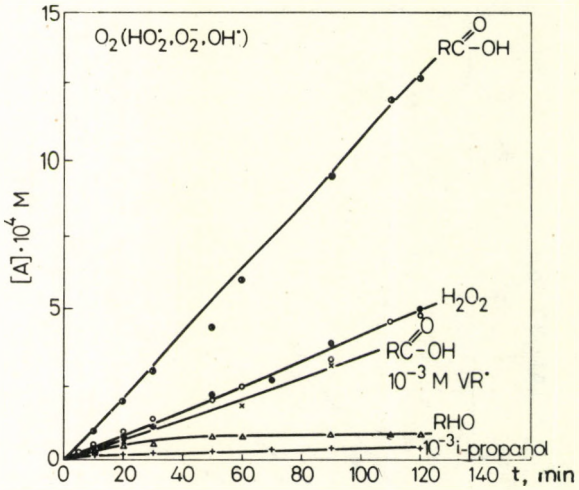

Fig. 2 The products of oxidation of p-xylene by $OH^{\cdot}$ and $HO_2^{\cdot}$ radicals as a function of time.
◑ = p-toluic acid, ○ = H_2O_2, △ = p-tolualdehyde.
In the presence of acceptors: ● = H_2O_2 (10^{-3}M i-propanol) + = p-tolualdehyde (10^{-3}M i-propanol) × = p-toluic acid (p-xylene emulsion containing 10^{-3}M iminoxyl radical)

DISCUSSION

G. R. FREEMAN
What was the temperature of the system?

I. MATUS
Investigations were carried out at room temperature.

G. R. FREEMAN
The reaction of N_2O with the organic radical indicates the occurrence of a chain. What was the chain length?

I. MATUS
It was about 4.

G. CHIRAKADZE
What is the solubility of p-xylene in water?

I. MATUS
At room temperature it is 1.2×10^{-3}M.

REGULARITIES IN THE O^-, O_2^-, O_3^- REACTIONS WITH HOMOLOGUES OF ORGANIC CATIONS

J. P. Suwalski, K. Bobrowski, Z. P. Zagórski
Department of Radiation Chemistry, Institute of Nuclear Research, Warsaw, Poland

Introduction

Our paper is devoted to studies on regularities in the O^-, O_2^-, and O_3^- reactions with homologues of tetraalkylammonium cations, symbolized in this paper by R_4N^+.

No data are available on the reactivity of these cations with primary and secondary products of water radiolysis. The direct measurements of changes in concentrations of species involved is practically impossible because in the U. V. below 300 nm the spectrum is not accessible for investigation. Cations of R_4N^+ show peaks from 210–220 nm (changing from tetramethyl to tetrabutylammonium hydroxide).

Therefore our investigations are based on the competition reactions of O_2 and R_4N^+ for O^- observed by pulse radiolysis on the other hand of the measurement of O_3^- formed in the reaction $O_2 + O^-$. The overall consumption of O_2 calculated as G_{-O_2} yields, was measured polarographically.

Experimental

All irradiations were performed with the beam of electrons of the linear electron accelerator LAE 13/9 operating in our laboratory in the Institute of Nuclear Research. The particular electron source and irradiation arrangement used in our laboratory have been described in Ref. /1/. All R_4N^+ hydroxides were checked for purity by spectrophotometric and polarographic methods. The different concentrations of O_2, N_2O and R_4N^+ in the solutions were adjusted by mixing in syringes. To avoid the absorption of CO_2 all alkaline solutions were prepared in CO_2-free glove box. The technique of O_3^- measurements is described in Ref. /2/.

Results

The reactivity of the oxide radical-ion O^- and the decay kinetics of the ozonide ion O_3^- have been investigated in aqueous solutions at pH 12.8 containing tetramethyl, tetraethyl, tetrapropyl and tetrabutylammonium ions, O_2 and N_2O by the pulse radiolysis method.

Figure 1 shows the resulting rate constants of tetraalkylammonium cations with O^- as a function of the chain length of the substituent in R_4N^+. Observed rate constants of the decay of O_3^- follow, of course, a similar pattern because the decay of O_3^- depends on the removal of O^-.

The observations of decay curves of the superoxide ion in a solution containing various concentrations of tetraalkylammonium cations and oxygen but without N_2O permits the determination of the rate constants for the reaction of O_2^- with tetraalkylammonium cations /3/.

Figure 2 shows the resulting rate constants of O_{2+}^- with these cations also as a function of the chain length of the substituent in R_4N^+. The G_{-O_2} value in different R_4N^+ solutions is shown in Fig. 3.

Discussion

Since the radiation chemistry of the tetraalkylammonium hydroxides in aqueous solutions has not been investigated yet, the only discussion of regularities may concern the closest analogue, which is the radiation chemistry of amines. The results are presented in Table 1 together with previously published k-values for amines.

One can see that the rate constants of amines with O^- show a rising trend similar to the present systems. However, contrary to tetraalkylammonium cation the rate constants of O^- with amines are close to being diffusion controlled $k \sim 10^{10}$ $M^{-1}s^{-1}$. The rate constants of O^- with tetraalkylammonium cations may be compared rather to the rate constants of OH with protonated amines.

Table 1

Rate constants ($M^{-1}s^{-1}$) for the reaction of OH with protonated (RNH_3^+), OH (and O^-, respectively) with unprotonated (RNH_2) aliphatic amines /5, 6/ and O^- with tetraalkylammonium cations in aqueous solutions

Amine	$k(OH + RNH_3^+)$	$k(OH + RNH_2)$	$k(O^- + RNH_2)$	Tetraalkyl-ammonium cations	$k(O^- + R_4N^+)$
Methyl-amine	0.12×10^9	4.2×10^9	7.5×10^9	tetramethyl	0.3×10^9
Ethyl-amine	0.50×10^9	6.2×10^9	8.65×10^9	tetraethyl	1.0×10^9
Propyl-amine	1.3×10^9	7.2×10^9	9.85×10^9	tetrapropyl	1.3×10^9
Butyl-amine	3.7×10^9	8.3×10^9	13.5×10^9	tetrabutyl	2.2×10^9

Possible R_4N^+ reaction with O_3^- was more closely investigated. The analysis of the decay curves of the ozonide ion with various concentration of R_4N^+ makes us conclude that all reactions of O_3^- studied have the same general character. They all involve as a rate-determining step the O_3^- dissociation into O^-. While O_3^- is rather unreactive towards R_4N^+ cations, the O^- radical ion is the reacting species in all reactions. This analysis also confirms the mechanism of Behar and Czapski /7/.

The dependence of the rate constants of O_2^- with tetraalkylammonium cations is remarkable and needs some comment.

In solutions without N_2O, when O_2^- was formed, we observed the build-up of a spectrum after the pulse that was identical to the spectrum of O_3^- /8, 9/. If we present the magnitude of the observed build-up (the difference between optical density D_{max} in maximum and optical density immediately after the pulse) as a function of the chain length (see Fig 4), and compare with the rate constants of these cations with O^- and O_2^-, respectively, one can suppose, that the rate constants of O^- and O_2^- with these cations are controlling the nature of the observed build-up. As it is the case in other properties and reactions of homologous series, also here the first member deviates more from other compounds. The deviation is particularly large in case when O_2^- is involved.

References

/1/ Z. P. Zagórski, J. Grodkowski, Z. Zimek, W. Roszczynko, Report IBJ 1564/XVII/C/B.

/2/ K. Bobrowski, J. P. Suwalski, Z. P. Zagórski, Int. J. Radiat. Phys. Chem. (in press).

/3/ J. P. Suwalski, K. Bobrowski, Z. P. Zagórski, submitted for publication.

/4/ N. Getoff, F. Schwörer, Int. J. Radiat. Phys. Chem. 1, 101 (1973).

/5/ M. Simic, P. Neta, E. Hayon, Int. J. Radiat. Phys. Chem. 3, 309 (1971).

/6/ P. G. Clay, M. Rashid, Int. J. Radiat. Phys. Chem. 3, 367 (1971).

/7/ D. Behar, G. Czapski, Israel J. Chem. 6, 43 (1968).

/8/ G. Czapski, L. M. Dorfman, J. Phys. Chem. 68, 1169 (1964).

/9/ Z. P. Zagórski, Z. Stuglik, J. Grodkowski, Roczniki Chemii 17, 571 (1973).

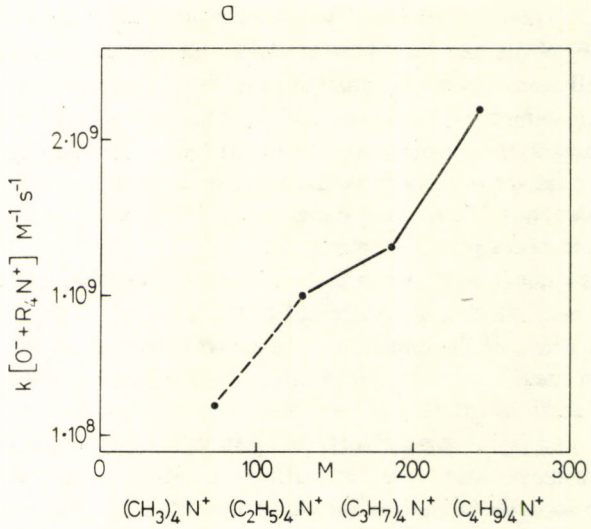

Fig. 1 Rate constants of tetraalkylammonium cations with oxide radical-ion O^- as a function of the chain length of the substituent in R_4N^+

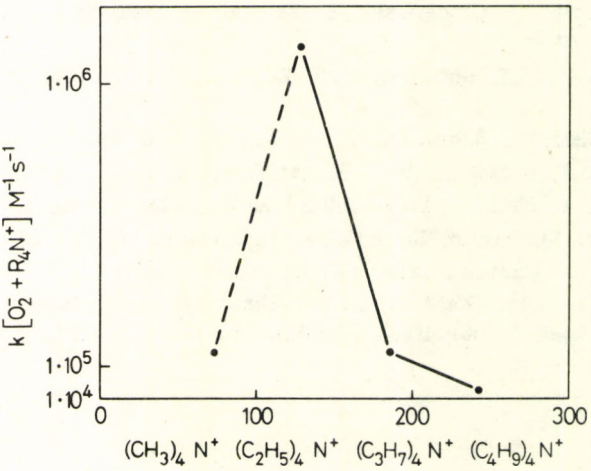

Fig. 2 Rate constants of tetraalkylammonium cations with superoxide radical ion O_2^- as a function of the chain length of the substituent in R_4N^+

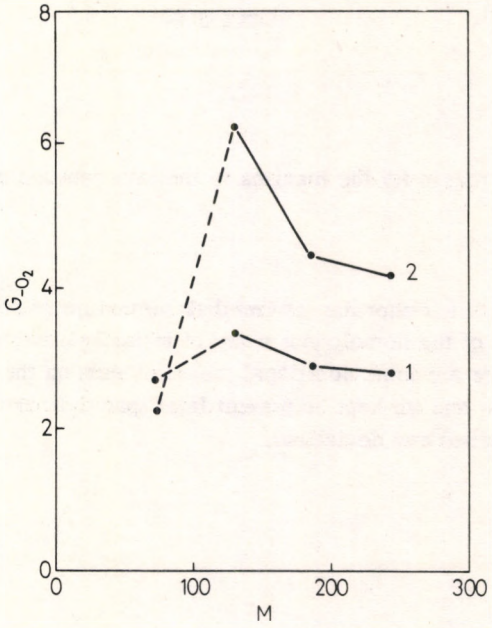

Fig. 3 Yield of O_2 disappearance as a function of the chain length in R_4N^+ in solutions with O_2 alone (curve 1) and with both O_2 and N_2O

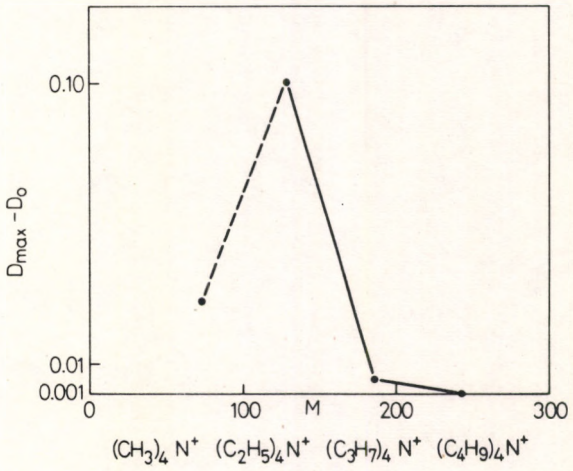

Fig. 4 Magnitude of the observed build-up (D_{max} - D_o) at 430 nm as a function of the chain length of the substituent in R_4N^+

G. R. FREEMAN

What was the reason for the maxima in the rate constant and (D_{max}-D_o) curves at $(C_2H_5)_4N^+$?

J. P. SUWALSKI

In my opinion it is rather the tetramethylammonium cation which deviates from the other members of the homologous series of tetraalkylammonium cations (cf. Figs 2 and 3). There are some additional measurements on the structure of R_4N^+ solutions in progress and we hope to present later speculations on the interpretation of observed regularities and deviations.

A STUDY OF RADIOLYSIS OF THIOACETAMIDE AND ACETAMIDE

S. E. Gvilava, H. M. Nanobashvili, S. G. Ignatashvili
Institute of Inorganic Chemistry and Electrochemistry of
the Georgian SSR Academy of Sciences,
Tbilisi, USSR

Only a limited amount of data is currently available in literature on the radiation chemical transformation of acetamide, while there are no data at all on the radiolysis of its sulphur analogue - thioacetamide.

It should be mentioned that these compounds, containing =O, =S, -SH, $-NH_2$ groups, are the most simple representatives of bifunctional compounds, therefore a study of their radiolysis is of great importance for the determination of the mutual influence of the functional groups contained in acetamide and thioacetamide. Besides, the establishment of the mechanism of thioacetamide and acetamide radiolytic transformation will promote the possibility of controlled performance or radiolysis of a number of sulphur-containing bifunctional compounds.

The present paper deals with a study of the radiation chemical transformation of the solutions of the above compounds.

Irradiation has been performed in atmospheric air on a Co-60 γ-unit with different dose rate values. Different physicochemical methods were used for the investigation of γ-radiolysis of solutions. Thioacetamide (TAA) was determined by the method of argentometric and acidimetric potentiometric titration. In the first case a silver plate was used as an indicator electrode with a saturated calomel counter-electrode, whereas in the second case a glass electrode was used as indicator with a saturated calomel counter-electrode.

Acetamide was determined by acidimetric potentiometric titration. Ammonia was measured by colorimetric method, elementary sulphur spectrophotometrically /1/ and sulphates nephelometrically.

The rate constant of the interaction of the examined compounds with OH radicals was determined by the method of competing scavengers: p-nitrozedimethylaniline (RNO) being used as standard substance /2-4/.

As a result of this work it has been established that elementary sulphur and ammonia are the basic radiolysis products of thioacetamide; the formation of sulphate and traces of hydrogen sulphide have also been observed.

The initial radiation chemical yield of thioacetamide transformation does not depend on concentration in the 0.001-0.1M solutions range and corresponds to 1.2molec/100 eV (Table 1).

The yield of elementary sulphur formation corresponds to the value of radiation chemical ammonia formation yield, i. e. $G(S^0) = G(NH_3) = (0.79 + 0.02)$ molec/100 eV (Fig. 1). In the range of the concentrations examined radiation chemical yields of ammonia and elementary sulphur formation are practically constant.

Table 1

γ-Radiolysis of thioacetamide aqueous solutions ($J = 0.65 \cdot 10^{16}$ eV/ml sec)

Concentration of initial solution, mole/l	Dose, eV/ml 10^{19}	Radiation-chemical yield of TAA transformation molec/100 eV
0.0010	2.41 - 4.82	1.15 ± 0.09
0.0025	1.2 - 7.2	1.02 ± 0.07
0.0050	2.41 - 24.0	0.86 ± 0.02
0.0100	1.2 - 16.9	0.90 ± 0.07
0.0250	11.5 - 46.1	0.92 ± 0.05
0.0500	11.5 - 46.1	1.19 ± 0.05
0.1000	11.5 - 46.1	1.20 ± 0.02

Accumulation of ammonia gives rise to a certain increase of pH. For instance, at a dose about $4.8 \cdot 10^{20}$ eV/ml the pH increases from 4 to 5.6.

Total transformation of thioacetamide was observed under irradiation of dilute solutions: for instance, under γ-radiolysis of 0.001M, 0.0025M and 0.005M thioacetamide with a dose of $1.2 \cdot 10^{20}$ eV/ml, 100%, 60% and 40%, of the amount initially present transforms, respectively.

Radiation-chemical transformation of thioacetamide depends on the dose rate (Fig. 2). While decreasing the dose rate from $J_1 = 0.65 \cdot 10^{16}$ eV/ml sec to $J_2 = 0.57 \cdot 10^{14}$ eV/ml sec the thioacetamide transformation yield increases from $G_1(-TAA) = 1.2$ molec/100 eV to $G_2(-TAA) = 12.1$ molec/100eV.

The above dependence is represented by a straight line plotting log G versus log s with a slope of about 0.5. This dependence indicates the occurrence of radical processes in the presence of competing reactions in the system.

It is noteworthy that the data obtained from γ-radiolysis of 0.05M thioacetamide solution (Fig. 3) indicate that the amount of transformed thioacetamide corresponds to the transformation of the $-NH_2$ group. This means that the sulphur-containing group of thioacetamide does not show protective properties towards the amine group, whereas this occurs in the case of thiourea /1/.

A comparatively high value of thioacetamide radiation chemical transformation yields is due to the great reactivity of this compound towards the radiolysis products of water. This is confirmed by the data obtained from determination of the k_{TAA+OH}

rate constant by the method of competing scavengers. The rate constant of the reaction

$$CH_3CSNH_2 + OH \xrightarrow{k_1} \text{product} \qquad (1)$$

corresponds to $k_{TAA+OH} = 7.6 \cdot 10^9$ 1. mole^{-1} sec^{-1}, whereas the rate constant of the recombination reaction

$$OH \cdot OH \xrightarrow{k_2} H_2O \qquad (2)$$

$$k_2 = 6.3 \cdot 10^9 \text{ 1. mole}^{-1} \text{ sec}^{-1} \quad /4/$$

This permits us to consider reactions (1) and (2) in thioacetamide radiolysis as being in competition.

A different situation is observed in radiation chemical transformation of acetamide (Fig. 4). The acetamide radiolysis process is accompanied with formation of ammonia, the values of acetamide transformation yields and of ammonia formation being mutually corresponding: $G(-AA) = G(NH_3) = 0.5$ molec/100 eV. Under the same conditions ($J = 0.65 \cdot 10^{16}$ eV/ml sec) the yield of radiation-chemical transformation of thioacetamide is 1.2 molec/100 eV. Therefore, radiation-chemical transformation of acetamide proceeds less effectively than the thioacetamide radiolysis.

As is known, thioacetamide is in thion and thiol forms in solutions /5/

$$CH_3 - C(=S)-NH_2 \rightleftharpoons CH_3 - C(-SH)=NH \qquad (3)$$

The radical products of the radiolysis of water, the OH radical, specifically, seem to attack the C – SH bond, resulting in the following reaction:

$$CH_3C(NH)SH + OH \longrightarrow S^0 + NH_3 + \dot{C}H_3 + CO \qquad (4)$$

In aerated solutions the contribution of the HO_2 radical should be taken into account

$$CH_3C(NH)SH + HO_2 \longrightarrow CH_3\dot{C}NH + S^0 + 2OH \qquad (5)$$

Reactions (4) and (5) permit us to conclude that the radiation-chemical transformation of thioacetamide in the presence of oxygen may proceed by the chain mechanism.

The formation of ammonia from thioacetamide and acetamide seems to occur through the participiation of a solvated electron.

Relative comparison of thioacetamide and acetamide radiolysis has shown that the transformation yield of the amino-group is much higher in the case of thioacetamide. This indicates the mutual influence between the -SH and $-NH_2$ groups in the radiation field.

Work in this direction is being continued.

References

/1/ S. E. Gvilava, H. M. Nanobashvili, N. G. Ignatashvili, Proc. Third Symposium on Radiation Chemistry, Akadémiai Kiadó, Budapest, 1972. pp. 1293–1299.

/2/ A. Henglein; W. Schnabel, J. Wendenburg, Practische Einführung in die Strahlénchemie, 1967.

/3/ I. Kraljic and C. N. Trumbore, J. Amer. Chem. Soc., 87, 2547 (1965).

/4/ J. Rabani, M. S. Matheson, J. Phys. Chem., 70, 261 (1966).

/5/ Yakovlev P. Ya., Razumova G. P., Thioacetamide – the Hydrogen Sulfide Substituent in the Analysis of Metals (in Russian). Moscow, 1963.

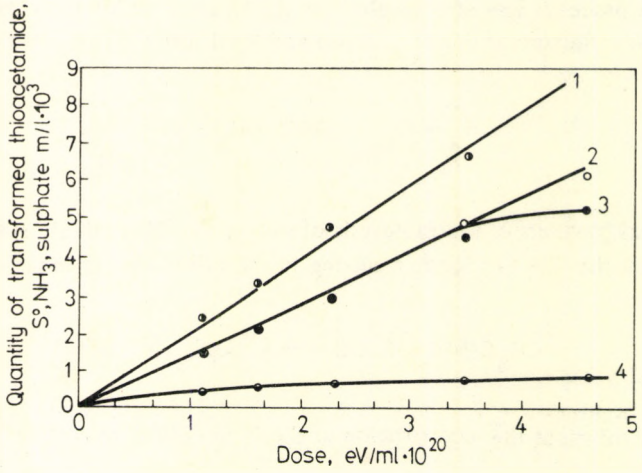

Fig. 1

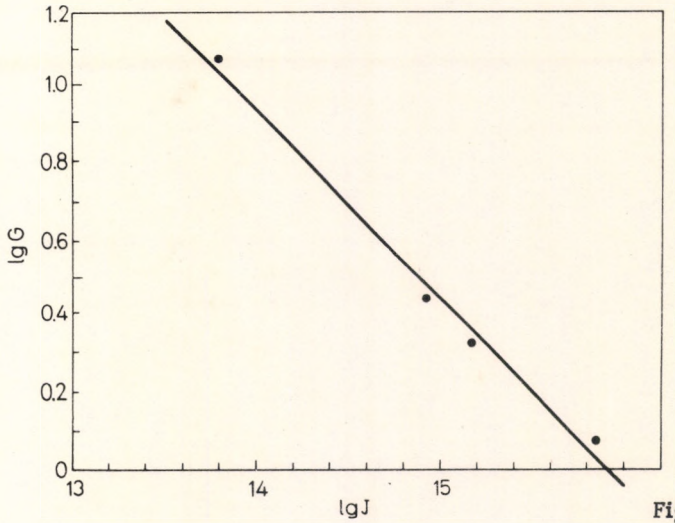

Fig. 2

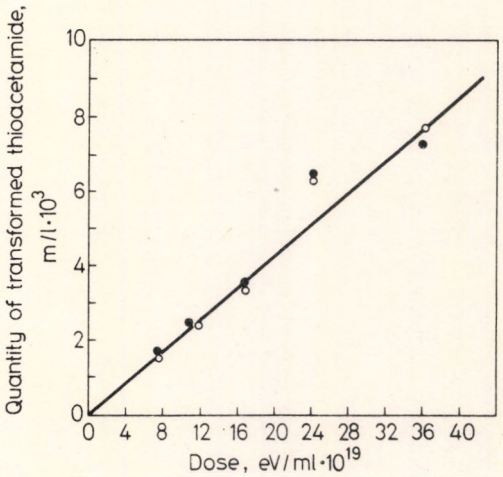

Fig. 3

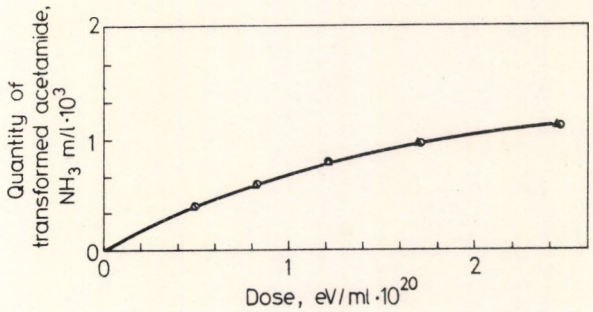

Fig. 4

FORMATION AND CONVERSION OF RADICALS IN IRRADIATED AQUEOUS DNP SOLUTIONS

V.A. Sharpatyi, N.V. Zakatova
Institute of Chemical Physics, Academy of Sciences of the USSR,
Moscow, USSR

In developing the investigations /1-3/ on the role of radicals in radiation damage of cells we studied the radiolytic properties of DNP in solution, the system being more complicated than the aqueous DNA solution /2/ and a less complicated one than the cell.

The following were used: DNP (M.W. 1.9×10^7 daltons, C_{DNA}: $C_{histone}$ = 1:2 and 1:1), NDA (M.W. 6×10^6 daltons) and summary histone preparations, obtained from thymus of calf by the method described in Ref. /4/. The samples were irradiated at 77, 195 and 273 K with Co^{60} γ-rays. In irradiated samples directly at 77 K and at higher temperatures, radicals were measured by the EPR method /2,3/ whereas after annealing phosphate ions and organic phosphate (i.e. phosphate ions that appear after the alkali treatment of the DNP solution) were determined according to methods of Ref. /5/, and malonaldehyde was analyzed by the thiobarbituric acid reaction as described in Ref. /6/. More precisely speaking the malonaldehyde (MA) analogues having -CHO-CH_2-CHR-groups were measured by this method. Studying the radiation chemical kinetics of these products at different conditions of irradiation it was possible to consider the mechanism of DNA radiation destruction, i.e. the decay of the sugar-phosphate chain of the biopolymer. This destruction is observed in the radiolysis of both the DNA solutions and the native cell /7,8/. The second main process of the DNA in the DNP-complex, the nucleic acid bases destruction, we studied observing the density absorption at λ = 260 nm, attributed to the chromophore groups of the bases /9/. The DNP histone fragment decay was measured through the deamination process i.e. through NH_3 formation according to Collyns /9/.

The values of the yields of analysed radiolysis products are given in Tables 1-4. From these data it was concluded that the main processes of DNP radiolysis in frozen aqueous solutions are the damage of chromophore groups and deamination (the histone fragment damage). The yield of these processes and the overall radical yield (at 77K) are of the same order. The $G(R^{\cdot}_{bp})$ increases with the increase of the DNP concentration. The overall yield of radicals increases to a smaller extent particularly in the case of the more concentrated solutions (Table 1). Besides this, the contribution of OH radicals to the overall radical concentration decreased. With the increase of the DNP concentration the yield of the radiolysis products increased. It was concluded from this fact

Table 1

G(R) in irradiated DNP and DNA solutions at 77K

Solution	G(ΣR)	$G(R^{\cdot}_{b.p.})$
DNP 0.6%, 1 : 1.7, air	0.6	0.08
2.3%, 1 : 1, argon	0.8	0.5
9%, 1 : 1.7, gel., air	1.2	0.8
9%, 1 : 1.7, gel., argon	1.3	1.0
DNA 1.56%, air	0.8	0.4

Table 2

G(-chromophore groups) in irradiated DNP and DNA solutions at 77, 195 and 273 K

Solution	77 K	195 K	273 K
DNP 0.6%, 1 : 1.7, air	0.3 ± 0.1	1.2 ± 0.1	1.8 ± 0.2
DNP +0.2 M inositol	0.5 ± 0.1	-	-
DNP argon	0.4 ± 0.1	-	-
1.8%, 1 : 2, air	0.57 ± 0.15	1.4 ± 0.1	3.1 ± 0.3
+0.2 M inositol	0.77 ± 0.15	-	2.2 ± 0.2
DNP argon	0.66 ± 0.15	-	-
+0.2 M inositol	0.70 ± 0.25	-	-
2.3%, 1 : 1, air	1.0 ± 0.2	-	-
DNA 0.2%, air		-	1.7 ± 0.2

Table 3

Yields of the radiolysis products in DNP solutions at 77 K, dose: 4.2 Mrad

Solution	G(MA)	$G(PO_4)$	G(org. phosph.)
DNP 0.6%, 1 : 1.7 air	0.0014	0.2[a]	0.025
DNP + 0.2M inositol	0.0004	0.013	-
DNP argon	0.0014	0.010[c]	0.025
DNP + 0.02 M inositol	0.0010	0.002	-
2.3%, 1 : 1, air	0.003[b]	0.03[b]	0.25[b]
DNA 1.56%, air	-	0.2[b]	0.45[b]

[a] post-effect + 100%, [c] post-effect + 150%, [b] dose 6 Mrad

Table 4

$G(NH_3)$ in irradiated biopolymer solutions at 77 and 195 K (the latter in parentheses)

Solution	Without inositol	0.2M inositol
Histone 0.6%, air	0.33 ± 0.03	0.32 ± 0.01
	(0.42 ± 0.07)	(0.18 ± 0.06)
DNA 0.6%, air	0.01 ± 0.01	0.01 ± 0.002
	(0.06 ± 0.006)	(0.04 ± 0.01)
DNP 0.6%, 1:1.7, air	0.15 ± 0.05	0.09 ± 0.01
DNP argon	0.04 ± 0.02	0.02 ± 0.01
DNP 1.08% 1:1, air	0.30 ± 0.03	0.10 ± 0.03
	(0.32 ± 0.02)	(0.13 ± 0.07)
DNP 1.4% 1:0.8, air	0.30 ± 0.10	-
DNP 1,4% 1:1.6, air	0.30 ± 0.15	0.16 ± 0.02
DNP 2.3% 1:1.6, air	0.45 ± 0.05	0.33 ± 0.04
argon	0.30 ± 0.03	0.03 ± 0.03

that the observed processes of the DNP radiolysis influence the radicals, mainly the products of water radiolysis e^-_{aq} and OH (H_2O^+).

As in the case of liquid-phase radiolysis /10/ the values of the nucleic acid bases and histone fragment destruction yields are as much as 150–200 times higher than those of the sugar-phosphate chain damage. It is necessary to underline that the yield of the biopolymer radicals (the primary radicals) does not depend on the fact whether O_2 is in the solution. The yield of the products of the DNA sugar-phosphate chain destruction does depend on it, as follows from the data of Table 3. It was observed in the experiments on the annealing of the DNP samples, containing O_2 and irradiated at 77K that during the disappearance of biopolymer radicals the peroxide type radicals, $\cdot RO_2$, arose. Their concentration increased in the temperature range 153 to 203K (Figs 1 and 2, the components are marked by arrows). In DNP solutions not containing O_2 instead of $RO\cdot_2$ the radical of thymine structure was observed in the same temperature range as in the case of the aqueous DNA solutions /2/. These radicals which appear in γ -irradiated DNP solutions also form under the action of UV light at 77K.

The data obtained enable one to conclude that the O_2 influenced the second stage of the biopolymer radicals conversion: $R^{\cdot}_{DNA} + O_2 = RO^{\cdot}_2$. Thus the O_2 presence in solution influenced the yield of the final radiolysis products of DNP. Addition of inositol to the DNP solution before the irradiation influenced the yields of the radiolysis products as well. The yield of the radiolysis product increased with increasing temperature of irradiated solution (Tables 2–4). All these facts could be explained in terms of the changes of the conditions of the radical conversion processes.

Analysing the data obtained for DNP intermediate system compared with the aqueous DNA solution and DNA in cell radiolysis given in literature /7,8/ we could now draw a conclusion on the main types of radical conversion, arising from the sugar fragment of DNA. It was shown /11,12/, that during the irradiation of frozen aqueous carbohydrate solutions OH (or H_2O^+) radicals attack C_α -H bonds (the α position counted from the -OH group). It was shown also that in the cases of monosaccharides and polysaccharides OH radicals attack all the H-$\dot{C}$-OH bonds /12/. Extending this finding to the 2-deoxyribose fragment we can say that the site of attack of OH radicals are C'_1, C'_3, C'_4 and C'_5 atoms, and 4 types of radicals might appear $\dot{C}'_1$, $\dot{C}'_3$ $\dot{C}'_4$ and $\dot{C}'_5$. It was shown earlier /3, 13/ that two types of primary sugar radical transformations are possible:

1. Dehydration (α-and β-elimination, as counted from the site of the free valency),

2. Isomerization with breaking the cyclic structure of the monomer link (in the case of free valency localization on C'_1-atom). Applying this conclusion to the case discussed we can say that the appearance of end phosphates groups when irradiating DNA solutions and cells is connected with the transformations of the primary radicals: $\dot{C}'_3$ gives $>C_3$-O-PO_3H and $\dot{C}'_1$, $\dot{C}'_4$ and $\dot{C}'_5$ give $>C_5$-O-PO_3H. This assumption is also supported by the equality G(5' phosph. group) = 3/4 G(phosph. groups, inorganic phosph.)/7/. The possibility of radical transformation through β-elimination of H_2O (or in our case end phosphate groups appearing) is supported by the result of the experiments on irradiated glucose (H_2O abstraction and allylic type radical appearance) /14/ and the lack of 3'OH end groups for balance products of sugar-phosphate band destruction /7,3/. The methane appearance during glucose irradiation /14/ supports the conclusion on the possibility of the primary radical C'_1 isomerization with breaking the cyclic structure of sugar bond.

After alkali treatment of the irradiated DNP solution (as in the case of DNA solution /7/ and cell /8/) the additional production of free phosphate took place (Table 3). Its formation is connected with the hydrolytic splitting /15/ of C-N bonds of nucleic acid bases containing saturated bonds (brought about by irradiation) or with the β -elimination of phosphate groups β -disposed to the double bonds /16/. The latter also appeared during irradiation. Taking into account the fact that the end 3'PO_4 and 3'-OH groups do not appear additionally after the alkali treatment of DNA solution /7/ and cell /8/, we can conclude that the additional inorganic phosphate arises mainly according the β-elimination reaction.

The nucleic acid bases destruction at 77K as follows from the data given in Table 2 can be attributed to the attack of electrons, at higher temperatures than that of electrons and OH radicals. However, the water radicals attack mainly histone fragment of DNP as shown by ESR spectra analysis. The results of ESR spectra analysis of the DNP and histone solutions are given in Table 5. Both in the DNP and in the histone solutions radicals were identified which have practically the same characteristics. It is a radical with the 6-component ESR line. This radical might appear because of end amino-group abstraction from lysine residue or guanidine from arginine

Table 5

Radicals identified in irradiated frozen aqueous DNP and histone solutions at 77 K, dose 6 Mrad

Radical	Number of HFS components	H, mT	Common width line, mT	Assumed structure of the radical	Temperature region of registration
R_1	5, 1:4:6:4:1 or	2	9	$-CH_2-\dot{C}H-CH_2$	histone soln.
R_1	1:2:2:2:1 and	2	9	$2H_+1H$(3.9mT)	77–190K
R_1''	1:2:1	2	4	2H(1.9mT)	
R_2	6, 1:3:4:4:3:1	2,3	12.5	$\dot{C}H_2-CH_2$	histone soln. 77-235K
R_2''	6, 1:3:4:4:3:1	2.1	11.2	$\dot{C}H_2-CH_2$	DNP soln 77-160K
R_3	2, 1:1	1.5	2.5	$=\dot{C}-O^-$	DNP and histone solns. 77–160K
R_4	3, 1:2:1	2.3	-	2H	DNP soln, to 160K
R_5	2, 1:1	-	2.2	anion-radical	DNP soln, 77-190K
R_6	8, 1:3:5:7:7:5:3:1	2	14	$-\dot{C}HH_3-CH_2$	DNP soln, 190-230 K or after UV light at 77K
R_7	asymm. line $g_{11} = 2.029$, $g_{\perp} \simeq 2.000$		5	$RO_2^{\cdot}$	DNP and histone solns. 150–205K
OH	2, asymm. doublet	4	10.5	OH	DNP and histone solns, 77-120K
e_{st}	1, singlet, $g \sim 2.001$	-	1	e_{st}	DNP and histone solns, 77–100K

residue as a result of electron attack. This conclusion is supported by the deamination data in the case of lysine /17/.

The peroxide type radicals observed in the case of irradiation of DNP, histone and serum albumin /18/ solutions have practically identical ESR line parameters (Table 5). It may be assumed that the free valency localizes at the same site, i.e. the albumen fragment. If this is true this means that the peroxide radical formation hinders free valency migration from histone-fragment of DNP complex to DNA-fragment during the annealing samples.

References

/ 1/ Emanuel' N.M. Trudy Moip, 7, 73 (1963).
/ 2/ Sharpatyi, V.A., Nadzimiddinova, M.T., Krugljakova, K.E., Emanuel, N.M. Doklady Akad. Nauk, 180, 112 (1968).
/ 3/ Sharpatyi, V.A., Proc. of III Tihany Symp. on Rad. Chem. 1973 Budapest, p. 1345.
/ 4/ Cramption, C.F., J. Biol. Chem. 206, 499 (1954).
/ 5/ Marsch, B.B., BBA, 32, 357 (1959).
/ 6/ Waravdekar, V.S., Saslav, L.D., J. Biol. Chem., 234, 1945 (1959).
/ 7/ Hagen, U., Bopp, A. Carry, S., Ullrich, M., Proc. I. Europ. Biophys. Congr., Vienna, 2, 105 (1971).
/ 8/ Lennartz, M., Coquerelle, Th. Hagen, U., Int. J. Rad. Biol., 28, 181 (1975).
/ 9/ Collyns, B., Okada, S., Rad. Res., 25, 526 (1965).
/10/ Sharpatyi, V.A. Izw. Akad. Nauk, ser. chim 1165 (1973).
/11/ Emanuel', N.M., Sharpatyi, V.A., Doklady Akad. Nauk, 177, 1142 (1967).
/12/ Sharpatyi, V.A. Doklady Akad. Nauk, 208, 1157 (1973).
/13/ Sharpatyi, V.A., Goldin, S.I., Izw. Akad. Nauk, ser. chim 1367 (1971).
/14/ Goldin, S.I., Ivko, A.A., Doklady Akad. Nauk (1975) in press.
/15/ Scholes, G., Weiss, J., Nature, 171, 920 (1953).
/16/ Bayler, C.R. Brammer, K.W., Jones, A.S. JACS 1903 (1961).
/17/ Sharpatyi, V.A. Zakatova, N.W. Minchadzidinova, D.R., Izv. Akad. Nauk, ser. chim. (1976) in press
/18/ Sharpatyi, V.A., Studia biophysica, 8 187 (1968).

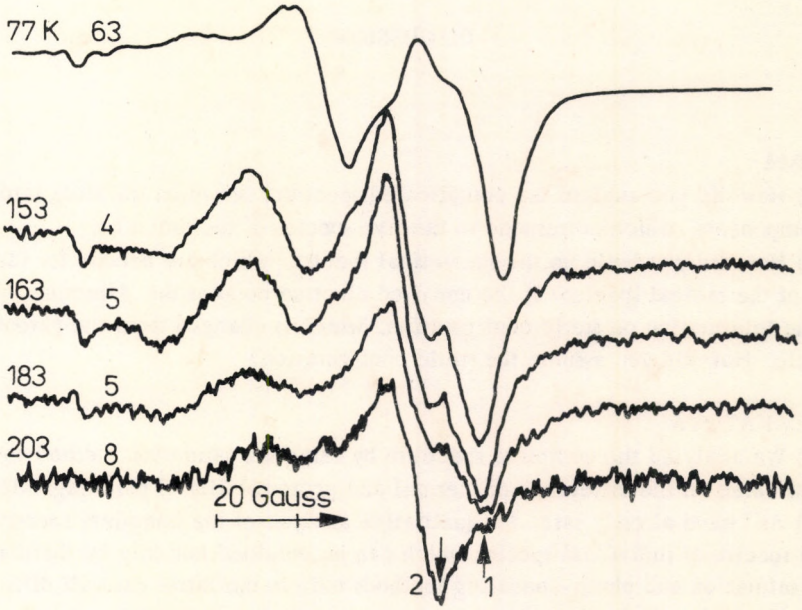

Fig. 1 ESR spectra of aerated 0.6% DNP solution irradiated at 77K measured at 77, 153, 163, 183 and 203K

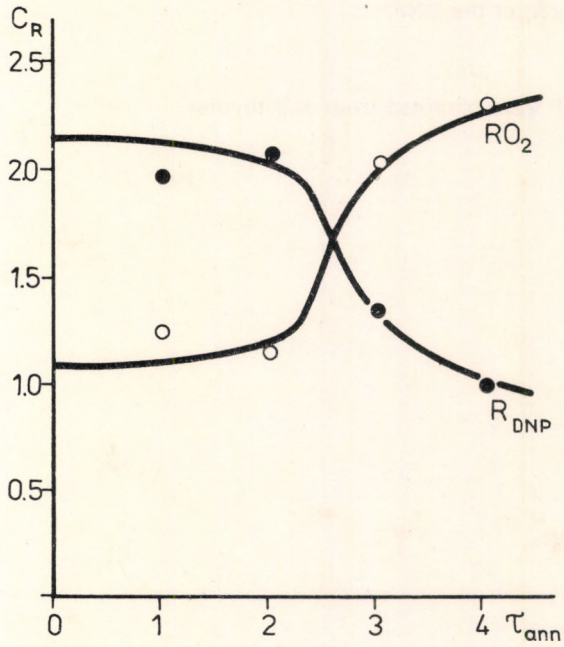

Fig. 2 The radical concentration change (arbit. units) in irradiated at 77K frozen DNP solution annealed: R_{DNP}-vert. arrow 1, RO_2 - vert. arrow 2, see Fig. 1.

J. SOHMA

(1) How did you analyse the complicated spectrum shown on the slide into the five components, which correspond to the five species of the radicals?

(2) How did you build up the theoretical spectra, which are needed for identification of the radical species? If the unpaired electron couples the β-protons, we need the information on steric configuration, which is changed from the parent molecule. How did you assume the steric configuration?

N. V. ZAKATOVA

(1) We analysed the complete spectrum by using the saturation method and other methods based on the difference of thermal and photostability of paramagnetic species.

(2) As I have already said, for qualitative analysis of the complete spectrum one needed spectra of individual species which can be obtained not only by thermal method, but by saturation and photo-annealing methods too. In the latter case all difficulties with configuration changes vanished.

R. A. HOLROYD

What is the source of the DNP?

N. V. ZAKATOVA

Samples of DNP were obtained from calf thymus.

RADIOLYSIS OF AQUEOUS SOLUTION OF ETHYLENE GLYCOL IN THE PRESENCE OF FERROUS SULPHATE, SULPHURIC ACID AND EXCESS OXYGEN

D. Bunn
School of Chemistry, University of Leeds, Leeds, England
R. C. Das
Department of Chemistry, University College of Engg, Burla, India

The mechanism of reactions taking place during the radiolysis of aqueous solutions of methanol, ethanol, t-butanol, ethylene etc. in the presence of $FeSO_4$, H_2SO_4, and oxygen have been studied by us /1-3/. As a part of the same scheme the present work has been undertaken.

Experimental

Purification of water. Doubly distilled water was distilled twice in a continuous stream of oxygen, firstly from alkaline permanganate and then from acid dichromate, the water vapour being passed in both the stages through a heated quartz tube at 800°C.
Reagents. 'AnalaR' ferrous ammonium sulphate (FAS) and twice-distilled ethylene glycol were used. Other reagents were either of 'AnalaR' or comparable purity.
Source. A Müller MG 300 constant potential X-ray unit with 5 mm Al window, operating at 280 kV and 10 mA, was used for irradiation. Irradiations were done in Pyrex glass syringes of 30 ml capacity.
Oxygenation. Experiments were carried out in oxygen-saturated conditions. The acidified FAS solution was pre-saturated by 15 minutes bubbling in medical grade, water scrubbed oxygen. One ml of concentrated solution of the substrate of appropriate concentration was stirred in and the solution drawn slowly into a Pyrex syringe for irradiation through a semi-capillary tube.
Estimation of ferric ion. Increase of ferric ion concentration was determined by measuring optical density of the sulphate complex at 304 nm relative to the initial solution.
Estimation of formaldehyde. Formaldehyde was estimated with chromotropic acid using the method developed by McFadyen /4/ and Bricker and Johnson /5/ modified to suit our concentration condition.

Results and discussion

In the absence of the organic substrate the reactions taking place in the system during radiolysis are the same as in the Fricke radiation dosimeter /6/.

$$H_2O \rightsquigarrow \left.\begin{matrix} H\cdot \\ e^-_{aq} \end{matrix}\right\} + \cdot OH + H_2O_2 + H_2 + H_3O^+ \qquad (1)$$

$$e^-_{aq} + H^+ \longrightarrow H\cdot \text{ (in excess of } H^+) \qquad (2)$$

$$H\cdot + O_2 \longrightarrow HO_2\cdot \qquad (3)$$

$$HO_2\cdot + Fe^{++} \longrightarrow Fe^{3+} + HO_2^- \qquad (4)$$

$$HO_2^- + H^+ \rightleftharpoons H_2O_2 \qquad (5)$$

$$H_2O_2 + Fe^{++} \longrightarrow Fe^{3+} + \cdot OH + OH^- \qquad (6)$$

$$\cdot OH + Fe^{++} \longrightarrow Fe^{3+} + OH^- \qquad (7)$$

In the presence of the organic substrate (RH), the hydroxyl radical also reacts with RH in competition with reaction (7).

$$\cdot OH + RH \longrightarrow R\cdot + H_2O \qquad (8)$$

In the presence of large excess of RH, reaction (8) swamps out reaction (7). The reaction of H· with organic substrates being rather slow /7/, it cannot effectively compete with reaction (3). The radical R , in the case of ethylene glycol as substrate, is obviously $HOCH_2\dot{C}HOH$.

Reactions following reaction (8) increase the ferric yield in the presence of organic substrates like alcohols, glycols, etc /8/.

Explanation of terms and experimental parameters. We define the quantity, Q, as the average number of Fe^{3+} ions produced by the reactions following reaction (8) per·OH radical derived from the sum of the reactions (1) to (8). The relative ferric yield, R_x, defined by the expression

$$R_x = \frac{\text{ferric yield in the presence of RH}}{\text{ferric yield in the absence of RH}} = \frac{G(Fe^{3+})_{RH}}{G(Fe^{3+})_{RH=O}}$$

is related to Q in the following way,

$$R_x = \frac{Q(G_{H\cdot} + G_{H_2O_2} + G_{\cdot OH}) + G_{H_2O_2} + 2G_{H\cdot}}{3G_{H\cdot} + 2G_{H_2O_2} + G_{\cdot OH}} =$$

$$= (Q-1)\,\frac{G_{H\cdot} + G_{H_2O_2} + G_{\cdot OH}}{3G_{H\cdot} + 2G_{H_2O_2} + G_{\cdot OH}} + 1,$$

writing $G_{H\cdot}$ in acid solution as including primary $G_{H\cdot}$ and $G_{e^-_{aq}}$. Thus,

$$(R_x - 1) = F(Q-1), \text{ where } F = \frac{G_{H\cdot} + G_{H_2O_2} + G_{\cdot OH}}{3G_{H\cdot} + 2G_{H_2O_2} + G_{\cdot OH}}\,.$$

The value of F under our experimental condition is determined as 0.499 ± 0.002. Thus, under our condition

$$(R_x - 1) = 0.499(Q-1).$$

Dewhurst /8/ first proposed a general reaction scheme for the radiolysis of aqueous aerated ferrous sulphate solution in the presence of organic compounds. On the basis of his mechanism, reaction (1) to (8) followed by processes (9) to (14) given below, the ferric yield (expressed as R_x, Q or G (Fe^{3+}) for a given dose of radiation would increase indefinitely until depletion of the reactants on increasing the proportion of the substrate, RH, at a particular concentration of ferrous ion /3/.

$$R\cdot + O_2 \longrightarrow RO_2\cdot \qquad (9)$$

$$RO_2\cdot + Fe^{2+} \longrightarrow Fe^{3+} + RO_2^- \qquad (10)$$

$$RO_2^- + H^+ \rightleftharpoons RO_2H \qquad (11)$$

$$RO_2H + Fe^{2+} \longrightarrow Fe^{3+} + RO\cdot + OH^- \qquad (12)$$

$$RO\cdot \begin{cases} + Fe^{2+} + H^+ \longrightarrow Fe^{3+} + ROH & (13) \\ + RH \longrightarrow ROH + R\cdot \text{ (This process recycles through reaction 9).} & (14) \end{cases}$$

Figure 1 gives the plot of R_x and $G(Fe^{3+})$ against $[RH] / [Fe^{2+}]_{av}$*. As can be seen, the ferric yield attains a limiting "plateau" value. The plateau formation and its actual value, in the case of methanol and t-butanol systems, are due to ineffective competition of reaction (14) with reaction (13) [$G(Fe^{3+})_{limit} \sim 30$; $R_{x(limit)} \sim 2$ or $Q_{limit} \sim 3$]/1, 2/. In the case of ethanol system, the main-course-reaction taking place at low $[H^+]$ and/or high $[Fe^{2+}]$, was identified as consisting of reactions (1) to (12) followed by

$$RO\cdot \longrightarrow R'\cdot \qquad (15)$$

$$R'\cdot + O_2 \longrightarrow R'O_2^{\cdot} \qquad (16)$$

$$R'O_2^{\cdot} + Fe^{2+} \longrightarrow Fe^{3+} + R'O_2^{-} \qquad (17)$$

$$R'O_2 + H^+ \rightleftharpoons RO_2H \qquad (18)$$

$$R'O_2H + Fe^{2+} \longrightarrow Fe^{3+} + R'O\cdot + OH^- \qquad (19)$$

$$R'O\cdot + Fe^{2+} + H^+ \longrightarrow Fe^{3+} + \text{stable organic products} \qquad (20)$$

This corresponds to $G(Fe^{3+})_{limit} \sim 45$, $R_{x(limit)} \sim 3$ and $Q_{limit} \sim 5$. The radicals R· and R'· for RH = EtOH, are CH_3CHOH and $\cdot CH_2CHO$ (or its hydrated form $CH_2CH(OH)_2$), respectively. The stable organic products (EtOH as substrate) include glycolaldehyde and formaldehyde which are formed by two simultaneous reactions /1, 2/

$$\cdot OCH_2CHO + Fe^{2+} + H^+ \begin{cases} \rightarrow HOCH_2CHO + Fe^{3+} & \ldots 20(a) \\ \rightarrow 2HCHO + Fe^{3+} & \ldots 20(b) \end{cases}$$

The "plateau" or limiting ferric yield in the ethylene glycol system is dependent on the $[H^+]$ and $[Fe^{2+}]_{av}$. Figure 2 shows the variation of $G(Fe^{3+})_{limit}$ with $[Fe^{2+}]_{av}$ at different acidities. It can be seen that both at high and low acidities the limiting ferric yield does not change with $[Fe^{2+}]_{av}$, beyond a certain value of the latter. The present paper gives the reaction mechanisms only under such high $[Fe^{2+}]_{av}$.

*Care was taken that in the experiments, the conversion of Fe^{2+} to Fe^{3+} never exceeded 10%. Under this condition, $[Fe^{2+}]_{av}$ is not much different from $[Fe^{2+}]_{in}$ and reactions of Fe^{3+} ion with radical intermediates do not play any important role.

Reactions at low $[H^+]$ and high $[Fe^{2+}]_{av}$. The limiting ferric yield in this condition corresponds to $Q_{limit} \approx 5$ as in the ethanol system. Hence it is assumed that similar reaction sequence takes place as in the case of ethanol as substrate [i.e. reactions (1) to (2) followed by (15) to 20]. The important feature of this reaction sequence is the reaction (15), which unequivocally takes place with $CH_3CH(O\cdot)OH$ ($RO\cdot$ of ethanol system). Because of the structural similarity between ethanol and ethylene glycol, a similar reaction can be assumed to be taking place with the corresponding radical of ethylene glycol. The radicals $R\cdot$, $RO_2\cdot$, $RO\cdot$, $R'\cdot$, $R'O_2\cdot$ and $R'O\cdot$ of ethylene glycol substrate are $HOCH_2\dot{C}HOH$, $HOCH_2CH(O_2\cdot)OH$, $HOCH_2CH(O\cdot)OH$, $\cdot CH(OH)CHO$ [or $\cdot CH(OH)CH(OH)_2$], $\cdot O_2CH(OH)CHO$ [or $\cdot O_2CH(OH)CH(OH)_2$)] and $\cdot OCH(OH)CHO$ [or $\cdot OCH(OH)CH(OH)_2$], respectively. The mechanism of the reaction (15) for RH = =ethylene glycol is,

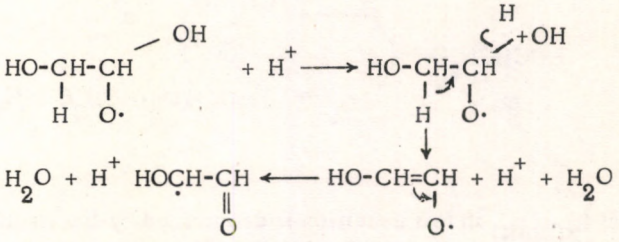

The ultimate stable organic end-products in this reaction mechanism are expected to be glyoxal (OHC-CHO), formic acid (HCOOH) and formaldehyde (HCHO) by processes analogous to reactions (20a) and (20b) of ethanol system. At very low concentrations, the yields of these organic products are very difficult to estimate, but formaldehyde has been quantitatively identified.

Reactions at high $[H^+]$ and high $[Fe^{2+}]_{av}$. - The limiting ferric yield decreases with the increase in $[H^+]$ as can be evident from Figure 3. At very high $[H^+]$, it equals to $Q_{limit} \approx 3$, $(R_{x(limit)} \approx 2$ and $G(Fe^{3+})_{limit}$ 31. A clue to the mechanism at high $[H^+]$ comes from the ESR work of Buley, Norman and Pritchett /9/ which shows that hydroxyl radical reacts with ethylene glycol molecule to form $HOCH_2\dot{C}HOH$ which, in very acidic solutions, is readily converted to $\cdot CH_2CHO$. In less acidic solutions the conversion is slow. The mechanism of the reaction is probably the following,

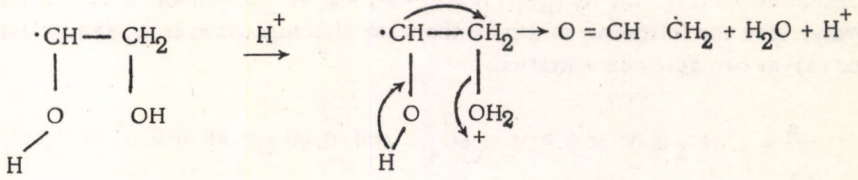

the driving force of the reaction being resonance stabilisation of the radical, $\cdot CH_2CHO$, i.e.

$$\cdot CH_2CH = O \longleftrightarrow CH_2 = CH - O\cdot$$

The radical $\cdot CH_2CHO$ is nothing but the radical $R'\cdot$ of ethanol system. Hence it is expected to undergo the same sequence of reactions as reactions (16) to (20) for ethanol system. This would give $Q_{limit} \sim 3$. The ultimate organic end-product is expected to be glycolaldehyde ($HOCH_2CHO$) and formaldehyde (HCHO). Of these, formaldehyde has been identified.

Reactions at intermediate $[H^+]$. In this condition, both the sequences are operative due to two competitive reactions,

$$HOCHCH_2OH \;(R\cdot) \xrightarrow{H^+} \cdot CH_2CHO \;(f_a)\;(R\cdot^*) \quad \ldots(a)$$

$$HOCHCH_2OH \;(R\cdot) \xrightarrow{+O_2} HOCH(O_2\cdot)\text{-}CH_2OH \;(f_b)\;(RO_2\cdot) \quad \ldots(b)$$

The value of $R_{x(limit)}$ in this condition is determined by the fraction f_a and f_b of the radicals which are converted to $R\cdot^*$ and $RO_2\cdot$, respectively. With all possible reactions which would regenerate $R\cdot$ suppressed by high $[Fe^{2+}]$, the yield $R_{x(limit)}$ is given by the expressions

$$Q_{overall} = f_b (Q_{RO_2\cdot}) + f_a (Q_{R\cdot}^{x}) = 5 f_b + 3 f_a$$

$$\text{and } (R_x - 1)_{limit} = F\,(Q-1)_{limit}$$

$$\text{For } F = 0.499,\ R_{x(limit)} = 3.00 f_b + 2.00 f_a$$

$$\text{therefore } \frac{f_a}{f_b} = \frac{3.00 - R_{x(limit)}}{R_{x(limit)} - 2.00}$$

By this relationship, the limits at high $[Fe^{2+}]$ of the data at 0.4 M and 0.05 M H_2SO_4 concentrations (Fig. 2), $R_{x(limit)}$ $(Fe^{2+} \to \infty) = 2.41 \pm 0.005$ and 2.92 ± 0.5 respectively, give the following values for the state of competition between reactions (b) and (a) at two acid concentrations,

$$\frac{f_a}{f_b} = 1.44 \pm 0.05 \text{ at } 0.4 \text{ M } H_2SO_4 \quad \text{and} \quad 0.09 \pm 0.06 \text{ at } 0.05 \text{ M } H_2SO_4$$

If the rate of the acid-catalysed reaction (a) is directly proportional to $[H^+]$, we can write,

$$\frac{f_a}{f_b} = \frac{k_a [H^+]}{k_b [O_2]}$$

From the value of f_a/f_b at 0.4 M H_2SO_4, taking $[H^+]$ = 0.505 M /10/. and O_2 = = 1.21×10^{-3} M /11/, one obtains

$$\frac{k_a(\text{apparent})}{k_b} = (3.4 \pm 0.1) \times 10^{-3}$$

References

/ 1/ D. Bunn and R.C. Das, Chem. Commun., 1970, 1456.
/ 2/ R.C. Das, Radiation Res. Rev., 3, 121 (1971).
/ 3/ R.C. Das, Ph. D. thesis, Leeds Univ. England (1969).
/ 4/ D.A. McFadyen, J. Biol. Chem., 158, 107 (1945).
/ 5/ C.E. Bricker and H.R. Johnson, Ind. Eng. Chem., Anal. Ed., 17, 400 (1945).
/ 6/ H. Fricke and E.J. Hart. J. Chem. Phys., 3, 60 (1935).
/ 7/ M. Anbar and P. Neta, Int. J. of Appl. Radiation & Isotopes, 18, 493 (1967).
/ 8/ H.A. Dewhurst, Trans. Farad. Soc., 48, 905 (1952).
/ 9/ A.L. Buley, R.O.C. Norman and R.J. Pritchett. J. Chem. Soc., B. 849 (1966).
/10/ T.F. Young, L.F. Maranville and H.M. Smith, "Structure of Electrolytic Solutions", Ed. W.J. Hamer, John Wiley, New York, 1959.
/11/ "Handbook of Physics and Chemistry", Chemical Rubber Publishing Co., 2nd ed, 1940.

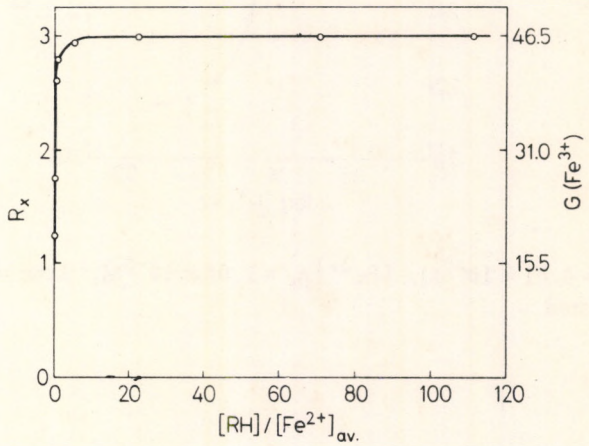

Fig. 1 $[Fe^{2+}]_{initial} = 1.00 \times 10^{-3}$M, $[H_2SO_4]$ = 0.05M, Dose = 914 rads, O_2-saturated

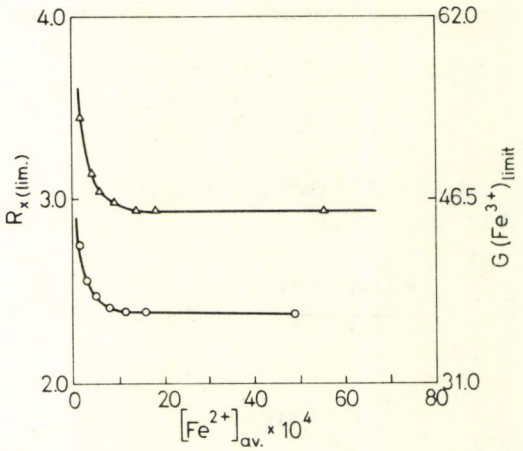

Fig. 2 -o- [RH] = 7.74×10^{-2}M, $[H_2SO_4]$ = 0.4 M Dose = 996 rads, O_2-saturated
-△- [RH] = 7.74×10^{-2}M, $[H_2SO_4]$= 0.05M, Dose = 893 rads, O_2-saturated

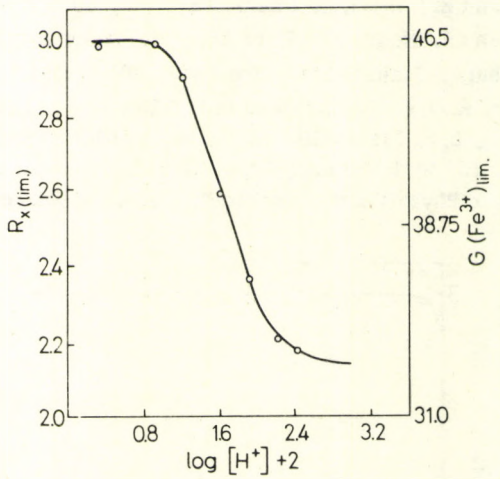

Fig. 3 [RH] = 4.61×10^{-2}M, $[Fe^{2+}]_{in}$ = 1.05×10^{-3}M, Dose = 941 rads, O_2-saturated

PART FOUR

MISCELLANEOUS PAPERS

THE ROLE OF LONG RANGE TUNNELLING IN ELECTRON TRANSFER PROCESSES WITH PARTICLES OTHER THAN TRAPPED ELECTRONS

R. F. Khairutdinov, K. I. Zamaraev
Institute of Chemical Physics of the Academy of Sciences of the USSR,
Moscow, USSR

The role of long range electron tunnelling in reactions with trapped electrons has been studied in many works (see, for example, /1,2/ and references therein). In this paper the experimental evidence is presented on the role of long range tunnelling in electron transfer reactions with particles other than trapped electrons, such as metal ions, aromatic and inorganic radical-ions and excited molecules.

1. Electron transfer from metal ions in low valence states to transition-metal complexes

Reactions

$$Cd(I) + Cr(VI) \longrightarrow Cd(II) + Cr(V) \quad (1)$$

$$Cd(I) + MN(VII) \longrightarrow Cd(II) + Mn(VI) \quad (2)$$

$$Cd(I) + Ag(I) \longrightarrow Cd(II) + Ag(0) \quad (3)$$

$$Ni(I) + Mn(VII) \longrightarrow Ni(II) + Mn(VI) \quad (4)$$

in vitreous 6M H_2SO_4-water solutions containing 0.05M or 0.16M $CdSO_4$, 1M $NiSO_4$ and various concentrations of $K_2Cr_2O_7$ (0 to 0.03M), $KMnO_4$ (0 to 0.5M) or $AgNO_3$ (0 to 0.06M) were observed at 77 K. Cd(I) and Ni (I) were produced by γ-irradiation of glasses at 77 K ($D=10^{19}$ ev/ml). The kinetics of reactions (1) – (4) were studied by measuring the decrease with the time of the intensity of Cd(I) and Ni(I) ESR spectra /3/. The decay curves for Cd (I) are given in Fig. 1. It is seen that the rates of Cd(I) decay depend on acceptor concentrations.

The rate of reaction (2) at 4.2 K is the same as at 77 K, while for reaction (1) the rate depends slightly on the temperature. The temperature independence of the rate of reaction (1) and the weak temperature dependence of the rate of reaction (1) indicate the tunnel mechanism of these processes. Reactions (3) and (4) also seem to proceed by the tunnel mechanism because of small diffusion coeficient

expected for water glasses at 77 K /2,4/. The decay curves for Cd(I) and Ni(I) are well described by the following equation which is characteristic for tunnel reactions

$$\frac{n(t,c)}{n(t,o)} = \exp\left(-\frac{\pi a^3}{6} C \ln^3 \nu t\right) \quad (5)$$

where n(t,c) is Cd(I) or Ni(I) concentration at a time t, C is Ag(I), Cr(VI) or Mn(VII) concentration, a and ν are parameters in expression for the dependence of the tunnelling rate constant k_t on the distance R between the reagents:

$$k_t = \nu \exp(-2R/a) \quad (6)$$

The values of a and ν which were obtained from experimental decay curves by minimizing the dispersion

$$\sigma^2 = \sum_{i=1}^{N} [n(t_i)_{exp} - n(t_i)_{theor}]^2 \quad (7)$$

as a function of two parameters a, ν for various C are summarized in Table 1. Note that at the moment these parameters should be considered as the average effective characteristics since more than one type of Cd(I), Ni(I), Cr(VI), Mn(VII), Ag(I) complexes can probably contribute to the experimentally observed decay process (e.g. complexes which contain in coordination sphere various number of SO_4^{2-} anions). It is seen from Fig. 1 that the theoretical curves which are obtained with the help of Eq. (5) and the values of a and ν from Table 1 are in a good agreement with the experimental data. The coincidence of the decay curves for 0.05M and 0.16M $CdSO_4$ allow us to rule out the possibility of electron transfer by consecutive jumps from Cd(I) to the neighbouring Cd(II).

Addition of 0.1M $CoSO_4$ or 0.1M $NiSO_4$ was found to produce no effect on Cd(1) radiation yield and its stability with time. Addition of $Ni(NH_3)_6Cl_2$ (0.02M) or $TlSO_4$ (0.1M) resulted in the decrease of Cd (I) yield, but not in the decay of Cd(I) with time. The absence of the electron transfer from Cd(I) to these acceptors can probably be explained by the different relations between their redox potentials in the solid matrix, i.e. E^0 /Cd(I):Cd(II)/ > E^0 /Co(I):Co(II)/. E^0/Ni(I):Ni(II)/, E^0 /Tl(0):Tl(I)/ and E^0 /Cd(I):Cd(II)/, < E^0 /Cr(V):Cr(VI)/, E^0 /Mn(VI):Mn(VII), E^0 /Ag(0):Ag(I)/. Decrease of Cd(I) radiation yield in the presence of $Ni(NH_3)_6Cl_2$ or Tl_2SO_4 can be explained by scavenging of electron-precursors of Cd(I). No influence of $CoSO_4$ and $NiSO_4$ on Cd(I) radiation yield is perhaps due to their small effeciency in competition for electron scavenging or due to the electron transfer from the excited states of Co(I)SO_4 and Ni(I)SO_4 to Cd(II). Addition of Cr(VI) results in the decrease of Ni(I) yield without any further decay with time. These data can also be explained

Table 1.

Donor	Acceptor	Matrix	T, K	ν, s^{-1}	a, Å	τ, s^{-1}			
						R=5Å	R=10Å	R=10Å	R=20Å
Reactions of inorganic ion-radicals									
NO_3^{2-}	CrO_4^{2-}	NaOH + H_2O	77	10^{20}	0.9	–	10^{-10}	10^{-6}	0.1
$AgNO_3$	SO_4^-	H_2SO_4 + H_2O	77	10^6	1.3	10^{-3}	10	-	-
$FeSO_4$	SO_4^-	H_2SO_4 + H_2O	4.2 to 77	10^7	1.8	10^{-5}	10^{-2}	1	10min
$K_4Fe(CN)_6$	O^-	NaOH + H_2O	4.2 to 77	10^{12}	0.8	10^{-7}	0.1	10h	-
Reactions of organic anion-radicals									
$(C_6H_5)_2^-$	$C_{10}H_8$	ethanol + ether	77	10^7	1.7	10^{-4}	10^{-2}	10	1h
Reactions between metal ions									
Cd(I)	$Cr_2O_7^{2-}$	H_2SO_4 + H_2O	77	10^{12}	1.4	10^{-9}	10^{-6}	10^{-3}	1
Cd(I)	MnO_4^-	H_2SO_4 + H_2O	4.2 to 77	10^{14}	1.3	10^{-11}	10^{-7}	10^{-4}	0.1
Ni(I)	MnO_4^-	H_2SO_4 + H_2O	77	10^{12}	1.2	10^{-8}	10^{-4}	10^{-1}	10min
Reactions of the excited molecules									
$C_{10}H_8^*$	CCl_4	ethanol	77–140	10^{14}	1	10^{-10}	10^{-5}	-	-

by assuming that Cr(VI) reacts only with electrons which are precursors of Ni(I). Thus, experimental results presented in this section indicate the possibility of long range electron tunnelling in reactions of metal ions in glasses.

2. Reactions between anion-radicals and transition metal complexes

Electron transfer from electron donors $FeSO_4$, $AgSO_4$ and $K_4Fe(CN)_6$ to electron acceptors – inorganic anion-radicals SO_4^- and O^- was observed at 77 K. The anion-radicals were produced by γ-irradiation of 6.5M NaOH – water or 6M H_2SO_4 – water glasses at 77 K. The average concentration of anion-radicals was much smaller than that of the added $FeSO_4$(0.05M), $AgSO_4$(0.06M) and $K_4Fe(CN)_6$ (0.3M). The decay kinetics was studied by the decrease with time of the intensity of ESR lines of O^- and SO_4^-. The experimental results are presented in Fig. 2. As it is seen from Fig. 2 the rate of the decay at 4.2 K is the same as at 77 K which indicates the nonactivated character of these reactions. The decay kinetics is well described by Eq. (5). Radiation yields of O^- and SO_4^- for fixed moments of time decrease exponentially with the increase of the donor particles concentration. All these facts indicate the tunnel mechanism of the electron transfer. Parameters a and ν which were obtained with the help of (5) by the same method as for processes (1) – (4) are summarized in Table 1.

3. Reactions of aromatic anion-radicals with aromatic molecules

Evidence for the existence of the long range electron tunnelling was also obtained for reactions of the type:

$$Ar_1^- + Ar_2 \longrightarrow Ar_1 + Ar_2^- \qquad (7)$$

where Ar_1 and Ar_2 are different aromatic molecules.
Kinetics of the decay at 77 K of biphenyl anion-radicals (ϕ_2) in the absence and in the presence of naphtalene (Nh) molecules in ethanol-diethyl ether glasses was studied. ϕ_2^- anion-radicals can be produced with high efficiency by γ-irradiation at 77 K of the solutions (D = 10^{19}ev/ml) containing ϕ_2(0.1M). ϕ_2^- spontaneously decayed at 77 K. The decay rate of ϕ_2^- anion-radicals, which was registered optically at 490 nm, increased after Nh addition. Decrease of temperature up to 4.2 K resulted in the total stop of ϕ_2^- decay in the absence and in the presence of Nh. Just as in the previous cases the tunnel mechanism of the electron transfer seems to be most probable for the process $\phi_2^- + Nh \rightarrow \phi_2 + Nh^-$ because of the extremely low mobility of the reagents even in the less rigid methylcyclohexane

glass /1/. Assuming that the spontaneous decay of $\phi\bar{2}$ and its reaction with Nh are independent processes one can write:

$$n/n_o = f_1(t/t_o) \cdot f_2(t/t_o) \tag{8}$$

$$f_2(t/t_o) = n/n_o \cdot [f_1(t/t_o)]^{-1} \tag{9}$$

where $f_1(t/t_o)$ and $f_2(t/t_o)$ are functions which describe $\phi\bar{2}$ decay by these two reactions separately. Parameters a and ν obtained from the experimental data with the help of (9) and (5) are summarized in Table 1. Note that in this case parameter ν is definitely temperature dependent. The value presented in Table 1 refers to 77 K.

4. Quenching of fluorescence in vitreous solutions by tunnel electron transfer reaction

The long range electron tunnelling was expected to be effective in reactions of excited molecules since the barriers for tunnelling from the excited states are smaller than in case of the ground states/1, 5/. We observed, together with Drs N. A. Sadovskii, V. N. Parmon and M. G. Kuzmin, the quenching of the fluorescence from the first singlet excited state of Nh by electron transfer to carbon tetrachloride. Figure 3 represents the corresponding fluorescence intensity decay curves. It is seen that for high concentrations of CCl_4 the decay curve is nonexponential. In principle, this fact can be explained in two different ways:

a) The kinetic curves observed may represent the sum of two exponentials, one of which describes the decay of free excited naphtalene and the other the decay of Nh in its complex form with CCl_4:

$$\frac{[M^*]}{[M^*]_o} = (1-\alpha)\ [\exp(-k_o t) + \frac{\alpha}{1-\alpha} \exp(-k_1 t)] \tag{10}$$

Here k_o and k_1 stand for the decay rate constants of the excited Nh in the free state and in the complex, respectively, α is the fraction of the complexed Nh.

b) The kinetic curves observed can represent the superposition of those for the spontaneous unimolecular decay with the rate constant k_o and of the decay by the electron transfer by tunnel mechanism to CCl_4. Assuming the random spatial distribution for CCl_4 molecules and bearing in mind that $[CCl_4] \gg [M^*]$ and $\ln \nu t \gg 1$ one can obtain the following expression to describe kinetics of such a process /5/:

$$\frac{[M^*]_t}{[M^*]_o} = \exp(-k_o t - A \ln^3 \nu t) \equiv \exp\ [-k_o t - A\ (D + \ln t)^3] \tag{11}$$

Here $A = \pi a^3/6$, $D = \ln \nu$, $N = C' \, 6 \times 10^{20}$, C is the concentration of CCl_4 in mole/l.

By minimizing the dispersion σ [Eq. (7)] of the theoretical curves in respect to experimental data the optimal sets of parameters a and ν were obtained for both situations. It is seen from Fig. 3 that Eq. (11) describes the experimental data much better than Eq. (10). The average for all the decay curves of Fig. 3 values of a and ν are summarized in Table 1. $\overline{k}_0$ is found to be equal to $(3.1 \pm 1) \times 10^6 sec^{-1}$ (k_0 in the absence of the acceptor is equal to $3.9 \times 10^6 sec^{-1}$). The marvelous fit of the experimental decay curves with the theoretical ones calculated with the help of Eq. (11), the coincidence of the decay curves for 77 K and 140 K (see Fig. 3) as well as the reasonable values obtained for a and ν support the tunnel mechanism of the reaction.

Note that the decay of phosphorescence intensity from the triplet excited state of Nh was found to obey the usual exponential law for all the concentrations of CCl_4 studied. On this ground electron tunnelling from this state to CCl_4 can be ruled out. Consequently long range electron tunnelling from excited naphtalene molecules to CCl_4 occurs from the singlet excited state of the donor.

The values of a and ν presented in Table 1 can be used to estimate the characteristic times $\tau = \nu^{-1} \exp(2R/a)$ of electron tunnelling over various distances. The result of such calculations are also presented in Table 1. It is seen that depending on the nature of reacting particles, electrons can tunnel during the periods of time from 10^{-10} sec up to 10 min. over the distances from several angströms up to several tens of angströms.

References

/1/ K. I. Zamaraev, R. F. Khairutdinov, Chem. Phys., 4, 181 (1974).

/2/ J. R. Miller, J. Phys. Chem., 79, 1070 (1975).

/3/ P. N. Moorthy, J. J. Weiss, Nature, 201, 1317 (1964).

/4/ R. F. Khairutdinov, Khimia vysokikh energii (in press).

/5/ R. F. Khairutdinov, N. A. Sadovskii, V. N. Parmon, M. G. Kuzmin, K. I. Zamaraev, Dokladi Akademii Nauk SSSR, 220, 888 (1975).

/6/ V. N. Parmon, R. F. Khairutdinov, K. I. Zamaraev, Fizika tverdogo tela, 16, 2572 (1974).

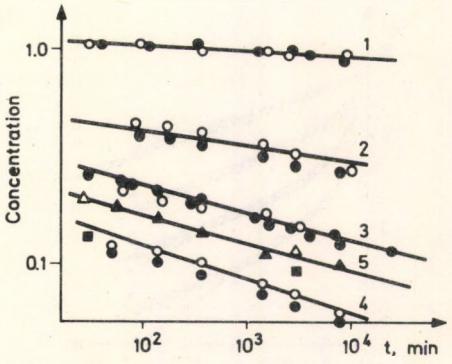

Fig. 1 Cd(I) decay curves for various concentrations of acceptors in 6M H_2SO_4 – water glasses at 77K. o Cd(II) =0.05M, ●, ▲, △, ■ – Cd(II) = 0.16M, 1 – in the absence of the acceptors, 2 – Cr(VI) = 0.02M, 3 – Cr(VI) = 0.04M, 4 – Cr(VI) = 0.06M, 5 – Mn(VII) = 0.05M. △, ■ – samples were immersed in Dewar vessel with liquid helium for the period between two measurements at 77K

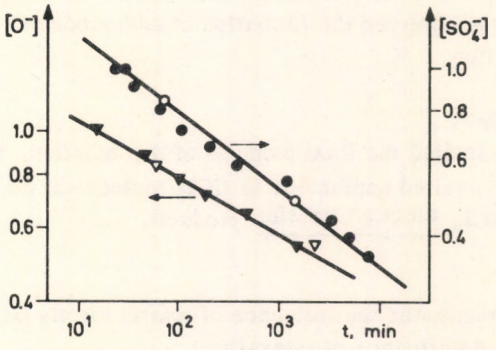

Fig. 2 O^- and SO_4^- decay curves at 77K (●, ▼) in 6M NaOH – water and 6M H_2SO_4 – water matrices containing 0.3M $K_4Fe(CN)_6$ and 0.05M $FeSO_4$ respectively. o, △ samples were immersed in Dewar vessel with liquid helium for the period between the two measurements at 77K

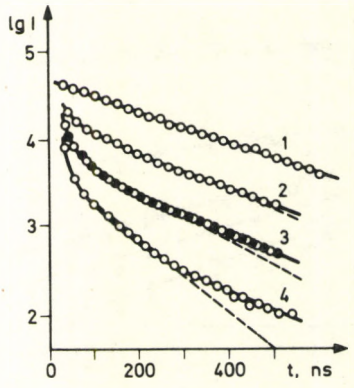

Fig. 3 Decay curves of Nh fluorescence in ethanol. o - 77K, • - 140K. Solid and dashed lines are the results of theoretical calculations with the optimal sets of parameters for Eq. (11) and Eq. (10) respectively

DISCUSSION

J. MAYER

Have you any evidence whether the reaction $Nh^{*} + CCl_4 \rightarrow Cl^{-} + CCl_3 + Nh^{+}$ proceeds? Have you observed the formation of such products? What is the driving force of this reaction?

R. F. KHAIRUTDINOV

We have not studied the final products of this reaction. We observed only electron transfer from excited napthalene to CCl_4 molecules. So I can write only the equation $Nh^{*} + CCl_4 \xrightarrow{\text{electron transfer}}$ products.

J. KROH

Have you investigated the influence of matrix history on the electron transfer to determine the significance of relaxation?

R. F. KHAIRUTDINOV

No, we have not. But I think that relaxation effect is negligible because of the temperature independence of the rate of the reaction.

G. R. FREEMAN

The frequency factors are $\nu \sim 10^{12} - 10^{14}\ s^{-1}$ and the distance parameters are $a \sim 1\text{Å}$. At what point can you distinguish between a tunnelling mechanism and an orbital overlap mechanism?

R. F. KHAIRUTDINOV

I speak about long range tunnelling. It is the reaction between particles, which are at a distance which is much longer than the sum of their radii. Tunnelling occurs due to the orbital overlap mechanism so I cannot distinguish between these two mechanisms.

G. R. FREEMAN

The term "tunnelling" is used often these days, and not all authors use it to mean the same thing. I would like to suggest that all authors who use the term include a definition of it in their paper. Would you please give the definition of tunnelling appropriate for your work?

R. F. KHAIRUTDINOV

I use the term "tunnelling" for the electron transfer reaction between two unmobilized particles, which are at a distance much longer than the sum of their radii, thus the reaction cannot proceed by thermal activation.

MATRIX ENDOR STUDIES OF THE ORIENTATION OF AMINE MOLECULES AROUND TRAPPED ELECTRONS IN γ-IRRADIATED AMINE GLASSES

Frank Q. H. Ngo*, Shoji Noda**, Larry Kevan
Department of Chemistry, Wayne State University, Detroit, Michigan, USA

Introduction

Solvated electrons produced in organic systems by ionizing radiation have excited considerable theoretical and experimental interest /1/. The kinetic features of electron solvation studied by pulse radiolysis, particularly in alcohols /2,3/, and the geometrical features studied by pulsed and double electron magnetic resonance techniques in alkanes /4/, ethers /5-7/, alcohols /5, 6, 8/ and even aqueous systems /9-11/ are beginning to emerge. The geometrical features are best studied in glassy matrices in which the electrons can be stabilized for relatively long times. Electrons are also solvated in glassy aliphatic amines /12-17/ but little structural information has yet been deduced for such systems. In primary and secondary amines it is easy to replace the NH protons by deuterons so that electron paramagnetic resonance (EPR) and electron nuclear double resonance (ENDOR) linewidth studies should yield structural data.

In EPR studies at 77K, the EPR linewidths of trapped solvated electrons are reported to be 24-25G for primary amines, 6.5-14G for secondary amines and 3-4G for tertiary amines /12, 15, 16/. The optical absorption spectra of these trapped, solvated electrons show small but noticeable spectral differences particularly in the maximum absorption wavelength, λ_{max}, for the three types of amines /12-14/. These spectral differences have been generally interpreted as due to differences in molecular dipole moment and molecular structure of the amines. The dipole moments of aliphatic amines decrease from primary to secondary to tertiary. However, no specific structural differences have been deduced.

In this study we have chosen sec-butylamine (SBA), diisopropylamine DIPA), and triethylamine (TEA) as representative primary, secondary, and tertiary amines, respectively. One objective is to deduce information about the molecular orientation of the various amines with respect to the electron by using partially deuterated amines. A second objective is to consider whether different size solvation shells account for the spectral differences between the primary, secondary and tertiary amines.

*Present address: Division of Biological and Medical Research, Argonne National Laboratory, Argonne, Illinois, USA

**Present address: Faculty of Engineering, Hokkaido University, Sapporo, Japan

Experimental

Amines bought from J. T. Baker Co. were purified as follows. The amine was first refluxed over potassium hydroxide pellets and then was repeatedly distilled under a nitrogen atmosphere. A middle portion of the distilled amine was collected, degassed, and treated with sodium-potassium alloy. The treated amine was stored in a bulb containing a freshly prepared potassium mirror to eliminate water remaining in the amine.

Partially deuterated amines, sec-butylamine-d_2(SBA-d_2) and diisopropylamine-d_1(DIPA-d) (with the NH protons replaced by deuterium), were prepared by repeatedly reacting the purified amine with D_2O (Stohler Isotope Co.). The percentage of deuteration can be adjusted by varying the volume percent of normal amine and D_2O. The final deuteration percentage was measured by mass spectrometry and nuclear magnetic resonance (NMR) spectroscopy.

The amine samples were sealed under vacuum in 7 mm I. D. spectrosil quartz tubing and quick frozen in liquid nitrogen to form glassy matrices. The samples were transferred at 77K to a ^{60}Co γ-source and irradiated in liquid nitrogen at dose rate of 0. 22 Mrad/hr. The primary, secondary, and tertiary amines were given total doses of 4. 8 Mrad, 3. 1 Mrad and 2. 0 Mrad, respectively, these doses correspond to the maximum yield of trapped electrons in these amines /7/. After irradiation, EPR and ENDOR measurements were immediately carried out in the dark to avoid electron decay and accidental photobleaching. The temperature during measurement was controlled by passing cold helium gas through a flow dewar in the ENDOR cavity.

EPR and ENDOR spectra were recorded with a Varian 4502 EPR spectrometer interfaced with a Varian E-700 ENDOR unit. ENDOR measurements were taken at a microwave power near the maximum intensity of the EPR microwave saturation curve of the trapped electron. The rf magnetic field was set near its maximum value of 5-6G.

Results

Primary amine:

In γ-irradiated sec-butylamine (SBA), we observe two distinct EPR signals, depending on the microwave power applied. The linewidths of these two signals are not changed when normal SBA is replaced by SBA-d_2. Figure 1 shows the first derivative of the EPR spectra at 0. 7 and 8 mW microwave power and 36K obtained from SBA-d_2. Using a microwave pover H_1=8mM, we observe a there line patern from which, by means of photobleaching and spectral subtraction, a broad singlet with a linewidth $\Delta H_{pp} \cong$ 23G could be obtained. This singlet, referred to here as signal A, has been reported and interpreted as due to a trapped electron in this amine /12, 17/. The main support for this interpretation appears to be that signal A can be bleached upon exposure to visible light. However, we have noticed that this EPR line has at least two peculiar features: (1) it has a similar microwave saturation curve to that of the

main three lines pattern with which it overlaps, (2) compared to other EPR signals of trapped electrons (for example to signal B of this amine and to those in DIPA and TEA), it is relatively stable to visible light.

On the other hand, when we reduce the microwave power by approximately one order of magnitude (H_1 = 0.7 mW), we observe that a much narrower singlet emerges from the broad background. This signal, referred to here as signal B, has a linewidth of ΔH_{pp} = 7G. To our knowledge this signal B has not been reported before. In addition to the dramatic difference in EPR linewidth compared to signal A, signal B is much more easily saturated by microwave power and more readily bleached by visible light.

ENDOR of both signals A and B has been attempted, however, only signal A ($\Delta H_{pp} \cong$ 23G) gave a response. The failure to obtain an ENDOR response from signal B ($\Delta H_{pp} \cong$ 7G) is probably due to the fact that the EPR signal is too weak. We have unsuccessfully tried to improve the conditions for ENDOR by using a partially deuterated sample (SBA-d_2) and also by varying the observation temperature. The matrix ENDOR line of signal A is shown in Fig. 2. The ENDOR linewidth ($\Delta \nu$) is 1.63 MHz in both SBA and SBA-d_2. Note that the signal-to-noise ratio of the ENDOR line is comparatively poor and that there is a slight contribution from the background radical (s). The radical contribution becomes more significant when the measurement temperature is lowered. However, the ENDOR line shown in Fig. 2 is mainly due to the bleachable component in the EPR spectrum.

Secondary Amine:

For a secondary amine, we have used undeuterated DIPA, 60% deuterated DIPA (60% of the NH protons being replaced by deuterons, DIPA-60% d) and 100% deuterated DIPA (100% of the NH protons being replaced by deuterons, DIPA-100% d). The percentage of deuteration was confirmed by NMR and mass spectroscopic measurements. The EPR spectrum of trapped electrons in γ-irradiated DIPA shows a singlet of linewidth ΔH_{pp} = 7.6 G which, within experimental error, does not change when NH protons are replaced by deuterons. Figure 3 shows the ENDOR spectra of the trapped electrons in DIPA and DIPA-100% d. The microwave power applied to obtain the ENDOR response did not saturate the background radical (s). As indicated by photobleaching, these ENDOR lines do not have a radical contribution. As shown in Table 1, the ENDOR linewidths in undeuterated and partially deuterated samples are essentially the same although the deuterated samples were reproducibly smaller when a relative comparison was made. Another interesting feature associated with the ENDOR spectra in DIPA is the existence of a pair of satellite ENDOR lines. These lines are better resolved in partially deuterated samples, as can be seen in Fig. 3. The distance between the satellite line at the high frequency side to the center of the matrix line is approximately 2 MHz. The intensity of the corresponding satellite at the low frequency side is smaller, a phenomenon generally observed for ENDOR spectra. A similar situation has been recently reported in the ethylene glycol/water matrix irradiated and measured at 4.2K /6/.

Tertiary Amine:

The EPR spectrum associated with the trapped electron in γ-irradiated triethylamine (TEA) is a very narrow singlet of linewidth $\Delta H_{pp} = 4G$, as reported by other workers /12, 15–17/. As in the case of DIPA, the saturation curve of this trapped electron by microwave power is distinctly different from that of the background rad-

Table 1

EPR and ENDOR linewidths of trapped electrons produced in γ-irradiated normal and partially deuterated diisopropylamines at 70K

Sample	EPR Linewidth	ENDOR Linewidth[a]	Measurement Temperature
DIPA	7.6 G	1.58 MHz	70K
DIPA-60% d	7.6 G	1.54 MHz	70K
DIPA-100% d	7.6 G	1.54 MHz	70K

[a] Estimated error is $\pm$ 0.02 MHz

Table 2

EPR and ENDOR linewidths of trapped electrons produced in γ-irradiated primary, secondary, and tertiary amine glasses at 77K

Amine	EPR Linewidths	ENDOR Linewidths[a]	ENDOR Satellite	Background radical contribution to ENDOR[b]	Measurement temperature
Signal B of SBA	7.0 G	No ENDOR	–	–	68–72 K
Signal A of SBA	23–24 G	1.63 MHz	No	Small	68–72 K
DIPA	7.6 G	1.58 MHz	Yes	None	67–70 K
TEA	4.0 G	1.89 MHz	No	None	40–70 K

[a] Estimated error is $\pm$ 0.02 MHz.

[b] Determined from ENDOR response at the same magnetic field after the sample was exposed to visible light.

ical (s). The EPR and ENDOR spectra of this trapped electron in TEA are shown in Fig. 4. Unlike that in DIPA, the ENDOR spectrum in TEA shows no satellite ENDOR lines. The matrix ENDOR linewidth ($\Delta\nu$= 1.89 MHz) in TEA is considerably larger than that in DIPA ($\Delta\nu$= 1.58 MHz). The EPR and ENDOR linewidths of the three amines are summarized in Table 2.

Discussion

The ENDOR responses observed in the present systems can be divided into two groups: the matrix ENDOR lines and the satellite ENDOR lines. The matrix ENDOR line which occurs at the free proton resonance frequency, can be interpreted as resulting primarily from dipolar interaction between the unpaired electron and the protons of the surrounding amine molecules /5, 18/, any contact interaction associated with these protons would shift the line away from the free proton frequency. The ENDOR linewidth decreases as the average distance to the dipolarly coupled protons increases, so if some of these protons are replaced by deuterons, the linewidth of the matrix ENDOR lines will be reduced. The satellite ENDOR lines, on the other hand, indicate some isotropic hyperfine interaction between the unpaired electron and its nearby protons. Such satellite ENDOR lines occur in pairs centered about the free proton frequency. However, the low frequency satellite ENDOR line is typically much weaker than the high frequency one.

Primary Amine:

In sec-butylamine, there appear to be two distinct EPR singlets: signal A and signal B. The interpretation that signal A is due to a trapped electron seems questionable for the reasons described in the results section. Furthermore, the rather broad EPR linewidth (ΔH_{pp} = 23 G) does not seem compatible with all other trapped electrons observed. Therefore, we suggest this signal is a radical species which is unstable to visible light. It is also possible that signal A is due to a trapped electron which is strongly coupled to nitrogen nuclei which broaden its EPR line and shorten its relaxation time. The EPR and ENDOR data obtained here are not sufficient to distinguish these possibilities; ^{15}N substitution is needed.

It is significant that we observe signal B at lower microwave power than for signal A. This is typical of trapped electron signals, so we assign this signal to a trapped electron. Other reasons that support this assignment are the following: (1) Signal B has a g-value close to the free spin value; (2) Signal B is very sensitive to visible light and has a saturation curve very different from that of the background radical (s); (3) The linewidth ΔH_{pp} = 7 G seems compatible with that for other trapped electrons in slightly polar systems. The weakness of signal B implies a relatively low concentration of trapped electrons, and suggests that SBA is an inefficient matrix for trapping electrons. This low trapping efficiency is perhaps not surprising in view of the low symmetry of the SBA molecule.

The identity of the EPR linewidth of signal B in both SBA and SBA-d_2 indicates that the spin of the electron has negligible contact interaction with the NH protons of the amine molecules. This appears to imply that the orientation of the amine molecules in the first solvation shell is such that the CH protons are closer to the trapped electron than are the NH protons.

Secondary amine:

There also appears to be no deuteration effect on the EPR linewidth for the trapped electron in di-isopropylamine, although there may possibly be a small effect on the matrix ENDOR linewidth. This indicates that there is nearly negligible hyperfine interaction involving the NH protons. The presence of a proton ENDOR satellite line and its enhancement in deuterated samples (DIPA – 100% d) imply that there is contact interaction between the unpaired electron and the CH protons, but not the NH protons.

In both SBA and DIPA we conclude that the electron does not interact significantly with the NH protons. Thus the electron is essentially in an alkane environment. A probable model for electron solvation is that the electron interacts with a methyl group from each of several amine molecules, in its first solvation shell. Interaction with CH and CH_2 protons is also possible but seems less probable due to steric factors. From electron spin echo modulation studies on ethers /7/ and alkanes /19/, it seems likely that there are 4–6 amine molecules in the first solvation shell. The similarity of the EPR linewidths in SBA and DIPA suggests that the distance from the electron to the first solvation shell protons is similar. Furthermore, the contact interaction inferred from the ENDOR data on DIPA suggests that the electron wavefunction is quite delocalized.

Tertiary Amine:

The linewidth (ΔH_{pp} = 4. 0 G) of the EPR line associated with the trapped electron in triethylamine is the narrowest among the three types of amines studied here. Note that this linewidth is very comparable to those observed for trapped electrons in alkane systems /1/. The similarity seems to indicate that in TEA the trapped electron is surrounded by alkyl protons with about the same geometry as for trapped electrons in alkane glasses. The absence of satellite ENDOR lines means that there is negligible contact interaction between the trapped electron and the closest alkyl protons. This is consistent with the larger EPR linewidth observed in SBA and DIPA.

As pointed out at the beginning of the discussion the matrix ENDOR linewidth decreases as the average distance to the dipolarly coupled proton increases. Since the matrix ENDOR linewidth in DIPA (1. 58 MHz) is less than in TEA (1. 89 MHz), this says that the dipolarly coupled protons are further away in DIPA. A quantitative

analysis assuming a nuclear spin packet linewidth of 100 Hz leads to a relation between the full width at half-height of the ENDOR line and the distance to purely dipolarly coupled protons/5/. Application to the data for DIPA and TEA gives a 0.2 Å distance difference. However, this does not mean that the trapped electron cavity in DIPA is larger than in TEA, because in DIPA the closest matrix protons to the electron have some contact hyperfine coupling and do not contribute to the matrix ENDOR line. The next nearest protons in DIPA, which we assume are purely dipolarly coupled to the electron, are $\sim$0.2A further away from the electron than the nearest protons in TEA.

The ENDOR results on TEA suggest that the 4 G EPR linewidth is due to purely dipolarly coupled protons. Then we can use Eq. (1) /4/ to calculate an average distance to the closest n equivalent protons. We assume n = 12 to 18

$$r(\text{Å}) = (40\, n^{1/2} / \Delta H_{pp})^{1/3} \qquad (1)$$

based on an analysis of electron spin echo modulation results /19/. These n values correspond to about 4–6 first solvation shell molecules interacting with the electron. The results are r = 3.3Å for n = 12 and r = 3.5Å for n = 18.

Summary

The NH deuteration experiments indicate that the alkyl protons of primary and secondary amines are closer than the NH protons to the trapped electron. The larger trapped electron EPR linewidths in primary and secondary amines compared to tertiary amines suggests a small contact hyperfine proton coupling, this is supported by the ENDOR data. The ENDOR and EPR results on trapped electrons in tertiary amines suggest that the proton interaction is purely dipolar and that the closest protons are $\sim$3.4Å from the electron. In the more polar primary and secondary amines the small proton contact interaction suggests that the closest protons are $<$ 3.4Å from the electron.

Acknowledgement. We are grateful for support of this research by the U.S. Army Research Office.

References

/ 1/ L. Kevan, Adv. Radiat. Chem. 4, 181 (1974).
/ 2/ J.H. Baxendale and P. Wardman, J. Chem. Soc. Faraday I, 69, 584 (1973).
/ 3/ W.J. Chase and J.W. Hunt, J. Phys. Chem., 79, 2835 (1975).
/ 4/ D.P. Lin and L. Kevan, Chem. Phys. Lett., in press.
/ 5/ J. Helbert, B.L. Bales and L. Kevan, J. Chem. Phys., 57, 723 (1972).
/ 6/ H. Hase, F.Q.H. Ngo and L. Kevan, J. Chem. Phys., 62, 985 (1975).
/ 7/ L. Kevan, M.K. Bowman, P.A. Narayana, R.K. Boeckman, V.F. Yudanov and Yu. D. Tsvetkov, J. Chem. Phys., 63, 409 (1975).
/ 8/ R.N. Schwartz, M.K. Bowman and L. Kevan, J. Chem. Phys., 60, 1690 (1974).
/ 9/ P.A. Narayana, M.K. Bowman, L. Kevan, V.F. Yudanov and Yu. D. Tsvetkov, J. Chem. Phys., 63, 3365 (1975).
/10/ B.L. Bales, M.K. Bowman, L. Kevan and R.N. Schwartz, J. Chem. Phys., 63, 3008 (1975).
/11/ S. Schlick, P.A. Narayana and L. Kevan, J. Chem. Phys. 64, 0000 (1976).
/12/ S. Noda, K. Fueki and Z. Kuri, Chem. Phys. Letters, 8, 407 (1971).
/13/ T. Ito, K. Fueki, A. Namiki and H. Hase, J. Phys. Chem., 77, 1803 (1973).
/14/ T. Shida, S. Iwata and T. Watanable, J. Phys. Chem., 76, 3683 (1972).
/15/ H. Tsujikawa, K. Fueki and Z. Kuri, J. Chem. Phys., 47, 256 (1967).
/16/ D.P. Lin and L. Kevan, J. Chem. Phys., 55, 2529 (1971).
/17/ T. Ito, S. Noda, K. Fueki and Z. Kuri, Can. J. Chem., 51, 2801 (1973).
/18/ J.S. Hyde, G.H. Rist and L.E.G. Eriksson, J. Phys. Chem., 72, 4269 (1968).
/19/ P.A. Narayana and L. Kevan, unpublished results.

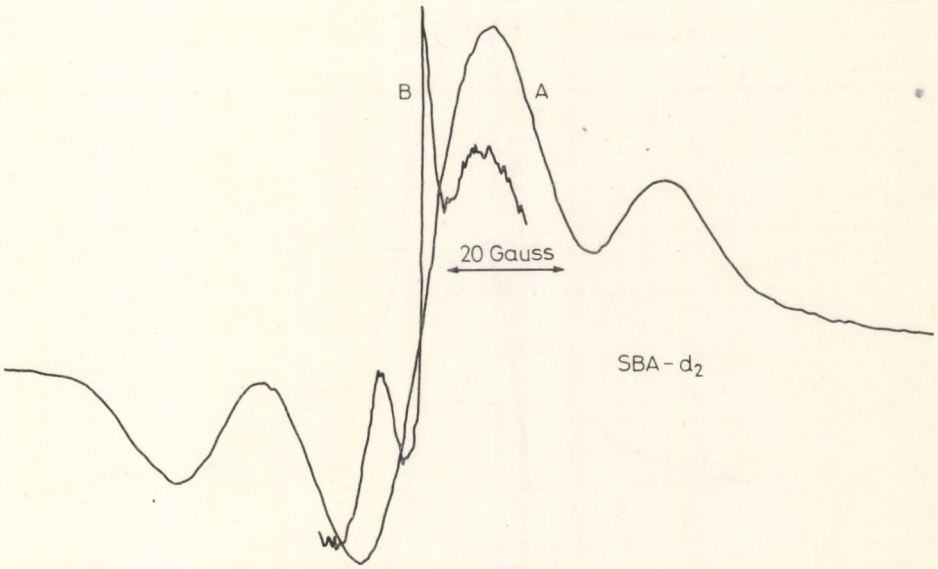

Fig. 1. EPR spectra obtained from γ-irradiated dideuterio sec-butylamine at 36 ± 2K showing two different signals, depending on the microwave power applied. Signal A is taken with P = 8 mW, H_m = 2G and signal B with P = 0.7 mW, H_m = 0.2G

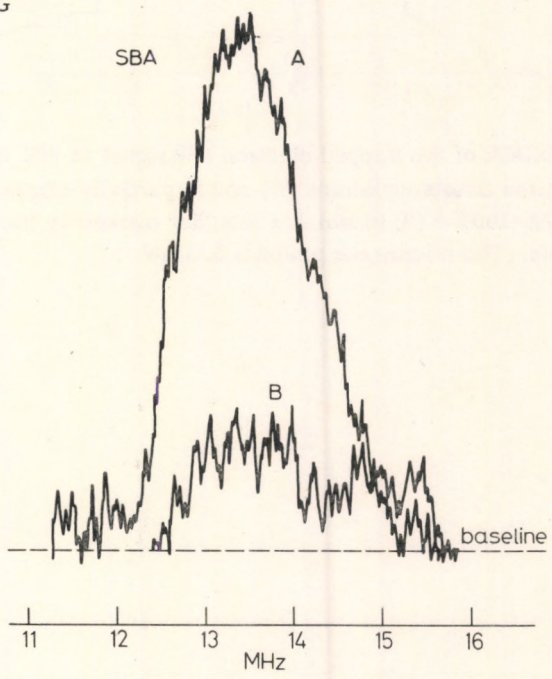

Fig. 2. Matrix ENDOR of EPR signal A of γ-irradiated sec-butylamine at 68K before (A) and after (B) photobleaching with visible light

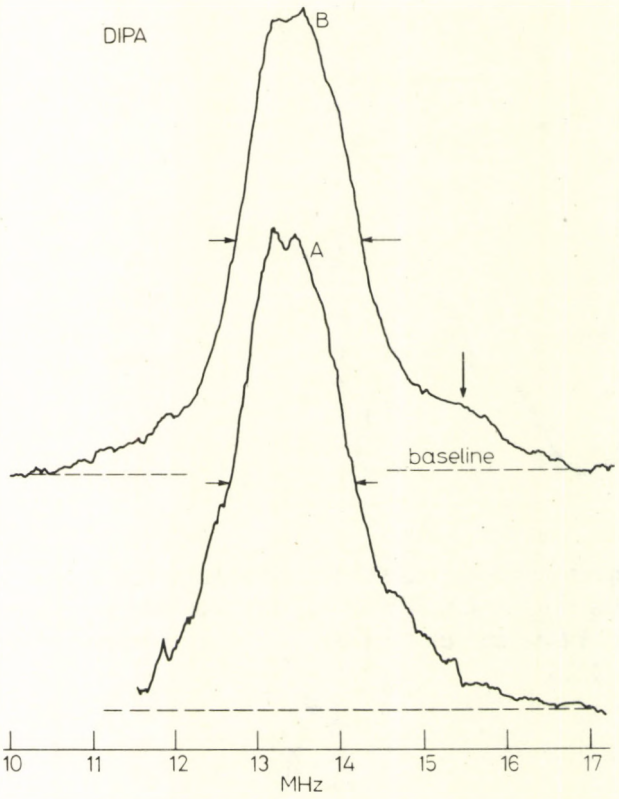

Fig. 3. Matrix ENDOR of the trapped electron EPR signal at 68K in γ-irradiated undeuterated diisopropylamine (A) and in partially deuterated diisopropylamine DIPA-100% d (B) in which a shoulder marked by the arrow is clearly observable. The microwave power is 3.5 mW

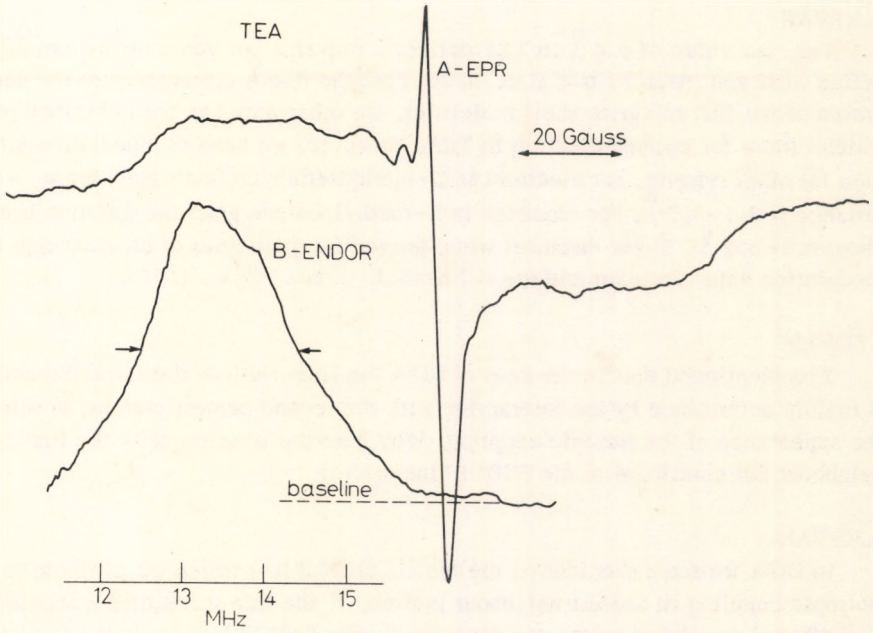

Fig. 4. Spectrum A shows the EPR of γ-irradiated triethylamine at 68K. Spectrum B shows the trapped electron while observing the EPR at the minimum of the derivative curve at 3.5 mW microwave power

DISCUSSION

Yu. D. TSVETKOV

Have you any idea about the arrangement of the second solvation shell of trapped electron in amine glasses?

L. KEVAN

No. To do this we need an experimental technique that is sensitive to much larger distances ($\gtrsim$10 Å) than we have now.

Yu. A. BERLIN

Is it correct to say that the value of radius between e^-_{tr} and H you have found may be attributed to the size of traps for the localized electron? Can you compare this value with data obtained by other authors?

L. KEVAN

Yes, our value of 3.4 Å in TEA defines a trap size but you must be careful to define what you mean by trap size. In our case the 3.4 Å corresponds to the nearest proton of the first solvation shell molecules. No other data has been obtained of which I know for trapped electron in TEA. However, we have obtained distance data for other systems. For electrons in 2-methyltetrahydrofuran glass the e_t^--H distance is 3.1-3.2 Å. For electrons in 3-methylpentane glass the distance is also about 3.1-3.2 Å. These distances were derived from analyses of electron spin echo modulation data. For example see L. Kevan, J. Chem. Phys., (1975).

J. SOHMA

You mentioned that in the case of DIPA the line width of the ENDOR spectrum is mainly determined by the interaction with the second nearest protons, in spite of the appearance of the isotopic coupling. Why does the coupling with the first nearest neighbour not contribute to the ENDOR line-width?

L. KEVAN

In DIPA we see a shoulder on the matrix ENDOR line which we attribute to isotropic coupling to nearest neighbour protons. If the line shape of this shoulder is estimated and this is subtracted from the matrix ENDOR line we will have a residual matrix ENDOR line that will be narrower than we reported. This corrected matrix ENDOR line will be mainly due to the next nearest neighbour protons. Protons which have much of an isotropic coupling, in this case the nearest neighbour protons, are split out from the free proton transport frequency and contribute little to the matrix ENDOR line.

I should mention that the semiquantitative relation of the matrix ENDOR linewidth and the minimum dipolar coupling distance is based on a very simple model which should be improved. We are currently trying to develop such an improved model which incorporates all dipolar interaction, forbidden spin transitions and dependencies on microwave and radio frequency magnetic field magnitudes.

CHEMICAL STATES OF RADIOACTIVE LANTHANIDE ATOMS IN Pr AND Nd FLUORINATED BETA-DIKETONATES

I. I. Gromova, Kh. M. Islamova, N. A. Lebedev, N. G. Zaitseva
Joint Institute for Nuclear Research, Dubna,
USSR

A large number of recent investigations dealing with the chemistry of fluorinated β-diketonates of rare earth elements (REE) offer the possibility of their use for different analytical purposes /1/. The consideration of the available data leads to the question whether these compounds can be used as a target material in the rapid separation and purification of lanthanides produced by nuclear reactions. Therefore, in the first place, we investigated the chemical states of the radioactive lanthanide atoms (Ln^*) formed by irradiating Nd and Pr trifluoroacetylacetonates and hexafluoroacetylacetonates with high energy protons.

The previous investigations dealing with the behaviour of radioactive atoms in irradiated β-diketonates /2–6/ indicate that the relative yields of the chemical forms depend on both the irradiation conditions and on the analysis method chosen.

In order to obtain complementary data which could provide better knowledge of the Ln^* stabilization process, we studied also the behaviour of Ln^* isotopes implanted into crystalline Nd hexafluoroacetylacetonates. The ion implantation procedure permitted simulation of the behaviour of a "hot" atom in the absence of any effects due to radiolytical processes induced by proton irradiation.

Experimental

The compounds of the $LnL_3 \times nH_2O$ (n = 1, 2) type, namely $Pr(TFA)_3$, $Pr(HFA)_3$, $Nd(TFA)_3$ and $Nd(HFA)_3$, were prepared by the method given in Ref. /7/.

Immediately before irradiation, they were recrystallized from hot benzene and the crystals were dried in a vacuum desiccator over $Mg(ClO_4)_2$.

High energy protons (E_p = 660 MeV) obtained from the JINR synchrocyclotron were used to irradiate the outgassed crystals and the solutions of the chelates in 0.1 M TBP/C_6H_6 (5 mg/ml) in sealed glass ampoules. The conditions of irradiation were as follows: the intensity of the external proton beam was about 10^{11} p/cm^2 × sec, the irradiation time was about 6 hours, and the dose of radiation received by the samples was ~ 20 Mrad /8/.

The lanthanum, cerium, praseodymium and neodymium radioactived atoms were obtained in the following types of reactions:

$$^{59}Pr\ (p, xpyn) \searrow$$
$$^{60}Nd\ (p, x'p'y'n) \nearrow \quad La^*,\ Ce^*,\ Pr^*,\ Nd^*,$$

$Ln^{*(1+)}$ ions were implanted using the isotope separator of the Department of Nuclear Spectroscopy and Radiochemistry (ref. /9/). The technique employed to produce carrier-free Ln* atoms with high specific activity and to prepare them for isotopic separation is described in Ref. /10/. Crystalline targets (90 – 110 mg/cm^2) designed for implantation, were prepared by desiccation of the $Nd(HFA)_3$ solution in acetone on glass plates (25 x 4) mm. Just prior to implantation, the samples were heated at 50°C during 40 min for the purpose of removing any possible defects. Separate $Nd(HFA)_3$ targets were used for the implantation of each of the isotopes as follows: Ce(A = 132, 134, 135, 137), ^{137}Pr, Nd (A = 138 and 139) and Tb (A = 148–151 154–156). The implantation was carried out at room temperature at 10^{-6} mm Hg during 15 min, the ion energy being 40 keV.

By taking the behaviour of Tb implanted ions as an example we investigated the effect of thermal annealing on the $Nd(HFA)_3$ crystals before and after implantation, the influence of the admixture of stable lanthanum in the form of $^{139}LaO^+$ ions, and the probability of implanting the accelerated Ln^{1+} ions into the $Zr(HFA)_4$ crystals, in which the metal central atom is of different chemical structure. These latter targets (13 – 16 mg/cm^2) were prepated just before implantation.

The chemical forms of radioactive Ln* atoms were analyzed using two techniques, i. e. distribution chromatography with a kieselguhr-filled column (l = 100 mm and d = 2 mm) and vacuum sublimation /3/.

In the first case the irradiated $LnL_3 \times nH_2O$ crystals were dissolved in a 0.1 M solution of TBP in C_6H_6. When the solutions percolated through the column, the compounds of the LnL_3 type were not retained on kieselguhr and were washed off by a 0.1 M solution of TBP in C_6H_6. Subsequently, the ligand-deficient forms $(LnL_{n-m})^{m+}$, (m = 1, 2), and Ln^{3+} ions were eluted by ethanol and 6M HCl, respectively.

Vacuum sublimation was employed only for an analysis of irradiated crystals of $Nd(HFA)_3$ and $Pr(HFA)_3$: this method is unsuitable for trifluoroacetylacetonate because of their low volatility. Sublimation was carried out at 140°C and 10^{-3} mm Hg for 1.5 h. After sublimation, we determined the relative abundances of individual radioactive isotopes both in the sublimates and residues, the weight loss in the chelate and the abundance of the corresponding lanthanide (Pr or Nd) in the residue and in the sublimate as well.

The samples obtained were analysed radiometrically using a Ge(Li) detector connected to the multi-channel pulse-height analyzer "Tensor"-4096 /11/, and the activations of the samples with implanted isotopes were measured by the device VA–M–146 (Vakutronik, DDR).

Results and Discussion

The chemical states of the Ln* atoms following the irradation of chelates with 660 MeV protons

Table 1 shows the relative quantities of the Ln* atoms stabilized in different forms as determined by distribution chromatography. These values are arithmetic means derived from several determinations ($N \geqslant 3$) with a r. m. s. error.

It follows from these data that the Ln* atoms stabilize mainly in the parent form. The substitution of water by TBP in the coordination sphere of the chelate complex and the following formation of the $LnL_3 \times 2TBP$ complexes /12, 13/ allow one to suppress the hydrolysis process and to eliminate its interference with the stabilization of the Ln* atoms as chelate forms with the complete number of ligands.

The complexometric analysis has shown that the relative retention value of Ln* coincides with the value of the relative amount of the target element (Pr and Nd). This coincidence can possibly indicate the rapid exchange of Ln* and Ln^{3+} in the C_6H_6-TBP solutions.

One could expect that exchange reactions would be less likely to occur in the solid phase during the sublimation of the irradiated crystals. The results for hexafluoroacetylacetonates are presented in Table 2. One can see here that in the case of the Pr chelate the relative amounts of radioactive isotopes and Pr macroquantities, passed into the sublimate, are rather close. As a result, the general picture of the Ln* distribution is similar to that obtained using distribution chromatography.

However, the sublimation of Ln* from $Nd(HFA)_3$ yielded considerably different results. Only 20 – 30% radioactive lanthanide isotopes including ^{130}Nd, passed into the sublimate, whereas about 80% of stable Nd was sublimated. This difference can be explained by the fact that the exchange reaction between the "hot" atom and the stable atom, i. e. $Ln^* + LnL_3 \longrightarrow Ln + Ln^*L_3$, depends on the chelate stability. In lanthanide series, the stability of complex compounds increase in going from lanthanum to lutecium. Therefore, the stabilization of the Ln* atoms as parent compounds is, in principle, more probable for Pr compounds than for Nd ones. It is possible that the sublimation analysis does not influence considerably the initial retention value.

The complexes $Pr(HFA)_3$ and $Nd(HFA)_3$ have practically the same radiolytical stability and the data (Table 2) suggest that they are destroyed at a rate of about 1% per 1 Mrad.

The chemical states of radioactive Ln*atoms implanted into crystalline Nd and Zr hexafluoroacetylacetonates

The results obtained from the analyses of the chemical states of Ln* atoms implanted into crystalline $Nd(HFA)_3$ and $Zr(HFA)_4$ are presented in Table 3. One can see that the relative yields of the Ln* chelate molecules, determined using

Table 1

Chromatographic yield of the Ln* chemical forms (%) for Pr and Nd beta-diketonates irradiated with 660 MeV protons

Chemical form	Ln^*	Crystals				Solutions			
		$Pr(TFA)_3$	$Pr(HFA)_3$	$Nd(TFA)_3$	$Nd(HFA)_3$	$Pr(TFA)_3$	$Pr(HFA)_3$	$Nd(TFA)_3$	$Nd(HFA)_3$
LnL_3	^{132}La	53^{+8}_{-}	79^{+4}_{-}	65^{+3}_{-}	50^{+9}_{-}	75^{+4}_{-}	81^{+0}_{-}	62^{+1}_{-}	73^{+10}_{-}
	$^{132,\ 135}Ce$	59^{+8}_{-}	70^{+4}_{-}	68^{+3}_{-}	59^{+3}_{-}	70^{+3}_{-}	71^{+5}_{-}	64^{+5}_{-}	67^{+7}_{-}
	^{138}Fr	61^{+4}_{-}	69	75^{+2}_{-}	75^{+2}_{-}	71^{+4}_{-}	–	–	–
	^{139}Nd	–	71	77^{+3}_{-}	59^{+14}_{-}	–	–	89^{+2}_{-}	66^{+6}_{-}
$(LnL_{3-m})^{m+}$ (M = 1, 2)	^{132}La	5^{+2}_{-}	3^{+1}_{-}	4^{+0}_{-}	15^{+5}_{-}	4^{+1}_{-}	5^{+1}_{-}	0	8^{+3}_{-}
	$^{132,\ 135}Ce$	5^{+1}_{-}	7^{+4}_{-}	6^{+1}_{-}	10^{+2}_{-}	6^{+2}_{-}	9^{+3}_{-}	2^{+1}_{-}	8^{+2}_{-}
	^{138}Pr	7^{+7}_{-}	12	0	0	0	–	–	–
	^{139}Nd	–	0	2^{+1}_{-}	16^{+11}_{-}	–	–	0	11^{+1}_{-}
Ln^{3+}	^{132}La	42^{+6}_{-}	18^{+3}_{-}	31^{+2}_{-}	35^{+4}_{-}	21^{+3}_{-}	14^{+1}_{-}	38^{+1}_{-}	19^{+7}_{-}
	$^{132,\ 135}Ce$	36^{+7}_{-}	23^{+3}_{-}	26^{+3}_{-}	31^{+2}_{-}	24^{+4}_{-}	20^{+5}_{-}	34^{+4}_{-}	25^{+5}_{-}
	^{138}Pr	32^{+3}_{-}	19	25^{+2}_{-}	25^{+2}_{-}	29^{+4}_{-}	–	–	–
	^{139}Nd	–	29	21^{+2}_{-}	25^{+11}_{-}	–	–	11^{+2}_{-}	23^{+6}_{-}

Table 2

The distribution of Ln* atoms between sublimates and residues (%) after the vacuum sublimation of Pr and Nd hexafluoroacetylacetonates

Beta-diketonate	Fraction	^{132}La	132, ^{135}Ce	^{138}Pr	^{139}Nd	Chelate amount			
						Irradiated chelate		Non-irradiated chelate	
						Gravimetric	Titrimetric	Gravimetric	Titrimetric
$Pr(HFA)_3$	Sublimate	51±4	68±6	65±3	–	90±4	88±5	93±2	93±0
	Residue	49±4	32±6	35±3	–	10±4	12±5	7±2	7±0
$Nd(HFA)_3$	Sublimate	20±3	34±1	27±6	27±1	80±6	80±6	92±0	91±0
	Residue	80±3	66±2	73±6	73±1	20±3	20±6	8±0	9±0

Table 3

Chemical states of Ln^* atoms (%) after their implantation into Nd and Zr hexafluoroacetylacetonates

β-diketonate	Ion implanted	Chromatography			Sublimation		Note
		LnL_3	$(LnL_{3-m})^{m+}$	Ln^{3+}	Passed to sublimate		
					Ln^*	$Me^{n+}(HFA)_n$ Me = Nd, Zr	
$Nd(HFA)_3$	$^{132, 134, 135, 137}Ce$	72±8	1±0	27±8	27±10	62±2	With thermal annealing of crystals before implantation
	$^{137}Pr^+$	71	0	29	30	70	
	$^{137}PrO^+$	81±3	1±0	18±2	not determined		
	$^{138, 139}Nd^+$	63±10	1±0	36±10	43±3	63±4	
	$^{138, 139}NdO^+$	87±3	0	13±3	86±4	88±3	
	$^{151, 154, 156}Tb^+$	65±3	1±0	34±8	93±4	78±8	
$Zr(HFA)_4$	$^{149, 150, 156}Tb^+$	not determined			84±4	72±5	Without annealing before implantation
	$^{150}Tb^+$	not determined			76	68	With thermal annealing after implantation
	$^{155}Tb^+$	not determined			48±1	75±0	Thermal annealing before implantation, uncontrolled admixture of $^{139}LaO^+$ in the $^{155}Tb^+$ beam
	$^{148}Tb^+$	14	1	85	not determined		With annealing before implantation
	$^{154}Tb^+$	not determined			4±2	94±1	

Table 4

The yield of $Ln^*(HFA)_3$ after the irradiation of $Nd(HFA)_3$ with 660 MeV protons and after the implantation of 40 keV $Ln^{*(+)}$ ions

Ln*	Chromatographic analysis		Sublimation analysis	
	660 MeV protons	40 keV $Ln^{*(+)}$	660 MeV protons	40 keV $Ln^{*(+)}$
Ce	59^{+3}_{-}	72^{+8}_{-}	34^{+1}_{-}	27^{+10}_{-}
Pr	75^{+2}_{-}	71	27^{+6}_{-}	30
Nd	59^{+14}_{-}	63^{+10}_{-}	27^{+1}_{-}	43^{+3}_{-}

chromatography, was practically the same (about 70%) for all of the Ln* atoms accelerated in the form of $Ln^{(1+)}$ ions and implanted into $Nd(HFA)_3$. In the case of Ln^*O^+ ions, this value increased to 80%, probably due to the fact that reformation reactions such as $Ln^* O^+ \dashrightarrow Ln^*(HFA)_3$ proceed to a large extent owing to the presence of oxygen in the ion implanted.

The sublimation analysis suggests that the thermal annealing of crystals does not affect, within experimental error, the formation of $Tb^*(HFA)_3$. However, the amount of Tb* stabilized in the chelated form was nearly twice as small as that in the case of implantation of the $^{155}Tb^{1+}$ ions, the beam of which contained the uncontrolled admixture of the $^{139}LaO^+$ ions. One can assume that in this case a considerably larger amount of damage occurs in the crystals, as compared with implantation of ultramicro amounts of $Ln^*(\gtrsim 10^{10}$ atoms/cm^2), and these damages hinder the formation of $Tb^*(HFA)_3$ molecules.

The extent of the damage of crystalline $Nd(HFA)_3$ probably depends on the size of the ion implanted. Figure 1 confirms this assumption by indicating that the stabilization of Ln* in the chelate form decreases with the increasing radius of the Ln* ion implanted.

The consideration of the implantation of $Tb^{*(+)}$ ions into crystalline $Zr(HFA)_4$ leads to the conclusion that the formation of $Tb^*(HFA)_3$ was unsubstantial possibly due to the fact that the larger Tb ions ($r = 0.93$ Å) cannot displace Zr ions ($r = 0.79$ Å) from the $Zr(HFA)_4$ lattice. In addition, one can assume that the defects produce disordered zones and prevent the reaction of $Tb^{*(1+)}$ with molecular fragments thus hindering the formation of the Tb* chelate. The results show that $Zr(HFA)_4$ is sublimed nearly completely (94%) after the implantation of $Tb^{*(1+)}$ ions into its crystals. This is understandable since the destruction of the thin layer of the substance induced by ion implantation (usually < 30 mg/cm^2) has no strong influence on the behaviour of the bulk material during sublimation. At the same time, the behaviour of the ions implanted and their reactions will be determined by the state of this surface layer proper.

On the basis of the analysis of the results characterizing the chemical behaviour of the same Ln* atoms introduced into crystalline $Nd(HFA)_3$ in different ways (by irradiation with 660 MeV protons or by ion implantation) (Table 4), one can conclude that the behaviour of radioactive Ln atoms is energy-independent.

References

/ 1/ R. Moshier and R. Sievers, Gas Chromatography of Metal Chelates, "MIR" Publishers, Moscow, 1967.

/ 2/ T. Tominaga, T. Sakai and K. Fujiwara, Bull. Chem. Soc. Japan, 44, 303 (1971).

/ 3/ N. G. Zaitseva, Kh. M. Islamova, Nguen Guin May and C. Ronneau, J. Inorg. Nucl. Chem. 37, 865 (1975).

/ 4/ N. G. Zaitseva, Kh. M. Islamova and Nguen Huyinh Mai, Radiochem. Radioanal. Lett. 16, 155 (1974).

/ 5/ H. Kawazu and M. Sakanoue, Radiochem. Radioanal. Lett., 16,373 (1974).

/ 6/ H. Meinhold and P. Reichold, Radiochim. Acta., 11, 175 (1969).

/ 7/ J. G. Stites, C. N. McCarty and L. L. Quill, J. Am. Chem. Soc. 70, 3142 (1948).

/ 8/ W. Stolz and K. Prokert, Kernenergie 8, 425 (1965).

/ 9/ V. P. Afanasiev, A. Vasilenko, I. I. Gromova, Zh. T. Zhelev, V. V. Kuznetsov, M. Ya. Kuznetsova, D. Monchka, Yu. Pomorsky, V. I. Raiko, A. V. Revenko, V. M. Soroko and V. A. Utkin, JINR Publication, 13-4763, Dubna, 1969.

/10/ F. Molnar, V. A. Khalkin and E. Hermann, PEPAN 4 1077 (1973).

/11/ V. S. Aleksandrov, F. Duda, O. I. Elizarov, G. P. Zhukov, G. I. Zabiyakin, Z. Zeidler, I. Zvolski, E. T. Kondrat, Z. V. Lysenko, V. I. Prikhodko, V. G. Grishin, V. I. Fominykh, M. I. Fominykh and V. M. Tsupko-Sitnikov, Izv. AN SSSR, ser. fiz. 34, 69 (1970).

/12/ J. W. Mitchell and Ch. V. Banks, Anal. Chim Acta 57, 415 (1971).

/13/ J. W. Mitchell and Ch. V. Banks, Talanta 19, 1157 (1972).

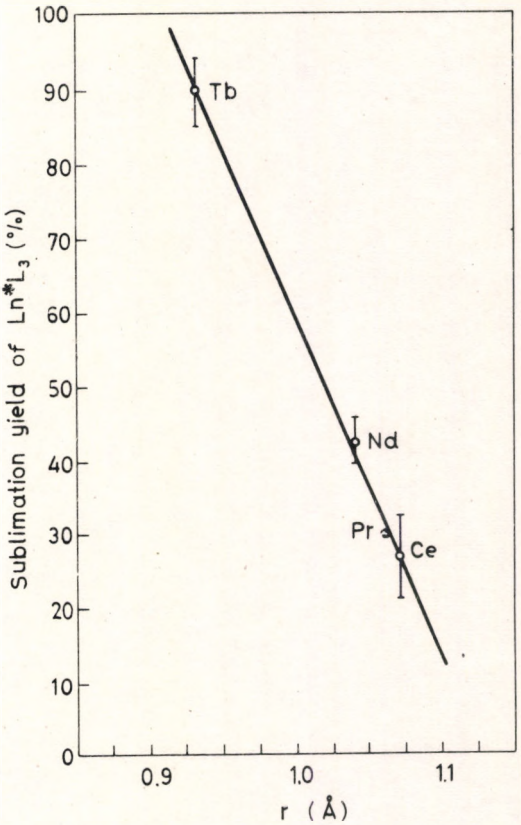

Fig. 1 The yield of labelled chelate molecules as a function of the radius of the Ln-ion implanted into $Nd(HFA)_3$ ($E_{Ln^{1+}}$ = 40 keV)

DISCUSSION

Z. SPURNY

I do not think that radiation effects of 600 MeV protons will be comparable with the influence of γ-radiation. Am I right?

N. G. ZAITSEVA

The radiolytic effect brought about by 600 MeV protons is comparable with that of γ-radiation. This has been shown for KCl as an example by Dolin and Bruesnueva. This is readily understandable if one considers high-energy proton absorption in a layer of the substance to be practically absent.

A THEORY OF ION PAIR RECOMBINATION TAKING INTO ACCOUNT TUNNELLING DECAY OF TRAPPED ELECTRONS

Yu. A. Berlin
Institute of Chemical Physics, The Academy of Sciences of the USSR,
Moscow, USSR

Irrespective of the corpuscular or electromagnetac nature of ionizing radiation its absorption in a substance leads to the formation of electrons with various initial energies as a result of primary, secondary, etc. processes. At the moment of the generation the major part of these electrons are "hot" i. e. their energy is higher than the average thermal energy of the surrounding molecules. But after a number of collisions, mainly inelastic ones, every fast electron transforms either into a thermalized and quasi-free or into a localized one.

Usually in non-polar condensed phase the second possibility is realized, the majority of electrons being localized at such distances from their "parent" cations that the energy of the Coulomb interaction between oppositely charged particles is higher than a thermal one. Such a system consisting of a positive ion and an electron formed from one and the same molecule and coupled by Coulomb attraction is called an ion pair /1–3/.

The investigation of the track structure has shown that in the case of low LET ionizing radiations a predominantly large number of these pairs may be considered as isolated ones because they do not overlap and do not interact with each other /2/. Their recombination plays an important role in a number of radiation-chemical transformations as well as in the mechanism of luminescence and electroconductivity induced by radiation in non-polar liquids and solids.

The decay of isolated ion pairs is usually believed to be caused by thermally activated electron "hopping" motion to the "parent" cation due to consecutive transitions from one localized state to another. This motion is analogous to random walk in Coulomb field and often may be described by a simple diffusion equation as has been shown by the author of the present paper /3/. However, it has recently been discovered that at sufficiently low temperatures the electron transfer from the initial trap to a neutral or charged reaction centre may be realized not only by random walk but also due to the direct quantum mechanical tunnelling /4–7/.

The purpose of this work is to describe the kinetics of ion pair recombination using a unified picture taking into account both the possibility of electron tunnelling transfer (ETT) from any trap being occupied by electron during its life-time and the stochastic motion of isolated ion pair components.

Let $P(\vec{r}, \vec{r}_o, t)\, d\vec{r}$ denote the probability that a trapped electron (e^-_{tr}) of an ion pair is to be found between the distances $\vec{r}$ and $\vec{r} + d\vec{r}$ from a positive ion at a time t if the charge separation was equal to $\vec{r}_o$ at zero time. Taking into consideration ETT and following the procedure described in Ref. /3/ it may be shown that P satisfies the equation:

$$\frac{\partial P}{\partial t} = D\left[\frac{1}{r^2}\,\frac{\partial}{\partial r}\left(r^2\frac{\partial P}{\partial r}\right) + \frac{\alpha}{r^2}\,\frac{\partial P}{\partial r}\right] - w_T(r)P \qquad (1)$$

with the initial condition

$$P(\vec{r}, \vec{r}_o, 0) = \delta(\vec{r}-\vec{r}_o), \qquad (2)$$

where D is the total diffusion coefficient of the ion pair components, α is the Onsager length defined as $e^2/(\varepsilon k T)$, e is the electronic sharge, ε is the dielectric constant of the medium, k is the Boltzmann constant, T is the absolute temperature, $W_T(r)$ is the probability of tunnelling recombination per unit time for the electron localized at the distance r from the "parent" cation.

The first term in the right hand side of Eq. (1) describes the random walk of ion pair components, the second their drift in the Coulomb field and the third represents ETT from a trap to the corresponding level of positive ion.

The problem expressed by Eqs (1, 2) can be solved by the method of prescribed diffusion /2/. According to this method $P(\vec{r}, \vec{r}_0; t)$ may be approximated by the function

$$P(\vec{r}, \vec{r}_0; t) = (4\pi D t)^{-3/2} \exp\left[-(\vec{r}-\vec{r}_0)^2/(4Dt)\right] F(t). \qquad (3)$$

Substituting (3) into (1), averaging the obtained expression over all possible directions of $\vec{r}_0$ and integrating over all r, we get the following ordinary differential equation for F:

$$\frac{dF}{dt} = -\gamma t^{-1/2} \exp\left[-r_0^2/(4Dt)\right]\left[t^{-1} + S(r_0, t)/(\alpha r_0)\right] F, \qquad (4)$$

where

$$\gamma = \alpha\,(4\pi D)^{-1/2};\quad S(r_0, t) = 2\int_0^\infty r\, W_T(r) \exp\left[-r^2/(4Dt)\right] \times \mathrm{sh}\left[r r_0/(2Dt)\right] dr.$$

Denoting $\mathrm{erfc}(z) = 1 - 2\pi^{-1/2}\int_0^z \exp(-\xi^2)\, d\xi$ and $\psi(r_0, t) = \int_0^t \gamma x^{-1/2} \exp\left[-r_0^2/(4Dx)\right] S(r_0, x)/(\alpha r_0)\, dx$ one can obtain that a solution of Eq. (4) can be expressed by the funcion

$$F(r_0, t) = \exp\left[-\alpha\, \mathrm{erfc}\left(r_0/\sqrt{4Dt}\right)/r_0 - \psi(r_0, t)\right], \qquad (5)$$

which represents the probability that all e_{tr}^- localized at the distance r_0 from their cation-pairs at zero time remain unneutralized at time t.

Formula (5) has been obtained using the assumption that all isolated ion pairs have the same characteristic dimension r_0. But in fact electrons are localized at different distances from positive ions due to the statistical nature of the electron interaction with surrounding molecules and a wide spectrum of their initial energies. Therefore in a real case the probability that charges of an ion pair have a life-time t before recombination must be characterized by the average value of F:

$$\overline{F}(t) = \int_0^\infty g(r_0) \exp[-\alpha \operatorname{erfc}(r_0/\sqrt{4Dt})/r_0 - \Psi(r_0, t)]\, dr_0, \qquad (6)$$

where $g(r_0)$ is the distribution of initial distances between components of ion pairs.

Expression (6) determines the general solution of our problem for arbitrary $W_T(r)$ and $g(r_0)$. Side by side with such general solution it is interesting to consider the dependence $\overline{F}$ on t for the actual form of $W_T(r)$.

Usually

$$W_T(r) = \nu \times \exp(-2\,kr), \qquad (7)$$

where ν is a frequency factor, k is the inverse characteristic distance for the attenuation of e_{tr}^- wave-function*. This dependence of the ETT rate on r leads to the following form of Ψ :

$$\Psi(r_0, t) = \nu/(8Dk^3 r_0)\{\exp[2k(r_0 + 2Dtk)][k(4Dtk + r_0) - 1] \times \operatorname{erfc}[(4Dt)^{1/2} k +$$

$$+ r_0/(4Dt)^{1/2}] - \exp[-2k(r_0 - 2Dtk)] \times [k(4Dtk - r_0) - 1] \operatorname{erfc}[(4Dt)^{1/2} k -$$

$$- r_0/(4Dt)^{1/2}] - 2\exp(-2kr_0)(kr_0 + 1) + 2\operatorname{erfc}[r_0/(4Dt)^{1/2}]\} \qquad (8)$$

If one accepts that $g(r_0) = 4\gamma^{3/2} \pi^{-1/2} r_0^2 \exp(-\gamma r_0^2)$ /3/, then it is possible to calculate $\overline{F}(t)$ by the substitution of (8) in (6) and the subsequent integration. The latter can be carried out only numerically.

* A more accurate formula must take into account the distortion of the potential barrier for e_{tr}^- by the Coulomb field of the cation. However, the estimates show that for the most part of non-polar substances this fact may have an influence on $W_T(r)$ only at such small distances which do not make a significant contribution to the value of the integral $S(r_0, t)$. Therefore the error in the calculation of $\overline{F}$ (t) connected with the neglect of the exact form of the barrier for e_{tr}^- is unimportant.

Figure 1 illustrates the variation of $\bar{F}$ with time obtained by means of the above-mentioned mathematical operations. The following values of parameters have been used in these calculations: $\gamma = 1.27 \times 10^{12}$ cm^{-2}, $D = 6.5 \times 10^{-5}$ cm^2/sec. and $\nu = 10^{13}$ sec^{-1}. We have also taken $k = 3.63 \times 10^{7}$ cm^{-1} corresponding to the trap depth$\sim$0.5 eV. The dashed curve has been plotted for the case when both ETT and random walk exert an influence on the kinetic of ion pair decay, while the solid one refers to the case when the only reason for the process is random walk of ion pair components.

From (8) one can obtain that for $t \to \infty$

$$r_0 \Psi(r_0, \infty) = R_T = \nu [1 - \exp(2 - 2kr_0)(kr_0 + 1)]/(4Dk^3) \qquad (9)$$

and hence

$$\bar{F}(t \to \infty) = \bar{F}_\infty = \int_0^\infty g(r_0) \exp[-(\alpha + R_T)/r_0] dr_0. \qquad (10)$$

Expression (10) allows us to calculate the quantity of the free ion yield G_{fi} as expressed by F_∞ and the total yield of geminate pairs G_i by the simple relation $G_{fi} = G_i \bar{F}_\infty$.

The important consequence of Eq. (10) consists in the fact that from a kinetic point of view the effect of ETT is equivalent to the interaction becoming stronger between components of isolated ion pairs. Indeed, Eq. (10) shows that ETT increases the effective range of the Coulomb potential by the radius R_T determining the dimension of the spherical zone around the cation inside which the electron has a small probability to escape recombination due to its stochastic motion because of the high rate of tunnelling from any trap situated in this zone to the "parent" positive ion.

It is interesting to note that in the framework of the present theory the expressions for $\bar{F}_\infty$ and G_{fi} differ from the well-known Onsager formula /8/ taking into account only the proccess of the electron "hopping" motion. Thus, for example, the value of $\bar{F}_\infty$ depends not only on the initial distance between components of the ion pair, but also on the magnitude of the electron diffusion coefficient. However, if $D \gg \nu/(4\alpha k^3)$ and the contribution of ETT in the mechanism of recombination is negligible, Eq. (10) gives

$$\bar{F}_\infty = \int_0^\infty \exp(-\alpha/r_0)\, g(r_0)\, dr_0. \qquad (11)$$

This expression agrees exactly with results obtained by Onsager /8/.

Finally let us describe the physical picture of the kinetics of the ion pairs recombination in condensed phase arising from our consideration.

According to Eqs (6) and (8), if t satisfies the inequalities

$$4Dtk^2 \ll 1, \tag{12}$$

$$4Dt \ll \bar{r}_0^2, \tag{13}$$

then $\Psi(r_0, t) = \nu t \exp(-2kr_0)$ and (6) may be reduced to the form

$$\bar{F}(t) = \int_0^\infty g(r_0) \exp[-\nu t \exp(-2kr_0)]\, dr_0. \tag{14}$$

The condition (12) means that t is much shorter than the period of time $\tau_i = 1/(4Dk^2)$ which is necessary for the displacement of electron to the characteristic distance of tunnelling $1/k$ by random walk. It is easy to show by differentiation of Eq. (6) with respect to time or directly from Eq. (4) that for such values of t

$$\frac{d\bar{F}}{dt} = -\int_0^\infty g(r_0)\, \nu \exp[-2kr_0 - \nu t \exp(-2kr_0)]\, dr_0. \tag{15}$$

Thus for ion pairs with the shortest life-time $\tau \ll \tau_1$ the rate of their recombination is determined mainly by the rate of direct ETT from the trap to the corresponding level of the positive ion and not by random walk of their components. However, the influence of the last process on the kinetics of ion pair decay increases gradually with t. In particular, it is manifested in the replacement of the considerably simple kinetical law (15) by the more intricate dependence [see Eqs (6) and (8)], which does not allow one to consider the recombination of ion pairs either as a first-order reaction or as a second-order one. The same situation is typical for many diffusion-controlled reactions /2,3/. Asymptotic expansions of Eq. (8) demonstrate directly that for large times $t \gg \bar{r}_0^2/(4D)$ the kinetics of recombination obey the pseudo-first-order law

$$\frac{d\bar{F}}{dt} = -\gamma[(1 + \nu/(4Dk^3\alpha)]t^{-3/2}\bar{F}, \tag{16}$$

which is completely analogous to the law obtained previously by Mozumder /2/ for the usual diffusion decay of the isolated ion pair.

References

/1/ V.L. Talrose, "Effects of the Electric and Magnetic Fields on the Phenomena and Chemical Processes Induced by Ionizing Radiation", Actions Chimiques et Biologiques des Radiations, ed. M. Haissinsky, 11 ser., 1967, Masson et Cie, Paris.

/2/ A. Mozumder, "Charge Particle Tracks and Their Structure", Advances in Radiation Chemistry, vol. I. eds M. Burton, J.L. Magee, Wiley-Interscience, New-York-London-Sidney-Toronto, 1969.

/3/ Yu. A. Berlin, Ph. D. Thesis, Moscow physical technical institute, USSR (1974).

/4/ K.I. Zamaraev, R.F. Khairutdinov, A.I. Mikhailov, V.I. Goldanskii, Dokl. Akad. Nauk SSSR, 199, 640 (1971).

/5/ A.I. Mikhailov, Dokl. Akad. Nauk SSSR, 197, 136 (1971).

/6/ Yu. A. Berlin, V.V. Kulakov, V.G. Nikolsky, Dokl. Akad. Nauk SSSR, 215, 887 (1974).

/7/ Yu. A. Berlin, V.V. Kulakov, B.G. Nikolsky, Int. J. Radiat. Phys. Chem. (in press).

/8/ L. Onsager, Phys. Rev., 54, 554 (1938).

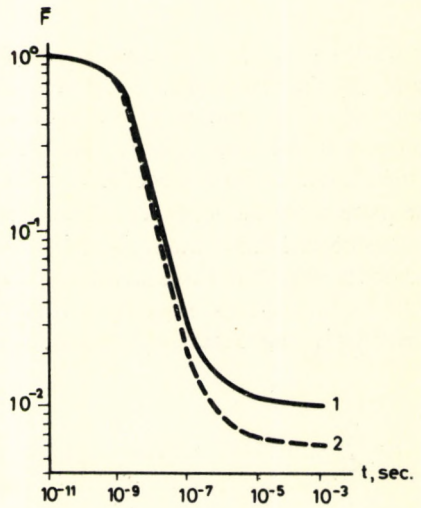

Fig. 1 Plot of $\bar{F}$ as a function of time t. Curve 1 – the case of the usual recombination of ion pairs caused by random walk of their component, curve 2 – the case when the recombination of ion pairs is a result of both electron tunnelling transfer and stochastic motion in the Coulomb field of the "parent" cation. In all the calculations the following parameter values have been used:
$\gamma = 1.27 \times 10^{12}\ cm^{-2}$, $D = 6.5 \times 10^{-5}\ cm^{-2}/sec$,
$k = 3.63 \times 10^{7}\ cm^{-1}$, $\nu = 10^{13}\ sec^{-1}$.

DISCUSSION

G. R. FREEMAN

(1) At what distance does tunnelling dominate the ion–electron recombination in a liquid alkane, say in n–hexane at 300K?

(2) At what distance would tunnelling dominate in an alcohol, say in methanol at 300K?

(3) The prescribed diffusion approximation is convenient for the solution of your problem, but it is not usually very accurate. In what way do you think that the prescribed diffusion approximation distorts your results? Would it tend to increase or decrease your estimates of the contribution of tunnelling?

(4) How is the tunnelling barrier height affected by the dielectric constant of the medium?

(5) What is the rationalization of the factor $e^{-\gamma r_0^2}$ in $g(r_0)$?

Yu. BERLIN

(1) In liquid n–hexane at 300K electron tunnelling makes a negligible contribution to the mechanism of the ion pair recombination. But for temperatures below about 100K tunnelling is very important for the kinetics of ion pair decay. The characteristic distances may reach several tens of Angströms.

(2) To answer this question it is necessary to have information about four parameters D, $\bar{r}_0$ ν and k. I have no such information just now. But I think that at room temperature tunnelling is unimportant for the kinetics of ion pair decay. The main contribution of tunnelling as I have mentioned above must be observed at lower temperatures.

(3) The prescribed diffusion approximation gives an accurate qualitative picture of ion pair recombination. But one can take into account that the accuracy of prescribed diffusion approximation increases with the increase of tunnelling contribution to the mechanism of recombination. So I think that method used for solving Eq(1) may be used for rather precise estimations of tunnelling contribution.

(4) The decrease of dielectric constant and the increase of the Coulomb interaction connected with this fact decrease the height of the barrier. This fact has been taken into account by the k factor in Eq. (7).

(5) The factor $e^{-\gamma r_0^2}$ in $g(r_0)$ is a typical exponential factor in Gaussian type distribution. Its physical meaning is well known and I cannot add anything to all the explanations published in the literature.

Yu. D. TSVETKOV

What type of r_0 distribution function did you use in your calculation?

Yu. BERLIN

We use for illustrative calculations the distribution of the form $g(r_0) = 4\gamma^{3/2}\pi^{-1/2}\exp(-\gamma r_0^2)r_0^2$.

R. SCHILLER

You have combined radial diffusion equation with a term which describes tunnelling. I think this is a very important step forward. I have, however, some doubts regarding the validity of the classical, causal form of the diffusion equation for the present case. The condition which refers to the mean free path to be much smaller than displacement of the diffusing entity seems not to be fulfilled if the distances are short enough for tunnelling to be effective.

Yu. BERLIN

The validity of diffusion equation has been discussed by us in a recent paper published in Int.. J. Radiat. Phys. Chem. But I would like to repeat here again that the present data about the mobility of electrons shows that the term "free path" has no meaning for an electron migrating by "hopping" mechanism. Instead of this term it is necessary to use the term "average hopping distance" which is only formally analogous to "mean free path". For systems where $\bar{1} \ll \bar{r}_0$ (*) we may use the diffusion equation for kinetic problems. It is important to note that the inequality (*) limits only the application of the first two terms in Eq. (1). The use of the last term of Eq. (1) has no limitations in terms of the condition (*). So if inequality (*) is satisfied the complete equation (1) is valid. This fact may be shown accurately by methods developed in my paper mentioned above.

H. WINCEL

You presented here the formal solution of the equation for ion-pair recombination.

(1) Did you investigate any correlation with real systems?

(2) What is the influence of variation of particular parameters (especially frequency factor) involved in the equation on the overall kinetic value of the process?

(3) Where is the electron affinity of the compound included?

Yu. BERLIN

(1) The data I have mentioned above (see Fig. 1) refer to liquid n-hexane at about 100K. Of course they are not experimental data only calculations with the parameters characteristic for this hydrocarbon. Unfortunately at the present time we have no experimental measurements which may be used for the comparison between the present theory and experiment. But I hope that such experiments will be carried out in the future.

(2) If we compare two systems with different frequency factors the contribution of tunnelling will be greater for the substance with higher ν.

(3) The electron affinity is included in the k factor.

ON THE THEORY OF RADIATION-INDUCED INITIATION OF CHAIN PROCESSES

V.L. Tal'roze, Yu. A. Berlin, I.K. Larin
Institute of Chemical Physics, Academy of Sciences of the USSR,
Moscow, USSR

Radiation-chemical initiation (RCI) of chain reactions is widely known and has been investigated for a number of unbranched (polymerization /1–3/, halogenation /4/, isotope exchange /5/, cracking /6/, low-temperature oxidation /7/), and branched (slow oxidation of organic compounds at an elevated temperature /8,9/) chain processes.

This paper deals with formal kinetics of the RCI of chain processes. A graphical method is used for representing a region in the logarithm of the dose rate vs. reciprocal temperature plot, which will be defined as the region of an efficient radiation-induced chemical reaction (ERC). The concept of efficiency implies four criteria to be met.

Initiation criterion (i-criterion). The rate W_{ir} of RCI reactions is higher than or equal to W_{it} of thermal initiation

$$W_{ir} \geq W_{it} \tag{1}$$

Here

$$W_{ir} = 10^{-2} \, GI \text{ of active species/cm}^3 \text{ sec} \tag{2}$$

where I stands for the dose rate expressed in eV/cm^3sec, G for the radiation yield of active species per 100 eV of energy absorbed. The overall initiation rate is

$$W_i = W_{ir} + W_{it} \tag{3}$$

Chain criterion (ν-criterion). The reaction is considered to be a chain one, when ν is higher than unity

$$\nu = \frac{W_p}{W_t} > 1 \tag{4}$$

where W_p is the chain propagation rate, W_t the chain termination rate.

Criterion of absolute rate (W-criterion). The reaction rate exceeds the necessary value

$$W \geqslant W_u \tag{5}$$

For practical purposes it is convenient to use the W-criterion as a condition for a sufficiently short time of conversion of the component p to a stipulated extent, for instance 1% - τ 0.01.

$$\tau_{0.01} < \tau_u \tag{6}$$

Criterion of a sufficiently intense radiation source (r- criterion). The source available ensures the necessary dose rate I_n

$$I \geqslant I_n \tag{7}$$

The definitions used are: N for the total compound concentration, cm^{-3}, n_m for the m component concentration, cm^{-3}, α_m for the molar fraction of the m component, k for the rate constant, sec^{-1} or $cm^3 sec^{-1}$ or $cm^6 sec^{-1}$. A for the pre-exponential factor of the Arrhenius equation, E for the activation energy, cal/mole, i for the elementary step index, p for an elementary step of chain propagation, b for an elementary step of chain branching, t for time or for the index of elementary chain-terminating process, T for absolute temperature or for the index of a thermal reaction, R for the universal gas constant, ∞ for the index of a value extrapolated to $T = \infty$, the number of primes above the relevant symbol indicates the reaction order.

1. Unbranched Chain Processes

The curves for the i-, ν-, W-, and r- criteria in this case (Fig. 1) were obtained by the following expressions:

i-criterion:

$$\log I > \log I_i = \log (k'_{iT} \alpha_i N + k''_{iT} \alpha_1 \alpha_2 N^2) - \log G \cdot 10^{-2} \tag{8}$$

Here $k'_{it} \alpha_i N$ corresponds to unimolecular, and $k''_{it} \alpha_1 \alpha_2 N^2$ to bimolecular initiation. Since the activation energy for unimolecular initiation E'_i is higher than that for bimolecular initiation E''_i, the first occurs at high, and the second at low temperatures.

ν-criterion:

$$\log I > \log I_{\nu=1} = \log\left[\frac{A''^2_p n_p}{10^{-2} a_{t2}} \exp(-2E_p/RT) - \frac{a_{t_1} A_p n_p}{10^{-2} a_{t2}} \exp\left(\frac{-E_p}{RT}\right) - \right.$$

$$\left. - \frac{A_i \alpha_i N \exp(-E_i'/RT)}{10^{-2} G} - \frac{A_i' \alpha_1 \alpha_2 N^2 \exp(-E_i''/RT)}{10^{-2} G}\right] \qquad (9)$$

where a_{t_1} and a_{t_2} are reciprocals of the characteristic lifetime of species before their decay by termination of first and second order in active center concentrations.

W-criterion:

$$\log I > \log I_w = \log\left[\frac{10^{-4} a_{t_2} \exp(2E_p/RT)}{\tau_u^2 A_p''^2 G10^{-2}} + \frac{10^{-2} a_{t_1} \exp(Ep/RT)}{\tau_u A_p'' G10^{-2}} - \right.$$

$$\left. - \frac{A_{i\alpha_1\alpha_2}'' N^2 \exp(-Ei''/RT)}{G10^{-2}} - \frac{A_{i\alpha_i}' N \exp(-E_i''/RT)}{G10^{-2}}\right] \qquad (10)$$

r-criterion:

$$\log I > \log I_n \qquad (11)$$

The desired ERC region in Fig. 1 is that of CEFD which obeys the four criteria.

It will be noted that a stringent condition for existence of the ERC region at not very high α is the fulfillment of condition $E_p < 1/2\, E_i'$ (E_p is the activation energy for chain propagation). When $E_p > 1/2\, E_i'$ for bimolecular termination, the curves for ν and i criteria do not cross and the ERC region does not exist.

A practical application of the method developed is illustrated in Fig. 2 for a chain reaction of hydrogen with chlorine, occurring at sufficiently high pressures, where first-order termination and generation of chains at the wall can be neglected. With a long chain the rate of propagation by H and Cl atoms are equal, and this enables one to express the concentrations of certain active species through concentrations of the others, as well as to use one-center approximation for the ERC region plot. The plots for relevant criteria are shown in the figure by curves denoted as i, ν, W and r. Absence of the vertical asymptote in the ν plot in the range of low temperatures is accounted for by the neglect of the first-order decay of active species. At a dose rate 10^{19} ev/cm^3 sec the reaction becomes mostly radiation-induced, of a chain nature, and will occur at rate ensuring the conversion of 1%

of the compound per 1 sec, with the dose rate and temperature lying within the ABCD region, which represents the sought ERC region. At τ_u = 10 sec, the ERC region embraces the dose rates and temperatures entering the plot ABC'D', and at τ_u = 100 sec – the plot ABC"D".

The results were obtained by computing the equations (8), (9), (10) that contained the following elementary rate constants: chain generation

$$H_2 + Cl_2 \longrightarrow 2Cl + H_2 \quad K = 1.66 \cdot 10^{-10} \exp(-47000/RT) \text{ cm}^3 \text{ sec}^{-1} *$$

radiation initiation of the chain

$$H_2 \rightsquigarrow 2H \qquad G(H) = 16.5 \text{ atoms/100 ev} **$$

$$Cl_2 \rightsquigarrow 2Cl \qquad G(Cl) = 21 \text{ atoms/100 ev} ***$$

chain propagation

$$H + Cl_2 \longrightarrow HCl + Cl \qquad k = 2.09 \cdot 10^{-9} \exp(-2200/RT) \text{ cm}^3/\text{sec}$$

$$Cl + H_2 \longrightarrow HCl + H \qquad k = 1.32 \cdot 10^{-10} \exp(-5500/RT) \text{ cm}^3/\text{sec}$$

chain termination

$$M + H + H \longrightarrow H_2 + M \qquad k_H[M] = 2.47 \cdot 10^{-13} \text{ cm}^3/\text{sec}$$

$$M + Cl + Cl \longrightarrow Cl_2 + M \qquad k_{Cl}[M] = 4.7 \cdot 10^{-14} \exp(800/RT) \text{ cm}^3/\text{sec}$$

$$M + H + Cl \longrightarrow HCl + M \qquad k_{H\text{-}Cl}[M] = 3.72 \cdot 10^{-10} \text{ cm}^3/\text{sec}$$

$$M = [H_2] = [Cl_2] \text{ cm}^{-3}$$

*All elementary rate constants are taken from Ref. /10/.

**The G(H) value was obtained by considering the processes $H_2^+ + H_2 \longrightarrow H_3^+ + H$, $H_3^+ + e^- \longrightarrow 3H$, the value $G(H_2^+)$ /11/, and assuming the yield of ions in hydrogen to be equal to that of dissociation.

***The G(Cl) value was obtained by considering the processes $Cl_2^+ + Cl_2 \longrightarrow Cl_3^+ + Cl$, $Cl_2 + e^- \longrightarrow Cl^- + Cl$, $Cl_3^+ + Cl^- \longrightarrow 4Cl$, the value $G(Cl_2^+)$ /11/, and assuming the yield of ions in chlorine to be equal to that of dissociation.

II. Branched chain processes

Here the plots of i- and r-criteria remain the same and have the same physical meaning as those for direct chain reactions. In Fig. 3 these curves are denoted as i and r. The chain criterion is replaced by the branching criterion (b-criterion). When it is met an isothermic reaction becomes auto-accelerated. The mathematical condition for the possibility of such a process, allowing for positive chain interaction, is /12/

$$a_{t_1} < C_{b_1} + \sqrt{4 k_b'' W_i} \qquad (12)$$

where $c_{b1} = A_b'' \alpha_b N \exp(-E_b/RT)$ is the reciprocal of the lifetime of active species before their decay by branching processes which are first-order regarding the concentration of active species, k_b'' is the rate constant of secont-order branching. From (3), (2), and (4) we obtain the condition for fulfillment of the b criterion

$$\log I > \log I_B = \log \{[a_{t1} - A_b'' \alpha_b N \exp(-E_B/RT)]^2 /4 \cdot 10^{-2} G k_b'' -$$

$$- A_i' \alpha_i N \exp[-E_i'/RT] /10^{-2} G - A_i'' \alpha_1 \alpha_2 N^2 \exp[-E_i''/RT] 10^{-2} G \} \qquad (13)$$

The criterion for "sufficiency" of the absolute rate can be obtained in terms of the chain branching theory developed by Semenov /12/. According to this theory, the amount of a compound that has reacted during a period of time t is

$$\Delta n \propto \frac{C_{b_1} W_i}{q} (e^{\sqrt{q}\, t} - 1) \qquad (14)$$

where

$$q = \begin{cases} (C_{b_1} - a_{t_1})^2 & \text{in the absence of chain interaction} \\ 4 k_b'' W_i - (C_{b_1} - a_{t_1})^2 & \text{on positive chain interaction} \\ 4 a_{t_2} W_i + (C_{b_1} - a_{t_1})^2 & \text{on negative chain interaction} \end{cases}$$

It follows from (14) that

$$\tau_{0.01} = \frac{2,3}{\sqrt{q}} \ln \left[\frac{10^{-2} \alpha_b N q}{C_{b_1} W_i} + 1 \right] \qquad (15)$$

Substituting (15) into (6) and expanding the exponent in series, we obtain for I in the absence of a chain interaction

$$\log I > \log I_w = \log \left\{ \alpha_b N / \tau_u G - a_{t_1} \exp (E_b/RT) / A''_b \tau_u G - W_{iT}/10^{-2} \right\} \quad (16)$$

On the rigth hand side of curve W in Fig. 3 the reaction proceeds at a rate sufficient for practical purposes, and the three criteria considered appear to be fulfilled in the region lying above the curve sections AB, BEC, and CD. Now if we draw a straight line of the r-criterion parallel to the x-axis, we obtain the ECDF region which is the ERC region sought.

So far we have not taken into account the second-order decay of active species, taking k''_t to be much smaller than k''_b. According to Semenov, the case $k''_t > k''_b$ corresponds to negative chain interaction. At the first stage the initial reaction step is auto-accelerated, then the process becomes slower and there is a smooth transition to a steady-state concentration of active centres, even if $a_{t1} < c_{b_1}$. In this case the chain length may become less than unity, i. e. the reaction will no longer be a chain process. Thus, taking into account the negative chain interaction, we have to ensure that after a constant reaction rate is attained the condition

$$\nu = \frac{W_p}{W_t - W_b} > 1 \quad (17)$$

is fulfilled. It can be seen from (17) that the specificity of a branched chain process disappears in this case, and the b-criterion can be obtained from the expression regarding to the existence of a chain (9), replacing a_{t_2} and a_{t_1} by the differences $k''_t - k''_b$ and $a_{t1} - c_{b1}$, respectively.

In a similar way, if the value $\tau_{0.01}$ calculated by equation (15) is much higher than the time τ_s of attaining a steady-state concentration – the latter being obtained by expression (18)

$$\tau_s = \frac{1}{\sqrt{q}} \ln \left[1 + \frac{2\sqrt{q}}{\sqrt{q} - (C_{b_1} - a_{t_1})} \right], \quad (18)$$

the W-criterion will be given by expression (10) with the same replacement of a_{t_1} and a_{t_2} as above. Qualitatively, the shapes of the curves for all the criteria controlling the ERC region will naturally be the same as for unbranched chains (Fig. 1).

The technique of finding the ERC region for branched processes is shown in Fig. 4 for the reaction of hydrogen with fluorine, the mechanism of which has been thoroughly studied /13/. The results have been obtained for a mixture containing, along with H_2 and F_2, also Ar and oxygen in a ratio $Ar:F_2:H_2:O_2 = 60:6:3:1$.

The use of the steady-state concentration method enebled us to solve the problem in the one-centre approximation, just as with straight chains, assuming first-order decay of active species and no interaction between the chains. At a dose rate of 10^{19}ev/cm^3 sec inside the ABCD region, the reaction $H_2 + F_2$ is a radiation-induced and a chain-branching one, and conversion of 1% of the compound occurs in $\tau_u = 0.1$ sec. Increase in τ_u by a factor of ten results in an expansion of the ERC region to the boundaries of the ABC'D' region.

The above results were computed by Eqs (8), (13), and (17) and by using the following elementary rate constants:

1. Chain generation:

$$F_2 + Ar \longrightarrow 2F + Ar \qquad k = 5.16 \cdot 10^{-9} \exp(-27300/RT) \text{ cm}^3/\text{sec}^*$$

2. Radiation initiation of chains:

$$F_2 \rightsquigarrow 2F \qquad G(F) = 21 \text{ atoms/100 ev}^{**}$$

$$H_2 \rightsquigarrow 2H \qquad G(H) = 16.5 \text{ atoms/100 ev}$$

3. Chain propagation:

$$F + H_2 \longrightarrow HF^* + F \qquad \text{not occurring in the calculation}$$

$$H + F_2 \longrightarrow HF^* + F \qquad k = 2 \cdot 10^{-10} \exp(-2400/RT) \text{ cm}^3/\text{sec}$$

4. Chain branching:

$$HF^* + H_2 \longrightarrow H_2^* + HF \qquad \text{not occurring in the calculation}$$

$$H_2^* + F_2 \longrightarrow H + F + HF \qquad k = 2 \cdot 10^{-17} \exp(-4500/RT) \text{ cm}^3/\text{sec}$$

5. Chain termination:

$$H_2^* + M \longrightarrow H_2 + M \qquad k = 0.85 \cdot 10^{-13} \exp(-100/\sqrt[3]{T})$$

$$H + O_2 + M \longrightarrow HO_2 + M \qquad k = 2.98 \cdot 10^{-33} \text{ cm}^6/\text{sec}$$

The above results show that the ERC region actually exists and the proposed theory can be successfully used for finding it.

*All rate constants were taken from Ref. /10/

**The G(F) value was obtained in the same way as G(Cl)

References

/ 1/ S.S. Medvedev, A.D. Abkin, P.M. Khomyakovskii, G.N. Gerasimov, V.F. Gromov, Yu.A. Chikin, V.A. Ningister, A.L. Auer, M.K. Yakovleva, L.P. Mezhirova, A.V. Matveeva, Z.G. Bezdubik. Vysokomol. Soedin. 2, 904 (1960).

/ 2/ A.D. Abkin. Trudy Vsesoyuzn. Soveshchanniya po Radiatsionnoi Khimii. M. Izd. Akad. Nauk SSSR, 1962, p. 430.

/ 3/ V.S. Ivanov. Radiatsionnaya Polimerizatsiya, Leningrad, "Khimiya", 1967.

/ 4/ R.V. Dzhagatspanyan, M.T. Filippov. Radiatsionnaya Khimiya Galoidsoderzhashchikh Soedinenii. Moscow, Atomizdat, 1973.

/ 5/ N.A. Kulazhenkova, I.K. Larin, V.L. Tal'roze. Dokl. Akad. Nauk SSSR, 207, 129 (1972).

/ 6/ A.V. Topchiev, I.V. Vereshchinskii, P.Ya. Glazunov, V.E. Glushnev, L.S. Polak, G.G. Ryabchikova, G.K. Sibirskaya, V.D. Timofeeva, N.Ya. Chernyak, Trudy II Vsesoyuzn. Soveshchaniya po Radiatsionnoi Khimii, Moscow, Izd. Akad. Nauk SSSR, 1962. P. 304

/ 7/ V.V. Saraeva, V.E. Pospelov, N.A. Bakh. Neftekhimiya, 7, 596 (1967).

/ 8/ N.M. Emanuel. Dokl. Akad. Nauk SSSR, 111, 1286 (1956).

/ 9/ M.A. Proskurnin, Yu.L. Khmel'nitskii, E.V. Barelko, I.I. Melikhova, A.G. Slepneva, Dokl. Akad. Nauk SSSR, 112, 886 (1957).

/10/ V.N. Kondratiev. Konstanty Skorostei Gazofaznykh Reaktsii. Moscow, "Nauka" 1970.

/11/ R.L. Platzman. Int. J. Appl. Rad. Isotop., 10, 116 (1961).

/12/ N.N. Semenov. O Nekotorykh Problemakh Khimicheskoi Kinetiki i Reaktsionnoi Sposobnosti. Moscow, Izd. Akad. Nauk SSSR, 1958.

/13/ E.M. Margolina. Mekhanizm i kinetika reaktsii ftora s vodorodom. Thesis, Moscow, 1971.

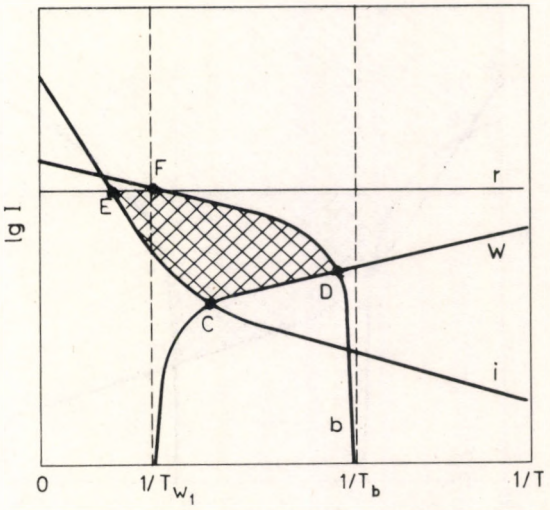

Fig. 1. Plots of i-, ν-, W- and r-criteria for unbranched chain processes. The ECDF region represents the ERC region where the four criteria are met

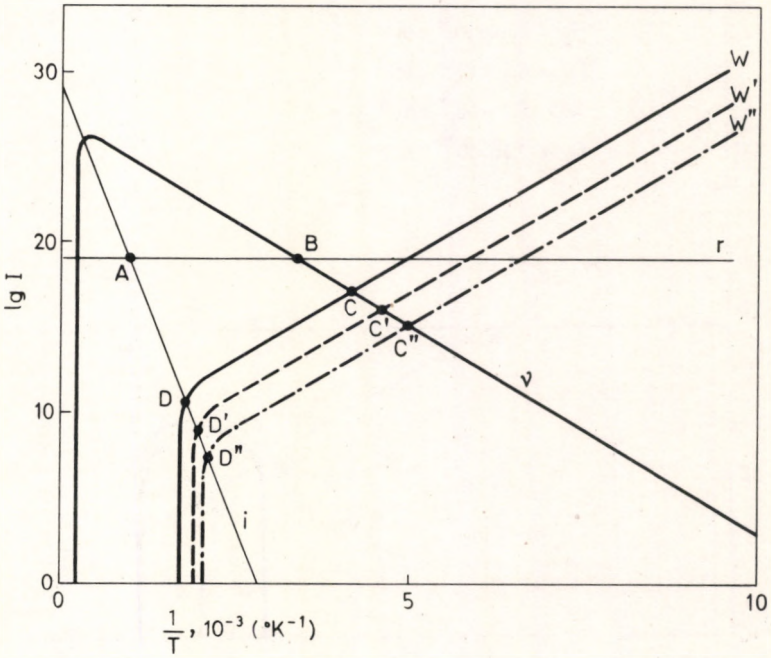

Fig. 2. Plots of i-, ν-, W- and r-criteria for an unbranched reaction of $H_2 + Cl_2$ curve for the W-criterion corresponds to $\tau_{0.01} = 1$ sec, W' to 10 sec, W" to 100 sec. The ABCD, ABC'D'ABC"D" regions represent ERC regions

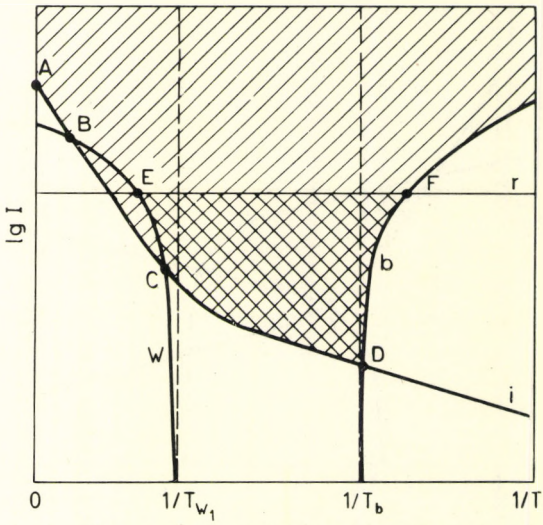

Fig. 3. Plots of i-, b-, W- and r-criteria for a branched reaction at $\tau_{0.01} < \tau_s$

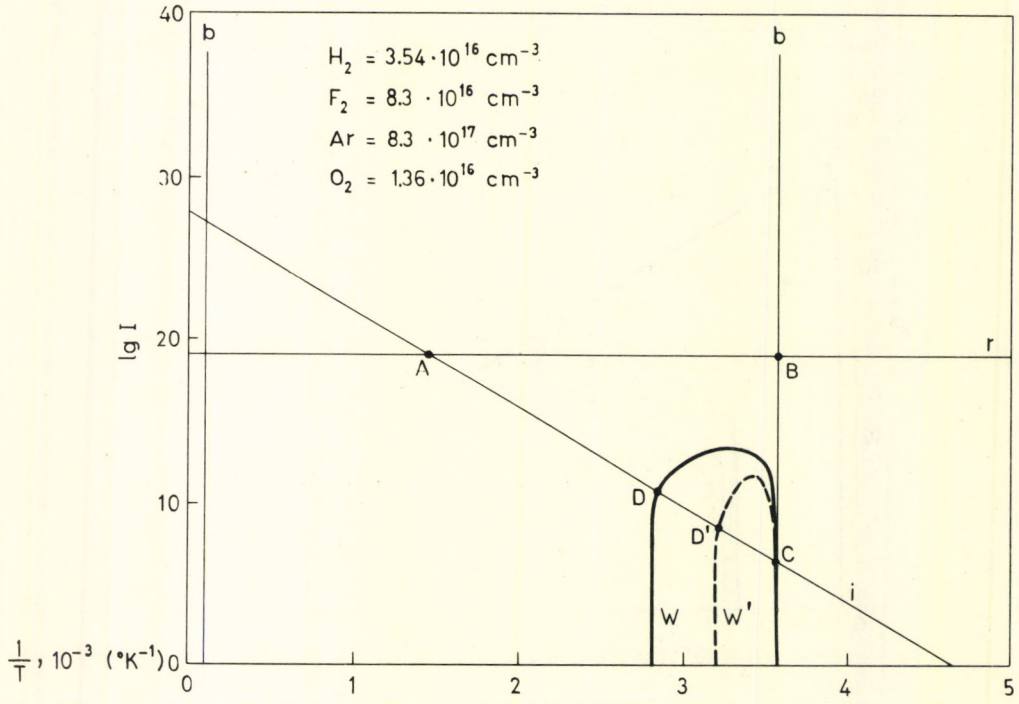

Fig. 4. Plots of i-, b-, W-, and r-criteria for a branched reaction of H_2 with F_2. Curve W corresponds to $\tau_{0.01} = 0.1$ sec, W′ to 1 sec. The regions ABCD and ABC′D′ represent ERC regions

ON THE POSSIBILITY OF SOLVATION OF AN EXCESS ELECTRON IN LIQUID HYDROGEN CHLORIDE

V. A. Zhigunov, G. I. Khaikin
Institute of Electrochemistry of the Academy of Sciences of the USSR,
Moscow, USSR

At present the solvation mechanism of the capture of excess electrons is known tc hold for a wide variety of liquids in a large polarity range. For these liquids the thermalization of subexcitation electrons and their capture does not involve any significant chemical changes of the molecules. It is of interest to elucidate the role of the solvation processes in the liquids in which the capture of a major portion of subexcitation and thermalized electrons by the molecules of the medium is accompanied by dissociation. As we know, hydrogen halides are typical representatives of this class of systems /1/. In our opinion, in the cases when the solvation mechanism is operative, an investigation of the properties of a solvated electron in liquids formed by simple diatomic molecules would be very useful for further development of the theoretical concepts regarding the nature of the solvated electrons.

This paper reports an investigation by means of microsecond pulse radiolysis on the solvated electron properties in liquid hydrogen chloride. Obviously, at present pulse radiolysis is the only method to be used for solution of the problem in question. Another well-known method, viz. the investigation of stable solutions of alkali metals, can hardly be used on account of an expectedly large value of the rate constant of the reaction of a solvated electron with the matrix. Moreover, as has been shown by our experiments, alkali metals (we used metallic sodium and potassium) do not dissolve in liquid HCl even in the presence of a special additive, 18-crown-6.

Liquid hydrogen chloride is a system most thoroughly studied from the point of view of its radiation-chemical behavior /2–4/. The analysis of the literature data on this subject suggests that the cross-section of a dissociative electron capture is relatively small, the fraction of thermalized electrons to the total number of subexcitation electrons is maximum and the probability of the capture of a solvated electron by the matrix is minimum among the hydrogen halides.

A linear accelerator U-12, generating electrons of the energy 3–4 MeV and with maximum current in the beam 120 ma was used as the source of electron pulses. The pulse width was about two microseconds.

The fast spectrophotometer used by us and the temperature control of the samples under the conditions of pulse irradiation as well as of the cells were described in detail before /5/.

For the detection of short-lived light absorbing species we used mainly a photomultiplier type FEU-39, by means of which we investigated the spectral range from 260 to 500 nm. For measurements in the IR-region we used a liquid-nitrogen-cooled indiumantimoninide detector which allowed us to perform measurements in the range éu to 2600 nm. The optical absorption spectra were measured by means of a digital recorder which recorded the instantaneous value of the signal at any given moment of time without recording it previously on a photographic film from the oscillograph screen.

High purity hydrogen chloride contained 0.005% chloroorganic products, 0.001% free chlorine, 0.002% water. The cells were filled in vacuum after evacuation down to 10^{-6} nm Hg and passing hydrogen chloride through a three-stage-system of low-temperature traps. The HCl purity was controlled from the electrical conductivity of the liquid immediately before its condensation in a special cell with platinum electrodes. The electrical conductivity of liquid HCl did not exceed 5×10^{-9} $ohm^{-1}cm^{-1}$ at 183 K, which is not much larger than the minimum electrical conductivity for this solvent as determined in Ref /6/.

The irradiation of liquid hydrogen chloride with a two-microsecond pulse of fast electrons results in the generation of a short-lived optical absorption in the UV-part of the spectrum. In the IR-region up to 2600 nm no optical absorption was detected. Knowing the spectral properties of solvated electrons in different liquids, we can conclude that in irradiated liquid HCl a solvated electron, if formed, under given experimental conditions lives for a period shorter than one microsecond (T=173 K).

Figure 1 shows the optical absorption spectra of irradiated hydrogen chloride at 173 with the dose in a 4,8 Krad pulse, measured directly at the end of the pulse and after 70 microsecond. It can be seen that the maximum of the absorption band shifts towards the long-wavelength region. The analysis of the disappearance of optical absorption at different wavelengths showed that in irradiated liquid HCl, at least two short-lived species, absorbing in the UV part of the spectrum are formed, which have strongly overlapping absorption bands but markedly different life-times.

Figure 2 gives the time dependences of the normalized concentrations of short-lived particles at 290 and 400 nm, which show that the half-lives differ nearly by a factor of 20.

At the wavelengths outside the 280–400 nm range the kinetics of disappearance of optical absorption remain unchanged. Here, evidently, we have to deal with individual optical absorption bands. Using the data on the kinetics of disappearance, we can separate the absorption spectrum of irradiated liquid HCl, taken at any moment of time, into individual bands. Figure 3 shows the absorption spectra of short-lived particles at the moment of time nearest to the end of the radiation pulse.

We have found $G \sim 3.9 \times 10^3/\varepsilon_{360}$ and $G \sim 1.5 \times 10^4/\varepsilon_{300}$ part. /100 eV. We can suppose that all of the hypothetical primary particles of the liquid hydrogen chloride radiolysis, by means of which the mechanism of radiolysis is described, it is the dichloride anion Cl_2^- and the chloride anion, existing according to /7/ in liquid HCl

in the form of HCl_2^-, which are the most probable species to exhibit optical absorption in the spectral range studied by us. By analogy with the optical absorption spectra of the dichloride-anion in water /8/, in alkali halide crystals /9/ and in some other irradiated systems, we can ascribe the absorption band with λ_{max} = = 360 nm to this species. The most likely main path of the dichloride-anion formation may be the reaction

$$HCl_2^- + Cl \longrightarrow Cl_2^- + HCl \qquad (1$$

At present the spectral characteristics of HCl_2^- in liquid hydrogen chloride are not known. At the same time it is known that phosphorus oxychloride dissolved in HCl has moderately basic properties and the system obeys equilibrium (2) /10/:

$$POCl_3 + HCl \rightleftharpoons POCl_2^+ + HCl_2^- \qquad (2)$$

However, in 10^{-2}M $POCl_3$ solution we could not record any optical absorption similar to that found in irradiated liquid HCl. For this reason, we think that the absorption and with λ_{max} = 300 nm can hardly belong to the chloride anion, though it is obvious that it should be formed mainly by the reaction

$$e^-_{therm} + 2HCl \longrightarrow H + HCl_2^- \qquad (3)$$

The main object of the further experiments was to find whether the formation of the species discovered by us could form without the participation of solvated electrons. At the same time, we obtained some data shedding light on the nature of the species with an absorption band at 300 nm.

It is known that the liquid-phase radiolysis of hydrogen chloride proceeds to a high extent, gives large yields of final products and high steady-state concentrations /2,3/. It was interesting to see how the spectral pattern of irradiated liquid hydrogen chloride changes as the molecular products H_2 and Cl_2 accumulate in the system.

Figure 4 shows the optical absorption spectra taken at 10 and 50 microseconds after the end of the irradiation pulse for the system in which about 10^{-2} M Cl_2 has accumulated.

The chlorine concentration was determined by means of a spectrophotometer with the use of the extinction coefficient value taken from /11/. By virtue of the fact that the spectrum did not depend on time and that the kinetics of disappearance of the optical absorption did not vary over the whole accessible spectral range, we could consider the spectrum in question as an individual absorption band, whereas the coincidence of the parameters of this band with those of the absorption band of Cl_2^- (Fig. 3) suggests that in the presence of molecular products, the radiolysis brings about only this species. The spectral pattern shown in Fig. 1 passes smoothly into the absorption band of Cl_2^- as final products accumulate. At small doses, when the

absorption band with the maximum at 300 nm is not yet completely suppressed, the absorption exhibits a structure which can be explained by the superposition of two individual bands of different intensity.

The experiment carried out by us was important in that it revealed a marked increase of the dichloride-anion concentration (approximately by a factor of 1.6), as compared with its concentration in pure liquid HCl containing no perceptible amounts of molecular chlorine. Evidently, this means that in the presence of considerable amounts of molecular products, the formation of the dichloride-anion can proceed not only by reaction (1), but also by another mechanism. Since the accumulation of molecular hydrogen should decrease the Cl_2^- concentration as the result of the reaction

$$H_2 + Cl \longrightarrow H + HCl \qquad (4)$$

we suppose that the reason for the phenomenon observed is the nondissociative capture of electrons by chlorine molecules. According to /12/, the electron capture by chlorine molecules has the threshold energy of the order of 1.6 eV. Therefore, unlike typical scavengers of free electrons, such as SF_6, Br_2, I_2, etc. these molecules can react only with non-free electrons, i.e. in the case of a liquid phase with solvated electrons. Thus, we can suppose that in liquid hydrogen chloride a certain portion of thermalized electrons undergoes solvation.

Evidently, the main reaction of electron disappearance, viz. the interaction with the matrix:

$$e_s^- + 2HCl \longrightarrow H + HCl_2^- \qquad (5)$$

has a rate constant not higher than $3 \times 10^6 M^{-1} sec^{-1}$ at 173 K, which for the half-life gives the relation:

$$2.5 \times 10^{-7} \text{ sec} < \tau_{\frac{1}{2}} < 10^{-6} \text{ sec.}$$

Thus, according to our data, already a nanosecond pulse radiolysis should result in the presence of solvated electrons in liquid hydrogen chloride, which can be observed by one or another method of detection.

The kinetics of disappearance of Cl_2^- in pure hydrogen chloride and in a solution of the final radiolysis products in hydrogen chloride are fairly well described by the law for a simple second order reaction. In both cases we obtain $2K = 7.2 \times 10^5/\varepsilon_{360}\ M^{-1}\ sec^{-1}$ at T = 173°K.

The kinetics of disappearance of optical absorption at wavelengths less than 290 nm are of a complex character and cannot be described by simple formal-kinetic laws.

Another important feature resulting from the change of the spectrum pattern with accumulation of molecular products is the suppression of the absorption band

with a maximum at 300 nm. Evidently, this points directly to the participation of solvated electrons in the reaction of the formation of a short-lived species having this absorption band.

In order to elucidate the mechanism of formation of this particle and to confirm the hypothesis of the participation of solvated electrons in the radiolysis, we studied also the solution of phosporus oxychloride in hydrogen chloride. We found that regarding its main parameters the optical absorption spectrum of an irradiated 0.01 M solution practically coincides with that of the dichloride anion. Its intensity is obviously higher than that of the absorption band of Cl_2^- in pure hydrogen chloride, while the absorption band with a maximum at 300 nm is absent. Taking into account that the solution is in equilibrium (2), we can reasonably suppose that the increase in the concentration of Cl_2^- is associated with a greater role of reaction (1). Moreover, the formation of a particle having an absorption band with $\lambda_{max} = 300$ nm should occur with the participation of solvated protons since in a basic solution they recombine effectively according to the reaction

$$HCl_2^- + H_2Cl^+ \longrightarrow 2\,HCl \qquad (6)$$

Thus, the obtained experimental data gives evidence of the formation of a short-lived species during the radiolysis of liquid HCl this being a product of the interaction of solvated electrons and protons and having an absorption band with a maximum at 300 nm. The elucidation of the properties and nature of this species is the object of further studies.

References

/ 1/ D. C. Christophorou, R. N. Compton, H. W. Dickson, J. Chem. Phys., 48, 1949 (1968), L. C. Christophorou, J. A. D. Stockdale, J. Chem. Phys., 48, 1956 (1968).

/ 2/ D. A. Armstrong, Can. J. Chem., 40, 1385 (1962).

/ 3/ R. C. Rumfeldt, D. A. Armstrong, J. Phys. Chem., 68, 761 (1964).

/ 4/ D. E. Wilsin, D. A. Armstrong, Radiation Res. Rev., 2, 297 (1970).

/ 5/ G. I. Khaikin, V. A. Zhigunov, P. I. Dolin, Khim. Vys. Energ. 5, 54 (1971).

/ 6/ G. Glockler, R. E. Peck, J. Chem. Phys., 4, 658 (1968).

/ 7/ H. F. Herbrandson, R. T. Dickerson, J. Weinstein, J. Amer. Chem. Soc., 76, 4046 (1954).

/ 8/ M. Anbar, J. K. Thomas, J. Phys. Chem., 68, 3829 (1964), G. G. Jayson, B. J. Parsons, A. J. Swallow, J. Chem. Soc., Faraday Trans. I, 9, 1597 (1973)

/ 9/ C. J. Delbecq, W. Hayes, P. H. Yuster, Phys. Rev. 121, 1043 (1961).

/10/ T. C. Waddington, F. Klanberg, J. Chem. Soc., 2332 (1960)

/11/ R. C. Rumfeldt, D. A. Armstrong, Can. J. Chem., 41, 1104 (1963).

/12/ D. C. Frost, C. A. McDowell, Can. J. Chem., 38, 407 (1960).

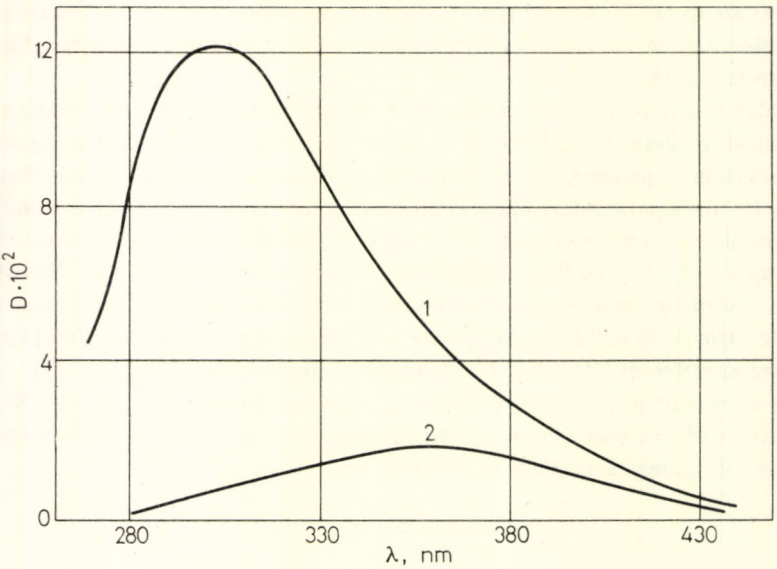

Fig. 1 Optical absorption spectra of irradiated liquid hydrogen chloride at 173 K: 1 – directly at the end of the electron pulse, 2 – after 70 microsecond

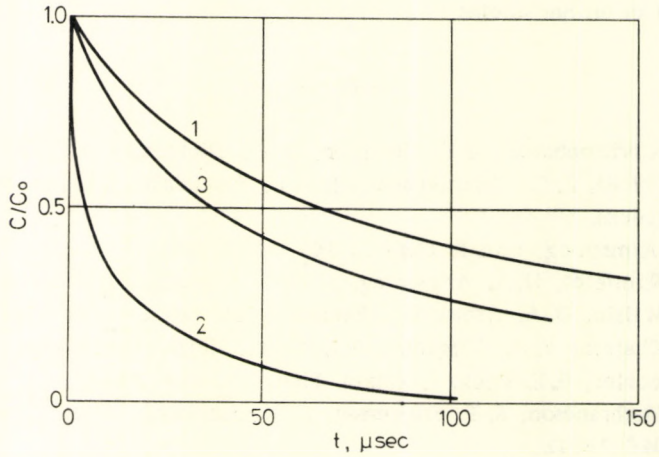

Fig. 2 Dependences of the normalized concentrations of absorbing species on time: 1 – λ = 400 nm, 2 – λ = 290 nm, 3 – λ = 360 nm, liquid HCl containing final radiolysis products, $[Cl_2] \simeq 10^{-2}$ M

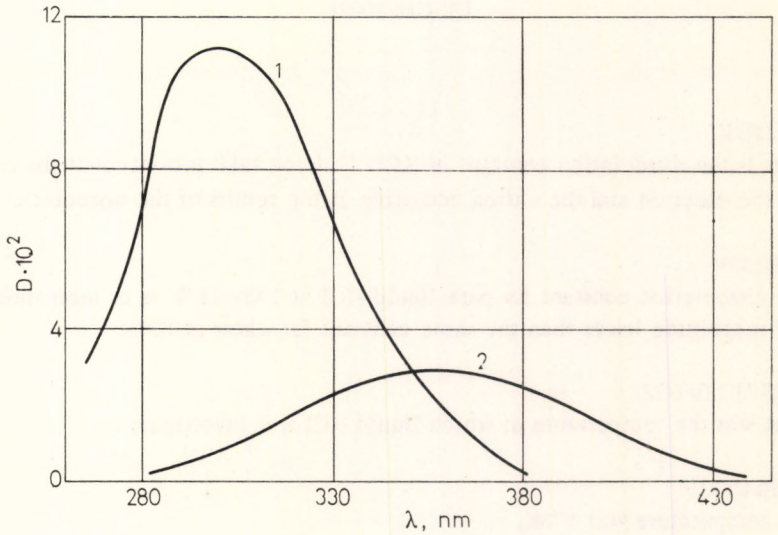

Fig. 3 Optical absorption spectra of short-lived particles of pure liquid HCl radiolysis at the end of the electron pulse

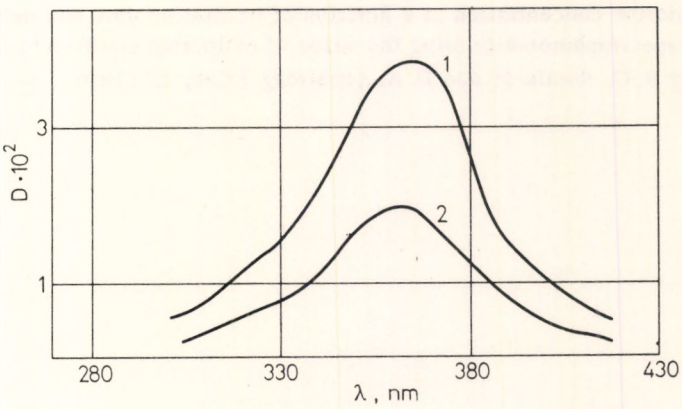

Fig. 4 Optical absorption spectra of irradiated liquid HCl containing molecular hydrogen and chlorine, $[Cl_2] \simeq 10^{-2}$ M: 1 – 10 microsecond after the end of the electron pulse, 2 – after 50 microsecond

J. KALECINSKI

What is the dissociation constant of HCl? Did you take into account the reaction between the electron and the cation occurring as the results of the dissociation?

V. ZHIGUNOV

The dissociation constant for pure liquid HCl at 173—187K is at least three orders of magnitude lower than the same constant for water at 293K.

R. K. BROSZKIEWICZ

What was the temperature at which liquid HCl was investigated?

V. A. ZHIGUNOV

The temperature was 173K.

R. K. BROSZKIEWICZ

Did you investigate the solutions of Cl_2 in HCl?

V. A. ZHIGUNOV

The chlorine concentration as a function of irradiation dose was determined by means of a spectrophotometer using the value of extinction coefficient taken from the paper by R. C. Rumfeldt and D. A. Armstrong [Can. J. Chem., 41, 1104 (1963)].

KINETICS OF PRESOLVATED ELECTRON REACTIONS IN CONCENTRATED SOLUTIONS

Gordon R. Freeman, Gerald L. Bolton
Chemistry Department, University of Alberta,
Edmonton, Canada

Several years ago Hamill proposed that electrons generated in water /1,2/ and alcohols /3/ could react before becoming solvated provided that the concentration of scavenger was large (>0.1 M). This was expected since there would be competition between trapping sites and scavenger molecules for the low energy quasifree electrons. (Hamill called the electrons "dry" or "mobile", but the term "presolvated" electron may be more suitable.) The unanticipated thing was that the relative rates of reaction with a series of scavengers was not the same for presolvated and solvated electrons. It must have seemed normal to Hamill that the electron cross section would vary with the energy and state of the electron, and that the variation would be different for different reactant molecules. But many other radiation chemists were slow to be convinced that the apparent differences were not artifacts. Subsequent work by Hamill and others /4–8/ has demonstrated beyond reasonable doubt that the differerences are real. Interest is now focussed on details of the reaction kinetics.

Several workers have found that scavengers such as benzene and phenol reduce the initial absorbance of solvated electrons at the end of a radiation pulse by an amount much greater than can be explained by the normal rate of reaction of solvated electrons with the scavenger. Figure 1 shows the optical absorbance at 690 nm during and after a 100 ns pulse of radiation in ethanol and ethanol containing 0.75 M benzene. Using the decay rate after the pulse to correct for similar decay during the pulse one obtains A_{io} for pure ethanol and A_i for 0.75 M benzene.

Decrease of the ratio (A_i/A_{io}) below unity represents scavenging of presolvated electrons. The effects of benzene and phenol concentration on this ratio in methanol and ethanol are shown in Fig. 2. Acetone also decreases (A_i/A_{io}) /8/. We have determined the relative efficiencies of acetone, phenol and benzene in their reactions with presolvated and with solvated electrons (Table 1). The efficiencies of benzene and acetone differ by only a factor of four in scavenging presolvated electrons, whereas they differ by a factor of three thousand in reacting with solvated electrons in methanol.

Our earlier model for the reaction of electrons in spurs /9/ did not allow for different reactivities of presolvated and solvated electrons. At that time the main

Table 1

Relative efficiencies of scavengers for reaction with presolvated and solvated electrons

Solvent	Solute	presolv. e^- [a]	solv. e^- [b]
CH_3OH	acetone	1.0	1.0
	phenol	0.41	0.0023
	benzene	0.23	0.0003
C_2H_5OH	acetone	1.0	1.0
	phenol	0.45	0.011
	benzene	0.27	0.0014

[a] The efficiency for reaction with presolvated electrons was taken proportional to $[f_{ps}/(1-p)]$, see Eq. (4).

[b] The efficiency for reaction with solvated electrons was taken proportional to $k(e^-_{solv} + S)$.

Table 2

Parameters for scavenging presolvated electrons, Eq. (4)

(To facilite comparison, n = 6, was used throughout)

Solvent	Solute	(1-P)	f_{ps}
H_2O	$(CH_3)_2CO$	0.024	1.0
$(CH_2OH)_2$*	$(CH_3)_2CO$	0.025	1.0
CH_3OH	$(CH_3)_2CO$	0.015	1.0
	C_6H_5OH	0.015	0.45
	C_6H_6	0.015	0.25
C_2H_5OH	$(CH_3)_2CO$	0.012	1.0
	C_6H_5OH	0.012	0.46
	C_6H_6	0.012	0.27

* In calculating the mol fraction of solute N_s, each ROH group was treated as a molecule of solvent. The number of mol of glycol in solution was therefore multiplied by two: N_s = mols acetone/[(mols acetone + (2 x mols glycol)].

interest was in explaining the square root concentration dependence of scavenging at low concentrations. Under those circumstances the probability of scavenging presolvated electrons was negligible. The model is easily extended so that it can focus on the high concentration region as well.

In general, scavenging may be possible during the last few collisions of the epithermal electron prior to localization. Reaction may also occur if the initial localization site contains a scavenger molecule. In liquids that form deep traps, electrons that are initially in shallow traps might migrate and react before settling into the equilibrium solvated state. However, the dependence of the reaction cross section on the energy and state of the electron is not known. Integration over this series of events may be approximately done by assuming that the presolvated electron, in the energy range where reaction is probable, encounters a number m_{ps} of molecules and that the average probability of reaction per encounter with a scavenger molecule is f_{ps}.

The probability ϕ_{ps} that a presolvated electron does not react with a solute that is present at mole fraction N_s is:

$$\phi_{ps} = (1-f_{ps}N_s)^{m_{ps}} \qquad = A_i/A_{io} \tag{1}$$

The value of m_{ps} is not the same for all electrons generated in a sample. It has a minimum value n equal to the number of molecules in the initial localization zone and may increase in a random way depending on the speed with which the electron settles into the solvated state.

$$m_{ps} = m + n \tag{2}$$

The encounters are counted from the time the electron energy has been degraded to the region where the electron is scavengeable. As the epithermal quasifree electron skitters through the liquid prior to localization, let the probability be P that it does not become localized at a given collision. The probability that it does become localized during m collisions is $(1-P^m)$. The distribution function for the number of collisions that an electron undergoes in its reactive state prior to localizations is

$$F(m) = d(1-P^m)/dm \qquad = -P^m \ln P \tag{3}$$

The initial optical absorbance in a solution relative to that in the pure solvent is equal to ϕ_{ps}, hence

$$A_i/A_{io} = \int_0^\infty F(m)\,(1-f_{ps}N_s)^{m+n}\,dm$$

$$= (\ln P)\,(1-f_{ps}N_s)^n \int_0^\infty P(1-f_{ps}N_s)^m\,dm \tag{4}$$

P, f_{ps} and n are adjustable parameters, although limitations are placed on one or more of them in a given series of systems.

The value of n is the minimum number of molecules that an electron meets after becoming scavengeable but before making the first diffusive jump in the solvated state. The value of n may vary with both solute and solvent. For example, n = 6 gave satisfactory agreement with our results from benzene and phenol solutions (Fig. 2), but n > 20 was required to fit the acetone solution results of Lam (Fig. 3). Increasing the value of n decreases the amount of curvature in the line.

The effect of temperature on the efficiency of scavenging presolvated electrons is smaller than the experimental scatter of the results (Fig. 2).

Finally, Lam and Hunt found a simple correlation between the rate constant for reaction of a solute with solvated electrons and the efficiency of that solute for scavenging presolvated electrons /10/. Figure 4 contains the correlation lines reported in Ref. /10/. C_{37} is the concentration of solute required to reduce (A_i/A_{io}) to 0.37 i.e. to e^{-1}. Figure 4 is a log-log plot of C_{37} against the rate constant for reaction of the solute with solvated electrons. The dashed lines have a slope of (-1), and results are presented for the four solvents water, ethylene glycol, methanol and ethanol. Solvated protons did not fit the correlation, lying much above the line formed by results from other scavengers such as carbon tetrachloride, acetone and monochloroacetate. Benzene and phenol do not fit the correlation either, they fall much below the correlation lines.

This interesting behavior requires more study. It gives information about the energy dependence of the electron reaction cross section of different solutes in liquids.

References

/ 1/ W.H. Hamill, J. Chem. Phys. 49, 2446 (1968).
/ 2/ W.H. Hamill, J. Phys. Chem. 73, 1341 (1969).
/ 3/ S. Khorana and W.H. Hamill, J. Phys. Chem. 74, 2885 (1970).
/ 4/ H.B. Steen, J. Phys. Chem. 74, 4059 (1970).
/ 5/ R.K. Wolff, M.J. Bronskill and J.W. Hunt, J. Chem. Phys. 53, 4211 (1970).
/ 6/ H.B. Steen, O. Kaalhus and M. Kongshaug, J. Phys. Chem. 75, 1941 (1941).
/ 7/ G.L. Bolton, Ph.D. Thesis, University of Alberta, 1974.
/ 8/ Y.K. Lam, Ph. D. Thesis, University of Toronto, 1974.
/ 9/ G.R. Freeman, J. Chem. Phys. 43, 93 (1965), ibid. 46, 2822 (1967).
/10/ Y.K. Lam and J.W. Hunt, Int. J. Radiat. Phys. Chem. 7, 317 (1975).

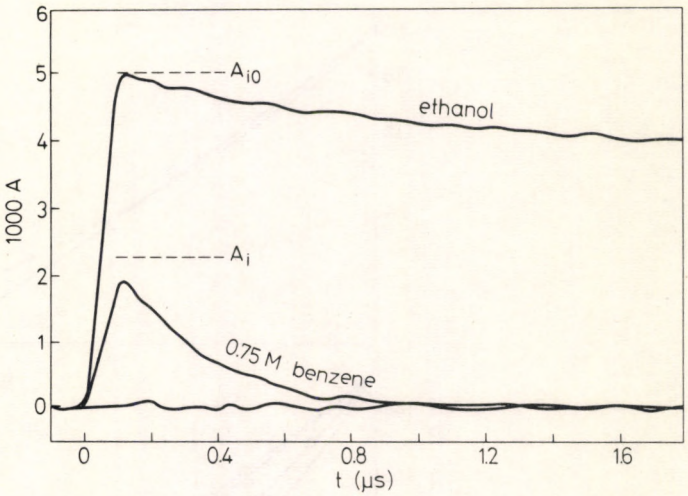

Fig. 1 Optical absorbance at 690 nm during and after a 100 ns pulse of 1.7 MeV electrons in ethanol containing 0.75 M benzene. T = 295K. Dose = 1.8 10^{16} eV/cm^3. A_i and A_{io} represent the initial absorbance corrected for decay during the pulse

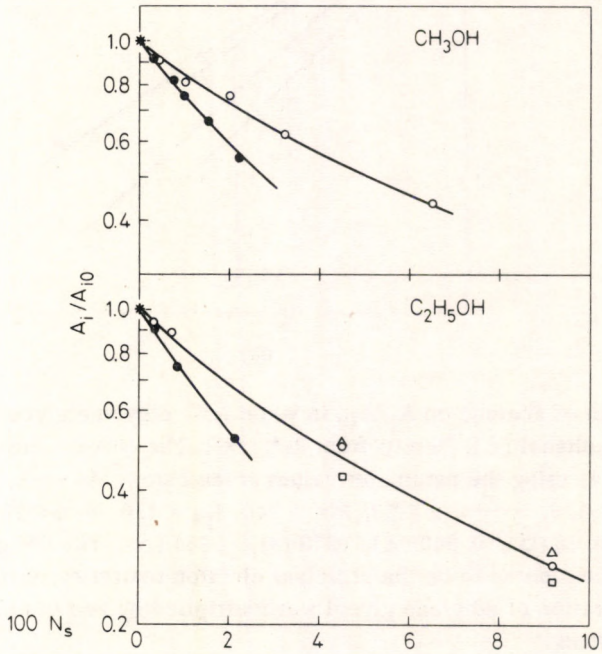

Fig. 2 Effect of benzene (○) and phenol (●) on the initial optical absorbance A_i of solvated electrons after a 100 ns pulse of radiation in methanol and ethanol. A_{io} is the initial absorbance in the absence of scavenger and N_s is the mol fraction of scavenger. ○, 295K; △, 275K; □, 234K; *, A_i/A_{io} = 1.0 for each set. The values of A_i were corrected for decay during the pulse due to scavenging of solvated electrons, using the rate constant measured after the pulse. The curves were calculated from Eq. (4), using the parameter values in Table 2

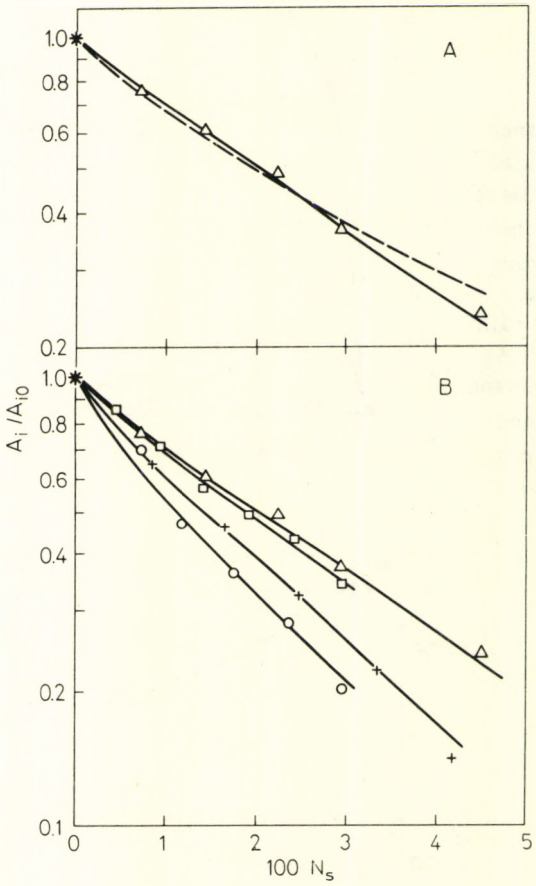

Fig. 3 Effect of acetone on A_i/A_{io} in water (□) ethylene glycol (△), methanol (+) and ethanol (○). Results from Ref. /8/. The curves were calculated from Eq. 4, using the parameter values given below. A: ----, n = 6, P = 0.975, f_{ps} = 1.0, ———, n = 20, P = 0.940, f_{ps} = 1.0. B: n = 20, f_{ps} = 1.0 and P = 0.95 (□), 0.940 (△), 0973 (+), 0.981 (○). The OH groups of the solvent are considered to be the principal electron scattering centers, so the concentration of ethylene glycol was multiplied by two in calculating N_s for those solutions

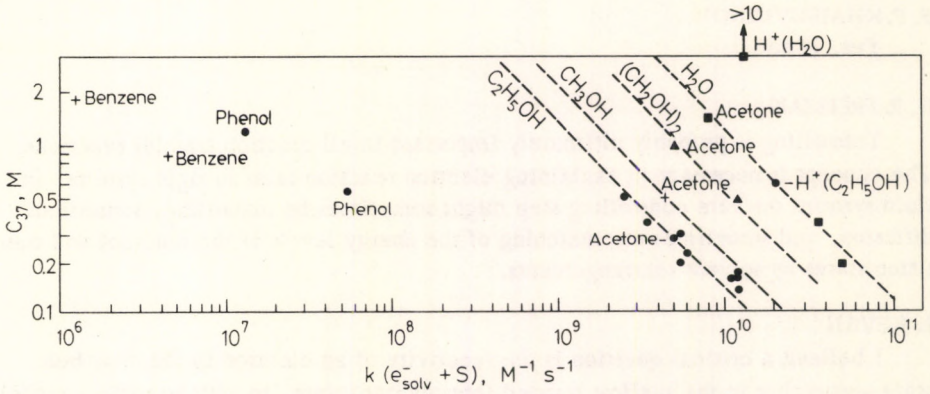

Fig. 4. Plot of C_{37} against $k(e^-_{solv} + S)$ for scavengers in water (■), ethylene glycol (▲), methanol (+) and ethanol (●). The four points labelled benzene and phenol are present results; the rest are from Ref. /10/. The dashed lines have slopes of (-1) and represent correlations suggested by Lam and Hunt/10/.

DISCUSSION

R. F. KHAIRUTDINOV

I want to draw the attention of investigators to another possible explanation of experimental data obtained by Prof. Freeman. This explanation is based on the ability of electron tunnelling, from traps to scavenger molecules. Electrons trapped in a matrix may tunnel to acceptors during the time interval of their existence in the traps before first diffusion jump. This model was first discussed in our paper in Chemical Physics 4, 181 (1974). Distances of electron tunnelling, obtained from the decrease of radiation yield in the presence of acceptors (5 to 10 Å) with the help of the formula for the tunnel model, are reasonable for characteristic time of diffusion jump at temperature used and for typical values of a and ν parameters. It is interesting that the abnormal properties of H^+ ions can be easily explained by their weak ability to capture solvated electrons because of low density of electron levels in H atom. As you know the resonance of electron levels of the initial and the final states is important for electron tunnelling. In a real situation the decrease of radiation yield is, I think, due to both tunnel and presolvated electron capture mechanisms.

G. R. FREEMAN

Can the tunnelling model explain curvature in the plot of log A_i/A_{io} ?

R. F. KHAIRUTDINOV

Yes, it can.

G. R. FREEMAN

Tunnelling is probably ultimately important in all electron transfer reactions. The concept is necessary in explaining electron reaction rates in rigid systems. In fluid systems the rate controlling step might sometimes be tunnelling, sometimes diffusion, and sometimes the matching of the energy levels of the reactant and transition states by solvent rearrangements.

L. KEVAN

I believe a critical question is the reactivity of an electron in the quasifree state versus that in the shallow trapped (presolvated) state. In your statistical model you assume reaction from a quasifree state. Can you really distinguish whether reaction occurs from a quasifree or shallow trapped state?

G. R. FREEMAN

We include the quasifree state in the category of "presolvated" states. The value $m_{ps} \sim 40$ required for benzene seems much too large for the main reaction probability to occur from a shallow trap. Benzene and toluene appear to react preferentially with quasifree electrons. By contrast, nitrous oxide appears to react preferentially with electrons in a localized state. The reaction probability as a function of electron energy varies from one solute to another.

H. J. ACHE

Do you see any correlation between the rate constants observed for presolvated or dry electrons and the rate constants observed for electron attachment in the gas phase (e. g. as reported by Christophorou)?

G. R. FREEMAN

No. The solutes for which we have determined reaction probabilities with quasifree (dry, if you prefer) electrons do not attach thermal electrons in the gas phase. Electron capture in the liquid phase is stabilized by the solvent. However, there is a qualitative correlation between our results and electron scattering cross sections as a function of energy, where scattering involves transient negative ion states.

V. TOLKATCHEV

Do you suppose that the reactivity of the presolvated electrons differ between first shallow trap and the next shallow trap?

G. R. FREEMAN

Yes. For solutes such as benzene whose reactions with electrons are endoergic, the reactivity is smaller when the trap is deeper. The second shallow trap would usually be deeper than the first.

Yu. A. BERLIN

What is the physical meaning of the m-parameters?

G. R. FREEMAN

m is the number of molecules that the electron encounters between the time when its energy has been reduced sufficiently that it can be scavenged, and the time that the electron is solvated. $m_{ps} = n + m$ includes the number of molecules in the initial solvation zone.

Yu. A. BERLIN

What is the value of electron mobility in methanol?

G. R. FREEMAN

About 1×10^{-3} cm^2/Vs. There is some disagreement about the exact value.

R. SCHILLER

I do not understand the time-scale of your results. You used solutions not more concentrated than 1 molar which results in an average electron lifetime not shorter than 100 ps with $k < 10^{10}$ $M^{-1}s^{-1}$. Now, Rentzepis and Hunt observed the solvated electron spectrum to be complete after a period of several picoseconds. How could you observe non-solvated electrons in your solutions?

G. R. FREEMAN

One should not use homogeneous kinetics concepts such as rate constants to describe nonhomogeneous kinetics systems. The reactions of electrons prior to solvation in alcohols are limited in time by the solvation process, which takes a few picoseconds in methanol at 300K. In the stochastic model we estimate the number of molecules that an electron encounters before its first diffusive jump from the solvated state, and the probability that one of the molecules will be a scavenger, and the probability that the electron reacts with the scavenger during an encounter.

M. MAGAT

I wonder (1) What is the distance covered by an electron, say in methanol, between the moment (or rather the energy state) in which it is able to react (say with benzene) and the moment the electron becomes solvated? (2) How many scavenger molecules, randomly distributed, the electron will meet on his way?

G. R. FREEMAN

The results indicate that the electrons in methanol encounter an average of about $(40/f_{ps})$ molecules while in the reaction energy range, before attaining the solvated state. If the scavenger is present at a concentration of 5 mol%, the electron would encounter an average of $(2/f_{ps})$ of them.

G. M. ZIMINA

Did I understand correctly that at the same concentration of acceptor (benzene, phenol, acetone) benzene is a worse acceptor of "dry" electrons than acetone?

G. R. FREEMAN

Yes, by a factor of about four in methanol and ethanol.

G. M. ZIMINA

In your opinion, in what time-interval does a pre-solvated electron become solvated?

G. R. FREEMAN

The electron seems to become localized in less than 1 ps. The complete solvation requires dielectric relaxation about the charge centre, wich is temperature dependent. It is a few picoseconds in methanol at 300K.

CORRELATION BETWEEN INHIBITION OF POSITRONIUM FORMATION BY AND CHEMICAL REACTION RATE OF ELECTRONS WITH SCAVENGER MOLECULES IN NONPOLAR LIQUIDS

Béla Lévay /1/ and Ole E. Mogensen
Chemistry Department, Danish Atomic Energy Research Establishment Ris, DK-4000 Roskilde, Denmark

The investigation of the behaviour of excess electrons in their liquid environment provides an important method for learning about the nature of matter /2/. The positron annihilation method has also been used successfully as a tool for studying the same subject /3/.

The correlation of results of radiation chemistry with positron annihilation, however, had not been attempted till very recently, when one of the present authors (O. E. M.) proposed a new model of Ps formation: the spur reaction model /4/.

Positronium, i. e., a bound state between an electron and a positron (Ps), is assumed to be formed by a reaction between a positron and an electron in the positron spur. This process competes with the recombination of the electrons and their parent positive ions ("geminate recombination") and also with the diffusion of electrons out of the spur. Reactions of the electrons or the positrons in the spur with the solvent molecules or with scavengers will also decrease the probability of Ps formation.

The aim of our present work was to test a very peculiar prediction of spur reaction model which we could have done using the recent results of Allen, Gangwer and Holroyd /5/ on chemical reaction rates of quasifree electrons on nonpolar liquids. They correlated their results with the quantity V_o, the work function of the electrons in their mobile state in the liquids. For C_2H_5Br the rate constants exhibited a maximum for a characteristic value of V_o, for CCl_4 the rate constants increased monotonously with decreasing V_o.

On the basis of the above experimental results of radiation chemistry the spur reaction model of Ps formation predicts at least a qualitatively similar kind of dependence on V_o for the Ps inhibition properties of C_2H_5Br and CCl_4, as was found for their electron reaction rate constants. The Ps inhibition property of a solute in a given solvent can be characterized by an inhibition coefficient which has the similar meaning to that of Schuler's relative scavenging constant/6/.

The Ps inhibition functions, i. e., relative o-Ps yields as a function of C_2H_5Br or CCl_4 concentration, have been determined for several nonpolar liquids and their mixtures by the conventional positron lifetime technique /3/. The results are presented in Fig. 1.

The inhibition functions in the order from right to left correspond to increasing inhibition constants as it is obvious that stronger inhibitors decrease the Ps yield at lower concentrations.

The spur reaction model of Ps formation results in a simple correlation between Ps inhibition function and scavenging function F (c):

$$P(c) = 1 - F(c) \tag{1}$$

The scavenging function is widely used in steady state scavenging experiments /6/ to describe the yield of a given product G(P) as a function of scavenger concentration:

$$G(P) = G_{fi} + G_{gi} F(c) \tag{2}$$

G_{fi} denotes the yield of "free ions", while G_{gi} represents the yield of "geminate ion pairs". Thus Eq. (1) has the meaning that the probability of Ps formation is proportional to the unscavenged fraction of "geminate electrons".

As for the explicit analytical form of F(c), Schuler and co-workers /6/ proposed the use of an empirical function

$$F(c) = \frac{(\sigma C)^{1/2}}{1 + (\sigma C)^{1/2}} \tag{3}$$

The Ps inhibition function corresponding to Eq. (3) would be

$$P(c) = \frac{1}{1 + (\sigma C)^{1/2}} \tag{3. a.}$$

Analysis of our measured Ps inhibition functions, however, suggested that we fit them with an other empirical expression using a second adjustable parameter in the exponent:

$$P(c) = \frac{1}{1 + (\sigma C)^{\alpha}} \tag{4}$$

which would correspond to the following scavenging function:

$$F(c) = \frac{(\sigma C)^{\alpha}}{1 + (\sigma C)^{\alpha}} \tag{4. a.}$$

The results of the fitting procedure are presented in Table 1. The last column contains the RMS deviation between the measured and calculated points. The data in parentheses represent the results when only the upper part of the total inhibition

Table. 1.

Summary of Results Obtained by Parameter Fitting of o-Ps Inhibition Functions Measured in Various Liquids and Liquid Mixtures

Solvent	V_0, eV	Inhibitor	σ, M^{-1}	α	$\sqrt{\Delta^2}$
n-tetradecane ($n-C_{14}$)	0.21	C_2H_5Br	3.9±0.4 (5.2)	0.61±0.01 (0.78)	0.032 (0.012)
		CCl_4	20.5±1	0.88±0.01	0.005
n-hexane ($n-C_6$)	0.00	C_2H_5Br	5.3±0.5 (8.2)	0.57±0.01 (0.74)	0.025 (0.005)
iso-octane ($iso-C_8$)	−0.26	C_2H_5Br	6.0±0.6 (10.3)	0.48±0.01 (0.62)	0.018 (0.005)
		CCl_4	46.0±1	0.67±0.01	0.006
neopentane ($neo-C_5$)	−0.35	C_2H_5Br	2.4±0.2 (2.8)	0.73±0.01 (0.83)	0.014 (0.004)
tetramethyl-silane (TMS)	−0.51	C_2H_5Br	1.04±0.1	0.94±0.01	0.011
		CCl_4	59.0±1	0.58±0.01	0.021
TMS + $n-C_{14}$ ($X_{TMS} = 0.49$)	−0.14*	C_2H_5Br	4.8±0.5 (7.8)	0.56±0.01 (0.75)	0.021 (0.002)
$n-C_6$+neo-C_5 ($X_{n-C_6} = 0.25$)	−0.26*	C_2H_5Br	4.3±0.5 (5.5)	0.55±0.01 (0.63)	0.014 (0.009)

* Calculated values from the V_0-s of the pure solvent components, assuming a linear relationship between V_0 and the mol fraction X

curve (P(c) > 0.6) was involved in the fitting procedure. In the case of C_2H_5Br the obvious reason for the difference between the two fitting procedures is due to the high concentration of C_2H_5Br.

In Fig. 1, the solid curves for C_2H_5Br and the dashed ones for CCl_4 are drawn using Eq. (4) with σ and α values calculated from total curve fitting (Table 1). The calculated curve for C_2H_5Br in TMS–$n-C_{14}$ mixture which is practically identical with the $n-C_6$ curve, is omitted.

In Fig. 2, positronium inhibition constants (σ, left side scale) are shown together Allen, Gangwer and Holroyd's /5/ electron rate constants (k, right side scale) as a function of V_o. The solid and dashed lines are graphic fits for C_2H_5Br and CCl_4 data, respectively.

The curves for C_2H_5Br in both cases exhibit a maximum for the same solvent (i. e., for the same V_o) and both curves are very much steeper from left to the maximum than from right to it. The CCl_4 curves, on the other hand, increase in both cases eith decreasing V_o.

Very convincing also is the fact that the points for the solvent mixtures, V_o values of which were adjusted to be close to the maximum, are situated reasonably well on a curve common with the pure solvents.

Thus the prediction of the spur reaction model of Ps formation proved to be valid for this very peculiar case and this fact seems to be the most severe test of this model until now. It is necessary to emphasize here, that the reaction rate of the spur electrons is only one factor which affects the process of Ps formation, and that there are several others which may modify, to a great extent, the very complex and compicated situation in the spur. The good qualitative correlation between these two quantities, howewer, demonstrates the decisive role of electron reaction rates on Ps formation – at least in those non-polar liquids of high electron mobility.

In principle the Ps inhibition coefficient has the same meaning as that of the relative scavenging constant in Schuler's phenomenological model for scavenging in hydrocarbons /6/ and the numerical values of these two quantities have to be the same or at least comparable. Unfortunately, however, we have hardly any data to make this comparison. Rzad and Bansal /7/ have measured the relative scavenging constant for C_2H_5Br in iso-octane and their $5M^{-1}$ value is very close to ours: $\sigma = 6 \pm 0.6\ M^{-1}$.

We have succeeded in fitting our Ps inhibition curves by Schuler's /6/ empirical scavenging function only if using a new fitting parameter (α) instead of the constant value (0. 5) in the exponent of concentration. This α, or more exactly α^{-1}, could be correlated with V_o in a qualitatively similar way as was found for the rate constants and Ps inhibition coefficients.

This correlation expresses the fact that our second fitting parameter (α) must be determined by the reaction rate constant of electrons and emphasizes the decisive role of V_o on the mechanism and kinetics of electron scavenging processes.

Because both σ and α^{-1} showed qualitatively similar dependence on V_o, it seemed to be obvious to look for their possible interrelationship.

This has resulted in a simple linear relationship

$$\alpha^{-1} = a'\sigma + b' \qquad (5)$$

where $a' = 0.21$ and 0.015 for C_2H_5Br and CCl_4 respectively, and $b' = 0.81$ for both from a graphic fit to the data.

The advantage of a relation like Eq. (5), if it proved to be valid also for other scavengers, would be the possibility of extracting a solvent-independent "number" for characterizing the "scavenging or inhibition strength" of the scavengers. For example $1/a' = 4.8$ and 67 for C_2H_5Br and CCl_4, respectively, could express that the latter is a stronger scavenger or Ps inhibitor than the former.

We have also tried to correlate our σ values measured for a given scavenger in different solvents to the k values for the same scavenger, and have got a reasonable linear correlation for log k vs. σ :

$$\log k = a\,\sigma + b \qquad (6)$$

where $a = 0.45$ and 0.065 for C_2H_5Br and CCl_4, respectively and $b = 10$ for both from a graphic fit to the data.

These special correlations stated here, however, are at present only tentative ones since data are too scarce to prove their general validity. In order to test them, and for our better understanding of the nature of matter, more experimental efforts are needed especially for extending the steady state scavenging measurements for liquids of low V_o. For this purpose Ps inhibition measurements can provide useful and important information for radiation chemistry and chemistry of Ps as well.

References

/1 / Visiting scientist from Department of Physical Chemistry and Radiology, Eötvös University of Budapest, 1088 Budapest, Hungary

/2 / E. J. Hart, and M. Aubar "The Hydrated Electron", Wiley, New York, 1970.

/3. a/ J. H. Green, and J. Lee "Positronium Chemistry", Academic Press, New York, 1964, b/ V. I. Goldanskii, Atomic Energy Review, 6, 3 (1968), c/ J. A. Merrigan, J. H. Green, and S. J. Tao. in "Physical Methods of Chemistry", A. Weissberger and B. W. Resitter, eds., Wiley, New York, 1972, Vol. 1, Part III. D, p. 501.

/4 / O. E. Mogensen, J. Chem. Phys., 60, 998 (1974).

/5 / A. O. Allen, T. E. Gangwer, and R. A. Holroyd, J. Phys. Chem. 79, 25 (1975).

/6 / J. M. Warman, K. -D. Asmus, and R. H. Schuler, Advan. Chem. Ser., No 82, 25 (1968).

/7 / S. J. Rzad, and K. M. Bansal, J. Phys. Chem., 76, 2374 (1972).

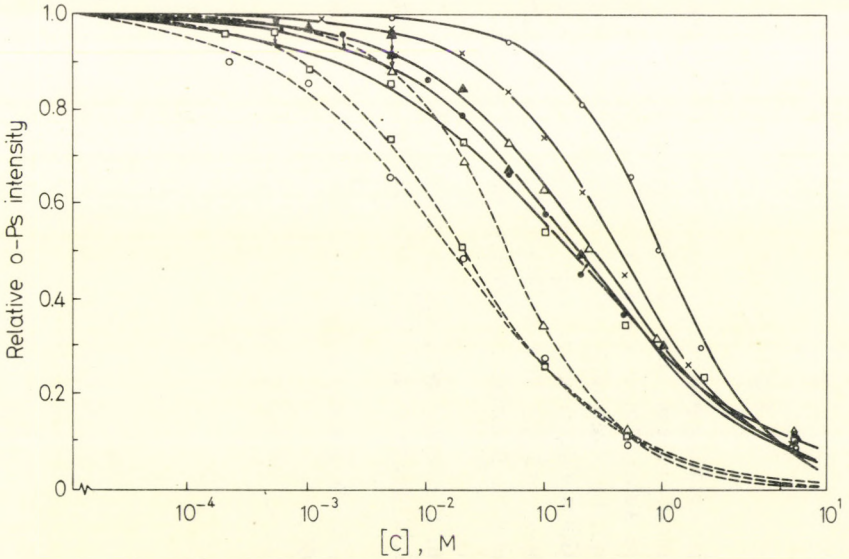

Fig. 1. Relative o-Ps intensities as a function of inhibitor concentration in various solvents. Symbols: △ n-C_{14}, ● n-C_6, □ iso-C_8, × neo-C_5, ○ TMS, ▲ TMS-n-C_{14} mixture. Solid curves for C_2H_5Br and dashed ones for CCl_4 for fitting to Eq. (4) with σ and α values in Table 1. (The solid curve for the TMS-n-C_{14} mixture is omitted.)

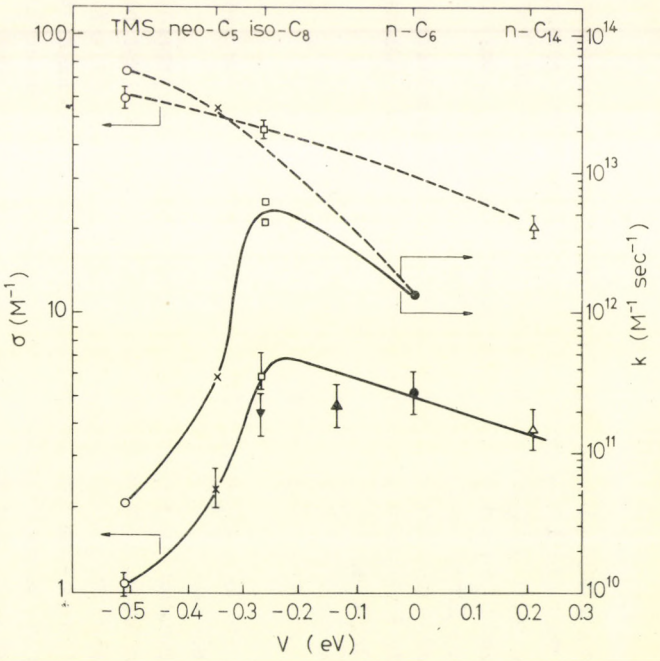

Fig. 2. Ps inhibition coefficients (σ, left side scale) and electron rate constants (k, right side scale) for reactions with C_2H_5Br (solid curves) and CCl_4 (dashed curves) as a function of V_0. Symbols: ▼ n-C_6-neo-C_5 mixture, others as in Fig. 1

Z-P. ZAGORSKI

Did you make investigations on solidified (frozen) organic systems?

B. LÉVAY

No! The idea is interesting, but the explanation of experimental results in the solid phase seems to be difficult.. Even the possibility of Ps formation is questionable in frozen organic systems.

R. SCHILLER

Could one make a difference between the electron-scavenging and positronium-scavenging mechanisms by investigating positron annihilation in the vapour of the scavenger?

B. LÉVAY

May be! It seems to be a very interesting idea. As regards to the experimental technique, it is possible to carry out such measurements.

QUANTITATIVE STUDIES IN THE γ-RADIOLYSIS OF LIQUID AND SOLID ALCOHOLS BY SPIN TRAPPING METHOD

V. E. Zubarev, V. N. Belevskii, L. T. Bugaenko
Department of Chemistry, Moscow State University,
Moscow, USSR

The spin trapping technique has been used to investigate the radiolysis of liquid alcohols. The method involves the trapping of unstable intermediates $\dot{R}$ formed in the radiolysis, by nitroso compound or nitrone to give a nitroxide as in the reaction:

$$\dot{R} + t\text{-BuNO} \longrightarrow R\text{-}N(\dot{O})t\ Bu$$

$$\dot{R} + Ph\text{-}CH = N(O)\,t\text{-}Bu \longrightarrow Ph\text{-}CHR\text{-}N(\dot{O})t\text{-}Bu$$

The resulting nitroxide has an ESR spectrum characteristic of $\dot{R}$. The alkoxy $R\dot{O}$, hydroxyalkyl radicals and H-atoms (in methanol) produced during radiolysis of alcohols have been detected by spin trapping method /1–5/. Primary radical yields were determined in γ-irradiated methanol /5, 6/.

In the present paper the radical yields in the γ-radiolysis of methanol, ethanol, 1-propanol and 2-propanol have been determined as a function of radiolysis temperature. Nitroso-tert.-butane (NtB) and C-phenyl-N-tertbutylnitrone (PBN) have been used as spin traps.

Experimental

Nitroso-tert.-butane (NtB) was prepared by the method of Stowell /7/, and C-phenyl-tert.-butylnitrone (PBN) was prepared by the method of Emmons /8/. The experimental techniques have been published earlier /5/. The samples were irradiated by Co^{60} γ-rays (dose rate 3×10^{16} eV/g. sec) at different temperatures. The total dose was not in excess of 2×10^{18} eV/g.

Results

PBN has been used for the determination of absolute radicals yields. The 0.02–0.5 M methanol solutions of PBN were irradiated at -196° as well as at the temperature range from $-90^{\circ}C$ to $+20^{\circ}C$. The solutions of PBN in ethanol, 1-propanol and 2-propanol were irradiated at $+20^{\circ}C$ and $-196^{\circ}C$ only. In the presence of

O_2 only alkoxy radicals were trapped by nitrone, while hydroxy-alkyl radicals and H-atoms reacted with O_2 to form peroxide radicals which produce no stable nitroxides.

In the ESR-spectra of evacuated samples there were detected the spin adducts of PBN with RO· and RĊHOH-radicals and H-atoms. The increase of PBN-concentration leads to the growth of the yields of RO-spin adduct $G(R_1)$ due to the competition between ROH and PBN for RO·-radicals.

$$R\dot{O} + ROH \xrightarrow{k_1} R\dot{C}HOH + ROH \quad (1)$$

$$R\dot{O} + PBN \xrightarrow{k_2} RO\text{-}PBN\ (R_1) \quad (2)$$

The steady-state concentration method gives the following equation:

$$\frac{1}{G(R_1)} = \frac{1}{G(R\dot{O})} + \frac{1}{G(R\dot{O})} \times \frac{k_1\,[ROH]}{k_2\,[PBN]} \quad (3)$$

The graphical solution of Eq. (3) gives both the initial yields of RȮ, G(RȮ) and the rate constants ratio k_1/k_2 /6/. The absolute rate constants of reaction (1) were determined in pulse radiolysis studies /9, 10/, where $k(CH_3\dot{O} + CH_3OH) = 2.62 \times 10^5$ and $k(C_2H_5OH + C_2H_5\dot{O}) = 1 \times 10^6$ 1/M sec at 20°C. According to our estimate the rate constants of spin trapping of RO-radicals by PBN are: $k(CH_3\dot{O} + PBN) = 1.2 \times 10^8$ and $k(C_2H_5\dot{O} + PBN) = 2 \times 10^8$ 1/M sec. The total spin adduct yields $G(\Sigma R) = G(R\dot{O}) + G(H) + G(R\dot{C}HOH)$ were determined in the absence of O_2. In concentration range of PBN between 0.1 and 0.5 M the total yields $G(\Sigma R)$ are independent of [PBN], i.e. all the radicals escaping from spurs are trapped by PBN. The $G(R\dot{O})$ and $G(\Sigma R)$ are listed in Tables 1 and 2.

Table 1

The radical yields $G(CH_3\dot{O})$ and $G(\Sigma R)$ radicals/100 eV depending upon the temperature of methanol radiolysis

t°C	20	0	-20	-40	-60	-80	-90
$G(\Sigma R)$	6.2	5.6	5.0	5.7	6.4	5.2	5.2
$G(CH_3\dot{O})$	2.5	2.2	1.95	1.85	1.7	1.5	1.4

Table 2

The radical yields $G(R\dot{O})$ and $G(\Sigma R)$ in γ-irradiated alcohols at 20°

Alcohols	Methanol	Ethanol	i-Propanol	2-Propanol
$G(\Sigma R)$	6.2	5.5	3.2	2.0
$G(R\dot{O})$	2.5	1.6	1.1	1.0

The primary $R\dot{O}$ yields (Table 2) determined by spin trapping agree well with the pulse radiolysis data for methanol and ethanol, $G(CH_3\dot{O}) = 2.0-2.5$, $G(C_2H_5\dot{O}) = 1.5$ /10/ and the estimate for 2-propanol $G(R\dot{O}) \simeq 1.0$ /11/. The principal primary radicals are $R\dot{O}$ and $R\dot{C}HOH$. The H-atom yields amount to about 5% of $G(\Sigma R)$.

If glassy alcohols containing 0.1–0.5 M PBN are γ-irradiated at $-196^{\circ}C$, the total radical yields $G(\Sigma R)$ measured at $-196^{\circ}C$ after irradiation are identical to those determined in the absence of PBN in pure alcohols. The electrons are completely trapped by 0.1 M PBN, however, the spin adduct of PBN with electron has decayed on warming to $-160^{\circ}C$ /6/. The $G(\Sigma R)$ determined after melting of glassy samples at $-50^{\circ}C$ was lower than that at $-196^{\circ}C$, in this case we have observed only the $R\dot{C}HOH$–spin adduct with PBN in all the alcohols studied. Thus electrons do not contribute in the radical yields determined by spin trapping method in solid after melting and in liquid. The difference between $G(\Sigma R)$ measured at $-196^{\circ}C$ and $-50^{\circ}C$ is equal to $G(e^{-}_{t2})$ – the yields electrons stabilized at $-196^{\circ}C$ (Table 3).

In glassy alcohols irradiated at $-196^{\circ}C$ the $R\dot{O}$-radicals were not observed. Mao and Kevan /3/ have suggested that the primary neutral radicals in γ-irradiated alcohols may be different in the liquid and in the glass. We have investigated the possibility of the $R\dot{O}$-radicals formation in radiolysis of methanol and ethanol in solid phase. We have chosen to use the trapping by NtB because of the greater sensitivity of the ESR spectra of the nitroxide to change in the nature of the trapped radical. The alcoholic solutions of 0.1 M NtB were irradiated by γ-rays in the range from $-90^{\circ}C$ to $-196^{\circ}C$. The ESR spectra were recorded at $-70^{\circ}C$ (Fig. 1). The relative yields of $R\dot{O}$ and $R\dot{C}HOH$-radicals formed at different temperature of irradiation are shown in Fig. 2. In alcohols irradiated at $-196^{\circ}C$ we observe mainly the nitroxide (I)$RCH(OH)N(\dot{O})tBu$ formed by the trapping of $R\dot{C}HOH$ and a small amount of RO-adduct, about 2% of $G(\Sigma R)$, i.e. nitroxide(II)$RO\text{-}N(O)tBu$.

The increase of irradiation temperature leads to the growth of the yields of nitroxide (II) and the decrease of the nitroxide (I). In γ-radiolysis of 0.1 M NtB solution in methanol at $-90^{\circ}C$ mainly $CH_3\dot{O}$ spin adduct (nitroxide II) was observed and very little nitroxide I. The identical situation takes place in radiolysis of ethanol, but the yields of nitroxide I are much higher.

The nitroxide (I)$HOCH_2\text{-}N(\dot{O})tBu$ as such is stable at $20^{\circ}C$ and is independent of the irradiation temperature being obtained by the irradiation at 20° /12, 13/ or

Table 3

The radicals yields $G(\Sigma R)$ in the alcohols, γ-irradiated at $-196^{\circ}C$ and measured at -196° and $-50^{\circ}C$

	t°C	CH_3OH	C_2H_5OH	1-propanol	2-propanol
$G(\Sigma R)$	−196	7.0	5.4	4.8	4.8
$G(\Sigma R)$	−50	4.5	3.2	3.0	1.9
$G(e^{-}_{tr})$		2.5	2.2	1.8	2.8

at -196° /5, 14/. It was shown in Ref. /14/ that nitroxide (I) decays in second-order reaction with nitroxide (III) HN(Ȯ)tBu, which is derived from the trapping of H-atoms or electrons followed by protonization:

$$HN(\dot{O})tBu + HOCH_2N(\dot{O})tBu \longrightarrow HN(OH)tBu + HOCH = N(O)tBu \qquad (4)$$

The nitroxide (III) was observed only "in situ" radiolysis with electron beam and rapidly disappeared when the electron beam was off. Thus the apparent yield of nitroxide (I) is equal to the difference between the yields of nitroxides (I) and (III). The rate constants for the reaction between H-atom and alcohols k(H+ROH) in liquid ethanol and propanols are ten times higher than that in methanol /15/. Therefore the yields of nitroxide (III) are reduced and the observed yields of nitroxide (I) are much higher than those in liquid methanol /4/.

The lowering of temperature in the range from $-130^{o}C$ to $-160^{o}C$ increases the viscosity of solid alcohols by several orders of magnitude /16/. This results in the decrease of the diffusion rate of RO-radicals to spin trap and in that of the observed yields of RO-adducts. Below $-175^{o}C$ the radicals were not trapped by NtB at all, and the RȮ-radicals and H-atoms react essentially with alcohols forming RCHOH-radicals, which are spin trapped upon warming above $-160^{o}C$ /6/ (see Fig. 2).

Discussion

The quantitative studies of aliphatic alcohols radiolysis by spin trapping method show that the most important primary radicals in the liquid are RȮ, RĊHOH, H-atoms and e_s^-. The radiolysis mechanism of these alcohols is, at least qualitatively, similar and the ion-molecular reaction (5) takes place both in liquid and in solid:

$$ROH^+ + ROH \begin{cases} \longrightarrow R\dot{O} + ROH_2^+ \\ \longrightarrow R\dot{C}HOH + ROH_2^+ \end{cases} \qquad (5)$$

The ratio of yields $G(\dot{C}H_2OH)/G(CH_3\dot{O}) = 1.3$ for methanol at $20^{o}C$ and depends on the temperature /6/. In the ESR-spectra recorded "in situ", with the electron beam on, there was detected a steady-state concentration of nitroxides as the result of the nitroxide I decay in reaction (4). Also the yield ratio $G(R\dot{C}HOH)/G(R\dot{O}) = 0.4$ for liquid methanol and ethanol found by Sargent and Gardy /17/ appear to be underestimated these results being in contrast with data of other authors /3, 5, 6/.

$G(R\dot{O})$ and $G(\Sigma R)$ in alcohols at $20^{o}C$ were shown to decrease from methanol to 2-propanol (Table 2), $G(CH_3\dot{O})$ and $G(\Sigma R)$ in methanol decrease with increasing radiolysis temperature (Table 3). The yields $G(R\dot{O})$ are plotted as a function of T/η in Fig. 3, where T is the radiolysis temperature (K) and η the viscosity of alcohols.

The $G(\dot{RO})$ seems to be proportional to T/η . The escape of RO-radicals from spurs into the bulk seems to be limited by the diffusion /6/. The decrease of $G(\Sigma R)$ at the lower radiolysis temperature (-90°C) appear to involve radical recombination in spurs: The non-scavengeable yield of ethylene glycol in methanol is 0.1-0.4 /18/. The growth of alcohol viscosity from methanol to 2-propanol hinders the radicals diffusion from the spur into the bulk, what results in the decrease of $G(\dot{RO})$ and $G(\dot{RCHOH})$. The radical recombination in spurs may probably account for the decrease of total yields of alcohol decomposition from methanol to 2-propanol /19/ as well as for the decrease of decomposition yield with the increase of LET.

The spin trapping experiments of irradiated alcohols in liquid and solid /1-6, 14, 17/ have shown that the alkyl radical adducts are not observed either after γ-irradiation or directly, during "in situ" radiolysis with electron beams /2, 17/. The alkyl radicals were not detected by the direct observation of ESR spectra from steady-state concentration of radicals formed during continuous radiolysis of pure alcohols with a beam of electrons /20/. Meanwhile hydrocarbons are formed in alcohol radiolysis and $G(C_2H_6) = 1.5$ in propanol and $G(CH_4) = 1.8$ mol/100 eV in 2-propanol are found. The low yields ($G \approx 0.5$) of CH_4, C_2H_6 and C_3H_8 in the radiolysis of methanol, ethanol and 1-propanol are accordingly due to the reaction (6) of dissociative electron capture proceeding in spurs /22/.

$$e^- + ROH_2^+ \qquad \dot{R} + H_2O \qquad (6)$$

These alkyl radicals seem to possess excess energy and react, forming hydrocarbons, still in the spur. The large yields of ethane and methane in propanols seem to involve the decomposition of excited alcohol molecules which leads to the formation of hydrocarbons and aldehydes /21, 23/.

References

/ 1/ J. A. Wargon, F. Williams, J. Amer. Chem. Soc., 94, 7917 (1972).
/ 2/ F. P. Sargent, E. M. Gardy, H. R. Fall, Chem. Phys. Lett., 24, 120 (1974).
/ 3/ S. W. Mao, L. Kevan, Chem. Phys. Lett. 24, 505 (1974).
/ 4/ F. P. Sargent, E. M. Gardy, Canad. J. Chem., 52, 3645 (1974).
/ 5/ V. E. Zubarev, V. N. Belevskii, L. T. Bugaenko, Vestnik Moscow State University, "Chemistry",, No. 3, 295 (1975).
/ 6/ V. E. Zubarev, V. N. Belevskii, L. T. Bugaenko, Dokladi Akad. Nauk USSR 226, 114 (1976).
/ 7/ J. C. Stowell, J. Org. Chem., 36, 3055 (1971).
/ 8/ W. D. Emmons, J. Amer. Chem. Soc., 79, 5739 (2957).
/ 9/ D. H. Ellison, G. A. Salmon, F. Wilkinson. Proc. Roy. Soc. Lond., A328, 23 (1972).

/10/ F.S. Dainton, J.Janovsky, G.A. Salmon, Proc. Roy. Soc. Lond., A327, 305 (1972)
/11/ R.V. Bensasson, J.K. Thomas, Int. J. Rad. Phys. Chem., 1, 185 (1969).
/12/ A. Ledwith, P.J. Russell, L.H. Sutcliff, Proc. Roy. Soc. Lon., A332, 151 (1973).
/13/ H. Toniguchi, H. Hatano, Chem. Letters, No. 6, 531 (1974).
/14/ V.E. Zubarev, V.N. Belevskii, L.T. Bugaenko "Chimia visokich energii" (in press) No. 6 (1976).
/15/ M. Anbar, P. Neta, J. Appl. Rad. Isotop. 18, 494 (1967).
/16/ A.C. Ling, J.E. Willarg, J. Phys. Chem., 72, 3349 (1968).
/17/ F.P. Sargent, E.M. Gardy, J. Phys. Chem. (in press) (1976).
/18/ J.H. Baxendale, P. Wardman "The Radiolysis of Methanol: Product Yields, Rate Constants and Spectroscopic Parameters of Intermediates", U.S. Dept. of Commerce Publ., No. NSRDS-NBS-54 (1975).
/19/ G.R. Freeman in "Actions Chimiques et Biologiques des Radiations" ed. M. Haissinky, Masson et Cie, Paris 14, 73 (1970).
/20/ F.P. Sargent, E.M. Gardy, J. Phys. Chem., 78, 1977 (1974)
/21/ A.I. Afanasiev, Candidat. dissertation. Moscow, 1972.
/22/ V.N. Belevskii, V.E. Zubarev, L.T. Bugaenko "Vestnik Moscow State University", Chemistry", No. 2, 184 (1975).
/23/ R.A. Basson, U.J.w.d. Linde, J. Chem. Soc. (A) (1969) 1618.

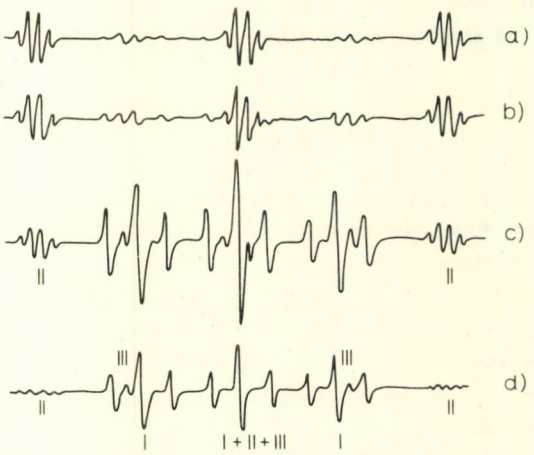

Fig. 1. The ESR-spectra observed in 0.1 M t-BuNO methanol solution after γ-radiolysis at different temperatures: a) -90°, b) -127°, c) -160°, d) -196°C. The spectra are recorded at -70°C

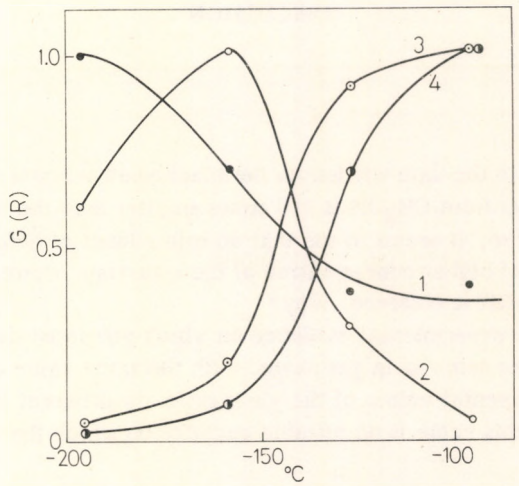

Fig. 2. The relative yields of RȮ and RĊHOH-radicals trapped by t-BuNO for γ -irradiated methanol (2,3) and ethanol (1,4) depending on the radiolysis temperature: RȮ (3,4), RĊHOH (1,2)

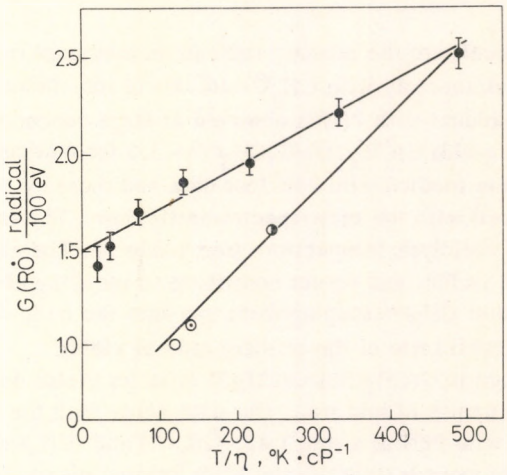

Fig. 3. The yields of RȮ-radicals as function of T/η : ● – methanol, ◑ – ethanol, ⊙ – 1-propanol, ○ – 2-propanol

J. SOHMA

(1) According to the data written on the blackboard the rate constant of hydrogen abstraction by $CH_3O^{\cdot}$ from CH_3OH is 100 times smaller than the formation rate of the spin-adduct. If so, it seems to me that no spin adduct of $\dot{C}H_2OH$ could be observed in the case of higher concentration of the spin-trap. However, apparently the spin-adduct of $\cdot CH_2OH$ is observed. Why?

(2) What is the experimental evidence on which you insist that reaction scheme in liquid phase is the same as in gas phase, with the same value of the yield ratio?

(3) The experimental values of the yield ratio are different from one researcher to another. Thus, this value is no suitable quantity on which the reaction scheme is discussed.

In our group the spin trapping experiments with BNB were carried out for irradiated alcohols methanol, ethanol and propanol, some of which were deuterated. In these experiments isotope effect in the yield ratio was found and the concentration dependences were studied. Based on these experimental results we believe that $CH_3O^{\cdot}$ is a precursor for a $\cdot CH_2OH$ radical both in the liquid and in the solid phase.

V. Y. BELEVSKI

(1) $\cdot CH_2OH$ -radicals are the primary radicals in methanol radiolysis, these radicals are formed simultaneously with $CH_3O^{\cdot}$-radicals in ion-molecule reaction (5). That is why $\cdot CH_2OH$-adduct with PBN is observed at large concentration of PBN.

(2) The ratio of yields $G(\dot{C}H_2OH)/G(CH_3O^{\cdot}) = 1.3$ for methanol at $+20^{\circ}C$, determined by spin trapping method with PBN (our data and those by Mao and Kevan /3/) as spin trap agrees well with the mass-spectrometric data. The ratio of yields rises with the decrease of radiolysis temperature (see Table 1). The electrons are completely trapped by 0.14 PBN and do not contribute to the CH_2OH-radical yield. $G(CH_3O^{\cdot})$ is the yield of $CH_3O^{\cdot}$ escaping from spur into the bulk. Therefore spin trapping data give the actual ratio of the primary radical yields.

(3) The difference in $G(CH_2OH)/G(CH_3O^{\cdot})$ ratio for yields determined by other authors is due to the nature of spin trap. Our data agree with the results of Mao and Kevan /3/ obtained with PBN as a spin trap. $\dot{C}H_2OH$ and $\cdot CH_3CHOH$ radicals are trapped by nitroso compounds (t-BuNO and BNB) forming nitroxide of the type

$$R - \underset{\underset{O\cdot}{|}}{N} - CH_2OH$$ /R=t-BuNO, or BNB/ which decays in a second-order reaction

with nitroxide $HN(\dot{O})$-tBu or H-BNB. These latter ones are derived from the trapping of H-atom or electron by nitro compound (e. g. reaction 4).

Secondary reaction of spin adduct $R\dot{C}HOH$ radicals with NtB and BNB results in the decreasing of the observed yields of this spin adduct.

Only PBN may be a good spin trap for quantitative studies in the γ-radiolysis of alcohols.

G. M. ZIMINA

I should like to know how the ratio

$$\frac{G(\dot{C}H_2OH)}{G(CH_3\dot{O})} = 1.3 \quad (t = 20^{\circ}C)$$

decreases with decreasing temperature?

V. Y. BELEVSKII

The ratio of yield, $G(\dot{C}H_2OH)/G(CH_3\dot{O})$ increases with the decrease of radiolysis temperature (see Table 1 in this paper). $G(\dot{C}H_2OH)/G(CH3\dot{O}) = 2.1$ at $-30^{\circ}C$.

ON THE RADIATION STABILITY OF SOME LIQUID CRYSTALS

M. Roder, K. Pintér, K. Ritvay
Central Research Institute for Physics, Budapest,
Hungary

Radiation chemical yields are known to depend markedly on the aggregate state of the irradiated parent compounds. While the energy absorbed in unit mass is practically independent of the state the yields and rates of transformation are drastically influenced by any phase change. The comparison of the solid and liquid or liquid and gaseous phase radiation chemistry of one and the same compound reveals fundamental differences /1/.

Hence the radiation chemical investigation of substances which have more than three aggregate states seems to be most promising both as a possible clue to phase effects and as a way of characterisation of these substances. Liquid crystalline compounds might give interesting answers on several questions raised in radiation chemistry.

The term 'liquid crystal' covers several aggregate states all of which are in an intermediary position between crystals of long range order and isotropic liquids of random molecular distribution. In the thermotropic liquid crystal compounds (in which the liquid crystalline phases are obtained by disruption of the crystal lattice due to thermal vibration) the different mesophases are characterized by the partial positional and orientational order of molecules.

In the smectic liquid crystalline phases the molecules are arranged in individual planes (layers). The longer axes of molecules are oriented in each layer toward a preferred direction which is perpendicular or tilted to the plane of the layer. The distribution of the molecular centres within the layers corresponds either to that of a two-dimensional liquid (unstructured layers) or to that of a two-dimensional lattice (structured layers).

The structure of the nematic liquid crystalline phase is much more mobile than that of the smectic phase. The periodicity of molecular arrangement of the smectic phases is absent in the nematic phase and the centres of the molecules are distributed at random as in isotropic liquids. However, on account of forces arising from their mutual interaction the molecules adopt a common average parallel orientation.

The cholesteric liquid crystalline phase is a special form of the nematic phase (twisted nematic crystalline phase). In this phase the arrangement of optically active molecules corresponds to planar uniformly twisted structure instead of the uniform parallel alignment characteristic to the nematics /2/.

The purpose of the present investigation was to determine the phase effect on the radiolytic stability of different liquid crystals. The studies were confined to a determination of the temperature dependence of the main gaseous product yields and the number of molecules converted to products less volatile than the liquid crystals studied.

EXPERIMENTAL

The derivatives of acetophenone were prepared by reacting the appropriate p-alkyloxybiphenyl compound with acetylchloride in the presence of aluminium chloride. The acetophenones obtained were recrystallized several times from ethanol. Ethyl p-ethoxybenzylidene-p'-aminocinnamate was prepared by the reaction of p-ethoxybenzaldehyde with p-aminoethylcinnamate in ethanol solution with subsequent recrystallization. p-Methoxybenzylidene-p-aminophenyl-n-pentanoate was synthesized by reacting p-methoxybenzylidene p-aminophenol with pentanoic anhydride in pyridine solution at room temperature. The crude product was repeatedly recrystallized from hexane. Synthesis of the other compounds was carried out according to methods in the literature /3-6/. Chemical composition of the products was verified by using elementary carbon-hydrogen analysis. The phase transition temperatures were determined by differential scanning calorimetry and differential thermo-analysis or by visual observation in a melting point capillary and thermal microscopy.

Radiolysis of each compound was carried out on quantities of about 0.5 g of the sublimed and carefully degassed, weighed material. These samples were sealed under vacuum in cells fitted with a break-seal. Irradiation was performed in a ^{60}Co gamma ray source with doses of $5.\ 10^{21}-10^{22}$ eVg^{-1} and average dose rate of $3.\ 10^{19}$ eV g^{-} h^{-1}. Temperature was regulated in the furnace with an accuracy of $\pm$ 2°C.

After irradiation the sample cells were sealed in a vacuum system combined with Toepler pump and separation and separation and fractionation of gaseous products from the condensed phase were performed by the freeze-thaw-pump technique. The overall gas yield was measured volumetrically. The collected fractions of gases were analyzed by gas chromatography. The quantity of products less volatile than the investigated compound was determined by measuring the residue of molecular vacuum distillation carried out at the sublimation temperature of the compound studied.

RESULTS AND DISCUSSION

Table 1 shows the liquid crystals studied together with their phase transition temperatures. Each compound was held unirradiated at the highest temperature applied for the same period of time as that of irradiation to determine whether there was any pyrolysis of the compound. The data of these pyrolytic studies indicated that heating left the compounds practically unchanged. This means that formation of products below this temperature is due solely to radiolytic effects.

Table 1

Phase-transition temperatures of the investigated compounds

Compounds	Temperature /°C/ of transition							
	C-S	C-N	C-Ch	S-S	S-N	S-I	N-I	Ch-I
p-Methoxybenzylidene p'-aminophenyl n-pentanoate		55					95	
p'-n-Butylphenyl p-n-butylbenzoyloxybenzoate		78					186	
Cholesteryl benzoate			145					178
p-n-Hexadecyloxybenzoic acid	90					129		
p-n-Pentyloxyphenyl acetophenone	90					139		
p-n-Heptyloxyphenyl acetophenone	95					136		
Ethyl p-ethoxybenzylidene p'-aminocinnamate	80			120	157		160	

C-crystalline phase, S-smectic liquid crystalline phase, I-isotropic liquid phase
N-nematic liquid crystalline phase,
Ch-cholesteric liquid crystalline phase,

Each compound was irradiated at a series of temperatures so that the effects in crystalline, liquid crystalline and isotropic liquid state could be observed. The quantity of the observed radiolytic products was proportional to the absorbed doses - over the dose range $5.\ 10^{21}-10^{22}$ eV g^{-1}.

Figure 1 shows the temperature and aggregate state dependence of the yields $G(H_2)$, $G(CH_4)$, $G(C_2H_n-C_4H_m)$ (this latter denoting different gaseous hydrocarbon products) and G(-M), the number of parent molecules converted into products less volatile than the parent compound for the radiolysis of p'-n-butylphenyl-p-n--butyl-benzoyloxybenzoate. A very slight rise in the $G(H_2)$-value was observed with increasing temperature whereas the increase of the other gaseous product yields was more significant. All these yields do not change appreciably at the phase transition temperatures. G(-M) increases slightly in the crystalline state with temperature but near the solid crystalline-nematic liquid crystalline phase transition temperature there was a rapid increase past which the temperature dependence became far less appreciable including the nematic liquid crystalline-isotropic liquid phase transition temperature. Similar aggregate state dependence was observed for the $G(H_2)$, $G(CO+N_2)$ and G(-M) values during the radiolysis of p-methoxy-benzylidene p'--aminophenyl n-pentanoate (Fig. 2).

In the case of cholesteryl benzoate which can form cholesteric liquid crystalline state, the gaseous yields increased with temperature but aggregate state dependence was not observed. In the crystalline state the G(-M) values indicated a small temperature dependence but near the crystalline-cholesteric liquid crystalline phase transition temperature it increased abruptly past which the change in the G(-M) became again slight (Fig. 3).

As the main aim of this investigation was to study the phase dependence of radiation stability and since the chemical characters of the investigated compounds were quite different, we did not intend to study the mechanism of product formation in detail.

The observed G(-M) values were found considerably higher than the sum of the other observed yields. On account of this we characterized the radiolytic stability by comparing the (G-M) values of different phase states. Any product, the yield of which contributes to G(-M), has a molecular weight higher than that of the parent molecule. Consequently they form by some bimolecular processes the rates of which are apparently rather inhibited in solid state. These processes are probably different reactions of heavy radical intermediates formed through some homolytic or heterolytic scission of bond of the parent molecule.

The variation of G(-M) with temperature shows that the radiation stability of each investigated compound does not change if the phase changes from nematic or cholesteric to isotropic liquid state. This means that in spite of intermolecular forces bringing about orientational order in the nematic and cholesteric liquid crystalline state the directions and rates of reactions which give radiolytic products do not change appreciably in comparison with the isotropic liquid phase.

In the cases shown in the figures some of gaseous product yields increased with increasing temperatures but the phase state conditions had no effect on them. These products are probably formed either by unimolecular dissociation reactions or by reactions of relatively light intermediaries which diffuse considerably rapidly even in solids. The increase of these yields with increasing temperature can be attributed to the lower probability of both collisional deactivation and radical recombination which do not lead to product formation.

The temperature and phase dependence of the radiolytic yields of the compounds p-n-hexadecyloxybenzoic acid, p-n-pentyloxyphenyl acetophenone and p-n-heptyloxyphenyl acetophenone which give the smectic liquid crystalline phase are shown in Figs 4, 5 and 6, respectively. All these figures show that in the crystalline and smectic phase the $G(-M)$ values increase slightly with temperature and do not change at this phase transition temperature. However, there is a strong increase of $G(-M)$ near the temperature of the smectic liquid crystalline to isotropic liquid phase transition. These results indicate that the nature and the rates of processes responsible for the product yields do not differ appreciably between the solid and smectic phase. It means that in spite of the mobility of the smectic layers in any direction parallel to their own plane the bimolecular reactions of bulk reactive species are hindered by the lamellar structure of the smectic crystalline phase to about the same extent as in solids.

Radiolysis of ethyl p-ethoxybenzylidene p-aminocinnamate giving two types of smectic phases (with structured and unstructured layers) shows that its radiation stability in the unstructured smectic phase is between those in the crystalline and isotropic liquid phase (Fig. 7).

In the case of smectic liquid crystals the course of the temperature dependence of different gaseous product yields is quite different from that of the nematic and cholesteric liquid crystals. This difference can be attributed not only to the difference of chemical structure of these compounds but, probably, partly to the specificity of smectic phase. This is particularly apparent from the results of the radiolysis of p-n-hexadecyloxybenzoic acid and ethyl p-ethoxybenzylidene p-aminocinnamate where the temperature dependence of $G(H_2)$ shows a maximum in the smectic phase.

From the experimental results obtained for the seven different compounds the following conclusions seem to be very probable:

1.) The radiation stability of compounds in the "more fluid" nematic and cholesteric liquid crystalline phase is about the same as in isotropic liquid phase.

2.) The radiation stability of compounds in the "rather rigid" smectic phase is nearly the same as that in the crystalline phase. The temperature dependence of gaseous product yields has an unusual course in the smectic crystalline phase.

Acknowledgement. Thanks are due to Dr. R. Schiller for the stimulation of the investigation presented.

References

/1/ Ausloos, P., Fundamental Processes in Radiation Chemistry, Interscience Publishers, New York, 1968.

/2/ Gray, G.W., Liquid Crystals and Plastic Crystals, Vol. 1, J. Wiley, New York, 1974.

/3/ Dewar, M.J., Goldberg, R.S., J. Org. Chem., 35, 2711 (1970).

/4/ Gray, G.W., J. Chem. Soc. 3733 (1956).

/5/ Ritvay-Emandity, K., KFKI Report 74-89 (1974).

/6/ Johnson, J.F., Porter, R.S., Liquid Crystals and Ordered Fluids, Pergamon Press, New York, London, 1970. p. 480.

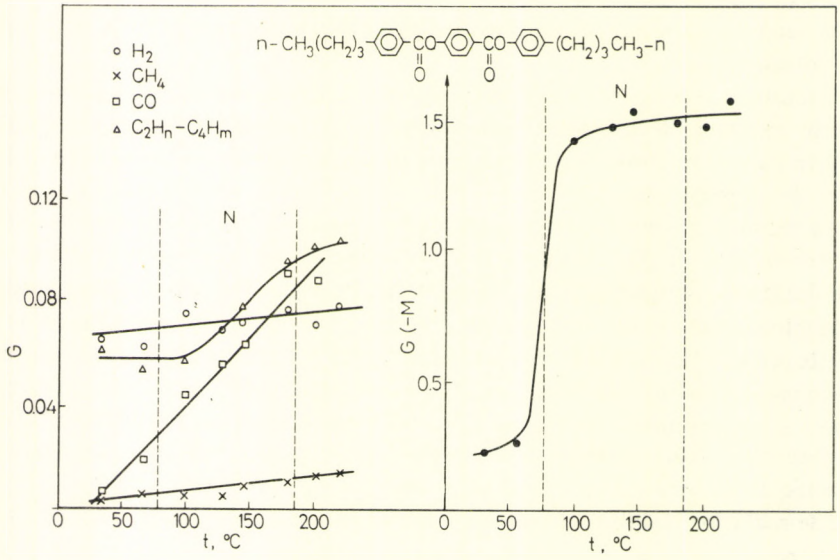

Fig. 1. Dependence of yields on the irradiation temperature of p'-n-butylphenyl--p-n-butylbenzoyloxy benzoate

Fig. 2. Dependence of yields on the irradiation temperature of p-methoxybenzylidene--p'-aminophenyl-n-pentanoate

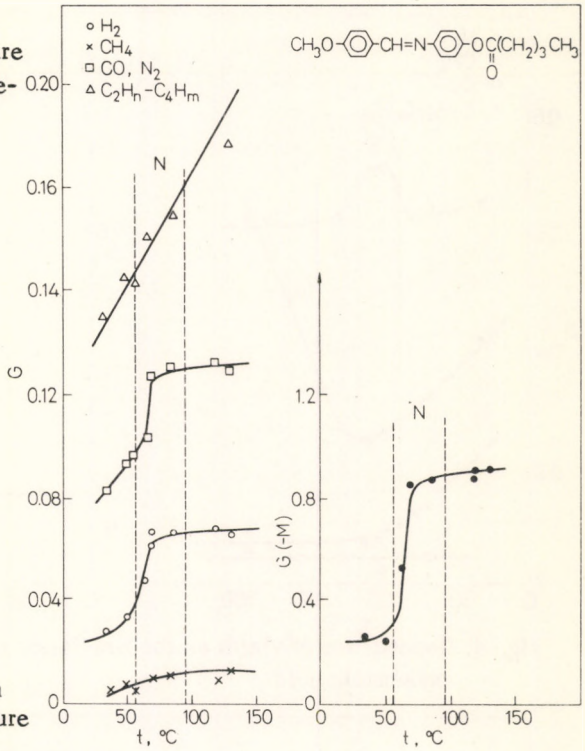

Fig. 3. Dependence of yields on the irradiation temperature of cholesteryl benzoate

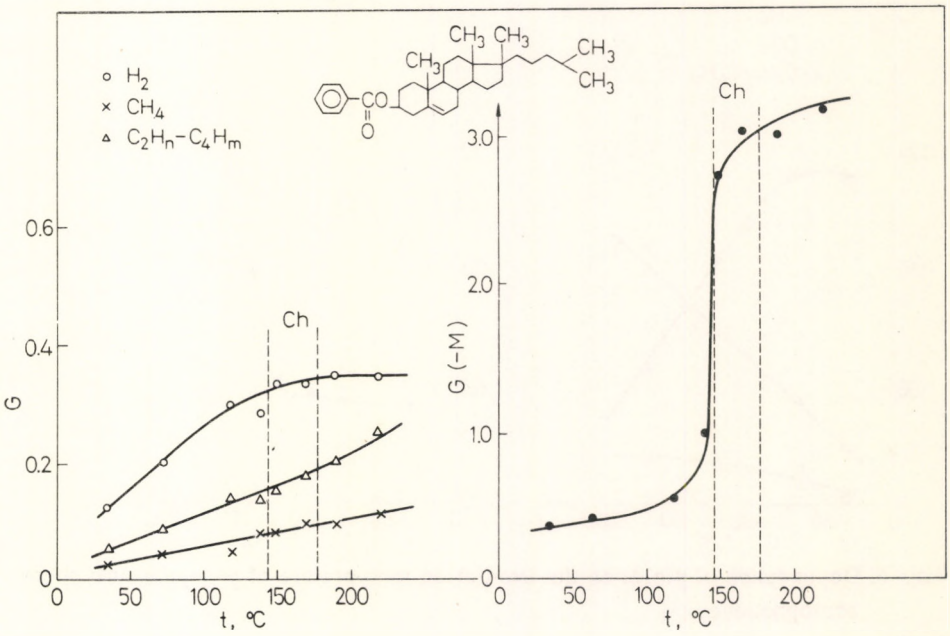

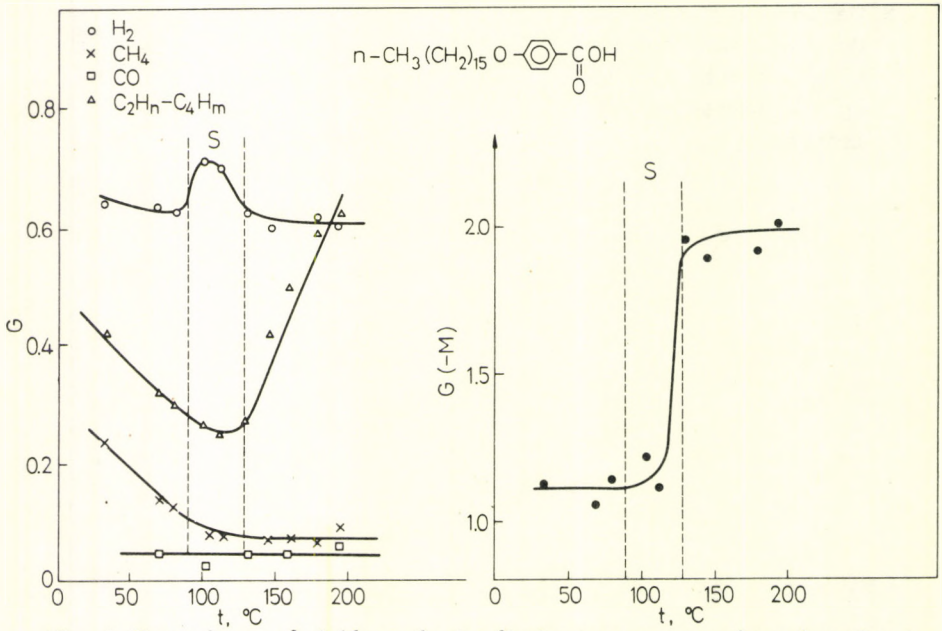

Fig. 4. Dependence of yields on the irradiation temperature of p-n-hexadecyl oxybenzoic acid

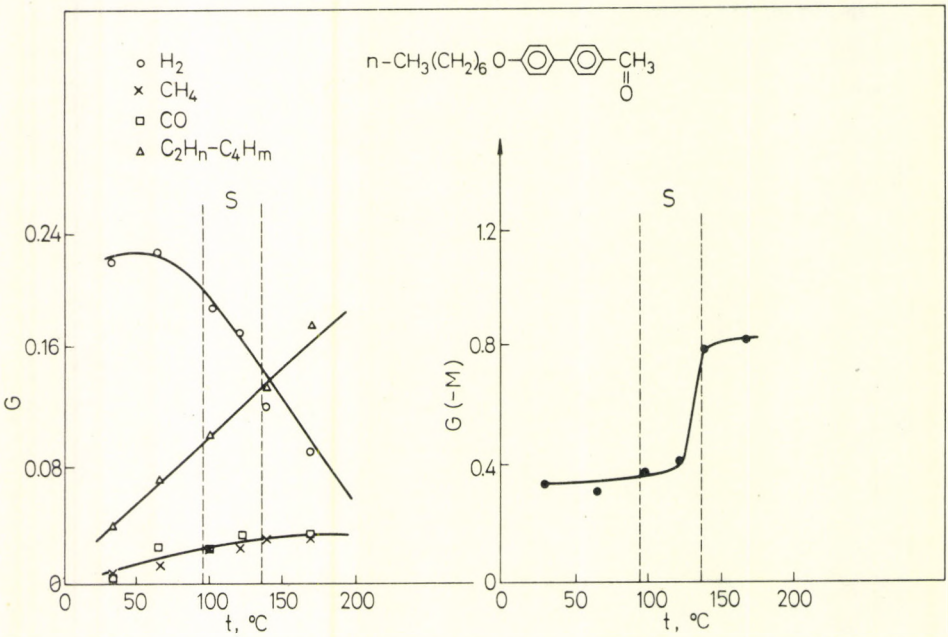

Fig. 5. Dependence of yields on the irradiation temperature of p-n-pentyloxyphenyl acetophenone

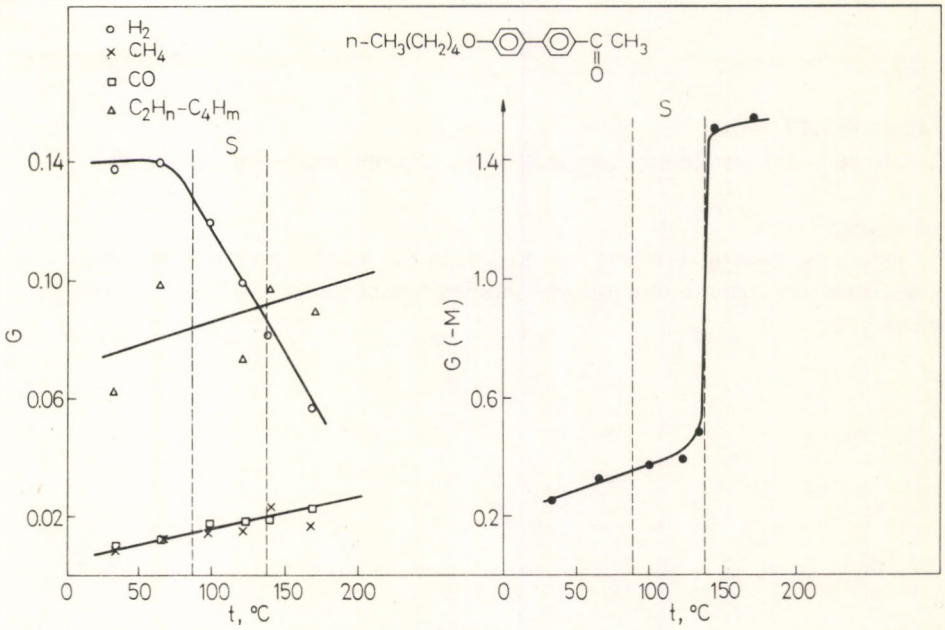

Fig. 6. Dependence of yields on the irradiation temperature of p-n-heptyloxyphenyl acetophenone

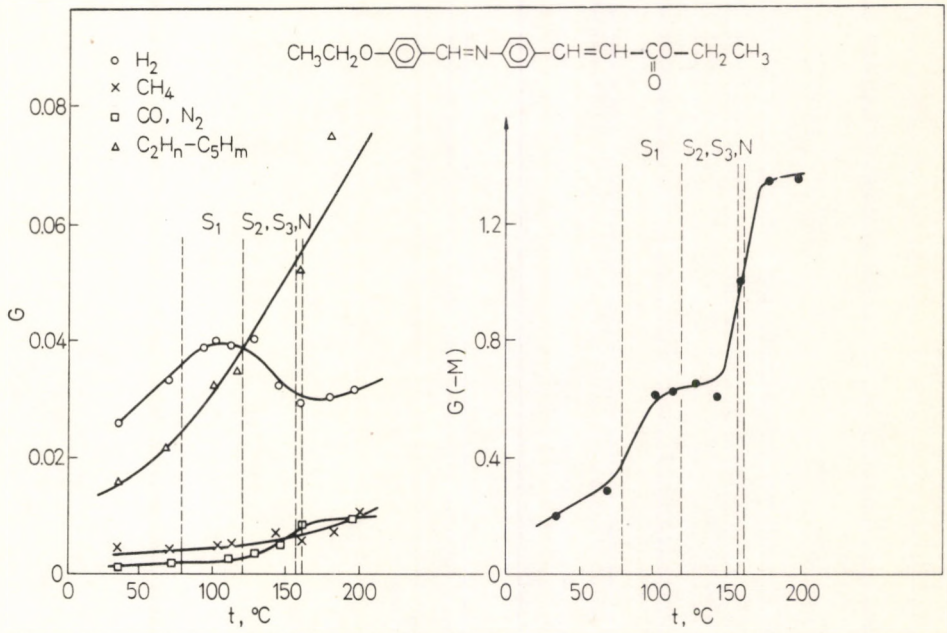

Fig. 7. Dependence of yields on the irradiation temperature of ethyl p-ethoxybenzylidene-p'-aminocinnamate

Yu. A. BERLIN

Have you investigated changes in physical properties of liquid crystals?

M. RODER

We have investigated only the changes in the melting point temperatures. Irradiation was found to diminish the temperature ranges of the liquid crystalline states.

ROLE OF N-ETHYLMALEIMIDE IN THERMORESTORATION OF RADIATION DAMAGE TO HYDRATED BACTERIAL SPORES

N. Grecz, G. Suchanek, T. Miura
Microbial Biophysics Laboratory, Biology Department,
Illinois Institute of Technology, Chicago,
Illinois, USA

The characteristic survival pattern associated with thermorestoration demonstrated in spores of the highly radioresistant organism Clostridium botulinum 33A suspended in oxic or anoxic water is shown in Fig. 1, where temperature during radiation was controlled at $0^{o}C$, to $100^{o}C$, and the time to deliver 0.8 Mrad was 50 min. The fact that 0.8 Mrad became progressively less efficient in killing spores between $0^{o}C$, and $75-85^{o}C$ is attributed to thermorestoration, or annealment of lethal radicals.

Thermorestoration in water is reminiscent of thermorestoration in vacuum or dry gaseous environments described elsewhere /10/. However, in vacuum the radicals being annealed are part of the spore itself, whereas in fully hydrated systems the important radical annealment appears to occur primarily in the water /5, 6, 8/. In N_2 under anaerobic conditions (Fig. 2), cell inactivation is thought to be due to the hydroxyl radical /2, 7/, while hydrated electrons and the hydrogen radicals seem to play no significant role. However H_2O_2 may be important since it has recently been shown that cell death from oxidizing species such as H_2O_2 /1/ and ozone /9/ can be correlated with DNA strand breaks in the case of radiation damage, DNA repair is invoked by the cell in response to the action of these agents. In the presence of oxigen, the hydrated electron as well as the hydrogen radical are converted into bactericidal species of relatively long half-life, the peroxyl and the perhydroxyl radical. The two important radiobiological effects of O_2 are that (i) radicals produced in its presence are not annealable /8/ and (ii) biological lesions produced in its presence, particularly DNA single strand breaks (SSB) cannot be repaired by direct rejoining of the SSB. This repair occurs in bacterial spores prior to germination, i.e. during or immediately after irradiation /3/, and is significantly related to the inherent radiation resistance of the various strains of sporeformers /4/. Since N-ethylmaleimide (NEM) has been described to have a radiobiological effect largely similar to that of O_2 it was of interest to investigate NEM in relation to the thermorestoration survival pattern of bacterial spores.

Results

a. Anoxic Conditions. In Fig. 3 the dotted lines represent those samples irradiated to 0.8 Mrad without NEM, i.e. under N_2 or O_2 alone. The solid line shows the

results for spores irradiated in the presence of 1 mM NEM. Under anoxic conditions NEM caused radiation sensitization as evident from the decrease in viable counts between approximately 10°C and 70–80°C, although sensitization was not as strong as that produced by O_2. The effect of NEM became thermoannealable at higher temperatures, since sensitization by NEM gradually diminished and became essentially nil above 80°C.

Controls indicated no difference in recovery of viability in samples which were not irradiated but subjected to heat for the same time as irradiated samples without NEM (dashed upper line) or with NEM (triangles). The increase in viable counts of samples receiving no radiation at approx. 60°C is due to spore activation. The fact that 1 mM NEM did not affect viable counts of unirradiated samples or irradiated samples at 80–95°C clearly suggests that NEM in this experiment was not toxic to spores and also that NEM had no detectable effect on spore heat resistance.

b. Oxic Conditions. Under oxic conditions the situation was just the reverse of that of anoxic samples (Fig. 4). Here 1 mM NEM offered radioprotection and the protection became gradually more pronounced as the temperature increased from 30 to 90–95°C, i. e. the NEM effect was subject to thermorestoration.

Discussion

At ambient temperatures, NEM scavenges electrons within its resonant molecule and thus sensitizes biological cells to radiation under anoxic conditions. Under oxic conditions, NEM has no detectable effect presumably because it competes with O_2 for electrons /7/. Our results are in agreement with the general idea that NEM and O_2 have a similar type of action. However, in addition, substantial differences have been observed between the action of NEM and that of O_2. These differences may be summarized as follows:

(i) the reaction product with NEM was distinctly thermoannealable, whereas the reaction product with O_2 could not be annealed at any temperature tested in this study,

(ii) NEM sensitized most efficiently at 20–40°C (in N_2), whereas O_2 sensitized at all temperatures with about the same efficiency,

(iii) the sensitizing effect of NEM was consistently small in contrast to the very large sensitization by O_2.

Supported by US – Hungary Int. Cooperation Program FHR 03/147, and US ARO-Grant No. DAHCO 4-75-G-0112.

References

/ 1/ Ananthaswamy, H. N., Eisenstark, A. and Johston, M., Am. Soc. Microbiol. Ann. Meet. (Abstr.) H63, p. 106. (1976).

/ 2/ Block, J., Lutjens, L. H. and RQSS, A. L. M. Radiat. Res. 30, 468, (1967).

/ 3/ Durban, E., Grecz, N. and Farkas, J., J. Bacteriol. 118, 129 (1974).

/ 4/ Farkas, J., Kang, T. W. and Grecz, N. Paper at British Spore Group Meet., Leeds, Dec. 16–18, 1975. (In press).

/ 5/ Friedman, Y. S. and Grecz, N., Acta Alim. 2, 209 (1973).

/ 6/ Friedman, Y. S. and Grecz, N., Acta Alim. 3, 251 (1974).

/ 7/ Johansen, I. and Howard-Flanders, P., Radiat. Res. 24, 184 (1965).

/ 8/ Suchanek, G., Miura, T. and Grecz, N., Radiat. Res. 40, 222 (1969).

/ 9/ Poliquin, L., Hamelin, C. and Chung, Y. S., Am. Soc. Microbiol. Ann. Meet. (Abstr.) H60, p. 106. (1976).

/10/ Powers, E. L. and Tallentire, A. In: Actions Chimiques et Biologiques des Radiations. Masson et Cie, Paris, (1968) pp. 3–67.

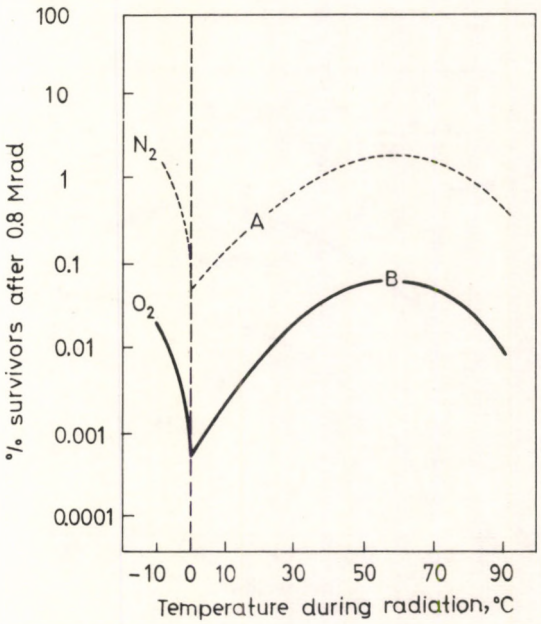

Fig. 1 Typical thermorestoration curves. Curve A is obtained when spores are irradiated in N_2-saturated water where the $\cdot OH$ radicals are the predominant lethal species and they are thermally annealed at elevated temperatures. Curve B is obtained when spores are irradiated in O_2-saturated water where $\cdot OH$, $\cdot O_2^-$ and $\cdot O_2H$ radicals are the predominant lethal species, and $\cdot OH$ radicals are thermally annealed, while the $\cdot O_2H$ are not annealed

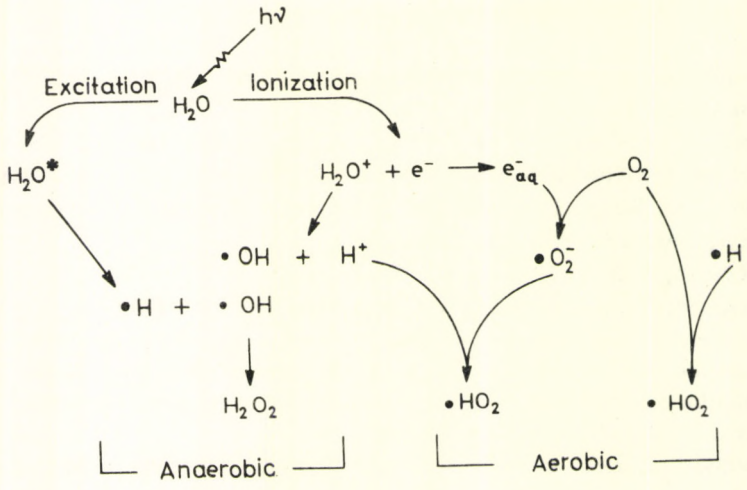

Fig. 2 Radiolysis products of water

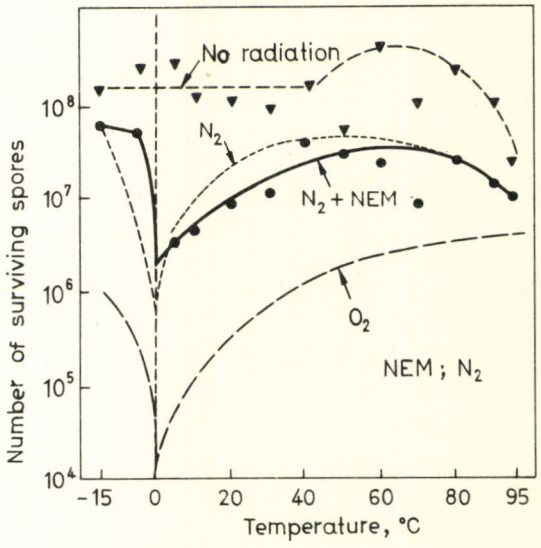

Fig. 3 Effect of 1 mM on thermorestoration pattern of spores of Clostridium botulinum 33A irradiated in distilled water saturated with N_2. Spore survival pattern in presence of NEM is compared with survival in distilled water containing no NEM and saturated with N_2, or alternatively saturated with O_2.

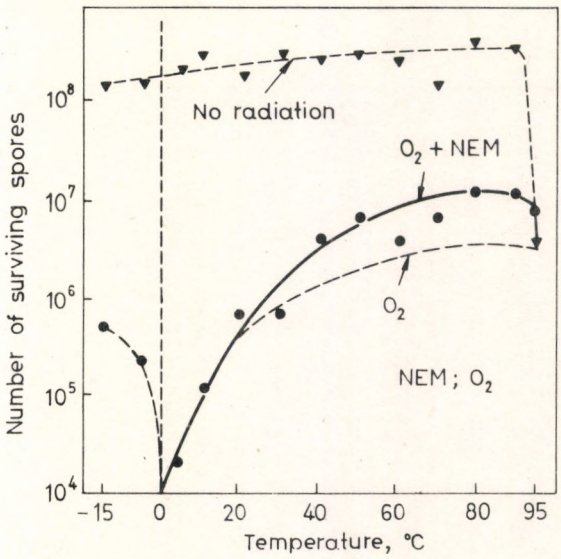

Fig. 4. Effect of 1 mM NEM on thermorestoration pattern of spores of Clostridium botulinum 33A irradiated in distilled water saturated with O_2.

STUDY OF TRACK STRUCTURE OF MULTICHARGED ION

E. A. Borisov, I. G. Kaplan, A. M. Miterev

The Branch of Karpov Institute of Physical Chemistry, Obninsk, USSR

Study of a charged particle track structure is of interest from many points of view /1, 2/. In radiation chemistry the so-called track effects make themselves evident in dependences of radiation chemical yield of radiolytic products on the LET of an ionizing particle. The well-known facts that in water radiolysis the yield of molecular hydrogen increases and the yield of stabilized electrons and free radicals decreases as LET increases are explained by diffusion-kinetic theory with non-uniform active particle distribution. LET-effects are particularly well known in radiobiology, in the dependence of RBE on LET /3, 4/.

Interpretations of the effects in liquid radiolysis by particles of various LET are based either on the occurrence of competitive reactions of excited particles or on the existence of thermal peaks at high LET; the thermal peaks accelerate decay into free radicals /5/ while at LET lower than 10 eV/Å radiation yield dependences on LET are fairly well accounted for by the conventional diffusion kinetics.

It is noteworthy that the nature of the dependence of radiation effects on LET generally changes if LET is higher than 20 eV/Å /3, 5, 6/. This presents a necessity to study the track structure of high LET particles in detail. Special attention should be paid to the physical stage of the radiolysis which consists of dissipation of ionizing particle energy together with the formation of primary active particles /7, 8/. Since LET values higher than 20 eV/Å are characteristic only of multicharged ions the present study is devoted to them.

In Ref. /9/ there has been proposed a qualitative model of a fission fragment track in water in the form of a cylindrical core of high ionization density surrounded by an extended sheath of low ionization density. The authors have taken as a core radius the value of 15 Å equalling the range of 100 eV electrons in water, the radius of the sheath was assumed to be equal to 60 Å.

Papers /10-18/ are devoted to calculations of spatial distribution of energy transferred to the medium by a heavy charged particle. In these papers special attention has been paid to the calculations of energy distribution absorbed from δ-electrons.

In the present paper our results on multiply charged ion track structure are reported. The spatial distribution of primary active particles, directly generated by a multiply charged ion as well as by electrons, has been obtained. The distribution of ionizations and excitations induced both by the δ-electrons and by the electrons of all subsequent generations has been determined analytically on the basis of the continuous loss model /19/ and numerically by Monte-Carlo method making use of a computer.

To find the spatial distribution of primary active particles formed by collisions of the ion with the molecules collisions were divided into knock-on and glancing ones. In the first region for inelastic scattering cross-section Rutherford's formula was used. In the case of glancing collisions a similar cross-section is expressed by Bethe's formula /20/.

In the validity-range of Rutherford's formula the value of the energy transferred is connected with a collision parameter p /21/.

$$\varepsilon = 2 Z_e^2 e^4 / mU^2 p^2 \qquad (1)$$

From this expression one can find the value of p_{max} beyond which in knock-on collisions no ionization of medium molecules by an ion occurs. For the effective charge of an ion the following expression holds /22/

$$Z_e = Z^{1/4} V/V_0, \qquad (2)$$

where Z and V are nuclear charge and ion velocity, respectively, and V_0 is the electron velocity on the first Bohr orbit. Then from Eq. (1) p_{max} is expressed as

$$p_{max}^2 = 2 Z^{1/2} \hbar/mI, \qquad (3)$$

where $\hbar$ is Planck's constant devided 2π , m denotes electron mass and I an ionization potential.

In particular for fission fragments with $Z \simeq 38$-54 estimations by formula (3) give $p_{max} \sim 3.5$ Å. p_{max} determines a cylindrical ionic core filled with ionized molecules and their fragments. The energy, released along the track of knock-on collisions is quite enough to ionize or dissociate all the molecules in a cylinder of 7 Å in diameter.

For the cases of glancing collisions Fano /21/ has obtained an expression for a differential cross-section which holds for allowed dipole transitions through an impact parameter. With the help of this expression it has been found /19/ that the density of particles $N_{on}(p)$ in the n-th quantum state, at a distance p measured from the

track axis, is well presented by the following relation

$$N_{on}(p) = 2\beta(f_{on}/E_{on})p^{-2}\exp[-\xi^2 p^2/2], \qquad (4)$$

where $\beta = \hbar^2 Z^{1/2} N/m$, $\xi = \kappa_0^{1/2} E_{on}(\hbar V)^{-1}$,

N is the number of molecules per unit volume, E_{on} is the transition energy, f_{on} the generalized oscillator strength and κ_0 presents a dielectric constant which takes into account the weakening of particle field due to medium polarization /23/.

From Eq. (4) it follows that $N_{on}(p)$ with the increase of a distance from the track axis decreases very sharply, the lower fragment the velocity – the sharper the density decrease.

Spatial distribution of ionizations and excitations induced by the δ-electrons has been obtained by us in Ref. /19/ on the basis of the continuous energy loss model. It was assumed that ion density might be determined from the density of energy losses which had to be divided by the average energy necessary for the formation of an ion pair (25-30 eV). A similar expression is valid also for excited particle density, hence the ratio of the number of excitations to the number of ionizations is close to one /24/.

For the density of δ-electron energy losses with energy spectrum $\sim \varepsilon^{-2}$ the following expression has been obtained /19/

$$q(r) = (\beta n/k^2 r^2)(k - r/r_{max}), \qquad (5)$$

where n is number of valency electrons, r_{max} is the electron range with the maximum energy $E_{max} = 2mV^2$, r is a distance from the track axis, k is an exponent in the range versus energy relation for slow electrons (see Ref. /25/).

$$R(\varepsilon) = \gamma \varepsilon^k$$

At $\kappa = 1$ expression (5) coincides with the results of study (cf. Ref. /11/).

For refinement of the results given by Eq. (5) as well as for calculating a detailed spatial distribution of primary active particles formed in δ-electron degradation, a numerical experiment by Monte-Carlo method making use of a computer was carried out. A given spatial part of the track in the form of a cylinder has been divided into five equal discs along the track axis and along the radius into a number of rings. Thus, spatial cells were obtained in which electrons were registered either in the case of their coming in from outside or their formation due to inelastic processes.

Having done the calculations with the help of the cross-sections of heavy particle-and-atom inelastic interaction obtained on the basis of the binary-encounter theory /26/ the spectrum of the electrons was divided into several energy groups. For each energy group the energy averaged over the spectrum and the weight of a

group in the total spectrum was determined. Then, one followed the slowing-down of electrons the energies of which were equal to mean energies of the electrons of corresponding groups in coordinate and energy spaces till their energy became lower than a certain value for which we took the potential of ionization. In a similar way the slowing-down of all the electrons, formed initially as δ-electrons were treated. Absorbed energies and all the acts of electron appeareance were introduced into the computer memory in the corresponding coordinate cells. This information was averaged over the number of cycles and was then printed.

As a following step the electron slowing-down due to elastic and inelastic collisions with molecules have been taken into account, energy losses in elastic collisions were neglected and only a change in the direction of electron motion was considered. In the case of an inelastic scattering both energy decrease of a bombarding electron and a change in the direction of its motion have been taken into account.

When an electron reached the energy of 50 eV its inspection in the coordinate space was stopped. In this case the probability of leaving the space cell for an electron with an energy less than 50 eV is was assumed to be equal to 0. Analogous treatment was used if a residual range $R(\varepsilon)$ became less than a minimum distance from a cell boundary.

A medium has been thought to be uniform and homogeneous and the assumption was made that all electrons of the medium molecules possess a bond energy which is equal to some average value.

The direction of δ-electron ejection relative to the direction of the multiply charged ion motion has been determined in Ref. /27/.

$$\cos\Theta_0 = (1+\lambda)/2\,\alpha(2+\lambda)^{1/2} \tag{6}$$

where $\alpha = v/v_2$, $\lambda = \varepsilon/I$, v is the ion velocity, v_2 some effective velocity of the medium molecule electrons determined from the relationship $mv_2^2 = 21$ and ε is the energy of the δ-electron.

A deviation angle of a bombarding electron from its initial direction after the i-th inelastic scattering has been determined in Ref. /20/.

$$\cos\Theta_i = (1-\Delta\varepsilon/E)^{1/2}, \tag{7}$$

where E is the energy of a bombarding electron and $\Delta\varepsilon$ the energy loss in a collision.

Electron elastic scattering by molecules of the medium has been calculated with an expression derived from electron scattering cross-sections on atoms in accordance with the additivity rule. For a scattering cross-section expressions have been used obtained with Thomas-Fermi potential in the form given in Ref. /20/

$$\sigma(\Theta) = (Z^2 e^4/4m^2 v^4)(\sin^2\Theta/2 + \alpha^2)^{-2}, \tag{8}$$

where $\alpha = 0,565\, Z^{1/3} S(2\pi e^4/hv)$, S = 0.66, Z is the atomic number, m, v, e, are mass, velocity and electron charge respectively. Azimuthal scattering angles were determined by generation of pseudorandom number /30/.

For a total cross-section of electron inelastic scattering on medium molecules a modified Stabler /28/ formula from Ref. /29/ was used

$$d\sigma/d\Delta\varepsilon = \pi e^4 (1+4I/3\Delta\varepsilon)/(E+2I)\Delta\varepsilon^2. \qquad (9)$$

In Table 1 there are presented calculation results obtained with a computer averaged over 1200 cycles for a track area with ion velocity 9×10^8 cm/sec. The data obtained are normalized for a single δ-electron.

From results of the calculation it may be seen that a relative weight of electrons with energy in the mean part of the degradation spectrum increases as the distance from the track axis also increases. Mean energy, necessary for an ion pair production at distances from the track axis $r > 10$ Å, is approximately equal to 38 eV. It has also been found that the ratio of the number of excitations to the number of ionizations is about 2. A higher number of excitations compared with that of ionizations is accounted for, on the one hand, by the fact that both in the initial energy spectrum and degradation spectrum the greatest number of the electrons have energy lower than I and, on the other hand, by the fact that discreteness of excitation levels has not been taken into account in the cross-section (9).

Figure 1 shows a comparison between spatial distribution of δ-electron energy losses obtained by two methods, i.e. according to the results of a numerical computer experiment (curve 1) and those calculated by formula (5) (curve 2) with K = 1. An agreement between the results obtained by different methods is quite satisfactory in the track region next to the axis ($r < 90$ Å). Only at those distances, measured from the track axis, which are close to the maximum track radius is the density of energy losses calculated according to Eq. (5) several times higher than that obtained by Monte-Carlo method. If one takes into account the fact that energy spectrum is proportional to ε^{-2} (by the help of which expression (5) has been derived) processes having higher total energy ($\sim$53,5 eV per an electron) than that of the initial spectrum given in the table ($\sim$30.6 eV) and also that value of k may be greater than unity – if one takes this into account, the best agreement between the calculated results obtained by these two methods may be achieved. One may come to the conclusion that the continuous model gives rather good results in a broad area of the track. Thus, in accordance with the obtained results the track of a multicharged ion, in particular of a fission fragment, can be presented in the form of a cylindrical ionic core with the diameter of about 7 Å surrounded by a cone-shaped excitation and ionization region (narrowing toward the end of the track) produced both by the direct action of an ion and by the δ-electrons. The density of ionizations and excitations directly produced by an ion beyond the ion core decreases sharply with the increase of the distance from the track axis, the lower the energy of multicharged ion, the sharper

Table

The results of a computer experiment

Interval over r, Å	Absorbed energy density, 10^{17}cm^{-3}	Ionic density, 10^{17}cm^{-3}	Mean energy per one ion pair formation, eV	Normalized electron		
				0-12.9	12.9-20	20-40
200-250	3.055	0.085	36.94	184.6	89.4	39.7
150-200	19.855	0.53	37.46	189.6	78.4	44.8
100-150	103.3	2.74	37.7	181	79.6	45.3
80-100	321.4	8.48	37.9	182.7	83.3	48
60-80	724.9	19.3	37.6	181.2	81.6	48
40-60	1.8×10^{3}	47.1	37.9	182	81.6	49.7
20-40	5.9×10^{3}	154.3	38.1	177	83.5	50.0
10-20	2.4×10^{4}	637.2	38.3	178	93	57
0-10	7.4×10^{5}	1.36×10^{4}	54.2(48*)	335	159.5	80.7
Initial spectrum				468.4	147	64

*without taking into account the energy of the δ-electron with $\varepsilon < I$

is the decrease of density. Concentration of ions and excited particles produced by the δ-electrons changes with the distance from the track axis roughly $r^{-2}(1-r/r_{max})$. The maximum radius of the track r_{max} decreases as ion energy decreases assymptotically to a curve "range-energy" for slow electrons.

As the multicharged ion slows down, its LET decreases. Meanwhile concentration of primary active particles at equal distances from the track-axis (at $r < r_{max}$) does not change practically along the track. This result is connected with the electron capture by a heavy charged ion due to its effective charge which changes proportionally to its velocity. As a result of this the dependence of inelastic scattering cross-section per ion energy is reduced. However, maximum energy of knocked-out electrons depends on the ion energy, therefore the maximum energy decreases with the decrease of ion energy, and this leads to the narrowing of the region of the δ-electron energy dissipation.

One obtains the result that the smaller the energy losses of the multicharged ion are, a the smaller is the area in which they scatter, and energy loss density (and consequently, the concentration of primary active particles) remain approximately constant at the given distance from the track axis (at $r < r_{max}$). A rapid decrease of energy loss density with increase of a distance from the track axis of the multicharged ion and a weak density dependence along the track (at $r < r_{max}$) results in dissipating of a part of ion energy beyond the limits of some effective radius in the same manner as in the case of low LET irradation. In the high density area along the track there is no actual dependence on LET.

1.
by Monte-Carlo method

density, $10^4 \rho(\varepsilon)$ eV^{-1}						
40-60	60-80	80-100	100-300	300-500	500-680	680-1.15 keV
23.8	15.9	15.9	8.7	7.9	8.64	0
26.6	18.1	15.7	9.6	7.6	6.6	0.27
29.2	21.4	16.6	10.8	7.9	4.3	0.48
28.7	21	16	10.9	8.2	3.7	0.47
29	22.3	18	11.7	7.9	2.8	0.46
31	23	18.3	12.7	7	2,5	0.44
32	24.8	20	13.8	5.9	2.3	0.42
38	30.6	26.5	12.3	5	1.8	0.37
40	25	16.5	5.2	0.78	0.27	0.08
26	14	8.7	2.44	0.5	0.22	0.05

As an example consider the influence of the track structure on methanol radiolysis brought about by fission fragments. From the obtained distribution of primary active particles it follows that radiation chemical yield of radical recombination, first increases with decrease of fragment energy, then passes through the maximum and then decreases. Such behaviour is associated with the fact that the radical concentration averaged over the track radius increases towards the end of the track and LET decreases. This conclusion is confirmed by experimental data /6/. High concentration of fragment ions in the track core necessarily increases the gaseous product formation that is also confirmed by the data on the yield of H_2 and CO /5, 6/.

The obtained distribution of primary particles in the track is valid for the multicharged ions with $Z > 10$ at not very high velocities ($v < 3 \times 10^9$ cm/sec). In case of particles with small charge such as protons, α -particles, which at the major part of their way possess a constant ionic charge, the track structure will be different to some extent. First, as such a particle slows down its LET increases while the energy dissipation area will narrow in the same manner as in the track of the multicharged ion. Consequently, concentration of the primary active particles towards the track end of the particle with a small charge will increase. It leads to the fact that radiolytic product yield dependences on LET in action of protons and α-particles on a substance will differ from those obtained under the action of the multicharged ions. The second peculiarity of light ion tracks is that the density of the δ electrons will be significantly lower and therefore distribution of ionized and excited states induced by them will not be continuous along the best part of the multicharged ion track.

References

/1/ U. Fano, Ann. Rev. Nucl. Sci. 13. 1 (1963).

/2/ A. Mozumder, In "Advances in Radiation Chemistry" , Eds. by M. Burton and J. L. Magee, Vol. 1, 1969. pp. 1-103.

/3/ G. W. Barendsen, In "Proc. Symp. on Microdosimetry". H. G. Ebert ed., Brussels, 1968.

/4/ B. M. Isaev, Yu. I. Bregadze, "Neitrony v radiobiologicheskom experimente". "Nauka", 1967.

/5/ M. Matsui, M. Imamura, "Let effect in the radiolysis of some organic liquids", IPCR Cyclotron Progr. Rept., 5, 93, (1971).

/6/ L. A. Bulanov, E. V. Starodubtseva, E. A. Borisov, Khimiya vysokikh energii, 6, 476 (1972).

/7/ R. L. Platzman, In "Radiation Biology and Medicine", W. D. Claus ed., Addison-Wesley, New York, 1956, pp. 15-72.

/8/ A. Kupperman, Nucleonics, 19, 38 (1961).

/9/ A. Mozumder, A. Chatterjee and J. L. Magee, In "Radiation Chemistry I. Advances in Chemistry Series 81", Washington, 1968, pp. 27-48.

/10/ D. I. Vaisburd, Yu. V. Volkov, A. M. Kol'chuzhkin, in "Radiatsionnye naruscheniya v tverdykh telach i zhidkostyach" "FAN", Tashkent, 1967, pp. 83-88.

/11/ J. J. Butts and R. Katz, Radiation Research, 30, 855, (1967).

/12/ E. J. Kobetich and R. Katz, Phys. Rev., 170, 391, (1968).

/13/ J. W. Baum, S. L. Stone and A. V. Kueher, In "Proc. of the Symposium on Microdosimetry", H. G. Ebert ed., Brussels, 1968, pp. 269-294.

/14/ Kudryaschov, A. M. Marennyi, V. I. Popov, O. M. Mescheryakova, Kosmicheskaya biologiya i meditsyna, 4, 35 (1970).

/15/ R. Katz and E. J. Kobetich, In "Charged Particle Tracks in Solids and Liquids", Eds. G. E. Adams et al., Cambridge, 1970, pp. 109-119.

/16/ A. Chatterjee, H. D. Maccabee, C. A. Tobias, Radiation Research, 54, 479 (1973).

/17/ J. H. Miller and A. E. S. Green, Radiation Research, 57, 9 (1974).

/18/ J. Fain, M. Monnin, M. Montret, Radiation Research, 57, 379 (1974).

/19/ A. M. Miterev, I. G. Kaplan, E. A. Borisov, Khimiya vysokikh energii, 8, 537 (1974).

/20/ N. F. Mott and H. S. W. Massey, "The Theory of Atomic Collisions" 3rd Edit., Oxford, Clarendon, 1965.

/21/ U. Fano, In "Charged Particle Tracks in Solids and Liquids", Eds. G. E. Adams et. al., Cambridge, 1970, pp. 1-7.

/22/ A. M. Miterev, W.A. Borisov, Atomnaya energiya, 36, 320 (1974).

/23/ E. Fermi, Phys. Rev., 57, 485 (1940).

/24/ I. G. Kaplan, V. E. Skurat, Khimiya vysokikh energii, 6, 252 (1972).

/25/ A. Mozumder, J. L. Magee, Radiation Research, 28, 203 (1966).

/26/ L. Vriens, In "Case Studies in Atomic Callision Physics I". Eds. E. W. McDaniel, M. R. C. McDowell, Amsterdam-London, 1969, pp. 335-398.

/27/ M. Gryzinski, Phys. Rev., 138, A305 (1965).
/28/ R. C. Stabler, Phys. Rev., 133A, 1268 (1964).
/29/ L. A. Vainshtein, V. I. Ochkur, V. I. Rakhovskii, A. M. Stepanov, Zh. Eksp. Teor. Fiz. 61, 511 (1972).
/30/ A. F. Akkerman, Yu. M. Nikityschev, V. A. Botvin, "Reshenie metodom Monte-Carlo zadach perenosa bystrych elektronov v veschestve", Izd. "Nauka", Kazakh. SSR, Alma-Ata, 1972.

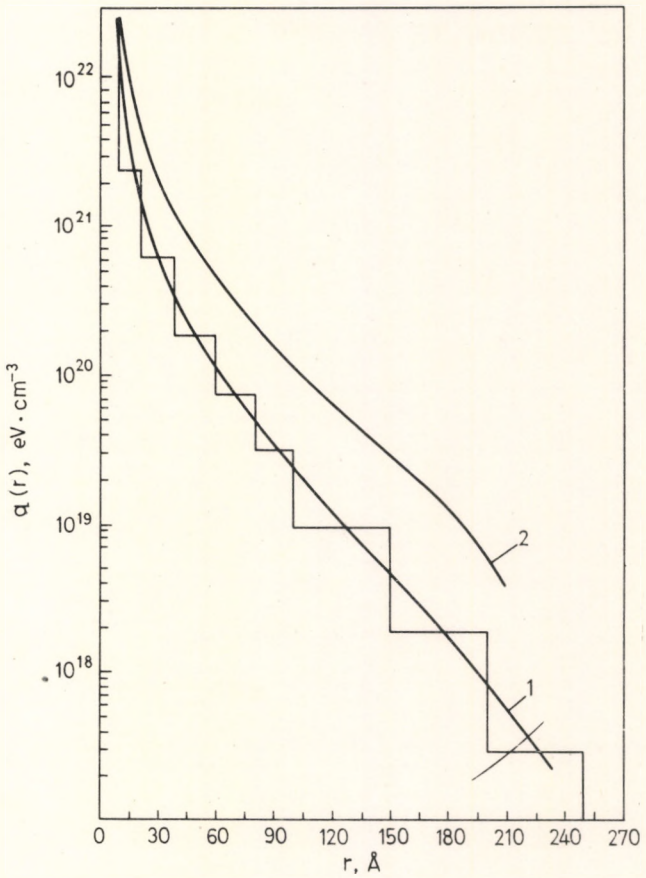

Fig. 1 Spatial distribution of δ-electron energy losses (see text)

INTERACTION OF HIGH-ENERGY ELECTROMAGNETIC RADIATION WITH MOLECULES

I. G. Kaplan, A. P. Markin
The Branch of Karpov Institute of Physical Chemistry,
Obninsk, USSR

In the process of irradiation of molecular mixtures by γ-quanta, one usually supposes that absorbed energy is distributed proportionally to the electron fraction of components. This assumption due to the fact that a large number of secondary electrons are produced per single γ-quantum (e. g. Co^{60} γ-quantum produces about 3×10^4 electrons), the energy of the secondary electrons is distributed nearly proportionally to the electron fraction of components. As a matter of fact electron fraction rule has been proved only for fast electrons ($E > 100$ eV), for slow electrons the situation is much more complicated /1, 2/. In the process of interaction γ-quantum undergoes numerous acts of inelastic scattering degrading to lower energies at which photoabsorption becomes a determining factor. Therefore, to study the processes of interaction of electromagnetic radiation with molecular systems is of interest.

First, consider the process of photoabsorption. Photoabsorption cross-section, when molecular electrons are described in terms of the molecular orbital approximation method (MO LCAO) and the knocked-out electron is regarded as a plane wawe. has the following form

$$\frac{dQ}{d\Omega} = \frac{\alpha}{\pi\omega} \sum_n q_n (\vec{e}, \vec{q}_n)^2 \left| \sum_{a\rho} C^n_{a\rho} \int \exp\left\{ i(\vec{k}-\vec{q}_n, \vec{R}_a + \vec{r}_a) \right\} \phi_{a\rho} d\vec{r}_a \right|^2 \quad (1)$$

where ω, $\vec{k}$, $\vec{e}$ denote frequency, wave vector and photon polarization vector, q_n is the photoelectron wave vector, α the fine structure constant, R_a the radius vector drawn from the origin of the coordinates to the nucleus of number a. The summation over n is carried out over all possible final states of the system. $C^n_{a\rho}$ coefficient at atom orbital $\phi_{a\rho}$ in molecular orbital n, ρ = 1s, 2s, 2p,... atom orbital type. Self-consistent values of $C^n_{a\rho}$ coefficients are taken from Ref. /3/. Formula (1) and all consequent expressions are given in atomic units (a. u.). Total cross-section of photo-ionization is obtained by averaging Eq. (1) over molecule orientations in space and integration over photoelectron ejection angles. The calculation has been made for an ethylene molecule since it contains electrons of three

types: valent π - and σ-electrons and inner K-electrons. The results of the calculation are given in Table 1.

As it may be seen from Table 1 photoionization cross-sections of σ-electrons $Q_5 - Q_7$ with increasing photon energy behave similarly to those of π-electrons Q_8 and their orders of magnitude are equal. Photoionization cross-sections of deeper lying σ-electrons Q_3 and Q_4 with the increase of photon energy decrease slower than $Q_5 - Q_8$ and at $E_{ph} \geq 500$ eV they exceed the latter ones almost by an order of magnitude. This difference in the cross-section behaviour is associated with the fact that the low lying molecular σ-orbital contains some addition of carbon-atom 1s-fractions. The addition of 1s-fuctions, insignificantly affecting the energy of the σ-state, considerably increases the possibility of photoionization from this state.

At E_{ph} exceeding the ionization threshold of K-electrons according to the data of Table 1, mainly K-electrons contribute to the cross-section which is in agreement with the calculations regarding photoeffect on atoms. Thus, at $E_{ph} = 1$ keV $\sum_{i=3}^{8} Q_i / \sum_{i=1}^{2} Q_i \approx 0.04$. Since the chemical bond only insignificantly affects the wave functions of the atomic 1s-electrons then at photon energies higher than the ionization potential of the K-electrons total cross-section of photoionization, taking into account all the molecular electrons, must be additive with respect to atomic cross-sections. For valency electrons the photoionization additivity must not take place.

To estimate the non-additivity of valency electron photoionization cross-section energy of incident quantum it is adequate to choose the simplest molecule, H_2. It presents antisymmetrized wave function of the final state $\Psi_{n,\vec{q}_n}$ in the form of the sum of products of Ψ_n ion wave function and the knocked-out electron wave function $V_{\vec{q}_n}$. Then taking into account the completeness of the set of ion wave functions the cross-section may by summed over all ionic states. For arbitrary two-electron systems

$$\frac{dQ}{d\Omega} = \frac{\alpha}{2\pi\omega} \sum_n q_n \left| \left\langle \Psi_{n,\vec{q}_n}(1,2) \right| \sum_{i=1}^{2} f_i \left| \Psi_o(1,2) \right\rangle \right|^2 = \qquad (2)$$

$$\approx \frac{\alpha}{\pi\omega} q \int \Psi_o^*(1,2)\,(f_1^+ + f_2^+)\,\Psi_{\vec{q}}(2)\Psi_{\vec{q}}^*(2')\,(f_1 + f_2)\Psi_o(1,2)\; d\tau_1\, d\tau_2\, d\tau_2$$

where the one-electron operator $f_i = -i\exp i(\vec{kr})\,(\vec{e}, \Delta)$, and $\Psi_o(1,2)$ is the wave function of the ground state of the set. When summing it has been assumed that the momentum of the knocked-out electron does not depend upon the state of the electron formed. The latter holds for a photon energy region being far from the threshold.

In calculation of H_2-molecular cross-cection the Weinbaum function has been taken as a wave function for the ground state [see Eq. (3) in Ref. /4/], the weight of ionic structure contribution being $\mu = 0.2644$. For equilibrium distance between nuclei $R_o = 1.431$ a. u. Slater effective charge is given as $\zeta = 1.1937$ /5/. At $\mu = 0$

Table 1

Photoionization cross-section from molecular levels of ethylene

E_{ph}(keV)	κ — electrons		σ — electrons					π — electrons
	Q_1 307.13	Q_2 307.11	Q_3 27.60	Q_4 21.29	Q_5 17.52	Q6 15.28	Q7 13.77	Q_8 10.09
0.3			0.(3)905	0.(3)714	0.(3)174	0.(3)277	0.(3)243	0.(3)245
0.4	0.(2)619	0.(2)555	0.(3)701	0.(3)454	0.(4)523	0.(4)556	0.(4)642	0.(4)781
0.5	0.(2)689	0.(2)712	0.(3)477	0.(3)283	0.(4)174	0.(4)241	0.(4)222	0.(4)318
0.6	0.(2)576	0.(2)643	0.(3)307	0.(3)217	0.(5)867	0.(4)156	0.(4)128	0.(4)147
0.7	0.(2)520	0.(2)455	0.(3)227	0.(3)159	0.(5)588	0.(5)884	0.(5)755	0.(5)759
0.8	0.(2)390	0.(2)372	0.(3)184	0.(3)113	0.(5)395	0.(5)519	0.(5)509	0.(5)430
0.9	0.(2)285	0.(2)313	0.(3)145	0.(4)852	0.(5)215	0.(5)310	0.(5)330	0.(5)262
1.0	0.(2)227	0.(2)242	0.(3)110	0.(4)687	0.(5)142	0.(5)188	0.(5)190	0.(5)167
2.0	0.(3)358	0.(3)360	0.(4)173	0.(4)114	0.(7)870	0.(6)184	0.(6)138	0.(7)805
3.0	0.(3)102	0.(3)105	0.(5)536	0.(5)341	0.(7)194	0.(7)482	0.(7)321	0.(7)135
4.0	0.(4)411	0.(4)417	0.(5)220	0.(5)141	0.(8)688	0.(7)186	0.(7)116	0.(8)378
5.0	0.(4)201	0.(4)200	0.(5)109	0.(6)693	0.(8)289	0.(8)865	0.(8)499	0.(8)141

Cross-sections Q_i are given in a.u (1a.u. = 0.27984×10^{-16} cm^2): the numbers under Q_i stand for potentials in eV: $0.(n)klm\ldots = 0.\underbrace{00\ldots0}_{n}klm$

Table 2

E_{ph}(keV)	$Q^{w}_{H_2}$	$Q^{HL}_{H_2}$	Q_H	$\frac{Q^{w}_{H_2}}{2Q_H}$	$\left(\frac{Q_{H_2}}{2Q_H}\right)_{exp.}$	$\left(Q^{w}_{H_2}\right)_0$	$\left(Q^{w}_{H_2}\right)_1$	$\frac{Q^{w}_{H_2} - \left(Q^{w}_{H_2}\right)_0}{Q^{w}_{H_2}}$
0.4	0.(4)458	0.(4)492	0.(4)135	1.70		0.(4)411	0.(5)217	0.103
0.6	0.(4)102	0.(4)112	0.(5)332	1.54		0.(5)918	0.(6)584	0.100
0.8	0.(5)346	0.(5)388	0.(5)122	1.42		0.(5)309	0.(6)237	0.107
1.0	0.(5)168	0.(5)186	0.(6)563	1.49		0.(5)152	0.(6)104	0.095
2.0	0.(6)148	0.(6)164	0.(7)503	1.47		0.(6)134	0.(8)932	0.095
4.0	0.(7)136	0.(7)150	0.(8)447	1.52		0.(7)125	0.(9)805	0.081
5.41	0.(8)486	0.(8)533	0.(8)155	1.57	1.44 ± 0.08	0.(8)448	0.(9)274	0.078
6.0	0.(8)334	0.(8)367	0.(8)108	1.55		0.(8)307	0.(9)195	0.081
8.0	0.(8)126	0.(8)137	0.(9)396	1.59		0.(8)116	0.(10)702	0.079
8.39	0.(8)106	0.(8)116	0.(9)335	1.58	1.45 ± 0.07	0.(9)975	0.(10)600	0.080
10.0	0.(9)578	0.(9)633	0.(9)181	1.60		0.(9)533	0.(10)326	0.078
15.0	0.(9)143	0.(9)156	0.(10) 44	1.63		0.(9)132	0.(11)803	0.077
20.0	0.(10) 53	0.(10)582	0.(10) 16	1.66		0.(10)491	0.(11)300	0.077

the Weinbaum function transforms into the Heitler-London function (HL). An electron knocked-out from a molecule has been described by a plane-wave normalized to unit volume.

The results of the calculations based on Eq. (2) averaged over molecular orientations and integrated over photoelectron ejection angles, for $\mu = 0.2644$ ($Q^{W}_{H_2}$) and $\mu = 0$ ($Q^{HL}_{H_2}$) are presented in Table 2. In the third column there are given the photoionization cross-sections of hydrogen atom calculated in the plane-wave approximation. [See Eq. (43) in Ref. /6/, this expression in the original reference is given with a misprint: the multiplier 1/3 has been omitted.] Photoionization cross-sections for H_2-molecule has earlier been calculated and estimation of non-additivity /6/ over the broad energy range from 100 eV up to 1 MeV has been carried out. The Heitler-London function has been taken as a ground state wave function. In this calculation only H_2-transitions into the ground and the first excited state have been taken into account. The sum of these partial photoionization cross-sections has been compared with the doubled hydrogen atom cross-section /6/. The value of non-additivity in photon energy range in question has appeared to be equal to 1.9—1.7.

Comparison between the results obtained earlier and those presented in this paper shows that in spite of the fact that in the present calculations the probability of H_2-ion formaton in all excited states has been taken into account, the additivity value is smaller than that in the previous calculation. This is due to the facts that:

1.) Heitler-London function used in Ref. /6/ for the ground state of H_2-molecule gives overestimated cross-section values in comparison with those obtained by a more precise Weinbaum function (see Table 2)

2.) in the calculation given a precise summation over all excited ionic states has been performed.

In calculation of the total cross-section taking into account ion transitions into different excited states we must use approximate wave functions since accurate ones do not exist.

The available experimental measurements /7/ have been performed only at two photon energies. The agreement between the calculation and experimental results can be considered to be good. Some overestimation of calculated values compared with those obtained experimentally is connected with the application of the plane-wave approximation.

In Table 2, partial photoionization cross-sections of H_2 with formation of H_2^+ in the ground $(Q^{W}_{H_2})_0$ and lower excited $(Q^{W}_{H_2})_i$ states are also presented. Wave functions of the ground and excited states of H_2^+ have been built up in the form of linear combinations of 1s slater orbitals. Each linear combination has had its own slater charge /8/ optimized for a distance between ionic nuclei $R_0 = 1.431$ a.u. In the last column of Table 2 a relative contribution into cross-section of the processes with H_2^+ formation in excited states has been evaluated. The H_2^+ ion in excited states is unstable to dissociation. It follows from the Table that the fraction of dissociative photoionization of H_2 is 8—10%.

Another process, competitive to photoabsorption, is Compton scattering. When considering γ-quantum scattering one assumes electrons to be free. It is due to the much higher energy of γ-quanta compared with that of electrons bound in molecules and solids. However, for electrons of inner shells such an approach when γ-quantum energy degrades becomes invalid. As a result of this δ-form Compton scattering line of free electron becomes broad /9/. Angular distribution of a scattered quantum given by classical Klein–Nishina formula /10/ changes. Particularly singnificant changes should be expected in the region of smaller angles. While the Klein–Nishina cross-section has a maximum at the scattering angle $\theta = 0$, the cross-section of Compton effect on a bound electron must decrease with a decreasing θ since the energy transferred to an atom at smaller scattering angles becomes insufficient for ionization.

Earlier experimental results of angular distribution of hard X-rays on light elements were analyzed in Heitler's monograph /10/. There a conclusion was made about full agreement between Klein–Nishina distribution and experimental data. In the region of smaller angles, however, no reliable measurements were presented at that time, this being associated with the difficulties of elastic component separation. Precise measurements of γ-quanta scattering with $\omega = 662$ keV have been made since 1960 /11–13/. They have shown that at small scattering angles experimantal cross-sections are sufficiently lower than those given by the Klein–Nishina formula, and at angles close to 180° they are even higher for heavy elements.

In Fig. 1 the results of calculation of scattering cross-section on K-electrons of some light elements /9/ are presented. For comparison the Klein–Nishina cross-section is presented as a continuous line. The greater is Z and the smaller are ω or θ the greater is the deviation from angular distribution given by the Klein–Nishina formula.

References

/ 1/ I.G. Kaplan. Dokl. Akad. Nauk SSSR 164, 842 (1965).
/ 2/ I.G. Kaplan, W.E. Skurat. Khimiya Wysokih Energii 6, 252 (1972).
/ 3/ W.E. Palke, W.N. Lipscomb. JACS 88, 2384 (1966).
/ 4/ I.G. Kaplan, A.P. Markin. Dokl. Akad. Nauk SSSR 184, 66 (1969) [Sov. Phys.-Doklady 14, 36 (1969)].
/ 5/ M.N. Adamov, W.P. Bulychev. Teor. i Eksp. Khimiya 2, 685 (1966).
/ 6/ I.G. Kaplan, A.P. Markin. Zh. Eksp. Teor. Fisik 64, 424 (1973)[Sov. Phys. – JETP 37, 216 (1973)].
/ 7/ B. Crasemann, P.E. Koblas, T.C. Wang, H.E. Birkeye, M.H. Chen. Phys. Rev. A9, 1143 (1974).
/ 8/ M.J. Feinberg, K. Ruedenberg, F.L. Mehler. Adv. Quant. Chem. 5, 28 (1970).
/ 9/ I.G. Kaplan, G.L. Yudin. Zh. Eksp. Teor. Fiz. 69, 9 (1975).
/10/ W. Heitler. The Quantum Theory of Radiation, Oxford, Clarendon Press, 1954.

/11/ Z. Suikowski, B. Nagel. Arkiv Fisik 20, 323 (1961).
/12/ J.W. Motz, G. Missoni. Phys. Rev. 124, 1458 (1961).
/13/ S. Shimuzu, Y. Nakayama, T. Makoyama. Phys. Rev. 140A, 806 (1965).

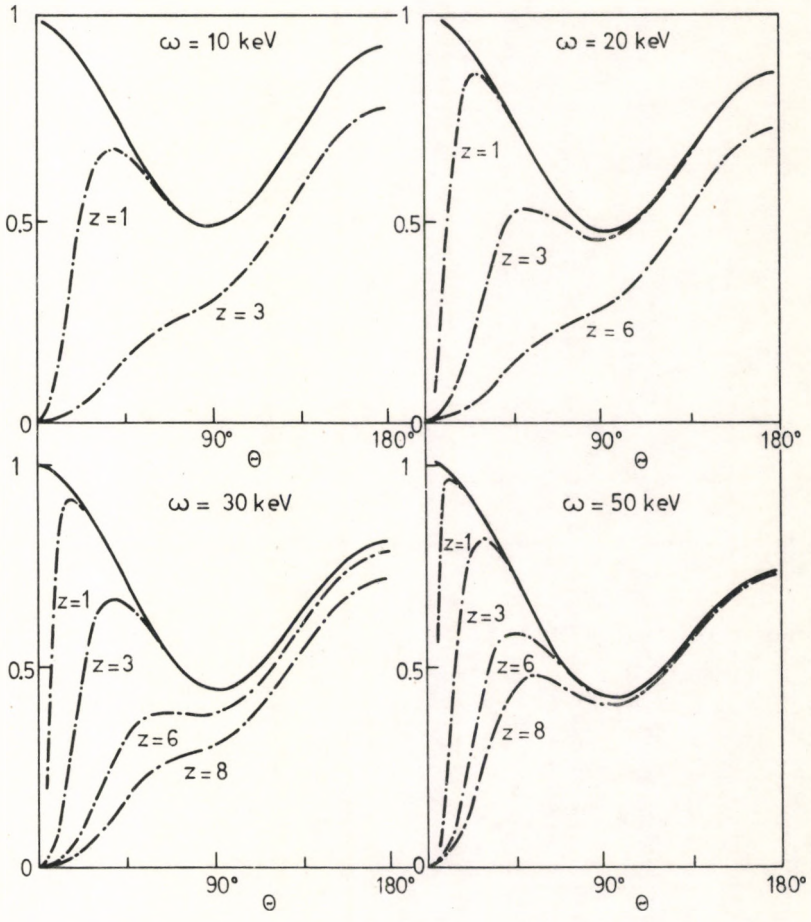

Fig. 1. Angular distribution at Compton effect on K-electrons. The continuous line corresponds to scattering on a free electron (Klein-Nishina cross-section)

STOCHASTIC TREATMENT OF DIFFUSION CONTROLLED REACTIONS IN THE CASE OF NON-HOMOGENEOUS CONCENTRATION OF THE REACTANTS

L. Botár, T. Vidóczy, I. Nemes
Central Research Institute for Chemistry of the Hungarian Academy of Sciences, Budapest, Hungary

1. Introduction

It has been recognized since long ago that one of the most important features of reaction mechanism in irradiated condensed systems is the non-uniform spatial distribution of radiolysis products. As a result, competition takes place between the chemical reactions and diffusion of these products.

This fact must be considered in any quantitative treatment aiming at the explanation of the dependence of the concentration of reaction products on time or on absorbed dose.

As most of the reactions of radiolysis products are diffusion controlled, a special branch of chemical kinetics has developed generally referred to as "diffusion kinetics" /1/. Though in principle they are closely related to what is known as "kinetics of diffusion limited reactions" /2/, the two fields were studied more or less independently.

By the middle of the last decade all the principal problems of inhomogeneous kinetics seemed to have been clarified, and obtaining a fair agreement with experimental data was thought to be merely a matter of a adequate physical model – and computing capacity. Thus the efforts of theoreticians were concentrated on studying the nature of primary physical events so as to provide a sound basis for the quantitative treatment of processes in the so called physico-chemical stage, therefore also for diffusion kinetics.

In the present paper we want to draw attention once again to chemical-kinetical methods which may be or have to be used in treating radiation chemical spur reactions.

From now on all the reactions will be supposed to be diffusion controlled, and only low LET radiations will be considered, characterized by the following properties:

1. overlapping of the spurs can be neglected /3/
2. about 90 % of spurs consists of no more than three pairs of primary products, and about 2/3 of radiolysis products are contained in this fraction /3/.

It will be seen that under such conditions a relatively simple stochastic treatment can be suggested, the kinetic behaviour of the system being considered as

a phenomenological consequence of elementary, spatially isolated random walk processes.

The random walk treatment must be preceded by a clearly stated spur model to prescribe initial conditions for the walking process.

2. Spur Simulation (Monte Carlo Method)

The low LET track is composed of a random sequence of more or less isolated "track entities": spurs, blobs and short tracks. Mozumder and Magee /1e/ investigated in detail the energy deposition in the course of track formation and the spatial distribution of these track entities by a Monte Carlo technique.

It is a direct logical continuation of the work of the above mentioned authors to use a Monte Carlo method in simulating a spur, i. e. the spatial distribution of "spur entities": radicals, ions and excited species formed during irradiation.

Let us consider a solution containing the solute molecules in a "strictly uniform" distribution. (The "strictly uniform" distribution is illustrated in Fig. 1a - it can be clearly seen that it is an extremely special realization of what is called uniform distribution in the theory of probability.)

The successive steps of spur simulation - in the case of two pairs of products - are illustrated in Figs 1b, f

i) the centre of spur is selected by random number generation with uniform probability (Fig. 1b)
ii) a direction is chosen at random – all the possible directions being a priori equally probable (Fig. 1c)
iii) a distance is selected by generating a random number with normal probability distribution $N(O: \sigma_1)$ (Fig. 1d)
iv) two further directions are chosen with uniform probability (Fig. 1e)
v) two distances are selected with normal probability distribution $N(O: \sigma_2)$ and divided into two sections with length ratio 1:2 (Fig. 1f). The "spur" generated in this way is shown in Fig. 2.

According to the method of diffusion kinetics the usual way to proceed consists of the steps:

a/ considering an extremely great number of such spurs,
b/ defining a "probabilistic concentration" function,
c/ setting up the material balance equation for this "concentration" (generally in differential form) the source term being assumed to be the reaction rate expression of "traditional" chemical kinetics (see Fig. 2).

Instead of following these steps, we have chosen a stochastic method – as has been indicated in the Introduction. In order to render the calculations simpler – i. e. to reduce the very heavy demans made on computing capacity – as a special case, a discrete solution model will be introduced in the next section.

3. The solution model

As a starting point, let us consider a solution model, idealized to the effect that solute and solvent molecules are supposed to be rigid bodies. (Such a model is presented, e. g., in the excellent textbook on chemical kinetics: /4/). A slightly modified version of this model is seen in Fig. 3a. As a further idealization, solvent molecules are supposed as being more symmetric, and to form an ordered set (see Fig. 3b). The last step of idealization results in a perfectly ordered and fixed set of solvent molecules, the motion of solute molecules being reduced to a sequence of rectilinear "steps" along the edges of a rectangular lattice from one lattice point to the other (see Fig. 3c).

4. Random walk on rectangular lattice (Monte Carlo Method)

The products of radiolysis, the spatial distribution of which have been generated by the Monte Carlo method, cannot be expected to fall into the lattice points of our idealized, "rectangular" solution model. It is quite natural to surmount this difficulty by displacing the radicals (or ions, or excited species) from their originally generated places to the nearest lattice points (see Fig. 4b, c). This done, we have arrived at the classical problem known as the "random walk in three dimensions". Though this problem has been thoroughly investigated in the theory of stochastic processes (treated in many textbooks), a general analytical treatment in the case of interacting walkers in three dimensions has not yet been presented. (The difficulties one has to face in this field can be realized by reading a paper dealing with random walk of two interacting walkers in one dimension /5/.

It seemed expedient therefore to proceed – instead of using analytical methods – by making use of the somewhat less general but in the given case more effective Monte Carlo method. The main features of this treatment are outlined in the following:

i) the strictly uniformly distributed scavenger molecules are
   a/ fixed and
   b/ "re-created" after reactions
ii) the ratio of walking probability of radicals (ions, excited species) equals their diffusion coefficients,
iii) the walk is symmetric, the probability of moving in any possible direction being equal to 1/6,
iv) each encounter of two radicals in a lattice point results in a chemical reaction, which will be referred to as
   a/ scavenging – if one of the reactants is a scavenger molecule
   b/ recombination – if solvent molecules are formed
   c/ combination – if identical radicals react,
v) radicals, leaving the "big cube" (see Fig. 4d) are supposed as being scavenged,
vi) the walking process comes to an end with all the products reacted.

The process of spur generation and random walk of the products performed sufficient times renders the statistical analysis of the results possible, a comparison being thus possible with experimental results.

5. Results

The computation was carried out for spurs consisting of one and two pairs of radicals with the following parameters:

1. One-pair spurs
   a/ initial distribution of radicals: N(0; 1) and N(0; 1.5) (the unit has been chosen equal to the length of edge of the unit cell in the rectangular lattice)
   b/ ratio of diffusion coefficients (D_A/D_B): 1/1 and 5/3
   c/ number of processes in one set: 2^{10}
   d/ number of sets submitted to statistical analysis: 2^4
2. Two-pair spurs
   a/ initial distribution of solvent decomposition: N(0; 1)
   b/ initial distribution of radicals: N(0; 1) and N(0; 5)
   c/ ratio of diffusion coefficients (D_A/D_B): 5/3 and 8/2
   d/ number of processes in one set: 2^6
   e/ number of sets submitted to statistical analysis: 2^3

The results of computations are shown in Figs 5a-c where $\bar{n}$ denotes the mean value of the numbers of combinations and recombinations in one set (in case of one-pair spur no combination is possible), d denotes the length of edge of the cell formed by scavenger molecules.

As 1/d is proportional to the 1/3 power of concentration, n plotted against 1/d makes possible a comparison between computed results and the so called "cube-root law" of irradiated aqueous systems.

It can be seen that by varying σ_2 and D_A/D_B, the run of the computed curves may vary in a wide range.

It must be emphasized that – like in the case of calculations in diffusion kinetics, performed in its initial periods /1. f/ – little effort was made to force numerical agreement with experimental data, the aim of the computations being to develop a feeling for the quantitative properties of the model.

6. Areas for future development

The main assumptions of our model were:

i) the scavenger molecules are a/ strictly uniformly distributed
b/ fixed
c/ re-created after reaction
ii) the walk takes place on a rectangular lattice
iii) the walking probability is supposed as being symmetric

None of these restrictive assumptions is an essential feature of the method – they were assumed only for making computation relatively simple. This means that with the above restrictions lifted, the flexibility of the model would make it possible to assimilate any further physical assumption, though it might even be the result of sophisticated considerations. On the other hand, the reality and applicability of theoretical considerations can be tested by stochastic (random walk) methods demanded by the theories. Calculations under less restrictive conditions are being made and will be published soon.

References

/1/ a Jaffe, G., Ann. Phys. Leipzig 42 303 (1913)
b Samuel, A. H., Magee, J. L., J. Chem. Phys. 21 1080 (1953)
c Ganguly, A. K., Magee, J. L., J. Chem. Phys. 25 129 (1956)
d Monchick, L., Magee, L. J., Samuel, A. H., J. Chem. Phys. 26 935 (1957)
e Mozumder, A., Magee, J. L., J. Chem. Phys. 45 3332 (1966)
f Kuppermann, A., in "Actions Chimiques et Biologiques des Radiations" vol. V 87 (1961)
g Schwarz, H. A., J. Phys. Chem. 73 1928 (1969)
/2/ a Smoluchowski, M., Ann. Physik 48 1103 (1915)
b Kirkwood, J. G., J. Chem. Phys. 14 180 (1946)
c Collins, F. C., Kimball, G. E., J. Colloid Sci. 4 425 (1949)
d Collins, F. C., Kimball, G. E., Ind. Eng. Chem. 41 2551 (1949)
e Noyes, R. M., in Progress in Reaction Kinetics vol. 1 129 (1961)
/3/ Mozumder, A., in Advances in Radiation Chemistry vol. 1. 1, (1969)
/4/ Weston, R. E., Schwarz, H. A., Chemical Kinetics, Prentice Hall (1972)
/5/ Schwarz, M., Poland, D., J. Chem. Phys. 63 557 (1975)

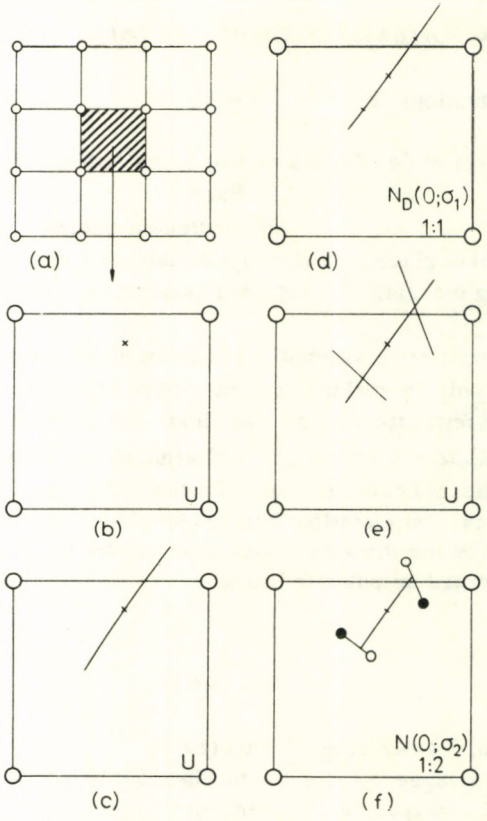

Fig. 1 Successive steps of the spur simulation

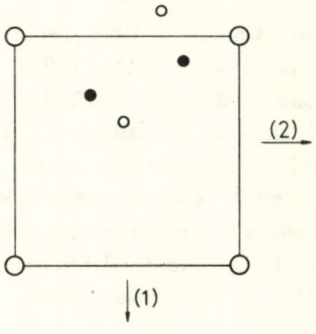

$$\frac{\partial c_R}{\partial t} = D\Delta C_R - (k_0 + \sum_i k_i c_i) c_{ij} + \sum_{ij} k_{ij} c_i c_j$$

Fig. 2 Two-pair spur generated by Monte Carlo technique ○:scavenger, ○,●:products of radiolysis, c_R:"concentration" of some of the products

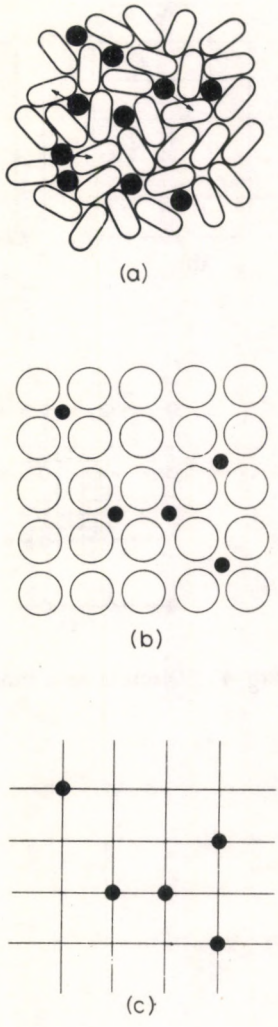

Fig. 3 Idealized solution model
a/ rigid body model (see Ref. /4/)
b/ as a/, with symmetric solvent molecules, forming an ordered set
c/ as b/, with the solvent molecules fixed

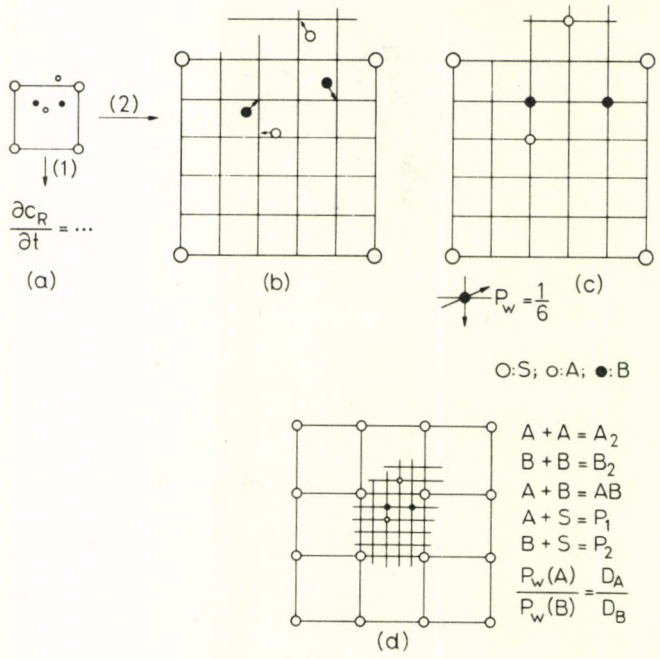

Fig. 4 Discrete spur model

Fig. 5 $\bar{n}$: average number of combinations and recombinations in one set (consisting of 2^{10} and 2^6 random walks)
d: length of edge of the cells formed by the strictly uniformly distributed scavenger molecules

a/ one-pair spur, a: N(0; 1), D_A:D_B=1:1 and 5:3
b: N(0; 1. 5), D_A:D_B=5:3

b/ two-pair spur, σ_2=1; o, ●:A_2; □, ■:B_2; ×, +:AB with D_A:D_B=5:3 and 8:2 respectively

c/ as b/ with σ_2=5

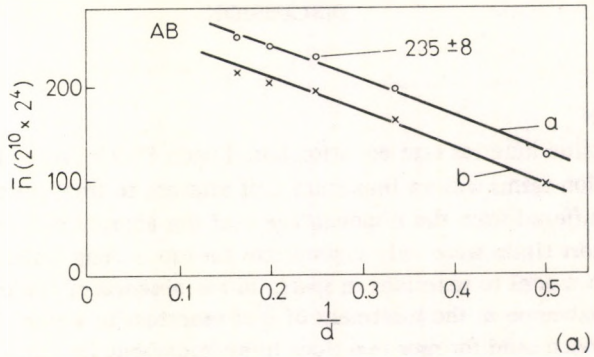
AB
235 ±8
a
b
$\bar{n}\,(2^{10}\times 2^4)$
200
100
0
0
0.1
0.2
0.3
0.4
0.5
$\frac{1}{d}$

(a)

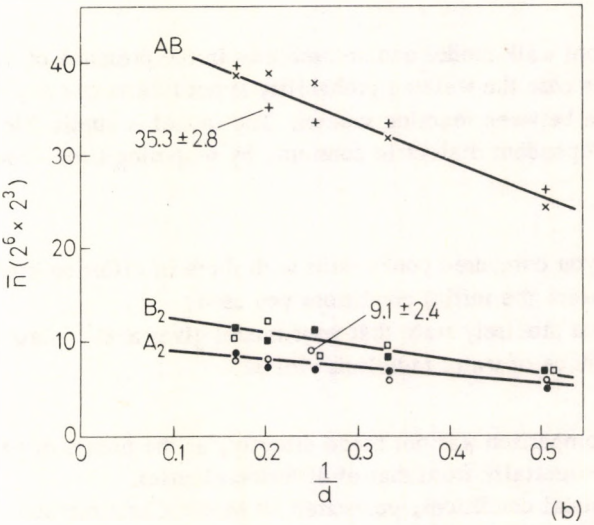
AB
35.3 ± 2.8
B_2
A_2
9.1 ± 2.4
$\bar{n}\,(2^6\times 2^3)$
40
30
20
10
0
0
0.1
0.2
0.3
0.4
0.5
$\frac{1}{d}$

(b)

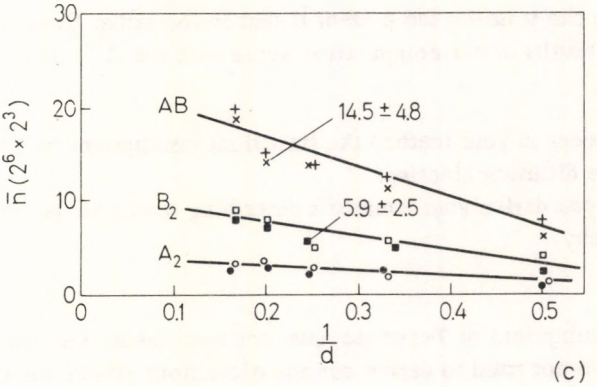
AB
14.5 ± 4.8
B_2
5.9 ± 2.5
A_2
$\bar{n}\,(2^6\times 2^3)$
30
20
10
0
0
0.1
0.2
0.3
0.4
0.5
$\frac{1}{d}$

(c)

Fig. 5

G. R. FREEMAN

The diffusion kinetics rate equation based upon Fick's law and homogeneous kinetics reaction terms was an important first attempt to treat reactions in spurs. However, it suffered from the disadvantage that the approximations used to describe the rates at short times were only appropriate for use at long times. The application of a stochastic model to reactions in spurs, in the absence of coulombic interactions, is a valuable advance in the treatment of spur reactions in water. The stochastic approach has been used for spur reactions in hydrocarbons for many years.

L. BOTÁR

The random walk model can be used also in the presence of coulombic interactions. In this case the walking probability is not symmetric any more and depends on the distance between reacting species. The model is applicable even in the case of time dependent dialectric constant, by supposing time dependent walking probabilities.

Yu. A. BERLIN

(1) Have you compared your results with those of diffusion kinetics?

(2) What were the initial conditions you used?

(3) Can you precisely state that your model gives a $C^{1/3}$ law for the concentration dependence of water radiolysis yields?

L. BOTÁR

(1) The comparison was not made directly, as the nature of parameters of our model differs essentially from that of diffusion kinetics.

(2) The initial conditions, generated by Monte Carlo method, are described in the text.

(3) All we can state for the present is that in the rather limited range of concentration the results of our computation agree with the $C^{1/3}$ law.

W. STILLER

Do you accept in your method the statistical assumptions made by Teramoto for deriving the diffusion kinetics?

(2) Could you derive your equations describing stochastic processes from the BBGKY-hierarchy?

L. BOTÁR

(1) The assumptions of Teramoto have not been taken into consideration.

(2) We have not tried to derive our equations from BBGKY chains and we hope that the treatment based on random walk conceptions – at least in the case of low LET spurs – will lead to the same results in a more direct way.

CORRELATION BETWEEN RADIATION-INDUCED CHEMICAL TRANSFORMATION OF SOME EPOXIDES AND THEIR STRUCTURE DETERMINED BY THE MOLECULAR ORBITAL METHOD

A. P. Meleshevich, E. G. Furman
The L. V. Pisarzhevsky Institute of Physical Chemistry, the Ukrainian Academy of Sciences, Kiev, USSR

At present an increased interest in radiation-induced transformations of heterocycles may be observed in relevant world publications. Epoxy compounds which are one of the most widely used classes of non-aromatic heterocycles possess a number of special properties due to the presence in the molecule of the strongly strained three-membered ring with oxygen and unusual valency of the atoms. It might be these particularities which influence the behaviour of epoxides under ionizing irradiation.

The methods of quantum chemistry now are being widely used for investigation of the structure of molecules and unstable intermediates. Epoxides have been poorly studied by quantum-chemical methods. There are some works /1–4/ employing EHT method /2, 3/ and referring to the epoxy cycle interaction with nucleophylic reagents. In the present work results of a quantum-chemical consideration of ethylene oxide /EO/, propylene oxide (PO), epichlorohydrin (ECH) as well as some products of their radiolysis are given. We supposed that evaluation of electron density distribution in epoxy molecules, bond strength characteristics, as well as the calculation of molecular ions and products of their decomposition would enable us to get some insight into the behaviour of these substances under ionizing irradiation.

Method

The calculations have been performed by the semiempirical method of the complete neglect of the differential overlap (CNDO/2) with the standard parametrization of Pople and Segal /5/. As a characteristic of the bond strength the values of the partitioned diatomic overlap suggested in Ref. /6/ were used. For calculations of the molecules their experimentally determined geometrical structures were given /7/. The molecular cation-radicals were calculated with the geometry of the parent molecules. Glycidic cation has been studied with invariable geometrical parameters of the three-membered ring, while the C–C bond length between the cycle and the substituent and the H–C–H angle of the latter were given to be 1.43 Å and 120°, respectively. The results on glycidic ion are presented for bisector conformation

where the H−C−H plane of the substituent is placed perpendicularly to the ring plane. The total energy of this conformation is 30.06 Kcal/mole, lower than that of the conformation in which the substituent plane is rotated by 90° from the bi-sector plane. This value is in good agreement with the figure reported in Ref. /8/. Conformations of other intermediates were given taking into account the reported data on valence angles and bond length variations in hydrogen carbon ions /9/. Geometry of $\dot{C}H_3$ and $\overset{+}{C}H_3$ particles has been optimized in dependence on C−H bond length at a given plane configuration and a valence angle of 120°. The full optimization of the geometry has been carried out for the $H\dot{C}O$ and $H\overset{+}{C}O$ species searching for a minimum of the total energy on all independent coordinates of the atoms by the variable metrics technique /10/. Geometrical parameters of the intermediates are listed in Table 1.

Results on experimental investigation of the radiolysis of epoxides are taken from the papers published elsewhere.

Table 1

The geometrical parameters of the studied intermediates

N	Species	Bond length, A°		Valence angle
1.	CH_3^+	C−H,	1.120	H−C−H, 120
2.	$\dot{C}H_3$	C−H,	1.105	H−C−H, 120
3.	HCO^+	C−H,	1.110	H−C−H, 180
		C−O,	1.177	
4.	$\dot{H}CO$ *	C−H,	1.111	H−C−O, 130°36′
		C−O,	1.219	
5.	CH_2^+	C−H,	1.140	H−C−H, 136
6.	$HC-CH^{+\cdot}$	C−H,	1.098	H−C−C, 180
		C−C,	1.282	
7.	$H_2CCO^{+\cdot}$	C−H,	1.070	H−C−C, 120
		C−C,	1.330	H−C−O, 180
		C−O,	1.150	
8.	$CH_4^{+\cdot}$	C−H,	1.140	H−C−H, 137°24′

* Full optimatization of the $H\dot{C}O$ radical within the framework of the CNDO/2 method is also reported in Ref. /11/

Results and Discussion

The molecular diagrams of the epoxides in Fig. 1 present the charge distribution and bond strength in the ground state of the molecules. For a long time the carbon-carbon bond was considered to be the weakest one in the epoxy cycle. However, the calculation confirms the suggestion put forward earlier /12/ about C−C bond being the strongest in the ring and C−O bonds being much weaker than the former one. A substituent attachment to the epoxy cycle causes the weakening of the bonds on its side.

Obtained data may be of use for interpretation of experimental results since they enable us to predict with a certain probability the bonds to be broken. Extensive experimental material on radiolysis of organic compounds reveals that splitting of the weakest bonds in a molecule predominates under radiation, in spite of an enormous energy of particles or quanta which is many orders of magnitude higher than that of any molecular bond. Such phenomena have their explanation in redistribution of the absorbed energy.

The ionization of molecules is one of the most important processes along with excitation when ionizing radiation interacts with a substance. We have obtained through the computation the electronic structures of the molecular epoxide ions the experimental study of which is extremely complicated. Redistribution of the charges on the atoms, spin density distribution, variation of the characteristic of the bond strength suggest the probable reactivity centres of the ionized molecules as well as bonds to be broken. Results of calculation of such cation-radicals as $EO^{+\cdot}$, $PO^{+\cdot}$, $ECH^{+\cdot}$ and glycidic cation are shown in Tables 2 and 3.

The variation of the partitioned diatomic overlap value is suggested in the CNDO/2 method as a tool for predicting the most probable place of a bond breakdown in an intermediate /6/. According to our calculations no significant decrease in the strength of any particular bond is observed in the ground state of EO molecular cation-radical. This is why it is rather difficult to predict the bond which breaks first in this species. In such a case an energetical balance of the primary products of the EO molecular ion decay through several possible pathways may be of use to shed light upon the most probable way of its degradation. A set of primary products, which arise as a result of the decay of an ionized molecule is reflected in the electron impact mass-spectrum of this substance. The order of peaks corresponds to fragment-ion abundances and thus the probabilities of their formation.

The mass-spectrometer of electron impact with electron energy of $70 \div 80$ eV is known to meet conditions of primary steps of radiolysis, though the following transformations are not quite identical expecially when dealing with condensed phase /13/.

In Table 4 the mass-spectra of electron impact of EO, PO and ECH are listed /14/. According to the set of the most intensive peaks in the mass-spectrum of EO a number of reactions of its molecular ion decay might be written. For the sake of convenience only the products of these reactions are presented in Table 5 together with their total energies ($E_{tot.}$) calculated by CNDO/2 method. The sums of the E_{tot} values are also listed in Table 5.

Table 2

Differences of the partitioned diatomic overlap values* between parent epoxide molecule and molecular cation

N	Cation	Bond						
		C_1-O	C_2-O	C_1-C_2	C_1-H	C_2-H	C_2-C_R	C − Cl
1.	$EO^{+\cdot}$	0.0118	0.0118	0.0062	0.0075			
2.	$PO^{+\cdot}$	0.0125	0.0158	0.0067	0.0065	0.0055	0.0079	
3.	$ECH^{+\cdot}$	0.0123	0.0163	0.0074	0.0068	0.0058	0.0095	0.0789
4.	Glycidic	-0.0185	0.0278	0.0591	0	-0.0021	-0.1741	

*Negative value of the difference corresponds to strengthening of the bond.

Table 3

Charges (q) and spin densities (p) in the molecular cations of the epoxides

N	Cation	Atoms									
		O		C_1		C_2		C(H)		Cl	
		q	p	q	p	q	p	q	p	q	p
1.	$EO^{+\cdot}$	0.2129	0.9132	0.1230	-0.0121			0.1353	0.0278		
2.	$PO^{+\cdot}$	0.1843	0.9125	0.0981	-0.0131	0.1784	-0.0063	-0.0454	0.0208		
3.	$ECH^{+\cdot}$	0.1825	0.9106	0.1001	-0.0127	0.1815	-0.0060	-0.0035	0.0208	0.0031	0.0016
4.	Glycidic	-0.0818		0.1981		0.1017		0.2660			

Table 4

Mass spectra of the electronic impact of EO, PO and ECH

N	Compound	Ion mass, a u.									
1.	EO	29	44	15	14	43	26	42	16	13	20
2.	PO	28	29	27	58	26	31	43	15	14	30
3.	ECH	57	27	29	49	31	62	28	42	26	15

Table 5

Characteristic of products of the EO molecular cation-radical decay by different pathways corresponding to tne mass spectrum of EO

Ion mass	Formula	Ion		Neutral species			Sum of E_{tot}, a. u.	Number of the reaction
		Number of bonds	E_{tot}(a. u.)	Formula	Number of bonds	E_{tot}(a. u.)		
29	HCO^+	2	-25.5135	$\dot{C}H_3$	3	-9.1173	-34.6308	(1)
44	Mol. ion	7	-35.2412	–	–	–	–	–
15	CH_3^+	3	- 8.6718	$H\dot{C}O$	2	-25.8886	-34.5604	(2)
14	CH_2^+	2	- 7.6313	CH_2O	3	-26.8313	-34.4626	(3)
43	$C_2H_3O^{+\cdot}$	6	–	H	0	–	–	(4)
26	$C_2H_2^{+\cdot}$	3	-19.0814	H_2O	2	-14.7396	-33.8209	(5)
42	$H_2CCO^{+\cdot}$	4	-33.3599	H_2	1	- 1.4746	-34.8345	(6)
16	$CH_4^{+\cdot}$	4	- 9.5002	CO	1	-25.0413	-34.5415	(7)

Since the CNDO/2 method is based on certain approximations, there are also restraints on energetical consideration of reactions in the course of which the number and the nature of bonds are changed if we compare the parent and final species. In our case it is correct to compare only such reactions the products of which have an equal sum of the number of bonds and equal ratio between the number of bonds in a pair of products (see Table 5). These are reactions (1–3), (5) and the second set of reactions (6) and (7). It should be kept in mind that in quantum-chemical treatment a multiplicity of a bond is not involved in calculation as a parameter, a bond being characterized only by its strength.

One can see from Table 5, that the energetically most favourable process is reaction (1), and others follow it in a sequence of an increase of the total energy sum of the pair of species arising in each reaction just according to the abundance of the ionic fragments in the mass-spectrum of EO. In the second group of reactions the sums of the total energies of products also give the correct sequence of the probability of the fragment-ion appearance. Decay of the molecular ion through less advantageous pathways should proceed evidently via its higher vibrational excited states.

The main gaseous products of EO radiolysis are hydrogen ($G = 0.6-0.8$), methane ($G = 0.5-0.6$), carbon monoxide ($G = 0.4-0.8$) and ethylene ($G = 0.4-0.5$)/15,16/. The conclusion may be drawn from the data on mass spectrometry and quantum chemical calculations that the major sources of methane in this case are $\dot{C}H_3$ radicals or $\overset{+}{C}H_3$ ions, while species $H\dot{C}O$ and $H\overset{+}{C}O$ serve as a source of carbon monoxide. Formation of hydrogen as one of the main products of radiolysis proceeds evidently by several pathways and also involve electronical excited states. Ethylene arises probably by reactions in which $\dot{C}\dot{H}_2$ or $\dot{C}\overset{+}{H}_2$ species take part but does not result from the two C–O bonds breakdown.

As is seen from Table 3, spin density in EO cation-radical is concentrated highly at the one oxygen atom. This species is likely to abstract hydrogen atom in a condensed phase giving rise to the oxonium ion.

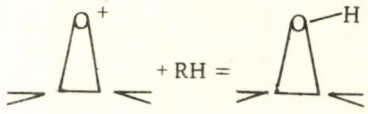

(8)

Formation of EO protonized molecule with a mass of 45 a. u. has been observed in a high-pressure mass-spectrometer in the range of $10^{-2} - 1$ torr /17/. The authors of Ref. /17/ believe that reactions proceeding under such conditions may take place in a condensed phase under irradiation as well. The oxonium ion breakdown in a condensed phase might occur through the addition of a slow electron resulting in an excited state formation. The same reaction according to the spin density distribution in the molecular cation-radical should occur in PO also.

The greatest decrease of the partitioned diatomic overlap value in $PO^{+\cdot}$ shows the C–O bond from the substituent side. It enables us to suppose the primary scission

of this bond and the following rupture of the carbon-carbon bond of the ring. The primary products of the $PO^{+\cdot}$ decay according to mass spectrometry data (Table 4) as well as to the molecular products of degradation determined by gas cromatography which are carbon monoxide, methane, hydrogen /16/ support this assumption.

As to the EO cation-radical, the most weakened bond in this species appears to be the C−Cl bond. Thus chlorine atom must be split off from this particle. Results of experimental investigation of ECH radiation-induced transformation support this view. Really, in the ECH electron impact mass spectrum (Table 4) the peak of 57 mass a.u., originating from C−Cl bond breakage, is the most intensive. The examination of stable products of this compound radiolysis also confirms the fact of prevailing rupture of the C−Cl bond. Thus, mass spectrometry of γ-irradiated ECH has shown under corresponding conditions the hydrogen chloride formation /18/. Electric conductivity of irradiated ECH revealed the kinetics of hydrogen chloride formation and its consumption in the secondary reaction with ECH. The product of this reaction, dichlorohydrin, is the major end-product of ECH radiolysis /19/.

Gaseous products of ECH radiolysis, carbon monoxide, ethylene, acetylene and hydrogene /16/, which arise as a result of the cycle bonds rupture in this case are due to glycidic cation decay. For this cation the strengthening of the C−O bond between the substituent and the cycle is inherent, the same being true for the removed C−O bond when it is compared with ECH molecule. At the same time the C−C bond in the ring and the C−O bond adjoining to the substituent decrease significantly the value of the partitioned diatomic overlap.

Accordingly, the second and the third peaks in the mass-spectrum of ECH in the order of their intensities are the mass of 27 and 29 a.u. These fragments may arise in the following reactions:

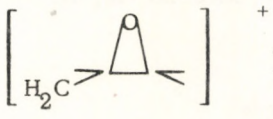

$$\rightarrow CH_2 = CH^+ + CH_2O \qquad (9)$$

$$\rightarrow CHO + CH_2 = CH_2 \qquad (10)$$

In conclusion we would like to point out that such a consideration does not of course reveal the whole complexity of transformations proceeding in a substance under ionizing radiations but to a certain extent it may be useful for interpretation of some details of radiation-induced reactions.

References

/ 1/ Yu. L. Frolov, S. M. Shostakovskii, G. I. Kagan, Theor. Exp. Khim. 5 153 (1969).

/ 2/ Z. M. Mulgakhmetov, A. V. Shchelkunov, K. A. Ajapberenov, I. I. Maj, Theor. Exp. Khim. 390 (1971).

/ 3/ T. Yonezawa, K. Simizu, H. Morimoto, H. Kato, Nippon Kagaku Zasshi, 90, 1196 (1969).
/ 4/ H. Fujimoto, M. Katata, Sh. Jamabe, K. Fukui, Bull. Chem. Soc. Jap., 45, 1320 (1972).
/ 5/ J. A. Pople, G. A. Segal, J. Chem. Phys., 44, 3289 (1966).
/ 6/ R. L. Flarry, Jr. D. Breen, D. L. Howland, Theor. Chim. Acta, 20, 371 (1971).
/ 7/ Tables of Interatomic Distances and Configuration in Molecules and Ions, London. Chem. Soc, Vol. 1, (1958).
/ 8/ W. C. Danen, J. Am. Chem. Soc, 94, 4835 (1972).
/ 9/ L. Radom, J. A. Pople, International Review of Science. Theor. Chem. Phys. Ser. one, v. 1, p. 71.
/10/ B. A. Murtagh, R. W. H. Sargent, Comput. J., 13, 185 (1970).
/11/ J. Pancir, Theor. Chim. Acta (Berlin), 29, 21 (1973).
/12/ A. P. Meleshevich, Usp. Khimii, 39, 444 (1970).
/13/ Sz. Ja. Psezseckij, Mechanism of radiation chemical reactions (in Russian) Khimija, 1968., p. 188.
/14/ A. Kornu, R. Masson, Mass spectrum catalog (in Russian) 1968.
/15/ T. Hoshino, K. Araki, M. Ishino, Annual Report of the Japenese Association for Radiation Research in Polymer, v. 1, 333, (1958–1959).
/16/ L. F. Kulish, A. P. Meleshevich, T. S. Antonovskaya, All-Union conference of epoxy monomers and polymers (in Russian), Dnepropetrovsk, 1974, p. 57.
/17/ A. Giardini-Guidoni, A. Mele, R. Platina, F. Zocchi, J. Chem. Soc. Faraday Trans., 71, 351 (1975).
/18/ A. Meleshevich, Y. Tabata, K. Ishigure, H. Kadoi, Ukr. Khim. Zhurnal, 41, 1013 (1975).
/19/ V. S. Zhiharyev, B. P. Zemskii, A. P. Meleshevich, Zh. Obshch. Khim. 43, 1377 (1973).

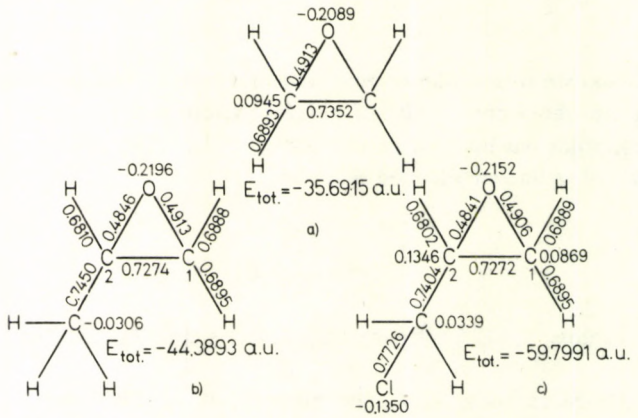

Fig. 1 Molecular diagrams of epoxides: a) EO, b) PO, c) ECH

acenaphthylene 377
acetamide 917
acetone 731, 897
acrolein 498
acrylamide 393
acrylamides n' substituted 406
  – substituted 401
acrylonitrile 419, 498, 513
  – urea channel complex 419
actinides 753
adamantane 37
ageing of polyester resins 545
alcohols 1017
aliphatic hydrocarbon radicals 853
alkaline earth nitrates 711
  – ice 679
alkali nitrates 711
alkene–diene mixtures 125
alkenes 147
N–tert alkylacrylamides 401
alkyl benzene sulphonate 837
  – iodides 809
  – naphthalene sulphonate 837
allyl palmitate 367
  – radicals 313
alpha irradiation 279, 656
amines 952
aminobenzylpenicillin 251
ammonia 264
anionic copolymerization mechanism 502
antibiotics 249
arenium ion 156
aromatic anion radicals 944
  – polyamides 471
aropol polyester 552
arsenic ions 761
arsenite ions 763

bacterial spores 1037
benzene 133
  – derivatives 40
  – styrene mixtures 133
benzonitrile 600
benzylpenicillin 250
bifunctional organic sulphur compounds 227
binary mixtures 43
biochemical systems 701
biopolymers 871
bromanil-tetrachloroquinone 377
bromodecane 330
Brønsted acids 209
butadiene–acrylonitrile rubber 527
butadiene–methylstyrene rubber 527
1–1' binaphthyl 303
n–butene–isobutene mixture 58
p–n butylbenzoyloxy benzoate 1032
p'n–butylphenyl benzoate 1032

$C_6H_4Cl_2$ 41
C_6H_4ClF 41

$C_6H_4ClNO_2$ 41
C_3–C_4 hydrocarbon mixtures 57
cadmium ions 947
cage effect 39
– reactions 39
canal complexes 413, 419
capture radius for radicals 321
carbocations 845
carbon tetrachloride 48
carboxybenzylpenicillin 251
cationic copolymerization mechanism 501
cationic polymerization 591, 599
cellulose 439, 664
– diacetate 667
– triacetate 667
cerium ions 777
N–cethyl acrylamide 367
N–cethyl methacrylamide 367
cethyl methacrylate 367
– vinyl ether 367
channel complexes 411
charge transfer 143
– complexes 201, 377, 583, 809
chelates 971
cholesteric state 1030
cholesteryl acrylate 367
– benzoate 1033
– methacrylate 367
– vinyl succinate 367
chloranil–tetrachloroquinone 377
chlorination of polyvinylchloride 457
chlorocomplexes of the platinum group 767
chromium ions 947
^{38}Cl replacement 41
Clostridium botulinum 1037
cloxacillin 250
coatings 545
Compton scattering 1058
conjugated dienes 132
copolymerization kinetics 499
cotton 439
crosslinking 337, 359, 482, 529, 536
crosslinking density 339
crystallinity 467
curing 535
– of polyester resins 545
cycloaddition 201, 613
cyclohexane 886
–N–ethylmaleimide mixture 613
N–cyclohexyl acrylamide 407
– methacrylamide 408
cyclopentane 77, 853
cyclopentene 853
cystine 702

D_2–alkylbenzene mixtures 155
D_2–arene 155
decane 330
n–decane 182, 333
degradation 434, 441, 449
– mechanism 437
dehalogenation 213
depolarization current 494
desoxyribonucleic acid 451, 745, 843, 924
desoxy ribose 742
dielectric depolarization spectroscopy 351
dielectric effects 721
dielectron 801
N–1,1–diethylpropylacrylamide 407
differential calorimetry 351
– thermal analysis 119
diffusion 513
– controlled reactions 793, 1061
1,2–dihydronaphthalene 592
dihydropirimidines 846
– diketonates of rare earths 963

dimer cation radical 592
dimethyl butane 184
N-2,4-dimethyl phenyl maleimide 584
diperoxides 567, 568
discrete spur model 1068
distribution of radicals 658
disulphide radical anion 703
DNA see desoxyribonucleic acid
DNP solutions 923
n-dodecane 171, 182
donor-acceptor pairs 613
doped organic glass 101
drugs 871
dry electrons 731
- electron reaction 194

n-eicosane 171
electroluminescence 487
electron attachment 163, 172
- mobility 172, 178, 179
- spin echo method 691
electron transfer 679, 941
- transfer reaction 330
- trapping 494
- tunnelling 944
emulsions 891, 903
ENDOR 951
energy transfer 57, 110
entanglements 339
enzymes 741, 827
epichlorohydrin 1071
epoxides 1071
ethane 49
ethanethiol 233
ethane-silicon oxide 243
ethanol 1003, 1017
ethidium bromide 874
ethyl bromide 164
- chloride 236
- p-ethoxybenzylidene-p'-aminocinnamate 1035
ethylene glycol 289, 931, 1005
- molecular levels 1054
- oxide 1071
ethylene propylene rubber 527
- vinylacetate copolymer 359
N-ethylmaleimide 1037
erythromycins 249, 255
excess electrons 1009
- electron solvation 991
excited states 57
extended chain polyethylene 313
eutectic mixture 393, 400

fabrics 577
ferric compounds 747
- ions 897, 931
ferrous ions 897, 931
- salt solutions 747
fibres 578
fillers 649
fluorescence 883
- quenching 945
forbidden ESR transitions 325
Fourier transform dielectric technique 351
free radical formation 521
fructose phosphates 827
fumaric nitrile 201

γ-globulin 701
glutathione, oxidized 701
glycidyl methacrylate 641
graft-copolymerization 497
grafting 513, 561, 569, 577, 663

H-atom abstraction 48, 725
H_2O^+-ion reactions 731
halobenzenium ions 212
n-heptane 182, 886
heptene-1 891
p-n heptyloxyphenyl acetophenone 1035

p-n hexadecyl oxybenzoic acid 1034
c-hexane 182
n-hexane 83, 162, 886
hexane-2,2-dimethylbutane 94
-2,3-dimethylbutane mixtures 93, 95
- vapour 519
1 hexene-cis 2, trans-4-hexadiene mixture 126
histone solutions 927
hopping 175
hot replacement 39
-tritium reactions 84
hydrated electron, reactions 793, 819
- recombination 801
hydrates 787
hydrogen atoms 247, 263
hydrogen chloride 991
- peroxide 853
- sulphide 268
- sulphide-ethylene mixture 268
hydrogenated polyethylene 314
hydroperoxides 563
hydroxymethyl radicals 271
human serum albumin 701

inhibiting effects 377
inhibition 603
- effects 470
- of Ps-formation 193
- of polymerization 386
inhibitor method 632
initiation of chain processes 981
inorganic ions 197
- organic polymer compositions 507
interspin distance 326
iodine scavenger 88
ion-molecule reactions 235, 796
- pair recombination theory 973
ionic copolymerization 497
- grafting 497
- polymerization 623, 645
iridium complexes 767
isobutene-thiourea channel complex 411
isobutene-vinylidene-chloride-thiourea complex 411
isobutylene 497
isomerization 158, 477
cis-trans isomerization 204
isooctane 182, 184
- ethanol chlorobenzene 296
iso-pentane 75
di-isopropyl amine 954
isothermal luminescence 698

ketyl radical 889

lanthanide atoms 963, 985
lanthanides 755
laser flash photolysis 449
- illumination 271
- photolysis 881
LET effect 655
light scattering apparatus 452
linen 439
liquid crystals 1027
lithium nitrate 713
luminescence 101, 139

magnesium nitrate 713
marble-polymer compositions 510
marlex 314, 348
mercapto-acids 219
metal-ions 941
methacrylamides, substituted 406
methacrylonitrile 626
methanol 29, 271, 725, 1003, 1017
- glass 272
p-methoxybenzylidene-p'-aminophenyl-n-pentanoate 1033
methyl cyclohexane 119, 698
- methacrylate 552

2-methyl-2-nitrosopropane spin trap 289
3-methylpentane 182
- glass 101
methyl propane 184
- radicals 725
- methyl styrene 497, 598, 625
mixed radiation dosimetry 295
molecular diagram of epoxides 1073
Monte Carlo method 387
multicharged ions 1043

-naphtol 465
natural rubber latex 477
neopentane 141, 184
neutralization of ions 49
neutron dosimetry 295
- irradiation 40, 243
nitrite ions 718
nitrobenzene 600
p-nitroso dimethyl aniline 739
-nitrostyrene 623
n-nonane 182
nuclear magnetic resonance 335
nucleic acids 742

n-octane 182
1-octene-1,7 octadiene mixture 127
OH-rate constants 739
oligo-diene urethane acrylate 532
one-electron reactions 701
optical bleaching 113
Ore model 189
organic cations 911
osmium complexes 767
oxidation 893
oxidative degradation 437, 445, 476
oxygen anion 947
- reactions 911
oxygen effect 600, 604
ozone anions 911

paraffin 325
penicillin 249
n-pentane 67, 73, 182, 854
cis-pentene-2 111
p-n-pentyloxyphenyl acetophenone 1034
peroxidation 562
peroxide yield 562
peroxy radicals 525, 566
phase diagram 383
- relaxation 692
phenothiazine 465
phenyl acetylene 498
N-phenylacrylamide 408
phenylethane thiol 233
N-phenylmethacrylamide 408
phosphorescence 101, 112
photoabsorption cross section 1053
photobleaching 421, 676
photochemical reactions 201
photoconductivity 685
photoionization cross section 1055
photolysis 621
- compared with radiolysis 205, 268
picosecond pulse radiolysis 819
pilot plant experiment 554
platinum complexes 767
- group metals 767
plutonium oxide ions 785
polarization interactions 793
polyacrylonitrile 517
polyamide fabrics 577
polyamides 465
polycaprolactam 656
polydimethyl siloxane 335
polyester resins 535, 545
polyethylene 171, 313, 348, 353, 359, 382, 491, 498, 517, 521, 561, 569, 649, 656, 663
polyethylene terephthalate 656
polyfunctional substances 527
polyisobutene 450

polyisobutylene 656
cis-1,4-polyisoprene 477
polymethyl methacrylate 450, 656
polymethyl vinyl ketone 451
polymorphic modifications 373
polyoxymethylene 332
polypropylene 351, 521, 563, 572, 656
polytetrafluoroethylene 431, 513, 521
polyvinyl chloride 505, 663
polyvinyl fluoride 663
- toluene 489
positron 189
positron lifetime measurement 191
positronium 189
- formation 737, 1009
- inhibition 1012
post scavenging technique 67
potassium nitrate 713
presolvated electron reactions 999
pressure effect 521
preglow luminescence 486
propane 49
- cyclopropane mixture 60
2-propanol 897
propanols 1019
propylene oxide 498, 1071
proteins 701
proton transfer 155
pulse radiolysis 591, 599, 749, 809, 819, 881
pulsed NMR 335
pyrimidine radicals 845
pyrogallol 465

quasi-free electron mobilities 184
quinhydrone 465

racemization 303
radiation chlorination 457
- curing of rubbers 527
- curing of polyester resins 535
- induced conductivity 171, 179
- protection 465
radical decay 313, 434, 566
radical-radical distance 326
- formation kinetics 445
- pairs 325
- stabilization 655
radio thermoluminescence 139
random walk model 1063
recoil T-atoms 83
- T-atom reactions 83
reduction of metal ions 777
- of platinum complexes 769
reprocessing of fuel elements 279
rhodium complexes 767
ribose 742
- monophosphate 742
ribonuclease 701

SF_6 52
scavenging presolvated electrons 1000
scintillators 489
sensitizing of copolymerization 583
silica gel 244
silicones 335
silk 663
sodium acetate hydrate 725
- hydroxide glass 675, 686, 691
- nitrate 713
- o-iodohippurate 861
sol-gel mixtures 341
solid state polymerization 365, 377, 387, 393, 401, 415, 419, 631
solvated electrons 271, 272, 882, 951
solvent effect 600, 605
sorption of water 668
spatial distribution of trapped electrons 691
spin trapping 29, 289, 1017
spur model 190
- simulation 1062

stroboscopic pulse radiolysis 819
strontium nitrate 713
structural data of monomers 368
styrene 133, 498, 569, 591, 882
- acrylonitrile mixture 552
sugar 742
sulphate anion 947
sulphur hexafluoride 165
surfactants 837

teflon 572
terpolymers 586
tetraalkyl ammonium cations 911
2-tetrahydro-2-methylfuran 31
tetra-methaerylate bis glycerolphthalate 530
tetramethyl butane 140
- hexane 140, 184
- pentane 184
thermoluminescence 485
thermomechanical curves 352
thermorestoration of radiation damage 1037
thioacetamide 917
thioacetic acid 223
thioacids 219
thioglycolic acid 220
thio-3-pentanethiol-5 227
-pentanol-5 227
thiourea 441
thiyl radicals 228
topochemical polymerization 365
track structure 1043
transient ion pairs 809
transiton metal complexes 941
trap size 961
trapped electrons 673, 679, 685, 691
tributyl phosphate-CCl_4-HNO_3 extraction system 279
trichloroethylene 165
triethylamine 960
trimethylbenzenes 159
trimethyl-oxydisilane methacrylate 527
triplet state 334
2,4,6 tri-tert butylnitrosobenzene 30
tritiated halobenzenes 210
tritio-deprotonation 211
tunnelling 488, 673, 698, 730, 941, 1006
- decay of trapped electrons 973

unsaturated polyester resins 535
urea 419
u. v. degradation of polyester resins 550

valence migration 334
vapour phase grafting 577
n-vinyl carbazole 393, 599
- acrylamide mixture 396
vinyl fluoride 663
- laurate 367
- n-butyl ether 497
N-vinyl phthalimide
vinyl pyridine 498
- oleate 367
vinylidene fluoride 663
viomycin sulphate 249, 253
viscose fabrics 577
vulcanisation 477, 533

waste waters 837
water 1005
water radiolysis 731
wetting 668
wood-plastic composites 551
wool 577

xylenes 158
p-xylene 903

WE RECOMMEND

RADIATION CHEMISTRY
Proceedings of the 1962 Tihany Symposium

Edited by J. Dobó

In English — 482 pages — 253 figures — 59 tables — 16×22 cm — Cloth

PROCEEDINGS OF THE SECOND TIHANY SYMPOSIUM ON RADIATION CHEMISTRY

Edited by J. Dobó and P. Hedvig

In English — 813 pages — 453 figures — 111 tables — 17×25 cm — Cloth

PROCEEDINGS OF THIRD TIHANY SYMPOSIUM ON RADIATION CHEMISTRY

Edited by J. Dobó and P. Hedvig

In English — In two volumes — 1458 pages — Numerous figures and tables — 17×25 cm — Cloth

FROM THE REVIEWS ABOUT THE ABOVE VOLUMES

"... The editors are to be congratulated upon the rapidity of publication in English and on the generally high standard of translation..."

CHEMISTRY AND INDUSTRY, London

"... For radiation chemists who have participated in this meeting and enjoyed excellent Hungarian hospitality, and for those who have not had that opportunity, this volume is most highly recommended as a source book..."

NATURE, London

"... This volume is therefore of considerable interest to readers in this country, as it provides, in English, a valuable entry to the radiation chemistry literature of a part of the world that has been especially active in the study of radiation effects..."

SCIENCE, Washington

Distributor
KULTURA
H-1389 Budapest, P.O.B. 149

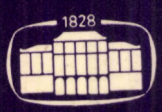

AKADÉMIAI KIADÓ, BUDAPEST